Underground Nuclear Testing in French Polynesia:

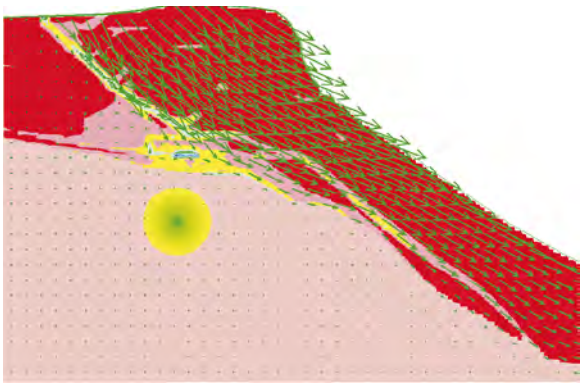

Stability and Hydrology Issues

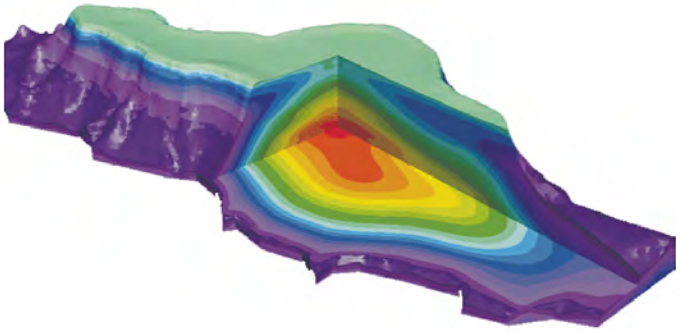

Volume I, General Results

International Geomechanical Commission
Charles Fairhurst, Chairman

Stability and Hydrology Issues Related to Underground Nuclear Testing in French Polynesia:

Volume I, General Results

A Report of the
International Geomechanical Commission

Charles Fairhurst, Chairman

Prepared under a contract with the University of Minnesota,
Minneapolis, Minnesota, U.S.A.

This report is published in three volumes: Volume I, *General Results*; Volume II, *Technical Analyses*; and Volume III, *Les Essais Nucléaires Souterrains en Polynésie Française: Stabilité et Hydrogéologie* (French language extracts from Volumes I and II). These volumes may be obtained from:

La Documentation Française
29, quai Voltaire
75344 Paris
Cedex 07
France

Printed in the United States of America.
This report has been reproduced from the best available copy.

On the cover : The upper figure shows calculated contours of plastic shear strain and displacement vectors at the Mururoa Atoll rim due to a 10-kilotonne explosion. Details of the calculations are described in Volume II, Chapter 5 of this report.

The lower figure shows a three-dimensional "cut-away" view of the temperature contours computed for the interior of Mururoa Atoll, in the natural condition — i.e. prior to underground nuclear testing. Details of the numerical calculations are given in Volume II, Chapter 6 of this report.

Members of the
International Geomechanical Commission

Chairman

Charles Fairhurst (U.S.A.)

Commission

Edwin T. Brown (Australia)

Emmanuel Detournay (Belgium/U.S.A.)

Ghislain de Marsily (France)

Victor Nikolaevskiy (Russia)

J.R. Anthony Pearson (Great Britain)

Lloyd Townley (Australia)

Technical Liaison

Pierre Bérest (France)

Brief biographical sketches of Commission members and main Consultants are given in Appendix A.

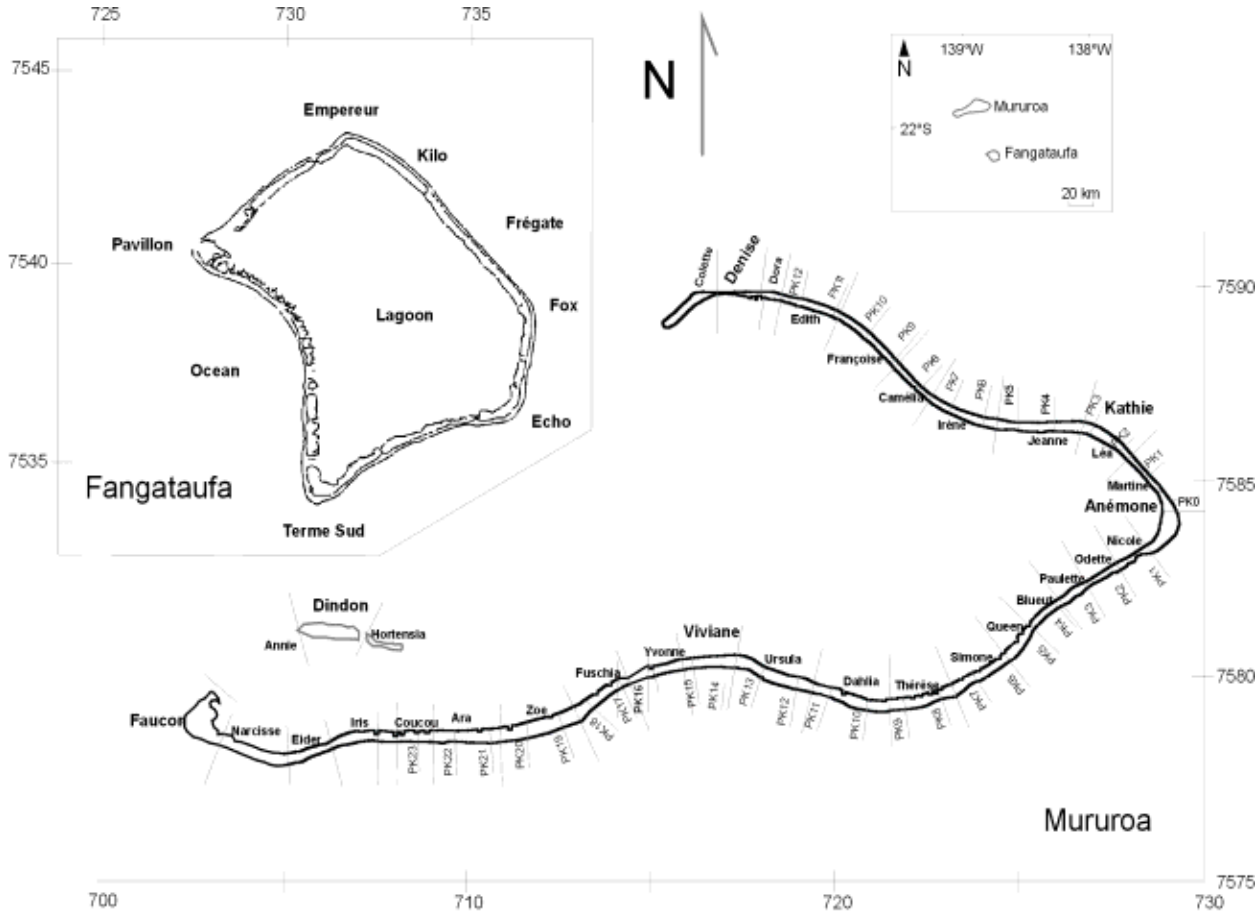

Local designations of the various sectors of Mururoa and Fangataufa. Local co-ordinates shown are Universal Transverse Mercator co-ordinates (in km) for the Southern Hemisphere. Correct relative geographical locations of the atolls are shown in inset diagram (upper right).

PREFACE

The French Nuclear Testing Programme

Gerboise bleue, a relatively low-yield explosion (estimated $60 \sim 70$ kt*), detonated in the Sahara desert, at Reggane, Algeria, on 13 February 1960, marked the debut of France as a nuclear power — some 15 years after the world's first nuclear explosion (Trinity) at Alamagordo, New Mexico, USA, on 16 July 1945. During those 15 years, the United States of America had detonated 196 explosions, the Soviet Union 84, and the United Kingdom 21. Except for 22 underground explosions at the Nevada Test Site in the United States, all of the 301 tests were conducted in the atmosphere. In November 1958, these three countries jointly declared a moratorium on testing. The moratorium lasted until September 1961.

In November 1961, after 4 atmospheric tests at Reggane, France proceeded to a series of 13 underground tests detonated deep within horizontal tunnels excavated in the Hoggar granite mass at In-Eker, some 560 km ESE of Reggane. This series concluded 16 February 1966, due, at least in part, to the political situation in Algeria. In the meantime, the United Kingdom, USA and USSR had signed the Limited Test Ban Treaty (5 August 1963), which banned nuclear testing in the atmosphere, outer space or under the open ocean.

Aldebaran, the first French test in the South Pacific, took place on 21 July 1966. It was an atmospheric explosion from a barge on the Mururoa lagoon, the first of a total of 41 atmospheric explosions: 37 on or near Mururoa (including Procyon, with a yield over 1 Mt*), and 4 on Fangataufa (including Canopus, with a yield over 1 Mt) (see figure on the following page). Five surface safety trials† were also carried out on Mururoa, 2 of which resulted in a (small) nuclear yield. Atmospheric tests ended 14 September 1974.

---

*1 Mt implies an energy release from, or *yield* of, a nuclear explosion equivalent to the detonation of one million tons of the chemical explosive tri-nitro-toluene (TNT) ($4.18 \cdot 10^{15}$ joules). 1 kt implies the energy release corresponding to 1,000 tons of TNT ($4.18 \cdot 10^{12}$ joules), which is the mechanical equivalent of 10^{12} calories of heat energy.

The Threshold Test Ban Treaty (1962), agreed to by the Soviet Union and the United States, placed an upper limit of 150 kt on the yield of underground tests. CEA (Bouchez and Lecomte 1996, Appendix, p. 113) claims that all underground tests conducted by France were below the 150-kt limit. International seismic monitoring results (see Vol. II, App. C) support this assertion.

†A safety trial involves detonation of an annulus of chemical explosive placed around the nuclear device to determine whether this explosion results in a nuclear explosion (or "yield").

Underground testing on the atolls began with two small tests (Achille and Hector) beneath the southern rim of Fangataufa on June 5, 1975, and November 26, 1975. By the time this series was completed in July 1991, a total of 131 underground tests had been conducted: 123 at Mururoa (73 under the rim and 50 under the lagoon) and 8 at Fangataufa (2 under the rim and 6 under the lagoon). An additional 10 underground safety trials, 3 of which resulted in a small nuclear yield[‡], were carried out on Mururoa. France announced its own moratorium on nuclear testing in September 1991.

Location of Mururoa and Fangataufa with respect to major continental land masses

The Final Campaign of Tests

Britain, the United States and Russia had already announced their readiness to adopt the proposed Comprehensive Test Ban Treaty, banning all nuclear weapons testing, when, in June 1995, President Chirac unexpectedly announced that France would conduct a limited number (not to exceed 8) of underground tests at Mururoa and Fangataufa before signing the Treaty[¶]. A total of 6 additional tests were carried out (4 at Mururoa and 2 at

[‡]Note that the 3 "nuclear" safety trials are included in the 134 underground tests listed in the appendix to Bouchez and Lecomte (1996). With the 6 tests of the 1995/1996 series, a total of (131 + 10 + 6 =) 147 underground tests and safety trials have been conducted on Mururoa and Fangataufa.

[¶]France signed this Treaty when it was adopted by the United Nations in 1996; it was approved by the French Parliament in March 1998. Britain, China, Russia and the United States have also signed the Treaty. The treaty has not yet taken force.

Fangataufa — all under the lagoons) between 5 September 1995 and 27 January 1996, when France announced that the series was complete. Between 13 February 1960 and 27 January 1996, France had carried out 210 nuclear tests, including the 15 safety trials. Details of all known tests worldwide (USA 1,030; USSR 415; France 210; China 45; U.K. 45, India 6; Pakistan 6[§]) are given in the table in Volume II, Appendix B.

The decision to conduct this final campaign, three years after all countries except China had stopped testing, provoked widespread concern and international protests that the tests, added to those already carried out, could result in severe adverse short-term[‖] and long-term consequences. Release into the environment of dangerously radioactive nuclides produced by the explosions and damage to the mechanical stability and hydrology of the atolls were the two principal issues.

Invitations to Study the Effects of Underground Tests

Responding to the concerns and protests, M. Hervé de Charette, the French Minister of Foreign Affairs, acting on behalf of President Chirac, invited two international groups to conduct separate, independent investigations of the consequences of the underground tests on Mururoa and Fangataufa.

The International Atomic Energy Agency (IAEA), headquartered in Vienna, agreed to examine the issue of radiological releases. An international conference to discuss the findings was held at IAEA headquarters in Vienna, 30 June 30–3 July 1998. The official report was released in August 1998.

Professor Charles Fairhurst, then President of the International Society for Rock Mechanics (ISRM), was asked to select and lead an independent group of international experts, designated as the International Geomechanical Commission (IGC), to study the stability and hydrology issues. The members of the IGC and support staff are listed in Appendix A, together with a brief biographical sketch of each member. This report presents the results of the IGC study.

Sources of Information

The Commission met several times (see box on page IX) with scientists of the Commissariat à L'Energie Atomique (CEA)** during the early phases of the study to obtain background information and to raise questions. Core samples from the Zoé borehole

[§] India detonated 5 underground tests, 11–13 May 1998; Pakistan announced 5 tests, 28 May 1998, then 1 on 30 May 1998. Some seismic detection experts have suggested that fewer than 5 devices were detonated on 28 May.

[‖] "Short-term", here, implies the period of testing to approximately 500 years from the cessation of underground testing. "Long-term" implies a period of the order of 10 000 years from the cessation of underground testing.

**Commissariat à L'Energie Atomique (CEA) is the French Atomic Energy Commission.

on the south-central rim of Mururoa, continuous from the surface through the carbonates and volcanics to a depth of 1100 metres were examined in the CEA headquarters at Bruyères le Chatel, south of Paris.

Commission members spent three days on Mururoa and Fangataufa (10–12 July 1996) and examined all accessible testing and affected areas on the rim by car and on foot. Both atolls also were studied at low altitude from a helicopter. Still and video-camera photographs were allowed without restriction.

On Mururoa, particular attention was paid to test area 1, where substantial volumes of the ocean-side rim have been undergoing continuous deformation for almost two decades, and test area 4, the most intensively used (in terms of total explosive yield per unit volume of rock) and the site of the large underwater slides induced by testing. On Fangataufa, fractures activated in the northeast rim in the vicinity of Kilo-Frégate were examined. This area is unique in that tests on Fangataufa were not conducted on the northeast rim. This implies that these fractures were *stimulated* by the seismic waves created by tests in other areas of the atoll — most probably, the large-yield tests under the lagoon.

Although, as mentioned earlier, the locations of individual tests (including depths) were not provided, the surface locations of many of the tests on the rim were visible from the air, especially on Mururoa.

Documents

The two-volume publication *The Atolls of Mururoa and Fangataufa — Volume 1, Geology, Petrology and Hydrogeology* (Guille et al. 1996) and *Volume 2, Nuclear Testing, Mechanical Lumino-Thermal and Electromagnetic Effects* (Bouchez and Lecomte 1996), available (in French[††]) at the start of the study, provided a comprehensive, general overview of CEA studies and the physical consequences of nuclear testing on the atolls. These were supplemented by a number of doctoral theses and publications of work related to the structure and hydrology of the atolls. Copies of reports by the three previous missions — the June 1982 mission led by the late Professor Haroun Tazieff (Tazieff 1982), followed, in October 1983, by a group from New Zealand, Australia and Papua, New Guinea, led by Mr. H. R. Atkinson (New Zealand MoFA 1984), and the Mission Scientifique de la Calypso, in July 1987, led by the late Commandant Jacques Cousteau (Fondation Cousteau, Paris 1988)[‡‡] were also provided.

[††] An English version of those parts of Vol. 2 related to underground testing (i.e. parts 4–9, plus appendix) was provided by DIRCEN/CEA for the benefit of the IAEA and the IGC groups. Publication of a complete, official, English version of Vol. 2 is planned by CEA/DASE.

[‡‡] Commandant Costeau's visit and findings concerning Mururoa also form part of the video "Tahiti, L'eau de feu," available from Equipe Cousteau, 7 rue Am d'Estaing, 75016, Paris (phone: +33 1 53 67 77 77; fax:+33 1 53 67 77 71)

Meetings of the International Geomechanical Commission

18–20 March 1996, Ecole des Mines & Bruyères le Chatel, Paris, France
Full Commission

27–29 May 1996, Minneapolis, Minnesota, USA
Stability Sub-Group and Consultants

30 May 1996, University of Paris VI, France
Hydrology Sub-Group and J. Hadermann

9–13 July 1996, French Polynesia: Tahiti; Mururoa & Fangataufa Atolls
Full Commission and CEA Officials

6–7 September 1996, University of Paris, France
Hydrology Sub-Group

21–22 September 1996, Chaska, Minnesota, USA
Stability Sub-Group and Consultants

20–21 December 1996, Cambridge, England
Full Commission and Consultants

14 February 1997, Montlhéry, France
E. T. Brown and Pierre Bérest

7–10 May 1997, Fontvieille, Provence, France
Full Commission and Consultants

28 June 1997, New York City, New York, USA
Stability Sub-Group

15–16 August 1997, Vienna, Austria
Hydrology Sub-Group and Pierre Perrochet (EPFL)

24–27 October 1997, Lewis, Wisconsin, USA
Full Commission, CEA Officials and Consultants

The documents were supplemented later by a more detailed and up-to-date series of 12 technical reports prepared by CEA scientists (again, in French and English). These documents, referred to here as DIRCEN/CEA Documents 1 through 12, have been used extensively by the Commission and are available through La Documentation Française (see the listing before the References for details).

Although the later-than-anticipated publication of these reports was an initial source of frustration to IGC members, it can be seen, in retrospect, to have had a positive effect in that members were obliged to concentrate on developing their own understanding of the mechanics of underground nuclear explosions and the effects of the explosions on the stability and hydrology of the atolls. This provided a greater insight, independently formed, that allowed a more critical review of the DIRCEN[¶¶]/CEA reports when they arrived.

More specific information would have allowed more detailed analyses in some instances. Coordinates of the Nestor, Priam and Tydée tests, for example, may have led to a better understanding of the factors governing the underwater slides produced by these tests. Why, for example, did the Tydée explosion provoke a slide approximately 2 km to the west of the explosion rather than on the directly adjacent slope, as would be expected? Were the Nestor and Priam slides of this more classical type and Tydée an *anomaly*, perhaps related to some local changes in the character of the underwater slopes?

Similarly, CEA scientists measured the temperature variations with depth in the emplacement boreholes prior to a substantial number of tests, but these data could not be made available to the IGC because, again, this information may identify individual test locations, which the CEA did not wish to reveal. These data would have allowed IGC to develop a more precise three-dimensional computer simulation of the hydrology of Mururoa. Eventually, after the IGC simulations had been completed, some data were made available in the form of minimum temperature contours (see Fig. 6.12). The comparison is considered to be very good, given the limited information available when the simulation was carried out.

It should also be acknowledged that, even if the precise coordinates of every test had been available to the IGC, significant uncertainty in the geomechanical characteristics of the rock in the vicinity of a test would remain — a consequence of the inherent heterogeneity in the mechanical properties of a rock mass such as the volcanics of the atolls.

[¶¶] DIRCEN (Direction des Centres des Essais Nuclèaires) is the Nuclear Testing Division of the CEA, the French Atomic Energy Commission.

A Final Note on Findings

In this report, the scientific bases for the IGC's conclusions are laid out in sufficient detail for colleagues to see how the conclusions were drawn. Notwithstanding the data limitations, it is believed that the Commission has been able to arrive at a good understanding of the stability and hydrological consequences of the underground testing and that the conclusions drawn are soundly based and robust.

An opportunity for open discussion of the IGC report will be offered in conjunction with the ISRM 9th International Congress on Rock Mechanics, which will be held 25–28 August 1999, in Paris. All interested colleagues are invited to participate in this discussion. IGC members will also prepare and submit papers based on this study for publication in international refereed scientific journals. Details on the session concerning underground nuclear testing will be announced in 1999 by the ISRM.[§§]

[§§] For details, please contact: Congrès ISRM, c/o G. Vouille, Ecole des Mines de Paris, 35 rue Saint Honoré, F-77305 Fontainebleau, France (telephone: +33-1-64.69.48.97 / telefax: +33-1-64.69.47.11 / email: congres.paris.99@cges.ensm.fr / internet: www.ensmp.fr/ISRM99

ACKNOWLEDGEMENTS

This report marks the conclusion of what was, officially, a one-and-a-half-year study, contracted between the Government of France and the University of Minnesota. The study has, in fact, taken almost three years to complete by the International Geomechanical Commission (IGC), an independent international group of experts assembled specifically for the study.

The delay in completion is not a result of inattention to the subject. On the contrary, it is primarily a consequence of the IGC's determination to establish a sound scientific and technical foundation on which to base its examination of the consequences of underground nuclear testing on the stability and hydrology of Mururoa and Fangataufa. It was necessary to undertake fundamental analyses on a variety of topics in order to make an independent assessment of the information and data provided by CEA (Commissariat à l'Energie Atomique) authorities. Some appreciation of the task can be gained from the topics covered in the appendices to the report. In many instances, these contain a summary only of the results of analyses. Considerable effort was often needed to develop the analyses.

It has been a special privilege and valuable experience to have worked with colleagues of the IGC and its two main consultant groups — Itasca Consulting Group, Inc., Minneapolis, U.S.A., for stability studies and administrative support; and Ecole Polytechnique Fédérale de Lausanne; (EPFL), Switzerland, for hydrology studies and computer graphics. Professor E. Detournay led and coordinated the stability studies; Dr. L. Townley and Professor G. de Marsily led and coordinated the hydrology studies.

Consultants Branko Damjanac and Peter Cundall, from Itasca, and Pierre Perrochet and Laurent Tacher, from EPFL, attended all IGC meetings (except for the initial meeting of the full Commission, in July 1996) and made invaluable contributions, in addition to preparing major portions of the analyses and material included in the report. Similarly, Professor Pierre Bérest, Ecole Polytechnique, Palaiseau, France, Technical Liaison between the IGC and French authorities, was an important asset.

The IGC had not worked together previously as a group, but soon established a very productive working environment. The mix of disciplines and the desire to comprehend both the underlying principles of ideas presented and the specific implications for the study led to stimulating and informative exchanges, improved understanding of the issues and, eventually, a stronger report.

The visit to Mururoa and Fangataufa and CEA geophysical installations in Tahiti, in July 1996, was a key element of the IGC study; it provided essential insights and understanding of the nuclear testing programme on the atolls that would not have been achieved otherwise. Senior scientific and technical personnel of DIRCEN/CEA (see footnotes in Preface, pp. vii and x) accompanied IGC members, providing briefings and commentaries and answering questions throughout the visit. Cameras and video recorders were allowed without restriction. The writer also visited the atolls in December 1996, as part of the International Atomic Energy Agency (IAEA) study group, and was able to re-examine areas of special interest with respect to atoll stability. Together with several technical discussions between DIRCEN/CEA staff and IGC (see the Overview), these exchanges supplemented appreciably the material presented in DIRCEN/CEA documents and reports. The considerable efforts taken to make these visits informative and pleasant by DIRCEN/CEA staff are sincerely appreciated.

Associates of individual IGC members have made important technical contributions to the study. Specifically, Dr. Carlos Carranza-Torres, formerly of the University of Minnesota, carried out the analyses and computer simulations for Appendices H.1 and I, and prepared graphical material. Also from the University of Minnesota, Dr. Igor Janković and Philippe Le Grand undertook the analyses and computer simulations for Appendix E, and Mrs. Haiying Huang carried out the three-dimensional analyses discussed in Chapter 5.4 (Figures 5.12–5.14). Dr. Anthony Smith of CSIRO Division of Land and Water performed a number of runs using the AQUIFEM-P program for the appendix on analysis of periodic groundwater flow. Professor P. A. Persson of the New Mexico Institute of Science and Mining Technology supplied information on the "yield" of TNT explosives for a footnote in the Overview.

The University of Paris VI, the Paris School of Mines and the Ecole Polytechnique generously made their facilities available to the IGC for several meetings.

Dr. Elena Luquet of the Institute of Physics of the Earth, Moscow, assisted Prof. Nikolaevskiy in his preparation of materials for the IGC.

Many individuals experienced in various aspects of the U.S. nuclear testing programme also provided valuable information and background details. Dr. Charles Archambeau (TRAC, Inc., Denver, Colorado), a distinguished seismologist, provided very helpful background information and constructive suggestions at an early stage of the IGC study; Norman R. Burkhard, Lawrence Livermore National Laboratory, Livermore, California, supplied a set of unclassified Proceedings of the Symposia on Containment of Underground Nuclear Explosions; Drs. John T. Cherry (President, Science Horizons, Inc., Missouri) and Theodore R. Butkovich (now retired), pioneers in much of the original efforts in analytical and numerical modelling of underground explosions, each provided valuable comments on early IGC studies, in interviews with Professor Nikolaevskiy; and Dr. Edward W. Peterson (S-cubed, San Diego, California) provided valuable insights into both the mechanics of cavity expansion and near-field damage (see Appendix D).

Preliminary drafts of sections of the IGC Report were sent for external review to distinguished international experts. Dr. B.H.G. Brady, Professor of Geomechanics and Executive Dean of Engineering, University of Western Australia, and Dr. Shunsuke Sakurai, Professor of Civil Engineering, Kobe University, Japan, and current President of the International Society for Rock Mechanics, each provided valuable, independent comments on the stability sections of the report (Chapters 3 through 5).

Colleagues involved in the IAEA technical studies, especially Robert Fry (Technical Director, IAC study, Vienna, Austria), Des Levins (ANSTO, Sydney, Australia), Lars Eric de Geer (Swedish Defence Ministry, Stockholm, Sweden), Eberhardt Mittelstaedt (Federal Maritime and Hydrographic Agency, Hamburg, Germany) and colleagues from IAEA Working Group 4, J. Hadermann (Paul Sherrer Institut, Villigen, Switzerland), H. Nitsche (Institute of Radiochemistry, Dresden, Germany), A. S. Sastratenaya (National Atomic Energy Agency, Jakarta, Indonesia) and G. Warnecke (IAEA, Vienna, Austria) provided many questions and comments that led to several changes and additions to the IGC Report.

Interactions with technical and administrative staff of the CEA — General M. Boileau, Colonels P. Delcourt and G. Corion and Mme T. Delpech; MM. Alain Barthoux, Jacques Bouchard, Jacques Bouchez, Yves Caristan, Christophe Guy and Jean-François Sornein — have been indispensable throughout the IGC study. At all times, IGC members have been received with exceptional courtesy and hospitality, notwithstanding the sometimes delicate balance and restraint required to avoid revealing details considered confidential, and to withhold comment where appropriate, in order to respect the independence of the IGC's findings. The particularly close interaction with Dr. Caristan and his associates, J. Bouchez and J.-F. Sornein, allowed the IGC to develop respect not only for their professional competence, but also for their diplomacy.

Associate Dean Steve L. Crouch monitored the project on behalf of the University of Minnesota and resolved, expeditiously, various administrative issues.

Several of the IGC members acted as hosts for the Commission meetings, all of which were important and memorable events. Anthony and Emma Pearson arranged the Cambridge, U.K. meeting; Ghislain and Gunilla de Marsily arranged the meeting in Provence, France; and Kathy Sikora and Itasca colleagues coordinated the meeting in Lewis, Wisconsin, U.S.A.

Professor Bérest, aided by M. B. Brouard of Ecole Polytechnique, undertook the very formidable task of translating and assembling all of the material for Volume III. This work has been reviewed carefully by IGC members and is an integral part of the IGC Report. We are greatly indebted to MM. Bérest and Brouard for completing this large, voluntary effort, which makes our report more readily accessible to a wider range of readers.

Kathy Sikora was the administrative coordinator for the IGC study, including arrangement of all meetings, preparation and distribution of minutes, communication with

members, and a multitude of other tasks, including the formidable challenge of finally integrating everything required to produce this report — an amazing feat. Chad Sylvain, of Itasca, converted and edited the graphics files, provided in a variety of formats by Committee members, consultants and DIRCEN/CEA, to produce the excellent illustrations in the report.

Donna Ahrens, independent scientific editor, supervised editorial integration of the report, cover design, preparation of the glossary, and all the many other editorial responsibilities.

My wife Margaret assisted in many ways, not the least of which was her uncomplaining acceptance of the many late nights and weekends (far more than anticipated) needed to complete the report, and typing and revising several sections of the final text.

To all of these, and many others, we express our sincere thanks and appreciation and hope that the result is considered to be one worthy of all their efforts.

Charles Fairhurst
Minneapolis

TABLE OF CONTENTS

LIST OF FIGURES

LIST OF TABLES

Chapter 1

CONSEQUENCES OF CONFINED NUCLEAR TESTS IN MURUROA AND FANGATAUFA

1.1 Introduction

The decision by France, in 1995, to resume underground testing of nuclear weapons in the South Pacific atolls of Mururoa and Fangataufa, led to worldwide protest and claims that underground testing, conducted from 1975 to 1990, had resulted in lasting damage to the stability and hydrology of the region and would lead to dangerous releases of radionuclides to the environment. President Chirac, in response, announced that two International Commissions of independent experts would be established by France to investigate the actual consequences of the tests with respect to these factors.

A Past President of the International Society for Rock Mechanics, Professor Charles Fairhurst, of the University of Minnesota, U.S.A., was asked in 1996 by the Government of France to set up an International Geomechanical Commission (IGC) to investigate the consequences of the underground nuclear tests carried out by France in Mururoa and Fangataufa (also referred to as the Pacific Test Centre, or PTC) for the mechanical stability and hydrological regime of the two atolls. The International Atomic Energy Agency (IAEA) was similarly asked to report on the radiological consequences of the tests. Because the hydrological consequences of the tests are directly related to the movement of radioactive materials, three members of the IGC also served on the IAEA group concerned with radionuclide transport through the rock. The composition of the IGC and its access to the French Ministry of Defence (through DIRCEN, CEA and DASE) and to the IAEA Commission are given in Figure 1.1. Brief biographical sketches of the IGC members and support staff are given in Appendix A of Volume II.

DIRCEN/CEA has provided a series of 12 documents (all available to the public and referred to here as DIRCEN/CEA Document No. 1, 2, etc.) that summarise all this information from the CEA (see listing following Chapter 1). According to DIRCEN/CEA Document No. 6, DIRCEN carried out a total of 147 underground experiments (including underground safety tests that took place in the carbonate layer) at the two atolls, yielding a total of 3.2 megatonnes (Mt), mostly on Mururoa (130 yielding 2.4 Mt and averaging 20 kt), with a small number of larger ones on Fangataufa (10 yielding 0.8 Mt and averaging 80 kt). The highest yields were below 150 kt, and more than half did not exceed 10 kt. For comparison, it may be noted that the aerial explosions over Hiroshima

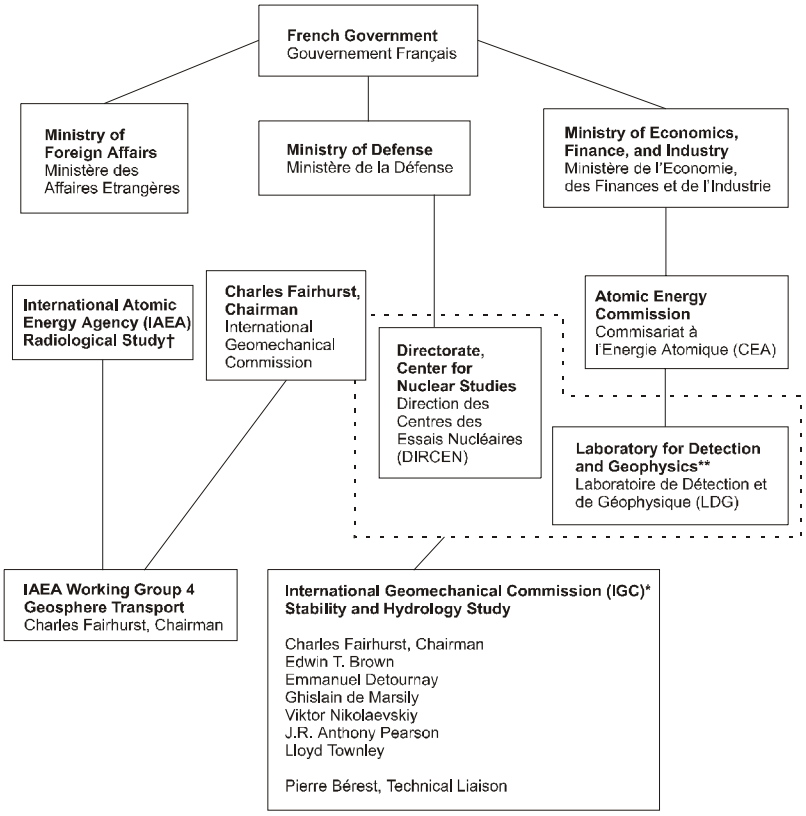

†Results of the IAEA study have been published in a series of reports (*The radiological situation at the atolls of Mururoa and Fangataufa*), prepared by an International Advisory Committee, E. Gail de Planque, Chairman, International Atomic Energy Agency, Vienna, 1998.

**Since 1996, LDG has been a division of the Département d'Analyse et de Surveillance de l'Environnement (DASE) [Department of Analysis and Surveillance of the Environment]

*The IGC was in contact with DIRCEN (for logistical aspects) and with LDG (for scientific aspects)

Figure 1.1 Composition of the IGC and interactions with other organisations involved in the atoll studies

and Nagasaki averaged 20 kt, and that thermonuclear tests of up to several Mt have been carried out. The underground test Cannikin (see Vol. II, App. D), conducted by the United States on 6 November 1971, on Amchitka Island, Alaska, at a depth of 1790 m in volcanics, had a yield of "less than 5 Mt". This exceeded the total yield of all 147 underground tests conducted in Mururoa and Fangataufa. An even larger underground explosion was detonated, apparently, in the Soviet Union ca 1983.

The first two underground explosions at the PTC were performed at Fangataufa in 1975 under the emerged part (the rim) of the atoll. From 1976 to 1980, all explosions were carried out under the rim at Mururoa. It was during this period that the 12 CRTV (Cavity Reaching the Top of the Volcanism) tests (see Fig. 1.11) occurred in test areas 1, 2 and 3 and that creep sliding was first observed on the northeast rim of Mururoa. From 1981 to 1986, all explosions were carried out at Mururoa, some under the rim and some under the lagoon. From 1987, all experiments were conducted under the lagoons, both at Mururoa and Fangataufa. These details come from DIRCEN/CEA Document No. 6; details of the dates of explosions are given in the Appendix to DIRCEN/CEA Document No. 2 and in Volume 2, Appendix C of the IGC report. Independent evidence from far-field seismic data also is presented in Volume 2, Appendix C of the IGC report.

The IGC was requested to visit the two atolls, which it did in July 1996 and where it was able to see the present state of the exposed parts of the atolls, particularly those lying above the sites of numerous tests. Commission members were also able to view the seismological and other monitoring stations on the atolls that will be maintained in the future by DASE. The Commission has been thoroughly briefed on the work carried out by the CEA and DASE in connection with the tests; this includes experiments done before and after the separate tests to establish the mechanical state and properties of the rock and the hydrological environment, and models developed to explain the changes that have been observed. There is little indication in the DIRCEN/CEA documents that significant attention was given to geomechanical issues during the early (pre-1980) phase of the testing programme. Although generic descriptions have been given for the mechanical effects of explosions (cavity and chimney formation, rock damage and deformation), there is little published data on the range and variation of such effects.

The Commission has held five full meetings. Two subgroups have been formed within the IGC — one on stability and one on hydrology — each of which has held various meetings with outside experts and consultants. Details are given in Table 1.1 and in the Preface to this volume.

The IGC is conscious of the concerns that have been expressed by various national and international groups during and after the series of tests. Some of these groups have already issued their own reports — for example, Tazieff (1982); Goguel (1982), henceforth referred to as the Tazieff report; New Zealand MoFA (1984), henceforth referred to as the Atkinson report; and Fondation Cousteau, Paris (1988), henceforth referred to as the Cousteau report — after visits to the atolls, and there have been suggestions (CRII-

Table 1.1 Members of the two IGC subgroups

Stability Subgroup		
Convenor	Emmanuel Detournay	
Members	Edwin T. Brown	
	Charles Fairhurst	
	Victor Nikolaevskiy	
	J. R. Anthony Pearson	
Liaison	Pierre Bérest	
Consultants	Peter Cundall	Itasca Consulting Group, Inc.
	Branko Damjanac	Itasca Consulting Group, Inc.
	Charles Archambeau	TRAC, Inc.
Hydrology Subgroup		
Convenor	Lloyd Townley	
Members	Charles Fairhurst	
	Ghislain de Marsily	
	J. R. Anthony Pearson	
Liaison	Pierre Bérest	
Consultants	Pierre Perrochet	Ecole Polytechnique Fédérale de Lausanne (EPFL)
	Laurent Tacher	Ecole Polytechnique Fédérale de Lausanne (EPFL)

RAD 1995; Vincent 1996) that catastrophic or incipiently catastrophic damage has been done to the two atolls (see, in a somewhat irreverent vein, the cartoon from New Zealand in Figure 1.2) in terms of large-scale structural collapse, surface subsidence, major fracturing and alteration in hydrological conditions; there have also been suggestions that members of the local population have suffered unacceptable irradiation. These reports and comments have been examined and concerns noted by the IGC. The Commission considers that some of its major tasks have been to assess these concerns (except the last, which is being addressed by the IAEA) in an expert and impartial fashion; to report on them in such a way as to allay fears where it considers them exaggerated; to alert the authorities of any unnoticed dangers; to suggest what could be done in the future to anticipate any major events (i.e. that might take place in the future as a result of the tests) and to mitigate their effects; and to report on the concerns in such a way as to allay fears where it considers them exaggerated. A relevant list of questions raised by these concerns is given in Table 1.2.

The time and resources available to the IGC have been such that the Commission has had to use readily available information to come to its conclusions. It has not been

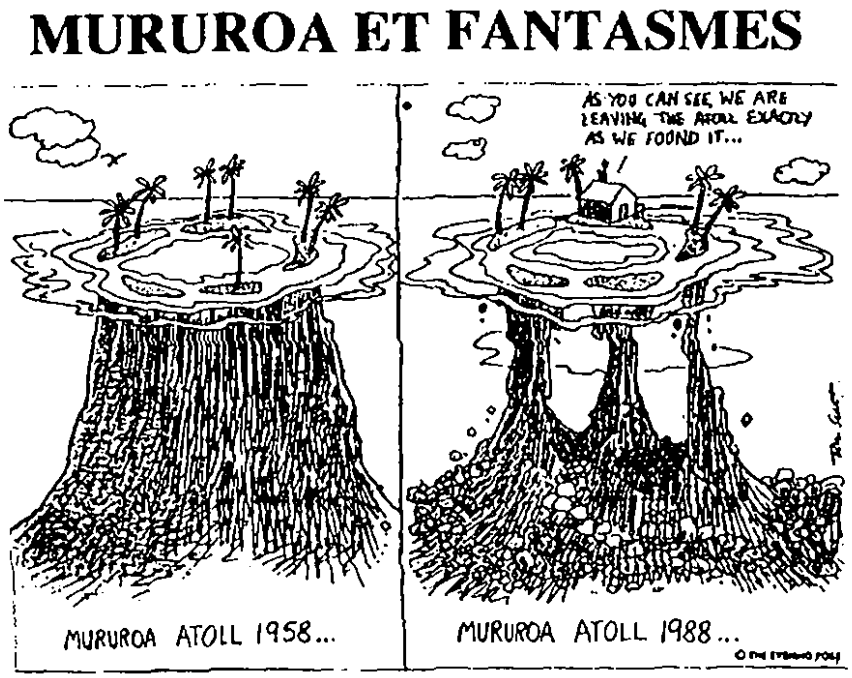

Figure 1.2 Cartoon published in the *Auckland Evening Post*

Table 1.2 Important questions to be answered by the IGC

*	Will further major settlement or subsidence take place at the exposed rim of the atoll?
*	Will further major slides take place along the ocean-facing slopes of the atolls?
*	Have major fractures been induced deep in the atolls — in particular, do those visible at the atoll surface represent major features connecting deep into the atoll rocks?
*	Have major changes in atoll hydrology (natural convection) been caused that will greatly accelerate transport of long-lasting radionuclides to the lagoon and ocean?

able to gather new data on site partly because the atolls, in the middle of the South Pacific, are remote, and also because access to the two atolls is strictly controlled; so all of its interpretations are based on the same data, or part of the same data, as that used by CEA/DASE. The IGC endeavoured to obtain, as far as possible, raw data on the factual observations in order to carry out its own interpretation of these observations. It also used some knowledge generally available on atoll structure and properties to produce its own estimates of parameters relevant to making essential predictions. Thus, it has been able to conduct a set of independent calculations to test and add to some of the more important results provided by DIRCEN/CEA. These calculations cover (i) the mechanical effects of the shock wave created by exploding a nuclear device within the atoll mass, including cavity formation, irreversible deformation of surrounding rock, settlement of the upper layers of the exposed reef, and its impact on the stability of the ocean slopes of the coral reefs; (ii) the immediately subsequent pore fluid flows induced by the cavity so formed and by the heating of surrounding rocks; and (iii) the long-term changes in the convection patterns in the atolls. These short- and long-term convective patterns in the rocks are the main cause of migration (transport) of radionuclides from the test cavity and its immediate neighbourhood to the surface of the atolls and, hence, to the environment. Predictions connected with (ii) and (iii) are precisely those that the IAEA has used in its assessment of radiological consequences.

The dominant feature of all these studies, as in all work connected with natural rock masses, is the uncertainty surrounding any data available on the rock mass properties of the atolls at and surrounding the test sites. (This feature is thus, to some extent, common to all underground works: tunnels, mines, oil exploration and production, waste disposal.) Although various geological, geophysical, mechanical and hydrological tests have been carried out by the CEA, the inhomogeneity of any natural rock mass means

that estimates for average values, together with some measure of their likely statistical variation, are all that can be used for calculations. Any opinion given will therefore refer to the "most likely" circumstance, the "range of possible" outcomes or the "worst-case" scenario.

The IGC report is presented in three parts (volumes). This, the first, is a summary version that avoids detailed technical analysis or discussion, seeking, rather, to present the relevant ideas, difficulties in interpretation and conclusions in a style accessible to the interested lay person, assuming a good general knowledge of scientific ideas and procedures. The second volume is a longer, more detailed version aimed at the expert reader and those determined to understand the full details of the work carried out, thus allowing them to draw their own conclusions, on the basis of known facts, about the consequences of the test series. The third volume contains a French translation, prepared by the IGC, of Volume I and parts of Volume II (Preface; Findings, Conclusions and Recommendations; and Chapter 1, Overview).

1.2 Information Available to the Commission

Because the two atolls were highly restricted areas from the day the French government decided to use them as test sites (and previously had no particular scientific or economic significance), the only directly available data about the atolls or about the tests conducted there are those provided by the French Government or its agencies. The Commission has also made use of generally available information about similar atolls or volcanic islands in the Pacific and about underground nuclear tests carried out at the Pacific Test Centre (PTC) and at other sites by other countries. The latter information includes seismic records collected and used in connection with Test Ban Treaties, whereby the sites and strengths of underground nuclear tests can be inferred from the seismic signals they emit.

We have no reason to suppose that any of the information given to us was other than accurate. However, the decision by the French Government not to allow the precise locations, including depths, nor the yield of each underground test to be revealed has had a pervasive limiting effect on data made available to the IGC. This lack of precise positional information has meant that potentially useful spatio-temporal correlations of geological and physical information could not be made, while almost no reliable information on interactions between tests carried out at neighbouring sites was available to us.

Initially, two comprehensive reports (Guille et al. (1996) and Bouchez and Lecomte (1996)) were the primary sources of information. Intended for a general scientific audience, and well-written for that purpose, these reports were derived from extensive investigations over many years. Although the IGC has drawn on these reports, they do not contain details of the kind needed for a thorough, critical review of the test programme. Barrillot (1996), whose recent text *Les essais nucléaires français 1960–1996* draws in part on these two reports, makes the following statement:

> *Comme nous l'avons remarqué à plusieurs reprises dans cette étude, les documents Dircen ne fournissent que des informations parcellaires, certes précises et éclairantes, mais les conséquences les plus graves des expériences réalisées font partie des omissions constantes qui risquent d'être masquées par l'abondance et la qualité des informations données sur des points de détail.* (p. 214)
>
> [As we have repeatedly noted in this study, the DIRCEN documents yield but fragmented information, admittedly precise and enlightening, while the most serious consequences of the explosions carried out form part of the regularly omitted information which is at risk of being masked by the abundant information of high quality provided on matters of detail.]

In the early stages of our investigation, we tended to echo these sentiments. However, the 12 DIRCEN/CEA documents mentioned earlier were not available to Barrillot when he made these comments. Nor were these more detailed documents initially available to us; they were transmitted to the IGC (and IAEA) as they were completed; their preparation (and translation) in time to be useful was a substantial challenge given that specific tests details had to be omitted. Despite the valuable information they contain, which has been used in the IGC study, important details are still missing.

It is possible that some of the information which we think DIRCEN/CEA needed and should have obtained to reach their conclusions had not been collected or had not been adequately interpreted. For example, laboratory values of rock strength are given, but estimates of important rock-mass parameters are not mentioned. Complete drilling and wellbore records, routinely collected in the petroleum industry, covering both the large-diameter holes down which the nuclear devices were lowered and the smaller diameter observation holes drilled into the cavities created by each explosion, should have been kept and analysed. They would have contained much useful information. Some wellbore tests evidently were made, and records kept of cavity refilling times and pressures. Some of these are reported, but full details are not given; these have been used to obtain permeabilities, but very little detail or discussion has been given about the methodology used. Estimates are reported, but, again, no discussion is given of the expected accuracy of the values so obtained, nor of their uniqueness, nor of their relevance to later convection patterns. When attempting to confirm the CEA results, the IGC has found either that there are points in the developments where we have to guess what unstated assumptions were made or that alternative and sometimes different conclusions can be drawn. Where temperature or tracer (tritium) measurements are reported and used, a similar situation is encountered.

It is true that the complexity of current mathematical models and computational software is such that, even in the case of published scientific papers, much is taken for granted. In addition, the French data and results have been obtained by a wide range

of workers, many of them at universities, some of whom may have inadvertently failed to include all necessary information in their own reports and theses, from which much of the DIRCEN/CEA documents are derived. Finally, it is clear that this most recent series of documents has been prepared long after the original work (started almost 25 years ago) was done, and so omissions and lack of justification may well be due to the unavailability of the original workers to supply what is missing; moreover, computing facilities were inadequate even 10 years ago to carry out analyses possible now.

These comments are not intended to suggest that interpretations made and actions taken by CEA scientists were incorrect, but simply to note that all the details involved were not available to the IGC. Faced with this lack of detail, and mindful of the generic uncertainty associated with geotechnical data, the IGC has been obliged to consider extreme cases in its analyses so as to cover all possibilities. Fortunately, even the most pessimistic assumptions with regard to short-term and long-term containment do not suggest that there are any serious consequences that need to be evaluated with any exactitude.

The quality of the data available to the IGC is summarised very qualitatively and subjectively, under various headings, in Table 1.3. The reason for the seemingly low quality of much of the data is the inevitable uncertainty surrounding measurements and, more particularly, their interpretation, made in a natural environment (as mentioned earlier), where inhomogeneity over all length scales means that the more local a measurement, the more the quantity measured can vary with spatial position. More measurements could have been made and a better estimate made of the range of variation to be expected. More care could have been taken in describing the models and calculations used in obtaining derived information, and more emphasis placed on the degree of uncertainty involved. Thus, arguments about local effects of particular explosions are meaningless if too much precision is sought; the size and shape of the cavity formed will be significantly dependent on the characteristics of that major part of the rock mass that is not brought to the surface as cores or cuttings; the latter can give only a good indication of the properties of the rock lying near the borehole concerned. Even if global quantities, such as the total fluid flux from the atoll rock (or coral) into the lagoon or the total seismic energy and momentum radiated into the far-field, are sought, there will remain a large measure of uncertainty. Model calculations are usually carried out only for averaged physical variables using averaged material parameters; this makes them illustrative rather than definitive. Nevertheless, the weight of what evidence the IGC has examined suggests that the uncertainties involved have not weakened its conclusions.

Table 1.3 Quality of data available for modelling and analysis

Type	*Sub-Type*	*Quality/Accuracy*
Geology		fair to good
Physical Properties	Densities	good
	Porosities	fair
	Thermal Conductivities	good
	Hydraulic Conductivities	poor
	Dispersion Lengths	poor
	Mechanical Properties	fair
Topography		good
Temperature		poor
Geothermal Flux		poor to fair
Convective Flux		wholly inferred and poor
Sites of Tests		partial
Magnitudes of Tests		fair to good
Tracer Tests		poor

1.3 Basic Structure and Geology of the Atolls

As explained in Chapter 2 of Bouchez and Lecomte (1996) and in Guille et al. (1996), and further discussed in Volume 2, Chapter 2 of this report, the two atolls form part of a chain of volcanic islands in the South Pacific. The vulcanism that gave rise to them is now no longer active under them, because they have moved away from the volcanic hot spot that created them. In that sense, they are as stable as the plate on which they sit. Some of the islands rise above sea level (e.g. Tahiti), while Mururoa and Fangataufa lie mainly below the surface with a coral rim, more complete in the case of Fangataufa than of Mururoa. In both cases, the relatively shallow lagoon within the rim is connected through hoas (channels) to the deeper ocean outside; tidal and wind actions raise and lower the surface level of the lagoons and exchange water daily through the hoas. This leads to a (roughly) monthly exchange of fluid between lagoon and ocean.

The coral rims (or reefs in the case of exposed islands) lie very close to the ocean level because of the growth patterns of coral. If too deeply submerged or if left dry for any

length of time, the coral dies. In the very long term, the islands are sinking very slowly over time, a process explicable in terms of global movements of the earth's surface; ice ages cause the sea level to fall and then rise over a rather shorter time scale than the slow sinking; the most recent period of glaciation is responsible for the emerged rim of dead coral. Submerged coral, on average, grows very gradually upward — perhaps more rapidly on the outer edges, giving rise to the visible rims; as the fragile and highly porous dead coral sinks below new growth, it is crushed by the weight above it and slowly altered chemically by the sea water percolating through it. In the case of Mururoa, the process has continued long enough for a (sedimentary) layer of about 400 m of calcareous rock (henceforth, conveniently referred to as carbonate) to sit above the less porous and less permeable basaltic rock that is the true basis of the islands. Figures 1.3 and 1.4 show in simplified form the relevant structure and shape of Mururoa and Fangataufa, respectively.

It is important to note that the average slopes of the deep basaltic flanks of the islands are mild enough to ensure that the basaltic bases are completely stable. (This has been questioned by at least one author (Vincent 1996), but standard theory and all available evidence points clearly to this conclusion.) It is only nearer the ocean surface, where the flank material is primarily composed of modified dead coral, that steeper, less stable slopes arise. Over the time scale (several million years) that the 400 m of calcareous rock have been formed, many slides have occurred on these slopes; so the composition of the edge material is partly calcareous to lower depths — 500–600 m deep around Mururoa, and slightly more around Fangataufa (see Fig. 1.5).

The observed changes in topography of the two atolls, particularly of Mururoa, caused by the test series are the result of changes taking place in the sedimentary rock and not in the underlying basalt. Much of our task in this context has been to review the explanations given by DIRCEN/CEA for these changes, to provide our own and to assess any likely future changes on the basis of existing knowledge and models. This is discussed in subsequent sections of this report. The most serious issues are

- settlement of the atoll rims,
- deep or superficial fracturing of the calcareous layer,
- sudden or slow slides on the flanks of the rims, and
- dispersion of radionuclides.

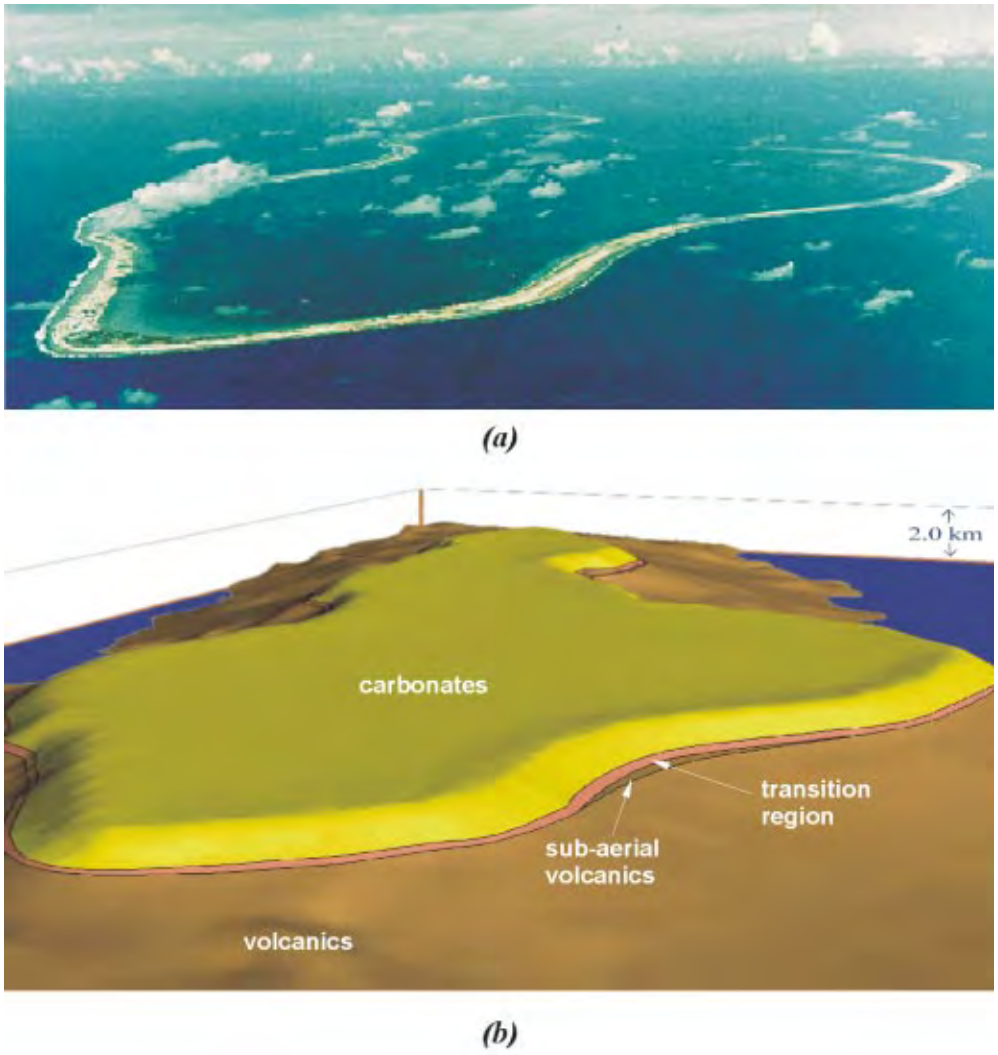

Figure 1.3 Mururoa: (a) aerial view; (b) bathymetric view (from same perspective) to a depth of 2.0 km (carbonates are shown overlying the volcanics; view is toward the southwest (S65°W, altitude 21° above horizon), with test area 1 in the foreground)

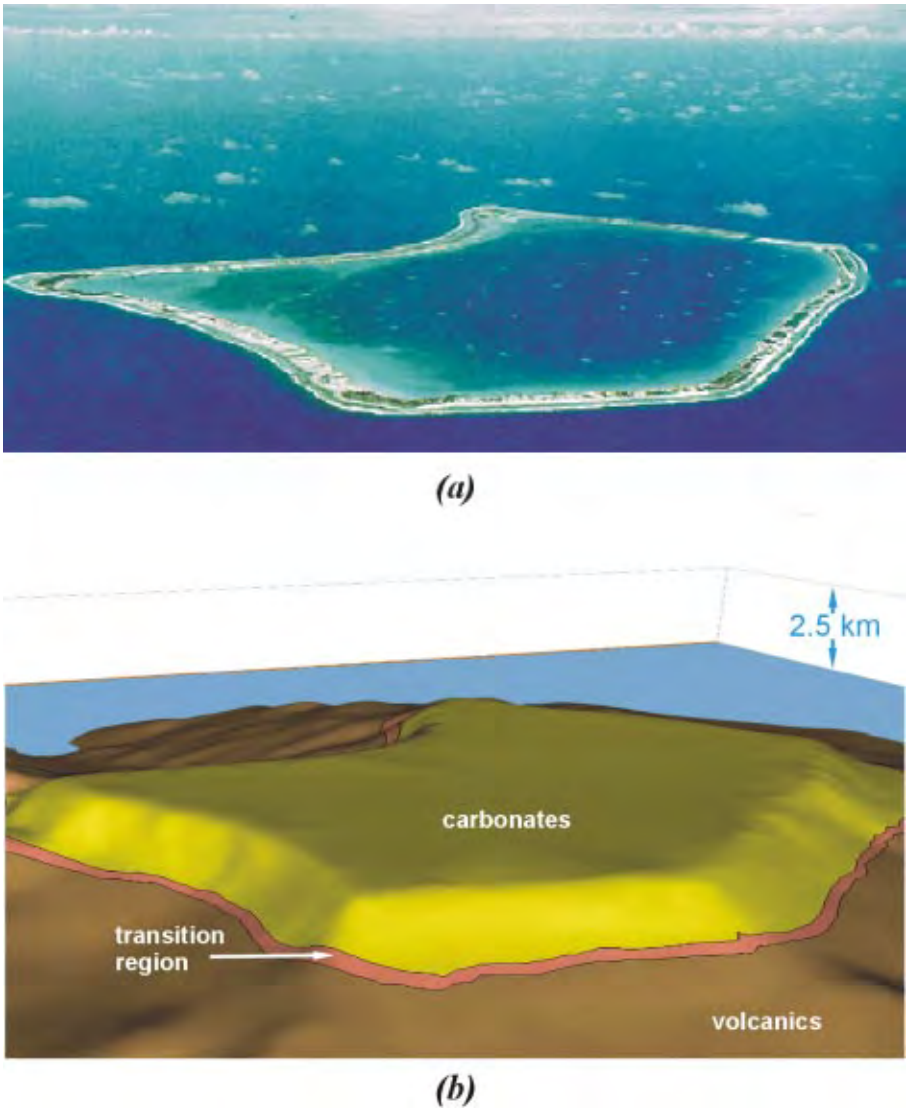

Figure 1.4 Fangataufa: (a) aerial view; (b) bathymetric view (from the same perspective) to a depth of 2.5 km (the flanks of Fangataufa descend more abruptly than do those of Mururoa; the carbonates are shown overlying the volcanics; view is toward the west (N68°W, altitude 27° above the horizon), with test area 1 on the left reef)

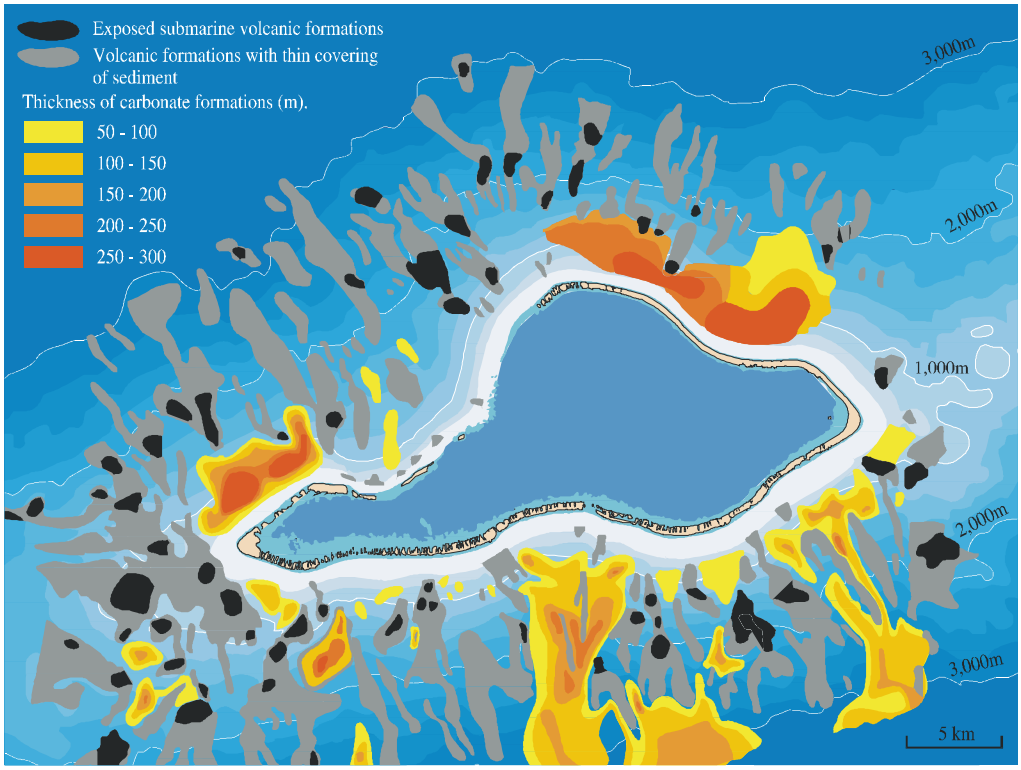

Figure 1.5 Distribution of sedimentary deposits and submarine outcrops on the flanks of Mururoa atoll (Guille et al. 1996, Fig. 23)

1.4 Basic Hydrology of the Atolls

Both the basalt and limestone are porous and saturated with salt water, the basalt being slightly permeable and the carbonate highly so; there are significant local variations, and hydraulic conductivity tends to be greater in the horizontal direction than in the vertical. Under natural conditions, there is a net flow of heat from the underlying basalt to the surface and sides of the atolls, known as the geothermal heat flux, caused by the higher underlying temperatures in the basaltic rock — the centre of the earth being much hotter than its surface. This vertical temperature gradient means that the salt water in the rock pores is driven upward by buoyancy, giving rise to large-scale overturning convection patterns. In the case of an atoll, this process is strongly enhanced by a simultaneous horizontal temperature gradient caused by (cooling from) the low ocean temperatures in the atoll flanks and by an inflow of sea water from the ocean (see Fig. 1.6). In the ocean itself, large-scale convection patterns involve the whole ocean; so, in tropical regions, the temperature profile is positive near the surface — i.e. the water gets colder with increasing depth.

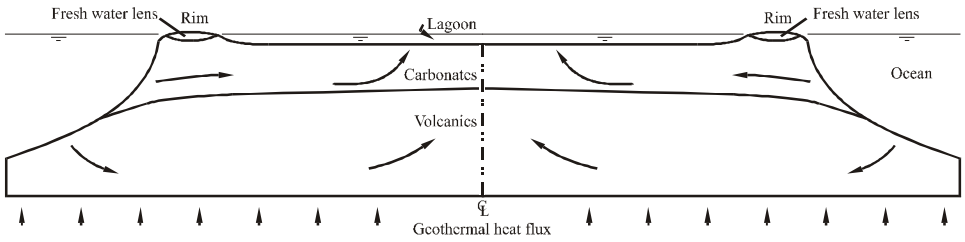

Figure 1.6 Schematic cross-section through an atoll (after Perrochet and Tacher 1997a)

Prediction methods for shallow and deep water circulation in the earth's crust are now well understood, and computational software is available in standard form, so predictions of steady flow patterns are as accurate as the porosity, permeability and temperature boundary conditions chosen to represent the rock mass concerned. Simple arguments show that, in the basalt, most of the heat is transferred by direct conduction and that the associated pore fluid circulation is slow enough (of the order of 1 cm/year for the volume-averaged Darcy velocity, which is equivalent to about 10 cm/year actual fluid velocity) for it to make only a minor contribution to heat transfer; in the carbonate, particularly in any karstic layer (one containing visibly large horizontal channels or voids arising from well-understood long-term physico-chemical processes) near the rim, the pore fluid flow will be more important, the relevant Darcy velocities averaging up to 1 m or more per year. These steady flow patterns are what we call global (i.e. on the full atoll length scale).

Firing a nuclear device at depths of between 600 and 1100 m involves, apart from any changes to the permeability and porosity caused by mechanical damage (discussed in Section 1.6), a sudden rise in temperature in the immediate vicinity of the explosion, which leads to large transient local temperature gradients and a rising plume of heated fluid. (A 1-kt explosion releases enough energy to warm up a million tonnes of water by 1 °C; in practice, this leads to a mean temperature rise of about 25 °C for a sphere with a 20-m radius.) In the basalt, this local effect can be simply superposed on the steady temperature and flow fields described earlier. In the carbonate, where the flow affects the temperature significantly, the changes in temperature and flow fields are more complicated but, qualitatively, the effect is the same. A very crude indication of the time scales involved can be given by saying that a thermal plume takes of the order of 50 years to rise through the 400 m of carbonate, and that the heated fluid moves rather faster than the maximum of the excess temperature field. By that time, the transient excess temperature energy has largely dissipated itself into the wider environment, mainly through conduction in the rock, and rapid convection in the ocean and atmosphere. After about 500 years, all thermal effects of the explosion have been dissipated.

1.5 Mechanical Effects of a Test Explosion

There is general agreement among experts about what happens when a nuclear device is exploded underground, and the IGC has made its own calculations to confirm what happens in the Mururoa/Fangataufa environment. As discussed in Volume 2, Chapter 3, well under the surface in the basalt, a large mass of gas at very high pressure is formed that expands the rock around it to form a cavity much larger than the original space occupied by the unexploded device. This happens so fast that a strong supersonic shock wave is propagated from the site of the explosion. As it moves away from point zero, the shock wave weakens until it becomes a sound (seismic) wave. This seismic wave is propagated all around and through the earth; for a large-enough release of energy in the explosion, this seismic signal can be detected and interpreted at seismic recording centres all over the globe. By the time a seismic wave is formed, all but a small proportion (say, 0.5 to 5% — depending upon the final outer elastic deformation) of the total energy in the wave has been lost.

There are two causes for a weakening of the strength of the wave. The first is the obvious and elementary one: it spreads itself over a near-spherical surface whose radius and, hence, surface area increase with time. For this reason alone, the energy and momentum per unit area decrease roughly as the inverse square of distance — or of time, since a sound wave moves with constant speed in a uniform medium. The second arises because the shock wave is very non-linear and dissipative in its early stages; some of its energy is left behind in the form of heat and altered state (free energy) of the rock. Attenuation resulting from dissipation decreases as the wave weakens, and is almost negligible in the far sonic region.

The rock is pushed outward and deforms during the passage of the wave. Near the centre, when the shock is strong, the stresses (loads/unit area) within the rock as it is deformed are large compared with those existing before the explosion — i.e. large compared to gravitational or tectonic stresses — and the process is independent of any but purely local rock characteristics. It can be expected to be spherically symmetric. At greater distances from the centre, the region (area) covered by the wave front shows more variation, and so spherical symmetry will be lost; an obvious example of this is provided by the wave reaching the ocean or atmosphere. At still greater distances, the pre-existing in-situ stresses will be larger than those caused by the passage of the sound wave, the distance depending on the vertical depth.

The passage of a shock wave is shown in Figure 1.7. The immediate result after the wave has passed away from the island (a matter of seconds) is shown diagrammatically in Figure 1.8. A cavity with molten rock (glass) at the bottom and on the sides is surrounded by a crushed zone beyond which is a much larger irreversibly deformed zone. The inner part of this deformed zone has sustained plastic shear failure, while the outer part displays discrete cracks (fractures); both zones may have dilated (expanded in terms of

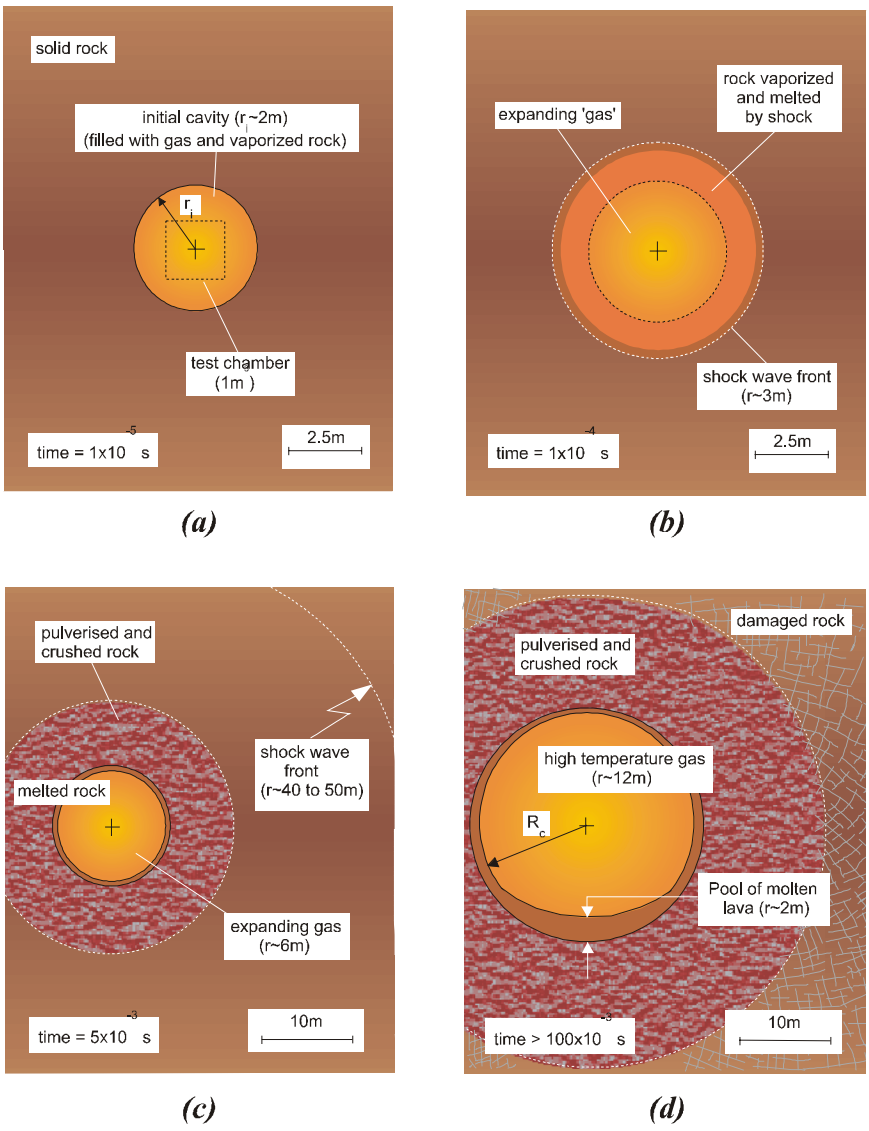

Figure 1.7 Stages of cavity formation and development during a nuclear explosion (Note: r_i is the radius of the "instantaneously" vaporized sphere; $r_i \simeq 2$ m for a 1-kt explosion — see Fig. 1.8 ; R_c is the final radius of the expanded cavity. $R_c \simeq 12$ m for a 1-kt (shallow) explosion on the atolls; at the greater depths, $R_c \simeq 10$ m for a 1-kt explosion)

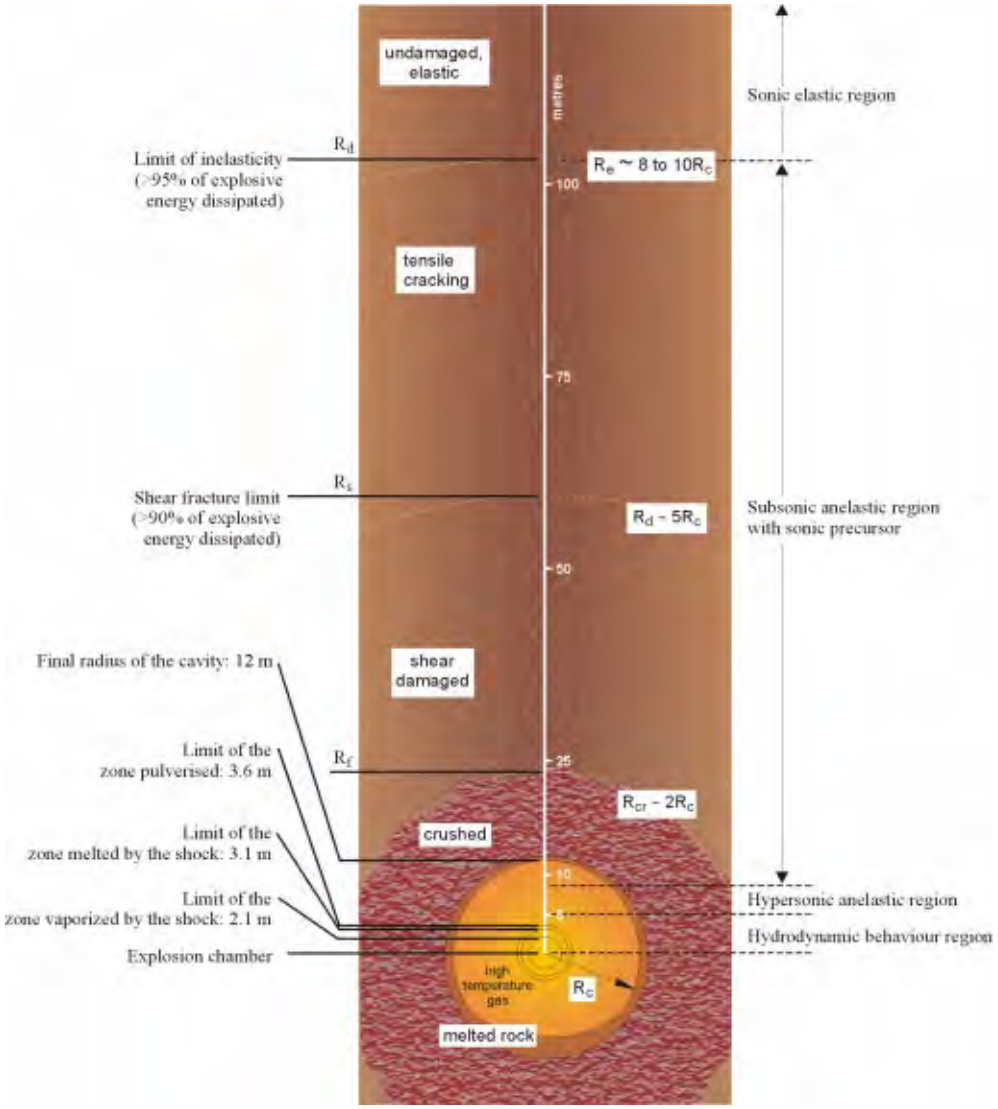

Figure 1.8 Presumed rock damage zones around a 1-kt nuclear explosion cavity in basalts at Mururoa and Fangataufa (the damage zones are expressed as multiples of the final cavity radius R_c; R_f, R_s and R_d refer to Fig. 3.6 in Vol. II) [after Bouchez and Lecomte (1996); see also Fig. 3.7]

volume occupied). Beyond this deformed (anelastic in the DIRCEN/CEA description) region, the rock is assumed to have been elastically deformed from its original state; all the rock is therefore in an altered stress state. There is little difference of opinion among the world's experts about this general picture, though, for any particular case, there have been disagreements about the precise details (size of zones, nature of rock deformation). We come back to this point later. It can be assumed that the volume of rock so affected increases directly with the energy of the explosion; this means that the radii of the various regions scale as the cube root of the energy.

Within hours of the explosion, it is found that the damaged rock above the cavity is not capable of remaining in place, a familiar enough experience when tunnelling through dry, weak material. The rock, therefore, collapses to form a "chimney" in and above the cavity. As pieces of rock fall into the cavity, or into the space left by pieces that fell down earlier, they "bulk up" and so occupy significantly more volume; in simple terms, the irregular-shaped lumps that fall off the top do not fit together very well at the bottom and so have free space between them. As the process of chimney collapse continues, the original free space in the cavity formed by the explosion is accounted for by the spaces between the fallen lumps; this process stops when the last lump to fall cannot fully separate from the bulk material above before it comes to rest on the lumps below. The height of the bulked chimney so formed is about equal to the radius of the fractured zone, where rock competent enough to form a roof is reached. Alternatively, undamaged rock can form an unsupported roof. Under subsequent stressing, such as caused by later nearby explosions, this bulked chimney material can transmit the stresses without major deformation.

This chimney formation is very important, because it greatly extends the effect of the explosion in terms of permeability enhancement of a large volume whose height is 5–8 times the radius of the cavity. It means that explosions whose centres are relatively close to the transition region between the basalt and carbonate can puncture the low-permeability basalt layer initially above them — and this is known to have happened — and communicate hydrologically directly with the high-permeability carbonate. In tests that took place at shallow depth in non-bulking dry material in the Nevada desert in the USA, the chimneys extended to the surface and formed a noticeable and localised depression of the surface. However, this did not occur on the atolls because the rocks are saturated and bulk more than do the alluvial sands of Nevada.

There are additional effects when the shock wave or strong sound wave reaches the bottom of the lagoon and then the sea surface, the exposed surface of the rim or the ocean on the atoll flanks. The sharp change in mechanical (acoustic) impedance leads to reflected and/or surface waves as well as to a weakened transmitted wave. The incident wave is essentially compressive and plane; the reflected wave will be essentially tensile; and the surface wave, progressively more important as the angle of incidence moves away from normal, will contain a significant shear component. Because most materials

can withstand a much larger (often a factor of 10) compressive than tensile stress, the reflected tensile wave is sufficient to detach a slab of material at the surface (spalling) which moves upward until the force of gravity sends it back to its original position; if the material is water, cavitation (temporary formation of vapour bubbles) is induced. This phenomenon can explain the apparent boiling that occurs in an area of the lagoon above the explosion centre just after firing, while irregularities in the topography of the lagoon bottom can lead to spouting. DIRCEN/CEA has further argued that the passage of the initial shock wave, together with the secondary shock wave caused by the return impact of the spalled slabs, is sufficient to explain the settlement that is evident in the atoll rim above the test sites (see Fig. 1.9).

We find this DIRCEN/CEA explanation for settlement unconvincing, and an alternative explanation in terms of shear failure is given in Volume 2, Chapter 5 of this report. In simple terms, the observed reduction in (vertical) thickness of the upper carbonate layer arises because the passage of the compressive shock wave squeezes the carbonate outward (horizontally) without any change in volume; the atoll rim becomes wider. A further consequence of this process is that the ocean slope of the atoll can be destabilised; so, the major slides noted in test area 4 (on the southwestern portion) can be partly attributed to this outward near-surface movement. However, either explanation will support the contention of DIRCEN/CEA that the observed settlements at the surface of the atoll are not directly connected to the explosion chambers. Figure 1.9 shows a plan view of settlements observed along the rim of Mururoa. (The seven test areas — four on the exposed rim and three in the lagoon — are outlined by red lines; see also Figure 1.11.)

As far as major fracturing is concerned, we note that the tips of fractures cannot travel as fast as the shock wave during its passage; therefore, those created then will remain short and probably isolated. Close to the initial cavities, the severe plastic deformation induced by the shock wave ensures that the stresses remain compressive; farther out, particularly in the elastic region, where tensile stresses can arise because of overall expansion, tensile failure and some fracturing can arise independent of the pressure within the cavity.

Strain energy release during fracture propagation will limit such fracture growth; at larger distances from the centre of the explosion, the pre-existing in-situ stresses will lead again to a compressive environment, except perhaps at the surface of the atoll. Some surface cracks have arisen because of slope instability. Figure 1.10 shows an aerial view of cracks developed due to slope movements in test area 1 on the northeastern rim of Mururoa. Whatever their cause, the IGC believes that it is incorrect to suppose that the surface cracks penetrate far into the atoll rock.

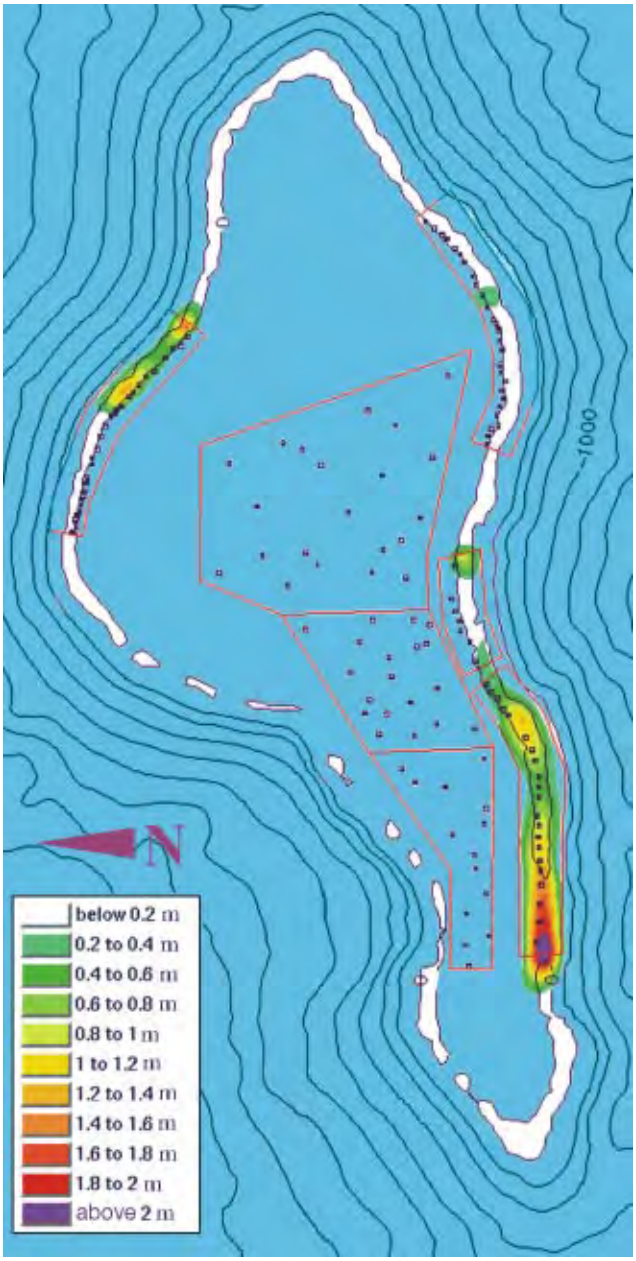

Figure 1.9 Areas of surface settlement produced by underground testing along the rim of Mururoa (based on DIRCEN/CEA 1996 settlement data)

Figure 1.10 Aerial photograph showing underwater extension fractures of the order of 2-m width in the vicinity of PK5N, Irène section (part of the aircraft runway strip, with protective wall, runs parallel to the bottom of the photograph; this region is outside test area 1) [photo courtesy of DIRCEN/CEA]

1.6 Hydrological Consequences of the Nuclear Explosions

There will be no residual changes in permeability in regions that are merely elastically deformed. In those that are irreversibly deformed, the permeability will tend to be reduced when crushing occurs and increased when the material is dilated. If the dilation is confined to small non-interacting microcracks, the enhancement may not be large; if, however, significant fracturing occurs, the enhancement will be large (many orders of magnitude in the basalt). Within the chimney, including the original cavity, the permeability becomes effectively (almost) infinite.

A large number of holes (wells) were drilled into the carbonates and underlying basalt and, while open to the rocks through which they were drilled, had some effect on the convection of pore waters in their neighbourhood. The large-diameter (1.5-m) holes, drilled to allow nuclear devices to be placed in the basalt, withdrew large volumes of water from the most permeable parts of the carbonates (karst layers) during drilling, conveying this water up the well to the rim surface or the lagoon bottom. In the case of those used for test explosions, they were filled with rubble, sand and cement slurry, to seal them off, before the devices were exploded. Thereafter, they had no influence on hydrological conditions, though it has been suggested that they can induce cracks (fractures) in the surrounding rocks caused either during the drilling phase or later, as a result of the shock wave, thus providing a potentially significantly enhanced pathway to the surface for hot fluid and any dissolved radionuclides.

Some of these large-diameter holes were not used for tests and so were left open, to some degree, to the surrounding rocks and/or to the surface. (This information came late in the IGC's investigations, and the effects have not been included in most of the detailed calculations.) Apparently, the holes were used to make measurements of radionuclide concentrations at the level of the lower karsts and in the carbonates generally. While open, because of their high hydraulic conductivity, they provide an enhanced pathway — to the surface or between the more conductive underground layers — for the pore fluid entering at the ocean flanks and moving inward and upward under pressure gradients within the porous rocks. Crude calculations suggest that this effect could be quantitatively significant over distances equal, for example, to the separation between test sites in test area 4 on Mururoa (though, since flow is normal to the line of test explosions in that area, there will be no significant interaction effects there).

Other, slightly offset and partly oblique, smaller-diameter (0.2-m) wells were drilled a few days (or weeks) after each test explosion to investigate (by coring and logging) the region of the cavities. All of these were sealed off after use, though portions of them may have been left full of water and in contact with the rock.

Neither DIRCEN/CEA nor IGC has attempted to analyse in any detail the short- and long-term effects of these man-made holes on pore fluid movement. The mixing model (see Vol. 2, Ch. 7) used to calculate tritium (and other radionuclide) concen-

trations within and fluxes through the carbonates has potentially taken full account of any enhanced convection. Of all the changes induced, those caused by cavity/chimney formation can be expected to dominate.

1.7 History of Tests — A Commentary

Figures 1.11 and 1.12 attempt to summarise the only direct information available (i.e. that provided by DIRCEN/CEA) on the distribution, location, timing and yield of the underground tests at Mururoa and Fangataufa. Most of the information is derived from DIRCEN/CEA Document No. 6 and the appendix of Bouchez and Lecomte (1996). Study of seismic records helps to confirm the test dates and add some detail to the relative magnitudes of individual tests (see discussion in Vol. II, App. C). Aerial photographs, some taken by IGC members and others supplied by CEA authorities, also indicate the surface location of many of the rim drilling sites on Mururoa, especially in test areas 3 and 4, where the tests were spaced approximately evenly along the inside perimeter of the rim. Figure 1.13 shows an aerial view, taken in July 1996, of test area 4 on Mururoa. In some cases, the IGC has been able to infer some helpful additional detail from verbal statements made by CEA/LDG to us or from the statistics of testing and calculations reported in the documents provided by DIRCEN/CEA.

It is clear that DIRCEN/CEA paid close attention to the ten years of prior underground test experience in other countries (see Vol. II, App. B), especially that reported for the Nevada Test Site (NTS) in the United States. The relative depths of the tests at the PTC were considerably greater than in the U.S. tests, so that direct release or *venting* of radionuclides to the atmosphere, which did occur in some of the nests at the NTS, was avoided (see Vol. II, App. D).

The predominantly underwater setting of the atolls effectively ruled out the less expensive and more informative option of testing from horizontal tunnels — as used in some of the U.S., Russian and earlier French tests in Hoggar (see Preface) — with subsequent investigation of the zones of damage around the explosion sites by supplementary tunnel excavations. Consequently, there is relatively little direct detail available on these zones in the atoll basalts. In this context, it is surprising that more careful use of drilling records was not made and reported.

It appears that inadequate attention was given to geomechanical issues during the initial stages of the underground programme at the PTC. It now is obvious, as shown in Chapters 4 and 5 of Volume II of this report, that noticeable untoward effects such as rim subsidence and slides could have been avoided if early tests had been conducted farther from the outer edges of the atolls (i.e. under the central portion of the atolls) and deeper into the basalt. Furthermore, penetration of chimneys into the transition layer

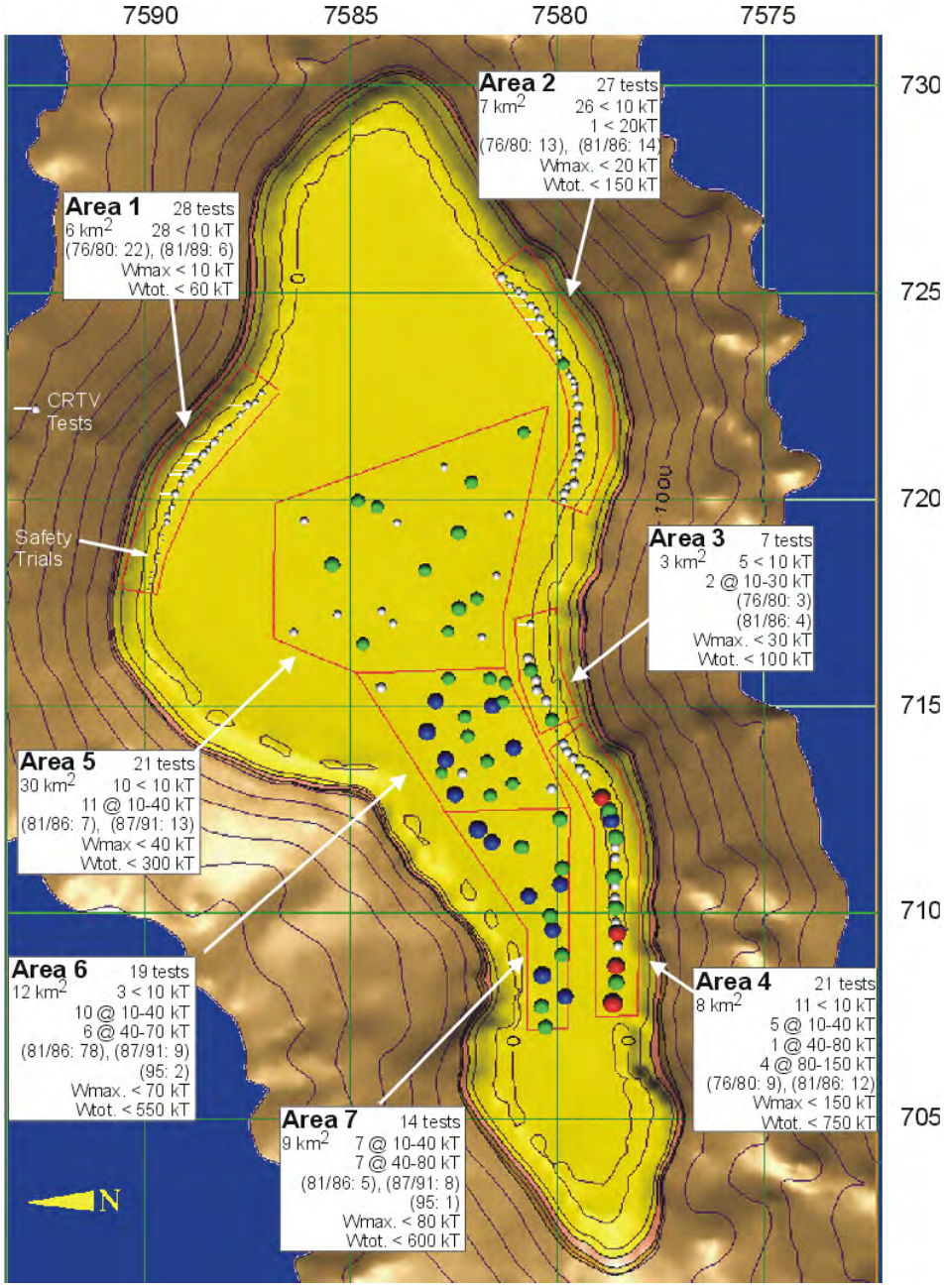

Figure 1.11 Details of underground tests conducted in each test area on Mururoa (provided by CEA/DIRCEN), together with a hypothetical distribution of underground nuclear tests in the test areas (contours are at 250-m intervals)

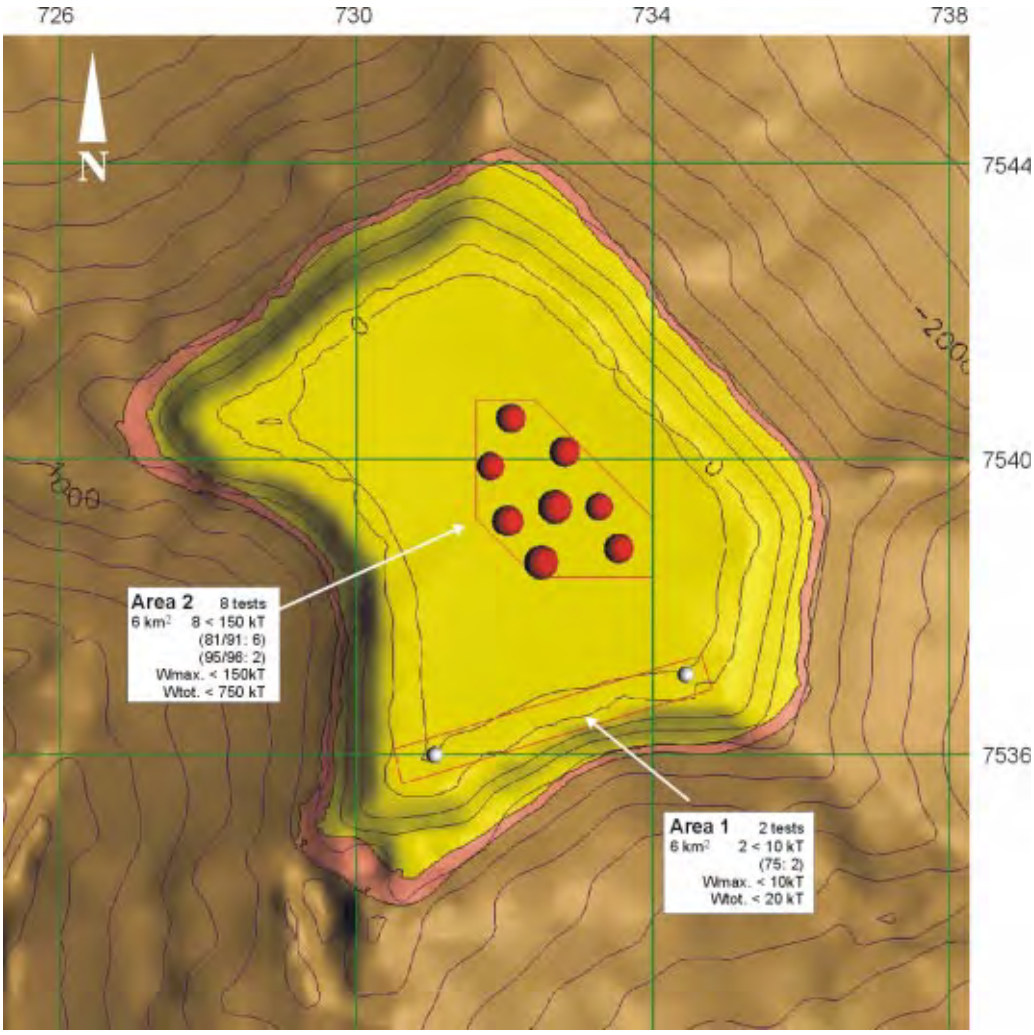

Figure 1.12 Details of underground tests conducted in each test area on Fangataufa (provided by CEA/DIRCEN), together with a hypothetical distribution of underground nuclear tests in the test areas (contours are at 250-m intervals)

Figure 1.13 Aerial view of western part of test area 4 on Mururoa taken in July 1996 (i.e. 16 years after rim testing ceased) from the ocean side, looking toward the lagoon (note that several test sites and settlements in the western end of test area 4 are underwater; see also Fig. 1.9)

or the carbonate proper, as occurred in 12 tests during the period 1976–1980* would thereby have been avoided. In another two early tests (Nestor and Enée), the quality of the volcanic cover proved to be inadequate to prevent early seepage of radionuclides from the chimney.

These last comments can easily be made in hindsight. However, it has been argued that working on land rather than offshore was thought to be inherently safer as far as operating hazards were concerned and, incidentally, much less expensive than lagoon testing.

Clearly, the slope failures on the southern rim of Mururoa,† the associated hydraulic waves‡ and the detection, in the 1970s, of a slow continuing deformation over a large

*see Vol. II, App. C, Table C.4, Category 3 (CRTV) tests

†Nestor (March 1977), Priam (November 1978), Tydée (July 1979)

‡see Vol. II, Ch. 5, and DIRCEN/CEA Document No. 7, Sect. V1

area of the northeast rim slope on Mururoa[¶] prompted a comprehensive review of the underground testing strategy, development of barge and platform technology to allow drilling of the large-diameter (1.5-m) holes in the lagoon (Bouchez and Lecomte 1996) and a progressive shift to lagoon testing, beginning in 1981[§]. The importance of these changes was underlined by the Tazieff Commission (Tazieff 1982). From 1987, all tests, save one small test in November 1989, were conducted under the two lagoons. Also, *since 1980, the minimal (volcanic) covering thickness has been 50 metres and, later, 100 metres* (DIRCEN/CEA Document No. 6, Fig. 7).[‖]

Except for two cases of inadequate (damaged) volcanic cover,[**] all of the 91 tests since 1980 appear to have been conduced with none of the earlier untoward local effects. In this regard, it is worth repeating that all of the slope instability and settlement issues examined in Volume II, Chapters 4 and 5 and associated appendices had their origin in problems resulting from the pre-1980 series of tests, although it appears that some temporary acceleration in the sliding on the southern rim of Mururoa atoll was precipitated by explosions remote from the shoreline. Also, neither the CRTV nor the Category 2 tests have had any significance with respect to stability and have only had negligible consequences with respect to hydrology or radionuclide release (IAEA 1998b).

The gradual change in the way tests were conducted (choosing deeper and more widely spaced point zeros, under the two lagoons rather than near the atoll flanks) leads us to conclude that, although few details are provided in the DIRCEN/CEA documents, the technical staff involved had probably analysed the situation facing them for each new test in as prudent and objective fashion as they could.

The highest concentration of energy release/unit rock volume was in test area 4 on Mururoa, which is where the most severe untoward events took place, followed by test area 2 in Fangataufa lagoon and test areas 6 and 7 in Mururoa lagoon. The slow restricted slide near test area 1 on Mururoa is not so easily attributed to large energy release (see Vol. II, Ch. 5), except as an impending natural process triggered and accelerated by relatively weak shock waves in a weak sedimentary layer.

[¶] see Vol. II., Ch. 5

[§] see Vol. II, App. C

[‖] These are pre-test design thicknesses calculated on the basis of the actual depth of the test in the volcanics and the chimney height calculated from the *chimney height versus yield* rule given in DIRCEN/CEA Document No. 6 (p. 6). The actual thickness of *intact* volcanic cover above a chimney was not routinely measured in later tests.

[**] Megarée (November 1985) in the Mururoa lagoon and Lycos (November 1989) in the Fangataufa lagoon (see Vol. II, App. C, Category 2 tests)

1.8 Major Issues

1.8.1 Local Mechanical Damage and Long-Term Stability of the Bulk Rock

It is convenient to develop the argument for test area 4 of Mururoa, where the concentration of test firings was greatest. From Figure 1.3, using the linearity argument relating volumes to energy of any test explosion, it can be deduced by simple arithmetic that the total cavity volume created was about 5 000 000 m^3, the total chimney volume created about 40 000 000 m^3 (0.04 km^3), the total damaged volume about 0.68 km^3 and the inelastically strained volume about 2.3 km^3; this assumes that none of the firings making up the total energy release of 750 kt overlapped in their effects. The total volume of the layer in which the tests took place can be computed as 8 km^2 times 600 m, or about 5 km^3, having used the fact that all tests took place at depths between 500 and 1100 m.

Because we do not know the precise locations of the firings, nor their strengths, we cannot calculate how much overlap there was between the damage regions of separate firings; the only information we have is a figure provided by the CEA in Tahiti that gives the proportion of nearest neighbor spacings that could be expected to lead to overlap of the fractured regions as 25%. Because of the greater density of firings in test area 4, we expect the proportion to be greater there. Noting the regularity of drilling sites along the line of the reef in test area 4, it could be argued that, at worst, these fractured regions form a continuous line about 7 km long just beneath the carbonate layer (see Vol. II, Fig. 1.6). What we can be sure of is that most of the 5 km^3 referred to in the last paragraph will have been inelastically strained. So far, no more than the geometry of spheres placed in a given volume has been involved in the argument.

A further question concerns the change in total volume of the 600-m-thick layer in which the cavities were formed. If we assume that there is no net change in density of the rock that is displaced, then the basaltic layer in question will occupy an extra 5 000 000 m^3. If we assume that the cavity volume is absorbed by an averaged increased density (decreased porosity) of the 5 km^3 of the layer material (i.e. no net change of the layer boundaries), then we get a mean reduction of 0.1% in porosity. If we assume that the cavity volume merely raises the 8 km^2 surface of the "land" above the layer, we get a rise of about 0.6 m; note that the actual outcome was a subsidence of between 1 and 2 m. If we assume that the slope of the atoll boundary bordering the test layer is merely pushed outward toward the ocean, then we get a mean horizontal displacement of about 1 m; because of the slides that took place, we have no conclusive evidence on what actually happened.

What these simple geometrical arguments show is that much more insight is needed into the local volume changes (compaction or dilatation) associated with the passage of the blast wave through the basalt and carbonate before any final conclusions can be drawn from the observed changes to the exterior of test area 4 on Mururoa. Volume 2, Chapter 3 of this report contains arguments challenging the simple explanations for settlement given by DIRCEN; this aspect is taken up in the next subsection.

The question now arises of whether the tests have destabilised the carbonate layer sufficiently for structural collapse to occur. We note, first, that, at a mean depth of 800 m, the raised rim is supported on the ocean side by a sloping mass of volcanic or sedimentary rock, so that the centres of all test firings should be at least 1 km horizontally from the ocean; on the lagoon side, the basaltic layer is continuous to the opposite slope. It is therefore clear that the damaged rock is surrounded and supported from the sides and below by wholly competent basaltic rock that has not been anelastically deformed. We believe that even the damaged rock is now fully able to support itself and the carbonate layer above it, despite a very extended network of chimneys and cracks (fractures) interlacing the volume in question. The impact on hydrology is discussed later.

1.8.2 Surface Settlement

Settlement (or subsidence) of the atoll rim, particularly in test area 4, is the most noticeable result of the test series (see Fig. 1.9). Monitoring in boreholes has shown that the residual compaction (reduction in porosity) and/or vertical compressive strain required to achieve this settlement is spread over the top 120 m of the carbonate layer. As stated above, this settlement is about 2 m, particularly if the formation of the cavities had led to an effective rise of 0.6 m. Two mechanisms to explain this can be invoked: a mean change in porosity of 1.5% in this upper layer of limestone will account for it (2 m reduction in 120 m) without lateral strain, while a mean lateral displacement of about 1 m at the ocean slope would achieve the same result without any change in porosity. In all cases, settlement was observed above the sites of tests (see Fig. 12 in DIRCEN/CEA Document No 7), so a generic process clearly was involved.

The directly available measured evidence is not conclusive on the matter. The DIRCEN/CEA documents are not fully explicit about the reasons for their views, but they seem to lean toward a pure matrix compaction effect, caused partly directly by the passage of a compressive wave, but primarily by the gravitational rebound of massive spalls (slabs detached by the tensile wave reflected from the surface) onto the friable upper levels of carbonate. (See Fig. 7-9 of Bouchez and Lecomte (1996) and the text following p. 69.)

The IGC finds this explanation unsatisfactory, because the carbonate rock involved is saturated (and was at the time of the tests). Even if the rock matrix were substantially damaged by the passage of the compressive blast wave and any reflected tensile wave, the time required to expel the necessary amount of pore fluid (to alter the porosity) from the relevant 120-m-thick layer would be long compared to the time taken for the observed settlement to occur. As mentioned earlier, the IGC favours an alternative rapid shear deformation mechanism, which, in simple terms, involves squeezing the relevant layer outward in a horizontal direction, thus reducing its vertical thickness, all at constant porosity. The arguments are detailed in Volume II, Chapter 4 of this report.

1.8.3 Slope Failure

The most spectacular events during the series were the sudden and delayed sliding of large sections of the slope, which took place between 1977 and 1980, at and beyond the western extremity of test area 4 (Mururoa). (For details, see DIRCEN/CEA Document No. 7, Ch. V.) An interesting feature is that the regions in which some of the most severe slides occurred, particularly those associated with Tydée, were not those closest to the test explosions concerned (see Fig. 1.14). Their consequences were major hydraulic waves that overwhelmed the part of the reef near the slides. It has been suggested that there could have been rapid release of radioactivity into the ocean, and even that vulcanism might have been triggered by this sliding.

Slope movement has taken place and is still being monitored along the northeast part of the rim, including the whole of test area 1. So far, the process appears to be as expected, and movement is slowing down, though there are places in which slides could occur in the future. The creep response of the chalky limestone in which the movement has already occurred is not well enough understood for it to be certain that the present slowing down of movement will not reverse and accelerate later — particularly if triggered by an otherwise relatively minor event. The lower intensity of shock waves striking the northeast slope (i.e. lower than those involved in the southwest area) may explain the absence of total failure. However, the chalky rock is of a different nature, with different physical properties, and so generalisations about slope weakening and collapse may be unjustified. What seems clear is that the slides will not involve the volcanic basement rocks and will be of the same general nature as those that occurred elsewhere around the rim in test area 4. Figure 1.15 provides a schematic summary of the various effects of a test under the rim of an atoll.

Various explanations can be proposed for the slides that occurred. Factors considered include:

(1) the basic weakness of the material, partly detrital, forming the slopes concerned;

(2) the high slope angle of the upper sections of the slopes concerned (i.e. slopes in a state of incipient collapse);

(3) possible spalling, analogous to the observations made on the horizontal portions of the atoll surface or, more probably, tensile failure associated with relatively minor strains in the direction the blast wave propagated;

(4) conversion of part of the energy of the blast wave into a surface wave (at the ocean/reef boundary), whose maximum strength occurs at other than the position on the slope closest to the explosion centre; and

Figure 1.14 Aerial view indicating the offshore region of Mururoa affected by the Tydée collapse

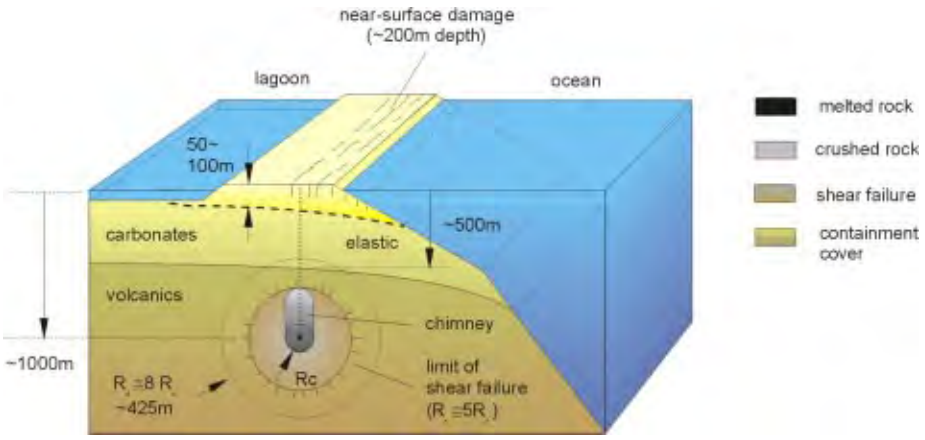

Figure 1.15 Schematic summary of damage due to an assumed 150-kt explosion at 1000-m depth under atoll rim (Note: chimney collapse develops minutes $\sim$ hours after explosion; DIRCEN/CEA Document No. 7, Fig. 1)

(5) lateral (horizontal) movement taking place in the upper carbonate layers as the blast wave reached the exposed sections of the reef, as described above in connection with settlement.

Straightforward calculations (carried out for the IGC), based on a compression wave striking a homogeneous rock having a uniform flat undisturbed slope, predict that failure should occur, if the wave is strong enough, or the rock is weak enough, in the region of the slope closest to the test explosion centre. However, some of the major slides occurred farther away from the explosion centre, and the IGC has had to conclude that local variations in slope topography and rock properties lie behind these otherwise paradoxical events. These issues are discussed in much more detail in Volume 2, Chapter 5 of this report. There we have also analysed the process of slope movement in test area 1, taking more realistic account than is provided in DIRCEN/CEA documents of

(a) the concomitant settlement process;

(b) the initiation and location of slip surfaces;

(c) the contribution of successive test explosions;

(d) the three-dimensionality of the process; and

(e) the consequences for the future.

Continued monitoring is obviously necessary: even a few days' warning of accelerated sliding would allow the local authorities to alert shipping and the inhabitants of the nearest inhabited atolls.

1.8.4 Enhanced Convection of Radioactive Material from the Explosion Sites to the Environment

This matter has been alluded to in a previous section. The greatest danger of rapid release to the environment arose from those tests, all of them "safety trials" (conducted using conventional explosives and not intended to go nuclear), that took place in the carbonate layer, where the natural permeability is greatest. For those tests that were completely contained in the basalt (i.e. where the chimney did not reach the interface of the basalt or transition material with more permeable layers), the dangers of rapid release are negligible, though there will be enhancement in the long term. For those tests, also conducted in the basalt, whose chimneys just reached the carbonate, early release of some of the radioactivity would have taken place on a time scale of about 10 years, a period which has already elapsed for most tests. Early release would have occurred before or as any hot water plume from the explosion reached the surface and should have been detected at the surface or at the lagoon bottom. The DIRCEN/CEA documents are not very precise on this matter, partly because they concluded that rapid release of all the mobile tritium did not constitute an important hazard and partly because adsorption onto the pore surfaces of the rock of the longer-lived and more toxic isotopes would have delayed the process of convecting them to the surface long enough for the plumes to dissipate.

IGC calculations have been undertaken to confirm and extend the French estimates of pre- and post-test-series global convection. There is no significant atoll-scale effect of the explosions in the sense that the total amount of water entering from the ocean and reappearing in the lagoons is virtually unaltered, and temperature distributions will be little affected. This conclusion can be drawn even though there remains considerable uncertainty about the details of the actual convection. However, where the rim surfaces have settled in the regions of greatest test firing density, or where substantial slides have occurred, very considerable changes in pore fluid circulation will have occurred; tidal effects will have changed on a local level.

The IGC has also done calculations to study the shorter-term effects of large energy release and chimney formation. These confirm, in a qualitative sense, the DIRCEN/CEA conclusions, although the range of post-test permeability distributions compatible with the observations and mechanical predictions is so wide that accurate quantitative prediction cannot be expected. The observations used cover cavity refilling times, pressure measurements connected with tides, vertical temperature profiles (as for Zoé) and tracer measurements at various depths and times.

An interesting observation is that vertical transport of pore fluid, and hence of radioactive tracers, in the several (about 5) wells on Mururoa drilled in connection with the test series that were not used and were left open may not be negligible by comparison with transport through the rock between the wells, even though the cross-sectional areas of the drilled wells were negligible compared with the total (horizontal) areal ex-

tent of the influence of any one explosion. This is because the vertical velocities in a well, driven by buoyancy forces, could be many orders of magnitude greater than the corresponding flow velocities in the rock mass.

In the case of one large (~100-kt) explosion, Lycos, on Fangataufa, a release of tritium clearly connected with that explosion was detected so soon after the explosion that the fact could only be explained by the presence of a highly conductive channel linking the explosion cavity to the karst layer where the tritium was detected. There were at least four such events on Mururoa (see Vol. II, App. C).

Such anomalies are not unexpected in a large non-uniform environment. Standard calculations undertaken in connection with large rock masses assume that the flow of pore fluid is governed by a rock property known as permeability, which is a consequence of (continuum approximation to) the overall connectivity of rock porosity. For predictions based on permeability to be relevant and realistic, the flows predicted must refer to mean values over surface areas (or bulk volumes) large compared with the specific geometrical features (pores, throats, fractures) that give rise to the pore connectivity. In practice, there will be some features (major fractures, karstic pipes and channels, highly conductive porous strata) that span the region for which predictions are sought; these can have significant, even dominant, overall effects. The values for permeability that have to be used in such cases will, it therefore turns out, depend both upon the size (length scale, typically 1 km in the case of the atolls) of the region in question and the size (typically, 10–50 m in the case of software used) of the individual volumes used in any discretised numerical simulation. This is true even when the nature of the rock is known exactly down to a very small (1 mm) length scale.

In the case of the two atolls of concern here, there is great uncertainty in our knowledge: we know that there will be statistical variations about any mean value, but we have little quantitative information; we suspect that there will be some regions of significantly higher hydraulic conductivity than the mean, but we cannot place them accurately with respect to any particular test location. To that extent, all DIRCEN and IGC calculations are representative rather than exact. An example is provided by the enhanced permeability in the various karstic layers (made quantitatively obvious by influxes during drilling operations), which ensures that much of the upward salt water flux under the lagoons is fed by sea water moving in along these layers, and that little of it comes from the underlying basalt. Within these conductive layers, tidal effects are clearly sensed. This separation between the time scales of circulation in basalt and carbonates is what distinguishes between the effects of radioactive releases contained within the basalt and those occurring within, or reaching directly into, the carbonate.

In the case of transport of tritium, a passive tracer, there is the added effect of kinematic dispersion, associated with the variation of pore scale velocities within the porous rock; this is particularly significant in highly fractured or inhomogeneous rock and is greatly enhanced by tidal motion. A consistent theory based on complete mixing within the carbonates can be found in Volume 2, Chapter 7 of this report.

1.9 Summary Findings, Conclusions and Recommendations

Most of these follow fairly obviously from what has been said in previous sections of this abbreviated account. Where additional findings or conclusions are reported, they have been introduced to paraphrase those that are given in the much more exhaustive version of the report (Volume II).

1. Approximately 5% of the volcanic rock lying between 500 and 1500 m below the surface, in both Mururoa and Fangataufa, has been damaged by the underground nuclear tests. There is no damage below 1500 m.

   Some of the early tests below the rim of Mururoa damaged the carbonates down to 200 m, leading to observable surface settlements of up to about 2 m; this affected about 3% of the total carbonate layer.

2. Associated with the damage in the carbonates on the southwest rim of Mururoa were a set of underwater slope failures, the largest of which involved some 0.1 km^3 of largely detrital material. On the northeast slope of Mururoa, a continuing creep deformation has persisted for almost two decades, made noticeable by long open surface fractures parallel to the rim on both the ocean and lagoon sides. Similar fractures have developed on the northeast rim of Fangataufa.

3. These settlements and fractures in the carbonates do not affect and are not in communication with the underlying volcanics; they are specific to the weakest or exposed rim portions of the carbonates.

4. With the exception of the northeast slope of Mururoa, which is still creeping (at a decreasing rate), and possibly (to a lesser extent) the northeast slope of Fangataufa (see Recommendation 14, below), the two atolls are everywhere stable and the volcanic bases structurally sound; the rubble-filled chimneys and cavities are effectively supporting the layers above them.

5. There have been no long-term (500–10 000 years) impacts on the global hydrology of either atoll.

6. Temperature increases in the vicinity of each explosion centre have led to detectable local increases in the upward groundwater movement. This increase in flow is greatest in the case of chimneys reaching into the carbonates. These increases will decay with time, and temperature effects will be imperceptible after 500 years.

Turning to the questions posed in Table 1.1, we can conclude specifically:

7. No further major settlement or subsidence directly attributable to the test series will take place on Mururoa or Fangataufa. There has not been, nor will be, any danger of induced volcanism.

8. One or more large underwater failures could occur in the carbonates on the flanks of the northeast rim of Mururoa, involving a total of up to 0.6 km^3 of material. (Slope movement in this region is being closely monitored, and adequate warning of accelerated creep should be available.) Similar failures might be possible on the northeast rim of Fangataufa, but these have not been monitored. No further slides can be envisaged on the southwest rim of Mururoa where they have already occurred.

9. Major fractures running deep into the atolls have not been created, while those visible at the surface do not extend into the volcanics.

10. Long-lasting changes have not been induced in the hydrology of the atolls. Radionuclide products of most of the nuclear explosions that took place are still well contained by an adequate covering of relatively impermeable volcanic rock. Those explosions within, or that had chimneys or damaged zones breaking into, the carbonates gave some early, but not environmentally significant, release of tritium, strontium and caesium into the lower portions of the carbonates (and thence into the lagoon or ocean).

11. The changes noted in 1 and 2 above are no more significant than natural changes, such as ocean water-level fall due to glaciation or coral growth and decay, to be expected in the short and long terms on Mururoa and Fangataufa. Coral atolls are developing continuously; historical evidence shows that topographical changes far greater than those attributable to the test series arise over long periods of time. Isolated events of the magnitude of the slides induced on Mururoa are known to occur periodically.

12. In populated regions in the rest of the world, greater changes, in quantitative terms, to hydrology and topography have been caused by common (and necessary) human activities — e.g. large-scale agriculture, mining and city building.

13. It is recommended that the current instrumentation system for measuring further deformation in the northeast region of Mururoa be maintained and monitored for the next 20 years (or until failure if this occurs sooner) to give adequate notice of possible impending collapse.

14. It is recommended that additional details leading to DIRCEN/CEA's conclusion that the visible creep on northeast Fangataufa has stabilised be released, to obtain independent assessment of any danger of larger underwater slides occurring there.

15. It is recommended that observations on the release of radionuclides into the lower carbonates and lagoons of Mururoa and Fangataufa be continued, and that additional analytic and numerical studies be conducted to better explain why extensive mixing appears to take place in the carbonates.

Finally, it is noted that the six tests of the 1995/1996 series were all exploded in the volcanics in the central parts of the atolls. Although no specific details concerning these tests have been provided to the IGC, it is clear that the tests avoided the dangers of slope collapse associated with rim tests. The ongoing monitoring of tritium released into the carbonates on both atolls should allow the effectiveness of the test containment to be assessed.

Appendix A

IGC BIOGRAPHICAL SKETCHES

Pierre Bérest graduated from Ecole Polytechnique (1970 and Ecole des Mines de Paris (Corps technique de l'état, 1973). He is an Associate Professor at Ecole Polytechnique, Palaiseau, France, as well as Director of the Laboratoire de Mécanique des Solides. Dr. Bérest is President of the French National Group of the International Society for Rock Mechanics and a member of the French Standing Committee for Nuclear Waste Disposal and the French Underground Storage Safety Commission.

Edwin T. Brown is a geomechanics engineer, with a Ph D in rock mechanics obtained from the University of Queensland, Australia, in 1969 and a D Sc(Eng), awarded by the University of London, U.K., in 1985 for published work in engineering rock mechanics. Currently, he is Senior Deputy Vice-Chancellor of the University of Queensland and was formerly Professor of Rock Mechanics and Dean of the Royal School of Mines at the then Imperial College of Science and Technology, London. Dr. Brown is a former President of the International Society for Rock Mechanics (1983–1987), a Fellow of the Australian Academy of Technological Sciences and Engineering and a Foreign Member of the Royal Academy of Engineering, U.K.

Ghislain de Marsily graduated as a mining engineer from the Paris School of Mines in 1963, and obtained a State Doctorate from the University of Paris in 1978. He is currently a Professor in the Earth Sciences and Natural Media Department of the University Pierre et Marie Curie (Paris VI) in Paris, France, where he teaches hydrology. Dr. de Marsily is a Fellow of the American Geophysical Union and a corresponding member of the French Academy of Sciences. He received an Honoris Causa Doctorate from the University of Quebec and was Editor of the *Journal of Contaminant Hydrology* for seven years. Dr. de Marsily has been a member of a Committee of the U.S. National Academy of Sciences for Environmental Management Technologies and is currently a member of the French Commission for the Evaluation of Research on Nuclear Waste Disposal.

Emmanuel Detournay graduated as a mining engineer from the University of Liège, Belgium, in 1976, and obtained a Ph D in geo-engineering from the University of Minnesota, Minneapolis, in 1983, where he is an Associate Professor in the Department of Civil Engineering. Prior to his current academic position, Dr. Detournay was a Senior Research Scientist at Schlumberger Cambridge Research, U.K.. His expertise is in petroleum geomechanics, with emphasis on mathematical modelling. He has

received several awards for his scientific and technological work, and he serves on the editorial boards of two international journals.

Charles Fairhurst obtained his Ph D in mining engineering from the University of Sheffield, England, in 1955. He is Professor Emeritus of Mining Engineering and Rock Mechanics, University of Minnesota, Minneapolis, U.S.A,; Chairman, Itasca Consulting Group, Inc., Minneapolis, U.S.A., and a member of the Advisory Committee on Nuclear Waste, U.S. Nuclear Regulatory Commission. A former President of the International Society for Rock Mechanics (1991–1995), Dr. Fairhurst is a member of the U.S. National Academy of Engineering and the Royal Swedish Academy of Engineering Sciences. He has received Honoris Causa Doctor of Engineering degrees from universities in St. Petersburg (Russia), Nancy (France), and Sheffield (England), and is an Honorary Visiting Professor at Tongji University (Shanghai, China).

Victor Nikolaevskiy obtained a Ph D in mechanics from Moscow State University, Russia, in 1960 and a D Sc (mining engineering) from the All-Union Institute of Oil and Gas, Moscow, Russia, in 1966. He was a Postdoctoral Fellow at The Johns Hopkins University (with C. Truesdell and J. Ericksen). Formerly a Professor of Applied Mathematics and Hydrodynamics at Moscow Civil Engineering University and the Moscow Gubkin Academy of Oil & Gas, Dr. Nikolaevskiy is now Head of the Laboratory of Geomechanics at the United Institute of Physics of the Earth, Russian Academy of Sciences. He is a member of the Russian National Committee on Theoretical and Applied Mechanics and the Russian Academy of Natural Sciences. From 1965 to 1982, Dr. Nikolaevskiy played a role in the Russian National Nuclear Program, specialising in mechanics of underground explosions and the dynamic strength of materials. His current fields of interest are the mechanics of geophysical processes and the applications of mechanics to oil and gas recovery.

Anthony Pearson obtained a Ph D in theoretical fluid mechanics from the University of Cambridge, England, in 1957. He is Professor Emeritus of Chemical Engineering at Imperial College, University of London, England, and is a Scientific Consultant for Schlumberger Cambridge Research. A former President and Gold Medalist of the British Society of Rheology, Dr. Pearson is a Foreign Associate of the U.S. National Academy of Engineering. He is an Honorary Professor at the universities of Wales and Birmingham, U.K.

Lloyd Townley obtained a Ph D in hydrology and hydrodynamics at the Massachusetts Institute of Technology, U.S.A., in 1983. Employed until recently by the Commonwealth Scientific and Industrial Research Organisation (CSIRO) in Perth, Western Australia, he became Perth Manager of the Centre for Groundwater Studies and a member of CSIRO's Minesite Rehabilitation Research Program. He has been a member of editorial boards for three international journals, as well as committees of the American Geophysical

Union and the International Association for Hydraulic Research. A former member of the National Committee on Water Engineering of The Institution of Engineers, Australia, Dr. Townley now works in private industry and is an Adjunct Associate Professor in the Department of Geology and Geophysics at the University of Western Australia.

Consultants

Peter Cundall obtained a Ph D in rock mechanics from Imperial College, London, in 1971. He has developed novel programmes and techniques in numerical modelling that find worldwide application in geomechanics, civil engineering and mining engineering. He is the originator of the distinct-element method that is used to model discontinuous systems, such as granular assemblies and rock masses, and is the chief developer of all Itasca Consulting Group programs: FLAC, UDEC, 3DEC and PFC. Dr. Cundall has published more than 60 papers on diverse topics, including shear-band genesis, micro-mechanics of soil and rock, fluid migration in jointed rock, and earthquake simulation of structures and foundations.

Branko Damjanac obtained a Ph D in civil engineering from the University of Minnesota in 1996. He has 15 years of experience in modelling and numerical simulations in the fields of rock mechanics and geomechanics for various research institutions and consulting companies. Dr. Damjanac currently is a Consulting and Code Development Engineer for Itasca Consulting Group, Inc., Minneapolis, U.S.A.

Pierre Perrochet has 15 years of experience in the fields of groundwater flow and transport modelling within various world-renowned research institutions. In 1992, he obtained a Ph D at the Swiss Institute of Technology (EPFL) in Lausanne, where, until recently, he was a Staff Scientist. Dr. Perrochet's research interests focus on regional fluid/thermal/chemical interactions, including theoretical and computational developments in numerical mathematics as well as the design of simulation methods operational for large, complex geophysical systems. He was recently elected Professor in quantitative hydrogeology at the University of Neuchatel, Switzerland.

Laurent Tacher obtained a Ph D in hydrogeology from the University of Neuchatel, Switzerland, in 1992. As a researcher at the Swiss Institute of Technology (EPFL) in Lausanne, he is mainly involved in geological and hydrogeological modelling, meshing and infography.

DIRCEN/CEA REFERENCES

References for the papers cited as DIRCEN/CEA documents Nos. 1–12 in the IGC are given below. These documents can be obtained from

La Documentation Française
29, quai Voltaire
75344 Paris
Cedex 07
France

DIRCEN/CEA, Document No. 1

Direction des Centres d'Expérimentations Nucléaires/Commissariat à l'Energie Atomique. "Lagoon Sediment Radioactivity in Mururoa and Fangataufa," in ***Geomechanical and Radiological Impact of Nuclear Tests at Mururoa and Fangataufa.*** Paris: La Documentation Française, 1998.

DIRCEN/CEA, Document No. 2

Direction des Centres d'Expérimentations Nucléaires/Commissariat à l'Energie Atomique. "Soil Radioactivity in Mururoa and Fangataufa," in ***Geomechanical and Radiological Impact of Nuclear Tests at Mururoa and Fangataufa.*** Paris: La Documentation Française, 1998.

DIRCEN/CEA, Document No. 3

Direction des Centres d'Expérimentations Nucléaires/Commissariat à l'Energie Atomique. "Environmental Monitoring in French Polynesia and on the Mururoa and Fangataufa Sites, Year 1994," in ***Geomechanical and Radiological Impact of Nuclear Tests at Mururoa and Fangataufa.*** Paris: La Documentation Française, 1998.

DIRCEN/CEA, Document No. 4

Direction des Centres d'Expérimentations Nucléaires/Commissariat à l'Energie Atomique. "Medium- and Long-Term Containment of Underground Nuclear Tests

at the CEP: Source Term Inventory and Worst-Case Impact Assessment," in ***Geomechanical and Radiological Impact of Nuclear Tests at Mururoa and Fangataufa.*** Paris: La Documentation Française, 1998.

DIRCEN/CEA, Document No. 5

Direction des Centres d'Expérimentations Nucléaires/Commissariat à l'Energie Atomique. "The Geological, Mechanical and Hydrogeological Environment of the Underground Nuclear Tests at Mururoa and Fangataufa," in ***Geomechanical and Radiological Impact of Nuclear Tests at Mururoa and Fangataufa.*** Paris: La Documentation Française, 1998.

DIRCEN/CEA, Document No. 6

Direction des Centres d'Expérimentations Nucléaires/Commissariat à l'Energie Atomique. "Overall Distribution and Characteristics of the Underground Nuclear Test Carried Out at Mururoa and Fangataufa and Their Effects on the Surrounding Media," in ***Geomechanical and Radiological Impact of Nuclear Tests at Mururoa and Fangataufa.*** Paris: La Documentation Française, 1998.

DIRCEN/CEA, Document No. 7

Direction des Centres d'Expérimentations Nucléaires/Commissariat à l'Energie Atomique. "Structural Integrity and Stability of the Atolls; Data and Modelling," in ***Geomechanical and Radiological Impact of Nuclear Tests at Mururoa and Fangataufa.*** Paris: La Documentation Française, 1998.

DIRCEN/CEA, Document No. 8

Direction des Centres d'Expérimentations Nucléaires/Commissariat à l'Energie Atomique. "Experimental Data on the Mobility of the Radionuclides Deposited By the Underground Tests at Mururoa and Fangataufa - Chapters 1 (Dissolution of Lava Formed by the Underground Tests), 2 (Retention of Radioelements Deposited by Underground Tests) and 3 (Mobility of Products Deposited by the Underground Safety Tests)," in ***Geomechanical and Radiological Impact of Nuclear Tests at Mururoa and Fangataufa.*** Paris: La Documentation Française, 1998.

DIRCEN/CEA, Document No. 9

Direction des Centres d'Expérimentations Nucléaires/Commissariat à l'Energie Atomique. "Current Underground Distribution of Radionuclides at Mururoa and Fangataufa," in ***Geomechanical and Radiological Impact of Nuclear Tests at Mururoa and Fangataufa.*** Paris: La Documentation Française, 1998.

DIRCEN/CEA, Document No. 10

Direction des Centres d'Expérimentations Nucléaires/Commissariat à l'Energie Atomique. "Fangataufa: Overall Assessment of the Short, Medium and Long

Term Radiological Situation of the Atolls of Mururoa and Fangataufa," in ***Geomechanical and Radiological Impact of Nuclear Tests at Mururoa and Fangataufa.*** Paris: La Documentation Française, 1998.

DIRCEN/CEA, Document No. 11
Direction des Centres d'Expérimentations Nucléaires/Commissariat à l'Energie Atomique. "Marine Data and Modelling," in ***Geomechanical and Radiological Impact of Nuclear Tests at Mururoa and Fangataufa.*** Paris: La Documentation Française, 1998.

DIRCEN/CEA, Document No. 12
Direction des Centres d'Expérimentations Nucléaires/Commissariat à l'Energie Atomique. "Guide de Surveillance Géomécanique des Atolls de Mururoa et Fangataufa," in ***Geomechanical and Radiological Impact of Nuclear Tests at Mururoa and Fangataufa.*** Paris: La Documentation Française, 1998.

DIRCEN/CEA Books — French Version *

Bouchez, Jacques, and Raphael Lecomte. (1995) ***Les Atolls de Mururoa et de Fangataufa (Polynésie Française),*** II. Les Expérimentations Nucléaires: Effets mécaniques. lumino-thermiques, électromagnétiques. Paris: Masson.

Guille, G., G. Goutière, J. F. Sornein, D. Buigues, A. Gachon and C. Guy. (1996) ***Les Atolls de Mururoa et de Fangataufa (Polynésie Française),*** I. Géologie - Pétrologie - Hydrogéologie: Edification et évolution des édifices. Paris: Masson.

* DIRCEN/CEA also made available to the IGC an official English translation of Guille et al. (1996) and a draft translation of the underground testing sections of of Bouchez and Lecomte (1996). References in the ICG report to page numbers and figures in these books refer to the English versions of both volumes; an official English translation of Bouchez and Lecomte (1996) is in preparation. Chapters 1–9 in the draft English version (referenced in the IGC report) correspond to Chapters 8–16 in the (official) French version of Bouchez and Lecomte (1996).

BIBLIOGRAPHY

Barrillot, B. (1996) Les Essais Nucléaires Française 1960-1996: Conséquences sur L'environment et la Santé. Lyon, France: Centre de Documentation et de Recherche sur la Paix et les Conflits.

Bouchez, J. and R. Lecomte (1996) The Atolls of Mururoa and Fangataufa (French Polynesia). II. Nuclear Testing, Mechanical Lumino-Thermal and Electromagnetic Effects (in Collaboration with J. Brugies, C. Guerrini, J.-F. Sornein, J.-L. Plantet and E. Blanc). Monaco: Musée Océanographique.

CRII-RAD (1995) Essais nucléaires (revue d'information de la CRII-RAD). Tech. Rep. 3, Commission de Recherche et d'Information sur la Radioactivité, Valence, France.

Fondation Cousteau, Paris (1988) Mission scientifique de la Calypso sur le site d'expérimentations nucléaires de Mururoa. Technical Report.

Goguel, J. (1982) L'évolution du cadre naturel. In *Rapport D'Haroun Tazieff*, no. Annex 2.

Guille, G., G. Goutière, J. F. Sornein, D. Buigues, A. Gachon and C. Guy (1996) The Atolls of Mururoa and Fangataufa (French Polynesia). I. Geology - Petrology - Hydrogeology, from Volcano to Atoll (translated by M.S.N. Carpenter). Monaco: Musée Océanographique.

IAEA (1998a) The radiological situation at the atolls of Mururoa and Fangataufa: Main report. Tech. rep., International Advisory Committee, Vienna.

IAEA (1998b) The radiological situation at the atolls of Mururoa and Fangataufa: Technical report, Vol. 4, Releases to the biosphere of radionuclides from underground nuclear weapon tests at the atolls, report by working group. Tech. rep., International Advisory Committee, Vienna.

IAEA (1998c) The radiological situation at the atolls of Mururoa and Fangataufa: Technical report, Vol. 3, Inventory of radionuclides underground at the atolls, report by working group. Tech. rep., International Advisory Committee, Vienna.

New Zealand MoFA (1984) Report of a New Zealand, Australian, and Papua New Guinea scientific mission to Mururoa Atoll. Tech. rep., New Zealand Ministry of Foreign Affairs, Wellington.

Tazieff, H. (1982) Rapport d'Haroun Tazieff sur l'ensemble de la mission scientifique en Polynesie Française. Tech. rep.

Vincent, P. M. (1996) The impact of underground nuclear explosions at Mururoa Atoll (South Pacific) and associated hazards. *Médecine: Re Nucléaire*, **11**(1).

GLOSSARY

Advection (of a solute) Transport of a solute by means of circulating waters in a porous medium, at the velocity of the water, and when the concentration of the solute is not sufficient to affect density of the water.

Barrier A coral reef situated offshore from an island or continent, sometimes forming a ring. Such a reef may later develop into an atoll by gradual subsidence of the central area.

Basalt A dark-coloured, fine-grained, volcanic rock composed of plagioclase feldspar, pyroxene and magnetite, with or without olivine, and containing not more than 53% SiO_2 by weight.

Carbonates For both atolls, the carbonate covering comprises limestones and dolomites; it varies between 130 m and 450 on Mururoa, and is approximately 230 m thick on Fangataufa.

Cavity Space formed around the test chamber following an underground nuclear explosion.

Chimney Rubble-filled zone of approximately cylindrical shape, formed after the cavity created by an underground nuclear explosion collapses. Chimney height is closely related to the yield and depth of the explosion.

Compaction (of carbonates) The act of forcing carbonate material together (consolidation) under pressure or impact to reduce porosity and yield a relatively denser mass.

Compression wave See **P wave**.

Conduction (of heat) Transport of heat through rock or water without any displacement of the pore water.

Convection (of heat) Transport of heat by means of circulating waters in a porous medium; the motion resulting in a fluid from the differences in density (due to thermal expansion) and the action of gravity is called ”natural convection”, whereas forced

convection represents the case where the velocity of the fluid is due to causes other than differences of density.

Coral rim A ring-shaped section of reef above sea level, forming the emergent part of an atoll.

Creep Continuous deformation of a material under steady load; behaviour of earth materials in response to factors such as time, temperature, pore pressure, and ambient stress level.

CRTV Nuclear tests in which chimneys reach the top of the volcanism.

Darcy A standard unit of measurement of permeability, with the dimension of an area (L^2) equivalent to the passage of 1 cm^3 of fluid of 1 centipoise viscosity flowing in 1 second under a pressure differential of 1 bar through a porous medium having a cross-sectional area of 1 cm^2 and a length of 1 cm. One Darcy is equal to $0.987 \cdot 10^{-12}$ m^2.

Darcy velocity A hypothetical discharge rate calculated assuming that water moves through the entire cross-sectional area in question. In practice, the water moves through interconnected pore-spaces that represent only a certain proportion of the total rock volume. Although the constant K has the dimensions of length per unit time (i.e. velocity), the Darcy velocity is evaluated from the product Ki.

Detrital Formed from fragmented material derived from the erosion of previously existing rocks (detrital deposits are commonly interbedded within carbonate formations).

Fault A fracture or zone of fractures along which there has occurred displacement of the sides relative to one another parallel to the fracture.

Flows (of sediment) Dislodging of sediment downslope involving a number of processes, notably debris flow, grain flow and liquefaction flow. Flows are sometimes regarded as a transitional stage between slides and turbidity currents.

Geothermal heat flow Heat flow from the inner earth.

Gravitational stresses Stresses resulting from the mass of overburden.

Ground zero The point on the surface of the water or the ground situated vertically below (in the case of atmospheric explosions) or above (in the case of underground explosions) the point of detonation (the zero point).

Hoa A hollow between motu (islets) on a barrier reef, allowing exchanges of sea water between ocean and lagoon.

Hydrothermal Pertaining to hot fluids that circulate within the earth's crust.

In-situ stress The stress existing at a point in the rock mass before the rock is disturbed.

Karst A type of internal modification of rocks developed specifically in limestone terrains as a result of variable degrees of dissolution by meteoric waters (karstic erosion, cavity), and characterised by enlarged fractures, enhanced porosity, caves and underground drainage, or, sometimes, sinkholes at the surface. Such features are recognised at varying depths within the body of a limestone and are related to past low sea levels or base levels.

Kilotonne Unit used to quantify the energy released by nuclear and thermonuclear explosions. It corresponds to the energy released by 1000 tons of a reference chemical explosive, tri-nitro-toluene (TNT), $4.18 \cdot 10^{19}$ Ergs or $4.18 \cdot 10^{12}$ Joules. For thermonuclear explosions the megatonne (Mt) is often used: 1 Mt = 10^3 kt.

Megatonne (Mt) A unit used to quantify the energy used by nuclear and thermonuclear explosions. It corresponds to the energy released by 1 million tonnes of the chemical explosive TNT. The kilotonne (1 kt = 0.001 Mt) is also sometimes used.

Motu A small islet made up of bioclastic material, situated on the reef rim of an atoll.

Nuclide An atomic species characterised by its mass number, atomic number and energy state. (see also **Radionuclide**)

P-(primary) wave Compression wave occurring after an earthquake or an underground nuclear explosion; the fastest vibration wave.

Permeability The ability to transmit water; the "matrix" permeability is governed mainly by the degree of communication between the pores. (see also **Porosity**).

Physico-chemical stress The stress state arising from chemical and/or physical changes in the rock (e.g. recrystallization, absorption of water, fluctuation of groundwater level).

Point zero See **Zero point**.

Pore water Water contained within the pores of a geological formation.

Porosity The ratio between the pore-space volume and the total volume of a rock sample or formation.

Radionuclide A radioactive atomic species.

Rayleigh wave Seismic wave, generated by an earthquake or an underground nuclear explosion, that affects only the superficial layers of the medium.

Reef See **Barrier reef**.

Rim See **Coral rim**.

S (secondary) wave Shear wave, propagating as a seismic wave, generated after an underground nuclear explosion.

Safety trial Detonation of an annulus of chemical explosive placed around a nuclear device to determine whether the explosion results in a nuclear explosion (or "yield").

Seismic wave Compression wave that propagates through the earth as a vibration, generated by an earthquake or an underground nuclear explosion.

Settlement In relation to underground nuclear testing, ground depressions caused by compaction of surface layers, due in part to the fall-back of layers that have risen in ballistic flight following slabbing.

Shear strength The value at which shear stresses exceed a limiting value, after which plastic deformation of the rock occurs; a measure of the rock's ability to withstand compression. Shear strength is related to specific values of pore fluid pressure.

Shock velocity Velocity of the shock front propagating in fluid or solid materials. This velocity depends on the nature of the medium and on the energy carried by the shock wave.

Slabbing See **Spalling**.

Slides The most widespread form of submarine slope instability, these may involve rock or soft sediment.

Spalling The upward or outward displacement of surface and near-surface layers of rock and sediment caused by the interaction of a compressional shock wave at a free surface. The shock wave may produce fragmentation or may cause only momentary parting of layers. Surface spalling associated with nuclear explosions occurs when a surface layer of rock separates from an underlying rock mass by a horizontal fracture generated by the reflected, downgoing tensile pulse from the explosion.

Subaerial volcanic rocks Overlying the submarine volcanics, these rocks were formed when the top of the volcano emerged from the ocean. They are more diverse and spatially variable than the submarine rocks. Rock types vary from massive basalts to volcanic cinder deposits.

Submarine rock falls Rock falls restricted to localised steep, near-vertical slopes.

Submarine volcanic rocks Rocks formed when the top of the volcano was still under sea level. On Mururoa and Fangataufa Atolls, these consist of pillow lavas and associated breccias, autoclastites and hyaloclastites.

Subsidence craters Following an underground nuclear test, a collapse of the cavity and formation of a chimney affecting layers up to the surface. In contrast to explosion craters, no near-surface material is expelled.

Transition zone Sedimentary layer, only a few metres thick, between the submarine and subaerial volcanics. The transition zone comprises two distinct layers: a sedimentary layer of calcareous, argillaceous or volcanic conglomeratic rock; and a layer of shallow submarine rocks, mainly highly brecciated lavas.

Vaporized zone The area in the immediate vicinity of the zero point where the rock has been melted and vaporized by the intense shock of the explosion.

Venting In the context of nuclear explosions, the transport of radioactive gases from the cavity created by the explosion to the surrounding rocks or even the biosphere via fractures or other pathways created by the explosion.

Wavelength Distance between two consecutive points of the same phase in an undulatory movement propagating in a straight line.

Yield The effective energy released in a nuclear explosion, manifested as shock or blast, thermal radiation and nuclear radiation. The residual nuclear radiation associated with the fission products, which amounts to about 10% of the total fission energy, is not included in the yield. Yield is usually expressed as TNT equivalent — the quantity of TNT that would release the same amount of energy if exploded. TNT equivalent is usually given in kilotonnes or megatonnes, one kilotonne of TNT being defined arbitrarily as $4.18 \cdot 10^{12}$ Joules.

Zero point The exact location where the nuclear testing device and measuring instrument container are positioned.

Underground Nuclear Testing in French Polynesia:

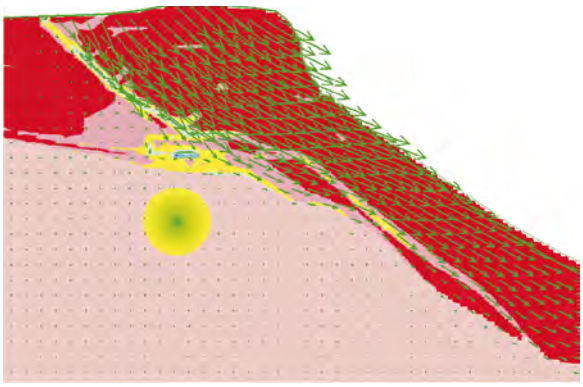

Stability and Hydrology Issues

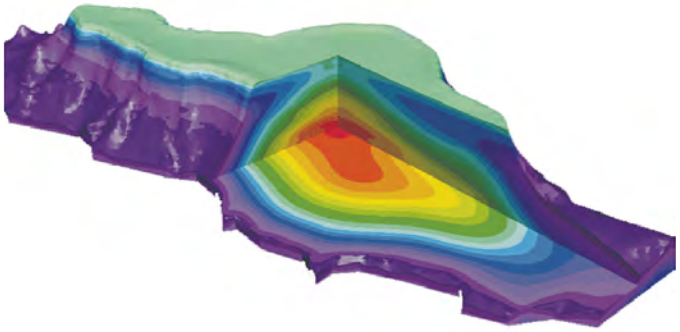

Volume II, Technical Analyses

International Geomechanical Commission
Charles Fairhurst, Chairman

Stability and Hydrology Issues Related to Underground Nuclear Testing in French Polynesia:

Volume II, Technical Analyses

A Report of the
International Geomechanical Commission

Charles Fairhurst, Chairman

Prepared under a contract with the University of Minnesota,
Minneapolis, Minnesota, U.S.A.

This report is published in three volumes: Volume I, *General Results*; Volume II, *Technical Analyses*; and Volume III, *Les Essais Nucléaires Souterrains en Polynésie Française: Stabilité et Hydrogéologie* (French language extracts from Volumes I and II). These volumes may be obtained from:

La Documentation Française
29, quai Voltaire
75344 Paris
Cedex 07
France

Printed in the United States of America.
This report has been reproduced from the best available copy.

On the cover : The upper figure shows calculated contours of plastic shear strain and displacement vectors at the Mururoa Atoll rim due to a 10-kilotonne explosion. Details of the calculations are described in Volume II, Chapter 5 of this report.

The lower figure shows a three-dimensional "cut-away" view of the temperature contours computed for the interior of Mururoa Atoll, in the natural condition — i.e. prior to underground nuclear testing. Details of the numerical calculations are given in Volume II, Chapter 6 of this report.

Members of the
International Geomechanical Commission

Chairman

Charles Fairhurst (U.S.A.)

Commission

Edwin T. Brown (Australia)

Emmanuel Detournay (Belgium/U.S.A.)

Ghislain de Marsily (France)

Victor Nikolaevskiy (Russia)

J.R. Anthony Pearson (Great Britain)

Lloyd Townley (Australia)

Technical Liaison

Pierre Bérest (France)

Brief biographical sketches of Commission members and main Consultants are given in Appendix A.

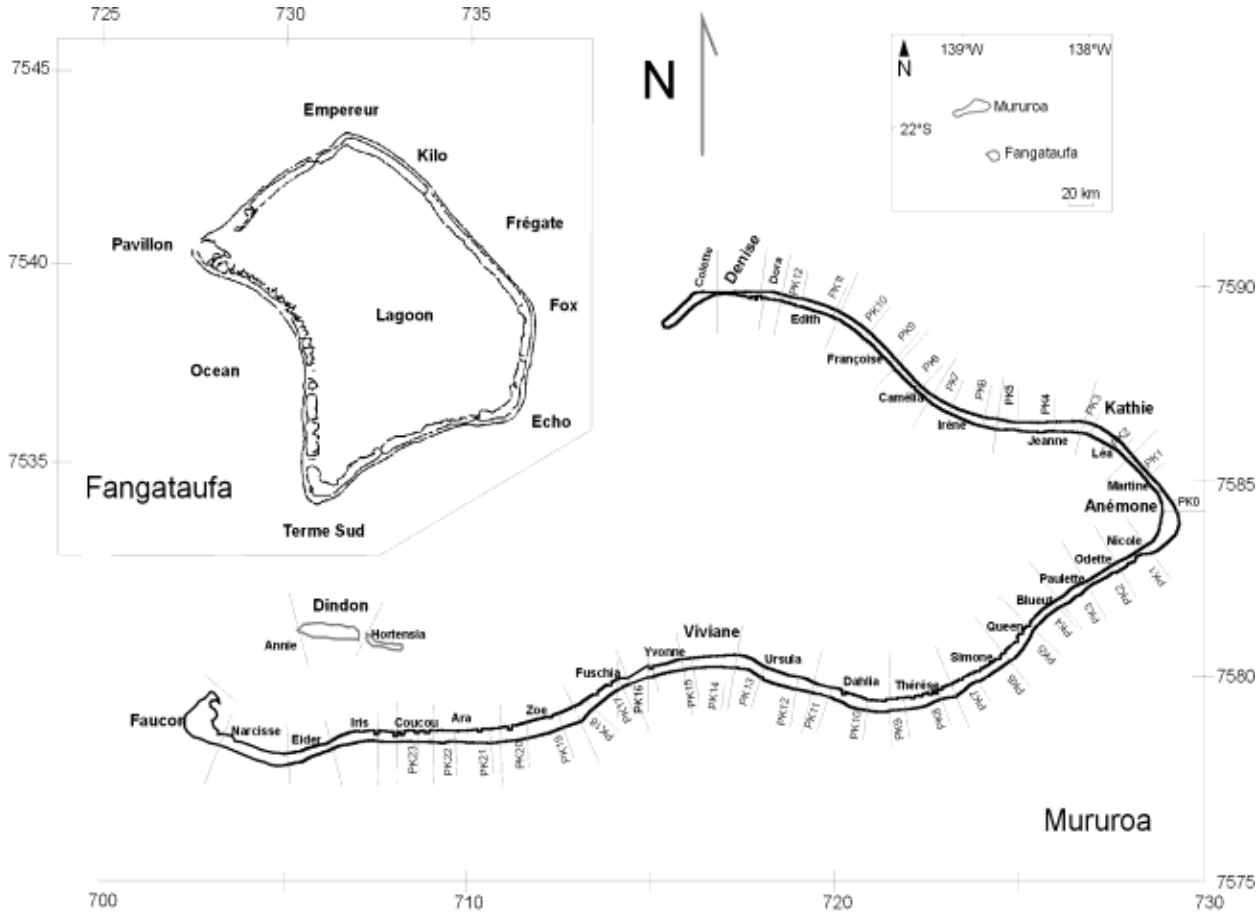

Local designations of the various sectors of Mururoa and Fangataufa. Local co-ordinates shown are Universal Transverse Mercator co-ordinates (in km) for the Southern Hemisphere. Correct relative geographical locations of the atolls are shown in inset diagram (upper right).

PREFACE

The French Nuclear Testing Programme

Gerboise bleue, a relatively low-yield explosion (estimated $60 \sim 70$ kt*), detonated in the Sahara desert, at Reggane, Algeria, on 13 February 1960, marked the debut of France as a nuclear power — some 15 years after the world's first nuclear explosion (Trinity) at Alamagordo, New Mexico, USA, on 16 July 1945. During those 15 years, the United States of America had detonated 196 explosions, the Soviet Union 84, and the United Kingdom 21. Except for the 22 underground explosions at the Nevada Test Site in the United States (see Appendix B), all of the 301 tests were conducted in the atmosphere. In November 1958, these three countries jointly declared a moratorium on testing. The moratorium lasted until September 1961.

In November 1961, after 4 atmospheric tests at Reggane, France proceeded to a series of 13 underground tests detonated deep within horizontal tunnels excavated in the Hoggar granite mass at In-Eker, some 560 km ESE of Reggane. This series concluded 16 February 1966, due, at least in part, to the political situation in Algeria. In the meantime, the United Kingdom, USA and USSR had signed the Limited Test Ban Treaty (5 August 1963), which banned nuclear testing in the atmosphere, outer space or under the open ocean.

Aldebaran, the first French test in the South Pacific, took place on 21 July 1966. It was an atmospheric explosion from a barge on the Mururoa lagoon, the first of a total of 41 atmospheric explosions: 37 on or near Mururoa (including Procyon, with a yield over 1 Mt*), and 4 on Fangataufa (including Canopus, with a yield over 1 Mt). Five surface safety trials† were also carried out on the surface of Mururoa, 2 of which resulted in a (small) nuclear yield. Atmospheric tests ended 14 September 1974.

---

*1 kt implies an energy release from, or *yield* of, a nuclear explosion equivalent to the detonation of 1 thousand tonnes of the chemical explosive tri-nitro-toluene (TNT) ($4.18 \cdot 10^{12}$ joules). 1 Mt implies the energy release corresponding to 1 million tonnes of TNT ($4.18 \cdot 10^{15}$ joules, which is the mechanical equivalent of 10^{15} calories of heat energy).

The Threshold Test Ban Treaty (1962), agreed to by the Soviet Union and the United States, placed an upper limit of 150 kt on the yield of underground tests. CEA (Bouchez and Lecomte 1996, Appendix, p. 113) claims that all underground tests conducted by France were below the 150-kt limit. International seismic monitoring results support this assertion (see Vol. II, App. C).

†A safety trial involves detonation of an annulus of chemical explosive placed around the nuclear device to determine whether this explosion results in a nuclear explosion (or "yield").

Underground testing on the atolls began with two small tests (Achille and Hector) beneath the southern rim of Fangataufa on 5 June 1975 and 26 November 1975. By the time this series was completed in July 1991, a total of 131 underground tests had been conducted: 123 at Mururoa (73 under the rim and 50 under the lagoon) and 8 at Fangataufa (2 under the rim and 6 under the lagoon). An additional 10 underground safety trials, 3 of which resulted in a small nuclear yield[‡], were carried out on Mururoa. France announced its own moratorium on nuclear testing in September 1991.

Location of Mururoa and Fangataufa with respect to major continental land masses

The Final Campaign of Tests

Britain, the United States and Russia had already announced their readiness to adopt the proposed Comprehensive Test Ban Treaty, banning all nuclear weapons testing, when, in June 1995, President Chirac unexpectedly announced that France would conduct a limited number (not to exceed 8) of underground tests at Mururoa and Fangataufa before signing the Treaty[¶] A total of 6 additional tests were carried out (4 at Mururoa and 2 at

[‡]Note that the 3 "nuclear" safety trials are included in the 134 underground tests listed in the appendix to Bouchez and Lecomte (1996). With the 6 tests of the 1995/1996 series, a total of (131 + 10 + 6 =) 147 underground nuclear tests and safety trials have been conducted on Mururoa and Fangataufa.

[¶]France signed this Treaty when it was adopted by the United Nations in 1996; it was approved by the French Parliament in March 1998. Britain, China, Russia and the United States have also signed the Treaty. The treaty has not yet taken force.

Fangataufa — all under the lagoons) between 5 September 1995 and 27 January 1996, when France announced that the series was complete. Between 13 February 1960 and 27 January 1996, France had carried out 210 nuclear tests[§], including the 15 safety trials. Details of all known tests worldwide (USA 1030; USSR 415; France 210; China 45; U.K. 45, India 6; Pakistan 6[‖]) are given in the table in Appendix B. More specific details related to the French underground tests in the South Pacific are presented in Appendix C.

The decision to conduct this final campaign, three years after all countries except China had stopped testing, provoked widespread concern and international protests that the tests, added to those already carried out, could result in severe adverse short-term** and long-term consequences. Release into the environment of dangerously radioactive nuclides produced by the explosions and damage to the mechanical stability and hydrology of the atolls were the two principal issues.

Invitations to Study the Effects of Underground Tests

Responding to the concerns and protests, the French Minister of Foreign Affairs, M. Hervé de Charette, acting on behalf of President Chirac, in September 1996, invited two separate international groups to conduct independent investigations of the consequences of the underground tests on Mururoa and Fangataufa.

The International Atomic Energy Agency (IAEA), headquartered in Vienna, agreed to examine the issue of radiological releases. The official report was released in August 1998. An international conference to discuss the findings was held at IAEA headquarters in Vienna, 30 June–3 July 1998.

A copy of the letter from M. de Charette (inviting Professor Fairhurst to lead the second study — on the stability and hydrology issues) is shown on the following pages. In responding to this invitation, Professor Fairhurst, then President of the International Society of Rock Mechanics (ISRM), noted that his (four-year) term of office would end within approximately one month, so he would not be conducting the study as President of ISRM. It was agreed, therefore, that he would select and lead an independent group of international experts, designated as the International Geomechanics Commission (IGC),

---

[§] The 210 tests can be broken down as follows: 45 atmospheric (4 Algeria, 41 South Pacific); 150 underground (13 Algeria, 137 South Pacific); 15 safety trials (5 surface, 10 underground — all South Pacific).

[‖] India detonated 5 underground tests, 11–13 May 1998; Pakistan announced 5 tests, 28 May 1998, then 1 on 30 May 1998. Some seismic detection experts have suggested that fewer than 5 devices were detonated on 28 May.

** "Short-term", here, implies the period of testing to approximately 500 years from the cessation of underground testing. "Long-term" implies a period of the order of 10 000 years from the cessation of underground testing.

14 septembre 1995

Le Ministre des Affaires Etrangères

Monsieur le Professeur,

L'engagement de la France de se joindre à la conclusion du Traité d'interdiction complète des essais nucléaires au plus tard en 1996 a conduit les autorités françaises à procéder à une ultime série d'essais. Ces essais souterrains, au nombre maximum de huit, se dérouleront au Centre d'Essais du Pacifique sur les atolls de Mururoa et de Fangataufa entre septembre 1995 et fin mai 1996.

Dans un souci de transparence, le Président de la République Française souhaite qu'une mission scientifique internationale procède a l'évaluation des effets de cette série d'essais sur l'environnement aussi bien du point de vue radiologique qu'au plan géologique et de la stabilité des atolls. Le Gouvernement français à décidé de confier la direction de cette mission à des experts ou à des organisations internationales dont la réputation scientifique est incontestable dans les domaines considérés.

A ce titre, considérant la réputation exceptionnelle que vous avez personnellement dans la communauté scientifique internationale, les responsabilités éminentes qui sont les vôtres en tant que Président de la Société Internationale de Mécanique des Roches, j'ai l'honneur de vous demander si vous accepteriez de conduire la mission scientifique dans le domaine de la stabilité des atolls et de l'hydrogéologie.

Si vous acceptiez cette responsabilité, il vous appartiendrait de préciser la composition de cette mission scientifique dont vous seriez seul juge, s'agissant en particulier du choix des experts. J'appelle toutefois votre attention sur l'intérêt que les pays de la zone Pacifique portent à cette mission.

Les autorités francaises mettront à la disposition de la mission scientifique l'ensemble des données disponibles concernant les études antérieures liées à la situation mécanique et hydrogéologique des atolls de Mururoa et Fangataufa.

Les frais engendrés dans le cadre de cette mission seront pris en charge par la France selon un protocole à établir avec vous.

Les Services des diverses administrations françaises concernées et notamment du Commissariat à l'Energie Atomique sont à votre disposition pour apporter les précisions que vous pourriez estimer nécessaires avant de prendre une décision que le Gouvernement français souhaite positive.

Il conviendra en particulier d'arrêter avec eux les dispositions pratiques concernant le calendrier, la nature et le volume des travaux. A cet égard, je peux vous assurer que les autorités françaises auront le souci de limiter autant que possible les contraintes à prendre en considération eu égard à la confidentialité des aspects militaires des essais.

J'ajouterai enfin que si vous estimez nécessaire pour la préparation de votre mission de venir sur les atolls, éventuellement avec d'autres experts, avant la fin de notre ultime campagne d'essais, les autorités françaises feraient leurs meilleurs efforts pour rendre cela possible.

Veuillez agréer, Monsieur le Professeur, l'expression de ma haute considération.

Hervé de CHARETTE

Professeur FAIRHURST
Président de la Société Internationale
de Mécanique des Roches

September 14, 1995

Ministry of Foreign Affairs

Dear Professor,

The commitment of France to sign the Comprehensive Test Ban Treaty no later than 1996 has led French authorities to carry out a final series of tests. These underground tests, no more than eight maximum, will take place at the Pacific Test Centre on the atolls of Mururoa and Fangataufa between September 1995 and the end of May 1996.

With a concern for openness, the President of the French Republic would like to have an international scientific mission undertake an evaluation of the effects of this series of tests on the environment from the points of view of the radiology, geology, and stability of the atolls. The French government has decided to entrust the direction of this mission to experts or international organisations whose scientific reputations are unquestioned in the fields concerned.

Considering the exceptional reputation that you have, in the international scientific community, and your special responsibilities as President of the International Society for Rock Mechanics, I am pleased to ask whether you would be willing to lead the scientific mission to investigate the stability and hydrology of the atolls.

If you accept this responsibility, you would be responsible for and the sole judge in defining the specific task of the scientific mission, particularly in the selection of the experts. However, I would call to your attention the particular interest of the Pacific Rim countries in this mission.

The French authorities will provide the scientific mission with all data regarding previous rock mechanics and hydrological studies of Mururoa and Fangataufa atolls.

The costs incurred in the conduct of this mission will be met by France according to a protocol to be arranged with you.

The services of the various relevant French administrative offices, particularly the Atomic Energy Commissariat (CEA), are at your disposal to answer any specific questions that you may wish to have answered before reaching what the Government hopes will be a positive decision.

In particular, it would be valuable to establish with these officials the schedule, nature and volume of the work to be done. In this respect, I assure you that the French authorities wish to minimise, so far as possible, the restrictions with respect to the confidentiality of the military aspects of these tests.

Finally, I would add that if you feel it necessary, in order to prepare for your mission, to visit the atolls with other experts before the end of our final testing programme, the French authorities will do their best to make this possible.

Yours sincerely,

Hervé de CHARETTE

Professor FAIRHURST
President, International Society for Rock Mechanics

to undertake the study. The members of the IGC and support staff are listed in Appendix A, together with a brief biographical sketch of each member.

Although most of the radioactivity and stability/hydrology studies have been pursued independently of each other, aspects of the stability and hydrologic consequences of the tests directly affect the radionuclide releases. To ensure that these consequences were taken into account, three members of the IGC group participated in the radiological study, at the invitation of the IAEA, as members of Working Group 4, Geosphere Transport.

This report presents the results of the IGC study.

IGC Study Procedure

Particular attention has been given, both by French authorities and Commission members, to ensuring the independence of the IGC study. The general topics of investigation, stability and hydrology were defined in the letter from M. de Charette, but the IGC made its own decision as to specific issues and procedures. Thus, although the letter refers to "*an evaluation of the effects of* ***this series of tests*** . . .", the Commission quickly decided that study of the effects of testing on the stability and hydrology of atolls must be framed within the context of the entire suite of 147 underground nuclear tests carried out on Mururoa and Fangataufa. Similarly, the choice of specific topics was made by the Commission. Some initial consideration was given, for example, to the seismic signal generated by an explosion — with respect to the accuracy of estimates of nuclear yield (see Appendix B), the potential for structural damage at large distances from the tests, and the generation of tidal waves by large underwater slides. In each case, it was decided that questions related to these effects could be answered adequately without detailed study by the Commission.

A master contract was established between the Commissariat à l'Energie Atomique (CEA) and the University of Minnesota, Minneapolis, USA, Professor Fairhurst's employer. All subsequent financial decisions were made by the University. Choice of IGC members, consultants and contractors was made independently of French authorities.

Commission studies and findings were confidential to IGC members only until October 1997 when, almost two years from the start of the study, CEA scientists were shown copies of several chapters of the IGC draft report. The Commission considered this necessary in order to ensure that data supplied by the CEA had not been used incorrectly. Although some explanatory comments and analyses have since been added to the Final Report, the findings and conclusions have not been changed.

The Commission placed emphasis on establishing a sound scientific framework on which to assess the consequences of underground nuclear tests on the stability and hydrology of Mururoa and Fangataufa. The results are presented in sufficient detail that their validity can be judged independently by others.

Sources of Information

The Commission met several times (see box on the following page) with CEA scientists during the early phases of the study to obtain background information and to raise questions. Core samples from the Zoé borehole on the south-central rim of Mururoa, continuous from the surface through the carbonates and volcanics to a depth of 1100 metres, were examined in the CEA laboratories at Bruyères le Chatel, south of Paris.

Commission members spent three days on Mururoa and Fangataufa, 10–12 July 1996, and examined all accessible testing and affected areas on the rim by car and on foot. Both atolls also were studied at low altitude from a helicopter. Still and video-camera photographs were allowed without restriction.

On Mururoa, particular attention was paid to test area 1, where substantial volumes of the ocean-side rim have been undergoing continuous deformation for almost two decades, and test area 4, the most intensively used (in terms of total explosive yield per unit volume of rock) and the site of the large underwater slides induced by testing. On Fangataufa, fractures activated in the northeast rim in the vicinity of Kilo-Frégate were examined. This area is unique in that tests on Fangataufa were not conducted on the northeast rim. This implies that these fractures were *stimulated* by the seismic waves created by tests in other areas of the atoll — most probably, the large-yield tests under the lagoon.

Although, as mentioned earlier, the locations of individual tests (including depths) were not provided, the surface locations of many of the tests on the rim were visible from the air, especially on Mururoa.

Documents

The two-volume publication *The Atolls of Mururoa and Fangataufa — Volume 1, Geology, Petrology and Hydrogeology (Guille et al. 1996)* and *Volume 2, Nuclear Testing, Mechanical Lumino-Thermal and Electromagnetic Effects* (Bouchez and Lecomte 1996), available (in French[††]) at the start of the study, provided a comprehensive, general overview of CEA studies and the physical consequences of nuclear testing on the atolls. These were supplemented by a number of doctoral theses and publications of work related to the structure and hydrology of the atolls. Copies of reports by the three previous missions — viz. the June 1982 mission led by the late Professor Haroun Tazieff (Tazieff 1982), followed, in December 1983, by a group from New Zealand, Australia and Papua, New Guinea, led by Mr. H. R. Atkinson (New Zealand MoFA 1984), and the

[††] An English translation of those parts of Vol. 2 related to underground testing (i.e. parts 4–9, plus appendix) was provided by DIRCEN/CEA for the benefit of the IAEA and IGC groups. Publication of a complete, official English version of Vol. 2 is planned by CEA/DASE.

Meetings of the International Geomechanical Commission

18–20 March 1996, Ecole des Mines & Bruyères le Chatel, Paris, France
Full Commission

27–29 May 1996, Minneapolis, Minnesota, USA
Stability Sub-Group and Consultants

30 May 1996, University of Paris VI, France
Hydrology Sub-Group and J. Hadermann

9–13 July 1996, French Polynesia: Tahiti; Mururoa & Fangataufa Atolls
Full Commission and CEA Officials

6–7 September 1996, University of Paris VI, France
Hydrology Sub-Group

21–22 September 1996, Chaska, Minnesota, USA
Stability Sub-Group and Consultants

20–21 December 1996, Cambridge, England
Full Commission and Consultants

14 February 1997, Montlhéry, France
E. T. Brown and Pierre Bérest

7–10 May 1997, Fontvieille, Provence, France
Full Commission and Consultants

28 June 1997, New York City, New York, USA
Stability Sub-Group

15–16 August 1997, Vienna, Austria
Hydrology Sub-Group and Pierre Perrochet (EPFL)

24–27 October 1997, Lewis, Wisconsin, USA
Full Commission, CEA Officials and Consultants

Mission Scientifique de la Calypso, in July 1987, led by the late Commandant Jacques Cousteau (Fondation Cousteau, Paris 1988)[‡‡] — were also provided.

The documents were supplemented later by a more detailed and up-to-date series of 12 technical reports prepared by CEA scientists (again, in French and English). These documents, referred to here as DIRCEN[¶¶]/CEA Documents Nos. 1 through 12, have been used extensively by the Commission and are available through La Documentation Française (see the listing after the References for details).

Although the later-than-anticipated publication of these reports was an initial source of frustration to IGC members, it can be seen, in retrospect, to have had a positive effect in that members were obliged to concentrate on developing their own understanding of the mechanics of underground nuclear explosions and the effects of the explosions on the stability and hydrology of the atolls. This provided a greater insight, independently formed, that allowed a more critical review of the DIRCEN/CEA reports when they arrived.

More specific information would have allowed more detailed analyses in some instances. Coordinates of the Nestor, Priam and Tydée tests, for example, may have led to a better understanding of the factors governing the underwater slides produced by these tests. Why, for example, did the Tydée explosion provoke a slide approximately 2 km to the west of the explosion rather than on the directly adjacent slope, as would be expected? Were the Nestor and Priam slides of this more classical type and Tydée an *anomaly*, perhaps related to some local changes in the character of the underwater slopes?

Similarly, CEA scientists measured the temperature variations with depth in the emplacement boreholes prior to a substantial number of tests, but these data could not be made available to the IGC because, again, this information may identify individual test locations, which the CEA did not wish to reveal. These data would have allowed IGC to develop a more precise three-dimensional computer simulation of the hydrology of Mururoa. Eventually, after the IGC simulations had been completed, some data were made available in the form of minimum temperature contours (see Fig. 6.12). The comparison is considered to be very good given the limited information available when the simulation was carried out.

It should also be acknowledged that, even if the precise coordinates of every test had been available to the IGC, significant uncertainty in the geomechanical characteristics of the rock in the vicinity of a test would remain — a consequence of the inherent heterogeneity in the mechanical properties of a rock mass such as the volcanics of the atolls.

[‡‡] Commandant Costeau's visit and findings concerning Mururoa also form part of the video "Tahiti, L'eau de feu," available from Equipe Cousteau, 7 rue Am d'Estaing, 75016, Paris (phone: +33 1 53 67 77 77; fax:+33 1 53 67 77 71)

[¶¶] DIRCEN (Direction des Centres des Essais Nucléaires) is the Nuclear Testing Division of the CEA, the French Atomic Energy Commission.

The CEA would have had some indication of these variations as a result of observations during the drilling of the emplacement holes. The Lycos test, for example, carried out under the Fangataufa lagoon on 27 November 1989, was designed to have a nominal cover of 140 m of intact volcanics above the chimney produced by the explosion. Tritium releases from this test were detected in the carbonates soon after the explosion (DIRCEN/CEA Document No. 9). This indicates that the permeability of the cover (and, hence, the velocity of the groundwater) was considerably higher than would be expected for intact volcanics.

CEA scientists have indicated that difficulties were experienced in drilling the Lycos emplacement hole, due to the poor quality of the volcanics above the (future) chimney region. It is believed that the annulus adjacent to the hole could have been disturbed significantly by the drilling to produce a "disturbed rock zone" (DRZ)[§§] in this annulus. Hence, even though the permeability of the concrete-filled hole would be low, this annulus would have a hydrological conductivity high enough to allow the early release of tritium.

Most cases of early tritium release are considered by CEA scientists to be associated with the CRTV tests. As indicated in Appendix C and Table C.1 (developed as part of the IAEA study of radionuclide releases), no releases have been detected to date for 121 of the 147 underground tests. This suggests that the covers overlying the chimneys produced by these tests are sufficiently intact and provide substantial barriers to groundwater and radionuclide flows from the chimney.

A Final Note on Findings

In this report, the scientific bases for the IGC's conclusions are laid out in sufficient detail for colleagues to see how the conclusions were drawn. Notwithstanding the data limitations, it is believed that the Commission has been able to arrive at a good understanding of the stability and hydrological consequences of the underground testing and that the conclusions drawn are soundly based and robust.

An opportunity for open discussion of the IGC report will be offered in conjunction with the ISRM 9th International Congress on Rock Mechanics, which will be held 25–28 August 1999, in Paris. All interested colleagues are invited to participate in this discussion. IGC members will also prepare and submit papers based on this study for publication in international refereed scientific journals. Details on the session concerning underground nuclear testing will be announced in 1999 by the ISRM.[***]

[§§] The development of a disturbed rock zone (DRZ) around underground excavations is a well-known phenomenon of concern in the sealing of underground nuclear waste repositories.

[***] For details, please contact: Congrès ISRM, c/o G. Vouille, Ecole des Mines de Paris, 35 rue Saint Honoré, F-77305 Fontainebleau, France (telephone: +33-1-64.69.48.97 / telefax: +33-1-64.69.47.11 / email: congres.paris.99@cges.ensm.fr / internet: www.ensmp.fr/ISRM99

ACKNOWLEDGEMENTS

This report marks the conclusion of what was, officially, a one-and-a-half-year study, contracted between the Government of France and the University of Minnesota. The study has, in fact, taken almost three years to complete by the International Geomechanical Commission (IGC), an independent international group of experts assembled specifically for the study.

The delay in completion is not a result of inattention to the subject. On the contrary, it is primarily a consequence of the IGC's determination to establish a sound scientific and technical foundation on which to base its examination of the consequences of underground nuclear testing on the stability and hydrology of Mururoa and Fangataufa. It was necessary to undertake fundamental analyses on a variety of topics in order to make an independent assessment of the information and data provided by CEA (Commissariat à l'Energie Atomique) authorities. Some appreciation of the task can be gained from the topics covered in the appendices to the report. In many instances, these contain a summary only of the results of analyses. Considerable effort was often needed to develop the analyses.

It has been a special privilege and valuable experience to have worked with colleagues of the IGC and its two main consultant groups — Itasca Consulting Group, Inc., Minneapolis, U.S.A., for stability studies and administrative support; and Ecole Polytechnique Fédérale de Lausanne; (EPFL), Switzerland, for hydrology studies and computer graphics. Professor E. Detournay led and coordinated the stability studies; Dr. L. Townley and Professor G. de Marsily led and coordinated the hydrology studies.

Consultants Branko Damjanac and Peter Cundall, from Itasca, and Pierre Perrochet and Laurent Tacher, from EPFL, attended all IGC meetings (except for the initial meeting of the full Commission, in July 1996) and made invaluable contributions, in addition to preparing major portions of the analyses and material included in the report. Similarly, Professor Pierre Bérest, Ecole Polytechnique, Palaiseau, France, Technical Liaison between the IGC and French authorities, was an important asset.

The IGC had not worked together previously as a group, but soon established a very productive working environment. The mix of disciplines and the desire to comprehend both the underlying principles of ideas presented and the specific implications for the study led to stimulating and informative exchanges, improved understanding of the issues and, eventually, a stronger report.

The visit to Mururoa and Fangataufa and CEA geophysical installations in Tahiti, in July 1996, was a key element of the IGC study; it provided essential insights and understanding of the nuclear testing programme on the atolls that would not have been achieved otherwise. Senior scientific and technical personnel of DIRCEN/CEA (see footnotes in Preface, pp. vii and x) accompanied IGC members, providing briefings and commentaries and answering questions throughout the visit. Cameras and video recorders were allowed without restriction. The writer also visited the atolls in December 1996, as part of the International Atomic Energy Agency (IAEA) study group, and was able to re-examine areas of special interest with respect to atoll stability. Together with several technical discussions between DIRCEN/CEA staff and IGC (see the Overview), these exchanges supplemented appreciably the material presented in DIRCEN/CEA documents and reports. The considerable efforts taken to make these visits informative and pleasant by DIRCEN/CEA staff are sincerely appreciated.

Associates of individual IGC members have made important technical contributions to the study. Specifically, Dr. Carlos Carranza-Torres, formerly of the University of Minnesota, carried out the analyses and computer simulations for Appendices H.1 and I, and prepared graphical material. Also from the University of Minnesota, Dr. Igor Janković and Philippe Le Grand undertook the analyses and computer simulations for Appendix E, and Mrs. Haiying Huang carried out the three-dimensional analyses discussed in Chapter 5.4 (Figures 5.12–5.14). Dr. Anthony Smith of CSIRO Division of Land and Water performed a number of runs using the AQUIFEM-P program for the appendix on analysis of periodic groundwater flow. Professor P. A. Persson of the New Mexico Institute of Science and Mining Technology supplied information on the "yield" of TNT explosives for a footnote in the Overview.

The University of Paris VI, the Paris School of Mines and the Ecole Polytechnique generously made their facilities available to the IGC for several meetings.

Dr. Elena Luquet of the Institute of Physics of the Earth, Moscow, assisted Prof. Nikolaevskiy in his preparation of materials for the IGC.

Many individuals experienced in various aspects of the U.S. nuclear testing programme also provided valuable information and background details. Dr. Charles Archambeau (TRAC, Inc., Denver, Colorado), a distinguished seismologist, provided very helpful background information and constructive suggestions at an early stage of the IGC study; Norman R. Burkhard, Lawrence Livermore National Laboratory, Livermore, California, supplied a set of unclassified Proceedings of the Symposia on Containment of Underground Nuclear Explosions; Drs. John T. Cherry (President, Science Horizons, Inc., Missouri) and Theodore R. Butkovich (now retired), pioneers in much of the original efforts in analytical and numerical modelling of underground explosions, each provided valuable comments on early IGC studies, in interviews with Professor Nikolaevskiy; and Dr. Edward W. Peterson (S-cubed, San Diego, California) provided valuable insights into both the mechanics of cavity expansion and near-field damage (see Appendix D).

Preliminary drafts of sections of the IGC Report were sent for external review to distinguished international experts. Dr. B.H.G. Brady, Professor of Geomechanics and Executive Dean of Engineering, University of Western Australia, and Dr. Shunsuke Sakurai, Professor of Civil Engineering, Kobe University, Japan, and current President of the International Society for Rock Mechanics, each provided valuable, independent comments on the stability sections of the report (Chapters 3 through 5).

Colleagues involved in the IAEA technical studies, especially Robert Fry (Technical Director, IAC study, Vienna, Austria), Des Levins (ANSTO, Sydney, Australia), Lars Eric de Geer (Swedish Defence Ministry, Stockholm, Sweden), Eberhardt Mittelstaedt (Federal Maritime and Hydrographic Agency, Hamburg, Germany) and colleagues from IAEA Working Group 4, J. Hadermann (Paul Sherrer Institut, Villigen, Switzerland), H. Nitsche (Institute of Radiochemistry, Dresden, Germany), A. S. Sastratenaya (National Atomic Energy Agency, Jakarta, Indonesia) and G. Warnecke (IAEA, Vienna, Austria) provided many questions and comments that led to several changes and additions to the IGC Report.

Interactions with technical and administrative staff of the CEA — General M. Boileau, Colonels P. Delcourt and G. Corion and Mme T. Delpech; MM. Alain Barthoux, Jacques Bouchard, Jacques Bouchez, Yves Caristan, Christophe Guy and Jean-François Sornein — have been indispensable throughout the IGC study. At all times, IGC members have been received with exceptional courtesy and hospitality, notwithstanding the sometimes delicate balance and restraint required to avoid revealing details considered confidential, and to withhold comment where appropriate, in order to respect the independence of the IGC's findings. The particularly close interaction with Dr. Caristan and his associates, J. Bouchez and J.-F. Sornein, allowed the IGC to develop respect not only for their professional competence, but also for their diplomacy.

Associate Dean Steve L. Crouch monitored the project on behalf of the University of Minnesota and resolved, expeditiously, various administrative issues.

Several of the IGC members acted as hosts for the Commission meetings, all of which were important and memorable events. Anthony and Emma Pearson arranged the Cambridge, U.K. meeting; Ghislain and Gunilla de Marsily arranged the meeting in Provence, France; and Kathy Sikora and Itasca colleagues coordinated the meeting in Lewis, Wisconsin, U.S.A.

Professor Bérest, aided by M. B. Brouard of Ecole Polytechnique, undertook the very formidable task of translating and assembling all of the material for Volume III. This work has been reviewed carefully by IGC members and is an integral part of the IGC Report. We are greatly indebted to MM. Bérest and Brouard for completing this large, voluntary effort, which makes our report more readily accessible to a wider range of readers.

Kathy Sikora was the administrative coordinator for the IGC study, including arrangement of all meetings, preparation and distribution of minutes, communication with

members, and a multitude of other tasks, including the formidable challenge of finally integrating everything required to produce this report — an amazing feat. Chad Sylvain, of Itasca, converted and edited the graphics files, provided in a variety of formats by Committee members, consultants and DIRCEN/CEA, to produce the excellent illustrations in the report.

Donna Ahrens, independent scientific editor, supervised editorial integration of the report, cover design, preparation of the glossary, and all the many other editorial responsibilities.

My wife Margaret assisted in many ways, not the least of which was her uncomplaining acceptance of the many late nights and weekends (far more than anticipated) needed to complete the report, and typing and revising several sections of the final text.

To all of these, and many others, we express our sincere thanks and appreciation and hope that the result is considered to be one worthy of all their efforts.

Charles Fairhurst
Minneapolis

TABLE OF CONTENTS

LIST OF FIGURES

LIST OF TABLES

FINDINGS, CONCLUSIONS AND RECOMMENDATIONS

This report describes the results of a three-year study of the effects of underground nuclear testing on the mechanical stability and hydrology of the atolls of Mururoa and Fangataufa in French Polynesia. The study was conducted by the International Geomechanical Commission (IGC), an independent group established specifically for the study.

Primary attention has been given to understanding, through analysis, the fundamental processes operative in an underground nuclear explosion and how these may affect the post-test conditions on the atolls. This understanding then served as a foundation on which to assess the information provided by the Commissariat à l'Energie Atomique (CEA) relevant to the stability and hydrology issues. Details of the analyses are presented in Chapters 2–7 of this Volume. The main findings, conclusions and recommendations are summarised below.

Findings and Conclusions

The comments below refer to the structural and hydrological effects on the atolls of the 137 underground nuclear tests and 3 "nuclear" safety trials on Mururoa[†††] and the 10 underground nuclear tests on Fangataufa, carried out between 1975 and 1996.

General

1. The volume of volcanic rock damaged by underground nuclear tests on Mururoa and Fangataufa is approximately 5%, in each atoll, of the total volume of the 500-m–1500-m interval within which the explosion-induced damage of the volcanics is confined (see App. H). There has been no damage to the volcanics below 1500 m.

   In addition, early (1975–1980) tests conducted in the volcanics under the rim of Mururoa resulted in explosion-induced deformation and fracturing in the upper 150–200 m of the carbonates, directly above the rim tests. Surface settlements of up to 2 m or more in some places were associated with these deformations (see

[†††] Three of the 10 underground safety trials conducted on Mururoa resulted in a small nuclear yield (see App. C, Table C.4, Category 3).

Fig. 1.23). The affected volume is approximately 3% of the 500-m thickness of the atoll carbonates (see App. H).

2. As discussed below, some of the rim damage on the southwestern rim of Mururoa resulted in underwater slope failures, contemporaneous with the explosions in 1977–1979. On the northeastern rim, a continuing creep deformation has persisted for almost two decades.

   Some test areas have been damaged more extensively than others (see App. H for details), but the underground test programmes have not significantly affected regions of the atolls outside these test areas. With the exception of the creeping deformation in the northeastern region of Mururoa, all areas of Mururoa and Fangataufa are now structurally stable, and there has been no change, on the atoll scale, either short-term or long-term*, of the overall mechanical stability of Mururoa and Fangataufa.

3. The main observable consequences of the underground tests are (a) underwater slope failures, (b) open, visible fractures on the surface, and (c) surface settlements. (All of these are included in the volumes described above.)

   The surface fractures are generally related to lateral displacements of the ocean slopes. These effects occur in the carbonates only. There is no reason to believe that slope failures or settlements have occurred in the underlying volcanics. Differences in the geology of the carbonates between the southwest-rim region of Mururoa and the northeast-rim regions of Mururoa and Fangataufa lead to important differences in the nature of the slope instabilities (see Overview, Section 1.7).

4. At least 95% of the energy released by the nuclear explosion underground is dissipated within a 500-m (or smaller) radius of the explosion source and at least 90% within a 250-m (or smaller) radius. The rock above the explosion collapses to a height of the order of 450 m by 55-m radius (or less), depending on the energy, so that a rubble-filled "chimney" exists around each explosion (see Overview).

5. There has been no significant impact on the long-term global hydrology of either atoll due to the underground tests and trials. (The long-term change in the total groundwater flow through the atolls is estimated to be no more than 1%; see Chapter 7, Section 7.5.)

*"Short-term", here, includes the period of testing to approximately 500 years from the cessation of underground testing. "Long-term" implies a period 500 to 10 000 years, or longer, from the cessation of underground testing.

6. Temperature increases in the vicinity of each explosion cause a local increase in the upward component of the natural groundwater velocity in the overlying volcanics. This increase declines approximately exponentially with time as the explosion heat is dissipated. The vertically upward Darcy velocity in the volcanics increases from a value of 8 mm/y prior to the tests, to values varying from 0.1 to 1.3 m/y at early times (one year after a test), depending on the modelling assumptions, for all cases where there is a good undamaged volcanic cover above the explosion chimney. This velocity decays to about one-half of the peak value after 10 years and stabilises to approximately 3 cm/y after 500 years. The Darcy velocity in the carbonates above the volcanics is not significantly affected by the tests. For tests with no or damaged volcanic cover, the velocities are increased almost fifty-fold in the volcanics above the explosion chimney. Also, for these tests, the velocities in the carbonates are increased from 2 m/y prior to the tests, to values of the order of 60 m/y after one year, decreasing to 5 m/y after 500 years.

7. Using the findings on which (5) above is based, it is possible to predict the transfer of radionuclides from the explosion cavities to the environment. The IGC estimated tritium release to the lagoons of both atolls and found good agreement with the observed values, thus supporting the estimated values of the velocities in the volcanics and carbonates. The tritium release peaked in Mururoa around 1997 and will peak in Fangataufa around 2000 and decay later. These concentrations of tritium in the lagoons are very small and of no radiological consequence.

8. The release of other nuclides to the environment was estimated by the International Atomic Energy Agency (IAEA 1998b) using the velocities provided by the IGC. The IAEA found the radiological consequences of these releases to be inconsequential.

9. In the long-term future (i.e. 20 000–60 000 years hence), new glaciation may make the ocean level drop by $100 \sim 150$ m. A freshwater aquifer will then develop in the limestone layer of the emerged islands. This carbonated layer may be contaminated with plutonium, leading to some potential risk to inhabitants. The IAEA (1998d) has evaluated this risk and concluded that it is of no significant concern.

Specific

Slope Failures

1. One or more large underwater ocean-slope failures could occur in the carbonates on the northeast rim region of Mururoa (test area 1).

   Continuing deformation of the ocean-side slope in this region has been observed since the late 1970s and could lead to one or more large underwater slope collapses in the future. The total volume undergoing deformation is approximately

0.6 km^3 — i.e. six times the volume of the initial collapse resulting from the Tydée explosion in 1979.

Measurements have clearly identified the movements as being due to localised creep-like deformations at a depth of approximately 500 m in a weak, sensitive, "chalky limestone" (see Fig. 5-9 and the related discussion in Chapter 5). Although there is some indication that the deformation rates are declining and may eventually cease, the accumulated strains in the chalky limestone over the past 20 years, approaching 0.5%, may have significantly damaged the chalky limestone so that an acceleration of the deformation to collapse in the future cannot be ruled out.

2. No further slope instabilities and/or major collapses related to the tests are expected on the southwest rim of Mururoa. The large underwater slope failures in this area (test area 4) occurred between 1977 and 1979 and were related directly, in location and time, to specific large-yield tests, such as Nestor, Priam and Tydée. The largest such slope failure (estimated volume of 0.1 km^3) occurred as a result of the Tydée explosion. This failure was followed by several smaller failures. Micro-seismic monitoring in the region indicates that there has been essentially no slope deformation since the tests.

3. Slope failures due to natural atoll-building processes will occur in the future, as they have in the (geological) past — evidenced by the accumulation of underwater sediments at depth in this and other areas.

Settlements

1. Computer modelling of the dynamic effects of underground explosions confirm the observations of surface settlements in the carbonates above the rim on the northeast (test area 1) and southwest (test areas 2, 3, 4) of Mururoa (see Fig. 1.23).

2. IGC calculations indicate that the primary mechanism responsible for these settlements is a constant-volume shearing, rather than the surface compaction suggested by CEA. The shearing mechanism also results in significant lateral deformation and fracturing of the carbonates on the shallow ($\simeq$ 150–200 m deep) underwater ocean slopes. Substantial fracturing of the carbonate reef slope was found in underwater observations by the Cousteau mission. (Some of the fracturing observed by the late Commandant Cousteau could be the result of natural collapse of the slopes.) Shear deformation will also occur on the lagoon side of the rim (see Vol. II, Fig. 1.25).

3. The settlements described above occur only in those parts of the rim test areas where the scaled depths of burial of the tests (see Ch. 4 and App. D, Fig. D.1) were relatively low. IGC analyses indicate that settlements of the lagoon floor resulting from tests conducted under the lagoon are probably much smaller than settlements resulting from tests conducted under the rim.

4. IGC calculations agree with CEA assertions that the surface settlements are superficial only — i.e., they are confined to the upper carbonates and do not extend to the volcanics; there is no direct communication between the surface settlements and the explosion cavity/chamber, as did occur at the NTS in the United States (see Fig. 1.24).

5. Settlements of 2 m or more have occurred in test areas 1 and 4 of Mururoa. Sections of test area 4 are now underwater (see Fig. 1.22). Vigorous coral building activity (of the order of several cm accumulation per year) has been observed in these areas, so that the settlements could be effectively "erased" over a period of 100–300 years. However, significant coral-growth activity above ocean level is unlikely, so that restoration of the reef to its previous above-water level does not seem possible.

Containment and Venting

1. Computer modelling calculations indicate the existence of an undamaged cover of volcanics above and around most tests, as in test area 1 (see Fig. 1.17) on Mururoa. Also, the depths of burial of the underground tests on Mururoa and Fangataufa are considerably greater than those found necessary for containment of the underground explosions at the Nevada Test Site in the United States. Thus, it is believed that all tests on Mururoa and Fangataufa have been contained (see App. D).

2. CEA scientists indicate that the top of the explosion-induced chimney did reach the top of the volcanics in 12 tests (the so-called "CRTV tests") conducted on the Mururoa rim during the period 1976–1980 (see Fig. 1.17).

3. Although venting in the classical sense of direct release of gaseous radionuclides to the atmosphere probably did not occur on the atolls, there is conclusive evidence, from CEA observations, of early (i.e. within several years of an explosion) "seeps" in the form of releases of tritium, strontium and caesium from the volcanics to the lower section of the carbonates, in about 15 of the 147 underground tests on the two atolls. This is clear indication that either (1) the volcanic cover has been significantly damaged by the explosion, as in the CRTV tests, or (2) the integrity and/or initial permeability of the volcanic cover above a particular test

(e.g. as in the Lycos test on Fangataufa) was significantly different from that anticipated. To date, only a small fraction of these releases has reached the lagoons (see App. S).

Hydrology

1. The overall hydrology of Mururoa and Fangataufa is typical of atoll hydrology and is well understood. (Much of this understanding of atolls results from CEA studies.)

2. The effects of nuclear testing will have essentially no effect on the long-term global hydrology of the atolls.

3. The considerable variations and heterogeneities of rock properties that exist both in the volcanics and the carbonates have only limited local influence on the pattern of groundwater flow. The karstic regions in the carbonates have a more global effect (see 4).

4. The hydrology of the carbonates is complicated considerably by the existence of numerous extensive, highly transmissive karstic layers at various horizons. These layers convey tidal influences of the ocean to the interior of the carbonates and generate intense mixing in the entire carbonate layer.

5. The complexity of flow in the carbonates introduces difficulties in understanding the flow from the volcanics through the carbonates. Analysis of observed tritium concentrations in the lower carbonates and releases into the lagoons of Mururoa and Fangataufa suggest that considerable mixing of water is taking place in the carbonates (see App. S).

6. A period of global glaciation some tens of thousands of years in the future would result in the development of a substantial lens of fresh water underground on both atolls, making it possible to support a resident population (see conclusion (8) under General Findings and Conclusions, above).

Volcanism

There is no possibility of renewed volcanism of the atolls as a result of the underground testing. The atolls are extinct volcanoes, no longer connected with the magmatic "hotspot" source from which they developed (see Ch. 2).

Seismic Hazard

The magnitude of the seismic wave produced by the underground nuclear tests in Mururoa and Fangataufa is much too small to affect the earthquake hazard in other regions of the earth's surface (see App. C).

Observations and Recommendations

Atoll Stability and Monitoring

Mururoa

The telemonitoring/instrumentation system proposed in DIRCEN/CEA Document No. 12 (see Overview) for continuous observation of the stability of the northeastern rim of Mururoa over the next decade is comprehensive. This surveillance system should allow adequate precautions to be taken to avoid any serious risks from the adverse effects of any slope collapse in this northeastern rim.

It is recommended that the current system of deformation-monitoring instruments now installed to measure deformation in the northeast region of Mururoa be maintained and monitored for the next 20 years — or until failure, if this occurs earlier. Information available at this time (20 years) should allow the stability of the slope — and the need for further monitoring — to be more reliably assessed. Acceleration of the creep rate, if it occurs, should provide ample advance warning of an impending collapse, sufficient to take appropriate precautionary safety measures on Mururoa and neighbouring atolls likely to be affected by a small tsunami. Waves of the order of 1–2 m, depending on the volume of the slide, similar to those that occurred as a result of the first of the several slope failures in test area 4 on Mururoa, could be generated.

Creep of the chalk in the northeastern region of Mururoa was observed to be affected by the seismic signal resulting from explosions occurring outside test area 1. This has relevance to slope deformations observed on the northeast rim of Fangataufa.

Fangataufa

Little information, other than that on microseismic activity, is available concerning the continuing deformations in the northeast rim of Fangataufa, but the geology is apparently similar to that of the northeast rim of Mururoa. No tests were conducted on this rim, but several large-yield explosions were carried out under the lagoon. It appears that the deformations on the rim have been stimulated by the seismic signal produced by these explosions. Some wide (30–40 cm or so) open fractures, apparently an enlargement and extension of existing fractures, are clearly visible, essentially parallel to the rim, in this region.

The volume of underwater slope undergoing deformation in the northeast rim region of Fangataufa appears to be smaller than in Mururoa and, according to CEA reports on local microseismicity, appears to have stabilised after the tests in 1992. Tests in 1995–1996 have not reactivated these deformations. It seems prudent to attempt to estimate the volume involved, continue to monitor the deformations and assess the potential for a serious underwater collapse. Release of some additional background details leading the DIRCEN/CEA to conclude that the northeastern rim of Fangataufa has stabilised is recommended.

No other serious structural instabilities due to underground testing on Mururoa and Fangataufa are anticipated by the IGC.

The current programme of measurement of release of radionuclides into the lower carbonates and to the lagoons of Mururoa and Fangataufa is providing valuable scientific insights into the operative hydrological process in the carbonates (see Appendices S and T). It is recommended (i) that these observations be continued, and (ii) that additional analytical and numerical modelling studies be conducted to better establish the influence of the karstic horizons on flow and the processes whereby extensive mixing of waters flowing into the carbonates take place.

Chapter 1

OVERVIEW

1.1 Introduction

This chapter provides a synoptic account of the principal results obtained by the International Geomechanical Commission from their technical review. The overview does not follow precisely the order of the chapters — rather, it seeks to present the IGC's findings in a comprehensive manner. This account is supplemented by graphical illustrations and comments intended to inform the general reader of underlying considerations that influenced the direction of the technical review. It also addresses issues which, although not mentioned explicitly in Chapters 2–7, have been raised in other technical or public discussions of underground nuclear testing at Mururoa and Fangataufa. A section entitled "Findings, Conclusions and Recommendations" was originally included at the end of this chapter; however, because of reader interest in this section, it now precedes the Overview chapter as a stand-alone summary.

1.2 Formation of the Atolls

The atolls of Mururoa and Fangataufa in the South Pacific Ocean are usually seen (Figs. 1.1a, 1.2a) as narrow fringes of coral reef, up to several hundreds of metres wide, rising no more than 2–3 m above the water and enclosing a lagoon. Severe storm swells can produce waves that completely submerge the reefs.

Take away the ocean cover (Figs. 1.1b, 1.2b), and these fragile structures are revealed to be just the upper limit of what are, in fact, underwater mountains of volcanic rock-basalt, topped with 300–500 m of limestone or carbonates, rising over 4 km above the earth's crust on the ocean floor.

These edifices were formed some 10~12 million years ago as the crustal plate passed over a hot-spot reservoir of molten magma which, breaking through fractures in the crust, flowed over and accumulated on the ocean floor, creating volcanic seamounts that, at their peak, rose more than 1 km above the ocean — appearing much as the island of Mehetia today (Fig. 1.3). The volcanic lava changed in character as deep submarine flows gave way to shallower deposits, aerial explosions of volcanic ash and, eventually, lava flows over the emerged island.

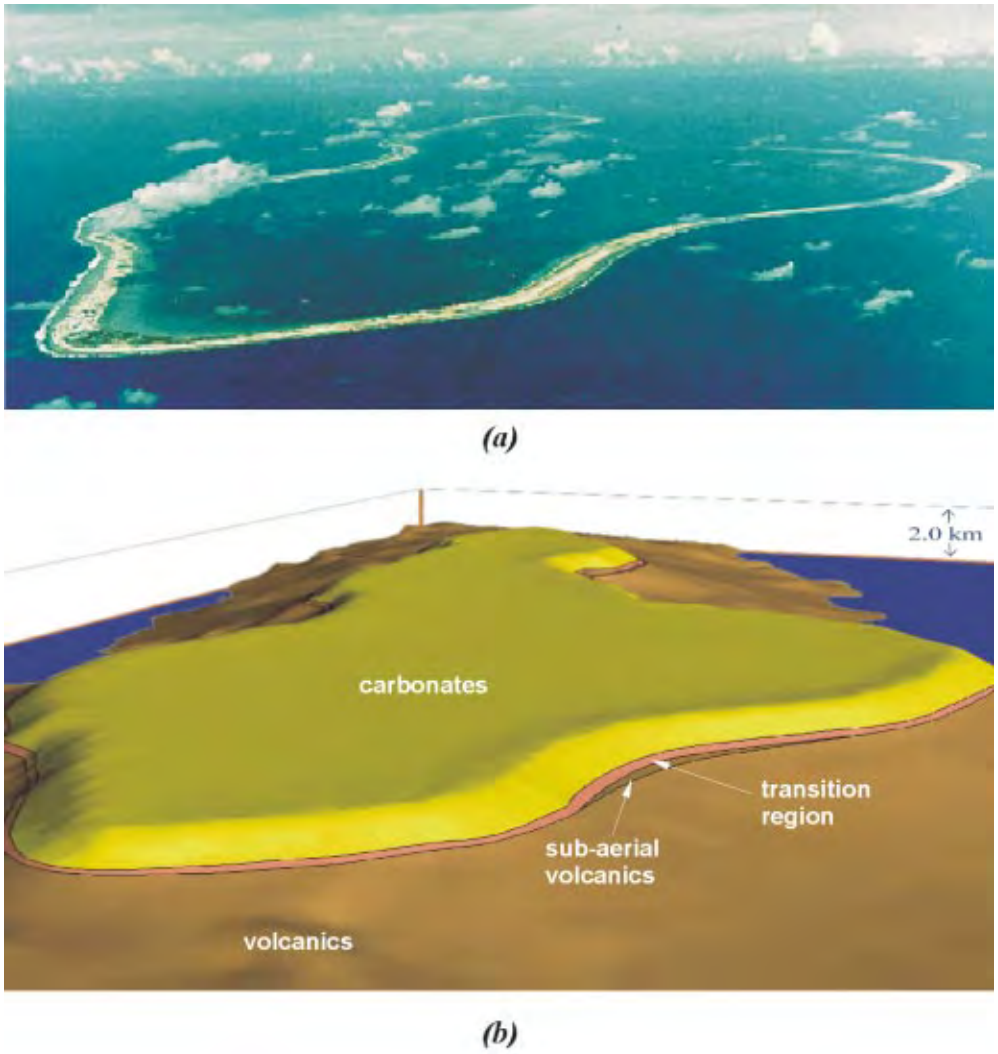

Figure 1.1 Mururoa: (a) aerial view; (b) bathymetric view (from same perspective) to a depth of 2.0 km (carbonates are shown overlying the volcanics; view is toward the southwest (S65W°, altitude 21° above horizon), with test area 1 (see Fig. 1.17) in the foreground)

Volcanic activity ceased after 1–2 million years, as the moving plate passed beyond the influence of the hot spot. The solid volcanic material gradually cooled and consolidated, causing the seamount to subside slowly into the ocean. Coral and algae became attached to the surfaces of the subsiding rock to form an outer apron of carbonate rock,

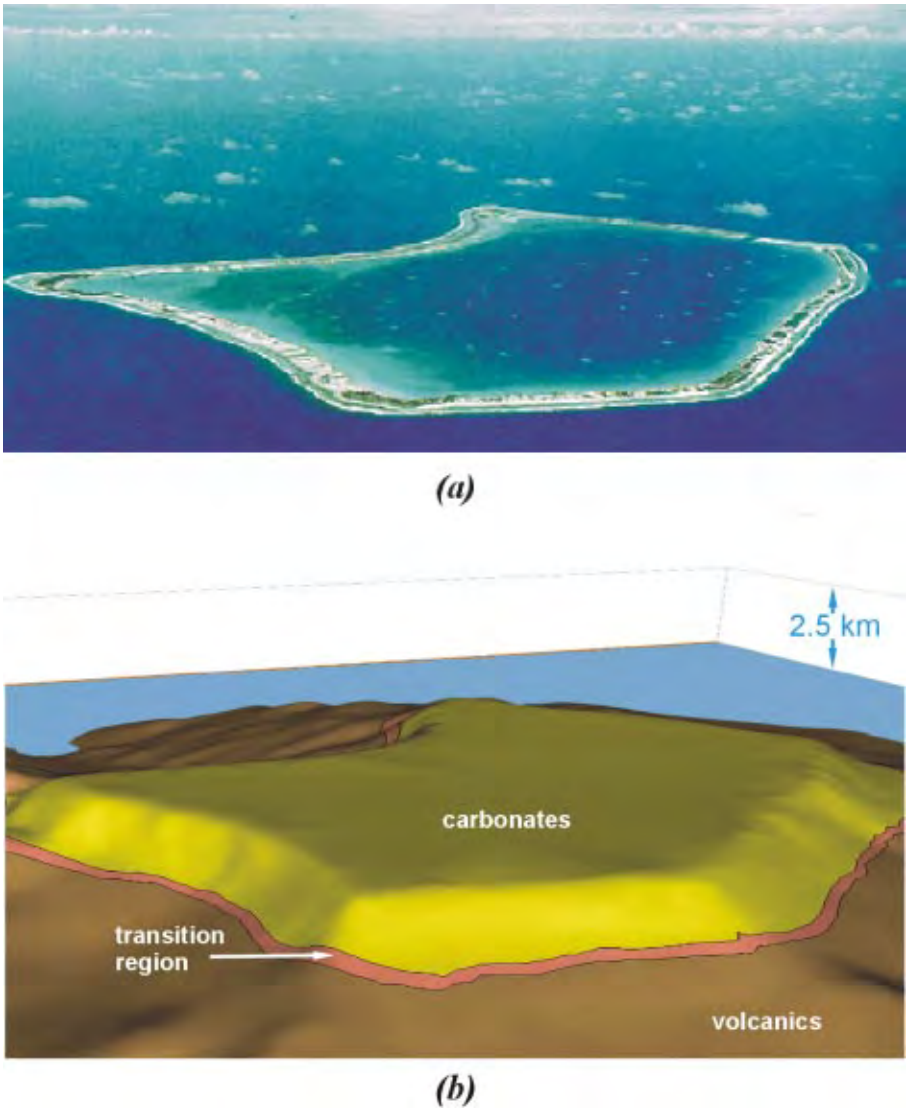

Figure 1.2 Fangataufa: (a) aerial view; (b) bathymetric view (from the same perspective) to a depth of 2.5 km (The flanks of Fangataufa descend more abruptly than do those of Mururoa; the carbonates are shown overlying the volcanics; view is toward the west (N68°W, altitude 27° above the horizon), with test area 1 on the left reef)

Figure 1.3 Aerial view of Mehetia

growing laterally in the upper 50–60 m of water penetrated by sunlight. Eventually, as the island submerged, coral growth extended to cover the entire surface, resulting in what is now the carbonate cover. In the almost 10 million years since activity ceased, the two islands have drifted more than 1000 km (approximately 11 cm per year) northwest from the hotspot, which is now located some 70 km southeast of Pitcairn Island. Today, Mururoa and Fangataufa are extinct volcanoes, far removed from their magmatic sources — hence, with essentially no possibility of being reactivated. A fuller discussion of the atoll-building process is given in Chapter 2.

The slow, progressive subsidence has been interrupted by cycles of global glaciation, ice ages which produce a relatively rapid drop of as much as 150 m in the level of the ocean (Fig. 1.4). The island has then re-emerged, and the carbonate island has been exposed to the elements, including rainfall (and associated alteration, dissolution, and precipitation processes, the effects of which are evident in the current lithology of the carbonate sediments). With the end of a glacial period, the island resubmerges to become saturated again with salt water. Some 3000 years ago, a change from a warm period to

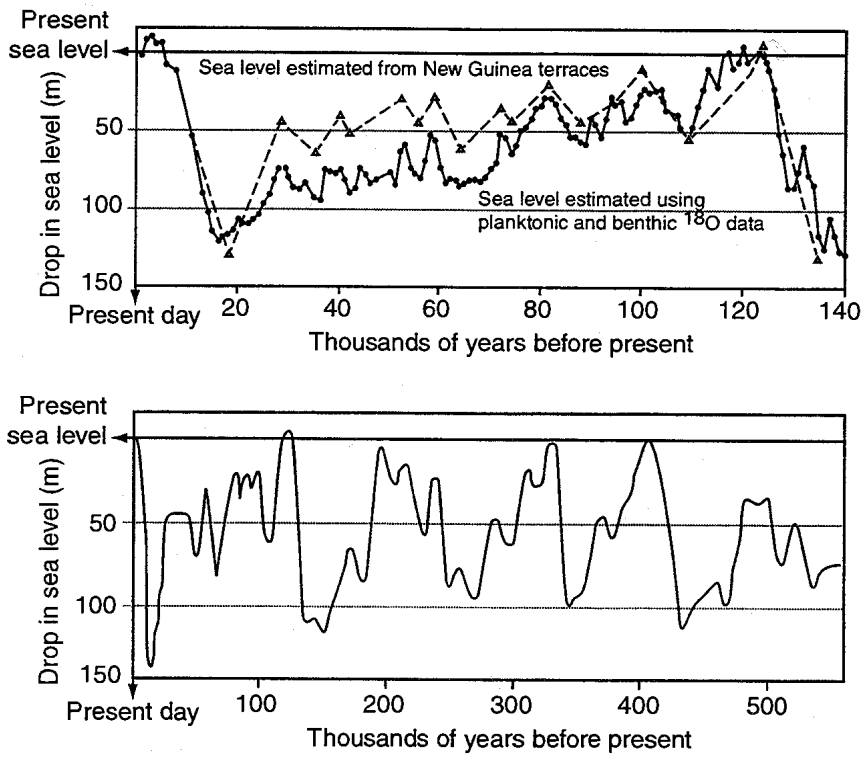

Figure 1.4 Variations in sea level over the past 500 000 years (top: Shackleton (1987); (bottom) Lalou et al. (1988))

the present cooler climate resulted in a drop of about 3 m in the ocean level (Fig. 1.4), accounting for the current above-water elevation of the reef.

Unable to accumulate much above water, the coral accretions have extended laterally. Because the accretions are relatively weak, the lateral extension tends to be self-limiting and may collapse periodically, either naturally or stimulated by seismic excitation — i.e. from a remote earthquake. Figure 1.5 shows accumulations of collapsed and eroded sediments to depths of more than 2 km around the atolls. More recent slope instabilities, collapses and surface displacements, a consequence of the underground explosions, are discussed in detail in Chapters 3 and 4 and, briefly, in Sections 1.5.3 and 1.5.4 of this Overview.

Figure 1.6 shows schematic cross-sections of the geology of the two atolls based on exploration core drilling and on seismic surveys. Note that the actual thicknesses of the formation variations are considerably less than indicated in the vertically exaggerated scale sections.

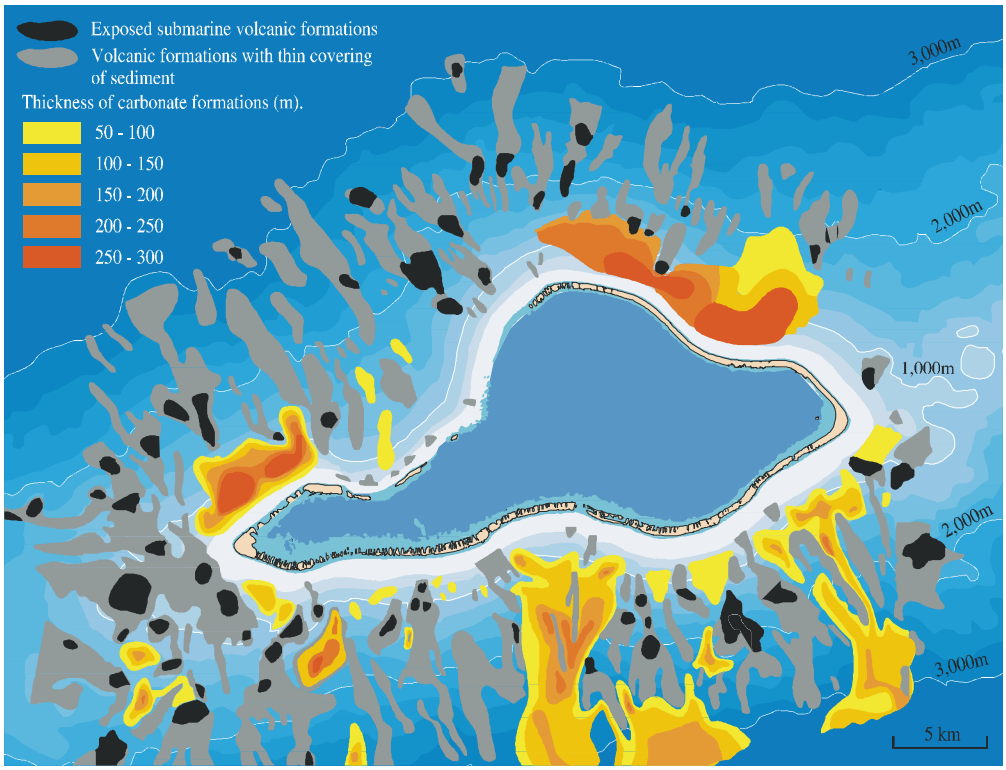

Figure 1.5 Distribution of sedimentary deposits and submarine outcrops on the flanks of Mururoa Atoll (Guille et al. 1996, Fig. 23)

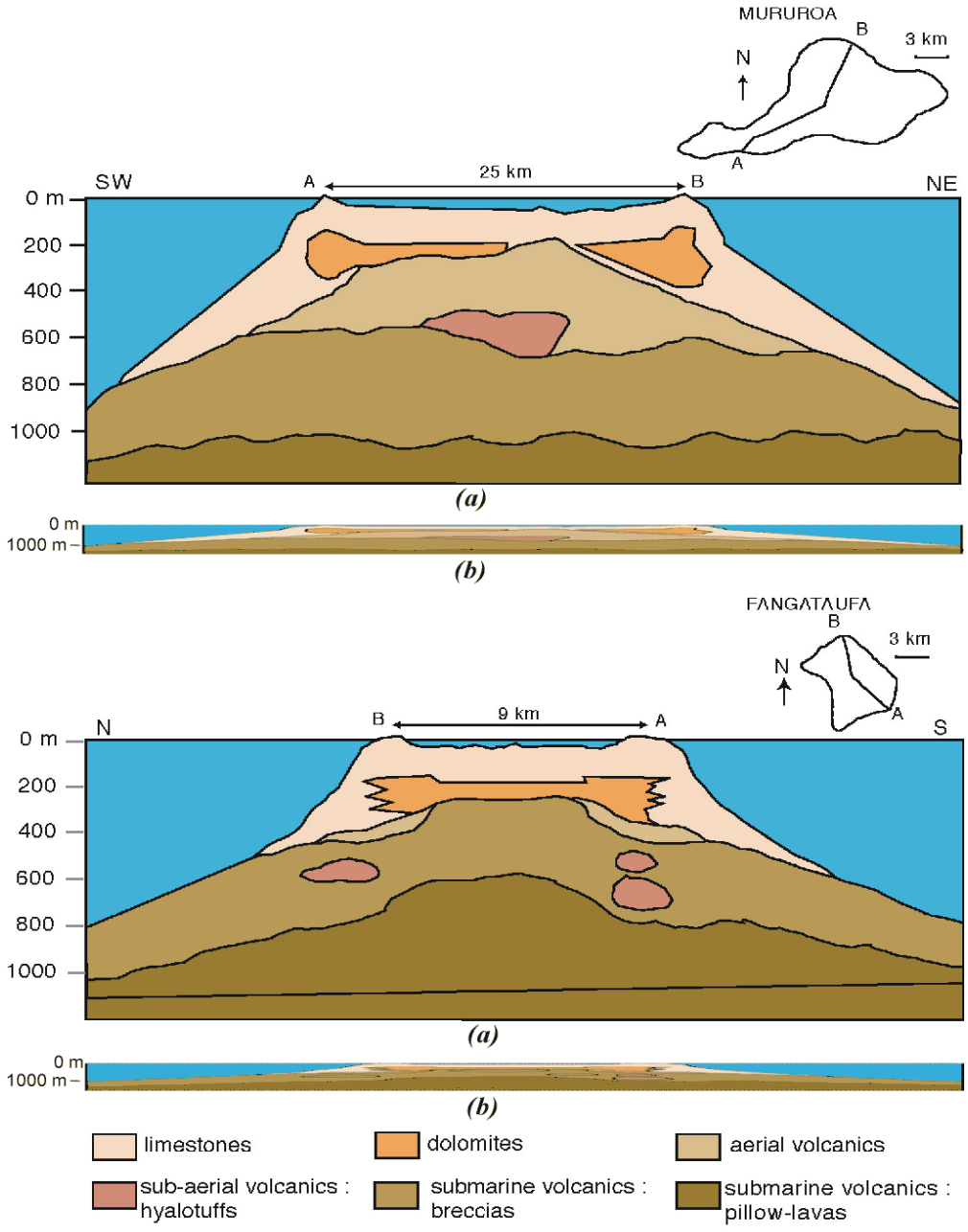

Figure 1.6 Schematic lithology of Mururoa and Fangataufa (modified after Buigues 1997; see also Figs. 2.5–2.8), showing exaggeration of ca 10:1 and reduced exaggeration of 2.1 (true scale versions are too “thin” to be interpreted)

1.3 The Mechanics of an Underground Nuclear Explosion

Before discussing the effect of underground nuclear explosions on the stability and hydrology of the atolls, it is necessary to develop some insight into the way in which energy released by a nuclear explosion is transferred to the rock mass around a device. The energy release or "yield" of a nuclear explosion is usually expressed in terms of the equivalent energy release of the chemical explosive TNT (trinitrotoluene). (Thus, a 100-kt nuclear explosion is considered to release as much energy ($4.18 \cdot 10^{14}$ joules*) as 100 000 tonnes of TNT.) However, the effects of a nuclear explosion on rock cannot be considered simply as a drastically scaled-up version of a chemical explosion. The virtually instantaneous nature of a nuclear reaction and the enormously higher rate at which the nuclear energy is initially generated introduce some effects that are fundamentally different from those produced by a chemical explosion. Chemical explosive energy is released at a rate determined by the velocity of detonation, which is of the same order as the speed of sound in the explosive — usually somewhat less than 10 km per second. Generation of nuclear energy occurs at the rate of electromagnetic radiation, which is more comparable to the speed of light (300 000 km per second). The initial pressures and temperatures of the nuclear explosion (i.e. in the initial test chamber volume) are correspondingly also much greater — of the order of 10^6 MPa and 10^6 K, or higher.

Triggering of the explosion in the container creates a fireball, which instantaneously vaporizes and melts rock (and the chamber that contains the device†). The radius of this vaporized zone is of the order of 2 m for a 1-kt explosion.‡ (This is the initial cavity radius, r_c, used in the calculations discussed in Chapter 3 and also in Fig. 1.7). The size of r_c (Fig. 1.9a) scales approximately as the cube root of the explosive yield, Y (i.e. $r_c \propto Y^{1/3}$).

This virtually instantaneous introduction of the high pressure "gas" (vaporized rock and container material) to the interior of the rock mass results in a high-intensity shock loading (Fig. 1.8) of the initial cavity walls. Figure 1.9 illustrates the development of the cavity for a 1-kt yield. A spherically diverging shock wave begins to propagate

---

*or 10^{14} calories of heat energy (4.18 joules is the mechanical equivalent of 1 calorie). The energy actually released by a TNT explosion varies somewhat around this assumed "standard" value (10^{12} calories/kt), depending on several factors, such as the initial density of the charge and surrounding (confining) medium (e.g. air or rock).

†At the Pacific Test Centre (PTC), the volume of the part of the container that receives the device is approximately 1 m^3. The actual nuclear "explosive", which can have a yield up to 150 000 tonnes in equivalent TNT (limited by the Threshold Test Ban Treaty (see Preface), occupies a small fraction of this volume. One cubic metre of TNT (specific gravity = 1.65) would have a yield of less than 2 tonnes. (A listing of all underground tests at the PTC, all of which were less than 150 kt, can be found in App. C of this report.)

‡The radius of this zone increases as $Y^{1/3}$, where Y is the explosion yield. Thus, the volume of this instantaneously vaporized zone increases in direct proportion to the yield. The initial pressure and temperature in this zone are, essentially, constant, independent of the yield.

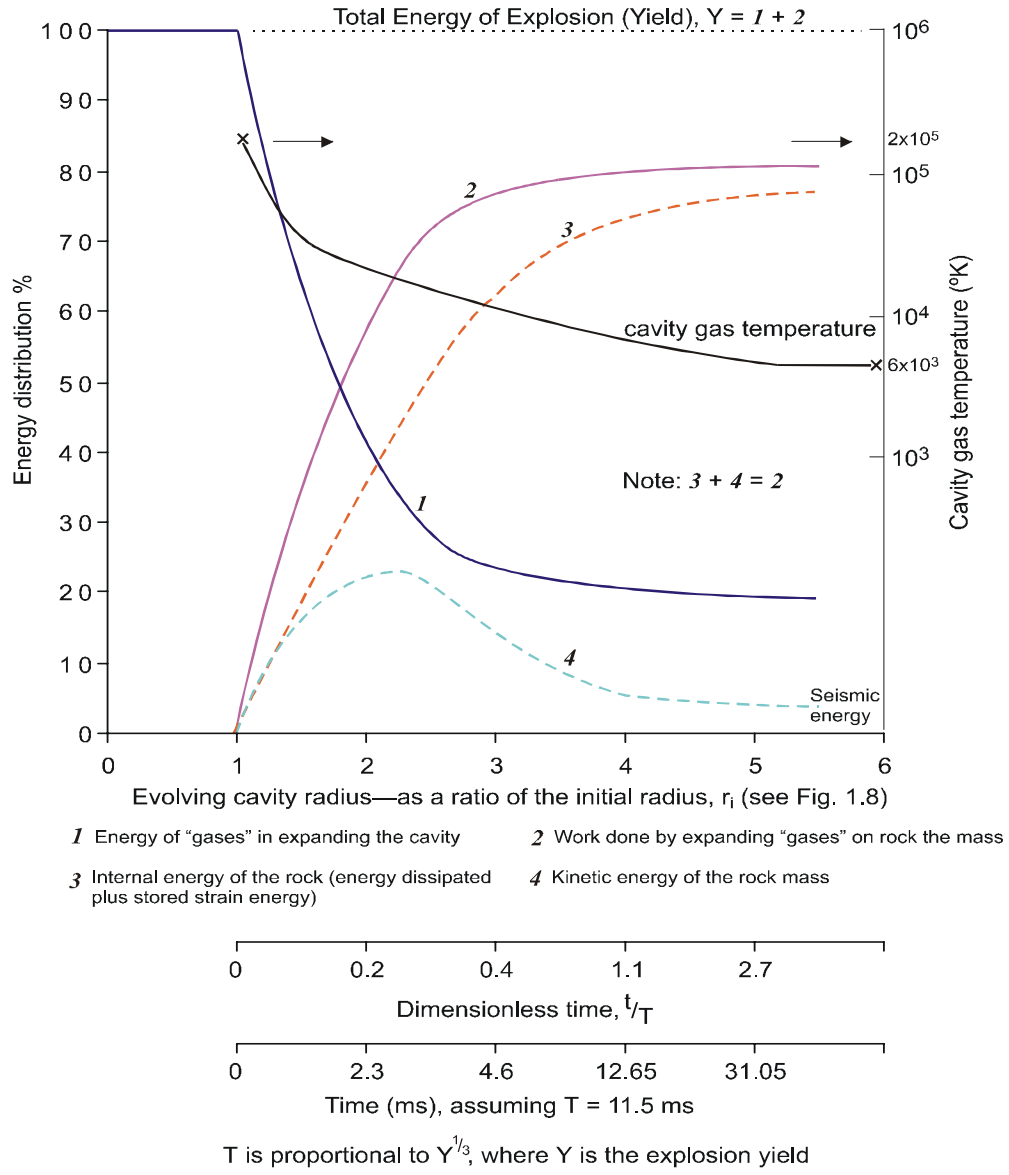

Figure 1.7 Distribution of explosion energy during early stages of cavity expansion (Note: (i) the final cavity radius in the volcanics, $R_c \simeq 6\, r_i$, from calculations in Chapter 3; (ii) this early distribution does not consider eventual dissipation of the energy. Except for the small amounts of seismic energy and elastic strain energy (mainly released by cavity rebound), all of the explosion energy is eventually dissipated in the vicinity of the cavity.)

Shock Waves and Plastic Waves

The word "shock" is popularly used as a synonym for impact or shaking (e.g. "seismic shock"), but we use its scientific meaning in this document.

A shock wave is a wave that travels faster than the usual speed of sound and has a characteristic steep front to its shape (in space and time).

However, not all steep-fronted waves are shock waves — a true shock forms in a material that gets stiffer with increasing load. The stress-strain curve of many rocks under intense compression looks like this . . . . . and the wave speed looks like this:

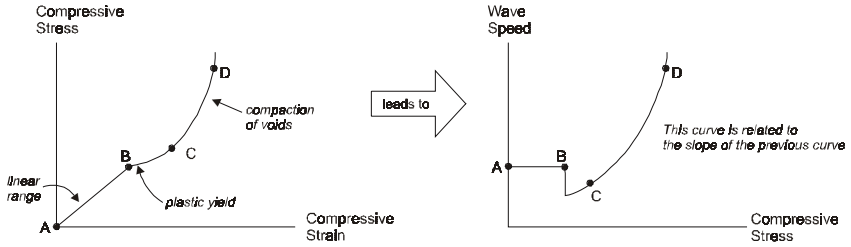

If we send a pulse through such a material, the response depends on the size (or "amplitude") of the pulse. For a small pulse (in the range A–B), the pulse travels at the usual speed of sound and its shape does not change. When the amplitude is larger (say, of stress level C), an elastic precursor develops because the main plastic part travels slower:

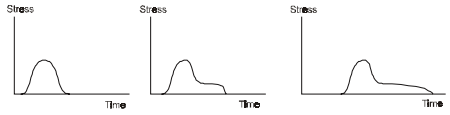

Evolution of a medium-amplitude pulse

For large pulses (e.g. at D), the reverse is true — higher amplitudes travel faster than lower amplitudes, so the pulse becomes steeper (or "shocks up"):

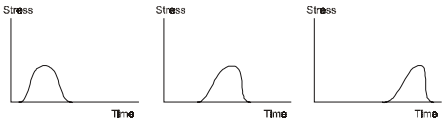

Evolution of a high-amplitude pulse

The nature of the wave generated by an explosion, therefore, changes as its amplitude decays with radius. It evolves from a shock wave close to the origin, to a plastic wave with an elastic precursor further out. At large distances, elastic seismic waves are observed.

Figure 1.8 Shock waves and plastic waves

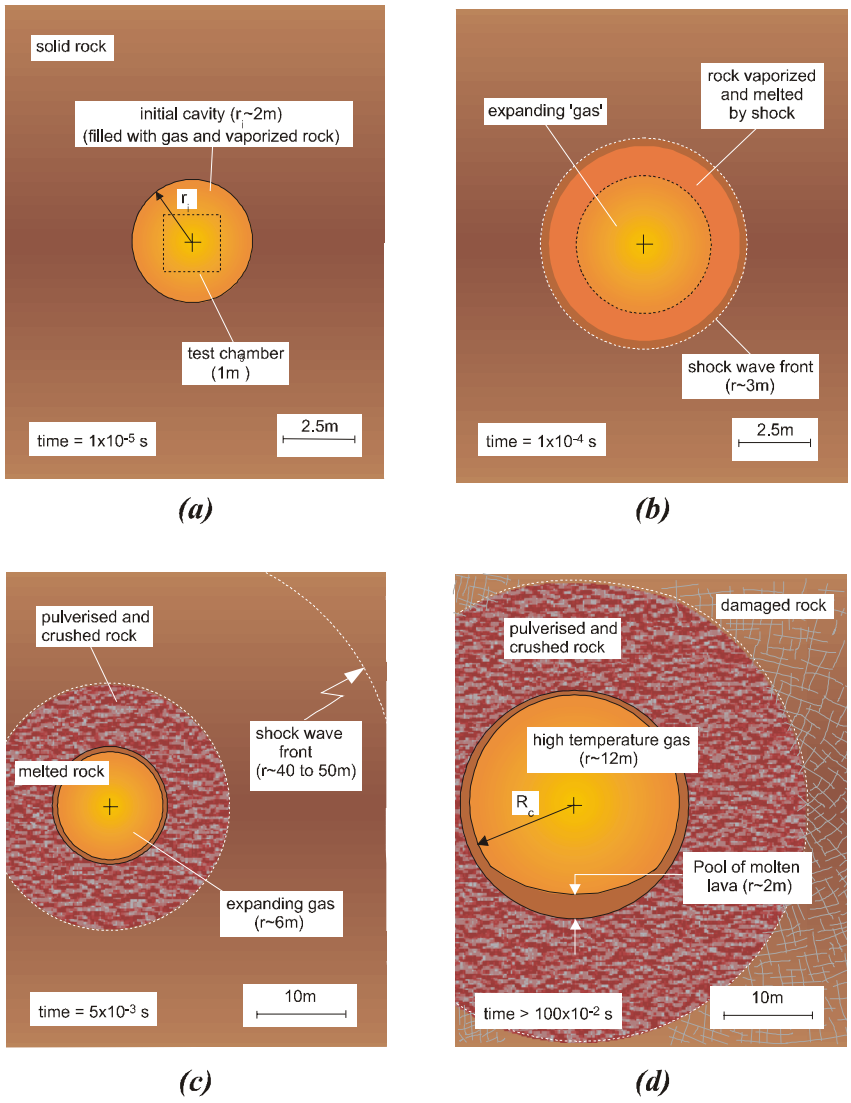

Figure 1.9 Stages of cavity formation and development during a nuclear explosion (Note: r_i is the radius of the "instantaneously" vaporized sphere; $r_i \simeq$ 2 m for a 1-kt explosion); Later stages of cavity expansion (to final size) and associated rock damage during a nuclear explosion (Note: R_c is the final radius of the expanded cavity. $R_c \simeq$ 12 m for a 1-kt (shallow) explosion on the atolls; at the greater depths, $R_c \simeq$ 10 m for a 1-kt explosion)

into the rock. Initially, the shock front vaporizes and then, as it progresses, melts rock immediately around the gas-filled cavity. According to Bouchez and Lecomte (1996), approximately 100 tonnes are vaporized and 210 tonnes are melted (per kt yield) during this initial period of wave propagation. The amount melted increases to 800 tonnes/kt yield during the later stages of shock wave loading and cavity expansion [Fig. 1.9c and 1.9d].

Two important features of the loading should be noted.

1. The high loading rate is such that the rock is intensely compressed over a relatively narrow spherical shell while the rock beyond this shell is (instantaneously) undeformed. The effect is physically equivalent to "ramming" the rock within the shell into a rigid (i.e. undeformed) outer boundary. Hence, the rock is subjected to compression in every direction (tangentially as well as radially). Thus, during this phase of the explosion process, there is no possibility of extensile crack generation or propagation.[¶]

2. The intense shock wave results in highly dissipative processes in the rock mass — i.e. much of the explosive energy is absorbed by the rock within a short distance of the explosion source. This is illustrated in Figure 1.7, which has been derived from analyses in Chapter 3. It is seen that 70% of the explosive energy is transferred from the pressurised, high-temperature gas into the rock within the order of 3 milliseconds. Most of the energy is transferred to the rock mass as "internal energy". Although this will include some elastic strain energy, the elastic component is likely to be small. It would appear, therefore, that a large fraction of the energy of an underground nuclear explosion is dissipated by inelastic deformation and heat very close to the explosive source. Based on the analyses in Chapter 3, it is found that more than 90% of the explosion energy is dissipated within a spherical radius of 5 R_c, and more than 95% within 10 R_c, where R_c is the final radius of the explosion cavity (see Fig. 1.10).

As noted earlier, the intensity of the initial shock loading is sufficient to produce melting directly at the shock front. Immediately beyond the initial cavity (radius r_i), the mean pressure of the shock wave in the "hydrodynamic" regime is so much higher than

[¶] It is for this reason that the molten lava,which contains a very large proportion of the radionuclides generated in the explosion, or radionuclides in gaseous or vaporized form, does not escape into the rock, but remains trapped in the cavity. The molten lava later solidifies, encapsulating the radionuclides. According to Bouchez and Lecomte (1996, p. 25), approximately 98% of all the elements with half-lives longer than 30 years is trapped in the lava. The radionuclides may become partially available for dissolution and transport in the groundwater as the lava eventually disintegrates over many hundreds or thousands of years.

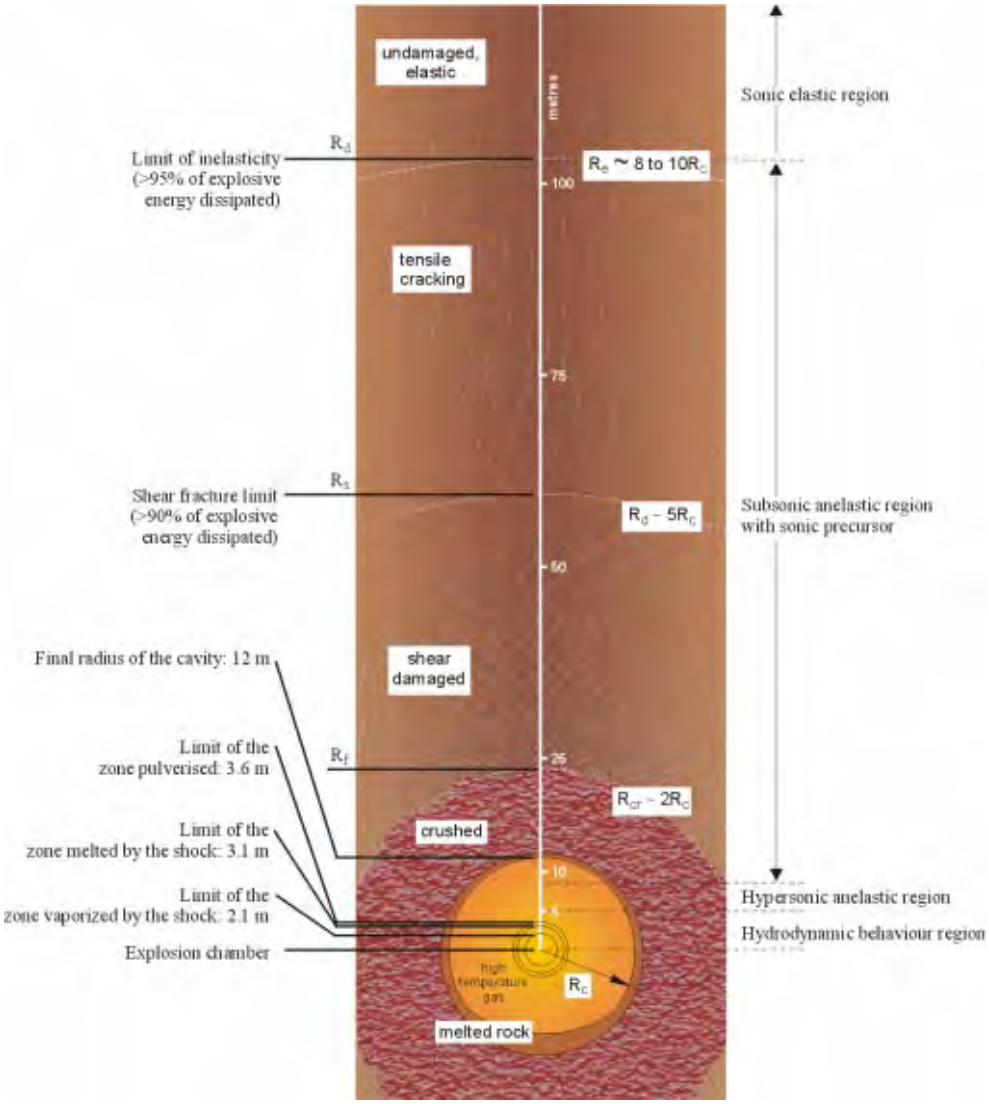

Figure 1.10 Presumed rock damage zones around a 1-kt nuclear explosion cavity in basalts at Mururoa and Fangataufa (The damage zones are expressed as multiples of the final cavity radius R_c, which increases in proportion to $Y^{1/3}$, where Y is the explosion yield in kt) [modified after Bouchez and Lecomte (1996); see also Fig. 3.7]

the rock shear strength that the rock behaves essentially as a (viscous) fluid. Beyond this "solid matrix melting radius,"

> *. . . over a distance of a few metres, the interstitial water is vaporized. As it expands, the high pressure steam shatters the matrix, which is divided into particulate fines. When the cavity later expands under the effect of the thrust of the gases, part of the zone of powdered rock is recompacted and partially sintered. It forms a low permeability shell around the cavity.* (Bouchez and Lecomte 1996, p. 42)

This suggests the possibility that, although subjected to intense inelastic deformation, the rock in this region could be "re-strengthened" by passage of the shock. Observations that the rock in the vicinity of the cavity radius appears to be intact, with substantial strength and elastic properties, have been made at the Nevada Test Site during post-test tunnelling investigations in the immediate vicinity of the explosion cavity – i.e. in the region $2\,R_c > R > R_c$. No such large-scale post-test investigations have been carried out at Mururoa or Fangataufa.

As the mean pressure at the shock front declines, due both to attenuation (through high dissipation) and the increasing area of the radially diverging shock front, the initially steep front will degrade progressively, and the rock will be less intensively damaged. Beyond a radius of the order of 8–10 R_c, no damage is inflicted on the rock mass.[§]

Figure 1.10 attempts to illustrate the changing character of rock damage that could be expected to develop at various distances from the explosion due to passage of the shock wave. In reality, of course, the zones of damage will not be distinct. However, any fractures induced in the immediate vicinity of the explosion will be shear fractures produced by sliding of the fracture surfaces over each other under compressive loading. They will not be the extensile radial fractures that are typical of dynamic loading situations where the net tangential stress is tensile (as will occur when the rise time of an explosive wave is much longer than in a nuclear explosion), and for quasi-static pressure loading of a cavity. At greater distances from the cavity, when the shock front (Fig. 1.10) has degraded considerably (so that the mean stress in the wave is now comparable to the deviatoric stress and the rise time of the wave is longer), some radial cracking will occur due to a tangential tension associated with the radial compression of the wave. Further out, the fractures degrade further, into cracks induced by inhomogeneities that generate localised tensions in the rock (as observed in the compressive loading of rock specimens under low or no confining stress). These cracks are likely to be unconnected and distributed throughout the rock mass, although pre-existing fractures could be extended.

[§] except for horizontal fractures opened by tensile stresses generated by wave reflections at interfaces between hard and softer rocks. Such fracture openings are frequently observed during post-test drilling.

Thus, the fractures formed during passage of the diverging shock wave are not likely to form connected pathways linking the cavity to the "undamaged" rock mass. It is in the outermost region, where the wave amplitude is approaching the limit below which it will propagate "seismically" (i.e. without damage to the rock) that small differences in rock strength and in-situ stresses become significant in controlling fracture extensions.

On the atolls, the horizontal in-situ stress will be less than the vertical stress (see Chapter 2, Section 2.6), so that the radial fractures will tend to extend preferentially upward in the vertical direction. However, the cracks produced by the diverging wave are not internally pressurised, as would be the case if they were penetrated directly by cavity gases, as in a number of practical situations — e.g. loading by (low-intensity) chemical explosives; the technique of hydraulic fracturing (used to stimulate oil field production); and the development of volcanic dykes by intrusion of molten magma. Also, the sub-horizontally layered structure of the volcanics will tend to inhibit propagation of vertical fractures. Some possible mechanisms for extension of fractures through internal pressurisation of the cavity by high-pressure fluids are discussed in Appendix D.

The formation of a 12-m radius cavity by a 1-kt nuclear explosion is essentially complete within 0.1 s of the explosion. This corresponds to an average rate of growth in radius of the cavity of more than 400 km/h! The initial rates are considerably higher, since the 0.1 s includes the deceleration phase as cavity expansion "comes to a halt" (see Fig. 1.7). Because the final cavity radius (R_c) and the time of cavity growth both increase in proportion to $Y^{1/3}$, where Y is the explosion yield, cavity expansion rates are largely independent of yield. Because there is very little increase in density of the rock due to the explosion, almost all of the cavity volume must be accommodated by (rapid) deformation of the elastic rock outside the damaged zone. This elastic deformation stores energy that is released or unloaded as the cavity gas pressure drops toward or below atmospheric. The cavity rebounds, and a tangential compression, tending to close the cavity, is induced around the cavity wall. This compression, referred to as the *stress cage*, will increase the tightness of any fractures in the damaged zone around the cavity. It seems probable, however, due to the pre-fractured nature of the volcanics at Mururoa and Fangataufa, that the intensity of the stress cage effect will be reduced. This topic is discussed in Appendix E.

As the gas cools, the pressure in the cavity continues to decrease with time and, in minutes or some hours, as the cavity pressure decreases toward the lithostatic pressure (imposed by the weight of overlying rock), the roof begins to collapse into the cavity. Typically, the collapse continues until the volume of broken pieces, or rubble, has progressed to a height 4–8 times the original cavity radius — i.e. when the volume of the original cavity has become effectively redistributed within the rubble (see Appendix I). Figures I.1 and I.2 show some observations of chimney height (H_c) as a function of cavity radius (R_c) [or, equivalently, explosive yield (Y)]. A value of $H_c = 5\,R_c$ has been assumed in most computations in this report.

1.4 Nuclear Testing on the Atolls

Atmospheric nuclear tests, either on or in the vicinity of the atolls, were carried out from 1966 to 1974, when they were abandoned in favour of underground tests on the atolls. Underground testing continued from 1975–1991 and again in 1995/1996. (A complete list of the underground tests is given in Appendix C.) Nuclear devices were detonated in the volcanics at the bottom of 1.5-m-diameter shafts drilled to a total depth varying between 500 m and approximately 1100 m, depending on the expected yield. Originally (1975–1981), the locations of the testing sites were constrained by the requirement to drill the holes from the rim surface. Several major failures of the ocean slope, starting in 1977 (DIRCEN/CEA Document No. 7) and culminating in the Tydée slope failure in July 1979 (see Fig. 1.11), accelerated development of the technology to allow drilling of the 1.5-m-diameter shafts from barges in the lagoons. Bathymetric surveys after the Tydée collapse indicated that a section of the ocean slope some 2 km in lateral extent, reaching from a depth of 1000 m to the surface, and averaging about 50 m in thickness (i.e. a total volume of the order of 0.1 km^3), collapsed with a velocity of 12 m/s (DIRCEN/CEA Document No. 7, p. 17). The sudden descent of rock in this way tends to pull the water adjacent to the slope downward. The filling of the depression thus created generates a hydraulic wave, or local tsunami, which breaks on the coast and propagates along and away from the atoll (see Bouchez and Lecomte (1996), Fig. 8-3). The Tydée slope collapse induced a hydraulic wave that covered part of Mururoa to a depth of 2.5 m, 90 s after the slide, and submerged the airstrip at Fangataufa, 40 km distant from the slide, to a depth of 2 m.

Figure 1.11 shows an aerial view indicating the offshore region affected by the Tydée collapse. The presumed location of the Tydée test is indicated. Figure 1.12 shows a similar view of the collapse region produced by the Nestor and Priam events. Note that the centre of the collapse region is approximately 3 km west of the shot point.

Starting in 1981, an increasing proportion of the tests was conducted beneath the lagoons, remote from the ocean slopes of the atolls. All tests after October 1986 were conducted under the lagoons, including the six tests of the (final campaign) of 1995–96. According to CEA scientists, the shot point (also referred to as the "zero point") of every underground test was located in the volcanics, either below the rim or below the lagoon.

The explosions in test area 1 of Mururoa — with some "assistance" from later, large explosions in the lagoon areas — have produced a different response of the rim slopes. Tests in test area 1 were of much smaller yield (average $\simeq$ 2 kt) than in test area 4 (average $\simeq$ 35 kt), and there have been no spectacular collapses to date. However, due to the presence of a weak "chalky limestone" formation in the carbonate lithology of the northeastern region (see Figs. 5.11 and 5.12), the tests in the northeastern region have stimulated a progressive "creep" deformation, first observed in 1980, that has continued to the present day (see Figs. 5.8 and 5.9). The total volume of rock involved in this

Figure 1.11 Aerial view indicating the offshore region of Mururoa affected by the Tydée collapse (the presumed location of Tydée and collapse limits have been added by IGC) [photographs provided by DIRCEN/CEA]

Figure 1.12 Aerial view indicating the offshore region of Mururoa affected by the Nestor (March 1977) and Priam (November 1978) collapses (see also Fig. 5.1) [original photographs provided by DIRCEN/CEA, limits of collapse added by IGC]

movement is estimated to be of the order of 0.6 km^3 — i.e. about six times the volume of the Tydée collapse. Large open fractures produced by these slope deformations are clearly visible in this region (see Figs. 1.13 and 1.14).

The northeastern rim of Fangataufa, where the geology also includes a weak chalky limestone formation, appears to have responded in similar fashion — i.e. fractures smaller than those on Mururoa did develop, essentially parallel to the shoreline, as a consequence of strain wave effects produced by the large tests in the Fangataufa lagoon. No tests were conducted under the northeastern rim of Fangataufa. The creep deformations in Fangataufa appear to have ceased since 1992. Figure 1.15 shows one of the fractures in this region.

Figure 1.16 shows a vertical cross-section normal to the shoreline, through the presumed location of the Tydée explosion (see Fig. 1.11). The shot point is shown at a depth of 987 m, but the shaft (emplacement hole) had been drilled to 1100 m (Bouchez and Lecomte 1996). The device became jammed at 987 m during loading into the hole (Bouchez and Lecomte (1996), p. 25). Although all underground tests in the atolls are believed to have had yields less than 150 kt (Bouchez and Lecomte 1996), Tydée has been estimated seismically to have been one of the largest underground tests on Mururoa up to that time — 115 kt (see App. B).‖

In Figure 1.16, it is assumed that the explosion had a yield of 150 kt and produced a cavity radius of R_c = 53 m and a chimney height of $H_c = 5\ R_c$ = 265 m. (Note, however, that chimney heights approaching 8 R_c appear possible in Mururoa and Fangataufa; see App. I, Fig. I.2). The profile of the ocean slopes and the depth of the carbonate-volcanic interface are taken from detailed bathymetric data supplied by the French Liaison Office.

At least two important characteristics of the atolls with respect to the effects of the underground explosions should be recognised in viewing Figure 1.16.

1. A distinct change in lithology (i.e. the transition zone from volcanics to carbonates) occurs between the explosion host rock and the rock surface (including the slopes). The overlying carbonates are mechanically weaker than the volcanics.

2. Because both rock types have considerable porosity (volcanics $\approx$ 20%; carbonates $\approx$ 30%) (see Chapter 2) and permeability and are, essentially, totally submerged; the rocks are fully saturated to the surface.

These characteristics are not present at the Nevada Test Site (NTS) in the United States — nor, probably, at other land-based underground testing sites.

If we accept, as discussed above, that the shock wave in the volcanics will degenerate into an elastic or "seismic" wave (i.e. causing no damage to the rock) beyond a radius of (8~10) R_c, then a cover of undamaged volcanics will exist between the damaged region

‖ Hyrtacos, 14 November 1990, detonated in Fangataufa, has been estimated at 118 kt (App. C)

Figure 1.13 Aerial photograph showing extension fractures generated by continuous creep deformation in the ocean slope of the northeastern rim of Mururoa in the vicinity of PK7.4N (Camélia zone), test area 1 (see frontispiece map of Mururoa; several relatively narrow (10 cm ∼ 20 cm) fractures (trending ENE) are visible on shore; larger fractures probably up to 2-m aperture, can be discerned under the deeper water) [photo courtesy of DIRCEN/CEA]

Figure 1.14 Aerial photograph showing underwater extension fractures of the order of 2-m width in the vicinity of PK5N, Irène section (see also Fig. 5.6); part of the aircraft runway strip, with protective wall, runs parallel to the bottom of the photograph; this region is outside test area 1 [photo courtesy of DIRCEN/CEA]

Figure 1.15 Underwater extension fractures of the order of 40-cm aperture on the northeastern rim of Fangataufa in the vicinity of Kilo-Frégate (no tests were conducted on the rim; fractures are stimulated by tests in the Fangataufa lagoon)

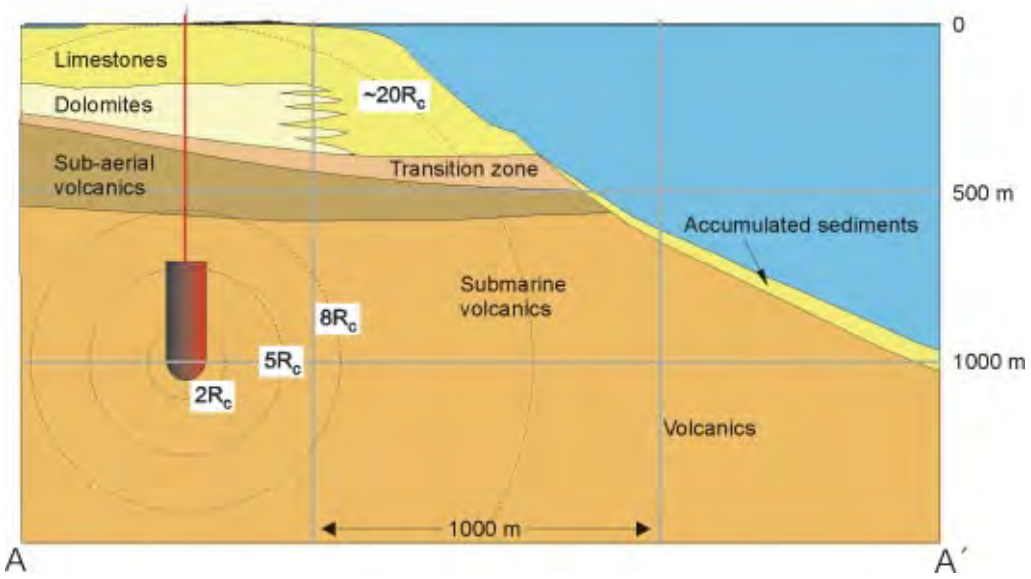

Figure 1.16 Schematic illustration of chimney (assuming $H_c = 5R_c$) formed due to a hypothetical 150-kt test under the rim in test area 4 (cf DIRCEN/CEA Document No. 7, Fig. 16) and radial extent of damage

around the explosion cavity and the base of the carbonates. However, when this seismic wave passes into the weaker carbonates, it may again cause damage, especially when the wave interacts with the surface. The fact that surface settlements of the order of 2 m or more have been observed on the carbonate rim above some explosion sites, and that major underwater slides have been provoked by some tests, indicate that such damage has in fact occurred. (An assessment of explosion damage to the atolls is presented in App. H.) Thus, understanding the mechanics of the interaction between the explosion and the entire rock mass to the surface is obviously important to an assessment of the atoll stability. Chapters 4 and 5 of this report examine these issues in detail.

The precise locations and yields of the individual underground tests conducted on Mururoa and Fangataufa are considered by the CEA to be militarily sensitive information and have not been revealed. Information has been provided on the distribution of tests by testing area. Upper bounds for total yield and several other pieces of statistical information are also included in documents issued by the French Liaison Office. Based on these sources and visual observations, it is possible to arrive at hypothetical distributions of the tests, with individual test yields and corresponding depths — to aid in visualising the intensity of damage in the various testing areas.

As noted earlier, French authorities have indicated that all of the 147 underground tests were detonated in the volcanics. In 12 of the tests, conducted between 1976–1980

(DIRCEN/CEA Document No. 6, Section 1.5), the chimney formed above the explosion cavity extended into the carbonates. These so-called CRTV (Chimney Reaching the Top of the Volcanism) tests (Category 3 tests, see App. C) present less of a barrier to the movement of water (and radionuclides) from the explosion cavity than those tests in which a cover of intact volcanics remains. This is considered in Chapter 7 in assessing the velocity of water flow from the chimney and is also of significance for estimating the rate of release of radionuclides contained in the water flowing through the cavity.

The white boxes in Figures 1.17 and 1.18 show the general details of the testing areas on Mururoa and Fangataufa, respectively, as provided by DIRCEN/CEA Document No. 6. These figures also show hypothetical (but not inconsistent with CEA data) distributions of underground tests for both atolls (including the CRTV tests on Mururoa). The region in which safety trials were conducted on Mururoa is also indicated. Circles of diameter 5 R_c, indicative of the extent of rock damage (including a chimney of height 5 R_c) associated with each test, are shown around each shot point. Clearly, the intensity of rock damage is highest in test area 4 on Mururoa. The probability of overlap or interaction between the damage zones of adjacent cavities will also be greatest in test area 4.

Figure 1.19 shows a vertical cross-section parallel to the coastline in test area 4 for the test distribution in Figure 1.17. This illustrates the potential overlap of rock damage zones.

Studies of the time required for an explosion cavity to fill with water (see Chapter 7) suggest that the region of significantly increased permeability around a cavity extends to a radius of the order of 2.5 R_c from the shot point and includes, of course, the chimney region. Figure 1.20 shows the enhanced permeability region for test area 4. Figure 1.21 shows the same regions for test area 1. It is seen that, even in test area 4, interaction between the zones of enhanced permeability is unlikely. Further comments on the possibilities of both structural and hydrological interaction between adjacent cavities are presented below.

The question of structural interaction, in which two adjacent cavities may tend to act as one larger cavity, has been analysed in Appendix H. It is shown there that, even for the extreme case where the strength of the rock separating the two cavities is reduced drastically, the effect on the rock mass is minimal except in the immediate vicinity of the two cavities.

Hydrological interaction between two adjacent cavities is discussed in Appendix F and in Chapter 7, Section 3.4. These analyses also confirm that essentially no interaction will occur, even for cavities that are quite close to each other.

It can be concluded, therefore, that effects in the vicinity of an underground test can all be considered as independent events — i.e. it is not necessary to consider interaction between tests. Analyses in Chapters 3–7 have been conducted on this assumption.

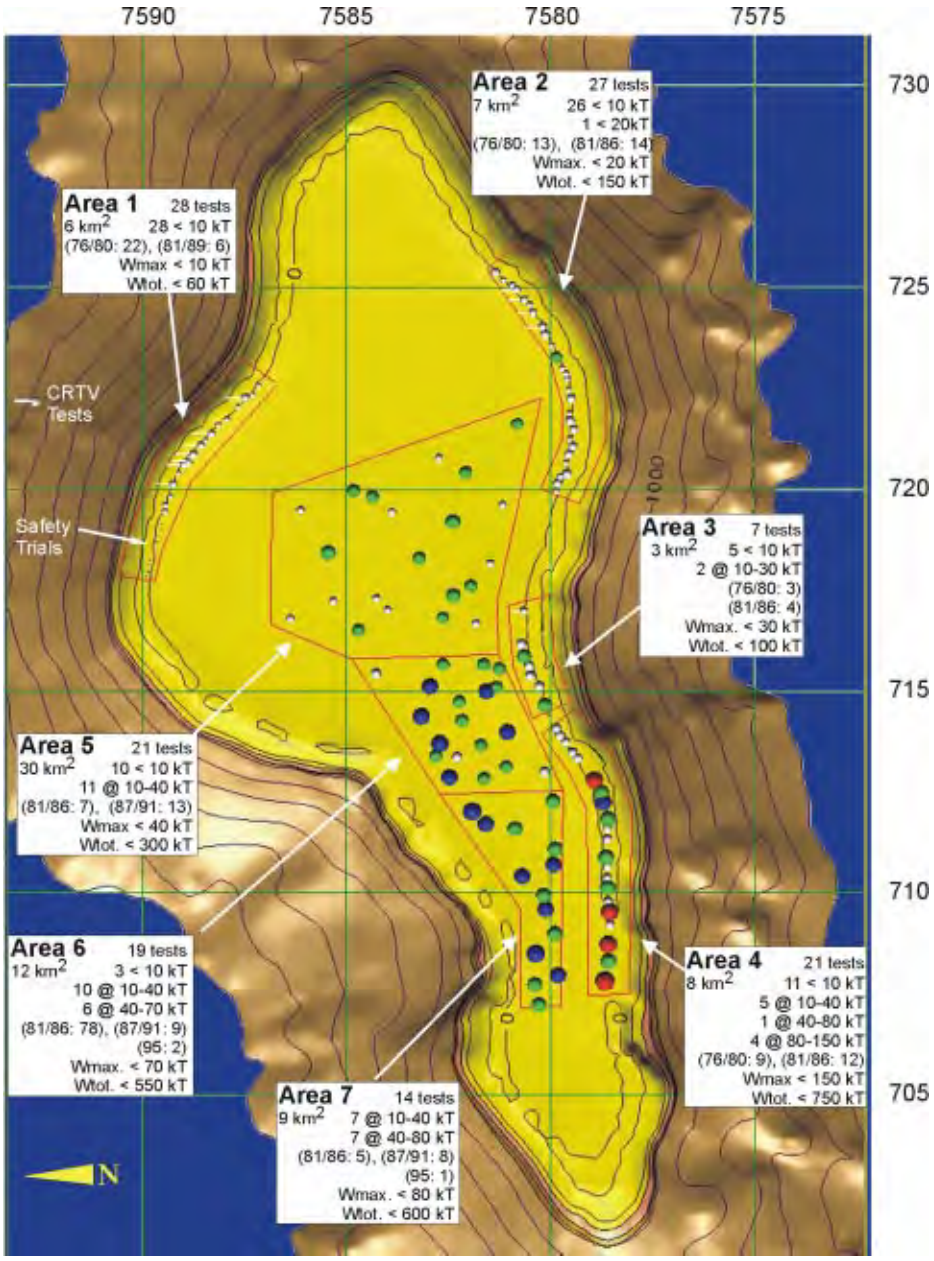

Figure 1.17 Details of underground tests in each test area on Mururoa (provided by DIRCEN/CEA), together with a hypothetical distribution of underground nuclear tests in the test areas (bathymetric contours around the atoll are shown at 250-m intervals down to 2 km below surface)

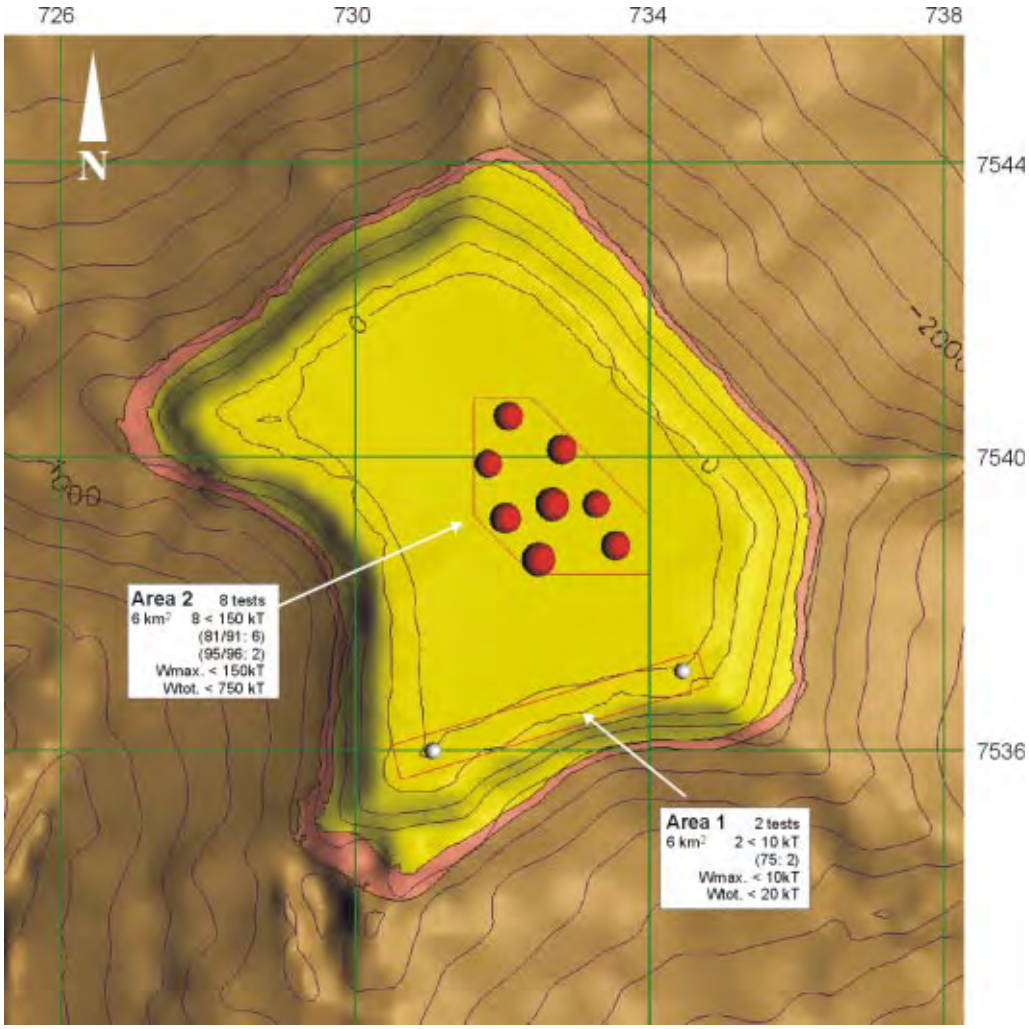

Figure 1.18 Details of underground tests in each test area on Fangataufa (provided by DIRCEN/CEA), together with a hypothetical distribution of underground nuclear tests in the test areas (bathymetric contours around the atoll are shown at 250-m intervals down to 2 km below surface)

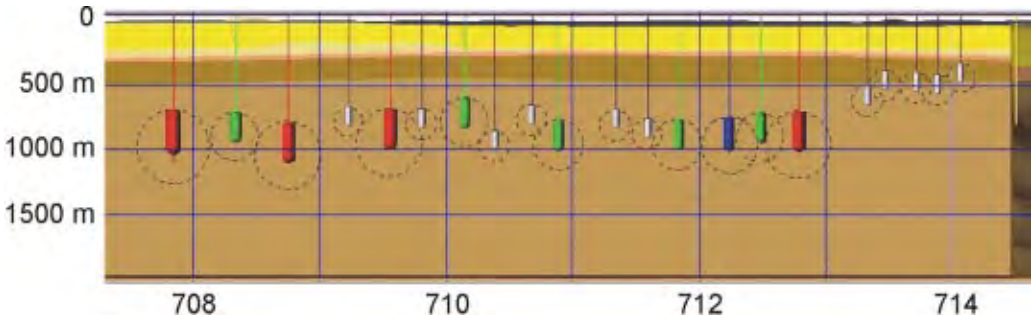

Figure 1.19 Hypothetical distribution of underground tests in test area 4 of Mururoa (Dotted circles, radius 5 R_c indicate the extent of fracture damage; coloured cylinders indicate collapse; chimney height is H_c = 5 R_c; colours indicate low (white) ($<$ 5 kt), intermediate (green) ($<$ 20 kt), high (blue) ($<$ 80 kt) and large (red) ($<$150 kt) explosions; the section is approximately parallel to the coast viewed from the ocean) (see also Fig. 1.17)

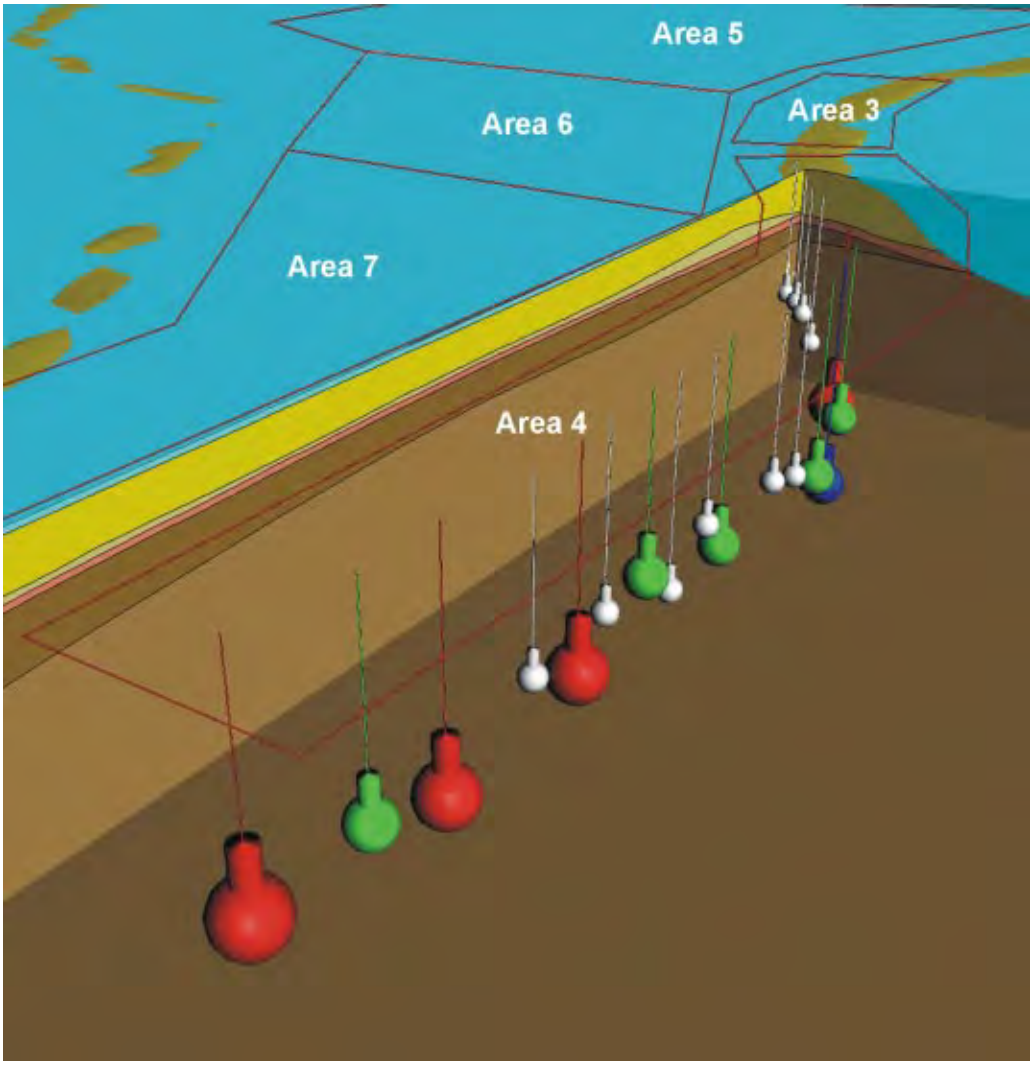

Figure 1.20 Schematic illustration of regions of enhanced permeability (R_p = 2.5R_c, H_c = 5 R_c) associated with underground tests in test area 4 on Mururoa; colours indicate low (white) (< 5 kt), intermediate (green) (< 20 kt), high (blue) (< 80 kt) and large (red) (<150 kt) explosions

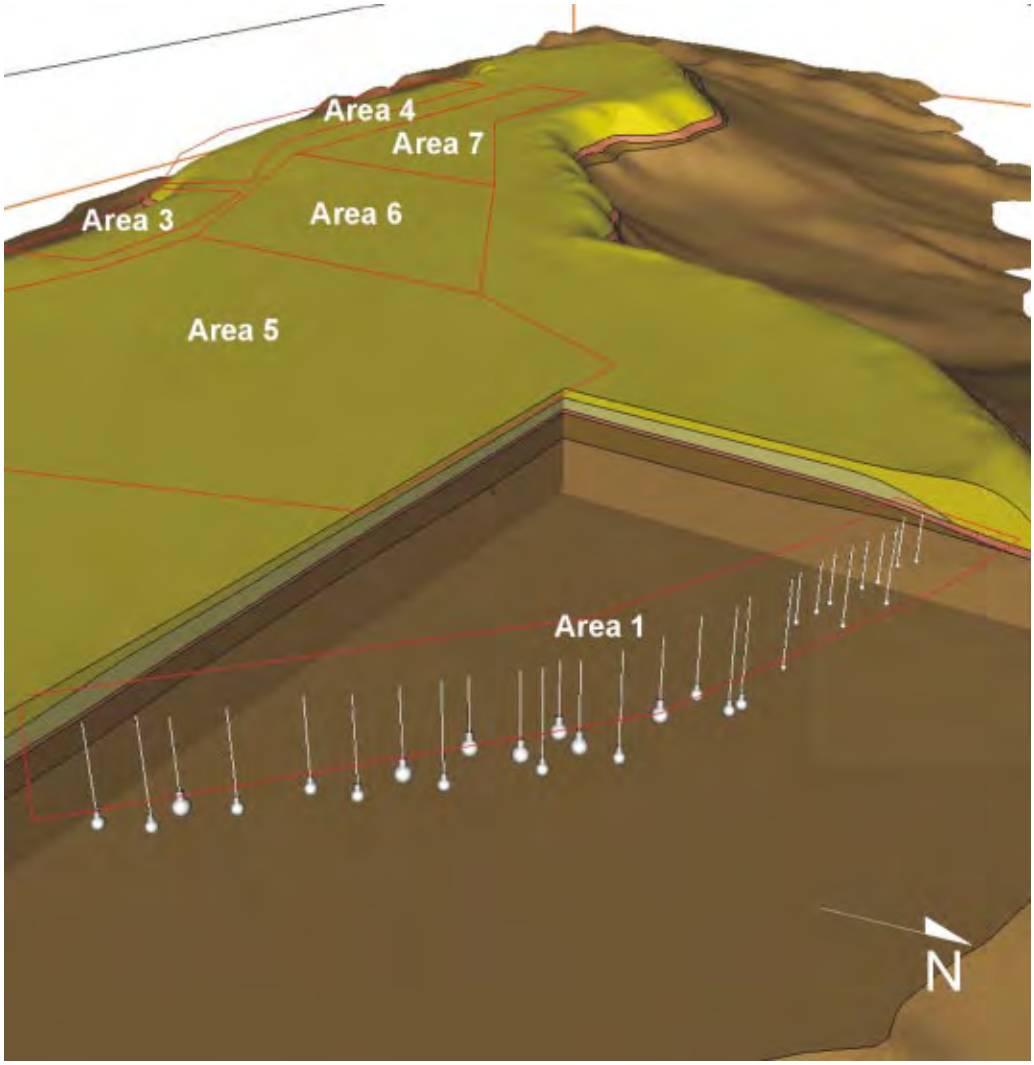

Figure 1.21 Schematic illustration of regions of enhanced permeability (radius R_p = 2.5 R_c; chimney H_c = 5 R_c) associated with underground tests in test area 1 on Mururoa (the white colour indicates low yield ($<$ 5 kt); all tests in test area 1 were below 10 kt; see Fig. 1.17)

1.5 Constraints on Analysis Imposed by Atoll Geology

1.5.1 Geological Variability and Uncertainty and Their Influence on the IGC Study

Variability in the mechanical and hydrological properties of rock masses is an inherent feature of geotechnical problems. Techniques of analysis allow consideration of *known* variability, particularly in numerical computational schemes, but the distribution and extent of the variability in geological systems are also largely unknown. This is due, in part, to the limited data available. Mururoa and Fangataufa are typical in this regard. The geological sections, such as those shown in Figure 1.6 (see also Chapter 2, Figs. 2.5–2.8), for example, are based mainly on cores from a very limited number (often no more than 5 or 6) of vertical boreholes drilled at various locations across the atoll, supplemented, in some cases, by inclined boreholes and by cuttings obtained during boring of the large-diameter emplacement holes. Considerable local variations in lithology in the space between the boreholes will go undetected. Vertical or near-vertical fracturing is particularly difficult to detect in the (vertical) boreholes. Some geophysical traverses have also been made (Guille et al. (1996), Figs. 27 and 61; DIRCEN/CEA Document No. 5, Figs. 2–4), but none of these interpretations show, reliably, detail on the local scale of significance in an individual test.

These limitations require a different strategy of analysis and design than is appropriate for the relatively well-defined "ample-data" problems in some of the other branches of applied analysis (Starfield and Cundall 1988).

The geological uncertainty at Mururoa and Fangataufa is compounded by the uncertainty introduced by data that exist but which were not made available for reasons of military security.

Together, these features of the IGC study dictate an approach that concentrates on developing an understanding of the general underlying physics and mechanics that govern the behaviour of the system to be analysed. The significance of variability in particular parameters of the problem can be more readily assessed when the analysis, numerical as well as closed-form, is carried out using appropriate dimensionless groups. This is particularly valuable with respect to the study of the complex effects of nuclear explosions on a rock mass, as demonstrated in Chapters 3, 4 and 5.

1.5.2 Heat and Groundwater Flow and Solute Transport

At the fundamental level, the flow of water through the interconnected pores and fractures of an atoll rock is governed by a number of inter-dependent or "coupled" processes. The main driving force is buoyancy; the temperature in the rock in the interior of the atoll is significantly hotter, due to heat flowing from the earth's crust at depth toward the surface, than that of the ocean water at the same level. The rock heats the pore water, causing it to expand and rise toward the surface.

The mean velocity of the water (in the pores) will depend on several factors, the most significant of which are the mechanical resistance to flow, usually measured in terms of a permeability, and the buoyancy field, which is given directly by the temperature field. It is usually assumed, as can be shown in this case, that the pore fluid is everywhere in thermal equilibrium with the rock through which it is flowing; this means that locally the water and the rock are at the same temperature. The temperature field is determined by two heat transfer mechanisms: one, heat conduction, takes place in any static medium (in this case, a water-saturated porous rock); the other, heat advection, is caused by the flow of water in the rock. Because all the flow channels in the rock are not equivalent, advection by the mean velocity is not equivalent to the actual advection that takes place. Dispersion therefore takes place and is often viewed as a velocity-dependent conductivity; oscillatory flows caused by tidal effects introduce a further complication, and can also be viewed as a dispersion.

The above processes can be described formally in terms of equations, presented in Chapter 6. Full consideration of all coupled interactions may make analytical solutions of the problem intractable or, in the case of numerical solutions, computationally intensive, and simplifications are often invoked.

In the basalt, where the permeability is relatively low, thermal conduction dominates the transport of heat; so the temperature field can be approximated without reference to advected heat transport (i.e. to the flow field); the latter is a perturbation. Even when a nuclear explosion creates a large generalised source of buoyancy in the basalt, thermal conduction dominates over advection except within the chimney and its near neighbourhood. To this extent, the temperature field is decoupled from the flow field.

Within the carbonates, however, the reverse is the case, and heat transport is dominated by the pore-fluid flow. The solution for either field — temperature or pore-fluid flux — is strongly coupled to the other. A suitable mathematical model is required, therefore, for the temperature field. The heat transport equation is given in Chapter 6 as (6.3) and (6.4); note that this introduces several more (continuum) parameters representing conduction (λ_s and λ_1), dispersion (α_L, α_T) and heat capacity **($(\rho c)_1$, $(\rho c)_s$)**. The thermal conductivity and heat capacities are, in practice, well-known to within the accuracies involved here; thermal conductivity is treated as a scalar, though, formally, it should be treated, like the permeability, $\boldsymbol{\kappa}$, as a tensor function of position. The thermal dispersion coefficients α_L and α_T are characteristic of the rocks; they reflect the connectivity (tortuosity) of the porous medium involved. Again, formally, they should be treated as two components of the dispersion tensor (of the 4^{th} rank) in the case of an isotropic medium.

In principle, both permeability and dispersion coefficients (dispersivities) can be obtained by inversion of data from steady-state experiments on heat and mass transfer in the relevant rocks. Neither IGC nor DIRCEN/CEA has attempted to do this in any systematic way, so values for dispersivities are taken from the literature, as in Table 6.2. The

matter is complicated by tidal effects (see Apps. U and V). Over many tidal periods (i.e. > 10 days), so that a mean continuum representation is relevant, the periodic reversing flows caused by tides cause additional dispersion, the mathematical form of which is, in general, different from that given in (6.4), because it does not depend in the same way on the mean velocity field, v. Because the driving force is different for the periodic flow, a different velocity field is induced. When solute or tracer transport is considered (as in the discussion of releases of tritiated water from the volcanics through the carbonates in Appendices S and T), separate (additional) transport equations are required. For a tracer like tritium, an equation of the form (6.4) is sometimes used, with the diffusive term corresponding to λ_1 neglected, and the left-hand side replaced by a more familiar material-derivative operator. For solutes that can adsorb and desorb from the inner surfaces of the porous rocks, an additional source/sink term is required as well (see (6.5) and (6.6)**)**. However, as is shown in Chapter 7, such a simple dispersivity-based approach proves not to be a suitable representation, and the much more general approach (developed by chemical engineers in connection with reaction engineering in porous catalyst beds — see Denbigh and Turner (1971) and Brenner and Edwards (1993)) — that introduces residence-time distributions and chromatographic exchanges is more appropriate. A very simple version, analogous to a perfectly mixed reactor model, is used in Appendix S to model the observed large-scale and unsteady tritium concentrations in the carbonates and lagoon.

These general considerations form the basis for much of the analysis discussed in Chapters 6 and 7.

1.6 Settlements

The main effects that can be observed on the atolls as a consequence of the underground tests are of two main types — surface settlements and slope instability. Both appear to be related primarily to tests conducted beneath the rim, although the geological conditions on the northeast rim of both Mururoa and Fangataufa are sufficiently sensitive to transient seismic effects that tests conducted under the lagoons can, and have, triggered slope deformations. It will be shown that settlements and slope deformations are, in fact, interrelated; however, we will discuss the two phenomena separately, in keeping with the presentations in Chapters 4 and 5.

One of the most visible results of the underground nuclear tests along the rim of Mururoa is the surface settlement. Figure 1.22 shows an aerial view (taken in July 1996) of test area 4 on the southern rim. (The surface zero point of some tests can be seen.) This region, approximately 2 m above ocean level before testing (DIRCEN/CEA Document No. 7, Fig. 20) is now under water. This indicates that settlements of the order of 2 m have been produced by the explosions. The settlements result from the interaction between the wave generated by the explosion and the top 150–200 m of the carbonates.

Figure 1.22 Aerial view of western part of test area 4 on Mururoa taken in July 1996 (i.e. 16 years after rim testing ceased) from the ocean side, looking toward the lagoon (note that several test sites and settlements in the western end of test area 4 are underwater; see also Fig. 1.23)

According to DIRCEN/CEA Document No. 7 (p. 10), the explosive wave

> *virtually instantaneously lowers the level of the rim within a radius of several hundred metres around the surface zero point. . . . The fraction of the coral rim gradually submerged because of such cumulated settling* [total settlement can be the result of effects from several tests] *(as much as 2 m in some places) represents about 15% of the ground initially above sea level.*

Viewed from the surface, these settlement troughs or basins (Fig. 1.23) appear to be similar to the subsidence features observed above many of the underground tests at the NTS in the United States, especially those conducted in non-welded tuff. CEA authorities emphasise, however, that there are essential differences between the two types of feature (see Fig. 1.24).

Thus,

(a) at the NTS, the subsidence basins are the surface expression of a collapse chimney that forms a continuous connection between the underground zero point and the

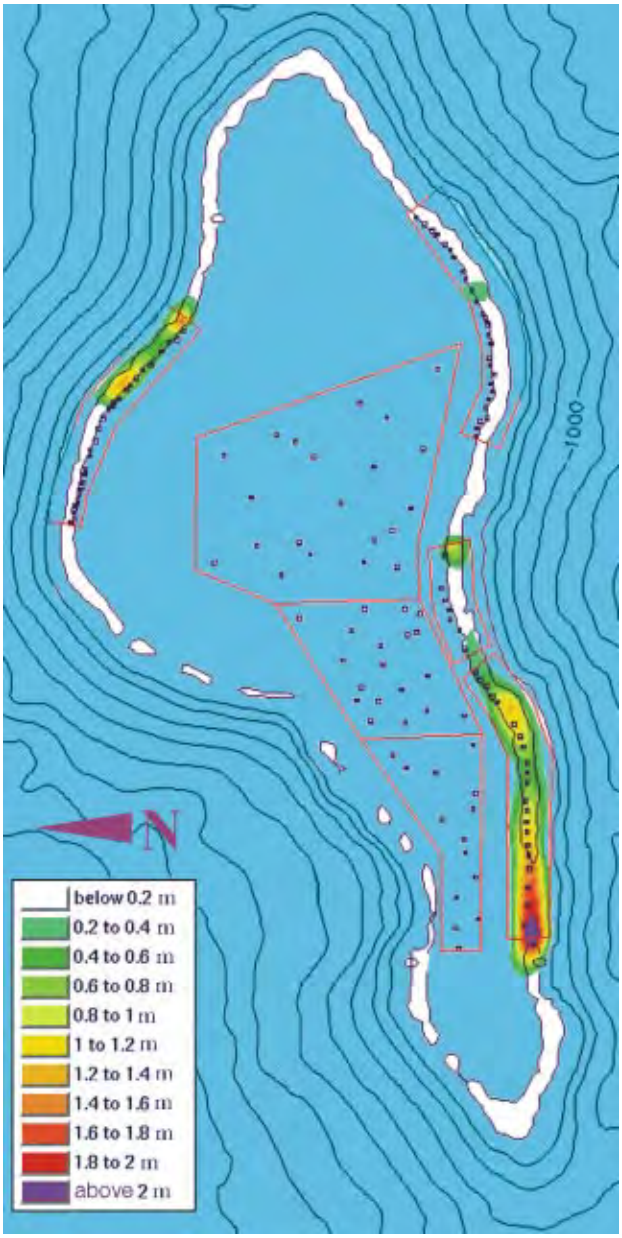

Figure 1.23 Areas of surface settlement produced by underground testing along the rim of Mururoa (based on DIRCEN/CEA 1996 settlement data) [According to Guille et al. (1996), p. 69, “Reef-building corals are currently proliferating at a remarkable rate” (of the order of 1 cm thickness per year) in the settlement regions. Thus, those areas of reef now under water could be restored to a surface elevation within a few hundreds of years.]

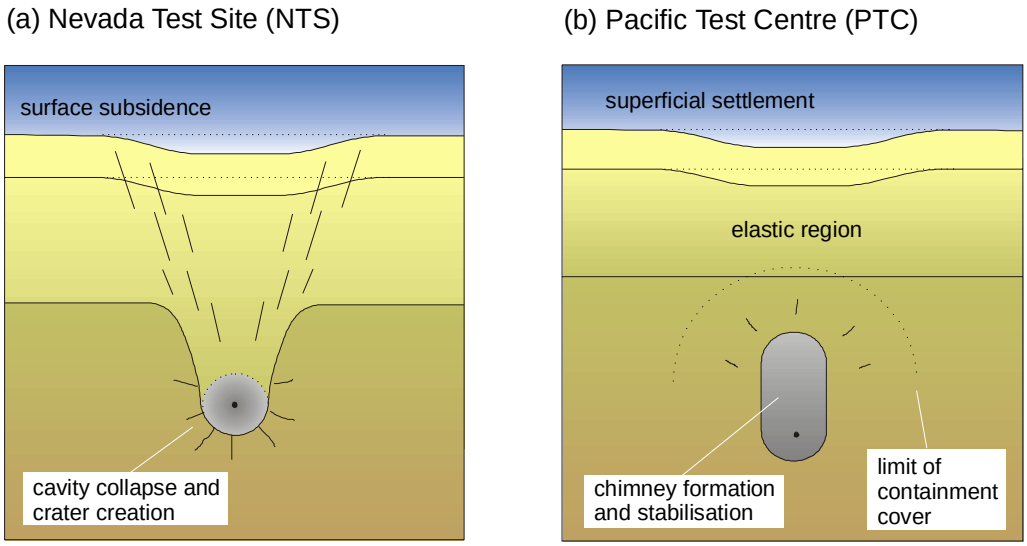

Figure 1.24 Comparison of subsidence occurring at the Nevada Test Site (NTS) with settlements produced by tests at the PTC (after Bouchez and Lecomte 1996, p. 77)

surface (Chapter 4, Fig. 4.5), resulting in high-permeability pathways directly from the explosion to the surface and possible "seepage" (see App. D) of the more volatile radionuclides to the accessible environment or biosphere; whereas,

(b) at the PTC, the depth of burst of the explosions was considerably greater (App. D), with the result that a zone of intact volcanic rock remains above the explosion chimney after a test. The radionuclides are thereby "contained" within the chimney, isolated from the surface (Chapter 4, Fig. 4.3). Hence, the settlement basins at the PTC are superficial only, affecting no more than the upper 100–200 m of the carbonates. This assertion has been examined in Chapter 4 of this report.

As mentioned earlier, the geological and hydrological situations at the two test sites are also quite different. At the PTC, relatively strong — although fractured — volcanics (basalt) are overlain by some 300 m–500 m of weaker carbonates (see Figs. 1.6 and 1.16). The volcanics and the carbonates are porous and saturated to the surface. At the NTS, volcanic tuff extends from below the zero point to the surface, and the water table is at a depth of about 300 m — i.e. the near-surface rock is unsaturated.

The situation at the PTC can be illustrated by reference to Figure 1.16, which is intended to represent the case of the Tydée test in area 4 — i.e. a yield approaching the maximum of 150 kt at a depth of 985 m, and a geological cross-section corresponding to that at the presumed location of Tydée. It is seen that the radius R~8 R_c, beyond which the volcanics are "essentially unchanged" by the passage of the explosion wave, remains

within the (outer regions of) the volcanics. On passing from the volcanics into the mechanically weaker carbonates, the wave may be capable of causing additional damage. As the wave approaches the surface, located at a radius of ~20 R_c, the influence of the lagoon and ocean interfaces become progressively more significant. Numerical modelling of the wave propagation, in which these influences are considered, is described in Chapter 4. It is found that the greater lateral restraint, due to the wider section of rock, tends to inhibit damage in the lower carbonates. In the narrower surface section, however, the rock is damaged. Under quasi-static loading, where water can be expelled from the rock pores or in the event that the rock is unsaturated (i.e. the pore spaces are not water-filled), then "damage" can occur through pore collapse and compaction.

The length (and duration) of the explosion wave varies approximately as the cube root of the yield [100 m (20 ms) for 1 kt; 500 (100 ms) for 150 kt] — i.e. similar to the cavity radius scaling. The larger the expected yield, the greater the depth of the burial of the test below the volcanic-carbonate interface. Thus, when the wave produced by a large test reaches the volcanic-carbonate interface, it will approximate a plane wave extended over a broad front and travelling toward the surface. Smaller, shallower tests will be correspondingly less extended and less uniform.

Numerical analyses of the effects of the explosion wave on the carbonates are described in Chapter 4. Results indicate that substantial surface settlement and lateral deformation will be induced in the upper carbonates by a process of equi-voluminal or *isochoric* shear. In this process, any reduction in the vertical elevation of the carbonates (i.e. settlement) must be accompanied by expansion elsewhere to maintain an overall constant volume of the rock mass subjected to inelastic deformation. Figure 1.25 illustrates that vertical contraction associated with a complex deformation pattern that includes lateral movement within the carbonate and on the ocean and lagoon slopes. The inelastic deformation occurs within the upper 300 m or so of the carbonates. This limited region of deformation is due, in large part, to the proximity of the ocean and lagoon slopes, which allow the lateral deformation to take place. At greater depths, the confinement imposed by the rock mass extending beneath the lagoon and toward the deeper ocean slopes (see Fig. 4.8), tends to limit lateral expansion and, consequently, vertical contraction. Similar reasoning suggests that low-yield explosions, which affect a relatively lower volume of rock (and, hence, are relatively more confined), will produce somewhat less vertical settlement than a high-yield explosion for the same scaled depth of burial. Note also that the lateral extension of the slopes indicated in Figure 1.25 will be underwater and thus not apparent from the land surface.

It is not possible to predict the magnitude of surface settlement due to the effect of one or more tests because the strength and deformability of the rock (coral) mass cannot be measured directly. (As mentioned earlier, this is a difficulty common to many large-scale geotechnical engineering problems.) Figure 1.26 shows a "generic" (dynamic) shear stress-strain response for a rock mass (e.g. coral). For applied stresses less than the

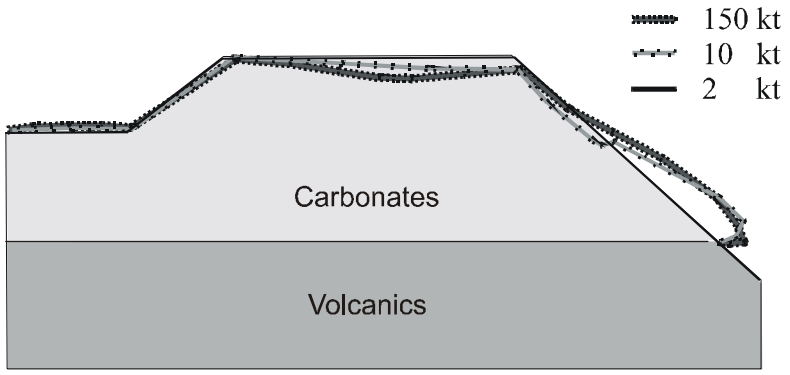

Figure 1.25 Surface and associated ocean and lagoon slope deformations produced by constant volume shear for different intensity explosions (at appropriate scaled depths of burial; see Ch. 4.5, Fig. 4.10)

elastic limit σ_A, the mass will respond essentially elastically, loading (OA) and unloading (AO) along the same path with no energy dissipation. (This is the situation for passage of a seismic wave through the medium). At higher wave amplitudes, the coral strength (σ_B) may be exceeded and the coral deformed along the path OBC, at which time the tail of the wave passes out of the region and the coral is unloaded along the "residual elastic" path CD, to a permanent displacement OD (recognised in this case as "settlement"). The energy abstracted from the wave is proportional to the area OABCD. A second wave (i.e. from another test) could then cause the same rock mass to be "re-loaded" along the path D′C′EF, increasing the displacement (and settlement) from OD′ to OF. The energy required for the increase (proportional to DCEF) is substantially less than for the first displacement. Because the stress and displacement magnitudes associated with the various stages (A . . . F), shown in Figure 1.26, are unknown *a priori*, it is obviously not possible to predict the magnitude of the final deformations.

Figure 1.26b shows an idealised form of Figure 1.26a that is sometimes used in numerical analysis. By appropriate choice of the parameters needed to define Figure 1.26b (i.e. peak and residual strengths and deformations, including the softening parameter, α, shown in Fig. 1.26b (see, also, Ch. 4, Section 4.4, and Table 4.2), it is possible to "match" the observed behaviour and, hence, arrive at "reasonable" rock-mass properties for use in future estimates. The need to "tune" model parameters in this way is also discussed in Chapter 3.5.4 with respect to the estimation of cavity radius.

CEA scientists (Bouchez and Lecomte,1996; CEA/DIRCEN Document No. 6) consider the surface settlements to result from compaction of the porous coral by the fallback impact of surface layers (slabs) of the coral that have been projected into the air by reflection of the explosion wave at the surface. While reflection slabs are developed in this way (see App. P), the IGC considers that the subsequent impact on the coral surface is

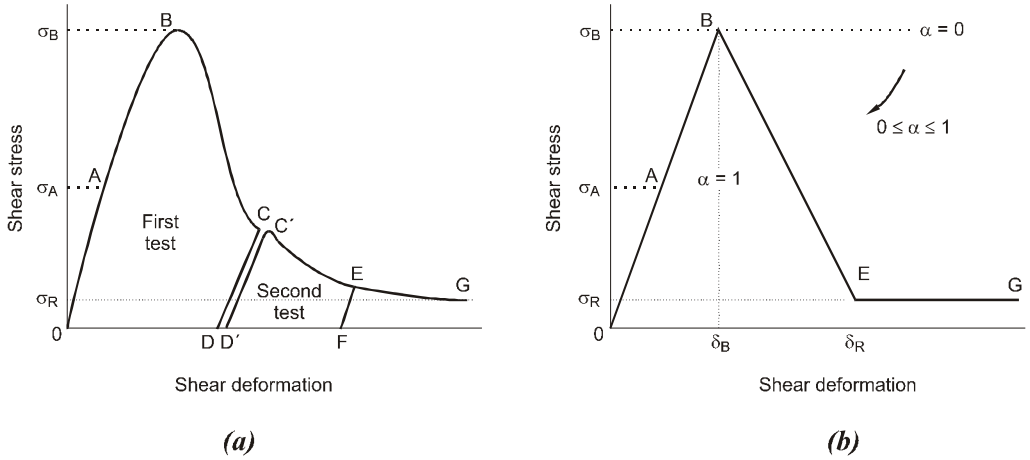

Figure 1.26 Typical (a) and idealised (b) "complete" load-deformation curves for rocks exhibiting softening behaviour (DD′ represents (time-dependent) deformation that occurs between the two tests)

unlikely to result in significant compaction. The carbonates are porous, but they are also saturated, and passage of the explosion wave — or the wave generated by the slab impact — will occur so rapidly (within a few tens of milliseconds; see Table 4.1 and App. P) that there is little opportunity for water to be expelled from the pores. Thus, compaction by pore collapse will be inhibited. The rock response will be that of an undrained medium. Passage of the explosion (compression) wave will raise the pore fluid pressure, reducing the effective stress and the resistance to shear and thus enhancing the isochoric shear deformation referred to earlier.

It should also be noted that, according to the settlement mechanism proposed by the IGC, tests conducted under the lagoons (hence, remote from the ocean flanks) are unlikely to produce settlements of the lagoon bottom (i.e. the top of the carbonates) since the large lateral extent of the carbonates around the zone of a test will inhibit lateral expansion and, in turn, inhibit vertical settlement. Reflection slabbing will still occur, but uplift and fallback impact of slabs are likely to be considerably attenuated in water compared to air.

Notwithstanding the difference in interpretation of the mechanics of the surface settlement, it is clear that the surface settlements observed at the PTC are definitely a superficial (surface-related) phenomenon caused by the passage of the explosive wave — i.e. there is no direct connection between the surface settlements and the top of the cavity chimney.

1.7 Slope Stability

1.7.1 Stability of the Atoll Flanks

Tests conducted in the volcanics beneath the rim on Mururoa have resulted in significant instabilities of the ocean slopes. Thus,

- several major underwater slides in the southwestern zone of the atoll, during the period 1977-80, in the vicinity of test areas 3 and 4 (DIRCEN/CEA Document No. 7);
- a creeping instability involving an extensive region in the northeastern zone was first identified in 1979. (The "sliding region" extends along the rim, over the entire test area 1 and into section PK4–PK 6, where no tests were conducted. This creep has been monitored continuously since 1979.);
- a creeping instability in the northeastern region of Fangataufa, near Kilo-Frégate, has been identified. No tests were conducted under this rim. Although the geology and the mechanics of creeping are similar to northeastern Mururoa, the creep activity seems to be declining.

As discussed below, the northeastern rims of the atolls appear to have been prone to periodic collapse over geological time. Much of the current deformation activity on the northeastern rim of Mururoa is considered to be the result of tests conducted under the rim during the first 3–4 years of underground testing (1976–80), although some large tests conducted in the lagoon also (starting in 1981) have had transient influences on the deformation (see Figs. 5.8 and 5.9 and the associated discussion in Section 5.4.2). Lagoon tests conducted at considerable distance from the rim were clearly a primary cause of the creeping deformations observed in 1988–92 on the northeastern region of Fangataufa, since, other than two small tests (each less than 10 kt) on the south rim in 1975, no rim tests have been conducted on Fangataufa.

As mentioned earlier, the underwater slides in the southwestern zone of Mururoa (test area 4), particularly those associated with the tests Nestor (19 March 1977), Priam (30 November 1978), and Tydée (July 25 1979), generated severe hydraulic waves which, especially in the case of Tydée, inundated parts of the atolls (DIRCEN/CEA Document No. 7, Section V) . These occurrences led to a careful re-evaluation of testing procedures (see Tazieff 1982) on the atolls and a decision to move tests from the rim toward the centre of the lagoon. Although three additional larger tests and one moderate test were conducted on the rim in 1980 [Thésée **(**estimated yield 78 kt; see App. C); Asios (78 kt); Diomède (51 kt); Eurypyle (26 kt)], it appears that (i) no very large tests (100~150 kt) were carried out on the rim after 1980 (see App. C); and (ii) none of the tests conducted since 1980 has created any new slope instabilities.

The above-mentioned tests on the southwest rim produced more or less immediate slope failure (DIRCEN/CEA Document No. 7), while those on the northeast rims resulted in a slow deformation that has continued for approximately two decades. The reason for this difference in behaviour can be found by studying the detailed geology of the rim regions.

1.7.2 Geology of the Atoll Rim

Detailed study of the bathymetric profile of Mururoa, supplemented by underwater photographs and video films, reveals the ocean flanks of Mururoa to consist of volcanic ridges radiating from the rim, with the valleys between the ridges filled to varying degrees with sediments derived largely from the overlying carbonates. The sediment accumulations reach 300 m in thickness in places (Fig. 1.5) and extend to as much as 3 km in depth.

The ridges and valleys appear to be the result of erosion that took place when the Mururoa volcanic edifice was above water. A similar pattern of erosion can be seen developing on the island of Mehetia today (Fig. 1.3). The accumulation of (carbonate) sediments results, in part, from erosion whenever the seamount emerges, due to a drop in ocean level during periods of glaciation (see Fig. 1.4), and in part also to periodic collapse of over-extended coral reef as it develops throughout the process of coral-building. The fact that the accumulations are thickest in the northeastern region of the rim (Fig. 1.5) suggests that this region is most prone to periodic collapse. A similarly large accumulation is seen on the northeast rim of Fangataufa (Guille et al. 1966, Fig. 80, p. 101). By contrast, except for a small region at depth in the vicinity of the Tydée slope collapse (Fig. 1.5), test area 4 on the southern rim shows relatively little accumulation.

Exploratory drilling has revealed significant differences in the detailed geology of the northern and southern slopes of Mururoa. In particular, the volcanics on the northern slope are overlain by an “apron” of weak, porous, chalky limestone that is absent from the southern slope (Figs. 5.11 and 5.12).

1.7.3 Numerical Modelling of Slope Stability

The IGC has conducted a series of numerical simulations, both two-dimensional (2D) and three-dimensional (3D), to investigate

(1) the relative stability of the southwestern and northeastern slopes in their natural condition prior to underground nuclear testing (a 2D static analysis was performed);

(2) the effect of underground tests on the slope stability (a 2D dynamic analysis was performed); and

(3) the potential for inducing slope instability at positions on the slope remote from the explosion point, as occurred with the slide induced by the Tydée explosion

(DIRCEN/CEA Document No. 7, Section V1, p. 12; a 3D dynamic analysis was performed).

1.7.4 Natural Stability

The natural stability of the two regions was examined in terms of their *factor of safety* against slope collapse. Upper and lower bounds of the factor were obtained, assuming that all units exhibited either (i) elastic-perfectly plastic (EPP) or (ii) elastic-perfectly brittle (EPB) behaviour, respectively. Several trial cases were run for each condition (EPP/EPB) to determine whether the slope was stable or unstable in each case. Although it is possible to narrow the strength decrement between each run, it was considered adequate to define the approximate range within which the slope changed from stable to unstable in each case. The results obtained in this way were as follows:

Factor of Safety	Rock Sample Properties		Rock Mass Properties
	Upper Bound (EPP)	Lower Bound (EPB)	Upper Bound (EPP)
Northeastern slope	2.0 ~ 2.5	1.4 ~ 1.7	1.5 ~ 1.6
Southwestern slope	2.5 ~ 3.3	2.0 ~ 2.5	—

As seen, the northeastern slope was significantly less stable than the southwestern slope.

Most of the values tabulated above are based on laboratory values of the strengths of the rock formations in the slopes, since no rock-mass strength values were given in the DIRCEN/CEA documents. Several runs were made, for the EPP case only (i.e. α = 0 in Fig. 1.26b), based on rock-mass strength estimates suggested in Chapter 2.5 of this report. The "unstable-stable" range was found to be 1.5 $\sim$ 1.67, with the "real" instability value probably closer to the 1.5 limit. No analysis was made for the EPB case, because there was no sound basis on which to choose a value for the softening parameter α (Fig. 1.26b). Clearly, however, the factor-of-safety would be lower than 1.5, and may approach *intrinsic* instability — i.e. a factor-of-safety of 1.0 or less. It is thus probable that the northeastern slope in its present profile could be close to instability and that additional loading, such as may result from future lateral accretion of coral or from explosions, would result in collapse of the upper carbonates.

1.7.5 Stability under Explosive Loading

The 2D dynamic analysis was carried out using the same boundary and loading conditions as for the analysis of settlements (see Fig. 4.8). Figure 4.11 indicates the contours of plastic shear strain produced in the carbonates by a 150-kt explosion detonated at a depth of 900 m, which is comparable to the larger tests conducted in test area 4. It is seen that a region of plastic shear develops parallel to the ocean slope over the full depth of the carbonates. Depending on the values assumed for the strength and softening parameters of the carbonates in the southwestern region, the slope could be stable or could

be immediately unstable over the full depth of the carbonates. The latter situation may have developed, in part at least, to produce the large rapid collapses that resulted from the Nestor and Priam tests. This must remain conjectural, since the locations of these tests with respect to the slope collapses (see Figs. 1.12 and 5.1) are not known.

In the case of Tydée, it is known that the main collapse occurred approximately 2 km west of the explosion point (see Fig. 1.11). To examine this case, a 3D dynamic analysis was carried out. In this model, it was assumed that all geological units along the rim had the same strength. Figure 5.14, for example, shows the vertical displacements resulting from the explosion at various locations on the ocean slope. It is seen (as expected) that effects (here, displacements) decrease with distance from the explosion. Assuming uniform properties, therefore, failure would most likely start on the slope at the point closest to the explosion. The probability of failure being initiated 2 km or so along the slope from this point would be small.

Two possibilities appear plausible:

(1) the material on the ocean slope at 2 km from the "nearest point" is much weaker than at points less than 2 km from the explosion; and

(2) irregularities in the slope surface lead to amplification or focusing of the explosion wave amplitude at 2 km, such that the material strength there is overcome.

A combination of (1) and (2) is also possible. As noted earlier, sediments do accumulate in valleys between the ridges on the flanks. The action of the wave on the interface between the flanks could produce a local increase in pore pressure in the sediments (which could include large blocks), leading to a major instability, rapid descent of the sediments and associated hydraulic wave effects. A somewhat related possibility is presented in Appendix R. The generally strong, brittle nature of the carbonates in the southwestern region, the relative absence of sediments at depth in this region, and the apparently low micro-seismic activity all combine to indicate that the southwestern slopes will remain mechanically stable in the absence of future testing on the rim of the atoll.

1.7.5.1 Northeastern Slope of Mururoa

Tests conducted in the immediate vicinity of test area 1 were of much smaller yield (all less than 10 kt) than those in test area 4, but the combination of relatively shallow depths of burial and the presence of weak chalky limestone resulted in a destabilising effect on the carbonates. Figure 1.27c shows the contours of plastic shear strain developed in the carbonates after a 10-kt explosion at a depth of 650 m in the volcanics in the northeastern rim. Comparing the plastic regions in Figure 1.27b (the static loading case) with those

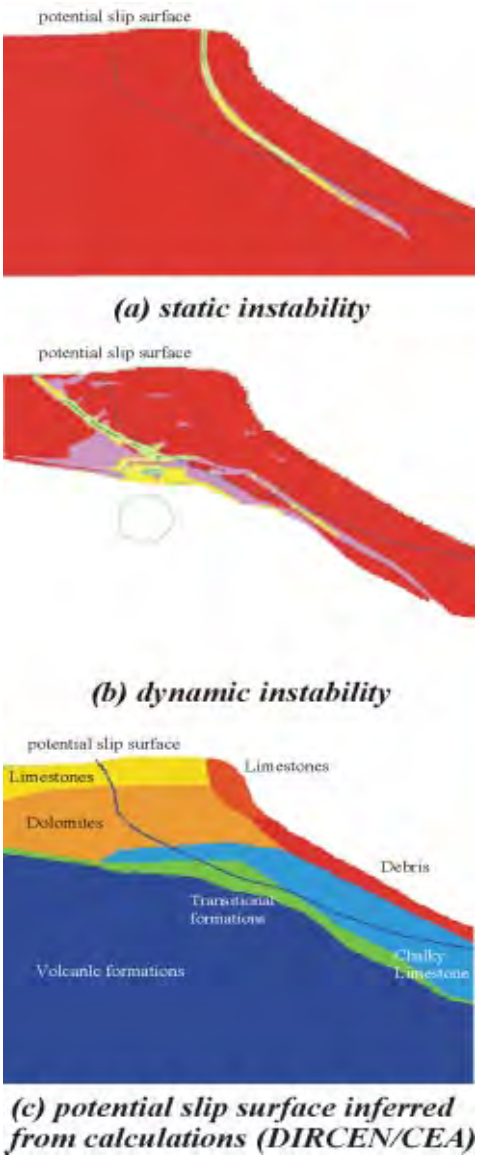

Figure 1.27 Calculated deformations of ocean slopes in the northeastern zone of Mururoa for both static and dynamic loading: (a) static deformation under gravitational and hydrostatic loading (contours of plastic shear strain for softening model and a factor-of-safety of 2.0; see Fig. 5.21); (b) deformation after dynamic loading (contours of plastic shear strain for softening model after a 10-kt explosion at a depth of 650 m; see Fig. 5.23); and (c) geotechnical model with potential slip surface superimposed (DIRCEN/CEA Document No.7; see Fig. 5.12) (Note: potential slip surface inferred from calculations by DIRCEN/CEA)

in Fig. 1.27a (the dynamic loading case), it is seen that the dynamic loading (which superimposes forces acting radially outward from the explosion onto the gravity forces of the static case) generates a more extensive zone of shear. The difference is particularly pronounced in the upper region of the rim, with a potential failure surface now extending under the entire rim into the lagoon. This failure surface is consistent with calculations by CEA scientists (see Fig. 1.27c) and suggests that the creeping deformations observed since 1980 in the northeastern region of Mururoa are due, in considerable measure, to the underground tests. The dynamic wave acts to form an inclined fracture in the upper, brittle formations of the carbonate and shearing of the chalky limestone. The fractured brittle formations result in additional loading and more rapid creep of the chalky limestone. The less extensive vertical fractures in the immediate vicinity of the ocean slope — visible tensile cracks with apertures up to 2 m or more in places (underwater) — are probably produced initially by static loading, to be extended as a result of movements induced by subsequent explosion effects (see Fig. 5.6).

Modelling of the effects of large explosions detonated at greater distance from the rim (e.g. lagoon tests) indicate that these can cause transient effects such as those observed in the measured deformations of the northeastern zone (Figs. 5.8 and 5.9). The transient increases in creep rate in November 1985 and 1987, for example, coincide with the detonations of Mégarée and Pélée, respectively, in test area 5. It seems plausible also that, for even larger tests, such as those conducted under the Fangataufa lagoon, the dynamic effect could be such as to produce even larger, longer-lasting deformation effects. In both cases, however, it seems likely that these effects will tend to attenuate with time.

1.7.5.2 Northeastern Slope of Fangataufa

According to CEA scientists, micro-seismic observations and direct topographic measurements at Fangataufa (DIRCEN/CEA Document No. 7, Section VII) indicate that testing has reactivated movements on existing fractures in the Kilo-Frégate region, but these movements appear to have essentially ceased since 1992: “The last campaign [1995/96] did not cause any significant increase in these movements” [DIRCEN/CEA Document No. 7, p. 38].

1.7.6 Potential for Further Instabilities on Mururoa and Fangataufa

The IGC agrees with the conclusions drawn by CEA scientists that

(1) ocean slopes on the southern rim of Mururoa are now stable and are likely to show no further changes due to the underground testing programme;

(2) the northeastern rim of Fangataufa is likely to continue its current apparent tendency to stabilise. Periodic monitoring for several (ca 20) years to confirm this impression is recommended.

With respect to the northeastern rim of Mururoa, the IGC acknowledges that measured deformations (see Figs. 5.8 and 5.9) show a trend toward lower rates that could imply eventual stabilisation (Bouchez et al. 1997). It is also possible, however, in view of the strain already sustained by the chalky limestone (ca 0.5%), that this rock formation could be entering a regime in which the strength of the chalk could fall significantly, leading to an acceleration of deformation and ultimate collapse. Given the large volumes of rock involved in these deformations and the possibility of hydraulic waves comparable to or larger than those experienced during the Tydée collapse, it is recommended that a careful programme of monitoring be continued for about 20 years, or until the future stability of this region can be assessed more reliably. It is expected that signs of accelerating deformation and ultimate collapse could be detected some weeks to several months in advance of an eventual failure. This would allow adequate time to alert anyone potentially at risk from a slope collapse.

In conclusion, the northeastern zone of Mururoa is essentially the only area where there is any residual concern for local stability. Changes introduced since 1980 (i.e. limiting the yield of rim tests and moving all tests to the lagoons) have avoided any additional stability-related consequences of underground testing elsewhere on the two atolls.

Underground testing has had no global stability consequences for either atoll. This is evident from consideration of the locally limited nature of stability effects in the test areas and is supported by the evidence (DIRCEN/CEA Document No. 7) that the average sea level at Mururoa over the past 17 years shows no departure from the trend observed over the same period in other regions of the South Pacific — i.e. there has been no effect of the underground nuclear tests on the overall stability of Mururoa. The same is very probably true for Fangataufa, but no specific sea-level measurements are available for this atoll.

1.8 Natural Flow of Groundwater in an Atoll

In general terms, the hydrology of an atoll is now well understood. (Studies of Mururoa and Fangataufa by CEA scientists have contributed significantly to this understanding.) The dominant groundwater flow is from the ocean toward the interior of the atoll, rising vertically toward the centre of the atoll lagoon (Fig. 1.28). The vertical component of flow is produced by "endo-upwelling". Water in the pores and fractures of the saturated interior of the rock mass is warmed by heat flowing from the earth's crust through the atoll toward the surface, creating thermal buoyancy forces in the water. The ocean water surrounding the atoll is colder and denser than the interior water, so that a circulation develops in which the ocean water flows from the atoll flanks toward the centre and upward toward the surface in the lagoon.

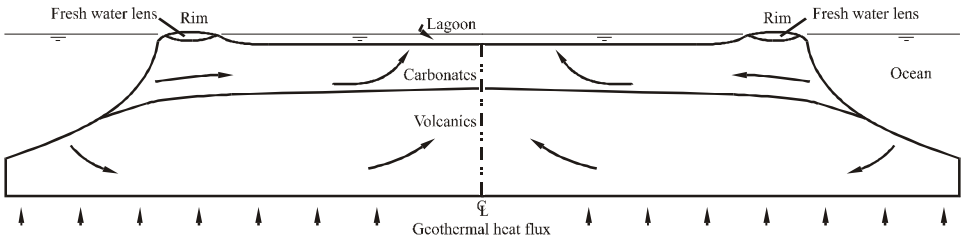

Figure 1.28 Schematic cross-section through an atoll (after Perrochet and Tacher 1997a)

The combination of thermal buoyancy and the relatively much higher permeability of the carbonates compared to the volcanics results in a characteristic temperature profile in the carbonates. The rock (and groundwater) temperature initially decreases with depth below surface but then begins to increase with increased depth. The temperature of the ocean water also exhibits a minimum temperature at a given depth.

1.8.1 Flow in the Carbonates

Determination of the minimum temperature and the depth at which it occurs at different locations across the atoll depend on the permeability and thermal properties of the carbonates and can be used to "calibrate" the groundwater flow model for the carbonates. This technique has been used by DIRCEN/CEA scientists and is confirmed by the IGC; it is discussed in Chapter 6, Section 3.

The main conclusion that can be drawn from the IGC numerical modeling studies of the temperature profiles are as follows. The temperature profiles in the carbonates can be explained almost equally well by any of several permeability regimes. The one considered most likely by IGC is a highly permeable karstic region in the lower carbonates, laterally interconnected so as to extend effectively across the atolls, with a transmissivity of 0.1 m^2/s (e.g. a 10-m thick layer with a 10^{-2} m/s permeability), covered by a thick series of coral with an average isotropic permeability of 10^{-5} m/s. (Several karstic horizons are observed in drillhole cores.) Alternatively, the carbonates could be made up of a single equivalent isotropic layer of $5{\cdot}10^{-4}$ m/s or a single anisotropic layer with horizontal and vertical permeabilities of 10^{-3} and 10^{-4} m/s, respectively.

1.8.2 Permeability of the Volcanics

The large-scale natural permeability of the volcanic rock has been established to be 10^{-7} m/s or lower. A higher volcanic permeability would result in a non-linear temperature versus depth profile in the volcanics. (The observed linear profile indicates that heat transfer occurs mainly by heat dispersion.) At higher permeabilities, some heat transfer would also occur by convection, producing an upwardly convex profile.

The 10^{-7}m/s upper bound is also confirmed by back calculations from the time required for cavities in the volcanics to fill with water after an underground explosion (Chapter 7).

The permeability measured on cores of volcanic rock is of the order of 10^{-10} m/s, indicating that flow in the volcanic rock mass occurs mainly via conductive, interconnected fractures that are not found in specimens of core size.

1.8.3 Darcy Flow Velocities

The studies described above yield estimates of the natural Darcy flux ("velocities") as follows:

in the carbonates	0.5–2 m/y in both the horizontal and vertical directions
in the volcanics	2 mm/y in the vertical; 5 mm/y in the horizontal

1.8.4 Pore Water Velocities

The Darcy fluxes (q) can be transformed simply into pore water velocity (v_i) if the rock porosity (ϕ) is known, using the relation

$$v_i = \frac{q}{\phi}$$

For the carbonates, ϕ is estimated to be approximately 30–40% — say, 35%. For the volcanics, a value of 10% is a reasonable estimate of the matrix porosity (ϕ_m) — i.e. the small-scale pores in the basalt. However, if the flow takes place in the fracture network with no exchange between the fracture walls and the matrix porosity, then a fracture-porosity value (ϕ_f) as low as 10^{-4} (i.e. 0.01%) could be appropriate.

With the above values [$(\phi_m)_{carb}$ = 35%; $(\phi_f)_{volc}$ = 0.01%; $(\phi_m)_{volc}$ = 10%], the interstitial pore (or fracture) velocities (v_i) are

volcanics	
with $\phi_m = 0.1$	v_i = 20 mm/y in the vertical direction; 50 mm/y in the horizontal direction
with $\phi_f = 10^{-4}$	v_f = 20 m/y in the vertical direction; 50 m/y in the horizontal direction
carbonates	
with $\phi_m = 0.35$	v_i = 1.5–6 m/y, both directions

1.9 Effect of Nuclear Explosions on Rock Permeability

The "damage" sustained by rock at various distances from an underground nuclear explosion has been discussed earlier (see Fig. 1.10; see also Chapter 3). It ranges from

vaporization of the rock to melting (and resolidification), compaction and shearing, and decreasing in intensity through minor, non-connected external cracking and, eventually, no damage. It is not possible to establish, reliably, the relation for each stage between "damage" and the resulting permeability. Regions most intensively affected by the explosive shock (e.g. the molten "skin") may be expected to exhibit a much lower permeability, while regions at a greater radial distance could increase in permeability. Non-monotonous changes in permeability can be explained by competition between pore collapse and fracturing under the action of the stresses developed behind the shock wave (Nikolaevskiy 1996). Also, the chimney collapse that occurs soon after an explosion serves effectively (via the chimney) to interconnect and/or "short-circuit" various regions of damage. No direct measurements appear to have been made of the post-explosion permeability in the various regions at the PTC. Indirect estimates have been attempted based on observation of the time required to fill the void volume of the "cavity plus chimney". The IGC's assessment (see Chapter 7) indicates that a permeability increase of the order of ten- to a hundredfold (depending on the radial extent considered — i.e. $R_{perm\,inc} \simeq 2.5\ R_c$) appears to be consistent with observed post-explosion filling rates.

1.9.1 Flow Around a Test Site After an Explosion

Water flowing to fill the cavity-plus-chimney produced by an explosion is quickly heated to between 25 °C and 50 °C above the pre-explosion rock and water temperatures. Because the volume of the cavity increases directly with the yield (i.e. energy released), the temperature is independent of the yield of the explosive. Within the chimney, a strong convective circulation mixes the water intimately. The heat dissipates slowly, by conduction in the rock and advection with the groundwater, generating a strong buoyancy flow and a high vertically upward velocity. This upward flow also dissipates more-or-less exponentially with time, reaching a steady-state value that is somewhat above the pre-test values (because of the locally increased permeability), in about 500 years.

Because this explosion-induced buoyant flow provides the main drive for transport of radionuclides from the cavity and chimney through the rock mass to the biosphere, a large variety of cases involving several different yields, depths of burial, etc., including tests where the chimney reached the carbonates, were simulated by numerical modelling. Details of these computations are presented in Chapter 7. Several general observations are worth noting. For an extreme (hypothetical) situation of a 150-kt explosion in which the chimney reached the carbonates and a cavity/chimney water temperature increased by 50 °C, the peak Darcy velocity (vertically upward) in the carbonates was found to be 58 m/y at its peak (after 1 y), averaging 18 m/y over 100 years. Thus, actual (interstitial) velocities in the carbonates (ϕ = 35%) would be of the order of 100–150 m/y in the early years. Tritium, a radionuclide that travels with the speed of the water (i.e. no delay or "retardation"), could arrive in the lagoon within 2–3 years of such an explosion.

The presence of a thick ($\simeq$ 50 m) karstic layer at the bottom of the carbonates can result in considerable dispersion and attenuation of the thermal plume (see Figs. 7.17 and 7.18) and will so reduce the vertical velocity in the carbonates.

Figure 1.29 shows extracts from Figures 7.17 and 7.18 comparing the thermal plume produced by a 150-kt explosion at the atoll rim for the periods 1 year and 50 years after the explosion. It is assumed that there is no cover of volcanic rock above the top of the chimney for the two situations: (i) where there is no karst layer above the cavity, and (ii) where a 50-m thick karstic layer exists above the cavity.

Where the large (150-kt) explosion occurs with 100 m of volcanic cover above the chimney, the peak Darcy velocity in the volcanics is of the order of 0.6–1.2 m/y.

For a small (5-kt) explosion with a volcanic cover of 15 m, the peak Darcy velocity in the volcanics ranges from 0.1–1.3 m/y, depending on the assumed permeabilities and the initial temperature increase. After 100 years, a steady velocity ranging from 0.03–0.3 m/y is reached.

Measurements by CEA (DIRCEN/CEA Document No. 9) indicate that tritium (^{3}H) has been detected in the lower carbonates (karstic layers) in several locations both on Mururoa and Fangataufa. This tends to confirm the overall impression that the depth of "intact" cover above most explosion chimneys has so far been sufficient to prevent any significant release of tritium (or any other radionuclides) to the carbonates. In a few ($\simeq$ 15) cases, however, rock conditions above the explosion chimney were not adequate to prevent rapid flow of groundwater from the chimney to the carbonates — and toward the lagoon.

1.9.2 Potential Short-Circuits Between Explosion Cavities and the Biosphere (i.e. Lagoon)

The heterogeneous nature of the depositional processes in both the volcanics and the carbonates, and fracturing and faulting associated with consolidation of the volcanics, including possible caldera-type events (e.g. in the Viviane sector of Mururoa), suggest the probability of substantial variability in hydraulic conductivity across the atoll. Could these variations be specifically large and extensive (e.g. lava tubes), such that they constitute effective "short-circuits" between the underground explosion chambers and the biosphere (rim, lagoon or ocean)? (See App. F for discussion.) DIRCEN/CEA scientists note that, in the drilling of more than 300 holes through the carbonates and volcanics (150 1.5-m emplacement boreholes, a similar number of post-shot radiochemical sampling holes and numerous geological exploration boreholes), no such "natural" short-circuits have been observed. Are these 300+ holes potential short-circuit pathways to the biosphere?

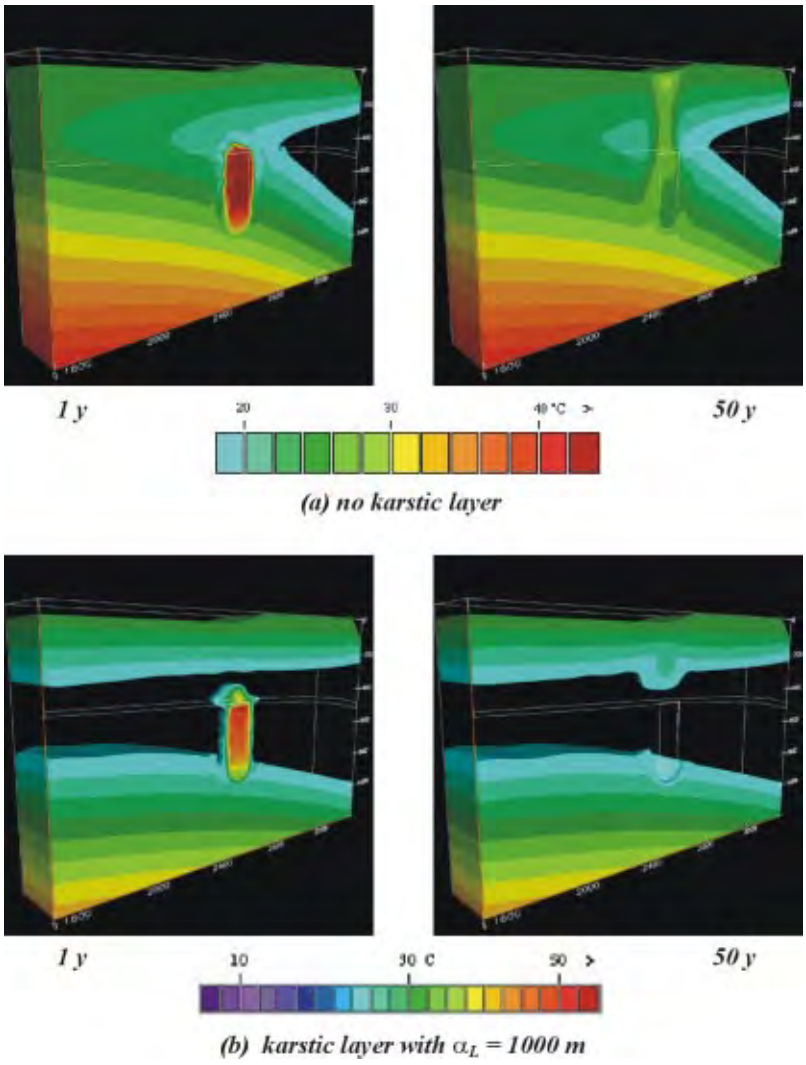

Figure 1.29 Thermal plume generated by a hypothetical 150-kt explosion detonated under the rim with no volcanic cover above the explosion chimney, at 1 year and 50 years after the test: (a) assuming no karstic layer at the base of the carbonates, and (b) assuming a karstic layer at the base of the carbonates [Note on scaling: The fluid temperature in the chimney is independent of explosive yield, Y (and, hence, of cavity size). The width of the initial plume (i.e. chimney diameter) is proportional to $Y^{1/3}$. The rate of decay of the thermal effects is approximately proportional to $Y^{2/3}$ (i.e. the temperature distribution in the vicinity of the plume at 1 yr for a 150-kt explosion would be similar to that for a 10-kt explosion after a period of 1 yr/$(15)^{2/3}$ = 2 months)]

1.9.3 Post-Test Radiochemical Sampling Holes

If left unplugged after recovery of cores of lava from each explosion cavity, the sampling holes would definitely constitute a direct pathway to the biosphere. DIRCEN/CEA scientists indicate that every such borehole was carefully sealed with cement throughout the entire length in the volcanics after removal of temporary casings, which were placed in the holes to prevent their collapse during use. The holes were not cemented in the carbonates. IGC has no information to suggest that these sealing operations were not carried out satisfactorily.

1.9.4 Emplacement Shafts

Drilling of the 150 or so[**], 1.5-m-diameter vertical shafts for underground placement of the nuclear devices at the prescribed explosion depth introduces a potential short-circuit to the biosphere. In each case, care was taken, as described by Bouchez and Lecomte (1996), to seal these holes above the expected chimney collapse region with 100 m or more of concrete plug. The composition of the plug was designed to ensure that the shock wave travelled less rapidly in the plug than in the rock mass, apparently with the intent of developing a "clamping" effect by expansion of the rock onto the plug during the explosion shock wave. Also, the chimney diameter associated with an underground explosion will vary from approximately 24 m for a 1-kt test to 105 m (i.e. 10 (yield)$^{1/3}$) for a 150-kt test.

Although sealing of the shaft itself was probably effective for most, if not all, tests, drilling can also damage the integrity of the rock in the vicinity of the shaft — i.e. in an annulus immediately outside the shaft. This region, referred to as the Disturbed Rock Zone (or DRZ), is of concern in the design of excavation seals for underground nuclear waste repositories. Given the relatively low in-situ stress state (see Chapter 2) at depth in Mururoa and Fangataufa, the extent of the DRZ should be negligibly small except where the rock mass is locally weak or disturbed and/or the height of undamaged volcanic cover above the chimney is small. This disturbed rock condition appears to have been the cause of early leakage of tritium into the lower carbonates in the case of the Lycos test under the lagoon of Fangataufa. The nominal depth of volcanic cover, 140 m, would normally have been sufficient to prevent such leakage.

Observations by DIRCEN/CEA in the lower carbonates indicate that there have been releases (leakages) of tritium, caesium and strontium from a relatively small number

[**]According to DIRCEN/CEA scientists, several (ca 5–10) of these shafts were drilled in the lagoon test regions on Mururoa but subsequently not used for an explosion. These holes were partially cased and capped with a cement plug a few metres thick at the top of the carbonates, but they were left open over the remainder of their length (i.e. in the carbonates and volcanics). The water in these holes is now sampled and forms part of the sampling well network. Although not associated with a direct source of radionuclides, as in the case where the holes were used for explosions, these open holes do increase the local permeability of the rock mass in their vicinity.

(15 or so of 147 tests) of the underground tests, although concentrations are not large. DIRCEN/CEA scientists assert that several of the observed releases in Mururoa are produced by the so-called CRTV tests — shallow, low-yield (< 8 kt) tests where the top of the chimney reaches the top of the volcanics.

Study of the tritium release has allowed the IGC to assess the validity of a "mixing model" (Appendix S) proposed to describe flow in the carbonates and of the estimated Darcy velocities in the volcanics above the chimneys.

The IGC hydrological modelling studies, referred to earlier in this discussion, have examined a range of conditions more extreme than those resulting from the tests conducted at Mururoa and Fangataufa. The case of a 150-kt test at a depth resulting in "no volcanic cover" (as shown in Fig. 7.18, for example) is much more severe than the 12 CRTV tests (essentially, no volcanic cover). According to DIRCEN/CEA scientists, all CRTV tests had a yield of "less than 10 kt". However, the situation assumed to exist in the Lycos test and, to some degree, perhaps, the Tydée test, as indicated in Figure 1.16, tends to approach the situation shown in Figure 7.18.

1.10 Effect of Slope Failures on Atoll Hydrology

As noted earlier, tests on the rim of Mururoa have resulted in substantial underwater slope failures on its southwest rim (test areas 3 and 4) and a large potential slide on the northeast rim (test area 1). On Fangataufa, long cracks have developed on the northeast flank, even though no tests were conducted directly on that rim. Some micro-seismic activity continues there, suggesting continuing deformation and fracture. The 1984 report by the Atkinson mission (New Zealand MoFA 1984) suggested that removal of an outer "protective apron" of low-permeability rock could adversely affect the hydrological regime:

> . . . *the Mission considers that an important point has been missed* [by DIRCEN/CEA scientists and the Tazieff mission (Tazieff 1982)] *regarding the potential risk of slumping i.e. the effect of any slump of the upper slope of the atoll is to strip the atoll of its outer protective impermeable skin. Recent reef research in the Caribbean and the Pacific has shown that maximum cementation and porosity reduction occurs along the outer margin and decreases towards the lagoon. Cementation and porosity reduction at Mururoa is likely to be greatest along windward southern margins. Submarine slides will remove this outer low permeability zone, thus increasing the probability of fluid movement between the ocean and the subsurface* . . . . (p. 97/97)

The IGC stability studies, presented in Chapter 4, show that slope failures that have already occurred, and slope failures in the future, will affect the carbonate layers and

not the volcanics. Removal of a portion of the ocean slope of the rim, as mentioned in the quotation above, does not create a major change in the general groundwater circulation of the atoll. Because water is moving laterally from the ocean to the interior of the carbonates, this flow is likely to be slightly increased (by a few percent), given the thickness of the slab of rock that is likely to slide, compared to the remaining amount of carbonates. This influence is minor compared to the general uncertainty with respect to the rock mass permeability for the carbonates, which do not constitute a significant barrier to the migration of the radionuclides.

1.11 Influence of Karst on Flow in the Carbonates

As noted in the Atkinson report (New Zealand MoFA 1984),

> *The subsurface limestone stratigraphy provides widespread laterally directed avenues of potential fluid motion, probably connecting with the oceans. Such avenues occur at depths of 8–10 m, 65 m, 90 m, 120–150 m, 280–290 m, 315–340 m, and 422 m.*

These karst horizons, of high permeability, have considerable influence on groundwater flow in the carbonates and, especially, the flow induced by underground explosions. As shown in Chapter 7, vertically upward (Darcy) velocities of 58 m/y (peak) and 18 m/y (average over 100 years) computed by neglecting the influence of any karst, were reduced to values of 2–5 m/y when one 50-m thick layer of karst was assumed at the base of the carbonates.

The karst also has a considerable effect on short-term transient phenomena. Measurements (DIRCEN/CEA Document No. 9) have shown that tidal effects in the ocean and the lagoon (the latter delayed some 20 minutes with respect to the ocean) create a sinusoidal pressure pulse in the atoll. This pulse results in an oscillatory movement of water in the rocks — especially in the carbonates. Modelling of how the flow in the carbonates is affected by these oscillatory effects is discussed in Appendices U and V. Although the effect probably does not greatly modify the overall flux of groundwater through the carbonates, it could influence the proportion of radionuclides transported in the water that eventually arrive at the lagoon by spreading horizontally the radionuclides arriving from the volcanics into the carbonates. If the spreading is ignored, then most of the radionuclides arrive in the lagoon; if it is represented by an equivalent very large lateral dispersion coefficient (as in the DIRCEN/CEA documents), then up to 50% of the radionuclide flux is said to be released to the ocean and the remainder to the lagoon.

1.12 Consequences of the Tests on Long-Term Hydrology of the Atolls

The global long-term effect of the 137 underground tests on Mururoa was examined using a three-dimensional model of the atoll. The model was first run in natural conditions,

confirming the general circulation pattern already discussed but including more details of the complex morphology of the atoll. One hundred thirty-seven (137) disturbances, each corresponding to a volume of 7 million m^3 of the volcanic rock in which the permeability was increased by 1000 (due to fracturing) compared to the background permeability (i.e. 10^{-4} m/s compared to 10^{-7} m/s), were introduced into the volcanics to represent the 137 underground tests. Since the locations of the tests are not known exactly, the test volumes were given locations that were, to some extent, random, but consistent with information provided by DIRCEN/CEA. The model was then re-run with the same endo-upwelling boundary conditions. This computation revealed that the total flux in the atoll was increased by just 1% as a result of the 137 tests. This result is consistent with that found in Appendix F. Assuming Mururoa to be approximately $300 \cdot 10^6$ m^2 in plan area and a volcanic test interval of 600 m (i.e. between 500 m and 1100 m), then the total of $137 \cdot 7 \cdot 10^6 \simeq 1 \cdot 10^9$ m^3 of "high-permeability volume" (v_i) is within a total volume (v_0) of the order of $300 \cdot 10^6 \cdot 600 \simeq 180 \cdot 10^9$ m^3. The fractional change (in this case, increase) in rock mass permeability is

$$\frac{v_i}{v_0} = \frac{1}{180} \tag{1.1}$$

or slightly more than 0.5%.

1.13 The Case of Fangataufa

The IGC did not perform any calculations specific to Fangataufa. Given the very similar nature of the geology and rock properties, the hydrologic situation will be very similar to that of Mururoa, both with respect to natural conditions and after underground tests. Indeed, the more "equi-dimensional" plan area of Fangataufa tends to increase the validity of two-dimensional axisymmetric numerical modelling results, compared to the more elongated atoll of Mururoa. Thus, the general conclusions drawn with respect to the hydrology of Mururoa are considered applicable also to Fangataufa.

1.14 Effect of Global Glaciation on Atoll Hydrology

As noted in Chapter 2, the atolls have experienced many periods of global glaciation since their formation. The net result of these glaciations is to lower the level of the Pacific Ocean by as much as 100–150 m in some cases. As noted earlier, in the discussion of Figure 1.4, a drop of 100 m in ocean level within the next 25 000–60 000 years appears likely. This would result in "re-emergence" of the atoll above the water and formation of a lens of fresh water, thinning to zero at each edge of the atoll but reaching a thickness of the order of 200 m under the centre of the "island". This can be expected to encourage habitation of the atoll, but it could possibly have adverse consequences due to possible release into the drinking water of long-lived radionuclides still remaining underground

from the testing period. This possibility was considered as part of the IAEA study, where it was concluded that the consequences would probably not be severe.

1.15 Long-Distance Effects of Seismic Waves Produced by Explosions at the PTC

The possibility that the nuclear explosions could trigger earthquakes is a concern sometimes raised in connection with underground nuclear testing. It could perhaps be argued that a large explosion in the immediate vicinity of an active fault that is already loaded (tectonically) close to slipping (i.e. about to produce an earthquake) could provide such a trigger, but these conditions do not apply at Mururoa and Fangataufa. This region is relatively quiet seismically, with activity concentrated in the crust (i.e. more than 4 km deep) around the Society Islands hotspot, situated between Tahiti and Mehetia (northwest of Mururoa), the hotspot of the Austral archipelago at the Macdonald seamount (south of Mururoa), and the hotspot of the Pitcairn Gambier archipelago located close to Pitcairn Island, southeast of Mururoa (Fig. 1.30). (The Pitcairn hotspot was responsible for the formation of Mururoa and Fangataufa.) These hotspots are all more than 1000 km from Mururoa and Fangataufa (Guille et al. 1996, pp. 7/8 and 33/4). Thus, there is essentially no possibility of renewed vulcanism at Mururoa and Fangataufa from the currently active volcanic regions in the South Pacific.

The intense seismic activity of the Pacific region is concentrated around the tectonic plate boundaries that make up the margins of the Pacific Ocean — the so-called Pacific "Ring of Fire"[††] (associated with the subduction zones shown in the top diagram in Fig. 1.30). These plate boundaries are all at least several thousands of km from Mururoa and Fangataufa — and the PTC.

As discussed earlier in this chapter (see Fig. 1.7), in Chapter 3 (Section 3.52), and in (Bouchez and Lecomte 1996) (Chapter 5, p. 91), approximately 95% or more of the explosive energy from an underground nuclear test is dissipated within a sphere of rock very close to the explosion (e.g. approximately a 400-m radius for a 150-kt explosion). The remaining 5% or less travels away as a diverging elastic wave, spreading over an ever-increasing spherical front and decreasing in amplitude with distance from the explosion. If the wave is truly elastic, the amplitude will decrease in direct proportion to the radial distance. In reality, energy dissipation (attenuation) will occur and the wave will decrease in amplitude more rapidly with distance.

> *...[R]esults show that these effects become extremely weak as the wave moves away from the test sites. For example, after a 100 kilotonne explosion, the ground movements recorded [by seismographs installed on islands*

[††] The "Ring of Fire" (or Circum-Pacific Belt) is named for the volcanoes generated on the land masses fringing the Pacific Ocean, where one plate "dives" below the other in the subduction zones. This Ring around the Pacific is the source of more than 90% of the world's earthquakes.

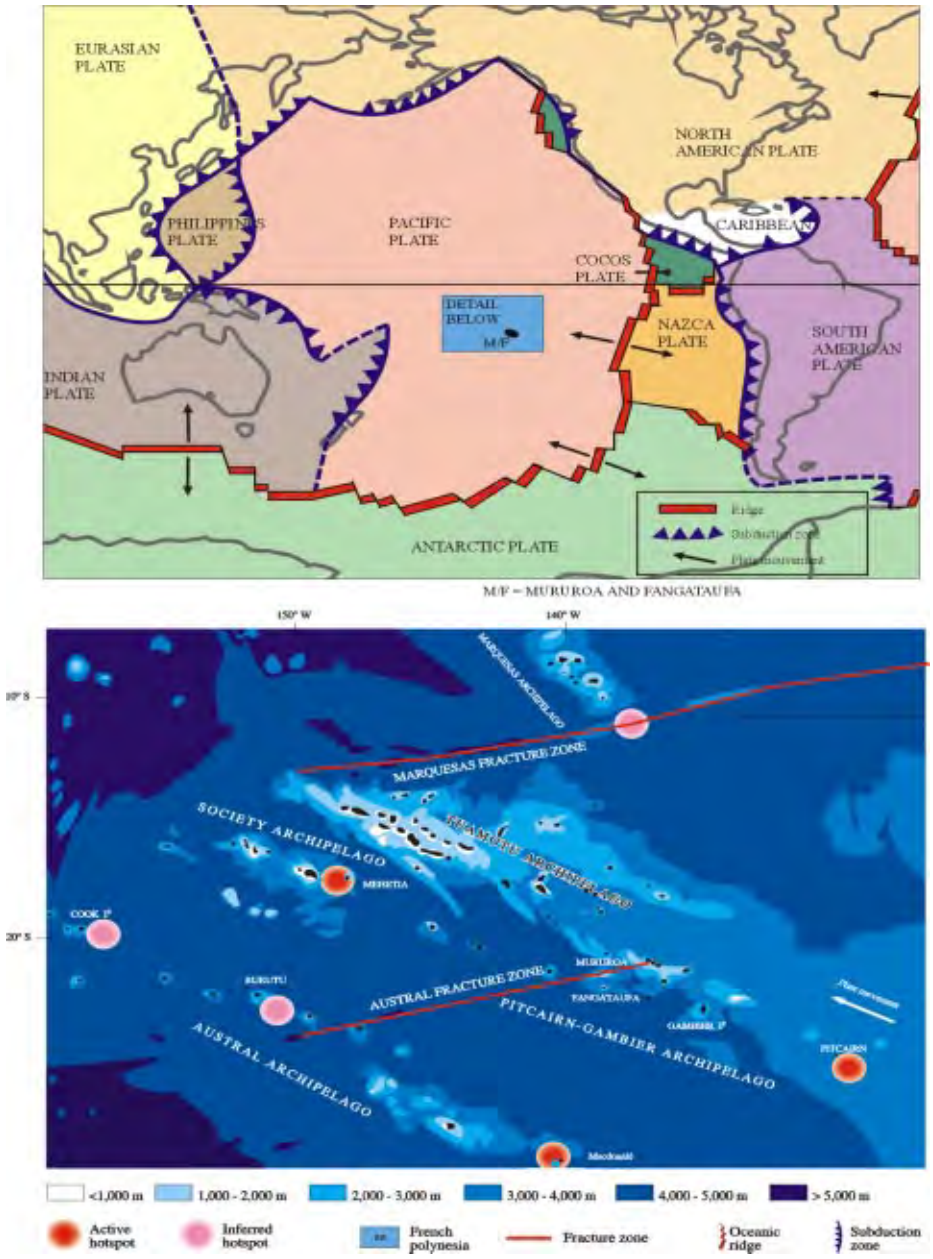

Figure 1.30 Top: Main lithospheric plates, mid-ocean ridges and subduction zones surrounding the Pacific Ocean — Bottom: Detail from top diagram showing alignment of island chains, fracture zones and location of identified and inferred hotspots near Mururoa and Fangataufa (Guille et al. 1996)

> *of Polynesia] 100 km away as the compression wave passes are less than 20 micrometres [0.02 mm], and are therefore completely imperceptible to people. For the same case of a 100 kilotonne explosion, the ground moves by no more than a few tenths of a micrometre at Papeete (Tahiti) more than 1200 km from Mururoa.* (Bouchez and Lecomte (1996), p. 96)

Local natural activities (winds, sea waves and swells, etc.) and industrial activities of populated areas will produce dynamic ground disturbances that are locally of the same order or larger than these remote effects of the explosions, which cannot be detected except by sensitive seismographs located in regions of low background noise. It is thus not credible that explosions at the PTC can influence earthquake activity thousands of kilometres from the tests.

A discussion of seismic estimates of the yield and location of individual tests at the PTC is given in Appendix C.

1.16 Monitoring of Atoll Stability

As discussed earlier in this chapter, underground explosions on the atolls have resulted in several substantial structural effects, including

1. In the Volcanics

   - a rubble-filled cavity chimney, around each explosion

     Most of these cavity-chimneys are contained within the volcanics, but 12 early tests, the so-called "CRTV tests" (Category 3; see App. C) produced a chimney that penetrated into the bottom section of the carbonates above the volcanics. Although these twelve tests resulted in some early release of radionuclides (see App. S), none of the explosion cavities represents any threat to structural stability, either locally above the cavity, or on the atoll scale (see App. H).

2. In the Carbonates

   - surface settlements, up to 2 m in places, of the exposed reef of Mururoa (see Fig. 1.23)

     Although these are considered by the IGC to be intimately associated with ocean slope deformations, the settlements do not represent a stability hazard.

   - slope collapses of the carbonates on the southwestern rim of Mururoa, during the period 1976-79

Subsequent underground tests on Mururoa have been conducted predominantly in the lagoon. There has been, apparently, no significant microseismic activity in the southwestern region since tests were moved to the lagoon. This strongly suggests that further structural effects of past testing on the southwestern flanks of the atoll are very unlikely.

- continuing slope deformations on the northeastern rim of Mururoa

  The volume of rock involved in these deformations (0.6 km^3) is approximately six times as large as that involved in the Tydée collapse, which produced a 3-m-high hydraulic wave that inundated a considerable part of Mururoa (DIRCEN/CEA Document No. 7, Section V.3) and covered the airstrip at Fangataufa, 45 km away.

  There is justifiable concern that simultaneous collapse of this volume of ocean slope could produce a hydraulic wave of the order of 6–8 m high in the immediate vicinity of the collapse (DIRCEN/CEA Document No. 12, Part 1), which could affect the nearest inhabited island of Tureia, some 110 km to the north of Mururoa. Tureia has an elevation of the order of 5 m above sea level.

  The slope region undergoing deformation consists of several somewhat distinct regions, and it seems unlikely that the entire volume would collapse at the same time (see Fig. 5.5). There is also evidence that the deformations have been decreasing in rate for several years, and hence may stabilise without any major collapse.

  Given the uncertainty and the potentially severe effects, it is prudent to monitor this region for a period of years into the future. The monitoring system proposed by CEA/DASE is briefly outlined below.

  The geology of the northeastern rim of Fangataufa, in the region between Empereur-Fox (see frontispiece and DIRCEN/CEA Document No. 7, Fig. 47), was also subject to creeping deformations and surface fracturing, stimulated by testing in the Fangataufa lagoon in the period 1988-91. According to CEA scientists, microseismic activity and fracture development declined after 1991 and ceased in 1993. The activity did not recur during the final tests in the Fangataufa lagoon in 1995/96. Thus, further monitoring of the Fangataufa slopes is not planned (DIRCEN/CEA Document No.12, Part 1).

1.16.1 Proposed Monitoring of the Northeastern Slope of Mururoa

Cessation of testing on Mururoa and Fangataufa has been followed by a programme of activities intended to restore, so far as possible, the surface environment to the natural condition prior to testing. Many of the structures associated with the tests have been removed and personnel reduced to a minimum. Future access will be strictly limited.

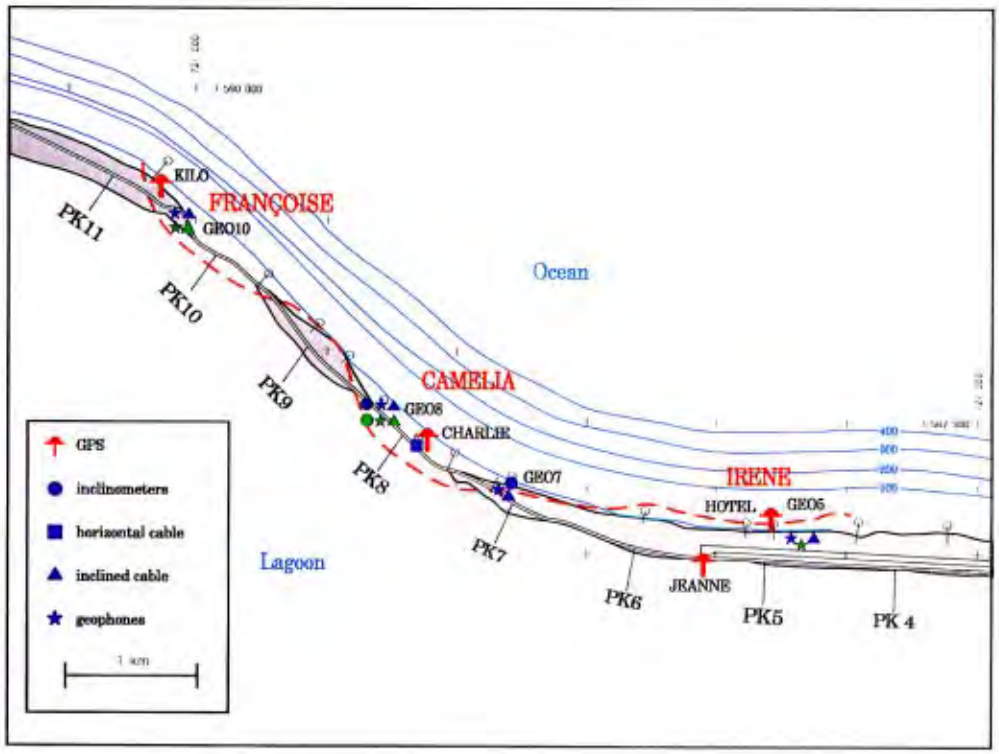

Figure 1.31 Monitoring system in the northern rim zone of Mururoa: plan view (after DIRCEN/CEA Document No. 7)

Fortunately, recent developments in remote sensing allow monitoring instruments on the atoll to be read and interpreted remotely — i.e. it is possible to develop a monitoring programme that requires minimal intrusion into the natural environment. The programme outlined by DIRCEN/CEA scientists will rely heavily on remote sensing.

The proposed instrumentation system, shown schematically in Figures 1.31 and 1.32 is essentially similar, although updated, to that in use since 1980 (see Fig. 5.6). The data acquired over the past 18 years have allowed CEA scientists to develop a very good understanding of the operative mechanics and rates of deformation of the deforming mass. This can serve as a valuable guide for predicting the future behaviour of the mass and establishing safety guidelines to ensure that any future instability does not result in a safety risk to personnel on Mururoa or anyone else in the region, including inhabitants of Tureia. (The probability of any serious wave consequences 110 km distant from Mururoa should be small — less than natural events in the region, such as storms and tsunamis.).

It is also characteristic of progressive creep-like (i.e. time-dependent) deformations of large rock slopes that collapse is preceded by a period of *accelerating creep* that

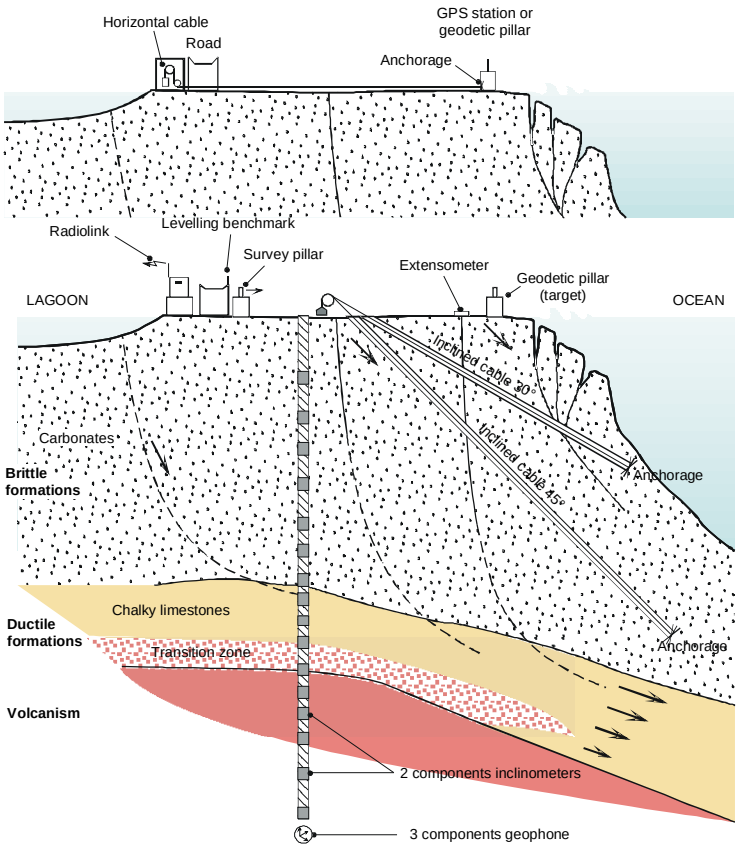

Figure 1.32 Monitoring system in the northern rim zone of Mururoa: sectional view (after DIRCEN/CEA Document No. 7)

can be detected readily by instrumentation such as that now installed at Mururoa. This system is now very comprehensive and includes sufficient redundancy to ensure adequate monitoring even in the event of failure or malfunction of some components.

The procedure to be followed to alert personnel of the risk of an impending collapse is based on the relative rate of current deformation measured by the horizontal cable extensometer (see upper diagram in Fig. 1.32; see also Fig. 5.8) and the inclined borehole extensometers (see the lower diagram in Fig. 1.32; see also Fig. 5.9), using the pre-1985 rate as the standard.

As noted in DIRCEN/CEA Document No. 12, the relative deformation rate, currently referred to as the VR [Vitesse Relative] is then translated into a risk level which is defined in terms of the anticipated delay before an (impending) major collapse. The definitions of these risk levels and delay times (i.e. before collapse) are shown below.

Table 1.1 Techniques used to monitor "normal" (expected) geomechanical evolution of the atolls

Technique	Immediate Risk	Delayed Risk	Type of Measurement	Regions Involved	Normal Frequency
Micro-Seismic Network seismographs & geophones	X	X	permanent	Mururoa	continuous measurement
Surface Topographic Network monitored by GPS spatial geodetic system		X	permanent	North Mururoa	daily
Extensometer Network		X	permanent	North Mururoa	daily
Inclinometer Network		X	permanent	North Mururoa	daily
Surface Geomorphology from satellite imaging		X	occasional	Mururoa & Fangataufa	annually
Atoll Topography from GPS survey		X	occasional	N & SE Mururoa	once every 3–5 years
Regional Geodetic Surveys		X	occasional	S. Tuamotu atolls	once every 3–5 years
Aerial Photography & Ground Surveys for surface fracturing		X	occasional	coral rim of Mururoa & Fangataufa	once every 5 years
SAR (Système Acoustique Remorqué) (towed acoustic system) for surface deformation		X	occasional	coral rim of Mururoa & Fangataufa	once every 5 years
Bathymetric & Lateral Sonar near-surface (30–300 m) underwater fracture monitoring		X	occasional	N & SE Mururoa	once every 5–10 years
Deep Underwater Geomorphology Survey (multi-sound and high resolution seismicity) by bathymetry		X	occasional	Flanks of Mururoa & Fangataufa	once every 10 years

Level 0	$VR < 2$	Normal situation
Level 1	$2 < VR < 7$	possibly transient (reversible situation); no immediate risk
Level 2	$6 < VR < 12$	possibly transient situation
Level 3	$VR > 12$	definitely leading to collapse; collapse in not less than one day

Although focused on the northeastern slope, the monitoring system will include components that will verify periodically the situation in other parts of the atoll. The system is considered to involve two parts: one, a routine, continuous system; the other, a complementary system to be introduced when an abnormal situation is detected. The two systems are summarised in Tables 1.1 and 1.2.

Any indication of risk will be communicated rapidly to personnel on site. Details of the procedures to be followed for alerting personnel, repair and updating of the system, etc. are provided in DIRCEN/CEA Document No. 12.

Table 1.2 Possible actions and complementary measures in the event of some unexpected development

Technique	Type of Intervention	Region of Concern	Frequency
Visual & photographic observation of the rim by aerial reconnaissance	occasional	Mururoa & Fangataufa	as needed
Mapping of the emerged zone by satellite imagery	occasional	Mururoa & Fangataufa	as needed
Complementary survey of surface topography	occasional	variable	as needed
Quantitative measurement of surface fracturing by radar SAR (towed acoustic system)	occasional	rim of Mururoa & Fangataufa	as needed

The current plan considers a 10-year period of monitoring. At the end of this period, a decision will be made as to whether or not the system should be continued. If continuation is considered necessary, then the system will be upgraded to include the improved instrumentation, monitoring and telemetering technology available at that time.

The IGC considers the system described in DIRCEN/CEA Document No. 12 to be well designed, using state-of-the-art technology, and sufficiently comprehensive to provide for the safety of all persons likely to be affected by a slope collapse, especially on the northeastern rim of Mururoa.

1.16.2 Proposed Monitoring for Fangataufa

DIRCEN/CEA Document No. 12 notes that observation of the northeastern rim of Fangataufa was terminated in 1996. IGC acknowledges that the volume of rock involved in slope deformation and fracturing on Fangataufa appears to be smaller than in Mururoa, and to have stabilised. However, it would be reassuring to make visual checks of the surface fracturing in the region (e.g. once every two years) to establish that no additional movements have in fact occurred. Alternatively, more details could be provided of the evidence on which DIRCEN/CEA scientists conclude that the situation on Fangataufa is stable.

Chapter 2

GEOLOGICAL AND GEOMECHANICAL SETTING

2.1 Introduction

French Polynesia covers an area in the South Pacific that extends some 2300 km from north to south and 2700 km from east to west. Its total land mass of 4000 km^2 occurs in five linear, sub-parallel chains of volcanic islands and atolls having generally NW-SE trends. Mururoa and Fangataufa atolls form part of the Tuamotu archipelago in the southeastern sector of French Polynesia (Fig. 2.1). Mururoa is located at 21°50'S, 138°53'W and Fangataufa at 22°14'S, 138°45'W. The atolls are approximately 1200 km from Tahiti.

Since the early 1960s, the geology of the two atolls has been studied extensively by geological and geophysical surveys, by a large number of deep vertical and deviated boreholes, by submarine observations made from remotely operated submersible vehi-

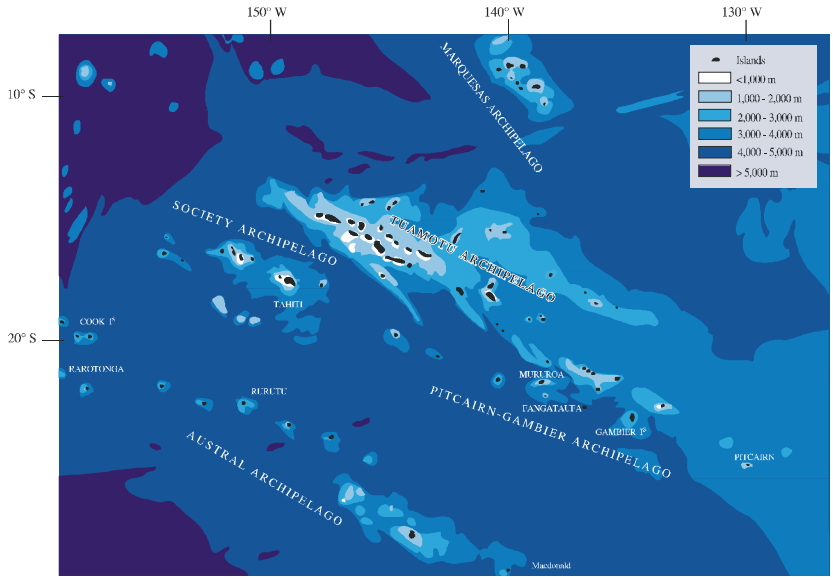

Figure 2.1 The islands of French Polynesia showing the ocean floor bathymetry (Guille et al. 1996)

cles, and by a range of laboratory tests and other studies. This chapter presents a synthesis of the geological and geomechanical setting in which the underground nuclear tests at Mururoa and Fangataufa were carried out. It draws heavily on a series of published papers and reports prepared in the main by geoscientists from the Direction des Centres d'Experimentations Nucléaires/Commissariat à l'Energie Atomique (DIRCEN/CEA), notably Buigues (1996), Buigues (1997), Buigues et al. (1992) and Guille et al. (1996), a number of unpublished sources, and observations made by Commission members. More specifically, use was made of the following sources:

- the published literature;
- published and unpublished reports of the DIRCEN/CEA;
- unpublished theses;
- logs of a number of boreholes;
- inspection and logging of borehole cores by Commission members;
- the reports of earlier commissions;
- published and unpublished test results and monitoring data provided by DIRCEN/CEA officers; and
- observations made by Commission members during site visits in July and December 1996.

2.2 Seamount and Atoll Formation

2.2.1 Plate Tectonics

The widely accepted model of Pacific atoll formation involves several stages, as illustrated in Figure 2.2. It invokes a number of concepts of modern geoscience, beginning with plate tectonics (Wegener 1924; Wilson 1970). This brief account of the model is a summary of those given by Buigues et al. (1992) and Guille et al. (1996).

The islands of French Polynesia sit on the Pacific plate which originates at the East Pacific Rise (Winterer 1973). The plate moves in direction N295° at about 11 cm/year toward the deep trenches of the western rim of the Pacific (Duncan and McDougall 1976), where it plunges under the Eurasian plate about 120 million years after its accretion at the East Pacific Rise. The relative motion of the two plates in the subduction zone triggers high-intensity earthquakes. In addition, some of the subducted material melts. Because the resulting magma is less dense than the upper mantle, it rises to the surface through zones of weakness in the crust to form a series of volcanoes located near ocean trenches.

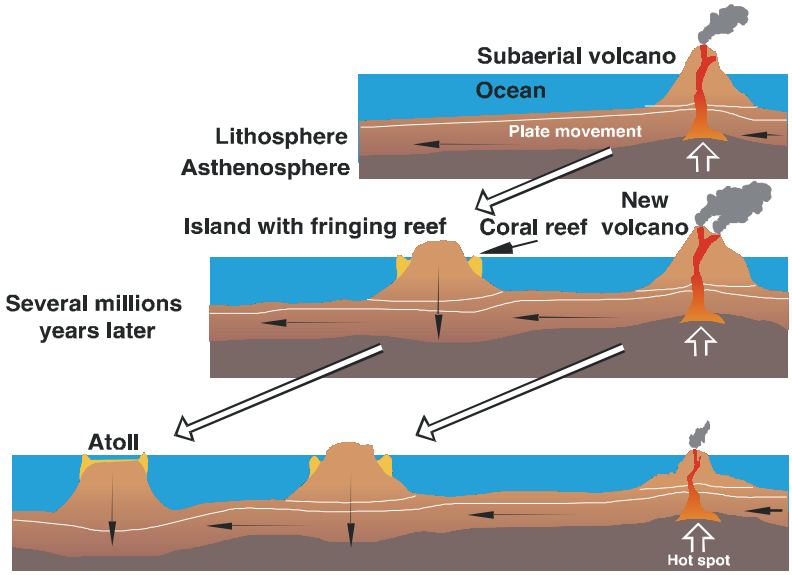

Figure 2.2 Stages in atoll formation (Guille et al. 1996)

Thus, the plate tectonics theory can explain the volcanic and seismic phenomena that occur around the Pacific Ocean and along the mid-ocean ridges. However, it alone cannot account for the several chains of islands and seamounts located on the Pacific plate. Indeed, dating carried out on the volcanic rocks forming these islands and underlying the atolls show that they are considerably younger than the oceanic crust on which they sit (Gillot et al. 1992). This suggests that they were formed in a within-plate setting away from the mid-ocean ridge at which the plate itself is formed.

2.2.2 Volcanic Activity

Wilson (1963) proposed an explanation of the formation of volcanic alignments of the Hawaiian island chain, which has become known as the "hotspot" model. It is believed that Mururoa and Fangataufa atolls were derived from a hotspot now located about 70 km to the southeast of Pitcairn Island (Gillot et al. 1992).

In the hotspot model, magma is generated from a fixed source of heat in the upper mantle beneath a drifting plate. Morgan (1971) suggests that hotspots are zones of significant thermal anomaly reflecting the influence of ascending mantle plumes that are believed to originate at the core-mantle boundary at a depth of 2900 km. The magma produced in this manner has a lower density than the surrounding mantle and so rises through zones of weakness in the crust to build up a volcano on the ocean floor. As the lithospheric plate moves over the underlying asthenosphere (Fig. 2.2), the volcano gradually drifts away from the hotspot and becomes extinct. If the hotspot activity con-

tinues, new volcanic islands are built up. If the velocity and direction of plate drift are unchanged over a long period of time, all of the islands will be aligned parallel to the direction of plate movement, with the oldest island being the furthest from the hotspot.

The development of volcanic structures, such as those now seen in Tahiti and those on which the atolls rest, requires the production of several thousands of cubic kilometres of lava. Their growth, at first underwater and then above sea level (Fig. 2.2), is necessarily rapid because only about two million years are available before the volcano drifts away from the magma source. It has been determined that the volcanic bedrocks at Mururoa and Fangataufa were formed 10.6–11.8 and 9.6–11.5 million years ago, respectively (Gillot et al. 1992; Guillou et al. 1993).

Most of the islands of French Polynesia exhibit a SE-NW orientation corresponding to the direction of drift of the Pacific plate. Mururoa atoll and its underlying seamount, however, clearly follow a N80° trend (Fig. 2.3). This is the dominant orientation of the Austral Fracture Zone. It is now believed that this fracture zone played a major role in the development of Mururoa, accounting for the atypical morphology of its volcanic seamount (Buigues et al. 1992). At Fangataufa, only 40 km away, the influence of this fracture zone is no longer apparent. The star-shaped morphology of this atoll (Fig. 2.4) reflects the eruption of lavas along rift zones that follow the main tectonic trends in the South Pacific (N170°, N80° and N115°).

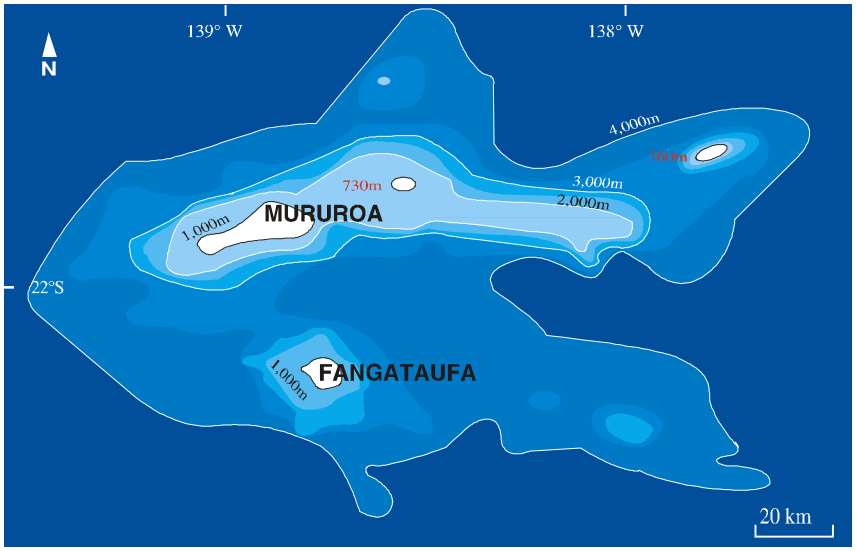

Figure 2.3 Bathymetric contours around Mururoa and Fangataufa atolls showing Mururoa as part of a 130-km-long submarine volcanic range oriented at N80°(Guille et al. 1996)

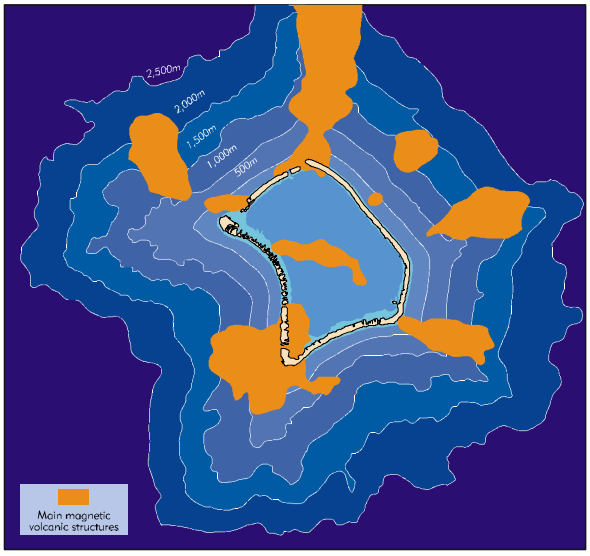

Figure 2.4 Bathymetric contours and the main submarine volcanic structures around Fangataufa (Guille et al. 1996)

2.2.3 From Volcano to Atoll

Once the aerial volcanic eruptions cease, the upper parts of the volcanic island are gradually destroyed by the effects of erosion. Subsidence of the island is associated with the increasing density of the underlying lithosphere during cooling as it moves away from the hotspot. In the Pacific, the rate of subsidence generally varies from 1.5 to 2.5 mm per year for recent islands down to a tenth of this amount for older islands (Guille et al. 1996).

Toward the end of volcanic activity, reef-forming organisms (mainly corals and calcareous algae) thrive around the shores of the volcanic island and build up a structure by the accretion and cementation of the fixed organisms, skeletal debris and finer-grained detrital material. During the early stages, it is the growth of organisms able to secrete a rigid skeleton that contributes most to reef construction. Corals are the most prolific of these reef builders. However, the bulk of the reef is made up of the products of biological disaggregation of living organisms, as well as the products of the mechanical erosion of skeletals under the action of sea swell, storms and cyclones (Buigues 1985; Buigues 1997).

Reef-building corals have to maintain themselves close to sea level (from 0 to 40–60 m) in order to proliferate. Reef growth is also influenced by water temperature, salinity, turbulence and turbidity and light (Hopley 1982). Thus, the coral can build up vertically only if the rate of subsidence of the island relative to sea level is similar to the rate required for coral growth. However, an additional factor has influenced reef development

in recent geological history. Several periods of glaciation (ice ages), especially during the Pleistocene (from 1.8 million years ago), have caused a series of sea level falls that have outpaced the rate of tectonic subsidence. The last period of glaciation (between 120 000 and 18 000 years ago) brought about a fall in sea level of approximately 120 m, which led to an average emergence rate of 1 to 1.5 mm per year for the edifice as a whole (Guille et al. 1996).

The fall in sea level is not continuous with time. During some periods when the sea level remains constant, terraced fringing reefs form around the emerging islands. During warmer periods, the rate of sea level rise is added to the subsidence rate, causing accelerated submergence and coral growth. The warmer climate that followed the last ice age caused the sea level to rise by about 10 mm/year between 12 000 and 3000 years ago. As is explained in Section 2.3.2 below, the geologies of both Mururoa and Fangataufa atolls show the effects of these sea-level variations in the form of sedimentary discontinuities and diagenetic fabrics, including karstification (Buigues 1996).

Further erosion of the volcanic edifice takes place during these periods of sea level change and reef building. The well-known atoll shape with its coral rim (Figs. 2.2 and 2.4) represents the final phase in the morphological evolution of volcanic islands. Darwin (1842) first suggested that atolls were built up on former volcanic islands submerged under the effect of their own weights and that coral growth at and just below sea level kept pace with subsidence. The first boreholes drilled deep into Pacific atolls (Emery et al. 1954; Ladd et al. 1953), as well as those at Mururoa and Fangataufa, have confirmed the general elements of Darwin's theory. The origin of atoll lagoons is still under investigation but is attributed partly to the erosive action of rainwater on the reef core during periods of reef emergence (Guille et al. 1996).

2.3 General Geology

2.3.1 Overview

The geologies of Mururoa and Fangataufa atolls and their underlying seamounts have been studied intensively over the past thirty years. In general terms, the geology is quite simple. Figure 2.5 shows the lithological sequences encountered in three deep boreholes at Mururoa, while Figure 2.6 shows a general geological cross-section of the atoll. Similarly, Figures 2.7 and 2.8 show typical lithologies encountered in boreholes and a general geological cross-section for Fangataufa. In both cases, the geological series consist of submarine and subaerial volcanics, transitional formations, and carbonates consisting of dolomites and limestones. The origins and natures of the various geological units at each atoll are outlined in Section 2.3.2, which is based on the accounts of Guille et al. (1996) and Buigues (1997).

Seismic reflection and borehole data have enabled the depths to the top of the volcanic basement to be determined. As shown in Figure 2.6, the greatest depth to the volcanic

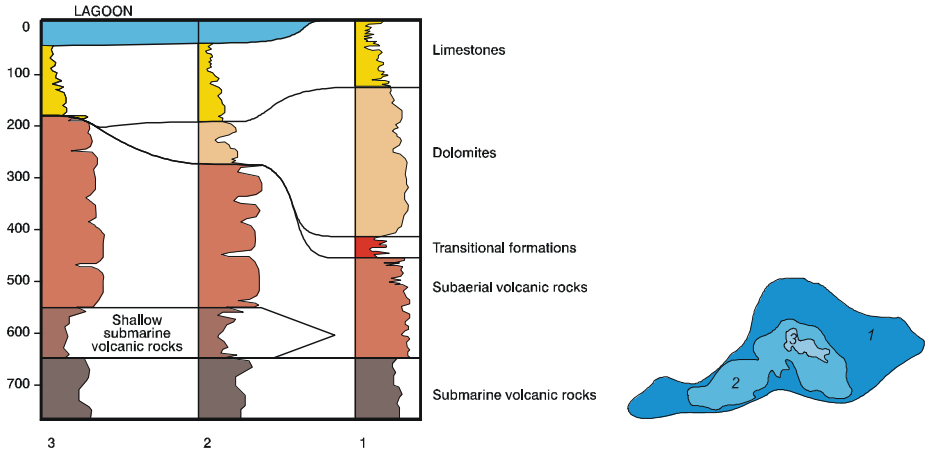

Figure 2.5 Typical lithological sequences encountered in three boreholes at Mururoa (Guille et al. 1996)

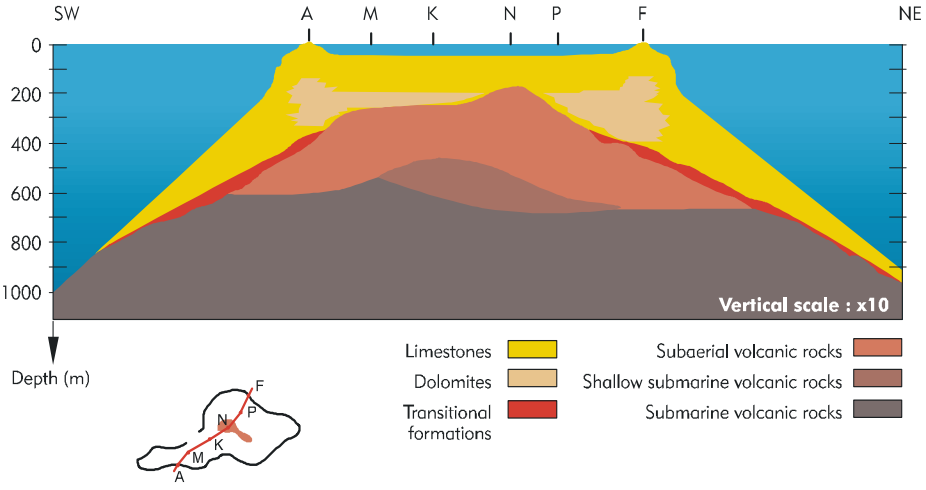

Figure 2.6 Geological cross-section of Mururoa (Guille et al. 1996)

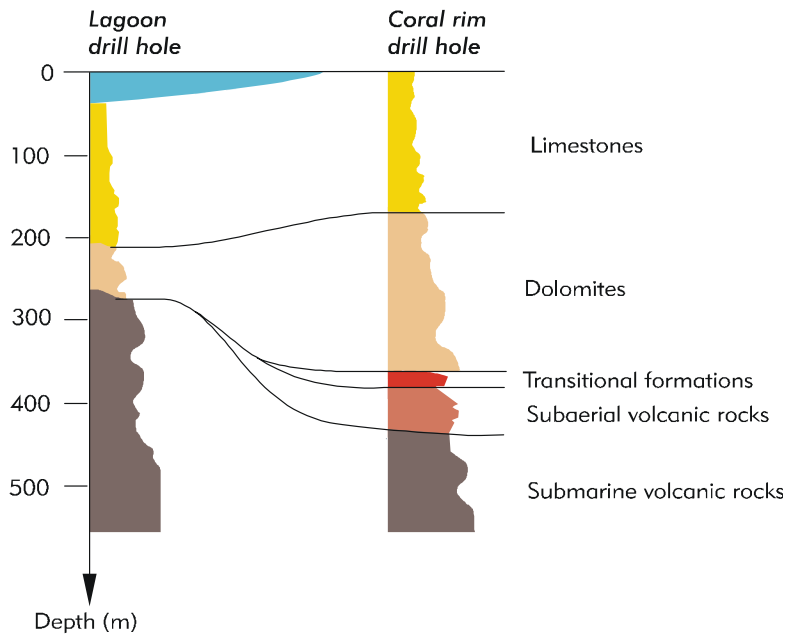

Figure 2.7 Typical lithological sequences encountered in boreholes drilled under the coral rim and under the lagoon at Fangataufa (Guille et al. 1996)

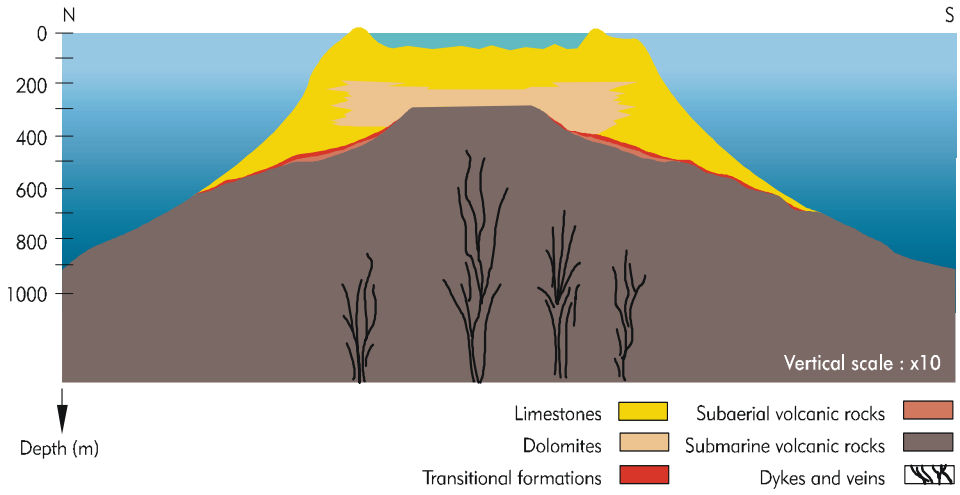

Figure 2.8 Sketch of geological cross-section of Fangataufa (Guille et al. 1996)

basement at Mururoa occurs on the flanks of the edifice outside the atoll rim. Under the atoll rim, the basement reaches a depth of more than 500 m. It is deeper in the north and at the eastern and western ends than it is in the south. The volcanics rise to a depth of 170 m under the centre of Mururoa. Under the lagoon, the strata dip at only 2–3° in the carbonates and at less than 10° in the volcanics. However, the dip is more pronounced near the atoll flanks, where it varies from 15° to 25° near the top of the volcanics (Guille et al. 1996). At Fangataufa, the summit of the volcanic pile occurs at a depth of about 270 m under a large part of the lagoon and at depths of 350-400 m beneath the coral rim (Fig. 2.8).

2.3.2 Geological Units

Submarine Volcanic Rocks — The submarine volcanic basements of both atolls, penetrated by drilling to depths of 1100 m below sea level (mbsl), consist of pillow-lavas and associated breccias, autoclastites and hyaloclastites. The base of the submarine volcano is built up from highly fluid (effusive) lava flows that spread very rapidly over a gently sloping surface to form tabular units. The effusive lavas observed in core samples show all the various stages of fragmentation, from thick flows of massive lava to highly brecciated flows. Subsequently, lava erupts in the form of pillow-shaped flows. The volcanic ejecta are characterised by intense fragmentation produced by thermal shock. In some locations, the finely brecciated volcanics (hyaloclastites) mark the transition from the submarine to the subaerial series.

The volcanic sequence at Mururoa constitutes a typical moderated alkaline series with a range of products, including basalts and trachytes. At Fangataufa, the geochemistry of the volcanic rocks is different; the submarine basalts are mainly tholeiitic (Guillou et al. 1990). Moreover, the occurrence of differentiated products is rare at Fangataufa. At both atolls, the volcanic rocks are affected by early stages of hydrothermal alteration caused by basalt-seawater interaction. The effect is more pronounced at Fangataufa (Dudoignon et al. 1992).

As a result of the methods of deposition and subsequent alteration, the submarine volcanics show two general types of structure: breccia of variable particle size in a clay matrix that may reach 80% of the total composition, or more massive fine-grained rock with a clay matrix of not more than 20% by volume.

Subaerial Volcanics — Between the submarine and subaerial volcanics there may be a transition zone characterised by two distinct facies: a sedimentary layer only a few metres thick, of calcareous, argillaceous or volcanic conglomeratic nature; and shallow submarine volcanic rocks, characterised by the presence of highly brecciated lavas.

The earliest subaerial eruptions associated with the gradual emergence of the volcano are mostly of an explosive nature. The lava comes immediately into contact with ocean water and breaks up into hyaloclastites. As soon as these hyaloclastites have built up above sea level, the magma no longer directly enters the water, and volcanic cinders

(scoriae) are formed by gas expulsion. When the height of the subaerial volcano reaches a few hundred metres above sea level, lava flows down the volcano flanks become predominant.

On Mururoa, the subaerial volcanic series is well developed beneath the central lagoon area, with a thickness exceeding 500 m, as well as throughout the southwestern sector, where they are about 400 m thick. They consist of volcanic ejecta, massive but thin lava flows, and highly vesicular lava that are all of mildly alkaline composition. The flows are of varied petrographic composition and are intercalated with red clayey layers corresponding to paleosols baked by subsequent lava flows (Guille et al. 1996).

At Fangataufa, the subaerial volcanics are alkali basalts and are present only under the rim, with thicknesses of up to 60 m. Similar rocks have been encountered at greater depths in some boreholes, but these rocks are considered to belong to intrusions (dykes and sills) emplaced during the subaerial eruptive stage.

As with the submarine volcanic rocks, the primary mineral phases at both atolls have been transformed not only by early hydrothermal activity but also by late leaching by meteoric waters (Dudoignon et al. 1989).

Transitional Formations — The discontinuous nature of the build-up of the volcanic basement is indicated by unconformities in the submarine volcanics, by erosion surfaces with argillaceous products or, more commonly, by carbonate-rich layers, particularly at Mururoa. These carbonate-rich layers suggest that the volcanic basement was colonised before the final cessation of volcanic activity. At Mururoa, carbonate-rich layers occur under both the lagoon and the rim. At Fangataufa, they occur only as coral debris deposits enclosed in volcanic rocks under the rim of the atoll (Buigues 1996; Buigues 1997).

The deepest recorded occurrence of carbonate rocks at either atoll is about 950 mbsl at Mururoa. Between the carbonate-rich layers, the volcanic sequence is 25–100 m thick. The thickest intercalated carbonate layer on the periphery of Mururoa occurs in the northern zone between 553 and 568 mbsl (Buigues 1996; Buigues 1997).

Carbonate Cap — The thickness of the sedimentary carbonate cap varies from 300–500 m at the atoll periphery and from 120–220 m at the centre. The lower portion of the carbonate cap under the rim and the lagoon of both atolls is dolomitised. Dolomite is distributed irregularly, or is absent, near the peripheries of the atolls. Under the lagoon, the top of the dolomite is located between 190 and 210 mbsl at both atolls. At Mururoa, the dolomite does not occur at the centre of the atoll above the highest volcanic peak at 170–180 mbsl (Fig. 2.6). At Fangataufa, the dolomite is distributed beneath the entire lagoon and above the flat volcanic top located close to 270 mbsl (see Fig. 2.8 from (Guille et al. 1996)).

A great diversity of sedimentary carbonate facies has been identified in drill core taken from all parts of the atolls. These include: coralgal (a mixture of corals and

coralline algae) and boundstone facies, which are typical of the reef crest; bafflestone facies, which are typical of sheltered areas; detrital deposits from various environments; and muddy facies, some typical of lagoons and some with plate-like corals typical of deep-sheltered areas (Buigues 1985; Buigues 1997). At the periphery, abundant slope deposits occur, as does pelagic infilling of karst features, which provide evidence of the submersion of a once emergent platform.

The calcareous deposits under the lagoon are generally poorly cemented. At Mururoa, they can be subdivided into three units of roughly equal thickness. The surface unit is predominantly sandy, and the intermediate unit consists of often lithified limestone interbedded with loosely cemented detrital deposits, while the lower unit contains mostly indurated beds that are commonly karstified.

On the atoll rim and, more particularly, on its flanks, the carbonate layers are cemented intensely from the surface down to 400–500 mbsl. Where present at greater depths, the carbonates are less well cemented and are highly porous. Generally, two main textures have been identified in the carbonates: a chalky and porous texture in which the original texture of primary calcite grains can still be identified and an indurated and better crystallised texture with cementation between the grains (Guille et al. 1996).

The carbonate cap contains many sedimentary unconformities, some soils and numerous karstic features that generally occur at the same depths on both atolls (Guyomard 1990). Figure 2.9 shows comparative facies and the sedimentary discontinuities, with their ages, encountered in boreholes drilled on Mururoa and Fangataufa.

2.3.3 Structural Features

Because of the way in which they were formed, the atolls do not display many of the structural features usually associated with continental rock masses. They have not been subjected to episodes of faulting, folding and metamorphosis, for example. The major structural features present are dykes and associated fracturing in the volcanics, layering in the volcanics, and sedimentary discontinuities and karstification in the carbonates. In addition, there is some jointing in the volcanics (Davies 1983) and some natural surface fracturing in the carbonates (Chevalier et al. 1968).

Faults and Dykes — A number of reports (Chauveau et al. 1967; Goguel 1982; Buigues 1982) have inferred faulting in the submarine volcanics at Mururoa mainly on the evidence of magnetic anomalies and seismic data. However, drill core taken from these areas shows that the "faults" represent dyke injections. There is no known evidence of active fault movements on the atolls for many millions of years (Davies 1983).

The eruptive production of the subaerial volcanics also implies some fracturing of the underlying submarine volcanics. This results in dykes, sills and veins being formed in the deeper volcanics. Dykes and veins at Fangataufa are illustrated in Figure 2.8. On both atolls, the dykes (faults) appear in swarms in specific areas. It is considered unlikely that they have any major geomechanical significance.

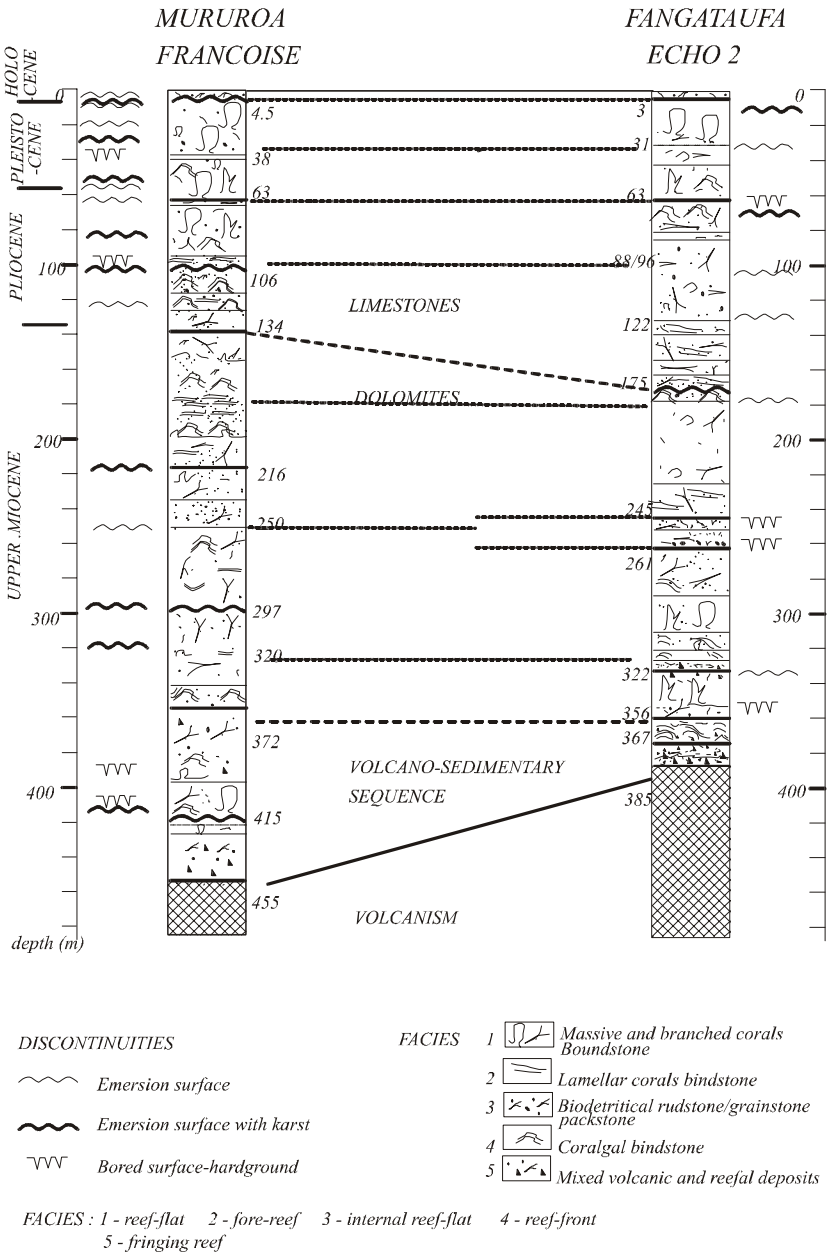

Figure 2.9 Comparative lithologies and the main sedimentary discontinuities and karst zones encountered in Mururoa and Fangataufa boreholes (Buigues 1996)

Layering in the Volcanics — Because they were formed by periodic episodes of volcanic activity, as outlined in Section 2.2.2, the volcanics are layered in a spatially variable manner. This layering is apparent in the cores obtained from deep boreholes. The thicknesses of layers in borehole cores have been measured by DIRCEN/CEA staff. Figure 2.10 shows a histogram of layer thicknesses measured for all boreholes drilled under the lagoons at Mururoa and Fangataufa. The layers were differentiated on the basis of density measurements. It is noteworthy that the most frequent layer thickness is 1 m, with a very large number of measurements at 2 and 3 m. The mean layer thickness is about 3.5 m, and the median is about 2 m. The boundaries between these layers do not necessarily represent in-situ mechanical discontinuities, nor are they always apparent to the eye. Any pre-existing or incipient sub-horizontal discontinuities are considered likely to have particular significance in chimney formation following underground nuclear blasts (see Chapter 3).

It is important to note that in about 300 deep boreholes drilled into the atolls for various purposes, no evidence has been found of the existence of the lava tubes found in other Pacific islands, including Tahiti.

Jointing and Fracturing — Reports of the earliest deep boreholes drilled at Mururoa (Chauveau et al. 1967; Deneufbourg 1967) refer to jointing in both the submarine and

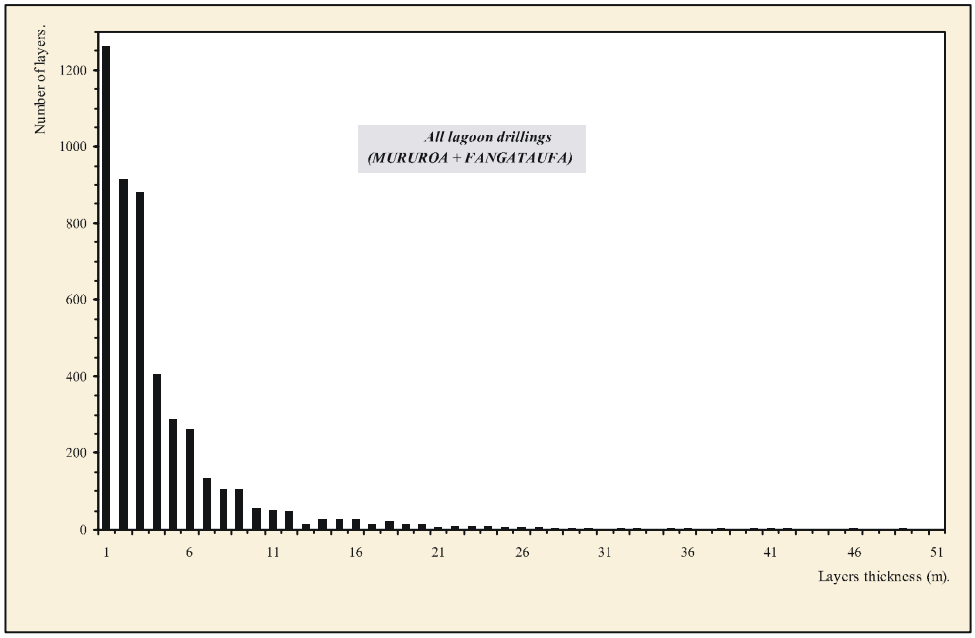

Figure 2.10 Histogram of constant density layer thickness in core recovered from beneath the lagoons at Mururoa and Fangataufa (DIRCEN/CEA Document No. 5)

subaerial volcanics. Deneufbourg (1967) reported 100% core recovery in the volcanics and referred to the joints as being filled with calcite, rust-brown clay or iron oxides. There is some doubt that zones of intense horizontal fracturing found in some core (Davies 1983) represent natural jointing; they are considered more likely to represent drilling breaks. Inspections of drill cores made by Commission members and others (e.g. (Davies 1983)) have found jointing to be often sub-vertical and, as a consequence, sparse. Some apparently healed and some open inclined joints were noted in the core taken from the Zoé borehole. These and the sub-vertical joints had rough, interlocking surfaces and occasionally had secondary minerals such as calcite on their surfaces. They appeared to have been formed as a result of cooling rather than by tectonic events.

Although it is understood that some early attempts were made to orient drill core and measure the joint orientations, no results of systematic discontinuity surveys of the type suggested by the International Society for Rock Mechanics (Brown 1981) are available. One valuable set of data provided by DIRCEN/CEA late in the study period was a set of logs of a small diameter vertical borehole drilled 3 years after the Eurytos test less than 20 m from the axis of the cemented test shaft. (The Eurytos test was carried out in the centre of the Mururoa lagoon on 19 April 1983 and had a yield in the 20–40 kt range.) The logs provided for the volcanics to the top of the chimney formed included the detailed local geology, neutron and temperature logs, permeabilities measured by pumping tests and fracture logs. Core recovery in the basalt was described as "excellent" (assumed to be close to 100%), and the mean spacing of discontinuities measured in the 250 m of volcanics above the chimney was 0.68 m. Except for vertical fractures (joints), no discontinuity orientations were given.

A number of observers, including Commission members, have noted extensive fissuring of the coral rims on both atolls. The question arises as to whether or not some of these fissures pre-date the underground nuclear tests or whether they have resulted from, or been reactivated by, the tests (Goguel 1982). There is clear evidence that many of the fractures observed at the surface and in the intertidal zone reflect surface displacements resulting from the underground tests (see Chapter 3). However, there is equally clear evidence that some fissuring pre-dates the testing.

Chevalier et al. (1968) report that, at the surface of the limestone conglomerate on the rim and in the intertidal zone at Mururoa, there are small superficial fractures either normal or parallel to the crest of the rim. They do not exceed 30–40 m in length, are occasionally offset at right angles, and are of recent origin (because they reflect the particulate structure of the reef conglomerate). Figure 2.11 shows a good example of a prominent fissure parallel to the shore in the Viviane zone.

Karstification — The presence of sedimentary unconformities and karstification on both atolls was noted in Section 2.3.2. These features, which have been studied extensively by Buigues (1982, 1985, 1996, 1997), are of potential importance to the hydrogeology of the atolls and so merit some discussion here. This account follows that of Buigues (1996). The major features described are illustrated in Figure 2.9.

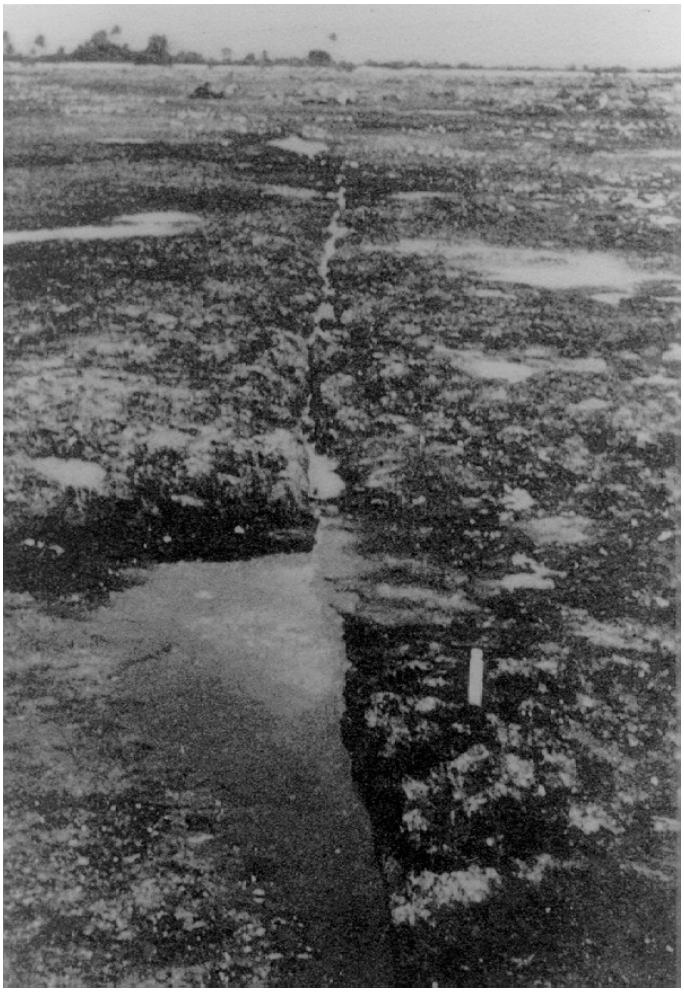

Figure 2.11 Natural longitudinal fissure in the conglomerate rim in the Viviane zone, Mururoa (Chevalier et al. 1968)

In the upper 80–100 m of the carbonate cap, karstification is more pronounced under the rim than under the lagoon; below 100 m, it occurs over the entire surface areas of both atolls. Under the rim, the first karstic surface, which is related to the Holocene/Pleistocene boundary, occurs at depths of between 6 and 10–15 m below surface. The Holocene sediments lie above a discontinuous surface of lithification marked by marine cementation.

At both atolls, important dissolutions with karstification and micritic infillings occur at depths of 90–100 m at the periphery. Karstification in the limestones extends down to a depth of 150 m under both the rim and the lagoon. Beneath both lagoons, karstification is present at the limestone-dolomite interface at 180–200 m and near the base of the dolomites at depths of 250–270 m. Beneath the rim, almost the entire sedimentary series is karstified, although some emersion surfaces occur between depths of 220 and 280 m. These surfaces correlate with sedimentary discontinuities across both atolls and are associated with changes in sea level.

At the base of the carbonate series below 310–350 m, karstification is particularly extensive in the massive dolomites. The karstic cavities are filled with successive marine sediments reflecting the complex detailed depositional histories of the carbonates.

2.4 Physical, Mechanical and Hydraulic Rock Properties

2.4.1 Scope

Just as the geology of Mururoa and Fangataufa atolls has been studied more intensively than probably any other atoll on earth, so have the properties of the volcanic and carbonate rocks forming their edifices been measured more intensively. Thousands of tests of one type or another have been carried out on core samples recovered from beneath the atolls. In-situ seismic, logging and permeability testing has also been carried out in selected boreholes (Bouchez and Lecomte 1996).

This section provides a summary of the test data available mainly in DIRCEN/ CEA reports. The data are presented and discussed under the three general headings of physical, mechanical and hydraulic properties. For this purpose, following the usual geomechanics usage, **physical properties** are taken to include properties derived from the compositions and phase relations of the rocks (e.g. densities, void ratios, water contents) and, where available, thermal properties. **Mechanical properties** are concerned with the responses of the rocks to either static or dynamic forces or stresses (e.g. elastic moduli, strengths, yield criteria, sonic-wave propagation velocities). Finally, **hydraulic properties** relate to the flow of water through the materials.

In geomechanics, it is necessary to distinguish between the rock material and the rock mass. **Rock material** is the term used to describe the intact rock between discontinuities; it might be represented by a hand specimen or a piece of drill core. The **rock mass** is the total in-situ medium containing bedding planes, joints and other structural

features. Rock masses are discontinuous and often have heterogeneous and anisotropic engineering properties (Brady and Brown 1993).

Section 2.4 is concerned only with the properties of the rock materials. Rock mass properties are considered in Section 2.5.

2.4.2 Physical Properties

Volcanics — The **water contents** (by weight) of the volcanics range from a very few percent for the freshest lava flows to 25% or even 30% for the highly altered submarine volcanics containing up to 80% clay minerals. The most common values are in the range of 10–15%, corresponding to an average **porosity** (by volume) of approximately 25%. The water contents of the subaerial volcanics are generally less than those of the submarine rocks.

The **densities** of the volcanic rocks have been determined in the laboratory and by geophysical borehole logging techniques. Table 2.1 shows the average saturated densities and longitudinal sonic velocities measured in the DIRCEN/CEA laboratories on volcanic samples taken from all depths under the rims and the lagoons of Mururoa and Fangataufa. The measured saturated densities vary between 1850 and 3150 kg/m^3. The lowest values are for ejecta from emergent volcanism (hyalotuffs); the highest are for lava flows rich in ferromagnesian minerals. In general, the subaerial volcanics are denser, with saturated densities mostly in the range 2400–2500 kg/m^3 than the submarine volcanics, for which the normal range is 2300–2350 kg/m^3 (except for the Zoé borehole). The spread of values as measured by the standard deviations is generally wider for the subaerial than for the submarine volcanics. The average values under the atoll rim are slightly lower than those under the lagoon, probably reflecting the greater presence of altered breccias with high clay contents under the rim.

The average saturated densities measured for samples taken from a band of approximately 100 m above "working points" in 55 boreholes give a mean value of 2470 $\pm$ 170 kg/m^3 for the volcanics. Measured values range from 2010 to 2870 kg/m^3, with a mode at 2350 kg/m^3. As in the case of the overall values, the densities of the submarine volcanics at Mururoa are generally lower than those of the subaerial rocks. At Fangataufa, the values lie within a narrower range, with an average of around 2550 kg/m^3, even though the volcanics rocks here are of predominantly submarine origin.

Some independent verification of the DIRCEN/CEA values is given by the results reported by Davies (1983) and shown in Table 2.2. These results were obtained at the laboratories of the then Bureau of Mineral Resources, Canberra, Australia, on four volcanic samples from Mururoa identified only by their depths. Note that the bulk densities quoted in Table 2.2 are dry densities rather than the saturated densities referred to above.

Bouchez and Lecomte (1996) report that the estimates of response of the volcanics to the blasts were determined "for a **standard material** having the average characteristics of the basaltic formations on Mururoa or Fangataufa":

Table 2.1 Laboratory measurements of saturated density and longitudinal sonic velocity for submarine and subareal volcanic rocks (after DIRCEN/CEA, Document No. 5)

BOREHOLES RIM	SUBAERIAL VOLCANICS				
	Number of measurements	Saturated density		Longitudinal velocity	
		Average kg/m^3	Standard Deviation	Average kg/m^3	Standard Deviation
FRANCOISE	346	2470	220	4405	785
QUEEN	42	2489	239	3689	735
DAHLIA	40	2760	310	4905	1115
FUCHSIA	20	2350	150	3385	905
ECHO 2	64	2380	250	4200	815
MURUROA+ FANGATAUFA RIM	TOTAL 512	WEIGHTED AVERAGE 2480		WEIGHTED AVERAGE 4330	
	SUBMARINE VOLCANICS				
	Number of measurements	Saturated density		Longitudinal velocity	
		Average kg/m^3	Standard Deviation	Average kg/m^3	Standard Deviation
FRANCOISE	120	2250	100	2475	540
QUEEN	13	2279	160	2590	480
DAHLIA	120	2310	310	3305	1230
FUCHSIA	17	2360	100	3150	615
ZOE	740	2480	130	4135	650
ECHO 2	429	2330	250	3895	430
MURUROA+ FANGATAUFA RIM	TOTAL 1439	WEIGHTED AVERAGE 2400		WEIGHTED AVERAGE 3915	

BOREHOLES LAGOON	SUBAERIAL VOLCANICS				
	Number of measurements	Saturated density		Longitudinal velocity	
		Average kg/m^3	Standard Deviation	Average m/s	Standard Deviation
LAGON 1	19	2490	400	4645	1175
NERITE 1	30	2610	270	4380	1155
	SUBMARINE VOLCANICS				
	Number of measurements	Saturated density		Longitudinal velocity	
		Average kg/m^3	Standard Deviation	Average m/s	Standard Deviation
LAGON 1	12	2230	250	2905	715

matrix density	2700	kg/m^3
mean density	2500	kg/m^3
mean porosity	12.5	%
water content (by weight)	5	%
latent heat of vaporization	2750	cal/g
latent heat of fusion	445	cal/g

Carbonates — The results of measurements of the physical properties of the carbonates are available for samples from Mururoa. As would be expected from the descriptions of these rocks given in Section 2.3.2 above, their porosities, densities and water contents vary widely, both vertically and laterally.

Largely because of the asymmetry of the central volcanic peak at Mururoa, which is offset to the south by approximately 1 km, there are differences between the properties of the carbonates to the north and those to the south of the atoll. In the north, there is a greater thickness of carbonate cover, greater thicknesses of dolomites at both the base and the top of the carbonate series and a significant deep soft chalky limestone formation near the outer slope (see Fig. 2.30). The properties of the soft chalky limestone (or chalk) have been studied extensively by Mariotti (1990) and by Mariotti and Bouchez (1989).

The limestones under the rim of Mururoa have an average **saturated density** of 2150 $\pm$ 100 kg/m^3. The average values for the dolomites are 2250 kg/m^3 in the south and 2450 kg/m^3 in the north. In the simulation of a particular test at Mururoa, DIRCEN/CEA used densities of 2200 kg/m^3 for a highly argillaceous formation separating the volcanics from the carbonates, 2300 kg/m^3 for the dolomites and 2200 kg/m^3 for the limestones.

The porosities and water contents of the carbonates can be expected to vary widely. Guille et al. (1996) indicate that the **porosity** of the deepest carbonates having a chalky and porous texture is about 40%. Mariotti (1990) and Mariotti and Bouchez (1989) measured the porosity of the chalk found between 440 and 490 mbsl in the outer northern slope as being between 37 and 45%.

In his examination of the Mururoa cores, Davies (1983) concentrated on the **transitional formations**. He estimated the porosity of the transitional zone as 20–40% in the Françoise borehole on the northern rim, with much of it around 30–40%, and 10–20% in the Lagon borehole under the lagoon, where the transitional zone consists almost entirely of detrital limestone. In general, there is no transition zone under the lagoon.

2.4.3 Mechanical Properties

Volcanics — The available data show quite clearly that the major mechanical properties of the volcanic rocks (compressive strengths, elastic moduli, longitudinal and shear wave velocities) vary with the water contents, porosities and densities of the samples on which measurements are made.

Table 2.2 Results of porosity, permeability, and density measurements on volcanic samples from Mururoa [after Davies (1983)]

Sample Depth	Effective Porosity[a]	Absolute Permeability[b] (mD)	Permeability[c] (mD)	Dry Bulk Density (kg/m^3)	Apparent Grain Density (kg/m^3)	Comments
551.7	30.1	29.5	1.9	1790	2610	whole core sample collapsed while drilling plug, but cylindrical plug remained essentially intact; minute fractures apparent in sample
601.6	1.3	0.006	–	2880	2920	cylindrical plug well-consolidated but minor traces of micro fractures and pinpoint porosity
672.3	9.5	0.005	–	2610	2890	cylindrical plug well-consolidated; main feature is a predominance of pinpoints to larger (up to 0.5 mm) porosity
811.7	20.3	6.4	1.8	2230	2800	cylindrical plug consolidated but contains a number of micro fractures around boundaries of various minerals and segments; some of the micro features are infilled

[a] % of bulk volume
[b] to Nitrogen perpendicular to core axis
[c] with respect to sea water

Figure 2.12 shows the relations between saturated density, water content, longitudinal velocity and uniaxial compressive strength* given by Bouchez and Lecomte (1996) for saturated volcanic rock taken from the same (un-named) borehole at Mururoa. Figure 2.13 shows a more detailed plot of the variation, with saturated density of longitudinal (P-wave) velocities measured by well-logging and laboratory techniques and for the volcanics from the Zoé and Françoise boreholes at Mururoa. Table 2.3 shows the variations with water content of the average saturated density (ρ_o), longitudinal or P-wave sonic velocity (V_L), shear wave velocity (V_T), shear modulus (G), bulk modulus (K), and Poisson's ratio (ν) measured in hundreds of laboratory tests on core samples of the subaerial and submarine volcanics. The results show clearly that, with the exception of Poisson's ratio, the values of these mechanical properties increase with increasing saturated density and decreasing water content (and porosity).

*Note on units: Throughout the DIRCEN/CEA documents, the bar is used as the unit of pressure and stress. In the SI system of units, the Pascal (Pa) is the correct unit of stress. 1 bar $\cong$ 100 kPa, or 1 kbar $\cong$ 100 MPa. The units used by DIRCEN/CEA will be retained here, but SI equivalents will be given as well.

Table 2.3 Average mechanical properties of volcanics at a range of water contents and saturated densities (DIRCEN/CEA Document No. 6)

Material	$\%H_2O$ in weight	ρ_0 (kg/m^3)	V_L (m/s)	V_T (m/s)	G (GPa)	K (GPa)	ν
Aerial	24	2000	2850	1396	3.9	11	0.34
Volcanic	17	2200	3470	1850	7.6	11	0.30
Formation	12	2350	3900	2000	9.4	23	0.33
	11	2400	4000	2062	19.2	25	0.32
	8	2500	4480	2060	11.0	36	0.37
	6	2600	4800	2842	21.0	32	0.23
	4	2700	5000	2962	23.7	36	0.23
	2	2800	5500	3088	26.7	49	0.27
Submarine	13	2100	2750	1510	4.7	9	0.29
Volcanic	12	2250	3510	1880	8.0	17	0.30
Formation	10	2300	3600	2000	9.2	18	0.28
	8	2360	3710	2020	9.6	20	0.29
		2500	4250	2550	16.2	23	0.22

The results presented thus far were obtained mainly from large numbers of standard laboratory characterisation and mechanical property tests using techniques such as those suggested by the ISRM (Brown 1981). In addition, more sophisticated undrained triaxial compression, hydrostatic compression and plate shock-compression tests were carried out (Bouchez and Lecomte 1996). The results available from the triaxial compression tests are generally presented as peak strength or yield envelopes on $1/2(\sigma_1 - \sigma_3)$ vs $1/2(\sigma_1 + \sigma_3)$ axes. Here, the minor principal stress$\sigma_3 (= \sigma_2)$ is the confining pressure in the triaxial compression test and the major principal stress, σ_1, is the axial stress at failure or yield. Sometimes the maximum shear stress $1/2(\sigma_1 - \sigma_3)$ is replaced by the maximum principal stress difference, often denoted by the symbol q. In some presentations of the results, $p = 1/2(\sigma_1 + \sigma_3)$, which gives the location of the centre of the Mohr's circle when the results are presented on shear stress-normal stress axes, is referred to as the mean stress. This is not strictly correct. In this case, the mean principal stress is $p = 1/3(\sigma_1 + 2\sigma_3)$.

Figures 2.14 and 2.15 show these curves for submarine and subaerial samples with a range of initial densities. As a general rule, the failure or yield stress at a given value of mean stress increases with increasing density, although there is some scatter, presumably reflecting differences in the compositions and degrees of alteration of the samples.

The values of the mechanical properties given in Table 2.3 and Figures 2.12 and 2.13 are typical of a wide range of volcanic rocks, including basalts (Lama and Vutukuri 1978;

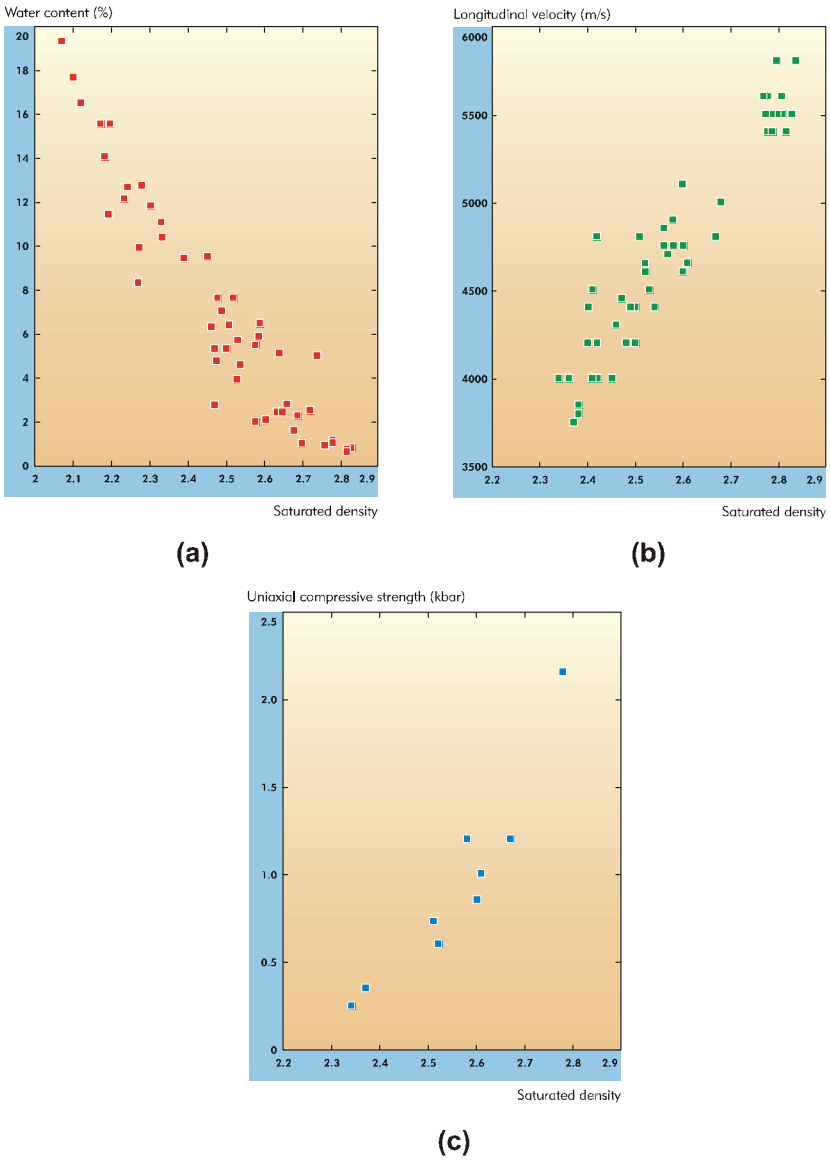

Figure 2.12 Correlations between saturated density (g/cm^3) and (a) water content, (b) longitudinal sonic velocity and (c) uniaxial compressive strength for volcanic rocks taken from the same drill core at Mururoa (Bouchez and Lecomte 1996)

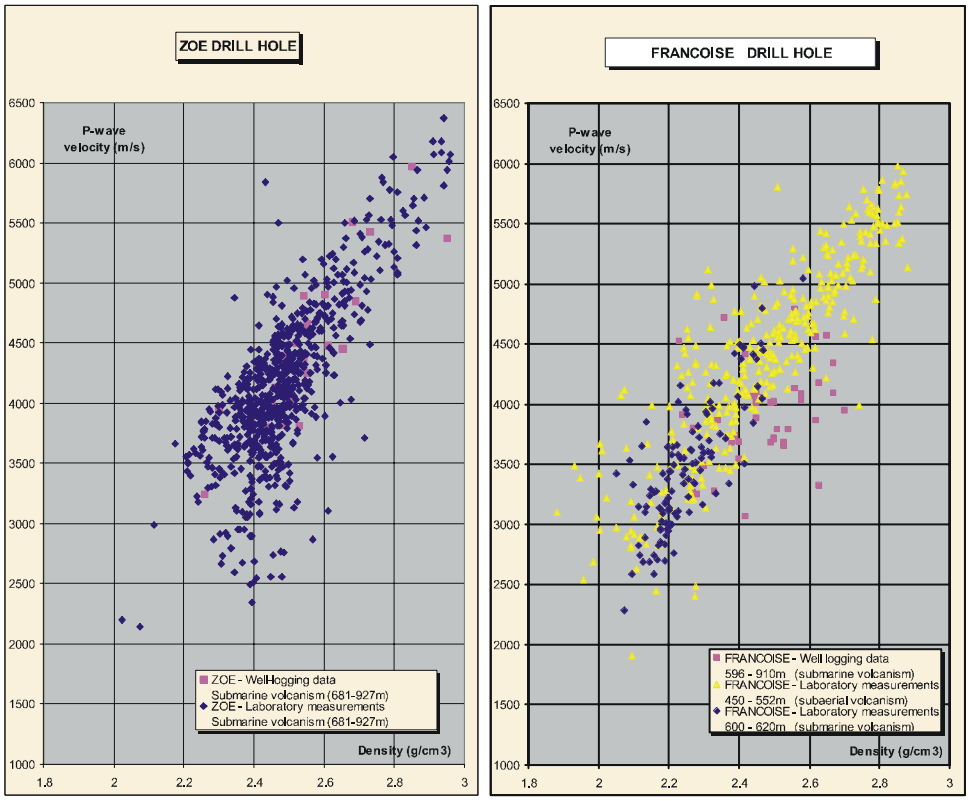

Figure 2.13 Variation of longitudinal sonic velocity with saturated density for volcanic rocks from the Zoé and Françoise boreholes (Bouchez and Lecomte 1996)

Schultz 1995; Vutukuri et al. 1974). The uniaxial compressive strength values shown in Figure 2.12 cover the wide range from approximately 20–220 MPa (0.2–2.2 kbar). These values fall within the weak to very strong categories in the classification system for the uniaxial compressive strengths of rock materials recommended by the International Society for Rock Mechanics (ISRM) (Brown 1981). The value of uniaxial compressive strength corresponding to the mean saturated density of the volcanics of 2400–2500 kg/m^3 is only about 50 MPa (0.5 kbar). This is a low value for fresh, intact igneous rocks such as basalt (Lama and Vutukuri 1978; Schultz 1995). It is important to note, however, that the basalts under the atolls have been altered by contact with sea water and show a high degree of brecciation.

Figure 2.16 shows the test data fitted by a model for saturated submarine volcanic rock with an initial saturated density of 2360 kg/m^3. The data and the curves fitted to them are in two parts: those up to a value of $(\sigma_1 + \sigma_3)/2$ of about 800 MPa (8 kbar), representing the behaviour of the "virgin" or unaltered rock, and that at higher pressures

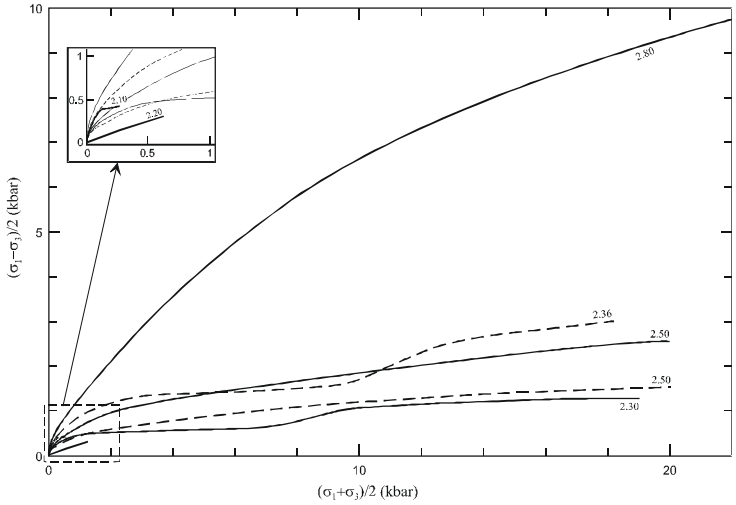

Figure 2.14 Failure curves for subaerial volcanics at various saturated densities (g/cm^3) (DIRCEN/CEA Document No. 6)

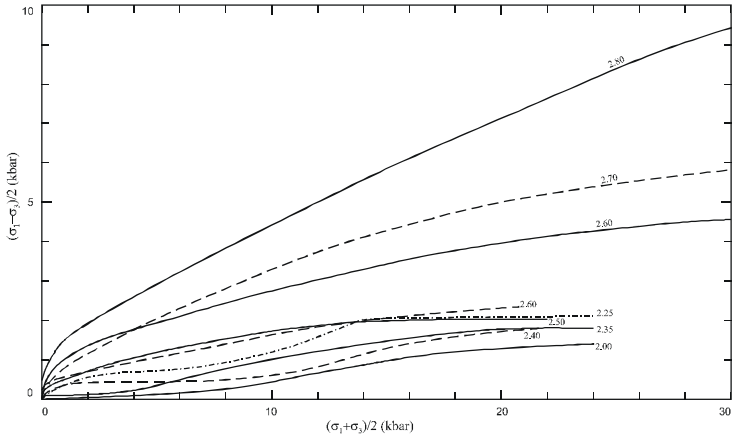

Figure 2.15 Failure curves for submarine volcanics at various saturated densities (g/cm^3) (DIRCEN/CEA Document No. 6)

which are sufficient to cause breakdown of the structure of the rock and/or phase changes in the water present. This straight-line portion of the envelope, when extrapolated back to the origin, represents the equivalent of Coulombic frictional behaviour with an angle of $\phi \cong 34°$, which is in the middle of the range given by Barton (1976) for the basic friction angle for basalt.

The peak strengths of volcanic rocks in the brittle range are well represented by a Hoek-Brown empirical strength criterion

$$\frac{\sigma_1}{q} = \frac{\sigma_3}{q} + \left(m_i \frac{\sigma_3}{q} + s \right)^{0.5} \tag{2.1}$$

where $m_i \cong 17$ and $s = 1.0$ for intact fine-grained volcanics (Hoek and Brown 1980; Hoek and Brown 1997). Analyses of data taken from the lower stress range of Figure 2.16 give a value of uniaxial compressive strength of q = 75 MPa, which is not inconsistent with the values given in Figure 2.12. It should be noted that most of the data shown in Figure 2.16 lie in the ductile rather than the brittle range of behaviour. At low values of confining pressure of less than 20 MPa, a Hoek-Brown failure envelope with q = 75 MPa, m_i = 17 and s = 1.0, gives equivalent Mohr-Coulomb shear strength parameters of c = 14 MPa and ϕ = 49°.

Relations of the type shown in Figure 2.16 are required for elasto-plastic calculations of the response of the rock mass to the blast in the inelastic region. The pressure-volume response of the rock must also be known. The required data were obtained by DIRCEN/CEA in drained, hydrostatic compression tests. Figure 2.17 shows, inter alia, the relation between confining pressure and the parameter $\mu = (\rho/\rho_0) - 1$ (where ρ is the saturated density at a given confining pressure and ρ_o is the initial saturated density) for submarine volcanic rock having an initial saturated density of 2360 kg/m^3.

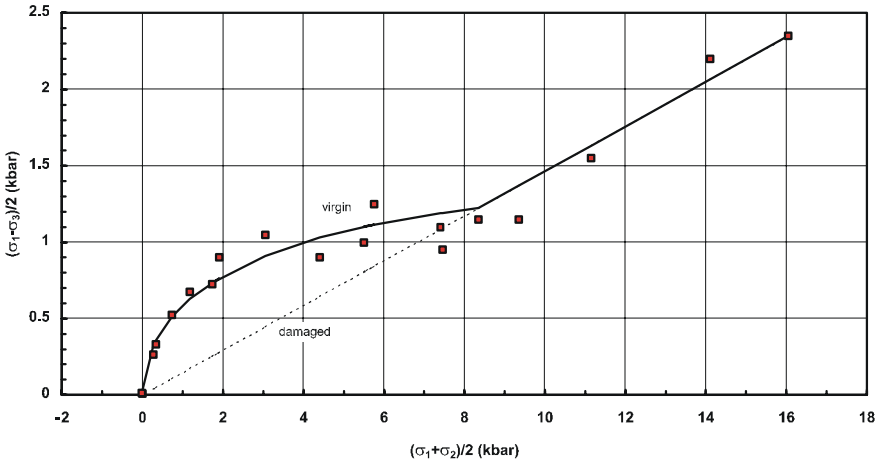

Figure 2.16 Failure curves for submarine volcanic rock with an initial saturated density of ρ_0 = 2360 kg/m^3 (DIRCEN/CEA Document No. 6)

The variability in the data available is illustrated by a comparison of the results shown in Figures 2.16 and 2.17 for undrained triaxial compression tests on submarine volcanics with an initial density of 2360 kg/m^3. Advice received from DIRCEN/CEA indicates that in Figure 2.17, pressure is given as $\frac{1}{3}(\sigma_1 + 2\sigma_3)$. On this basis, the "residual" value of friction angle for the broken material is calculated from the data as ϕ = 8°,

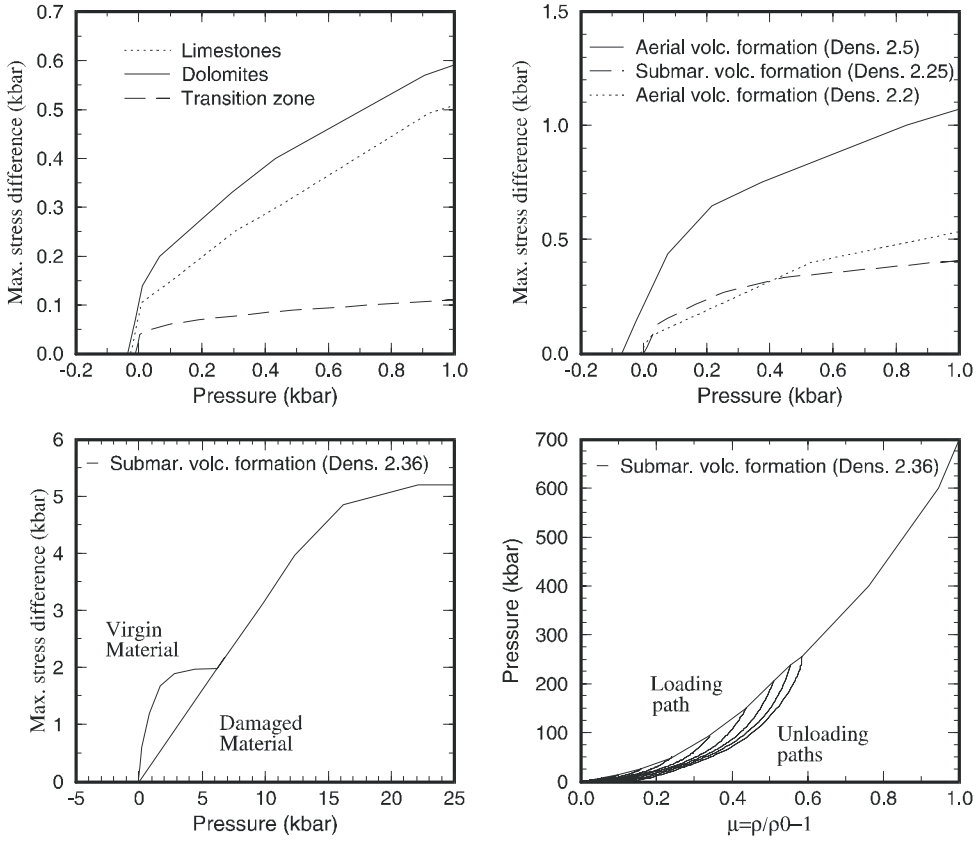

Figure 2.17 Failure curves for representative rock types used by DIRCEN/CEA in calculations (DIRCEN/CEA Document No. 6, Appendix)

compared with the more reasonable value of $\phi = 34°$ calculated from the data of Figure 2.16. The peak strength envelope for the virgin material shown in Figure 2.17 may be approximated by a bi-linear Mohr-Coulomb envelope with a cohesion and friction angle of $c = 32$ MPa and $\phi = 30°$ in the initial section and values of $c = 105$ MPa and $\phi = 13°$ in the upper section. The c- and ϕ-values for the initial section are consistent with a value of uniaxial compressive strength of $\phi_c = 110$ MPa. It is considered likely that the unusually low values of friction angle indicated by these results arise from the fact that the tests were carried out on saturated samples at very high confining pressures under undrained conditions without pore pressure measurement so that the results are presented in total stress terms. (Under these conditions, undrained tests on saturated clays give a friction angle of zero on total stress axes.)

The data described above apply only for quasi-static loading conditions. They do not describe the behaviour of the rock under the high shock-loading conditions generated

Table 2.4 Average mechanical properties of dolomites from Mururoa

Saturated Density (kg/m^3)	Water Content (%)	Tensile Strength (MPa)	Uniaxial Compressive Strength (MPa)	Young's Modulus (GPa)
1800	31	0.5–1	4–5	1.5–2.5
2000	23	1–2	8–10	2–4
2200	16	2–3	10–12	5–9
2450	8.6	4.5–6.5	40–60	12–18

immediately following the blast. In order to assist the development of an understanding of this response, planar shock-compression tests were carried out on plates of submarine and subaerial volcanic rocks subjected to extremely high impact pressures of up to 60 GPa (600 kbar). When they exceed a limiting value known as the Hugoniot elastic limit, these pressures cause material collapse by pore closure, grain crushing or plastic deformation. The relation between pressure and some measure of the density produced at that pressure (the specific volume or the ratio of the current to the initial density) is known as the Hugoniot curve or simply the Hugoniot (e.g. Chabai (1963) and Zel'dovich and Raizer (1967)).

Figure 2.18 shows the Hugoniot for volcanic rock with an initial density of 2400 kg/m^3 (Bouchez and Lecomte 1996). The values of the Hugoniot elastic limit measured in the volcanics of varying initial densities show some scatter but generally increase with increasing initial density and decreasing initial water content or porosity. The measured values are in the range 100–500 MPa (1–5 kbar). Further details of the nature and calculation of the Hugoniot curve are given in Appendix J.

Carbonates — With the exception of those of the chalky limestone studied by Mariotti (1990), the mechanical properties of the carbonates have not been studied in the same detail as those of the volcanics. Generally, the carbonates can be expected to be weaker, to have lower stiffnesses, and to exhibit plastic behaviour more readily than the volcanics.

Figure 2.17 shows the idealised failure or yield envelopes for limestones, dolomites and the transition zone rocks used by DIRCEN/CEA in numerical modelling.

Table 2.4 shows the ranges of the average mechanical properties of the dolomites from Mururoa measured at a range of saturated densities and water contents. As would be expected, the tensile and compressive strengths and Young's moduli increase with increasing density and decreasing water content. The measured uniaxial compressive strengths of 4–60 MPa (40–600 bar) are in the range classified as weak-to-strong according to the classification system recommended by the ISRM (Brown 1981) and are typical of carbonate rocks (Vutukuri et al. 1974; Hoek and Brown 1980).

Undrained triaxial compression tests were carried out on dolomites with the range of saturated densities shown in Table 2.4. Figure 2.19 shows the differential axial stress

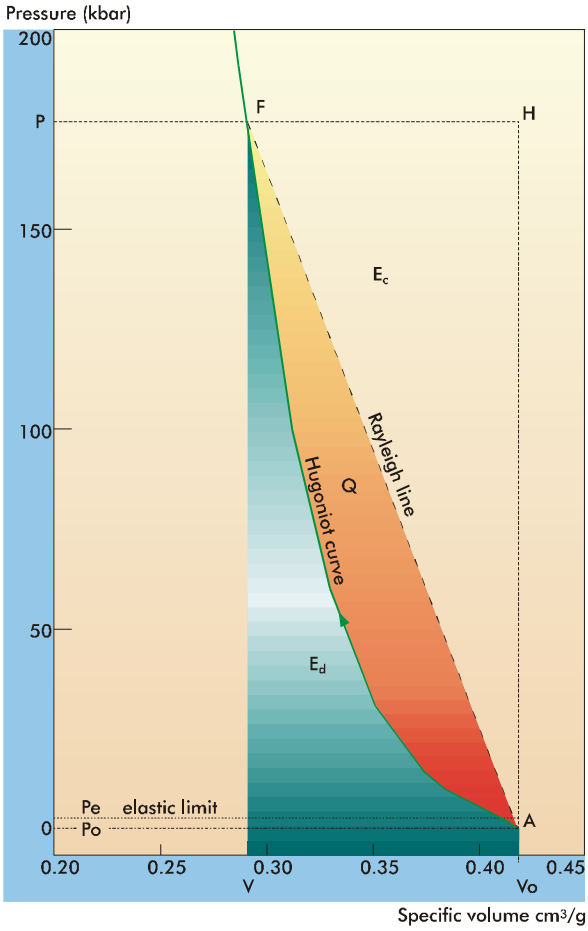

Figure 2.18 Hugoniot curve for volcanic rock with an initial density of 2400 kg/m^3 (Bouchez and Lecomte 1996)

($\sigma_1 - \sigma_3$) vs axial strain curves recorded in a uniaxial compression test and in triaxial compression tests carried out at confining pressures of σ_3 = 100 MPa (1 kbar) and 400 MPa (4 kbar) on dolomites having an initial saturated density of 2200 kg/m^3. Note that these confining pressures are very high by normal geomechanics standards. These stress-strain curves indicate strain-hardening plastic deformation of the dolomite at both confining pressures used. Even for the densest dolomite tested (that with ρ_o = 2450 kg/m^3), strain-hardening behaviour occurs at a confining pressure of 50 MPa (0.5 kbar).

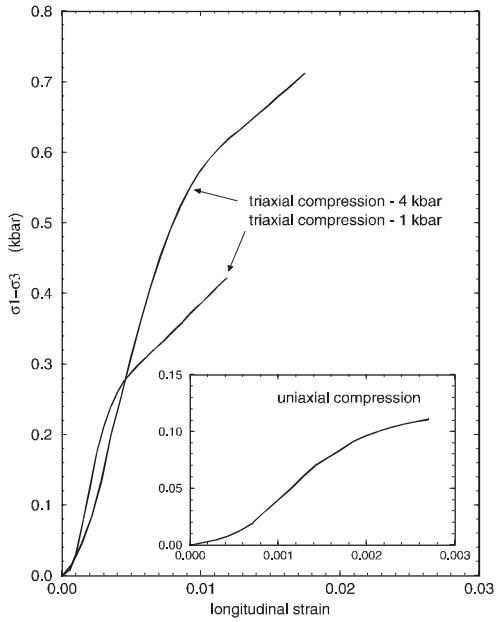

Figure 2.19 Differential axial stress-axial strain curves obtained in triaxial compression tests on dolomite with an initial saturated density of ρ_0 = 2200 kg/m^3 (provided by DIRCEN/CEA)

The maximum principal stress difference ($\sigma_1 - \sigma_3$) vs the mean principal stress $\left(\frac{1}{3}(\sigma_1 + 2\sigma_3)\right)$ envelope for the ρ_0 = 2200 kg/m^3 dolomite is shown in Figure 2.20. The values of $\sigma_1$used in preparing this plot are understood to correspond to the maximum stresses reached in tests such as those illustrated in Figure 2.19. Thus, the envelope may not be taken to represent a locus of points corresponding to a common stage (e.g. initial yield, peak strength in the brittle range, residual strength) in the stress-strain histories of the specimens. Analysis of the data shown in Figure 2.20 gives an indicative value of uniaxial compressive strength of q = 15 MPa for the ρ_0 = 2200 kg/m^3 dolomite. This is slightly outside the range of values given in Table 2.4, but it seems reasonable.

As noted earlier, Mariotti (1990) carried out a detailed study of the mechanical behaviour of the chalky limestone or soft chalk found at depths of between 440 and 490 mbsl in the outer northern slope at Mururoa. This study included permeability, hydrostatic compression, triaxial compression, cyclic loading, and creep tests carried out on mainly 50-mm-diameter by 100-mm-long samples taken from borehole core. The test results were used to develop elasto-plastic and viscoplastic models for the constitutive behaviour of the material. Some of the results were summarised by Mariotti and Bouchez (1989).

The porosity of the chalk varied from 37% to 45%. Uniaxial compressive strength averaged 5 MPa (50 bar), which means that it would be classified as a weak rock. In triaxial compression tests at confining pressures of 1.5 and 3.0 MPa, values of Young's moduli in the range 0.3–1.7 GPa were measured. As expected, Young's modulus was found to vary inversely with porosity. It was found that the results of the quasi-static undrained triaxial compression tests could be interpreted using the critical-state soil-mechanics principles (Schofield and Wroth 1968) as adapted for soft rocks (e.g. Brown and Yu (1988)). At confining pressures of up to 3 MPa (30 bar), the chalk showed mildly brittle failure characteristics with a progressive increase in pore pressures throughout the tests. The higher porosity specimens showed ductile behaviour at a confining pressure of 3MPa (30 bar). Figure 2.21 shows an example of the test results. The critical-state model fitted to the results used values of Coulomb friction angle at the critical state of $\phi' = 33^\circ$ at $\sigma_3 = 1.5$ MPa and $\phi' = 27^\circ$ at $\sigma_3 = 3.0$ MPa, with an overall value of $\phi' = 31^\circ$ being finally chosen for the model used in numerical analyses. These are reasonable values compared with those given, for example, by Barton (1976).

Undrained cyclic load tests were also carried out on samples subjected to confining pressures of 1.5 and 3.0 MPa (15 and 30 bar). The increment of deviator stress applied was $\pm$ 0.5 MPa ($\pm$ 5 bar) about the pre-established mean at frequencies of 0.1–1 Hz for 30 to 100 cycles. The results showed that this cyclic loading quickly built up excess pore pressures which, depending on the level of the initial loading, could induce significant deformation and, eventually, rupture of the samples.

Drained and undrained confined compression tests at constant effective and constant total stress, respectively, allowed the viscoplastic response of the material to be studied and the relevant model parameters to be determined. Constant deviator stresses of up to 80% of the maximum attainable at the particular confining pressure (1.5 or 3.0 MPa — i.e. 15 or 30 bar) were applied for periods of up to 13 000 sec (3.6 hours). In none of the tests did tertiary creep failure result, although creep did occur, with the rate of deformation generally increasing with the value of the constant deviator stress for a given confining pressure.

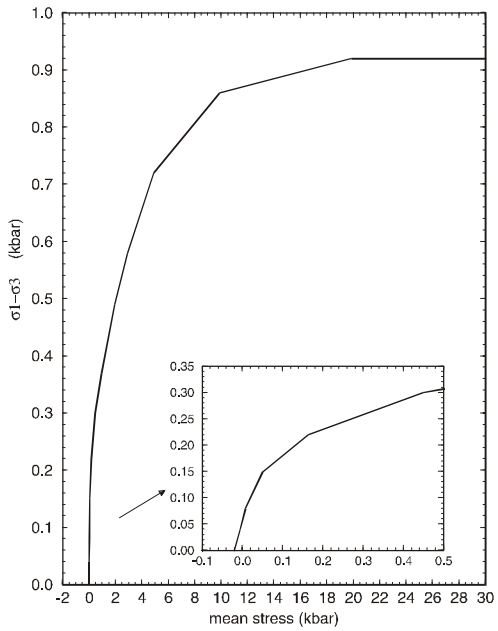

Figure 2.20 Failure or yield curve for dolomite with an initial saturated density of 2200 kg/m^3 (provided by DIRCEN/CEA)

2.4.4 Permeability

Units — When fluid flows under differential pressure through a medium in a single direction, the flow rate, Q, is related to the gradient of the head in the direction of flow, i, by Darcy's law:

$$Q = Ki \tag{2.2}$$

where K is the hydraulic conductivity or coefficient of permeability.

Strictly, K is a second-order tensor which has three principal directions in the three-dimensional case. Special test methods and analytical techniques have been developed to determine the principal values of the hydraulic conductivity for anisotropic rock masses (e.g. Hsieh and Neuman (1985), Hsieh, Neuman, Stiles and Simpson (1985)). In the present case, tests of these types were not carried out, and the data are not available to permit the hydraulic conductivity tensor to be evaluated. Accordingly, as in many other cases, K will be evaluated as a scalar quantity here and in Section 2.5.2, concerning rock mass permeability.

The value of the hydraulic conductivity, which has the dimensions LT^{-1}, is not only a property of the material through which the flow is taking place but is also a function of the kinematic viscosity of the fluid. The permeability, k, which is a property of the

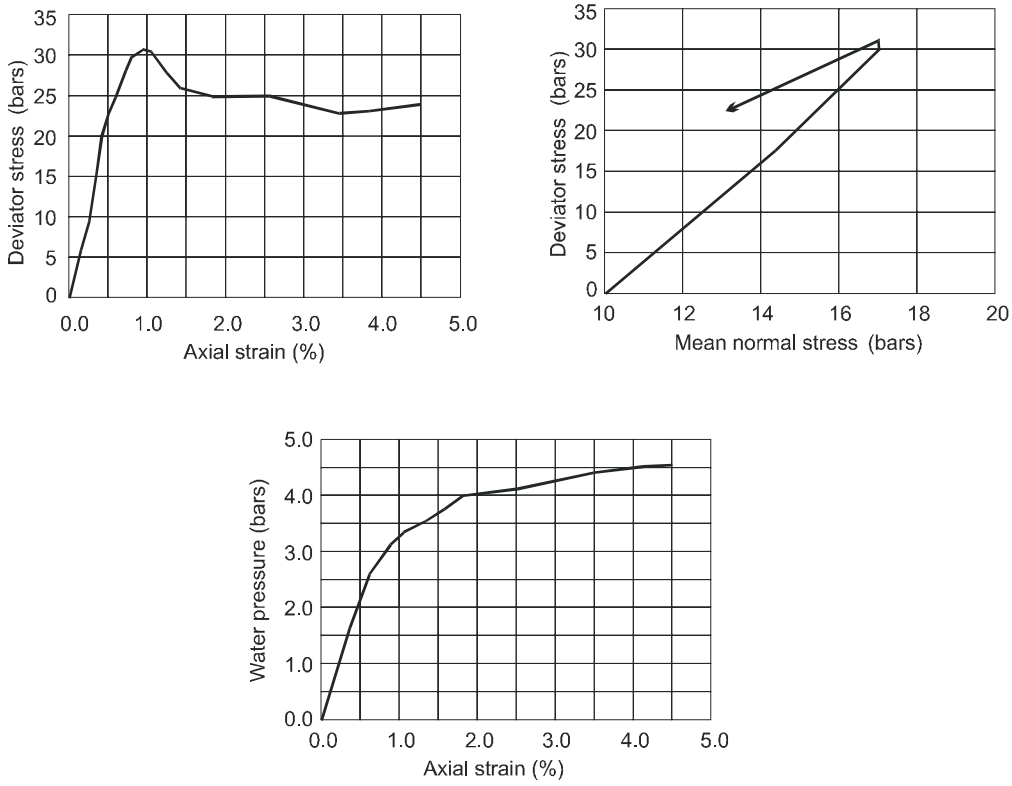

Figure 2.21 Results of an undrained triaxial test on soft chalk from the northern slope of Mururoa tested at a confining pressure of 1 MPa (10 bar) (after Mariotti 1990)

material alone, has the dimensions L^2. The unit is the Darcy (D), such that 1D $\cong 10^{-12}$ m^2. For water under standard conditions, this corresponds to a value of K of 10^{-5} ms^{-1}. This is usually taken as the unit of hydraulic conductivity, coefficient of permeability or simply permeability and is often referred to as the Darcy permeability.

The permeabilities encountered in rocks vary between 10^{-3} ms^{-1} (100 D), the permeability of sand, and 10^{-14} ms^{-1} (Brace 1980). The boundary between "permeable" and "impermeable" formations is generally taken to occur at 10^{-9} ms^{-1} (0.1 mD).

Volcanics — On the scale of a core sample, the measured values of permeability of the submarine volcanics are in the range 10^{-11} to 10^{-8} ms^{-1} ($10^{-3}$to 1 mD) (Guille et al. 1996). These very low values arise from a lack of inter-connectivity of the pores and the presence of significant amounts of clay in some of the rock types. The subaerial volcanics are more diverse and spatially variable than the submarine rocks. Rock types vary from massive basalts having zero or very low permeability to volcanic cinder deposits with porosities above 30% and matrix permeabilities of about 10^{-7} ms^{-1} (10 mD)

(Guille et al. 1996). Table 2.2 shows values of permeability with respect to sea water of 1.8 and 1.9 mD ($\cong 2 \cdot 10^{-8}$ ms^{-1}) determined independently by Davies (1983).

In-situ permeabilities have also been determined by in-situ pump testing in boreholes. If a 10–20 m test length is used, a small number of the layers in the volcanics may be involved, as may small numbers of discontinuities. Guille et al. (1996) report that, for sequences composed of massive lava flows or rocks containing pores filled with alteration products, the permeability is often below or at the threshold of sensitivity of the test method at 10^{-9} ms^{-1} (0.1 mD). The more common vesicular and brecciated lavas give permeabilities in the range 10^{-8} to 10^{-7} ms^{-1} (1–10 mD). In the high-porosity pyroclastic rocks, the permeability can reach 10^{-6} ms^{-1} (100 mD) on this scale.

Carbonates — The carbonates generally have higher and more highly varying permeabilities than the volcanics. On the scale of core samples, the dolomites may have very low permeabilities of the same order as those of the volcanics. The uncemented, coarse-grained carbonate conglomerates have moderate to high permeabilities of, say, 10^{-5} to 10^{-4} ms^{-1}. The karstic formations have very high permeabilities that cannot be measured on the scale of core samples.

Mariotti (1990) obtained values of permeabilities in the range 10^{-6} to 10^{-5} ms^{-1} (0.1–1.0 D) in laboratory tests on the soft chalky limestone from the northern slope of Mururoa.

2.5 Rock Mass Properties

2.5.1 Mechanical Properties

Volcanics — As noted earlier, it is essential in rock engineering to distinguish between the mechanical properties of the rock material as discussed in Section 2.4 above and those of the in-situ rock mass. Unfortunately, in the present case, there is a paucity of the core logging data, test data, observations of the field performance of engineered structures, and back-analyses on which estimates of rock mass properties are usually based.

In a study of the limits on strength and deformation properties of jointed basaltic rock masses from a number of sites, Schultz (1995) concluded that the tensile and cohesive strengths of basaltic rock masses are generally one to two orders of magnitude lower than the corresponding values for the intact basalts. The shear strengths of joints in basalts vary considerably from flow to flow and with normal stress magnitudes and surface roughness. Schultz (1995) quotes values of friction angle in the range 29°–46°. Figure 2.22, adapted from Hoek and Brown (1980, 1997), illustrates the concepts of intact rock, a single joint, jointed rock, and the rock mass in a basaltic lava flow sequence.

A widely used method of estimating the strengths of rock masses is the empirical criterion developed by Hoek and Brown (1980, 1977). The generalised Hoek-Brown

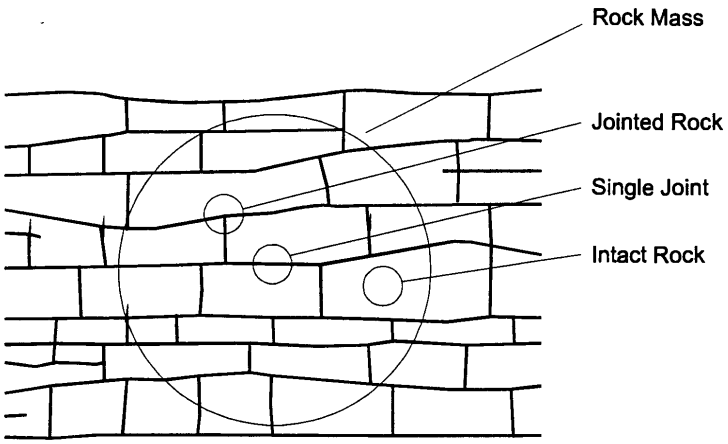

Figure 2.22 Schematic geometry of a basaltic lava flow sequence (after Hoek and Brown 1980 and Schultz 1995)

strength criterion is given by

$$\sigma_1' = \sigma_3' + q\left(m_b \frac{\sigma_3'}{q} + s\right)^a \tag{2.3}$$

where σ_1' and σ_3' are the major and minor principal effective stresses at failure; m_b, s and a ($0.5 \leq a \leq 0.65$) are dimensionless parameters depending on the characteristics of the rock mass; and q is the uniaxial compressive strength of the intact rock.

For intact rock, $s = 1.0$. In most cases, $a = 0.5$ — in which case, (2.3) reduces to (2.1) — but it may increase to 0.65 for very poor quality rock masses, for very weak rocks and for coal. In the case of the volcanics at Mururoa and Fangataufa, it is consistent with experience elsewhere to take $a = 0.5$.

The parameters m_b and s decrease as the quality of the rock mass decreases. The quality of the rock mass is represented by a Geological Strength Index (GSI), which, for all but poor-quality rock masses, is equivalent to Bieniawski's Rock Mass Rating (RMR), a quantity which may be determined routinely in rock engineering site investigations (Bieniawski 1976). Unfortunately, as noted above, no such determinations have been made for the atoll rock masses.

Examination of the core from the Zoé borehole suggests that a high proportion of the volcanic rock mass is of very good quality (RMR = 80–100), some is of good quality (RMR = 60–80) and a small proportion is at the higher end of the fair range of quality (RMR = 40–60). For purposes of illustration, Hoek-Brown rock mass strength curves have been calculated for intact rock, for RMR = 90 (representing the best quality rock

mass), for RMR = 80 (representing the "typical" or "average" quality rock mass) and for RMR = 55 (representing the likely poorest quality rock mass).

The parameters m_b and s corresponding to each value of GSI or RMR are given by

$$\frac{m_b}{m_i} = \exp\left(\frac{GSI - 100}{28}\right) \tag{2.4}$$

where m_i is the value of m for the intact rock, and

$$s = \exp\left(\frac{GSI - 100}{9}\right) \tag{2.5}$$

The extensive sets of results analysed and presented by Hoek and Brown (1980) and Hoek and Brown (1997) indicate that generally m_i = 17 for basalts and m_i = 18 for pyroclastic breccias. It seems reasonable, therefore, to assume that m_i = 17 in the case of the volcanic rocks from the atolls.

The data presented previously show that q = 75 MPa is a reasonable value for "typical" or standard volcanic rock with ρ_0 = 2360 kg/m^3. Using this value of q and values of m_b (for m_i = 17) and s calculated for GSI = 90, 80 and 55, from (2.4) and (2.5), respectively, the relations between σ_1 and σ_3 at failure for a range of rock mass qualities may be calculated from (2.3). The results are shown in Figure 2.23 for values of σ_3 of up to 100 MPa. Note that, in general, the peak strength for a poor quality rock mass with GSI = 55 is only about half that for a very good quality rock mass with GSI = 90.

Just as the strength of the in-situ rock mass will be less than that of the intact rock, so will the modulus of the rock mass be reduced. Table 2.3 gives measured average values of the shear modulus, G, of about 10 GPa (0.1 Mbar) and Poisson's ratio, ν, of 0.3 for volcanics with ρ_0 = 2360 kg/m^3. For isotropic elastic materials, G and ν are related to the modulus of deformation or Young's modulus, E, by

$$G = \frac{E}{2\,(1 + \nu)} \tag{2.6}$$

For G = 10 GPa and ν = 0.30, this gives E = 26 GPa, which is a reasonable value. For volcanic rock masses with RMR varying down to 55, the in-situ modulus might be expected to vary between this upper limit and, say, E = 10 GPa.

The rock mass properties for the volcanics derived in this section are consistent with those published by (Arthur et al. 1997) for the slightly denser basalts encountered in the underground works for the 'Muela Hydropower Project, Lesotho:

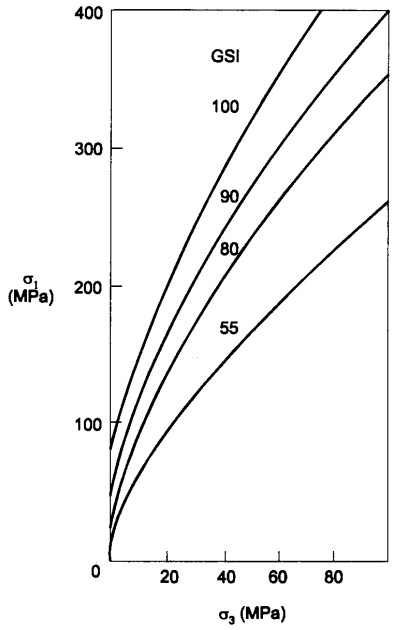

Figure 2.23 Estimated rock mass strengths for volcanic rocks with a range of rock mass qualities and an intact compressive strength of 75 MPa

Density	2700–2750	kg/m^3
Unconfined Compressive Strength (intact rock)	20–82	MPa
Deformation Modulus	13–19	GPa
Friction Angle	40–50	degrees
Cohesion	2–4	MPa

Carbonates — Because of the wide variability in the rock mass quality and the intact rock strengths of the carbonates, it is difficult to estimate their global or overall rock mass properties with any degree of confidence. Clearly, the values can be expected to vary over an extremely wide range. Given that Hoek and Brown (1997) give general values of m_i of 7 for chalk and 8–10 for limestones, a value of $m_i = 8$ will be taken for purposes of illustration. On the basis of the data presented earlier, an overall value of q = 15 MPa will be assumed. Based on the limited data available and the inspection of the core from one borehole, an overall or "mean" value of GSI = RMR of 70 will be used for the carbonates.

Using these presumptive values of input data, a general Hoek-Brown rock-mass strength envelope for the carbonates may be calculated. Particular interest exists in the strength of the carbonates at low effective normal stresses for the purposes of slope

stability analysis rather than that at the higher confining pressures used in the triaxial compression tests reported previously. At values of σ_3' of less than 1.0 MPa, the Hoek-Brown rock-mass strength envelope referred to above may be represented by a straight line to a very good approximation. This gives an estimated "mean" or overall unconfined compressive strength of the rock mass of 2.8 MPa and equivalent Mohr-Coulomb shear-strength parameters of $c' = 0.62$ MPa and $\phi' = 42.4°$. It must be emphasised that these are estimated mean or overall peak-strength parameters for the large and quite diverse carbonate rock mass. Nevertheless, they seem reasonable. Suitable design parameters for broadly based calculations might be $c' = 0.5$ MPa, $\phi' = 40°$.

In slope-stability analyses, use is made of a basic or residual friction angle for rock surfaces. It is useful to note that the values of basic friction angle of 30° for chalk, 27°–37° for dolomite and 33°–40° for limestone given by Barton (1976) are consistent with the values estimated here and those used previously for low confining or normal effective stresses.

2.5.2 Permeability

It is the permeability on the scale of the rock mass rather than the permeability on the scale of a core specimen or an individual discontinuity that will be one of the governing factors in determining the nature and rates of flows through the atoll edifice. Estimates of the large-scale permeability of the volcanics, in particular, have been made on the basis of pumping tests in boreholes, from studies of the times taken for the chimney to be refilled with water following a blast (Bouchez and Lecomte 1996) and from modelling of thermal exchanges between the edifice and the ocean (Guille et al. 1996; Henry et al. 1996). These tests will be reviewed further in Chapters 6 and 7.

As noted above, the borehole pumping tests gave values of permeability in the volcanics in the range 10^{-9} to 10^{-6} ms^{-1} (0.1–100 mD). Estimates of the time required to fill the cavities and chimneys with water following the blast are available for almost 50% of the underground tests. Numerical modelling using the finite-element method has been used by DIRCEN/CEA to obtain estimates of the permeability of the surrounding rock mass. In the modelling runs, a damaged zone radius of 1.6 times the radius of the cavity was assumed, with the permeability in this region taken as $2 \cdot 10^{-6}$ ms^{-1} (200 mD). A storage coefficient of 10^{-5} m^{-1} was used for the surrounding rocks. Figure 2.24 shows a histogram of the average maximum values of rock mass permeability used to provide good fits to the observations. In around 90% of all cases, the rock mass permeability is less than $3 \cdot 10^{-7}$ ms^{-1} (30 mD). The maximum value estimated was $1.2 \cdot 10^{-6}$ ms^{-1} (120 mD), but it should be noted that the estimates are considered to be conservative (DIRCEN/CEA Document No. 5). These values, which are at the top end of the range measured in borehole pumping tests, seem reasonable.

If the temperature distribution calculated within the edifice assuming particular permeabilities and other properties corresponds with measured values, then it may be in-

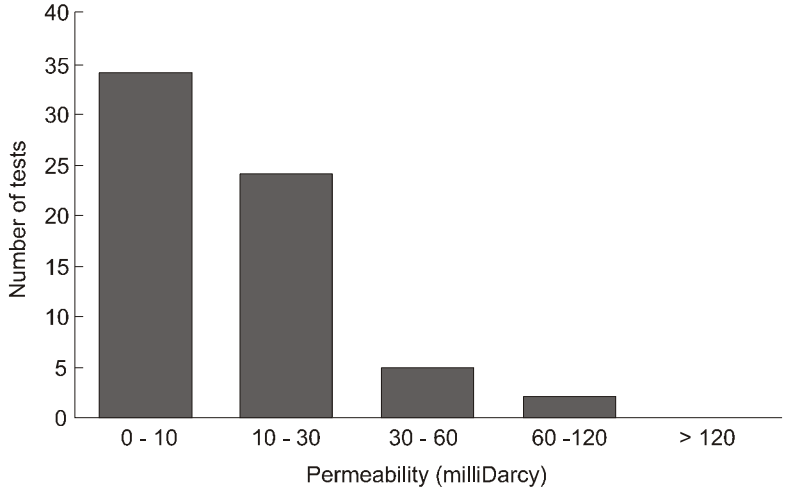

Figure 2.24 Average maximum permeability of the volcanic rock masses surrounding underground tests deduced from cavity-chimney rewatering data (DIRCEN/CEA Document No. 5)

ferred that the chosen values of permeability are reasonable. Guille et al. (1996) report successful thermal convection modelling of this type in which the rock mass permeabilities used were 10^{-5} ms^{-1} (1.0 D) in the upper carbonates, 10^{-4} ms^{-1} (10 D) in the lower carbonates and 10^{-7} ms^{-1} (10 mD) in the volcanics.

Further detailed modelling by Henry et al. (1996) suggests that the average large-scale permeability of the volcanics cannot be more than a few tens of mD. This is consistent with the results obtained from studies of the refilling times of cavity-chimney structures. These values are toward the higher-permeability end of the results assembled by Brace (1980) for igneous rocks at depths of greater than 500 m.

As is shown in Chapter 3, at equilibrium after an underground nuclear test, the rubble-filled cavity and chimney is surrounded by a zone in which the rock has been subjected to intense shear failure and a further zone of damage involving discrete fracturing of the rock. On the basis of all the evidence available, the best estimates that can be made of the orders of magnitude of the in-situ permeabilities in these zones in the volcanics are:

Rubble-Filled Cavity	10^{-2} ms^{-1}	(1000 D)
Shear Failure Zone	10^{-5} ms^{-1}	(1 D)
Damaged Zone	10^{-6} ms^{-1}	(100 mD)
Undamaged Zone	10^{-7} ms^{-1}	(10 mD)

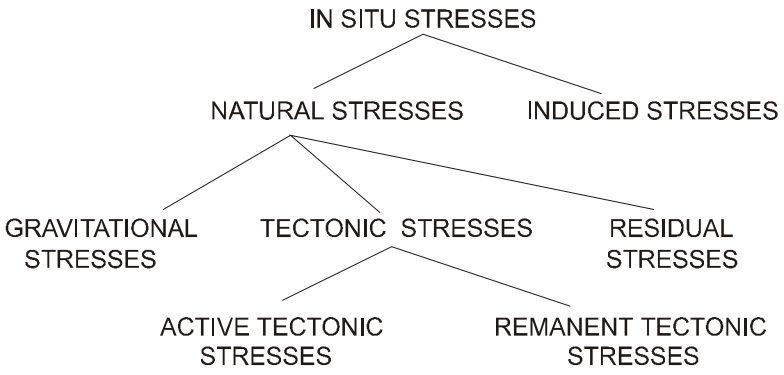

Figure 2.25 Components of in-situ stress (after Bielenstein and Barron 1972)

2.6 In-Situ Stresses

The stresses existing within a rock mass before disturbance, the in-situ stresses, can exert a major influence on the responses of the rock mass to drilling and excavation processes and on the flow of fluids through the rock mass. Measuring or estimating the in-situ stresses is usually considered to be an important prerequisite for the analysis and prediction of the behaviour of underground excavations in rock (Hoek and Brown 1980). In the case of the underground nuclear tests at Mururoa and Fangataufa atolls, the in-situ stresses can be expected to influence, in particular, chimney development and the flow of water through joints and fractures in the volcanics.

No evidence has been found of any in-situ stress measurements having been made at Mururoa and Fangataufa or of stress fields having been inferred from other measurements. A major difficulty exists in this case in that entry into the test zones in order to make in-situ measurements was clearly impossible. However, the site would appear to have been a suitable one for the application of the down-hole hydraulic fracturing method of stress measurement in the deeper volcanics. It is widely acknowledged that it is rarely possible to calculate the in-situ stresses at a given site from first principles (Brady and Brown 1993). The only available alternative in the present case, therefore, is to attempt to reach conclusions about the likely nature of the in-situ stress fields from considerations of the geological histories of the atolls.

Discussions of the states of stress in rock masses may be complicated by the use of varying and often conflicting terminologies. The terminology used here is that suggested by Bielenstein and Barron (1972) and adapted by Brown and Windsor (1990). This system is illustrated in Figure 2.25.

The in-situ stress is the stress that exists at a point in the rock mass at a given time. It is the stress existing before we disturb the rock mass at or very close to the point of interest. The in-situ stress may itself be influenced by previous engineering activity nearby. If the point is within the zone of influence of a future excavation, the creation

of the excavation will perturb the in-situ stress field producing a resultant state of stress. It is this stress that will influence the performance of the excavation and the response of the rock surrounding it.

Induced stresses are man-made stress components arising from the removal or addition of material. They are superimposed on natural stresses that exist prior to any excavation. The natural stress field can be composed of gravitational stresses (due to the mass of overburden), tectonic stresses and residual stresses. Tectonic stresses may be active tectonic stresses (due to the active present-day straining of the Earth's crust) or remanent tectonic stresses. (Due to past tectonic events, these stresses have only been partially relieved by natural processes.)

The concept of residual stress is one that often causes controversy and so requires careful definition. Hyett et al. (1986) identify residual stress as "the stress state remaining in the rock mass, even after the originating mechanism(s) has ceased to operate. The stresses can be considered as within an isolated body that is free from external tractions; neither are they caused by the action of body forces or thermal gradients, etc.".

In addition to the gravitational, tectonic and residual stresses represented in Figure 2.25, some authors also identify thermal and physico-chemical stresses. Thermal stresses are those stresses resulting from temperature variations. They may be local in nature or may form part of the tectonic stress. Physico-chemical stress is the stress state set up as a result of chemical and/or physical changes in the rock — e.g. recrystallisation, absorption of water, fluctuation of groundwater level (Hyett et al. 1986).

The most probable sources of regionally uniform, broad-scale tectonic stress fields are the major forces acting at lithostatic plate boundaries. As well as discussing the nature of these forces, Zoback and Zoback et al. (1989) also identified more localised sources of tectonic stress, including flexural stresses caused by surface loads supported by the strength of the lithosphere (e.g. sediment deposition or volcanic loading, mountain building and erosion), by subsurface loads required for isostatic compensation of topography (i.e. adjustment of lithospheric density in response to variability of the overlying load), by down-bending of the oceanic lithosphere in subduction zones, and by membrane stresses generated by the motion of plates over an Earth of varying radius of curvature.

While these various mechanisms can be expected to influence the stresses in the lithospheric plate underlying the atolls (Fig. 2.2), it is difficult to argue that they will have any significant influence on the in-situ stresses in the volcanic rocks in which the underground nuclear tests were carried out.

The geological history of the atolls outlined in Section 2.2 suggests that gravitational stresses are likely to exert the major influence on the pre-test in-situ stresses under the atolls. A common starting point for discussions of gravitational stress is to assume a condition of zero lateral strain or complete lateral restraint during the development of gravitational loading by the superincumbent rock. For an isotropic, elastic rock mass,

the horizontal normal components of total stress are then given by

$$\sigma_x = \sigma_y = \frac{\nu}{1-\nu}\,\sigma_z \tag{2.7}$$

where ν is the Poisson's ratio of the rock mass, and σ_z is the total vertical normal stress, usually assumed to be given by

$$\sigma_z = \gamma\ z \tag{2.8}$$

where γ is the unit weight of the rock, and z is the depth below surface. For typical values of Poisson's ratio of 0.20–0.25, (2.7) gives the ratio of horizontal to vertical stress (K), as 0.25–0.33, which is very much lower than the values commonly observed near the surface in continental rock masses (Brown and Windsor 1990).

Erosion may reduce the vertical stress according to (2.8) and the horizontal stress by a lesser amount according to (2.7), leading to in-situ states of stress having high values of K, particularly at shallow depths. Analysis of this problem also indicates that the K-value decreases as the depth increases, approaching the pre-erosion value when the current depth at the point of interest is significantly greater than the depth of overburden removed (Brady and Brown 1993).

The application of even this simplified approach to the atolls is problematic. Because of the way in which the atolls and their seamounts were formed, the assumption of complete lateral restraint during the development of gravitational loading will not be satisfied. The more deeply buried rocks, particularly those well removed from the peripheries of the seamounts, are likely to have experienced close to full lateral restraint during the more recent phases of their geological histories, but even the simple assumptions made in the development of (2.7) and (2.8) will not be satisfied near the submarine boundaries of the edifice. At the periphery, one principal effective stress must act normal to the slope and be equal to zero. (In addition, hydrostatic normal stresses will act on the submarine slopes.) The other two principal effective stresses will lie in the plane of the slope. Their values will be influenced by local slope morphology.

Thus, it is concluded that the nature of the gravitational stress field is likely to vary across the zones affected by the underground nuclear tests. It is difficult to conclude that the horizontal components of gravitational stress will anywhere be greater than the values estimated by (2.7). The vertical stresses are likely to be well approximated by a form of (2.8) that takes into account the varying unit weights of the superincumbent strata. As an illustration, Figure 2.26 shows the results of a simple calculation of the variation of total vertical stress with depth at the site of borehole 1 in Figure 2.5.

In addition to the gravitational stresses, there could be some local remnant tectonic stresses arising from the intrusions associated with the deposition of the subaerial and aerial volcanics. However, the effects of contraction and, presumably, of jointing on

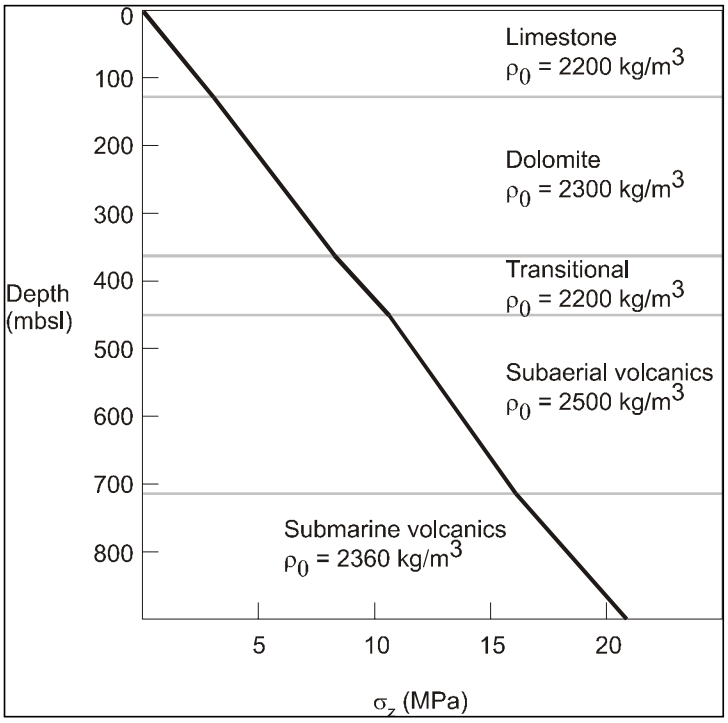

Figure 2.26 Estimated vertical stresses at the site of borehole 1 in Fig. 2.5

cooling are considered likely to have relieved these stresses, at least partially, to help produce a low horizontal stress environment. There could also be some physico-chemical modification of the stress field locally associated with mineral dissolution and alteration, most notably the dolomitisation of the carbonates. Here again, it is difficult to conclude how these effects could significantly modify the likely gravitational/vertical-stress, low/horizontal-stress regime in the first 1000 m below the surfaces of the atolls.

Stresses within a rock mass must be self-equilibrating — that is, although they may vary both in magnitude and sign within the mass, the integrated value of the stresses acting across any planar area will always result in a force equal to that imposed across that area by the force at the boundaries of the rock mass. Thus, for the depths of concern in the underground nuclear tests, the total force across a vertical plane through the atoll will be essentially that produced by the hydrostatic pressure of the Pacific Ocean, while the total force across a horizontal plane will be that produced by the total weight of the overlying (saturated) rock mass. As seen in Figure 2.27, the forces produced in the atolls by tectonic stresses acting in the ocean floor plate will be small at depths less than 2000 m or so. Because most rock masses tend to “relax” over time, reducing the potential energy of the mass, the absolute magnitude of in-situ stresses will also tend to decline in magnitude.

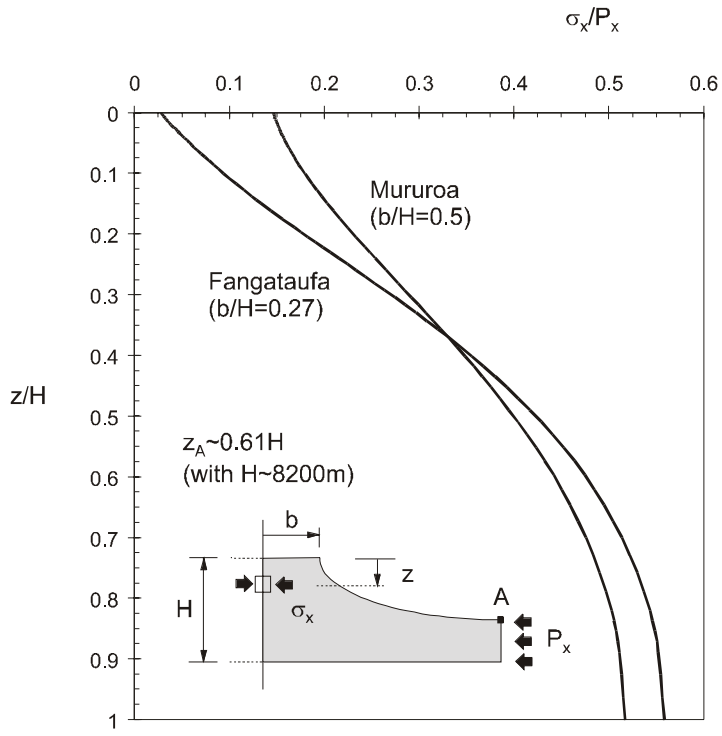

Figure 2.27 Normal stresses induced along the vertical axis of Mururoa and Fangataufa due to a unit normal stress in the upper crust (ocean floor)

Note that the analysis on which Figure 2.27 is based assumes that the normal stress (σ_x) is applied after the seamount is formed and deforms elastically. Any stresses or stress changes in the crust prior to that time would probably not be transmitted to the upper atoll. It is thus more correct to interpret the above diagram as indicating that an increase in compressive stress, σ_x, will cause a change of approximately 0.15 σ_x at the centre of the region of Mururoa — i.e. parallel to the long axis. The normal stress change parallel to the short axis (b/H) $\simeq$ 0.1 would be essentially nil, with a change of 0.025 σ_x at Fangataufa. Tensile changes (i.e. **reductions** in compressive stresses) may induce fracturing in the deeper parts of the atoll and, hence, may not be transmitted to the upper parts.

In summary, then, the available evidence and analysis of the situation suggest that the best estimate of the general state of in-situ stress under the atolls is that given below.

1. The total vertical stress is given by

$$\sigma_z = \sum \gamma_i \, z_i \tag{2.9}$$

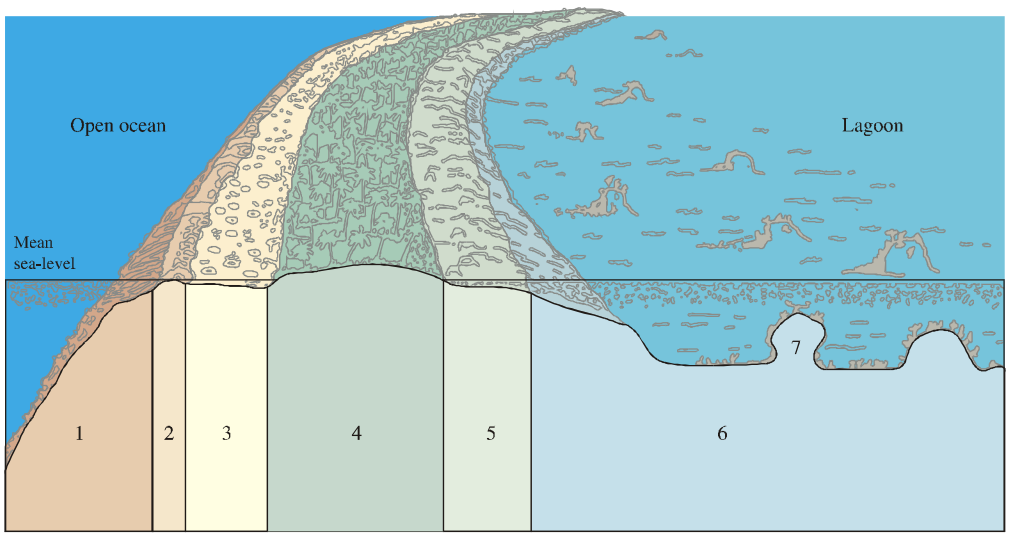

Figure 2.28 Cross-section of the Mururoa coral rim showing (1) outer slope, (2) algal ridge, (3) outer reef platform, (4) emerged zone, (5) inner platform, (6) lagoon and (7) knolls and patches (Guille et al. 1996)

where γ_i, z_i are the saturated unit weights and thicknesses of the superincumbent strata.

2. Near the periphery of the atoll, the horizontal total stresses at depth z are given by

$$\sigma_x = \sigma_y = \gamma_w z \tag{2.10}$$

where γ_w is the unit weight of water.

3. In the central and deeper portions of the volcanics, there may be an additional component of horizontal total stress arising from lateral restraint during deposition (up to the value given by (2.7)) or tectonic forces (as shown in Fig. 2.27).

2.7 Submarine Atoll Slopes

2.7.1 Slope Morphology

Figure 2.28 shows a typical cross-section of the Mururoa coral rim. The coral rim is submerged to the northwest of the atoll, where a channel 4500 m wide and 1 m to 9 m deep has formed. In the southern sector, erosion has cut parallel channels called hoa in the coral rim. The hoa define emerged islets called motu and connect the ocean and lagoon waters. Hoa and motu also exist on parts of the Fangataufa rim.

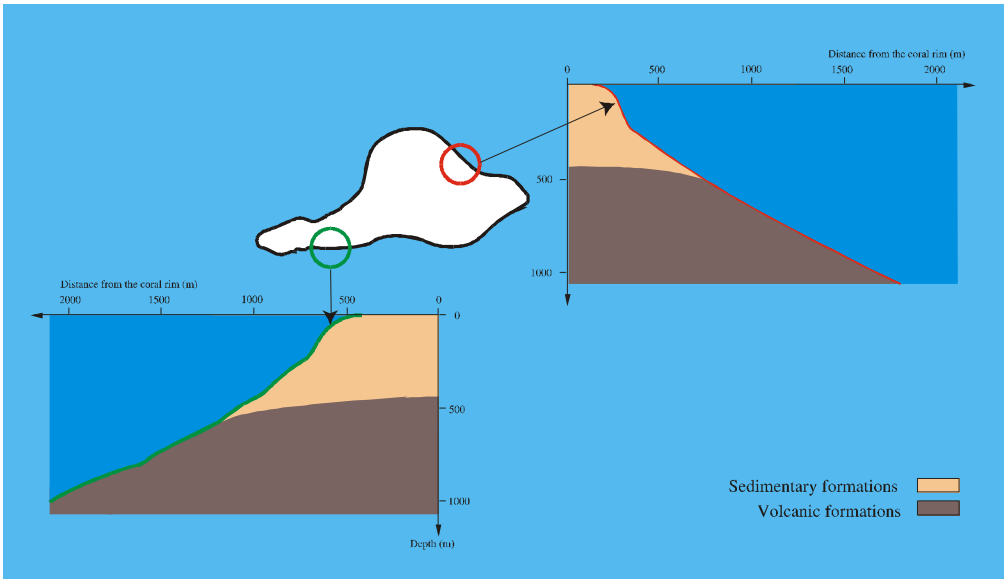

Figure 2.29 Typical overall slope profiles of the north and south zones, Mururoa (Guille et al. 1996)

The submerged outer portion of the atolls consists of the outer reef platform, the algal ridge made up of spurs and grooves, and the outer slope, which begins at depths of greater than about 10 m. Coral grows continuously on this outer slope down to about 60 m. As is shown in Figure 2.29, the outer slopes of Mururoa average 20–30° from the surface down to 80–100 m, where there is an almost vertical drop of 100–150 m. Below about 250 m, the slopes flatten progressively from 45° to 10° at about 2000 m and eventually merge with the abyssal plain at depths of greater than 3000 m. The outer slopes of Fangataufa have similar overall profiles to those of Mururoa (Guille et al. 1996).

At a more detailed level, there are differences between the southern and northern slopes of Mururoa, and between the southwest and south-southeast slopes and the northwest, northeast and eastern slopes of Fangataufa. The southern slopes of Mururoa and the SW and SSE slopes of Fangataufa have been eroded more substantially than the slopes on the opposite sides of the atolls. The southern slopes have been eroded to produce alternating volcanic escarpments and valleys below 500–600 m.

Carbonate sediments have accumulated on all slopes, but they are less thick in the mid-slope regions of the more heavily eroded southern slopes. Large volumes of sedimentary materials in deep water below these slopes outside concave areas of the atoll periphery suggest that they may have resulted from old submarine slides. By contrast, the northern slope of Mururoa, and the northwest, northeast and eastern slopes of Fangata-

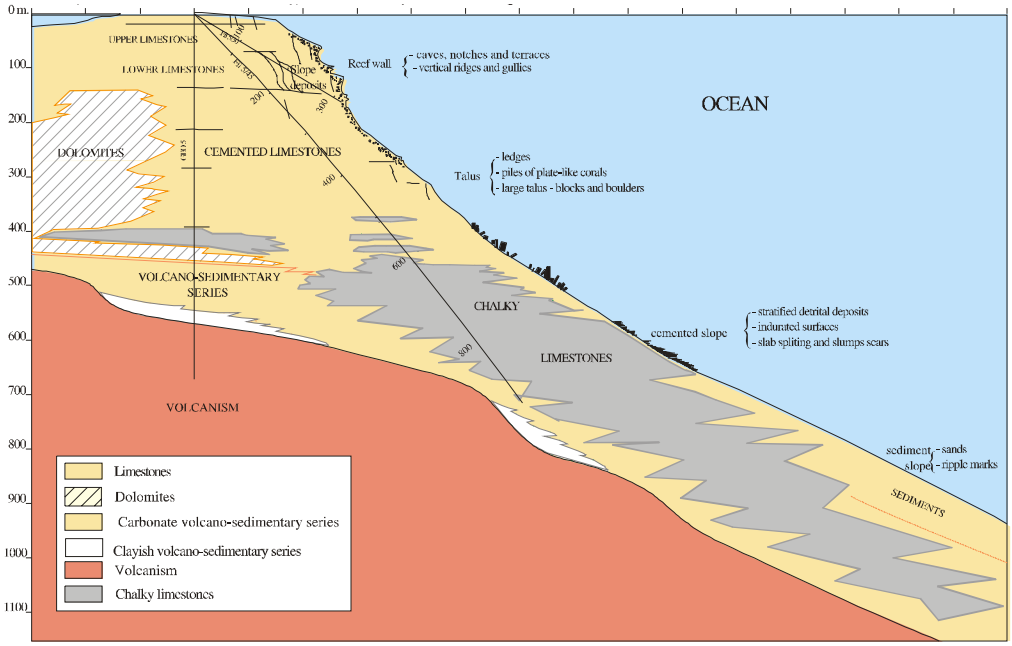

Figure 2.30 Geology and slope profile, northern zone at PK5, Mururoa (DIRCEN/CEA Document No. 5)

ufa are smoothed out by sediments, and the accumulation of sediments in deep water is more widespread in these areas. Natural submarine slope failure processes are discussed in Section 2.7.2 below.

The upper portions of the slopes above depths of about 1000 m are of special interest in terms of the long-term integrity of the atolls. Figure 2.30 is a cross-section showing the geology and a summary of the submarine observations made of the northern slope of Mururoa from a Remote Operated Vehicle (Buigues 1997). Above 100 m, the slope is at about 20° and is interrupted by a number of terrace levels. From about 100 to 250 m, there is an almost vertical cliff interrupted locally by notches and terraces providing evidence of sea level changes. Below the cliff to 300–350 m, the slope is at about 45°, and its surface is covered with talus. From 300–350 to 500 m, calcareous debris of all sizes is found on slopes of 30°–35° . Between 500 and 600–650 m, the surface sediments are occasionally lithified, and the average slope is 25°–30°. Below 600–650 m, the slope surface is covered uniformly with calcareous sands, and the slope gradually decreases, reaching 10° at 2000 m.

Figure 2.31 shows a more detailed cross-section of the northern Mururoa slope down to a depth of about 200 m. Buigues (1996) and Buigues (1997) note that the terraces ob-

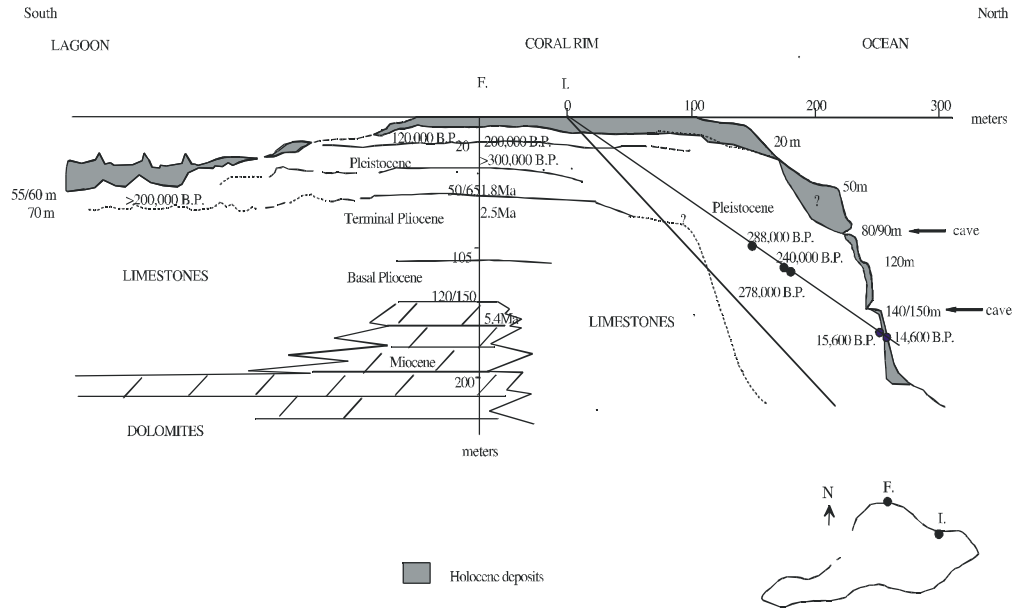

Figure 2.31 Detailed submarine slope profile with ages, northern zone, Mururoa (after Buigues 1996)

served at depths of 10, 20, 40 and 55/65 mbsl may correspond to the tops of successive carbonate platforms of Pleistocene and, probably, Pliocene ages. The vertical walls at 110–120 and 200–230 mbsl are features that have been observed in carbonates at similar depths at several other sites, including Eniwetok atoll (Colin et al. 1986), Tahiti (Salvat 1986), the Bahamas (Grammer and Ginsberg 1992) and Belize (James and Ginsburg 1979). The cave-like heterogeneities at 80–90 and 120–150 mbsl are interpreted by Buigues (1996) and Buigues (1997) as recording former sea level positions during the Pleistocene, when the atolls emerged above the sea. The feature at 120–150 mbsl probably corresponds to the last maximum of emersion 18,000 years ago. As in the case of the vertical walls, similar features have been noted in carbonate atolls and islands at similar depths in the Pacific and elsewhere (e.g. Grammer and Ginsberg (1992), Grammer and Ginsberg (1992)). The talus present below about 250 mbsl at Mururoa and elsewhere probably derives, at least in part, from erosion occurring during these periods of emergence.

According to Guille et al. (1996),

> *Volcanic outcrops appear at the depths of 600 m in some parts of the southern and northwestern sectors, and at generally greater depths (1000 m) towards the northeast. These outcrops, of a more or less radial orientation with the respect to the emerged atoll rim, delimit valleys filled to variable ex-*

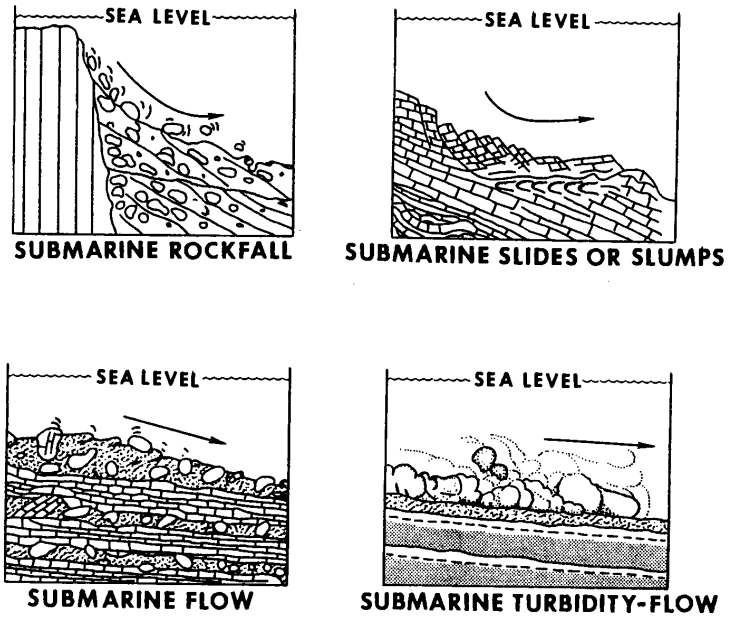

Figure 2.32 Main types of submarine slope instability (Dott 1963)

tent material of sedimentary origin. In the northeastern and northwestern sectors, these valleys become wider and the relief is smoothed out by deposits; the topography is broken only in places by small volcanic outcrops at water depths of more than 1000 m. By contrast, the valleys are marked to the south. Sediments have accumulated here from a depth of 2500 m down to the abyssal plain.

2.7.2 Slope Instability Processes

Submarine slope instability is a significant geological process. Varnes (1975) suggests that "the largest of all slope movements appears to have occurred on the bottom of the sea". Goguel (1982) (see also Section 2.9) argues that slides on the atoll slopes are part of normal marine geological processes. Prior and Coleman (1984) provide an overview of the types of submarine instability based on a classification by Dott (1963). The four main types are illustrated in Figure 2.32.

Submarine rock falls are restricted to localised steep, near-vertical slopes. An example of this type of instability at Mururoa and the accompanying accumulation of blocks of coral is illustrated in Figures 2.30 and 2.31 and discussed in Section 2.7.1 above.

Slides of both rock and soft sediment are the most widespread form of submarine slope instability. Submarine slides involving hundreds and even thousands of cubic

kilometres of material have occurred in most of the world's oceans (Prior and Coleman 1984). Those on the flanks of the Hawaiian ridge are among the largest in the world (Moore et al. 1994). Submarine slides may take either rotational (circular or non-circular) or translational (block or slab slide) forms. Some of the instabilities that have occurred on the atolls and in other carbonate environments (Mullins et al. 1986) are of this type. Surface fractures such as that shown in Figure 2.11 are found along the rims of most Polynesian atolls, including Mururoa and Fangataufa. They appear to be tension cracks created by the effects of gravity on the outer atoll slopes, and possibly by forces associated with the downslope flow of sediments. However, there is no evidence that these submarine slides on Mururoa and Fangataufa atolls have reached into the underlying volcanic rocks, as they have in the flanks of the Hawaiian Ridge (Moore et al. 1994).

Flows of sediment downslope involve a number of processes, notably debris flow, grain flow and liquefaction flow (Prior and Coleman 1984). Flows are sometimes regarded as a transitional stage between slides and turbidity currents (see below). Natural flows may be caused by the forces of gravity, earthquakes and storm wave action. There is evidence that nearby explosions can also cause the downslope flow of submarine sediments on the atolls (Bouchez and Lecomte 1996).

Turbidity currents or flows complete the general categorisation of submarine slope instabilities. They are probably not as important in the current context as the other types of instability. Turbidity flows involve the downslope transport of sediment, which is supported by the upward component of fluid turbulence within the current. They are believed to occur off the mouths of major rivers where high density water/sediment plumes move downslope into deeper water. However, turbidity currents are also considered to be triggered by, and to occur in association with, submarine slides and debris flows (Prior and Coleman 1984). It is possible that they may have been associated in this way with the debris and grain flows that have occurred on the submarine slopes of the atolls.

Of particular interest to considerations of the stability of the atoll slopes under the influence of underground nuclear explosions is the phenomenon of liquefaction, which causes downslope flows of sediment but may also be associated with submarine slides. Put simply, the process is one in which cyclic loading arising from an earthquake, an explosion or wave action produces a build-up of excess pore pressure under undrained or partially undrained conditions. In loose granular materials, the increase in pore pressure results from a deformation (compaction) of the solid skeleton under cyclic loading. The increase in pore pressure will lead to a reduction in the effective normal stress in the slope and, therefore, in the shear strength that can be developed by the slope material. If the shear strength is exceeded by the downslope shear stress, then shear failure can occur. Cyclic loading can also lead to a degradation of the shear strength of some geological materials. In the extreme case, the pore pressures can become so high that a mass of material "liquefies" and flows down the slope.

Natural submarine failures of this type have occurred in a range of materials under earthquake and storm wave-loading conditions (e.g. Seed (1968), Seed and Rahman (1978), Lee and Edwards (1986)). Clearly, there have been submarine slope failures and the downslope transport of significant volumes of material during the geological histories of the atolls (Guille et al. 1996; Bouchez and Lecomte 1996). It must be concluded that the sediments accumulated on the outer atoll slopes remain susceptible to the forms of instability discussed above.

Bouchez and Lecomte (1996) indicate that the underground nuclear tests carried out under the southwestern rim of Mururoa in 1977, 1979 and 1980 "effectively destabilised sediments on the atoll flanks." Bouchez and Lecomte (1996) argue that the tremors associated with the explosions can produce liquefaction and rapid downslope movements of slope debris and sediments. They say that, in some cases, the underlying carbonate rock, including a small part of the outcropping coral on the outer rim, can be "dragged down" by the shear forces associated with the submarine "avalanche". This can produce cliff collapses, rock slides and degradation of the submarine slopes. If the volume of the consequent slope failure is large enough, suction of the water above the sliding blocks can produce large hydraulic wave trains that can submerge the atoll rim (DIRCEN/CEA Document No. 7, Section V.3, pp. 15–18; (Bouchez and Lecomte 1996)).

Bouchez and Lecomte (1996) also report that the Tydée event on 27 July 1979 triggered the sliding of several tens of millions of cubic metres of slope material. The biggest wave of the resulting hydraulic wave train submerged the atoll rim approximately 1-1/2 minutes after the start of the collapse. The maximum rim submergence recorded was 2 m in the failure zone. Subsequent surveys showed that a new, almost vertical, cliff and outer slope profile had been formed.

Davies (1983) makes the interesting point that slope instabilities involving the outer portions of carbonate rock can have a marked effect on the hydrology of the atoll. He argues that the outer skin of the limestone slopes are more highly cemented and of lower porosity than the bulk of the carbonate rock mass. Removal of this less permeable skin through rock slides will serve to increase the ease of vertical and horizontal water transport through the carbonates.

2.7.3 Summary

The present morphology of the atoll slopes and the nearby sea floor shows that instabilities of the outer atoll slopes have occurred throughout their geological histories. These instabilities are likely to have involved rock falls, rock slides, debris and grain flows and flows caused by liquefaction. There is no reason to suppose that these instability processes will not continue to operate in the future. Such processes are typical of atolls and carbonate islands in the Pacific and elsewhere.

Experience of underground nuclear tests under the rim of Mururoa has shown that the loadings produced by explosions can cause, or accelerate, incipient submarine rock slides and slope sediment instabilities.

2.8 Quality and Adequacy of Available Data

The question arises as to the quality and adequacy, for the Commission's purposes, of the data reviewed in this chapter. Uncertainties about the quantity and quality of the data available imply some degree of uncertainty about the conclusions reached from numerical modelling, in particular.

Because of the range of data that, ideally, is required for the studies reported in Chapters 3–7, it is difficult to assign numerical ratings to the quality and adequacy of the data available in each category and sub-category. Accordingly, a simple three-point qualitative scale will be used in which the data are described as being good, fair of poor. On this basis, Table 2.5 presents a summary assessment of the quality and adequacy, for the Commission's purposes, of the data reviewed in this chapter.

The **general geology** of the atolls has been studied in great detail over the past 30 years. The geological history, petrology and stratigraphy are especially well understood. Although it is less of a complicating factor on the atolls than it is on many sites, the structural geology has not been studied in as much detail as other aspects of geology. Geophysical studies have contributed to the development of some understanding of the structure of the atolls.

Data on the **engineering geology** and detailed local geology at test sites are largely lacking. Borehole and core logging to establish standard engineering geology and rock engineering parameter (e.g. fracture frequency and orientation, RQDs, fracture condition, rock material strength indices) would have been very helpful. As noted in Section 2.6, no in-situ stresses were measured.

Like the geology, the **topography** and morphology of the atolls, including the submarine slope morphology and bathymetry, have been studied in great detail over a period of some 30 years. Although a greater degree of local detail may have been an advantage for the purposes of slope stability studies, the quality and quantity of these data are quite adequate for the Commission's needs.

The **physical properties** of the various rock materials, including their densities, porosities and thermal properties, are as well-established as could reasonably be expected, taking their natural variability into account.

Although they have been studied in some detail, the **mechanical properties** of the rocks are not as well known as the Commission ideally requires. The distinction between rock material and the rock mass is made in Section 2.4.1. Uniaxial compressive strength measurements have been made on large numbers of small specimens of the rock materials. The triaxial compression tests were often carried out at confining pressures that were too high and without the pore pressure measurement or control required for the reliable establishment of effective stress strength or yield criteria. The determination of reliable mechanical properties in the shock and dynamic loading ranges is a difficult undertaking. Limited amounts of useful data are available. No data are available on the

Table 2.5 Quality and adequacy of available data

Category	**Sub-Category**	**Quality/Adequacy**
Geology	Petrology	Good
	Stratigraphy	Good
	Structural Geology	Fair
	Engineering Geology	Poor
	In-Situ Stresses	Poor
Topography	Surface Topography	Good
	Submarine Slopes	Good
	Bathymetry	Good
Physical Properties	Densities	Good
	Porosities	Fair
	Thermal Conductivities	Good
Mechanical Properties		
1. Rock Materials	Unconfined Compressive Strengths (static)	Good
	Strength/Yield Criteria (static)	Poor
	Strength/Yield Criteria (dynamic)	Poor
	Deformabilities (static)	Poor
2. Rock Masses	Strength/Yield Criteria (static)	Poor
	Strength/Yield Criteria (dynamic)	Poor
	Deformabilities (static)	Poor
Hydraulic Conductivities		
1. Rock Materials		Fair
2. Rock Masses		Fair

mechanical properties of the rock masses. The IGC has made its own estimates of these properties from the data available (Section 2.5.1).

Hydraulic conductivities of the rock materials and of the rock masses in a number of states have been measured or estimated by a variety of means. The summary of order of magnitude values given for the rocks and rock masses in Sections 2.4.4 and 2.5.2, respectively, are judged to be fair estimates for the purposes of the numerical modelling presented in Chapters 6 and 7.

2.9 Concluding Remarks

The following comments by the renowned French geologist, the late Professor J. Goguel, are taken from Appendix 2 of the Tazieff Report (Tazieff 1982). They illustrate some of the geological uncertainties associated with Mururoa and Fangataufa[†].

After a general discussion of the geological evolution of atolls, Professor Goguel continues:

> *Returning to Mururoa - and Fangataufa - the sea-beam diagrams (which, regrettably, do not extend beyond the foot of the talus) show that the talus undulates about a series of protruding ridges, which contain pinnacles. These ridges seem to be part of the volcanic edifice - lines of* [small] *cones or* [volcanic] *emissions through fissures. Although this view is widely accepted, it is an impression only; one would prefer to be sure. An effort should be made to obtain proof, by dredging, underwater dives, measurement of the magnetic field and gradient at depth in the region or by any other means.* [see Fig. 1.5, produced after Professor Goguel's comments, below[‡].]
>
> *If we assume, tentatively, that these ridges are part of the volcanic framework, then the talus of coral debris, the weak materials occupying the valleys between the ridges, represent the main sliding risk, and are clearly identified* [on the sea beam diagrams]. *If the precise bathymetric surveys had been deep enough, which was not the case, this interpretation could have been verified by establishing the presence of cones* [or volcanic fissure intrusions] *alongside the valleys.*
>
> *Accepting this interpretation, the main zones of small valleys of coral debris can be seen* [from the sea beam diagrams] *to be in the south, the western*

[†] Phrases shown in square brackets have been added to clarify the meaning of the original French text.

[‡] Professor Goguel apparently is referring to the sea beam (bathymetric) diagrams mentioned in the first paragraph. The figure (post-1982; Guille et al. 1996, Fig. 23), shows the results of bathymetric observations to greater depth, as he recommended (see last sentence of first paragraph). The new results, extending to a depth of 2000 m, confirm the existence of the volcanic ridges.

part, the south-centre, southeast and northeast. These can be considered as the zones of risk.

As to the NW, opposite the passes, this could perhaps correspond to a particularly large zone of ancient sliding, which may have cut into the volcanic basement, at a time such that recolonisation by coral was not complete, giving rise to the passes, precisely in the "notched" part of the atoll contour.

In the SE, how significant are the so-defined risk zones, and what could be the consequences? It should be recalled that the slides under consideration would affect the detrital carbonate apron only, which has no influence - except insofar at it contributes to the rock surcharge [vertical loading] *- on the confinement of the tests. Thus, these slides do not involve any risk of release of radioactivity.*

They may affect the atoll surface, even quite substantially; the road could be under water, but this would still be a local problem, with no major safety implications either locally or more distant. The most serious consequences arising from this [slide] *phenomenon- the recurrence of which may be unavoidable, are the hydraulic effects, against which a passive protection system has been installed.*

Of course, it would be valuable to be able to determine the [allowable] *yield of the explosions as a function of their distance from the external talus* [slope], *so as to be able to* [design to] *avoid any sliding. To the extent that the explosion may act as a simple trigger, I am not sure that this procedure, which has been adopted, can be considered reliable, in a situation* [such as we have] *where the "reserve of stability" can not be calculated precisely for the current situation.*

Calculations of slope stability by soil mechanics principles are subject to severe limitations.

The first difficulty arises in the definition of the geometry of the model used in the calculations; one is limited to two-dimensional or axi-symmetric (cylindrical) models while, in reality, the unstable mass is confined within some form of small valleys.

It is the transition zone that exhibits the worst mechanical properties. This zone consists of clays, resulting from the alteration of volcanic rocks that were exposed on the surface. It is perhaps an over-simplification to assume that this zone is a continuous layer between the volcanic massif and the coral carbonate formations. The coral reef barrier around the volcanic massif has emerged at various times [in its history] *and has been covered, at least partially, by alluvium produced by alteration of the above-water vol-*

canics, and by volcanic projections or flows, altered to varying degrees in places. Some borings (e.g. Zoé) have shown intercalations of coral reef carbonates within volcanics, and the possibility that such intercalations were more frequent above the level of the present carbonate crown cannot be ruled out. Thus, the transition zone may be less continuous than assumed in the model now used.

The main difficulty in all soil or rock mechanics calculations is that we do not know the initial stress distribution. This will not be hydrostatic in regions where there is relief, i.e. where equilibrium exists under conditions of very low stress.

To overcome this difficulty, Mr. CARISTAN[¶] *uses an original and ingenious method, in which he assumes that each layer of the model is unstressed when laid down, and behaves elastically when loaded by* [the weight of] *subsequent layers. Unfortunately, certain processes violate this hypothesis - in particular, dolomitisation, which involves a change in volume, and must introduce a redistribution of stresses. One can also imagine that, during deposition, certain layers will reach limiting equilibrium and yield, the stresses being transferred onto neighbouring layers; but there is no method of calculating the effect of these processes on the stress distribution.*

For these reasons, I believe that a calculation of slope stability by soil mechanics can not be considered, by itself, to provide a definitive result. It can provide comparisons only, or allow evaluation of the effect of various changes [in assumed conditions]. *I recommend, therefore, that the calculation performed for the NE slope be repeated, using the same hypotheses, for the SW and South slopes, which we know have failed after having been stable earlier. Only such a comparison of results (often expressed, improperly, as a "safety factor") will allow us to obtain some idea of the risk presented by the NE slope.*

Conclusion

From the above discussion [more extensive than the extract quoted above] *we may deduce that the changes in the geological setting produced by the* [underground nuclear] *tests are of the same nature as those which have or would have resulted from natural evolution* [of the atolls] *over a much longer period. We do not know, however, how to convert the effect of the explosions into an acceleration of the rate of natural geological change; different effects behave very differently in this regard.*

[¶] Currently, Head of Laboratoire de Détection et de Géophysique (LDG).

This implies that these changes do not introduce any new forms of risk (tidal waves have occurred in the past). Certain disturbances may result from carrying out the tests, but these are entirely technical problems, which it should be possible to solve.

Considerable advances have occurred in computer modelling capabilities, particularly in the application to geological materials and situations in the 16 years since Professor Goguel wrote the comments above, but the uncertainty, variability and data-limited character of problems remain unchanged. The analyses of the slope failures in the southwestern and northeastern regions of Mururoa described in Chapters 4 and 5 of this report were carried out using essentially the same modelling procedure for both (as recommended by Prof. Goguel, above), with appropriate changes to include the particular geological features of each regions. Fully three-dimensional models are now available and have been used to illuminate certain aspects of the IGC study.

All of these improvements in modelling capabilities notwithstanding, we can offer no definite reason why the Tydée slide occurred on the rim some 2 km or so to the west of the explosion. This must be related to some (unknown) local heterogeneity or anomaly that was not included in the three-dimensional model. The pre-explosion bathymetric profile does not indicate the existence of any discernible geometrical feature such as the volcanic ridges and valleys discussed by Professor Goguel.

Chapter 3

NEAR-FIELD MECHANICAL DAMAGE

3.1 Introduction

An underground nuclear explosion creates a large cavity around point zero* (the location of the nuclear device), typically within less than one-tenth of a second (see Fig. 3.1) following detonation of the bomb. This cavity is surrounded by a region where the rock has experienced irreversible changes to its structure, ranging from melting and crushing caused by the passage of a very strong shock wave, to some inelastic deformation of the rock (the degree or intensity of damage depending on the distance from point zero). Within a few hours, the cavity collapses as it is filled by rock blocks and debris resulting from the formation of a chimney directly above the created opening.

The primary objective of this chapter is to assess critically the information published by DIRCEN/CEA regarding the size of the cavity, the nature and extent of the damaged rock region around the cavity and the height of the chimney. This assessment relies on published data pertaining to other underground nuclear testing sites and on mathematical modelling and numerical simulation using rock properties provided by DIRCEN/CEA.

The secondary objective is to provide an introductory description of the complex phenomena by which the thermal energy liberated by the nuclear explosion is used to create the cavity and damage the rock, as well as basic technical information (such as the scaling laws and transformation of thermal into mechanical energy) that is detailed further in the accompanying appendices.

3.2 Phenomenology of an Underground Nuclear Explosion

3.2.1 Preamble

The detonation of a nuclear explosion quasi-instantaneously generates an energy, Y (the "yield"), which is then converted into other forms of energy through a sequence of processes, as follows.

First, the device and some surrounding rock (as well as some water) are vaporized. A fraction of the initial energy released by the explosion, δY, is expended (mainly as a latent heat of vaporization and melting) in that process. The volume of vaporized

*often referred to as the "working point" in U.S. nuclear testing literature and by DIRCEN/CEA Document No. 6, p. 21

rock, which corresponds to a cavity with initial radius r_c, is proportional to the released energy Y, or "yield" of the explosion; in other words, $r_c = \bar{r}_c Y^{1/3}$, with the constant $\bar{r}_c$ depending, among other things, on the initial density of the rock.

Second, the cavity expands from an initial radius r_c to a final radius R_c. The final cavity volume is also proportional to Y — i.e. $R_c = \overline{R}_c Y^{1/3}$. The energy available for the expansion phase, $(1 - \delta)Y$, is initially in the form of internal energy of the gases contained in the cavity. The expansion of the gas can be assumed to follow the perfect gas law; during this expansion the gas does work on the surrounding rock, initially generating a strong shock wave. While the shock is strong enough, some of this work is transformed into irreversible heat in the rock and dissipated by a phase change (vaporization of water, melting of the rock). With increasing distance from point zero, the stress wave becomes weaker and transforms first into a plastic wave responsible for shear failure and damage of the rock, and then into an elastic wave at a distance $R_d = \overline{R}_d Y^{1/3}$.

Most the energy liberated by the device (at least 95%) is thus expended in an approximately spherical volume of rock of radius R_d, containing a cavity of radius R_c centred at point zero. The remainder of Y (at most, 5%) is transferred outside this sphere and converted in approximately equal amounts into stored elastic energy and radiated seismic energy. According to DIRCEN/CEA documents (Bouchez and Lecomte 1996; DIRCEN/CEA Document No. 7), the coefficients $\overline{R}_c$ and $\overline{R}_d$ for the nuclear explosions at the Pacific Test Centre (PTC) are approximately equal to 12 m/kt$^{1/3}$ for shallow and 100 m/kt$^{1/3}$ for low-yield (hence, shallow depth of burial) explosions, and 10 m/kt$^{1/3}$ and 80 m/kt$^{1/3}$ for large-yield (more deeply buried) explosions. For example, a nuclear explosion with a yield of 150 kt (about $6.3 \cdot 10^{14}$ Joules), purportedly the maximum yield achieved at the PTC, would create a cavity of radius of about 53 m inside a damaged volume of rock with outer radius of about 530 m (according to the values of $\overline{R}_c$ and $\overline{R}_d$ quoted above). The seismic energy liberated by such an explosion would be approximately equivalent to an earthquake of magnitude 6.0.

The following text describes in more detail the processes by which the initial released energy Y is transformed into other forms of energy. It provides an introduction to the mathematical models developed further in this chapter and in Appendices J to M. (A description of the near-field mechanical effects of an underground explosion can also be found in Bouchez and Lecomte 1996.)

3.2.2 Propagation of the Shock Wave in the Rock

The energy generated quasi-instantaneously by the nuclear reaction is predominantly radiated to short distances, where it first causes vaporization of both the bomb material and the surrounding rock. Production of gases allows the initial energy to be transformed into internal energy of the gases, a large portion of which is then available to perform mechanical work. Further vaporization of the rock takes place, mainly from the action of an extremely intense shock wave propagating through the rock. The efficiency of

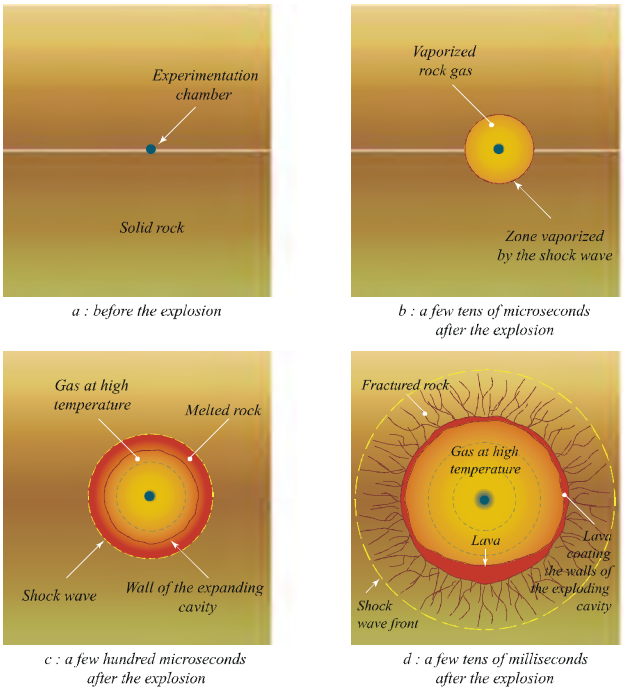

Figure 3.1 Cavity formation (after Bouchez and Lecomte 1996; see also Fig. 1.7)

conversion of the energy of the nuclear device into mechanical energy — i.e. the "coupling" between the nuclear device and the surrounding rocks, is related directly to the amount of gas produced by the energy release. Strong "coupling" occurs, for example, when the nuclear device is exploded in carbonates and/or water-saturated rocks, due to the release of large amounts of CO_2 gas or H_2O vapour, while a low efficiency would be achieved by exploding the nuclear device in a large empty cavity (a technique known as "decoupling").

At the end of the vaporization phase (which takes place within nanoseconds to a few tens of microseconds after the detonation), the situation can be idealised as corresponding to an "initial" cavity approximately 30 m^3 in volume for a 1-kt explosion, filled by gases at extremely high pressure. This marks the onset of cavity expansion, under the mechanical action of the compressed gases.

The early stage of the expansion is associated with the radial propagation of an intense shock wave in the rock, which results in melting of the rock in the immediate vicinity of the cavity, intense crushing and fragmentation of the rock further away, and radial acceleration of the rock to expand the cavity. In this early stage of cavity expansion, the shock front is spreading much faster than the elastic waves, and a single-front structure exists. (This is seen in Fig. 3.2, for example, for the radial pressure profile at

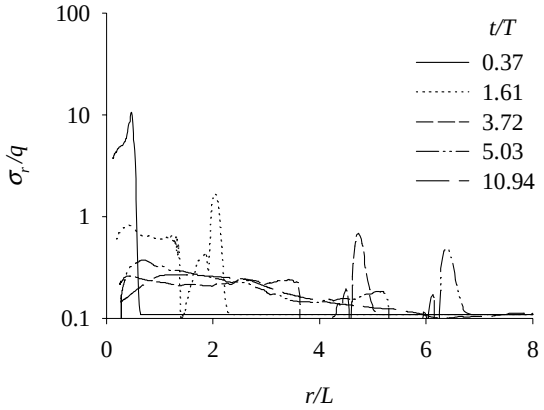

Figure 3.2 Radial stress profiles (r is the distance from the point zero, t is the time after the explosion, and L and T are the characteristic length and time defined in Section 3.5.4)

$t/T = 0.37$.) However, due to the spherically divergent motion and energy dissipation, the velocity of the shock front decreases progressively, leading eventually to the appearance of an elastic precursor ahead of the main shock jump. (This double-front structure of the shock wave is linked to the existence of a kink at the elastic limit in the Hugoniot curve — see App. J for details.) Further spreading of the shock causes a continuous decrease of the pressure jump until the elastic limit of the rock is reached. From this point, the wave becomes essentially elastic, and the double-front structure disappears. The distance from point zero at which the wave becomes elastic corresponds to the outer radius, R_d, of the damage zone discussed in Section 3.2.2. Note that, depending on the magnitude of the in-situ stress, some discrete tensile fractures may develop beyond radius R_d.

Numerically calculated profiles of radial and tangential stresses (in a spherical coordinate system centred at point zero) at different times after an explosion are shown in Figures 3.2 and 3.3. Similarly, the histories of the radial and tangential stresses at different distances from point zero are shown in Figures 3.4 and 3.5. (Note that the results shown in Figs. 3.2–3.5 do not exhibit the double-front structure of the plastic wave, because a smooth Hugoniot curve was assumed in the calculations.)

3.2.3 Melting, Crushing and Fracturing of the Rock

Energy dissipation during the phase of cavity expansion is associated with melting, fragmentation and crushing, shear failure and associated flow, and tensile failure of the rock caused by the passage of the shock wave. The different modes of rock fracturing that occur are mainly controlled by the magnitude of the stress and the duration of load.

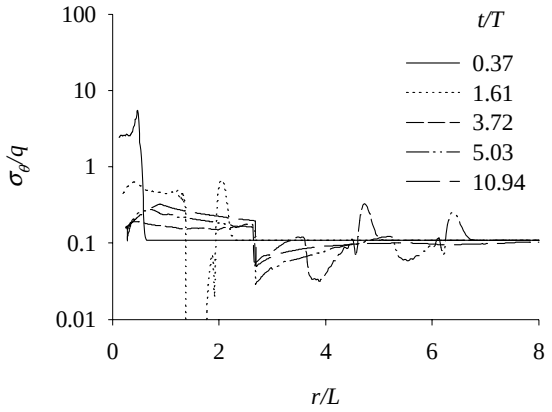

Figure 3.3 Tangential stress profiles (r is the distance from the point zero, t is the time after the explosion, and L and T are the characteristic length and time defined in Section 3.5.4)

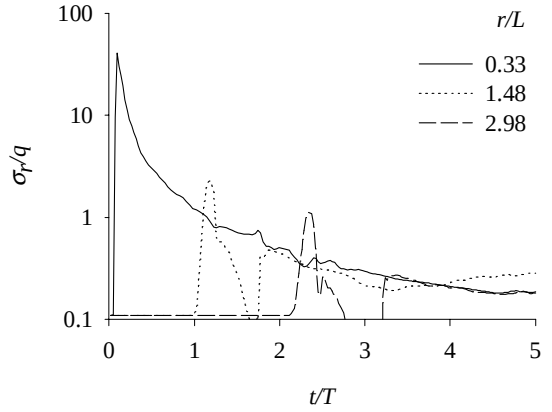

Figure 3.4 Radial stress histories (r is the distance from the point zero, t is the time after the explosion, and L and T are the characteristic length and time defined in Section 3.5.4)

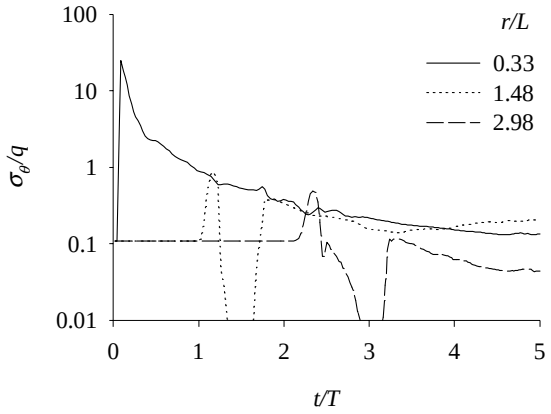

Figure 3.5 Tangential stress histories (r is the distance from the point zero, t is the time after the explosion, and L and T are the characteristic length and time defined in Section 3.5.4)

Figure 3.6 shows a conceptual picture of the damage in the rock at the end of cavity expansion phase. Several zones can be recognized: (i) the cavity of radius (R_c) filled with gas, (ii) molten rock ($R_c < R < R_m$), (iii) crushed rock ($R_m < R < R_f$), (iv) rock fractured by shear failure ($R_f < R < R_s$), (v) rock deformed inelastically by shear ($R_s < R < R_d$), and (vi) discrete tensile fractures ($R_d < R < R_e$). Although discrete zones have been identified in this conceptual picture, in reality, the transition between different modes of rock failure is progressive and graduated.

The molten and crushed rock regions result from conditions that occur when the mean stress during the passage of the shock wave is much larger than the shear strength of the rock. Indeed, the ratio of the pressure at the shock front to the shear strength of the rock is typically three orders of magnitude (i.e. a factor of 1000) in the molten rock zone and one to two orders of magnitude in the crushed rock region. In these regions, the response of the rock to passage of the shock wave is essentially that of a fluid. It is thus adequate to limit the description of the dynamic rock response to the Hugoniot, which is the relation between the specific volume jump and the pressure jump across the shock front (see App. J). The Hugoniot curve can be used to estimate the heat production and the shock front velocity as a function of pressure jump. The degree of fragmentation in the crushed rock zone decreases with distance from point zero, reflecting a progressively diminishing maximum stress level experienced by the rock during the shock.

In the shear failure region, the rock has experienced, during the shock, shear stresses that are typically of the same order of magnitude as the mean stress. The behaviour of the rock during failure can then be adequately described within the framework of classical elasto-plastic theories, with a non-linear failure envelope. Shear failure of the rock

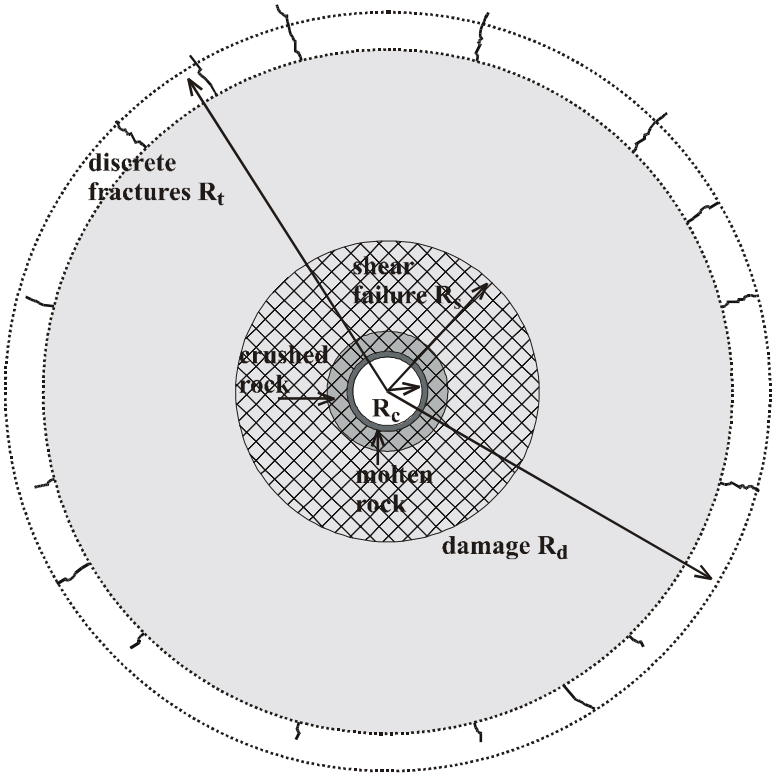

Figure 3.6 Damage zones in the rock produced by the shock wave diverging from a nuclear explosion

leads to a fragmentation of the rock generally associated with an increase of the pore space and concomitant irreversible volumetric expansion of the rock and a dramatic loss of strength. The failed rock is characterised by virtually zero cohesion, but it retains significant frictional resistance. Note that the dilatant behaviour of the rock during shear failure could increase significantly the seismic signal of the underground explosion (Rodionov et al. 1971).

There could be a region outside the damaged rock region where discrete tensile fractures exist. The existence of tensile cracks is of concern if the fractures reach the ground surface or very permeable rock formations, as they would then provide a pathway for the release (venting) of radioactive gas. The propagation of these cracks is driven by tensile stresses that are induced, if the lithostatic stress is not large enough, by the outward radial displacement of the rock required to accommodate the formation of a cavity and, possibly, the irreversible volumetric expansion of the rock in the damaged rock region. Radial fracturing will thus be prevented if the depth of burial of the nuclear device is large enough. Also, the fine stratification of the basalts (with interbeds of porous rocks)

at the PTC is likely to inhibit the propagation of the tensile cracks. The development of these cracks dissipates very little mechanical energy, which can thus be ignored in the overall energy balance.

Finally, it must be noted that some mechanical effects during an explosion are peculiar to the saturated rock environment of the PTC. Indeed, underground nuclear explosions at other military testing sites (Semipalatinsk, NTS, Hoggard) took place in low-porosity or unsaturated porous rocks, although a small number of explosions was carried out in oil-bearing rocks in the former USSR (Glass 1974; Bakirov and Bakirov 1981), in attempts to stimulate hydrocarbon production. These oil-bearing rock formations are characterised by a porosity (about 20%) similar to that of the basalt at the atolls of Mururoa and Fangataufa (porosity ranges from 10%–30%). Pore collapse was found to be a dominant mode of failure[†] in the oil formations, and no long tensile fractures were observed (Schock et al. 1980; Bovt and Nikolaevskiy 1981; Durham 1981).

The mechanical consequence of the presence of a saturating pore fluid is twofold: first, the Hugoniot is modified, as discussed in Appendix J; and second, pore pressure generated by the explosion (because the rock deformation is essentially undrained over the timescale of interest) is responsible for an effective reduction of the rock shear strength.

3.3 Scaling Laws

Valuable insights into the complex mechanical response of a rock mass to the intense loading induced by an underground nuclear explosion can be gained through dimensional analysis. Such an analysis also enables formulation of the requirements for the applicability of scaling laws (such as the proportionality between the cavity volume, $\mathcal{V}_c$, and the yield, Y), which take into account geometrical similarity of the process (Rodionov et al. 1971).

First, it is useful to introduce a length scale L and a time scale T to identify an underground explosion with an energy release (or yield) Y in a rock characterised by a peak unconfined compressive strength[‡] q, and a compressional wave speed C:

$$L = \left(\frac{Y}{q}\right)^{1/3} \tag{3.1}$$

[†] It is worth mentioning that attempts to use an underground nuclear explosion as a means to stimulate oil reservoirs were rather short-lived, as the rock permeability around point zero was found to be decreased due to pore collapse. Similar attempts in the USA to stimulate production from gas reservoirs apparently were also unsuccessful.

[‡] Note that other measures of rock strength, such as the approximately constant shear strength that is characteristic of rocks at very high effective confining pressure, could have been used in the definitions of L and T.

$$T = \frac{L}{C} \tag{3.2}$$

Consider, first, the final cavity radius, R_c, which can be expressed as¶

$$R_c = \eta_c L \tag{3.3}$$

where $\eta_c(\mathcal{S})$ is a number that is a function of a set $\mathcal{S}$ of (dimensionless) parameters that characterise the geomechanical environment (in-situ stress, physical and mechanical properties of the rock), the "coupling" of the nuclear device (see Section 3.2.2), and the depth of burial. It is convenient to express the dependence of η_c upon these parameters as

$$\eta_c = \eta_c \left(\mathcal{S}_Y, \mathcal{S}_{\text{stress}}, \mathcal{S}_{\text{coupling}}, \mathcal{S}_{\text{rock}}\right) \tag{3.4}$$

where $\mathcal{S}_Y$ denotes the subset of parameters dependent on the yield; $\mathcal{S}_{\text{stress}}$ is the subset that depends on the in-situ stress (function of the depth of burial); $\mathcal{S}_{\text{coupling}}$ is the subset characterising the coupling; and $\mathcal{S}_{\text{rock}}$ is the subset of parameters describing the mechanical response of the rock. For our purpose, we restrict the content of these sets to the following independent dimensionless parameters:

$$\mathcal{S}_Y = \left\{\frac{t_y}{T}, \frac{h}{L}\right\} \tag{3.5}$$

$$\mathcal{S}_{\text{stress}} = \left\{\frac{\sigma_o}{q}\right\} \tag{3.6}$$

$$\mathcal{S}_{\text{coupling}} = \{\delta\} \tag{3.7}$$

$$\mathcal{S}_{\text{rock}} = \left\{\frac{C^2\rho}{q}, \frac{q_r}{q}, \nu, \phi, \psi, \phi_r, \psi_r, \cdots\right\} \tag{3.8}$$

In the above, t_y is a "relaxation time", which describes the time scale of the drop of rock strength from peak to residual value; h is the depth of burial; $\sigma_o = \rho g h$ is the lithostatic stress at point zero (with ρ = the rock density and g = the acceleration of gravity); δ is a number characterising the efficiency of conversion of the energy released by the nuclear explosion into mechanical energy available to expand the cavity (see Section 3.5); q_r is the residual strength of the rock; and $\nu, \phi, \psi, \phi_r, \psi_r$ comprise a series of numbers further describing the mechanical response of the rock. Note that the rock has been assumed to be homogeneous in this analysis.

¶ Strictly speaking, R_c should be viewed at this stage as the characteristic dimension of the cavity — not as the radius, which implies spherical symmetry.

The limits between the various zones of damage around the cavity can be expressed in a form similar to (3.3) and (3.4). For example, the radius, R_d, (or, more exactly, the characteristic dimension) of the boundary between the intact and the damaged rock region can be written as

$$R_d = \eta_d L \tag{3.9}$$

with

$$\eta_d = \eta_d \left(\mathcal{S}_Y, \mathcal{S}_{\text{stress}}, \mathcal{S}_{\text{coupling}}, \mathcal{S}_{\text{rock}}\right) \tag{3.10}$$

Consider, now, the practically important cases characterized by

$$\frac{t_y}{T} \ll 1 \tag{3.11}$$

$$\frac{h}{L} \gg 1 \tag{3.12}$$

Under these conditions, the subset $\mathcal{S}_Y$ does not enter the parameter list of either η_c or η_d, which then become constants independent of the explosion yield[§]. In other words, the problem becomes geometrically similar with respect to the yield Y, as the dependence of R_c and R_d (and other limits between zones) on Y is through the scaling length, L (which is the only length entering the problem definition), only. Note that the particular case of geometrical similarity, which hinges on the fulfillment of the conditions (3.11) and (3.12), is embodied in the classic scaling laws

$$R_c = \overline{R}_c\, Y^{1/3} \tag{3.13}$$

$$R_d = \overline{R}_d\, Y^{1/3} \tag{3.14}$$

where both coefficients $\overline{R}_c$ and $\overline{R}_d$ are independent of Y. Obviously, the ratio of two lengths, such as R_c/R_d, does not depend on Y under conditions of geometrical similarity.

The results of nuclear underground tests worldwide are generally reported in the form of particular values for $\overline{R}_c$, $\overline{R}_d$, and other scaled values (in the traditional unit of m/kt$^{1/3}$); this suggests that the conditions of geometrical similarity are essentially fulfilled for underground nuclear explosions.

3.4 DIRCEN/CEA Estimates of Cavity and Damage Dimensions

The DIRCEN/CEA estimates of the final cavity dimension and limits of the various zones of damage are given by Bouchez and Lecomte (1996) and are summarised here in

[§] It is assumed, of course, that finite limits η_c or η_d exist for both $t_y/T \to 0$ and $h/L \to \infty$. Note also that the cases characterised by $t_y/T \gg 1$ and/or $h/L \ll 1$ are physically meaningless.

Table 3.1 and in Figure 3.5. Further details are given in DIRCEN/CEA Document No. 5, which also provides a relation between the chimney height H_c, the yield Y, and the depth of burial h. According to DIRCEN/CEA Document No. 6, these numbers are derived from field data obtained from small boreholes drilled for *post-mortem* radiochemical sampling of the lava, with some confirmation from numerical simulations.

Table 3.1 Summary of DIRCEN/CEA estimates of zones around a nuclear cavity

vaporized rock[a]	$\overline{r}_c$	$\sim$	2.1 m/kt$^{1/3}$
molten rock	$\overline{r}_m$	$\sim$	3.1 m/kt$^{1/3}$
final cavity[b]	$\overline{R}_c$	$\sim$	12 m/kt$^{1/3}$
	R_c	$\sim$	100 $(Y/h)^{1/3}$
shear failure[c]	$\overline{R}_s$	$\sim$	40 m/kt$^{1/3}$
inelastic deformation[d]	$\overline{R}_d$	$\sim$	$80 - 100$ m/kt$^{1/3}$
chimney height[e]	H_c	$<$	1100 $(Y/h)^{1/2}$

[a] $\overline{r}_c$ is scaled outer radius of the vaporized rock zone
[b] $\overline{R}_c$, R_c are scaled and final cavity radius, respectively
[c] $\overline{R}_s$ is scaled outer radius of the failed rock region
[d] $\overline{R}_d$ is scaled outer radius of the region of inelastic deformation of the rock, corresponding to the damaged/intact rock interface
[e] H_c is chimney height

Several comments need to be made concerning the DIRCEN/CEA discussion of shock wave effects.

- The DIRCEN/CEA documents, (for example, Bouchez and Lecomte 1996), use the term "fractured rock" and "fracture extension limit" for what has been denoted here as "(shear) failed rock" and "limit, or outer radius, of the shear failure region". The word "fracture" is used in this report exclusively in the context of tensile cracking of the rock. Note that Figure 3.7 is somewhat misleading, as it indicates a connected network of quasi-radial fractures extending directly from the cavity, through the crushed and shear failed-rock regions; indeed, this depiction, together with the term "fracture", suggests that long tensile cracks exist in these zones. CEA scientists agree that such cracks are unlikely in these zones. (Fig. 1.9 presents an interpretation showing shear cracking separating more distant tensile cracks from the cavity.) Finally, the term "crushed rock" is used in this text to denote what is identified as "pulverised rock" in Bouchez and Lecomte (1996) (although the term "crushed" is also sometimes used in that text).

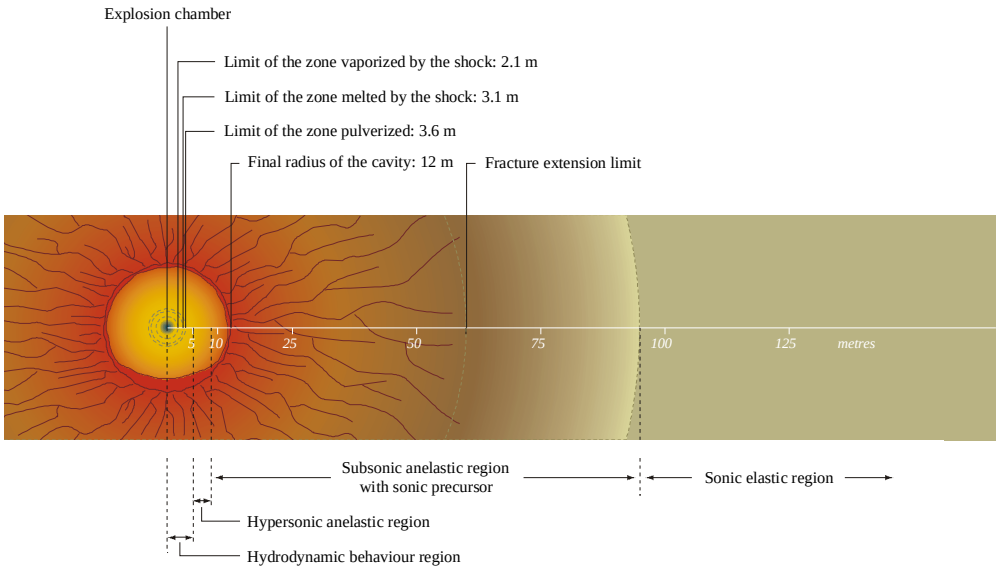

Figure 3.7 Rock damage induced by a 1-kt nuclear explosion (with some limits as defined by Bouchez and Lecomte 1996)

- For depths of burial, h, in the range 500–700 m, the expression for R_c as a function of Y and h, quoted in Table 3.1, is approximately equivalent to $\bar{R}_c \sim 12$ m/kt$^{1/3}$.

- The quantity of vaporized and melted rock actually depends on the specific heat of vaporization and density of the rock. For a depth of 1100 m, the expression becomes $\bar{R}_c \sim 9.7$ m/kt$^{1/3}$. The values quoted in Table 3.1 must be regarded as averages. In Bouchez and Lecomte (1996), the total weight of melted rock per kilotonne is shown to vary from approximately 500 t/kt for a rock density of 2100 kg/m^3 to about 900 t/kt for a density of 2700 kg/m^3.

3.5 Estimation of Size of Cavity and Damage Zone

3.5.1 Preamble

This section discusses estimates of the radius of the cavity ($\overline{R}_c$) and the outer radius of the damaged rock region ($\overline{R}_d$) for the underground nuclear explosions carried out at the PTC. The discussion follows three lines of argument: (i) an empirical approach making use of published data from other test sites; (ii) a numerical simulation of the dynamics of an underground explosion; and (iii) a quasi-static cavity-expansion model providing upper bounds to $\overline{R}_c$ and $\overline{R}_d$. The discussion is preceded by an analysis of the transformation of the thermal energy liberated by the nuclear reaction into mechanical energy.

3.5.2 Mechanical Energy Available for Deformation of the Rock

Part of the energy liberated by the nuclear explosive device is consumed in the vaporization of the metal container, water and surrounding rock in a few tens of microseconds following the detonation. The energy "lost" in vaporization, Y_v, is conveniently expressed as a fraction, δ, of the total energy Y liberated by the nuclear explosion — i.e., $Y_v = \delta Y$. The remainder of the energy, $Y_o = (1 - \delta)\, Y$, is assumed to have been completely transformed into internal energy of the gas as the shock leaves the vaporized rock region, which is taken to correspond to time t_o (see Fig. 1.8).

Energy Y_o is, in principle, available to perform mechanical work through expansion of the cavity, which corresponds essentially to the "initial" region of vaporized rock. Indeed, the "initial" state at time t_o can be described as a cavity of radius r_c in a rock mass filled with a gas at uniform pressure p_o and uniform temperature T_o. (The values of initial pressure and temperature are extreme, with $p_o \approx 10^5$ MPa and $T_o \approx 10^5$ °C.) Beyond time t_o, the cavity will expand under the action of the gas pressure to reach a final radius, R_c. Note that time t_o can advantageously be taken to correspond to the origin of time in the description of the processes associated with mechanical deformation of the rock; thus, the word "initial" will be used to describe states at the time t_o following the firing of the nuclear device.

At the end of the cavity expansion phase, the initial energy, Y_o, of the gas will be partitioned into (i) heat generated at the shock-wave front (40–50%), (ii) heat generated by irreversible plastic deformation of the rock beyond the shock region (30–40%), (iii) locked-in internal energy through phase changes (less than 5%), (iii) elastic (strain) energy in the intact rock surrounding the damaged region (less than 8%), (iv) kinetic energy that is radiated seismically (less than 5%), and (v) some residual internal energy, Y_r, left in the gas inside the cavity (a few percent). The fraction $(1 - \delta)$ is often referred to as the "mechanical efficiency" of the nuclear explosion. As discussed previously, many factors influence the efficiency, the most important one being the "coupling" between the nuclear device and the surrounding rock (Fig. 1.8).

Under similar conditions (and neglecting the initial cavity and presence of the device), the mass of basalt vaporized by the shock is proportional to the released energy (Butkovich 1971,1974; DIRCEN/CEA Document No. 6. The fraction, δ, of the total energy released by the nuclear explosion that is consumed by vaporization of the basalt is thus independent of Y and can be written as

$$\delta = e_v \overline{M}_v \tag{3.15}$$

where e_v is the specific latent heat of vaporization, and $\overline{M}_v$ is the mass of vaporized basalt per unit total energy release. Also, the outer radius, r_c, of the vaporized zone can be expressed as

$$r_c = \overline{r}_c Y^{1/3} \tag{3.16}$$

where

$$\overline{r}_c = \left(\frac{3\overline{M}_v}{4\pi\rho_o} \right)^{1/3} \tag{3.17}$$

with ρ_o denoting the initial (saturated) density of the basalt. According to the DIRCEN/CEA documents (Bouchez and Lecomte 1996, DIRCEN/CEA Document No. 6), $e_v \approx 2750$ cal/gr, $\overline{M}_v \approx 70$ t/kt[‖] and $\rho_o \approx 2360$ kg/m^3; hence, $\delta \approx 19\%$ and $\overline{r}_c \approx 1.92$ m/kt$^{1/3}$. The value $\overline{r}_c \approx 1.92$ m/kt$^{1/3}$ compares well with $\overline{r}_c \approx 1.8$ m/kt$^{1/3}$ computed by Butkovich (1971) for granite.

An upper bound for the radius of the vaporized zone can be calculated by assuming that all of the energy Y is transformed into an internal energy of the vaporized rock (i.e. that the kinetic energy is zero):

$$\overline{r}_{c,\max} = \left(\frac{3}{4\pi h_v} \right)^{1/3} \tag{3.18}$$

where h_v is the internal energy of vaporization[**]. For example, for granite, $h_v \approx 58.4$ GPa yields $\overline{r}_{c,\max} \approx 5.53$ m/kt$^{1/3}$.

The value of the energy fraction $\delta \approx 19\%$ is also comparable to calculations showing that about 25–30% of the explosion energy was spent in evaporation and melting of tuff in the Rainier event at NTS (Johnson et al. 1959).

Finally, the initial pressure of the gas in the cavity produced by vaporization of the rock can be computed from the adiabatic gas expansion law:

$$pV^\gamma = p_o V_o^\gamma \tag{3.19}$$

$$pV = (\gamma - 1)e \tag{3.20}$$

where V is the specific volume (volume per unit mass), γ is the effective gas constant, e is the specific internal energy of the gas, and the subscript o denotes a quantity at initial time t_o. At the onset of the cavity expansion phase, the specific gas volume, V_o, and the internal energy, e_o, are given by

$$V_o = \frac{1}{\rho_o} \qquad e_o = \frac{Y_o}{M_v} = \frac{(1-\delta)}{\overline{M}_v} \tag{3.21}$$

where M_v is the mass of the vaporized rock (equal to $\overline{M}_v Y$) and ρ_o is the density of the intact basalt. The initial pressure p_o of the gas in the cavity can then be deduced from

[‖] The number quoted in Bouchez and Lecomte (1996) is larger (i.e. 100 tons of vaporized rock/per kt).

[**] Strictly speaking, there is a smooth transition between the different states (mixtures of solid and gaseous phases) upon unloading as a function of the internal energy attained by the material immediately behind the shock (Zel'dovich and Raizer 1967).

(3.20) and (3.21) to be

$$p_o = \frac{(1-\delta)\,(\gamma\ -1)}{\rho_o \overline{M}_v} \tag{3.22}$$

The average pressure in the vaporized rock (after the process of vaporization by the shock is complete) is thus independent of the total initial energy of the device. Using the values for δ, ρ_o, and $\overline{M}_v$ pertaining to the tests at PTC, and taking the gas constant $\gamma \approx 1.7$, the initial pressure p_o of the gases in the cavity is estimated to be about 80 GPa.

3.5.3 Empirical Evidence

One way to assess the plausibility of the DIRCEN/CEA estimates of the size of the cavity and the damaged zone is to compare these estimates with data obtained from other testing sites. A useful comparison between sites can be made on the basis of the scaling laws. Thus, both R_c and R_d can be expressed as follows (see Section 3.3):

$$R_c = \eta_c L \tag{3.23}$$

$$R_d = \eta_d L \tag{3.24}$$

where L is the characteristic length $(Y/q)^{1/3}$, and η_c and η_d are two numbers, functions of several dimensionless parameters that characterise the efficiency of the nuclear explosion, the rock response, the state of stress, etc. The numbers η_c and η_d can be computed from the quoted values of $\overline{R}_c$, $\overline{R}_d$, provided that the rock strength, q, is known; indeed, from (3.23) and (3.24),[††]

$$\eta_c = \overline{R}_c q^{1/3} \tag{3.25}$$

$$\eta_d = \overline{R}_d q^{1/3} \tag{3.26}$$

Although the number η_c (or η_d) is expected to vary from site to site, it is likely to remain of the same order. Thus, a comparison between sites can be made on the basis of η_c and η_d. Table 3.2 gives a compendium of data pertaining to underground nuclear explosions and the corresponding values of η_c and η_d; it can be seen that the values of η_c and η_d for the PTC are generally of the same order as the values reported for other sites. It can be said, therefore, that experiences from other sites are consistent with values for the size of the cavity and the damaged rock region that have been published by DIRCEN/CEA (Bouchez and Lecomte 1996; DIRCEN/CEA Document No. 6).

[††]The traditional unit of $\overline{R}_c$and $\overline{R}_d$ is [m/kt$^{1/3}$]; this can be converted into a SI unit according to the relation m·kt$^{-1/3}$ = 6.21·10^{-3} MPa$^{-1/3}$.

Table 3.2 Summary of available data on size of cavity and damaged zone [in m/(kt)$^{1/3}$] created by an underground explosion in rock (Michaud 1970, Heuze 1983, Bovt et al. 1990, Bouchez and Lecomte 1996)

	site	rock	q (MPa)	$\overline{R}_c$	$\overline{R}_d$	η_c	η_d
1	PTC	basalt	110	12	100	0.36	2.98
2	Hoggard	granite	100 - 200	7	26	0.20 - 0.25	0.78 - 0.94
3	Hardhat NTS[a]	Climax granite	110 - 150	10	140 - 200	0.30 - 0.33	4.64 - 6.59
4	Semipalatinsk	granites	100 - 200	8 - 10	140	0.23 - 0.36	4.03 - 5.08
5	Oil reservoir in USSR	limestone	50	10	100 - 200	0.23	2.28 -4.57
6	Gas reservoir in USA	sandstone	20 - 35	8 - 12	140 - 200	0.13 - 0.20	2.36 - 4.06
7	Rainier NTS[a]	tuff	2 - 35	15	37.5	0.16 - 0.30	0.40 - 0.76

[a] additional data on the properties of rocks at NTS taken from Lama and Vutukuri (1978)

3.5.4 Numerical Simulation

For this study, numerical simulations of underground nuclear explosions have been carried out using a computer programme developed specifically for this purpose. Although highly idealised, the calculations were performed using rock parameters that pertain to the nuclear tests at the PTC. The main objective of the numerical modelling is to calculate the equilibrium (i.e. final) size of the cavity and extent of the various damaged regions and to assess the dependence of these dimensions on the in-situ stress. Secondary objectives of the simulations are to confirm the validity of the scaling laws and to evaluate the robustness of the numerical simulation through examination of the sensitivity of the results to unknown parameters.

The mathematical model on which the numerical algorithm is based is described in Appendix K, while certain numerical considerations — together with a verification problem — can be found in Appendix L. These appendices illustrate the degree of complexity involved in these calculations, even though the numerical simulations are made for a highly idealised problem in which critical simplifications have been introduced (e.g. spherical symmetry, material homogeneity, relatively simple material response) and which also neglect of the presence of pore fluid. These simplifications have important implications. For example, the assumption of spherical symmetry implies that the influence of stress gradient, stress anisotropy and rock heterogeneity on the size and shape of the cavity and the damaged rock region cannot be assessed. Also, outside the stress regime for which the rock behaves essentially as a fluid (in the immediate vicinity of the cavity), the material is assumed to behave as a frictional cohesive material, with no tensile strength, that experiences a quasi-instantaneous loss of strength once the failure criterion is reached.

All of the calculations were performed on the assumptions that (i) the underground explosions at the PTC occurred inside the submarine volcanic formation and (ii) the

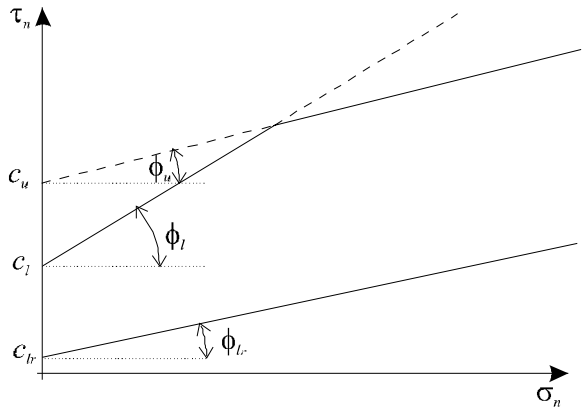

Figure 3.8 Peak and residual shear failure criterion for volcanics, as used in simulation of explosion effects (see Table 3.3)

Table 3.3 Mechanical properties of the basalt used in the simulation of events at the PTC (see Fig. 3.8)

density	ρ_o	2360	kg/m^3
bulk modulus	K	20000	MPa
shear modulus	G	9600	MPa
friction angle	ϕ_l	30°	
friction angle	ϕ_u	13°	
cohesion	c_l	32	MPa
cohesion	c_u	105	MPa
residual cohesion	c_{lr}	0	
residual friction angle	ϕ_{lr}	8°	
tensile strength	σ_t	0	

damage was contained within that formation. The mechanical properties for this rock, taken from DIRCEN/CEA Document No. 6, Appendix, are shown in Table 3.3, with reference to Figure 3.8. (The Hugoniot curve used in the shock calculations is shown in Fig. L.2; see App. L).

There are two specific features of the constitutive model of the basalt that require further discussion, as they directly affect the outcome of the calculations. First, the rock is assumed to behave elastically until failure. In other words, the elastic limit is assumed to coincide with the peak shear-strength criterion, with the consequence that the zone of inelastic damage (identified earlier as $R_s < R < R_d$) cannot be predicted by the numerical model. Thus, $R_s = R_d$; however, the symbol R_d will be used to identify the outer radius of the failure zone consistent with our definition that the rock outside the region of radius

R_d behaves elastically, even though tensile fractures could perhaps develop in this region under certain in-situ stress conditions. Second, a small "relaxation" time, t_y (of the order of ms; see App. K, Fig. K.2), is introduced to give a time scale for the weakening of the rock from peak to residual strength (see App. K and Fig. K.2 for details). As discussed below, knowledge of the material behaviour under these loading conditions and rates is virtually non-existent, and t_y is considered as an extra degree-of-freedom that is used to "tune" the outcome of the numerical computations.

The numerical simulations begin at the end of the vaporization phase (i.e. the origin of time is taken to correspond to the previously identified time t_o). Hence, the initial geometry of the model is defined by the radius r_c of the zone of vaporized rock, given in (3.17), and the initial conditions correspond to the initial gas pressure, p_o, in the cavity, computed according to (3.22), and a uniform isotropic stress of magnitude σ_o in the medium. Here, $\overline{r}_c = 1.92$ m/kt$^{1/3}$ and $p_o = 80$ GPa. The evolution of the pressure, p, as a function of the cavity radius is computed using the gas law (3.19), noting that the cavity expansion is adiabatic and that the mass of gas inside the cavity remains unchanged (see App. L for details).

The result of a particular simulation is illustrated in Figure 3.9, which shows the evolution of the cavity radius with time for a 1-kt yield. [Due to the dependence of the solution on the relaxation time t_y, the scaled curve shown in Figure 3.9 is not truly "universal" (i.e. independent of Y), but the influence of the magnitude of the yield is weak.]

The main goal of the calculations, however, is to predict the final dimensions of the cavity and the damaged region. The scaling factors computed from four numerical simulations of an underground nuclear explosions at the PTC are shown in Table 3.4.

Three parameters were varied in these simulations: the yield Y (1, 10 kt), the initial stress magnitude σ_o (12, 24 MPa), and the relaxation time t_y (5, 10 ms). Using the material properties listed in Table 3.3 and the definitions (3.1) and (3.2), the two yields can be translated into the following values of length scale L and time scale T : $L =$ 33.6 m and $T = 11.5$ ms for $Y = 1\,kt$, and $L = 72.3$ m and $T = 24.8$ ms for $Y = 10$ kt. The isotropic stress, σ_o, is taken as the pre-existing vertical stress at point zero; the two values $\sigma_o = 12$ and 24 MPa correspond to a depth of burial h of approximately 500 and 1000 m, respectively, in a rock of average density (2.5 gm/cm^3). The values of t_y are chosen in the calculations to "match" the DIRCEN/CEA estimates for the cavity radius ($\overline{R}_c \sim 12$ m/kt$^{1/3}$) and the outer radius of the damage zone ($\overline{R}_d \sim 90$ m/kt$^{1/3}$). Because t_y/T is close to unity for smaller yields (e.g. $t_y/T \sim 0.5$ for $Y = 1$ kt and $t_y/T \sim 0.25$ for $Y = 10$ kt), the condition (3.11) for geometrical similarity is not strictly met, and the numerical solution deviates slightly from the scaling laws represented by (3.13).

Note that a comparison of the results for simulations 1 and 2 provides a test of the correctness of the code. Indeed, these two simulations correspond to different yields, the same initial stress and different relaxation times t_y — but chosen so that $t_y/T = 0.43$ in

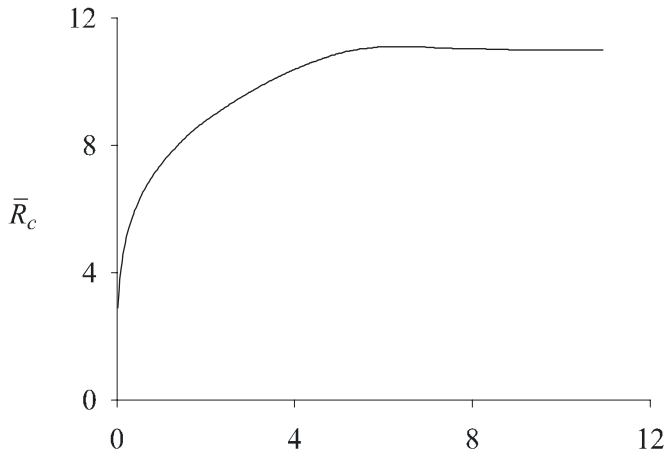

Figure 3.9 Evolution of the scaled cavity radius, $\overline{R}_c$, as a function of the dimensionless time t/T. The cavity radius evolves from the initial value $\overline{r}_c$ (corresponding to the outer radius of the vaporized rock region) to the final equilibrium radius, $\overline{r}_c$. Computations were performed for the case σ_o = 12 MPa, Y = 1 kt, t_y = 5 ms; note that the cavity "rebounds" slightly after reaching its maximum size (i.e. for t/T $>$ 6). The rebound corresponds to the (partial) release of the elastic strain energy imparted to the rock by the outgoing shock wave.

Table 3.4 Scaling factors (all expressed in m/kt$^{1/3}$) for the cavity radius $\overline{R}_c$, crushed zone $\overline{R}_f$, damaged zone $\overline{R}_d$, and tensile fracture zone $\overline{R}_e$

Case	Y (kt)	σ_o (MPa)	t_y (ms)	$\overline{R}_c$	$\overline{R}_f$	$\overline{R}_d$	$\overline{R}_e$
1	1	12	5	11.0	13.4	89.8	100.4
2	10	12	10.8	11.0	13.3	90.4	101.9
3	1	24	5	9.3	11.9	55.5	59.0
4	1	12	10	9.8	12.4	80.8	96.0

both cases. As can be seen from Table 3.4, the scaling factors are virtually identical for the two simulations. This is expected, since the numbers η in (3.23) and (3.24) should be identical for both cases.

Case 2 from Table 3.4 illustrates the sensitivity of the numerical results to the initial stress. The increase in initial stress from 12 MPa to 24 MPa (i.e. 100%) causes a reduction of the radius of the damaged zone by 40%; the effect on the cavity radius is smaller (16%). The DIRCEN/CEA estimate of the dependence of the cavity radius on the initial stress (or depth of burial), given in Table 3.1 for the same case, yields a reduction of the cavity radius by 21%.

Numerical simulations reveal that the relaxation time, t_y, the parameter characterising the time delay over which the rock is assumed to lose its strength, has a significant influence on the predicted size of the cavity. In the simulations, the relaxation time t_y was varied between 5 ms and 10 ms, resulting in a variation of the scaled cavity radius, $\overline{R}_c$, between about 9.8 m/kt$^{1/3}$ and 12 m/kt$^{1/3}$ (for calculations pertaining to $Y = 1$ kt and $\sigma_o = 12$ MPa). Knowledge of rock softening at these time scales (less than 1 second) is, however, virtually non-existent; hence, t_y should be viewed as a "fudging" parameter whose value is adjusted simply to match predicted cavity dimensions — or, in the case of CEA, cavity dimensions and surface settlements — with those observed (Bouchez and Lecomte 1996; DIRCEN/CEA Document No. 6, Appendix).

Such a large sensitivity of predicted results to a parameter that is essentially unknown obviously weakens conclusions reached on the basis of numerical simulations. Such sensitivity to input parameters (either to the relaxation time or to others unexplored in this study, such as rock dilatancy or the residual strength of the rock) also highlights some of the uncertainty of using numerical modelling as a predictive tool, especially for large-scale situations and rock-loading conditions that cannot be simulated in typical laboratory tests. A critical assessment of the literature on underground nuclear experiments indicates that in the papers reviewed, good matches between numerical results and field data were obtained *a posteriori*, with a series of parameters adjusted to match experimental measurements (Institute for Defense Analysis 1970; DIRCEN/CEA Document No. 6, Appendix).

3.5.5 Cavity Expansion Model

An alternative approach, which is expected to give an upper bound to the cavity radius and size of the damage zone, is to assume that all of the initial energy of the gas (at the end of the vaporization phase) is available to perform a quasi-static expansion of the cavity.

The problem of a pressurised cavity in an infinite elastoplastic medium is characterised by the existence of a limiting internal pressure p_c (also referred to as the "cavi-

tation pressure"[‡‡]). Unbounded quasi-static growth of a cavity takes place if the internal pressure is maintained at the cavitation pressure. In Appendix M, the cavitation pressure p_c and the ratio $\xi_* = R_c/R_d$ are determined by considering the self-similar problem of a cavity expanding quasi-statically from a zero initial radius. For the purpose of the analysis reported in Appendix M, the rock is assumed to be characterised by a single peak and residual failure envelope and to be perfectly brittle — i.e. the rock loses strength abruptly once it fails.

The essence of the upper-bound determination of R_c and R_d is to match the energy available in the gas to perform quasi-static expansion of the cavity. According to the cavity expansion model, the cavitation pressure can be written as

$$p_c - \sigma_o = \Pi q' \tag{3.27}$$

where Π is the dimensionless cavitation pressure. The parameter q' (giving the scaling) is a modified strength which accounts for the influence of the in-situ stress (σ_o) in a frictional material:

$$q' = q + (N_\phi - 1)\sigma_o \tag{3.28}$$

where N_ϕ is a number dependent only on the peak friction angle. Both Π and ξ_* are functions of a set of numbers characterising the rock. Note that the dependence of Π and ξ_* upon Young's modulus E, uniaxial strength q, and in-situ stress σ_o is through the small number q'/E.

Note, finally, that the stresses are everywhere compressive if

$$\sigma_o \geq \frac{q}{3} \tag{3.29}$$

If σ_o is less than the minimum value given by (3.29), the maximum radial extent of tensile fractures is obtained by determining the scaled radius $\xi_t = R/R_c$ at which the net hoop stress (i.e. the sum of the (tensile) hoop stress induced by cavity expansion and the (compressive) in-situ rock stress) vanishes in the elastic region. This radial distance may be expressed as

$$\frac{\xi_t}{\xi_*} = \left[\frac{q'}{(N_\phi + 2)\sigma_o}\right]^{\frac{1}{3}} \tag{3.30}$$

The simplest approach to calculate R_c is to assume that the initial energy in the gas, Y_0, is used entirely to expand the cavity (see also App. M). The work used to expand the

[‡‡] "cavitation pressure" (i.e. the pressure at which the cavity develops) used here is different from the "cavitation pressure" in fluid mechanics (i.e. the pressure at which the vapour bubbles form in a low-pressure region when liquid is accelerated to high velocities—the cause of blade erosion in pumps, turbines, etc.)

cavity at constant pressure from an initial volume $\mathcal{V}_o$ is

$$W = \Pi q' (\mathcal{V}_c - \mathcal{V}_o) \tag{3.31}$$

Imposing $W = Y_o = (1 - \delta)\, Y$ with $\mathcal{V}_o = 0$ gives the final cavity volume

$$\mathcal{V}_c = \frac{(1 - \delta) Y}{\Pi q'} \tag{3.32}$$

and the cavity radius

$$R_c = \alpha' L' \tag{3.33}$$

In the above, L' is a new characteristic length

$$L' = \left(\frac{Y}{q'} \right)^{1/3} \tag{3.34}$$

and α' is a number given by

$$\alpha' = \left[\frac{3(1 - \delta)}{4\pi\, \Pi} \right]^{1/3} \tag{3.35}$$

Upper-bound estimates for $\overline{R}_c$, $\overline{R}_d$, and $\overline{R}_t$, as computed with the quasi-static cavity expansion model for the mechanical properties of the basalt given in Table 3.3, are listed in Table 3.5 for both $\sigma_o = 12$ MPa and $\sigma_o = 24$ MPa.

Table 3.5 Scaling factors $\overline{R}_c$, $\overline{R}_d$, $\overline{R}_e$ (all in m/kt$^{1/3}$) predicted by the cavity expansion model

σ_o (MPa)	$\overline{R}_c$	$\overline{R}_d$	$\overline{R}_t$
12	18.1	94.9	124.4
24	16.9	83.9	92.1

As expected, the scaling factors predicted by the cavity expansion model are larger than estimates obtained by numerical simulation (compare with Table 3.4).

The above calculations make no reference to the presence of pore fluid. The pore fluid influence can be taken into account indirectly by modifying the rock properties, assuming that the deformation is undrained (see, for example, App. Q in the context of the slope stability calculations). For the particular case of concern here, it is sufficient to set the peak friction angle ϕ_l to zero. (The residual friction ϕ_{lr} is left unchanged, however, as setting ϕ_{lr} to zero would render the broken basalt equivalent to a fluid — since c_{lr} is assumed to be zero — which is obviously not physically plausible.) Calculations show that the values of $\overline{R}_c$ and $\overline{R}_d$ are not affected significantly by setting $\phi_l = 0$.

3.6 Chimney Formation

Following cavity formation and the passage and attenuation of the shock wave outwards from the cavity, the static stresses will be redistributed around the cavity. The magnitudes and distribution of the tangential static stresses induced around the periphery of the cavity will depend on the magnitudes of the vertical and horizontal in situ stresses and the internal pressure within the cavity. As the gases inside the cavity cool with time following expansion of the cavity and there is possibly some seepage of the gases into the surrounding rock, the pressure inside the cavity can be expected to fall to well below the original lithostatic pressure. At the same time, the melted rock around the periphery of the cavity will begin to solidify and will also tend to accumulate at the bottom of the cavity under the action of gravity.

Under these conditions, and because the cavity can be up to several tens of metres in diameter in the fractured basalt, progressive collapse of the crushed and sheared rock above the cavity will commence. The caved zone or chimney will propagate upward until it stabilises naturally. This process usually occurs over a period ranging from a few minutes to a few hours after the explosion. The progress of chimney formation is accompanied by a series of micro-seismic events that have been recorded (Bouchez and Lecomte 1996, Fig. 5.11). The structure of the volcanic rock mass as illustrated in Figure 2.22 exerts a significant influence on chimney formation. In the crushed and sheared zones, the blocky nature of the rock mass illustrated in Figure 2.22 will be accentuated, and blocks will fall progressively into the cavity in an unravelling mechanism under the influence of gravity.

Eventually, the progress of the upward expansion of the chimney will be arrested by one or a combination of three major mechanisms.

1. As the chimney forms progressively, there will be a further redistribution of stresses around the periphery of the caved zone. The concentration of horizontal compressive stresses above the chimney in the mechanism known as arching (Brady and Brown 1993) may become sufficient to hold or clamp the remaining blocks of rock in place.

2. Alternatively, the chimney front may encounter a largely unfractured rock layer a few metres in thickness (see Section 2.3.3), which, with the possible assistance of horizontal stresses transmitted through it, remains stable and so arrests the propagation of the chimney.

3. Finally, if neither of these two causes arrests chimney formation, the cavity and chimney zones ultimately will become completely filled with broken rock so that no further unravelling failure is possible. As the broken rock accumulates in the cavity and then in the chimney zone, it occupies a greater total volume than it occupied in situ. In mining this phenomenon is known as bulking. A given mass

of broken rock in the form of rubble may occupy a volume that is, say, 20–30% greater than the volume that the same mass occupied in situ. Eventually, upward propagation of the caved zone will be arrested because there will no longer be any free volume available into which new blocks may fall. Indicative calculations of the possible limits to chimney zone height based on this concept are given in Appendix N. The calculated range of approximately 5–10 times the cavity radius is consistent with observations made by DIRCEN/CEA using post-event drilling from surface into the zone surrounding the cavity (Bouchez and Lecomte 1996). Assuming a cylindrical collapse chimney, a value of $H_c/R_c = 8$ (see App. H) indicates a "bulking factor" of the order of 18% only. This is lower than that usually observed in most mine caving operations, and suggests that the volcanic material above the caving is fractured to small sizes (order of several cm).

3.7 Concluding Remarks and Discussion

None of the information or results of analysis that have been reported in this chapter has given ground to either contradict or question the validity of DIRCEN/CEA data regarding the size of the cavity, the extent of the damaged region, and the height of the chimney. This assessment relies on a comparison of these data with worldwide experience, on mathematical modelling, on numerical simulation, and on consideration of the consequences of geological heterogeneity — in the case of the atolls of Mururoa and Fangataufa.

Perhaps the most compelling argument that the DIRCEN/CEA data are adequate comes from an examination of the empirical evidence at other testing sites in combination with scaling laws to account for the difference of rock strengths. Numerical simulations of an idealised underground explosion also gave results that are "close" to the radius of the cavity and the size of the damaged rock region reported by DIRCEN/CEA. The significance of these results must be tempered, however, by the recognition that these predictions are rather sensitive to some parameters (such as the relaxation time) that are essentially unknown. (Hence the good fit of the numerical predictions with DIRCEN/CEA data was in part the result of appropriately selecting these parameters.) Nonetheless, useful information has resulted from the numerical simulations, such as the influence of the in-situ stress (which reflects the depth of burial) on the size of the cavity and the extent of the region where tensile cracks could possibly exist. A strong argument in support of the DIRCEN/CEA data regarding the scaling factors $\overline{R}_c$ and $\overline{R}_d$ also comes from considerations of the quasi-static cavity expansion model, which yields upper bound estimates of these quantities.

Another robust argument on the maximum size of the chimney relies simply on volumetric considerations using values of the bulking factor that are compatible with mining experience. Although DIRCEN/CEA estimates of the chimney height H_c are within the

presumed range, CEA notes that the inverse square root relationship between H_c and depth of burial h (DIRCEN/CEA Document No. 6) is empirical.

It must be noted, finally, that the geological setting of the atoll is unique and that there could be effects associated with the particular topography of this site (a "submarine mountain") that would not have been experienced elsewhere (for example, and speculatively, a reflected wave on the atoll flank causing further damage around the cavity). Nuclear explosions that have been set off inside a mountain (tests carried out by France in the Hoggar in the early 1960s, or some tests carried out in the former USSR) provide perhaps the closest equivalent to the tests at the PTC. However, information on these tests is scarce.

Concerns have been raised in the past that long fractures could be created following a nuclear explosion that would directly connect the cavity to the permeable carbonates, thus enabling effective venting of radioactive gases into the permeable layer. However, an analysis of the stress histories during dynamic loading and residual stress states in the vicinity of the cavity suggests the improbability of the existence of such cracks. At low depth of burial, tensile fractures could develop in the vicinity of the damaged-intact rock interface, but they would tend to be prevented from connecting directly with the cavity because of the compressive stress "cage" that may exist around the opening, at least during the early stages after the initial explosion. The development of long continuous fractures is also likely to be inhibited by the fine stratification of the basalt and the interbedding of rigid basalt and porous carbonates.

Chapter 4

SURFACE SETTLEMENT OF THE ATOLLS

4.1 Introduction

Geodesic surveys carried out by DIRCEN/CEA between 1977 and 1996 have revealed that all the land testing areas of Mururoa have suffered settlements as a result of underground testing. Figure 4.1 shows the cumulative settlement along the road as measured during the testing program. As can be seen in Figure 4.1, the settlement has reached about 2 m in some places (test area 1, north zone). Actually, parts of the rim of Mururoa, initially only about 1–2 m above sea level, are now submerged (test areas 2, 3, 4, south zone). Note that the settlements can be referred to an approximate location on the map of Mururoa, shown in Figure 4.2, by means of the distance in kilometres (*PK, points kilometriques*),* measured along the road from the most easterly point of the road, for both the north and south segments of the rim.

According to Bouchez and Lecomte (1996), the settlement reflects compaction of the upper 120 m or so of the carbonates, taking place quasi-instantaneously after an explosion (see below). However, concern has been raised that the surface settlement is actually indicative of the existence of subsidence craters, similar to those that have formed at the Nevada Test Site (NTS) and at Semipalatinsk. These subsidence craters are the manifestation of a continuous damage of the rock (or soil) and chimney-type collapse from the point of the explosion to the ground surface — the region of damage then providing a potential relatively high-permeability pathway for the direct release of radioactive gases into the atmosphere (as has been observed at the NTS, for example; see App. C).

The objective of this chapter is to provide an explanation of the settlement phenomena observed at the atolls. The discussion and analysis focus on (i) assessment of the likelihood of a direct connection through damaged rock between the explosion chamber and the ground surface, and (ii) the mechanism of deformation revealed in the surface settlements. It is argued, notably on the basis on empirical knowledge, that the surface settlement is unlikely to be the expression of subsidence craters. Rather, the settlement is most probably associated with a mechanism of irreversible deformation of the carbonates, which is apparently disconnected from the damage around the explosion

*On the atoll of Mururoa, the point of origin for the (PK) distances along the road is located on the easternmost point of the road near Anémone, the easternmost part of the atoll (Fig. 4.2).

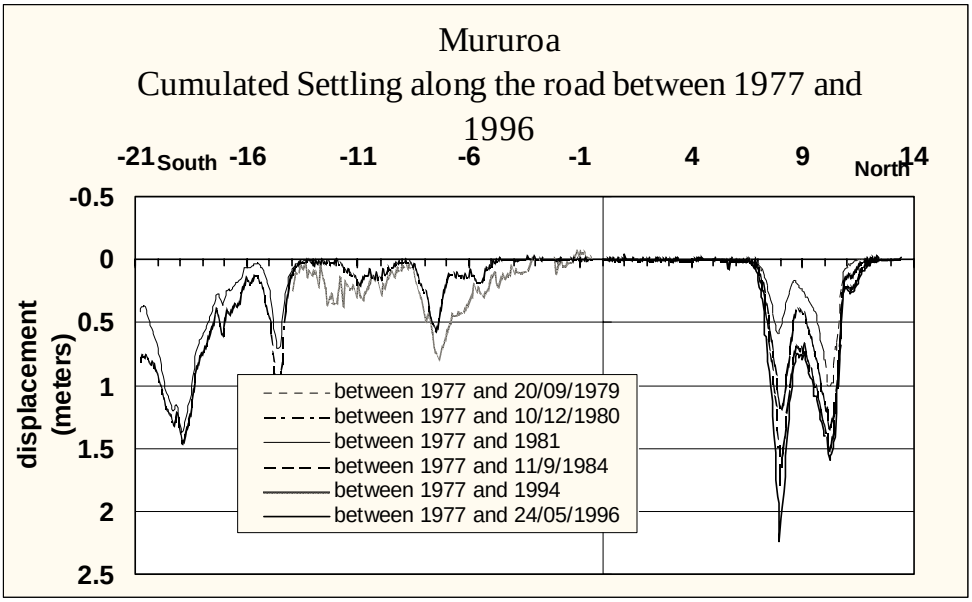

Figure 4.1 Cumulative settlement along the road (DIRCEN/CEA Document No. 7, Fig. 11) (Note that tests on the southern rim extended to PK 24. Measurements of settlements could not be made in the region beyond PK 24 South because this region, originally about 1.5–2.0 m above ocean level (DIRCEN/CEA Document No. 7, Fig. 20) settled below water level — i.e. was inaccessible)

point. However, compaction of the surface layers does not appear to be a plausible primary mechanism of "instantaneous" settlement, as it would require expulsion of a large amount of pore water in an extremely short amount of time. Instead, a shear deformation mechanism is proposed, which involves irreversible lateral movement of the submerged flanks of the atoll. A variety of arguments, detailed in the chapter, are presented to support the shearing mechanism, including results of numerical simulations involving the propagation of a stress pulse in yielding carbonates layers. Finally, this analysis further suggests a connection between the settlement and the stability of the atoll flanks.

4.2 DIRCEN/CEA Interpretation of Surface Settlements

According to Bouchez and Lecomte (1996), surface subsidence is a consequence of the compaction of carbonates (from the surface up to a depth of 120 m), which is caused when a surface layer (or layers) of carbonates is thrown into ballistic flight and falls back to impact the underlying formations (see Fig. 4.3). This sequence of events is described in more detail below.

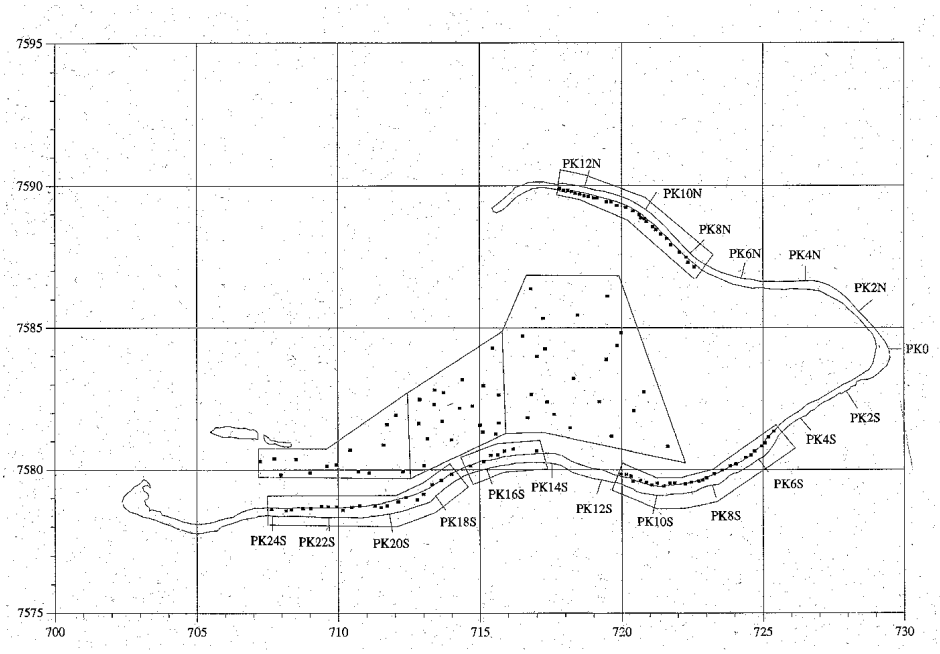

Figure 4.2 Map of Mururoa showing the relation between PK distances and testing areas on the rim (after DIRCEN/CEA; presumed individual test locations have been added) (Note that settlements shown in the figure for test area 4 extend only to PK 215)

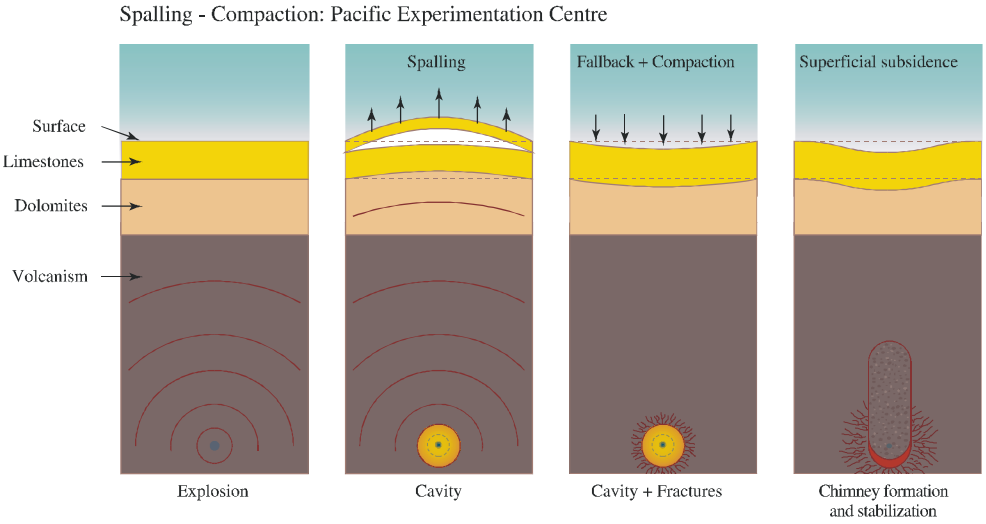

Figure 4.3 Mechanism of settlement at PTC (Bouchez and Lecomte 1996)

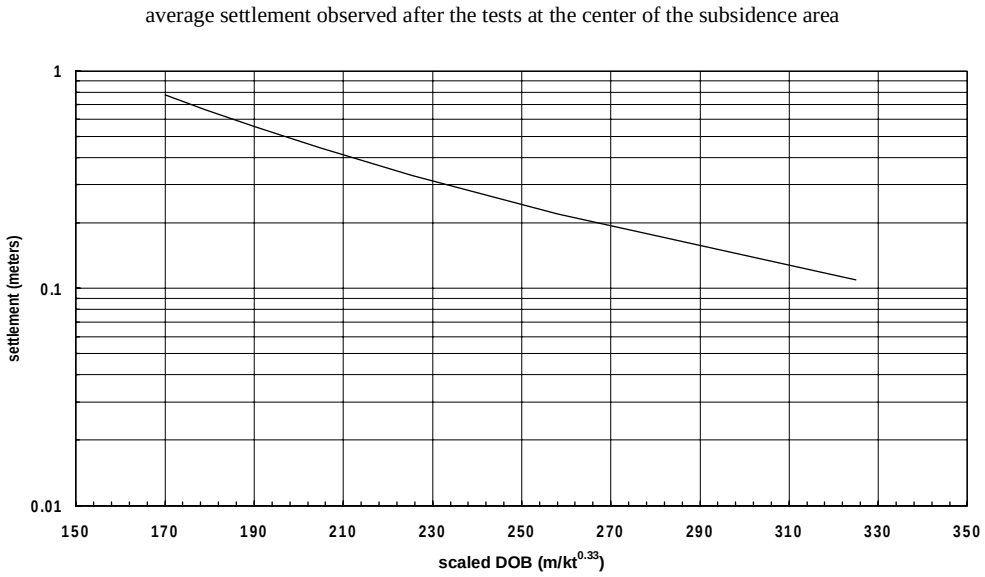

Figure 4.4 Empirical relation between the average vertical displacement at the center of the settlement area and the scaled depth of burial (DOB), $\overline{h} = h/Y^{1/3}$ (DIRCEN/CEA Document No. 6, Fig. 19)

After the ascending wave reflects from the free surface, superposition of the incident and reflected waves creates tension and, subsequently, separation of a layer at a depth of the order of one or two tens of metres. The separated layer then goes into ballistic flight at an initial velocity equal to the average velocity inside the layer at the moment of separation. After rising, the layer falls back due to gravity and elastic forces (bending of the layer) and impacts the underlying carbonates, thus generating a compressive wave. This wave then moves from the surface of impact into the interior of both the spalled layer and the underlying rock, causing compaction in both. The empirical curve shown in Figure 4.4 relates the average settlement and the scaled depth of burial, $\overline{h} = h/Y^{1/3}$, according to DIRCEN/CEA Document No. 6.

Bouchez and Lecomte (1996) also stress the difference between the situation at the PTC and that at other sites, such as the NTS and Semipalatinsk, where subsidence craters have developed following underground testing (see Fig. 4.5 and Section 4.1). The distinct mechanism of subsidence/settlement is attributed to the following two factors:

(1) difference in the depth of burial (tests have been conducted at greater relative depth at the PTC [see Fig. 4.6 giving the minimum scaled depth of burial, $\overline{h}_{\min}$, as a function of the yield, Y, according to DIRCEN/CEA (Caristan 1997) and App. D).

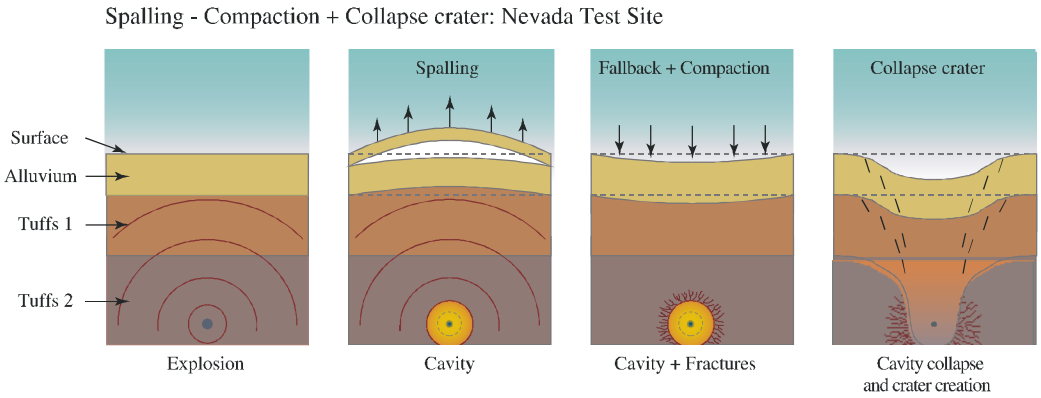

Figure 4.5 Mechanism of subsidence at the NTS (Bouchez and Lecomte 1996)

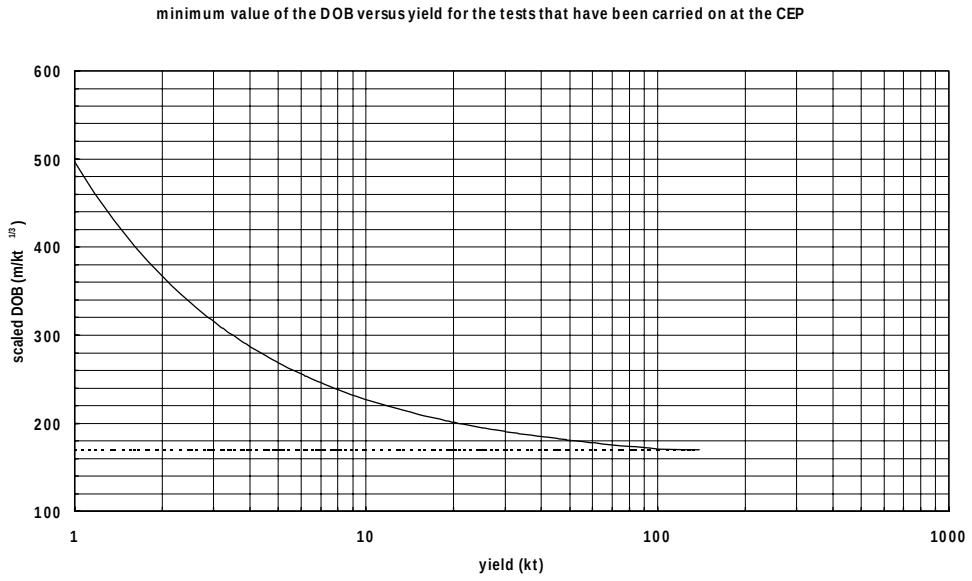

Figure 4.6 Relation between yield Y and reduced minimum scaled depth of burial $\overline{h}_{min}$, according to DIRCEN/CEA (presentation by Y. Caristan at Mururoa, July 1996; actual data points lie above the curve shown)

(2) nature of the surface layers (at both the NTS and Semipalatinsk, the top layers consist of virtually cohesionless soil (alluvium at the NTS, loess at Semipalatinsk), in contrast to the limestones and carbonates found at the atolls of Mururoa and Fangataufa).

4.3 Discussion

4.3.1 Dimensional Analysis Considerations

As a prelude to discussion of the DIRCEN/CEA interpretation of the mechanism of surface settlement, dimensional analysis is revisited in the context of the surface phenomena of concern here. According to the dimensional analysis presented in Section 3.3, the influences of both yield Y and depth of burial h on the nature of the phenomena induced by an underground explosion can be combined into a single parameter, the reduced depth of burial[†] $\overline{h} = hY^{1/3}$. In other words, similar phenomena would occur under constant $\overline{h}$, all other parameters being kept the same.

The direct influence of the gravitational field was ignored[‡] in the scaling considerations of Section 3.3, as well as in the geometrical characterisation of the atoll rim. Neglect of both effects is admissible provided the explosion is "deep" (i.e. $h/L \gg 1$, where $L = (Y/q)^{1/3}$ is the length scale) and that the process of interest (such as the formation of the cavity) is also "deep". However, in analysing the surface effects caused by an underground nuclear explosion, the influences of both gravity and the shape of the rim cannot be automatically disregarded. In fact, the geometry of the rim appears to be of crucial importance in explaining the nature of the deformation mechanism near the surface of the atoll. (As discussed below, the rim geometry enters essentially through the dimensionless ratio of w/λ, where w is the width of the rim and λ the wavelength of the stress pulse, which is related to length scale L).

The influence of the gravitational field can be assessed by studying the limiting case of an explosion in a heavy viscous fluid (Sedov 1992). For this particular case of a material without strength, scaling considerations indicate that the process is similar with respect to the number $Y/\rho g h^4$, in contrast to Y/qh^3 for the case of a weightless solid. It is not known whether similarity is strictly maintained under conditions where both strength and gravity effects are significant, although ad hoc scalings, such as $Y/(\rho g h^4 + qh^3)$, have been proposed (Rodionov et al. 1971). There is evidence to suggest that systematic deviation from a scaling in $\overline{h}$ (i.e. in Y/qh^3) exists when gravity effects are expected to be significant (Rodionov et al. 1971; Butkovich and Lewis 1973). For example, experimental data for the explosion cratering process appear to follow an empirical $Y/h^{3.4}$

[†]The scaled depth of burial, $\overline{h}$, is essentially equivalent to the ratio h/L appearing in the subset $\mathcal{S}_Y$ (introduced in Section 3.3).

[‡]Gravity was introduced indirectly through the magnitude σ_o of the in-situ stress at point zero, as $\sigma_o = \rho g h$.

scaling law[¶] (Rodionov et al. 1971). Both scalings are used below in reporting the thresholds for the reduced depths of burial at which various surface phenomena have been observed. (For that purpose, a second, reduced, depth of burial, $\overline{h}'$, is defined according to $\overline{h}' = h / Y^{1/3.4}$.)

4.3.2 Connection with the Explosion Chamber

The experience accumulated from many underground nuclear tests performed at various testing sites (including NTS and Semipalatinsk) indicates that a reduced depth of burial (either $\overline{h}$ or $\overline{h}'$) indeed controls the nature of the surface effects. As expected, these effects decrease in severity with increasing depth of burial (Rodionov et al. 1971). Different phenomena arise depending on the reduced depth of burial, which can be ordered as follows with increasing $\overline{h}$ or $\overline{h}'$:

(1) explosion craters associated with the expulsion of soil and the collapse of the cavity (at very shallow depth, the bottom of the craters extends to below the location of the nuclear device);

(2) subsidence craters caused by collapse of the cavity and formation of the chimney, affecting layers up to the surface (there is no expulsion of near-surface material, although spalled layers rise in ballistic flight); and

(3) settlement caused by compaction of the surface layers due in part to the fallback of layers that have risen in ballistic flight following slabbing (in some cases, mounds have also been observed).

Empirical rules have been established to define the ranges of scaled depth of burial over which these different processes take place. Thus, explosion craters are limited to $\overline{h} < 61$ m/kt$^{1/3}$, and gases from explosions are contained for $\overline{h} > 107$ m/kt$^{1/3}$, according to Butkovich and Lewis (1973) (who are presumably drawing upon experience at the NTS; see App. D). Rodionov et al. (1971) state that explosion craters have not been observed beyond $\overline{h}' = 65$ m/kt$^{1/3.4}$ in clay and $\overline{h}' = 120$ m/kt$^{1/3.4}$ in alluvium and loess; they also report the formation of subsidence craters for nuclear explosions in the range $100 < \overline{h}' < 200$ m/kt$^{1/3.4}$.

The suggestion that settlements at the atoll surface are associated with subsidence craters can be dismissed on several counts.

1. The stated minimum depth of burial $\overline{h}_{\min}$ at the PTC is larger than the depths at which subsidence craters form, according to empirical evidence. Indeed, values of $\overline{h}_{\min}(Y)$ provided in DIRCEN/CEA Document No. 7 (see also Fig. 4.6) indicate

[¶] The power 3.4 can be thought to reflect a situation intermediate between a strength-dominated (power 3) and a gravity-dominated (power 4) regime.

that the explosions always took place at depths $\overline{h}'$, larger than 200 m/kt$^{1/3.4}$. (For example, $\overline{h}$ =170 m/kt$^{1/3}$ (see App. D) with a 150-kt explosion translates into $\overline{h}' = 207$ m/kt$^{1/3.4}$).

2. Subsidence craters have generally been observed in alluvium. If the depth of burial is insufficient, collapse of the cavity and formation of the chimney can affect layers of soil up to the surface (see Fig. 4.5). Indeed, rupture of the layers in unconsolidated materials can extend over distances, above the cavity, that are well beyond the estimated chimney height at the PTC (at most, H_c is equal to $5R_c \sim 6R_c$), because the bulking factor in unconsolidated materials is very small, unlike in rocks. In contrast, chimneys at the PTC are generally expected to be confined to the basalt and, in any case, are always covered by a thick layer of competent carbonates.

3. There is a large difference between the time scale of the settlements observed at the PTC, which are quasi-instantaneous,[§] and the time scale of the chimney collapse (of the order of a few hours) that would trigger the formation of a subsidence crater.

4. Measurements carried out by the CEA, using gamma logging techniques, of the distance between radioactive probes implanted in the walls of boreholes have shown that the surface settlement is consistent with vertical deformation extending to depths of 120 m in the upper carbonates (Bouchez and Lecomte 1996).

5. Subsidence craters have, in general, a larger height-to-radius ratio and a steeper slope at the edges than for the settlements on Mururoa.

In view of the above arguments and evidence, the explosions at PTC appear to have been completely contained. Therefore, the surface settlement can only be explained by a "superficial" deformation mechanism — i.e. one that affects the near-surface carbonates but which is disconnected from the damaged rock around the explosion chamber. Most likely, the irreversible deformation of the "weak" carbonate (limestone and dolomite) formations near the surface is produced by the seismic (elastic) wave arriving from deeper, competent (basalt) rock.

4.3.3 Mechanism of Settlement

Although there is agreement between the CEA and the IGC with respect to the "superficial" nature of the processes leading to permanent settlements of the atoll surface, the basic mechanism of compaction invoked by DIRCEN/CEA does not appear plausible

[§] In the south zone of Mururoa, most of the settlement takes place within 10 seconds after the explosion. In the north zone, there are long-term components (time scale of months and years) to the settlement, which are associated with the stability of the atoll flank.

for the conditions at the PTC. As a basis to refute the compaction scenario, consider the following information (some excerpted from DIRCEN/CEA reports).

1. The carbonates (as well as the volcanic rocks) are fully saturated with water.

2. The surface settlement takes place within seconds after the explosion (Bouchez et al. 1997). [There is no significant evolution of the settlement with time, except in the northern zone of Mururoa (see Fig. 4.1 and Chapter 5).]

3. The settlement is greater for a given yield and depth of burial when the test takes place in an area that has already been used for testing (Bouchez and Lecomte 1996).

These observations appear to contradict the compaction mechanism. A transient increase in the stress (due to the explosion pressure pulse) in a saturated rock will not generate a significant volumetric plastic deformation (collapse of the pore space) but, rather, a transient increase in pore pressure. Because the increase in pore pressure is transient and the settlement takes place instantaneously (at most, one or two seconds after the wave arrival), the settlement cannot be explained as consolidation — i.e. as a reduction in volume due to drainage of water. Indeed, the time scale, T_c, for consolidation of a layer of thickness, H, and diffusivity, D, *under conditions of sustained loading*, is $T_c = H^2/D$. Taking $H \simeq$100 m and $D \simeq$ 10–100 m^2/s yields $T_c \simeq$ 1.5 – 15 min, which is at least two orders of magnitude larger than the observed time of the phenomenon.

It is worth noting that all instances where the compaction mechanism has been observed, such as at Semipalatinsk, have occurred in unsaturated loess under conditions of a "flat" ground surface.

Also, observation No. 3 is not consistent with our understanding of the behaviour of porous materials. Indeed, porous materials harden as they compact. Furthermore, a pre-consolidated (already compacted) material will generally not compact more than an unconsolidated material.

Finally, as discussed in detail in Appendix P, deformation of the upper carbonates is caused predominantly by the upward-propagating incident wave and not by the (downward-propagating) wave generated by impact of the spalled layers with the underlying carbonates at the end of their ballistic flight, as argued by Bouchez and Lecomte (1996). Under ideal conditions, (i.e. no dissipation, rectangular pulse shape) the wave generated in the superficial carbonates by the impact is identical to the incident compressive wave. (The amplitude of the pulse generated by the impact could be larger—at most twice—than the amplitude of the incident wave if the acoustic impedance of the underlying rock is larger than the acoustic impedance of the spalled layer.) However, it is more likely that more than one layer will be spalled, which will eventually result in a

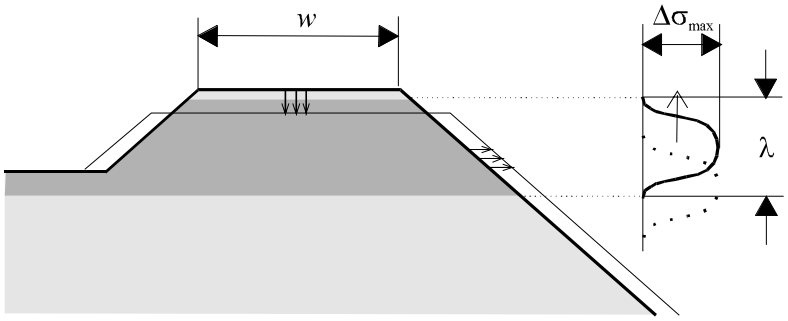

Figure 4.7 Alternative mechanism for surface settlements

series of compressive pulses, each of progressively smaller amplitude and duration than that of the incident wave. Thus, spalling will have an effect on the settlements, but this effect is certainly smaller than the effect of the original, upward-propagating incident wave.

4.4 Alternative Mechanism for Surface Settlements

4.4.1 Shearing Deformation

The alternative mechanism behind the surface settlement is illustrated schematically and idealised to a plane wave process in Figure 4.7. Here, the view is taken that, over the time scale of the passage of the pressure pulse, the response of the water-saturated carbonates to the dynamic loading is essentially undrained. Under undrained conditions, deformation of the carbonates is approximately isochoric (zero volume change)[‖]. Hence, the dominant mechanism of deformation is shearing, and the permanent surface displacement that occurs quasi-instantaneously must therefore be accommodated predominantly by lateral displacement of the flanks of the atolls.

In addition to the condition of water saturation of the carbonates, several other key elements contribute to the plausibility of the proposed mechanism: the nature of the initial effective stress state; the ratio of the width, w, of the atoll rim to the wavelength, λ, of the stress pulse; and the magnitude of the energy flux provided by the stress pulse. Each of these is reviewed below.

4.4.2 Initial Stress State

The initial stress state in the carbonates is characterised approximately by (i) a vertical principal stress of magnitude corresponding to the weight of the overlying rock; and (ii) isotropic horizontal stresses of magnitude given by the water pressure at the depth

[‖] Undrained volumetric deformation of the carbonates is expected to be predominantly elastic, unlike the deviatoric deformation.

of concern (see Chapter 2). It follows, therefore, that the initial effective stress ($\sigma_{ij}^{o\prime} = \sigma_{ij}^{o} + p\delta_{ij}$, where σ_{ij}^{o} denotes the Cartesian components of the initial stress and p the pore pressure) is essentially uniaxial. The consequences of the absence of an effective lateral confinement are twofold. First, the undrained compressive strength q_u of the carbonates remains close to their unconfined compressive strength q, since, then,

$$q_u = q + N_\phi \gamma' d/3 \tag{4.1}$$

where $N_\phi = (1 + \sin\phi)/(1 - \sin\phi)$ (ϕ denoting the drained friction angle), γ' is the buoyant (submerged) unit weight, and d is the depth; hence, q_u increases with depth at a rate of about 1 MPa per 100 m. Second, the carbonates will probably undergo significant softening beyond failure. As discussed in Sections 4.4.4 and 4.5, the magnitude of the observed surface displacement can be explained only by invoking strength softening.

4.4.3 Wave Length of the Stress Wave

The magnitude of the ratio $\delta = \lambda/w$ between the length λ of the pulse and the width w of the rim, taken at the surface of the atoll, is evidently a significant control parameter. This can be seen by examining the two limits of (i) short ($\delta \ll 1$) and (ii) long ($\delta \gg 1$) wavelengths.

- Short wavelength limit ($\delta \ll 1$). Deformation of the rock during the passage of the stress wave is essentially uniaxial (provided that the effects of the curvature of the wave are negligible). In other words, the rock deforms only in the direction of the wave propagation, as in a plane p-wave. Under these limiting conditions, very little surface settlement is expected, since permanent deformation can be accommodated only by volumetric strain — i.e. by compaction, which is minimal in view of the saturation of the carbonates. The limit $\delta \ll 1$ is expected to yield a lower bound to the surface settlement.

- Long wavelength limit ($\delta \gg 1$). The state of stress induced dynamically is approximately uniaxial; i.e. the only non-zero dynamic stress component is the vertical component. In this case, a permanent vertical strain is consistent with a predominantly isochoric deformation, since a lateral horizontal strain (perpendicular to the rim) is allowable, as discussed above. The limit $\delta \gg 1$ corresponds obviously to an upper bound to the surface settlement (this bound is computed below).

The order of the ratio δ varies from 0.1 to 1 for the experiments carried out under the rim of the atoll of Mururoa, taking $w \simeq$ 300–700 m. This range of variation for δ can be deduced from Table 4.1 which lists, among other parameters, the estimated length λ of the stress pulse at the base of the carbonates, for three different orders of magnitude of the yield ($Y = 2$, 10, 150 kt). Thus, the conditions regarding the wavelength to width ratio δ lie somewhere between the short and long wavelength limits, and numerical

modelling is needed, in principle, to provide some quantitative statements with respect to the magnitude of the settlement s. It can be stated, however, that the settlement s is expected to increase with Y, since δ as well as the energy flux increase with Y.

Table 4.1 Minimum depth of burial $h_{\min}$, pulse duration ΔT, amplitude $\Delta\sigma_{\max}$, wavelength λ, and energy flux $\mathcal{F}$, for three values of the yield Y

Y kt	$h_{\min}$ m	ΔT[a] ms	$\Delta\sigma_{\max}$[a] MPa	λ m	$\mathcal{F}$ MJ/m^2
2	465	24	29	68	1.3
10	495	37	56	103	7.4
150	900	99	38	272	9.0

[a] Values for ΔT and $\Delta\sigma_{\max}$ are computed from empirical expressions provided by DIRCEN/CEA Document No. 7 (see App. O). Wavelength λ and energy flux $\mathcal{F}$ are then computed using (4.4), assuming a saturated density $\rho = 2200$ kg/m^3 in the carbonates and a compressional wave speed of $V_p = 2750$ m/s.

4.4.4 Energy Flux and Maximum Settlement

An upper bound for the surface settlement s for the long wavelength limit may be computed using the following arguments, based on several approximations.

Let $\mathcal{F}$ denote the vertical energy flux (energy crossing a horizontal unit area) transmitted through the base of the carbonates, vertically above point zero, by the stress pulse emitted by the nuclear explosion. Assuming a plane wave, $\mathcal{F}$ can be expressed as

$$\mathcal{F} = \rho \int_0^{\lambda} \dot{u}^2 d\xi \tag{4.2}$$

where $\dot{u}$ denotes the particle velocity. After adopting the waveform given in (O.1) and also noting that, under plane wave conditions,

$$\Delta\sigma = \rho V_p \dot{u} \tag{4.3}$$

$\mathcal{F}$ can also be written as

$$\mathcal{F} = \frac{3}{16}\rho\lambda\dot{u}_{\max}^2 = \frac{3\Delta T(\Delta\sigma_{\max})^2}{16\rho V_p} \tag{4.4}$$

where V_p is the compressional wave speed velocity, ΔT is the pulse duration, and $\Delta\sigma_{\max}$ is the stress amplitude. Estimates of $\mathcal{F}$ above point zero for three different orders of magnitude of the yield (Y = 2, 10, 150 kt) can be found in Table 4.1.

An upper-bound estimate, $s_{\max}$, of the maximum settlement may then be obtained by assuming that all the wave energy is used in plastic yielding of the carbonates:

$$s_{\max} = \frac{2\mathcal{F}}{2\alpha q_u - \gamma' H} \tag{4.5}$$

where H denotes the thickness of the carbonate layer that is deforming plastically, γ' is the average submerged (buoyant) unit weight of the carbonates, and α is a number ($0 < \alpha \leq 1$) that accounts for the strength softening ($\alpha = 1$ for a perfectly plastic material — i.e. without loss of strength — and $\alpha = 0$, corresponding to a perfectly brittle material with zero residual strength). In writing (4.5), the work of the gravitational forces, as well as the work against the water pressure along the flank of the atoll, has been taken into account.

A comparison of the upper-bound estimate, $s_{\max}$, using information from Table 4.1 with the empirical curve of Figure 4.4 suggests that softening needs to be invoked to explain the magnitude of s. Consider, for example, a 150-kt explosion which is, according to the CEA, the maximum yield of weapons tested at the PTC. According to (4.5), with $H = 100$ m and $\alpha = 1$, and Table 4.1, $s_{\max} \approx 0.7$ m, which is still smaller than the observed settlement. Note, however, that the settlement can be made arbitrarily large by introducing material softening — i.e. by taking $0 \leq \alpha < 1$.

4.5 Numerical Modelling

A series of numerical simulations was carried out to investigate further the plausibility of the shearing mechanism proposed to explain the surface settlement of the atoll caused by dynamic loading. As discussed above, the ratio, δ, of the wavelength λ of the pulse to the width w of the rim is the parameter that essentially controls the mechanism of deformation of the rim. On the basis of information provided by DIRCEN/CEA, it is estimated that δ varies from about 0.1 to 1 (the latter value corresponding to the maximum yield of 150 kt). Thus, the main issue to be addressed by numerical modelling is whether these estimated values δ are large enough to be consistent with the proposed shearing mechanism, which has been justified so far for the long wavelength limit ($\delta \gg 1$) only. In effect, because δ is directly related to the yield of the explosion, we are interested in exploring the influence of Y on the mechanism of deformation.

The computations were carried out using the finite-difference code *FLAC* (Itasca Consulting Group, Inc. 1995) on the basis of the two-dimensional model shown in Figure 4.8. These calculations were complemented by a three-dimensional simulation of a 150-kt explosion using the code *FLAC*^{3D} (Itasca Consulting Group, Inc. 1997). (The 3D simulation was carried out with the twofold objective of modelling the settlement and the destabilisation of the slope caused by an explosion; see Chapter 5 and Appendix Q for details). Particulars of the two-dimensional numerical simulations are presented in Appendix O; the main features and assumptions of the model are summarised below.

- The analyses are carried out in two steps: first, a quasi-static calculation to determine the initial stresses, followed by a dynamic calculation with pulse loading at the bottom of the model. Plane-strain conditions are assumed in both cases.

- For the purpose of the dynamic analysis, the basalt is modelled as an elastic material and the carbonates as a plastic strain-softening Tresca material. Also, some water on the lagoon and ocean sides of the atoll is explicitly modelled, to simulate the fluid-solid interaction along the submerged flanks of the rim. Modelling of the carbonates as a cohesive, frictionless, and plastically incompressible material is intended to approximate the undrained response of these rocks under dynamic conditions. It follows, therefore, that the dynamic pore pressure response is not modelled explicitly in these calculations. Finally, strength softening is introduced in order to predict "large enough" surface settlements. (Strength softening could result from a combination of cohesion loss and undrained pore pressure increase associated with a compactive tendency of the carbonates during failure.)

- The carbonates (and the basalt) are assumed to be isotropic and homogeneous. Thus, the general increase of strength with depth is ignored in this model, as is the existence of layers of varying properties. These approximations are considered to be of little consequence as far as the main objective of this analysis is concerned, which is to examine the influence of the yield on mechanism of failure and on the relative surface settlement**

- The stress pulse is applied at the bottom of the model as a plane wave. The amplitude, $\Delta\sigma_{\max}$, and the duration, ΔT, of this applied pulse are computed for a given yield, Y, and distance from point zero, following the empirical formulae established in DIRCEN/CEA Document No. 7. Note that the distance from point zero is here taken to be the difference in depth between the centre of the explosion and the transition between the basalt and the carbonates. Because the pulse propagates as a plane elastic wave in the basalt section of the model, there is no attenuation of the wave in the basalt, and the wave form is chosen in order to apply the "correct" loading at the base of the carbonates.

The three cases mentioned earlier, corresponding to yields, Y, of 2, 10 and 150 kt, have been simulated numerically. The results are summarised in Figure 4.9, which shows the maximum surface settlement as a function of the scaled depth of burial scaled to the yield. Figure 4.10 represents the initial configuration of the model and the configuration after passage of the pressure pulse (with the deformation exaggerated 50 times) for the three cases considered. In Figures 4.11 to 4.13, contour levels of the plastic shear

**Increase of strength with depth would tend to concentrate the damage in the near-surface region of the rim.

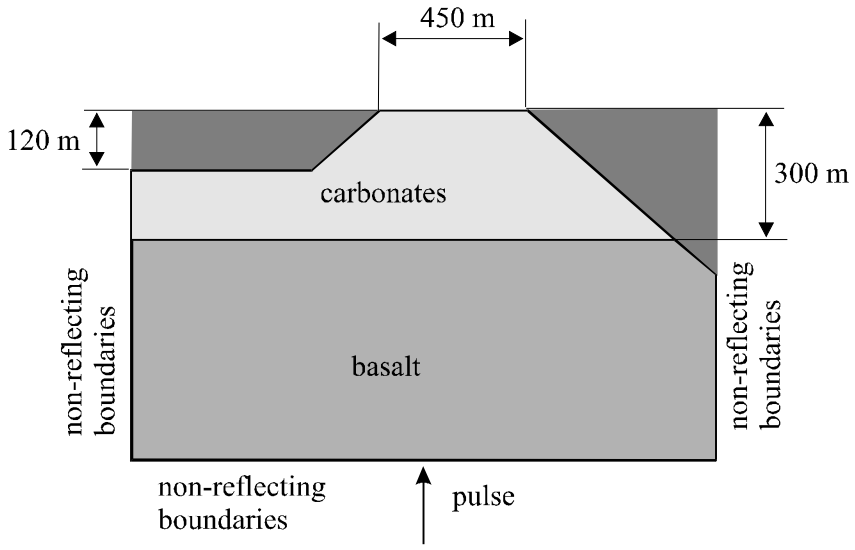

Figure 4.8 Geometry of the two-dimensional model used for numerical modelling of the surface settlement. Note that the 120 m depth of water in the lagoon is used to account for both the water and the soft sediments accumulated at the bottom of the lagoon. (The boundary conditions shown on this sketch are those used for the dynamic analysis.)

strain, vertical displacements, and the displacement vector field are shown for a 150-kt explosion at a depth of 900 m. These figures show clearly that plastic shear deformation is a major cause of the settlement.

The numerical results also demonstrate the dependence of the maximum settlement on the ratio w/λ — i.e. although the pressure amplitude at the base of carbonates, $\Delta\sigma_{\max}$, is larger after the 10-kt explosion than after the 150-kt explosion (Table 4.1), the settlement after the 150-kt explosion is larger as a consequence of the longer wave length (or duration of the positive phase of the pressure pulse).

The mode of permanent deformation of the atoll rim, illustrated in Figures 4.11, 4.12 and 4.13, suggests a connection between the surface settlements and possible submarine slope instability. During nearly isochoric deformation, the settlement of the atoll rim must be compensated by horizontal lateral displacement (predominantly to the side of the ocean) of the atoll's flanks. The plastic shear strain resulting from deformation of a perfectly plastic or strength-softening material tends to localise, forming shear bands (Fig. 4.11). These calculations suggest that some portions of the rim, outlined by the slope on the ocean side and the shear bands, could further destabilise under the action of gravity, depending on the magnitude of the plastic shear strain accumulated along the shear bands. As further discussed in Chapter 5, the deep destabilisation of the atoll flanks in the northern zone of Mururoa (test area 1) appears to be consistent with the predictions of this numerical model.

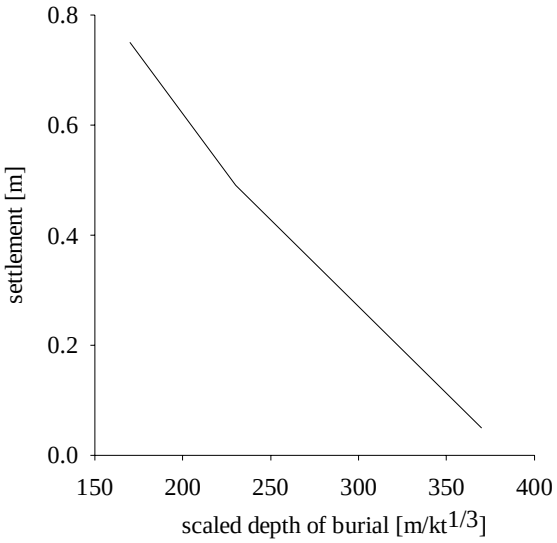

Figure 4.9 Settlement as a function of the scaled depth of burial (computed for $Y = 2, 10, 150$ kt)

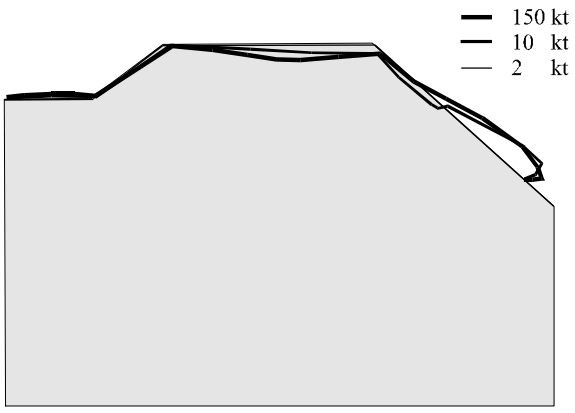

Figure 4.10 Exaggerated (50x) deformation of the model (maximum displacements = 1.32 m)

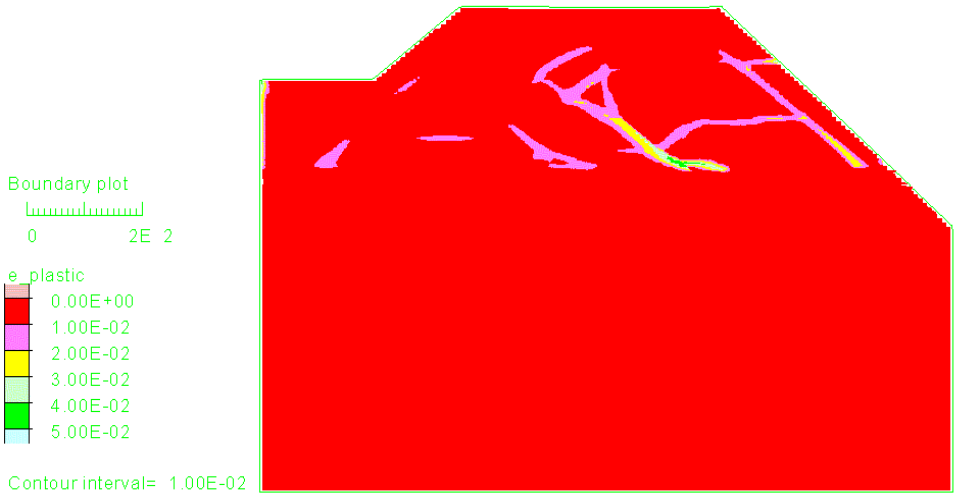

Figure 4.11 Contours of plastic shear strain after a 150-kt explosion

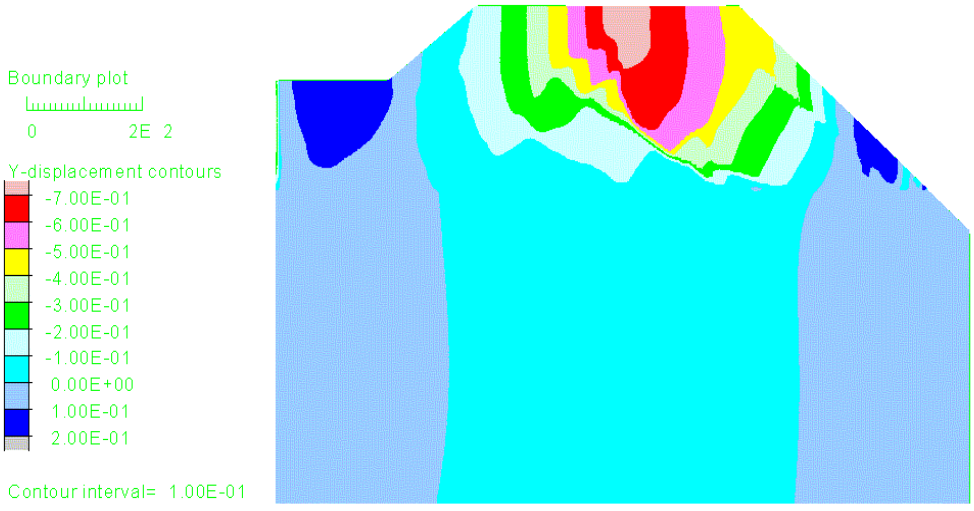

Figure 4.12 Contours of vertical displacements after a 150-kt explosion at a scaled depth of burial of 900 m

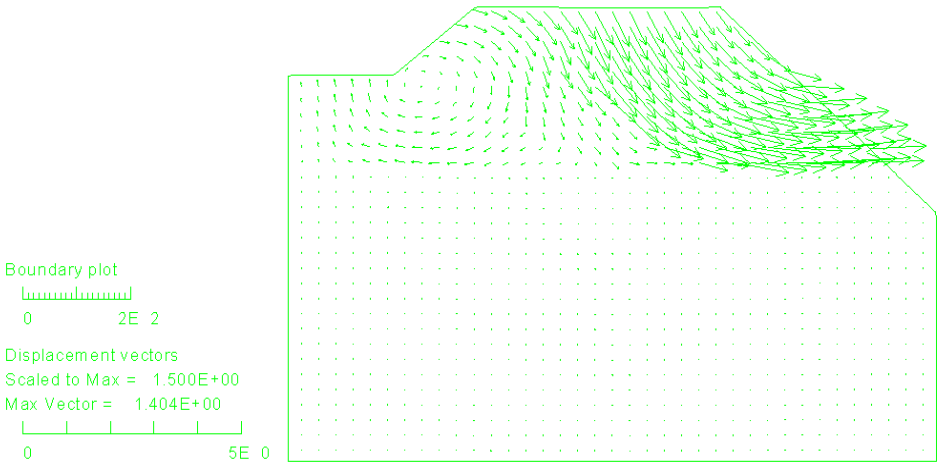

Figure 4.13 Displacement vector field after a 150-kt explosion at a scaled depth of burial of 900 m

The results shown have been obtained using the strength-softening constitutive model. Because it is not possible to characterise the softening behaviour of the rock mass on the scale of the atoll rim using standard laboratory and in-situ tests, the softening parameters (see Appendix O) used in this analysis were selected to match the settlements reported by DIRCEN/CEA (Fig. 4.4). Sensitivity of the settlement magnitude to the softening parameters is demonstrated in Table 4.2, where the maximum settlement for a 10-kt explosion is listed as a function of the softening parameters.

In order to simulate the effect of cumulative damage, two consecutive explosions of the same yield, Y, of 2 kt have been modelled. The maximum settlement is 0.05 m after the first explosion and 0.14 m after the second explosion. Hence, the incremental settlement due to the second explosion is larger than the initial settlement. This result, which is to be expected since the material exhibits softening, is consistent with field

Table 4.2 Settlement as a function of softening parameters (c_p is the peak cohesion; c_r is the residual cohesion; D_y is the plastic shear strain when cohesion reaches the residual value c_r)

c_r/c_p	D_y	$d_{\max}$ m
0.08	0.008	0.49
0.07	0.007	1.52
0.1	0.01	0.17

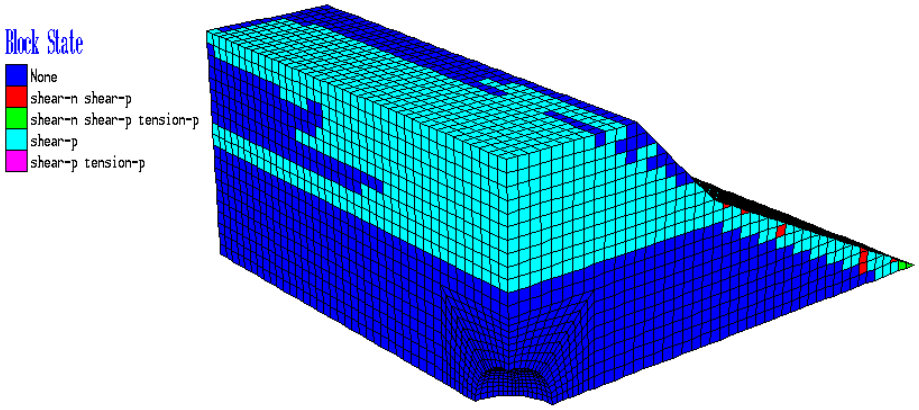

Figure 4.14 Indicators of plastic deformation due to a nearby explosion, calculated from the three-dimensional model

observations reported by DIRCEN/CEA. Some limited simulations were also carried out to investigate the influence of slabbing on the magnitude of the settlement. Under similar conditions, the results suggest that the impact of the spalled layer will tend to increase the total settlement (see Appendix P).

Finally, the results of a three-dimensional simulation of a 150-kt explosion at a depth of 900 m under the rim (in the southwestern zone of Mururoa) are displayed in Figures 4.14 and 4.15. In this calculation, described in Appendix Q, the volcanics are assumed to be elastic and the carbonates to be elastic-perfectly plastic. Figure 4.14 indicates the extent of the region, along the rim, where the carbonates are damaged by the explosion, while Figure 4.15 provides an idea of the extent of the rim affected by the settlement.

4.6 Concluding Remarks

The analysis presented in this chapter supports the contention of DIRCEN/CEA that the observed settlements at the surface of the atoll are not directly connected to the explosion chamber. (The term “connection” is used in this context to describe a situation in which collapse of the cavity roof results in permanent damage directly from the cavity to the surface.) In other words, our analysis gives support to the claim that surface settlements reflect a “superficial” deformation mechanism that is “disconnected” from the damage near the explosion chamber.

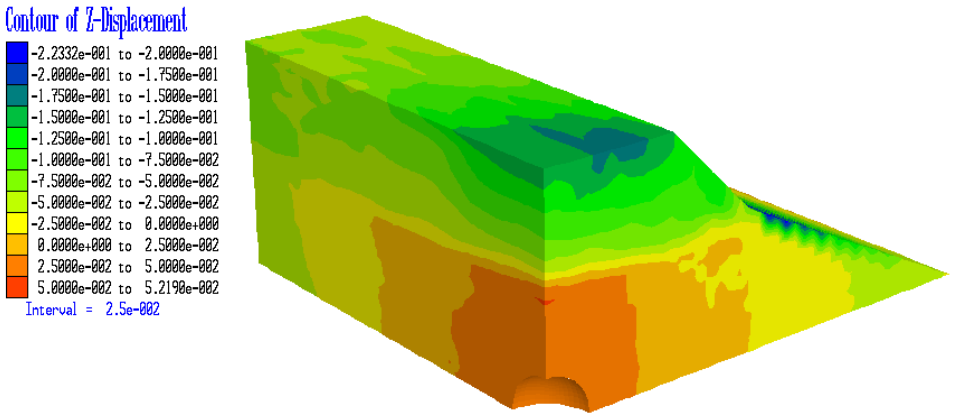

Figure 4.15 Contours of vertical displacements ("settlements") due to a nearby explosion, calculated from the three-dimensional model

However, considering the information available, it appears improbable that the settlements are associated primarily with compaction of the carbonates near the surface. Instead, the settlement is considered to be the result of predominantly isochoric deformation, with the irreversible vertical displacement being compensated by lateral movement of the flanks of the atoll rim. (Compaction is not ruled out entirely, but it is believed to be a secondary mechanism.) As confirmed by numerical modelling, the necessary condition for the validity of this mechanism is that the wave length of the pressure pulse must be of the same order of magnitude as the width of the atoll rim.

The significance of the proposed mechanism of settlement is that it suggests a link between settlement and damage or instabilities of the flanks of the atoll. The fractures on the submarine slopes of Mururoa in test area 4 that were observed by the divers of the Cousteau mission (Fondation Cousteau, Paris 1988) could very well be a manifestation of the damage to the carbonates associated with the settlement. It is also probable that at least some of the damage and fractured blocks of rock observed were "superficial" sediment accumulations on the slopes that had been dislodged and disturbed by the wave reflection effects of the underground tests. The link between the settlement and deep destabilisation of the rim is further examined in Chapter 5 in the context of the study of the slope stability in the northern zone of Mururoa.

Chapter 5

STABILITY OF THE ATOLL FLANKS

5.1 Introduction

The underground nuclear testing at Mururoa has caused destabilisation of the atoll flanks in the form of either submarine slope failures in the southwestern zone or slow (creeping) movements of some parts of the rim in the northern zone of the atoll (DIRCEN/CEA, Document No. 10). Some destabilisation of the flanks has also taken place in Fangataufa's northeast zone.

The slope failures in the southwest of Mururoa occurred between 1977 and 1980. The largest of these events, involving three successive rock slides with a total volume of 0.36 km^3, was triggered by the Tydée explosion, which took place on 25 July 1979. The first rock slide, with an estimated volume of 0.11 km^3, occurred immediately after the explosion and induced significant hydraulic phenomena. Parts of the atoll were actually submerged by hydraulic waves that reached a height of 2.5 m in some places.

In the northern zone of Mururoa, destabilisation of the flanks involves slow movement of large portions of the rim toward the ocean. These movements were detected in 1979, following the establishment of an extensive monitoring programme (put into operation after the Tydée events). Three separate destabilised zones have been outlined, the largest one (in the region named Camélia) encompassing a volume of about 0.6 km^3.

The objective of this chapter is (i) to review the field evidence of destabilisation of the atoll flanks and evaluate the CEA interpretation of this evidence, and (ii) to provide an independent assessment of the mechanisms of destabilisation of the flanks, using numerical modelling. One of the issues addressed here is whether the nuclear testing has merely accelerated a natural process or whether it has indeed caused a destabilisation that would not have occurred otherwise. Also, the connection between settlement and the stability of the flanks is further established.

5.2 Evidence of Destabilisation of the Atoll Flanks

5.2.1 Southern Zone of Mururoa

The strongest underground nuclear tests on Mururoa were conducted in test area 4, under the rim in the southwestern part of the atoll. Those tests provoked a series of slides and failures of the atoll flanks between 1977 and 1980. The largest slide produced waves in the ocean that completely submerged part of the rim.

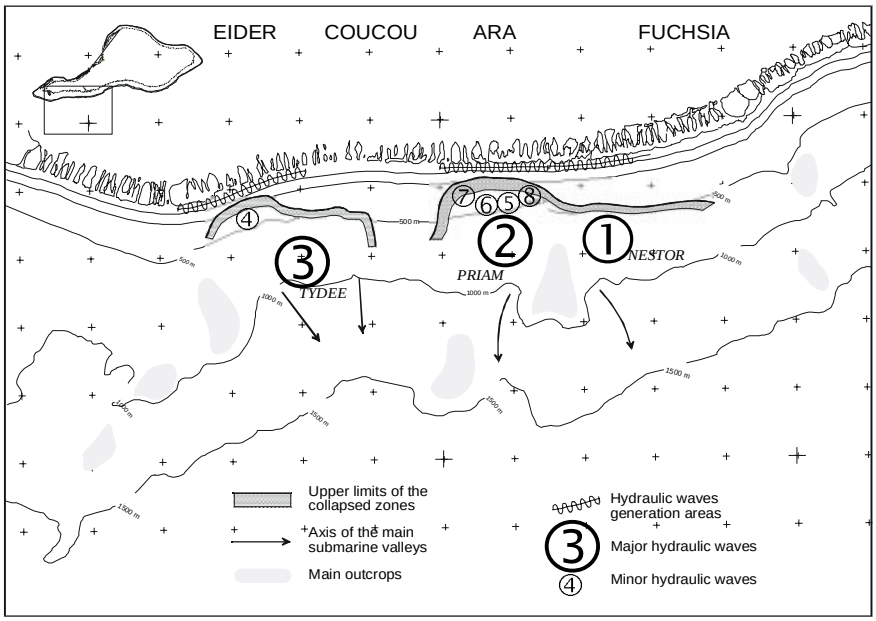

Figure 5.1 Limits of the destabilised zones in the southwestern part of Mururoa atoll (DIRCEN/CEA Document No. 7, Fig. 13)

The shapes and locations of the major rock slides in the southwestern part of the atoll are shown in Figure 5.1. These instabilities were triggered by Nestor (March 1977), Priam (November 1978), and Tydée (July 1979) explosions. As noted above, the most severe damage to the atoll flanks was caused by Tydée, which induced three successive rock slides. The first slide, involving a volume estimated at 0.11 km^3, occurred within seconds of the explosion, the second one three hours later, and the third one after 23 days. Bathymetric profiles before and after the Tydée rock slides are shown in Figure 5.2. According to DIRCEN/CEA Document No. 7, the zone affected by Tydée is 2 km wide and 1000 m deep, with the total destabilised volume estimated at 0.36 km^3.

Geophysical investigations have revealed that the volcanic base was not affected by the slides. Further monitoring (geodetic measurements and microseismic monitoring) has also indicated that no further destabilisation has taken place in that zone.

5.2.2 Northern Zone of Mururoa

Evidence of an ongoing process of destabilisation in the northern zone of Mururoa came initially from geodetic surveys. These measurements revealed (unlike in the south) a continuing increase in the settlement with time — see Figures 5.3 (showing plots of settlement profiles at different times) and 5.4 (showing histories of the vertical displacements at five different locations marked as PK points).

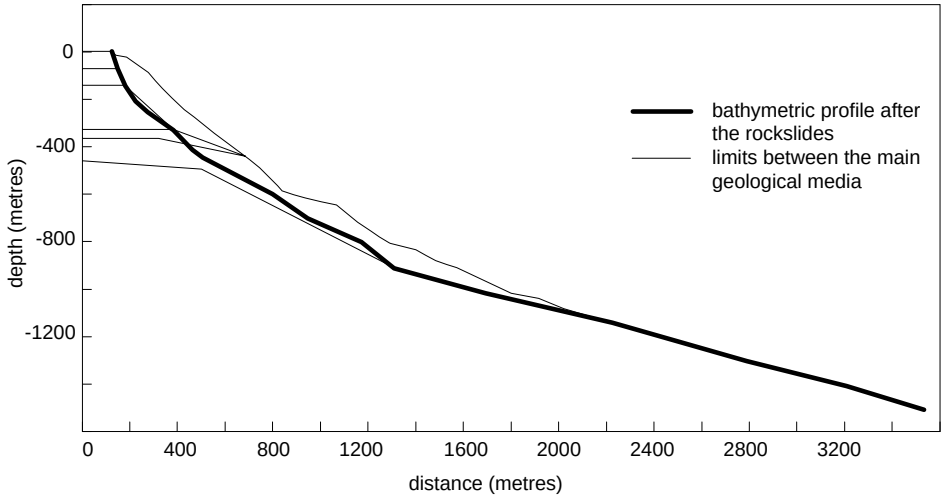

Figure 5.2 Bathymetric profiles before and after the rockslides

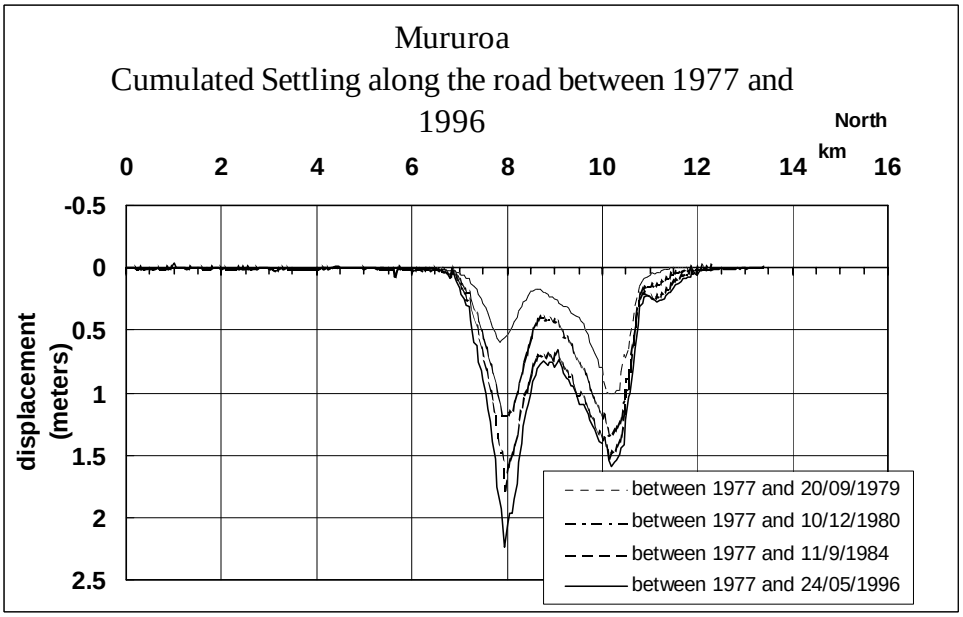

Figure 5.3 Detail of accumulated settlement along the road between 1977 and 1996 (DIRCEN/CEA Document No. 7, Fig. 11 (detail))

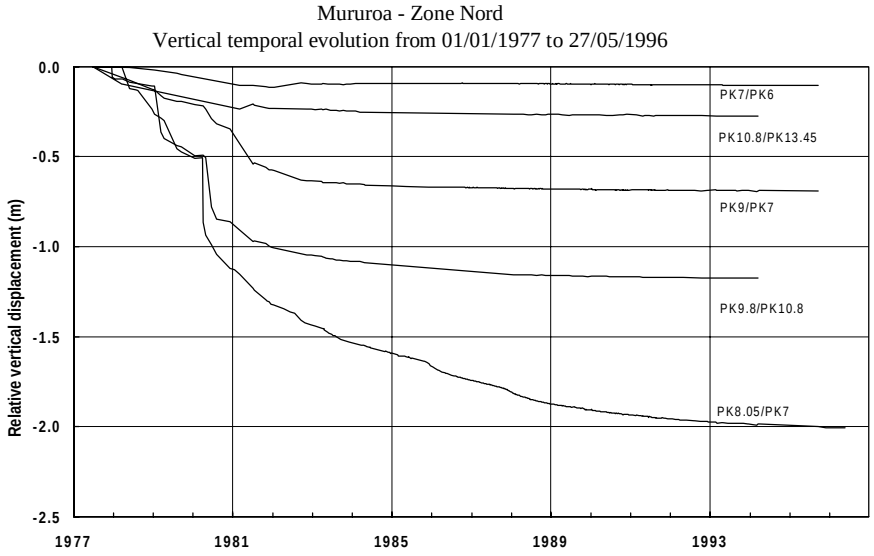

Figure 5.4 Histories of vertical displacement PK points in the northern zone (DIRCEN/CEA Document No. 7, Fig. 21)

Three potentially unstable regions, named Irène, Françoise and Camélia, have been identified (Fig. 5.5). These regions, which are delimited by a system of cracks, are slowly moving toward the ocean. The movements are monitored continuously at the surface and at depth (DIRCEN/CEA, Document No. 7). Some of the elements of the monitoring system are shown in Figures 5.6 and 5.7. (There is also a network of surface seismographs and deep geophones.)

The monitoring system has provided indisputable evidence of the seaward motion of the destabilised zones. This can be seen, for example, in Figure 5.8, which shows the time record of the horizontal movement of reference point "6C" on the seashore at the center of the Camélia zone. A similar trend can also be observed on the inclinometer records in the Camélia zone (Fig. 5.9). Both figures indicate that the motion is gradually decelerating, except for short periods of acceleration that are triggered by underground nuclear tests.

Inclinometer measurements in the Camélia zone reveal the existence of a sharp discontinuity in the horizontal displacements at a depth of about 400 m. The discontinuity is located within the very weak chalky limestone formations (Fig. 5.10). This measurement, and the presence of open cracks on the lagoon side along the rim, suggest the existence of a deep-seated sliding mechanism that involves shearing through the chalky limestone. (The maximum volume of the rock potentially destabilised by this kinematic mechanism is about $6 \cdot 10^8$ m^3.) The other sliding mechanism, manifested by the open

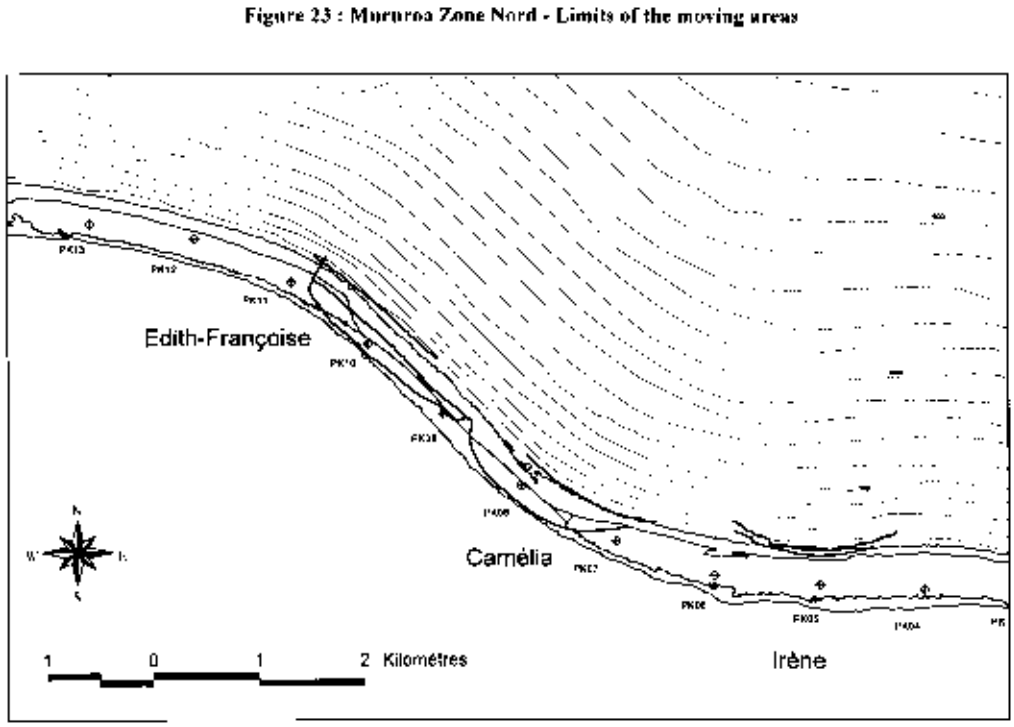

Figure 5.5 Limits of the moving areas in the northern part of Mururoa Atoll (DIRCEN/CEA Document No. 7, Fig. 22)

cracks on the ocean side along the rim (some with openings up to 3 m wide), is superficial and might eventually destabilise smaller volumes of the rock. The cracks that form the Irène and Françoise zones are on the ocean side of the rim (some below the water level; see Fig. 1.14).

5.3 DIRCEN/CEA Interpretation

5.3.1 Southern Zone

According to DIRCEN/CEA Document No. 7, several tests carried out in the southwestern part of Mururoa engendered stresses that destabilised sediments and coral structures on the sides of the atoll. The destabilisation process is attributed either to fragmentation of the material or to liquefaction. A simple analysis is conducted in which the potential zones of yielding are assessed by identifying the regions where the stresses during dynamic loading violate the yield condition. (In this analysis, the stress consists of the sum of the initial stresses and the stresses induced by the explosion, which are computed according to the empirical rule given in Appendix Q, assuming plane wave propagation

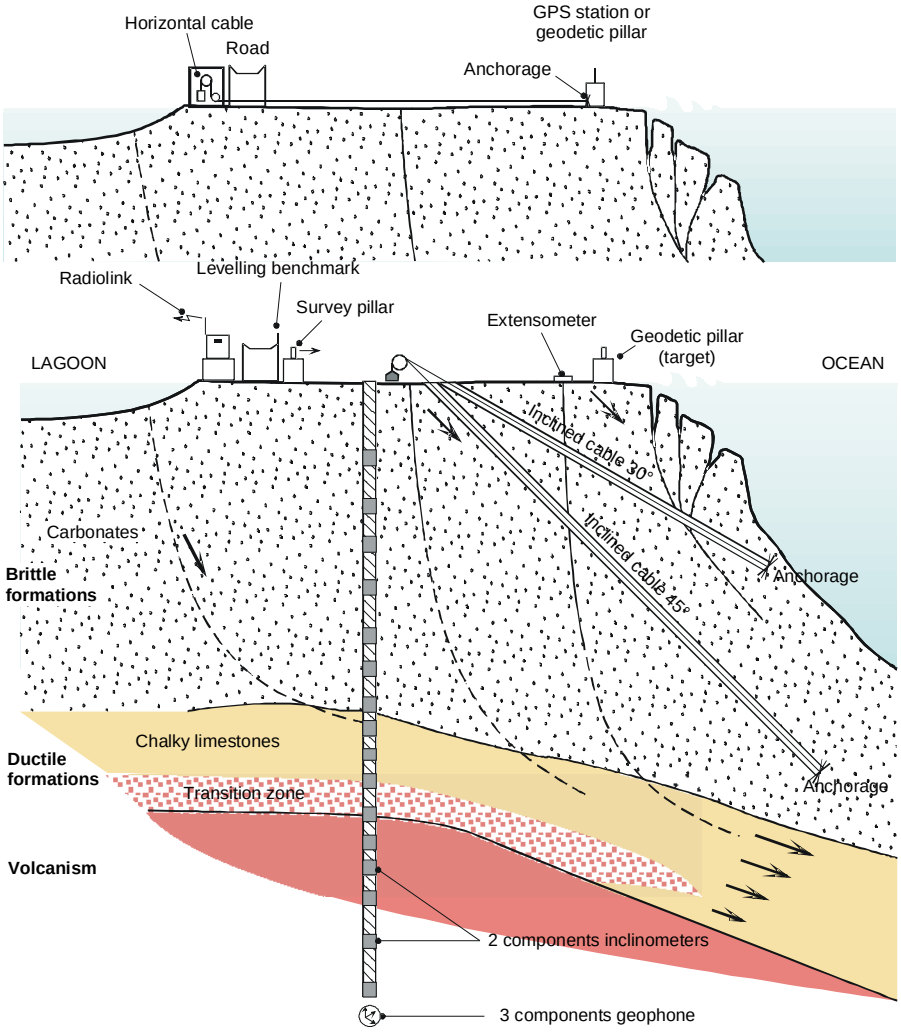

Figure 5.6 Monitoring system in the northern zone of the atoll (DIRCEN/CEA Document No. 7, Fig. 24)

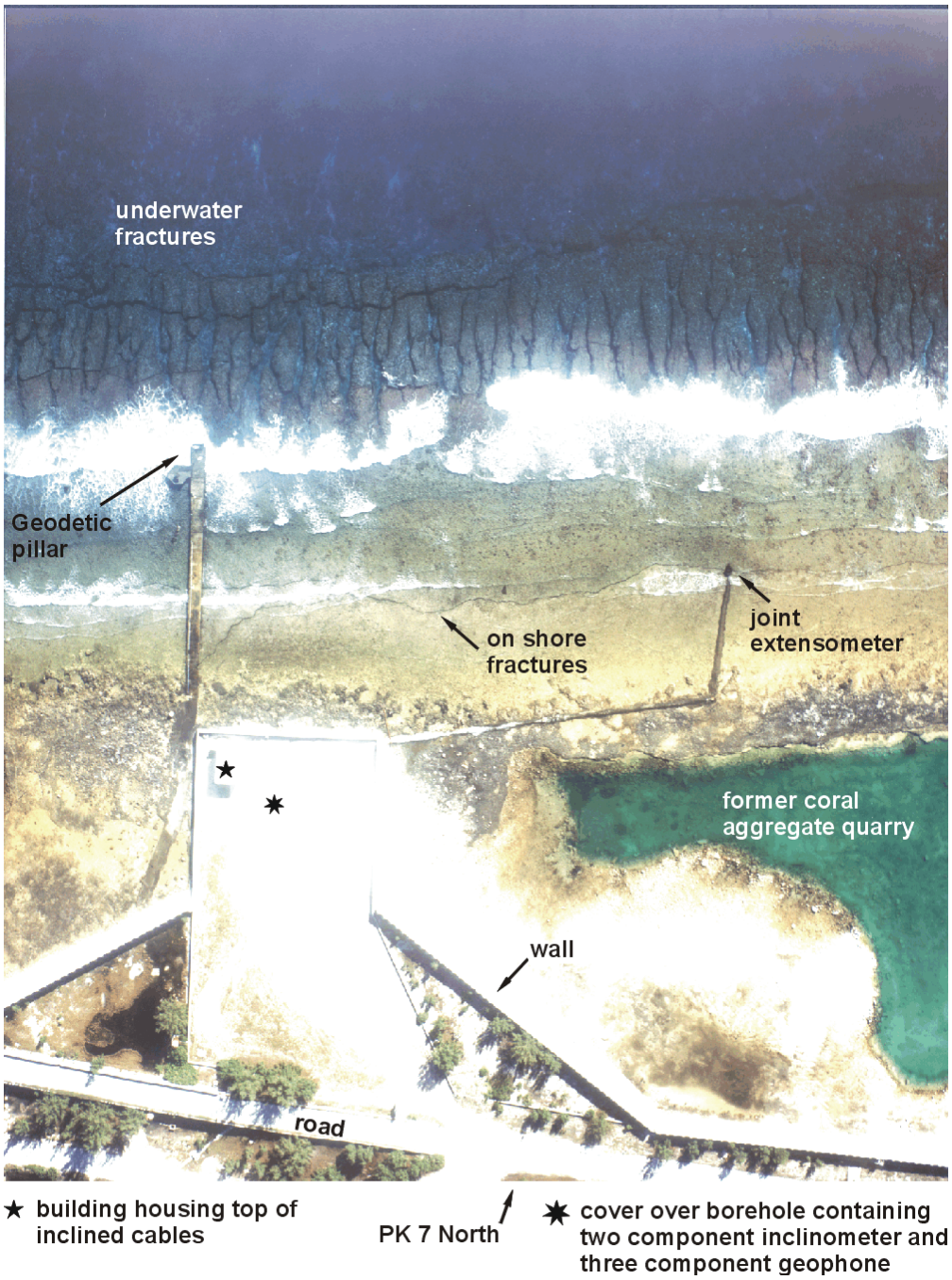

Figure 5.7 Aerial view of the monitoring system in the northern zone of the atoll

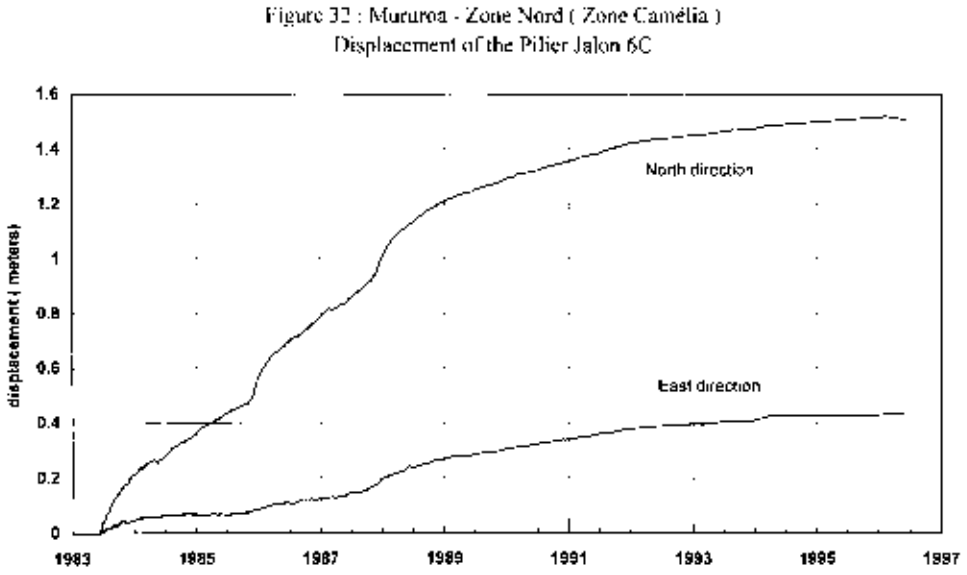

Figure 5.8 Horizontal displacement of the point in Camélia zone (after DIRCEN/CEA Document No. 7, Fig. 32)

in the direction radial from the explosion point.) Following the rock slides, an empirical rule was devised to constrain the yield and location of an explosion in order to limit the stresses caused by the explosion; this criterion is to limit the impulse, defined as

$$I = \int_0^t \Delta P(\tau) d\tau \tag{5.1}$$

(where ΔP denotes the dynamic mean stress increase), to less than a certain critical level.

5.3.2 Northern Zone

Interpretation of the ground movements in the northern zone of Mururoa is described in DIRCEN/CEA Document No. 7 and in the paper by Bouchez et al. (1997). It is stated that explosions in the area have caused plastic deformation of the chalky carbonates and localised fractures within the upper carbonate strata. The DIRCEN/CEA position, as presented in DIRCEN/CEA Document No. 7, may be summarised as follows.

The volcanic platform is stable. Deep-seated shearing of the chalky limestone is associated mainly with creep deformation driven by gravity under the weight of the more rigid carbonate formations but, also, with some plastic deformation caused by the tests. The velocity of the creep increases temporarily following dynamic loading, but the rate of deformation returns to the previous level after a couple of months. Because the

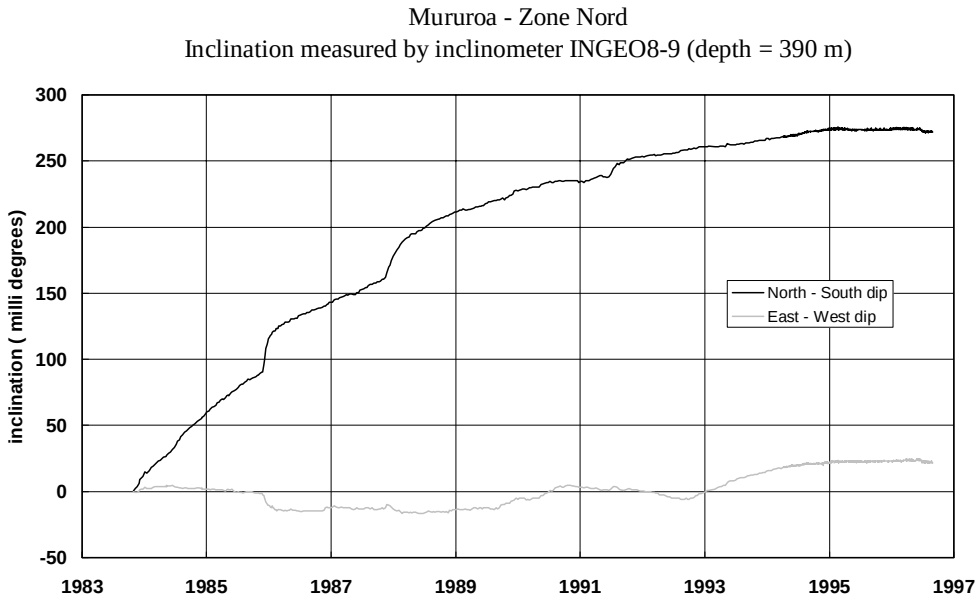

Figure 5.9 Inclinometer measurements in Camélia zone (DIRCEN/CEA Document No. 7, Fig. 34)

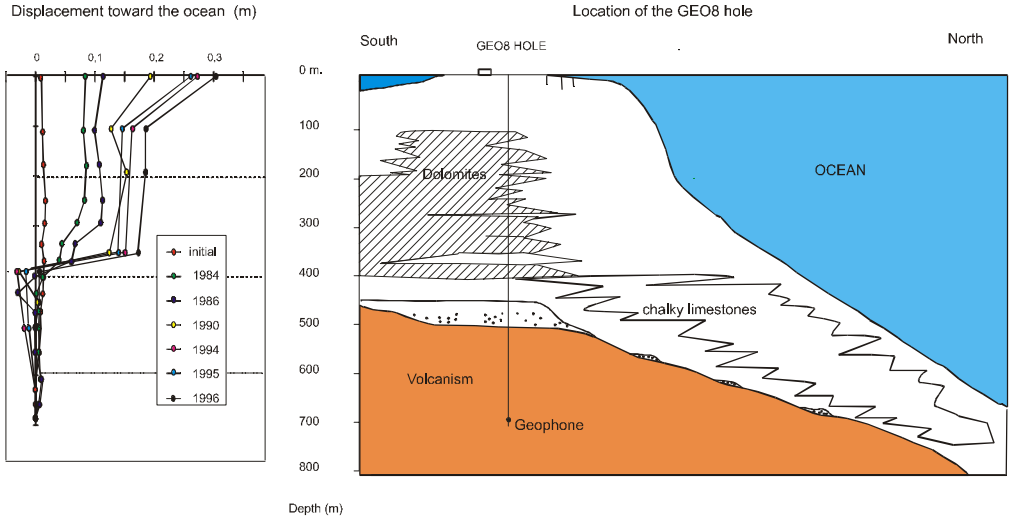

Figure 5.10 Successive profiles of the hole in Camélia zone inferred from inclinometry (after DIRCEN Document No. 7, Fig. 29)

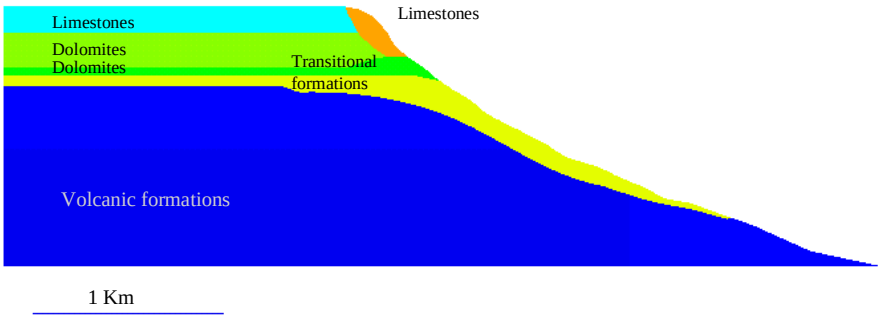

Figure 5.11 Geomechanical model of the slope in the southwestern part of the atoll (DIRCEN/CEA Document No. 7, Fig. 16)

creep rate is observed to have decreased by about one order of magnitude since 1980, when movements were first detected, the deformations are still in the so-called transient, or primary creep, phase. (The present strain rate is estimated to be of the order of $5 \cdot 10^{-13}$ s^{-1}.) The trend is toward stabilisation and it is likely that no rupture will take place. Furthermore, tertiary creep (the phase of accelerated creep rate that eventually leads to failure) has not been observed in laboratory tests on the chalky limestone. (This feature is attributed to the compactant nature of this type of material.) However, if the secondary or steady-state creep stage is reached at some time in the future, it is unlikely that this will take place in less than several hundred years.

The potential failure surfaces are identified from the monitoring system (borehole inclinometry, extensometers, GPS and geodetic measurements), together with "factor of safety" analysis. In particular, for the Camélia zone, the factor of safety analysis identifies the most probable slip surface (indicated on Fig. 5.12) as a steep surface through the carbonates, emerging in the coral rim on the lagoon side. This surface connects with the chalky limestone at a depth of about 400 m and exits on the atoll flank (ocean side) at a depth of about 800 m. The existence of this surface corresponds closely with visible fractures on the rim, just inside the lagoon.

The results of a two-dimensional dynamic, coupled (fluid-solid) elasto-plastic analysis carried out to simulate the effects of a distant underground nuclear explosion (Y = 65 kt, at a distance of about 10 km) are also reported in DIRCEN/CEA Document No. 7. This simulation indicates a very rapid (of the order of 1 hour) dissipation of the excess pore pressure induced by dynamic loading. However, the simulation underestimates the magnitude of the displacement observed in the field (2 cm in the upper carbonates rather than 10 cm). This is likely due to the existence of a network of fractures that is not

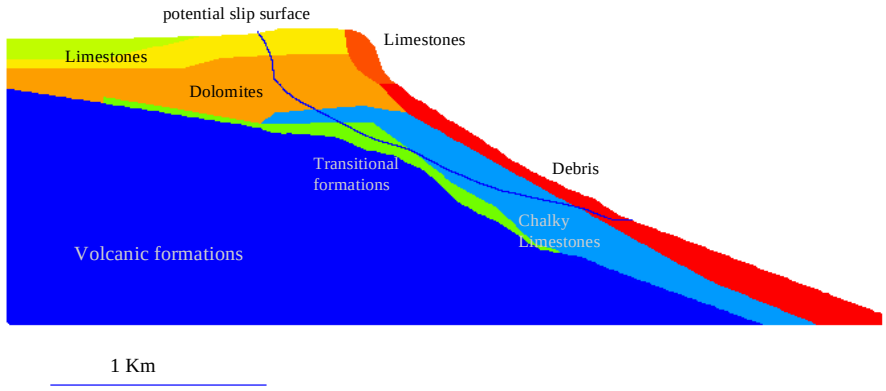

Figure 5.12 Geomechanical model of the slope in the northern part of the atoll (DIRCEN/CEA Document No. 7, Fig. 30)

represented in the numerical model, although CEA scientists indicate that a 10-cm displacement could be obtained from their simulation by a small modification of the values of the parameters assumed in their model (Personal Communication).

Finally, the possibility that all of the rock involved in the active Camélia zone (calculated to be about 0.6 km^3) will collapse at once is excluded because of the compartimentalisation of the rock mass into subzones. The most likely rock slide delimited in part by the open fractures on the ocean side is estimated to amount to 0.04 km^3. The sea wall erected on the atoll to safeguard the living area would be sufficient protection for the smallest rock slide but not for the largest slide (i.e. 0.6 km^3), which would cause complete submersion of the atoll rim.

5.4 Discussion

5.4.1 Southern Zone

Results of a three-dimensional numerical model of a 150-kt explosion 900 m under the rim (reported in Chapter 4) suggest that potential instability of a superficial lens involving the transition formation can be expected. Figure 5.13 shows a view of the indicators of the plastic deformation experienced after dynamic loading. As can be seen from the contours of vertical displacement plotted in Figure 5.14, comparatively larger displacements are predicted along the slope; these displacements are indicative of larger plastic deformation and, thus, greater damage. Slope collapse during dynamic loading cannot be predicted by this simulation, since a perfectly plastic material has been assumed. (As discussed in Chapter 4, the predicted displacement induced during dynamic loading can be made as large as possible, depending on the assumed softening parameters.)

Both Figures 5.13 and 5.14 show that the damage (plastic deformation) of the slope produced by a test under the rim decays as a function of the distance from the detonation point if the strengths of the various geological units are assumed to be uniform along the rim. However, the three major slides (Tydée, Priam, and Nestor) that were triggered in the southwestern zone were located at a greater distance from the point of explosion, in apparent contradiction to the results of the numerical simulation. For example, the closest point of the Tydée rock slide is estimated to be at least 2 km away from the explosion point. Variations in material properties and localised geometry (i.e. ridges and valleys) along the ocean slopes of the rim appear to be the likely explanation of this apparent anomaly. Appendix R describes a possible mechanism by which a slope can be destabilised by a distant explosion under the rim.

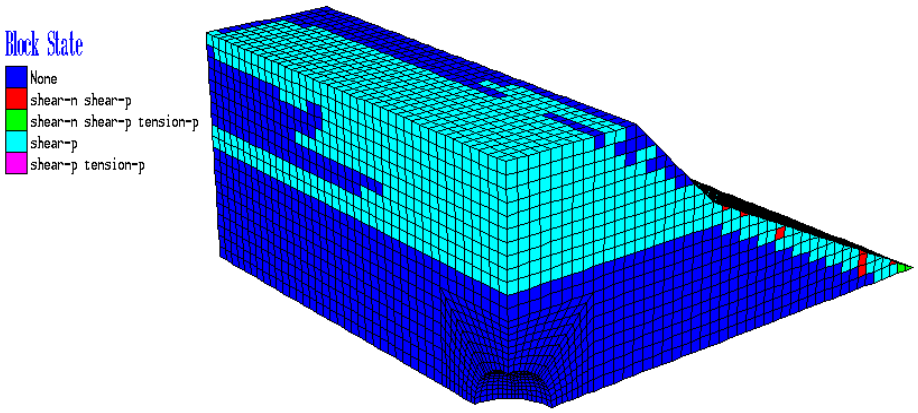

Figure 5.13 Indicators of plastic deformation in the vicinity of an underground explosion near the ocean slope, calculated from the three-dimensional model — rear view

5.4.2 Northern Zone

Little information is given by the CEA about the scenario or sequence of events that caused the onset of the process of slope destabilisation; the only reference to the origin of the movements can be found in DIRCEN/CEA Document No. 7 and in Bouchez et al. (1997). In these documents, mention is made of a factor of safety analysis which suggests that yielding of the chalky limestone layer takes place when the dynamic stresses due to an 8-kt explosion at a depth of 800 m are superimposed onto the initial stress. Yielding of the chalky limestone then leads to the development of a fracture in the upper brittle carbonates.

As stated in Section 5.5, the IGC's view is that the fundamental mechanism of slope destabilisation observed in the northern zone of Mururoa is identical to the one invoked to explain the settlement. However, the manifestation of this mechanism is somewhat

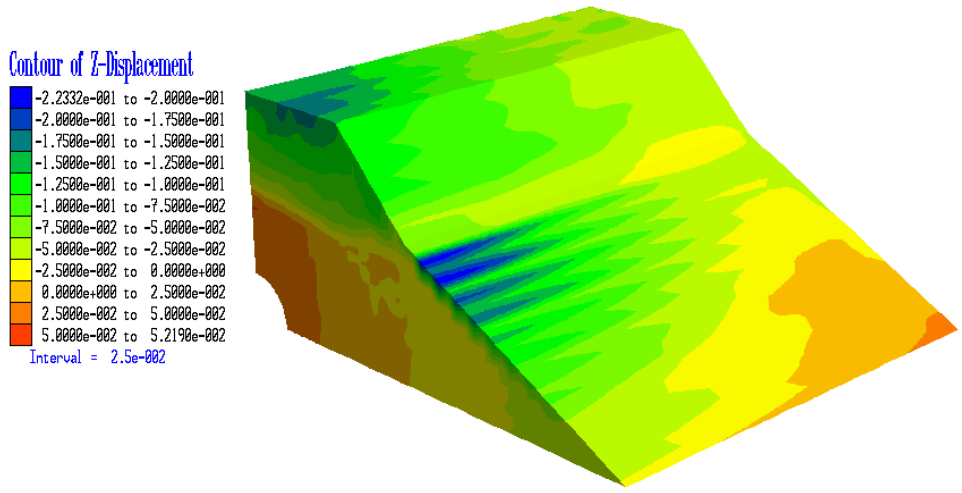

Figure 5.14 Contours of vertical displacement in the vicinity of an underground explosion near the ocean slope, calculated from the three-dimensional model — front view

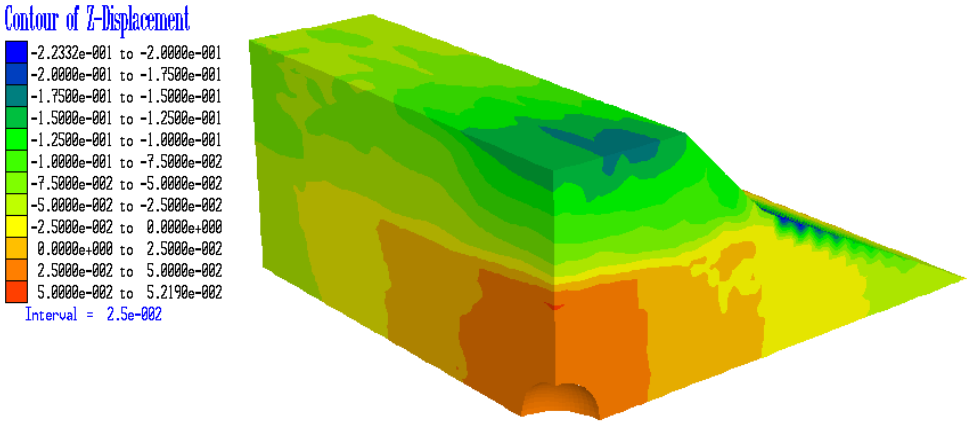

Figure 5.15 Contours of vertical displacements in the vicinity of an underground explosion near the ocean slope, calculated from the three-dimensional model — rear view

different in the southern and the northern parts of the atoll because of differences in the local geology (compare Figs. 5.11 and 5.12).

In the northern zone of the atoll, the stress pulse associated with the explosion causes yielding not only in the chalky limestones, *but also in the upper carbonates*. A deep-seated failure surface eventually develops in the upper carbonates essentially because of the existence of the weak chalky limestone layer in which significant irreversible deformation is taking place, but also because of the brittle nature of the upper carbonates under the stress conditions that exist at the atoll (see the discussion in Section 5.5 and Fig. 5.23, which shows the predicted slip surface in the upper carbonates). Depending on a variety of factors (yield of the explosion, material property, softening parameters), a failure surface could be created after one test or after a series of tests in test area 1. Such a failure surface enables the development of a mechanism, which is shown conceptually in Figure 5.12. In contrast, it does not appear that the explosions have created deep-seated failure surfaces in the southern zone. This is probably because of differences in the geological setting between the northern and southern rim sections.

Further destabilisation of the slopes by nuclear explosions outside test area 1 appear to have taken place. For example, it is quite clear from the "jumps" in the extensometer and inclinometer records (see Figs. 5.8 and 5.9) that two tests, Megarée, on 26 November 1985, and Pélée, on 19 November 1987, had a significant effect on the deformation of the slopes in the Camélia zone.

The possible collapse of the slopes in test area 1, associated with the deep-seated failure mechanism, is controlled, in large measure, by the mechanical behaviour of the chalky limestone. Slope failures are unlikely as long as this material compacts and hardens during shearing; however, a slope collapse would be triggered if the chalk starts to soften with deformation. The chalky limestone enters an irreversible transition toward a granular behaviour beyond 1% deformation, according to Mariotti (1990) and DIRCEN/CEA Document No. 7. (Undrained triaxial experiments carried out by Mariotti (1990) also show softening, beyond 1% deformation, caused by pore pressure build-up associated with the shear-compactant behaviour of the chalky limestone.) An order-of-magnitude calculation suggests that the strain accumulated in the chalky limestone layer to date is of this order. Thus, assuming an average strain rate of 10^{-11} s^{-1} over the 18 years since 1980 gives a total strain to date of 0.06%, which is likely to be an underestimate. Also, a displacement of the order of 1 m, distributed uniformly over a 100-m-thick layer, corresponds approximately to 1% deformation. These "back-of-the-envelope" calculations indicate that it is not inconceivable that the conditions in the northern zone could lead to collapse of the slopes.

Table 5.1 Material properties of geological units included in the two-dimensional models (after DIRCEN/CEA Document No. 7)

No.	geological formation	ρ kg/m^3	E GPa	ν	v_s m/s	v_p m/s	c MPa	ϕ °
1	peripheral	2400	14.5	0.4	1468	3598	5	35
2	upper limestone	2050	6	0.3	1060	1984	1.5	45
3	lower limestone	2250	14	0.3	1546	2894	4	25
4	dolomite under the lagoon	2200	11	0.3	1386	2594	4	25
5	dolomite under the rim	2450	17.4	0.4	1592	3901	5	35
6	transition	2200	11	0.3	1386	2594	1	30
7	debris	2150	4.4	0.4	855	2094	1	40
8	volcanic rocks	2350	29	0.2	2267	3702	8	55
9	chalky limestone	2000	1	0.3			0.5	30

5.5 Numerical Modelling

5.5.1 Introduction

The problem of slope stability at Mururoa was investigated using numerical modelling. The objectives of these calculations were twofold:

- to assess the factor of safety of the slope against collapse under natural conditions for both the southern and the northern zones of the atoll; and
- to understand the mechanisms of destabilisation of the slope in the northern zone.

The modelling effort discussed in this section is concerned exclusively with two-dimensional models (both plane-strain and axisymmetric); it complements the three-dimensional calculations of surface settlement and slope stability reported in Section 5.4. (Recall that the three-dimensional model is concerned with a generic segment of the rim in the southwestern part of the atoll.)

The geological units that have been included in the two-dimensional models are based on the cross-sections of the rim of Mururoa shown in Figures 5.11 (southwest) and 5.12 (north). The corresponding material properties are listed in Table 5.1 (DIRCEN/CEA Document No. 7).

5.5.2 Safety Factor Calculations

A set of calculations was undertaken to assess the safety factors of the slopes under gravity and hydrostatic pressure loading (see Appendix Q for details). The approach used to compute the factor of safety differs from that adopted by DIRCEN/CEA Document No. 7, which is based on elastic stress calculations. Here, the safety factor is defined as the (single) number by which the strength of all the geological units involved must be reduced in order to cause collapse of the slope. This definition is more realistic than

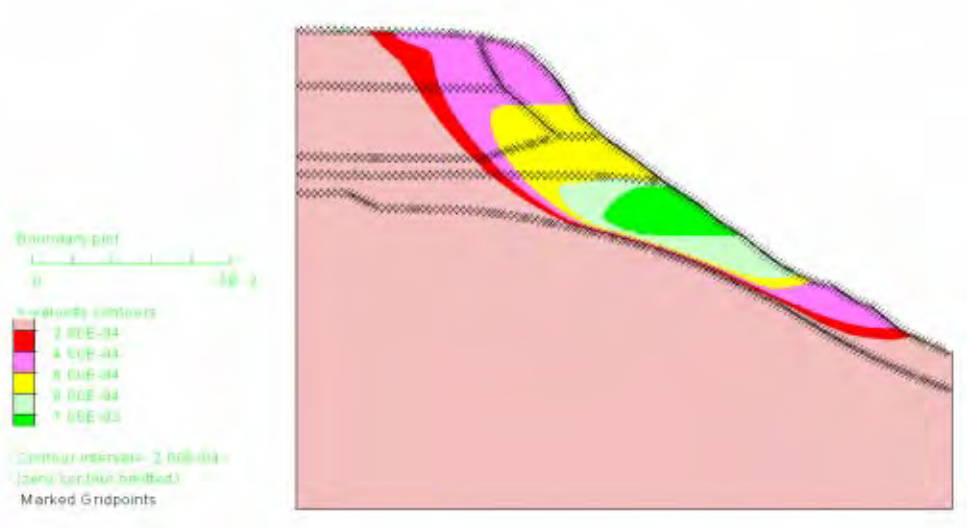

Figure 5.16 Slope in the southwestern zone — contours of steady-state horizontal velocity for $\Phi_u = 3.3$

one based on elastic stresses, since it involves an actual simulation of the slope failure. (Experience suggests that this approach also leads to a smaller — and, thus, more conservative — estimate of the factor of safety than a calculation based on elastic stresses.) Furthermore, this approach enables the post-peak behaviour of the materials to be taken into account. Upper and lower bounds to the factor of safety can be computed by assuming the material to be elastic-perfectly plastic and elastic-perfectly brittle, respectively.

Computation of the upper bound, Φ_u, of the safety factor is carried out by assuming a perfectly plastic Mohr-Coulomb yield condition for all geomechanical units. For the southwestern part of the atoll, Φ_u is estimated to be in the range 2.5∼3.3; for the northern zone, Φ_u = 2.0∼2.5. The lower value of the safety factor in the northern zone of Mururoa is a direct consequence of the presence of the weak chalky limestone in that zone. The area and the shape of the unstable portion of the rim can be seen from the contours of the horizontal velocity at failure. (See Figs. 5.16 and 5.17 for the southwestern and the northern zones, respectively.) The volume and the shape of the least stable part of the slope in the north of the atoll agree with the values predicted by DIRCEN/CEA Document No. 7. However, the safety factor computed by DIRCEN/CEA Document No. 7 for the north slope is about 3 — larger than our upper-bound estimate.

Computation of the lower bound, Φ_l, of the safety factor (calculated by assuming an elastic perfectly brittle behaviour) yields the following values: Φ_l = 2.0∼2.5 for the southwest and Φ_l = 1.4∼1.7 for the north. Again, the factor of safety is lower in the north than in the southwest.

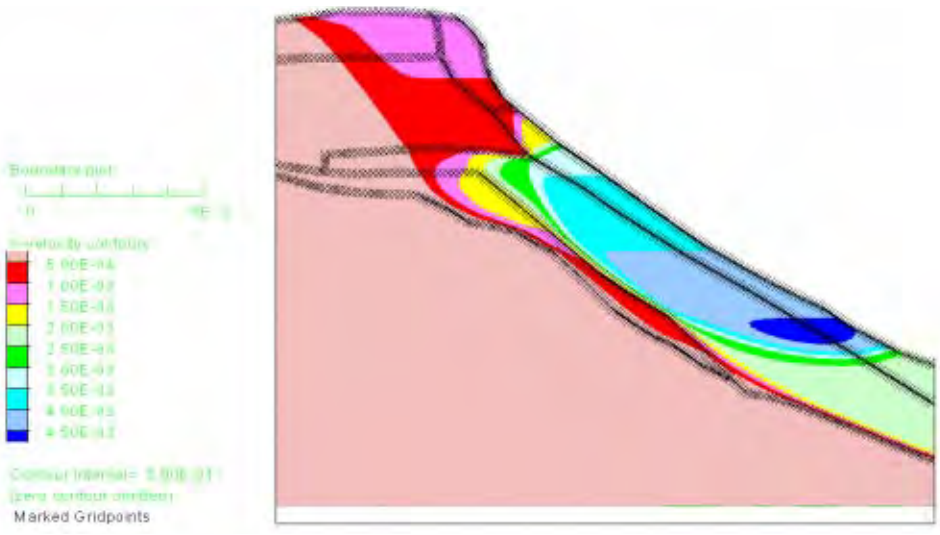

Figure 5.17 Slope in the northern zone — contours of steady-state horizontal velocity for a safety factor $\Phi_u = 2.5$

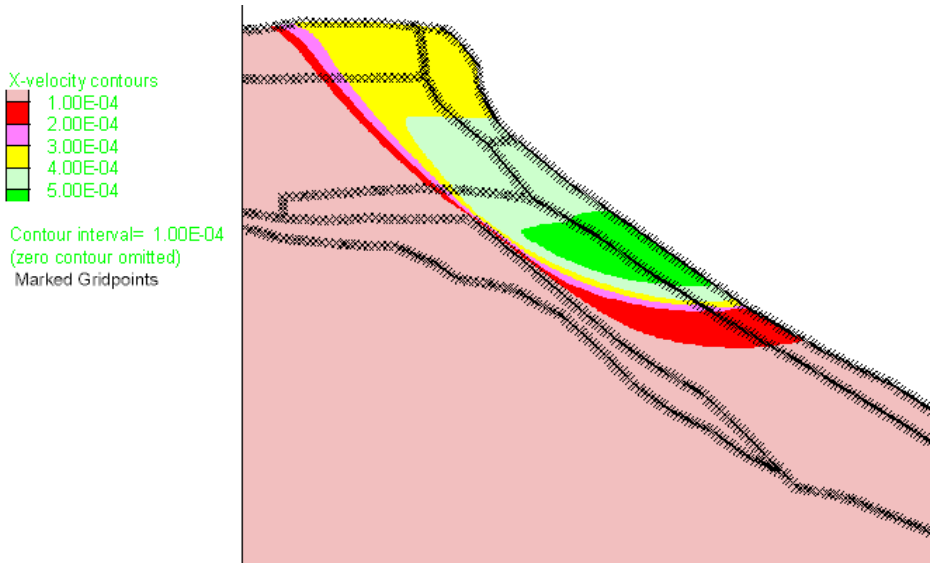

Figure 5.18 Slope in the northern zone (assumed rock-mass properties) — contours of steady-state horizontal velocity for a safety factor $\Phi_u = 1.67$

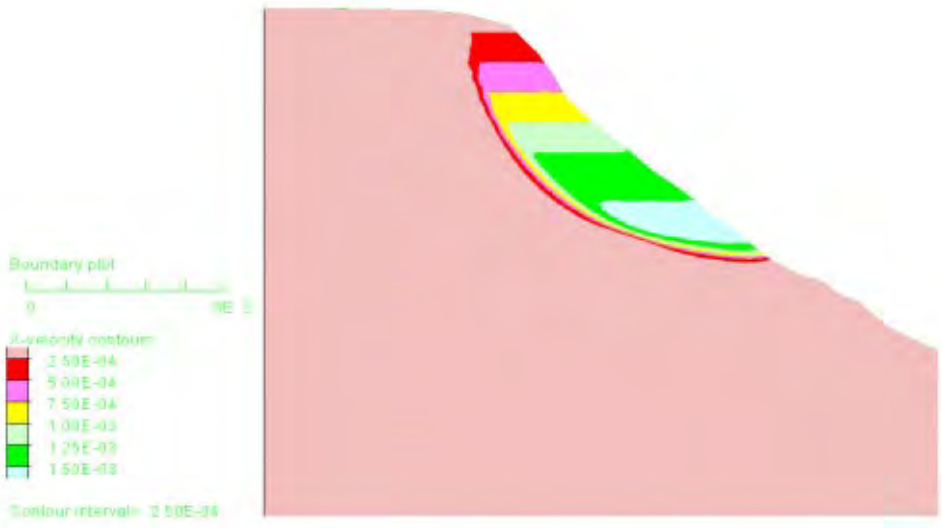

Figure 5.19 Slope in the southwestern zone, softening model — contours of steady-state horizontal velocity for a safety factor $\Phi = 2.5$

Calculations of the safety factor, assuming strain-softening parameters for the carbonates identical to those used for the dynamic stability calculations, give a value Φ = 2.0∼2.5 for the southwestern zone (Fig. 5.19) and Φ = 1.7∼2.0 for the northern zone (Fig. 5.20). As expected, these values of Φ are within the range defined by the lower and upper bounds. A plot of contours of plastic shear strain in the northern zone, for the critical factor $\Phi = 2.0$ (shown in Fig. 5.21), supports the conjecture that the fractures visible on the ocean side of the rim are part of the natural process of destabilisation of the atoll sides.

Finally, a comparison between the results obtained with plane-strain and axisymmetric models indicates that curvature of the rim in the northern part of the atoll does not have a significant effect on stability of the sliding regions.

It must be emphasised that the values of Φ given above are the factors by which the strengths of the intact rock materials given in Table 5.1 must be reduced in order to produce limiting equilibrium of the slopes. As has been noted in Section 2.5, the overall strengths of in-situ rock masses are less than those of the corresponding intact rock materials (determined on the laboratory scale). This means that the real in-situ factors of safety are likely to be lower than the calculated values so that the slopes will be closer to limiting equilibrium than the calculated values might suggest. The upper bound of safety factor for the slope in the north zone, using rock mass properties calculated based on estimated GSI for different geological units, was calculated to be 1.5∼1.67 (Fig. 5.18).

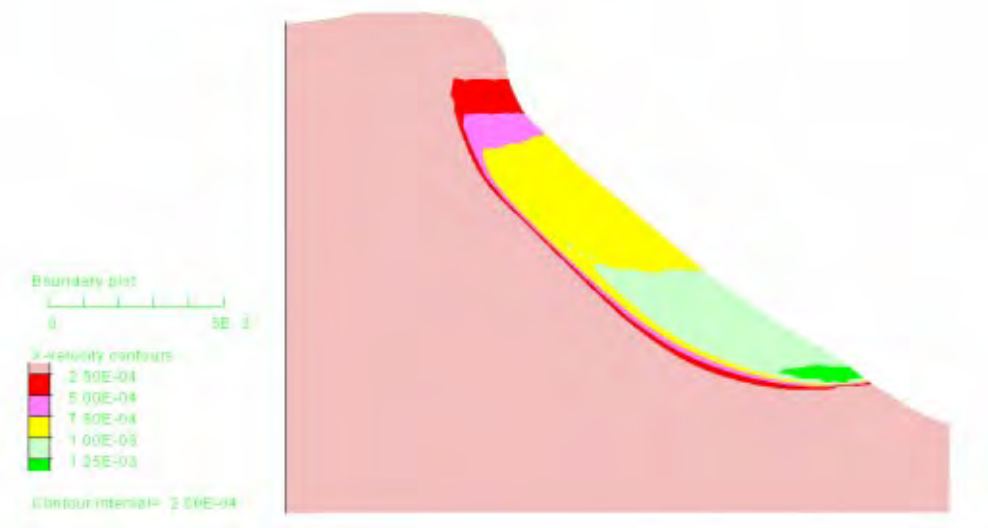

Figure 5.20 Slope in the northern zone, softening model — contours of steady-state horizontal velocity for a safety factor $\Phi = 2.0$

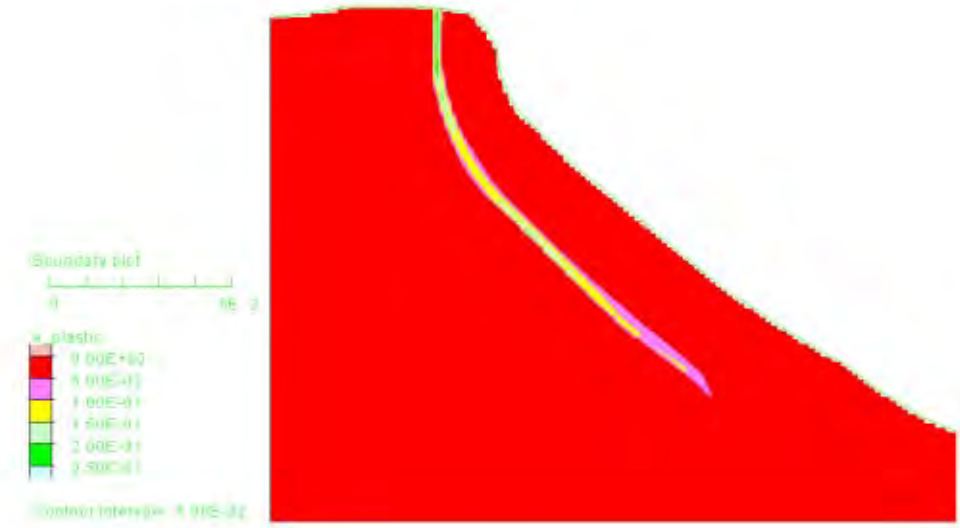

Figure 5.21 Slope in the northern zone, softening model — contours of plastic shear strain for a safety factor $\Phi = 2.0$

5.5.3 Destabilisation of the Slopes in the Northern Zone of Mururoa

Another set of numerical simulations was carried out to model the destabilisation of the northern slope of Mururoa. Both the initial damage caused by an explosion under the rim and the subsequent further destabilisation of the slope by a distant explosion were analysed by numerical modelling. The main objectives of these calculations were to assess whether:

(1) underground explosions in test area 1 were indeed capable of inducing irreversible damage in the carbonates, leading ultimately to destabilisation of large blocks of rock (deep-seated shearing mechanism); or

(2) a sufficiently powerful distant explosion could have caused further destabilisation of the slope in the northern zone of the atoll, following the initial damage induced by explosions in that zone.

Consider, first, the modelling of the initial damage caused by underground explosions in test area 1. A 10-kt explosion (according to DIRCEN/CEA Document No. 6, this was the largest yield of explosions in that area) at a depth of 650 m is simulated using a two-dimensional model in which the effect of the explosion is modelled as a P-wave source applied at the boundary of a cylindrical cavity. (The cavity radius is taken to correspond to the radius of the damaged zone; the amplitude and duration of the positive phase of the pressure boundary condition are calculated from the scaling law; see Appendix Q for details.) Note that, in this model, the carbonate formations are assumed to be strain softening. Results of this simulation, shown in Figures 5.22 (displacement vector field) and 5.23 (contours of plastic shear strain), clearly indicate the existence of a failure mechanism, which involves the formation of an inclined fracture in the brittle formations and shearing of the chalky limestone layer. The additional loading on the chalky limestone layer, caused by damage of the brittle formations, is evidently responsible for triggering the creep process. These results suggest that the deep-seated failure mechanism in the northern zone was indeed caused by the underground tests in area 1, since this failure surface does not correspond to the more "superficial" shearing surfaces predicted by the factor of safety computations.

The predicted failure surface on the lagoon side of the rim is generally consistent with field observations and DIRCEN/CEA interpretation of the monitoring records*. (Movements across these outer fractures have been either reactivated or enhanced by

*The shear fracture in the carbonates predicted by the model emerges at the surface of the rim, further inside the lagoon than suggested by DIRCEN/CEA Document No. 7. However, the predicted orientation and location of the fracture could very well have been affected by the "shear-only" failure criterion enabled in the numerical model. It is likely, in reality, that, close to the surface, the shear slip would change to vertical tensile cracks, thus reducing the distance inside the lagoon.

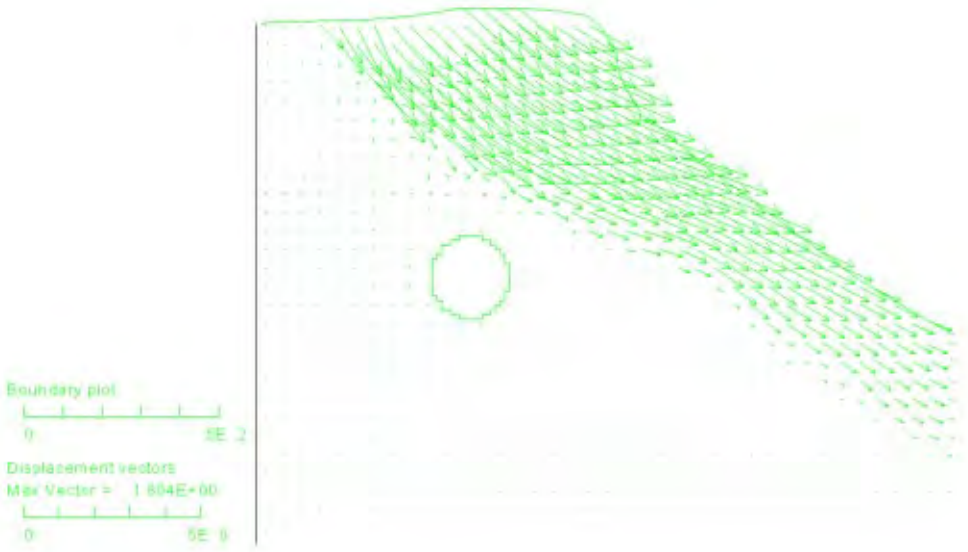

Figure 5.22 Displacement vector field after a 10-kt explosion at a depth of 650 m

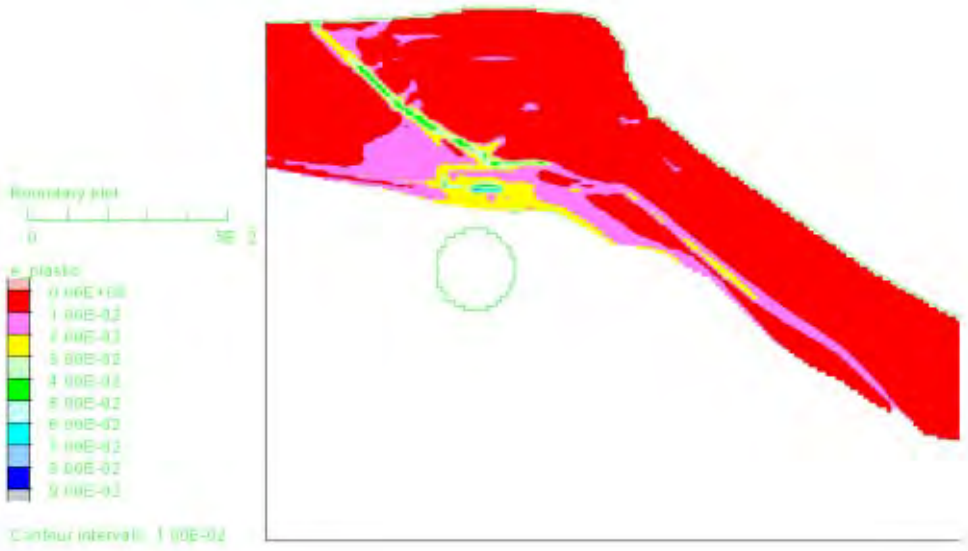

Figure 5.23 Contours of plastic shear strain after a 10-kt explosion at a depth of 650 m

the dynamic loading.) The observed destabilisations in the northern zone of Mururoa are generally consistent with the model proposed in Chapter 4 to explain the observed surface settlements. The fact that, in contrast to the southwestern zone, settlements did not stabilise rapidly in the northern zone is very likely due to the difference in geological structure between the two zones of the atoll rim and, especially, to the existence of a weak chalky limestone layer in the north.

Consider, next, the numerical simulations of the effects of distant explosions on the stability of the northern rim of Mururoa, already weakened by testing in area 1. Three calculations were performed to simulate a 40-kt test at distances, d, of 5 km and 10 km from the north slope, and a 70-kt explosion at a distance of 7 km. The two calculations (for Y = 40 kt at d = 5 km, and Y = 70 kt at d = 7 km) are intended to simulate the effect of the most powerful explosion in the lagoon, in test areas 5 and 6, respectively. The parameters Y = 70 kt and d = 7 km presumably characterise the tests Megarée (November 1985) and Pélée (November 1987), which left a strong signature on the data records of the extensometers and inclinometers installed in the Camélia zone.

Simulation of the distant explosions involve far-field and near-field models. The role of the far-field model is to propagate, in an elastic half-space, a stress wave generated at the outer boundary of the damaged zone around the explosion point, up to the boundary of the near-field slope model. The near-field model is the same as that used to simulate the effects of a 10-kt explosion under the rim; the initial state of the model incorporates the damage induced by the 10-kt explosion.

Results of the numerical simulation are shown in Figures 5.24–5.27. Contours of the horizontal-displacement increments (caused by the explosion) are plotted in Figures 5.24 and 5.25 for a 40-kt explosion at a distance of 5 km and 10 km, respectively, from the north slope. It can be seen from these figures that the 40-kt explosion at d = 5 km induces a displacement that can be as large as 3 cm, while the effect of the same yield at a distance of 10 km is insignificant. Finally, the results of the simulation for Y = 70 kt and d = 7 km are presented in Figures 5.26 (contour of the horizontal-displacement increment) and 5.27 (plot of incremental displacement vectors). For this simulation, the maximum incremental displacement is about 2.5 cm.

These simulations suggest that distant explosions in the lagoon could indeed have further destabilised the northern slope. In particular, the results of the numerical modelling for a 70-kt explosion at a distance of 7 km are consistent with the observations that the most powerful explosions in area 6 have had a significant impact on the movements of the destabilised rock masses. It is worth re-emphasising that these induced movements are possible only because of the damage inflicted to the slope by the explosions under the rim.

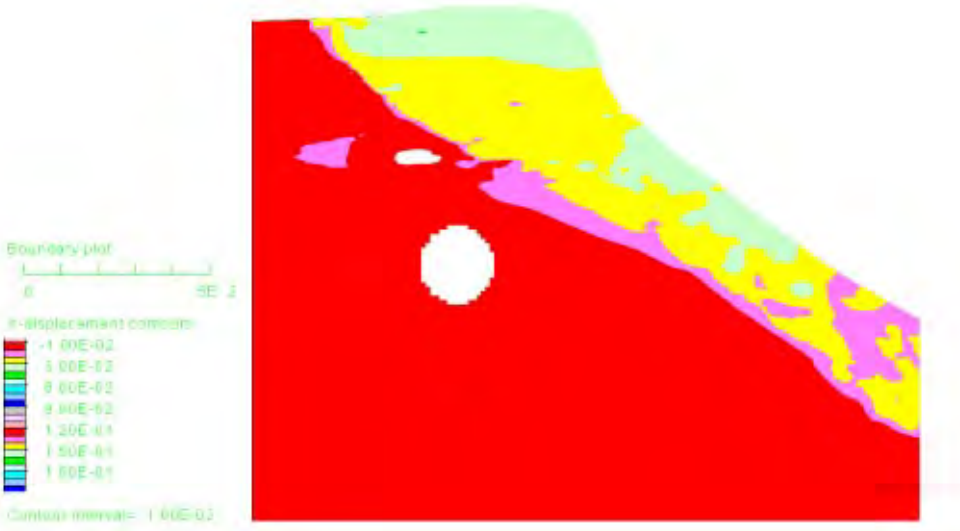

Figure 5.24 Contours of horizontal displacements on the northeast rim after a 40-kt explosion at 5 km

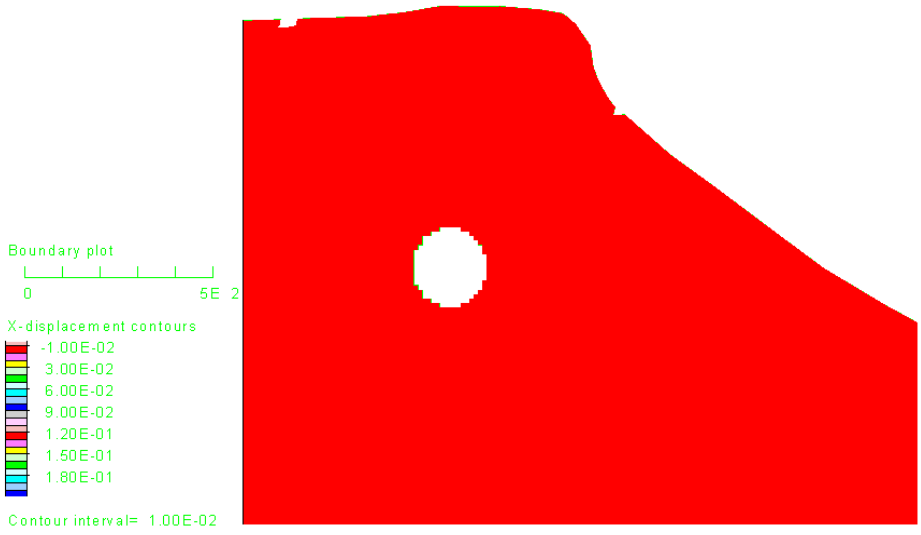

Figure 5.25 Contours of horizontal displacements on the northeast rim after a 40-kt explosion at 10 km

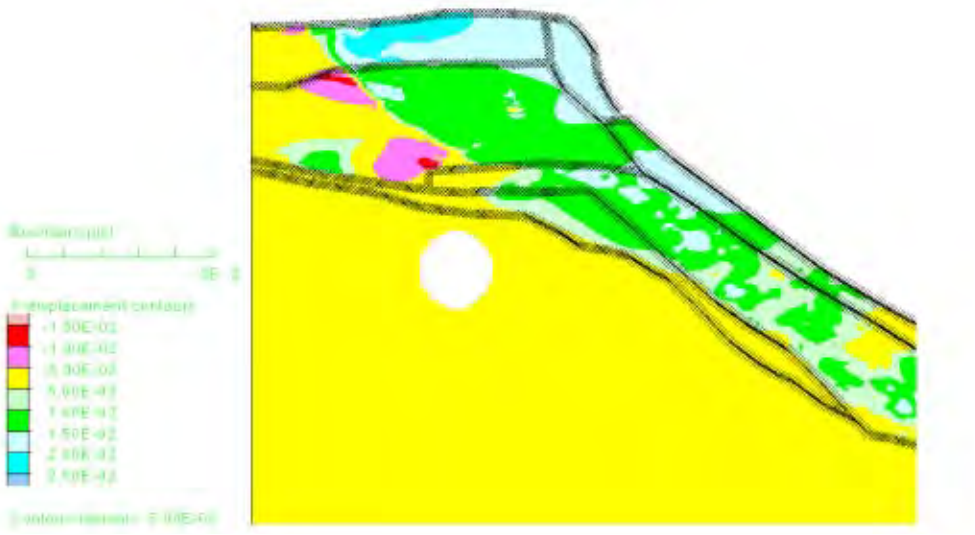

Figure 5.26 Contours of horizontal displacements after a 70-kt explosion at 7 km

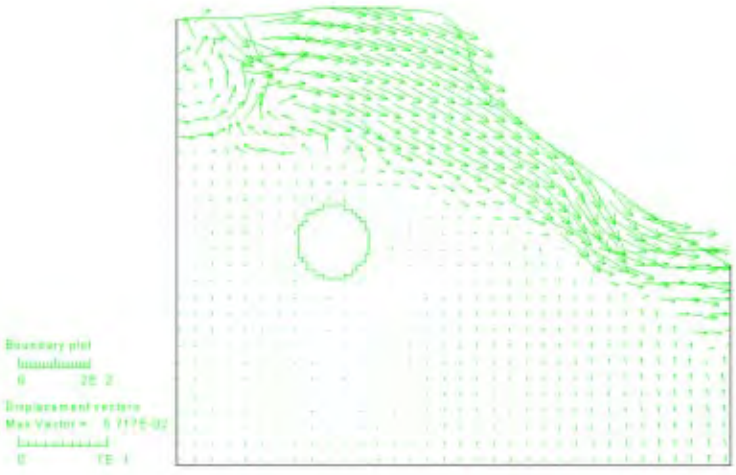

Figure 5.27 Displacement vector field after a 70-kt explosion at 7 km

5.6 Conclusions

There is an ample body of evidence, provided by DIRCEN/CEA Document No. 7, to support the claim that significant destabilisation of the flanks of Mururoa has occurred as a result of the underground nuclear testing. This destabilisation has taken different forms: massive sudden failures of accumulated sediments and debris in the southwestern zone, "shaving-off" of the rim, and slow seaward movement of large destabilised blocks of rock in the northern zone of the atoll.

Insights provided by numerical modelling allow us to address tentatively the issue of whether the underground testing has merely accelerated a natural process of evolution of the atoll flanks or instead has caused slope failures that would not have taken place otherwise. The answer appears to be that both situations have arisen.

On the one hand, it is clear that the ocean slopes of the atoll of Mururoa are not far from critical equilibrium under natural conditions. Indeed, numerical computations on the basis of information provided in DIRCEN/CEA Document No. 7 show that the factor of safety for the slope under gravity loading is between 1.4 and 3. (The factor of safety is smaller in the northern zone and depends on the assumed strength-softening parameters.) The potentially unstable lenses, under gravity loading alone, appear to be superficial both in the north and south of the atoll. Furthermore, numerical simulations of explosions under the rim (in the south as well as in the north) also indicate that materials on the atoll flanks yield during dynamic loading. However, the question of whether these lenses are actually failing rather than yielding cannot be answered by numerical modelling because the answer depends on the softening characteristics of these rocks, which are not known.

On the other hand, results of numerical modelling indicate that the carbonates are damaged by explosions under the rim. The horizontal radius of damage around a vertical axis through point zero (in the volcanics) is large, of the order of hundreds of metres. The most convincing evidence of this inflicted damage is the "instantaneous" surface settlement caused by explosions. As discussed at length in Chapter 4, the settlement is associated with "deeper" destabilisation of the atoll flanks, which manifests itself differently in the north and in the south of the atoll due to differences in the geomechanical conditions between the two regions. Despite their low yield (less than 10 kt), explosions under the rim in the north of Mururoa have caused irreversible deformation and have generated failure surfaces in the upper carbonates due to the presence of the weak chalky limestone layer. Together, the induced fractures in the carbonates and the weak chalky limestone layer delimit massive blocks of rock which are essentially resting on the inclined chalky limestone layer and slowly moving toward the ocean. This deep-seated failure mechanism appears to be the consequence of underground explosions, since it is unlikely that it would have developed as part of the natural process of destabilisation of the atoll flanks.

Finally, in our opinion, the question of the long-term stability of the north slope cannot be answered with any certainty. The creep response of the chalky limestone is not understood well enough to ensure reliable long-term predictions of the stability of the north slope. Although there is evidence, from the monitoring data, that the movement of the slope is stabilising, there is no certainty that the rate of variation of the displacement will continue the present steady decrease. Furthermore, the chalky limestone could already very well have undergone a large enough strain to cause an irreversible loss of cohesion, in which case it would behave essentially as a cohesionless granular material (i.e. $C = 0$ in Table 5.1), and a reduced ability to resist further deformation.

Chapter 6

ATOLL HYDROLOGY PRIOR TO NUCLEAR TESTING

6.1 Introduction

Hydrological issues at Mururoa and Fangataufa Atolls can be divided into two groups: those related to the natural hydrological system in atolls of this kind, and those related to the effects of underground nuclear testing. The first group provides the context within which the impacts of nuclear testing can be considered and is the focus of this chapter.

For the purposes of this study, hydrology includes the processes related to the flow of groundwater within the atolls, driven by differences in temperature and salinity, as well as by tides and other variations in ocean levels. In general, the surface hydrology of the atolls is of little interest, because rainfall on the rim of the atolls quickly becomes groundwater or is returned to the atmosphere by evapotranspiration.

To understand the conditions on the atolls prior to nuclear testing, the following questions must be addressed.

- What are the geological structure and the physical properties of the atolls, especially those which influence or control the movement of groundwater? Can the structure and physical properties be inferred from available data?
- What are the natural directions and rates of groundwater flow in the atolls?
- What are the effects of tidal fluctuations on groundwater movement and transport of heat and solutes?

To answer these questions, the basic approach taken in this chapter is to identify the important issues and processes, to review relevant earlier studies and, where necessary, to make additional calculations or assessments to elucidate the issues.

Figure 6.1 is a schematic cross-section through an atoll, showing groundwater flow directions under natural conditions prior to testing. Following introductory discussions in Section 6.2 about island hydrology, Section 6.3 provides an analysis of natural circulation at atoll scale and of the resulting structure and physical properties of the system. Section 6.4 then summarises our understanding of the natural hydrological system at Mururoa and Fangataufa prior to the tests.

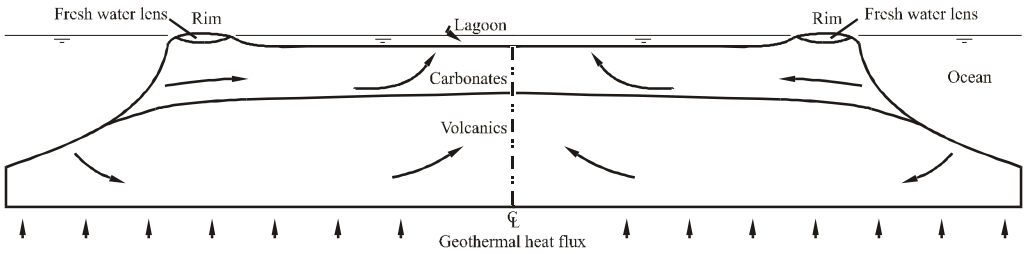

Figure 6.1 Schematic cross-section through an atoll (after Perrochet and Tacher 1997a)

6.2 Major Hydrological Processes on Atolls

There have been many previous studies of atoll hydrology, and the processes observed on these other atolls are relevant to the study of Mururoa and Fangataufa. Some of the atolls for which significant hydrological studies have been carried out are listed in Table 6.1. This table shows the locations of previous studies, references in the open literature and a brief reference to the types of hydrological issues of importance. A reference book edited by Vacher and Quinn (1997) provides the most up-to-date summary of the state of the art.

6.2.1 The Geological Structure of Atolls

The accepted conceptual model of an atoll is that of a cone of volcanic rocks overlain by carbonates formed by the growth and decay of limestone reefs as the volcanics subsided beneath sea level over geological time. Between these two zones is a *transition zone* — a term which is not precise because it includes many types of materials, such as clays formed during weathering of the volcanics at a time when they were above sea level, and also because the transition zone does not occur continuously at all locations.

Several of the papers listed in Table 6.1 provide good descriptions of the geology of atolls, especially within the carbonate zone. Carbonates are certainly not uniform in structure or even of one type. While most carbonates are limestone, originating from massive or branching corals, some limestone has been transformed into dolomite due to inflow of magnesium-rich seawater into the limestone over geologic time (Rougerie and Wauthy 1993). While some of the limestone is very porous and permeable, many atolls have relatively impermeable limestone caps known as beachrock (Underwood et al. 1992). The carbonate region often contains layers of karst (highly permeable, even cavernous limestone) formed by dissolution of carbonates by fresh water during periods when the sea level was relatively steady over long periods of time and considerably lower than at present (Buigues 1996; Buigues 1997).

In principle, geophysical methods can provide considerable detail about the internal structure of atolls, within both the carbonate and basalt zones (see Section 2.3). Seismic and magnetic methods have been applied at Bikini and other atolls in the Marshall Is-

Table 6.1 Atolls for which relevant hydrological studies have been carried out

Atoll	References	Hydrological Issues
Arno Atoll, Marshall Islands	Cox (1951)	freshwater lens, tidal fluctuations
Bikini Atoll, Marshall Islands	Swartz (1958)	geothermal structure
Davies Reef, Great Barrier Reef, Australia	Oberdorfer and Buddemeier (1986)	groundwater flow processes
Deke Island, Pingelap Atoll, Eastern Caroline Islands	Ayers and Vacher (1986)	freshwater lens, tidal efficiency
Enjebi Island, Parry Island, Enewetak Atoll, Marshall Islands	Arnow (1954), Swartz (1958), Wheatcraft and Buddemeier (1984), Herman and Wheatcraft (1984), Saller (1984), Samaden et al. (1985), Herman et al. (1986), Oberdorfer et al. (1990)	geothermal structure, hydrogeochemistry, atoll-scale flow, freshwater lens, tidal effects
Ifalik Atoll, Caroline Islands	Arnow (1955)	freshwater lens, tidal efficiency
Kapingamarangi Atoll, Caroline Islands	McKee (1956)	freshwater lens, tidal fluctuations
Kwajalein Island, Marshall Island	Hunt, Jr. and Peterson (1980)	freshwater lens, tidal efficiency
Majuro Atoll, Marshall Islands	Hamline and Anthony (1987), Anthony et al. (1989), Griggs and Peterson (1993)	freshwater lens, tidal efficiency, hydrogeochemistry
Mururoa Island, French Polynesia	Rougerie and Wauthy (1993), Henry et al. (1996)	geothermal structure, atoll-scale flow
Swains Island, Tokelau Group	Lam (1974)	tidal effects
Tarawa Atoll, Republic of Kiribati	Lloyd et al. (1980), Volker et al. (1985)	freshwater lens
Tikehau Atoll, Tuamotu Archipelago, French Polynesia	Rougerie and Wauthy (1993)	geothermal structure, endo-upwelling

lands (Dobrin and Perkins 1954; Raitt 1954; Alldredge et al. 1954) but also at Mururoa Atoll (Ruzie and Gachon 1985; Buigues et al. 1992).

6.2.2 Natural Flow of Groundwater in an Atoll

In very general terms, the hydrology of a natural atoll is well understood. Generally, two different flow systems are present; these are described below and in Figure 6.1.

1. The first system is very superficial and consists of fresh to moderately saline water that infiltrates the ground above sea level, due to recharge by rainfall, and flows laterally toward the ocean and the lagoon. This freshwater forms a “lens” on top of denser seawater in the sand and calcareous rim of the atoll. Its thickness

can range from a few metres to some tens of metres, mostly depending on the maximum width and ground elevation of the rim. If, for instance, the water table elevation under the rim, due to recharge, is 1 m, then, according to the Ghyben-Herzberg relation, the thickness of the freshwater lens would be of the order of 40 m. The coefficient 40 between the elevation of the water table and the depth of the seawater interface is equal to $(\rho_s - \rho_f)/\rho_f$, where ρ_s and ρ_f represent the density of seawater and freshwater, respectively (e.g. de Marsily 1986, p. 223). Because of tidal fluctuations, a gradual transition from freshwater to seawater is observed over a thickness of some 10 m (Oberdorfer et al. 1990). This freshwater lens is the unique source of freshwater for human consumption on an atoll.

2. The second system is the deeper seawater that saturates the lower part of the calcareous cover of the atoll, underneath the freshwater lens, and the underlying volcanic rocks. Generally speaking, the permeability of the limestone is much higher than that of the volcanics, and most of the flow in this second system occurs in the limestone. Two mechanisms have been shown to generate groundwater flow in this saltwater. The first one, known as *bow pressure*, is related to the general ocean current that surrounds the atoll; because of a small pressure difference between the upstream and downstream ends of the atoll (with respect to the ocean current), a small horizontal groundwater flow exists in the atoll in the same direction as the ocean current. The second mechanism is known as *endo-upwelling* and has a vertical component upward. It is considered more significant than bow pressure, especially in the case of interest here. This vertical flux is due to thermal buoyancy forces. Because of the natural geothermal heat flux in the earth's crust, the solid atoll conducts heat to the surface and is warmer than the surrounding ocean water, which typically is around 4 °C at depths greater than 1 km. Thus, the water in the pores or fractures of the atoll is warmer than the surrounding seawater, and therefore lighter, due to water thermal expansion. A general circulation pattern is thus infiltration of seawater along the flanks of the atoll and flow of this water towards its centre and vertically upward to the lagoon. This mechanism has been observed in several atolls and is thought to explain the generally high biological productivity of lagoons, because the flux of deep seawater is rich in nutrients (Rougerie and Wauthy 1993; Samaden et al. 1985; Henry et al. 1996; Swartz 1958). Superposed on this upwelling flow are periodic tidal fluctuations, which can generate larger velocities than the upwelling ones, especially if the tide inside the lagoon lags slightly behind the tide in the ocean. This oscillating velocity is, however, in general of zero average and responsible for generating mixing in the atolls, especially in the high-permeability karstic layers of the carbonates.

6.2.3 Hydrological Processes and Governing Equations

Hydrological processes of interest in atoll hydrology include groundwater flow through porous and fractured rock, transport of heat, and transport of solutes. Even though the volcanic and carbonate rocks in atolls are generally fractured and exhibit variability at many scales, it is commonly accepted to represent the rock by an equivalent porous medium when considering groundwater flow at the atoll scale. It is thus necessary to adjust the permeability of this equivalent porous medium so that it accounts, in a global sense, for the effect of fractures and heterogeneities, when the flux of water, heat and solutes are calculated. This conceptual model, as applied in all other hydrological studies of atolls, is adopted for all of the analyses described in this report. The governing equations that describe flow and transport in porous or fractured media, and which were used by the IGC in its calculations, are presented briefly below.

In mathematical terms, groundwater flow in a porous medium is described by Darcy's Law:

$$\boldsymbol{q} = -\frac{\boldsymbol{\kappa}}{\mu}\left(\nabla p + \rho\,\boldsymbol{g}\right) \tag{6.1}$$

where $\boldsymbol{q}$ is a vector of specific discharge or Darcy flux (volume per unit time per unit cross-sectional area of porous medium [e.g. ms^{-1}]), $\boldsymbol{\kappa}$ is the permeability tensor [m^2], μ is dynamic viscosity of the fluid [$\mathrm{kg\,m}^{-1}\mathrm{s}^{-1}$], $p(x, y, z, t)$ is pore pressure [Nm^{-2}], ρ is fluid density [$\mathrm{kg\,m}^{-3}$], and $\boldsymbol{g} = g \nabla z$ is the vector of acceleration due to gravity [ms^{-2}] oriented upward. ∇ denotes a spatial gradient, bold lower-case symbols are vectors, and bold upper-case symbols are tensors. The Darcy flux must satisfy an equation of conservation of mass for the fluid phase, of the form:

$$\frac{\partial(\phi\rho)}{\partial t} + \nabla \cdot \rho\,\boldsymbol{q} = 0 \tag{6.2}$$

where ϕ is the porosity of the medium [-]. The $\cdot$ symbol between ∇ and $\rho\boldsymbol{q}$ denotes "scalar product". In the context of coupled flow and transport of heat, both ρ and μ vary with temperature T according to appropriate constitutive laws.

A similar balance equation is solved for the advective-conductive-dispersive transport of heat:

$$\left[\phi\,(\rho c)_l + (1-\phi)\,(\rho c)_s\right]\frac{\partial T}{\partial t} + (\rho c)_l\,\boldsymbol{q}\cdot\nabla T = \nabla\cdot\left[\phi\boldsymbol{\Lambda}_l + (1-\phi)\,\lambda_s\,\boldsymbol{I}\right]\nabla T \tag{6.3}$$

where $(\rho c)_l$ and $(\rho c)_s$ are the volumetric heat capacity [$\mathrm{Jm}^{-3}\,\mathrm{K}^{-1}$] of liquid and solid phases, respectively, $\lambda_s\,\boldsymbol{I}$ [$\mathrm{Jm}^{-1}\,\mathrm{s}^{-1}\,\mathrm{K}^{-1}$] is the thermal conduction tensor of the solid (assumed to be isotropic), $\boldsymbol{I}$ is the identity matrix, and $\boldsymbol{\Lambda}_l$ [$\mathrm{Jm}^{-1}\,\mathrm{s}^{-1}\mathrm{K}^{-1}$] is the hydrodynamic thermal dispersion tensor of the liquid. The latter can be written in the form given by Nikolaevskii (1959) for the dispersion of any conservative quantity (heat or tracer) as:

$$\mathbf{\Lambda}_l = (\rho c)_l \left[(\alpha_L - \alpha_T) \frac{\boldsymbol{v} \otimes \boldsymbol{v}}{\| \boldsymbol{v} \|} + \alpha_T \| \boldsymbol{v} \| \boldsymbol{I} \right] + \lambda_l \boldsymbol{I} \tag{6.4}$$

where α_L and α_L [m] are longitudinal and transverse thermal dispersivities, $\lambda_l \boldsymbol{I}$ is the isotropic thermal conduction tensor of the liquid, and $\boldsymbol{v} = \boldsymbol{q}/\phi$ is the pore velocity vector. The symbol $\otimes$ denotes "tensorial" (or dyadic) product.

For solute transport, a very similar balance equation is (see, for example, de Marsily 1986):

$$\phi \frac{\partial C}{\partial t} + (1 - \phi) \rho_s \frac{\partial F}{\partial t} = \nabla \cdot \boldsymbol{D} \nabla C - \nabla \cdot \boldsymbol{q} C \tag{6.5}$$

where C is the solute concentration [kg m^{-3}], F is the amount of solute sorbed on the solid [kg kg^{-1}], if any, ϕ is the porosity, ρ_s is the density of the bulk porous medium, $\boldsymbol{D}$ is the dispersion tensor [m^2 s^{-1}], and $\boldsymbol{q}$ is the Darcy flux given by (6.1). If there is no interaction between the solute and the solid rock, then the second term on the left-hand side disappears. Otherwise, an evolution equation for F in terms of C has be to specified to make the system of equations determinate. For isotropic media, the dispersion tensor $\boldsymbol{D}$ is oriented with its principal directions parallel and perpendicular to the velocity vector (one longitudinal component and two transverse components). It is given by Nikolaevskii (1959) as:

$$\boldsymbol{D} = \left[(\alpha_L - \alpha_T) \frac{\boldsymbol{q} \otimes \boldsymbol{q}}{\| \boldsymbol{q} \|} + \alpha_T \| \boldsymbol{q} \| \boldsymbol{I} \right] + \phi d \boldsymbol{I} \tag{6.6}$$

where α_L and α_T are the longitudinal and transverse solute dispersivities [m] (which, numerically, are different from and larger than the thermal diffusivities above), and d is the molecular diffusion coefficient in porous media, which is only a fraction of the molecular diffusion coefficient in free water (in general, 10–70%) due to tortuosity. This molecular diffusion coefficient is often neglected with respect to the first term in (6.6).

An alternative formulation to the flow equations (6.1) and (6.2) is based on the use of an equivalent hydraulic head

$$H_0 = \frac{p}{\rho_0 g} + z \tag{6.7}$$

where $\rho_0 = \rho(T_0)$, and T_0 is a chosen reference temperature (Perrochet and Tacher 1997a). In terms of H_0, Darcy flux can be written:

$$\boldsymbol{q} = -\boldsymbol{K}_0 \frac{\mu_0}{\mu} \left[\nabla H_0 + \frac{(\rho - \rho_0)}{\rho_0} \nabla z \right] \tag{6.8}$$

where $\boldsymbol{K}_0 = \boldsymbol{\kappa} \rho_0 g / \mu_0$ [ms^{-1}] is the hydraulic conductivity tensor at $T = T_0$. The conservation equation becomes:

$$S_0 \frac{\partial H_0}{\partial t} + \nabla \cdot \boldsymbol{q} = -\frac{1}{\rho} \frac{\partial \rho}{\partial T} \left(\phi \frac{\partial T}{\partial t} + \boldsymbol{q} \cdot \nabla T \right) \tag{6.9}$$

where the specific storativity S_0 [m^{-1}] combines the effects of the compressibilities of the liquid and the porous matrix. This form of the flow equation is not commonly used, and a simplified form, referred to as the Boussinesq approximation, is often used (e.g. in CEA calculations). The simplification keeps the variation of the water density with temperature in (6.8) and neglects all other variations, equivalent to setting to zero the right-hand-side of (6.9). However, the IGC decided to systematically use the complete form of (6.9).

The forms of Darcy's Law given in (6.1) and (6.8) assume that the porous medium is anisotropic. When we assume that flow through fractured rock behaves like flow in a porous medium, we are assuming that the flow can be described at a bulk scale by a linear gradient law of the form of Darcy's Law, with effective values of permeability or hydraulic conductivity that allow the correct (observed) flows to be calculated, given the correct (observed) gradients of pressure or head.

To make predictions of groundwater flow and transport of heat or solutes, it is necessary to define the geometry of a flow system, the physical properties of the porous medium and of the fluid itself, and boundary conditions, such as temperatures or fluctuating water levels, which drive the flow. Of these, the most difficult to determine are often the physical properties of the medium — in particular, the equivalent or effective hydraulic conductivities. The estimation of these properties, or of values of parameters that represent these properties in a mathematical model, requires a significant effort in the study of any natural hydrogeological system.

Aquifer properties are best estimated by using all available sources of information. These can include direct measurements, such as small-scale parameter tests on core samples, and indirect measurements based on observing piezometric heads, temperatures and concentrations in the field, and inferring aquifer properties by calibrating appropriate models. Even the so-called direct measurements are really obtained by model calibration, where the model may be as simple as Darcy's Law applied to a one-dimensional column. The general problem of inferring material properties is known as the inverse problem, and a number of different types of information can be used to address this problem at Mururoa and Fangataufa Atolls.

6.2.4 Tidal Fluctuations

Many early studies of atoll hydrology used measurements of tidal fluctuations in water table elevations (and piezometric heads at depth) to infer aquifer properties. The term *tidal efficiency* is used to describe the way the amplitude of water table fluctuations decays with distance from the coast. The efficiency is high in highly permeable aquifers or in confined aquifers with a small aquifer-storage coefficient, and the full tidal amplitude is then observed far from the coast.

There are numerous analytical solutions to simple mathematical representations of this problem. In an infinitely long idealised aquifer with spatially uniform transmissivity and storage coefficient, for example, the amplitude of fluctuations drops off exponentially with distance from the coastline (Jacob 1950, Ferris 1951). Wheatcraft and Buddemeier (1981) applied a solution by Williams et al. (1970) for a finite-length aquifer to the Enewetak Atoll.

Lam (1974) analysed tidal fluctuations using a numerical model of groundwater flow in a two-dimensional cross-section. Such a model has the advantage that it can include the effect of zones with different hydraulic properties, such as a relatively impermeable limestone cap or a highly permeable karst. Most published analyses of tidal effects focus on the response in shallow boreholes, to depths of 25 m or so. However, Oberdorfer et al. (1990) simulated tidal effects to a depth of 1277 m, at the interface between carbonates and basalt at Enewetak Atoll. Maximum tidal velocities were of the order of 10^{-5} ms^{-1}.

Oscillating flows in a porous medium can cause increased dispersion. Webster and Taylor (1992) showed the possibility of increased dispersion, which they described as rotational dispersion, when velocity fluctuations in different directions are out of phase — i.e. the oscillations are not uni-directional. Certainly there is field evidence, and considerable support from modelling as well, to show that there is significant mixing of the interface between fresh water and sea water and that this is enhanced by tidal oscillations. Oberdorfer et al. (1990) used a density-coupled flow and transport model with small timesteps to resolve the tidal cycle. This showed that mixing is so large that in order to simulate the same effect with a steady flow and transport model, it would be necessary to use extremely large dispersivities, which would be considered unreasonably large in other circumstances. The same would be expected to apply to transport of heat, because the transfer of heat by conduction to the solid matrix provides an exchange mechanism that could lead to increased effective spreading in a similar manner. Underwood et al. (1992) supported the view that tidal oscillations are critical in controlling mixing and the structure of the freshwater lens in atolls.

6.3 Groundwater Flow at Mururoa and Fangataufa

6.3.1 General Description According to CEA Documents

The general picture of flow in an atoll given in Section 6.2.2 applies to Mururoa and Fangataufa. The superficial freshwater system is known to exist (e.g. in the *base vie* area of the rim, which is the widest section), but it is very shallow and contains brackish water. It has been reported (Caristan 1997) that the lens is only metres thick. Such a thin layer of fresh water under the rim of the atolls would have negligible effects on the movement of groundwater at depth within the atolls, as shown in Section 6.3.7. It is presently unexploited (all water consumed in Mururoa was either imported or desalinised from seawater), but it could represent a resource for a very small community or become

significant if a drop in sea level (e.g. during glaciation) makes the rim wider and raises its elevation, as will be seen in Section 7.6.2. The *bow-pressure* flow has not been reported, and it would not be very significant, compared to the endo-upwelling flow, because the ocean current in this area is rather weak (estimated to be 0.1 m/s). However, the *endo-upwelling* flow is definitely present and has been shown by temperature measurements in vertical boreholes in the atoll (Figures 6.2 and 6.3).

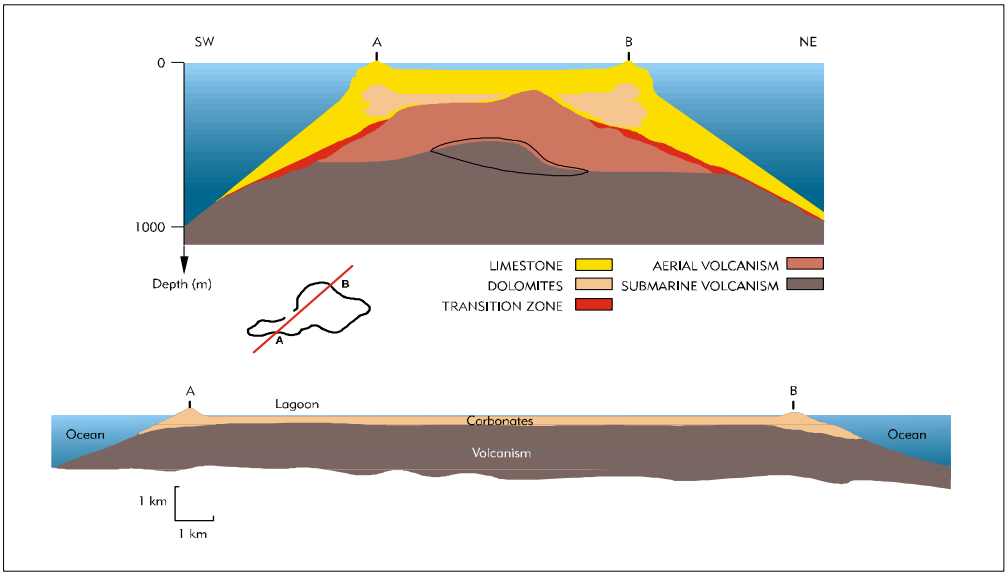

Figure 6.2 Idealised cross-section through Mururoa Atoll (Bouchez and Lecomte 1996)

The hydrogeological system of Mururoa Atoll is described in detail in Guille et al. (1996). However, there are no direct and compatible observations of heads and flows at Mururoa or Fangataufa that might allow the estimation of bulk-scale effective hydraulic conductivities. The CEA has used a number of types of data to infer values or relative values of conductivity. These include observations of (i) the thermal structure of the atolls, (ii) observations of flows within vertical drill holes, (iii) the rate of refilling of the chimney after many tests, and (iv) tidal fluctuations of piezometric heads within the karst. Also, an attempt was made to confirm the estimated hydraulic conductivity by geochemical measurements in the water of some boreholes. The CEA has used the finite-element code METIS (Goblet 1981) for its calculations. The results are presented in DIRCEN/CEA documents and in Guille et al. (1996), Bouchez and Lecomte (1996) and Henry et al. (1996), and will be discussed below. The general conclusion from all of this work is that the volcanics and carbonates have effective (isotropic) hydraulic conductivities of about 10^{-7} ms^{-1} and 10^{-4}–10^{-5} ms^{-1}, respectively. The values in the carbonates are consistent with those found at other atolls (Oberdorfer et al. 1990).

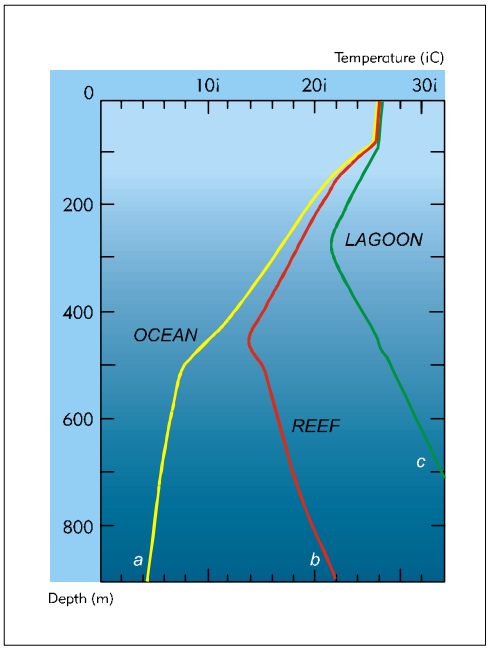

Figure 6.3 Idealised thermal profiles (Guille et al. 1996)

There is little doubt, however, that the volcanics and carbonates at Mururoa and Fangataufa are fractured, so that the above figures are effective conductivities that include the role of the fractures. Some of these fractures may be connected over significant distances, but there is no specific evidence to support this suggestion. Underground nuclear testing has certainly affected the nature of fracturing in the near field of each test, but it may or may not have caused fracturing over larger distances. Data from a drillhole called Nérite show natural fractures in the volcanics and new fractures induced by the nuclear test Eurytos within the chimney and up to 20 m above the chimney. The age of the fractures can be determined based on the presence or absence of weathering products on the surfaces of the fractures.

By current standards of practice, neglecting to collect systematic data on fracturing from every drillhole may be considered unacceptable, but much less was known about the role of fractures at the time of the first underground tests, in the mid-1970s, than is known today. The science of flow and transport in fractured media has been advancing rapidly since the mid-1980s, but it is still a long way from maturity. Even if detailed analyses of fractures were available at Mururoa and Fangataufa, it would be very difficult, if not impossible, to predict effective hydraulic conductivities of the volcanics and carbonates based on fracture geometry analyses.

6.3.2 Modelling of the CEA Results by IGC

The IGC's assessment of the hydrology of Mururoa and Fangataufa Atolls depends on the available field data, the primary source for which is the CEA. Data have been obtained from published CEA reports (Guille et al. 1996; Bouchez and Lecomte 1996), from documents prepared by the CEA in the course of this study (DIRCEN/CEA, Document Nos. 4–11), and from papers in the open literature published by the CEA staff and their scientific collaborators. Where possible, studies of other atolls or of relevant physical processes have also been used.

Data — Available data on the hydrology of the two atolls are of three types: qualitative information about the geology of the atolls (see Chapter 2), temperature data, and qualitative information about hydrothermal alteration within the volcanic rocks.

It is believed that the CEA measured temperature profiles in a significant number of boreholes at Mururoa and Fangataufa. However, only a selection of profiles was made available for interpretation by the IGC. These include the following:

(1) two idealised profiles beneath the rim and the lagoon at unspecified locations (Guille et al. 1996) (very similar profiles were published by Atkinson et al. (New Zealand MoFA 1984) and Rougerie and Wauthy (1993), based on data provided to Atkinson et al. by the CEA);

(2) an indication of the relative positions of these two profiles on a generalised cross-section through one of the atolls (Guille et al. 1996) (the thermal profile beneath the lagoon in this case, however, does not match the profile in (1).);

(3) a second generalised cross-section (Bouchez and Lecomte 1996), which is slightly different from (2) and more consistent with the profiles in (1);

(4) profiles at three sites at Mururoa known as Lagon (under the lagoon), Viviane and Fuchsia (under the south rim) (Henry et al. 1996);

(5) a profile measured at a site on Mururoa known as Zoé (under the south rim) (DIRCEN/CEA Document No. 5; also presented by Rougerie and Wauthy (1993));

(6) six temperature profiles measured at Fangataufa Atoll (provided by DIRCEN/CEA); and

(7) a map showing hand-drawn contours of the minimum temperature in temperature profiles on Mururoa Atoll (provided by DIRCEN/CEA). (This map became available only after all IGC hydrologic modelling studies had been completed.)

None of the data were provided in digital form. In essence, the data consist of a number of lines on graphs that were digitised to facilitate the IGC's analyses. Figure

6.2 shows the idealised cross-section corresponding to (3), and Figure 6.3 shows the temperature profiles described in (1), together with the ocean thermal profile.

Temperature profiles like those shown in Figure 6.3 were obtained by the CEA using downhole thermistors in open (uncased) boreholes. Whether the temperatures obtained in this way are characteristic of ambient temperatures at the level at which they are measured is an interesting question. If groundwater flow is horizontal past a vertical open hole, temperatures in the borehole can be expected to represent groundwater temperatures when the thermal perturbation caused by drilling has decayed (after several months). If there is any possibility of a vertical component of flow, or an oscillatory flow due to tidal influences, the issue is not as easily resolved. To complicate matters further, when the temperature gradient is inherently unstable (e.g. with hotter water at depth), there exists the possibility of setting up convection cells within an open borehole. This possibility is more likely when a borehole is inclined (Ecole des Mines de Paris 1985).

Temperature data were collected by the CEA partly to facilitate the identification of highly permeable (karst) horizons in the carbonates at particular elevations within boreholes. This is possible if a temperature anomaly occurs, with a deviation from profiles of the kind shown in Figure 6.3. The CEA investigated the reasonableness of temperature profiles and concluded that they provided a reasonable indication of ambient groundwater temperatures. We accept this assertion and agree that the data are sufficiently accurate to allow analysis of the kind which follows.

Evidence for geothermal convection or endo-upwelling is not limited to temperature profiles. Other evidence includes recent studies of dolomitisation (Rougerie and Wauthy 1993), which argue that in-flowing sea water provides the source of magnesium for ion substitution with calcium carbonate to form dolomite. Geochemical alteration and weathering within the volcanics (Guy et al. 1992) also provide — qualitative if not quantitative — support for the conceptual model of convection. Henry et al. (1996) attempt to apply this argument quantitatively; however, their arguments supporting particular rates of groundwater flow in the volcanics are not conclusive.

Qualitative Interpretation of Thermal Data — It is interesting to attempt to interpret the temperature profiles without resorting to sophisticated modelling of coupled flow and transport of heat. Stallman (1960, 1965) suggested that temperature measurements might provide a method of measuring rates of groundwater flow, and he analysed the effects of sinusoidally varying surface temperatures on subsurface temperatures in the presence of vertically downward infiltration. Bredehoeft and Papadopulos (1965) determined the expected shape of the temperature profile through a region of vertical groundwater flow with known temperatures at either end. They showed that with steady upward flow, the profiles are generally convex, the degree of curvature depending on the thermal conductivity or, more generally, on the effective longitudinal dispersion coefficient. In the limiting case in which the conductivity or dispersion coefficient becomes infinitely large, the thermal profile becomes linear.

At first glance, all available thermal profiles in the volcanics at Mururoa are relatively linear with depth. Because groundwater flow is very slow in this region, advection and dispersion would be negligible; the shape of the profiles therefore suggests the dominance of conduction over advection in this region. The profiles are also relatively linear in the carbonates, where the upward flow is not only much faster, but also oscillates due to tidal influences. By comparison with Figure 2 of Bredehoeft and Papadopulos (1965), the profiles in the carbonates correspond to values of vL/D less than 0.5 or 1, where v is (the time-averaged) vertical upward velocity, L is the thickness of the carbonates, and D is an effective thermal dispersion coefficient. This implies that D/vL is greater than 1 or 2, from which an effective longitudinal dispersivity, D/v, would be between L and $2L$, when defined relative to the long-term average velocity. By simple examination of the field data, it appears therefore that there must be a significantly enhanced effective longitudinal dispersivity in the carbonates, perhaps caused by tide-induced oscillations in the vertical velocity. However, it is shown below that fluctuations in vertical velocity would be expected to vary with depth throughout the carbonates, so that the effective dispersion coefficient should also vary with depth. This simple analysis based on a uniform value of D still suggests the dominance of dispersion over vertical advection in the carbonates.

Modelling by the CEA — The data presented in Figures 6.2 and 6.3 have been interpreted and modelled by Guille et al. (1996) and Bouchez and Lecomte (1996). Further modelling has been carried out by Henry et al. (1996) for a complete idealised cross-section through Mururoa Atoll. Finally, some modelling has recently been carried out by the CEA for an idealised radially symmetric cross-section through Fangataufa Atoll. All modelling by the CEA was carried out using the code METIS (Goblet 1981), which solves the equations for density-coupled transport of water and heat in a two-dimensional cross-section.

The purpose of the reports by Guille et al. (1996) and Bouchez and Lecomte (1996) was to describe general principles — in particular, to explain the general concept of endo-upwelling and to present an approximate calibration of a model to the observed thermal profiles. Guille et al. (1996) conclude that effective hydraulic conductivities are about 10^{-7} ms^{-1} in the volcanics and 10^{-4} – 10^{-5} ms^{-1} in the carbonates.

Henry et al. (1996) present sensitivity analyses, using various combinations of hydraulic conductivities in the volcanics and carbonates. They show that without advection in the carbonates, which occurs when the hydraulic conductivity of the carbonates becomes sufficiently large, heat would be transported only by conduction, and observed thermal profiles could not be explained. The authors conclude that large-scale effective hydraulic conductivities are about 10^{-7} ms^{-1} in the volcanics and $3 \cdot 10^{-4}$ ms^{-1} in the carbonates.

Results of modelling by Henry et al. (1996) of an idealised radially symmetric cross-section through Fangataufa Atoll (provided by CEA) show good agreement between

measured and predicted thermal profiles for three temperature profiles beneath the rim at a radius of 3370 m (minimum temperature about 16.5 °C at a depth of 300 m), for a fourth profile beneath the lagoon at radius 1500 m (minimum 20 °C at 260-m depth), for a fifth profile at radius 900 m (minimum 21 °C at 260-m depth) and, finally, for a sixth profile at a radius of 500 m (minimum 21.5 °C at 260-m depth). These results were obtained using effective hydraulic conductivities of 10^{-7} ms^{-1} in the volcanics and $3 \cdot 10^{-4}$ ms^{-1} in the carbonates, with a 10-m layer to represent karst at the base of the carbonates, with a conductivity of 10^{-1} ms^{-1}. Effective porosities were 0.1 in the volcanics and 0.3 in the carbonates and karst.

In all modelling by the CEA, movement of heat is assumed to occur by advection and conduction-dispersion. Dispersion is represented in the classical way, with longitudinal and transverse dispersion coefficients being equal to the product of the magnitude of the local pore velocity and longitudinal and transverse dispersivities, respectively. As suggested in Section 6.3.2 (*Qualitative Interpretation of Data*), the small effective hydraulic conductivities in the volcanics lead to small velocities and, therefore, negligible advection and dispersion; thus, the transport of heat is dominated by conduction. In the carbonates, however, the velocities are three orders of magnitude larger, and tidal fluctuations increase the dispersion coefficient, so that dispersion dominates both advection and conduction as the primary mechanism for transport of heat.

6.3.3 Verification by the IGC

Modelling the density-coupled transport of water and heat is fundamental to this study. All modelling was carried out by Perrochet and Tacher (1997a) on behalf of the IGC, using a commercial code known as FEFLOW (Diersch 1996). In order to test the equivalence of METIS and FEFLOW, at least under certain conditions, an effort was made to reproduce a number of results obtained by the CEA, both to verify the CEA results and to detect possible inconsistencies.

Simulations for a Full Cross-Section Through Mururoa Atoll — The first verification runs were aimed simply at reproducing results obtained by Henry et al. (1996) for an idealised cross-section through Mururoa Atoll. A finite-element mesh was generated with 517 bilinear quadrilateral elements, digitised from Henry et al. (1996).

To ensure a fair comparison (i.e. to be consistent with the assumptions made by Henry et al. (1996)), FEFLOW was run using the Boussinesq approximation and constant values of viscosity and of the coefficient of thermal expansion for water. The Boussinesq approximation includes the dependence of density on temperature in the momentum equation (6.8) but not in the continuity equation (6.9) (Nield and Bejan 1992; Perrochet and Tacher 1997a); it is implemented in FEFLOW by setting the right-hand side of (6.9) to zero. Boundary conditions included zero fluid flow and a geothermal heat flux of 4500 $Jd^{-1}m^{-2}$ along the base of the cross-section, piezometric heads along the top and flanks of the atoll computed using observed ocean temperatures (Fig. 6.3), and a

constant coefficient of thermal expansion for water of $\beta = 2.6 \cdot 10^{-4}$ K^{-1} (Perrochet and Tacher 1997a). The assumption of fixed head across the top of the "rim" is equivalent to considering a section of the atoll where the rim is submerged such that all water in the section has seawater salinity. The physical properties of the rocks, given in Table 6.2, are known from the literature and confirm the numbers used by the CEA.

Temperature distributions obtained with the two models (Fig. 6.4) agree relatively well (compare Figs. 6.4a and 6.4b). However, the pathlines computed by FEFLOW (Figure 6.4d) are slightly different from the velocity vectors in Figure 6.4c of Henry et al. (1996); they clearly show the existence of a stagnation point beneath the rim of the atoll, consistent with water from under the flooded rim flowing both inward toward the lagoon and outward toward the ocean.

A finite-element mesh with only 517 elements would generally be considered today to be very coarse; therefore, further FEFLOW simulations were performed with a much finer grid, with about 20 000 linear triangular finite elements. The Boussinesq approximation was removed, so that density effects were included in the continuity equation, and nonlinear models were introduced into FEFLOW for the dependence of both density and viscosity of water on temperature (Perrochet and Tacher 1997a). (It is common to represent the dependence of density on temperature as a linear relationship (i.e. as the tangent to the true function at a given reference temperature) and with a slope, β, known as the coefficient of thermal expansion; in this study, however, the function has been generalised to a 6^{th}-order polynomial, so that β itself is a 5^{th}-order polynomial function of temperature.) These changes were all aimed at improving the accuracy of FEFLOW simulations. With a finer grid and these changes to the model, the temperatures predicted in the interior of the atoll were larger (Perrochet and Tacher 1997a), such that slightly higher hydraulic conductivities would be required in the carbonates in order to match observed temperature profiles.

In general, the results presented by Henry et al. (1996) are reasonable; however, results obtained with FEFLOW with a finer mesh and more complete mathematical formulations can be expected to be more rigorously consistent with the geometry and boundary conditions assumed for any particular simulation.

Simulations for Half a Cross-Section Through Mururoa Atoll — A second set of comparisons was performed, based on simulations of flow in a cross-section extending only halfway through an atoll. Some simulations were two-dimensional, based on the assumption that the atoll is long and narrow, such that nearly all cross-sections are identical. However, others were radially symmetric, based on the assumption of a circular atoll. Table 6.2 describes the various cases that were considered and the respective set of parameters that was used. The simulations were designed to be similar to those presented by Guille et al. (1996) and Bouchez and Lecomte (1996).

The model domain and finite-element grid used in IGC simulations are shown in Figure 6.5. The domain is 5 km long and 1200 m deep. The zone of lower carbonates is

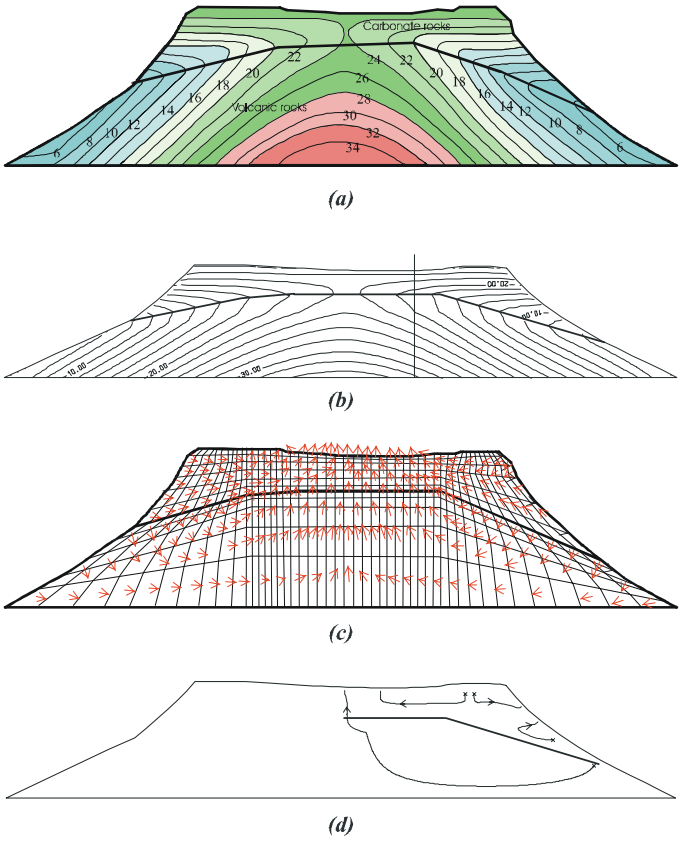

Figure 6.4 Comparison of predictions of geothermal circulation by the CEA and IGC: (a) isotherms predicted by Henry et al. (1996); (b) isotherms obtained using FEFLOW with the same parameters as Henry et al. (1996); (c) finite-element mesh and velocity vectors from Henry et al. (1996); (d) typical pathlines obtained using FEFLOW (Figures (a) and (c) are reprinted from Henry et al. (1996), pp. 2087–2109, with permission from Elsevier Science.)

based on Figure 6-1 of Bouchez and Lecomte (1996), but this division of the carbonates into two homogeneous zones is only one of many possible conceptualisations. As in the earlier comparisons with results by Henry et al. (1996), the initial simulations adopted the Boussinesq approximation, with a constant coefficient of thermal expansion $\beta = 2.6 \cdot 10^{-4}$ K^{-1}. Boundary conditions were as in the full atoll cross-section considered above, with prescribed heads on the whole of the upper boundary and the flank of the atoll.

In fact, neither Guille et al. (1996) nor Bouchez and Lecomte (1996) provide sufficient information to allow a precise comparison of their results with new calculations using FEFLOW. As a result, Figure 6.6 shows three similar simulations (Cases 1, 2, 3 of Table 6.2) using a hydraulic conductivity of 10^{-7} ms^{-1} in the volcanics, 10^{-4} ms^{-1} in the lower carbonates, and, in one case, 10^{-5} ms^{-1} in the upper carbonates (Perrochet and Tacher 1997a). Figure 6.6b also differs from Figures 6.6a and 6.6c in that the cross-section is radially symmetric.

None of the three simulations agrees well with the CEA results. The latter shows a minimum water temperature below the rim of about 14 °C, at the interface between the volcanics and the carbonates, and a minimum of 22–23 °C at the centre of the atoll. In contrast, the 22 °C isotherm in FEFLOW simulations penetrates no further than one-third of the distance from the rim to the centre of the atoll, and groundwater temperatures in the centre of the atoll are systematically higher than in CEA calculations.

Figure 6.7 shows corresponding pathlines for the three simulations shown in Figure 6.6. The flow patterns are relatively similar, and horizontal and vertical velocities are very similar to those computed by the CEA. Horizontal velocities are of the order of 6 or 7 mm y^{-1} in the volcanics, and of the order of 1 my^{-1} in the carbonates. Vertically upward velocities in the carbonates are of the order of 0.5–2 my^{-1} near the centre of the atoll, where significant upward flow occurs. The apparent focusing of flow toward the centre of the lagoon is quite real, in the sense that the spatial distribution of flux entering the floor of the lagoon shows that fluxes are much greater near the centre. It should be noted that regions in the volcanics that do not contain flowlines are not regions of no flow but, in fact, receive from and discharge to the overlying carbonates, as shown in Figure 6.4d.

What is particularly interesting in Figure 6.7 is the flow pattern beneath the rim of the atoll, a detail not explored by the CEA in its calculations. In all the simulations using FEFLOW, the boundary condition along the top of the rim was a prescribed head condition, with equivalent head equal to zero and temperature set to 26 °C. Ignoring tidal effects, which are presumed to be smoothed out in these steady calculations, this boundary condition corresponds to the rim of an atoll at locations where the rim is flooded. In this situation, seawater is drawn downward into the atoll to depths of 100–200 m beneath the rim, before flowing either to the ocean or to the lagoon. All flow patterns of this type have a stagnation point beneath the rim or a stagnation ring in axisymmetry.

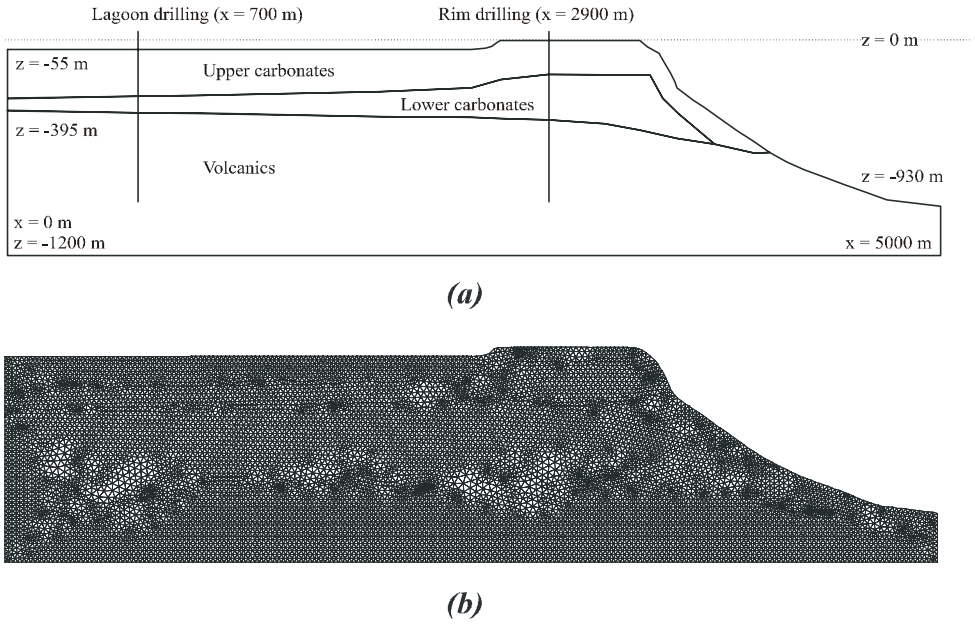

Figure 6.5 (a) Model domain, and (b) finite-element mesh used for comparison with results presented by Guille et al. (1996) and Bouchez and Lecomte (1996) (Perrochet and Tacher 1997a)

In Figure 6.6a, the temperature inversion in the carbonates dies out about 1 km from the centre of the atoll. Near the centre of the atoll, the temperature at the base of the carbonates is higher than in the lagoon, allowing the development of local free convective cells. (Rayleigh numbers calculated *a posteriori* near the centre of the atoll are about 100 in the carbonates, 2.5 times the critical value for such an instability.) These cells are not seen in the simulations of Henry et al. (1996), because the distance from the shore to the centre of the atoll is less in that case. They are not seen in Figure 6.6b, because radially inward (centripetal) velocities are greater near the centre of the atoll in the radial case, and these larger velocities prevent the instabilities from occurring. The same is true in Figure 6.6c, where, even in a non-radially symmetric case, velocities are larger because of the zone with larger hydraulic conductivity. The reason why they are not seen in the CEA calculations may be that the resolution of the mesh used by the CEA was too coarse for them to appear. There is no field evidence that such convection cells occur at Mururoa or Fangataufa, but it is nevertheless interesting that with parameters close to those used by the CEA, the FEFLOW simulation with a fine mesh in a non-radially symmetric cross-section shows a behaviour quite different from that observed or predicted by the CEA. The existence or absence of these local convective cells, however, does not have a significant impact on the resulting magnitude of the upward velocity field.

Table 6.2 Numerical values of parameters used in FEFLOW for fitting to the observed thermal profiles

Parameters		Carbonates	Volcanics
Base Case 1, vertical 2D cross-section			
horizontal hydraulic conductivity	ms^{-1}	10^{-4}	10^{-7}
vertical hydraulic conductivity	ms^{-1}	10^{-4}	10^{-7}
porosity		40%	10%
specific storage coefficient	m^{-1}	10^{-5}-10^{-4}	10^{-5}-10^{-4}
medium thermal conductivity	$Wm^{-1}K^{-1}$	2	2.5
water thermal conductivity	$Wm^{-1}K^{-1}$	0.65	0.65
medium volumetric heat capacity	$10^6Jm^{-3}K^{-1}$	2.2	2.2
water volumetric heat capacity	$10^6Jm^{-3}K^{-1}$	4.2	4.2
medium thermal longitudinal dispersivity	m	10	10
medium thermal transversal dispersivity	m	1	1
water salinity	gL^{-1}	34	34
water density and viscosity		high-order function of temperature	high-order function of temperature
In the Boussinesq approximation, the water thermal expansion coefficient is taken as constant ($\beta = 2.6 \cdot 10^{-4}\kappa^{-1}$) and the viscosity is assumed constant			
Case 2, axisymmetric version of Case 1, same parameter values			
Case 3, vertical 2D cross-section			
upper-carbonate isotropic hydraulic conductivity		10^{-5}	
upper-carbonate isotropic porosity		30%	
lower-carbonate isotropic hydraulic conductivity (thickness75-315 m; see Fig. 6.5)		10^{-4}	
lower-carbonate isotropic porosity		40%	
Case 4, vertical 2D cross-section			
isotropic hydraulic conductivity in carbonates		$5 \cdot 10^{-4}$	
Case 5, vertical 2D cross-section			
horizontal hydraulic conductivity in carbonates		10^{-3}	
vertical hydraulic conductivity in carbonates		10^{-4}	
Case 6, vertical 2D cross-section			
bottom karstic layer in carbonates, 10 m thick, hydraulic conductivity		10^{-2}	
remaining isotropic carbonate layer, hydraulic conductivity		10^{-2}	
Case 7, three-dimensional calculations			
upper-carbonate isotropic hydraulic conductivity		10^{-5}	
upper-carbonate isotropic porosity		40%	
lower-carbonate anisotropic horizontal hydraulic conductivity, 100 m thick		10^{-3}	
lower-carbonate anisotropic horizontal vertical conductivity, 100 m thick		10^{-4}	
lower-carbonate isotropic porosity		40%	

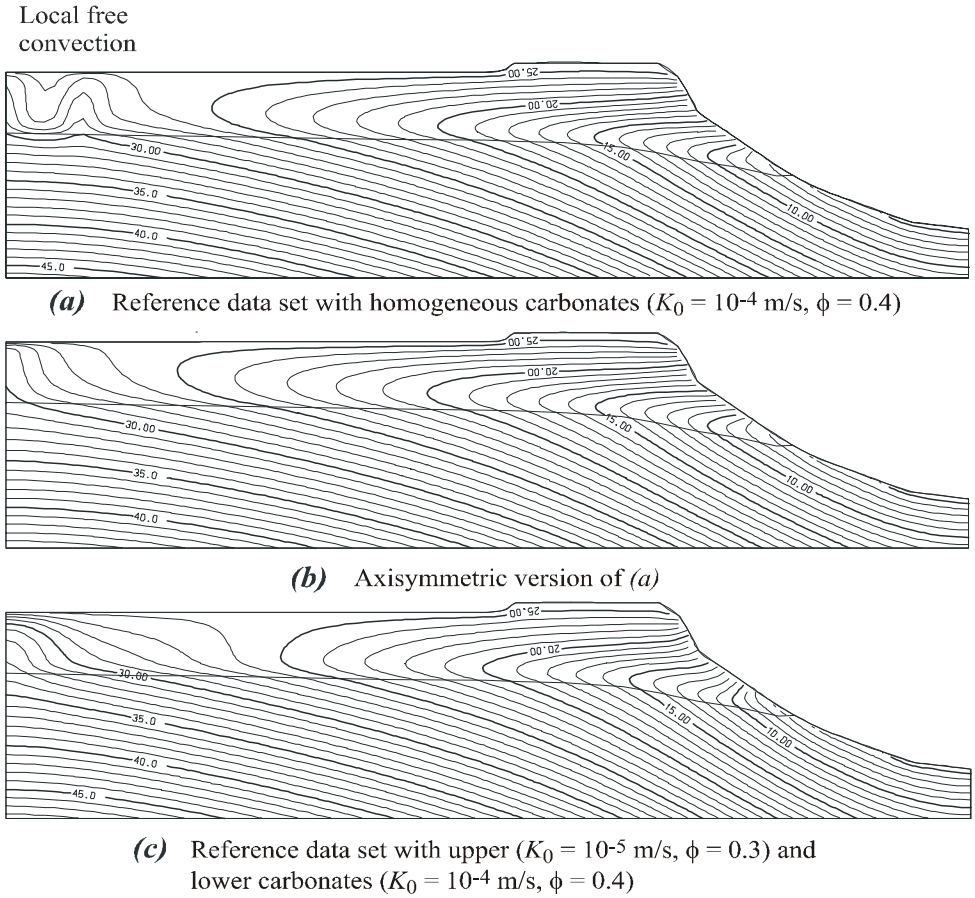

Figure 6.6 Predicted isotherms for Cases 1, 2, and 3 of Table 6.2 (Perrochet and Tacher 1997a): (a) Case 1, vertical 2D cross-section; (b) Case 2, axisymmetric cross-section; (c) Case 3, vertical 2D cross-section with two carbonate layers

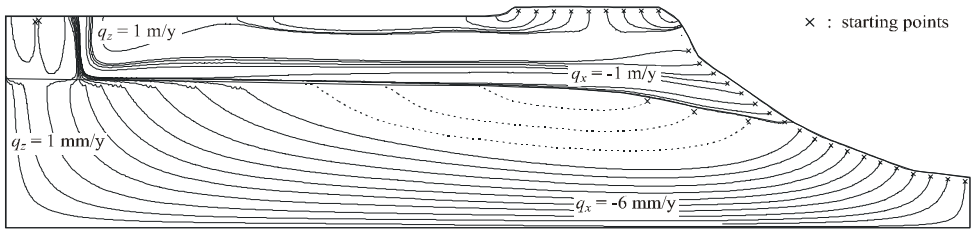

(a) Reference data set with homogeneous carbonates ($K_0 = 10^{-4}$ m/s, $\phi = 0.4$)

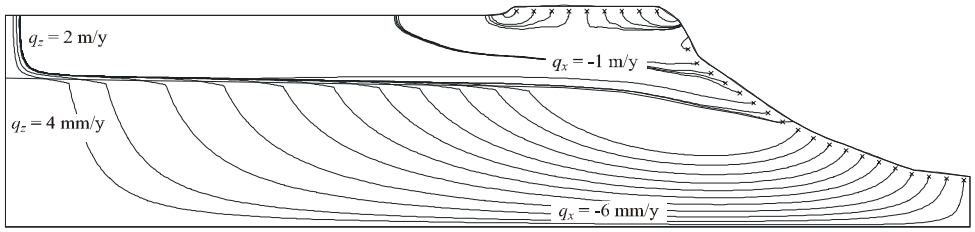

(b) Axisymmetric version of *(a)*

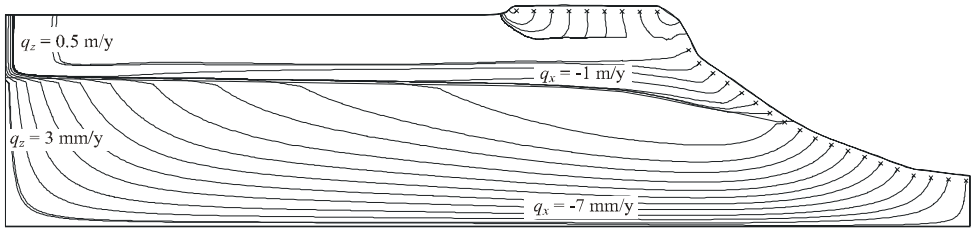

(c) Reference data set with upper ($K_0 = 10^{-5}$ m/s, $\phi = 0.3$) and lower carbonates ($K_0 = 10^{-4}$ m/s, $\phi = 0.4$)

Figure 6.7 Pathlines and Darcy fluxes (mm/y in the volcanics and m/y in the carbonates) for the three simulations shown in Figure 6.6 (Perrochet and Tacher 1997a), Cases 1–3 of Table 6.2: (a) Case 1, vertical 2D cross-section; (b) Case 2, axisymmetric cross-section; (c) Case 3, vertical 2D cross-section with two carbonate layers

General Assessment of CEA Results — In general, modelling performed by the CEA using METIS is consistent with the available data and has been verified by comparison with independent calculations using FEFLOW. Modelling by the CEA used coarse grids and adopted the Boussinesq approximation, whereas FEFLOW allows calculations with much higher resolution and is based on non-linear constitutive relations that express the dependence on temperature of fluid density and viscosity. In principle, FEFLOW is capable of producing more accurate results, in the sense of being more consistent with the true solution for any given combination of geometry, material properties and boundary conditions. Nevertheless, from many points of view, the results obtained and published by the CEA are good results that support the phenomenon of endo-upwelling and suggest that long-term average groundwater flow directions are generally inward, from the ocean toward the lagoon.

Alternatives That Match Observed Thermal Profiles — Four simulations with different combinations of aquifer properties were made in an attempt to "calibrate" the model — i.e. select optimal parameters (Cases 3, 4, 5, 6 of Table 6.2). The temperature logs are shown in Figure 6.8 and the corresponding thermal profiles and flow paths in Figures 6.6 – 6.7 and 6.9 – 6.10. It could be argued that all four of these simulations fit the observations. They agree well under the rim, but they do not agree as well under the lagoon, because the elevation of the interface between volcanics and carbonates is very approximate in the model. Thus, the elevation of the temperature minimum in Figure 6.9a is not as important conceptually as the slope of the thermal gradient in the carbonates. The different simulations clearly indicate significantly different velocities in different parts of the model domain. Nevertheless, in the absence of more data, all of these simulations are generally consistent with the data and must be accepted as possible alternatives to other scenarios, at least in the absence of further information.

Sensitivity to Increased Dispersion — As discussed in Section 6.2.4 and further down in Section 6.3.6, it is known that tidal oscillations can cause increased mixing in the medium, which is sometimes approximately accounted for by artificially increasing the dispersion coefficients. In the previous runs, the thermal dispersivities used were not artificially increased (see Table 6.2, values of 10 m and 1 m for longitudinal and transverse dispersivities, respectively, both in the volcanics and in the carbonates, which would correspond to the average fracture length). This tidal mixing effect is much more important in the carbonates than in the volcanics due to the much larger velocities in the former. In order to test the effect of an increase in dispersivity, a run was made with a longitudinal dispersivity of 10 000 m and a transverse dispersivity of 1 m. The results show that such a dramatic increase of the thermal longitudinal dispersivity does not affect the thermal profiles significantly. It is concluded, therefore, that it is reasonable to try to "calibrate" the flow model without artificially increasing the dispersivity, because the thermal profiles are not sensitive to this dispersivity. However, as will be shown in Chapter 7, for the transport of solute, the influence of tidal mixing seems to be much more significant,

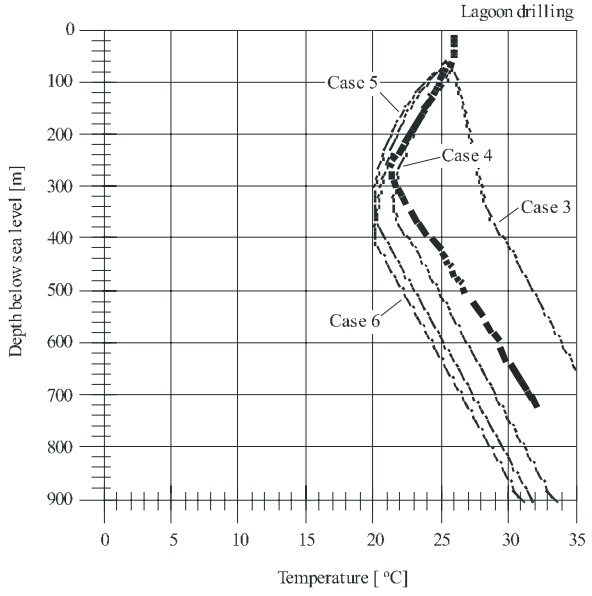

(a)

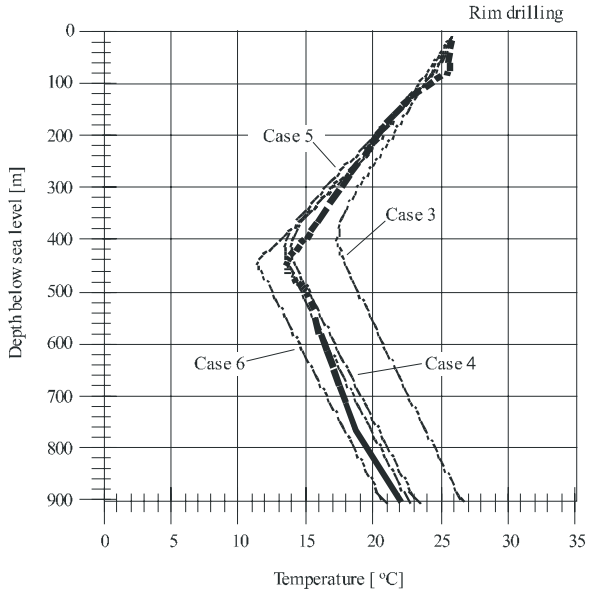

(b)

Figure 6.8 Calculated temperature profiles in drillholes under (a) lagoon and (b) rim for Cases 3, 4, 5 and 6 of Table 6.2 (observed profiles are shown with a thick line) (Perrochet and Tacher, 1997a)

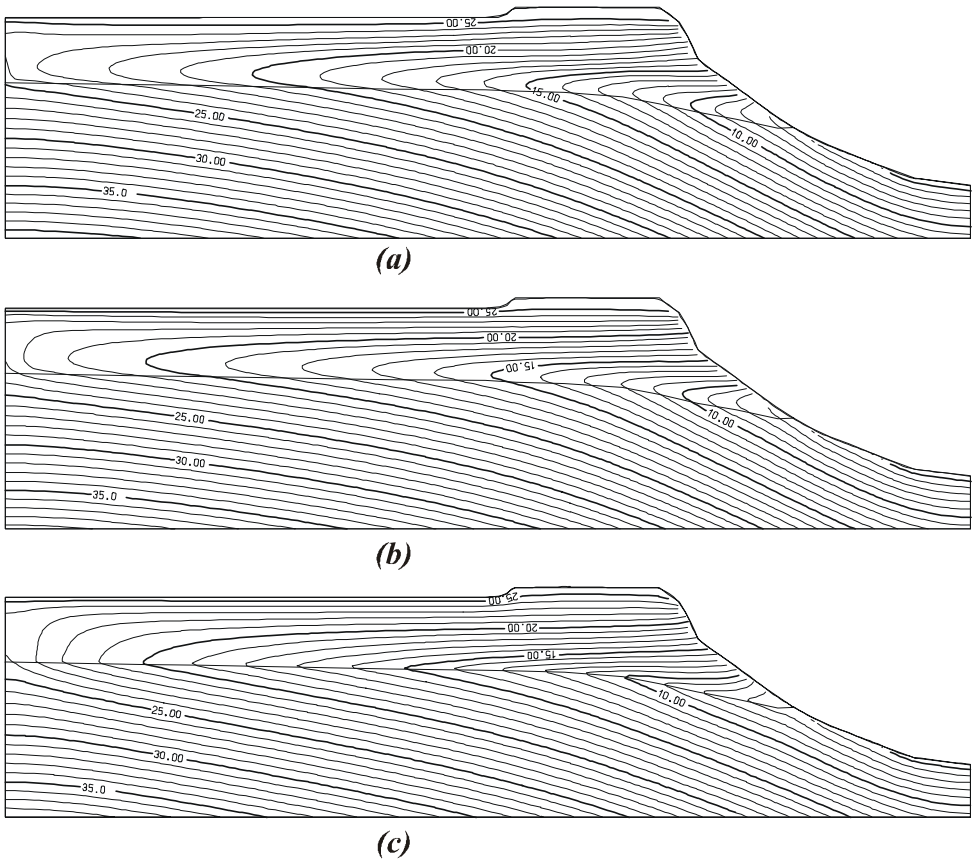

Figure 6.9 Predicted isotherms for Cases 4, 5 and 6 of Table 6.2 (Perrochet and Tacher 1997a): (a) Case 4, isotropic hydraulic conductivity in carbonates; (b) Case 5, anisotropic hydraulic conductivity in carbonates; (c) Case 6, two layers in carbonates

and a special type of model will have to be used to account for the observed distribution of tritium in the carbonates.

Sensitivity Analyses in a Two-Dimensional Cross-Section — From the outset, it should be noted that the atolls of Mururoa and Fangataufa are three-dimensional and that neither a two-dimensional plane section nor a radially symmetric section is a good approximation of any section through either of the atolls. It could be argued that parts of Mururoa, particularly toward the western end, behave more like a plane section, whereas the eastern end of Mururoa and all of Fangataufa possibly behave more like a radially symmetric section. However, given the computational effort required to make any of the groundwater simulations, and the lack of a full three-dimensional description of the atolls, sensitivity analyses were made with the idealised two-dimensional and radially symmetric sections.

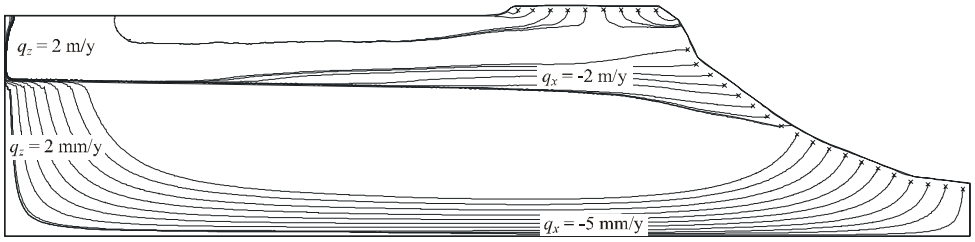

(a) Reference data set with homogeneous carbonates and K_{carb} increased by a factor of 5 to 5 • 10^{-4} m/s

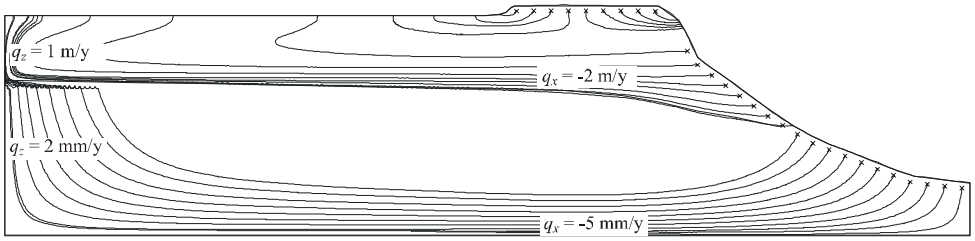

(b) Reference data set with anisotropic carbonates K_H / K_V = 10^{-3} / 10^{-4}

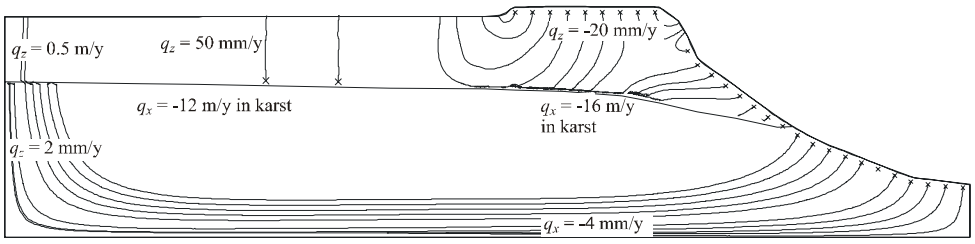

(c) Reference data set with a karstic layer and K_{carb} decreased by a factor of 10 to 10^{-5} m/s

Figure 6.10 Pathlines and Darcy fluxes (mm/y in the volcanics and m/y in the carbonates) for the three simulations, shown in Figure 6.9, of Table 6.2 (Perrochet and Tacher 1997a): (a) Case 4, isotropic hydraulic conductivity in carbonates; (b) Case 5, anisotropic hydraulic conductivity in carbonates; (c) Case 6, two layers in carbonates

These sensitivity studies (Perrochet and Tacher 1997a) demonstrate the following.

1. Decreasing the hydraulic conductivity in the volcanics by one order of magnitude to 10^{-8} ms^{-1} does not significantly affect the spatial distribution of temperatures.

2. Increasing the hydraulic conductivity in the volcanics by one order of magnitude to 10^{-6} ms^{-1} decreases the temperature at the interface between volcanics and carbonates, at any particular distance from the centre of the atoll but, more importantly, results in temperature profiles in both the volcanics and the carbonates that are curved, unlike the observations shown in Figure 6.3. A hydraulic conductivity of 10^{-7} ms^{-1} therefore appears to be an upper limit for the volcanics.

3. Increasing the hydraulic conductivity in the carbonates by one order of magnitude to 10^{-3} ms^{-1} significantly increases the extent to which ocean water is drawn into the atoll, resulting in a temperature inversion at all distances from the centre of the atoll, not only near the rim.

4. Introducing into the carbonates a thin layer of extremely high conductivity, 10^{-2} ms^{-1}, to represent a karst near the interface between volcanics and carbonates, has a similar effect and ensures that the minimum temperature in any temperature profile occurs in that layer.

5. Increasing the depth of the domain of simulation from 1200 m to 2000 m has negligible effects on the spatial distribution of temperatures.

6. Decreasing the geothermal heat flux from 4500 to 3000 Jd^{-1} m^{-2} decreases temperatures deep in the volcanics and changes the slope of the geothermal profile within the volcanics to a value that is too small compared to observations, but which does not have a significant impact on temperatures within the carbonates, which are more influenced by ocean temperatures along the flank of the atoll.

Three-Dimensional Simulations — Toward the end of the IGC's study, the CEA provided ocean bathymetric data and a digital representation of the base of the carbonates at Mururoa, at approximately 100-m spacing, and a map of the temperature at the base of the carbonates, interpolated from an unknown number of measurements. These data allowed simulation of geothermal convection in three dimensions.

A three-dimensional model was constructed using FEFLOW to a depth of 1700 m below sea level (Case 7 of Table 6.2). The three-dimensional finite-element grid has a resolution of the same quality as that used by Henry et al. (1996). Hydraulic conductivities were set to anisotropic values of 10^{-3} and 10^{-4} ms^{-1} in the horizontal and vertical directions, respectively, in the bottom 100 m of carbonates, and an isotropic 10^{-5} ms^{-1} in the upper carbonates. Figure 6.11 shows three-dimensional images of Mururoa illustrating the thermal structure inside the atoll. The temperature inversion in the carbonates

is clearly evident, as is the fact that the penetration of cooler water into the atoll depends on the three-dimensional geometry of the atoll.

Figure 6.12 compares the minimum temperatures observed by the CEA (and contoured by hand) with temperatures at the interface between the volcanics and the carbonates in our three-dimensional simulation. The agreement is reasonably good, even though the IGC's results are strongly influenced by the geometry of the atoll, and probably not sufficiently influenced by the unknown spatial variability in material properties. If the data had been provided earlier, it might have been possible to calibrate the model somewhat better. Such an exercise, using minimum temperatures in geothermal profiles as surrogates for the complete vertical profiles in an inverse or model calibration procedure, would have been an interesting and novel piece of work.

6.3.4 Effects of a Freshwater Lens

In regions where the rim is above sea level, there would normally be a thin freshwater lens, with a lower boundary reflecting the shape of a slightly curved water table. In order to demonstrate that this is the case, separate calculations were performed using FEFLOW to solve the equations for movement of water, heat and salt — i.e. to predict the so-called thermohaline convection, taking proper account of the effects of both heat and salt on density without the Boussinesq approximation. As an example, a recharge rate of 0.73 my^{-1} was applied to the water table and the recharge water was assumed to be fresh (with zero salinity) at 26 °C. The case considered was Case 6 of Table 6.2, with a thin karst layer, as shown in Figures 6.9c and 6.10c. Longitudinal and transverse solute dispersivities were 50 m and 5 m, respectively, and free water molecular diffusion coefficient was $2{\cdot}10^{-9}$ m^2 s^{-1}. Figure 6.13a shows the spatial distribution of salinity in gL^{-1} (parts per thousand), varying from 0 for fresh water to 34 for seawater. A freshwater lens with a wide mixed zone can clearly be seen. The maximum depth of the 17 isohaline is about 100 m below sea level, which, with a maximum water table elevation of about 2.6 m, demonstrates that the Ghyben-Herzberg approximation applies reasonably well to an isohaline at half the maximum salinity. Figure 6.13b shows that temperatures within the atoll are almost identical to those computed without consideration of the freshwater lens, as in Figure 6.9c; the lens affects temperatures only locally in the vicinity of the lens under the rim. Finally, Figure 6.13c shows that the pathlines are very similar to those under a flooded rim, except beneath the rim (Fig. 6.10c), where there is no longer any tendency for water to flow downward from the top of the rim to the karst.

Solution of the thermohaline convection problem shows that a freshwater lens has only local effects under the rim. The example shown in Figure 6.13 uses a recharge rate significantly larger than might be expected and therefore results in a much deeper freshwater lens than has been observed. It follows that flow patterns beneath the non-flooded portions of the rim at Mururoa and Fangataufa are probably qualitatively similar to those shown here, but the depth of penetration of the lens is probably much smaller.

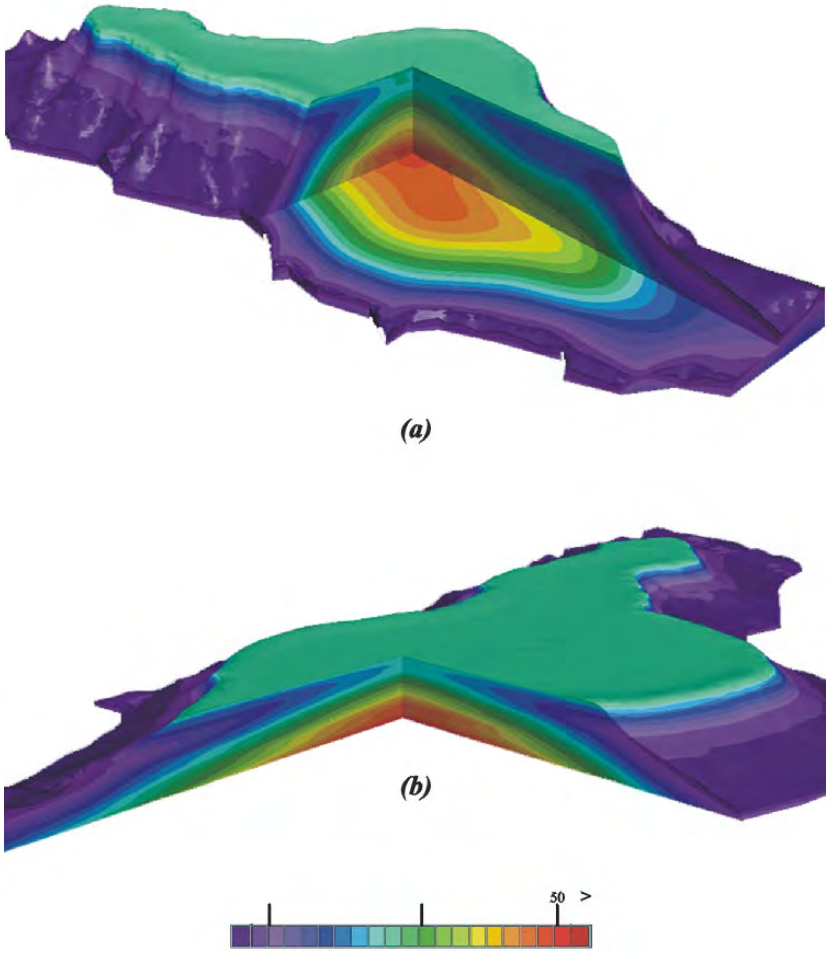

Figure 6.11 Two views of the simulated three-dimensional thermal structure within Mururoa Atoll (Perrochet and Tacher 1997a): (a) vertical expansion 3; (b) vertical expansion 1

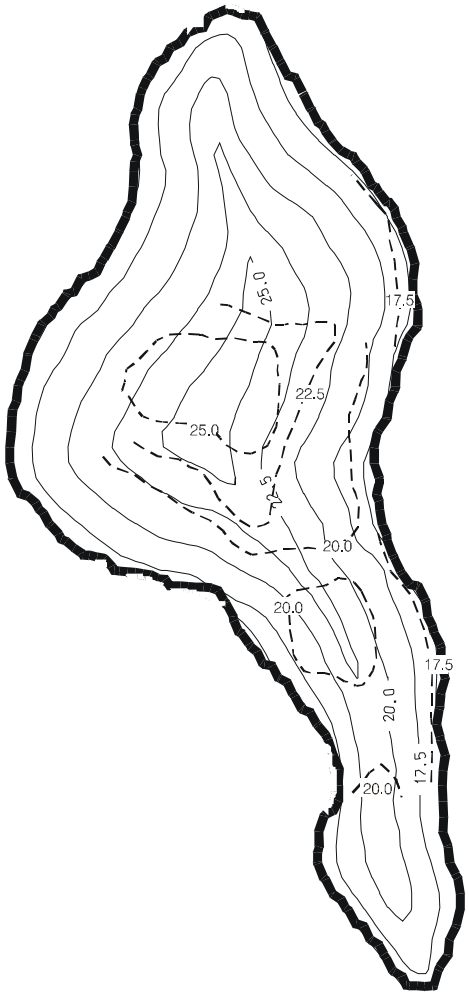

Figure 6.12 Comparison of predicted isotherms calculated with the 3D model at a distance of about 50 m above the volcanics-carbonates interface in Mururoa (solid lines), with isotherm contours, provided by DIRCEN/CEA, in the karstic layer near the base of the carbonates (dotted lines) (Perrochet and Tacher 1997a)

The fact that temperature fields are similar with and without the freshwater lens supports the argument that large-scale features of the temperature and velocity fields within an atoll can be assessed without solving the complete thermohaline convection problem.

6.3.5 Groundwater Velocities and Residence Times

Figures 6.7 and 6.10 show a number of possible flow patterns within two-dimensional sections in the atolls of Mururoa and Fangataufa. While they differ in detail, there are many common features.

First, it must be emphasised that the calculations of natural geothermal circulation are steady-state calculations that do not include the influences of tidal, seasonal or any

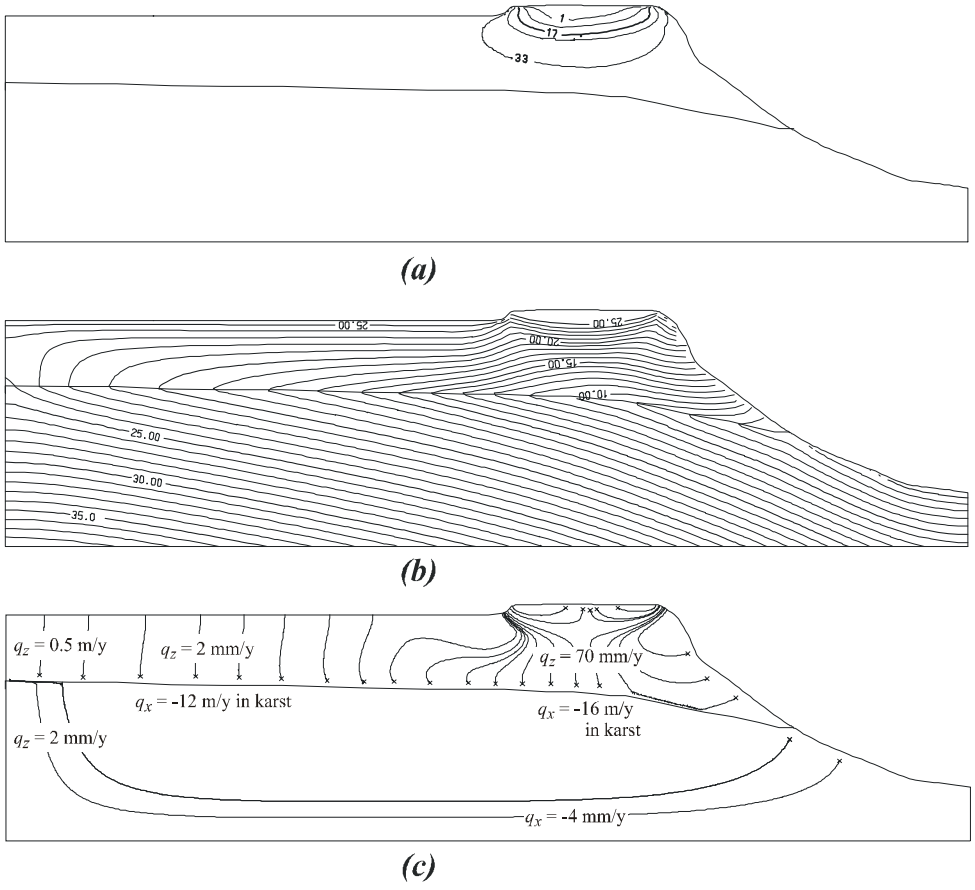

Figure 6.13 (a) Salinity (parts per thousand), (b) temperature (°C) and (c) pathlines and Darcy fluxes (mm/y in the volcanics and m/y in the carbonates), taking into account the existence of a freshwater lens (Perrochet and Tacher 1997b)

other changes in boundary conditions. With that in mind, velocities in the volcanics are generally of the order of 5 mm y^{-1} radially inward and of the order of 2 mm y^{-1} vertically upward where the flow rises to the carbonates. The difference between these values depends simply on the aspect ratio (the ratio of length to thickness) of the volcanics. Velocities in the carbonates are of the order of three orders of magnitude greater — i.e. of the order of m y^{-1} instead of mm y^{-1}, essentially because hydraulic conductivities are three orders of magnitude higher in the carbonates than in the volcanics.

The flow patterns in Figure 6.10 seem to suggest that flow in the volcanics occurs mainly near the base of the volcanics, rising towards the centre of the atoll. This is an artifact of the way pathlines are drawn, starting at equally spaced starting points just inside the flank of the atoll. In fact, the flow throughout the volcanics is relatively uniform, and, as described in relation to Figure 6.7, the region which appears to carry little flow receives inflow from and discharges to the carbonates.

The region carrying water from the rim toward the ocean has been described above. With the exception of this region, flow is generally from the ocean toward the lagoon. In most scenarios, the flow direction in the carbonates is horizontal under much of the lagoon; in Figure 6.10c, however, the flow directions are nearly vertical. In this scenario, the karst is so effective at transporting water laterally that water under the flooded rim is drawn downward to the karst under the rim and rises vertically from the karst under the lagoon. While this scenario may be extreme, it suggests that a heterogeneous carbonate layer with multiple karst layers would act as a system of aquifers and aquitards, with the karst carrying water horizontally and the intermediate carbonates allowing leakage between karst layers.

While travel times can be inferred from velocities (a lateral distance of 5000 m with an average Darcy flux of 5 mm y^{-1} and a porosity of 0.1 implies a travel time of 100 000 years in the volcanics), there exists a more systematic way of showing groundwater ages, as described first in the groundwater literature by Goode (1996). Perrochet and Tacher (1997a) describe how this method can be implemented using FEFLOW, in parallel with density-coupled geothermal convection, by using the capacity of FEFLOW to solve a solute balance equation to represent the equation for groundwater age. Figure 6.14 shows an example of groundwater ages for a case similar to that shown in Figure 6.6a (Case 1 of Table 6.2), but without the Boussinesq approximation and with non-linear constitutive relations. Groundwater ages in the volcanics increase from zero at the flank of the atoll to more than 150 000 years in the centre. In the carbonates, the ages are young near the flank of the atoll, under the rim where water is drawn downward, near the centre of the atoll (where, for this particular scenario, for which there is no evidence at Mururoa, there are convective cells drawing lagoon water down toward the base of the carbonates) and, interestingly, along the floor of the lagoon (where younger water appears to be drawn into the carbonates by dispersion). The latter effect results in a small zone of water more than 10 000 years old within the carbonates. Because a transport equation is solved

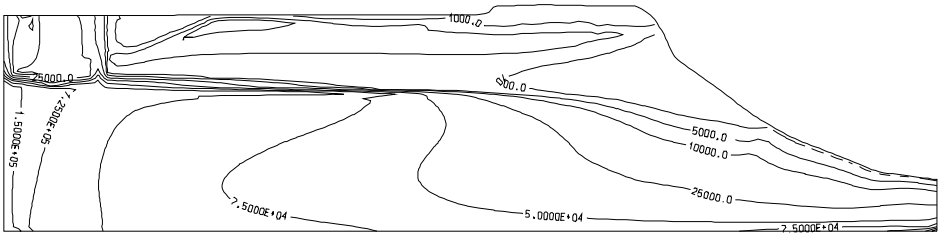

Figure 6.14 Groundwater age, for a case similar to that in Figure 6.7(a), with α_L = 10 m (the numbers indicate the groundwater age in years) (Perrochet and Tacher 1997a)

for groundwater age, the results, at least in the carbonates, are somewhat sensitive to assumptions about the dispersivities, α_L and α_T, which are not well known.

6.3.6 The Magnitude and Effects of Tidal Fluctuations and Resulting Dispersion

Superimposed on the steady flow pattern discussed thus far is the effect of tides. Figure 24 of DIRCEN/CEA Document No. 5 shows that the tidal signal within the lagoon at Fangataufa is 5–10% lower in amplitude and lags behind the ocean tide by about 20 minutes, because significant quantities of water flow through a narrow artificial channel in the rim twice in each tidal period. The piezometric head at the base of the carbonates beneath the lagoon, however, is almost in phase with the ocean tide and only slightly smaller in amplitude. Data of this kind are very significant because they suggest a high degree of connectivity between the ocean and possible karst horizons over large horizontal distances. The same phenomenon is observed at Mururoa; however, because the rim is naturally open, the tidal oscillations in the lagoon are almost in phase with those in the ocean. To a certain extent, the fact that we have considered the possibility of a karst layer in Case 6 of Table 6.2 is due to the phenomena to be discussed in this section.

Tidal fluctuations in velocities are not trivial, and a significant volume of water can flow into and out of an atoll during each tidal cycle. Consider a cross-section 5000 m long and 1200 m deep, with $S_0 = 10^{-5}$ m^{-1}. If the difference between maximum and minimum heads at all points in the aquifer during each 12-hour tidal cycle (twice the amplitude) were 0.8 m, then the total volume of water flowing into and out of a 1-m slice of aquifer in each tidal cycle would be 48 m^3. If such a volume were to enter the carbonates primarily in thin karstic layers, the corresponding velocities would be much greater than steady velocities due to geothermal convection. To be specific, the peak volumetric flow rate into the atoll would be 302 m^{3}d^{-1} for each 1-m slice, corresponding to a maximum Darcy flux of 30.2 md^{-1} into a karst layer 10 m thick.

The magnitude of tidally induced velocities can be determined much more systematically by a variety of methods. Appendix U presents an approximate analytical solution based on idealising flows within an atoll as being essentially vertical within the carbonates and essentially horizontal within an underlying karst aquifer. Perrochet and Tacher

(1997b) used FEFLOW to confirm the validity of the analytical solution: tidal effects were computed independently of geothermal effects, using small timesteps to resolve the fluctuations in heads and velocities over many tidal cycles. Appendix U presents an alternative finite-element approach which represents tidal fluctuations in terms of sinusoids and computes the spatial distribution of amplitudes and phase lags directly, without timestepping (Townley 1993). In all of these analyses, the density effects represented in the non-zero right-hand side of (6.9) can be taken into account in a steady flow field, but ignored in separate calculations of the cyclic perturbations in heads and fluxes due to tides.

Dispersion Due to Tidal Oscillations — As discussed in Section 6.2.4, several authors have found evidence that salinity distributions within atolls are significantly influenced by tidal oscillations. There is also a theoretical explanation for this phenomenon, at least conceptually, in that an oscillatory motion can be shown to cause mixing, at least in the presence of some kind of trapping or exchange mechanism.

Figures 7 and 8 of DIRCEN/CEA Document No. 9 show observed spatial distributions of tritium in the karst at the base of the carbonates for both Mururoa and Fangataufa Atolls. DIRCEN/CEA Document No. 10 describes a simple model of the spreading of tritium and other radioisotopes within the carbonates, in which the effective dispersion coefficient is considered to be proportional to the product of the maximum tidal velocity, U_a, and a traditional dispersivity, α. The resulting dispersion coefficients are very large, but, consistent with the findings of Oberdorfer et al. (1990), the modelling results provide qualitative agreement with field observations. From a number of points of view, however, the form of the effective dispersion coefficient appears to be incorrect; thus, an alternative approach was followed by the IGC.

In order to consider the process of dispersion in the presence of oscillations, a new moment analysis was performed (App. V) to extend the results of Okubo (1973). Okubo's model assumes that a solute of interest can be distributed between a flowing zone and trapped zones, or between a mobile and immobile (sorbed) phase, with a simple exchange coefficient between the two zones or phases. This model could be considered to apply to a karst aquifer, with a very conductive channel and slow-moving or dead-end zones to the side of the channel, or to flow in a porous medium, with solute sorbing to and desorbing from the surfaces of the solid matrix. In the context of heat, heat could also transfer to or from an immobile zone. The result of the moment analysis is that an effective asymptotic longitudinal dispersion coefficient can be as large as:

$$D = \frac{U_a^2 \, P}{32 \, \pi} \tag{6.10}$$

where P is the period of the fluctuations. Dispersion due to velocity fluctuations is independent of the steady flow on which fluctuations are superimposed and can be superimposed on any estimate of dispersion due to steady flow (e.g. Watson (1983)). Compared

to the effective dispersion coefficient proposed by the CEA (DIRCEN/CEA Document No. 10), (6.10) suggests that the appropriate dispersivity to use in the CEA's expression should be spatially varying and proportional to $U_a P$ — this, in turn, being proportional to the particle excursion distance during each tidal cycle.

The possibility of increased spreading due to oscillating flows has implications for geothermal convection, both under natural conditions and following underground nuclear tests, and for the transport of radionuclides. In an extensive karst layer, which is a real possibility at Mururoa and Fangataufa, based on observed piezometric heads beneath the lagoon, oscillations in horizontal velocities may cause large horizontal dispersion, even though the dominant geothermal gradients and velocities are in the vertical direction. Within the carbonates, the oscillating vertical velocities may also cause enhanced vertical dispersion. Okubo's (1973) model, which has been further developed here, contains several parameters that are completely unknown in the context of heat and solute transport at Mururoa and Fangataufa. Nevertheless, we believe that (6.10) provides qualitative support for spreading mechanisms, which may be important but which would not normally be included in a model that does not explicitly simulate tidally oscillating velocities. There are, however, no available density-coupled codes that represent effective dispersion using (6.10) or similar forms; at the same time, it would not have been feasible during this study to run density-coupled codes with small enough timesteps to resolve tidal cycles.

The use of dispersivities to represent physical dispersion is therefore problematic, because the choice of appropriate values of dispersivities depends on the scale of the problem, on the precise nature of the quantity being transported, and on the way that quantity interacts with the surrounding medium. All the thermal steady results presented above use dispersivities α_L and α_T in the classical way — i.e. without artificially increasing them (see Table 6.2) — because without new research and data, there is no adequate basis for deciding which increase is necessary to describe the effect of tidal fluctuations. However, an additional test made with increased thermal dispersivities proved that the thermal problem is less sensitive to tidal mixing than the solute transport problem (see Section 7.4.2).

The IGC did not have adequate information to fully describe and model the consequences of tidal fluctuations; however, in Section 7.4.2, a mixing model that accounts for tidal mixing is presented, and its results appear to be reasonably consistent with tritium measurements in the carbonates and in the lagoons of both Mururoa and Fangataufa.

6.4 Summary and Discussion

Mururoa and Fangataufa Atolls are typical of many atolls, with a volcanic core (comprising submarine and subaerial basalts) overlain by carbonates (limestone and dolomite) derived from corals. The volcanic rocks, although fractured to some extent, have a very low effective hydraulic conductivity. The carbonates are highly variable, with regions of very low conductivity and layers of highly conductive karst. Groundwater flows naturally from the flanks of the atolls inward and upward toward the lagoon. Rates of water movement are much lower in the volcanics — typically, three orders of magnitude lower than in the carbonates. Tidal fluctuations are believed to cause enhanced mixing of salt and heat, although appropriate theoretical models for this phenomenon are not available. The implication of tidal mixing is that dispersion coefficients at any point in space would probably depend on the amplitude of tidal velocities, rather than on the steady velocity at that point.

The IGC simulations of natural hydrogeothermal convection made with the FEFLOW code are generally in agreement with earlier simulations by the CEA and show that the observed geothermal profiles can be matched with a number of plausible combinations of hydraulic conductivities in the volcanic and carbonates zones.

The major conclusions that can be drawn with confidence from this modelling work are not very different from those presented by the CEA.

1. The large-scale natural hydraulic conductivity of the volcanic rocks is of the order of 10^{-7} m/s. This very important piece of information is well established — in fact, this value is an upper limit; lower values could also be used. The reason is that with a higher volcanic hydraulic conductivity, the lower part of the temperature profiles would no longer be linear (thus showing that heat transfer occurs mostly by conduction) but would show an upward convexity due to heat transfer by convection. Given that the volcanic rock hydraulic conductivity, as measured on cores, is about 1000 times lower, this shows that flow in the volcanics occurs mainly in a set of fractures with an unknown density and aperture distribution. For example, assuming smooth fractures with parallel walls, such a hydraulic conductivity could result from one vertical fracture every 10 m, with an aperture of 0.1 mm, or from one fracture every 1 m, with an aperture of 0.02 mm, etc. But real fractures are neither parallel nor smooth, so their actual densities and apertures can be much larger.

2. Different arrangements of hydraulic conductivities in the carbonates can explain the observed temperature profiles. The one considered the most likely by the IGC is a lower, highly permeable karstic layer above the volcanics, with a transmissivity of 0.1 m^2/s (e.g. a 10-m layer with a 10^{-2} m/s hydraulic conductivity), covered by a thick series of carbonates with an average isotropic hydraulic conductivity of

10^{-5} m/s. Alternatively, the carbonates could be made of one single equivalent isotropic layer of $5 \cdot 10^{-4}$ m/s or a single anisotropic layer with horizontal/vertical hydraulic conductivities of $10^{-3}/10^{-4}$ m/s.

3. These numbers produce estimates of the natural Darcy fluxes at the centre of the atoll, as given below.

in the volcanics:	2 mm/y in the vertical and 5 mm/y in the horizontal directions
in the carbonates:	0.5 to 2 m/y in both the vertical and horizontal directions

4. These Darcy fluxes can be transformed into pore water velocities, if the rock porosity is known. For the carbonates, a reasonable estimate is 20–40% — say, 30%. For the volcanics, an average value of 25% is given to the matrix porosity (i.e. the small-scale pores in the basalt). However, if the flow takes place in the fracture network without any exchange with the matrix porosity on the fracture walls, then a porosity value as low as 10^{-4} could be used. Using these numbers, one obtains:

in the volcanics, with matrix porosity:	10 and 20 mm/y, vertically and horizontally
in the volcanics, with fracture porosity:	25 to 50 m/y, vertically and horizontally
in the carbonates:	2 to 7 m/y, both vertically and horizontally

5. The whole focus of this section has been on Mururoa Atoll or idealised cross-sections intended to represent sections through Mururoa. Although no specific calculations were carried out for Fangataufa, there is no reason to expect that the behaviour on Fangataufa should be fundamentally different.

Chapter 7

HYDROLOGICAL IMPACTS OF UNDERGROUND NUCLEAR TESTS

7.1 Impacts of Underground Nuclear Explosions

The effects of underground nuclear explosions are both local — in the vicinity of each test — and at the atoll scale. Important questions about these effects follow.

- What are the hydrological processes that occur immediately following an underground nuclear explosion?
- What can be learned from the rates at which cavities are refilled with water about fracturing and modified physical properties of the rock due to the explosions and/or about the natural conditions of the rock prior to the explosions?
- What are the directions and rates of groundwater flow near each cavity that are induced by the sudden release of heat during the explosions?
- What can be learned from observed distributions of radionuclides in the atolls that might affect our interpretation of atoll structure and hydrology?
- Are there long-term effects on the directions and rates of groundwater flow in the atolls?
- Are there long-term implications for water quality in freshwater lenses beneath the rim of the atolls?
- What are the likely effects of climate change and/or changes in sea level?

Section 7.2 considers the effects in the near field of individual tests over very short times scales, up to a period of weeks or months, while Section 7.3 focuses on the medium term, perhaps some hundreds of years, until such time as the thermal energy released by nuclear explosions has dissipated. Section 7.4 analyses the observed distribution of tritium in the carbonates, as interpretation of these data aids evaluation of the predictive capacity of our models. Section 7.5 returns to circulation at the atoll scale, as in Chapter 6, but with an emphasis on the very long term, when the impact of the tests is due only to modification of the structure of the atoll. Section 7.6 addresses possible future scenarios, such as the effects of climate change, and Section 7.7 summarises the IGC's findings on the hydrology of Mururoa and Fangataufa Atolls after the tests.

7.2 Impacts Over Very Short Time Scales

The complex processes of cavity expansion during a nuclear explosion were described in Chapter 3, which emphasised mechanical effects and the final geometry of the cavity and chimney. This section focuses on the influence of these effects on hydrological processes — i.e. the movement of water and heat. A recent review by Kersting (1996) describes the hydrological phenomena associated with an explosion that is independent of the French experience at Mururoa and Fangataufa Atolls.

7.2.1 Cavity, Chimney Formation and Fracturing

The physical processes that occur within the first fractions of a second after an underground nuclear explosion are described in Section 3.2. From a hydrological point of view, our primary interest is in the net effect of the explosion in terms of creating a cavity and, possibly, a surrounding fractured zone, but there is also some interest in the possibility of movement of fluids over significant distances in very short time periods, as discussed in Chapter 3.

Under natural conditions, before a test, the rock throughout the atoll is saturated with water that has a salinity roughly equal to that of seawater. The pressure distribution in the pore water is slightly above the hydrostatic values, because of the natural thermal gradient and the natural geothermal circulation described in Chapter 6, thus driving the upward flow from the flanks of the atoll toward the lagoon. The nuclear explosion produces a cavity within which all material, including water, is vaporized. At the same time, the process of cavity expansion causes pressures in the pore fluids in the surrounding rock to rise beyond their ambient levels. The extent to which this occurs has not been estimated, and no direct data were obtained in the course of French nuclear testing. This pore pressure may have some effect on the fracturation of the rock.

The radius of a spherical cavity, r_c, produced by an underground test scales as the 1/3-power of the yield of the test, ϵ (Section 3.2.1). The height of a chimney, h_c, which forms when the roof of the cavity collapses is proportional to r_c and therefore to $\epsilon^{1/3}$. The constants of proportionality for these relations are discussed in Sections 3.5 and 3.6. The geometry of the chimney can be predicted by theoretical analyses, but oblique drilling by the DIRCEN/CEA after most tests provided estimates, based on observations of changes in drilling rates and loss of drilling fluid, of the size of the chimney. Of particular interest is the fact that the volume of the combined cavity and chimney is proportional to r_c^3 and, therefore, to ϵ. For purposes of hydrological modelling, the following relations will be used:

$$r_c = 12\,\epsilon^{1/3} \tag{7.1}$$

$$h_c = 5\,r_c \tag{7.2}$$

Fracture propagation is discussed in detail in Section 3.2.3. Nearly all the evidence for fracturing following underground nuclear tests is indirect, although some cores were taken in the damaged zone by the CEA and analysed for fracture density. In general, fractures are formed in the region of plastic deformation surrounding an explosion — not in the region of elastic deformation. Fractures tend not to propagate easily through other fractures; thus, if basalts are layered with weaker zones between layers, the propagation of fractures in the vertical direction may be inhibited.

Figure 7.1 represents the position of the damaged and fractured zones surrounding a cavity (see Chapter 3), where the permeability might be increased. There is, however, great uncertainty about the net effect of the explosions on this permeability. The IGC developed a set of alternative patterns of permeability increase in the different zones, to be introduced in the hydrological modelling. They are summarised in Figure 7.2 and Table 7.1 and are referred to as Scenarios F0, F1, F2 and F3. For simplicity, they were taken as concentric discrete layers with different (constant) permeabilities. Scenario F0 assumes no damage in the surrounding rocks except in the chimney, while Scenario F3 is considered as extreme, with increases of permeabilities by factors ranging from 1000 to 10 000. This scenario is compatible, however, with the simulations performed by Hochstein and O'Sullivan (1985), which are based on model calibration of a 10-kt test at a depth of 550 m. Scenario F1 considers a lower increase of permeability (from 5 to 100), while Scenario F2 considers a permeability increase by a factor of 10 only in the zone above the chimney. Note that in Scenario F3, a thin molten-rock layer is added (1 to 1.1 r_c) to the cavity's lower hemisphere (permeability = 10^{-11} ms^{-1}). In all cases, the permeability of the undamaged volcanics (at distances larger than 10 r_c from the zero point) is taken as constant and equal to 10^{-7} ms^{-1} — i.e., the upper limit of the values calibrated on the thermal profiles in boreholes prior to explosions, as discussed in Chapter 6. In the chimney, the permeability is very large and is taken as 10^{-2} ms^{-1} for all scenarios. In the overlying carbonates, the permeability is taken as 10^{-4} ms^{-1}, as calibrated on the thermal profiles in Chapter 6.

As will be shown in Section 7.2.3, the choice between the four different scenarios was made by comparing calculations with these four scenarios and the available data on the filling rates of chimneys after the tests. It will be shown that Scenarios F1 and F2 seem to be more consistent with these data than Scenario F3.

7.2.2 Changes in Temperature

When the roof of the initial spherical cavity starts to collapse, the cavity is filled with hot gases, and the walls of the cavity are lined with molten or rapidly crystallising rock. The collapse and creation of the chimney occurs in a few hours and stops when the rubble touches and provides sufficient support for the final roof. Thermal energy contained within the initial spherical cavity becomes distributed throughout the rubble, because, although heat is transferred through the outer walls of the cavity, the temperatures within

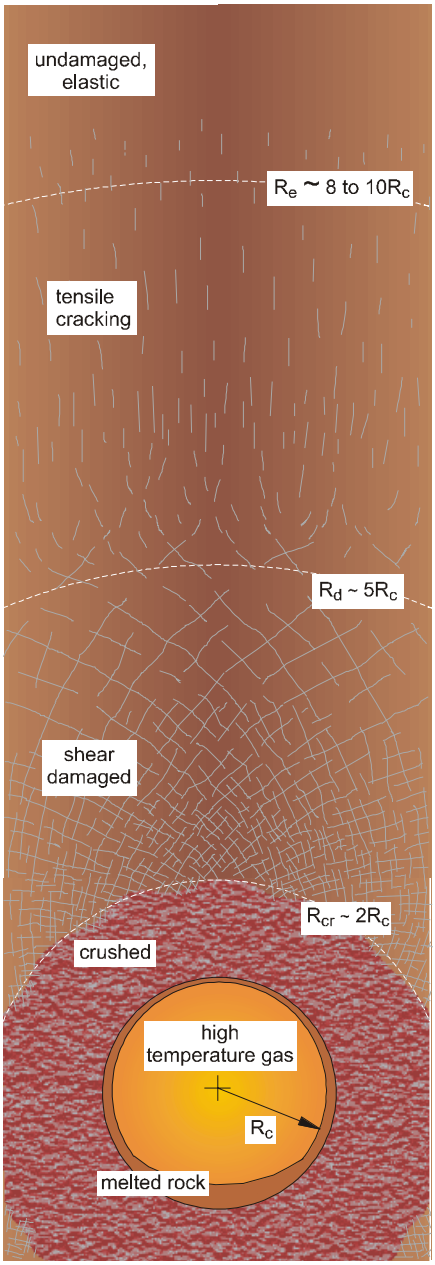

Figure 7.1 Position of the damaged and fractured zones surrounding a cavity (see also Vol. II, Fig. 1.9)

Table 7.1 Scenarios for distributions of hydraulic conductivity in the volcanics intended to represent possible fracturing in damaged zones around cavity

Hydraulic Conductivity (ms^{-1})	F0	F1	F2	F3	Radii
K0	10^{-7}	10^{-7}	10^{-7}	10^{-7}	regional background
K1	10^{-7}	10^{-5}	10^{-7}	10^{-3}	$r_c - 2r_5$
K2	10^{-7}	$5 \cdot 10^{-6}$	10^{-7}	$5 \cdot 10^{-4}$	$2r_c - 3r_5$
K3	10^{-7}	10^{-6}	10^{-7}	$5 \cdot 10^{-4}$	$3r_c - 4r_5$
K4	10^{-7}	$5 \cdot 10^{-7}$	10^{-7}	$5 \cdot 10^{-4}$	$4r_c - 5r_5$
K5	10^{-7}	10^{-6}	10^{-6}	10^{-4}	volcanic cover
K6	10^{-7}	10^{-7}	10^{-7}	10^{-4}	$5r_c - 10r_5$

Note:
F0 – no fracturing
F1 – radially decreasing intensity of fracturing
F2 – no fracturing except in volcanic cover above chimney
F3 – extensive fracturing

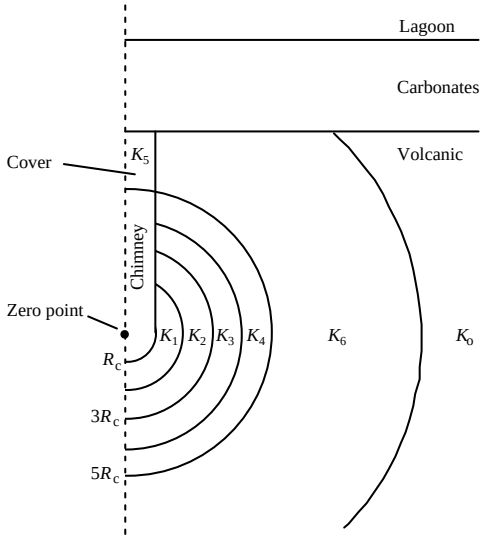

Figure 7.2 Spatial distribution of potentially damaged zones near a cavity: alternative patterns of permeability increase in the different zones (see Table 7.1) (Perrochet and Tacher 1997a)

small pieces of rock inside the cavity rapidly equilibrate with the surrounding gases. To a first approximation, all of the thermal energy inside the spherical cavity at the time when chimney formation starts becomes distributed throughout the volume of the combined cavity and chimney, including the volume of the rubble.

The temperature reached inside the chimney depends on how much of the energy released in an explosion initially remains as thermal energy inside the cavity. There is no precise way of determining the distribution of energy, but in general, about 20% is said to remain inside the cavity, and less than about 15% escapes the region of plastic deformation to become elastic or seismic energy which propagates far from the explosion. The remainder of the energy (65–70%) is used in deformation processes in the damaged zone surrounding the cavity, causing the rock to flow and fractures to be formed. The energy used in deformation processes is ultimately converted to thermal energy — i.e. high pressures in the growing cavity cause the rock to deform and, in doing so, the rock gains temperature. It can be argued, therefore, that, even though 20% of the energy remains inside the chimney, 60–90% of the energy remains as heat inside the damaged zone, extending to a radius of, perhaps, 5 r_c. The transfer of mechanical energy to radii outside r_c and transformation into heat are very rapid (fraction of seconds), but it can be argued that it is reasonable to ignore this initial distribution of heat outside r_c in any hydrological calculations, because heat would be conducted from the chimney to the same radii relatively rapidly (weeks), thus achieving almost the same result.

Temperature is a measure of thermal energy per unit volume. Because both the thermal energy and the volume of the combined cavity and chimney produced by an explosion are proportional to the yield, it follows that the initial temperature in a chimney is independent of the yield. That is, regardless of the yield of an underground nuclear explosion, the temperature inside the resulting chimney some short time after the explosion depends mainly on the coefficients that express how r_c and h_c depend on the yield, for a particular combination of rock type and ambient stress conditions.

Perrochet and Tacher (1997a) show that the temperatures may depend somewhat on the initial porosity of the rock, but the net result is that, within a few days after a nuclear explosion in basalt, the temperature increase in the cavity, chimney and surrounding rock is between 25°C throughout the volume of the chimney, depending on how much of the energy is assumed to remain within 5 r_c. If an explosion were to occur at a location where the ambient temperature was 30°C, the temperature in the chimney some days after the explosion would be 55°C to 80°C. This temperature would be reached even before the chimney, initially filled with gas, had refilled with water (see Section 7.2.3). The temperature is well below boiling point, especially at the depths of the explosion, where the high ambient pressures cause the boiling point of water to be much higher than 100°C.

7.2.3 Refilling of the Chimney — Description and Interpretation of the Data

Shortly after a test, the initially hot gases in the chimney cool, the pressure inside the chimney drops to less than the ambient hydrostatic pressure at that depth, and groundwater from the surrounding region is effectively sucked back into the cavity and chimney. Therefore, during a period of days to weeks, the chimney refills with water. A small proportion of the water comes from condensation of gaseous water in the cavity, but most of it flows into the cavity from the surrounding rock.

After the first underground tests at Mururoa, the DIRCEN/CEA attempted to drill vertical holes into the top of the chimney to ascertain the height of the chimney and to perform other tests (coring of the lava at the bottom of the cavity, for analysis). Because drilling through the rubble in the chimney was very difficult, directional drilling techniques were later used to construct an inclined drillhole (see Bouchez and Lecomte 1996). The hole started vertically near the surface, some tens of metres away from test site, but deviated obliquely when reaching the explosion depth so as to intersect the chimney and ultimately core the lava at the bottom of the cavity. During construction of the first drillholes of this type, water entered the cavity via the drillhole; in a couple of cases, gases are believed to have escaped. Once proper techniques were used to prevent blowout of gases, it was possible to obtain information (usually qualitative, but sometimes quantitative) about the rate of pressure increase within the chimney as water was filling up the chimney. In effect, the chimney acted as a large pumping well — attracting water toward it at an ever-decreasing rate until the chimney was nearly full. The pressure of the gas remaining at the top of the chimney reached values close to hydrostatic, thus preventing further inflow. In principle, and in practice, data of this kind allow estimation of the aquifer properties of the rock near the cavity, much as a large-scale pumping test.

The data obtained were not always precise. For large tests, they were generally limited to observations of whether refilling was complete by the time the inclined drillhole was finished. For small tests, pressure sometimes was measured in a gas sampling line installed into the chimney prior to the test. In some cases, measurements of static water levels within the drill hole were made at different times. In general, it was found that refilling times were longer for large tests, essentially because the ratio of volume to surface area of the chimney increases with the yield of the test, and water to refill the volume can flow in only through this surface area.

In order to analyse these data, DIRCEN/CEA used the METIS code (Goblet 1981) for the atoll-scale geothermal convection calculations described in Chapter 6. The code was modified specifically to allow for the refilling and repressurisation of the chimney. Simulations were started with an initial reduced pressure in the empty chimney; this caused water to flow toward and into the chimney. Timestep by timestep, the cumulative volume of water inside the chimney was determined, allowing calculation of a new gas pressure above the free water surface in the chimney (due to compression of the gases remaining in the cavity) and calculation of pressure at all locations beneath that free water

surface. These new pressures, calculated on the surface of the chimney, were applied as boundary conditions for the subsequent timestep. Thermal effects were ignored in these calculations, largely because water movement due to pressure differences were much greater than those due to temperature differences — at least over the period of days to weeks of refilling. Initial overpressuring in the surrounding region was also ignored. As examples of this kind of analysis, the DIRCEN/CEA (DIRCEN/CEA Document No. 5) has released a number of sensitivity analyses showing the effects of hydraulic conductivity, K, and specific storativity, S_0, on the filling rates, as well as data and simulations for a 14.5-kt and a 3.2-kt test.

Even though only a limited amount of data is available, the IGC has used it to check the methodology for interpreting effective hydraulic properties near the chimney after nuclear explosions. This approach is described in detail by Perrochet and Tacher (1997a). An axisymmetric model with a very fine mesh was used for the calculations. The cavity and chimney were not part of the mesh, because prescribed head boundary conditions were applied at the wall of the chimney, to induce flow into the chimney. Similarly to DIRCEN/CEA, simulations were performed with no consideration of thermal effects, which are considered not to affect the short time-scale interpretations. The simulations were performed using the finite-element code FEFLOW (Diersch 1996), without modifying the code to adjust the boundary conditions inside the cavity as it filled. This is contrary to what had been done by DIRCEN/CEA. In order to simulate the effect of filling the chimney, it was decided to run the calculation in eight periods, during each of which the inflow to the chimney was 10% of the chimney volume. During each such period, the boundary head for nodes along the wall of the chimney was set either to the elevation of the node, for nodes above the chimney water level at the start of the period, or to the elevation of water in the chimney, for all nodes below that level. Pressure increase in the gas cap was also neglected. This methodology is an approximation to the better method programmed into METIS for DIRCEN/CEA's calculations. Numerical experiments have shown, however, that ignoring the time-varying boundary conditions in the chimney and the gas pressure build-up leads to predicted filling times within 5% of those based on the more correct boundary conditions, for a chimney at great depth and filling only to 80% capacity (Perrochet and Tacher 1997a).

As a first stage in this exercise, an attempt was made to reproduce the DIRCEN/CEA results of sensitivity runs for two tests with yields of 10 kt and 100 kt (DIRCEN/CEA Document No. 5, Fig. 17). Insufficient information has been provided to allow a perfect comparison, but reasonable assumptions have been made for unknown quantities, such as the chimney volumes and porosities used in their calculations. Whereas the DIRCEN/CEA simulations were based on a homogeneous hydraulic conductivity of 10^{-7} ms^{-1} throughout the medium (i.e. no damage to the rock), the IGC has considered the four permeability scenarios described in Section 7.2.1, Figure 7.2 and Table 7.1, in order to assess the sensitivity of the results to fracturing in damaged zones surrounding the cavity (Perrochet and Tacher 1997a).

Comparisons were performed using only a single value of specific storativity, S_0 = 10^{-5} m^{-1}, because DIRCEN/CEA sensitivity analyses showed that this was the value best matching the observations and also because this value is reasonable for basalt. For both yields, scenario F0 led to somewhat slower filling rates than DIRCEN/CEA's, probably because of slight differences between the IGC's calculations and theirs, due to an incomplete definition of the problem by DIRCEN/CEA (DIRCEN/CEA Document No. 5). Scenario F1 led to significantly faster filling, and scenario F3 was so fast that it could not be compared on the same plot. Scenario F2 led to slightly faster filling than F0, as expected. This phase of the comparisons simply confirmed that the simpler modelling techniques used by the IGC were comparable with those used by DIRCEN/CEA. They showed that filling times (to 80% full) would be of the order of 10 days for a 10-kt test and 40 days for a 100-kt test if there were little damage to surrounding rock outside the chimney.

Two sets of observations were made available to IGC, for a 14.5-kt and a 3.2-kt test (DIRCEN/CEA Document No. 5, Fig. 21). DIRCEN/CEA matched the filling rate with a model based on a regional background hydraulic conductivity of $6 \cdot 10^{-8}$ ms^{-1} and an increased conductivity of $2 \cdot 10^{-6}$ ms^{-1} within a radius of 2.3 r_c from the location of the explosion. IGC calculations for Scenarios F0, F1 and F2 are shown in Figure 7.3, together with IGC calculations using the scenario adopted by DIRCEN/CEA (Perrochet and Tacher 1997a). IGC calculations using the DIRCEN/CEA permeability scenario shown in Figure 7.3 are close to, but do not exactly match, the observations because, as before, not enough information has been provided to allow a complete definition of the problem. Scenarios F0 (no damage) and F2 (damage to the zone above the chimney) agree reasonably well with the data, at least as well as the DIRCEN/CEA scenario. Scenario F1 (permeability increase by factors of 5 to 100) would result in filling much faster than observed. It appears that the data obtained in the field for this 14.5-kt test are consistent with very little damage to the surrounding rock except above the chimney.

The second set of data provided to the IGC are observations of pressure in the chimney for a 3.2-kt test (DIRCEN/CEA Document No. 5, Fig. 22; note, however, that the time after the test should be in hours rather than days). These data have been converted to filling rates, as described by Perrochet and Tacher (1997a), and IGC calculations are shown in Figure 7.4. In order to match the observations, DIRCEN/CEA used a conductivity of $5.5 \cdot 10^{-7}$ ms^{-1} as a regional background value and $2 \cdot 10^{-6}$ ms^{-1} within a radius of 2.5 r_c. The IGC scenario F1 matched the data far better than scenarios F0 and F2 in this case. This finding is consistent with the DIRCEN/CEA finding that hydraulic conductivity needed to be greater in order to explain the faster rate of filling.

It is interesting that, in order to match field observations, DIRCEN/CEA chose to modify the regional background value rather than the near-field distribution of conductivities, especially when it is known that the explosion is likely to affect rock in a spherically symmetric manner, with damage decreasing with distance from the explosion. The

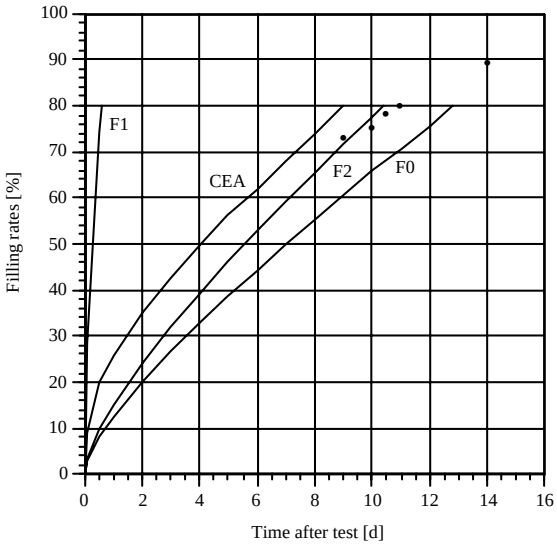

Figure 7.3 Comparison of measured and predicted filling rates for a 14.5-kt test (Perrochet and Tacher 1997a)

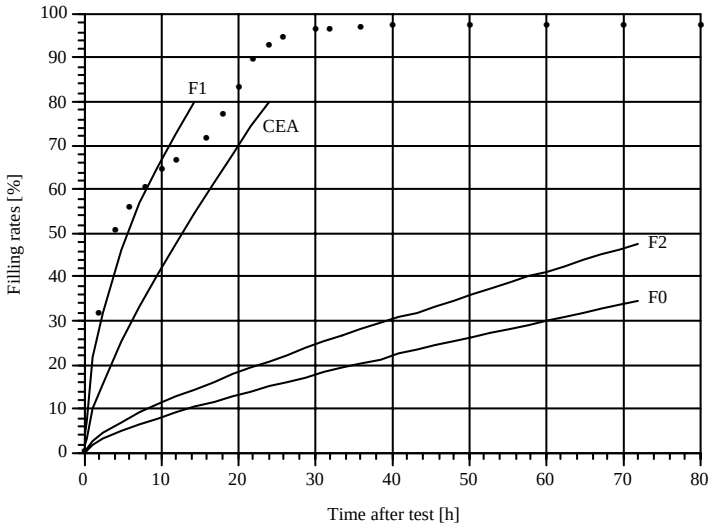

Figure 7.4 Comparison of measured and predicted filling rates for a 3.2-kt test (Perrochet and Tacher 1997a)

explanation for this is that DIRCEN/CEA (Sornein 1997) viewed these data as providing confirmation of an upper bound on regional conductivities, rather than as providing detailed information about local damage.

Estimates of filling times are available for nearly half of the underground nuclear tests carried out at Mururoa and Fangataufa Atolls. DIRCEN/CEA used the technique described above to estimate effective hydraulic conductivities (regional background value) for each test and has provided the results in the form of a histogram (DIRCEN/CEA Document No. 5, Fig. 22). This histogram shows the range of values of regional background conductivity, given an assumed value of $2{\cdot}10^{-6}$ ms^{-1} within a radius of 1.6 r_c. Even though the parameter on which the calibration has been performed is not the one that might have been expected, the results are nonetheless interesting. More than half of the estimates of regional conductivity are less than 10^{-7} ms^{-1}; another 40% are between 10^{-7} and $3{\cdot}10^{-7}$ ms^{-1}. Given that studies of geothermal convection at the atoll scale described in Chapter 6 imply a regional conductivity of the order of 10^{-7} ms^{-1}, these results suggest that, if that value were chosen as a fixed parameter, and if filling rates were used to calibrate an effective conductivity within a radius of 1.5 or 2 r_c, nearly all tests would imply values less than 10^{-5} ms^{-1} in that zone, and IGC's F1 scenario would significantly overestimate the extent of damage.

7.2.4 Convection Inside the Chimney

Once the chimney is full of water, the temperature of the water inside the chimney becomes almost constant everywhere within the chimney volume, because of natural convection. Natural convection occurs in all fluids (e.g. in water or air), whenever there are temperature-induced density differences that are inherently unstable, such as with hot fluid beneath cold fluid, as is the case in the chimney. It also occurs in porous media, where water moves much more slowly than in open water bodies. However, the criteria for the onset of convection are somewhat different, because of the different physical laws describing flow in these situations. A chimney created by a nuclear explosion contains rubble and has an overall porosity of about 20–30%. The volume of the chimney is more like rockfill in a dam wall or an ocean breakwater than a porous medium. Convection probably occurs more as it does in an open water body than in a porous medium. As a result, even small temperature differences of the order of 1°C are probably sufficient to cause rapid overturning and mixing by convection, with velocities on the order of metres per hour, a phenomenon which equalises temperatures and solute concentration within a chimney in a matter of days.

Independent evidence for this phenomenon is provided, for instance, by research on the potential use of caverns in rock salt to store gas. Geothermal data for a 35-m-high cavern constructed between depths of 930 and 965 m show normal geothermal gradients in clay and limestone to a depth of 700 m; a smaller gradient between 700 m and 930 m, due to the much higher thermal conductivity of rock salt; and a much smaller gradient

in the cavern itself. This is clear evidence of very effective thermal convection in the cavern (Bérest et al. 1996). Although such a cavern is not a perfect analogue, especially since it is not filled with rubble, it does provide evidence that convection will occur in a fluid-filled subterranean region with an unstable geothermal gradient, so as to equalise temperatures in that region and provide mixing and spreading in the whole volume of any solute present in the water.

7.3 Geothermal Convection Cells Near Chimneys in the Medium Term

Once the cavity and chimney are full of water, the dominant process of hydrological interest is the growth and decay of a second geothermal convection cell in the rock surrounding the chimney, superimposed on the rapid convection cell that exists inside the chimney. This second convective movement is caused by the temperature and density differences between hot water in the chimney and cooler ambient water in the surrounding basalt. This phenomenon has been described by Bouchez and Lecomte (1996), both qualitatively and somewhat quantitatively. The convection cell is essentially radially symmetric, with hot water rising vertically above the chimney and cool ambient water entering the bottom and sides of the chimney. Convection provides a mechanism for dissipation of heat, in that heat is carried upward by the rising water at the same time as it is being transported outward in all directions by conduction.

There is very little published literature that is directly relevant to underground nuclear tests or to thermal convection problems which are, in some ways, analogous. One reason for this is the political and military sensitivity of nuclear testing; in addition, however, most of the tests in the USA (for example, at the Nevada Test Site), were carried out in the unsaturated zone, where such a phenomenon does not occur in the water phase. A major concern related to tests carried out in the saturated zone was that the formation of a "chimney" above each test could provide a vertical conduit for radionuclides to migrate toward laterally extensive aquifers that are intersected by the chimney. Several papers by Brikowski (1991, 1993a, 1993b) address this issue, but his solutions are not directly applicable to the situation at Mururoa and Fangataufa, where the major focus is on vertical transport toward the water table or the lagoon.

From a fluid mechanics perspective, an underground nuclear test can be considered to be an instantaneous release of heat into a large, highly permeable chamber at some depth within an infinite half-space. Despite a wealth of literature on natural and forced convection in porous media (see the excellent reviews by Nield and Bejan (1992) and Bejan (1995)), there has been little theoretical work on instantaneous point sources of heat, and apparently none on instantaneous sources within a cavity of finite extent. A paper by Poulikakos (1985) on an instantaneous point source is relevant and interesting, especially because it considers the problem of coupled release of heat and mass (by dissolution of a concentrated source), but it cannot be directly applied.

In the absence of relevant theoretical results, the best way to proceed is to use numerical methods. Numerical modelling by DIRCEN/CEA was referred to by Atkinson et al. (New Zealand MoFA 1984) in their 1984 report (Annex V, Fig. 22), but few details were provided. Hochstein and O'Sullivan (1985, 1988) used these data to develop a two-dimensional model of steady natural convection in Mururoa Atoll and thermal convection models for 10-kt and 100-kt tests at depths of 550 m and 1000 m, respectively. The authors first determined values of hydraulic conductivity and porosity for different geological zones to match a single observed temperature profile at the Zoé site. They then modelled the thermal convection patterns which developed following an instantaneous increase in temperature in zones representing the chimneys for both tests. By present standards, the finite-difference grids they used were very coarse: a typical cell size was 100 m x 200 m; the chimney for a 10-kt test was represented by a single cell 50 m x 50 m in section; and the calculations were two-dimensional only, for a slice 100 m thick, although there is some suggestion that Hochstein and O'Sullivan (1988) used three parallel slices to allow some degree of three-dimensionality. The authors concluded that upward velocities above a chimney could be of the order of 25–150 my^{-1}. Although similarly large values will be suggested below for some special cases, it appears that these large values may partly be a consequence of the coarse resolution in their grid.

The following sections review the modelling carried out by DIRCEN/CEA and then present the results of modelling conducted by the IGC, where symmetry is ensured by considering a single explosion at the centre of a circular atoll. The problem is then examined more generally with full three-dimensional modelling of geothermal convection cells under the rim of an atoll. Finally, the issue of interaction between tests is considered, at least qualitatively.

7.3.1 Model Description

Modelling of convection near a chimney was carried out by DIRCEN/CEA; one synthetic example is described by Bouchez and Lecomte (1996) and in DIRCEN/CEA Document No. 4. Figures 6-4 and 1 in those two documents, respectively, are almost identical. They show that for a 100-kt test, with 140–150 m of volcanic cover with hydraulic conductivity enhanced by a factor of 10 relative to the background conductivity of 10^{-7} ms^{-1} (i.e. IGC's scenario F2 in Table 7.1), the initial temperature difference in the chimney of 25°C decays to zero over a period of about 500 years. The vertical velocity in the cover decays initially at a slow rate, but relatively faster at later times, reaching the upward velocity induced by the natural geothermal gradient after 400 years. During the first five years, the Darcy flux above the chimney exceeds 0.25 my^{-1}. It is difficult to interpret this Darcy flux, however, because the actual velocity depends on the effective porosity of the cover; and that, in turn, depends on whether the cover acts as a porous or as a fractured medium. In reality, it will be a combination of both.

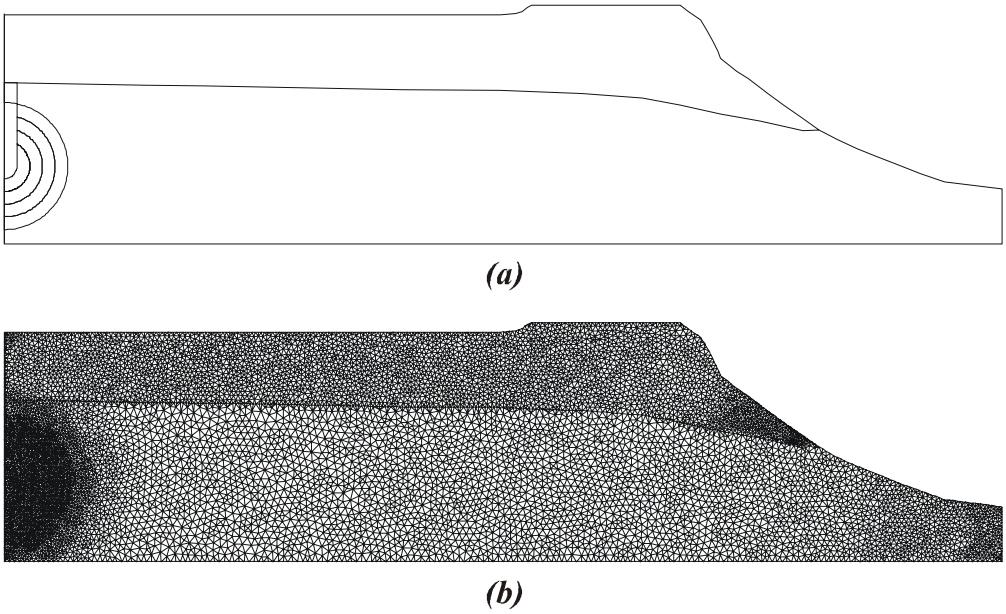

Figure 7.5 (a) Geometry of model following an explosion at the centre of an atoll, and (b) corresponding finite-element mesh (Perrochet and Tacher 1997a)

Any calculation of convection in an axisymmetric domain requires boundary conditions on the outer boundary. Because the natural geothermal circulation in an atoll leads to sloping isotherms, it is technically not possible to have a perfectly radially symmetric plume rising above a chimney, unless the test is located at the centre of the atoll. Thus, in order to study the convection patterns in radial symmetry, the IGC decided to consider the case of a test located exactly at the centre of a circular atoll in order to satisfy perfectly the requirements for radial symmetry.

Figure 7.5a shows a conceptual model for an axisymmetric slice through a circular atoll in which a nuclear explosion has been carried out at the centre. The section is 5000 m long and 1200 m deep. The depth and dimensions of the cavity and chimney depend on the yield of a test, as do the locations of zones of different hydraulic conductivities, as defined in Figure 7.2 and Table 7.1, which also depend on the yield. An example of a finite-element mesh is shown in Figure 7.5b. Typical node spacings are 2 m in the chimney, 4-8 m in the surrounding fractured zone, 12 m in the carbonate zone, and 25 m in the volcanics.

Simulations were performed for a number of combinations of yield, initial temperature increase in the chimney, thickness of volcanic cover, and spatial distribution of hydraulic conductivity. Details of the calculations are presented by Perrochet and Tacher (1997a). The yield of a test was considered to be either 5 kt (a relatively small explosion,

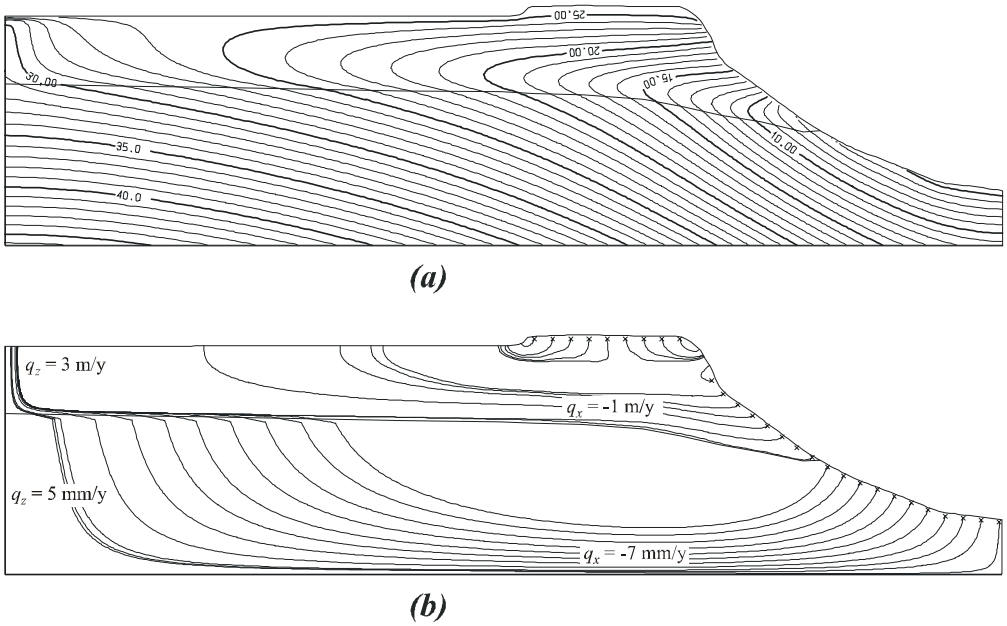

Figure 7.6 (a) Predicted isotherms and (b) pathlines and Darcy fluxes for a radially symmetric atoll, as initial conditions prior to an explosion at the centre of the atoll (Perrochet and Tacher 1997a)

requiring a small thickness of cover) or 150 kt (the upper limit of test yields at Mururoa and Fangataufa). Initial temperature differences were assumed to be either 25°C or 50°C, as discussed in Section 7.2.2. Volcanic cover (between the top of the chimney and the carbonates) was assumed to have thicknesses of 15 m and 100 m — these being reasonable values for small and large yields, respectively — or 0 m, for the case of a chimney touching the carbonates. DIRCEN/CEA Document No. 6 describes the latter as a CRTV test, in which the Chimney Reaches the Top of the Volcanism. Hydraulic conductivity distributions were considered to be F0 to F3, as defined in Table 7.1.

A separate finite-element mesh was designed for each yield and depth of cover, so that r_c and h_c and the zones for different hydraulic conductivities could be represented properly. Initial conditions were as shown in Figure 7.6, representing an axisymmetric simulation using non-linear representations of density and viscosity in FEFLOW, as described in Section 6.2.3. Boundary conditions at the bottom and ocean boundaries were the same as those used for long-term geothermal circulation in Section 6.3.3.

Scenario Description — Four groups of runs were performed to assess different issues. The first set focused on the effects of hydraulic conductivity variations, due to the degree of fracturing, for a 5-kt test with shallow cover. The second set was identical except for a larger initial temperature increase. The third set considered 150-kt tests with

deeper cover. The fourth set examined the effects of 150-kt tests with no cover, specifically to assess the impact of large CRTV tests. This fourth set of tests is extreme and hypothetical, because all CRTV tests were less than 10 kt (DIRCEN/CEA Document No. 6).

All simulations were run for a period of 500 years. During the course of the calculations, FEFLOW computes piezometric heads, temperatures and velocities at all nodes in the finite-element mesh. Visualising the results is not easy, because the flow field is dynamic and changing. Perrochet and Tacher (1997a) present results for all runs as plots of temperatures and velocities at a number of locations of interest immediately above the chimney, both on the axis of the axisymmetric plume and off-axis. Some results are also presented as plots of isotherms and pathlines at specific times. In fact, these pathlines would not be followed exactly by any particle of water, because they are plotted using instantaneous velocities at a specific time, whereas, in reality, while a particle travels from one location to another, the velocity in the domain changes. The results are plotted this way because FEFLOW cannot currently compute the true tracks of individual particles in transient flow fields. Nevertheless, the plots do allow the directions of flow to be visualised at any instant.

Figures 7.7 and 7.8 show the results for a simulation of a 150-kt test with 100 m of volcanic cover (a 25°C increase in temperature in the chimney) and no increase of hydraulic conductivities outside the chimney — i.e. scenario F0 in Table 7.1. Figure 7.7 is qualitatively similar to Figure 6.3 of Bouchez and Lecomte (1996), but there are some differences. Figure 7.7 is plotted without any stretching of scales, contrary to Figure 6.3 by Bouchez and Lecomte (1996), so the region shown is 1200 m deep and extends to a radius of 1500 m from the centre of the atoll. Throughout the period of the simulation, temperature changes occur essentially within a radius of 200–300 m; thus, the smaller radius of influence (400 m) used by Bouchez and Lecomte (1996) is not unreasonable. Because Figure 7.7 is based on calculations that extend to the flanks of the atoll and include the natural geothermal heat flux, all temperatures are higher than the DIRCEN/CEA calculations. The characteristics of the evolution of the thermal plume, however, are the same. At early times, the chimney remains hot and well-mixed, and heat is transported from the chimney mainly by conduction. After 50–100 years, the original natural isotherms are all distorted upward, and the radius to which isotherms are distorted is greatest. After 500 years, the heat originally released in the cavity has dissipated into the surrounding medium; the chimney acts as a region of enhanced hydraulic conductivity; the small flow reaching the centre of the atoll as part of the endo-upwelling process is slightly increased; and the uniform temperature in the chimney, due to continuing convection within the chimney, causes regional isotherms to be deflected both upward and downward.

Figure 7.8 shows corresponding instantaneous pathlines, as described above. For periods of more than 1 but less than 100 years, the temperature in the chimney is suffi-

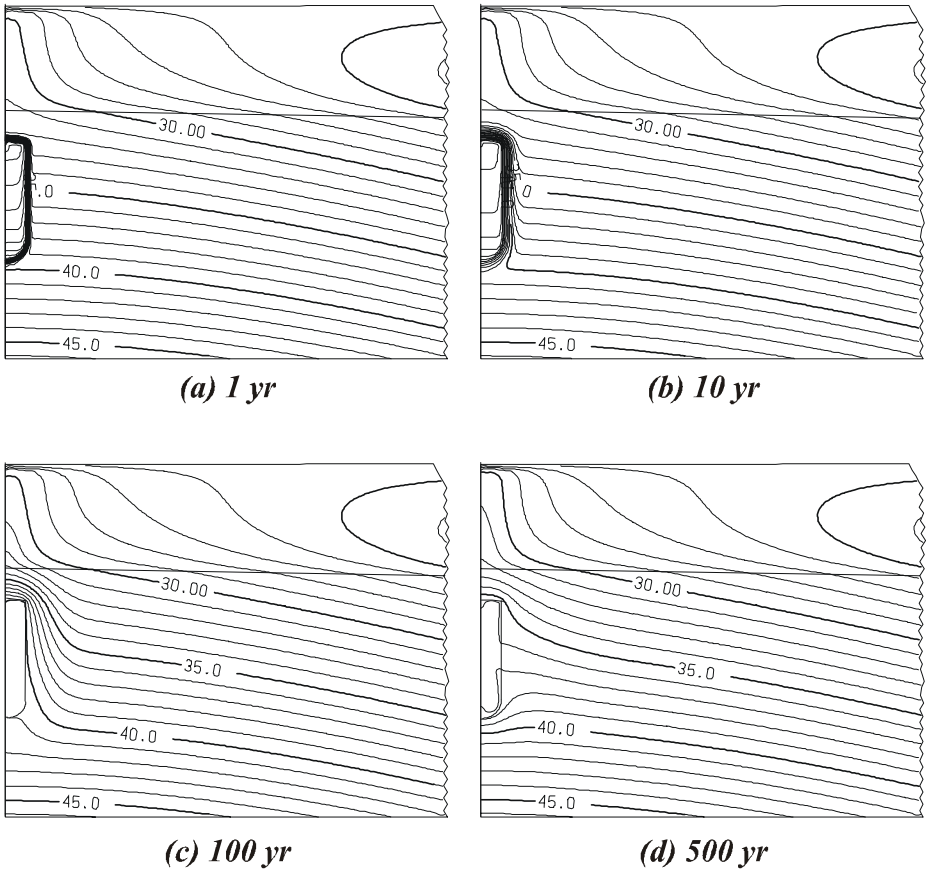

Figure 7.7 Isotherms for a 150-kt test with 100 m of volcanic cover, a 25°C initial temperature increase, and no increase of hydraulic conductivity beyond the chimney, Scenario F0 (Perrochet and Tacher 1997a)

ciently high to drive a local geothermal circulation cell in the surrounding rocks; water rises vertically above the chimney to the carbonates and enters the base of the chimney from the lower part of the volcanics; and some flow recirculates from the upper toward the lower part of the chimney wall. For such a flow pattern to exist, there must be a circular ring surrounding the chimney where the groundwater velocity is zero — i.e. the axisymmetric equivalent of a stagnation point. Within 100 years, this stagnation ring migrates inward toward the chimney, resulting in the disappearance of the dipole-like behaviour and a transition toward focused flow through the chimney, more because of its increased hydraulic conductivity than because of thermal effects.

Figure 7.8 shows only flow directions and does not provide any indication of relative velocities. The fact that pathlines appear to be bundled together along the base of

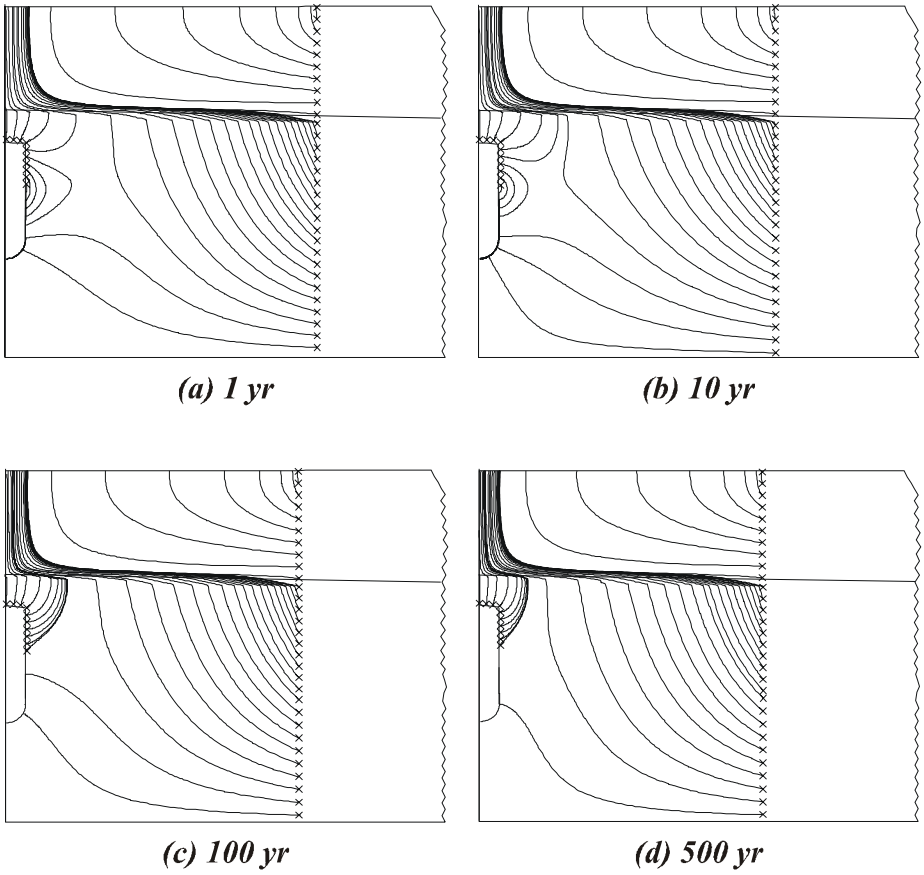

Figure 7.8 Pathlines for a 150-kt test with 100 m of volcanic cover, a 25°C initial temperature increase, and no increase of hydraulic conductivity beyond the chimney, Scenario F0 (Perrochet and Tacher 1997a)

the carbonates and immediately above the chimney is the result of the large contrast in hydraulic conductivity between the volcanics and the carbonates, such that most of the natural flow in the volcanics has to rise through the carbonates near the centre of the atoll (see, also, Figure 7.6b, before the test). It is interesting that water rising from the chimney toward the carbonates does so over an area of radius of up to about $4r_c$ at early times, during the existence of the dipole, but ultimately over an area of radius of about $2r_c$. It is also significant that there is no circulation cell within the carbonates and the flow in that region is predominantly upward.

Figures 7.7 and 7.8 are typical of results for tests within the volcanics, with some degree of volcanic cover, and with little damage to the surrounding rock. Figures 7.9 and 7.10 show analogous results for a 150-kt explosion with 100 m of volcanic cover, but, this time, with a 50°C initial increase in temperature and a high degree of damage, as defined by scenario F3 in Table 7.1. This scenario is somewhat extreme, in that it results in an effective conductivity to a radius of $10r_c$, equal to or greater than the conductivity in the carbonates. The simulation can therefore be expected to have some features in common with cases with no cover.

The main features shown in Figure 7.9 are (i) within a very short period of time, an identifiable "bubble" of hot water rises toward the lagoon through the carbonate zone, and (ii) even after 500 years, the isotherms are still significantly different from the pre-test distribution, to a radius of nearly 1000 m. In many ways, the pathlines shown in Figure 7.10 help to explain the isotherms in Figure 7.9. At all times, there is a convection cell in which water is rising in the centre of the chimney; however, by the end of 10 years, there is some suggestion that this cell is weakening in intensity and shrinking. After 500 years, there are two cells — one circulating in the original sense within the chimney, but the other operating in the reverse sense, with water rising around and within the damaged zone of radius $10r_c$, then plunging downward, just outside the chimney, to the base of the aquifer.

The scenario summarised in Figures 7.9 and 7.10 is extreme, and sensitivity studies on refilling times, described in Section 7.2.3, suggest that the damage due to an underground nuclear test is unlikely to be this severe. The reason for showing these results is to illustrate the fact that, even though the geometry of the geothermal flow system in such a situation is quite different from the more likely situation shown in Figures 7.7 and 7.8, the magnitudes of groundwater velocities, as will be shown below, are not enormously different.

Velocities — We now turn our attention to groundwater velocities, in the form of Darcy fluxes, for a number of possible scenarios. The fluxes are computed at 11 points whose locations are shown relative to r_c, h_c and the height of volcanic cover, C, in Figure 7.11.

Figure 7.12 shows time variations in temperature and Darcy flux after a 5-kt test with 15 m of cover and an initial temperature increase of 25°C, assuming no fracturing

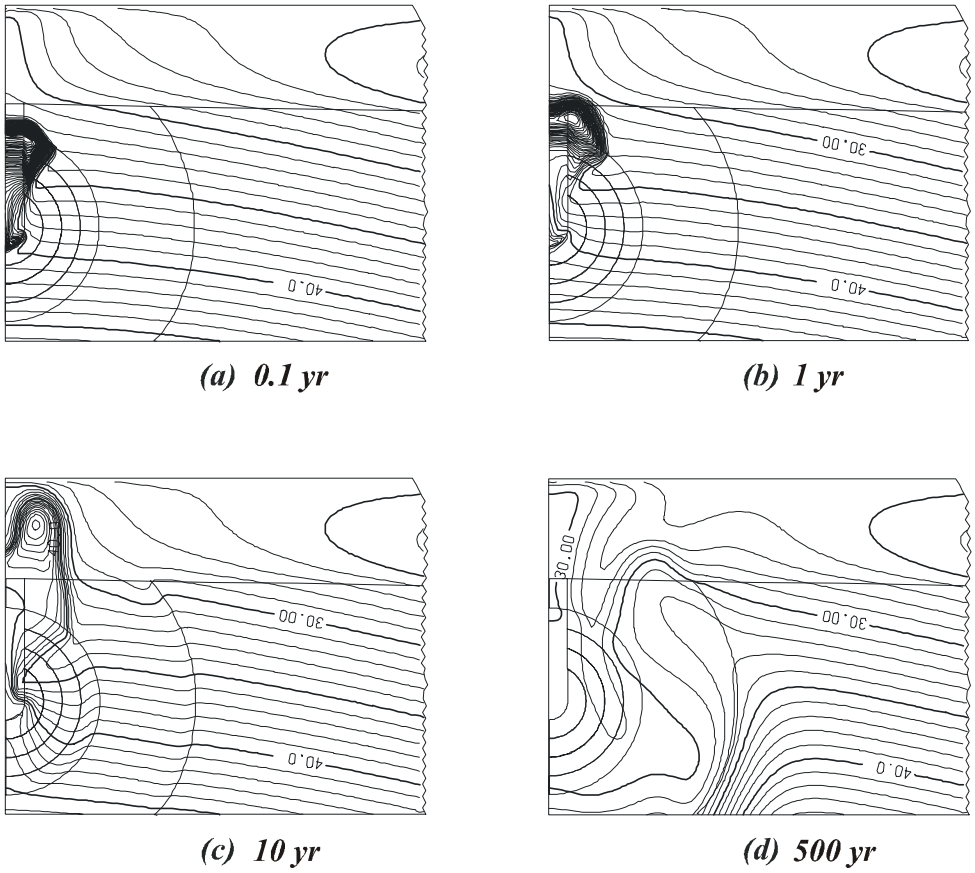

Figure 7.9 Isotherms for a 150-kt test with 100 m of volcanic cover, a 50°C initial temperature increase, and significantly higher hydraulic conductivities to $10\,r_c$, Scenario F3 (after Perrochet and Tacher 1997a)

outside the chimney (scenario F0 in Table 7.1). The two upper plots show temperatures, and the two lower plots show fluxes. In each case, the time scale is magnified in the right-hand plot, to show the first 10 years of the corresponding 500-year simulation. In general, in the zone of volcanic cover above the chimney, both temperature and velocity decline with radius and height above the chimney. Apart from a short period of less than six months, the highest temperatures and velocities appear to decline in a manner very similar to that described by Bouchez and Lecomte (1996, pp. 58–62). The highest Darcy flux, observed at a point 5 m above the chimney, is about 0.12 my^{-1}.

Increasing the hydraulic conductivity in the cover immediately above the chimney by a factor of 10 (scenario F2 in Table 7.1) results in a maximum Darcy flux above the chimney of nearly 0.6 my^{-1}, an increase by a factor of almost 5. Significant increases in

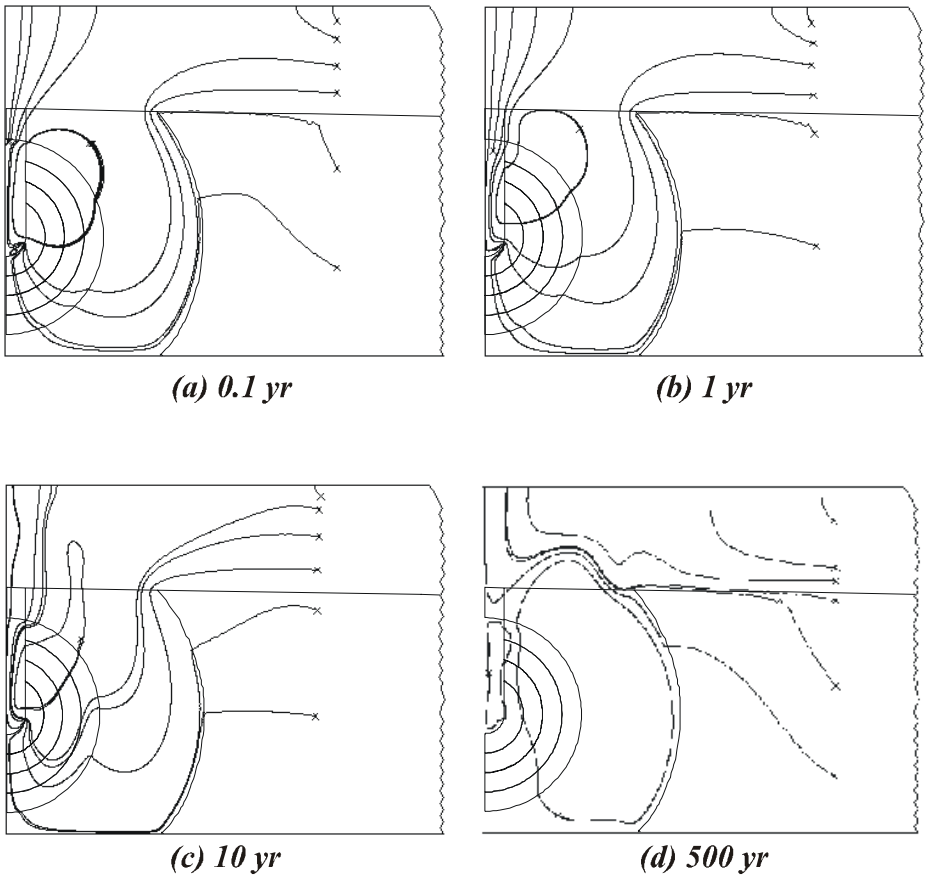

Figure 7.10 Pathlines for a 150-kt test with 100 m of volcanic cover, a 50°C initial temperature increase, and significantly higher hydraulic conductivities to $10\,r_c$, Scenario F3 (after Perrochet and Tacher 1997a)

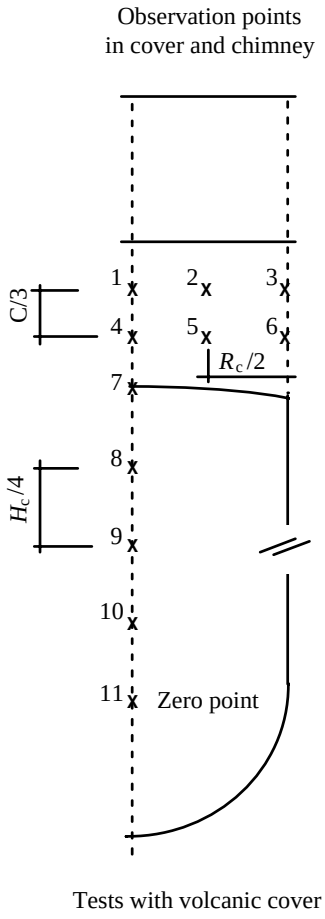

Figure 7.11 Locations of points where fluxes are computed (Perrochet and Tacher 1997a)

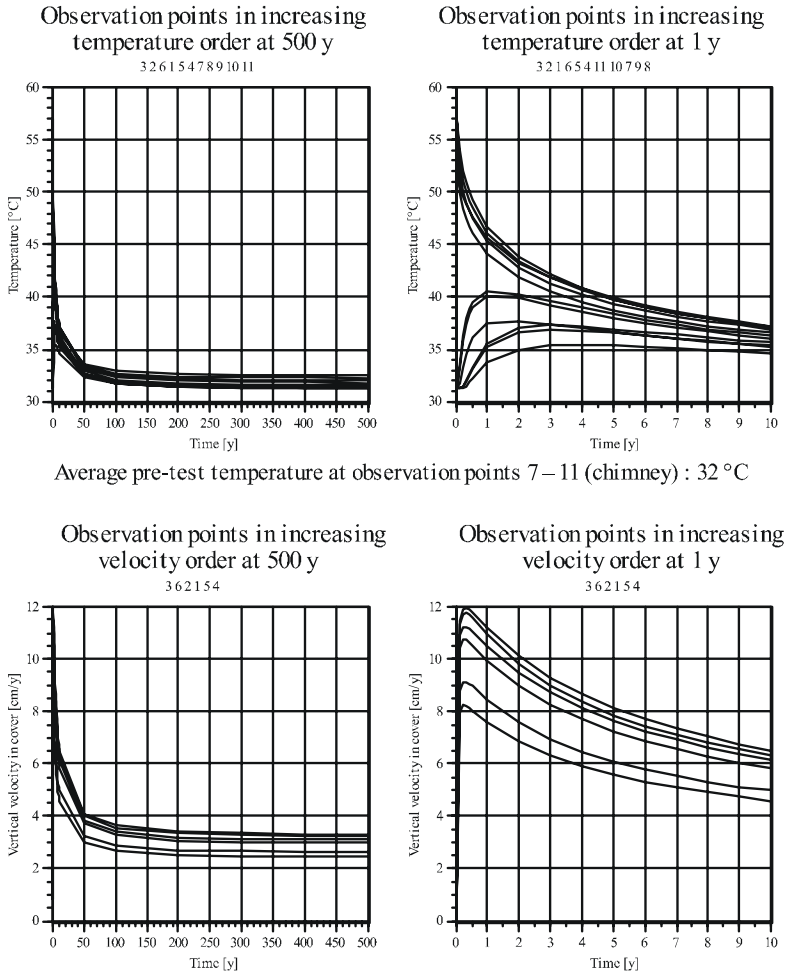

Figure 7.12 Time variation of temperatures and Darcy fluxes following a 5-kt test with 15 m of volcanic cover, a 25°C initial temperature increase, and no increase of hydraulic conductivity beyond the chimney, Scenario F0 (Perrochet and Tacher 1997a)

conductivities to a radius of $5r_c$ (scenario F1) result in a maximum Darcy flux of nearly 1.4 my^{-1}. Despite these differences, the rates of decrease in temperature are almost the same in all three cases, indicating that dissipation of heat is dominated by conduction and that very little heat is carried away by the convectively driven flow. In all cases, the fluxes decay to almost steady values after about 100 years, and to 0.03, 0.15 and 0.3 my^{-1} for scenarios F0, F2 and F1, respectively, after 500 years. These values should be compared with a vertical flux of about 0.008 my^{-1} prior to the tests, the long-term increase being due to physical damage in and around the chimney, which causes a focusing of flow through that region.

Vertical velocities in the carbonates above the cover are hardly affected by the geothermal convection below, because all flows are naturally orders of magnitude larger in the carbonates. The upward Darcy fluxes remain about 3 my^{-1}, as shown in Figure 7.6b.

An almost identical set of simulations with an initial temperature increase of 50°C for a 5-kt test shows very similar time distributions of temperatures and Darcy fluxes (Perrochet and Tacher 1997a). The maximum fluxes 5 m above the chimney are 0.24, 1.3 and 3.3 my^{-1} for Scenarios F0, F2 and F1, respectively; these values are double or a little more than double the previous maxima. This simply confirms that the buoyancy forces that drive the convective circulation are almost proportional to temperature differences, as in many other natural geothermal flow systems. Since there are natural bounds on the temperature increases caused by nuclear explosions, it is therefore not possible for Darcy fluxes to rise without bound to values orders of magnitude higher than those described here.

Increasing the yield of an explosion increases the size of the chimney and the damaged region; however, because thermal energy is mainly dissipated by conduction, the time taken for the larger amount of heat initially stored in the chimney to dissipate is also increased. Figure 7.13 shows changes in temperatures and Darcy fluxes for the case illustrated in Figures 7.7 and 7.8 (150-kt test, 100-m volcanic cover, 25°C initial temperature increase, Scenario F0). Temperatures and fluxes decay significantly more slowly than shown in Figure 7.12. The maximum flux at a point 33.3 m above the chimney (one-third the thickness of the cover) is about 0.09 my^{-1}, a little lower than shown in Figure 7.12, but somewhat farther from the chimney.

With conductivity scenarios F2 and F1, the same 150-kt test has little effect on the variations of temperature with time, once again showing the dominance of conduction. The corresponding maximum Darcy fluxes are 0.64 and 1.25 my^{-1} (for Scenarios F2 and F1, respectively). For all three cases, these maximum fluxes appear to be lower than for a 5-kt test, but the fluxes are being compared at different locations. What is interesting, however, is that they are certainly of the same order of magnitude as for the smaller tests, indicating, again, that velocities depend on buoyancy forces, which, in turn, depend on temperature differences, which are essentially independent of the yield of a test.

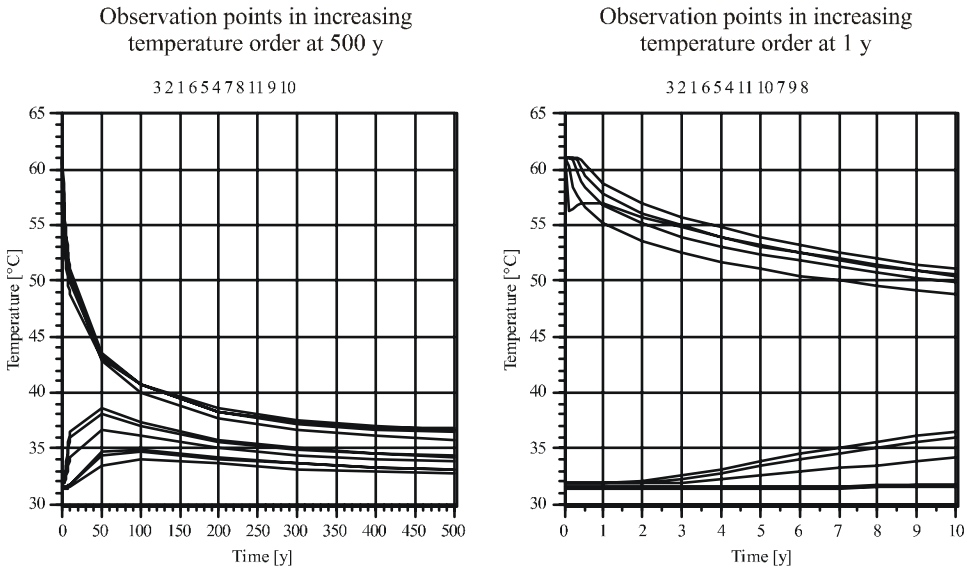

Figure 7.13 Time variation of temperatures and Darcy fluxes following a 150-kt test with 100 m of volcanic cover, a 25°C initial temperature increase, and no increase of hydraulic conductivity beyond the chimney, Scenario F0 (Perrochet and Tacher 1997a)

Figure 7.14 shows temperatures and fluxes corresponding to Figures 7.9 and 7.10, for a 150-kt test with 100 m of volcanic cover, a 50°C initial temperature increase, and significantly higher hydraulic conductivities, to $10\,r_c$ (Scenario F3). In this extreme case, the maximum Darcy flux is about 70 my^{-1}; after about 3 years, however, the flux drops to around 20 my^{-1}, before declining steadily over a period of 300 years. At approximately that time, Darcy fluxes at the observation points become negative for nearly 100 years, indicating that the geothermal convection pattern is still unstable and continuing to evolve.

Another extreme case is when there is no volcanic cover (CRTV test, the chimney reaches the carbonates). In this case, observation points are as shown in Figure 7.15. Figure 7.16 shows results for a 150-kt test with a 50°C initial temperature increase and no damage outside the chimney (Scenario F0). Temperatures and upward fluxes in the carbonates above the chimney rise and then fall as the bubble of hot water rises toward the surface. Peak fluxes in the carbonates reach about 50 my^{-1} and take about 50 years to drop to 10 my^{-1}. Combining extreme fracturing (e.g. scenario F3) with the possibility of zero volcanic cover leads to smaller peak fluxes, but significant fluxes would then occur over a larger area in plan (Perrochet and Tacher 1997a).

7.3.2 Effects of Tests Conducted Beneath the Rim of an Atoll

All the results described in Section 7.3.1 assume radial symmetry for a nuclear test conducted at the middle of a circular atoll. The IGC results show that, for simple scenarios, with damage represented by conductivity scenarios F0, F1 or F2, the geothermal convection cell caused by a nuclear explosion has little influence on the atoll-scale circulation beyond a radius of a few hundred metres. It is therefore possible to imagine that the assumption of radial symmetry may be reasonable even for tests conducted far from the centre of an atoll.

In order to test this hypothesis, three-dimensional simulations were performed for nuclear tests under the rim of an atoll. For these calculations, a three-dimensional mesh was developed to represent a slice 300 m wide, extending from the centre of an atoll to the ocean boundary. The distance of 300 m in the longshore direction represents half the distance between adjacent tests — i.e. the spacing between tests was assumed to be 600 m. One face of the slice passes through the centre of a chimney; because it is a plane of symmetry (if we imagine an infinite line of equally spaced tests), it is represented as a no-flow boundary, for movement of both water and heat. The other face, halfway between adjacent tests, is also a plane of symmetry and is also represented as a no-flow boundary. The interface between volcanics and carbonates is at a depth of 430 m below sea level at the centreline of the chimney, and the depth of burst is assumed to be 750 m below sea level. For a 150-kt test at this location, the chimney would reach the carbonates. (There would be no volcanic cover.) Hydraulic conductivities are assumed to be 10^{-7} ms^{-1} in the volcanics, 10^{-4} ms^{-1} in the carbonates, and 10^{-2} ms^{-1} in the

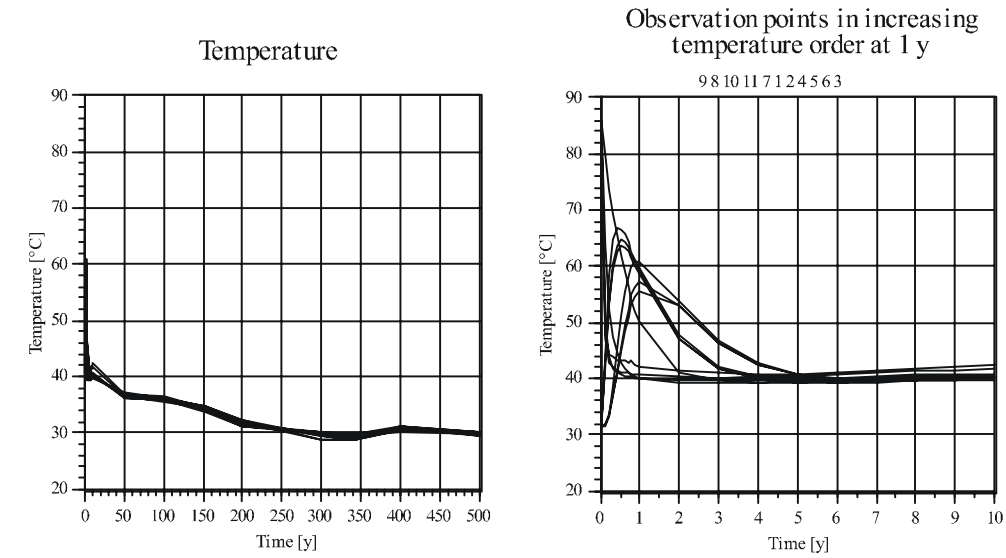

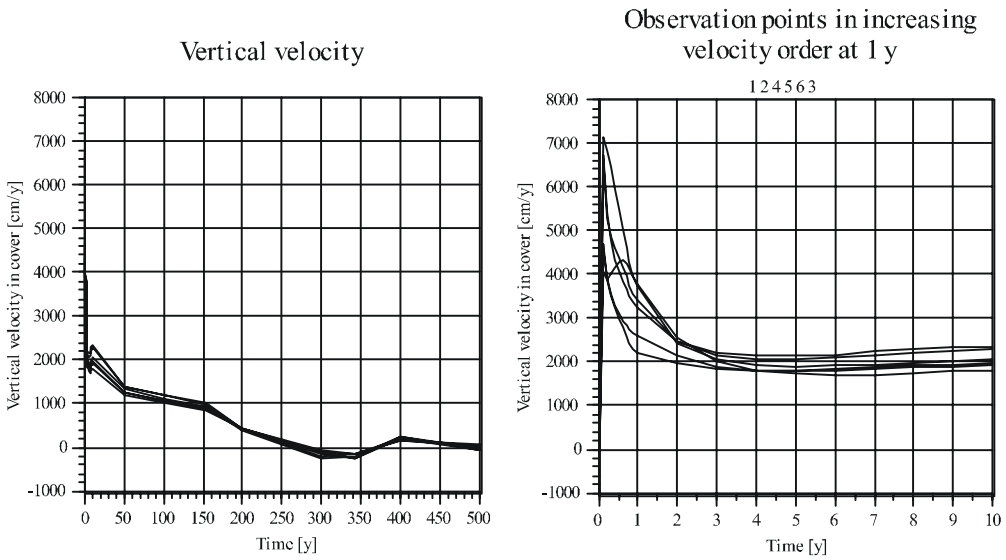

Figure 7.14 Time variation of temperatures and Darcy fluxes following a 150-kt test with 100 m of volcanic cover, a 50°C initial temperature increase, and significantly higher hydraulic conductivities to $10\,r_c$, Scenario F3 (Perrochet and Tacher 1997a)

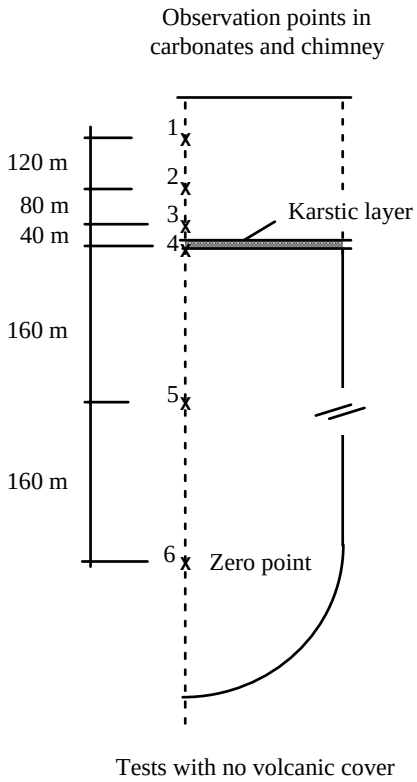

Figure 7.15 Locations of points where fluxes are computed for cases with no cover (Perrochet and Tacher 1997a)

chimney, with no damage outside the chimney (scenario F0 in Table 7.1). Typical node spacings in a three-dimensional mesh of this type are 2–5 m in the chimney, 5–10 m in damaged zones, and 10–50 m elsewhere.

Figure 7.17 shows isotherms following a 150-kt test with a 50°C temperature increase. (The black region to the right of each image represents temperatures less than 18°C.) The almost vertical migration of a bubble of heat is clearly visible. Figure 7.18 shows isotherms following a 150-kt test with a 50°C temperature increase and a 50-m-thick karstic layer at the base of the carbonates. Figure 7.19 shows corresponding variations in temperatures and fluxes for periods up to 200 years. Breakthrough of heat at each of the observation points (see Figure 7.15) occurs at times of maximum Darcy flux, indicating the clear dominance of advection over thermal conduction in the carbonates. Compared to results at the centre of an atoll (cf. Fig. 7.16), temperatures and fluxes decline much faster under the rim. This is partly because the natural geothermal convection at atoll scale allows advection of some heat in the centripetal direction, whereas no such

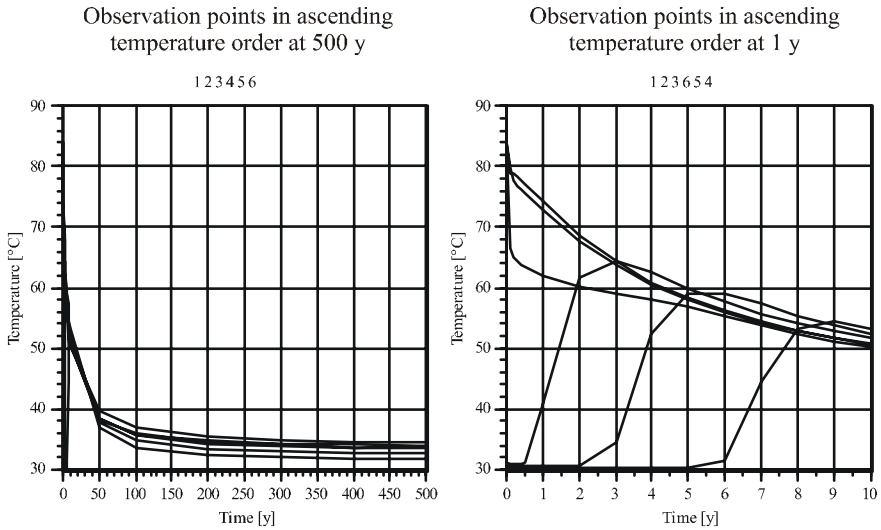

Average pre-test temperature at observation points 4–6 (chimney): 34°C

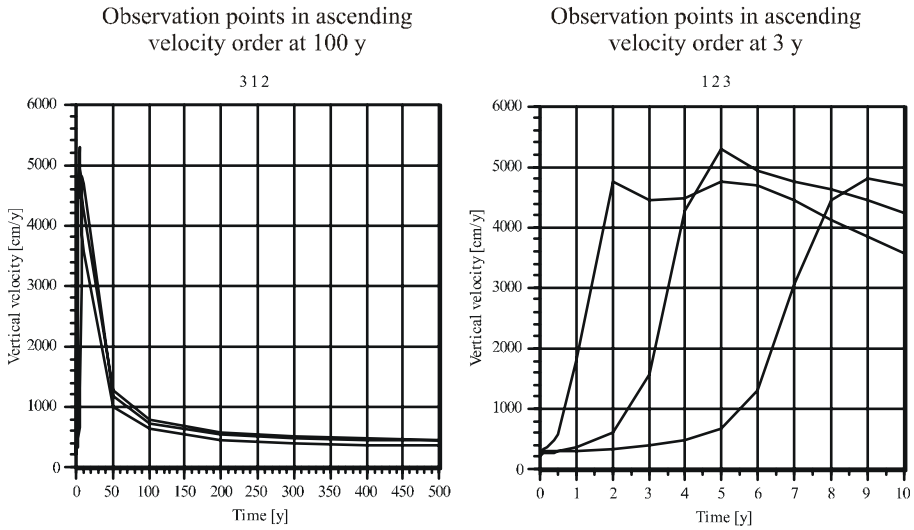

Average pre-test vertical Darcy velocity at observation points 1–3 (above chimney): 200 cm/y

Figure 7.16 Time variation of temperatures and Darcy fluxes following a 150-kt test with no volcanic cover, a 50°C initial temperature increase, and no increase of hydraulic conductivity beyond the chimney, Scenario F0 (Perrochet and Tacher 1997a)

lateral movement of heat can occur at the centre of an atoll. The ambient temperatures are also lower under the rim, so buoyancy forces are also diminished.

These results show that the results of the axisymmetric calculations given in Section 7.3.1 provide velocities and rate of decay of temperature and velocities that are higher than those obtained for three-dimensional calculations made under the rim. For safety studies, where the rate of release of radionuclides into the environment is important, it is therefore conservative to use the axisymmetric results to predict the hydrological behaviour of the atolls.

7.3.3 Safety Trials in the Carbonates

Ten underground safety trials were carried out at Mururoa Atoll (DIRCEN/CEA Document No. 6) (see Vol. II, Figs. 1.17 and Tables C.3 and C.7). In these tests, a nuclear device was placed in a conventional shaft and traditional chemical explosives were detonated in order to test the safety of the nuclear device. Seven safety trials did not "go nuclear" (see App. C), so plutonium was dispersed in the immediate vicinity of the test; four of these took place in carbonates at a depth greater than 280 m, and three were in the volcanics. Three safety trials released a small amount of fission yield, equivalent to roughly 0.2 kt each; all of these were in lower carbonates, at a depth greater than 280 m. All safety trials are presumed to have taken place under the rim of the atoll; however, their exact locations were not provided.

Safety trials that did not go nuclear resulted in a minimal amount of physical disturbance in the subsurface and did not release sufficient heat to cause local geothermal cells as a mechanism for transport for radionuclide migration. Those that went nuclear, on the other hand, resulted in cavities and chimneys and released heat. In order to assess the impact of safety trials, a 0.2-kt explosion at a depth of 280 m in the carbonates was simulated by Perrochet and Tacher (1997a). Cavity and chimney dimensions are mildly sensitive to the nature of the rock, but, because there is little information on the effect of nuclear explosions in saturated carbonates, the explosion was assumed to create a chimney with radius of 7 m and height of 35 m — the same dimensions as would be assumed in basalt. The initial temperature increase was assumed to be 50°C, taking the initial temperature in the chimney to 81°C. No damage was assumed outside the chimney because the carbonates are very porous and already very permeable (see Chapter 3).

Figure 7.20 shows temperatures and Darcy fluxes at points 1, 2 and 3, at distances of 20 m, 10 m and 0 m, respectively, above the top of the chimney. The relatively slow decline in temperature at point 1, once it has reached its maximum, suggests the existence of an advectively dominated rising plume rather than dissipation of heat by conduction. The peak Darcy fluxes at points 1 and 2 occur almost immediately after the trials. Average values during the period of 200-600 days are of the order of 7–10 my^{-1}, about 10 times larger than natural upward flows in the carbonates.

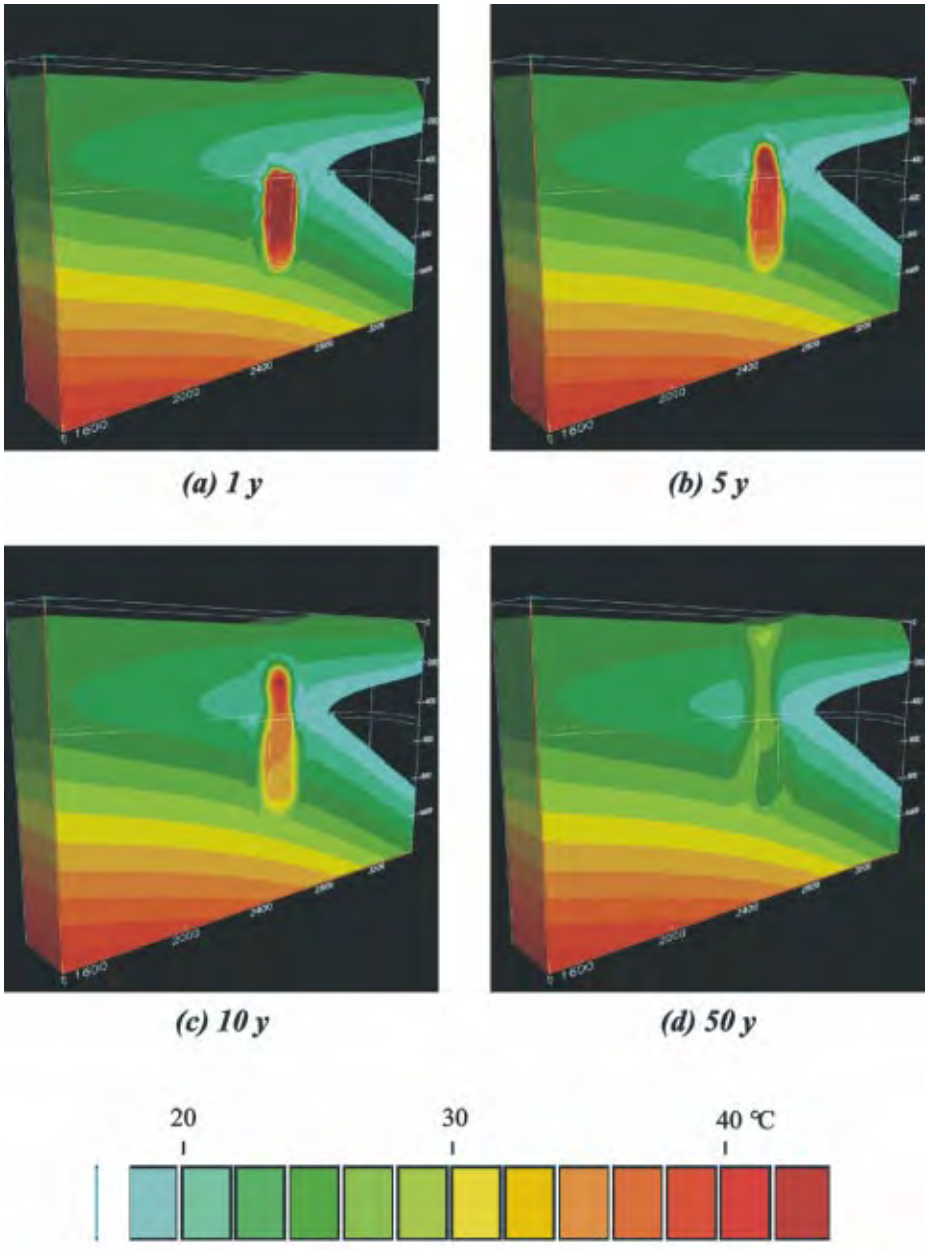

Figure 7.17 Three-dimensional images of isotherms following a hypothetical 150-kt test under the rim of an atoll, with no volcanic cover, a 50°C initial temperature increase, and no increase of hydraulic conductivity beyond the chimney, Scenario F0 (no tests of this magnitude were carried out with no volcanic cover) (Perrochet and Tacher 1997a). (See note on scaling of these images — Fig. 1.29.)

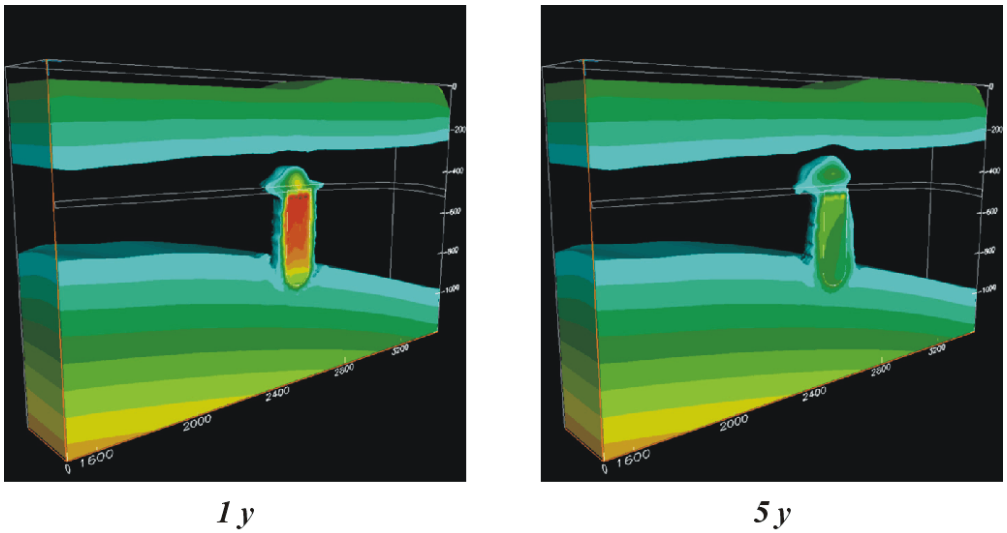

Figure 7.18 Three-dimensional images of isotherms following a hypothetical 150-kt test under the rim of an atoll, with no volcanic cover, a 50°C initial temperature increase, no increase in hydraulic conductivity beyond the chimney, Scenario F0 and a 50-m-thick karstic layer at the base of the carbonates (Perrochet and Tacher 1997a). (See note on scaling of these images — Fig. 1.29.)

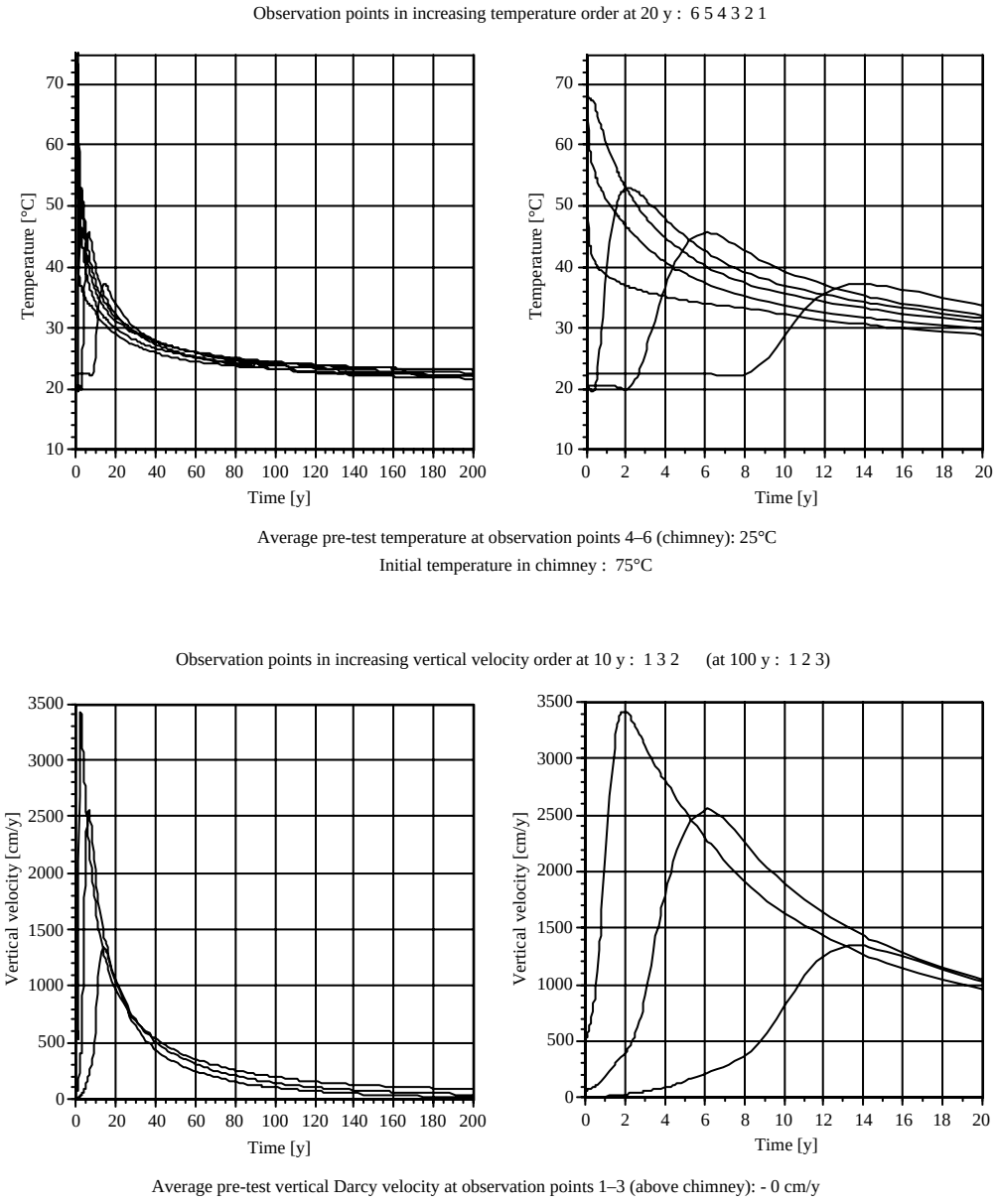

Figure 7.19 Time variation of temperatures and Darcy fluxes following a hypothetical 150-kt test under the rim of an atoll, with no volcanic cover, a 50°C initial temperature increase, and no increase of hydraulic conductivity beyond the chimney, Scenario F0 (no tests of this magnitude were carried out with no cover) (Perrochet and Tacher 1997a)

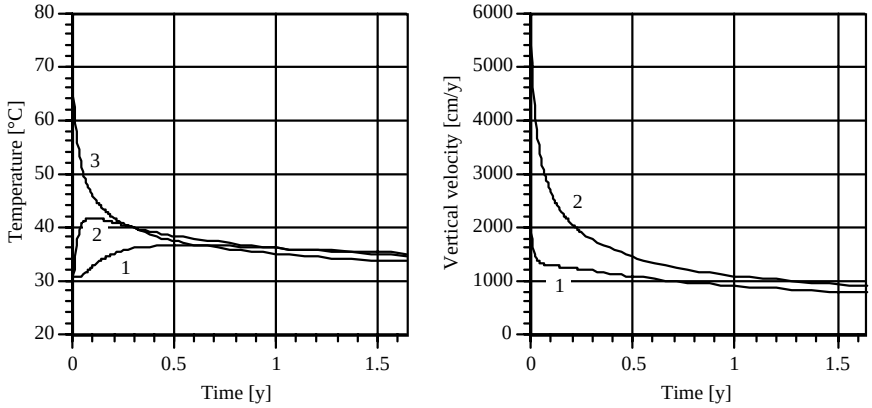

Figure 7.20 Time variation of temperatures and Darcy fluxes following a 0.2-kt safety trial at a depth of 280 m in the carbonates, with a 50°C initial temperature increase and no increase of hydraulic conductivity beyond the chimney (after Perrochet and Tacher 1997a)

7.3.4 Interaction Between Adjacent Tests

In some areas of the Mururoa rim, the number of tests is large; therefore, the spacing between tests must be small. Overlapping of damaged zones (in particular, fractured zones) from tests made on the rim at short distances from each other was discussed in Chapter 3**.** As far as convective flow around each test site is concerned, it is possible to give bounds to potential consequences of overlapping. As shown in Section 7.3.2 for the three-dimensional calculations, each test in a line of regularly spaced tests of equal magnitude under the rim behaves as if there were a no-flow boundary halfway between adjacent tests. If the tests are not of equal magnitude, or if they are not shot at the same elevation, the no-flow boundary exists, but it is not quite halfway between the tests. Thus, compared to a single test, the net effect of closely spaced tests is to limit the volume of rock from which water can flow toward the chimney and to reduce the flux and the velocity above the chimney. Flow can indeed originate only from the domain bounded by the no-flow planes, compared to the unbounded domain surrounding a single test. Even if the damaged zones overlap, the zone of increased permeability will be essentially in the plane joining the two chimneys, whereas the flow toward the chimney will be essentially perpendicular to that plane. The increase in permeability, therefore, would not have a significant effect and should be well within the uncertainty in the permeability scenarios F0–F3, which were used in Section 7.3.1. (See also App. F, Fig. F.6.)

7.3.5 Summary

The IGC reports three major findings:

1. The vertical velocity above a test site is not as sensitive to the permeability scenario as may have been expected. The reason for this is that water leaving the chimney toward the surface must be replaced by water flowing radially toward the cavity and chimney. Even if the rock is damaged at some distance from the chimney, this water must eventually come from undamaged zones, where the permeability in the volcanics is small. For example, for a 150-kt test, if the extreme scenario F3 (with permeability increase by a factor of 10 000) is used, the velocity above the chimney is increased only by a factor of 5 compared to scenario F2 (with permeability increase by a factor of 10).

2. Because the cavity and chimney are "well-mixed reactors", due to their constant internal convection, the uncontaminated water entering the chimney is instantly mixed with the contaminated water inside the chimney. As a result, it can easily be shown that the concentration in the chimney decreases exponentially with time. The time needed to transfer to the carbonates (a conservative radionuclide initially present in the chimney water, such as tritium, can be calculated as a function of the ratio of the Darcy velocity above the chimney to the height of the chimney; see Appendix S). Typical values are tens to hundreds of years. Sorbed radionuclides would take much longer. Radioactive decay also must be taken into account during this transfer.

3. The vertical velocity above a test is almost independent of the yield of the test. This is also due to the fact that the volume of the cavity and chimney scales linearly with the yield, which makes the temperature increase constant. Thus, the buoyancy forces are of the same order whatever the yield. On the other hand, when the temperature increase is changed from 25°C to 50°C, the velocity is almost doubled.

Table 7.2 provides a summary of the velocities in the volcanics and the carbonates for several types of tests analysed above. In order to further simplify and group the various tests that were performed over the years, it was decided to select a few typical values of the Darcy velocity above the chimneys for use by the IAEA (1998b) in radionuclide transport modelling. These velocities are:

- for tests with volcanic cover, for any yield, 1 my^{-1} in volcanics, 2 my^{-1} in carbonates;
- for CRTV tests or tests with a damaged volcanic cover, for any yield, 20 my^{-1} in carbonates and volcanics; and

Table 7.2 Summary of predicted velocities due to geothermal convection cells

	Type 1	Type 2	Type 3	Type 4	Type 5	Type 6
Volcanic Cover (m)	15	100	0 (CRTV tests)	damaged volcanic cover (scenario F3)	0 (safety trials that did not go nuclear)	0 (safety trials that did go nuclear)
Yield (kt)	5	150	150	150	0	0.2 kt at depth of 280 m
Peak Darcy Velocity in Volcanics (my^{-1})	0.1 – 0.3[a]	0.6 – 1.2[a]	irrelevant, since no volcanic cover	68 my^{-1} at peak (1 month)	irrelevant, since no volcanic cover	irrelevant, since no volcanic cover
Asymptotic Steady Darcy Velocity in Volcanics (my^{-1})	0.03 – 0.3[a] after 100 y	0.3 after 200 y	irrelevant	20 my^{-1} on average over 50 years	irrelevant	irrelevant
Darcy Velocity in Carbonates (my^{-1})	2	2 – 3	58 at peak (1 month), decaying rapidly to 18 on average, over 100 y	$\sim$ 30 for the first tens of years	2 – 3	55 for a few days, stabilising at 11 after 1 y
Number of Tests in This Category	121	0?	12, but with yields of 5 – 10 kt	4	4	3

[a] the range depends on the permeability scenario and the initial temperature increase

- for safety trials in carbonates: 11 my^{-1} if the tests went critical, 2 my^{-1} if they did not.

Because the actual velocities decrease with time, these velocities (assumed constant in the IAEA transport model) are taken as averages for the first tens of years, and are therefore conservative estimates later on.

7.4 Assessment of Observed Tritium Distributions

7.4.1 Observed Distributions of Tritium in the Karst

As shown (e.g. by Nikolaevskiy 1990), radionuclides can be transported in porous media away from a nuclear cavity by gases or fluids. DIRCEN/CEA Document No. 9 (Figs. 7 and 8) provides data on the observed spatial distributions of tritium (^{3}H), strontium (^{90}Sr), caesium (^{137}Cs) and plutonium (^{239}Pu) measured in so-called karstic horizons of the carbonates at Mururoa and Fangataufa, above the volcanics, from a limited set of observation holes. The IAEA sampling campaigns on the same boreholes provide additional measurements of these distributions (Section 6 of (IAEA 1998b)). These data are limited in that the number of sampling locations is relatively small. On the other hand, they are extremely significant because they provide direct evidence for the fact

that radionuclides have been transported to the base of the carbonates in some locations but not in others. Figures 7.21 and 7.22 from DIRCEN/CEA Document No. 9 show the spatial distribution of tritium in the karst at Mururoa and Fangataufa in 1996.

The contour maps provided by DIRCEN/CEA show a considerable amount of structure. According to DIRCEN/CEA, these maps were prepared with considerably more data than just the measurements in the boreholes indicated on the maps (e.g. numerous additional boreholes, explicit knowledge of geological variability, site conditions, and the location of all the nuclear tests) — none of which has been available for our interpretation. It has been explained that a number of nuclear tests, known as CRTV tests, had chimneys that reached the base of the carbonates, allowing rapid release of radionuclides to the carbonates. Furthermore, there were four tests (three at Mururoa (Enée, Nestor and Mégarée) and one at Fangataufa (Lycos)) for which the volcanic cover may not have been as competent as in most situations, generating faster release of radionuclides from the volcanics to the carbonates. The spatial distribution of radionuclides therefore provides an indication of the locations of those tests which may have caused releases to the carbonates.

In addition to the measurements of concentrations in the carbonates, radionuclide concentrations were also measured in the lagoons of both atolls. Because the rate of exchange of water between the lagoons and the ocean has been estimated both by DIRCEN/CEA (Document 11) and by IAEA (1998e), these concentrations can be transformed into a flux of radionuclides released from the carbonates to the lagoons. It is then possible to obtain a rough estimate of the transfer of radionuclides from the volcanics through the carbonates to the lagoons.

In order to explain the observed data, DIRCEN/CEA has developed quasi-three-dimensional models of flow and transport of radionuclides in the carbonate layers of the two atolls (DIRCEN/ CEA Document No. 10). The models are not described in sufficient detail to be reproduced by others, but they seem to have the following features. Each model has several horizontal layers, over a thickness of 250 m of carbonates, with the lowest layer representing a karst horizon. Layers are connected by highly conductive vertical elements to represent pathways through the carbonates from the karst to the lagoon. The models compute steady flow and unsteady transport of radionuclides. The steady centripetal flow field is driven by prescribed effective heads at the ocean and lagoon boundaries (the extrema of each horizontal layer and the whole of the upper layer within the lagoon). These heads are calculated to take into account the dependence of density on temperature at the ocean boundary. The unsteady transport uses an effective dispersion coefficient which attempts to account for the effects of tidal fluctuations on the dispersion process, as discussed in Section 6.3.6. The calibrated values of this dispersion coefficient (based on the tritium concentrations in the carbonates) are 10^{-3} and $5 \cdot 10^{-4}$ m^2 s^{-1} in the longitudinal and transversal directions with respect to the average velocity. This model also assumes a 10-m-thick karst layer at the bottom of the carbonates, where the Darcy velocity is calibrated at 10 my^{-1}.

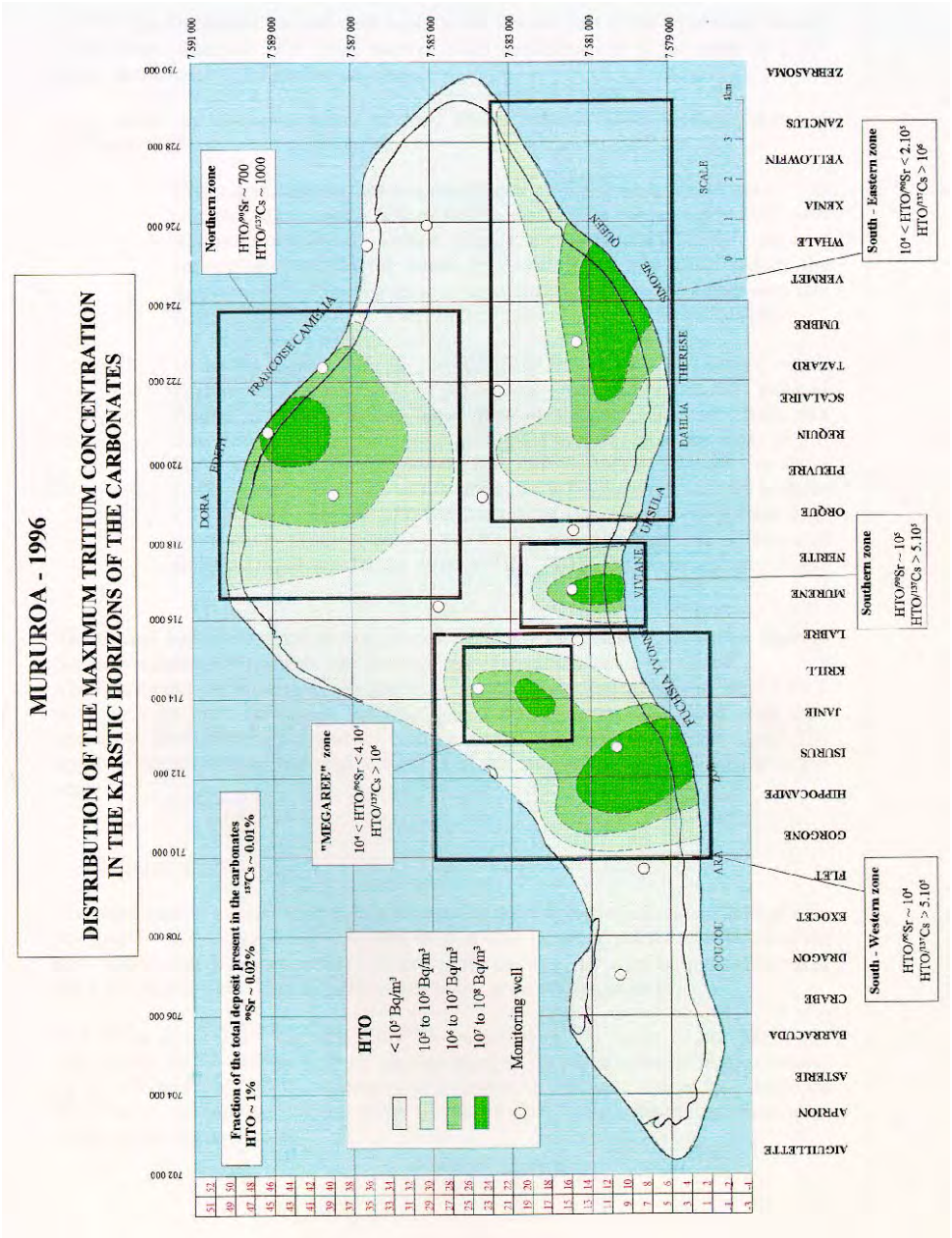

Figure 7.21 Spatial distribution of maximum tritium concentrations in the karstic horizons of carbonates at Mururoa in 1996 (DIRCEN/CEA Document No. 9)

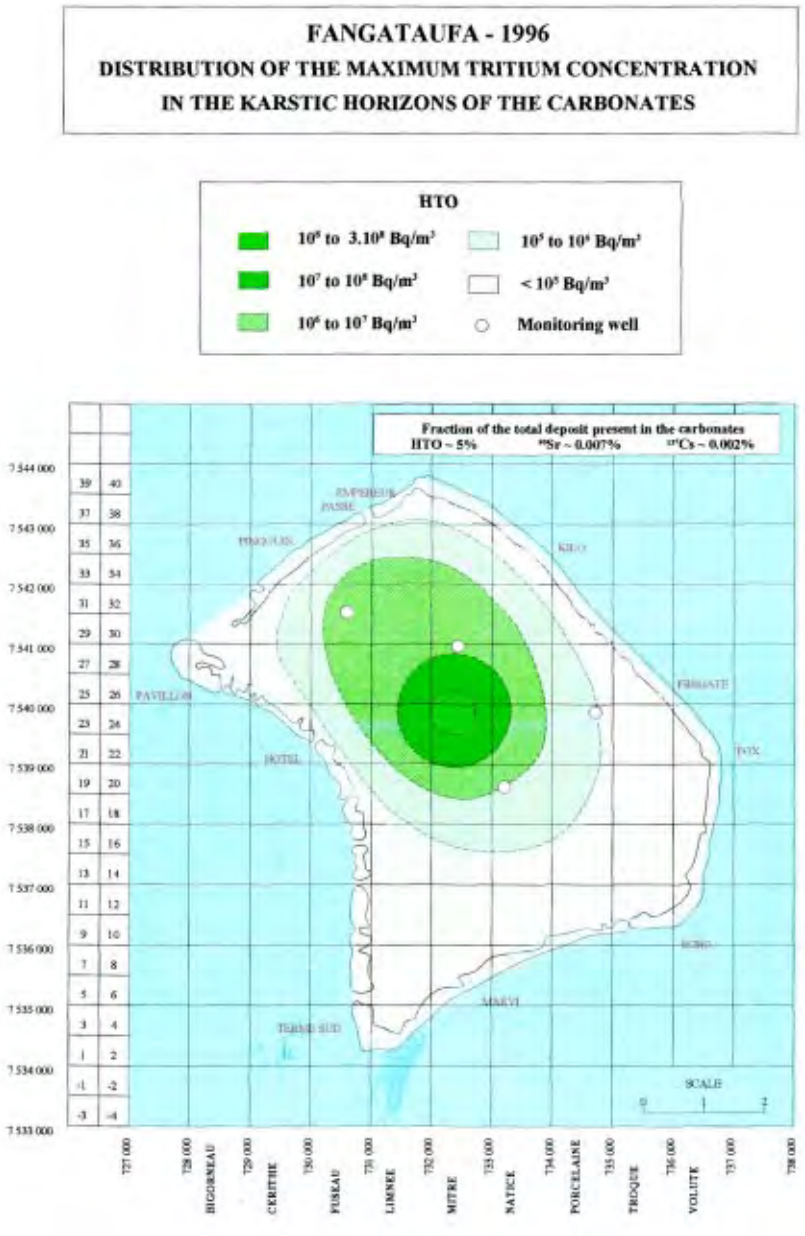

Figure 7.22 Spatial distribution of maximum tritium concentrations in the karstic horizons of carbonates at Fangataufa in 1996 (DIRCEN/CEA Document No. 9)

The model receives a radionuclide flux from the volcanics which has been estimated for three categories of tests: the CRTVs, the four tests where the volcanic cover is considered weak (Enée, Nestor, Mégarée and Lycos), and the three safety tests shot in the carbonates that went nuclear. The other tests are considered not to have released radionuclides to the carbonates. The flux of nuclides to the carbonates is estimated from the rate at which the water in the chimneys is flushed while being constantly mixed. This is itself a decaying function of time, because of the cooling of the chimneys, as shown in Section 7.3.1. These rates were estimated by DIRCEN/CEA in Document No. 8, using a convection model in the volcanics similar to the one described in Section 7.3.1. This modelling approximately represents the observed distribution of tritium, caesium and strontium in the carbonates and the observed flux to the lagoons.

7.4.2 A Model of Tritium Release Based on Mixing in the Carbonates

The IGC used a different set of models to represent the release of radionuclides from the volcanics to the carbonates and their subsequent transfer to the lagoons. The objective of this modelling was essentially to determine whether the convective model of Section 7.3.1 adequately represented the flow around a cavity and, therefore, predicted a release of radionuclides from the volcanics consistent with the observations. For this purpose, only tritium was considered, as tritium is integrally released to the water phase in the chimney after a test and is not sorbed by the rocks; it is therefore an excellent tracer of groundwater circulation. The other radionuclides (caesium, strontium, plutonium, etc.) are partly contained in the molten lava or sorb onto the rock surfaces; they are not conservative tracers. While their transfer to the environment is fundamental in studying the radiological consequences of the tests, this is the task entrusted to the IAEA in this analysis (Section 5 of IAEA (1998b)). The role of the IGC was to estimate the flow and velocities for the radionuclide transfer models used by IAEA; tritium was considered as a means of understanding and quantifying the flow.

To this end, a simplified "mixing model" was developed for tritium transport in the carbonates and compared with a "piston flow" model and an "advection-dispersion" model, similar to the one used by DIRCEN/CEA. These comparisons are reported in Appendices S and T. The mixing model was found to be the one most coherent with the observations. This model assumes :

- constant mixing of tritium in the cavity and chimney water at each test site and release of this water to the carbonates with the calculated Darcy velocities given in Section 7.3.5. (The release thus decays exponentially with time, because of tritium half-life and mixing in the chimney; the initial tritium inventory for each test was estimated by IAEA (1998c));
- tritium leaving the volcanics enters the carbonate layer, represented as a well-mixed "reservoir", with no delay for transfer through the volcanic cover, which

is pessimistic (see App. S). (The rationale for using a mixing model in the carbonates is the observation that tritium is spread over a considerable thickness and volume of the carbonates throughout each test zone; however, the amount of tritium reaching the lagoons is very small (a few percent of the total inventory stored in the carbonates, for the cumulated release over 20 years)). This shows that the distribution of the residence times of tritium in the carbonates is uneven — a small fraction is released rapidly while a large fraction stays in the pore water. A mixing model is one simple way to represent such a residence time distribution; the cause of the mixing may be the tidal effect and, possibly, the effects of the drilling of new test wells during the period of active testing);

- release of tritium from the carbonates to the lagoons by the average natural Darcy flux estimated by IGC in the three-dimensional calculation (Section 6.3.3) for natural conditions, which are not affected globally by the tests (see Section 7.5.1 below). This Darcy flux is assumed to have the tritium concentration of the mixed carbonate reservoir); and

- release of tritium from the lagoons to the ocean because of the daily tidal flow in and out of the lagoons. (These lagoons are again assumed to be well mixed, and the knowledge of the average water residence time in the lagoons, estimated by both DIRCEN/CEA and IAEA (1998e), makes it possible to estimate the total annual flux of tritium to the lagoons from the measurement of the average tritium concentration in the lagoon water.

All the parameters of this simplified mixing model can be estimated independently (in general, within a factor of two) from the estimated yield of the tests and the IGC hydrogeologic calculations — in particular, the values of Darcy velocities for each test category (Section 7.3.5). All 137 tests in Mururoa and 10 tests in Fangataufa (as given by DIRCEN/CEA Document No. 6**)** were taken into account and grouped together by periods of 5 years. The calculated inventory in the carbonates and annual release in the lagoons for both atolls were then compared with the estimated inventories in the carbonates (obtained by sampling water in a total of 16 boreholes in Mururoa and 4 boreholes in Fangataufa) and the estimated flux of tritium to the lagoons (based on the measured concentrations in the lagoon water). The agreement was surprisingly satisfactory, with an overestimate by the model of the flux to the lagoons by a factor of less than two and an overestimate of the tritium inventory in the carbonates by a factor of 2 to 10. Overestimating the flux and inventory is, of course, conservative with respect to the radionuclide release. Figure 7.23 shows the calculated evolution of the tritium flux in the Mururoa and Fangataufa lagoons over the years.

The results of this analysis indicate that the estimated velocities describing the rates at which contaminated water from the explosion chambers would reach the carbonates

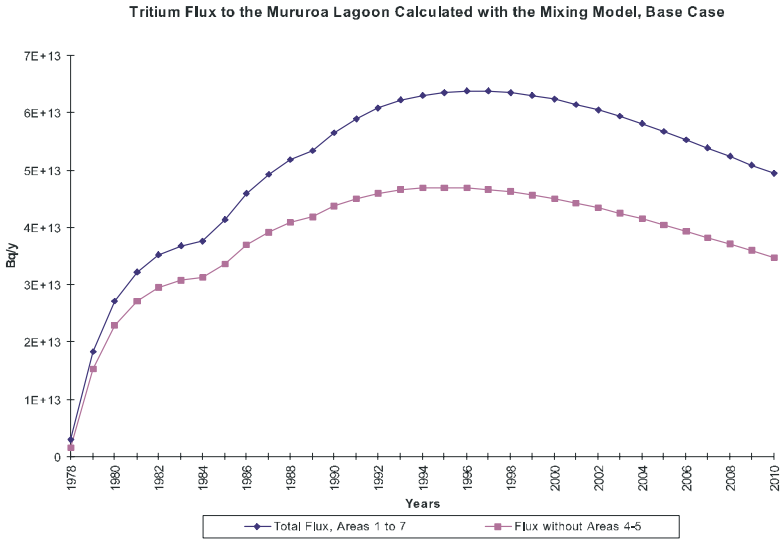

(a)

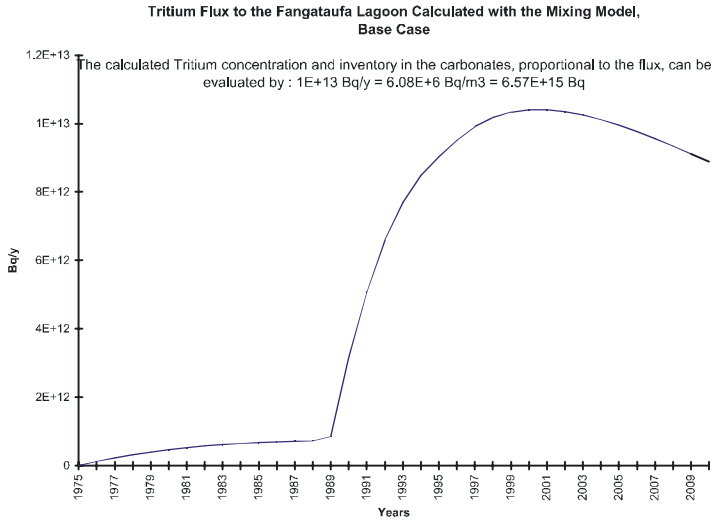

(b)

Figure 7.23 Calculated tritium release to the Mururoa (a) and Fangataufa (b) lagoons using the IGC mixing model; in (a), the upper curve assumes that all seven test areas at Mururoa release tritium, while the lower curve excludes any flux from test areas 4 and 5 (see App. S)

are reasonable. These numbers are clearly very important for estimating the radiological consequences of the tests. Table 7.3 provides a summary of the times of transport of conservative (non-sorbing) tracers based on the simple models presented in Appendix S.

Table 7.3 Summary of travel times for transport of conservative tracers (see Table 7.2 for definition of test type)

Tests Type	Time for Tracer to Reach Carbonates[a] (y)	Time for Tracer to Reach Lagoon (y)	Time for Emptying 90% of the Tracer from the Cavity[b] (y)
1	< 1	45	275
2	< 1	30	800
3	almost instantly	2	15
4	almost instantly	3	12
5	instantly	30	irrelevant (no cavity)
6	instantly	8	2

[a] assuming a fracture porosity in volcanics of 10^{-4} (with negligible diffusion in the rock matrix), a porosity in the carbonates of 0.3, and 300 mm of carbonates

[b] tritium would almost totally disappear by decay in ten half-lives (i.e. 123 years)

7.5 Geothermal Circulation at Atoll Scale in the Long Term

The local geothermal circulation induced by each underground nuclear test gradually loses intensity due to dissipation of heat by conduction and, in some extreme circumstances, by advection. After a period of 500 years, the main hydrological impact of nuclear tests at Mururoa and Fangataufa will be the effect they have had on the structure of the atolls, in the sense that each test has created a chimney with an enhanced effective hydraulic conductivity.

7.5.1 Effects of Chimneys on Atoll-Scale Permeability

It is instructive to examine the general influence of one or more heterogeneities in the rock structure on the global permeability of a rock mass. We assume that the heterogeneity can be represented as an ellipsoidal volume, which could represent, on the large scale, a nuclear explosion chimney or a lava tube, for example. The effect of such heterogeneities on the global permeability of a porous medium has been studied by Janković and Barnes (1997) and is exemplified below and in Appendix F using a computer code that they developed which represents heterogeneities in three dimensions by large permeability contrasts.

As an example, Figure 7.24 shows a typical flow pattern around a highly conductive ellipsoidal cavity (void). This cross-section corresponds to the horizontal plane. The semi-major axis of the ellipsoid is 5 m along the x-direction, and the semi-minor axis is 2 m. A uniform flow is applied upstream in the x-direction, with a head gradient of 0.1. In the absence of the ellipsoid, the head contours would be perpendicular to the x-axis, and a particle of water would follow the x-axis from left to right. When the ellipsoid is introduced, the head contours deviate around the cavity, as shown in Figure 7.24. The same particle of water would deviate toward the cavity as it travels perpendicularly to the head contours. The quasi-hydrostatic head within the ellipsoid is balanced by its very high conductivity, so that the particles "rush" through the cavity from the higher head in the rock on the left to the lower head on the right.

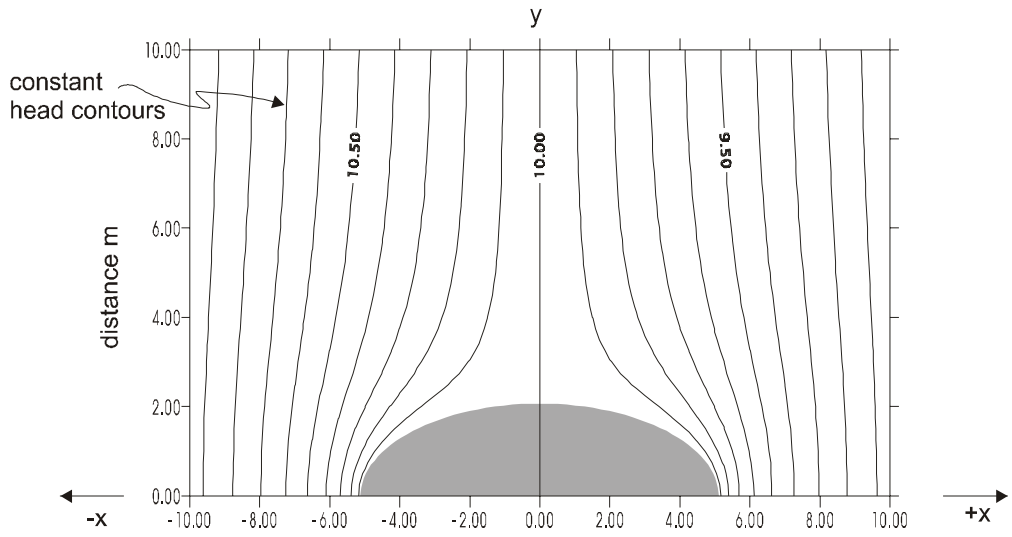

Figure 7.24 Head contours around an ellipsoidal cavity in a uniform flow field (Janković and Barnes 1997)

Another example is given in Figure 7.25, where three mutually orthogonal sections through a three-dimensional flow field are shown, in which 1000 spheroidal inhomogeneities were introduced. Because the plots show only those intersections with the planes defined by the cross-sections on the lower-right plot, most of the spheroids cannot be seen. The flow is in the C-C′ direction; thus, the piezometric head contours on the upper-left plot do not show a clear gradient. (This cross-section is approximately a section of constant head.) The inhomogeneities cover about 30% of the volume of the cube. They are three orders of magnitude more conductive than the background. This

example contains both prolate (elongated) spheroids and oblate (squashed) spheroids of random orientation; hence, the medium should be isotropic. In both examples, it is seen that the distortion of the head contours (which would all be straight lines in the absence of inhomogeneities) is significant only in the vicinity of the individual inhomogeneities.

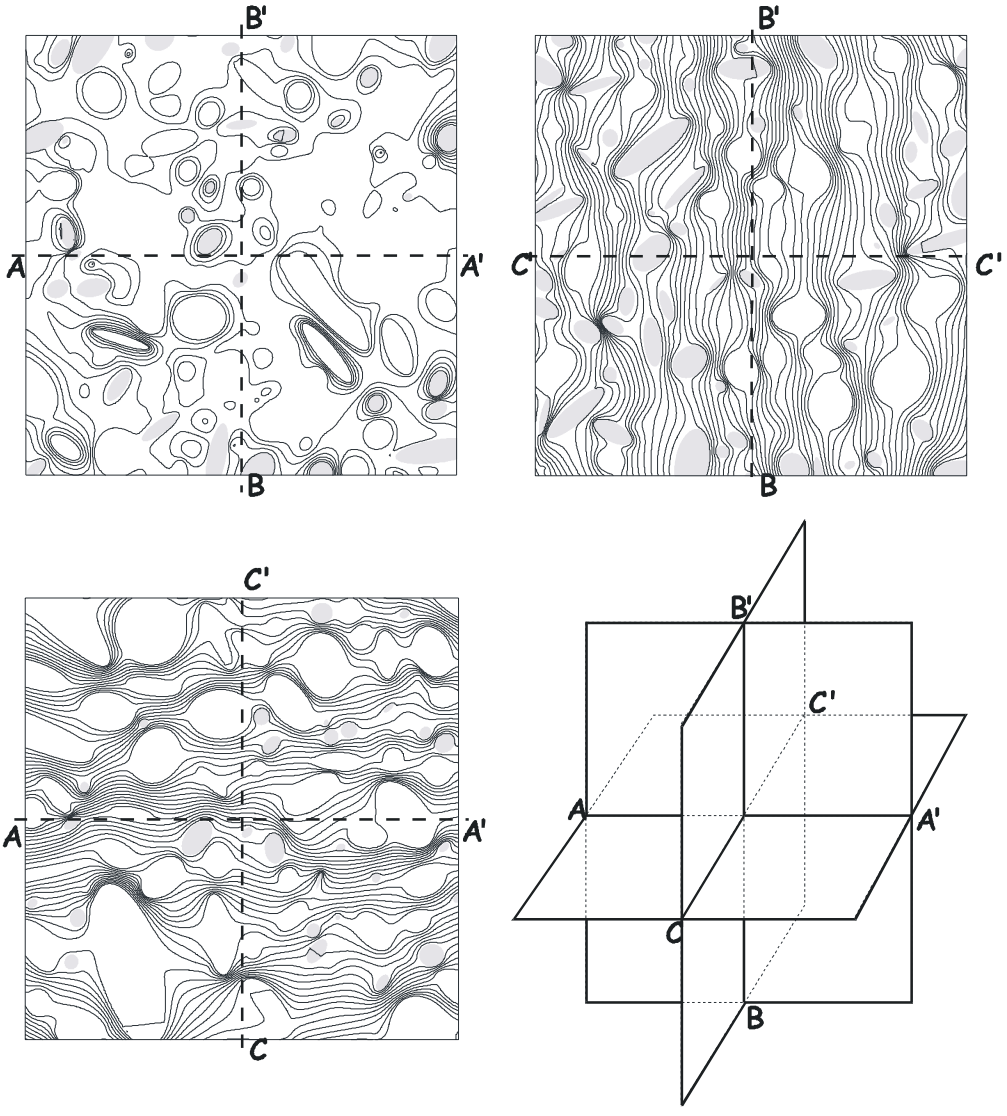

Figure 7.25 Intersection of three planes with constant head surfaces for 1000 spheroidal heterogeneities in a uniform flow field (Janković and Barnes 1997)

Using Janković´s code (Janković and Barnes 1997), it is possible to calculate the equivalent permeability of the medium containing many inhomogeneities as the size of the domain is increased. A series of computer runs was carried out for the ellipsoidal cavities of Figure 7.24, using domains of progressively increasing size to surround the ellipsoid. As V_e / V diminishes, the equivalent permeability K_e can be expressed as

$$\frac{K}{K_e} = 1 - \frac{V_e}{V} \tag{7.3}$$

where K is the permeability of the background medium,
V_e is the volume of the ellipsoid, with very large permeability compared to the background (in practice, equivalent to a void), and
V is the volume of the domain containing the ellipsoid. (The ratio V_e/V is a measure of the density of ellipsoids in the medium.)

Thus, when the volume of the domain, V, becomes large compared to the volume of the ellipsoid, the equivalent permeability, K_e, tends to the background permeability. As will be seen in the next section, the effect of the presence of 137 chimneys in the Mururoa atoll on the global permeability of the volcanics must be very small, according to these theoretical results, since the total volume of the damaged zones for all cavities is very small compared to the volume of the atoll. The overall geothermal flow in the volcanics in the atoll, when the thermal phase due to the tests is over (i.e. after about 500 years) must therefore be very close to the original value prior to the tests.

7.5.2 Long-Term Impacts on Geothermal Circulation

In Section 6.3.3, a three-dimensional model of the natural geothermal flow in the Mururoa atoll was constructed using FEFLOW (Perrochet and Tacher 1997a). In order to verify the theoretical results outlined in the previous section, this model was run again, introducing medium zones of high permeability (representing both the chimneys and the damaged zones of each test) at a time when the heat generated by the tests has disappeared. In each test area, as described in DIRCEN/CEA Document No. 6, the test location was chosen at random and given damaged zones with a prismatic shape of size 20 000 $m^2 \cdot$ 350 m, with the top reaching the carbonates. Thus, the total volume of the damaged zones for the 137 tests is 0.96 km^3 — i.e. 0.15% of the volume of the volcanics in the model. Simulations were carried out with permeabilities of 10^{-6}, 10^{-5}, and 10^{-4} ms^{-1} in these damaged zones. For all cases, the temperature distribution in these zones was virtually identical to the pre-test values. If we compare the total discharge from the carbonates to the lagoon before the tests, calculated by the model at 60 000 m^3 per day, to the one calculated with the 137 damaged zones with the highest permeability (10^{-4} ms^{-1}), we find that the increase is less than 1%.

These results confirm the theoretical results given in the previous section and show that the effects of the tests on the natural hydrology of the atoll at the global scale, after the decay of the heat pulse (about 500 years), is negligible. The effects of the radioactivity contained in the chimneys in the long term is discussed in IAEA (1998a) and IAEA (1998e).

7.6 Extreme Events

Although the long-term impact of the tests on atoll-scale circulation is perhaps insignificant, it is important to consider the potential impacts of extreme events that could modify the hydrologic system in the future. Such events include possible slope failures, which may modify the physical structure of the atolls, and changes in the regional climate, which could modify boundary conditions. In each case, the concern is that hydrological transport processes could be modified in a manner that may not have been anticipated without these analyses.

7.6.1 Slope Failures

Slope failures of various magnitudes have occurred during and following several of the underground nuclear tests on the atolls, and there is a region in test area 1 at Mururoa in which the ocean slopes have been deforming continuously since at least 1980 (see Chapter 5). It is likely that there will continue to be mass movements from the flanks of Mururoa and Fangataufa Atolls over geologic time, because such movements are natural processes on all atolls. The important question is: "What is the probable impact of such movements on the hydrology of the atolls?"

A slope failure removes a layer of geologic materials from the flank of the atoll. In the case of the Tydée test in 1979, the thickness of material removed was of the order of 100 m. Because all geologic materials provide resistance to groundwater flow, removal of such material modifies the geometry of the groundwater system and the spatial distribution of material properties. It has been suggested that carbonates along the flanks of the atolls are potentially more highly cemented and, therefore, less permeable than in other zones. Removal of a low-conductivity layer on the flank of the atoll would certainly modify local rates of flow. Since there is no information on the difference of permeability in the carbonates on the flanks of the atolls compared to the interior, it is very arbitrary to try to simulate this effect. It can be said, however, that the IGC did not include any low-permeability layer on the flanks of the atolls in any of the simulations presented earlier. Therefore, the rates of release estimated by the current simulations may be seen as including the effect of the removal of a low-permeability layer on the flank of the atolls.

It is also important to note that flow generally enters the atolls at the levels where radioactivity is present in the atolls. Thus, it is unlikely that removal of a layer of material

from the flank of an atoll could significantly increase the rate of transfer of radionuclides to the ocean at those depths. Perhaps the most significant potential impact would be if a failure occurred of sufficient size to remove part of the atoll where radionuclides are present in large quantities. Such a failure is considered unlikely.

7.6.2 The Glaciation Scenario

In this section, we investigate the likely hydrologic situation in Mururoa and Fangataufa in a hypothetical future climatic situation: that of a new glacial period worldwide, which would result in a drop in sea level and affect the hydrology of the atolls. Such a scenario is almost certain to occur in the future, although it is difficult to predict when. Several climate models have been built (see, for example, SKI (1997) for a review) based on the Milankovich theory, which suggests that the climate may become colder within 10 000–20 000 years, even colder within 50 000–60 000 years, after a brief warmer phase, then cold again at 100 000 years. Based on what happened during the last glaciation, which ended about 10 000 years ago, the sea level could drop as much as 100 or 150 m, due to the accumulation of ice in the cold regions of the earth's surface. The climate in the atolls will also change, but this is less predictable (probably colder and wetter) and of less consequence than the drop in sea level. Note that, during glaciation, a 100-m drop in sea level could occur in a few thousand years, whereas the rate of subsidence of an atoll by readjustment of the mantle is of the order of 150 m in one million years (see, for example, Guille et al. (1996)), which is negligible compared to the former.

We will estimate the extent of the freshwater lens that will develop in the atolls, after they have become islands with a ground elevation between 50 and 150 m above sea level, receiving recharge from rainfall. The shape of a freshwater lens in a carbonate island has been studied extensively (see, e.g., Raeisi and Mylorie (1995)). Because of the difference in density between seawater and freshwater, seawater is "pushed" down by the rainfall recharge water that infiltrates the porous limestone, and an interface develops at depth, separating the two types of water. In natural conditions, the thickness of the transition zone between the two waters, on an island in an ocean with tides, can be of the order of a few metres, up to ten metres. When pumping wells are installed, this thickness can increase up to some tens of metres.

To predict the shape of the interface, common simplifications are to assume the medium to be homogeneous and isotropic (neglecting the existence of a karst layer, which may be pessimistic) and the interface to be sharp (neglecting the transition zone thickness) and to neglect the vertical components of the velocity field with respect to its horizontal components, the so-called classical "Dupuit" assumption. Using the Ghyben-Herzberg relation, based on the density difference between the two types of water, which states that the depth of the sharp interface below sea level is equal to 40 times the elevation of the water table above sea level, one can derive the following relation (e.g. Henry (1964), Fetter (1972) , Bear (1972), Vacher (1988)):

$$h^2 = \frac{R}{K(1+\alpha)}(2Mx - x^2) \tag{7.4}$$

$$z = \alpha h \tag{7.5}$$

where h is the elevation of the water table above sea level (m),
z is the depth of the interface below sea level (m),
R is the mean annual recharge rate by infiltration (m/s),
K is the limestone permeability (m/s),
x is the distance inland from the shoreline (m),
M is the half-width of the island (m),
α is the density contrast $\rho_f/(\rho_s - \rho_f)$ (in this case, α = 40), and
ρ_s,ρ_f are the mass per unit volume of seawater and freshwater, respectively 1025 and 1000 kg m^{-3}.

The shape of the water table and of the interface for Mururoa and Fangataufa were calculated with the following parameters:

half-width of the island, M:	Mururoa 5 km, Fangataufa 3 km
recharge rate, R:	0.4 m/y, as in Vacher (1988) for carbonate islands in a similar climate
permeability, K:	10^{-4} m/s, as estimated from fitting the flow model on temperature data (see Ch. 6)

The results are presented in Figure 7.26 and show that the depth of the interface can be as much as 350 m below the future sea level for Mururoa and 200 m for Fangataufa. Such a lens obviously could be exploited in the future for freshwater supply on the emerged island.

Can the existence of the underground tests be of consequence in terms of potential contamination of the freshwater lens by radionuclides in this glaciation scenario? Given the likely time of occurrence of this scenario (i.e. more than 10 000 years in the future), only plutonium (Pu) is of concern, since all the caesium (Cs) and strontium (Sr) will have decayed away.

The seven safety trials performed in the carbonates, four of which did not go nuclear, were conducted between 1976 and 1980 on the rim of Mururoa at a depth greater than 280 m. If the sea level were lowered by 100 or 150 m, the safety trials would be at a depth of 130 to 180 m below the future sea level. As can be seen from Figure 7.26, the trial sites would be in the freshwater lens if they were exploded inland at a distance of 350 m from the future shoreline, for the 150-m drop in sea level, or 700 m inland for the

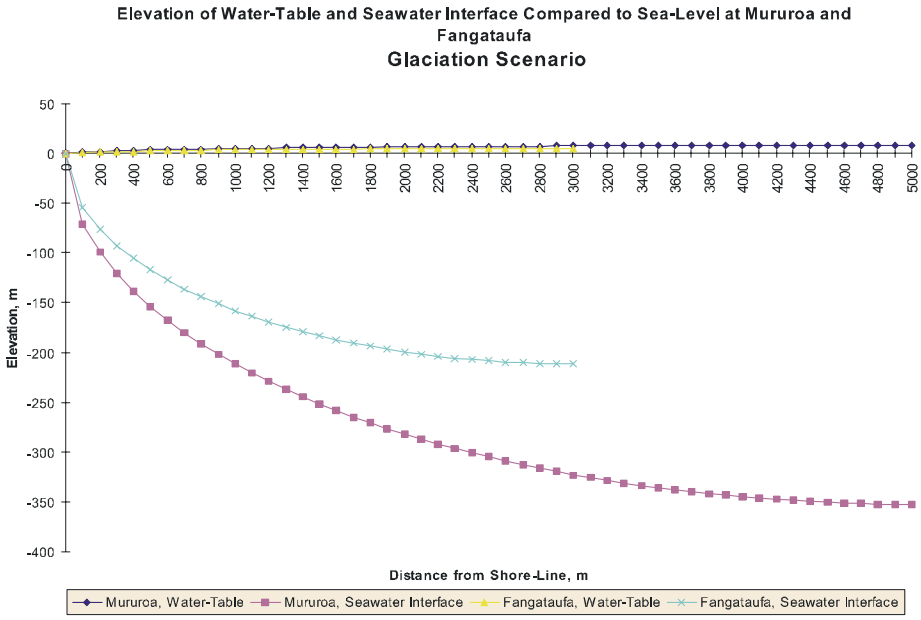

Figure 7.26 Water table and saltwater interface during glaciation at Mururoa (magenta) and Fangataufa (blue)

100-m drop. The rim is of the order of 400 to 600 m wide, and the trial holes were on the lagoon side of the rim, sometimes even built on a platform some tens of metres into the lagoon from the rim. Furthermore, a drop in sea level of 100 m or 150 m would displace the shoreline seaward by about 200–240 m, given a seaward slope of the atoll of 50° (see DIRCEN/CEA Document No. 5, Fig. 9). Thus, there is every reason to believe that the sites of the safety trials would be inside the freshwater lens during a period of glaciation.

Will there still be plutonium from the safety trials available for dissolution at the time of the next glaciation? Given the centripetal flow velocity in the carbonates before the glaciation, Pu will have been transported inland. If we assume, for instance, a Darcy velocity of 1 m/y, a porosity of 30%, a K_d for Pu of 0.5 m^3/kg (IAEA 1998b), and a carbonate density of 2200 kg/m^3, we obtain a retardation factor for plutonium transport of 2500 and a transport distance inland of 13 m in 10 000 years. We can thus conclude that Pu will still be in the vicinity of the sites of the safety trials.

The presence of Pu in the carbonates under the rim is therefore of concern for a glaciation scenario. However, it is difficult to determine the Pu concentration in the water pumped from a well in the freshwater lens. First, the wells will probably be drilled toward the centre of the island rather than toward the shoreline, since the seawater interface is at greater depth in the centre and the risk of upconing of the saltwater interface is lower. Second, if a well is drilled close to the shoreline, the resulting drawdown may

raise the level of the interface by upconing and, thus, bring the site of the safety trials below the seawater interface and, hence, outside the freshwater lens. Third, the likelihood that a well will be drilled exactly at the location of a safety trial is rather small. Last, not all the water extracted from the well will come from the deeper section containing the Pu source.

Furthermore, most of the Pu slowly released from the volcanics to the carbonates by all of the other 144 tests prior to the onset of the glaciation will still be in the carbonates, strongly sorbed to the rock. This Pu will also be in the freshwater lens and could be extracted by pumping wells. Thus, the glaciation scenario is one that could possibly lead to significant consequences for future inhabitants of the atolls. These consequences have been examined in detail by the IAEA team investigating the radiological consequences of underground nuclear testing on the atolls (IAEA 1998a, 1998b, 1998e).

7.7 Conclusions

The impact of nuclear tests on the hydrology of the atolls needs to be evaluated at the four different times listed below.

1. For very early times (seconds to weeks), the impact is local but rather strong. Water is vaporized, then condensed again, and a strong flux of water is sucked back into the cavity and chimney generated by the explosion until they are filled.

2. For a considerable period of time (up to 500 years), the flow field is strongly perturbed, compared to the pre-test situation, by convective cells that develop both inside the chimney (thus making it a well-mixed reactor) and outside the chimney in the damaged or undamaged zones. These convective cells decay with time, as the heat released by the test is slowly dissipated in the medium. The flow velocity above the chimney is directed from the volcanics to the carbonates and varies significantly, depending on the depth of the tests and the intensity of the damage to the rock (including those cases where the chimney reaches the carbonates). However, velocity does not vary much with the yield. The transfer to the carbonates of the water from the chimney is rather rapid, requiring only a few years, but the rate at which the chimneys release their water is quite low, because the flux is not very large, and the water initially contained in the chimney is constantly diluted and mixed with the incoming clean water. The time for 90% of the water initially present in the chimneys to be transferred to the carbonates varies between 12 years (for CRTV or highly damaged zones) to 800 years (for undamaged zones). Only radionuclides that are not sorbed by the rock (e.g. tritium) would be released in the same time frame, whereas sorbed nuclides, or nuclides trapped in the lava at the bottom of the cavities, would be released more slowly.

The transfer of water from the carbonates to the lagoon or to the ocean is apparently very slow. It has been shown that the major fraction of tritium, for example, that has been transferred from the volcanics to the carbonates is still present in the carbonates 20 years after its release. It seems that the carbonates act as a large "mixing tank", spreading the water released from the volcanics both horizontally and vertically, with little release to the lagoons or to the ocean; the flux of tritium to the lagoons is expected to peak in the year 2000, at a value 10% above the 1997 level, in Fangataufa; the flux appears to have peaked in 1997 in Mururoa. The rate of transfer of radionuclides to the environment has been estimated by the IAEA team established to examine the radiological consequences of underground nuclear testing on the atolls (IAEA 1998b).

3. After 500 years, the flow pattern in the two atolls will be very close to the initial pattern before the tests. Some slow convective cells will remain in the chimneys, creating mixing and distorting the isotherms around each test site. Because most radionuclides will have decayed to insignificant levels (except plutonium), the potential consequences of the tests will depend on the rate of release and transfer of plutonium in the environment, as analysed by the IAEA (1998b).

4. In the very long term (i.e. around 10 000 to 60 000 years), when a new worldwide glaciation may cause the ocean level to drop by 100 or 150 m, the flow pattern may change considerably. A thick freshwater lens will develop in the carbonates and reach a thickness of 200–350 m. In this case, the location of the safety trials that were shot in the carbonates at depths below 280 m may now be within the freshwater lens. The plutonium present in these zones (as well as the plutonium transferred from the volcanics to the carbonates and sorbed to the carbonates) will still be present and may thus cause a threat to people living on the island and taking their water supply from deep wells drilled in the carbonates. It is likely that wells inadvertently drilled close to the locations of the safety trials may have plutonium concentrations that exceed drinking standards. But the probability that such a scenario will occur is rather low and furthermore very difficult to estimate.

Although these conclusions are based on many assumptions and on a limited set of observations, it is believed that they provide a reasonable picture of the situation. It is recommended, however, that a continuous monitoring of the hydrology of the site be maintained for at least 300 years, to verify that no unexpected release of radionuclides in the environment occurs. This duration of 300 years is consistent with the French regulations for the monitoring of surface storage of low-level radioactive wastes and with the recommendations recently made in a French parliamentary report (Bataille 1997) that Mururoa and Fangataufa be considered as waste storage sites.

This monitoring should be conducted in the boreholes available on the atolls, and in the lagoons, on a yearly basis. Additional monitoring studies should be conducted to interpret these measurements, thus improving the understanding of the transfer of radionuclides through the volcanics and the carbonates to the environment, and refining the predictions.

Appendix A

IGC BIOGRAPHICAL SKETCHES

Pierre Bérest graduated from Ecole Polytechnique (1970 and Ecole des Mines de Paris (Corps technique de l'état, 1973). He is an Associate Professor at Ecole Polytechnique, Palaiseau, France, as well as Director of the Laboratoire de Mécanique des Solides. Dr. Bérest is President of the French National Group of the International Society for Rock Mechanics and a member of the French Standing Committee for Nuclear Waste Disposal and the French Underground Storage Safety Commission.

Edwin T. Brown is a geomechanics engineer, with a Ph D in rock mechanics obtained from the University of Queensland, Australia, in 1969 and a D Sc(Eng), awarded by the University of London, U.K., in 1985 for published work in engineering rock mechanics. Currently, he is Senior Deputy Vice-Chancellor of the University of Queensland and was formerly Professor of Rock Mechanics and Dean of the Royal School of Mines at the then Imperial College of Science and Technology, London. Dr. Brown is a former President of the International Society for Rock Mechanics (1983–1987), a Fellow of the Australian Academy of Technological Sciences and Engineering and a Foreign Member of the Royal Academy of Engineering, U.K.

Ghislain de Marsily graduated as a mining engineer from the Paris School of Mines in 1963, and obtained a State Doctorate from the University of Paris in 1978. He is currently a Professor in the Earth Sciences and Natural Media Department of the University Pierre et Marie Curie (Paris VI) in Paris, France, where he teaches hydrology. Dr. de Marsily is a Fellow of the American Geophysical Union and a corresponding member of the French Academy of Sciences. He received an Honoris Causa Doctorate from the University of Quebec and was Editor of the *Journal of Contaminant Hydrology* for seven years. Dr. de Marsily has been a member of a Committee of the U.S. National Academy of Sciences for Environmental Management Technologies and is currently a member of the French Commission for the Evaluation of Research on Nuclear Waste Disposal.

Emmanuel Detournay graduated as a mining engineer from the University of Liège, Belgium, in 1976, and obtained a Ph D in geo-engineering from the University of Minnesota, Minneapolis, in 1983, where he is an Associate Professor in the Department of Civil Engineering. Prior to his current academic position, Dr. Detournay was a Senior Research Scientist at Schlumberger Cambridge Research, U.K.. His expertise is in petroleum geomechanics, with emphasis on mathematical modelling. He has

received several awards for his scientific and technological work, and he serves on the editorial boards of two international journals.

Charles Fairhurst obtained his Ph D in mining engineering from the University of Sheffield, England, in 1955. He is Professor Emeritus of Mining Engineering and Rock Mechanics, University of Minnesota, Minneapolis, U.S.A,; Chairman, Itasca Consulting Group, Inc., Minneapolis, U.S.A., and a member of the Advisory Committee on Nuclear Waste, U.S. Nuclear Regulatory Commission. A former President of the International Society for Rock Mechanics (1991–1995), Dr. Fairhurst is a member of the U.S. National Academy of Engineering and the Royal Swedish Academy of Engineering Sciences. He has received Honoris Causa Doctor of Engineering degrees from universities in St. Petersburg (Russia), Nancy (France), and Sheffield (England), and is an Honorary Visiting Professor at Tongji University (Shanghai, China).

Victor Nikolaevskiy obtained a Ph D in mechanics from Moscow State University, Russia, in 1960 and a D Sc (mining engineering) from the All-Union Institute of Oil and Gas, Moscow, Russia, in 1966. He was a Postdoctoral Fellow at The Johns Hopkins University (with C. Truesdell and J. Ericksen). Formerly a Professor of Applied Mathematics and Hydrodynamics at Moscow Civil Engineering University and the Moscow Gubkin Academy of Oil & Gas, Dr. Nikolaevskiy is now Head of the Laboratory of Geomechanics at the United Institute of Physics of the Earth, Russian Academy of Sciences. He is a member of the Russian National Committee on Theoretical and Applied Mechanics and the Russian Academy of Natural Sciences. From 1965 to 1982, Dr. Nikolaevskiy played a role in the Russian National Nuclear Program, specialising in mechanics of underground explosions and the dynamic strength of materials. His current fields of interest are the mechanics of geophysical processes and the applications of mechanics to oil and gas recovery.

Anthony Pearson obtained a Ph D in theoretical fluid mechanics from the University of Cambridge, England, in 1957. He is Professor Emeritus of Chemical Engineering at Imperial College, University of London, England, and is a Scientific Consultant for Schlumberger Cambridge Research. A former President and Gold Medalist of the British Society of Rheology, Dr. Pearson is a Foreign Associate of the U.S. National Academy of Engineering. He is an Honorary Professor at the universities of Wales and Birmingham, U.K.

Lloyd Townley obtained a Ph D in hydrology and hydrodynamics at the Massachusetts Institute of Technology, U.S.A., in 1983. Employed until recently by the Commonwealth Scientific and Industrial Research Organisation (CSIRO) in Perth, Western Australia, he became Perth Manager of the Centre for Groundwater Studies and a member of CSIRO's Minesite Rehabilitation Research Program. He has been a member of editorial boards for three international journals, as well as committees of the American Geophysical

Union and the International Association for Hydraulic Research. A former member of the National Committee on Water Engineering of The Institution of Engineers, Australia, Dr. Townley now works in private industry and is an Adjunct Associate Professor in the Department of Geology and Geophysics at the University of Western Australia.

Consultants

Peter Cundall obtained a Ph D in rock mechanics from Imperial College, London, in 1971. He has developed novel programmes and techniques in numerical modelling that find worldwide application in geomechanics, civil engineering and mining engineering. He is the originator of the distinct-element method that is used to model discontinuous systems, such as granular assemblies and rock masses, and is the chief developer of all Itasca Consulting Group programs: FLAC, UDEC, 3DEC and PFC. Dr. Cundall has published more than 60 papers on diverse topics, including shear-band genesis, micro-mechanics of soil and rock, fluid migration in jointed rock, and earthquake simulation of structures and foundations.

Branko Damjanac obtained a Ph D in civil engineering from the University of Minnesota in 1996. He has 15 years of experience in modelling and numerical simulations in the fields of rock mechanics and geomechanics for various research institutions and consulting companies. Dr. Damjanac currently is a Consulting and Code Development Engineer for Itasca Consulting Group, Inc., Minneapolis, U.S.A.

Pierre Perrochet has 15 years of experience in the fields of groundwater flow and transport modelling within various world-renowned research institutions. In 1992, he obtained a Ph D at the Swiss Institute of Technology (EPFL) in Lausanne, where, until recently, he was a Staff Scientist. Dr. Perrochet's research interests focus on regional fluid/thermal/chemical interactions, including theoretical and computational developments in numerical mathematics as well as the design of simulation methods operational for large, complex geophysical systems. He was recently elected Professor in quantitative hydrogeology at the University of Neuchatel, Switzerland.

Laurent Tacher obtained a Ph D in hydrogeology from the University of Neuchatel, Switzerland, in 1992. As a researcher at the Swiss Institute of Technology (EPFL) in Lausanne, he is mainly involved in geological and hydrogeological modelling, meshing and infography.

Appendix B

KNOWN NUCLEAR TESTS WORLDWIDE 1970–1998

Between 13 February 1960 and 27 January 1996, France carried out 210 nuclear tests, including 15 safety trials.

After completion of the final series of underground tests by France, on 27 January 1996, and 2 underground tests by China, also in 1996, no nuclear tests were reported worldwide until 11 May 1998, when India announced that it had exploded three underground nuclear devices (a fission device, a low-yield device, and a thermonuclear device) in the desert at Pokhram, 330 miles southwest of New Delhi. The Swiss Federal Institute of Technology reported a magnitude of 5.2, equivalent to approximately 10 kt (Sharma 1998) . Two additional explosions took place in India on 13 May 1998, followed by one on 30 May 1998.

Pakistan announced that it had detonated five tests on 28 May 1998, followed by one on 30 May 1998. Some seismic detection experts have suggested that fewer than five devices were detonated on 28 May 1998.

Details of all known tests worldwide (USA 1,030; USSR 415; France 210; China 45; U.K. 45, India 6; Pakistan 6) as of August 1998 are given in Table A.1, which is modified from the table produced by the U.S. Natural Resources Defense Council (NRDC) in 1997.

Table B.1 Known Nuclear Tests Worldwide: 1945–1969 (after NDRC, 1997)

Known Nuclear Tests Worldwide: 1945-1969 (National Resources Defense Council, 1997)

Year	*A = atmospheric; U = underground*										Total
	United States		Soviet Union		United Kingdom		France		China		
	A	U	A	U	A	U	A	U	A	U	
1945	1										1
1946	2										2
1947											0
1948	3										3
1949			1								1
1950											0
1951	15	1	2								18
1952	10				1						11
1953	11		5		2						18
1954	6		10								16
1955	17	1	6								24
1956	18		9		6						33
1957	27	5	16		7						55
1958	62	15	34		5						116
1959											0
1960							3				3
1961		9/1*	58	1			1	1			71
1962	39	55/2	78	1		2**		1			178
1963	4	41/2						3			50
1964		39/6		9		2		3	1		60
1965		37/1		14		1		4	1		58
1966		44/4		18			5/1*	1	3		76
1967		39/3		17			3		2		64
1968		52/4		17			5		1		79
1969		45/1		19					1	1	67

(continued on next page)

Known Nuclear Tests Worldwide: 1970-1996 (National Resources Defense Council, 1997)

Year	United States		Soviet Union		United Kingdom		France		China		Total
	A	U	A	U	A	U	A	U	A	U	
	A = atmospheric; U = underground										
1970		38/1		16			8		1		64
1971		23/1		23			5		1		53
1972		27		24			3/1		2		57
1973		23/1		17			5/1		1		48
1974		22		21		1	7/2		1		54
1975		22		19				2		`	44
1976		20		21		1		4/1	3	1	51
1977		20		24				7/2	1		54
1978		19		31		2		10/1	2	1	66
1979		15		31		1		10	1		58
1980		14		24		3		11/1	1		54
1981		16		21		1		12			5-
1982		18		19		1		9/1		1	49
1983		18		25		1		9		2	55
1984		18		27		2		8		2	57
1985		17		10		1		8			36
1986		14		0		1		8			23
1987		14		23		1		8		1	47
1988		15		16		0		8		1	40
1989		11		7		1		8/1			28
1990		8		1		1		6		2	18
1991		7				1		6			14
1992		6						0		2	8
1993								0		1	1
1994								0		2	2
1995								5		2	7
1996								1		2	3
Total	**215**	**815**	**219**	**496**	**21**	**24**	**50**	**160**	**23**	**22**	**2046#**
	1030		**715**		**45**		**210**		**45**		

* Number after / beginning in 1961 in the U.S. column represents PNEs (Peaceful Nuclear Explosion). In the French column number after / represents safety tests.
** All UK underground tests were conducted in the U.S.
*** Does not include Hiroshima, Nagasaki explosions Aug. 6, 9, 1945. These two explosions are included in some lists.
// Grand total includes one underground explosion by India conducted on May 18, 1974.

Appendix C

FRENCH UNDERGROUND TESTS AT CEP (PTC)

C.1 Seismic Estimates of Explosion Yield and Location of Underground Tests

C.1.1 Yield

As with earthquakes, underground nuclear explosions produce elastic waves that radiate from the explosion source. The amount of energy released at the source of the earthquake or explosion can be estimated from the amplitude and frequency characteristics of the waves as detected by sensitive seismograph stations around the world. This energy release is usually expressed as a volume *magnitude* (m_b), which is calculated as the logarithm of the amplitude of the P-volume waves (compressional or *push*) waves emanating from the energy source, corrected for attenuation.

> *The results, dependent on the test site, are not very precise. For example, it has been determined that the relative error in the yields announced by New Zealand for tests at the Pacific Test Centre is greater than 100% in 20% of the cases. Conventionally, it is estimated that, without calibration explosions, the seismic method provides an estimate with a margin of error of between -50% and +100%, that is, a factor of 2. This is at present the only method for non-intrusive monitoring of countries likely to carry out nuclear tests.*[*] *(Bouchez and Lecomte 1996, pp. 99–100)*

C.1.2 Location

As with earthquakes, the location at which an underground nuclear explosion occurs can be estimated by comparing the differences in time of arrival of the seismic waves from the explosion at many seismograph stations surrounding the explosion source. The accuracy of the location depends on the orientation of the array of stations around, and their distances from, the explosions source. Figure C.1 shows two attempts to locate underground nuclear tests conducted at the PTC. The limited accuracy is evident, but the tests are clearly associated with the PTC.

---

[*] More precise (i.e. within +/- 5%) determinations of the yield of an underground explosion are made by radio-chemical analysis of cores of the lava in the base of the explosion cavity obtained from on-site post-test drilling (see Bouchez and Lecomte 1996, pp. 52–53).

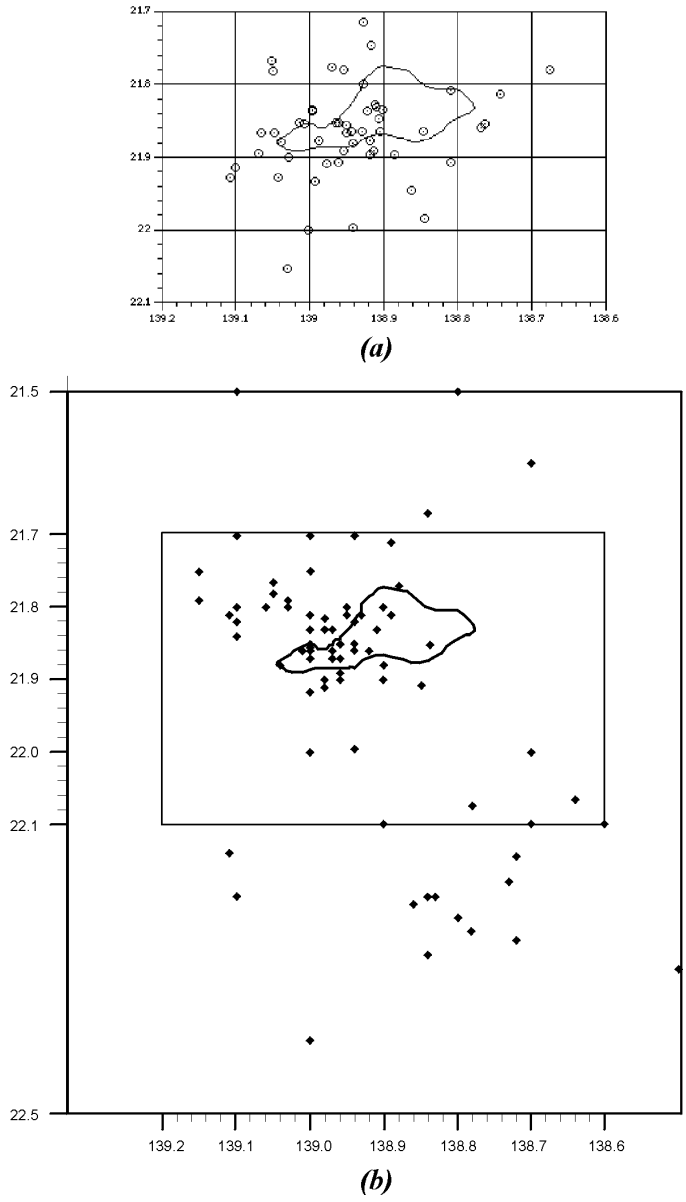

Figure C.1 Examples of two attempts to remotely locate underground nuclear explosions on Mururoa: (a) plot of NRDC seismic location coordinates (presented by B. Barrillot (1996), pp. 369–374, with reference to R. Norris et al., *Nuclear Weapons Handbook*, Vol. V, pp. 405–419); (b) based on data in *Bull. Int. Seismic Centre* and other sources (kindly furnished to Dr. V. Nikolaevskiy by Dr. E. Luquet). (It is seen that the locations are sufficient to identify the explosion source as being at the Pacific Test Centre, but not the position within the PTC.)

C.1.2.1 Rarotonga Observatory

The seismic station on the island of Rarotonga, one of the Cook Islands (New Zealand), is approximately 2000 km west of Mururoa and Fangataufa *on a direct uninterrupted line*. Separated from the PTC by the Pacific Ocean, Rarotonga also receives the so-called *T-(Third) wave* (much slower than a P-wave), which is generated in the water by the interaction of the explosion P-wave at the rock-water interface of the rim slope. The T-wave tends to propagate with little attenuation over a more or less constant depth interval known as the SOFAR Channel, defined by salinity and temperature characteristics of the ocean water. Upon reaching an island (e.g. Rarotonga), the T-wave becomes partially reconverted to a P-wave in the rock and is detected by the seismograph. With the relative proximity of Rarotonga to the PTC, plus the T-wave arrivals, this station *has a detectability close to 1 kilotonne* (Bouchez and Lecomte 1996, p. 96).

Figure C.2 shows the positions of seismic stations worldwide and reports the detection of high- and low-yield events at the PTC.

The magnitudes and yield estimates shown in the tables below are those provided by the Rarotonga seismic station.

C.1.3 Yield Estimates for Underground Tests at the PTC

Tables C.1–C.6 are published with the kind permission of Dr. Lars Erik de Geer, Chairman of Working Group No. 3, for the IAEA Study, The Radiological Situation at the Atolls of Mururoa and Fangataufa (see (IAEA 1998c)) and are referred to in Chapters 6 and 7 and Appendices S and T of this report. Explanation of the tables is as given in IAEA (1998c), p. 65:

> ***Estimated Yields and Other Data on the 147 Underground Nuclear Tests at CEP,[†] the French Test Site in the Pacific***
>
> *French underground nuclear test explosions at CEP. The tables give the official time, name and yield classification of all 147 French underground nuclear experiments in the Pacific . . . . It thus includes the 3 nuclear yield safety explosions and the 7 safety trials with no observed nuclear yield. The official yields are classified as less than 5 kt (A), between 5 and 20 kt (B) and above 20 kt but less than 150 kt (C). The non-nuclear yield safety trials are classified by the letter S. The numerical body wave magnitudes and yield estimates given are adapted from measurements at the New Zealand seismic laboratory at Rarotonga. The measured magnitudes are given with two decimals [m_b] and the estimated yields as integers in kt irrespective of actual accuracy. The smallest yield adopted is 1 kt for all but the non-*

[†] CEP - Centre d'Expérimentations du Pacifique (in English, PTC = Pacific Test Centre)

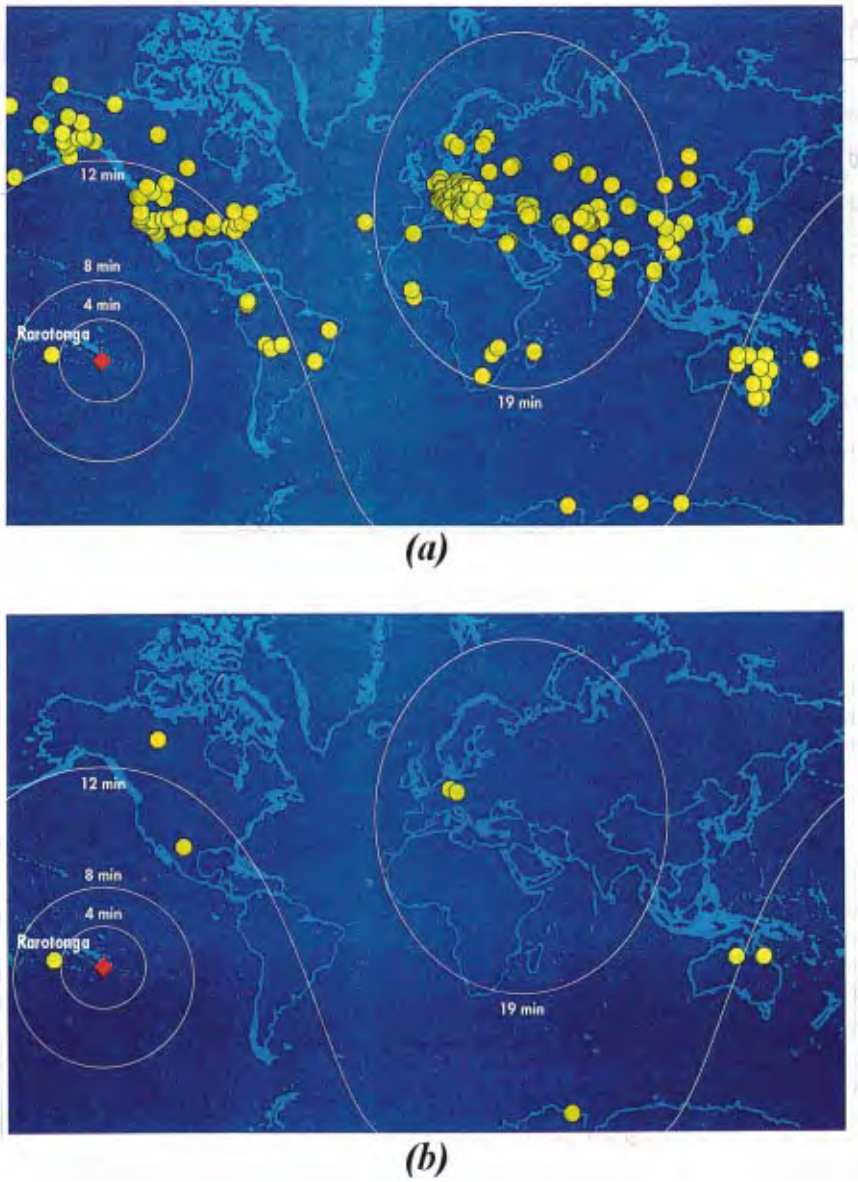

Figure C.2 Positions of seismic stations: (a) that recorded a high-yield underground test carried out at the PTC (The white contours represent the propagation times of the P-wave, which takes less than 20 minutes to reach the antipodes of the source.); (b) that recorded a low-yield underground nuclear test carried out at the PTC (Only a few particularly sensitive stations were able to detect this test.) (Bouchez and Lecomte 1996, Figs. 9.4 and 9.5)

nuclear yield safety trials. . . . the error can well be a factor of two or more in the estimated yields, with larger errors for the smaller explosions.

Table C.1 Tests conducted under Fangataufa rim

Year	Date	Time	Name	Category	m_b[a]	Y(kt)
1975	5 Jun	18:15	Achille	A	5.33	22
	26 Nov	0.48	Hector	B	5.23	17
			Total Fangataufa Rim		**2 tests**	**39 kt**

[a] m_b = measured magnitudes

Table C.2 Tests conducted under Fangataufa lagoon

Year	Date	Time	Name	Category	m_b	Y(kt)
1988	30 Nov	17:55	Cycnos	C	5.87	103
1989	10 Jun	17:30	Cyzicos	C	5.75	74
	27 Nov	17:00	Lycos	C	5.81	87
1990	26 Jun	18:00	Cypsélos	C	5.86	100
	14 Nov	18:12	Hyrtacos	C	5.92	118
1991	29 May	19:00	Périclyménos	C	5.88	106
1995	1 Oct	23:30	Ploutos	C	5.85	97
1996	27 Jan	21:30	Xouthos	C	5.58	46
			Total Fangataufa Lagoon		**8 tests**	**731 kt**

Table C.3: Tests conducted under Mururoa rim

Year	Date	Time	Name	Category	m_b	Y(kt)
1976	3 Apr	17:07	Patrocle	A	4.20‡	1
	11 Jul	0:30	Ménélas	B	5.09	11
	22 Jul		Calypso	S		0¶
	30 Oct	23:00	Ulysse A	A	4.20†	1
	5 Dec	23:00	Astyanax	A	4.20†	1
1977	19 Feb	23:30	Ulysse B	B	4.81	5
	19 Mar	23:01	Nestor	C	5.59	47
	2 Apr	23:30	Oedipe	A	4.20†	1
	28 Jun		Andromaque	S		0‡
	6 Jul	23:00	Ajax	B	5.40	27
	12 Jul		Clytemnestre	S		0‡
	12 Nov	1:30	Oreste	A	5.20	15
	24 Nov	17:00	Enée	C	5.61	53
	17 Dec	22:00	Laocoon	A	5.09	11
1978	27 Feb	23:00	Polyphème	A	4.03	1
	22 Mar	17:30	Pylade	A	5.09	11
	25 Mar	17:30	Hécube	A	4.20†	1
	1 Jul	17:00	Xanthos	A	4.20†	1
	19 Jul	18:00	Arès	B	4.40§	2
	26 Jul	23:00	Idoménée	A	4.73	4
	2 Nov	18:00	Schédios	A	4.55	2
	14 Nov		Aphrodite	S		0‡
	30 Nov	17:32	Priam	C	5.70	65
	17 Dec	18:04	Etéocle	A	5.15	13
	19 Dec	16:57	Eumée	B	5.09	11
1979	1 Mar	17:24	Penthésilée	B	4.95	7
	9 Mar	16:37	Philoctète	B	5.15	13
	24 Mar	16:38	Agapénor	B	4.95	7
	4 Apr	18:07	Polydore	B	4.85	6
	18 Jun	23:27	Pyrrhos	B	4.73	4
	29 Jun	18:56	Egisthe	C	5.40	27

continued on next page

‡None of these eleven (all category A) tests under the rim of Mururoa were detected at Rarotonga because of the weak signals. They were assigned a magnitude of 4.1, corresponding to a yield of 1 kt.

¶safety trial without nuclear yield(categories 6 and 7 in Table C.7)

§Two events were missed during record changes. Data from Yellowknife seismic array in Canada were adopted, in these cases, by the New Zealand laboratory after correction.

continued from previous page

Year	Date	Time	Name	Category	m_b	Y(kt)
	25 Jul	17:57	Tydée	C	5.90	115
	28 Mar	19:56	Palamède	A	5.15	13
	19 Nov	17:53	Chrysotémis	A	4.20†	1
	22 Nov	19:15	Atrée	A	4.73	4
1980	23 Feb	18:03	Thyeste	A	4.32	1
	3 Mar	17:56	Adraste	A	5.07	11
	23 Mar	19:37	Thésée	C	5.77	78
	1 Apr	19:31	Boros	B	5.25	18
	4 Apr	18:33	Pélops	B	4.37	2
	16 Jun	18:27	Euryple	C	5.37	26
	21 Jun	17:01	Ilus	B	5.01	9
	6 Jul	17:27	Chrysès	B	4.77	5
	9 Jul		Léda	S		0‡
	19 Jul	23;47	Asios	C	5.77	78
	25 Nov	17:53	Laerte	A	4.47	2
	3 Dec	17:33	Diomède	C	5.62	51
1981	27 Feb	23:28	Brotéas	A	4.95	8
	6 Mar	17:27	Tyro	A	4.40	2
	28 Mar	17:23	Iphiclès	B	4.77	5
	8 Jul	22:23	Lyncée	B	5.32	22
	11 Jul	17:17	Eryx	A	4.95	8
	18 Jul	17:43	Théras	A	4.47	2
	3 Aug	18:33	Agénor	C	5.21	16
	6 Nov	17:03	Léto	A	4.20†	1
	11 Nov	17:07	Proclès	B	4.55	3
	5 Dec	16:58	Cilix	B	4.81	5
1982	20 Feb	17:33 *	Aéropé	A	4.58	3
	24 Feb	18:15	Déiphobe	A	4.20†	1
	23 Mar	17:07	Evénos	A	4.20†	1
	31 Mar		Aéson	S		0‡
	27 June	17:00	Laodice	A	4.37	2
	1 Jul	17:02	Antilokos	C	5.28	20
	21 Jul	17:03	Pitane	A	4.47	2
	27 Nov	17:02	Procris	A	4.20†	1
1983	25 Apr	17:33	Automédon	A	4.25	1
	18 Jun	17:31	Bruisis	A	4.58	3
	20 Jul	20:30	Battos	B	5.04	10

continued on next page

continued from previous page

Year	Date	Time	Name	Category	m_b	Y(kt)
	3 Dec	16:58	Linos	A	4.73	4
1984	8 May	17:26	Démophon	A	5.32	22
	12 Jun	17:16	Aristée	B	4.47	2
	27 Oct	17:16	Achaon	B	4.54	3
	1 Dec	16:51	Milétos	A	4.17	1
1985	30 Apr	17:29	Ceryon	B	5.12	13
	3 Jun	17:30	Talaos	B	5.07	11
	24 Oct	17:50	Héro	A	4.47	2
	24 Nov	16:01	Zétès	B	4.81	5
1986	26 Apr	17:02	Hyllos	B	4.77	5
	6 May	16:58	Céto	A	4.75	5
	27 May	17:15	Stéhénelos	B	4.67	4
	10 Nov	16:58	Hésione	A	4.87	6
	6 Dec	17:10	Pénéléos	A	4.99	9
1989	25 Nov		Daunus	S		0‡
Total Mururoa Rim					**76 tests**	**970 kt**

Table C.4: Tests conducted under Mururoa lagoon

Year	Date	Time	Name	Category	m_b	Y(kt)
1981	10 Apr	17:57	Clymène	B	4.95	8
	8 Dec	16:47	Cadmos	B	5.17	15
1982	20 Mar	17:03	Rhésos	B	5.23	17
	25 Jul	18:02	Laios	C	5.65	56
1983	19 Apr	18:53	Eurytos	C	5.53	40
	25 May	17:31	Cinyras	C	5.55	42
	28 Jun	17:46	Oxylos	B	5.46	33
	4 Aug	17:14	Carnabon	C	4.95	8
	7 Dec	17:28	Gygès	B	5.17	15
1984	12 May	17:31	Midas	C	5.65	56
	16 Jun	17:44	Echémos	C	5.47	34
	2 Nov	20:45	Acaste	C	5.47	34
	6 Dec	17:29	Memnon	C	5.63	53
1985	8 May	20:28	Nisos	C	5.82	89
	7 Jun	17:40	Erginos	B	4.77	5
	26 Oct	16:35	Codros	C	5.25	18
	26 Nov	17:42	Megarée	C	5.64	54
1986	30 May	17:25	Galatée	C	5.43	31
	12 Nov	17:02	Nauplios	B	5.34	23
	10 Dec	17:15	Circé	C	5.45	32
1987	5 May	16:58	Jocaste	B	4.77	5
	20 May	17:05	Lycomède	C	5.42	30
	6 Jun	18:00	Dircé	B	4.54	3
	21 Jun	17:55	Iphitos	C	5.17	15
	23 Oct	16:50	Hélénos	C	5.62	51
	5 Nov	17:30	Pasiphaé	B	5.25	18
	19 Nov	16:31	Pélée	C	5.69	62
	29 Nov	17:59	Danaé	B	4.65	3
1988	11 May	17:00	Nélée	C	5.28	20
	25 May	17:01	Niobé	C	5.79	83
	16 Jun	17:15	Antigone	A	4.77	5
	23 Jun	17:31	Déjanire	B	5.42	30
	25 Oct	17:00	Acrisios	A	4.37	2
	5 Nov	16:30	Thrasymedès	C	5.59	47
	23 Nov	17:01	Phérès	C	5.57	44
1989	11 May	16:45	Epéios	B	5.21	16

continued on next page

continued from previous page

Year	Date	Time	Name	Category	m_b	Y(kt)
	20 May	17:59	Técmessa	A	4.47	2
	3 Jun	17:30	Nyctée	C	5.28	20
	24 Oct	16:30	Hypsipyle	C	5.28	20
	31 Oct	16:57	Erigone	B	5.28	20
	20 Nov	17:29	Tros	B	5.40	28
1990	2 Jun	17:30	Telèphe	B	5.42	30
	7 Jun	17:30	Megapenthès	B	4.65	3
	4 Jul	18:00	Anticlée	B	5.25	18
	21 Nov	17:00	Thoas	C	5.49	36
1991	7 May	17:00	Melanippe	A	4.25	1
	18 May	17:15	Alcinoos	C	5.21	16
	14 Jun	18:00	Pitthée	C	5.40	28
	5 Jul	18:00	Coronis	A	3.80	1
	15 Jul	18:10	Lycurgue	C	5.47	34
1995	5 Sep	21:30	Thétys	B	4.93	8
	27 Oct	22:00	Aepytos	C	5.52	39
	21 Nov	21:30	Phégèe	C	5.22	17
	27 Dec	21:30	Thémisto	C	5.29	
		Total Mururoa Lagoon			**54 tests**	**1443 kt**

Table C.5 Number and yield of tests of Mururoa and Fangataufa

Location	Number	Total Yield (kt)	Average Yield (kt)
Mururoa Rim	83	970	13 [a]
Mururoa Lagoon	54	1443	27
Mururoa Total	137	2413	19
Fangataufa Rim	2	39	20
Fangataufa	8	731	91
Fangataufa Total	10	770	77
Total CEP	147	3183	23

[a] Average yields are for nuclear tests only — i.e. safety trials are excluded.

Table C.6 Comparison of estimates of total yield (kt) based on seismic records with information provided by French authorities

Atoll	French Values	This Study	
		Best Estimate	Range (95% confidence limits)
Mururoa	2400	2413	2390–3065
Fangataufa	800	770	641–1174
Total	3200	3183	3180–4058

C.1.4 Potential Releases of Radionuclides from Underground Testing at the PTC

Most cases of early tritium release are considered by CEA scientists to be associated with the CRTV tests. As indicated in Table C.7 and Figure C.3 (developed primarily for the IAEA study of radionuclide releases (IAEA 1998b)), no releases have been detected to date for 121 of the 147 underground tests. This suggests that the covers overlying the chimneys produced by these tests are sufficiently intact and provide substantial barriers to groundwater and radionuclide flows from the chimney.

Table C.7 Categories of Sources and Potential Release of Radionuclides Produced by Nuclear Testing in Mururoa and Fangataufa (after IAEA 1998b)

Category 1	the majority of the nuclear tests (121 of the 137) — i.e. where a significant thickness of essentially undamaged volcanic cover exists above the test chimney (see Note 1 below)
Category 2	4 tests where tritium releases to the karst have been detected even though the minimal depth of (low-permeability) volcanic cover should be high enough (140 m in the case of the Lycos tests at Fangataufa) to prevent this. French Liaison Office suggests that, in these cases, the original volcanic cover was relatively weak, such that drilling of the 1.5-m borehole (for installation of the nuclear device at depth) created an annulus of damaged rock around the hole. This annulus acts as a high-permeability conduit from the chimney to the base of the carbonates, allowing early release of tritium from the chimney.
Category 3	12 relatively shallow CRTV (Chimney Reaching Top of the Volcanism) tests in which the chimney came into immediate contact with the base of the carbonates (karst). All CRTV tests are on Mururoa [7 tests carried out (1976–81) in test area 1; 4 in test area 2 (1976–80); 1 in test area 3 (1976–80)]. Together with Category 2 tests, the CRTV tests would produce a total of 16 tritium (and strontium, caesium) release locations on the atolls. Measurements reported in DIRCEN/CEA Document No. 10 (Figs. 1-4;8) suggest at least 4 "leaky" holes at Mururoa, and 1 (Lycos) at Fangataufa. (Some of the concentration contours shown in these diagrams — especially for Mururoa — could encircle more than one leaky hole (i.e. the releases could be produced from several such holes relatively close to each other).
Category 4	3 safety trials conducted (1976–81) in test area 2 (Mururoa rim) at a depth greater than 280 m in the carbonates, in which a (small) nuclear explosion (average yield 0.15 kt) resulted from each trial. Assuming that the resultant cavity radius (R_c) scales according to the same cube-root law as the cavities in the volcanic rock (i.e. $R_c = 12\ Y^{1/3}$ m, where Y is the nuclear yield in kt), we obtain, for $Y = 0.15$ kt, a cavity radius of approximately 7 m. It is probably sufficient to assume that the radionuclide inventory in each of these three trials will be similar in composition to those in the larger tests, but directly proportional, in quantity, to the yield of the explosive. (See Notes 2 and 3 below.)
Category 5	4 safety trials conducted in test area 1 (Mururoa rim), at a depth greater than 280 m in the carbonates, where there was no nuclear yield. In these cases, the plutonium contained in the device that was tested (estimated to be 3.7 kg plutonium oxide per trial) remains at depth. There are essentially no craters associated with these safety trials, but radial fracturing will occur around the seat of the chemical explosion (see (IAEA 1998c), App. 1, pp. 81–82, for names and dates of trials; also see Notes 2 and 3 below)
Category 6	3 safety trials conducted at depth in the volcanics (Mururoa rim). None of these trials resulted in a nuclear explosion. There are essentially no craters. Approximately 3.7 kg of plutonium (per trial) remains at depth from these trials. (see (IAEA 1998c) and Notes 2 and 3 below)
Category 7	Radioactive waste produced by surface safety trials has been deposited in two shafts on the Mururoa rim, just west of test area 1 in the volcanic rock, at a depth of about 1200 m. The total quality of alpha activity was 10 TBq, equivalent to the plutonium from one trial. Because most of the plutonium was incorporated into cement and buried at depth in the volcanic zone, this waste represents a much lower safety hazard than the safety trials (Categories 4 and 5) carried out in the carbonate zone.

Note 1 The 134 underground tests listed in the Appendix to Bouchez and Lecomte (1996) include the 3 Category-4 safety trials, but do not include the 6 tests (4 at Mururoa, 2 at Fangataufa) carried out in 1995–96 (see also the table in Barrillot (1996), p. 178).

Note 2 It is probable that explosions in the carbonates will produce compaction and pore collapse, leading to a lower permeability in the zone around the seat of the explosion—so it would be conservative to assume no permeability change due to the explosion

Note 3 The safety trials were all conducted in the general vicinity of Dora/Denise (at the westerly end of test area 1) on Mururoa—i.e. slightly east of the most northerly portion of the Mururoa rim.

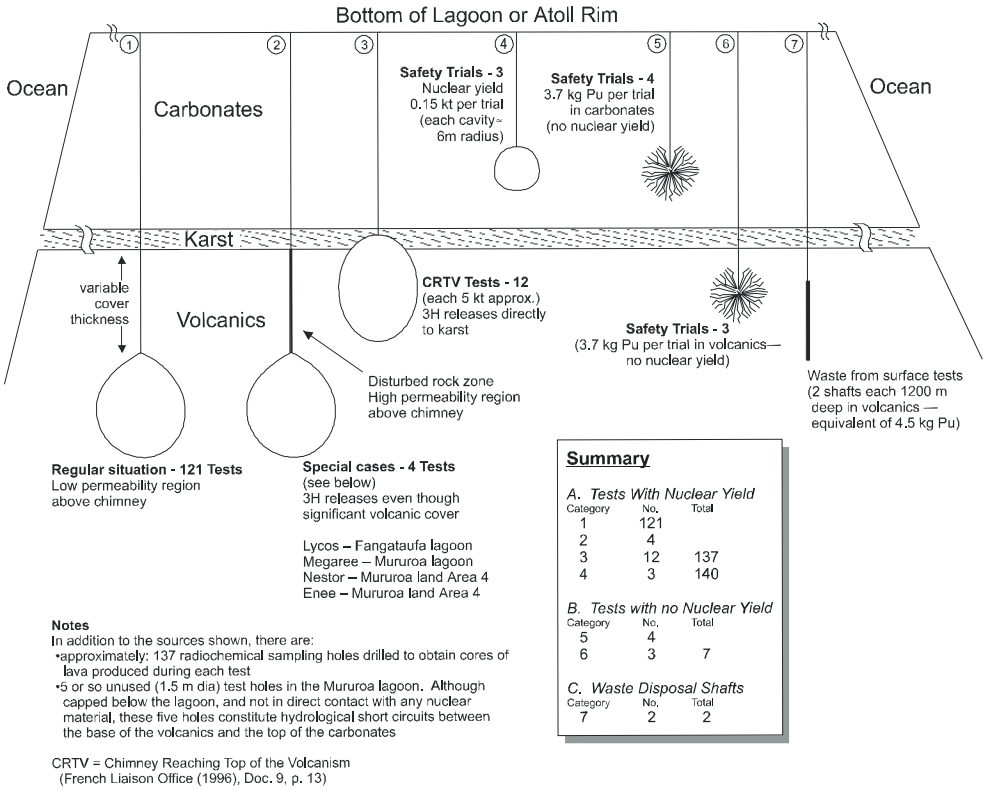

Figure C.3 Sources of potential release of radionuclides produced by nuclear testing in Mururoa and Fangataufa

Appendix D

CONTAINMENT AND VENTING OF UNDERGROUND NUCLEAR EXPLOSIONS

The principal reason for the decision to switch from atmospheric to deep underground nuclear tests was the desire to contain the explosions* — i.e. to prevent the direct release of radionuclides into the atmosphere, a phenomenon known as *venting*.

The United States has defined two types of Containment Failure (OTA 1989) — ventings and seeps.

> '*Ventings' are prompt, massive uncontrollable releases of radioactive materials. They are characterized as active releases under pressure, such as when radioactive material is driven out of the ground by steam or gas." "Baneberry", in 1970, is the last example of an explosion that "vented".*
>
> '*Seeps', which are not visible, can only be detected by measuring for radiation. Seeps are characterized as uncontrolled, slow releases of radioactive material with little or no energy.*
>
> *Late-time seeps are small releases of noncondensable gases that usually occur days or weeks after a vertical drillhole test. The noncondensable gases diffuse up through the pore spaces of the overlying rock and are thought to be drawn to the surface by a decrease in atmospheric pressure (called "atmospheric pumping").*

The Baneberry explosion referred to in the quotation produced a spectacular plume of steam and dust and involved a large ($2.5 \cdot 10^{17}$ Bq) release of radionuclides to the atmosphere, reaching several hundreds of metres into the sky (see OTA (1989), p. 33). The event prompted a major review of U.S. rules for containment of underground explosions, particularly with respect to the depth of burial of the explosive device. Prior to the Baneberry explosion in 1970, the U.S. rule for containment, based on the cube-root scaling law (i.e. that the linear dimensions of explosion effects in rock scale directly as

*The first underground test, code-named Pascal A, was conducted by the United States on 26 July 1957 at the Nevada Test Site. The device was detonated at the bottom of a 152-m deep "open" hole. (Even so, 90% of the fission products were contained underground (OTA 1989)).)

the cube root of the explosive energy) was, approximately (when converted into metric units)

$$D.O.B. = 91.5\,Y^{1/3} + (60\sim100)\,m \tag{D.1}$$

[The actual rule, expressed in feet, was Depth (ft) = 300 $Y^{1/3}$ "plus a few hundred feet".] After Baneberry, the rule was revised to

$$S_d = \frac{D.O.B.}{Y^{1/3}} = 122\,m/kt^{1/3} \tag{D.2}$$

where $D.O.B.$ is the actual depth of burial in m, Y is the explosive yield in kt, and S_d is the scaled depth of burial.

As indicated in the quotation above, according to U.S. authorities, there have been no ventings of U.S. underground nuclear explosions since the revised containment rule was adopted.

Presumably, this statement includes Cannikin, a test of the Spartan warhead conducted on Amchitka Island, Alaska, on 6 November 1971, which had *"a reported yield of 'less than five megatons'. This test, by far the highest-yield underground test ever conducted by the United States, was too large to be safely conducted in Nevada."* † (OTA 1989). Additional details of the Cannikin test can be found in Claassen (1978).

The "less than 5 Mt" yield of the Cannikin test was greater than the total yield of all 147 underground tests on Mururoa and Fangataufa. The latter total is given as 3.2 Mt by CEA; essentially the same value has been estimated from independent seismic observations (see App. C).

According to data provided by CEA (DIRCEN/CEA Document No. 6, Fig. 6, shown as Fig. D.1), the scaled depths, S_d, of underground tests on Mururoa and Fangataufa were considerably greater than those used by the United States — viz $800 > S_d > 170$ m/kt$^{1/3}$, for 137 of the 147 tests conducted; S_d was greater than 800 m/kt$^{1/3}$ for the remaining 10 tests. Because the maximum depth for tests on the atolls was 1100 m, the lower limit of 170–200 probably applies to the higher yield tests.

The Atkinson Mission (New Zealand MoFA 1984) to Mururoa and Fangataufa concluded that

> *venting of gaseous and volatile fission products from the test sites does occur at the time of detonation. There is evidence that the amount is greater than would be expected simply through the back-packing of the placement bore being "less than perfect".*

† *The predictions of ground motion suggested that an unacceptable amount (in terms of claims and dollars) of damage would occur to structures if the test were conducted in Nevada* (OTA 1989).

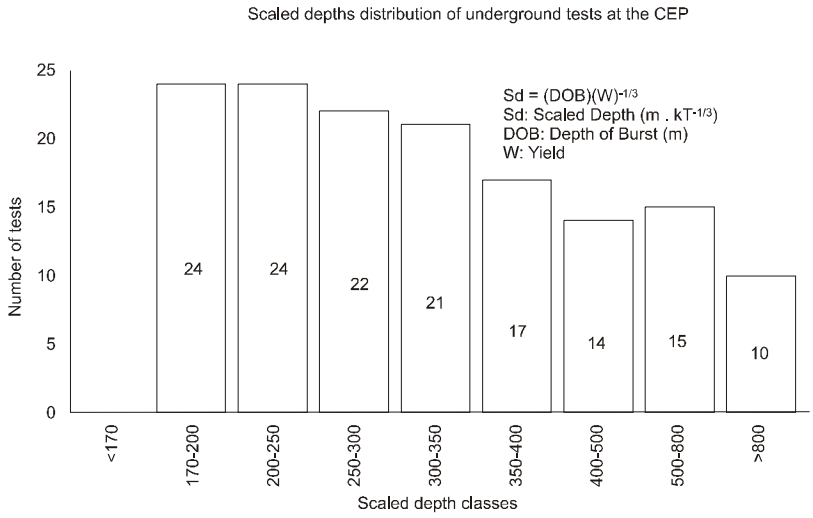

Figure D.1 Distribution of scaled depth of burial "burst" of underground tests at the CEP (DIRCEN/CEA)

The evidence cited is based on a test to measure the concentration of tritium (^{3}H) in air, sampled from the coral rim very close to the surface on Mururoa in test area 2 (see Fig. 1.17. A concentration level of 500 Bq was measured in the sampled air. It was noted (New Zealand MoFA 1984) that this

> *. . . corresponds to 4.8 Bq m^{-3} in the sampled air. An acceptable derived air concentration (DAC) for members of the general public exposed continuously to tritiated water vapour is 2.7 kBq m^{-3} (1/100 of the occupational DAC), a factor of 560 times that measured. . . . . Were it not for weapon testing by France, the tritium level in surface waters near Mururoa would be about 0.1 Bq l^{-1} — a factor of 5000 times lower than that measured in the absorbed water vapour.*

The Atkinson Mission visited Mururoa 25–29 October 1983. A total of 27 underground tests were conducted in area 2, including 13 during the period 1976–80 and 14 between 1981–1986 (see Fig. 1.17). The last two rim tests prior to the visit took place 18 June and 20 July 1983 (not necessarily in test area 2). It seems difficult, therefore, to attribute the tritium concentration measured in a test in October 1983 to a release coincident with a specific explosion.

Continuing seeps, or releases, of tritium, strontium and caesium from a number of tests into the lower carbonates have been observed and are continuously monitored by CEA scientists (DIRCEN/CEA Document No. 9). These results are considered in detail

in Appendices S and T of this (IGC) report, as a means of assessing the velocity of groundwater flow predicted by numerical modelling.

It would seem that the releases observed at Mururoa and Fangataufa, both during the Atkinson mission and by CEA scientists, fall within the U.S. definition of seeps, rather than ventings. In summary, it seems very probable that venting of underground tests as defined by the United States has not occurred at Mururoa and Fangataufa.

Appendix E

EXPLOSIVE INJECTION OF RADIONUCLIDES BEYOND THE CAVITY WALL

The discussion of fracturing of the rock mass in Section 1.3 of the Overview (Ch. 1) was concerned exclusively with the effects of the outgoing shock wave. It was asserted that the triaxially compressive nature of the outgoing wave would not allow extensile (i.e. "opening") fractures to occur; hence, no radionuclides could enter the rock mass around the cavity. In addition, elastic rebound of the rock mass, after outward motion of the cavity ceases, tends to produce a compressive stress *containment cage* acting tangentially around the cavity wall. This stress cage will tend to close any radial extensile fractures that may have begun and will prevent new fractures from starting. However, observation of what has been referred to as *prompt* or *early-time* injection of thin veins of radioactive lava in this region tends to question this assertion. U.S. scientists have also suggested that the gas pressure history at later times during the explosion process may allow tangential tensions to be generated in the cavity wall. These may be sufficient to produce fractures that could then propagate, resulting in venting of cavity gases. These phenomena are discussed below. (This appendix does not consider the trace quantities of radionuclides (e.g. iodine-131) sometimes detected due to releases after drilling to sample the cavity lava (Bouchez and Lecomte 1996, p. 52)).

E.1 Stress Containment Cage

Figure E.1 and explanations are taken from the report *The Containment of Underground Nuclear Explosions* (OTA 1989).

> *At first, the explosion creates a pressurized cavity filled with gas that is mostly steam. As the cavity pushes outward, the surrounding rock is compressed* [Fig. E.1a]. *Because there is essentially a fixed quantity of gas within the cavity, the pressure decreases as the cavity expands. Eventually the pressure drops below the level required to deform the surrounding material around the cavity. Once the shock wave has passed, however, the material tries to return (rebound) to its original position* [Fig. E.1c]. *The rebound creates a large compressive stress field, called a "stress containment cage", around the cavity* [Fig. E.1d]. *The physics of the stress containment*

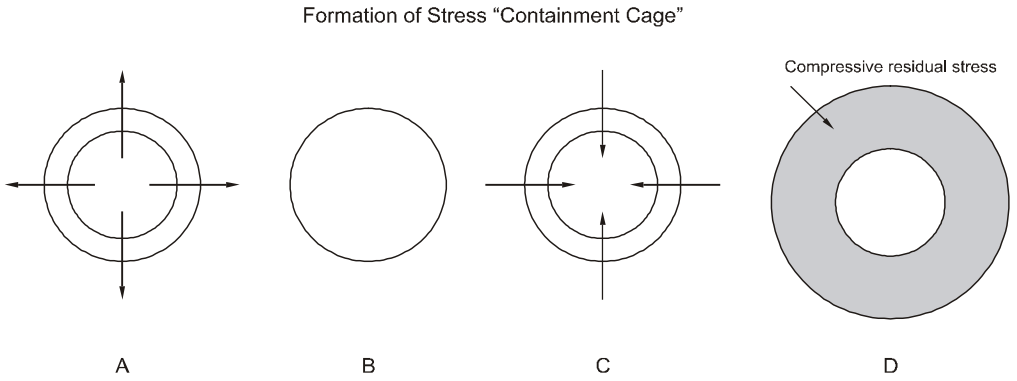

1) Cavity expands outward and deforms surrounding rock. 2) Natural resistance to deformation stops expansion. 3) Cavity contracts (rebounds) from elastic unloading of distant rock. 4) Rebound locks in compressive residual stress around cavity.
SOURCE: Modified from Lawrence Livermore National Laboratory.

Figure E.1 Formation of stress containment cage (OTA, 1988)

> *cage is somewhat analogous to how stone archways support themselves. In the case of a stone archway, the weight of each stone pushes against the other and supports the archway. In the case of an underground explosion, the rebounded rock locks around the cavity forming a stress field that is stronger than the pressure inside the cavity. The stress "containment cage" closes any fractures that may have begun and prevents new fractures from forming.*

Of course, the stress cage is destroyed once chimney collapse occurs, but the cage would exist long enough to inhibit the formation and propagation of extensile cracks (i.e. during the initial phase of high cavity temperature and gas pressure).

The amount of stored (i.e. elastic) energy available to "drive" the rebound will depend on the elastic properties and strength of the rock mass. If the rock mass is fractured, it will have, effectively, a low modulus and a low strength. This, in turn, will tend to result in low stored energy, low rebound and low containment stress. Proffer and Halda (1993), discussing tests at the NTS (USA), comment as follows:

> *Small scale laboratory and field experiments have verified that such residual stress fields are formed by explosions conducted in homogeneous materials. However, the few successful measurements obtained within the severe environments produced by nuclear events suggest that the actual residual stresses may be weaker than calculated or may decay very rapidly. It has been conjectured that the absence or reduction of residual stress might be a consequence of the faults and joints which are present in the geologic host medium.*

> *Shear displacements of faults and joints, sometimes extending a meter, are routinely observed on reentry. Since these non-homogeneous discrete motions occur within the confines of the residual stress fields calculated by the continuum models, they clearly have the potential to significantly alter the formation of a confining stress field.*

In their paper, Proffer and Halda (1993) describe numerical modelling studies using the discontinuum code UDEC (Itasca 1993) , in which discrete joints and faults are included. It is found, as may be expected, that the magnitude of stress containment generated by dynamic elastic rebound of a jointed mass compared well to that obtained in the same rock mass when there are no joints.

It also seems probable that time-dependent relaxation of stresses acting on joints and fractures will progressively reduce the stress containment, even before the onset of chimney collapse.

E.2 Prompt (Early-Time) Injection

Post-test excavations at the NTS have revealed (Smith et al. 1996) occasional thin "stringers", or fine fractures, in the region $R_c < R < (2-3)\ R_c$ beyond the cavity. These fractures contain thin coatings of lava, similar in chemical composition to the lava within the cavity. This is a strong indication that these stringers are formed by injection of radionuclides directly from the cavity — i.e. propagation of one or more tensile fractures directly from the cavity into the rock beyond. It is believed that these fractures, which may have been present in the rock before the explosion, are generated or opened by gas pressure in the cavity **after** passage of the shock wave.

U.S. scientists indicate that overlap between the later stages of the outgoing wave and the wave reflected from the surface can result, in some cases, in a brief period during which a net tangential tension may develop at the cavity wall, opening a fracture into which very hot cavity gases are injected. These gases melt the fracture surfaces — the molten lava then traps the radionuclides in the gases and solidifies.

The scaled depths of burial for tests on the atolls were considerably greater than at the NTS. It is not known whether such wave interaction would be able to generate a net tension sufficient to allow this injection. CEA scientists indicated that no such stringers have been encountered in post-shot drilling at CEP. Because the horizontal stress is less than the vertical stress in the rock, it seems likely that any such fractures at CEP would tend to propagate vertically upward — i.e. in the region that later collapses to form the cavity chimney — so that some part of any such induced fractures would be incorporated within the chimney. (However, the same argument could be applied to tests at the NTS.)

Also, the in-situ stress state may not have the dominant influence on the orientation of fractures in the immediate vicinity of the cavity, especially those occurring at this early period in the explosion loading history. As outlined earlier in this section, it is not

considered feasible, in view of the highly compressive environment during shock wave loading, that these stringers are generated during passage of the outgoing shock wave only.

E.3 Late-Time Cavity Pressure Increase

The cavity pressure history of an underground explosion is important to understanding containment phenomena and test design. If the pressure some time after passage of the shock wave is sufficient to generate tensile tangential stresses around the wall of the cavity, it may be possible to generate and extend tensile fractures directly from the cavity into the rock.

Peterson et al. (1991) have examined the possibility that, as the cavity pressure gradually cools, heat conducted from the gas into the cooler rock walls may cause spalling of rock from the wall as water in the porous, saturated rock is vaporized. The authors refer to this as a "popcorn"-ing effect, in which vaporization of water in the pores causes the rock to spall, the heat of the spalled rock and vapour then becoming available to "re-heat" the cavity gases. The calculations involve considerable uncertainty concerning

> *how rapidly energy can be transferred among the various different phases and the different regions within the cavity. This is important because of the great variation in the specific energy of the entering material which depends mainly on its original range from the explosion. Moreover, at relatively late times, condensed rock phases may exist as liquid pools or frozen crusts, making it less likely that these phases will remain in thermal equilibrium with the gas phase. Thus, we cannot accurately know the amount of energy residing within the gas phase which exerts pressure on the cavity wall. Despite these complexities, it is possible to place useful bounds on the amount and timing of material mixing and the resulting pressure and temperature within the cavity.*

Material above the amount produced by shock melting

> *can be mixed into the cavity by the thermally induced pop-corning process, which will remain operative as long as the cavity gas is hotter than the boiling temperature of water (e.g. 585 K) corresponding to the instantaneous cavity pressure (e.g. 98 bar). For cavity temperatures greater than this, heat transfer from the cavity gas to the wall will vaporize the pore water within the rock, causing microfracturing and/or spalling of the wall material. It is important to realize that this process is not simply a consequence of the final post-shock state of the wall, but rather depends on the current state of the cavity. Thus, to estimate the amount of material which can*

> *be thermally spalled into the cavity, it is necessary to determine the cavity temperature and pressure as a function of the added mass. This was accomplished by post processing of a SKIPPER/CHEST* [the numerical code used by the authors] *ground motion simulation in which the cavity mass had been held constant at 18 Mg/kt. After the motion had stopped, spherical shells of previously-shocked wall material were incrementally added to the cavity, and the equilibrium temperature and pressure were calculated based on the evolving values of the mass. energy, and volume within the cavity.*
>
> *[*Figure E.2*] illustrates the variation of cavity pressure and temperature with added mass, assuming thermal equilibrium within the cavity. Starting from a highly dissociated vapor state at nearly 10,000 K, the addition of roughly 50 Mg/kt of wall material cuts the pressure in half, from 96 to 48 bars, and reduces the cavity temperature to the rock vaporization temperature of 3740 K (corresponding to the 48 bar pressure). With further addition of mass, the temperature continues to decrease, because the added mass reduces the energy per unit mass. Conversely, the pressure begins to gradually increase because (1) the energy of the incoming rock contributes to the energy of the cavity and (2) the gamma (gas expansion coefficient) of steam is greater than that of rock vapor. This upward trend persists for mass additions up to 1450 Mg/kt, but the gradually rising pressure never exceeds the initial value of 96 bars. It is noted that such increases in cavity pressure have been observed in the field . . . and they are, according to our model, a direct consequence of heat transfer from condensed rock to steam vapor, i.e. a consequence of equilibration.*

E.4 Discussion

The mechanism considered by Peterson et al. (1991) has some features similar to the early time shock wave shattering of rock due to vaporization of interstitial water, described in Bouchez and Lecomte (1996, p. 4 and quoted in Section 1.3 of the Overview). These later-time effects are a consequence of the slower process of heat transfer from the cavity gas to the cooler rock mass — and a subsequent transfer back into the cavity. The time scale associated with the behaviour shown in Figure E.2 is of the order of minutes~some tens of minutes after the explosion. (Comparison with Fig. 1.7 illustrates the evolution of cavity temperature from the early cavity expansion phase into the final cavity regime.)

The late-time increase in cavity pressure, albeit small, possibly could provide the conditions necessary to allow opening of cracks directly from the cavity wall and escape of radionuclide-contaminated gases into the rock mass. Because the lateral stresses in

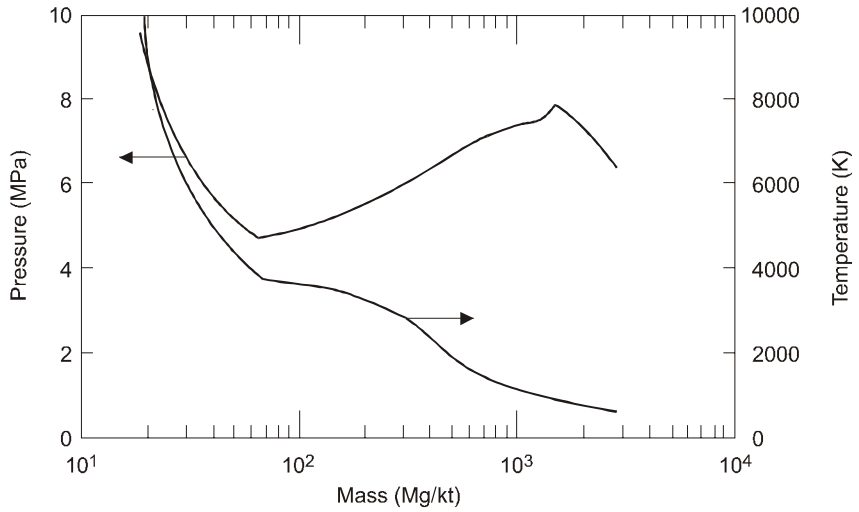

Figure E.2 Cavity pressure and temperature versus the amount of mass during mixing and equilibration of wall material (Pressure and temperature are calculated from known values of cavity mass, volume, energy and composition.) (Peterson et al. 1991)

situ are lower (in compression) than the vertical (or overburden) stresses (both at the NTS and the atolls), fractures would tend to extend preferentially vertically upward. Although the fractures will tend to extend as enlarging elliptical "discs" (with the (imaginary) lower vertex within the cavity), much of the fracture would probably be included in the chimney collapse when it occurs. Chimney collapse will usually start when the cavity pressure falls below lithostatic (i.e. due to the weight of the overlying rock) pressure, which is of the order of 14 MPa at 600 m and 25 MPa at 1100 m depth; thus, the phenomenon considered in Figure 1.16 may be eliminated by chimney collapse.

The possibility that venting would occur (as in the U.S. definition — see App. D) was a principal concern that helped to stimulate the interest in late-time cavity pressures. Given the greater depths of burial of tests at the Pacific Test Centre compared to those of the NTS, the relative probability of this phenomenon should be reduced at Mururoa and Fangataufa.

Ultimately, the most direct information on the containment achieved in the underground tests on Mururoa and Fangataufa is provided by the observed releases of tritium, which travels with the (particle) velocity of the groundwater. From evidence to date, discussed in Appendices S and T, it would appear that the majority of the tests were fully contained, with late-time seeps (using the U.S. terminology) at 16 or so (of the 147) test locations — most of which are tests where the cavity chimney reached the top of the volcanism (i.e. the CRTV tests). (See Fig. 1.17, Fig. C.3 and Table C.7.)

Appendix F

INFLUENCE OF HOLLOW SPHEROIDAL INHOMOGENEITIES IN A POROUS MEDIUM

It is instructive to examine the general influence of one or more heterogeneities in the rock structure on the permeability of the rock or rock mass. We will assume that the inhomogeneity can be represented as a spheroidal void, such as shown in Figure F.1. (The spheroid is an ellipsoid that is generated by revolving an ellipse about one of its axes.) On the micro-scale, this void could represent pore spaces between grains in a porous medium, the solution cavities often found in carbonate rock, etc. On the larger scale, the void could be a nuclear explosion cavity, lava tube, etc. (These results are based on studies by Janković (1997); see also Janković and Barnes (1997). Note that the numerical codes used by Janković allow the inhomogeneities to be of lower or higher permeability than the surrounding medium. Since we are concerned here with "cavities" or "voids" in the medium, we have focused attention on inhomogeneities that have a much higher permeability than the surrounding medium.)

The inhomogeneities were represented in a computer (potential flow) simulation by spheroids of high permeability in a three-dimensional medium of average conductivity (i.e. of the order of 10^{-5} m/s). Note that this computer code allows computation of heads only. Actual flow (streamlines) would occur along the local head gradient — i.e. perpendicular to the contours of constant heads.

Figure F.1 shows a typical result for flow around a highly conductive spheroidal cavity (void). The cross-section shown corresponds to the horizontal plane. The semi-major axis of the prolate spheroid is 5 m, the semi-minor axis is 2 m, and it is centred on the xyz-origin. A uniform flow is applied upstream (direction of -x) at a rate corresponding to a head drop of 10 cm per metre from left to right in the x-direction (i.e. the direction of x increasing) along which the spheroid is aligned. The x-axis is also the axis of (rotational) symmetry for the spheroid.

In the absence of the cavity, a particle travelling in the water from left to right in the x-direction (i.e. down the head gradient) would follow a path parallel to the x-axis — i.e. perpendicular to the local head contour. After the water-filled cavity (the "inhomogeneity") is introduced, the head contours deviate around the cavity, as shown in Figure F.1. The same particle would now deviate toward the cavity — again, in order to remain perpendicular to the local head contour. The quasi-hydrostatic pressure

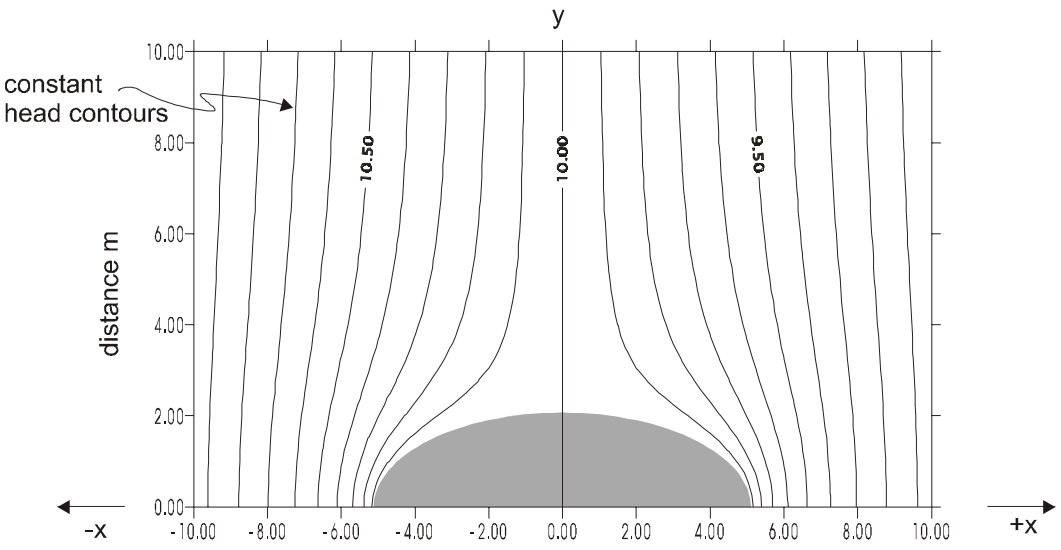

Figure F.1 Head contours around a spheroidal cavity in a uniform flow field (heads decrease from 11.00 m along the extreme left ordinate to 9.00 m along the extreme right-hand ordinate)

within the water-filled cavity tends to reduce the flow rate through it, but the very high conductivity allows the fluid to "rush" through the cavity from the higher head in the rock medium (on the left) to the lower head (on the right).

F.1 Equivalent Permeability of a Porous Medium Containing an Inhomogeneity

Using Janković's code (Janković and Barnes 1997), the spheroidal inhomogeneity in Figure F.1 can be surrounded by an imaginary stream "cell," using the method of images discussed below. The cell is effectively a rectangular "tube" of square cross-section placed symmetrically around the cavity, as shown in Figure F.2. Flow along the cell is uniform from left (AA) to right (BB), as in Figure F.1.

The pressure head acting on planes normal to the flow can be determined and, from this, a measure of the average head loss through the cell. Since the specific discharge (Darcy velocity) is given, this allows an equivalent conductivity (k_e) to be computed for the cell with the internal cavity. As the size of the cell around the single inhomogeneity is increased, the effect on the overall hydraulic conductivity (k) of the medium becomes progressively less.

A series of computer runs was carried out for the spheroidal cavity of Figure F.1 using cells of progressively increasing size to surround the spheroid. It was found that

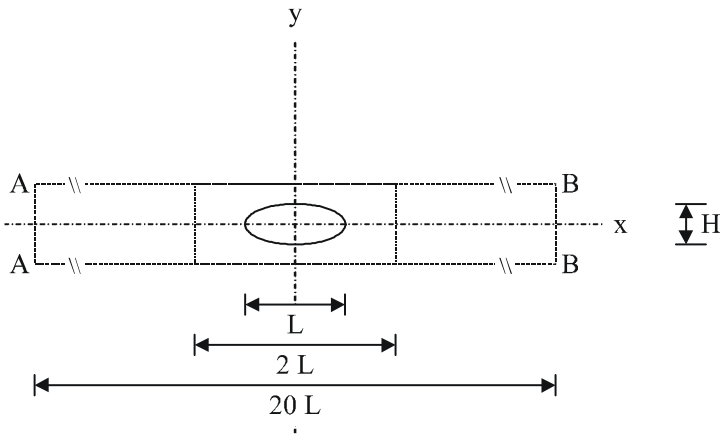

Figure F.2 Rectangular stream cell, of variable length AB ($2L$~$20L$) and square cross-section in the yz-plane (see Fig. F.6) and variable height BB, enclosing the spheroid of major axis (L), minor axis (H). (For the results shown in Fig. F.3, L = 10 m, H = 4 m, and the distance between measuring planes AA, BB was varied between $2L$ = 20 m and $20L$ = 200 m)

the equivalent conductivity (k_e) could be represented well by the expression

$$\frac{k}{k_e} = 1 - \frac{V_e}{V_t} \tag{F.1}$$

where k is the hydraulic conductivity of the medium, k_e is the equivalent conductivity of the cell (with cavity), V_e is the volume of the spheroid, and V_t is the volume of the cell.

Thus, as the volume of the cell (V_t), which could be considered as the space available between spheroidal inhomogeneities, becomes large compared to V_e, then the effective conductivity (k_e) approaches the conductivity of the medium (k) without inhomogeneities.

The percentage error, as computed from the ratio

$$\frac{k_{e_{computational}} - k_{e_{Eq.(1)}}}{k_{e_{Eq.(1)}}} \tag{F.2}$$

for different sizes of cell, is shown in Figure F.3. It is seen that the error is less than 2% is all cases.

Figure F.4 shows (a) the arrangement of spheroids around the central spheroid.

A confirmation (obtained by three-dimensional finite-element analysis) of this result is provided by the observation in Section 7.5.2 of this report.

If we compare the total discharge from the carbonates to the lagoon before the tests, calculated by the model at 60 000 m^3 per day, to the one calculated with the 137 damaged

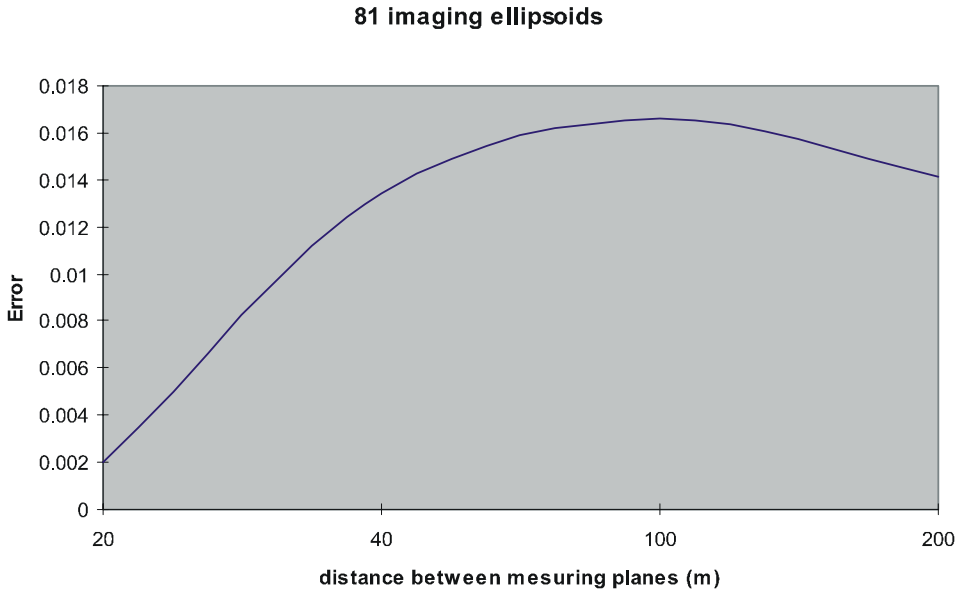

Figure F.3 Error, as computed by (F.2) in the computed hydraulic conductivity of a cell compared to the actual equivalent conductivity (k_e) for various sizes of square-sided cell surrounding a single spheroidal cavity (semi-major axis = 5 m, semi-minor axis = 2 m; see Fig. F.1)

zones with the highest permeability (10^{-4} ms^{-1}), we find that the increase is less than 1%.

Further details of the computational procedures used to arrive at this result are given in Janković and Barnes (1997).

F.2 Method of Images

As mentioned in the discussion of Figure F.1 above, introduction of the inhomogeneity into the medium causes the potential flow field to deviate from the previously uniform pattern. In calculating the effect of the inhomogeneity on the resistance to flow in the medium, we wish to ensure that this total flow through and past the inhomogeneity is "contained" within the (imaginary) boundaries (the four sides) of the rectangular cell shown in Figure F.2 — i.e. that flow enters at one end (say, AA) of the cell and leaves at the other (say, BB), and that no fluid enters or leaves across the four sides. Thus, we must ensure that these sides are, in fact, no-flow boundaries.

A technique frequently used to achieve this in analysis is to introduce a second inho-

mogeneity, identical to the first but displaced from it (a "mirror image" about the desired plane of symmetry), as shown in Figure F.4(i).

Conditions of symmetry dictate that the plane mid-way between the two inhomogeneities will be a no-flow boundary (i.e. there will be no-flow normal to this plane).

Superposition of two inhomogeneities as shown in Figure F.4(ii) will similarly ensure that the plane mid-way between the (now four) inhomogeneities will be a no-flow boundary. However, the process of going from F.4(i) to F.4(ii) destroys the symmetry along the plane in F.4(i) — since now there are two inhomogeneities on the right of the original inhomogeneity and only one on the left. Addition of another inhomogeneity

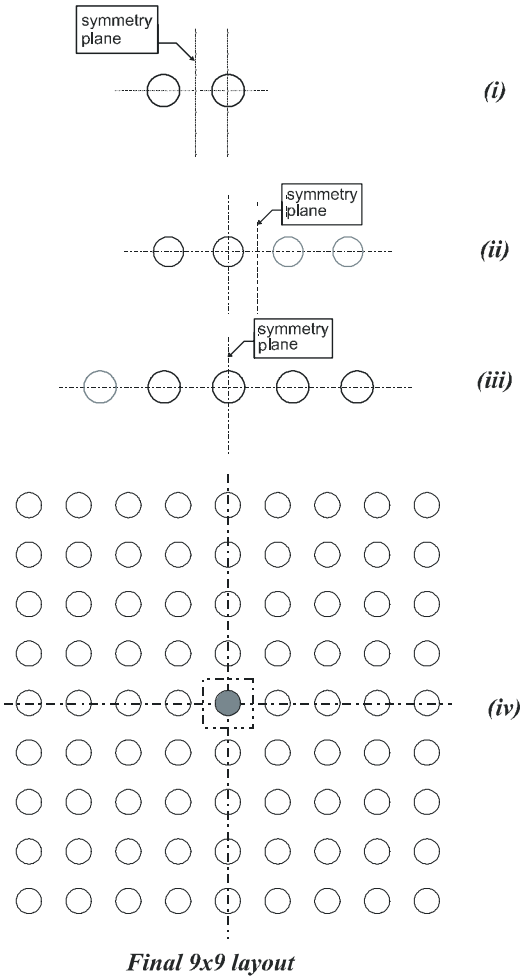

Figure F.4 Successive steps of adding mirror image spheroidal inhomogeneities in order to establish rectangular no-flow boundaries for the stream cell shown in Figure F.2

to the left as in F.4(iii) would move the plane of symmetry to the axis of the original inhomogeneity, introducing a small degree of asymmetry to the flow along the planes of symmetry established in F.4(i) and F.4(ii) — i.e. they are no longer strictly no-flow boundaries. This asymmetry along the previously symmetric boundaries can be reduced by introducing additional inhomogeneities, along the same line shown in Figures F.4(i)–(iii). In this way, the symmetry planes shown in Figures F.4(i) and (ii) will tend to be restored as no-flow boundaries. Repeating the same process above and below the initial inhomogeneity, as shown in Figure F.4(iv) will similarly establish no-flow boundaries on the planes mid-way between the first layers of inhomogeneities above and below the initial inhomogeneity. The 9×9 array shown in Figure F.4(iv), established in this way, allows a very good approximation to the no-flow cell boundaries required for the stream cell shown in Figure F.2. Variation of the centre-centre spacing between adjacent inhomogeneities will thus vary the size of the square cross-section of the cell. The distance upstream and downstream of the planar array of 81 inhomogeneities is varied from $2\,L$ to $20\,L$, as shown in Figure F.2.

Figure F.5 shows three mutually orthogonal sections through a (three-dimensional) field of (overall) uniform flow containing 1000 spheroidal inhomogeneities. In this case, the inhomogeneities are, on average, 1000 times more permeable than the background.

The flow shown in Figure F.6 is intended to represent groundwater flow around a series of explosion cavities (with chimneys) aligned essentially perpendicular to the flow, which is directed from the ocean slope along the atoll and the lagoon. This arrangement of cavities is similar to the situation in rim test areas, especially on Mururoa. The axis AA1 can be considered to be parallel to the rim shoreline; BB1 is vertical. It is seen that the pattern of uniform flow is changed only in the immediate vicinity of the cavities — even for the two closest cavities. This indicates that there is very little hydrological interaction between explosion cavities, even when they are relatively close to each other.

In all cases (Figs. F.1, F.5 and F.6), it is seen that the distortion of the constant head contours — which would all be straight lines in the absence of the inhomogeneities — is significant only in the vicinity of the individual inhomogeneities.

F.3 Lava Tubes

Lava tubes are long, tunnel-like voids sometimes formed in sub-aerial volcanics. They are formed

> *as a result of the surface solidification of a lava flow during the last stages of its activity. A frozen crust forms over still mobile and actively flowing liquid rock as a result of surface cooling. A dwindling supply of lava may then cause the molten material to drain out from under the crust and leave long cylindrical tunnels.* [see **lava caves**, in Macropaedia, Vol. VI p.83, Encyc. Britt. (Chicago) 15th Ed. 1975]

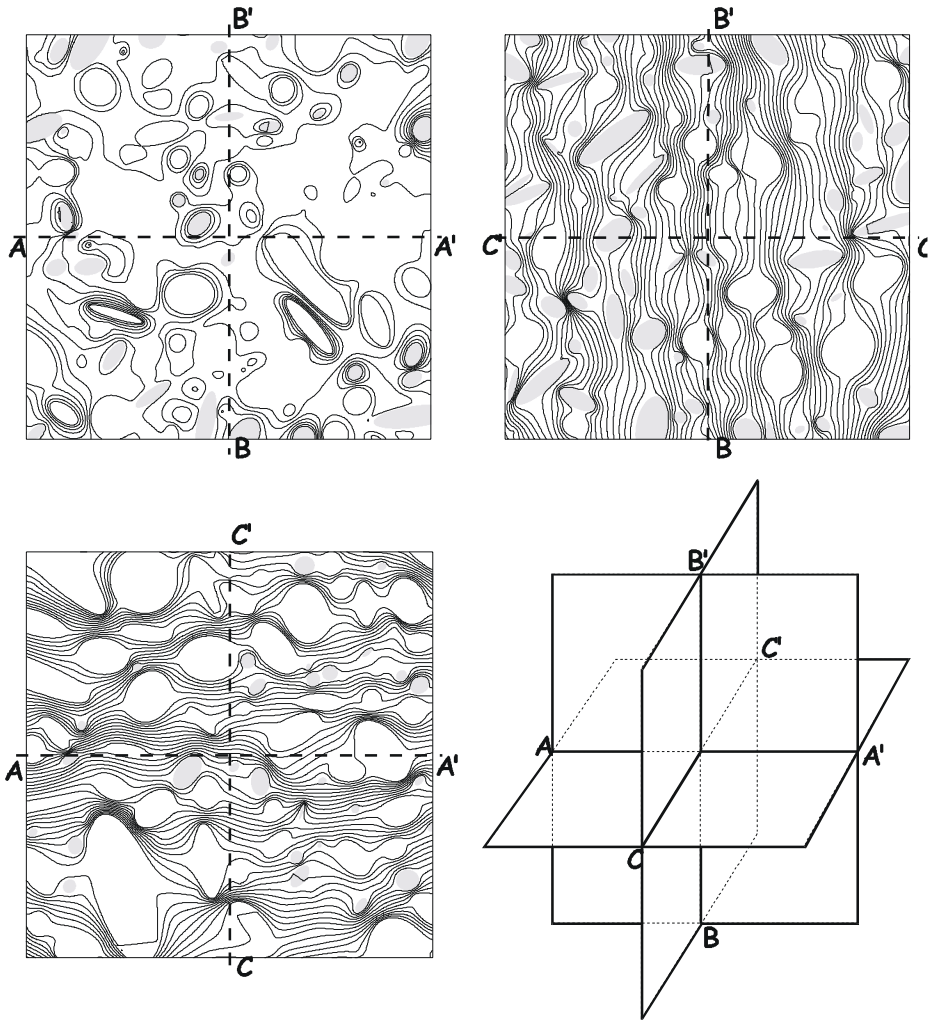

Figure F.5 Intersections with constant head surfaces for 1000 spheroidal inhomogeneities in a uniform flow field (inhomogeneities are, on average, 1000 times more permeable than the background; flow is from C to C)

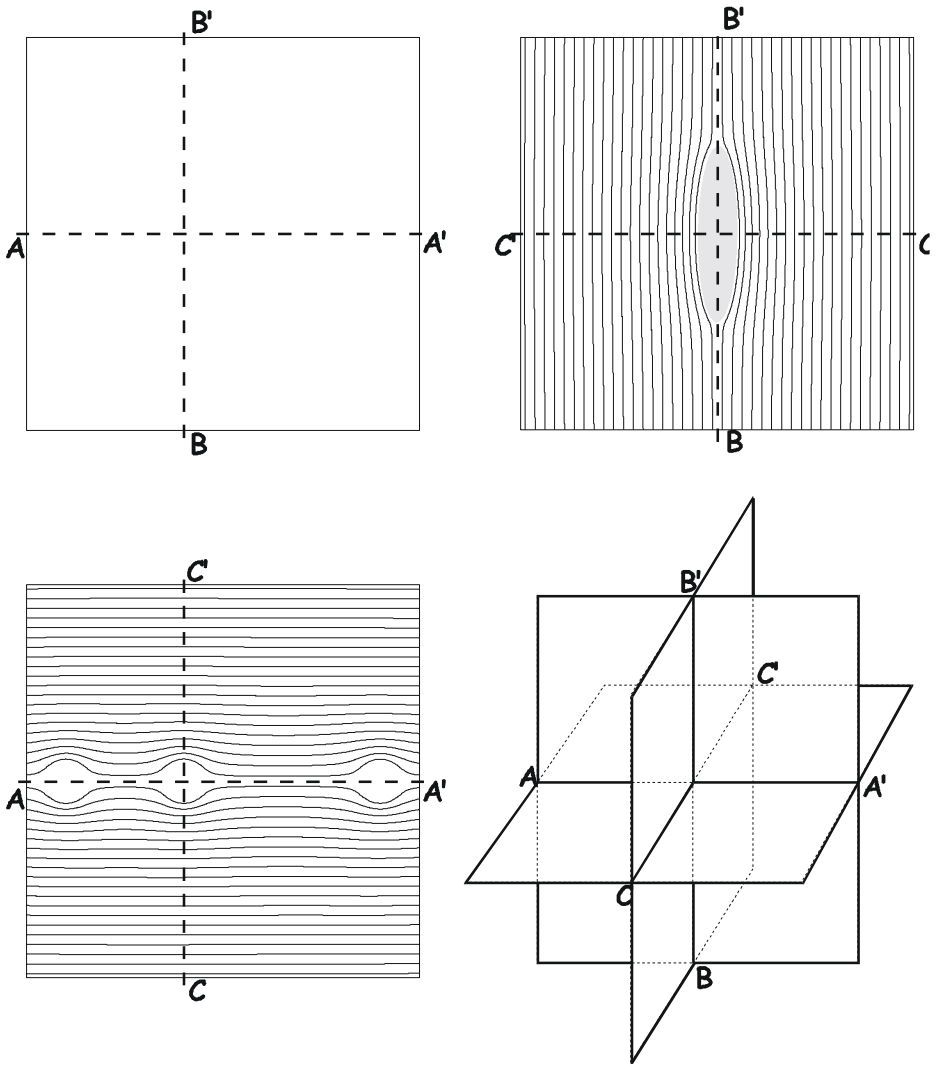

Figure F.6 Effect of three spheroidal inhomogeneities on a previously uniform flow field (flow is from C to C^1)

Lava tubes may be up to several metres in diameter and can extend for kilometres in length. Impressive examples of lava tubes can be found on Hawaii and other recent volcanic islands. It has been suggested that lava tubes at depth in the volcanics could serve as fast conduits for flow of radionuclide-contaminated groundwater from the vicinity of the explosion cavities towards the biosphere.

If lava tubes exist in Mururoa and Fangataufa, they most probably will be located (as noted in the quotation above) in the sub-aerial volcanic series, which are found in the upper sections of the volcanics (see Figs. 2.6 and 2.7) — hence, above (or in the upper part of) the explosion chimneys. Because the radionuclide-contaminated groundwater rises from the explosion sites toward the lagoon, lava tubes, which will be more or less horizontal, would appear to have the potential to serve as fast conduits for the contaminated groundwater.

It seems probable, however, that any such tubular voids would tend to become filled with sediments and also to collapse under the accumulated weight of overlying rock as the volcanic seamount subsided. CEA scientists indicate that no evidence of lava tubes has been found in any of the more than 300 drillholes associated with the underground tests on the atolls.

If the lava tubes did not extend as an interconnected system across the full width of the atoll, their effect on the flow field would be restricted to the region of the lava tubes — i.e. forming one or more spheroidal inhomogeneities, with an effect on the regional flow similar to that discussed earlier in this appendix. Even allowing that one or more lava tubes did extend as a continuous conduit across the atoll, which seems very improbable, they would have a negligible influence compared to the areally much more extensive karst horizons in the overlying carbonates. The influence of the karsts is recognised and is considered in the analysis of radionuclide pathways to the biosphere. Thus, it can be assumed that any possible influence of lava tubes on flow is effectively included in the effect of the karst horizons.

Appendix G

THE *LE MONDE* MAP

G.1 The *Le Monde* Map of 4 October 1995

The map shown in the upper part of Figure G.1 appeared in the journal *Le Monde* on 4 October 1995, four months after President Chirac announced the decision to conduct a final campaign of underground nuclear tests. When it appeared, DIRCEN/CEA authorities vigorously denied the authenticity of the map and the information that it contained. The map has since been reproduced in several publications, including CRII-RAD (1995) and Barrillot (1996).

The map in the lower part of Figure G.1 (Fig. 12 of DIRCEN/CEA Document No. 7) indicates the regions where, according to the CEA, fractures have occurred along the rim of Mururoa.

Since large-scale fractures have an obvious association with structural stability, the IGC took particular interest in the *Le Monde* map and the fractures shown on it. The locations where fractures are indicated on the map were visited — on foot where possible, otherwise by helicopter flight at low altitude along the rim. The widths of individual fractures observed during the IGC visit were of the order of 10–30 cm, although these appeared to increase in width in deeper water toward the ocean. Some fractures and, in the case of the southern rim, slope failure lines, were also visible from the air. Longitudinal fractures were also seen from the ground, slightly below water level, parallel to the northeast rim of Fangataufa. On the northeast rim of Mururoa, the region where fractures are shown parallel to the coast is known to have been deforming continuously since the late 1970s. An extensive monitoring system has recorded these deformations (DIRCEN/CEA Document No. 7, Sec. VI). The origin and implications of the deformations are discussed in Chapter 4 of the IGC report.

Comparing the *Le Monde* and DIRCEN/CEA maps, it is seen that there is some correspondence between the regions where longitudinal fissures are indicated. The apertures indicated on the *Le Monde* map are considerably larger than those observed by the IGC, although apertures of 1–2 m can be seen underwater on the northeast slope of Mururoa (Figs. 1.13 and 1.14). Also, although the longitudinal fractures are extensive, the lengths and apertures indicated in the *Le Monde* map appear to be exaggerated.

The most westerly longitudinal fracture on the southwest rim in the *Le Monde* map appears to indicate the region where the Priam and Nestor tests induced underwater slope

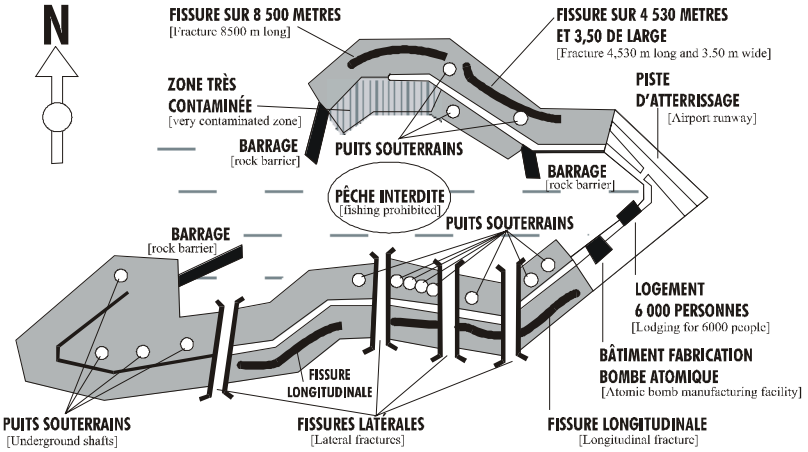

La carte ci-dessus représente un relevé de l'atoll de Mururoa effectué en juin 1980 par les services militaires de la base. En grisé apparaissent le zones interdites. Au nord, la "zone très contaminée", aujourd'hui nettoyée, provient des retombées d'un essai atmosphérique antérieur. Le plus significatif réside dans le présence d'importantes fissures latérales et longitudinales qui auraient été comblées depuis. Quinze ans plus tard et après une centaine de tirs supplémentaires, on peut s'interroger sur l'amplitude de la "fracturation" de l'atoll. —La une du Monde, le 4 octobre 1995

[The map above is a plot of Mururoa atoll prepared in June 1980 by the military authorities of the base. Areas where access is prohibited are shown in grey. The area indicated as "zone très contaminée", now cleaned up, was the result of fallout from one of the earlier atmospheric tests (on the atoll). Most significant are the large lateral and longitudinal fissures which have since been filled. Fifteen years later and after hundred more tests, one may wonder about the extent of fracturing of the atoll.]

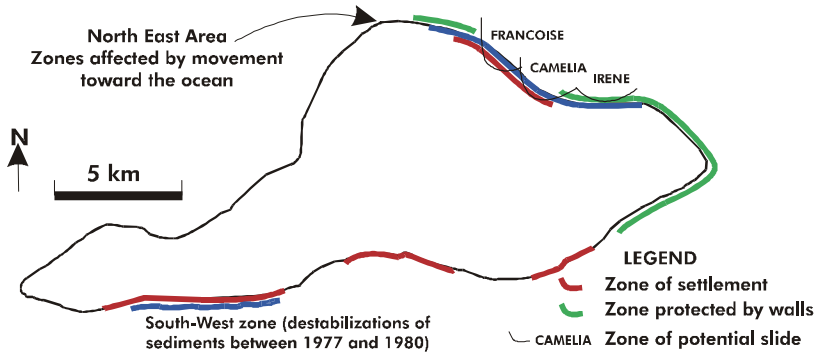

Figure G.1 Upper — map of Mururoa published in the journal *Le Monde* on 4 October 1995; Lower — map reproduced from Figure 12, DIRCEN/CEA Document No 7;

failures in 1977/78; the similar, but larger Tydée slide of 25 July 1979 is not shown (see DIRCEN/CEA Document No. 7 and Figs. 1.11 and 1.12 of this report).

Although a careful search of the southern rim was made (on foot in the accessible parts and from a helicopter along the entire rim) during their visit in July 1996, IGC members could find no evidence of the lateral fractures indicated on the *Le Monde* map. With a width indicated to be of the order of metres, these would have been difficult to overlook, even if filled. IGC members were also unable to find any structural geological reason why such a pattern of fractures would develop, or any mechanism by which they could open to the extent indicated.

The shafts shown on the *Le Monde* map are apparently intended to represent some of the test locations. These can be compared with the locations shown in Figures 1.17 and 1.18 of the Overview. The number of underground tests carried out on the Mururoa rim by the end of 1980 was 42 (Bouchez and Lecomte 1996). The nature of the barriers at the ocean inlet to the lagoon is unknown. CEA officials indicate that no such physical barriers were constructed. None could be seen by the IGC from the air.

Fishing in the lagoon is forbidden because of the danger of poisoning from eating fish infected with ciguatera, a disease that exists to varying degrees in waters near atolls in the South Pacific (Garnett 1998).

In summary, it would appear that the locations of the longitudinal fractures show some correspondence with recent official data, whereas other details of the *Le Monde* map are either inaccurate or wrong.

Appendix H

ROCK DAMAGE FROM UNDERGROUND NUCLEAR TESTS

H.1 Structural Interaction Between Adjacent Explosion Cavities

Detonation of an underground explosion in proximity to an existing cavity may result in additional structural damage between the resulting two cavities (i.e. more than the total damage produced by two non-interacting cavities). The dynamic interaction between the outgoing shock wave and the wall of the existing cavity and chimney will produce some damage. However, since the first cavity and chimney will be filled with rubble and water, the impedance contrast with the surrounding rock will be less than if the cavity was open and empty. Also, the damage region around the first cavity will tend to "deflect" the incoming wave to some extent. Even so, some additional damage could result, and the presence of the two adjacent cavity/chimneys in close proximity may result in interaction between the two and more extensive deformation — possibly extending to the surface. The discussion below examines this possibility.

The relatively high concentration of large-yield explosions in some of the testing areas, such as test area 4 in Mururoa, has been discussed in Chapter 1. Figure 11 in DIRCEN/CEA Document No. 6, reproduced as Figure H.1, provides statistics on the "distances between a new test and the nearest previous test at the CEP", expressed in terms of R, defined as the ratio

$$R = \frac{D}{R_{c1} + R_{c2}} \tag{H.1}$$

where D is the centre-to-centre distance between the two explosion points, R_{c1} is the cavity radius created by the "nearest previous test", and R_{c2} is the cavity radius created by the second test. R varies from 2.5 to more than 15. As shown in Figure H.1, 9 of the 147 underground tests conducted on the two atolls involved a value of R between 2.5 and 3.5. The yields of individual tests — and the values of R_{c1} and R_{c2} — are not given, so that the absolute spacing between any two cavities cannot be determined. For tests that are relatively close together, the spherical regions of appreciably fractured rock generated around each explosion shot point may overlap and weaken the column of rock between the two cavities so that the load-carrying ability of the column will be much reduced. In such a situation, will the region above the two explosion cavities (and associated chimneys) cause collapse of the overlying rock?

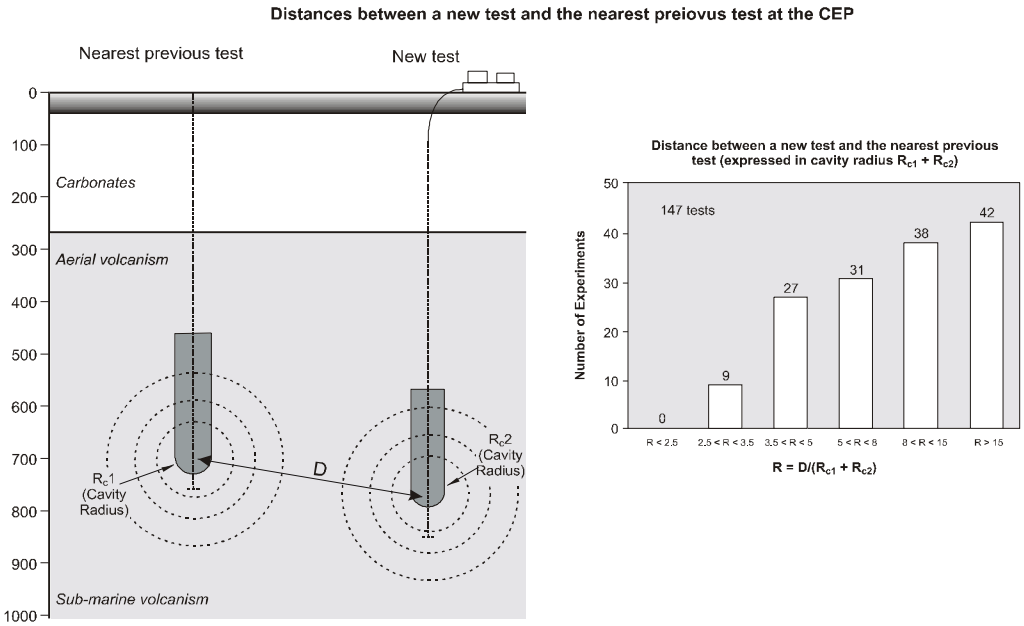

Figure H.1 Spacing between a new test and the nearest previous test at the PTC (DIRCEN/CEA Document No. 6, Fig. 8)

Three cases have been analysed.

First, in order to establish a reference condition, the case of a single 150-kt test (the maximum yield allowed under the Limited Test Ban Treaty) exploded at a depth of 1000 m below the surface in the volcanics was analysed. The thickness of the carbonates overlying the volcanics was 500 m. The mechanical properties of the intact rocks and rock masses were those considered to be representative of the weakest of those in which tests were conducted at the PTC. These are summarised in Table H.1.

According to DIRCEN/CEA Document No.6,

- The radius (R_c) of the cavity produced by a deeply buried explosion in the PTC is, approximately,

$$R_c = 10\,Y^{1/3} \quad \text{metres} \tag{H.2}$$

- The height (H_c) above the zero point (i.e. the explosion origin) of the collapse chimney is given by the expression

$$H_c = 1100\left(\frac{Y}{h}\right)^{1/2} \tag{H.3}$$

Table H.1 Mechanical properties of volcanics and carbonates assumed in the analysis of stress distribution and deformations around two interacting explosion cavities

		Intact Rock Properties					Rock Mass Properties[a]		
Rock		σ_{ci} MPa	m_i	a	K GPa	G GPa	GSI	m_b	s
Carbonates		15	8	0.5	4.8	1.6	70	2.74	0.036
Volcanics	undamaged	75	17	0.65	8.33	3.84	30	1.395	$4.9 \cdot 10^{-4}$
	fractured	75	17	0.65	8.33	3.84	10	0.683	$4.54 \cdot 10^{-5}$

[a] The rock mass properties are based on values suggested in Chapter 2, Section 2.5.1. The values of m_b and s, used to define the Hoek-Brown envelope for the rock mass, are derived from the GSI rating, as follows:

$$m_b = mi \exp(\frac{GSI - 100}{28})$$
$$s = \exp(\frac{GSI - 100}{9})$$

where Y is the explosion yield in kt, and H is the depth, in m, to the zero point.

(Note: In order to accommodate the mesh element size used in the numerical model, some slight modifications to cavity dimensions have been introduced; these are shown in [ ] after the calculated dimensions.)

Thus, for a test of 150 kt at 1000 m, the cavity radius (R_c) will be approximately 53 m [50 m] and the chimney height (H_c) will be 426 m [400 m] (i.e. approximately 8 R_c). The chimney and original cavity will be filled with the broken rock (rubble) produced by the fallen rock and with water in the voids. For the analysis, it is assumed that the explosion fractures and substantially weakens the rock within a radius (R) of 5 R_c [250 m] around the explosion.

The cavity is assumed to be subjected to the far-field stresses produced by

(1) the gravitational load in the vertical direction — i.e. $\sigma_v = \rho_r g h$, where σ_v is the vertical stress at depth, h, ρ_r is the average rock mass density, and g is the acceleration due to gravity;

(2) the hydrostatic stress ($\sigma_h = \rho_w h$) in the horizontal direction, resulting from the lateral load on the atoll flanks produced by the ocean water (density ρ_w); and

(3) the "stress cage" effect (see App. E) is represented approximately by increasing the vertical (gravitational) and horizontal (hydrostatic) stresses by 20%.

Figure H.2a shows the resulting field of deformations around the single cavity/chimney for the above-mentioned conditions. It is seen that (i) the inelastic region is confined to

the vicinity of the explosion; (ii) a substantial elastic region of volcanic rock remains above the top of the chimney; (iii) the carbonates remain elastic; and (iv) the maximum (downward) displacement at the surface (approximately 1 mm) (Fig. H.2b), due to the cavity/chimney, is approximately 1 mm.

The second case considers two identical (150-kt) cavities, spaced at $D = 5\ R_c = 265$ [250 m], centre to centre — i.e. with a column of rock 150 m wide, 400 m high and (2 R_c =) 100 m "thick" between the two cavities. Again, it is assumed that the rubble- and water-filled cavities/chimneys are empty and dry. The resulting maximum displacement at the surface (Fig. H.2b) is increased to approximately 5 mm.

The third case assumes an ultra-conservative situation in which the rock column between the two cavities has no strength — i.e. for purposes of the numerical analysis, this column is removed, so the two cavities are replaced by one slot of the full width ($7\ R_c \simeq$ 371 m [350 m] between the outer extremities of the two chimneys. This case is shown in Figure H.3.

It is seen that, even with these ultra-conservative assumptions, the deformation induced in the overlying carbonates remain elastic, with maximum (downward) displacement at the surface of 80 mm.

Compared with the 2 m of surface settlement produced by the stress wave that is generated by large explosions, this elastic deformation is negligibly small, even for the extreme conditions assumed above.

It is concluded, therefore, that significant structural interaction between cavities is very unlikely in any of the testing areas of Mururoa and Fangataufa.

H.2 Volume of Rock Damaged by Underground Testing

H.2.1 Volcanics

As discussed in Chapter 3 and summarised in Section 1.3, each underground nuclear test produces a spherical cavity, radius R_c ,around the explosion point. This cavity becomes filled with broken rock or rubble, resulting from the collapse of the roof of the cavity up to a height (H_c), which varies between 5 R_c and 8 R_c above the explosion point (i.e. centre of the cavity). The rock beyond the cavity wall is damaged by the explosion, but to a progressively decreasing intensity with radial distance from the explosion point. From analyses such as those presented in Chapter 2 and post-test observations reported from both the USA and the former USSR test programmes, it appears that

(1) the radius (R_t), beyond which the explosion energy does not damage the rock, is approximately (8–10) R_c (Approximately 95–99% of the explosive energy is dissipated within this region; the remaining 1–5% is radiated elastically — i.e. as seismic energy — beyond (8–10) R_c); and

(2) the load-carrying ability of the rock is not degraded substantially beyond 5 R_c.

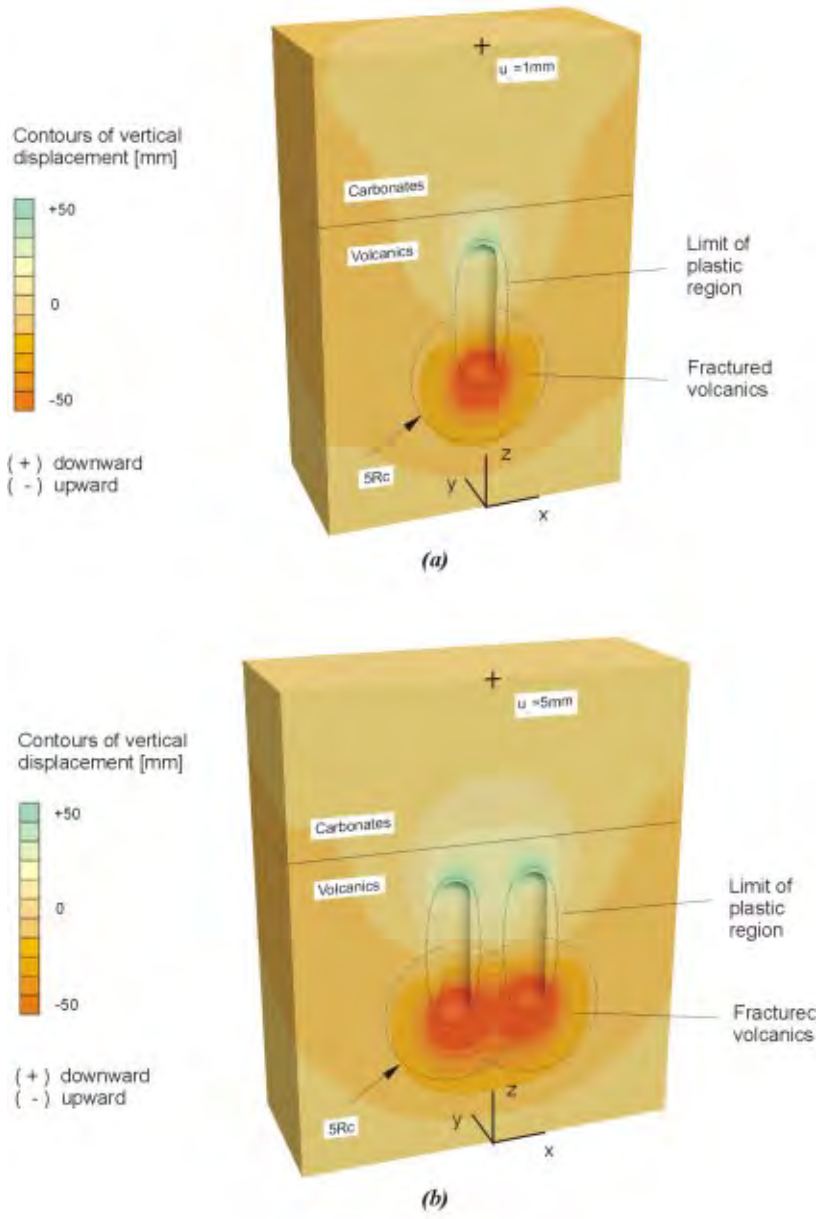

Figure H.2 Inelastic (perfectly plastic) and elastic regimes and vertical displacements (u) in the vicinity of two explosion cavities (i.e. cavities plus chimneys) with damaged (fractured) rock around the cavities)

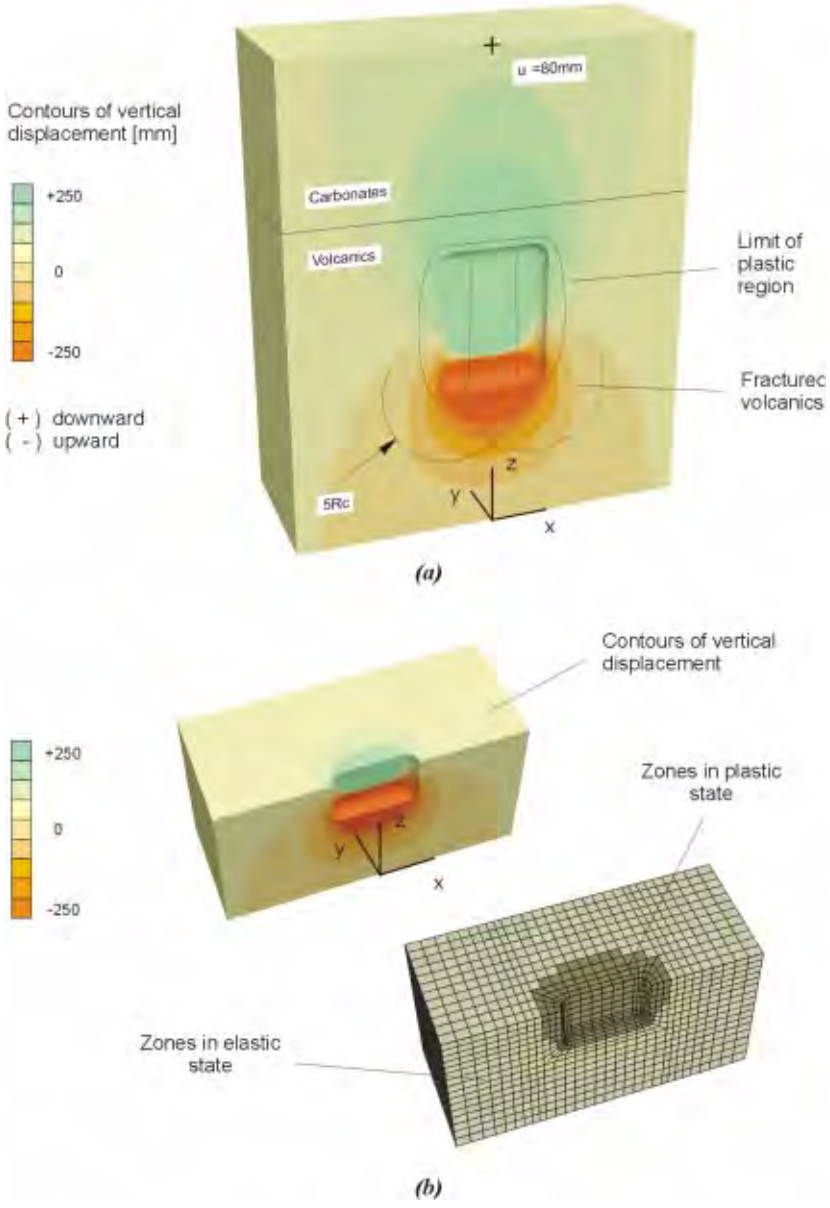

Figure H.3 Inelastic (perfectly plastic) and elastic regimes and vertical displacements (u) in the vicinity of two explosion cavities (i.e. cavities plus chimneys) with “zero-strength rock” between the cavities)

IGC calculations indicate that more than 90% of the explosion energy is dissipated in the rock inside the 5 R_c radius. The volume of the cavity (V_c) is directly proportional to the energy release, or yield (Y), of the explosion; R_c is thus proportional to $Y^{1/3}$. At the PTC, post-test drilling indicates that the relation between cavity radius and yield may be expressed as

$$R_c = a\, Y^{1.3}\,\mathrm{m} \tag{H.4}$$

where a is approximately 12 m/kt$^{-1/3}$ for shallow (usually low-yield) tests and 10 m/kt$^{-1/3}$ for deep (usually high-yield) tests.

According to DIRCEN/CEA, all underground tests at the PTC were conducted in the volcanic rock at depths between 500 m and 1100 m. A 150-kt test conducted at the maximum depth of 1100 m would produce a damage region 10 R_c = 10 · 10· 150$^{1/3}$ = 530 m below the explosion — i.e. to a depth of 1630 m. However, recognising that most tests were well below 150 kt (the average yield of tests on Mururoa was 17.5 kt; the average yield of tests on Fangataufa was 80 kt), we will assume that all damage was confined to the 1-km depth interval from 500 m (the top of the volcanics) to 1500 m on the two atolls. We will also assume, to be conservative (i.e. to overestimate the cavity and damage volumes), that a is 12 m/kt$^{-1/3}$ for all tests, independent of the yield or depth. The volume of volcanic rock, V_{D10}, that extends to the start of the elastic (or seismic) region (i.e. $R = R_t$) is, then,

$$\begin{aligned} V_{D10} &= 4\pi/3\,\left(10 \cdot 12\, Y^{1/3}\right)^3 \\ &= 7.2 \cdot 10^6\, Y\,\mathrm{m}^3 \end{aligned} \tag{H.5}$$

or

$$V_{D10} = 7.2 \cdot 10^{-3}\, Y\,\mathrm{km}^3 \tag{H.6}$$

Similarly, the volume of volcanic rock (V_{D5}) that is damaged to a radius of 5 R_c is, then

$$V_{D5} = 0.9 \cdot 10^{-3}\, Y\,\mathrm{km}^3 \tag{H.7}$$

where Y is in kt.

We can then calculate the total volume of damaged rock in each test area, as a proportion of the total volume bounded by the plan test area (see Figs. 1.17 and 1.18) and the 1-km-thick damage interval (see Tables H.2 and H.3).

Table H.2 Fractional damage volumes in test areas of Mururoa

Test Area	No. of Tests	Yield (kt)		Plan Volume V_R (km^3)	Volume Damage			
		Total	Avg	(assuming 1-km vertical interval)	km^3		%	
					V_{D10}	V_{D5}	$\frac{V_{D10}}{V_R}$	$\frac{V_{D5}}{V_R}$
1	28	< 60	< 2.1	6	0.43	0.05	7.2	0.1
2	27	< 150	< 5.6	7	1.09	0.14	15.6	1.9
3	7	< 100	< 14.3	3	0.72	0.09	24.0	3.0
4	21	< 750	< 35.7	8	5.40	0.68	67.5	8.4
5	21	< 300	< 14.3	30	2.16	0.28	7.20	0.9
6	19	< 550	< 28.9	12	3.96	0.50	33.0	4.1
7	14	< 600	< 42.9	9	4.32	0.54	48.0	6.0
Total	137	< 2400	< 17.5	75	17.28	2.16	23.0	2.9

Note: Differences between total damage and the sum of individual test area damage values is due to "rounding up" of yield values for all of the test areas (total = 2510 kt, compared to 2400 kt for round-up of total values from DIRCEN/CEA).

Table H.3 Fractional damage volumes in test areas of Fangataufa

Test Area	No. of Tests	Yield (kt)		Plan Volume V_R (km^3)	Volume Damage			
		Total	Avg	(assuming 1-km vertical interval)	km^3		%	
					V_{D10}	V_{D5}	$\frac{V_{D10}}{V_R}$	$\frac{V_{D5}}{V_R}$
1	2	< 20	< 10	6	0.15	0.02	2.5	0.3
2	8	< 750	< 94	6	5.40	0.68	90.0	11.0
Total	10	< 770	< 77	12	5.55	0.7	46.3	5.7

The above values for fractional damage volumes refer to the rectangular volumetric *boxes* within which the test regions have been defined (test areas by CEA; 1-km vertical interval by IGC; see Fig. H.4).

It must be noted, however, that the rectangular boxes defined above are integral parts of much larger volumes of rock. From computer calculations based on the bathymetric contours (Tacher 1998), the cross-sectional area of the atoll at the 500-m depth level is 212 km^2; at the 1500-m level it is 434 km^2. The total volume of volcanics across the Mururoa atoll within the 500-m to 1500-m interval is approximately 311 km^3 (rather than the 75 km^3 used in the table above.)*

*These values for Mururoa have been obtained by (artificially) terminating the 500-m and 1500-m contours around the eastern tip of the rim at approximately the same distance from the rim as the contours around the remainder of the atoll. The actual contours extend more than 100 km to the east, so this artificial cut-off is again conservative — i.e. the actual volume between the 500-m and 1500-m contours is much larger.

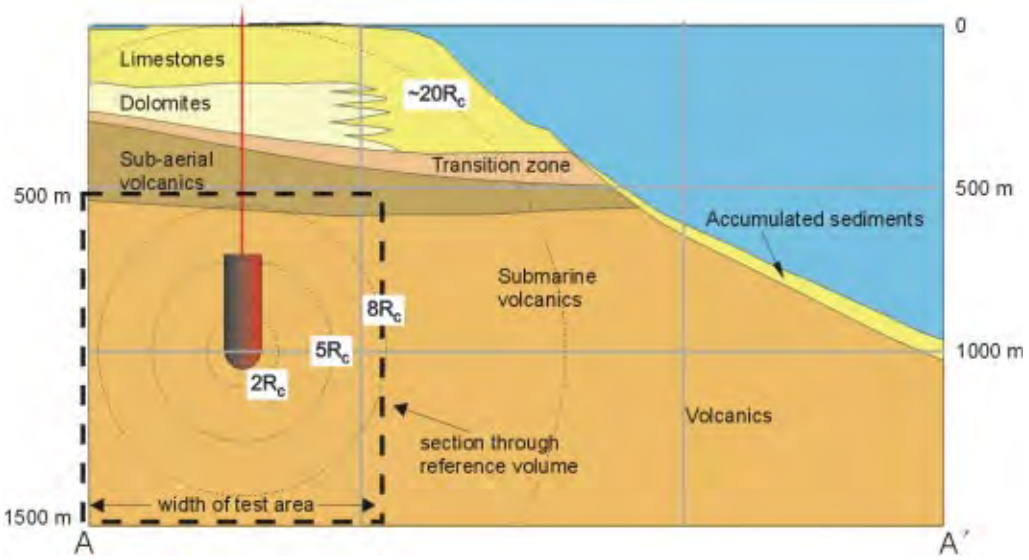

Figure H.4 Cross-section through test area 4 of Mururoa along AA' (see Fig. 1.11) showing cross-section of the "box" (volume V_R) used in calculation of fractional damage volumes in Table H.2

When considered as part of this larger volume, the 23% (V_{D10}) and 2.9% (V_{D5}) values calculated above are, more correctly, 5.5% and 0.7%, respectively, for the damaged volcanic rock in the 500-m to 1500-m interval of Mururoa. The volcanics below 1500 m are not damaged by the underground nuclear tests.

Similarly, for Fangataufa, the cross-sectional areas of the 500-m and 1500-m contours are 69 km^2 and 188 km^2, respectively. The actual volume of volcanics between the 500-m and 1500-m levels is 116 km^3 (rather than the 12 km^3 used in the table above). In this case, the 46.3% (V_{D10}) and 5.8% values (V_{D5}) are then, more correctly, 4.6% and 0.6%. Again, the volcanics below 1500 m are not damaged by the underground tests.

It is also worth noting that the 311 km^3 volume of the 1-km interval from 500 m to 1500 m on Mururoa represents an increase of 156 km^{3}compared to the volume occupied in this interval by the vertical projection of the surface profile of the atoll [area 155 km^2 (Guille et al. 1996, p. 96, Fig. 57)]. The corresponding increase on Fangataufa is 71 km^3 [116 km^3–45 km^3 (Guille et al., op. cit.)]. These volume increases are, of course, all on the ocean side of the exposed rims of the atolls. Thus, the rim test locations at depth in the volcanics are not as close to the volcanics/ocean slope interface as appears from the surface plots shown in Figures 1.17 and 1.18. The "added volume" of volcanics between the explosion point and the ocean slope is also apparent from Figure H.4 (which is modified from Fig. 1.16).

H.2.2 Carbonates

As discussed in Chapter 3, explosions detonated in the volcanics under the exposed rim of the atolls can often result in damage to the overlying carbonates. This is especially the case in Mururoa, where 83 rim tests were carried out, compared to only 2 (small-yield) events in Fangataufa.

In rim tests, the strain wave generated by the explosion passes from the volcanics into the overlying, mechanically weaker carbonates, and interacts with the upper 150–200 m of these formations and the associated underwater carbonate slopes to produce inelastic deformation and fracturing. In some cases, substantial underwater slope failures (e.g. the Nestor, Priam, and Tydée events in test area 4 of Mururoa, where slope failure volumes up to 0.1 km^3 were estimated, have occurred. In the northeastern rim of Mururoa, a large region of the ocean slope (estimated volume 0.6 km^3) has been deforming continuously — since 1979 at least —stimulated by the underground explosions (including some explosions under the lagoon). In other cases, no major slope failures have been reported, but surface settlements have been measured. These settlements have exceeded 2 m in some cases. Figure 1.23 shows a plan view of the observed settlements on the Mururoa rim.

According to the analysis presented in Chapter 4 (See Fig. 4.10), the settlements are the result of volumetric shearing of the upper 150–200 m of the carbonates. An estimate of the volume of rock affected in this way can be obtained by multiplying the total areal extent of settlement on the rim by a thickness of 200 m. Proceeding in this way, the "damaged" volume of carbonates is estimated to be approximately 2.5 km^3, or 3% of the total volume of approximately 77 km^3 [500 m thickness $\cdot$ 155 km^2 area of Mururoa (Guille et al. 1996; Fig. 57, p. 96)] of the carbonates. Of the above 2.5 km^3, approximately 70% is located in test area 4 and 20% in test area 1 (See Fig. 1.23).

It should be noted that surface settlement of the bottom of the lagoon resulting from the explosion wave is much less likely, due to the absence of the free (lateral) surfaces that exist on each side (and particularly the ocean side) of the exposed rim. It has been assumed that settlement of the carbonates under the lagoon does not occur, or is negligibly small.

H.3 Summary

- Cavity interaction

  Even for very conservative assumptions of cavity size, proximity and residual strength of the rock mass surrounding two adjacent explosion cavities (with chimneys), the extent of structural interaction is very small. In general, therefore, the overall structural integrity of the atoll surface has not been significantly affected by the underground tests at the Pacific Test Centre.

- Structural damage

  Using conservative estimates (i.e. damage extending to 10 cavity radii), no more than approximately 5% of the rock in the 1-km depth interval within which all explosion damage to the volcanics is contained has been even minimally damaged by the underground nuclear tests on Mururoa and Fangataufa. Considering the damage region in which some loss of rock strength may occur (i.e. extending 5 cavity radii around the explosion), this percentage is reduced to less than 1%.

  Some additional damage to the carbonates has taken place in the vicinity of some rim tests on Mururoa. This is estimated to affect 3% of the 500-m-thick layer of carbonates across Mururoa.

  Although the proportion of the volume of damaged rock varies from test area to test area, the analysis in the first part of this appendix indicates that the overall structural integrity of the volcanics has not been significantly impaired, even in the most extreme cases of high-yield tests exploded in close proximity to each other.

Appendix I

VARIABILITY IN EXPLOSION CAVITY RADIUS FOR TESTS AT THE PTC

Essentially all of the analyses in the IGC report are based on average values of the various parameters (permeability, rock strength, etc.) involved in the analyses. As noted frequently in the text (see, for example, Overview Section 1.5.1), while average values are useful in providing an understanding of the overall behaviour of the system under study, it is even more important to be aware of the consequences of variations in these parameter values on the behaviour of the system. Dimensional analysis is a valuable step toward this end, but data on the actual performance of the system, especially where they are sufficient to allow an assessment to be made of the variability in this performance, are invaluable. Unfortunately, in all of the information supplied in the DIRCEN/CEA documents there is very little data that allows the variability to be estimated.

Some potentially useful graphs showing test results were presented by Dr. Y. Caristan of DIRCEN/CEA to members of the Atkinson Mission in October 1984, and are included in the Atkinson Report (New Zealand MoFA 1984), but without scales on the graphs! [It was simply indicated on the graphs that some scales were logarithmic, others linear.] Apparently, the actual values were considered to be confidential — and remain so.

Using the additional results provided in the DIRCEN/CEA documents and associated information provided to IGC, an attempt has been made to establish approximate scales for the graphs in Figures I.1, I.2 and I.3. The results are shown below. Based on these assumed scales, some additional information (e.g. values of the slopes of the regression curves) has been provided. The curves are as on the original graphs — only the line $R_c/Y^{0.33} = 100\,h^{-0.33}$ has been added in Figure I.1, and the line $H_c = 5\,R_c$ in Figure I.2.*

---

*According to DIRCEN/CEA Document No. 6, field experimental data at the PTC are best fitted by the following relations:

$$H_c = 1100\ (Y/h)^{0.5} \qquad \text{(i)}$$

$$R_c = 100\ (Y/h)^{0.33} \qquad \text{(ii)}$$

Substituting for Y from (ii) in (i) gives

$$H_c = 1.1\,R_c^{1.5}$$

Thus, for $Y = 150$ kt at $h = 1100$ m depth, $R_c = 51.5$ m, $H_c = 406$ m and $H_c/R_c = 7.9$

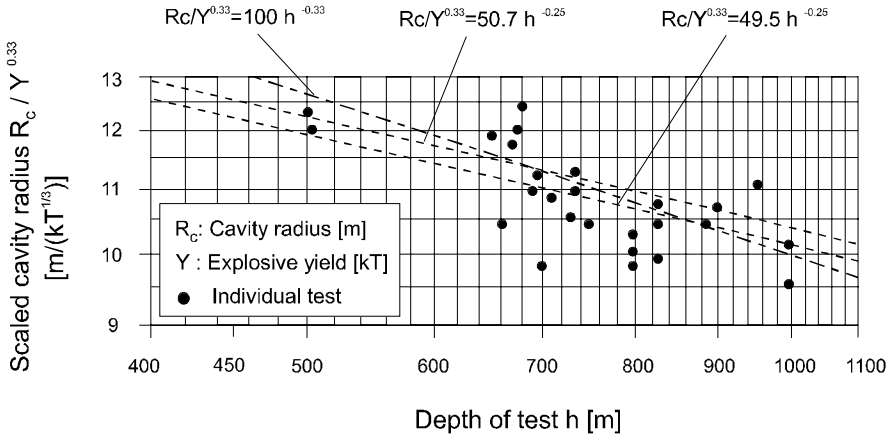

Figure I.1 Underground data for scaled cavity radius ($R_c / Y^{0.33}$) as a function of depth of test in Mururoa and Fangataufa (after New Zealand MoFA 1984, Caristan appendix). Note that, for the figures in this appendix, the scale for each axis was omitted on the original graphs in New Zealand MoFA (1984); the scales shown are the IGC estimates based on other data supplied in DIRCEN/CEA documents. The two dotted lines with a slope that varies apparently as $h^{-0.25}$ are on the original (1984) diagrams, although no relation is given. The line showing a slope with a dependency of $h^{-0.33}$ has been added by the IGC.

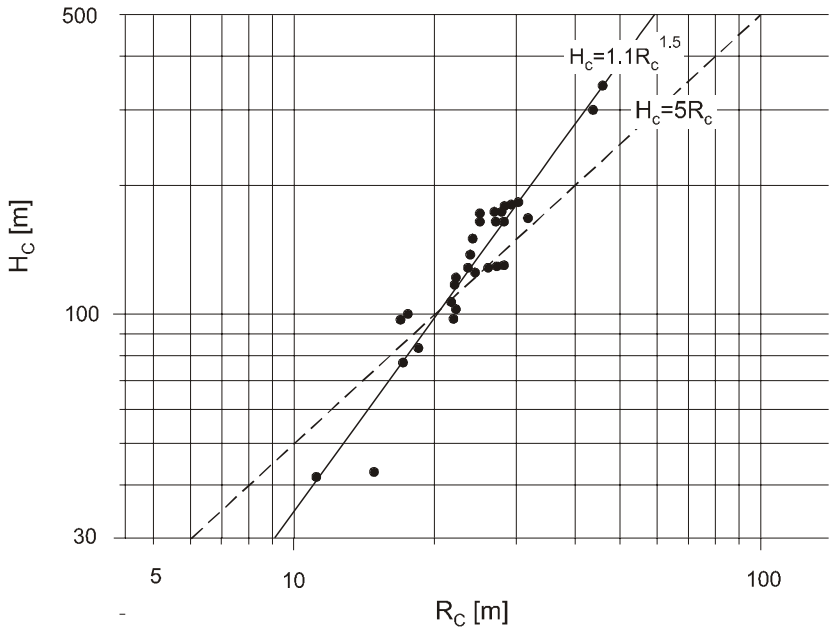

Figure I.2 Log-log plot of measured chimney height (H_c) as a function of measured cavity radius (R_c) (after New Zealand MoFA 1984, Caristan appendix) (See note in caption for previous figure; the solid line is in the original (1984) figure, but the slope $H_c = 1.1\, R_c^{1.5}$ has been added, and the line $H_c = 5\, R_c$ has been added.)

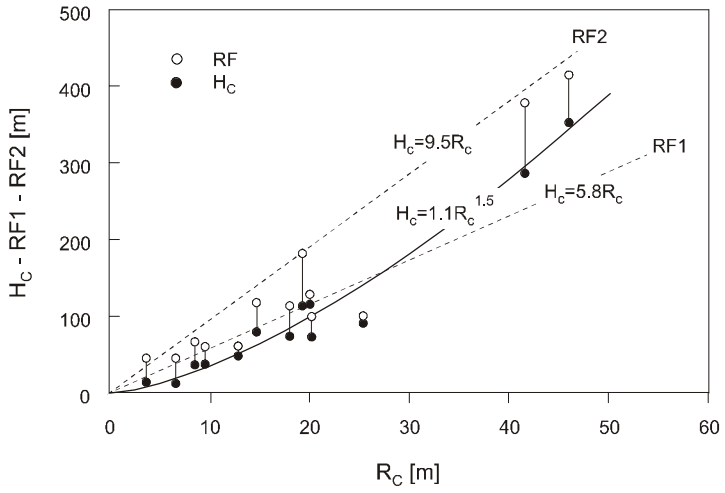

Figure I.3 Examples of variability in cavity radius produced by underground nuclear tests in Mururoa and Fangataufa (after New Zealand MoFA 1984, Caristan appendix) (See note on scales of axes in the caption to Fig. I.1; the solid line and two dotted lines are in the original (1984) figure, but the equations for each line have been added.)

Appendix J

SHOCK WAVES IN SOLIDS

J.1 Introduction

Small perturbations produce elastic waves in solids. Perturbations stronger than the material strength cause the material to deform plastically. Depending on the intensity of the perturbation, the plastic wave can travel at subsonic or supersonic speed. The weaker, plastic perturbations are associated with a subsonic plastic wave that has a characteristic double structure, with the plastic wave lagging behind an elastic precursor. Very strong perturbations generate plastic waves that travel faster than the speed of sound and "overtake" the elastic precursor, forming a shock.

The perturbations associated with a nuclear explosion produce a shock wave in the surrounding rock. The shock front is a domain in space where the pressure, particle velocity, density and internal energy change suddenly. Although the change is in reality always continuous (due to dissipative processes that exist in real materials), it is convenient to represent the shock front as a mathematical discontinuity.

J.2 Hugoniot

In 1887 Hugoniot used the conservation laws to derive equations relating the density ρ (or specific volume V), particle velocity v, internal energy e, and the pressure p (on both sides of a planar shock front) and the speed U of the shock wave

$$\begin{aligned} \rho\,(U - v) &= \rho_0 U \\ p - p_0 &= \rho_0 v U \\ e - e_0 &= (p + p_0)\,(V_0 - V)\,/2 \end{aligned} \tag{J.1}$$

The equation of state, relating e, V and p:

$$p = p(V, e) \tag{J.2}$$

is required to provide, with (J.1), a sufficient set of equations to completely specify conditions on both sides of the shock front.

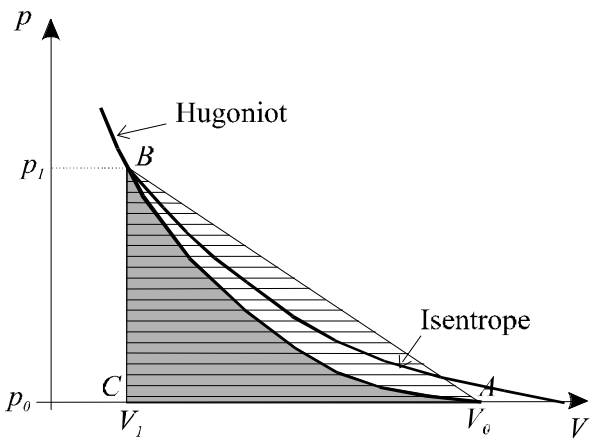

Figure J.1 The Hugoniot curve

The Hugoniot curve (Fig. J.1), a relation between the pressure p and the volume V, connects points in the pressure-specific volume plane corresponding to different shock intensities. The increase in internal energy across the shock front is equal to the area of the triangle ABC (horizontally hatched) in Figure J.1. (The shaded area between points A and B would be equal to the increase of internal energy if the Hugoniot was an equilibrium curve.)

It can be assumed that behind the shock, the rock unloads isentropically. The unloading isentrope, which must be above the Hugoniot curve (Fig. J.1), can be calculated from the Mie-Grüneisen form of the equation of state:

$$p = p_c(V) + \Gamma(V)\frac{c_v T}{V} \tag{J.3}$$

where $p_c(V)$ is the cold compression curve, $\Gamma(V)$ is the Grüneisen coefficient, and c_v is the specific heat at constant volume.

J.3 Water Influence on Shock Compression

Underground nuclear experiments have confirmed the influence of fluid content in the rock on the mechanical effects (coupling) of an explosion. The presence of water (or other fluid) may, under a given set of conditions (i.e. the same rock mass and energy released by the explosive device), significantly increase the mechanical efficiency of the detonated device.

It is assumed that there is no relative movement between the solid and fluid components of the rock mass during the nuclear explosion and subsequent deformation of the rock mass. Two other assumptions are used in our analysis:

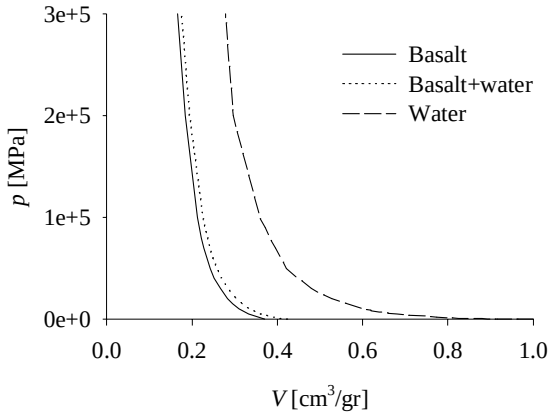

Figure J.2 The Hugoniots in $p - V$ plane

1. The solid and the fluid components of the rock mass are in mechanical equilibrium immediately after the shock (i.e. the pressures are equal).

2. The solid and fluid components of the rock mass are not in thermal equilibrium after the shock — the temperatures and specific energies of the solid and the fluid are different.

With these assumptions, it is possible to derive the Hugoniot curve and release isentrope for a homogenised mixture, provided that the Hugoniot and the equation of state are known for each component. The Hugoniot curve for a completely saturated basalt (20% porosity) is calculated using a numerical program; the Hugoniots for non-porous basalt (Chabai 1963), water, and a saturated, 20% porosity basalt are shown in Figure J.2.

The same principles and methods are used to construct the release isentropes, irrespective of a phase change of one or all components. For example, if the shock intensity is such that water vaporizes while the rock remains solid, a small unloading will cause fracturing of the rock (because of the large difference in compressibility between the rock and the steam), and the assumption of mechanical equilibrium between the rock and the steam will still be acceptable.

J.4 Shock Heating of the Rock

Thermal conduction can be neglected during cavity expansion and shock wave propagation. At the time scale of cavity expansion, the rock temperature changes as a function of mechanical effects only. After compression of the rock by the shock, the increase in internal energy, equal to the area of the triangle V_0AV_1 in Figure J.3, can be divided (Zel'dovich and Raizer 1967) into:

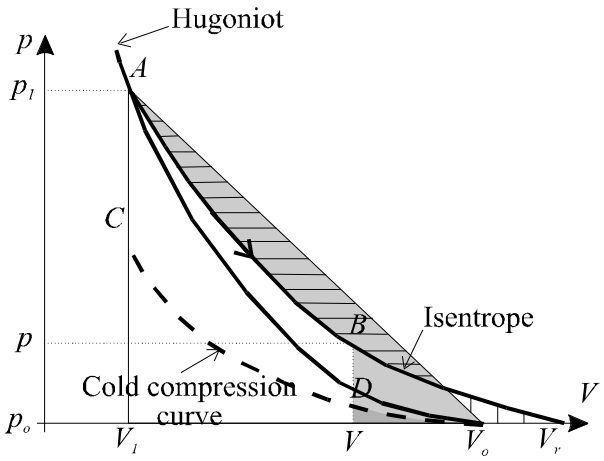

Figure J.3 Irreversible internal energy in equilibrium state

(1) elastic internal energy (the area V_0CV_1 under the cold compression curve), and

(2) thermal internal energy (the difference between the area of the triangle V_0AV_1 and the area V_0CV_1 under the cold compression curve).

The elastic internal energy is completely recoverable, while only a part of the thermal internal energy is recoverable. When a non-porous rock unloads after the shock to the initial pressure p_o, its temperature is increased relative to the pre-shock temperature. This increase in temperature is due to irrecoverable thermal energy, equal to the difference between the horizontally and vertically hatched area—the difference (Fig. J.3) between the area of the triangle V_0AV_1 and the area under the unloading isentrope V_rAV_1 (Zel'dovich and Raizer 1967). The increase in temperature ΔT after complete unloading can be calculated from the formula for the increase in irrecoverable thermal energy as a function of the temperature change (assuming that the specific heat c_p is constant over the range of temperature change ΔT):

$$e_t = \left(\text{area}_{V_0AV_1} - \text{area}_{V_rAV_1}\right) = c_p \Delta T \tag{J.4}$$

where $c_p = (\partial H/\partial T)_p$ is the specific heat at constant pressure, and H is the enthalpy.

The temperature of an arbitrary state can be calculated from the equation of state (J.3) if two other state variables (p and V) are known. However, as mentioned earlier, relation (J.3) is not very useful, since the cold compression curve $p_c\,(V)$ cannot be measured over the range of volumes (and pressures) of interest. Consider the case of a material that has been shocked to a state corresponding to the point $A\,(V_1,\ p_1)$ (Fig. J.3). Unloading takes place along the release isentrope, and point $B\,(V,\ p)$ is an equilibrium state. The internal energy at point B is equal to the shaded area V_0ABV. If we assume that the equilibrium

Table J.1 Heat capacity constants

	a	$b \cdot 10^3$	$c \cdot 10^{-5}$
	Joule/kg °K	Joule/kg °K^2	Joule/kg °K^3
granite	965	254	296
basalt	902	402	122

pressure p is small relative to the pressure p_1 after the shock, then the area under the cold compression curve (V_0DV) — the elastic internal energy — is a small portion of the total internal energy (area V_0ABV), and we can calculate the increase in temperature ΔT from the following equation:

$$e_t = \text{area}_{V_0ABV} = \int_{T_0}^{T_0+\Delta T} c_p(T)\,dT \tag{J.5}$$

It is not correct to use c_p in (J.5) because the pressure is not constant (i.e. there is a difference between p and p_o). However, since the difference between specific heats at constant volume and constant pressure is not large over a wide range of temperatures, the error introduced by this simplification is not large.

At high temperatures (above room temperature), the specific heat c_p can be expressed by an empirical relation of the type

$$c_p(T) = a + bT + cT^{-2} \ \left[\text{Joule/kg °K}\right] \tag{J.6}$$

The values of the coefficients in (J.6) for granite and basalt, as reported by Birch et al. (1942), are shown in Table J.1.

Profiles of the variation in temperature and internal energy in the rock at steady state, as a function of radial distance from the shot point, after a 1-kt explosion at the PTC, are shown in Figures J.4 and J.5.

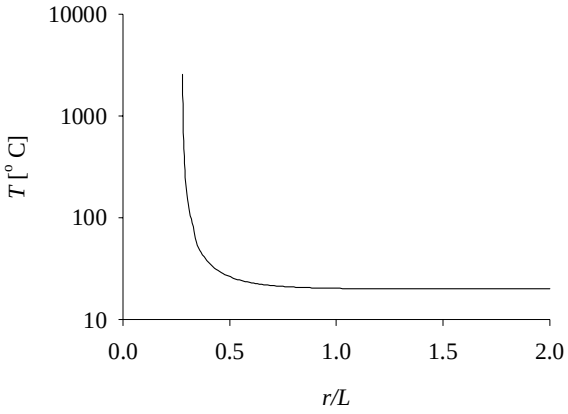

Figure J.4 Temperature profile

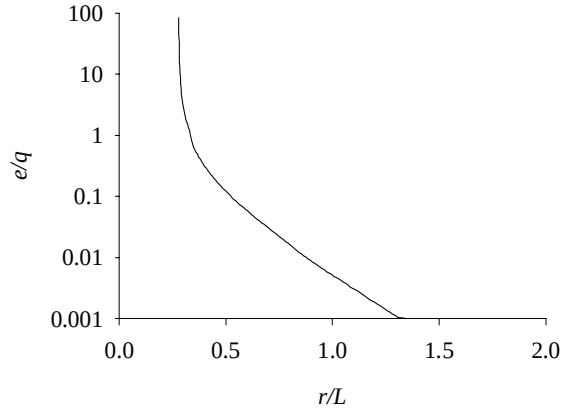

Figure J.5 Internal energy profile

Appendix K

MATHEMATICAL MODEL OF THE NEAR-FIELD MECHANICAL RESPONSE

K.1 Balance Laws

The model invokes conservation of momentum and mass, written in the Lagrangian form and assuming spherical symmetry, as follows:

momentum

$$\rho \frac{dv}{dt} = \frac{\partial \sigma_r}{\partial r} + \frac{2(\sigma_r - \sigma_\theta)}{r} \tag{K.1}$$

mass

$$\frac{d\rho}{dt} + \rho \left(\frac{\partial v}{\partial r} + 2\frac{v}{r} \right) = 0 \tag{K.2}$$

where v is the radial velocity, $\boldsymbol{\sigma}$ is the stress tensor (with the indices r and θ denoting radial and tangential component), r is the radial coordinate, and t is the time. Although the equation of energy conservation is not necessary for solution of the problem, it is instructive to check the global energy balance independently at every timestep during numerical simulation of the problem.

The rate of deformation tensor $\boldsymbol{D}$ can be reduced to the following two non-trivial components

$$D_r = \frac{\partial v}{\partial r} \tag{K.3}$$

$$D_\theta = \frac{v}{r} \tag{K.4}$$

which can each be decomposed into an elastic and plastic strain rate:

$$D_r = D_r^e + D_r^p \tag{K.5}$$

$$D_\theta = D_\theta^e + D_\theta^p \tag{K.6}$$

K.2 Constitutive Relations

K.2.1 Constitutive Relations at High Pressures

When the pressure is large compared to the shear strength of the rock, as is the case for the stress levels achieved in the rock mass surrounding the nuclear explosion, the deviatoric part of the stress tensor can be neglected. The constitutive relations between the mean stress (i.e. pressure) p, the spherical part $\mathrm{tr}\,\epsilon$ of the (Green–Saint Venant) strain tensor $\boldsymbol{\epsilon}$, and the internal energy e may be written as

$$p = f(\mathrm{tr}\,\boldsymbol{\epsilon}, e) \tag{K.7}$$

The equation of state for solids (K.7) cannot be determined directly for the range of strain and pressure generated in the rock mass in the vicinity of the nuclear explosion. Instead, Hugoniots (discussed in Appendix J) are measured experimentally and used in mathematical models.

As the shock propagates into the rock, it decays in intensity. Eventually, the pressure becomes comparable to the shear strength, and the complete tensor relation between stress and strain must be considered.

K.2.2 Elasto-plastic Constitutive Relations

It is assumed that rock material exhibits linearly elastic behaviour if the stress state does not satisfy the condition for plastic deformation (i.e. the yield condition). Linearly elastic relations between the components (in a spherical coordinate system) of the strain and stress tensors for an isotropic material can be written (in rate form), as

$$D_r^e = \frac{1}{E}\left(\dot{\sigma}_r - 2\nu\,\dot{\sigma}_\theta\right) \tag{K.8}$$

$$D_\theta^e = \frac{1}{E}\left[(1-\nu)\,\dot{\sigma}_\theta - \nu\dot{\sigma}_r\right] \tag{K.9}$$

where the dot above the σ denotes the Lagrangian (material) time derivative.

K.2.2.1 Yield Conditions

The following conditions for shear and tensile plastic deformation are used in this study:

Mohr-Coulomb shear yield condition $\quad f_s = \sigma_1 - \sigma_3 N_\phi + 2c\sqrt{N_\phi} \geq 0$

tension yield condition $\quad f_t = T - \sigma_3 \geq 0,$

where σ_1 and σ_3 are principal stresses, such that $\sigma_1 \leq \sigma_3$. (Compressive stresses are negative.) Therefore, the strength parameters required to define the yield behaviour of

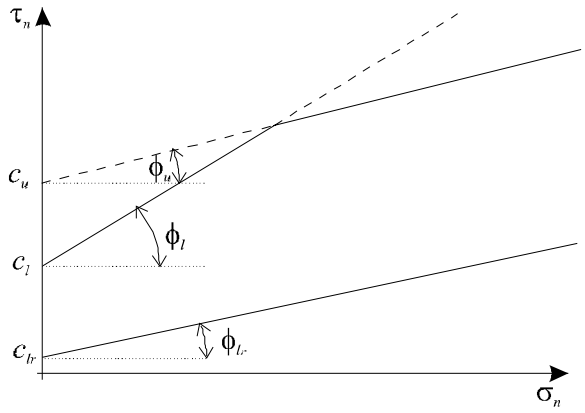

Figure K.1 Shear yield condition

the material are: (i) the cohesion c, (ii) the friction angle ϕ, and (iii) the tensile strength T. The parameter N_ϕ is defined as

$$N_\phi = \frac{1+\sin\phi}{1-\sin\phi} \tag{K.10}$$

The additional condition for the tensile strength is:

$$T \leq \frac{c}{1+\sin\phi} \tag{K.11}$$

A classical Mohr-Coulomb failure condition assumes constant cohesion c and friction angle ϕ. Here, however, a bilinear yield condition, characterised by two pairs of strength parameters (c_l, ϕ_l) and (c_u, ϕ_u) valid over two ranges of $(\sigma_1+\sigma_3)/2$ (as shown in Fig. K.1), is used as an approximation of a (more realistic) non-linear condition.

Generally speaking, the strength of the rock is dependent on the loading rate and reduces with increased duration of the load. Taking into account the stress history at a particular point in the problem being considered, the rate dependence of the strength is simulated by simple relations for the cohesion and friction with the duration $\bar{t}$ of the shear yield at the point:

$$\begin{aligned} c_l &= c_l\left(\bar{t}\right) \\ \phi_l &= \phi_l\left(\bar{t}\right) \\ c_u &= c_u\left(\bar{t}\right) \\ \phi_u &= \phi_u\left(\bar{t}\right) \end{aligned} \tag{K.12}$$

A typical form of the functional relations (K.12) used in the analysis is shown in Fig-

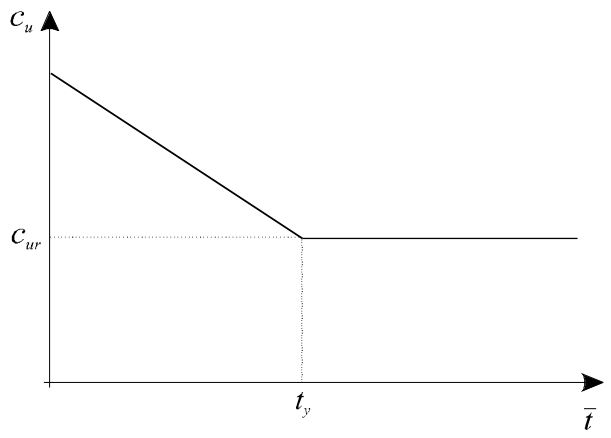

Figure K.2 Strength relaxation as a function of time

ure K.2. The strength of the rock changes also as a function of the plastic deformation—rock can rarely be considered a perfectly plastic material. Here, the amount of plastic shear strain ϵ^{ps} has been used as a hardening (or softening) parameter:

$$\begin{aligned} c_l &= c_l\left(\epsilon^{ps}\right) \\ \phi_l &= \phi_l\left(\epsilon^{ps}\right) \\ c_u &= c_u\left(\epsilon^{ps}\right) \\ \phi_u &= \phi_u\left(\epsilon^{ps}\right) \end{aligned} \tag{K.13}$$

where

$$d\epsilon^{ps} = \left[\frac{1}{2}\left(d\epsilon_1^{ps} - d\epsilon_m^{ps}\right)^2 + \frac{1}{2}\left(d\epsilon_2^{ps} - d\epsilon_m^{ps}\right)^2 + \frac{1}{2}\left(d\epsilon_3^{ps} - d\epsilon_m^{ps}\right)^2\right]^{1/2} \tag{K.14}$$

$$d\epsilon_m^{ps} = \frac{1}{2}\left(d\epsilon_1^{ps} + d\epsilon_3^{ps}\right) \tag{K.15}$$

The softening functions used in the analysis are similar to the relaxation shown in Figure K.2: a strength parameter decreases linearly as the plastic shear strain ϵ^{ps} changes between zero and the characteristic value ϵ_y.

K.2.2.2 Flow Rules

The flow rules define the non-linear, plastic deformation of the material. The principal plastic components of the rate of deformation tensor, D_i^{ps} (with $i = 1, 2, 3$) can be written as a function of the plastic potential for shear yielding $g_s(\sigma_i)$ (where σ_i denotes the principal stress components)

$$D_i^{ps} = \dot{\lambda}_s \frac{\partial g_s}{\partial \sigma_i} \tag{K.16}$$

while the plastic tensile strain rate D_i^{pt}, as a function of the plastic potential for tensile yielding $g_t(\sigma_i)$, is

$$D_i^{pt} = \dot{\lambda}_s \frac{\partial g_t}{\partial \sigma_i} \tag{K.17}$$

The tensile flow rule is assumed to be associated:

$$g_t = -\sigma_3 \tag{K.18}$$

However, the shear flow rule

$$f_s = \sigma_1 - \sigma_3 N_\psi \tag{K.19}$$

can be either associated

$$\psi = \phi$$

or non-associated

$$\psi \neq \phi$$

where ψ is the dilation angle.

Because the spherical symmetry of the problem enforces symmetry of the strain rates and stresses, that is:

$$\begin{array}{lll} \text{case 1:} & D_1 = D_r, & D_2 = D_3 = D_\theta \\ \text{case 2:} & D_1 = D_2 = D_\theta, & D_3 = D_r \end{array} \tag{K.20}$$

and

$$\begin{array}{lll} \text{case 1:} & \sigma_1 = \sigma_r, & \sigma_2 = \sigma_3 = \sigma_\theta \\ \text{case 2:} & \sigma_1 = \sigma_2 = \sigma_\theta, & \sigma_3 = \sigma_r \end{array} \tag{K.21}$$

Since the plastic potential (K.19) represents a pyramid in stress space, relations (K.21) imply that yielding always takes place at the "corner", which, in this particular case, means that the plastic potential is ill-defined (Fig. K.3). Since picking just one of the planes intersecting at the corner would result in plastic strains that violate relations (K.20), we have assumed that corners of the potential surface are rounded in such a way that the plastic strain rate is diagonal with respect to the two intersecting planes (see Fig. K.3). The plastic shear strain rate can then be written (Drescher 1991):

$$\text{case 1:} \quad \begin{array}{l} D_1^{ps} = 2\dot{\lambda} \\ D_2^{ps} = -\dot{\lambda} N_\psi \\ D_3^{ps} = -\dot{\lambda} N_\psi \end{array} \tag{K.22}$$

$$\text{case 2:} \quad \begin{array}{l} D_1^{ps} = \dot{\lambda} \\ D_2^{ps} = \dot{\lambda} \\ D_3^{ps} = -2\dot{\lambda} N_\psi \end{array} \tag{K.23}$$

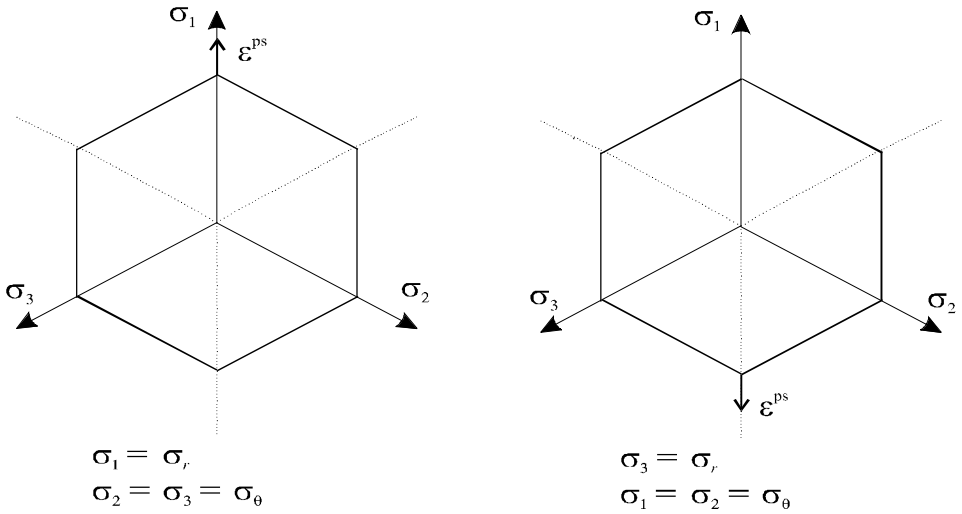

Figure K.3 Plastic potential and plastic shear strain in π-plane ($\psi = 0$)

The same reasoning also holds for tensile yielding:

$$\text{case 1:} \quad \begin{aligned} D_1^{pt} &= 0 \\ D_2^{pt} &= -\dot{\lambda} \\ D_3^{pt} &= -\dot{\lambda} \end{aligned} \tag{K.24}$$

$$\text{case 2:} \quad \begin{aligned} D_1^{pt} &= -\dot{\lambda} \\ D_2^{pt} &= -\dot{\lambda} \\ D_3^{pt} &= 0 \end{aligned} \tag{K.25}$$

Tensile "yielding" means fracturing of the rock. Any plastic tensile strain subsequent to fracturing either opens or closes the fracture. Therefore, a negative strain must first close the open fracture, after which the compressive stress will increase. The model simulates such a response, since plastic tensile strains are accumulated (if different from zero) and compressive stresses do not develop before the plastic tensile strains are reduced to zero.

Appendix L

NUMERICAL SIMULATION OF THE NEAR-FIELD MECHANICAL RESPONSE

L.1 Introduction

Many numerical codes for simulating the near-field response of a rock mass to a nuclear explosion have been developed over the last five decades in countries involved in the testing of nuclear weapons. One of the first codes, developed for the numerical solution of spherically symmetric, hydrodynamic-elastic-plastic models, was *UNEC* (Underground Nuclear Explosion Code), produced in the 1950s at the Lawrence Radiation Laboratory (LRL), Livermore, U.S.A. (Butkovich 1965). The next version of *UNEC*, called *SOC* (and also developed at the LRL), included more complex constitutive relations (e.g. strain rate effects). The two-dimensional code *TENSOR* (Maenchen and Sack 1964) was developed to analyse cylindrically symmetrical problems. All of these codes are based on a Lagrangian description of the mechanical processes and use the finite difference method for integration of the differential equations. A short description of the codes and their application to simulation of explosions at the Nevada Test Site (NTS) can be found in publications by Cherry (1967), Cherry et al. (1968), Butkovich (1965) and Holzer (1966). More recently, Mariotti and Thomas (1994) have developed the code *ARMOR*, inspired by *SOC* and *TENSOR*, for the simulation of underground nuclear explosions at the PTC.

The code *BOUM* (Damjanac 1996) has been written specifically at the request of the IGC to perform numerical simulation of the near-field response of a rock mass to a nuclear explosion. The intention in developing this code was not to implement very complex constitutive models of material behaviour, but to develop a simple model that would allow assessment of the effects and overall significance of all the relevant parameters.

The original Lagrangian formulation for numerical simulation of elastic-plastic flow, presented by Wilkins (1964) and Cundall [see the *FLAC* manual (Itasca Consulting Group, Inc. 1995)], has been retained. Spherical symmetry is assumed—a pressure wave originating at the boundary of a sphere diverges in an infinite, isotropic, homogeneous material. The mathematical model described in Appendix K has been solved using the finite difference method. The numerical solution has been programmed in *FISH*, a programming language built into the Itasca codes (Itasca Consulting Group, Inc. 1995). Because the general methods of the numerical procedure are well described in the lit-

erature (Maenchen and Sack 1964; Wilkins 1964; Holzer 1966; Cherry 1967; Itasca Consulting Group, Inc. 1995), they will not be repeated here.

This appendix describes the initial and boundary conditions used for the dynamic calculation, some algorithmic issues pertaining to the modelling of shock propagation, and particulars of the numerical simulations; it also compares the results of the numerical code with the published results of measurements and numerical simulations of the Hardhat underground nuclear explosion at the NTS.

L.2 Initial and Boundary Conditions

The initial state for the dynamic calculations corresponds to the end of the process of rock vaporization by the shock wave (which has been identified as time t_o). The initial state is thus characterised by an isotropic stress of magnitude σ_o in the rock, an initial spherical cavity of radius r_c formed by vaporization of the rock, and an initial pressure p_o applied to the wall of the cavity.

The initial radius r_c of the vaporized rock can be calculated from (3.17). Once the initial size of the cavity has been established, it is necessary to determine the boundary condition in terms of the radial velocity or pressure as a function of time. Four assumptions have been made in the analysis of cavity expansion (see also Radionov et al. 1971):

1. The initial velocities are zero and the initial energy is simply the internal energy of the gases inside the vaporized zone.
2. The pressure in the cavity is homogeneous.
3. The gas in the cavity behaves as a perfect gas.
4. The process of cavity expansion is adiabatic.

Combining the equation of state of a perfect gas and an equation for the adiabat yields an expression for the energy $Y_c(t)$ of the gas inside the cavity as a function of the volume $\mathcal{V}(t)$:

$$Y_c(t) = \frac{p_o \mathcal{V}(t)}{\gamma - 1}\left[\frac{\mathcal{V}_o}{\mathcal{V}(t)}\right]^{\gamma} \tag{L.1}$$

In particular, (L.1) gives a value for the initial pressure $p_o = p(0)$ as a function of the initial energy $Y_o = Y_c(0)$ of the gas in the cavity,

$$p_o = \frac{Y_o(\gamma - 1)}{\mathcal{V}_o} \tag{L.2}$$

and the boundary conditions

$$p(\mathcal{V}) = p_o\left(\frac{\mathcal{V}_o}{\mathcal{V}}\right)^{\gamma}$$

The coefficient γ is the effective gas constant. The initial energy Y_o, used in equation (L.2) is not the total energy Y of the device, but differs by the term $e_v \rho_0 \mathcal{V}_0$, which represents the latent heat of vaporisation:

$$Y_o = Y - e_v \rho_o \mathcal{V}_o = (1 - e_v \overline{M}_v) Y = (1 - \delta)\, Y$$

where e_v is the latent heat of vaporisation per unit mass.

L.3 Viscosity

In some simple cases of one-dimensional shock propagation, the Hugoniot equations (i.e. the balance laws across the shock front), together with the equilibrium equations, suffice to determine the motion of the shock front and also provide the needed boundary conditions at the shock front. The numerical solution is then obtained within the domain where all field variables are smooth while the shock front is a moving boundary of the domain.

The general numerical solution for shock propagation using the finite difference method, where the shock is automatically accommodated everywhere in the grid, "suffers" from the numerical dispersion that appears behind the shock front. According to von Neumann (Richtmyer and Morton 1967), this computational difficulty can be resolved by devising a method whereby artificial dissipative mechanisms (viscosity and heat conduction) take place across the shock front. Then, in such a calculation, the shock appears as a near discontinuity with the approximately correct jump and the correct speed of propagation. The artificial viscosity is chosen to be proportional to the square of the velocity gradient

$$q = k_q \frac{1}{V_0} \left(\frac{\partial v}{\partial r} \right)^2 \Delta a^2 \tag{L.3}$$

where k_q is a dimensionless coefficient, V_0 is the specific volume in the reference state, and Δa is the size of the grid zone. Use of the "quadratic" artificial viscosity gives good results since the shock thickness is then independent of the shock strength.

The following procedure has been devised to properly approximate the Hugoniot in the numerical solution with a finite thickness of the shock and to incorporate physical dissipation into the numerical solution. As mentioned earlier, the Hugoniot curve is constructed on the assumption of a jump (discontinuity) in pressure and specific volume across the shock and gives a relation between jumps in pressure, specific volume and internal energy. For example, the shock intensity in Figure L.1 is such that the material changes from state (p_o, V_o) to state (p_1, V_1) and the increase in energy is equal to the area of the triangle $V_0 C V_1$. In the finite difference numerical simulation, with finite thickness of the shock zone (due to dissipation across the shock), the field variables change across the shock in discrete jumps (from the initial state through states A and B

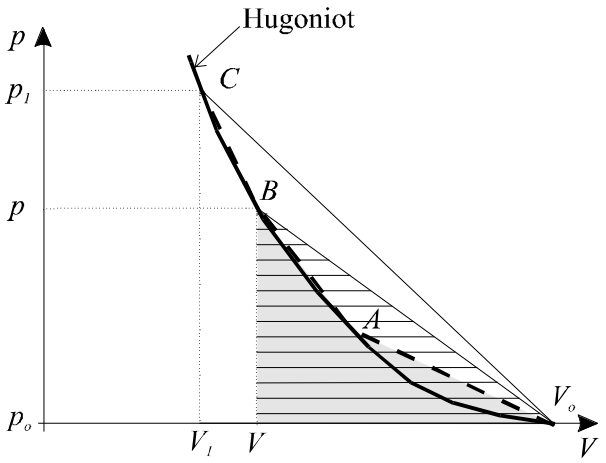

Figure L.1 Numerical approximation of energy increase across the shock front

to the final state C) that are smaller than the total jump across the shock. If the Hugoniot curve were to be used as an equilibrium curve, the relation between pressure and volume behind the shock would be correct (as given by the Hugoniot curve), but the increase in internal energy would be incorrect, being equal to the area under the polygonal line V_0ABC (instead of being equal to the area V_0CV_1, the jump implied by the Hugoniot curve). In order to properly approximate the increase in internal energy, the viscous forces are added across the shock, in such a way that, for example at state B, although this is not behind the shock, the work of the viscous forces is equal to the difference between the area of the triangle V_0BV and the area under the polygonal line V_0AB. Consequently, the increase in internal energy behind the shock (state C) must be equal to the area of the triangle V_0CV_1.

Artificial, quadratic viscosity is added to the physical dissipation only if, for a given domain discretisation, physical dissipation is insufficient to damp out numerical dispersion. Artificially dissipated energy (around 10%) is compensated for by an increase in the initial energy Y_o.

L.4 Particulars of the Numerical Simulations for PTC

The material properties used in the numerical simulations of underground nuclear explosions at the PTC are shown in Chapter 3 as Table 3.3 and in Figure L.2 (Hugoniot curve). The initial pressure in the cavity was calculated to be $p_o = 80$ GPa; the scaled initial cavity radius was $\overline{r}_c = 1.92$ m/kt$^{1/3}$.

A non-uniform grid was used in the simulations. For example, for a 1-kt simulation, the zone size increases linearly from 0.3 m at the cavity boundary to 1.0 m at the far-field boundary of the numerical model. The size of the model (e.g. 500 m for the 1-kt

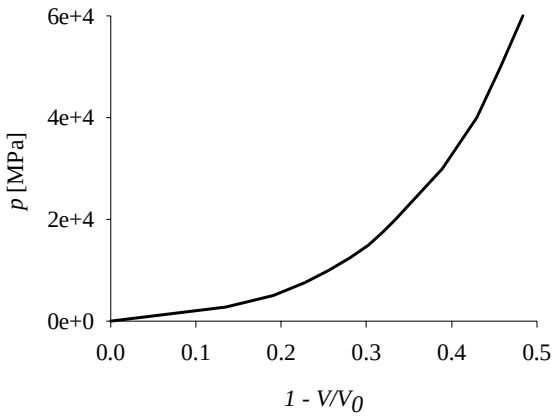

Figure L.2 The Hugoniot curve for the volcanic submarine formation

simulation) was chosen to contain the domain of inelastic deformation of the rock mass and to provide sufficient time (before reflection of the seismic wave from the far-field boundary) to capture the complete evolution of the cavity radius. Because models for different yields are almost geometrically similar, the computational cost does not change as a function of the yield if satisfactory discretisation lengths are rescaled accordingly. The average simulation time on a 100 MHz Pentium PC was approximately 16 hours.

L.5 Verification

It is not possible to verify the numerical solution since there is no analytical solution for this type of problem. Instead, results obtained with *BOUM* were compared with published monitoring results and numerical solutions of the Hardhat event. This underground nuclear explosion at NTS was particularly well monitored: stresses, displacements and velocities were measured at different distances from the point of the explosion. The measurements and different numerical solutions of the mathematical models can be found in the published literature (Butkovich 1965; Butkovich 1971; Holzer 1966; Cherry 1967; Rodean 1971). The energy of the explosion was about 5 kt, and the initial pressure inside the sphere of vaporized rock ($r = 3.15$ m) was 130 GPa (Rodean 1971). The explosion was in a relatively non-porous granite with a small percentage of water content. The magnitude of the initial (hydrostatic) stress was assumed to be $\sigma_o = 10$ MPa. The mechanical properties used in the calculations are shown in Table L.1 and Figure L.3 (Holzer 1966).

The numerical solution obtained by the *BOUM* code is compared with results and measurements published by Rodean (1971), in Figures L.4 and L.5. The agreement between the measured and calculated stress history at 42 m distance (Fig. L.4) is quite

Table L.1 Assumed mechanical properties of the granite used in the simulation of the Hardhat event

density	ρ_0	2670	kg/m^3
bulk modulus	K	36100	MPa
shear modulus	G	31500	MPa
friction angle	ϕ_l	30°	
friction angle	ϕ_u	0°	
cohesion	c_l	50	MPa
cohesion	c_u	2000	MPa
residual cohesion	c_{lr}	0	
residual friction angle	ϕ_{lr}	5°	
tensile strength	σ_t	0	

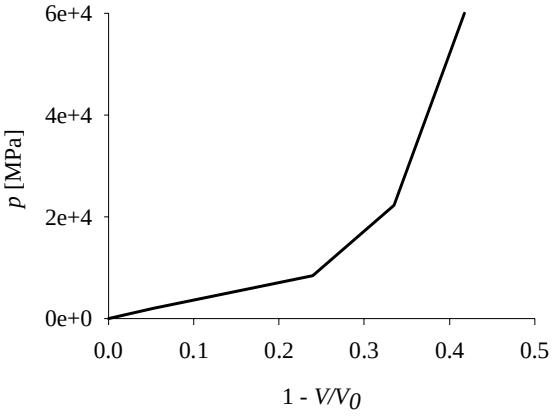

Figure L.3 Assumed Hugoniot curve for the Hardhat granite

good. Comparison of the evolution of the cavity as a function of time simulated by the two different numerical codes (Fig. L.5) shows that: (i) the calculated final radii of the cavity are in good agreement, and (ii) the calculated time scales for evolution of the cavity are quite different. The difference in time scale (a factor of approximately 4 in this case) can be attributed to the "relaxation time" of the granite, which is not given in the published literature.

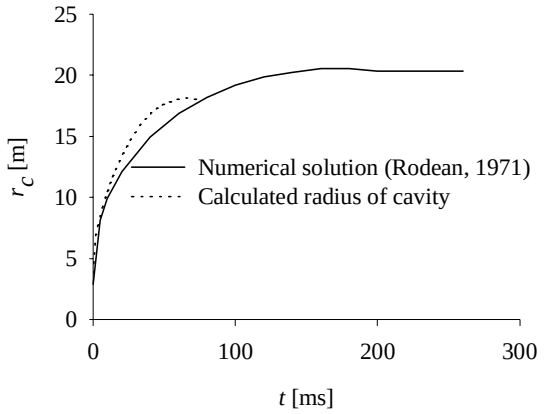

Figure L.4 Cavity expansion

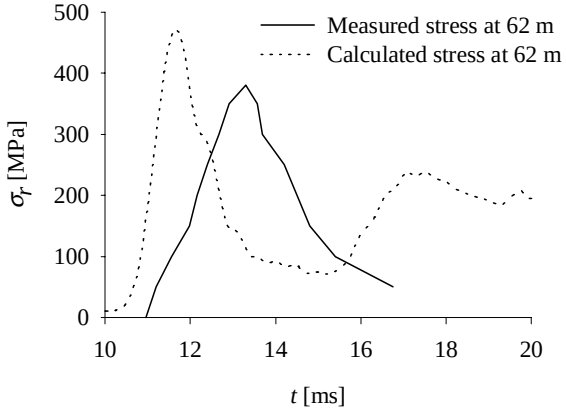

Figure L.5 Stress history at 62 m from the location of the explosion

Appendix M

QUASI-STATIC CAVITY EXPANSION OF A PRESSURISED CAVITY IN AN INFINITE MEDIUM

M.1 Introduction

An upper bound to the final radius of the cavity and to the outer radius of the damaged rock region created by a nuclear explosion can be obtained from considerations involving the quasi-static expansion of a pressurised spherical cavity in an infinite medium. Such a problem is characterised by the existence of a limiting internal pressure p_c, generally referred to as the cavitation pressure, for which unbounded growth of the cavity takes place. The cavitation pressure p_c, as well as the (constant) ratio ξ_* of the radius of the elastoplastic boundary over the current cavity radius, can be determined by treating the self-similar problem of a spherical cavity expanding from a zero initial radius (Hill 1950; Collins and Stimpson 1994). This appendix outlines the solution of p_c and ξ_* for an elastoplastic, perfectly brittle material, and the application of this solution for the determination of an upper bound to the final cavity radius r_c created by a nuclear explosion of yield Y.

In the general problem of cavity expansion, the mechanical fields (e.g. velocity and stress) are functions of both position (radius r) and an evolution parameter (such as the current cavity radius a) which varies monotonically with time t. (Time is not an intrinsic independent variable here, because the quasi-static nature of the problem considered and the rate independence of the material response.) However, the problem of a cavity expanding from a zero cavity radius can be expressed in terms of the single similarity variable $\xi = r/a$. It then follows that the partial differential equations (in terms of the position variable r and the evolution variable a) can be transformed into ordinary differential equations in ξ using the following transformation rules:

$$\frac{\partial}{\partial r} = \frac{1}{a}\frac{d}{d\xi} \tag{M.1}$$

$$\dot{(\,)} = (v - \xi)\frac{1}{a}\frac{d}{d\xi} \tag{M.2}$$

where $\dot{(\,)}$ denotes the Lagrangian "time" derivative (material "time" derivative) and v the particle "velocity". (Note that the terms "time" derivative and "velocity" are to be understood as rates of change with respect to a.)

M.2 Governing Equations

The equilibrium equations reduce to a single equation (Sokolnikoff 1956), which can be directly expressed in terms of the similarity variable $\xi = r/a$:

$$\frac{d\sigma_r}{d\xi} + 2\frac{\sigma_r - \sigma_\theta}{\xi} = 0 \tag{M.3}$$

The failure and post-failure responses of the material are assumed to be characterised by both a Mohr-Coulomb failure criterion (described in terms of a peak uniaxial compressive strength q and a peak friction angle ϕ) and a Mohr-Coulomb residual yield criterion (described by a residual uniaxial compressive strength q_r and a residual friction angle ϕ_r). It is further assumed that the material is perfectly brittle — i.e. once the failure criterion is met, the strength parameters drop abruptly from their peak (q, ϕ) to their residual values (q_r, ϕ_r).

Due to the spherical symmetry of this problem, the stress at failure must be on an "edge" of the Mohr-Coulomb failure surface. Furthermore, noting that σ_r is the most compressive stress, the failure criterion can be written as

$$\sigma_r - \frac{q}{N_\phi - 1} = N_\phi \left(\sigma_\theta - \frac{q}{N_\phi - 1} \right) \tag{M.4}$$

where $N_\phi = (1+\sin\phi)/(1-\sin\phi)$. Similarly, the residual yield criterion can be written as

$$\sigma_r - \frac{q_r}{N_\phi^r - 1} = N_\phi^r \left(\sigma_\theta - \frac{q_r}{N_\phi^r - 1} \right) \tag{M.5}$$

where $N_\phi^r = (1+\sin\phi_r)/(1-\sin\phi_r)$.

It is convenient to introduce the limiting value of the stress invariant $S = -(\sigma_r - \sigma_\theta)/2$ for both peak and residual state. From the yield conditions (M.4) and (M.5),

$$S_o^l = \frac{3}{2}\frac{N_\phi - 1}{N_\phi + 2}(\sigma_o + \frac{q}{N_\phi - 1}) \tag{M.6}$$

$$S_o^{lr} = \frac{3}{2}\frac{N_\phi^r - 1}{N_\phi^r + 2}(\sigma_o + \frac{q_r}{N_\phi^r - 1}) \tag{M.7}$$

where σ_o is the magnitude of the far-field isotropic stress. The ratio of limiting deviators is referred to as χ ($0 \le \chi \le 1$):

$$\chi = \frac{S_o^{lr}}{S_o^l} \tag{M.8}$$

At failure and in the residual yield state, the rate of deformation consists of an elastic and a plastic part (see Appendix K for details)

$$D_{ij} = D^e_{ij} + D^p_{ij} \tag{M.9}$$

The elastic component D^e_{ij} is related to the stress rate through Hooke's law, (K.8) and (K.9), and the plastic component D^p_{ij} is given by the flow rule

$$D^p_{ij} = \lambda \frac{\partial g}{\partial \sigma_{ij}} \tag{M.10}$$

where the potential function $g(\sigma_{ij})$ is of the Mohr-Coulomb type. Since the stress is on an edge of the potential surface, there are equal contributions to the strain rate increment from the two potential planes, and

$$D^p_r = -2\lambda \tag{M.11}$$

$$D^p_\theta = \lambda N_\psi \tag{M.12}$$

where N_ψ is the dilatancy factor, which is defined in terms of the dilatancy angle ψ ($0 \le \psi \le \phi$) as

$$N_\psi = \frac{1+\sin\psi}{1-\sin\psi} \tag{M.13}$$

Eliminating λ in (M.11) and (M.12) yields

$$2D^p_\theta + N_\psi D^p_r = 0 \tag{M.14}$$

M.3 Stress Field

M.3.1 Elastic Zone

The stresses in the elastic region ($\xi > \xi_*$) are given by Lamé's solution (Sokolnikoff 1956; Timoshenko and Goodier 1987)

$$\sigma_r = -\sigma_o + (\sigma^*_r + \sigma_o)\left(\frac{\xi_*}{\xi}\right)^3 \tag{M.15}$$

$$\sigma_\theta = -\sigma_o - \frac{1}{2}(\sigma^*_r + \sigma_o)\left(\frac{\xi_*}{\xi}\right)^3 \tag{M.16}$$

where σ^*_r is the radial stress at $\xi = \xi_*$. The radial stress σ^*_r can be computed by noting that the material on the elastic side of the elasto-plastic boundary is about to fail, i.e. the stresses satisfy the failure criterion (M.4). Indeed, substituting σ_θ at $\xi = \xi_*$ according to (M.16) in (M.4) yields

$$\sigma^*_r = -\frac{2q + 3N_\phi \sigma_o}{N_\phi + 2} \tag{M.17}$$

M.3.2 Plastic Region

Determination of the stresses in the plastic region ($1 < \xi < \xi_*$) requires solving a first order differential equation in σ_r, obtained by combining the equilibrium equation (M.3) with the residual yield criterion (M.5)

$$\frac{d\sigma_r}{d\xi} + \frac{2(N_\phi^r - 1)}{N_\phi^r}\frac{\sigma_r}{\xi} = \frac{2q_r}{N_\phi^r \xi} \tag{M.18}$$

Solution of (M.18) with the boundary condition $\sigma_r = \sigma_r^*$ at $\xi = \xi_*$, together with (M.5), gives the stress field in the plastic region

$$\sigma_r = \frac{q_r}{N_\phi^r - 1} + \left(\sigma_r^* - \frac{q_r}{N_\phi^r - 1}\right)\left(\frac{\xi_*}{\xi}\right)^{2(N_\phi^r - 1)/N_\phi^r} \tag{M.19}$$

$$\sigma_\theta = \frac{q_r}{N_\phi^r - 1} + \frac{1}{N_\phi^r}\left(\sigma_r^* - \frac{q_r}{N_\phi^r - 1}\right)\left(\frac{\xi_*}{\xi}\right)^{2(N_\phi^r - 1)/N_\phi^r} \tag{M.20}$$

where the term $\sigma_r^* - \frac{q_r}{N_\phi^r - 1}$ can be expressed as

$$\sigma_r^* - \frac{q_r}{N_\phi^r - 1} = -\frac{2S_o^l}{3}\left[2 + \chi\frac{N_\phi^r + 2}{N_\phi^r - 1}\right] \tag{M.21}$$

in view of (M.17), (M.6), and (M.7).

Because the cavitation pressure p_c corresponds to $\sigma_r = -p_c$ at $\xi = 1$, a relation between p_c and ξ_* can be established using (M.19)

$$\xi_* = \left[-\frac{(N_\phi^r - 1)p_c + q_r}{(N_\phi^r - 1)\sigma_r^* - q_r}\right]^{\frac{N_\phi^r}{2(N_\phi^r - 1)}} \tag{M.22}$$

Alternatively, the stresses in the plastic region can be expressed in terms of the cavitation pressure by substituting ξ_* in (M.19) and (M.20) by the expression given by (M.22)

$$\sigma_r = \frac{q_r}{N_\phi^r - 1} - \left(p_c + \frac{q_r}{N_\phi^r - 1}\right)\xi^{-2(N_\phi^r - 1)/N_\phi^r} \tag{M.23}$$

$$\sigma_\theta = \frac{q_r}{N_\phi^r - 1} - \frac{1}{N_\phi^r}\left(p_c + \frac{q_r}{N_\phi^r - 1}\right)\xi^{-2(N_\phi^r - 1)/N_\phi^r} \tag{M.24}$$

M.4 Velocity Field in the Plastic Region

M.4.1 Differential Equation

Expressing the total deformation rate in terms of the radial velocity v

$$D_r = \frac{\partial v}{\partial r} \qquad D_\theta = \frac{v}{r} \tag{M.25}$$

and writing the plastic deformation rate as the difference between the total deformation rate and the elastic deformation rate, the flow rule (M.14) transforms into

$$N^r_\psi \frac{d\widetilde{v}}{d\xi} + 2\frac{\widetilde{v}}{\xi} = a(2D^e_\theta + N^r_\psi D^e_r) \tag{M.26}$$

where the change of coordinates $\xi = r/a$ has been taken into account. The inhomogeneous term in (M.26) is calculated using the stress solution (M.19) and (M.20), the constitutive relations (K.8) and (K.9), and the consistency condition

$$\dot{\sigma}_r = N^r_\phi \dot{\sigma}_\theta \tag{M.27}$$

The right-hand side of (M.26) can thus be rewritten as

$$a(2D^e_\theta + N^r_\psi D^e_r) = \frac{a\lambda\dot{\sigma}_r}{2G} \tag{M.28}$$

where λ is a number given by

$$\lambda = \frac{1}{(1+\nu)N^r_\phi}[N^r_\phi N^r_\psi + 2 - 2\nu(N^r_\phi + N^r_\psi + 1)] \tag{M.29}$$

Note that for an incompressible, frictionless material ($\nu = 0.5$, $N^r_\phi = 1$, and $N^r_\psi = 1$), $\lambda = 0$. Using the differentiation rule (M.2), the expression for the Lagrangian derivative $\dot{\sigma}_r$ can readily be derived from (M.19)

$$\dot{\sigma}_r = \frac{4\eta S^\ell_o}{a}\left(\frac{v}{\xi} - 1\right)\left(\frac{\xi}{\xi_*}\right)^{2(1-N^r_\phi)/N^r_\phi} \tag{M.30}$$

where the number η is defined as

$$\eta = \frac{1}{3N^r_\phi}\left[2\left(N^r_\phi - 1\right) + \chi\left(N^r_\phi + 2\right)\right] \tag{M.31}$$

Note that $0 \le \eta \le 1$ and that $\eta = 1$ if the material is perfectly plastic ($\chi = 1$).

Taking into account (M.28) and (M.30), the compatibility equation (M.26) is finally written as

$$N^r_\psi \frac{d\widetilde{v}}{d\xi} + 2\frac{\widetilde{v}}{\xi}\left[1 - \lambda\eta\kappa\left(\frac{\xi}{\xi_*}\right)^{2(1-N^r_\phi)/N^r_\phi}\right] = -2\lambda\eta\kappa\left(\frac{\xi}{\xi_*}\right)^{2(1-N^r_\phi)/N^r_\phi} \tag{M.32}$$

M.4.2 Velocity Boundary Conditions

Consider now the velocity at the elastic/plastic interface, $\xi = \xi_*$. If the material is perfectly brittle (i.e. if $\chi < 1$), a material point will experience a velocity jump at $\xi = \xi_*$ as it passes from the elastic to the plastic side of the elastoplastic boundary. Let quantities on the elastic side of the elasto-plastic interface be assigned the superscript $^{[+]}$ and on the plastic side the superscript $^{[-]}$. For example, $v_*^{[+]}$ and $v_*^{[-]}$ denote the velocity on the elastic and the plastic side of the interface, respectively.

If the displacement u of a material is "small", the difference between the Lagrangian and Eulerian time derivative can be neglected. It then follows that the following exact expression for the velocity v

$$v = \frac{\partial u}{\partial a}\left(1 - \frac{\partial u}{\partial r}\right)^{-1} \tag{M.33}$$

can be simplified to

$$v = \frac{\partial u}{\partial a} \tag{M.34}$$

The approximation embodied in (M.34) implies that the displacement u is necessarily of the form

$$u(r, a) = a\widetilde{u}(\xi) \tag{M.35}$$

and, therefore,

$$\widetilde{v} = \widetilde{u} - \xi\frac{d\widetilde{u}}{d\xi} \tag{M.36}$$

The above expressions (M.34), (M.35) and (M.36) are applicable only in the elastic region and near the elastoplastic interface. They are used below to derive an expression for the velocity jump across the interface.

Consider first the velocity on the plastic side of the interface. In the elastic region, the displacement field is given by the Lamé solution (Sokolnikoff 1956; Timoshenko and Goodier 1987)

$$\widetilde{u} = \frac{\kappa\xi_*^3}{3\xi^2} \tag{M.37}$$

Hence, from (M.36) and (M.37), the radial velocity on the elastic side of the elastoplastic interface is derived to be

$$v_*^{[+]} = \kappa\xi_* \tag{M.38}$$

Consider next the velocity on the plastic side of the interface. First, note that the displacement is necessarily continuous at the interface; therefore, the tangential strain ε_θ is also continuous across $\xi = \xi_*$ — i.e. $\varepsilon_\theta^{[+]} = \varepsilon_\theta^{[-]}$, according to the Maxwell compatibility condition. The velocity jump is thus associated with the jump of the radial strain ε_r.

Strains on the plastic side consist of an elastic and a plastic part; hence, the (total) radial strain can then be expressed as $\varepsilon_r^{[-]} = \varepsilon_r^{e[-]} + \varepsilon_r^{p[-]}$; the plastic component of radial strain is related to the tangential component by the flow rule (M.14) as $\varepsilon_r^{p[-]} = -2/N_\psi \varepsilon_\theta^{p[-]}$. When the plastic component of tangential strain is expressed in terms of total and elastic components (i.e. $\varepsilon_\theta^{p[-]} = \varepsilon_\theta - \varepsilon_\theta^{e[-]}$), the former equations allow the radial strain on the plastic side to be computed as

$$\varepsilon_r^{[-]} = \varepsilon_r^{e[-]} - \frac{2}{N_\psi}\left[\varepsilon_\theta - \varepsilon_\theta^{e[-]}\right] \tag{M.39}$$

The strains $\varepsilon_\theta^{e[-]}$ and $\varepsilon_r^{e[-]}$ are then computed from Hooke's relations (K.8) and (K.9), with the stresses σ_r and σ_θ given by (M.19) and (M.20). An explicit expression for $\varepsilon_r^{[-]}$ can then be deduced from (M.39), taking into account that $\varepsilon_\theta = \widetilde{u}/\xi = \kappa/3$ on the interface. Finally, the velocity $v_*^{[-]}$ on the plastic side of the interface is determined from (M.36), noting that $\varepsilon_r = d\widetilde{u}/d\xi$

$$v_*^{[-]} = \kappa\xi_*\left[1 + (1-\chi)\gamma\right] \tag{M.40}$$

where

$$\gamma = \frac{2(1-\nu)(N_\phi^r + 2) - 2\nu N_\phi^r N_\psi - 4\nu N_\psi}{3(1+\nu)N_\phi^r N_\psi} \tag{M.41}$$

It can be shown that $\gamma \geq 0$. The velocity is continuous at the interface ($v_*^{[-]} = v_*^{[+]} = \kappa\xi_*$) if the material is frictionless and incompressible ($\gamma = 0$) or if the material is perfectly plastic ($\chi = 1$).

M.4.3 Solution for the Radial Velocity in the Plastic Zone

The velocity field in the plastic zone is determined from the differential equation (M.32) in conjunction with the boundary condition

$$\widetilde{v} = v_*^{[-]} \qquad \text{at} \qquad \xi = \xi_* \tag{M.42}$$

The velocity v cannot be solved in closed form, however, unless some approximations are made to (M.32).

An approximate solution of the velocity field can readily be obtained by neglecting the term with the small number κ in the left-hand side of (M.32). Solution of the resulting simplified differential equation, together with the boundary condition (M.42), yields

$$\widetilde{v} = \left[1 + (1-\chi)\gamma + \mu\right]\kappa\xi_*\left(\frac{\xi_*}{\xi}\right)^{2/N_\psi^r} - \mu\kappa\xi_*\left(\frac{\xi_*}{\xi}\right)^{(N_\phi^r - 2)/N_\phi^r} \tag{M.43}$$

where μ is a number defined as

$$\mu = \frac{2\lambda\eta N_\phi^r}{2(N_\phi^r + K_p^{*\prime}) - N_\phi^r N_\psi^r}$$

An improved approximation relies on expanding in a Taylor series the term $2\eta\lambda\kappa(\widetilde{v}/\xi)\cdot(\xi/\xi_*)^{2(1-N_\phi)/N_\phi}$ in (M.32). By retaining the first two terms of this expansion, a linear first order differential equation is obtained with the solution given by

$$\widetilde{v} = \left[1+\mu+(1-\chi)\gamma - \beta_1\kappa\right]\kappa\xi_*\left(\frac{\xi_*}{\xi}\right)^{2/N_\psi^r} - \mu\kappa\xi_*\left(\frac{\xi_*}{\xi}\right)^{(N_\phi^r-2)/N_\phi^r} \tag{M.44}$$

$$+2\eta\lambda\kappa^2\xi\left[\frac{1+2\beta_2}{2+N_\psi^r} - \frac{\beta_2}{1+N_\psi^r}\left(\frac{\xi}{\xi_*}\right)\right] \tag{M.45}$$

In the above, the new numbers β_1 and β_2 are defined as

$$\beta_1 = \frac{2\lambda\eta\left[1+(1+\beta_2)N_\psi^r\right]}{(N_\psi^r+2)(N_\psi^r+1)}$$

$$\beta_2 = \left(\frac{1-\lambda\eta\kappa}{N_\psi^r} - \frac{1}{N_\phi^r} + \frac{3}{2}\right) + \frac{\lambda\eta}{N_\psi^r} \tag{M.46}$$

M.5 Elastoplastic Interface and Cavitation Pressure

The position of the elasto-plastic interface ξ_* is finally determined from the velocity solution using the boundary condition $v=1$ at $\xi=1$. Using the approximation (M.43) of the velocity field, the following transcendental equation in ξ_* is obtained

$$\left[1+(1-\chi)\gamma+\mu\right]\xi_*^{(K_p^{*\prime}+2)/N_\psi^r} - \mu\xi_*^{2(N_\phi^r-1)/N_\phi^r} = \frac{1}{\kappa} \tag{M.47}$$

Note that solution of the equation for ξ_* based on the improved approximation (M.44) for v is hardly different from the value of ξ_* predicted by (M.47).

Finally, an expression for the cavitation pressure p_c is derived from (M.22)

$$\frac{p_c}{S_o^l} = \frac{2}{3}\left[2+\chi\frac{N_\phi^r+2}{N_\phi^r-1}\right]\xi_*^{2(N_\phi^r-1)/N_\phi^r} - \frac{q_r}{(N_\phi^r-1)S_o^l} \tag{M.48}$$

It is convenient to introduce a dimensionless cavitation pressure Π as follows

$$p_c - \sigma_o = \Pi q' \tag{M.49}$$

where

$$\Pi = \frac{1}{N_\phi+2}\left\{\left[2+\chi\frac{N_\phi^r+2}{N_\phi^r-1}\right]\xi_*^{2(N_\phi^r-1)/N_\phi^r} - \chi\frac{N_\phi^r+2}{N_\phi^r-1}\right\} \tag{M.50}$$

and

$$q' = q + (N_\phi-1)\sigma_o \tag{M.51}$$

M.6 Cavity Size Created by an Underground Nuclear Explosion

An upper bound for the final cavity volume $\mathcal{V}_c$ created by a nuclear explosion of yield Y can be computed using the cavitation pressure. The calculation of $\mathcal{V}_c$ described below is slightly different from the approach described in Section 3.5.5, since it takes into account the initial volume $\mathcal{V}_o$ of the cavity (corresponding to the vaporized rock) and the residual energy of the gas, Y_r, left after expansion of the cavity. Using

$$\left(\frac{\mathcal{V}_c}{\mathcal{V}_o}\right)^{\gamma-1} = \frac{Y_o}{Y_r} \tag{M.52}$$

deduced from (3.19) and (3.20), and equating the mechanical work $W = \Pi q'(\mathcal{V}_c - \mathcal{V}_o)$ to the energy change $Y_o - Y_r$ in the gas, we obtain the following equation, to be solved for the dimensionless cavity volume $v_c = \mathcal{V}_c/\mathcal{V}_o$

$$v_c + \omega v_c^{1-\gamma} - (1+\omega) = 0 \tag{M.53}$$

where ω is a number defined as

$$\omega = \frac{(1-\delta)\rho_o}{\Pi M_v q'} \tag{M.54}$$

Because ω is a number $O(10^2)$ and the effective gas constant $\gamma \simeq 1.7$, the solution of (M.53) is given approximately by

$$v_c \simeq \omega \tag{M.55}$$

which is actually the solution (3.32). The quality of this approximation simply reflects the fact that the initial volume $\mathcal{V}_o$ is negligible compared to $\mathcal{V}_c$ and that the residual energy Y_r can be neglected.

Appendix N

HEIGHT OF CHIMNEY PRODUCED BY AN UNDERGROUND NUCLEAR EXPLOSION

Calculation of the chimney height H_c is based on the simple consideration that the maximum height is attained when both the cavity and the chimney are filled by rock blocks and debris produced by the formation of the chimney, assuming a certain shape of the chimney and taking into account the bulking of broken rock. Thus,

$$\mathcal{V}_c = B\mathcal{V} \tag{N.1}$$

where $\mathcal{V}_c$ is the cavity volume, $\mathcal{V}$ is the volume of the chimney, and B is the bulking factor.

First, assume the chimney to be cylindrical with a flat top (see Fig. N.1). (This is consistent with observations made in mining environments in horizontally bedded strata.)

Here, the chimney volume $\mathcal{V}$ consists of $\mathcal{V}_1$, the volume of the cylinder above the top of the cavity, and $\mathcal{V}_2$, the shaded volume (see Fig. N.1). These volumes and $\mathcal{V}_c$ can be expressed in terms of the cavity radius r_c and the chimney height H_c as follows

$$\mathcal{V}_c = \frac{4}{3}\pi R_c^3 \tag{N.2}$$

$$\mathcal{V}_1 = \pi R_c^2 (H_c - R_c) \tag{N.3}$$

$$\mathcal{V}_2 = \frac{\pi}{3} R_c^3 \tag{N.4}$$

From the above expressions and (N.1), it is readily deduced that

$$H_c = \frac{2}{3} R_c \left(\frac{2}{B} + 1\right) \tag{N.5}$$

Thus, if $B = 0.2$ (a low value),

$$H_c = 7.33\ R_c$$

and if $B = 0.4$ (a high value),

$$H_c = 4\ R_c$$

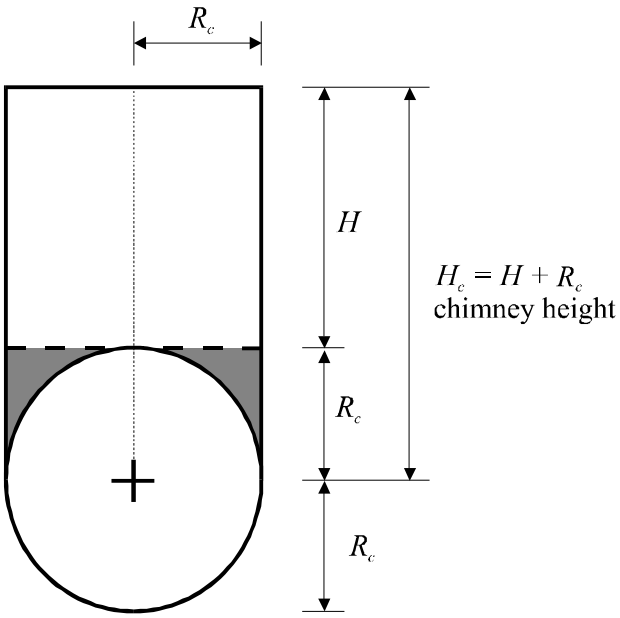

Figure N.1 Cylindrical chimney

These provide reasonable limits for the height of the chimney and are consistent with CEA observations (DIRCEN/CEA 1998b). (Perhaps B could be reduced to 0.15, in which case, $H = 9.56\,R = 9.56\,R_c$ in the extreme case.)

An alternative approach is to assume that the chimney takes the form of an ellipsoid, so that its greatest width could exceed $2\,R_c$.

If a, b, c are the lengths of the semi-axes of the ellipsoid, then its volume $\mathcal{V}_e$ is

$$\mathcal{V}_e = \frac{4}{3}\pi\ a\,b\,c$$

For the purposes of the exercise, let $b = c$:

$$\mathcal{V}_c = \frac{4}{3}\pi\ a\,b^2$$

To a very good approximation, this is the total volume to be filled. The material available is that contained in the volume $\mathcal{V} = \mathcal{V}_e - \mathcal{V}_c$. Thus, in the limit,

$$\mathcal{V}_e\,B = \mathcal{V}_c\,(1 + B) \tag{N.6}$$

On substitution, this reduces to

$$a = \frac{R_c^3\ (1 + B)}{b^2\,B} \tag{N.7}$$

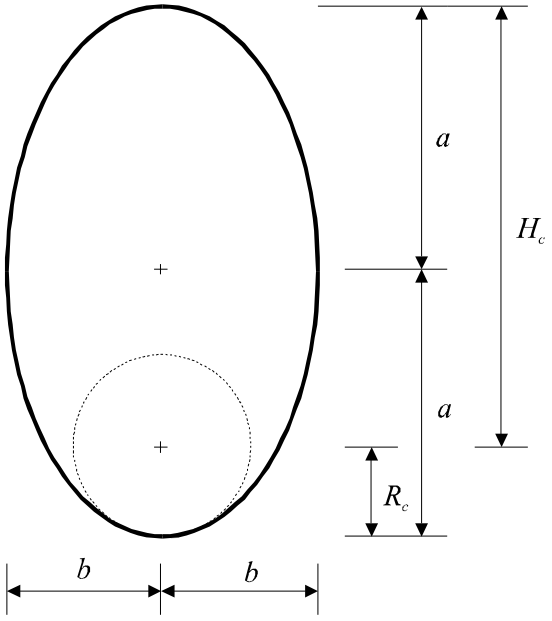

Figure N.2 Ellipsoidal chimney

In order to obtain some illustrative solutions, let b be a multiple of r_c (i.e., $b = k\,R_c$). Then,

$$a = \frac{R_c}{k^2}\left(1 + \frac{1}{B}\right) \tag{N.8}$$

It follows therefore that

$$H_c = R_c(2\,a - 1) \tag{N.9}$$

Hence,

$$H_c = 2R_c\left[\frac{1}{k^2}\left(1 + \frac{1}{B}\right) - 1\right] \tag{N.10}$$

Consider some values for k and B. If $k = 1.2$, $H_c = 6.3\,R_c$ for $B = 0.20$ and $H_c = 2.9\,R_c$ for $B = 0.40$; if $k = 1.5$, $H_c = 3.6\,R_c$ for $B = 0.20$ and $H_c = 1.3\,R_c$ for $B = 0.40$. It is difficult to imagine a case in which $b \gg R_c$. Value $k = 1.5$ would appear to be a reasonable upper limit.

Figure N.3 shows a comparison between two cylindrical cavities/chimneys (flat and arched roof in each case) and an equivalent ellipsoidal cavity/chimney — all for a 150-kt explosion:

(1) $H_c = 5\,R_c$, the standard chimney/cavity ratio used in most of this report;

(2) $H_c = 7.7\ R_c$, the cavity calculated for a 150-kt explosion at a depth of 1100 m using the empirical expression (DIRCEN/CEA Document No. 6) $H_c = 1100\ (Y/h)^{1/2}$, where Y is the explosive yield in kt and h is the depth of burial in m. A cavity of these dimensions — with $R_c = 10\ Y^{1/3} = 53$ m (for $Y = 150$ kt) — is obtained from (N.5), when $B = 0.19$; and

(3) an ellipsoidal cavity that

   (a) is of equivalent volume to the high, flat-roofed cavity $H_c = 7.7\ R_c$; and

   (b) intersects the cavity at its full (horizontal) width.

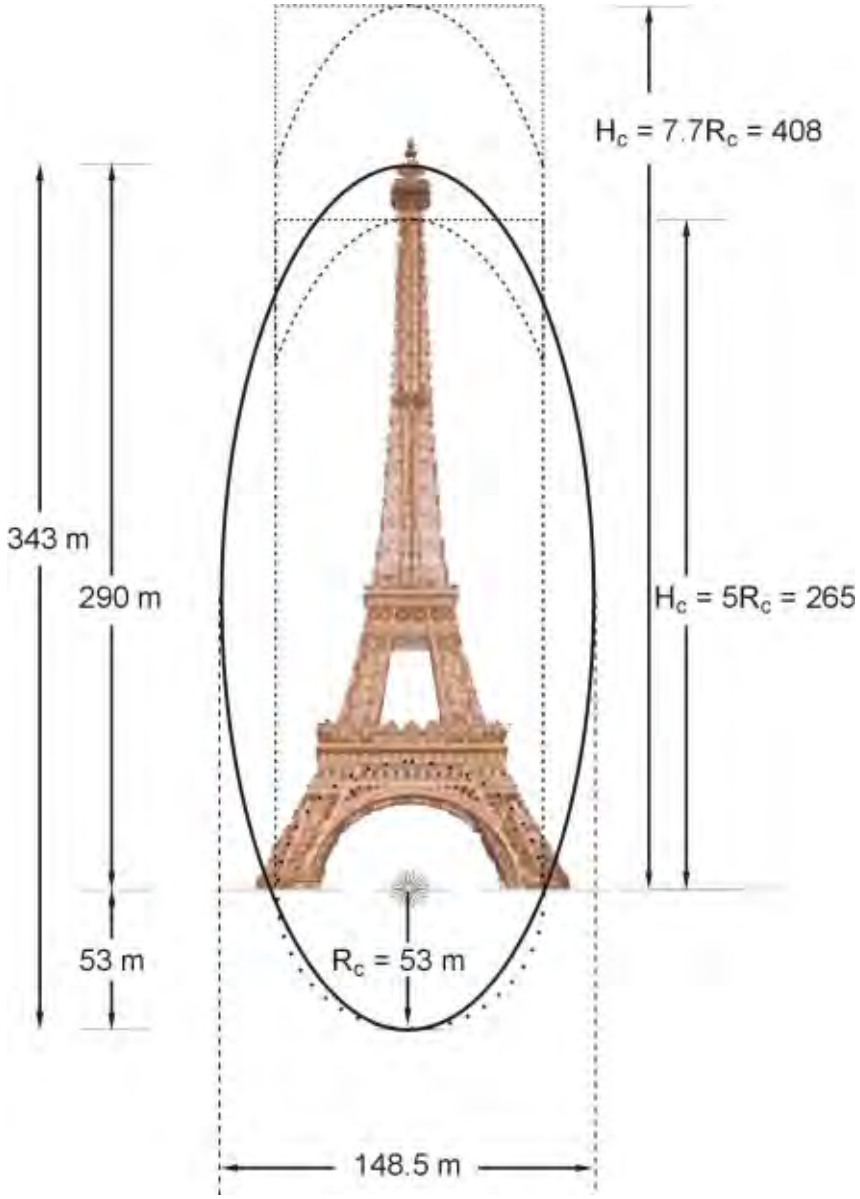

Figure N.3 Comparative dimensions of cylindrical (flat or arched roof) and spheroidal (i.e. ellipsoid of rotation with K = 1.4) chimney/cavity produced by a 150-kt yield (Y) nuclear explosion at a depth of 1100 m at the PTC (cavity radius R_c = 10 Y; cylindrical chimney height H_c = 5 R_c (first case) and 1100 $(Y/h)^{1/3}$ = 7.7 R_c (second case). The spheroidal cavity/chimney is of the same volume as the 7.7 R_c flat roof cylindrical cavity/chimney; the Eiffel Tower is 318.7 m high, including the TV tower, and 127.5 m wide at the base)

Appendix O

NUMERICAL MODELLING OF SURFACE SETTLEMENT OF THE ATOLLS AT THE PTC

This appendix describes some aspects of the calculations carried out with the code *FLAC* (Itasca Consulting Group, Inc. 1995) to analyse settlement of the surface of the atoll produced by dynamic loading. All the computations were performed using the two-dimensional model shown in Figures O.1 and O.2. Note that a volume of water on the lagoon and ocean sides of the atoll has been explicitly taken into account in this analysis to simulate the fluid-solid interaction on the submerged flanks. A uniform grid is used to discretise the model. The size of a zone (element) was selected to be 6.5 m, at least 10 times smaller than any length of the problem analysed. The wavelength of the pressure pulse for a 2-kt explosion is about 66 m.)

The numerical modelling was carried out in two steps. First, a quasi-static computation was made to determine the initial stresses due to gravity and water loading (through explicit representation of water in the model). This was followed by a dynamic calculation involving pulse loading at the bottom of the model. Different boundary conditions on the bottom and sides of the discretised domain are used for the two steps: "roller" boundary conditions (zero normal displacement, zero shear stress) for the quasi-static calculations, as shown in Figure O.1; and non-reflecting boundary conditions for the dynamic analysis, as shown in Figure O.2.

All the materials in the model (water, basalt, carbonates) are assumed to be isotropic and homogeneous. The following material models have been used in the numerical analysis.

- The water is treated as an elasto-plastic material characterised by a bulk modulus $K = 2$ GPa, zero shear modulus and zero tensile strength, to simulate a non-viscous compressible fluid.
- The basalt is modelled as a linearly elastic material with Young's modulus E = 12.9 GPa, Poisson's ratio ν = 0.28, and a saturated density, ρ = 2,200 kg/m^3.
- The carbonate is assumed to behave as an elasto-plastic Tresca material with strength softening beyond failure for the dynamic calculations, but as an elastic material for the preliminary quasi-static analysis. The parameters assigned to this material are: E = 12.9 GPa, ν = 0.28, ρ = 2200 kg/m^3, compressive strength q_u =

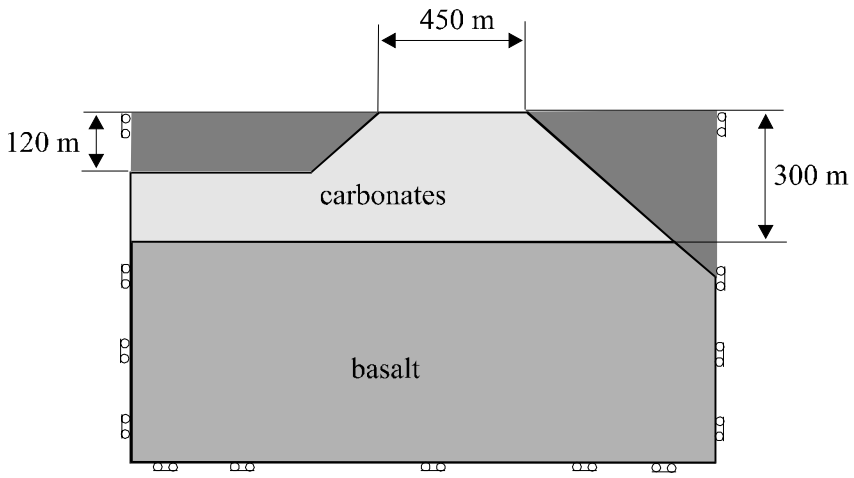

Figure O.1 Geometry of the model and boundary conditions for quasi-static gravity loading.

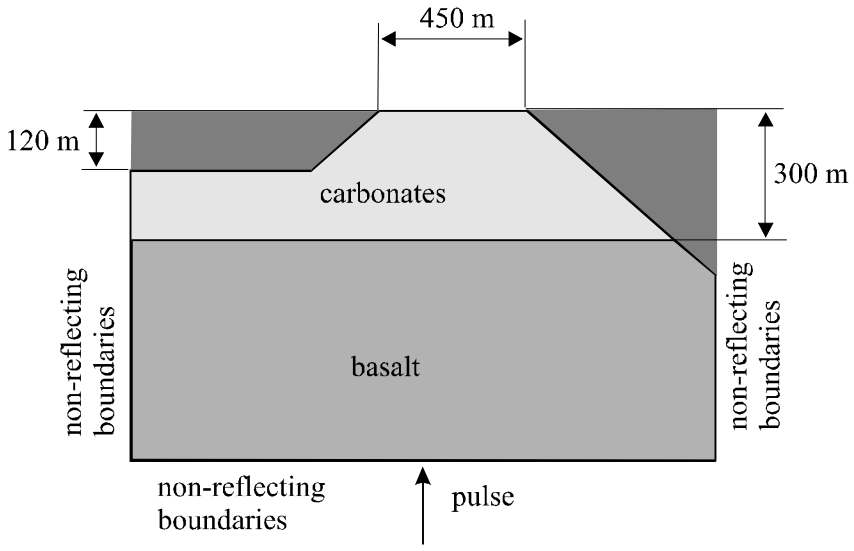

Figure O.2 Model with dynamic interaction between the rock and the water

8 MPa, friction angle $\phi = 0$, and dilation angle $\psi = 0$. (The material is assumed to be plastically incompressible.) The cohesion softening is a bi-linear function of accumulated plastic shear strain: the cohesion drops from the peak value, at zero plastic shear strain, to a residual value (8% of the peak cohesion) after 0.8% of plastic shear strain. After reaching the residual value, the cohesion is independent of the plastic shear strain.

Increase in the undrained compressive strength, q_u, with depth (due to increase of the effective confining pressure) is neglected in this analysis — i.e. $q_u = q$. Numerical simulations have indicated that variation of the carbonate strength, due to either (i) change of the effective stress or (ii) alternation of soft and hard layers, does not change fundamentally the proposed mechanism of deformation, although it does influence the magnitude of the computed settlement. However, as noted in the main text, the magnitude of the settlement is ill-defined since it is very sensitive to the assumed softening modulus.

The pressure pulse, applied at the bottom of the model as a plane wave (see Fig. O.2), is defined by

$$\Delta\sigma = \Delta\sigma_{\max}\left(\frac{1-\cos 2\pi t/\Delta T}{2}\right) \tag{O.1}$$

where the amplitude, $\Delta\sigma_{\max}$, and the duration of the positive phase, ΔT, are deduced from the empirical formulae* given in DIRCEN/CEA Document No. 7

$$\Delta\sigma_{\max} = K\left(\frac{R}{Y^{1/3}}\right)^{-1.75} \tag{O.2}$$

$$\Delta T = 4.3\cdot R^{0.31}\cdot Y^{0.23} \tag{O.3}$$

In the above dimensionally inconsistent equations, $\Delta\sigma_{\max}$ is expressed in bars, ΔT in milliseconds, the explosion yield, Y, in kilotons and the distance, R, from point zero in metres. Also, K is a constant that is assigned the numerical value of $1.5\cdot 10^6$. Calculation of $\Delta\sigma_{\max}$ and ΔT of the pulse loading applied at the bottom of the model is based on the distance, R, from the explosion to the interface between the basalt and the carbonates. Because the pulse propagates as a planar elastic wave in the basalt layer of the model, there is no attenuation of the wave, and the "correct" loading is applied at the base of the carbonates. Note, finally, that R is calculated as the difference between the minimum depth of burial, $h_{\min}$, and the thickness, H, of the carbonates. Here H = 300 m and $h_{\min}(Y)$ is deduced from Figure 4.6.

*In DIRCEN/CEA Document No. 7, it is the maximum overpressure $\Delta P_{\max}$ (i.e. the mean value of the three principal stresses induced dynamically) that is given by an expression similar to (O.2), rather than the stress increase $\Delta\sigma_{\max}$ in the direction of propagation of the plane wave as in (O.2). Depending on the value of Poisson's ratio, $\Delta\sigma_{\max}/\Delta P_{\max}$ may vary between 1 (incompressible medium) and 3.

Appendix P

SURFACE SPALLING DUE TO ELASTIC WAVE REFLECTION

P.1 Introduction

Separation or "spalling" of the surface layer of the rock when the compressive strain pulse from an underground explosion reaches the surface can often be recognised on the near-field accelerographs of underground nuclear tests and can also affect far-field records (Burdick et al. 1983). The surface layer of the rock separates from the underlying rock mass by a fracture generated parallel to the surface by the tensile pulse reflected from the surface. The energy trapped in the slab (or spall) between the surface and the fracture lifts the spalled layer into a ballistic flight. Depending on the shape and amplitude of the initial compressive pulse, several slabs may be generated by a repetition of the reflection process at the fracture surface. Each slab rises to some height before falling back under gravity to impact the ground. The impact radiates additional wave energy into the ground. Therefore, spalling provides additional energy for possible plastic deformation of the superficial layers of the rock mass. The mechanics of the spalling and subsequent impact processes are discussed in greater detail below.

P.2 Mechanics of Spalling

It is assumed that the rock is linearly elastic, homogeneous and isotropic, and that the plane wave is incident normally to the free surface. Given the maximum overpressure $\Delta\sigma_{\max}$, duration ΔT of the positive phase of the wave arriving at the free surface, the shape of the wave and the tensile strength of the rock σ_t, it is possible to calculate the number of spalled layers, their thickness and initial velocities (Rinehart 1960). A rectangular pulse shape is assumed for simplicity. This shape gives an upper bound for the thickness of the spalled layer and its initial velocity (see Fig. P.1), and can be generalised easily to a wave of arbitrary shape. Only one layer will be spalled by a rectangular pulse, and spalling occurs only if $\Delta\sigma_{\max} \geq \sigma_t$.

The solution is constructed by superposition of the arriving compressive, upward-propagating wave and the *image* tensile, downward-propagating wave generated by reflection of the compressive wave at the free surface. A net tension will occur first in the rock when the tensile wave front passes beyond the "tail" of the outgoing (equal amplitude) compressive pulse. This occurs at the depth $\Delta h_{\max}$ below the free surface, given

by the expression

$$\Delta h_{\max} = \frac{1}{2} C \Delta T \tag{P.1}$$

This condition defines the thickness of the spall. At the instant of tensile fracturing, both the spalled layer and the underlying rock are unstressed (i.e. the outgoing compression and the reflected tension "cancel" each other everywhere in the slab). The initial (upward) velocity $\dot{u}_{\text{ini}}$ of the spalled layer is then given by

$$\dot{u}_{\text{ini}} = \frac{2\Delta\sigma_{\max}}{\rho C} \tag{P.2}$$

i.e. the sum of the velocities of the compressive and the *image* tensile wave. The maximum height reached by the surface layer during flight is a function of the initial (upward) velocity of the layer at the moment of spalling and the forces acting on the layer—i.e. gravity and the elastic forces induced in the layer by bending as the fracture develops laterally (see Fig. P.2).

The average (downward) acceleration of the ground surface above the explosion point zero is found (from accelerograph records; DIRCEN/CEA Appendix to Document No. 6) to be 12.8 m/s^2, i.e. greater than the acceleration of gravity. This implies that the elastic forces (in the region of the outer radius of the still-connected slab) add to the gravitational forces to increase the downward acceleration of the slab during the ballistic flight. However, these elastic forces affect the rebound height only; they do not change the velocity of the falling slab at the moment of impact on the underlying rock. (The downward velocity of impact in the elastic model must be equal to the upward velocity of the layer at the moment of spalling.) It is the velocity of impact that defines the amplitude of the generated pressure wave. Assuming that gravity is the only force acting on the layer during ballistic flight, the maximum height reached can be calculated as

$$u_{\max} = \frac{\dot{u}_{\text{ini}}^2}{2g} \tag{P.3}$$

Accelerograph records reveal that the acceleration of the slab as it falls is less than the acceleration during upward flight, indicating some dissipation of energy on the way up (possibly due to lateral fracturing). The relation between the radius R_{eq} (see Fig. P.2) and the equilibrium displacement $u_{\max}$ at the center of a thin plate which is being "torn away" from a rigid base (Murakami and Aoki et al. 1987) is given by the expression

$$R_{\text{eq}}(\alpha) = \left[\frac{\alpha u_{\max} (2ED)^{1/2}}{K} \right]^{1/2} \tag{P.4}$$

where $\alpha = 4$ for a uniform pressure (the "blister test", Fig. P.2), $\alpha = 2$ for a concentrated force at the centre, $D = E\Delta h^3/[12(1-\nu^2)]$, and K is the rock toughness. Equation (P.4)

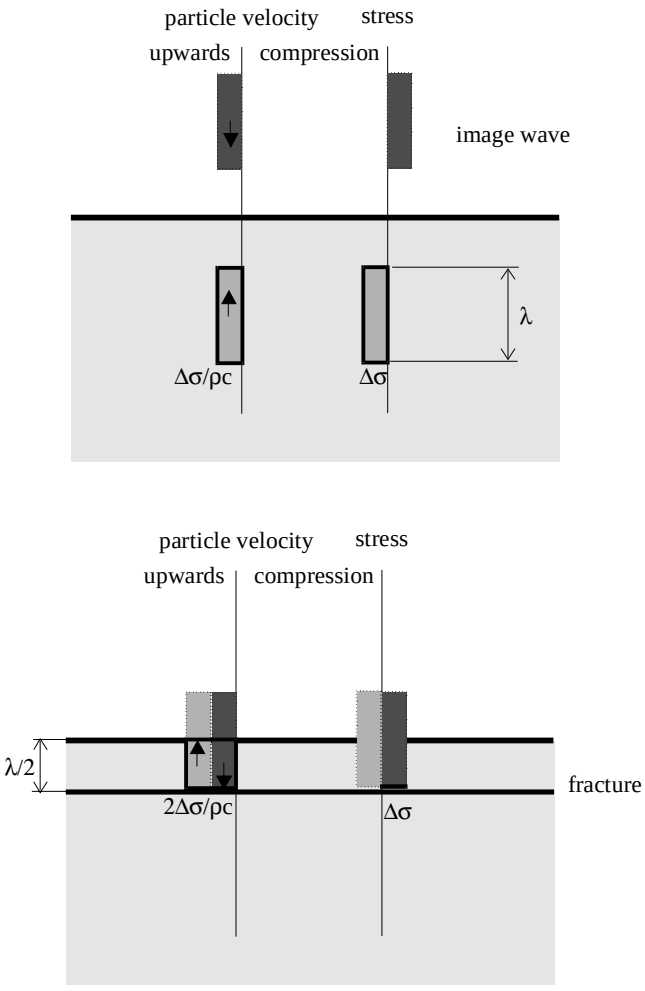

Figure P.1 Wave reflection and spalling

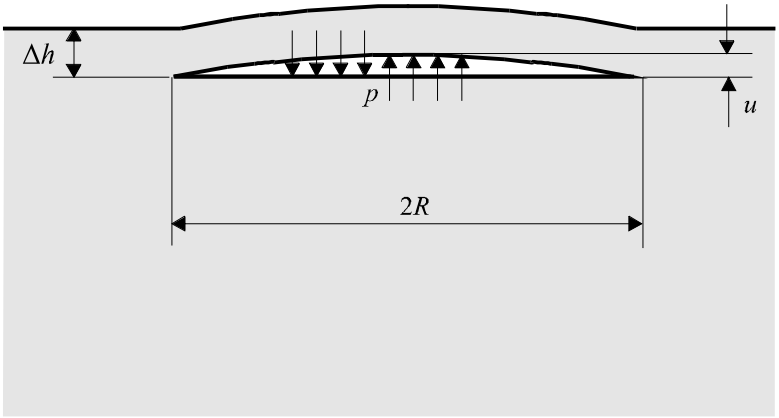

Figure P.2 Spalling of the surface layer

can be used to estimate the radius R of the spalled layer, based on the thickness of the layer Δh, and the maximum height $u_{\max}$ reached during the flight of the slab.

The spall falls back to impact the underlying rock (with a velocity which, if we ignore any energy dissipation, must be equal to the initial upward velocity $\dot{u}_{\text{ini}}$, given by P.2). The solution for a slab or layer of constant thickness moving vertically downwards at uniform velocity can be represented as the superposition of two planar waves (Fig. P.3):

(1) a compressive wave propagating downward, with downward particle velocity $\dot{u}_1 = \Delta\sigma_{\max}/\rho C$, and corresponding stress $\Delta\sigma_{\max}$; and

(2) a tensile wave propagating upwards, with downward particle velocity $\dot{u}_1 = \Delta\sigma_{\max}/\rho C$, and corresponding stress $-\Delta\sigma_{\max}$.

The compressive wave reflects from the free lower boundary of the layer as a tensile wave, while the tensile wave reflects from the free upper boundary as a compressive wave. When the layer impacts the underlying rock (which has the same acoustic impedance as the spalled layer), the compressive wave is transmitted across the interface into the half-space without any reflection. Consequently, the resultant compressive stress, equal to $\Delta\sigma_{\max}$, propagates from the interface symmetrically (i.e. from below and above) until the upward-propagating tensile wave completely reflects from the free upper boundary of the spalled layer. From that moment, a rectangular compressive pulse with amplitude $\Delta\sigma_{\max}$, particle velocity $\dot{u}_1 = \Delta\sigma_{\max}/\rho C$ and wave length $C\Delta T$ propagates downward. This wave is identical to the incident wave.

It should be noted that the maximum stress that can be generated by the impact is

$$\Delta\sigma \leq 2\Delta\sigma_{\max}$$

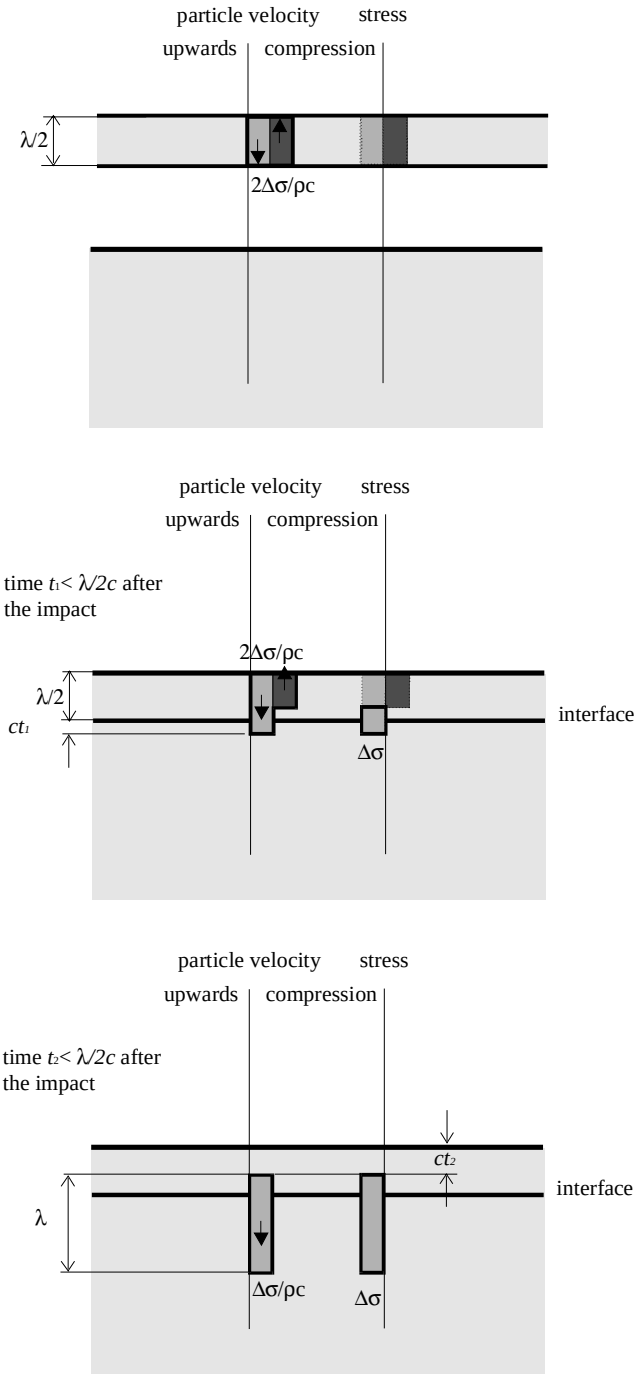

Figure P.3 Impact of the spalled layer

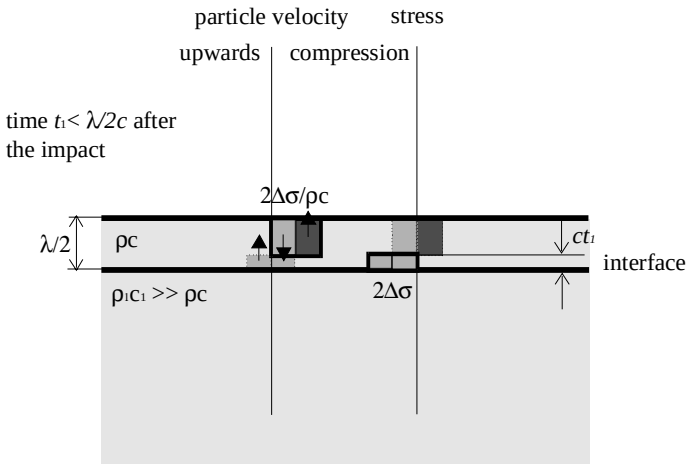

Figure P.4 Maximum induced stress

If the acoustic impedance of the underlying rock is much larger than the acoustic impedance of the spalled layer, the downward-propagating compressive wave will be reflected (upward) after the impact as a compressive wave (see Fig. P.4). Superposition of the downward- and upward-propagating compressive waves generates an impact stress equal to $2\Delta\sigma_{\max}$.

For the case where the initial compressive pulse arriving at the surface is triangular (with an instantaneous rise time), the number of spalled layers is $n = \Delta\sigma_{\max}/\sigma_t$. The thickness of each layer Δh is given by the expression

$$\Delta h = \frac{1}{2} C \Delta T (\sigma_t / \Delta\sigma_{\max}) \tag{P.5}$$

and the initial velocity of the first spalled layer is

$$\dot{u}_{\text{ini}} = \frac{2\Delta\sigma_{\max} - \sigma_t}{\rho C} \tag{P.6}$$

The initial velocity of each subsequently spalled layer is progressively smaller than that of its predecessor (since the peak stress is reduced). If the rise time of the pressure pulse is finite, two cases can occur: (i) a single layer is spalled, or (ii) a single layer is spalled and is succeeded by a large number of very thin layers or dust particles (Rinehart 1960). In any case, $\Delta h_{\max} < C\Delta T/2$ and $\dot{u}_{\text{ini}} < 2\Delta\sigma_{\max}/(\rho C)$.

Table P.1 summarises the values for the rebound height (P.3), thickness of the spalled layer (P.1) and radius of spalled zone (P.4) for different yields and corresponding depths of burial assuming the rectangular pulse shape. (The tensile strength σ_t is assumed to be $\sigma_t = 1$ MPa.) The estimates obtained assuming a triangular pulse shape (with instantaneous rise time), listed in Table P.2, seem to be in better agreement with observations at the PTC than the results for a rectangular pulse shape, given in Table P.1.

Table P.1 Rectangular pulse — spalling calculations

Y	h	$\dot{u}_{\text{ini}}$	$u_{\max}$	$\Delta h_{\max}$	$R_{\text{eq}}(2)$
kt	m	m/s	m	m	m
2	465	1.59	0.13	47	710
10	495	3.66	0.68	69	2060
150	900	6.23	1.98	154	6440

Table P.2 Triangular pulse — spalling calculations

Y	h	$\dot{u}_{\text{ini}}$	$u_{\max}$	$\Delta h_{\max}$	n	$R_{\text{eq}}(2)$
kt	m	m/s	m	m		m
2	465	1.25	0.08	9.64	4	165
10	495	3.31	0.55	6.21	11	310
150	900	5.88	1.73	8.18	18	680

Appendix Q

NUMERICAL MODELLING OF SLOPE STABILITY AT THE PTC

The effect of underground explosions on the stability of the submarine slopes on Mururoa atoll was analysed numerically for both static and dynamic loading. Because a two-dimensional model is not always a satisfactory approximation for dynamic analysis of slope stability (it is unable to account for (i) a different angle of incidence of the loading wave relative to the dip direction of the slope, and (ii) a spherically symmetric dynamic source), the numerical simulations of the slopes were conducted with both two-dimensional (*FLAC*) and three-dimensional (*FLAC3D*) finite-difference numerical codes (Itasca Consulting Group, Inc. 1995; Itasca Consulting Group, Inc. 1997).

Q.1 Modelling Methodology

Static analysis of the safety factor of the slopes was conducted in three steps.

1. The initial stresses due to gravity and hydrostatic pressure of the water in the ocean were calculated. Linearly elastic material behaviour and homogeneous elastic properties were assumed to generate a simple initial stress state in equilibrium with the loading on the slope. (Measurements of in-situ stresses were unavailable.)

2. The material model of the rock mass was "switched" from linearly elastic to perfectly plastic, Mohr-Coulomb (properties listed in Table 5.1), and the stresses corrected accordingly.

3. The safety factor Φ of the slope with respect to failure was calculated in a series of successive calculations by reduction of the cohesion, c, and the tangent of the friction angle, $\tan\phi$, uniformly in all geological formations, i.e. $c' = c/\Phi$ and $(\tan\phi)' = \tan\phi/\Phi$. The largest Φ which resulted in a stable configuration (i.e. equilibrium as the steady-state condition) was considered to be the factor of safety of the slope.

The pore pressure in the rock was assumed to correspond to the pressure imposed by the average level of the ocean surface. The calculations were done uncoupled — i.e. the pore pressure was assumed to be independent of the mechanical deformation.

The first two steps of the dynamic analysis were the same as for the static analysis. During the dynamic simulations, the change of effective stresses was ignored and the rock mass was assumed to behave as a pressure-insensitive material because

- for the duration of the pressure pulse, the rock mass deforms essentially as if under undrained conditions; and
- Skempton's coefficient B is almost unity.

Therefore, although the material is fully saturated, the third step of the dynamic analysis was conducted uncoupled (i.e. the pore pressure field was not explicitly simulated), using undrained elastic parameters and simplifying the Mohr-Coulomb yield condition to the Tresca yield condition. The effective cohesion used in the Tresca condition was calculated from the expression:

$$c_u = c\cos\phi - \frac{\sigma_1^{'} + \sigma_3^{'}}{2}\sin\phi \tag{Q.1}$$

The history of the overpressure in the near field of the explosion was assumed to be

$$p(t) = \frac{1}{2}\Delta p\left(1 - \cos\frac{2\pi t}{T}\right) \tag{Q.2}$$

The amplitude Δp (10^5 Pa) was calculated from the empirical relation as a function of yield Y (kt) and distance R (m) (DIRCEN/CEA Document No. 7):

$$\triangle p = K\ (R/Y^{1/3})^n \tag{Q.3}$$

The constant K depends on the medium surrounding the zero point; typically, it is in a range between $1.2 \cdot 10^6$ and $1.6 \cdot 10^6$. The value of n is of the order of -1.75. The duration, T, of the pressure pulse was suggested to be

$$T = 4.3R^{0.31}Y^{0.23} \tag{Q.4}$$

where T is in ms.

Viscous, non-reflecting boundary conditions were applied along the artificial boundaries of the model in the dynamic analysis in order to absorb outgoing kinetic energy. The acoustic impedance of the water differs but is not negligible compared to the acoustic impedance of the rock mass, so it was not justified to apply either stress-free (i.e. stresses do not change during the dynamic simulation) or non-reflecting boundary conditions along the water-rock interface. Thus, a volume of water associated with the slopes was modelled explicitly (discretised by the finite difference grid) as a compressible, non-viscous fluid.

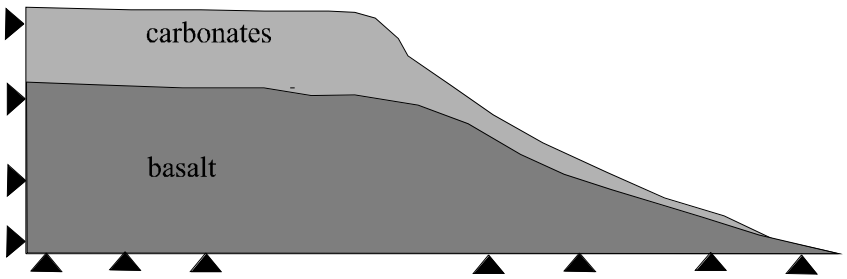

Figure Q.1 Model of the slope in the southwestern part of the atoll used in quasi-static calculations

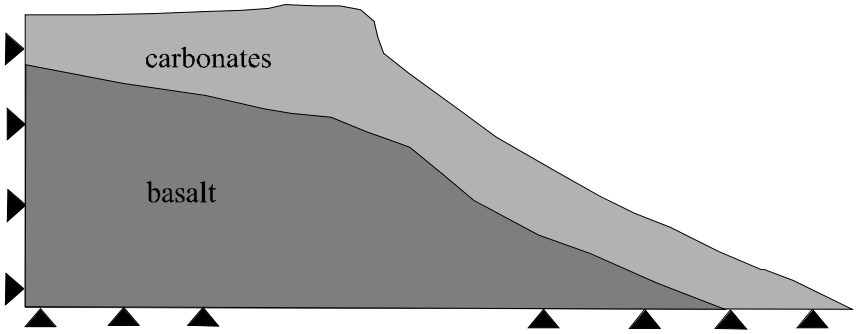

Figure Q.2 Model of the slope in the northern part of the atoll used in quasi-static calculations

Q.2 Two-dimensional Model

Q.2.1 Static Calculations

The geometry and boundary conditions of the slope models used to represent the southwestern and northern parts of the atoll were as shown in Figures Q.1 and Q.2, respectively. The zone size in the models was approximately 15 m. The effect of the water in the ocean was taken into account as a hydrostatic pressure applied along the slope contours.

Q.2.2 Dynamic Calculations

The geometry and boundary conditions of the slope models in the southwestern and northern parts of the atoll were as shown in Figures Q.3 and Q.4, respectively. In the first two steps of the analysis, “rollers” (i.e. no displacement normal to the boundary, free displacements tangential to the boundary) were used at the far-field boundaries of the model. The zone size in the models was approximately 12 m.

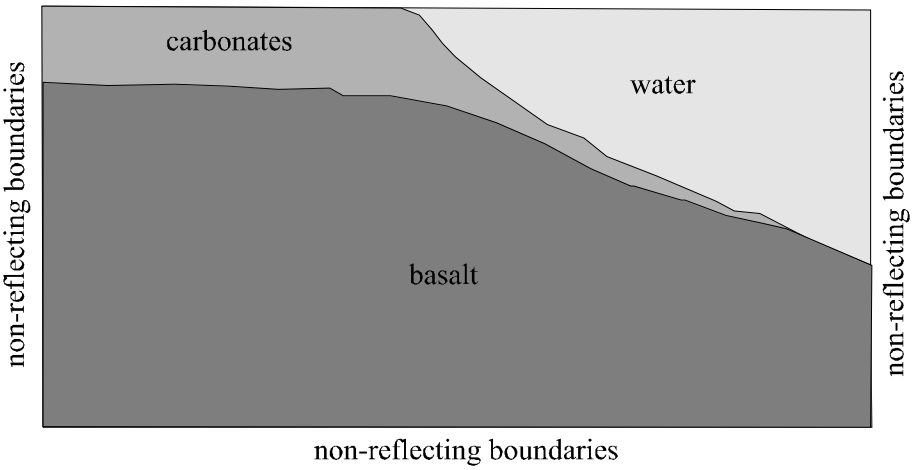

Figure Q.3 Model of the slope in the southwestern part of the atoll used in dynamic calculations

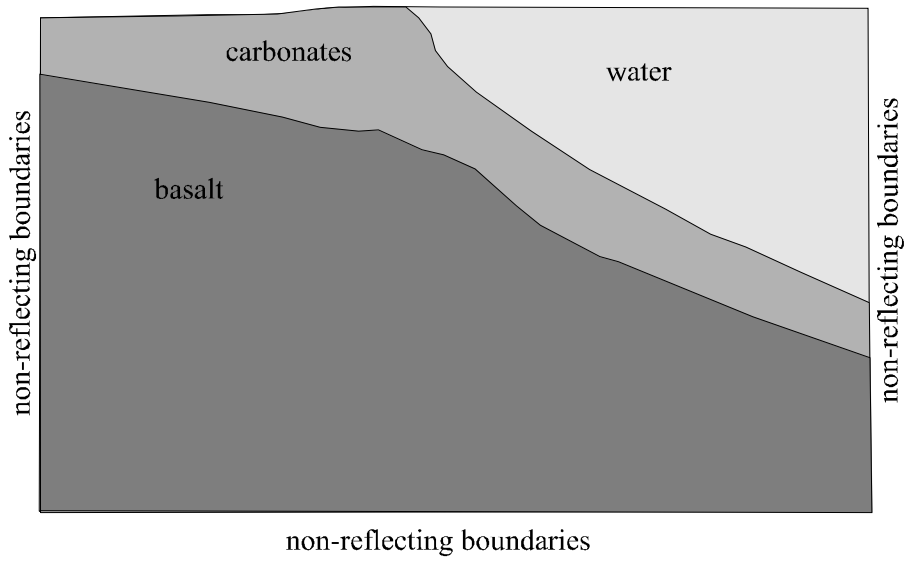

Figure Q.4 Model of the slope in the northern part of the atoll used in quasi-static calculations

Q.3 Three-dimensional Model

A three-dimensional model of the southern rim of Mururoa Atoll was generated in order to take into account three-dimensional effects in the stability analysis. The geometries of the slope contour and different geological formations in the typical cross-section (parallel to the dip direction of the slope) were simplified to those shown in Figure Q.5 (the geological formations were as defined in Table 5.1). The model assumed symmetry relative to the plane parallel to the dip direction of the slope through the point zero. The length of the model, along the slope (i.e. normal to the plane of the section shown), was 2000 m; the depth was taken to be equal to the assumed 1000-m depth of burial of the simulated explosion.

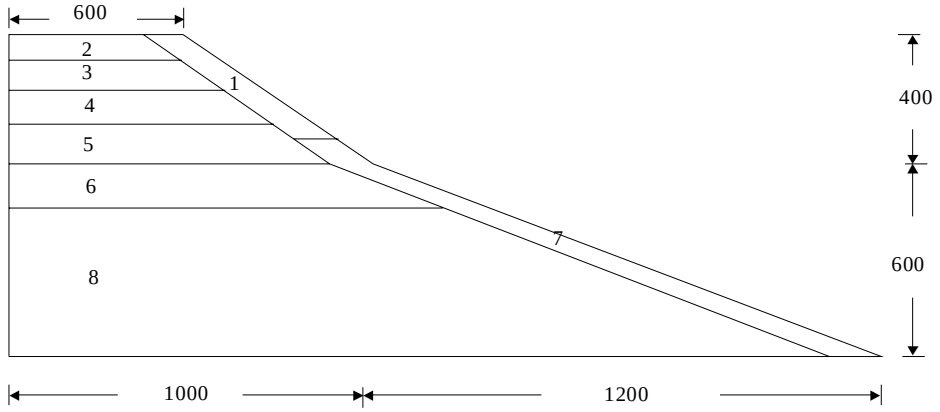

Figure Q.5 Numerical model for the south slope of the atolls. The geometry of the slope is shown in metres (see Table 5.1 for definition of zones)

Appendix R

SOUTH SLOPE FAILURE AT MURUROA: AN ALTERNATIVE MECHANISM

R.1 Introduction

The Tydée event on July 25, 1979, caused underwater landslides on the south rim of Mururoa immediately after the event as well as after delays of three hours and 23 days. The location and extent of the failed mass are illustrated in Figures 18 and 19 of DIRCEN/CEA Document 7. The mechanism is unusual because the landslide occurred at a position on the slope that does not correspond to the shortest distance from the dynamic source to the slope face. In fact, the vector from the source to the location of the landslide is almost tangential to the slope. Hence, the presumed ground motion was almost normal to the direction of slip. We explore here the possibility that a mechanism exists in which slope failure is initiated by motion in the transverse direction by assuming that the failure consists of a single block sliding on a sloping base that is subjected to transverse motion. We justify the simplification by noting that the rock slide appears to consist of soft material (debris, transition and limestone—see the table on p. 14 of DIRCEN/CEA Document No. 7), while the base is composed of harder material (volcanic rock—see Fig. 19 of DIRCEN/CEA Document No. 7). There is a natural transition in acoustic impedance that tends to decouple the propagation of a wave within the base from the resulting motion of the surface material.

Simple analyses are performed here that account, in part, for the three-dimensional nature of the problem. The objectives are: first, to determine if conditions for slip initiation are met; second, to estimate the resulting magnitude of sliding that occurs; and, third, to assess material properties that are consistent with the observed landslides.

R.2 Sliding-Block Analysis—Conditions for Slip Initiation

To perform a sliding-block analysis, we need the motion and period of the pulse at the location of the slope. Assume that Tydée had a yield of 150 kt at a depth of 1.1 km and that it is located between 2 and 5 km (in the horizontal direction) from the slope. First,

we use the formula in DIRCEN/CEA Document No. 7 (p. 9)*:

$$\Delta\sigma_{\max} = K\ \left[(R/Y)^{1/3}\right]^{-1.75} \qquad \text{(bar,m,kt)} \tag{R.1}$$

where $1.2 \cdot 10^6 \leq K \leq 1.6 \cdot 10^6$. Using the lower value for K and the higher value for the radial distance, we obtain a lower bound of $\Delta\sigma_{\max}$ = 0.72 MPa. Similarly, the upper bound is Δp = 3.9 MPa, using the remaining data values. The corresponding particle velocities were then estimated from the following formula, valid for a plane wave:

$$\dot{u} = \frac{\Delta p}{C\rho} \tag{R.2}$$

Using a p-wave velocity, $C = 3150$ m/sec, and a density of 2360 kg/m^3, from Table 2.1 in Chapter 2 of this report, for submarine volcanism in the Fuchsia region, we obtain particle velocities of 0.1 m/sec and 0.52 m/sec, respectively, for the 5-km and 2-km distances. As a check, the radial particle velocities can also be estimated from the formula given on p. 21 of DIRCEN/CEA Document 6, derived from measurements made in the field:

$$V_{\text{radial}} = \left[0.114\ (R/Y)^{1/3}\right]^{-1.74} \qquad \text{(m/sec,km,kt)} \tag{R.3}$$

which yields 0.11 m/sec and 0.49 m/sec for the two cases. The values of 0.1 m/sec and 0.5 m/sec were used in further calculations.

In order to estimate accelerations, some assumptions must be made about the waveform of the pulse. The shape of the initial pulse seen in simulations (Damjanac 1996) suggests a cosine function:

$$\dot{u} = \ddot{u}\left[\frac{1 - cos(2\pi\ t\ T)}{2}\right] \tag{R.4}$$

for t $\geq$ T, where T is the pulse duration and $\ddot{u}$ is the peak velocity. The peak acceleration is then

$$\ddot{u} = \pi\ \dot{u}\ /\ T$$

The pulse width is estimated using the formula given in DIRCEN/CEA Document No. 7 (p. 9):

$$T = 4.3\ R^{0.31}\ Y^{0.23} \tag{R.5}$$

*In DIRCEN/CEA Document No. 7, it is the maximum overpressure $\Delta P_{\max}$ (i.e. the mean value of the three principal stresses induced dynamically) that is given by an expression similar to (R.1), rather than the stress increase $\Delta\sigma_{\max}$ in the direction of propagation of the plane wave as in (R.1). Depending on the value of Poisson's ratio, $\Delta\sigma_{\max}/\Delta P_{\max}$ varies between 1 (incompressible medium) and 3.

Table R.1 Slope stability conditions

Material	c	ϕ	ρ	$\ddot{u}$	α ($F \leq 1$)
debris	1.0	40°	2150	1.1	≥29°
transition	1.0	30°	2200	1.1	≥0°
upper limestone	1.5	45°	2005	1.1	≥53°
debris	1.0	40°	2150	0.18	≥60°
transition	1.0	30°	2200	0.18	≥53°
upper limestone	1.5	45°	2005	0.18	≥60°
debris	1.0	40°	2150	0.5	≥60°
transition	1.0	30°	2200	0.5	≥45°
upper limestone	1.5	45°	2005	0.5	≥60°

which yields 0.18 s and 0.15 s for the two cases (5-km and 2-km distance, respectively). The corresponding accelerations are then calculated as 0.18 g and 1.1 g.

To determine whether part of the slope surface will start to slip, we assume that the sliding mass consists of a uniform layer of thickness H (in the direction normal to the face) resting on a slope. Because the vector from the source is approximately parallel to the strike of the slope, we can use vector addition to combine the dynamic acceleration and the in-plane gravity component for an element of the sliding layer. Neglecting the vertical component of the dynamic acceleration, the total "driving" shear stress is

$$\tau_{\text{drive}} = \rho\, H \sqrt{\ddot{u}^2 + g^2 \sin^2 \alpha} \tag{R.6}$$

where g is the gravitational acceleration. The resisting shear stress is

$$\tau_{\text{resist}} = c + g\, \rho\, H\, \cos\alpha\, \tan\phi \tag{R.7}$$

where c is the cohesion and ϕ is the friction angle. Failure will occur if the ratio of these stresses, F, is less than unity:

$$F = \frac{c + g\, \rho\, H\, \cos\alpha\, \tan\phi}{\rho\, H \sqrt{\hat{\ddot{u}}^2 + g^2 \sin^2 \alpha}} \tag{R.8}$$

This equation is used to determine the slope angle necessary for incipient failure, given various values of acceleration and material properties. The results are given in Table R.1, where c is in MPa, ρ is in kg/m^3, $\ddot{u}$ is in units of g, and a block height, H, of 100 m is assumed. Note that all cases are statically stable for slope angles of at least 54°.

The first three rows of Table R.1 are for the upper-bound case, the second three rows are for the lower-bound case, and the final three rows are for an intermediate value of acceleration. The materials correspond to those tabulated in DIRCEN/CEA Document No. 7 (p. 14). It appears that only the higher acceleration (event at 2-km distance) leads to results that are compatible with the observation that sliding occurred immediately after the explosion. Note that the actual pre-explosion slope angles are in the range of 25° to 55°.

R.3 Sliding-Block Analysis—Displacements

Newmark (1965) provided a simple analysis for the slip displacement, δ, accumulated by a block resting on a horizontal, frictional base that is accelerated for a given time:

$$\delta = \frac{v^2}{2g\tan\phi} 1 \left(\frac{1 - \tan\phi}{A} \right) \tag{R.9}$$

where A is the (constant) acceleration of the pulse, and v is its peak velocity.

We capture the spirit of Newmark's approach with a *FLAC3D* simulation of a block resting on an inclined plane. The block representing the slope is given a horizontal velocity pulse of cosine shape, and the resulting motion of the block is calculated as a function of time. The calculation is performed for the lowest strength and highest acceleration given in Table R.1, and for two slope angles: 26° and 45°. Down-slope displacements of 0.07 cm and 1.2 cm, respectively, are recorded. The implications of this displacement are discussed in the conclusions below.

R.4 Factors Not Considered—Uncertainties

There is likely to be considerable variation in material properties, particularly in the cohesive component of strength, due to repeated prior loading cycles. Also, the actual slope surface is irregular — a series of ridges and valleys eroded during the emergent phases of atoll formation (see Figs. 1.3 and 1.5).

The effects of focusing, trapping, or amplification at layers, interfaces or free surfaces are not considered. For example, a normally incident wave reflected at a free surface will produce velocity (and acceleration) amplitudes that are double those of the incident wave in the far field. This effect is seen within a distance of half a wavelength from the free surface. Similar amplification occurs when a wave passes from high impedance to medium to low impedance. There may also be wave conversion: for example, a P-wave that encounters a medium surface at grazing incidence will convert some of its energy to a Rayleigh wave.

The dynamic wave, even when it is travelling parallel to the slope surface, will induce dynamic pore pressures in the saturated material. However, the effective mean stress is

likely to increase (in the compressive sense), since the pore pressure increment will be smaller than the total stress increment, in a material that does not soften isotropically. Therefore, the effective normal stress on the slip surface will increase during the pulse, thereby reducing the tendency for slip. Thus, it seems that the stated conclusion (of very low slip displacement) would not be affected by inclusion of pore fluid in the calculation.

R.5 Conclusions

Slope failure is likely for a 150-kt event located 2 km from the slope, assuming a cohesion of 1 MPa and a friction angle between 30° and 40°. However, the accumulated displacement — for constant strength — is of the order of centimetres. In order to explain a landslide (with displacements of many metres), we need to assume that the material softens, such that its strength falls below that necessary for static stability after some displacement (of the order of cm only) is induced by the explosion wave(s). In this case, the final displacement would be limited only by factors such as changing geometry (e.g. the failing mass moving to a flatter sliding surface).

The phenomenon of softening, although very likely, is almost impossible to quantify for large volumes of material. A quantitative "prediction" of the displaced volume of material in the landslides induced by the Tydée event is therefore impossible.

In order to reach the conclusions noted above, a mechanism is considered in which dynamic motion in the strike direction of the slope induces a shear stress that exceeds the strength of surface material, leading to collapse in the dip direction after some drop in strength. There are alternative hypotheses, but these are considered to be less plausible.

Appendix S

MODEL OF TRITIUM RELEASE BASED ON MIXING IN THE CARBONATES AT THE PTC

S.1 Introduction and Objective

In this appendix, we attempt to evaluate flow and transport in the carbonates by using a simple mixing model to take account of tidal effects. The primary objective is to test the assumptions and parameter values of spatially distributed flow models presented in Chapter 7 and in Perrochet and Tacher (1997a) by showing that measurements of tritium (HTO) concentrations at the atoll scale are consistent with the modelling results. Such comparisons with actual radionuclide measurements help to develop confidence in the flow models developed by the IGC and in the transport and release models developed subsequently by the IAEA.

S.2 Flux of HTO in the Carbonates and to the Lagoons

Measurements of concentrations of HTO in the carbonates performed by both the IAEA and DIRCEN/CEA show that a large amount of HTO is present in the carbonates — of the order of several 10^{15} Bq for each atoll. Comparing this amount with the current annual flux of HTO into the lagoons (see Table S.1) and assuming that the present flux has been maintained for 20 years, the cumulative amount of HTO having left the carbonates is of the order of $0.7 \cdot 10^{15}$ Bq at Mururoa and $0.2 \cdot 10^{15}$ Bq at Fangataufa. Thus, a large amount of HTO is stored in the carbonates, and HTO is released to the lagoons very slowly.

Based on the observed spatial distribution of HTO in the carbonates (Figs. 7.21 and 7.22), particularly in test area 1 at Mururoa, HTO seems to have been "diffused" from the rim toward the interior of the lagoon, over a distance of about 4 km, during a period of 20 years. This is about 200 my^{-1}, whereas the calculated horizontal pore velocities in the carbonates are of the order of less than 10 my^{-1}. The most likely explanation for this spreading is lateral mixing due to tidal effects, as discussed in Sections 6.2.4 and 6.3.6.

It is very difficult to determine whether some of the HTO released to the carbonates has been transferred to the ocean, or if most of it has spread toward the interior of the atolls. From the steady-state model of geothermal circulation presented in Chapter 6, the direction of flow in the carbonates is toward the interior, thus suggesting the absence

Table S.1 Annual flux of HTO into lagoons in 1996

Atoll	Average HTO Concentrations in Lagoons ($Bq\ m^{-3}$)	Daily Flow into Lagoons[a] ($m^3\ d^{-1}$)	Annual HTO Flux into Lagoons ($Bq\ y^{-1}$)
Mururoa	1000	$100 \cdot 10^6$	$37 \cdot 10^{12}$
Fangataufa	600	$42 \cdot 10^6$	$9 \cdot 10^{12}$

[a] based on estimates by DIRCEN/CEA, which are larger than those of the IAEA in Deleersnijder and Tartinville (1997)

of significant releases to the ocean. However, mixing due to tidal influences may have spread some of the HTO into the ocean as well. Based on a comparison of the amount of HTO released in area 1 over the years and the amount still present in the carbonates (with radioactive decay taken into account — see Section S.6), the hypothesis of no-release into the ocean is not incompatible with the measurements. In area 4, however, the same analysis shows that some release to the ocean may have occurred, but this area is known to have been perturbed by mechanical instabilities, thus making it possible that communication between the rim and the ocean in the carbonates is easier. We will thus consider as a "worst case" the hypothesis that all radionuclides released from the volcanics to the carbonates end up in the lagoons — not in the ocean. We do not imply that direct release to the ocean is impossible — in fact, we believe that there is local evidence of this phenomenon. However, there are no hard data to allow us to estimate the flux of water to the ocean; therefore, we take the conservative view that all transfer from the volcanics through the carbonates ends up in the lagoons.

Sampling of water in the carbonates, as performed by both DIRCEN/CEA and the IAEA (IAEA 1998e), seems to indicate a rather uniform concentration of HTO over the vertical, for a thickness of several hundred metres at the sampling points. Because these sampling points are within vertical boreholes, it is possible that the mixing that made this concentration homogeneous over the vertical occurred in the boreholes only — not in the carbonates. However, we will presume that the data imply that the observed HTO distribution is indicative not only of the karst layers, as assumed by DIRCEN/CEA, but also of significant thickness of the carbonates. Several such thicknesses will be considered. A possible explanation for vertical mixing is the effect of tides. The assumption of mixing over a large thickness of the carbonates leads to an increase of the inventory of HTO in the carbonates compared to that given by DIRCEN/CEA, which assumed that the measured HTO was distributed only over a 50-m dolomitic karst layer with a porosity of 20% at the bottom of the carbonates. This increases the rate of nuclide release from the volcanics, but it is obviously conservative.

We know from hydrothermal modelling that the steady flow in the carbonates is first

horizontal and centripetal from the ocean toward the interior, and then vertically upward. Vertical Darcy velocities in the carbonates have been estimated by IGC to be in the range of 0.5 to 2 my^{-1} in the centre of the atoll. Globally, in the three-dimensional modelling of Mururoa, the net flux of water to the lagoon has been estimated to be 60 000 m^3 d^{-1} — i.e. an average Darcy velocity of 0.137 my^{-1}over the 160 km^2 of the lagoon. The porosity of the carbonates is of the order of 30%. If we assume vertical "piston flow" from the base of the carbonates to the lagoon, over a thickness of 300 m, the transfer time for HTO would be between 45 and 650 years. This is obviously incompatible with the data, since HTO has been observed in the lagoons from 1987 onward. (No data are available from before 1987.) Thus, the piston-flow model for transfer in the carbonates can be ruled out. A test of this model, with increased velocities and transfer times of 1 to 20 years (App. S), shows that this model cannot account for the observed flux to the lagoon and the inventory.

Another model for transfer of HTO through the carbonates could be an advection-dispersion model in the vertical direction. Such a model accounts for the existence of preferential paths in which the advective velocity could be much higher than the average. Using the same average advective velocity as in the piston-flow model, a large dispersive term would make it possible to have early breakthrough, long before the advective front. In order to have breakthrough in less than 10 years, it would be necessary to use a very large longitudinal dispersivity in the advection-dispersion equation, of the order of 100 m or more. (The dispersion coefficient is the product of the dispersivity by the average velocity.) While such large dispersivities could be explained by the tidal effect, as suggested by DIRCEN/CEA and in Section 6.3.6, introducing them into the transport equation has the net effect that the early breakthroughs are followed by a rapid increase of the HTO flux to the lagoon and, thus, of the concentration in the lagoon. This again contradicts the observations, which indicate that the concentration in the lagoon seems to have been fairly constant over the last ten years, whereas the incoming flux of HTO from the nuclear test is increasing (as will be shown below). A test of this model (provided in App. T) shows its inability to account for both the flux to the lagoon and the inventory.

Having ruled out both the piston-flow and the advection-dispersion models, we suggest that a mixing model may be adequate to represent the transfer of HTO and other radionuclides through the carbonates. This model assumes that the horizontal areas, where HTO has invaded the carbonates, behave as "well-mixed" reservoirs (i.e. that the HTO spreads over a significant vertical thickness of the carbonates) and is well mixed with a homogeneous concentration over this thickness. Several thickness values will be considered. A small percentage of this water is transferred annually to the lagoons and accounts for the observed concentration in the lagoon water. This is plausible because of the mixing effect of the tide; it is not inconsistent with the few observations of a fairly homogeneous distribution of HTO over the vertical, and locally over the horizontal, and will be shown to be compatible with both the estimated releases of HTO from

the volcanics and the flux of HTO to the lagoons. Because of the very large volume of water stored in the carbonates, the concentration in the carbonates builds up slowly, and the small average flux of HTO to the lagoon is approximately constant, thus providing an explanation for the absence of large variations of the concentration of HTO in the lagoons over the years. This model is in better agreement with the observations than DIRCEN/CEA's advective-dispersive model, which does not reproduce the almost constant level of HTO in the lagoons.

Is a mixing model for HTO transport in the carbonates incompatible with the heat transfer model used by the IGC to account for the thermal profiles in the volcanics and carbonates? The answer is no. Indeed, the effect of mixing (e.g. due to tidal fluctuations) is much more significant for a tracer like HTO than for heat, for which the temperature constantly equilibrates between water and solid. To confirm this, a thermal profile in the Mururoa atoll was calculated with the code FEFLOW, with an artificial increase of the thermal conductivity by taking a longitudinal thermal dispersivity of 10 000 m, equivalent to increasing the mixing. The results showed very little difference in the thermal profile, confirming that intense mixing in the carbonates would not drastically change the thermal profile.

S.3 The Carbonate Mixing Model

This section describes in detail a proposed mixing model of the carbonates. The model is composed of three types of "reservoirs" in series. The first is the chimney above each individual test. Within such a highly permeable chimney, a convective cell develops, causing an intense mixing within the cavity. It is assumed that the concentration of any radionuclide is maintained uniform within the chimney at all times. This well-mixed reservoir loses water through the top of the chimney, with a Darcy velocity, V_D, either through the volcanic cover, if there is one (category 1), or directly to the carbonates for tests known to have leaking covers (category 2) or for CRTV tests (category 3). The flux of water coming out of the chimney is thus the product of this Darcy velocity multiplied by the cross-sectional area of the chimney, $\pi\, r_c^2$, where r_c is the radius of the chimney. By continuity, the chimney receives the same amount of water, either from below or from the sides, which mixes rapidly, and it is easy to establish the variation with time of the concentration in the chimney, taking radioactive decay into account:

$$C(t) = C_0\, \exp(-\Lambda\, t) \tag{S.1}$$

where

$$C_0 = \frac{A_0}{2\,\pi\, r_c^2\, h'_c\, \epsilon} \tag{S.2}$$

is the initial concentration in the cavity, A_0 is the initial inventory of HTO in Bq, $h'c$ is the height of the chimney (equal to 5.666 r_c, taking into account the volume of the lower

hemisphere of the cavity), ϵ is the porosity of the chimney (assumed to be 30%), and

$$\Lambda = \lambda + \frac{V_D}{h'_c \, \epsilon \, R} \tag{S.3}$$

where λ is the decay constant of the radionuclide of interest (equal to $(\ln 2)/T$, where T is the half-life), and R is a retardation coefficient to account for sorption on the rubble.

The flux of radionuclides leaving the chimney and transferred to the carbonates is, thus, $\pi \, r_c^2 \, V_D \, C(t)$. The time for this flux to reach the carbonate is a function of the thickness of the volcanic cover and its porosity. For CRTV and category-2 tests with a damaged cover, this delay is zero. For category-1 tests, however, the most likely scenario, based on interpretation of the filling rates of the chimneys in Section 7.2.3, is that the volcanic cover has an effective hydraulic conductivity of the order of ten times the undisturbed value. If this is the case, fractures in the volcanic cover must have a larger aperture than the undisturbed fractures, which is consistent with the mechanical interpretation of the consequences of a test; transfer through the volcanic cover will take place through these fractures. A conservative estimate of the fracture porosity is 1% (one fracture of 1-mm aperture every 10 cm). With a Darcy velocity above a chimney estimated to be of the order of 1 my^{-1} or more, at early times, and a thickness of cover on the order of 100 m, the delay between the flux leaving the chimney and reaching the carbonates is of the order of a year. This delay will be ignored, even for the category-1 tests. This is certainly conservative, but it will be shown later to be consistent with the observations. This does not mean that the category-1 tests release their contents as quickly as the CRTV or category-2 tests (the Darcy velocity above a CRTV or category-2 test is about 20 times larger than for a category-1 test); it means only that the thickness of the volcanic cover does not provide a time delay for non-sorbing radionuclides such as HTO, which "leak" into the carbonates at the same rate as the flow through the chimney.

The second reservoir is the carbonate layer, with a given (variable) thickness and a selected horizontal area, S. Into this "reservoir", which is assumed to be perfectly mixed by the tidal effects discussed above, enters a decaying radionuclide flux from a chimney. A vertical radionuclide flux leaves the reservoir toward the lagoon.

Let V'_D be the vertical average natural Darcy velocity in the carbonates, directed upward to the lagoon. (With the three-dimensional model, the IGC estimated this to be of the order of 0.137 my^{-1} at Mururoa.) Note that this Darcy velocity is much smaller than that above a chimney, because the heat in the chimney creates strong buoyancy forces. These forces are only local, and the natural Darcy velocities at the large scale are essentially undisturbed by the tests, as we have shown. The flux entering the lagoon is thus $V'_D \, S$. Taking radioactive decay into account, the differential equation representing the evolution of the concentration $C'(t)$ in the carbonates as a function of time is

$$\frac{dC'}{dt} = -\left(\lambda + \frac{V'_D\, S}{V}\right) C' + \frac{\pi\, r_c^2 V_D}{V}\, C(t) \tag{S.4}$$

where V is the volume of the carbonate reservoir equal to $L\, S\epsilon'$, L is the thickness of the reservoir, and ϵ' is the porosity of the carbonates.

The solution of this equation is

$$C'(t) = \frac{\pi\, r_c^2 V_D\, C_0}{V(\Lambda - \Gamma)} \left[\exp(-\Gamma t) - \exp(-\Lambda t)\right] \tag{S.5}$$

where $\Gamma = \lambda + V'_D\, S/V = \lambda + V'_D\, /\, (L\, \epsilon')$.

Note that the somewhat arbitrary selection of area S, over which the spreading of the nuclides occurs, is irrelevant as far as flux to the lagoon is concerned: if this area is too large, the concentration in the carbonates will be smaller, but the total flux to the lagoon will remain the same. Because we will try to validate this model against both the observed concentrations in the carbonates and the flux in the lagoons, the uncertainty on area S is not important as far as the flux to the lagoon is concerned. It can be used to check whether the calculated concentrations in the carbonates are in reasonable agreement with the measured ones, with a credible estimate of S. Note also that the thickness, L, of carbonates in which the mixing occurs is an adjustable parameter. DIRCEN/CEA assumed mixing over 50 m of dolomite with a porosity of 20% (DIRCEN/CEA Document No. 9) to estimate the inventory of nuclides in the carbonates. Later, we will use 300 m (i.e. the full thickness of the carbonates), which is more conservative and also more consistent with the observed distributions over the vertical. Sensitivity tests with smaller thickness will also be made.

One could argue that the mixing occurs over 150 m instead of 300 m, but the net result would then be to reduce the inventory in the carbonates by a factor of 2 and to make the model produce slightly less constant concentrations in the lagoon, contrary to the observations. We believe that the uncertainty in the concentration distribution in the carbonates is higher than a factor of 2, and we therefore propose to adopt the conservative 300-m thickness of the carbonate layer. It may be, however, that the upper 50 m of the carbonates do not participate in the mixing and are "short-circuited" by the flux leaving the mixed reservoir to the lagoon by a few fractures with low porosity (and without delay). There are no data to further refine our model; we therefore keep the simple and conservative approach described above. Note that a flux from the reservoir to the ocean could easily be added and would amount to increasing the constant Γ by the ratio of the additional flux leaving the reservoir to the reservoir volume.

The above model needs to be further developed when several successive tests are considered, with fluxes arriving in the same carbonate reservoir but at different times and different rates. It can easily be shown that, in this case, the concentration $C'(t)$ in the reservoir is given by

$$C'(t) = A_0 \exp(-\Gamma t) + \Sigma_i A_i \exp[-\Lambda_i (t - t_i)] \tag{S.6}$$

with

$$A_0 = \frac{C'(t_k) - \Sigma_{i=1}^{k} A_i \exp[-\Lambda_i (t_k - t_i)]}{\exp(-\Gamma t_k)} \tag{S.7}$$

$$A_i = \frac{\pi r_{ci}^2 V_{Di} C_{oi}}{V (\Gamma - \Lambda_i)} \tag{S.8}$$

where t_i is the time of a new test, and all subscripts i relate to the properties of test i. In (S.6), the summation over i is extended to all the tests prior to time t and each time a new test is added — e.g. at time t_k, the constant A_0 is re-initialised using (S.7).

The third reservoir is actually the lagoon. The lagoon could be modelled as a well-mixed reservoir with a nuclide flux entering the carbonates from the second reservoir and a flux leaving the lagoon through the daily exchange with the ocean. Because the residence time in this third reservoir is of the order of tens of days (compared to years for the other two), this third reservoir will not be modelled; we only compare the flux leaving the carbonate reservoir toward the lagoon to the observed flux exiting the lagoon, obtained as the product of the measured concentration in the lagoon and the annual flux of water transiting through the lagoon. As we have seen, this flux is relatively constant in time.

S.4 Selection of Parameters for the Transport Model in the Carbonates

The carbonate mixing model depends upon a number of parameters that need to be estimated. The initial concentration of HTO in each chimney, C_0, depends on the yield of the test. The initial inventory of HTO has been estimated by the IAEA (IAEA 1998c) for classes of yields between 1 kt and 150 kt. Although the inventory does not vary linearly with yield, we have chosen to interpolate linearly between the values given in Table S.2.

The decay constant $\Lambda = \lambda + V_D / (H_c' \epsilon)$ depends on the unknown Darcy velocity, V_D, which applies to the fluid flow above the chimney. This Darcy velocity was estimated based on detailed numerical calculations (see Section 7.3.5) and was found to be almost independent of the yield of the test. The range of average velocities for the first 10–50 years after a test is 0.1–1.3 my^{-1} for category-1 tests and 20–40 my^{-1} for category-2 and category-3 tests.

As a base case, it was decided to use the values 1 my^{-1}, for category-1, and 20 my^{-1}, for category-2 and category-3 tests. These values have also been used in the radionuclide-release model described by the IAEA (IAEA 1998b) — in fact, the primary objective of this mixing model is to check that these average velocities are not unreasonable on the basis of available information. These Darcy velocities are prescribed, not

Table S.2 Amount of tritium produced by tests of different yields (IAEA 1998c)

Yield (kt)	HTO Inventory (T Bq)
0.45 (safety test)	0
1	1360
5	1360
10	1620
20	2360
25	2730
50	4570
60	5300
100	8270
150	12 000

calibrated; however, variations by a factor of 2 will be analysed below. Note that, for a given velocity, the larger the yield, the smaller is Λ, meaning that small cavities release their tritium faster than large cavities. Since the inventory and the total flux above a cavity do not scale with the yield, a zone where many small tests were carried out will release more tritium than a zone where a small number of large tests, with the same total yield, was carried out.

The decay constant $\Gamma = \lambda + V'_D / L\ \epsilon'$ depends on the average Darcy velocity, V'_D, in the carbonates at atoll scale, which has been estimated at 0.137 my^{-1} for Mururoa. We assume a 300-m average thickness, L, of the carbonates, but we will study the sensitivity of predictions to values of 200, 100, and 50 m. The porosity of the carbonates, ϵ', is assumed to be 30% and is not varied.

The last model parameter is the horizontal area S, over which HTO spreads in the carbonates. This area will be estimated on the basis of the maps of HTO distribution as observed from the sampling holes (Figs. 7.21 and 7.22). This is, of course, a parameter with a significant uncertainty, as the number of sampling holes is very limited: 16 at Mururoa and 4 at Fangataufa. The uncertainty may reach a factor of 2, but we have shown that this will affect only the calculated concentration in the carbonates, not the flux to the lagoon nor the inventory.

Because this information is available only for that year, we will estimate S for 1996, but it will not make any difference to use an area S that grows with time (which is certainly the case — the HTO "spreads" horizontally with time by tidal mixing). This parameter will also be varied by a factor of two. Table S.3 summarises the set of uncertain parameters to be studied for both atolls.

Table S.3 Model parameters to be tested in the carbonate mixing model

Model Parameter	Parameter Value(s)
carbonate thickness	300 m; sensitivity = 200, 100 and 50 m
vertical Darcy velocity in carbonates at atoll scale	0.137 my^{-1} sensitivity = half or twice this value
Darcy velocity above chimney for category-1 tests	1 my^{-1} sensitivity = half or twice this value
Darcy velocity above chimney for category-2 and -3 tests	20 my^{-1} sensitivity = half or twice this value

S.5 Application of the Mixing Model to Fangataufa

We first apply the model to Fangataufa, where the number of tests is small (10). All tests are category-1 tests, shot between 1975 and 1996, except Lycos, which was shot on 27 November 1989 and which is known to have leaked (a category-2 test). The yields of these 10 tests have been estimated by the IAEA (IAEA 1998b), which determined that the values are consistent with various totals provided by DIRCEN/CEA. The estimates are reproduced in Table S.4.

Considering the HTO distribution at Fangataufa in 1996 (Fig. 7.22) and the results of measurements made by IAEA in 1996-1997 (IAEA 1998e), there is clearly one central leak of HTO under the lagoon, spreading toward the rim. This leak is probably due to the Lycos test. Area S, where the HTO is distributed, is estimated, based on this map, to be 12 km^2, with an average concentration of $4{\cdot}10^6$ Bq m^{-3}. The flux to the lagoon is estimated to be $9{\cdot}10^{12}$ Bq y^{-1}, based on the concentration of lagoon water and daily flow. The inventory in the carbonates is estimated to be $4.3{\cdot}10^{15}$ Bq. This number is based, for consistency, on 300 m of HTO-containing carbonates, with a porosity of 30%, over a 12-km^2 area, at the estimated concentration of $4{\cdot}10^6$ Bq m^{-3}. This is larger than the DIRCEN/CEA estimate, for which 50 m of karst with a porosity of 20% was used.

It is assumed in the calculations that all tests are shot on 1 January of each year; concentrations are calculated only for 1 January of each subsequent year. The concentration in the carbonates, the inventory in the carbonates, and the flux into the lagoon have been calculated with the analytical expressions (S6–S8) using a spreadsheet. The results are given in Figure S.1b, which represents the HTO flux to the lagoon from the carbonates from 1976 to 2010; the conversion factor for the concentration and the inventory are given in Figure S.1b. The HTO concentration and total inventory in the carbonates have an identical shape, since these three curves are all proportional to the concentration. These figures clearly show that the Lycos test in 1989 is indeed the major source of HTO in the carbonates, since the rapid increase in concentration occurred immediately after 1989.

Table S.4 Estimated yields of tests at Fangataufa Atoll (after IAEA (1998a))

Year	Name	Yield (kt)
1975	Achille	20
1975	Hector	20
1988	Cycnos	103
1989	Cysicos	74
1989	Lycos	87
1990	Cypselos	100
1990	Hyrtacos	118
1991	Periclymnos	106
1995	Ploutos	97
1996	Xouthos	46

Table S5 compares the estimated concentration, flux to lagoon and inventory with the results of the mixing model at Fangataufa, for the base case and for a number of combinations of parameter values, to test the sensitivity of the model to uncertain parameters. All results are calculated for the year 1996. After the base case, all parameters are varied in turn by a factor of two (except the carbonate thickness, for which three values are tested), while all other parameters take their base-case values.

No attempt was made to calibrate the model. All the base-case parameters were selected *a priori* from earlier estimates. Nevertheless, the base case seems to be reasonably consistent with the observations.

The sensitivity study shows a large dependence on the thickness of the reservoir; a thickness smaller than 300 m would require a significant decrease of all the fluxes from the volcanics from category-1 or -2 tests. It appears, therefore, that the 300-m thickness leads to a conservative estimate of the fluxes passing from the volcanics to the carbonates. The sensitivity to the velocities in the chimneys for category-1 and -2 tests shows that these parameters are not very sensitive; however, the larger values for both categories would give overestimates for all three observations, while the smaller values would still be acceptable. The base-case values for these chimney velocities therefore seem to be on the conservative side. The flux to the lagoon is very sensitive to the average velocity in the carbonates, while the concentration and inventory are not — as one would expect. The base-case average velocity in the carbonates is the only acceptable value. As expected, area S has no impact on the flux to the lagoon and the inventory, while the concentration varies almost linearly with this parameter. The base-case value, again, seems the best choice, on the conservative side.

In summary, and for this first attempt at Fangataufa, we believe that the carbonate mixing model, with the selected Darcy velocities above the chimneys for category-1 and -2 tests, is consistent with the data available at Fangataufa and matches the measured flux of HTO to the lagoon and the few measured concentrations in the carbonates. There is

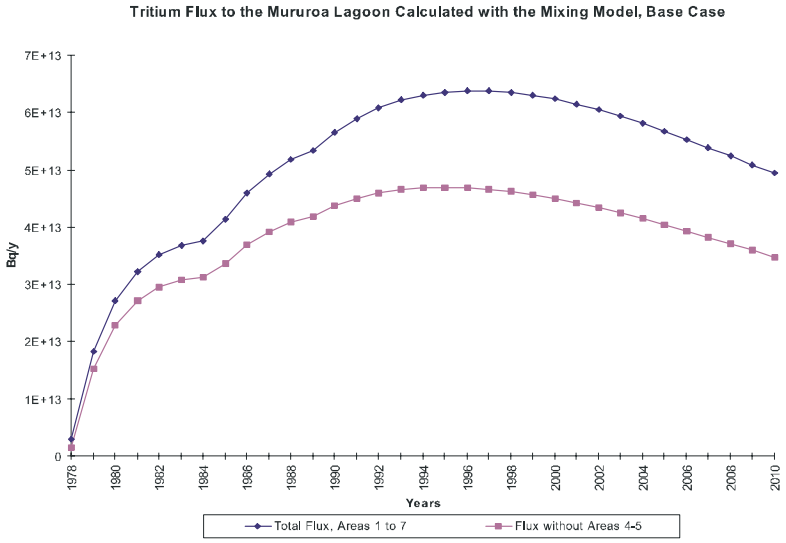

(a)

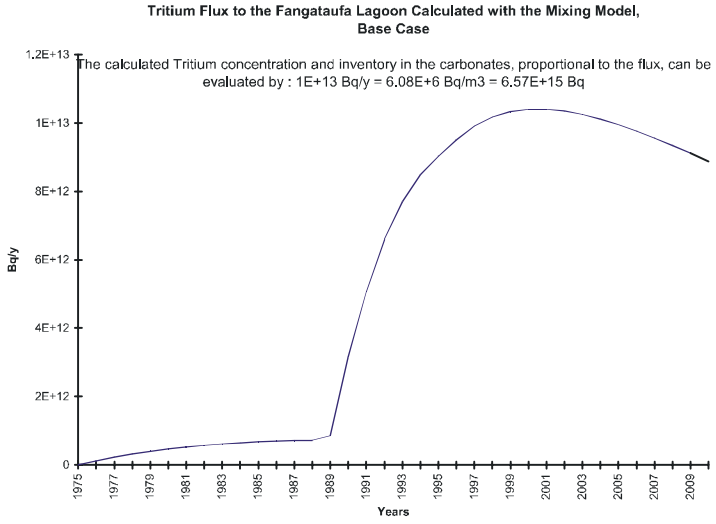

(b)

Figure S.1 Calculated tritium release to the Mururoa (a) and Fangataufa (b) lagoons using the IGC mixing model

Table S.5 Mixing model HTO results for Fangataufa, for 1996: Base case and sensitivity study

Test Case	Concentrations in Carbonates	Flux to Lagoon	Inventory in Carbonates
	(10^6 Bq m^{-3})	(10^{12} Bq y^{-1})	(10^{15}Bq)
Estimated Values from observations	4	9	4.3 (3 in DIRCEN/CEA Doc. No. 9)
Base Case, L = 300 m V_D for Cat. 1 = 1 my^{-1} V_D for Cat. 2 = 20 my^{-1} V'_D in Carbonates = 0.137 my^{-1} Area S = 12 km^2	5.79	9.51	6.25
Reduced Thickness, L = 200 m	8.65	14.2	6.23
Reduced Thickness, L = 100 m	17.1	28.2	6.16
Very Low Thickness, L = 50 m	33.6	55.2	6.04
Reduced Velocity V_D = 0.5 my^{-1} for Category1	4.71	7.75	5.09
Increased Velocity V_D = 2 my^{-1} for Category 1	7.75	12.7	8.37
Reduced Velocity V_D = 10 my^{-1} for Category 2	4.66	7.66	5.03
Increased Velocity V'_D = 40 my^{-1} for Category 2	6.54	10.8	7.06
Reduced Velocity in Carbonates V'_D = 0.5·0.137 my^{-1}	5.81	4.77	6.27
Increased Velocity in Carbonates V'_D = 2·0.137 my^{-1}	5.75	18.9	6.21
Reduced Area, (0.5·S)	11.6	9.51	6.25
Increased Area (2 S)	2.89	9.51	6.25

no need to include in the model any leak to the ocean; however, if such a leak were added (e.g. of the same order of magnitude as the leak to the lagoon), it would not significantly alter the results, as the total inventory transferred to the lagoon (and thus to the ocean as well, if of the same order of magnitude) is negligible compared to the total inventory in the carbonates.

S.6 Application of the Mixing Model to Mururoa

Looking at the HTO distribution in the carbonates in Mururoa (Figure 7.21), it is clear that a single application of the model to the entire atoll would be inappropriate: several plumes of HTO can be seen, linked to the seven test areas, as defined by DIRCEN/CEA (Document No. 6). The same mixing model was thus applied successively to the seven areas, with the same parameters as for Fangataufa. For each area, area S and the average concentration of HTO were taken from DIRCEN/CEA Document No. 9 and IAEA (1998e).

The average yield per area, the number and the years of the tests (for a period of 5 years) are known from the DIRCEN/CEA documents for each category (1, 2, or 3). The tests are grouped for calculations for the years 1978, 1984, 1989, or placed at the exact years for the most recent ones. The yields of category-2 tests are based on IAEA (1998c) estimates.

Note that the category-2 Enée test may not be in test area 3, but in test area 4, because it is a category-C test (< 150 kt), and there are no such tests in test area 3 according to DIRCEN/CEA (Document No. 6). However, there is evidence of a significant leak in the Murène 16 observation hole, immediately to the north of test area 3, which is attributed to Enée. Alternatively, this observation could be due to a category-2 test in test area 6.

Also note that in test area 5, area S of the present distribution of HTO is apparently non-existent, unless some of the plumes attributed to test area 2 or 3 are due to some of the tests in test area 5. This is a difficulty in our attempt to understand the transfer in the carbonates and will be discussed further. An area of 4 km^2 was used to define the reservoir for test area 5.

From the observed HTO distribution summarised in Table S.6, the total inventory in the carbonates at Mururoa can be calculated. For consistency, we used a thickness (300 m) in the carbonates over which the observed HTO concentration is assumed to be constant and a porosity of 30%; the inventory for 1996 is, then, $30 \cdot 10^{15}$ Bq, which is larger than the DIRCEN/CEA (Document No. 9) estimate, which was based on only 50 m of carbonates ($4.2 \cdot 10^{15}$ Bq). The HTO flux to the Mururoa lagoon is estimated for 1996 at $37 \cdot 10^{12}$ Bq/y, using the observed concentration in the lagoon and the conservative DIRCEN/CEA estimate of the daily flow.

Figure S.1a presents, for the base case, the evolution of the calculated HTO flux to the Mururoa lagoon with time, from 1978 to 2010, and Table S.7 presents, for 1996, the

calculated concentration for each area, the total flux to the lagoon, and the total inventory in the carbonates; these last two quantities are also calculated separately, with test areas 4 and 5 excluded from the summation, for reasons that will be explained below. Figure S.1a also presents the HTO flux to the Mururoa lagoon when the flux from test areas 4 and 5 is excluded. In Table S.7, base-case results are given first, followed by sensitivity studies where the major parameters are decreased or increased by a factor of two, except for the carbonate thickness, for which three values are considered, as for Fangataufa.

In general, the calculated concentrations are in reasonable agreement with the observed ones, except for test areas 4 and 5. For test area 4, the calculated concentration is larger than the estimate by a factor of two. This can be interpreted as a possible indication of the existence of a significant direct leak from the carbonates to the ocean. Such a leak is rather more likely in this area because of the mechanical instability that developed and the sliding that occurred, which may have facilitated communication between the carbonates and the ocean.

For test area 5, the calculated concentration is much higher than those measured in that area (two boreholes at 6 and $7{\cdot}10^4$ Bq/m^3). Note that this, along with test area 7, is one of the two areas where no CRTVs or category-2 tests were shot. Thus, one could say that the Darcy velocity of 1 m/y adopted for the category-1 tests is too large: however, it is consistent with the observations in test area 7 and in test area 1. We think, therefore, that either the sampling boreholes were not adequate to estimate the HTO concentration in test area 5 or that the volcanic rock in this area is more resistant and provides better confinement than in the other areas (or that the tests may have been deeper). One can also note that the average yield of the area 5 tests is small, 14.3 kt, compared to that for area 6 or 7.

For test area 1, the calculated concentration is consistent with observation. It is, however, very interesting to realise that the present level of HTO in the carbonates cannot be attributed to the early CRTV tests only: each CRTV test produced an estimated 1360 TBq of HTO; 18 years later, for the 7 CRTV tests, this amounts to a residual of 3500 TBq of HTO by radioactive decay only. For an area of 10 km^2 with a concentration of 10^7 Bq/m^3, a 300-m thickness of carbonates and a porosity of 30%, the present inventory is of the order of 9000 TBq — i.e. about three times larger than the residual HTO from the CRTVs. To explain the present level of HTO with the CRTVs only, we would need to assume that the area is 3 km^2 or that the thickness of the carbonate mixing layer is 100 m, without any losses — but this is not really consistent with the observations. While this scenario cannot be totally ruled out, it is much more likely that the present level of HTO is due, in part, as assumed by the model, to the leakage of category-1 tests, thus validating (or at least not invalidating) the estimated Darcy velocity of 1 m/y in the undamaged volcanic cover. The Darcy velocity of 20 m/y for the CRTVs cannot be validated in test area 1 at this late date: with any value of Darcy velocity larger than 2.5 m/y, more than 90% of the HTO in each CRTV cavity would have leaked into the

carbonates in 18 years. Note that there is no need to include any release of HTO to the ocean to match the observations, as indicated earlier for Fangataufa; however, if such a leak were included with the same order of magnitude as the leak to the lagoon, it would not change the results significantly, because the flux is very small compared to the inventory.

For test area 6, the calculated concentration is slightly higher than the observations, indicating that the leaks may be overestimated by the model. In general, the base-case value seems to be in reasonable agreement with the observations, particularly if the fluxes coming from test areas 4 and 5 are excluded from the summation. Even so, the calculated values are still conservative.

The model is very sensitive to the carbonate thickness; assuming a smaller thickness than 300 m would require an almost proportional reduction of the leaks from the volcanics. The sensitivity to the velocities above the chimneys is slight — but greater for category-1 tests, where the base-case value seems the best choice. The category-2 tests were too few (3) and old (1977 and 1988), and the category-3 tests too old (12 in 1978) to be of any remaining significance compared to the very large number of category-1 tests. This was not the case for Fangataufa, where the category-2 Lycos test still had a significant effect. The sensitivity to the average Darcy velocity in the carbonates is large for the flux to the lagoon, with the base case having the most likely value, on the conservative side. The sensitivity to area S is also large.

S.7 Conclusion

The approach used in this appendix to understand how nuclides released from the volcanics to the carbonates eventually reach the environment is based on a very simple mixing model to represent the carbonates. This model has been shown to be reasonably consistent with the observations, without any calibration of its parameters, which have all been estimated independently or based on earlier models developed by the IGC.

The major difference between this model and the model proposed by DIRCEN/CEA is that the carbonates act as a large reservoir for the radionuclides: we estimate that the total inventory stored in the carbonates is much higher than has been estimated by DIRCEN/CEA, because we have assumed that HTO was distributed at a constant concentration over the whole thickness (300 m) of the carbonates. This is, of course, a very conservative assumption.

With this model and assumption, the available data on the flux to the lagoon and the concentration in the carbonates have been used to evaluate the reasonableness of the rate of release of HTO from the chimneys in the volcanics for Category 1, 2 and 3 tests. We conclude that the Darcy velocities of 1 m/y (for category 1) and 20 m/y (for categories 2–3) can be used with some confidence to predict radionuclide release from the volcanics to the environment. These Darcy velocities lead to higher release rates

Table S.6 Parameters for the carbonates mixing model for Mururoa

Area	1	2	3	4	5	6	7
Surface S of HTO plume, km^2	10	8	2.5	4	4	4	4
Observed average HTO concentration, 10^7 Bq/m^3	1	1	1.5	1	~ 0	1	1
Category-1 tests (average yield and when they occurred)	2.4 kt: 22 in 1978 5 in 1984 1 in 1990	5.5 kt: 13 in 1978 14 in 1984	14.3 kt: 3 in 1978 4 in 1984	35.2 kt: 8 in 1978 12 in 1984	14.3 kt: 7 in 1984 13 in 1989 1 in 1991	27.6 kt: 7 in 1984 9 in 1989 2 in 1995	43 kt: 5 in 1984 8 in 1989 1 in 1995
Category-2 tests (average yield and when they occurred)			53 kt: 1 in 1977 [a]	47 kt: 1 in 1977[b]		54 kt: 1 in 1985[c]	
Category-3 (CRTV) tests (average yield and when they occurred)	5 kt: 5 in 1978	5 kt: 4 in 1978	5 kt: 1 in 1978				

[a] Enée
[b] Nestor
[c] Megarée

Table S.7 Mixing model HTO results for Mururoa, for 1996: Base case and sensitivity study

Test Case	Conc. Area 1 10^7 Bq/m^3	Conc. Area 2 10^7 Bq/m^3	Conc. Area 2 10^7 Bq/m^3	Conc. Area 4 10^7 Bq/m^3	Conc. Area 5 10^7 Bq/m^3	Conc. Area 6 10^7 Bq/m^3	Conc. Area 7 10^7 Bq/m^3	Flux to Lagoon 1-7 10^{12} Bq/y	Invent. 1-7 10^{15} Bq	Flux to Lagoon 1-3 + 6-7 10^{12} Bq/y	Invent. 1-3 + 6-7 10^{15} Bq
Estim. Values	1	1	1.5	1	0	1	1	37	30	37	30
Base Case	**1.1**	**1.0**	**1.6**	**2.0**	**1.1**	**1.7**	**1.0**	**63.8**	**41.9**	**46.9**	**30.8**
L = 200 m	1.7	1.5	2.4	3.0	1.6	2.6	1.5	95.1	41.7	69.8	30.6
L = 100 m	3.2	2.9	4.6	5.9	3.2	5.1	3.0	186	40.8	137	29.9
L = 50 m	6.1	5.6	8.7	11.4	6.2	10.0	5.9	358	39.2	262	28.7
V_2 = 10 m/y	1.1	1.0	1.5	2.0	1.1	1.6	1.0	62.8	41.2	45.9	30.2
V_2 = 40 m/y	1.1	1.0	1.6	2.0	1.1	1.8	1.0	64.0	42.1	47.1	30.9
V_1 = 0.5 m/y	0.8	0.7	1.3	1.3	0.6	1.2	0.5	42.4	27.8	32.4	21.3
V_1 = 2 m/y	1.5	1.5	2.1	3.3	2.0	2.7	1.9	98.4	64.6	69.4	45.6
V_{carb} halved	1.1	1.0	1.6	2.0	1.1	1.7	1.0	32.1	42.2	23.6	31.0
V_{carb} doubled	1.1	1.0	1.6	2.0	1.1	1.7	1.0	126	41.4	92.4	30.4
S halved	2.2	2.0	3.2	4.1	2.1	3.5	2.0	63.8	41.9	46.9	30.8
S doubled	5.6	5.1	7.9	10.1	5.4	8.7	5.1	63.8	41.9	46.9	30.8

from the volcanics than those assumed by DIRCEN/CEA and to concentrations in the carbonates, inventories and fluxes to the lagoons that are larger than those observed. We believe that the IGC's estimates are reasonable and on the conservative side.

This attempt to use measured nuclide distributions in the carbonates and lagoons to validate assumptions and models has included only HTO data, although Sr, Cs and Pu data are also available. This is because HTO is a perfect tracer of water and can thus be used to understand the hydrology of the atolls. If we had tried to use the other nuclides, it would have been necessary to take retardation factors into account. The assumption of there being no delay for transfer from the top of the chimney to the carbonates, for the case of an existing volcanic cover, would not have been reasonable.

As we have seen, direct release to the ocean cannot be ruled out with the present data. Because there is some evidence that leaks to the ocean are taking place in some areas, such as test area 4, we recommend that the fluxes of nuclides in the environment be estimated according to two extreme scenarios: one in which release occurs only to the lagoon, and one in which release occurs only to the ocean.

Appendix T

TEST OF A PISTON-FLOW MODEL AND A DISPERSION MODEL FOR TRITIUM RELEASE AT THE PTC

T.1 Piston Flow Model

The piston-flow model is based on the assumption that the flux released to the carbonates, as given by the product of the concentration in the chimney (see Eq. (S.1)) multiplied by the Darcy velocity in the chimney, is simply transferred to the lagoon with a time lag of 1, 2, 5, 10, 15 or 20 years. This time lag is assumed to be the convective transfer time through the carbonates. Radioactive decay is taken into account during this transfer, but mixing is not. The flux arriving to the lagoon is simply the sum of all the releases of each group of tests, as given for the mixing model (Appendix S). The only parameters involved in this model are the transfer time, from 1 to 20 years, and, of course, the velocities in the chimney for category-1, -2 or -3 tests.

Four cases were run with this piston-flow model: two for Fangataufa, and two for Mururoa (Figs. T.1 and T.2). Two cases were examined for each atoll: (a) the base case, where the chimney velocities are 1 and 20 m/y, for category-1 and category-2 and -3 tests, respectively (the results show that, for the base case, the flux to the lagoon is much too high, about two orders of magnitude higher than the observed flux); and (b) a second case in which the velocities in the chimney were reduced by a factor of 166, to match approximately the observed flux to the lagoon. Although the flux is now of the correct order, the time-variation of this flux is not consistent with the rather stable flux observed, and the inventory of tritium in the carbonate is now about two orders of magnitude too low compared to the observations.

These results show that piston-flow is not a realistic model for flow in the carbonates. The assumption of a rapid transit of the HTO flux from the volcanics to the lagoon is not consistent with the observations.

T.2 Dispersion Model

The dispersion model assumes convective and dispersive transfers in the carbonates. For each group of tests, as used in the mixing model, the following analytical solution of the dispersion equation is used:

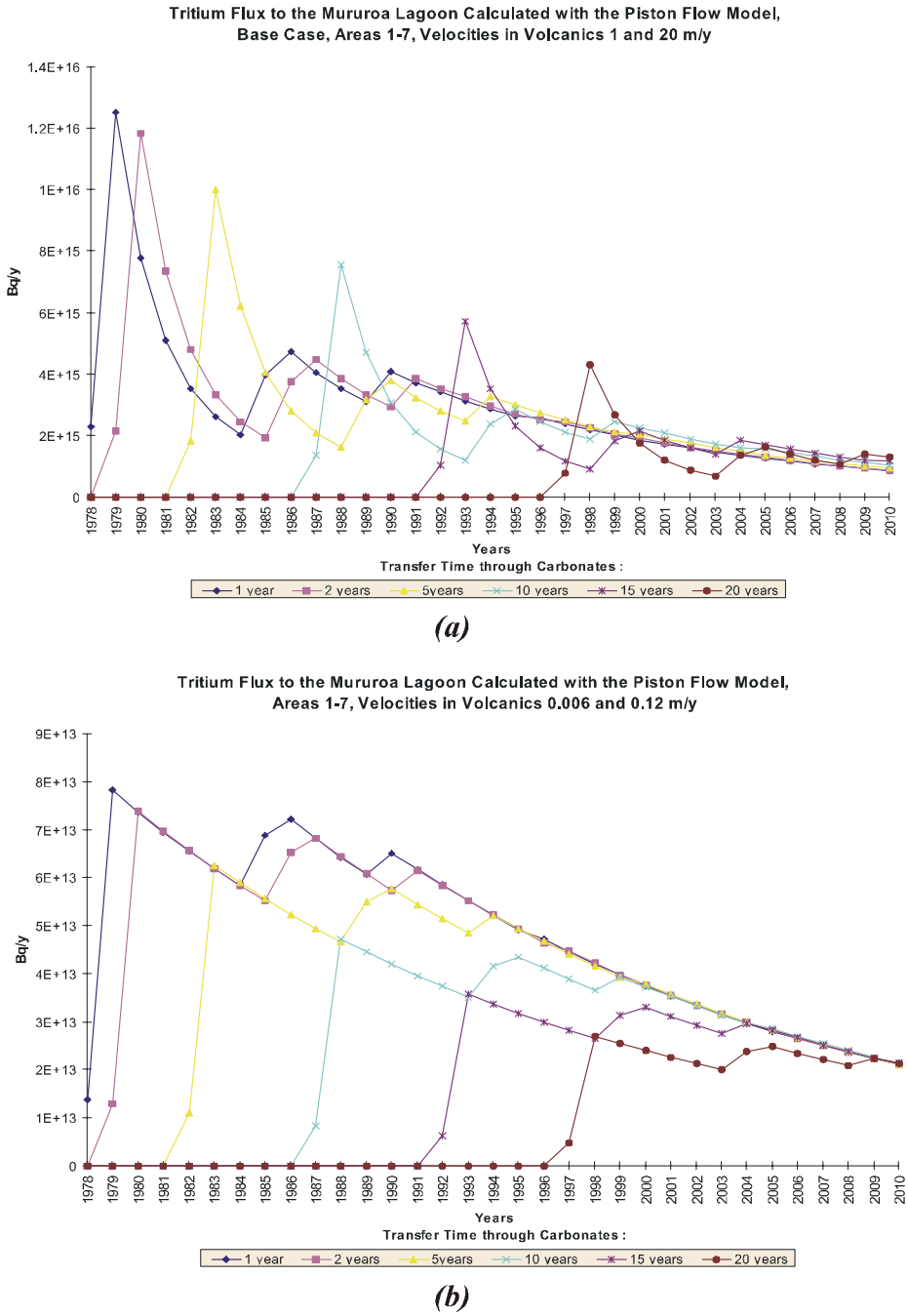

Figure T.1 Tritium flux to the Mururoa lagoon calculated with the piston-flow model: (a) Base case, areas 1–7, velocities in volcanics 1 and 20 m/y; (b) areas 1–7, velocities in volcanics 0.006 and 0.12 m/y

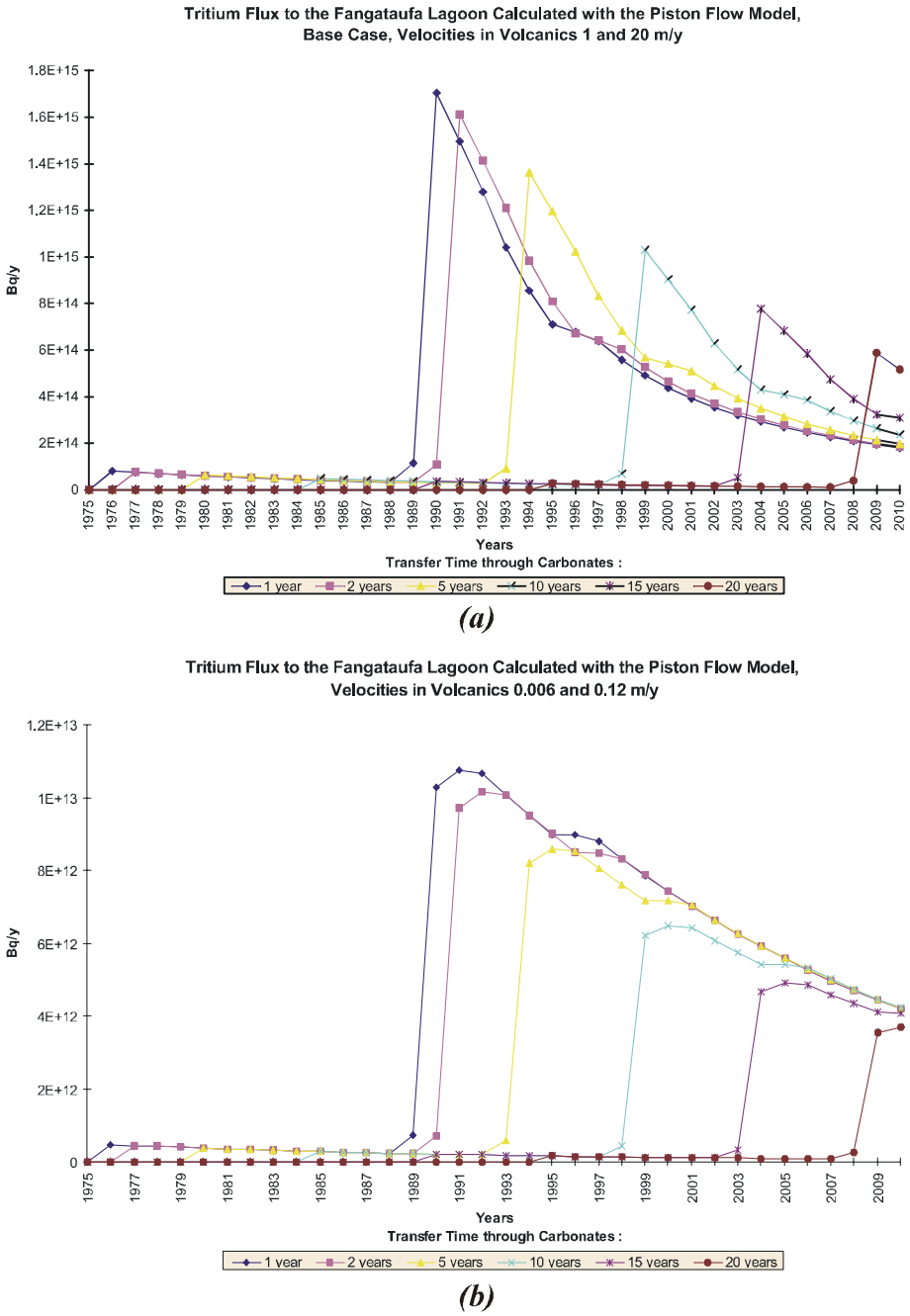

Figure T.2 Tritium flux to the Fangataufa lagoon calculated with the piston-flow model: (a) Base case, velocities in volcanics 1 and 20 m/y; (b) Velocities in volcanics 0.006 and 0.12 m/y

$$C(x,t) = \frac{C_0}{2}\exp\left(\frac{Ux}{2D}\right)\exp(-\Lambda t)\left\{\begin{array}{l}\exp(-\beta x)\,\mathrm{erfc}\left[\frac{x-t\sqrt{(U/\varepsilon)^2+4(\lambda-\Lambda)D/\varepsilon}}{2\sqrt{Dt/\varepsilon}}\right] \\ +\exp(\beta x)\,\mathrm{erfc}\left[\frac{x+t\sqrt{(U/\varepsilon)^2+4(\lambda-\Lambda)D/\varepsilon}}{2\sqrt{Dt/\varepsilon}}\right]\end{array}\right\} \quad \text{(T.1)}$$

where:

$$\beta = \sqrt{\left(\frac{U}{2D}\right)^2 + \frac{(\lambda-\Lambda)\varepsilon}{D}}$$

λ is the decay constant of HTO,

Λ is the decay constant of the source term (see S.3 of App. S),

D is the dispersion coefficient, product of Darcy velocity U (m/s) by the dispersivity α in (m),

ε is the porosity,

x is the distance, here the thickness of the carbonate layer, and

t is the time.

Equation (T.1) is valid for an injection at decaying concentration. The flux coming from the volcanics is transformed into a flux reaching the lagoon. As with the piston-flow model, all groups of tests are simply summed to calculate the total release to the lagoon. The parameters of the model are the Darcy velocity, U, and the dispersivity, α, along with the chimney Darcy velocities for category-1, -2 and -3 tests.

The model was run for both atolls, with five tests for each (see Fig. T.3). The Darcy velocity in the carbonates was varied from 0.5 to 3 m/y, and the dispersivity from 100 to 1000 m. The chimney velocities were also varied. The results show that, in order to obtain an early release, as observed in the field, it is necessary to use large dispersivities, from 200 to 1000 m. Such large values could be due to tidal mixing. Again, however, the flux to the lagoon is too large, and increases rapidly with time, contrary to observations. If the velocities in the chimneys are reduced (to 0.002 and 0.4 m/y), then it is possible to match the observed flux to the lagoon, but the inventory in the carbonates would then be much too low — by a factor of about 50. Although this model shows a much smoother evolution of the flux to the lagoon with time, it is unable to account for the inventory and flux to the lagoon as observed and, therefore, is considered unacceptable.

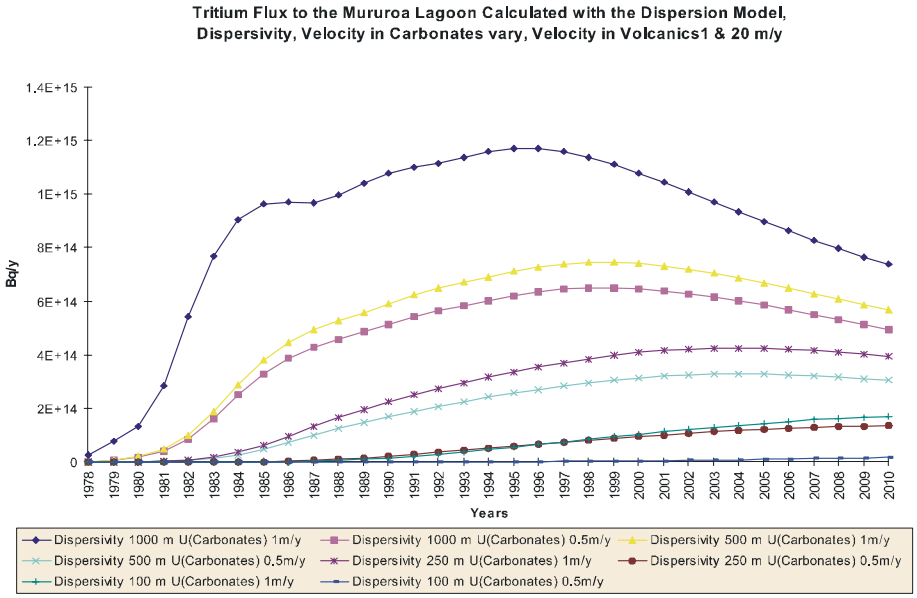

(a)

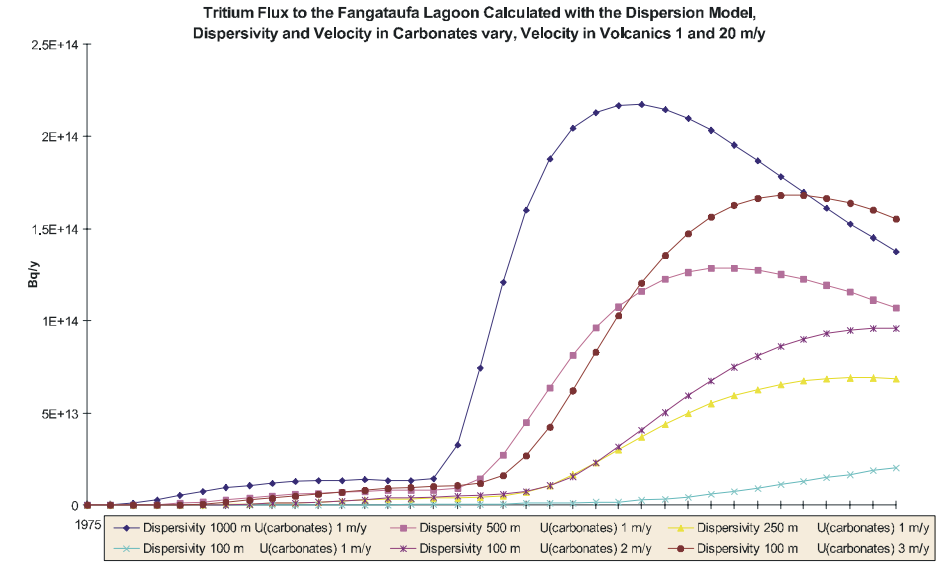

(b)

Figure T.3 Tritium flux to the (a) Mururoa and (b) Fangataufa lagoons calculated with the dispersion model: Dispersivity, velocity in the carbonates vary, velocity in volcanics 1 and 20 m/y

Appendix U

ANALYSIS OF PERIODIC GROUNDWATER FLOW

U.1 One-Dimensional Vertical Flow in the Carbonates

Consider, first, the behaviour of a one-dimensional vertical column of porous medium driven by fluctuating heads at both its upper and lower boundaries, perhaps with a difference in phase between the fluctuations. Flow in such a column is described by, for example, Bear (1972):

$$S_0 \frac{\partial \phi}{\partial t} = K \frac{\partial^2 \phi}{\partial z^2} \tag{U.1}$$

where $\phi(z,t)$ represents piezometric head $[L]$, S_0 is the specific storativity $[L^{-1}]$, and K is the vertical hydraulic conductivity $[L^1 T^{-1}]$.

Suppose that boundary heads can be expressed in the form

$$\Phi = \Phi_s + Re\{\Phi_p \exp(i\omega t)\} \tag{U.2}$$

where Φ_s is the steady component of the boundary head, $\Phi_p = \Phi_{pr} + i\Phi_{pi}$ is a complex number representing the magnitude and phase of a component of boundary head which is sinusoidal or periodic in time, $\omega = 2\pi/P$ is the angular frequency of a fluctuation with period P, and $Re\{\cdot\}$ is an operator which takes the real part of a complex number.

Equation (U.2) can also be written in the forms

$$\Phi(t) = \Phi_s + \Phi_{pr} \cos \omega t - \Phi_{pi} \sin \omega t \tag{U.3}$$

$$\Phi(t) = \Phi_s + \Phi_{pa} \cos(\omega t + \tau_\Phi) \tag{U.4}$$

where $\Phi_{pa} = |\Phi_p| = (\Phi_{pr}^2 + \Phi_{pi}^2)^{0.5}$ is the amplitude of the periodic fluctuation of boundary head and τ_Φ is the phase angle in radians (see, e.g. Churchill et al. 1976), given by $\tau_\Phi = \arg\{\Phi_p\} = \tan^{-1}(\Phi_{pi}/\Phi_{pr})$, with $-\pi \leq \tau_\Phi \leq \pi$. However, the use of (U.2) simplifies the form of the analytical solutions that follow.

The mathematical functions arg and $\tan^{-1}$ are multi-valued, since they return angles measured in radians. By convention, most software implementations of these functions return principal values in the range $-\pi$ to π. For convenience, however, we define *time*

to peak, t_Φ, in the range $0 < t_\Phi < P$, as the time in each period when the periodic boundary head has its maximum value:

$$\begin{aligned} t_\Phi = F(\tau_\Phi)P &= \left[1 - \frac{\tau_\Phi}{2\pi}\right] P \qquad 0 \le \tau_\Phi \le \pi \\ &= \left[-\frac{\tau_\Phi}{2\pi}\right] P \qquad -\pi \le \tau_\Phi \le 0 \end{aligned} \tag{U.5}$$

The function F, defined by (U.5), converts an angle in the range $-\pi$ to π to a fraction between 0 and 1. A phase angle of $\pi/4$, for example, corresponds to a time to peak of 0.875 P and a phase angle of $-\pi/2$ corresponds to 0.25 P.

Because (U.5) is a linear differential equation and the boundary conditions take the form of (U.2), it follows that $\phi(z,t)$ can be written as

$$\phi(z,t) = \phi_s(z) + Re\{\phi_p(z)\exp(i\omega t)\} \tag{U.6}$$

where ϕ_s is the steady component of head and $\phi_p = \phi_{pr} + i\,\phi_{pi}$ is a complex number representing the magnitude and phase of a component of head that is sinusoidal or periodic in time. As above, $\phi(z,t)$ can be written

$$\begin{aligned} \phi(z,t) &= \phi_s(z) + \phi_{pr}(z)\cos\omega t - \phi_{pi}(z)\sin\omega t \\ &= \phi_s(z) + \phi_{pa}(z)\cos(\omega t + \tau_\phi(z)) \end{aligned} \tag{U.7}$$

where $\phi_{pa} = |\phi_p| = (\phi_{pr}^2 + \phi_{pi}^2)^{0.5}$ is the amplitude of the periodic component of head and τ_ϕ is the phase angle (in radians), given by $t_\phi = \arg\{\phi_p\} = \tan^{-1}(\phi_{pi}/\phi_{pr})$. As in (U.5), we define the time to peak, $t_\phi(z)$, in the range $0 < t_\phi(z) < P$, as the time when the periodic component of head has its maximum value. Because heads at all locations are linked by the differential equation (U.1), the amplitude and phase of head are always functions of z.

Substituting (U.6) into (U.1) leads to separate ordinary differential equations for the steady and periodic components of head:

$$K\,\frac{d^2\,\phi_s}{d\,z^2} = 0 \tag{U.8}$$

$$K\,\frac{d^2\,\phi_p}{d\,z^2} - i\omega\,S_0\,\phi_p = 0 \tag{U.9}$$

Equation (U.8) is the usual steady-state flow equation, while (U.9) has an extra term and is a differential equation for the complex variable ϕ_p. Once these two differential equations have been solved, the complete solution for $\phi(z,t)$ is given by (U.6) or (U.7).

Solutions for the differential equations depend on boundary conditions. The general solutions of (U.8) and (U.9) are:

$$\phi_s = C_1 z + C_2 \tag{U.10}$$

$$\phi_p = D_1 \cosh az + D_2 \sinh az \tag{U.11}$$

where C_1 and C_2 are real constants determined by the boundary conditions for (U.8), $a^2 = i\omega S/T = 2\pi i\, S/TP$, and D_1 and D_2 are complex constants determined by the boundary conditions for (U.9).

Consider a one-dimensional domain that extends from $z = 0$ at the surface to $z = -D$. If $\phi = \Phi_0$ at $z = 0$ and $\phi = \Phi_D$ at $z = -D$, substituting these boundary conditions into (U.10) and (U.11) leads to $C_1 = (\Phi_{0s} - \Phi_{Ds})/D$, $C_2 = \Phi_{0s}$, $D_1 = \Phi_{0p}$ and $D_2 = (\Phi_{0p} \cosh aD - \Phi_{Dp})/\sinh aD$, from which

$$\phi_s = \frac{\Phi_{0s}(z + D) - \Phi_{Ds}\, z}{D} \tag{U.12}$$

$$\begin{aligned}
\phi_p &= \frac{\Phi_{0p}(\sinh aD \cosh az + \cosh aD \sinh az) - \Phi_{Dp} \sinh az}{\sinh aD} \\
&= \frac{\Phi_{0p}(\sinh b \cosh b(\frac{z}{D}) + \cosh b \sinh b(\frac{z}{D})) - \Phi_{Dp} \sinh b(\frac{z}{D})}{\sinh b} \\
&= \frac{\Phi_{0p} \sinh b(1 + \frac{z}{D}) - \Phi_{Dp} \sinh b(\frac{z}{D})}{\sinh b}
\end{aligned} \tag{U.13}$$

where

$$b^2 = a^2 D^2 = 2\pi i\, \frac{D^2 S_0}{KP} \tag{U.14}$$

which depends directly on $D^2 S_0/KP$. This non-dimensional ratio is always important in solutions of the groundwater flow equation and can be interpreted as a non-dimensional response time — i.e. as the ratio of the column response time, $D^2 S_0/K$, to the period of fluctuations, P.

Being a complex number, the periodic solution ϕ_p contains two types of information: amplitude and phase. The amplitude of fluctuations decays with distance from both boundaries, but the decay distance depends on the properties of the porous medium and the depth of the column. The solution is logically presented by graphing the amplitude of head relative to the amplitude of fluctuations at the upper boundary, as a function of z/D and $D^2 S_0/KP$. The ratio of amplitudes is given by:

$$\left|\frac{\phi_p}{\Phi_{0p}}\right| = \left|\frac{\sinh b\left(1+\frac{z}{D}\right) - \frac{\Phi_{Dp}}{\Phi_{0p}}\sinh b\left(\frac{z}{D}\right)}{\sinh b}\right| \tag{U.15}$$

Figure U.1 shows the spatial distribution of amplitude, as given by (U.15), with Φ_{Dp} and Φ_{0p} equal and perfectly in phase, for four values of D^2S_0/KP. When this ratio is small, the fluctuations in piezometric head occur far from the boundaries. Conversely, when the ratio is large, the fluctuations die out rapidly with distance from the boundaries.

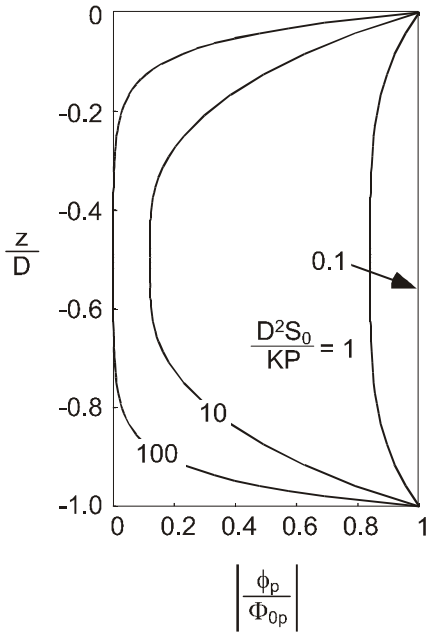

Figure U.1 Spatial distribution of amplitude of heads in the carbonates with $\Phi_{Dp} = \Phi_{0p}$

The phase $\tau_\phi = \arg\{\phi_p\} = \tan^{-1}(\phi_{pi}/\phi_{pr})$ can be calculated directly. Alternatively, we can express the phase as the lag between the forcing at the upper boundary, Φ_{0p}, and the response, $\phi_p(z)$. This lag is to be given by

$$\begin{aligned}\Delta\tau_\phi &= \arg\{\phi_p\} - \arg\{\Phi_{0p}\} = \arg\left\{\frac{\phi_{Dp}}{\phi_{0p}}\right\} \\ &= \arg\left\{\frac{\sinh b(1+\frac{z}{D}) - \frac{\Phi_{Dp}}{\Phi 0p}\sinh b(\frac{z}{D})}{\sinh b}\right\}\end{aligned} \tag{U.16}$$

Utilising (U.5), we can express the lag as a fraction of a period, and this is shown in Figure U.2. The lag is small when D^2S_0/KP is small; however, for large D^2S_0/KP (when the amplitude is negligibly small), the lag can be more than one period.

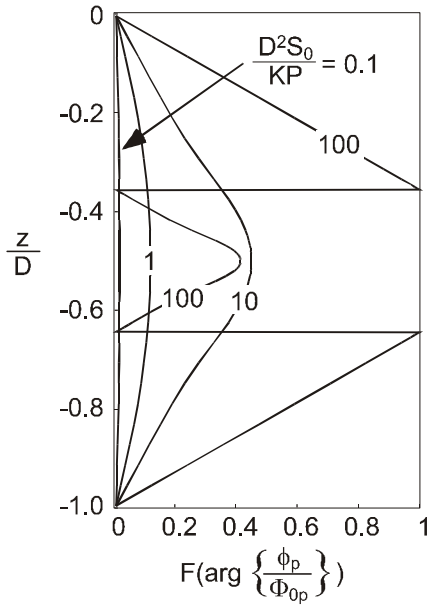

Figure U.2 Spatial distribution of lag between boundary heads and heads in the carbonates with $\Phi_{Dp} = \Phi_{0p}$

Figure U.3 shows three-dimensional representations, for four different values of D^2S_0/KP, of the fluctuations in head (U.13) over two periods, assuming that the peak tidal level at both ends of the column occurs when t/P = 0, 1 and 2.

One issue of interest is the magnitude and direction of flows within the column. By differentiating (U.13) and (U.14), the steady and periodic components of flow in the upward direction are given by

$$q_s = K\,\frac{\Phi_{Ds} - \Phi_{0s}}{D} \tag{U.17}$$

$$q_p = \frac{K}{D}\left\{\frac{b\left[\Phi_{Dp}\cosh b(\frac{z}{D}) - \Phi_{0p}\cosh b(1+\frac{z}{D})\right]}{\sinh b}\right\} \tag{U.18}$$

If the steady components of the boundary heads are equal, (U.17) confirms that the steady flow through the column is zero. Figure U.4 shows how the amplitude of the periodic component of flow (normalised with respect to $K\Phi_{0p}/D$) varies in space for four values of D^2S_0/KP. When D^2S_0/KP is small, the normalised inflow is the smallest —

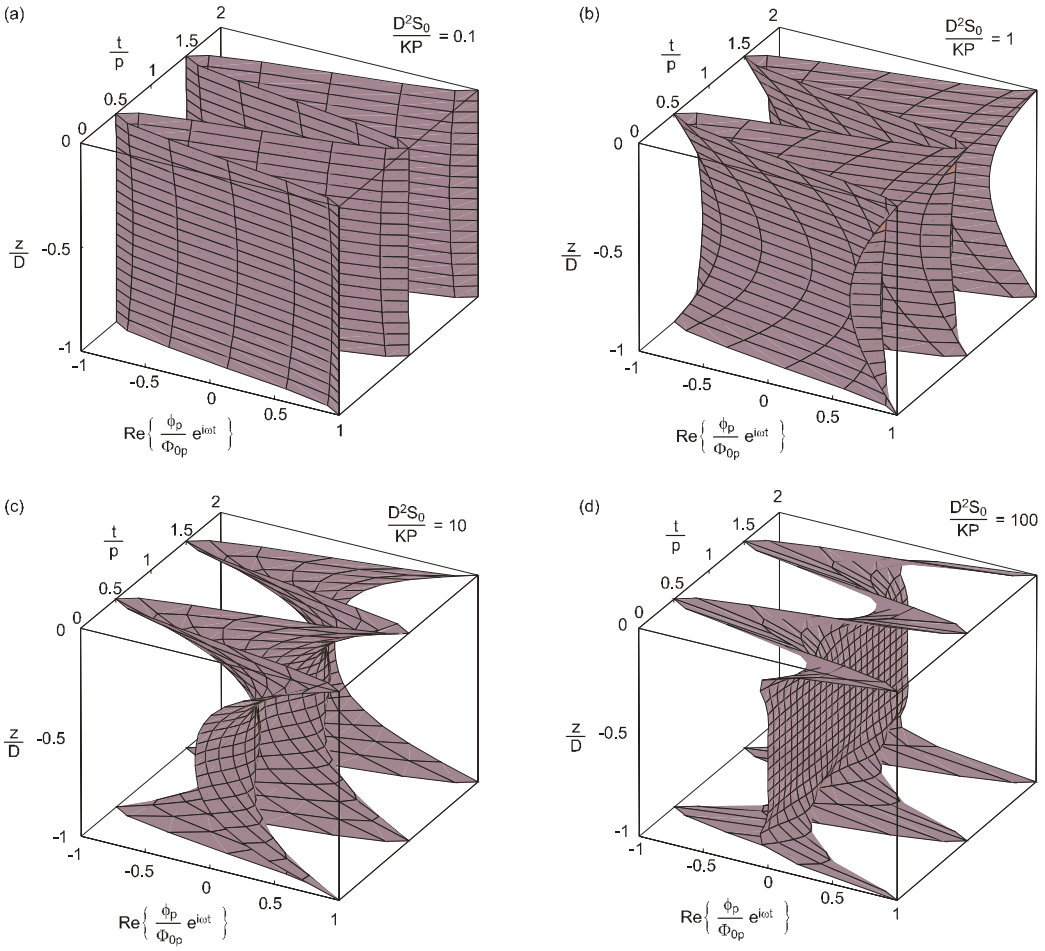

Figure U.3 Three-dimensional representations of heads in the carbonates

i.e. the flattest V-shaped curve in the figure. As D^2S_0/KP increases, the "V" becomes sharper, until the last curve, when the "V" becomes more U-shaped. Flows near the middle of the carbonates are largest for intermediate values of D^2S_0/KP. Figure U.5 shows that the phase lag of q_p relative to Φ_{0p} is even more interesting, partly because flows in the lower half of the carbonates are upward when flows in the upper part of the carbonates are downward.

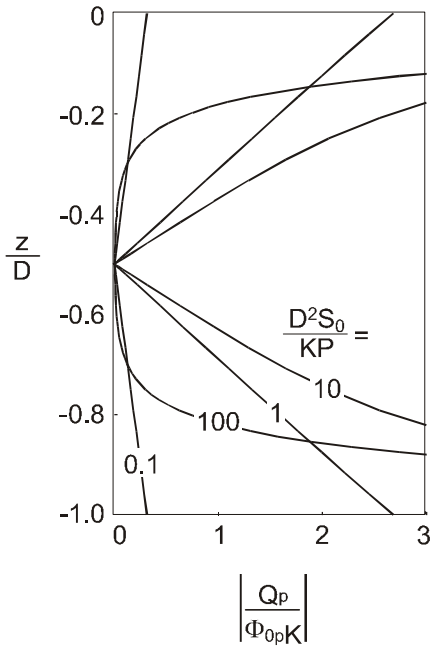

Figure U.4 Amplitude of flows in the carbonates

Of special interest are the fluctuations in flow at the bottom of the column. The steady flow is constant, or possibly zero, throughout the column; however, the periodic component of the specific discharge is given by (U.18) evaluated at $z = -D$:

$$q_{Dp} = \frac{K}{D}\left[\frac{b\left(\Phi_{Dp}\cosh b - \Phi_{0p}\right)}{\sinh b}\right] \tag{U.19}$$

The fluctuation in flow at the base of the column depends linearly on the fluctuations in boundary heads at the ends of the column.

Figure U.6 shows how q_{Dp} varies in time for four values of D^2S_0/KP. For very small and very large values of D^2S_0/KP, the upward flow at $z = -D$ is most positive at t = 0.75 P and 0.875 P, respectively, with a very slightly higher lag for values of D^2S_0/KP between about 3 and 12. This implies that the upward flow reaches its maximum gen-

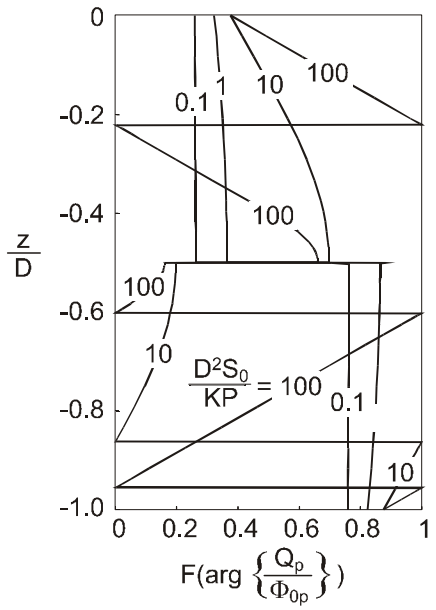

Figure U.5 Phase lag of upward flow in the carbonates relative to Φ_{0p}

erally between 0.25 P and 0.125 P ahead of the peak in Φ_{0p}. When D^2S_0/KP is very small, the magnitude of $q_{Dp}D/\Phi_{0p}K$ is very small — i.e. $|q_{Dp}|$ is much less than would occur if there were a head drop of $|\Phi_{0p}|$ over the length of the column. When D^2S_0/KP is large, $|q_{Dp}|$ is much greater than would occur if there were a head drop of $|\Phi_{0p}|$ over the length of the column, because of the very steep head gradients that occur near the boundary (see Figs. U.1 and U.3).

All of the results presented here are affected by differences in magnitude and phase between Φ_{0p} and Φ_{Dp}, but the details have not been explored.

U.2 Horizontal Flow in a One-Dimensional Karst Aquifer Coupled to Overlying Carbonates

The previous analysis presupposes that the boundary conditions at both the top and bottom of the carbonate zone are known. Now we consider a conceptual model in which the carbonate zones at Mururoa and Fangataufa Atolls are represented by a continuum of adjacent vertical columns for which the boundary conditions at the bottom of each column depend on the behaviour of a horizontal karst aquifer that traverses the atolls at the base of the carbonate zone. This situation is illustrated in Figure U.7.

The justification for this conceptual model relies on the assumption that the karst is sufficiently conductive to transmit ocean water horizontally toward the centre of the atoll with little loss in head. If the loss in head were completely negligible, there would be

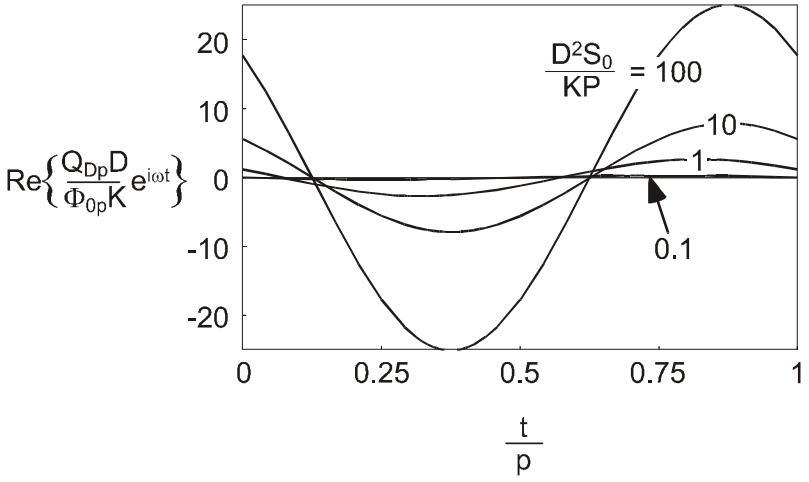

Figure U.6 Time variation of upward flow at $z = -D$, for four values of $D^2 S_0 / K P$: 0.1, 1, 10 and 100 (the largest amplitude corresponds to the largest $D^2 S_0 / K P$)

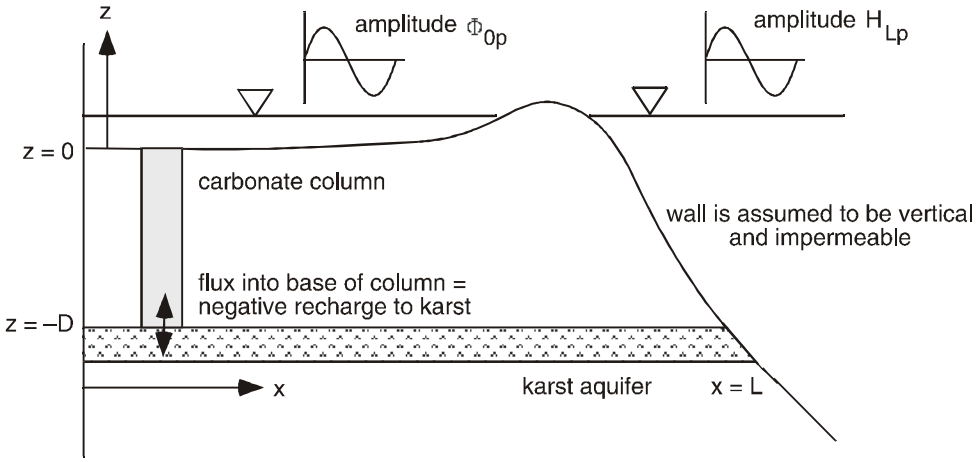

Figure U.7 Conceptual coupled model of the carbonate and karst

no need to consider this coupling, as all flow from the karst to the lagoon above would be essentially vertical and the model considered in Section U.1 could be used alone with sufficient accuracy. If the head loss in the karst is small but non-negligible, flow in the carbonates will still be almost vertical as long as $L >> D$, but there would be some small lag between tidal fluctuations in the ocean and head fluctuations in the karst beneath the centre of the atoll. In all cases, a coupled model integrates the flows within the karst and allows a direct calculation of flows and particle trajectories within the karst.

Flow in a homogeneous one-dimensional aquifer of thickness B is described by the aquifer flow equation (e.g. Bear 1972)

$$S \frac{\partial h}{\partial t} = T \frac{\partial^2 h}{\partial x^2} + R \tag{U.20}$$

where $h(x, t)$ represents head $[L]$, S is the aquifer storage coefficient [-], T is the aquifer transmissivity $[L^2T^{-1}]$, and $R(x, t)$ represents distributed net recharge $[LT^{-1}]$. In a confined aquifer, h is piezometric head, S is equal to S_0B, where S_0 $[L^{-1}]$ is specific storativity, B is the actual thickness of the aquifer, and T is equal to KB, where K is the horizontal hydraulic conductivity.

Suppose that fluxes between the underlying volcanics and the karst are negligible relative to those between the karst and the carbonates. Recharge, R, is then the net flow from the carbonates to the karst, or, if negative, the anticipated flow from the karst to the carbonates. If R can be represented as the sum of steady and periodic components, then, as in Section U.1, h can be represented in the same way. All the analysis for the aquifer flow equation is analogous to that presented above, so only an outline of the analysis is presented here.

Suppose that R can be expressed in the form

$$R(x, t) = R_s(x) + Re\{R_p(x) \exp(i\omega t)\} \tag{U.21}$$

Let us assume initially that R is spatially uniform. Substituting (U.21) into (U.20) leads to two separate differential equations for the steady and periodic components of h, respectively:

$$T \frac{d^2 h_s}{dx^2} + R_s = 0 \tag{U.22}$$

$$T \frac{d^2 h_p}{dx^2} - i\omega S h_p + R_p = 0 \tag{U.23}$$

With a no-flow boundary at $x = 0$ and a prescribed head boundary at $x = L$, the solution to this problem can be found by superimposing (adding) the solutions from Townley's (1995) Examples 1 and 2:

$$h_s = H_{Ls} + \frac{R_s}{2T}\left(L^2 - x^2\right) \tag{U.24}$$

$$h_p = H_{Lp}\left[\frac{\cosh c\frac{x}{L}}{\cosh c}\right] + Z_p\left[1 - \frac{\cosh c\frac{x}{L}}{\cosh c}\right] \tag{U.25}$$

where H_{Ls} and H_{Lp} represent the steady and periodic components of head at the ocean end of the karst aquifer, $Z_p = R_p / i\omega S$, and

$$c^2 = 2\pi i\,\frac{L_2 S}{T P} \tag{U.26}$$

where $L_2 S/T P$ is a non-dimensional response time for the karst aquifer — i.e. the aquifer response time relative to the period P. The quantity Z_p represents the amplitude of the fluctuation of head that would occur throughout the aquifer, due to periodic recharge alone, if the transmissivity of the aquifer were zero.

In the situation of interest, R is not spatially uniform, but is given by the downward flux (net recharge) from an imaginary set of vertical columns of carbonate at each point x along the length of the karst aquifer. From (U.17) and (U.19), we get

$$R_s = -Q_s = -K\,\frac{\Phi_{Ds} - \Phi_{0s}}{D} \tag{U.27}$$

$$R_p = -Q_{Dp} = -\frac{K}{D}\,\frac{\left(b\,\Phi_{Dp}\cosh b - \Phi_{0p}\right)}{\sinh b} \tag{U.28}$$

The differential equations (U.22) and (U.23) then take the form

$$T\,\frac{d^2 h_s}{dx^2} - \frac{K}{D}\,h_s = -\frac{K}{D}\,\Phi_{0s} \tag{U.29}$$

$$T\,\frac{d^2 h_p}{dx^2} - i\omega S\,h_p - \frac{K}{D}\,b\coth b\,h_p = -\frac{K}{D}\,b\,\mathrm{csch}\,b\,\Phi_{0p} \tag{U.30}$$

Equation (U.29) is different in form from (U.22); however (U.30) is identical in form to (U.23), so the existing solution (U.25) can be used with slightly different coefficients. The solutions to (U.29) and (U.30) are

$$h_s = H_{Ls}\left(\frac{\cosh d\,\frac{x}{L}}{\cosh d}\right) + \Phi_{0s}\left(1 - \frac{\cosh d\frac{x}{L}}{\cosh d}\right) \tag{U.31}$$

$$h_p = H_{Lp}\left(\frac{\cosh e\,\frac{x}{L}}{\cosh e}\right) + Z_p^*\left(1 - \frac{\cosh e\frac{x}{L}}{\cosh e}\right) \tag{U.32}$$

where

$$d^2 = \frac{L^2 K}{DT} \tag{U.33}$$

$$e^2 = L^2 \frac{i\omega s + \frac{K}{D}\coth b}{T} = 2\pi i \frac{L^2 S}{TP} + \frac{L^2 K}{DT} b\coth b = c^2 + d^2 b\coth b \tag{U.34}$$

$$Z_p^* = \frac{\frac{K}{D} b\,\mathrm{csch}\, b}{i\omega s + \frac{K}{D} b\coth b}\Phi_{0p} = \frac{d^2 b\,\mathrm{csch}\, b}{c^2 + d^2 b\coth b}\Phi_{0p} = \frac{d^2}{e^2} b\,\mathrm{csch}\, b\,\Phi_{0p} \tag{U.35}$$

A variable like d is commonly found in analytical solutions where there is leakage from one aquifer to another through an aquitard. The variables e and Z_p^*, which are fundamental to the solution (U.32), combine the influence of d and the non-dimensional response times for the carbonate and karst that are embedded in b and c, respectively.

Note that the periodic boundary conditions in the ocean and the lagoon enter the solution through H_{Lp} and Z_p^*, respectively, with the latter depending directly on Φ_{0p}. When arguments of the hyperbolic functions coth and csch are small (i.e. sufficiently less than 1), we can write

$$b\coth b = 1 + \frac{b^2}{3} + O[b^4] \tag{U.36}$$

$$b\,\mathrm{csch}\, b = 1 - \frac{b^2}{6} + O[b^4] \tag{U.37}$$

Although e^2 and Z_p^* in (U.33) and (U.34) could be simplified and rewritten in terms of b^2, c^2 and d^2, this does not appear to offer any significant advantages.

The fluxes in the karst aquifer can be found by differentiating (U.31) and (U.32). Thus,

$$Q_s = T\left(\frac{\Phi_{0s} - H_s}{L}\right) d\left(\frac{\sinh d\,\frac{x}{L}}{\cosh d}\right) \tag{U.38}$$

$$Q_p = T\left(\frac{Z_p^* - H_p}{L}\right) e\left(\frac{\sinh e\,\frac{x}{L}}{\cosh e}\right) \tag{U.39}$$

As before, if the average heads in the ocean and lagoon are equal, the steady component of flow is zero. An indicative value for the amplitude of horizontal displacement of a particle of water due to fluctuating heads can be determined by integrating the horizontal flux over a quarter of a period while the particle is moving in one direction, and

correcting for aquifer thickness and the effective porosity, n, of the karst. This can be shown to be given by

$$\delta_x(x) = \frac{|Q_p(x)|\,P}{2\pi\,Bn} \tag{U.40}$$

This quantity is not rigorously correct, because as soon as a particle moves from its original position, it experiences a different $Q_p(x)$. However $\delta_x(x)$ still provides a useful relative measure of displacement.

In principle, it would be nice to display examples of the solution (U.32) for a wide range of non-dimensional parameters, as in Section U.1. However (U.32) depends on three non-dimensional ratios: D^2S_0/KP, as in Section U.1, as well as L^2S/TP and L^2K/DT. We therefore choose to select a smaller range of parameter values and to show solutions that may be relevant to Mururoa.

Suppose the carbonate has parameters D = 300 m, $S_0 = 10^{-5}$ m^{-1}, K = 10 md^{-1} and P = 0.5 d, and that the karst has L = 3000 m, $S_0 = 10^{-5}$ m^{-1}, $K = 10^4$ md^{-1}, and B = 1 m (so that $S = 10^{-5}$ and $T = 10^4$ m^{2}d^{-1}). We therefore have D^2S_0/KP = 0.18, L^2S/TP = 0.018 and L^2K/DT = 30. These non-dimensional ratios suggest that the whole atoll responds quickly to changes in pressure, although the karst is ten times more responsive than the carbonate.

Figures U.8 and U.9 show the amplitude and phase of heads in the karst, assuming a 0.4-m tidal amplitude and no lag between the ocean and the lagoon. It can be seen that there is about a 10% diminution in amplitude at the centre of the atoll, with a phase lag of about 0.08 of a period — i.e. about 1 hour. For a first attempt, these results are quite close to those cited in DIRCEN/CEA Document No. 5. To facilitate visualisation of this behaviour, Figure U.10 shows a three-dimensional version of these results over two periods.

The results can be presented in many forms, but Figure U.11 shows one quantity of interest, the flux in the karst aquifer at three locations — i.e. at the ocean boundary and at distances 0.2 and 0.4 of the length of the karst inside the atoll. The fluxes are presented as physical values, in m^{2}d^{-1}. In the analytical solution, the karst aquifer is presumed to be 1 m thick, but similar results would be achieved with any thickness and modified values of hydraulic conductivity and specific storativity to achieve the same transmissivity and aquifer storage coefficient in the karst. If we do imagine the karst to be 1 m thick, the flux in m^{2}d^{-1} is equal to specific discharge in md^{-1}. This can be converted to a particle velocity by dividing by the effective porosity in the karst. If this is 0.1 or 0.01 (imagine a karstic solution channel 1 m wide every 10 or 100 m around the perimeter of the atoll), the instantaneous peak velocity for this case is 39.5 or 395 md^{-1}.

Integrating velocity leads to the displacement of a particle from its average position. The amplitude of displacement is equal to the amplitude of velocity divided by angular frequency $\omega = 2\pi/P$; thus, at the ocean entrance to the karst layer, particles would

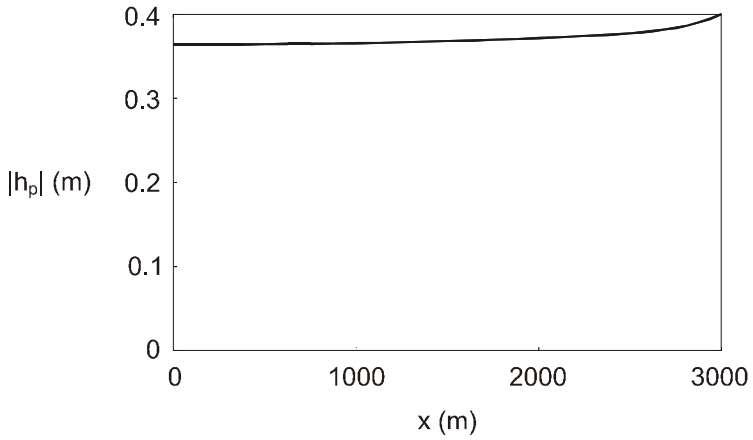

Figure U.8 Amplitude of heads in the karst with initial estimates of parameters

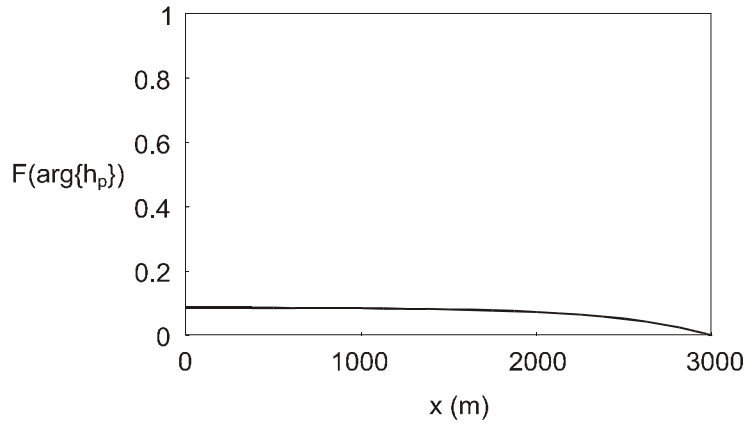

Figure U.9 Lag of heads in the karst relative to the tidal forcing

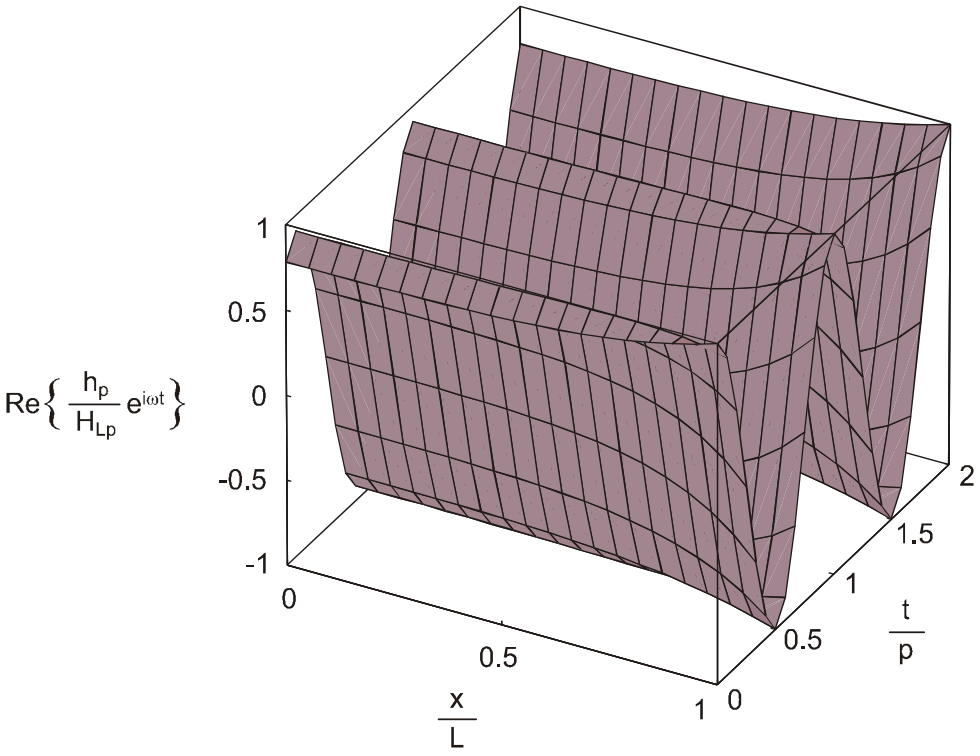

Figure U.10 Three-dimensional representation of heads in the karst

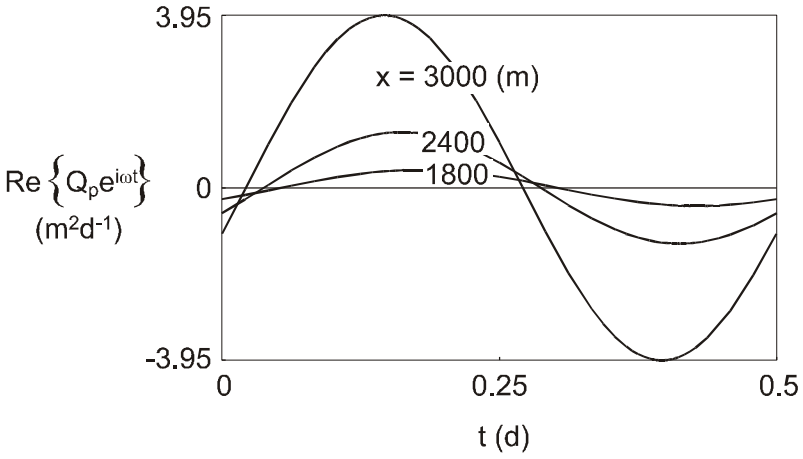

Figure U.11 Flux in the karst with initial parameter values

move backward and forward between 6.3 and 63 m in every tidal cycle. It is hard to imagine that these excursions would not cause significant mixing in the karst and, possibly, significant weakening of any thermal plume reaching the karst from the volcanics below. We can therefore imagine movement of radionuclides over wider and weaker plumes, but with further modification due to fluctuations in vertical velocities within the carbonate zone.

As an indication of the sensitivity of these results to various parameters, Figures U.12 to U.14 show results with the original parameters and some parameters modified, as shown in the figure captions.

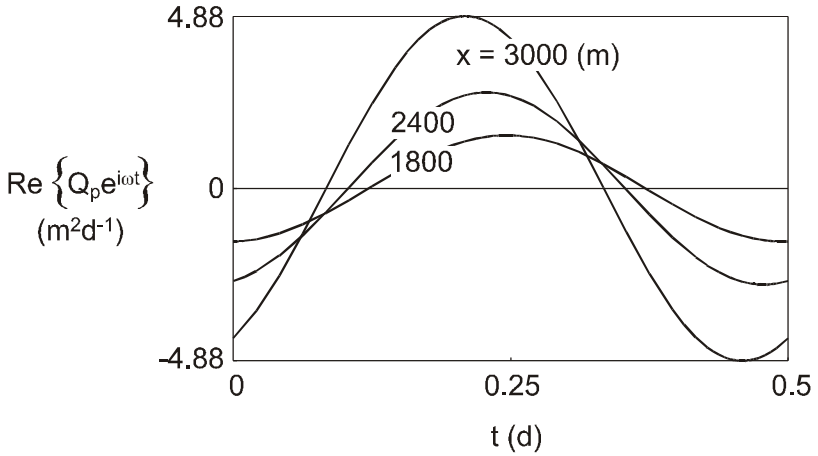

Figure U.12 Flux in the karst with initial parameter values, but with conductivity in the carbonate reduced to 1 md^{-1}

As a final remark, at any location along the karst aquifer, the solution provides the amplitude and phase of head so that the fluctuations within the overlying vertical column can be computed. These calculations have not been performed systematically, but for the initial parameters used here, the amplitude of vertical specific discharge at the ocean boundary is 0.0075 md^{-1}. (This is not quite what we would see in the atoll, because the analytical model described here has a vertical impermeable wall in the carbonates at the edge of the atoll. The analytical model is likely to be more accurate at some distance from the boundary.) With an effective porosity of 0.1 or 0.01, and integrating over half a tidal cycle, an indicative vertical excursion distance is 12 to 120 mm per tidal cycle. As piezometric head in the karst rises, slightly lagged behind the lagoon, water flows downward from the lagoon and upward from the karst into the carbonate. There is a location near the middle of the carbonate (a node in the oscillations) where the fluctuations in heads and fluxes is zero. However, the fluctuations below and above that location will certainly contribute to increased spreading of any solute.

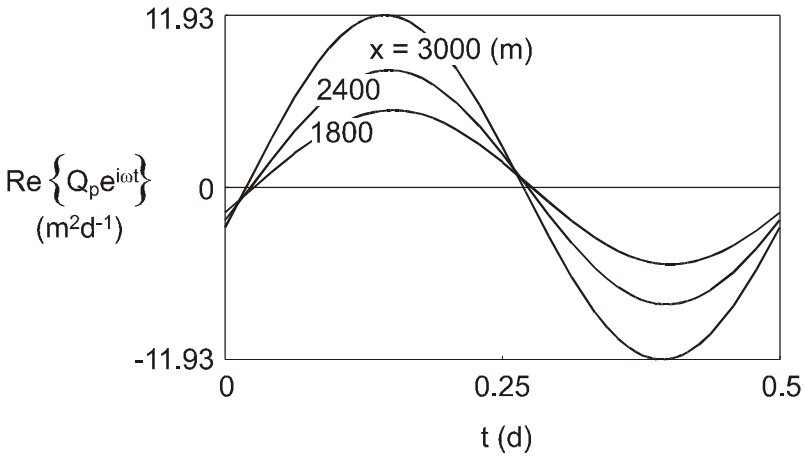

Figure U.13 Flux in the karst with initial parameter values, but with conductivity in the karst increased to 10^5 md^{-1}

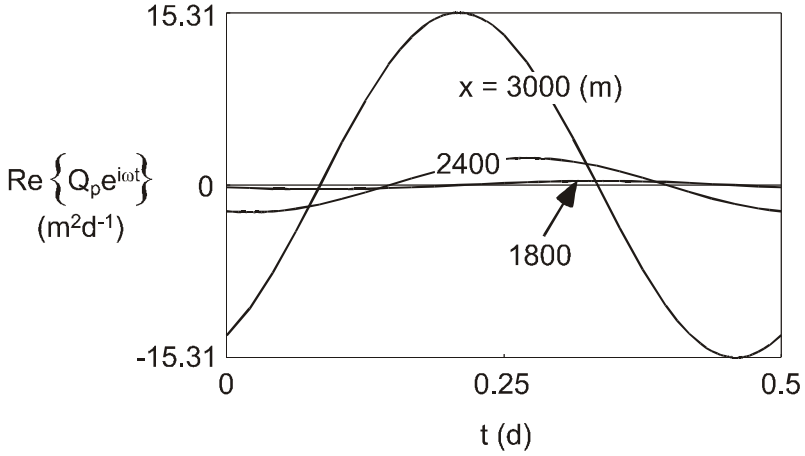

Figure U.14 Flux in the karst with initial parameter values, but with specific storativity in the carbonate increased to 10^{-4} m^{-1}

The one-dimensional analysis presented has been generalised to a radially symmetric karst aquifer, but the results are not presented here.

U.3 A Two-Dimensional Periodic Finite-Element Model

The above analysis can be extended to a linear finite model in the following way (Townley 1993). Many numerical models of aquifer flow can be written in the form

$$\boldsymbol{S}\frac{d\boldsymbol{h}}{dt} + \boldsymbol{K}\boldsymbol{h} = \boldsymbol{f} \tag{U.41}$$

where $\boldsymbol{h}(t)$ is a vector of nodal heads, $\boldsymbol{S}$ is a storage matrix, $\boldsymbol{K}$ is a conductivity or transmissivity matrix, and $\boldsymbol{f}(t)$ is a forcing vector containing recharge terms and boundary conditions. Suppose that $\boldsymbol{f}$ can be represented as a sum of steady and periodic components

$$\boldsymbol{f} = \boldsymbol{f}_s + Re\{\boldsymbol{f}_p \exp(i\omega t)\} \tag{U.42}$$

where $\mathbf{f_s}$ represents the steady or long-term average forcing, and $\boldsymbol{f}_p$ represents the complex amplitude of forcing with frequency ω. If $\boldsymbol{K}$ is independent of time, the solution can be represented as

$$\boldsymbol{h} = \boldsymbol{h}_s + Re\{\boldsymbol{h}_p \exp(i\omega t)\} \tag{U.43}$$

where $\boldsymbol{h}_s$ is the average or long-term average vector of heads, and $\boldsymbol{h}_p$ contains complex amplitudes of head fluctuations with frequency ω.

Substituting (U.42) and (U.43) into (U.41) leads to the result that $\boldsymbol{h}_s$ and $\mathbf{h_p}$ satisfy

$$\boldsymbol{K}\boldsymbol{h}_s = \boldsymbol{f}_s \tag{U.44}$$

$$(i\omega\boldsymbol{S} + \boldsymbol{K})\boldsymbol{h}_p = \boldsymbol{f}_p \tag{U.45}$$

where both $\boldsymbol{f}_p$ and $\boldsymbol{h}_p$ are, in general, complex. Solving for $\boldsymbol{h}_p$ is computationally equivalent to solving a steady-state problem, except that all matrices contain complex numbers instead of reals.

The above algorithm has been implemented in a two-dimensional linear triangular finite-element model called AQUIFEM-P (Townley 1993). AQUIFEM-P can be used for aquifers that are two-dimensional in plan or for flow in two-dimensional vertical sections.

AQUIFEM-P has been applied to a vertical section through Mururoa Atoll, using the finite-element grid shown in Figure U.3b. Steady flow was ignored by setting fixed head boundary conditions along the floor of the lagoon and along the flank of the atoll. Tidal fluctuations were represented with an amplitude of 0.4 m along the same boundaries.

The rim of the atoll was assumed to act as a no-flow boundary, corresponding to the case of an exposed rim with a shallow freshwater lens.

Results are difficult to show in the form of contours because the amplitudes of fluctuations in head and specific discharge vary over many orders of magnitude. All runs used $K = 8.64 \cdot 10^{-3}$ md^{-1} in the basalt and $K = 8.64$ md^{-1} in the carbonate layer. Three different scenarios were considered, with $K = 864$, $K = 8640$ and $K = 86\,400$ md^{-1} in a karst layer 10 m thick. The maximum particle excursion distance (twice the amplitude of displacement) occurs consistently at the ocean entrance to the karst layer. Assuming an effective porosity of 0.1 in the karst layer, the maximum excursion distance is 1.3 m, 7.1 m and 16.7 m for these three cases, respectively. With an effective porosity of 0.01, these distances would be ten times larger. Despite the fact that the analytical results presented in Section J.2 are based on a section 3 km in length (versus 5 km in the two-dimensional section), and in spite of minor differences in conductivities (due to rounding of 8.64 to 10), the two models are remarkably consistent.

A complete spatial analysis of fluctuations is beyond the scope of this appendix. However, it is interesting to note that the horizontal fluctuations in the karst beneath the centre of the rim are about half the maximum value at the flank of the atoll. Given the uncertainties in all hydrogeological parameters, it is sufficient to say that tidal forcing appears to result in significant displacement of groundwater at the frequency of the twice daily tides. This effect is likely to occur even when superimposed on the steady flow due to thermohaline convection and, thus, to generate intense mixing in the carbonates of the atolls.

Appendix V

EFFECTIVE DISPERSION IN A PERIODIC FLOW FIELD

V.1 Basic Equations

Consider a homogeneous one-dimensional infinite domain ($-\infty < x < \infty$) and the system of equations describing periodic advection, reversible first-order sorption and first-order decay

$$\frac{\partial c}{\partial t} = -v(t)\frac{\partial c}{\partial x} - \alpha f - \lambda c \tag{V.1}$$

$$\frac{\partial s}{\partial t} = f - \lambda s \tag{V.2}$$

$$f = r\,(c - s) \tag{V.3}$$

where c is a solute concentration, s is the "sorbed concentration", f is the rate of solute exchange between the sorbing and fluid phases, $v(t) = V_o \cos(2\pi t/T)$ is the oscillating velocity with amplitude V_o and period T, λ is a decay constant, α is the volumetric ratio of sorbing to fluid fractions in a porous medium, and r is a reversible exchange coefficient.

A similar system of equations was analysed by Okubo (1973), in an attempt to predict mixing in tidal estuaries. However, Okubo's solution is inconsistent with the assumptions. The solution presented below is therefore an improvement on his results.

The above system of equations can be manipulated and simplified to a single differential equation in terms of c. Substituting (V.3) into (V.2) yields

$$\frac{\partial s}{\partial t} = r\,c - (r + \lambda)\,s \tag{V.4}$$

which gives, after integration,

$$s = r\,e^{-(r+\lambda)t}\int_0^t e^{(r+\lambda)u}\,c\,du + s(x,0)\,e^{-(r+\lambda)t} \tag{V.5}$$

Differentiating (V.5) with respect to time and substituting into equation (V.2) gives

$$f = r\,c - r^2\,e^{-(r+\lambda)t}\int_0^t e^{(r+\lambda)u}\,c\,du - r\,s(x,0)\,e^{-(r+\lambda)t} \tag{V.6}$$

Equation (V.1), describing transport in the fluid phase, then becomes

$$\frac{\partial c}{\partial t} + \alpha\,r\,c - \alpha\,r^2\,e^{-(r+\lambda)t}\int_0^t e^{(r+\lambda)u}\,c\,du - \alpha\,r\,s(x,0)\,e^{-(r+\lambda)t} = -v(t)\,\frac{\partial c}{\partial x} - \lambda c \tag{V.7}$$

Note that the terms involving λ in the left-hand side of (V.7) account for the decay of the sorbed fraction.

Multiplying (V.7) by $e^{(r+\lambda)t}$, differentiating with respect to time and simplifying by $e^{(r+\lambda)t}/(r+\lambda)$, results in

$$\begin{aligned}\left(\frac{1}{r+\lambda}\right)\frac{\partial^2 c}{\partial t^2} + \left(1+\frac{\alpha r+\lambda}{r+\lambda}\right)\frac{\partial c}{\partial t} + \lambda\,\left(1+\frac{\alpha r}{r+\lambda}\right)c \quad = \\ -\left(v + \frac{1}{r+\lambda}\,\frac{\partial v}{\partial t}\right)\frac{\partial c}{\partial x} - \left(\frac{v}{r+\lambda}\right)\frac{\partial}{\partial t}\left(\frac{\partial c}{\partial x}\right)\end{aligned} \tag{V.8}$$

which is the equation that will be considered for moment analysis.

V.2 Moment Analysis

Analysis of the zeroth, first and second moments of the function $c(x,t)$ is presented below. Without loss of generality, c is standardised by its initial integral (mass in the fluid phase), and $s(x,0) = c(x,0)$ (initial saturation of the sorbing phase) is assumed to be symmetric around $x = 0$ with initial variance $\sigma_o^2/2$. Furthermore, the function $c(x,t)$ and its space derivatives are assumed to vanish at $x = \pm\infty$.

The ith moments of $c(x,t)$ are defined as

$$M_i(t) = \int_{-\infty}^{\infty} x^i\,c(x,t)\,dx \tag{V.9}$$

M_o is the mass in the fluid phase, M_1 is the average coordinate of the centre of mass, and $M_2 - M_1^2$ is the variance of the solute distribution around its centre of mass.

V.2.1 Zeroth Moment

Applying (V.9) to (V.8) gives the differential equation for M_o:

$$\left(\frac{1}{r+\lambda}\right)\frac{\partial^2 M_o}{\partial t^2} + \left(1+\frac{\alpha r+\lambda}{r+\lambda}\right)\frac{\partial M_o}{\partial t} + \lambda\,\left(1+\frac{\alpha r}{r+\lambda}\right)M_o = 0 \tag{V.10}$$

Given initial equilibrium between the fluid and sorbing phases, this equation can be solved for the conditions $M_o(0) = 1$ and $\partial M_o/\partial t(0) = -\lambda$. The solution is $M_o(t) = e^{-\lambda t}$, which does not depend on the sorption parameters α and r.

V.2.2 First Moment

In a similar manner, the first moment is obtained as the solution of

$$\left(\frac{1}{r+\lambda}\right)\frac{\partial^2 M_1}{\partial t^2}+\left(1+\frac{\alpha r+\lambda}{r+\lambda}\right)\frac{\partial M_1}{\partial t}+\lambda\left(1+\frac{\alpha r}{r+\lambda}\right)M_1 = -\left(v+\frac{1}{r+\lambda}\frac{\partial v}{\partial t}\right)M_o-\left(\frac{v}{r+\lambda}\right)\frac{\partial M_o}{\partial t} \tag{V.11}$$

with conditions $M_1(0) = 0$ and $\partial M_1/\partial t(0) = V_o$. The latter is obtained by evaluating the first moment of (V.7) at $t = 0$.

The solution $M_1(t)$ cannot be given here because of its size. However, after an integer number of periods $t = nT$, the first moment is

$$M_1(nT) = \frac{V_o T\alpha\left(1-e^{-nTr(1+\alpha)}\right)e^{-nT\lambda}}{Tr\,(1+\alpha)^2+\frac{4\pi^2}{Tr}} \tag{V.12}$$

The above equation indicates that the centre of mass is shifted in the direction given by the sign of the flow velocity at $t = 0$. When decay is present, this shift is only temporary. For parameter values compatible with groundwater dynamics, the maximum shift should generally be less than 1 m.

V.2.3 Second Moment

The second moment is obtained as the solution of

$$\left(\frac{1}{r+\lambda}\right)\frac{\partial^2 M_2}{\partial t^2}+\left(1+\frac{\alpha r+\lambda}{r+\lambda}\right)\frac{\partial M_2}{\partial t}+\lambda\left(1+\frac{\alpha r}{r+\lambda}\right)M_2 = 2\left(v+\frac{1}{r+\lambda}\frac{\partial v}{\partial t}\right)M_1+\left(\frac{2v}{r+\lambda}\right)\frac{\partial M_1}{\partial t} \tag{V.13}$$

with $M_2(0) = \sigma_o^2/2$ and $\partial M_2/\partial t(0) = -\lambda\sigma_o^2/2$. The latter condition is also readily obtained by the evaluation of the second moment of (V.7) at $t = 0$. Again, the solution $M_2(t)$ is too complex to be given here; however, for $t = nT$, it simplifies to

$$M_2(nT) = \left\{ \frac{\sigma_o^2}{2} + \frac{nV_o^2\,T^2\alpha}{Tr\,(1+\alpha)^3 + \frac{4\pi^2}{Tr}\,(1+\alpha)} \right.$$
$$\left. + \left[\frac{2V_o^2\,T^2\alpha\,(1-\alpha)}{T^2r^2\,(1+\alpha)^4 + 16\pi^2\,(1+\alpha)^2} + \frac{2V_o^2\,T^2\alpha}{\left(Tr\,(1+\alpha)^2 + \frac{4\pi^2}{Tr}\right)^2} \right] (e^{-nTr(1+\alpha)} - 1) \right\} e^{-nT\lambda} \tag{V.14}$$

and the variance of the function $c(x,t)$ at $t = nT$ is given by

$$\sigma^2(nT) = M_2(nT) - M_1^2(nT) \tag{V.15}$$

Equation (V.14) indicates that the presence of decay makes the variance tend to zero as time tends to infinity. Without decay, the variance would asymptotically increase linearly with time.

V.3 Diffusive Analytical Model

Time-discontinuous solutions of (V.7) can possibly be approached by an alternative model equation. To be useful and accurate, this equation must allow for analytical solutions and provide the same moments at $t = nT$. The parameters of the equation should also not depend on the initial condition.

Given the periodicity of the flow and since the temporal shift of the first moment is not only very small but somewhat arbitrary as well (initial direction of the periodic velocity), M_1 will be assumed to be zero and only the moments M_o (mass in the system) and M_2 (variance) will be considered.

It has been found that the above conditions are all satisfied with the diffusive equation

$$\frac{\partial c}{\partial t} = D(t)\,\frac{\partial^2 c}{\partial x^2} - \lambda c \tag{V.16}$$

involving decay and a time-dependent equivalent diffusion (or "dispersion") coefficient. In effect, moment analysis of this equation yields $M_o(t) = e^{-\lambda t}$, $M_1(t) = 0$ and

$$M_2(t) = \sigma^2(t) = \left(2\int_0^t D(u)\,du + \frac{\sigma_0^2}{2} \right) e^{-\lambda t} \tag{V.17}$$

which is fully compatible with the second moment given in (V.14).

Equating (V.17) with the full, sinusoidal, time-continuous version of the second-moment equation (V.14) (i.e. $M_2(t)$, not $M_2(nT)$) leads, after time differentiation, to the continuous function $D(t)$. However, this step is not necessary, since the discontinuous solutions of interest require the integral of $D(t)$ over a given number of periods. In

effect, for unit Gaussian or "step" initial distributions around $x = 0$, analytical solutions of (V.16) at elapsed times $t = nT$ have the forms

$$c(x, nT) = e^{-nT\lambda} \frac{\sigma_0}{\sqrt{\sigma_0^2 + 4\int_0^{nT} D(u)\,du}} e^{-\left(\frac{x^2}{\sigma_0^2 + 4\int_0^{nT} D(u)\,du}\right)} \tag{V.18}$$

where the initial variance per unit mass in the system is $\sigma_o^2/2$, and

$$c(x, nT) = \frac{e^{-nT\lambda}}{2}\left[\operatorname{erf}\left(\frac{a - x}{2\sqrt{\int_0^{nT} D(u)\,du}}\right) + \operatorname{erf}\left(\frac{a + x}{2\sqrt{\int_0^{nT} D(u)\,du}}\right)\right] \tag{V.19}$$

where a is the half-length of the step distribution around the origin (in this case, the initial variance per unit mass $\sigma_o^2/2$ is $a^2/3$).

Consequently, analytical solutions at $t = nT$ can be obtained by direct substitution in (V.18) or (V.19) of the quantity

$$\int_0^{nT} D(u)\,du = \frac{nV_0^2T^2\alpha}{2\left[Tr\,(1+\alpha)^3 + \frac{4\pi^2}{Tr}(1+\alpha)\right]} + \left\{\frac{V_0^2T^2\alpha\,(1-\alpha)}{T^2r^2\,(1+\alpha)^4 + 16\pi^2\,(1+\alpha)^2} + \frac{V_0^2T^2\alpha}{\left[Tr\,(1+\alpha)^2 + \frac{4\pi^2}{Tr}\right]^2}\right\}\left[e^{-nTr(1+\alpha)} - 1\right] \tag{V.20}$$

obtained from the comparison of (V.17) and (V.14) at $t = nT$. Here, the contribution of the first moment in (V.15) has been neglected ($M_1(nT) \approx 0$, always very small), but it could easily be taken into account if a more accurate evaluation were required.

The second term in (V.20) becomes rapidly constant, while the first one gains an order of magnitude after every ten periods. Examination of (V.20) reveals that if the equivalent transient diffusion introduced in (V.16) were of the alternative form

$$D(t) = D_o + K_o\,e^{-r(1+\alpha)t} \tag{V.21}$$

with

$$D_o = \frac{V_o^2\,T\,\alpha}{2\left[T\,r\,(1+\alpha)^3 + \frac{4\pi^2}{Tr}(1+\alpha)\right]} \tag{V.22}$$

and

$$K_o = -r\,(1+\alpha)\left[\frac{V_o^2\,T^2\,\alpha\,(1-\alpha)}{T^2r^2\,(1+\alpha)^4+16\,\pi^2\,(1+\alpha)^2}+\frac{V_o^2\,T^2\,\alpha}{\left(Tr\,(1+\alpha)^2+\frac{4\pi^2}{Tr}\right)^2}\right] \tag{V.23}$$

it would yield the same integral quantity at $t = nT$ as in (V.20). Therefore, the equivalent diffusion induced by the process of periodic sorption/desorption can be expressed with the above steady and transient components. When reasonable hydrological parameters are enforced, the latter vanishes rapidly. Discontinuous solutions of excellent accuracy are obtained with the linear diffusion model upon substitution of

$$\int_0^{nT} D(u)\,du = D_o\,nT \tag{V.24}$$

in (V.18) or (V.19).

Note, finally, that the equivalent diffusion function (V.21) is not affected by decay and that its steady part, D_o, has a maximum value for selected sorption parameters α and r. Simultaneous solution of the zeros of $\partial D_0/\partial r$ and $\partial D_0/\partial\alpha$ yields $\alpha = 1$ and $r = \pi/T$ — in which case, the maximum is

$$D_o^{\max} = \frac{V_o^2 T}{32\pi} \tag{V.25}$$

Moreover, the equivalent diffusion tends to zero when α and r tend to zero, and it also tends to zero when r tends to infinity. In this latter case, sorption is instantaneous, and the initial condition is simply submitted to periodic advection about the origin with an apparent oscillating velocity retarded by the factor $(1 + a)$.

V.4 Remarks

When physical diffusion is present in the system, the same procedure may be carried out. In such a case, the right-hand side of (V.1) and (V.7) is complemented by the term $d\partial^2 c/\partial x^2$, where d is the coefficient of molecular diffusion.

Consequently, the right-hand side of (V.8) includes the additional terms

$$d\,\frac{\partial^2 c}{\partial x^2}+\frac{d}{r+\lambda}\frac{\partial}{\partial t}\left(\frac{\partial^2 c}{\partial x^2}\right) \tag{V.26}$$

which affect only the second moment equation.

In effect, (V.10) and (V.11) and their initial conditions remain the same, while (V.13) becomes

$$\left(\frac{1}{r+\lambda}\right)\frac{\partial^2 M_2}{\partial t^2}+\left(1+\frac{\alpha r+\lambda}{r+\lambda}\right)\frac{\partial M_2}{\partial t}+\lambda\left(1+\frac{\alpha r}{r+\lambda}\right)M_2$$
$$= 2d\,M_o+\left(\frac{2d}{r+\lambda}\right)\frac{\partial M_o}{\partial t}+2\left[v+\frac{1}{r+\lambda}\frac{\partial v}{\partial t}\right]M_1+\left(\frac{2v}{r+\lambda}\right)\frac{\partial M_1}{\partial t} \tag{V.27}$$

with the initial conditions $M_2(0)=\sigma_o^2/2$ and $\partial M_2/\partial t\,(0)=2d-\lambda\sigma_o^2/2$.

Integration of (V.27) yields, at $t=nT$, a second moment similar to (V.14) but complemented by the addition of

$$\left(\frac{2ndT}{1+\alpha}-\frac{2\alpha d}{r\,(1+\alpha)^2}\,(e^{-nTr(1+\alpha)}-1)\right)e^{-nT\lambda} \tag{V.28}$$

The analogy based on the diffusion equation (V.21) involving decay and transient equivalent diffusion then results in the coefficients

$$D_o=\frac{V_o^2 T\,\alpha}{2\left[Tr\,(1+\alpha)^3+\frac{4\pi^2}{Tr}\,(1+\alpha)\right]}+\frac{d}{1+\alpha} \tag{V.29}$$

and

$$K_o=-r\,(1+\alpha)\left\{\frac{V_o^2 T^2\alpha\,(1-\alpha)}{T^2r^2\,(1+\alpha)^4+16\,\pi^2\,(1+\alpha)^2}+\frac{V_o^2 T^2\alpha}{\left[Tr\,(1+\alpha)^2+\frac{4\pi^2}{Tr}\right]^2}\right\}+\frac{\alpha d}{1+\alpha} \tag{V.30}$$

Molecular diffusion thus affects both the steady and transient parts of the equivalent diffusion (dispersion) by the addition of a very simple contribution. In the steady component, D_o, this contribution is, logically, the original diffusion retarded by the factor $(1+\alpha)$.

V.5 Numerical Verification

These theoretical results have been verified using a finite-element numerical model simulating periodic advection with first-order sorption kinetics and decay. Comparison of the linear-analytical results with numerical results at regular intervals nT are excellent at all times past ten periods. These results are valid for both initial Gaussian and "step" distributions (analytical solutions (V.18) and (V.19)), confirming that the equivalent diffusion does not depend on the initial condition but is solely a function of the retarded physical diffusion, periodic velocity and sorption parameters.

DIRCEN/CEA REFERENCES

References for the papers cited as DIRCEN/CEA documents Nos. 1–12 in the IGC are given below. These documents can be obtained from

La Documentation Française
29, quai Voltaire
75344 Paris
Cedex 07
France

DIRCEN/CEA, Document No. 1

Direction des Centres d'Expérimentations Nucléaires/Commissariat à l'Energie Atomique. "Lagoon Sediment Radioactivity in Mururoa and Fangataufa," in ***Geomechanical and Radiological Impact of Nuclear Tests at Mururoa and Fangataufa.*** Paris: La Documentation Française, 1998.

DIRCEN/CEA, Document No. 2

Direction des Centres d'Expérimentations Nucléaires/Commissariat à l'Energie Atomique. "Soil Radioactivity in Mururoa and Fangataufa," in ***Geomechanical and Radiological Impact of Nuclear Tests at Mururoa and Fangataufa.*** Paris: La Documentation Française, 1998.

DIRCEN/CEA, Document No. 3

Direction des Centres d'Expérimentations Nucléaires/Commissariat à l'Energie Atomique. "Environmental Monitoring in French Polynesia and on the Mururoa and Fangataufa Sites, Year 1994," in ***Geomechanical and Radiological Impact of Nuclear Tests at Mururoa and Fangataufa.*** Paris: La Documentation Française, 1998.

DIRCEN/CEA, Document No. 4

Direction des Centres d'Expérimentations Nucléaires/Commissariat à l'Energie Atomique. "Medium- and Long-Term Containment of Underground Nuclear Tests

at the CEP: Source Term Inventory and Worst-Case Impact Assessment," in ***Geomechanical and Radiological Impact of Nuclear Tests at Mururoa and Fangataufa.*** Paris: La Documentation Française, 1998.

DIRCEN/CEA, Document No. 5
Direction des Centres d'Expérimentations Nucléaires/Commissariat à l'Energie Atomique. "The Geological, Mechanical and Hydrogeological Environment of the Underground Nuclear Tests at Mururoa and Fangataufa," in ***Geomechanical and Radiological Impact of Nuclear Tests at Mururoa and Fangataufa.*** Paris: La Documentation Française, 1998.

DIRCEN/CEA, Document No. 6
Direction des Centres d'Expérimentations Nucléaires/Commissariat à l'Energie Atomique. "Overall Distribution and Characteristics of the Underground Nuclear Test Carried Out at Mururoa and Fangataufa and Their Effects on the Surrounding Media," in ***Geomechanical and Radiological Impact of Nuclear Tests at Mururoa and Fangataufa.*** Paris: La Documentation Française, 1998.

DIRCEN/CEA, Document No. 7
Direction des Centres d'Expérimentations Nucléaires/Commissariat à l'Energie Atomique. "Structural Integrity and Stability of the Atolls; Data and Modelling," in ***Geomechanical and Radiological Impact of Nuclear Tests at Mururoa and Fangataufa.*** Paris: La Documentation Française, 1998.

DIRCEN/CEA, Document No. 8
Direction des Centres d'Expérimentations Nucléaires/Commissariat à l'Energie Atomique. "Experimental Data on the Mobility of the Radionuclides Deposited By the Underground Tests at Mururoa and Fangataufa - Chapters 1 (Dissolution of Lava Formed by the Underground Tests), 2 (Retention of Radioelements Deposited by Underground Tests) and 3 (Mobility of Products Deposited by the Underground Safety Tests)," in ***Geomechanical and Radiological Impact of Nuclear Tests at Mururoa and Fangataufa.*** Paris: La Documentation Française, 1998.

DIRCEN/CEA, Document No. 9
Direction des Centres d'Expérimentations Nucléaires/Commissariat à l'Energie Atomique. "Current Underground Distribution of Radionuclides at Mururoa and Fangataufa," in ***Geomechanical and Radiological Impact of Nuclear Tests at Mururoa and Fangataufa.*** Paris: La Documentation Française, 1998.

DIRCEN/CEA, Document No. 10
Direction des Centres d'Expérimentations Nucléaires/Commissariat à l'Energie Atomique. "Fangataufa: Overall Assessment of the Short, Medium and Long

Term Radiological Situation of the Atolls of Mururoa and Fangataufa," in ***Geomechanical and Radiological Impact of Nuclear Tests at Mururoa and Fangataufa.*** Paris: La Documentation Française, 1998.

DIRCEN/CEA, Document No. 11
Direction des Centres d'Expérimentations Nucléaires/Commissariat à l'Energie Atomique. "Marine Data and Modelling," in ***Geomechanical and Radiological Impact of Nuclear Tests at Mururoa and Fangataufa.*** Paris: La Documentation Française, 1998.

DIRCEN/CEA, Document No. 12
Direction des Centres d'Expérimentations Nucléaires/Commissariat à l'Energie Atomique. "Guide de Surveillance Géomécanique des Atolls de Mururoa et Fangataufa," in ***Geomechanical and Radiological Impact of Nuclear Tests at Mururoa and Fangataufa.*** Paris: La Documentation Française, 1998.

DIRCEN/CEA Books — French Version *

Bouchez, Jacques, and Raphael Lecomte. (1995) ***Les Atolls de Mururoa et de Fangataufa (Polynésie Française),*** II. Les Expérimentations Nucléaires: Effets mécaniques. lumino-thermiques, électromagnétiques. Paris: Masson.

Guille, G., G. Goutière, J. F. Sornein, D. Buigues, A. Gachon and C. Guy. (1996) ***Les Atolls de Mururoa et de Fangataufa (Polynésie Française),*** I. Géologie - Pétrologie - Hydrogéologie: Edification et évolution des édifices. Paris: Masson.

* DIRCEN/CEA also made available to the IGC an official English translation of Guille et al. (1996) and a draft translation of the underground testing sections of of Bouchez and Lecomte (1996). References in the ICG report to page numbers and figures in these books refer to the English versions of both volumes; an official English translation of Bouchez and Lecomte (1996) is in preparation. Chapters 1–9 in the draft English version (referenced in the IGC report) correspond to Chapters 8–16 in the (official) French version of Bouchez and Lecomte (1996).

BIBLIOGRAPHY

Alldredge, L. R., F. Keller and W. J. Dichtel (1954) Magnetic structure of Bikini atoll. Tech. Rep. Professional Paper 270-L, U.S. Geological Survey.

Arthur, L. J., C. M. Wagner and B. Hein (1997) Lesotho Highlands Water Project — Design of the 'Muela hydropower station. *Civil Eng.*, **120**(Special Issue 1), 43–53.

Bakirov, A. A. and E. A. Bakirov (editors) (1981) Applications of Underground Nuclear Explosions in Oil Recovery (in Russian). Moscow: Nedra.

Barrillot, B. (1996) Les Essais Nucléaires Française 1960-1996: Conséquences sur L'environment et la Santé. Lyon, France: Centre de Documentation et de Recherche sur la Paix et les Conflits.

Barton, N. (1976) The shear strength of rock and rock joints. *Int. J. Rock Mech. Min. Sci. & Geomech. Abstr.*, **13**(9), 255–279.

Bataille, C. (1997) Rapport sur l'évolution de la recherche sur la gestion des déchets nucléaires à haute activité. Tech. Rep. 541, Sénat no. 179, Office Parlementaire d'Évaluation des choix Scientifiques et Technologiques, Paris.

Bear, J. (1972) Dynamics of Fluids in Porous Media. New York: American Elsevier.

Bejan, A. (1995) Convection Heat Transfer. New York: John Wiley & Sons, Inc., 2nd edn.

Bérest, P., J. Bergues, B. Brouard, G. Durup and B. Guerber (1996) A tentative evaluation of the M.I.T. *Solution Mining Research Institute*, (Spring Meeting, Houston).

Bielenstein, H. U. and K. Barron (1972) In situ stresses. In *Proceedings of the 7th Canadian Rock Mechanics Symposium (Edmonton)*, pp. 3–14, Ottawa: Dept. of Energy, Minerals and Resources.

Bieniawski, Z. T. (1976) Rock mass classification in rock engineering. In Z. T. Bieniawski (editor), *Proceedings of the Symposium on Exploration for Rock Engineering (Johannesburg)*, pp. 97–106, Rotterdam: A. A. Balkema.

Birch, F., J. F. Schairer and H. C. Spicer (editors) (1942) Handbook of Physical Constants. New York: Geological Society of America, Special Papers No. 36.

Bouchez, J., Y. Caristan and C. Mariotti (1997) Stabilité des pentes sous-marines de l'atoll de Mururoa sous sollicitations dynamiques. *Revue Française Géotechnique*, **78**, 3–13.

Bouchez, J. and R. Lecomte (1996) The Atolls of Mururoa and Fangataufa (French Polynesia). II. Nuclear Testing, Mechanical Lumino-Thermal and Electromagnetic Effects (in Collaboration with J. Brugies, C. Guerrini, J.-F. Sornein, J.-L. Plantet and E. Blanc). Monaco: Musée Océanographique.

Bovt, A. N. and V. N. Nikolaevskiy (1981) Dilatancy and mechanics of underground explosion (in Russian). *Itogi nauki i techniki, Ser. Mech. def. tv. tela*, **14**, 129–169.

Brace, W. F. (1980) Permeability of crystalline and argillaceous rocks. *Int. J. Rock Mech. Min. Sci. & Geomech. Abstr.*, **17**(5), 241–251.

Brady, B. and E. T. Brown (1993) Rock Mechanics for Underground Mining. London: Chapman & Hall, 2nd edn.

Bredehoeft, J. D. and I. S. Papadopulos (1965) Rates of vertical groundwater movement estimated from the Earth's thermal profile. *Water Resources Res.*, **1**(2), 325–328.

Brenner, H. and D. A. Edwards (1993) Macrotransport Processes. Stoneham, Mass.: Butterworth-Heinemann.

Brikowski, T. H. (1991) Estimation of hydrologic transport of radionuclides from below water table tests using analytic models. Tech. Rep. CONF-9109114, Lawrence Livermore Laboratories.

Brikowski, T. H. (1993a) Estimating movement of groundwater from a pond or large-radius conduit. *Ground Water*, **31**(3), 393–400.

Brikowski, T. H. (1993b) Flow between aquifers through filled cylindrical conduits: Analytic solution and application to underground nuclear testing sites. *J. Hydrology*, **20**(8), 115–130.

Brown, E. T. (editor) (1981) Rock Characterisation, Testing and Monitoring - ISRM Suggested Methods. Oxford: Pergamon Press.

Brown, E. T. and C. R. Windsor (1990) Near surface in situ stresses in Australia and their influence on underground construction. In *Proceedings of the 7th Australian Tunnelling Conference (Sydney)*, pp. 18–48, Canberra: The Institution of Engineers, Australia.

Brown, E. T. and H. S. Yu (1988) A model for the ductile yield of porous rock. *Int. J. Rock Mech. Min. Sci. & Geomech. Abstr.*, **12**(6), 679–688.

Buigues, D. (1982) Sédimentation et Diagenèse des Formations Carbonatées de L'atoll de Mururoa (Polynesie Française), Thèse 3^e Cycle. Master's thesis, Université de Paris XI.

Buigues, D. (1985) Principaux Facies et Leur Répartition Dans L'Atoll de Mururoa, vol. 3, pp. 249–255. Moorea, French Polynesia: Antenne Museum - EPHE.

Buigues, D. (1996) Mururoa and Fangataufa: Sea-level changes, karstification and the atoll morphology. *Mém Géol. France*, **169**, 373–382.

Buigues, D. (1997) Geology and hydrogeology of Mururoa and Fangataufa, French Polynesia. In H. L. Vacher and T. M. Quinn (editors), *Geology and Hydrogeology of Carbonate Islands*, vol. 1, chap. 13, pp. 433–451, Amsterdam: Elsevier.

Buigues, D., A. Gachon and G. Guille (1992) L'atoll de Mururoa (Polynésie Française), I. Structure et évolution géologique. *Mém. Soc. Géol. France*, **163**(5), 645–657.

Burdick, L. J., T. Lay, D. V. Helmberger and D. G. Harkrider (1983) Implications of records from the spall zone of the Amchitka tests to nonlinear losses in the source region and to elastic radiation by spall. Tech. Rep. / Annual Technical Report to ARPA, WCCP-R-84-03, Woodward-Clyde Consultants.

Butkovich, T. R. (1965) Calculation of the shock wave from an underground nuclear explosion in granite. *J. Geophys. Res.*, **70**(4), 885–892.

Butkovich, T. R. (1971) Influence of water in rocks on effects of underground nuclear explosions. *J. Geophys. Res.*, **76**(8), 1993–2011.

Butkovich, T. R. and A. E. Lewis (1973) Aids for estimating effects of unerground nuclear explosions. Tech. Rep. UCRL-50929 Rev. 1, Lawrence Livermore Laboratory, Livermore, California.

Caristan, Y. (1997) Personal communication.

Chabai, A. J. (1963) Synthesis of shock Hugoniots for rock materials. In C. Fairhurst (editor), *Rock Mechanics (Proceedings of the 5th Symposium, University of Minnesota, May 1962)*, pp. 347–366, Pergamon Press, Oxford.

Chauveau, J. C., F. Deneufborg and J. A. Sarcia (1967) Observations sur l'infrastructure de l'atoll de Mururoa (archipel des Tuamotu), Pacific sud. *Comptes rendus de l'Académie des Sciences de Paris, Série D*, **265**, 1113–1116.

Cherry, J. T. (1967) Computer calculations of explosion-produced craters. *Int. J. Rock Mech. Min. Sci. & Geomech. Abstr.*, **4**(1), 1–22.

Cherry, J. T., D. B. Larson and E. G. Rapp (1968) A unique description of the failure of a brittle material. *Int. J. Rock Mech. Min. Sci. & Geomech. Abstr.*, **5**, 455–463.

Chevalier, J.-P., M. Denizot, J.-L. Mougin, Y. Plessis and B. Salvat (1968) Etude géomorphologique et bionomique de l'atoll de Mururoa. *Cahiers du Pacifique*, **12**, 1–144.

Churchhill, R. V., J. W. Brown and R. F. Verhey (1976) Variables and Applications. New York: McGraw-Hill, 3rd edn.

Claassen, H. C. (1978) Hydrologic processes and radionuclide distribution in a cavity and chimney produced by the Cannikin nuclear explosion, Amchitka Island, Alaska, U.S. Tech. Rep. Professional Paper 712-D, U.S. Geological Survey.

Colin, P. L., D. M. Devaney, L. Hillis-Colinvaux, T. H. Suchanek and J. T. Harrison (1986) Geology and biological zonation of the reef slopes, 50-360 m depth at Eniwetok Atoll, Marshall Islands. *Bull. Marine Sci.*, **38**(1), 111–128.

Collins, I. F. and J. R. Stimpson (1994) Similarity solutions for drained and undrained cavity expansions in soils. *Géotechnique*, **44**(1), 21–34.

CRII-RAD (1995) Essais nucléaires (revue d'information de la CRII-RAD). Tech. Rep. 3, Commission de Recherche et d'Information sur la Radioactivité, Valence, France.

Damjanac, B. (1996) Numerical simulation of the near-field response of a rock mass to an underground nuclear explosion. Tech. Rep. International Geomechanical Commission, Itasca Consulting Group.

Darwin, C. R. (1842) The Structure and Distribution of Coral Reefs. London: Smith, Elder & Co.

Davies, P. J. (1983) Structural integrity and hydrology of Mururoa Atoll. In *Report of a New Zealand, Australian and Papua New Guinea Scientific Mission to Mururoa Atoll*, pp. 77–119, Wellington: New Zealand Ministry of Foreign Affairs.

de Marsily, G. (1986) Quantitative Hydrogeology, Groundwater Hydrology for Engineers. New York: Academic Press.

Deleersnijder, A. and B. Tartinville (1997) A simple model of the tracer flux from the Mururoa lagoon to the Pacific. *Appl. Math. Lett.*, **10**(5), 13–17.

Denbigh, K. G. and J. Turner (1971) Chemical Reactor Theory. Cambridge: Cambridge University Press.

Deneufbourg, F. (1967) Les forages de Mururoa. *Cahiers du Pacifique*, **13**, 47–58.

Diersch, H. J. (1996) Interactive, graphics-based finite-element simulation system FEFLOW for modeling groundwater flow, contaminant mass and heat transport processes. Tech. Rep. WASY Ltd., Berlin.

DIRCEN/CEA (1998a) Overall Assessment of the Short, Medium and Long Term Radiological Situation of the Atolls of Mururoa and Fangataufa. No. Document No. 10, Paris: La Documentation Française.

DIRCEN/CEA (1998b) Overall Distribution and Characteristics of the Underground Nuclear Tests Carried Out at Mururoa and Fangataufa and Their Effects on the Surrounding Media. No. Document No. 6, Paris: La Documentation Française.

DIRCEN/CEA (1998c) Structural Integrity and Stability of the Atolls; Data and Modelling. No. Document No. 7, Paris: La Documentation Française.

Dobrin, M. B. and B. Perkins (1954) Seismic studies of Bikini Atoll. Tech. Rep. Professional Paper 260-J, pp. 487-505, U.S. Geology Survey.

Dott, R. H. (1963) Dynamics of subaqueous gravity depositional processes. *Bull. Am. Assoc. Pet. Geologists*, **47**, 104–128.

Drescher, A. (1991) Analytical Methods in Bin-Load Analysis. Elsevier, Amsterdam.

Dudoignon, P., C. Destrigneville, A. Gachon, D. Buigues and B. Ledesert (1992) Mécanismes des altérations hydrothermales associées aux formations volcaniques de l'atoll de Mururoa. *Comptes Rendus de l'Académie des Sciences de Paris*, **314**(II), 1043–1049.

Dudoignon, P., A. Meunier, D. Beaufort, A. Gachon and D. Buigues (1989) Hydrothermal alternation at Mururoa Atoll (French Polynesia). *Chem. Geol.*, **76**, 385–401.

Duncan, R. A. and I. McDougall (1976) Linear volcanism in French Polynesia. *J. Volcanology & Geothermal Res.*, **1**, 197–227.

Durham, W. B. (1981) Direct observation of explosively induced damage in sandstone with application to reservoir stimulation. *Scanning Electron Microscopy*, **1**(1981/1), 583–594.

Ecole des Mines de Paris (1985) Détermination expérimentale de la vitesse d'écoulement de la nappe géothermique du dogger en région parisienne

(rapport final). Tech. Rep. 1985-RD/43, ARMINES, Centre d'Informatique Géologique Fontainebleau.

Emery, K. O., J. I. Tracey and H. S. Ladd (1954) Geology of Bikini and nearby atolls. Tech. Rep. Professional Paper 260-A, U.S. Geological Survey.

Ferris, F. G. (1951) Cyclic fluctuations of water level as a basis for determining aquifer transmissibility.

Fetter, Jr., C. W. (1972) Position of the saline interface beneath oceanic islands. *Water Resources Res.*, **8**, 1307–1314.

Fondation Cousteau, Paris (1988) Mission scientifique de la Calypso sur le site d'expérimentations nucléaires de Mururoa. Technical Report.

Garnett, H. M. (1998) 'Ciguatera'. Presented at the International Conference on the Radiological Situation at the Atolls of Mururoa and Fangataufa (Vienna, 30 June – 3 July, 1998).

Gillot, P. Y., Y. Cornette and G. Guille (1992) Age (K-Ar) et conditions d'édification du soubassement volcanique de l'atoll de Mururoa (Pacifique Sud). *C.R. Acad. Sci. Paris*, **314**(Série II), 393–399.

Glass, I. I. (1974) Shock waves and man. Technical Report, University of Toronto, Institute of Aerospace Studies.

Goblet, P. (1981) Modélisation des transferts de masse et d'énergie en aquifère. Ph.D. thesis, University of Paris VI, Paris School of Mines.

Goguel, J. (1982) L'évolution du cadre naturel. In *Rapport D'Haroun Tazieff*, no. Annex 2.

Goode, D. J. (1996) Direct simulation of groundwater age. *Water Resources Res.*, **32**(2), 289–296.

Grammer, G. M. and R. N. Ginsberg (1992) Highstand versus lowstand deposition on carbonate platform margins: Insight from Quaternary foreslopes in the Bahamas. *J. Marine Geol.*, **103**, 125–136.

Guille, G., G. Goutière, J. F. Sornein, D. Buigues, A. Gachon and C. Guy (1996) The Atolls of Mururoa and Fangataufa (French Polynesia). I. Geology - Petrology - Hydrogeology, from Volcano to Atoll (translated by M.S.N. Carpenter). Monaco: Musée Océanographique.

Guillou, H., R. Brousse, P. Y. Gillot and G. Guille (1993) Geological reconstruction of Fangataufa Atoll, South Pacific. *J. Marine Geol.*, **110**, 337–391.

Guillou, H., G. Guille, R. Brousse and J. M. Bardintzeff (1990) Evolution de basaltes tholéiitiques vers des basaltes alcalins dans le substratum volcanique

de Fangataufa (Polynésie Française). *Bull. Soc. Géol. France*, **8**(VI/3), 537–549.

Guy, C., J. Schott, C. Destrigneville and R. Chiappini (1992) Low-temperature alteration of basalt by interstitial seawater, Mururoa, French Polynesia. *Geochemica et Cosmochimica Acta*, **56**(12), 4169–4189.

Guyomard, T. (1990) Sédimentation et Diagénèse Du Sondage Echo II de L'atoll de Fangataufa (Polynésie Française); Correlations Avec Mururoa. Mémoire DEA, Université de Paris XI.

Henry, H. R. (1964) Interfaces Between Salt Water and Fresh Water in Coastal Aquifers. Water Supply Paper, U.S. Geological Survey.

Henry, P., C. Guy, R. Cattin, P. Dudoignon, J.-F. Sornein and Y. Caristan (1996) A convective model of water flow in Mururoa basalts. *Geochemica et Cosmochimica Acta*, **60**(12), 2087–2109.

Hill, R. (1950) The Mathematical Theory of Plasticity. The Oxford Engineering Science Series, New York: Oxford University Press.

Hochstein, M. P. and M. J. O'Sullivan (1985) Geothermal systems created by underground nuclear testing. In *Proceedings of the 7th New Zealand Geothermal Workshop (University of Auckland, New Zealand, November 1985)*, pp. 149–154, Auckland: University of Auckland, Geothermal Institute.

Hochstein, M. P. and M. J. O'Sullivan (1988) Geothermal systems created by underground nuclear testing. In *International Scientific Symposium on a Nuclear Test Ban (Las Vegas, January 1988)*.

Hoek, E. and E. T. Brown (1980) Underground Excavations in Rock. London: Institution of Mining and Metallurgy.

Hoek, E. and E. T. Brown (1997) Practical estimates of rock mass strength. *Int. J. Rock Mech. Min. Sci. & Geomech. Abstr.*, **34**(8), 1165–1186.

Holzer, F. (1966) Calculation of seismic source mechanisms. *Proc. Roy. Soc. London, Ser. A*, **290**, 408–429.

Hopley, D. (1982) The Geomorphology of the Great Barrier Reef — Quaternary Development of Coral Reefs. New York: John Wiley & Sons.

Hsieh, P. A. and S. P. Neuman (1985) Field determination of the three-dimensional hydraulic conductivity tensor of anisotropic media 1. Theory. *Water Resources Res.*, **21**(11), 1655–1665.

Hsieh, P. A., S. P. Neuman, G. K. Stiles and E. S. Simpson (1985) Field determination of the three-dimensional hydraulic conductivity tensor of anisotropic

media 2. Methodology and application to fractured rocks. *Water Resources Res.*, **21**(11), 1667–1676.

Hyett, A. J., C. G. Dyke and J. A. Hudson (1986) A critical examination of basic concepts assocaited with the existence and measurement of in situ stress. In O. Stephansson (editor), *Proceedings of the International Symposium on Rock Stress and Rock Stress Measurements (Stockholm, 1986)*, pp. 387–396, Luleå: Centek Publishers.

IAEA (1998a) The radiological situation at the atolls of Mururoa and Fangataufa: Main report. Tech. rep., International Advisory Committee, Vienna.

IAEA (1998b) The radiological situation at the atolls of Mururoa and Fangataufa: Technical report, Vol. 4, Releases to the biosphere of radionuclides from underground nuclear weapon tests at the atolls, report by working group. Tech. rep., International Advisory Committee, Vienna.

IAEA (1998c) The radiological situation at the atolls of Mururoa and Fangataufa: Technical report, Vol. 3, Inventory of radionuclides underground at the atolls, report by working group. Tech. rep., International Advisory Committee, Vienna.

IAEA (1998d) The radiological situation at the atolls of Mururoa and Fangataufa: Technical report, Vol. 6, Doses due to radioactive material present in the environment or released from the atolls, report by working group. Tech. rep., International Advisory Committee, Vienna.

IAEA (1998e) The radiological situation at the atolls of Mururoa and Fangataufa: Technical report, Vol. 5, Transport of radioactive material present within the marine environment, report by working group. Tech. rep., International Advisory Committee, Vienna.

Institute for Defense Analysis (Arlington, Virginia) (1970) Proceedings of the ARPA seismic coupling conference. Tech. Rep. ARPA-T10-71-13-1, Report to Battelle Columbus Laboratories.

Itasca Consulting Group, Inc. (1993) UDEC (Universal Distinct Element Code) Version 2.0. Minneapolis.

Itasca Consulting Group, Inc. (1995) FLAC (Fast Lagrangian Analysis of Continua) Version 3.3. Minneapolis.

Itasca Consulting Group, Inc. (1997) FLAC3D (Fast Lagrangian Analysis of Continua in 3 Dimensions) Version 2.0. Minneapolis.

Jacob, C. E. (1950) Flow of Ground Water, pp. 321–386. New York: John Wiley.

James, N. P. and R. N. Ginsburg (1979) The Seaward Margin of Belize Barrier and Atoll Reefs. Oxford: Blackwell Scientific Publications, Int. Assoc. of Sedimentologists, Special Publication No. 3.

Janković, I. (1997) High-Order Analytic Elements in Modeling Groundwater Flow. Ph.D. thesis, University of Minnesota.

Janković, I. and R. Barnes (1997) Three-dimensional flow through large numbers of spheroidal inhomogeneities. *Submitted to J. Hydrology*.

Johnson, G. W., G. G. Higgins and C. E. Violet (1959) Underground nuclear detonations. *J. Geophys. Res.*, **64**(10), 1457–1470.

Kersting, A. B. (1996) The state of the hydrologic source term. Tech. Rep. UCRL-ID-126557, Lawrence Livermore National Laboratory.

Ladd, H. S., E. Ingerson, R. C. Townsend, M. Russell and H. K. Stephenson (1953) Drilling on Eniwetok Atoll, Marshall Islands. *Bull. Am. Assoc. Petr. Geologists*, **37**(10), 2257–2280.

Lalou, C., J. L. Reyss and R. Boichard (1988) Relations entre certains aspects de la sédimentaion carbonatée dans le golf arabo-persique et les niveaux de stagnation concomitante de la mer au cours des 500 000 dernières années. *C. R Acad. Sci. Paris*, **307**, 1211–1216.

Lam, R. K. (1974) Atoll permeability calculated from tidal diffusion. *J. Geophys. Res.*, **79**(21), 3073–3081.

Lama, R. D. and V. S. Vutukuri (1978) Handbook of Mechanical Properties of Rocks, vol. 2. Clausthal: Trans Tech Publications.

Lee, H. J. and B. D. Edwards (1986) Regional method to assess offshore slope stability. *ASCE J. Geotech. Eng.*, **112**(5), 489–509.

Maenchen, G. and S. Sack (1964) The Tensor code. In *Methods in Computational Physics*, vol. 3, pp. 181–210, Academic Press, Inc., New York.

Mariotti, C. (1990) Propriétés Rhéologiques de Roches Tendres - Etudes Expérimentales et Numériques. Ph.D. thesis, Ecole Centrale des Arts et Manufactures, Paris.

Mariotti, C. and J. Bouchez (1989) Différences rhéologiques sous pression de confinement entre des craies tendres naturelles et synthétiques. In V. Maury and D. Fourmaintraux (editors), *Rock at Great Depth (Proceedings of the ISRM/SPE International Symposium, August 1989, Pau)*, pp. 93–99, Balkema, Rotterdam.

Mariotti, C. and F. Thomas (1994) Loi de comportement ARMOR pour géomatériaux sous chargement dynamique. *J. de Physique IV*, **4**, C8577–C8582.

Moore, J. G., W. R. Normark and R. T. Holcom (1994) Giant Hawaiian landslides. *Ann. Rev. Earth & Planetary Sci.*, **22**, 119–144.

Morgan, J. (1971) Convection plumes in the lower mantle. *Nature*, **230**, 42–43.

Mullins, H. T., A. F. Gardulski and A. C. Hine (1986) Catastrophic collapse of the west Florida carbonate platform margin. *Geology*, **14**(2), 167–170.

Murakami, Y. and S. Aoki et al. (editors) (1987) Stress Intensity Factors Handbook. New York: Pergamon Press, 1st edn.

National Resources Defense Council (1997) Table of known nulcear tests worldwide: 1945-1969/1970-1996.

New Zealand MoFA (1984) Report of a New Zealand, Australian, and Papua New Guinea scientific mission to Mururoa Atoll. Tech. rep., New Zealand Ministry of Foreign Affairs, Wellington.

Newmark, N. M. (1965) Effects of earthquakes on dams and embankments. *Géotechnique*, **15**(2), 139–159.

Nield, D. A. and A. Bejan (1992) Convection in Porous Media. New York: Springer-Verlag.

Nikolaevskii, V. N. (1959) Convective diffusion in porous media. *J. Appl. Math. & Mech.*, **23**(6), 1492–1503.

Nikolaevskiy, V. N. (1990) Mechanics of Porous and Fractured Media. Singapore: World Scientific.

Nikolaevskiy, V. N. (1996) Geomechanics and Fluidodynamics. Dordrecht, The Netherlands: Kluwer.

Oberdorfer, J. A., P. J. Hogan and R. W. Buddemeier (1990) Atoll island hydrogeology: Flow and freshwater occurrence in a tidally dominated system. *J. Hydrology*, **120**, 327–340.

Okubo, A. (1973) Effect of shoreline irregularities on streamwise dispersion in estuaries and other embayments. *Netherlands J. Sea Research*, **6**, 213–224.

OTA (1989) The containment of underground nuclear explosions. Tech. Rep. OTA-ISC-414, U.S. Congress, Office of Technology Assessment, U.S. Government Printing Office, Washington, D.C.

Perrochet, P. and L. Tacher (1997a) Mathematical modeling of hydro-thermal processes in Mururoa atoll. Tech. Rep. International Geomechanical Commission (University of Minnesota), École Polytechnique Fédérale de Lausanne, Laboratoire de Géologie.

Perrochet, P. and L. Tacher (1997b) Personal communication.

Peterson, E., K. Lie, N. Rimer, R. Nilson and G. Higgins (1991) Thermodynamic evolution of nuclear cavities. In *Proceedings of the 6th Symposium on Containment of Underground Nuclear Explosions (University of Nevada, Reno, September 1991)*, vol. 1, pp. 257–274, Livermore, California: Lawrence Livermore National Laboratory.

Poulikakos, D. (1985) On buoyancy induced heat and mass transfer from a concentrated source in an infinite porous medium. *Int. J. Heat Mass Transfer*, **28**(3), 621–629.

Prior, D. B. and J. M. Coleman (1984) Submarine Slope Instability, pp. 419–455. Chichester: John Wiley & Sons.

Proffer, W. J. and E. J. Halda (1993) Distinct element modeling of late-time containment phenomena. In *Proceedings of the 7th Symposium on Containment of Underground Nuclear Explosions (CONF-9309103)*, vol. 2, pp. 61–85, Lawrence Livermore National Laboratory.

Raeisi, E. and J. E. Mylorie (1995) Hydrodynamic behavior of caves formed in the freshwater lens of carbonate islands. *Carbonates & Evaporates*, **10**(2), 207–214.

Raitt, R. W. (1954) Seismic refraction studies of Bikini and Kwajalein Atolls. Tech. Rep. Professional Paper 260-K, U.S. Geological Survey.

Richtmyer, R. D. and K. W. Morton (1967) Difference Methods for Initial-value Problems. Interscience Publishers, 2nd edn.

Rinehart, J. S. (1960) On fractures caused by explosions and impacts. *Q. Colorado School Mines*, **55**(4), 1–155.

Rodean, H. C. (1971) Nuclear-Explosion Seismology. Oak Ridge, Tennessee: U.S. Atomic Energy Commission.

Rodionov, V. N., V. V. Adushkin, V. N. Kostiuchenko, V. N. Nikolaevskii, A. N. Romashov and V. M. Tsvetkov (1971) Mechanical Effects of an Underground Explosion. Moscow: Nedra.

Rougerie, F. and B. Wauthy (1993) The endo-upwelling concept: From geothermal convection to reef construction. *Coral Reefs*, **12**, 19–30.

Ruzie, R. and A. Gachon (1985) Apport des techniques géophysiques à L'Etude des carbonates dans les atolls: Application à L'Atoll de Mururoa. In *Proceedings of the Fifth International Coral Reef Congress (Tahiti, 1985)*, vol. 3, pp. 381–388.

Salvat, B. (1986) Le Littoral Corallien, vol. 3, pp. 9–24. Paris: Multipress Editions.

Samaden, G., P. Dallot and R. Roche (1985) Atoll d'Eniwetok: Système géothermique insulaire à l'état naturel. *La Houille Blanche*, **2**, 143–151.

Schock, R. N., H. C. Heard, R. P. Swift and O. R. Walton (1980) In situ fracture related to energy and resource recovery. In *Proceedings of the 7th International AIRAPT Conference (Le Creusat, 1979)*, vol. 2, pp. 902–912, Oxford: Oxford University Press.

Schofield, A. N. and C. P. Wroth (1968) Critical State Soil Mechanics. London: McGraw-Hill.

Schultz, R. A. (1995) Limits on strength and deformation properties of jointed basaltic rock masses. *Rock Mech. & Rock Eng.*, **28**, 1–15.

Sedov, L. I. (1992) Similarity and Dimensional Methods in Mechanics. Boca Raton, Florida: CRC Press, 10th edn.

Seed, H. B. (1968) Landslides during earthquakes due to soil liquefaction. *ASCE J. Soil Mech. & Foundations Div.*, **94**(SM5), 1055–1121.

Seed, H. B. and M. S. Rahman (1978) Wave-induced pore pressure in relation to ocean floor stability of cohesionless soils. *Marine Geotech.*, **3**(2), 123–150.

Shackleton, N. J. (1987) Oxygen isotropes, ice volumes and sea level. *Quartern. Sci. Rev.*, **6**, 183–190.

Sharma, A. (1998) India sets off three nuclear blasts. *St. Paul Pioneer Press*, (May 12), Associated Press.

SKI (1997) Glaciation and hydrology workshop on the impact of climate change and glaciations on rock stresses, groundwater flow and hydrochemistry — past, present and future. Tech. Rep. 97:13, Swedish Nuclear Inspectorate.

Smith, D. K., R. J. Nagle and J. M. Kenneally (1996) Transport of gaseous fission products adjacent to an underground nuclear test cavity. *Radiochimica Acta*, **73**, 177–183.

Sokolnikoff, I. S. (1956) Mathematical Theory of Elasticity. New York: McGraw-Hill.

Sornein, J.-F. (1997) Personal communication.

Stallman, R. W. (1960) Notes on the use of temperature data for computing ground-water velocity. In *Proceedings of the 6th Assembly on Hydraulics (Nancy, France, 1960)*, vol. 1, rapp. 3, pp. 1–7, Paris: Société Hydrotechnique de France, Also in Methods of Collecting and Interpreting Ground-Water Data (R. Bentall, Compiler), USGS Water-Supply Paper 1544-H, pp. 26-46, 1963.

Stallman, R. W. (1965) Steady one-dimensional fluid flow in a semi-infinite porous medium with sinusoidal surface temperature. *J. Geophys. Res.*, **70**(12), 2821–2827.

Starfield, A. M. and P. A. Cundall (1988) Towards a methodology for rock mechanics modelling. *Int. J. Rock Mech., Min. Sci. & Geomech. Abstr.*, **25**(3), 99–106.

Swartz, J. H. (1958) Geothermal measurements on Eniwetok and Bikini atolls. Tech. Rep. Professional Paper 260-U, U.S. Geological Survey.

Tacher, L. (1998) Personal communication.

Tazieff, H. (1982) Rapport d'Haroun Tazieff sur l'ensemble de la mission scientifique en Polynesie Française. Tech. rep.

Timoshenko, S. P. and J. N. Goodier (1987) Theory of Elasticity. New York: McGraw-Hill.

Townley, L. R. (1993) AQUIFEM-P: A periodic finite element aquifer flow model: User's manual and description, version 1.0 (plus software). Tech. Rep. 93/13, CSIRO Division of Water Resources.

Townley, L. R. (1995) The response of aquifers to periodic forcing. *Adv. Water Resources*, **18**(3), 125–146.

Underwood, M. R., F. L. Peterson and C. I. Voss (1992) Groundwater lens dynamics of atoll islands. *Water Resources Research*, **28**(11), 2889–2902.

Vacher, H. L. (1988) Dupuit-Ghyben-Herzberg analysis of strip-island lenses. *Geol. Soc. America Bull.*, **100**, 508–591.

Vacher, H. L. and T. M. Quinn, Eds. (1997) Geology and Hydrogeology of Carbonate Islands. Amsterdam: Elsevier Science BV.

Varnes, D. J. (1975) Slope movement in the western United States. In E. Yatsu, A. D. Ward and F. Adams (editors), *Mass Wasting (Proceedings of the 4th Guelph Symposium on Geomorphology, University of East Anglia, 1975)*, pp. 1–18, Norwich: Geo Abstracts Ltd.

Vutukuri, V. S., R. D. Lama and S. S. Saluja (1974) Handbook on Mechanical Properties of Rocks, vol. 1. Clausthal: Trans Tech Publications.

Watson, E. J. (1983) Dispersion in oscillating pipe flow. *J. Fluid Mech.*, **133**, 233–244.

Webster, I. T. and J. H. Taylor (1992) Rotational dispersion in porous media due to fluctuating flows. *Water Resources Res.*, **28**(1), 109–119.

Wegener, A. (1924) The Origins of Continents and Oceans. London: Methuen, Translated from the 3rd German Edition by J.G.A. Skerl.

Wheatcraft, S. W. and R. W. Buddemeier (1981) Atoll island hydrology. *Ground Water*, **19**(3), 311–320.

Wilkins, M. L. (1964) Calculation of elastic-plastic flow. In *Methods in Computational Physics*, vol. 3, pp. 211–263, Academic Press, Inc., New York.

Williams, J. A., R. N. Wada and R. Wang (1970) Model studies of tidal effects on groundwater hydraulics. Tech. Rep. 39, University of Hawaii, Water Resources Research Center.

Wilson, J. T. (1963) A possible origin of Hawaiian Islands. *Canadian J. Physics*, **41**, 863–870.

Wilson, J. T. (1970) Continents Adrift: Readings from Scientific American. San Francisco: W. H. Freeman.

Winterer, E. L. (1973) Sedimentary facies and plate tectonics of equatorial Pacific. *Bull. Am. Assoc. Petr. Geologists*, **57**, 265–282.

Zel'dovich, Y. B. and Y. P. Raizer (1967) Physics of Shock Waves and High-Temperature Hydrodynamic Phenomena. Academic Press, London.

Zoback, M. L. and M. D. Zoback et al. (1989) Global patterns of tectonic stress. *Nature*, **341**(6240), 291–298.

GLOSSARY

Advection (of a solute) Transport of a solute by means of circulating waters in a porous medium, at the velocity of the water, and when the concentration of the solute is not sufficient to affect density of the water.

Bar Unit of pressure. 1 bar = 1.01972 kilograms weight per centimetre squared, or 10^5 Pascals (Pa). The atmospheric pressure is approximately 1 bar (often expressed as 1000 millibar). Multiples: 1 kilobar (kb) = 10^3 bar; 1 megabar (Mb) = 10^6 bar.

Barrier A coral reef situated offshore from an island or continent, sometimes forming a ring. Such a reef may later develop into an atoll by gradual subsidence of the central area.

Basalt A dark-coloured, fine-grained, volcanic rock composed of plagioclase feldspar, pyroxene and magnetite, with or without olivine, and containing not more than 53% SiO_2 by weight.

Breccia A type of rock formed mostly of angular fragments (grain size less than 2 mm), cemented by finer material.

Calcite A form of calcium carbonate, containing variable amounts of magnesium.

Carbonates For both atolls, the carbonate covering comprises limestones and dolomites; it varies between 130 m and 450 on Mururoa, and is approximately 230 m thick on Fangataufa.

Cavity Space formed around the test chamber following an underground nuclear explosion.

Cementation Process that binds together the loose bioclastic debris and contributes to lithification of the atoll reef.

Chimney Rubble-filled zone of approximately cylindrical shape, formed after the cavity created by an underground nuclear explosion collapses. Chimney height is closely related to the yield and depth of the explosion.

Compaction (of carbonates) The act of forcing carbonate material together (consolidation) under pressure or impact to reduce porosity and yield a relatively denser mass.

Compression wave See **P wave**.

Conduction (of heat) Transport of heat through rock or water without any displacement of the pore water.

Convection (of heat) Transport of heat by means of circulating waters in a porous medium; the motion resulting in a fluid from the differences in density (due to thermal expansion) and the action of gravity is called "natural convection", whereas forced convection represents the case where the velocity of the fluid is due to causes other than differences of density.

Conglomerate Cemented gravel with rounded pebbles or granules (i.e. greater than 2 mm in size) making up more than 50% of the rock.

Coral rim A ring-shaped section of reef above sea level, forming the emergent part of an atoll.

Coupling In reference to nuclear explosions, this term refers to the process and proportion of the energy of a nuclear explosion that is mechanically transmitted to the surrounding rock. It is related directly to the amount of gas produced by the release of thermal energy.

Creep Continuous deformation of a material under steady load; behaviour of earth materials in response to factors such as time, temperature, pore pressure, and ambient stress level.

CRTV Nuclear tests in which chimneys reach the top of the volcanism.

Darcy A standard unit of measurement of permeability, with the dimension of an area (L^2) equivalent to the passage of 1 cm^3 of fluid of 1 centipoise viscosity flowing in 1 second under a pressure differential of 1 bar through a porous medium having a cross-sectional area of 1 cm^2 and a length of 1 cm. One Darcy is equal to $0.987 \cdot 10^{-12}$ m^2.

Darcy's Law A law that describes the rate of movement of water through porous media. It states that the rate of movement of water through porous media is proportional to the hydraulic gradient; it can be expressed as u = Ki, where u is the volume of water transmitted through a unit cross-sectional area per unit time, K is the hydraulic conductivity (linearly proportional to permeability), and i is the unit

change in the head through unit length of flow path (otherwise termed hydraulic gradient).

Darcy velocity A hypothetical discharge rate calculated assuming that water moves through the entire cross-sectional area in question. In practice, the water moves through interconnected pore-spaces that represent only a certain proportion of the total rock volume. Although the constant K has the dimensions of length per unit time (i.e. velocity), the Darcy velocity is evaluated from the product Ki.

Decoupling In reference to nuclear explosions, this term refers to the technique for minimising the proportion of energy of a nuclear explosion that is transmitted mechanically to the surrounding rock (see also **Coupling**).

Detrital Formed from fragmented material derived from the erosion of previously existing rocks (detrital deposits are commonly interbedded within carbonate formations).

Dolomite A mixed carbonate of calcium and magnesium; also a sedimentary rock type formed of this mineral.

Dolomitised Affected by the process of dolomitisation whereby limestone is wholly or partly converted to dolomite rock or dolomitic limestone by the replacement of the calcium carbonate (calcite) by magnesium carbonate.

Dry density Mass/volume ratio of a soil or rock sample measured when the sample is dry and there is no water in the voids or pores (see also **Saturated density**).

Dyke An intrusion of (volcanic) rock cutting through the previously existing strata. Most dykes are vertical or near-vertical, having pushed their way through the overlying country rock.

Endo-upwelling Geothermal circulation resulting when the groundwater rises near the centre of an atoll and cool ocean water is drawn inward across the flanks of the atoll to support that upward flow.

Explosion craters Caused by the expulsion of soil and collapse of the cavity following an underground nuclear test sufficiently close to the surface.

Factor of safety In slope stability analysis, the (single) number by which the strengths of all the geological units involved have to be reduced in order to cause collapse of a slope.

Fault A fracture or zone of fractures along which there has occurred displacement of the sides relative to one another parallel to the fracture.

Flows (of sediment) Dislodging of sediment downslope involving a number of processes, notably debris flow, grain flow and liquefaction flow. Flows are sometimes regarded as a transitional stage between slides and turbidity currents.

Fringing reef A coral platform formed around an island and lying very close to the shore.

Geothermal heat flow Heat flow from the inner earth.

Gravitational stresses Stresses resulting from the mass of overburden.

Ground zero The point on the surface of the water or the ground situated vertically below (in the case of atmospheric explosions) or above (in the case of underground explosions) the point of detonation (the zero point).

Hoa A hollow between motu (islets) on a barrier reef, allowing exchanges of sea water between ocean and lagoon.

Hugoniot curve A plotted line representation of the locus of all the thermodynamic states accessible by shock from a given initial state.

Hugoniot relations The three-jump discontinuity between the variables characteristic of the state of a material. Named after the scientist who established them, these relations describe the conservation of mass, momentum and energy during the instantaneous transition from a quiescent state to a loaded state.

Hyaloclastite Volcanic breccia formed underwater, composed of glassy fragments greater than 4 mm in size and often associated with pillow lavas.

Hydrostatic pressure The pressure exerted by the overlying water in the absence of fluid movements.

Hydraulic gradient A measure of the change in groundwater head over a given direction for a unit distance (see also *Darcy's Law*).

Hydrothermal Pertaining to hot fluids that circulate within the earth's crust.

Induced stresses Man-made stress components arising from the removal or addition of material; they are superimposed on natural stresses that exist prior to any human action.

In-situ stress The stress existing at a point in a rock mass before the rock is disturbed.

Karst A type of internal modification of rocks developed specifically in limestone terrains as a result of variable degrees of dissolution by meteoric waters (karstic erosion, cavity), and characterised by enlarged fractures, enhanced porosity, caves and underground drainage, or, sometimes, sinkholes at the surface. Such features are recognised at varying depths within the body of a limestone and are related to past low sea levels or base levels.

Kilotonne Unit used to quantify the energy released by nuclear and thermonuclear explosions. It corresponds to the energy released by 1000 tons of a reference chemical explosive, tri-nitro-toluene (TNT), $4.18 \cdot 10^{19}$ Ergs or $4.18 \cdot 10^{12}$ Joules or $1 \cdot 10^{12}$ calories. For thermonuclear explosions the megaton (Mt) is often used: 1 Mt = 10^3 kt.

Liquefaction A process in which cyclic loading (arising from an earthquake, an explosion or wave action) produces a build-up of pore pressure, under undrained or partially undrained conditions, causing failure and plastic flow of sediment.

Lithostatic pressure The released pressure exerted at depth due to the weight of overlying rocks.

Logging Measurement of the characteristics of the geological formations, carried out in a drillhole by downhole geophysical measurements.

Mean density Total mass of the solid and liquid parts of a porous rock sample divided by the overall volume of the sample.

Mean porosity The pore volume as a percentage of the overall volume of a porous sample.

Megatonne (Mt) A unit used to quantify the energy used by nuclear and thermonuclear explosions. It corresponds to the energy released by 1 million tonnes of the chemical explosive TNT. The kilotonne (1 kt = 0.001 Mt) is also sometimes used.

Motu A small islet made up of bioclastic material, situated on the reef rim of an atoll.

Nuclide An atomic species characterised by its mass number, atomic number and energy state. (see also **Radionuclide**)

P-(primary) wave Compression wave occurring after an earthquake or an underground nuclear explosion; the fastest vibration wave.

Permeability The ability to transmit water (see also *Darcy's Law*); the "matrix" permeability is governed mainly by the degree of communication between the pores. (see also **Porosity**).

Physico-chemical stress The stress state arising from chemical and/or physical changes in the rock (e.g. recrystallization, absorption of water, fluctuation of groundwater level).

Pillow lava Submarine volcanic flow forming a jumbled heap of pillow-shaped units.

Point zero See **Zero point**.

Pore water Water contained within the pores of a geological formation.

Porosity The ratio between the pore-space volume and the total volume of a rock sample or formation.

Radionuclide A radioactive atomic species.

Rayleigh wave Seismic wave, generated by an earthquake or an underground nuclear explosion, that affects only the superficial layers of the medium.

Reef See *Barrier reef.*

Residual stress Stress state remaining in the rock mass even after the originating mechanism(s) has ceased to operate.

Rim See *Coral rim.*

S (secondary) wave Shear wave, propagating as a seismic wave, generated after an underground nuclear explosion.

Safety Trial Detonation of an annulus of chemical explosive placed around a nuclear device to determine whether the explosion results in a nuclear explosion (or "yield").

Saturated density Mass/volume ratio of a soil or rock sample measured when all of the pores or voids are filled with water. (see also **Dry density**).

Seismic pulse Created by an underground nuclear explosion, the pulse propagates long distances in the geological environment.

Seismic ray Path followed by a seismic wave. In an isotropic medium, this path is perpendicular to the wave front.

Seismic wave Elastic wave that propagates through the earth as a vibration, generated by an earthquake or an underground nuclear explosion.

Settlement In relation to underground nuclear testing, ground depressions caused by irreversible strains in surface layers induced by the dynamic wave transmitted through the rock overlying the explosion.

Shear strength The value at which shear stresses exceed a limiting value, after which plastic deformation of the rock occurs; a measure of the rock's ability to withstand compression. Shear strength is related to specific values of pore fluid pressure.

Shock velocity Velocity of the shock front propagating in fluid or solid materials. This velocity depends on the nature of the medium and on the energy carried by the shock wave.

Slides The most widespread form of submarine slope instability, involving rock or soft sediment.

SOFAR SOund Fixing And Ranging channel, a water layer in the ocean, usually located between 500 and 1500 m in depth, where the propagation velocity of the waves is the lowest, due to local salinity and temperature characteristics of the ocean. Waves trapped in the SOFAR channel propagate within it over very long distances with little attenuation.

Spalling The upward or outward displacement of surface and near-surface layers of rock and sediment caused by the interaction of a compressional wave at a free surface. The wave may produce fragmentation or may cause only momentary parting of layers. Surface spalling associated with nuclear explosions occurs when a surface layer of rock separates from an underlying rock mass by a horizontal fracture generated by the downgoing tensile pulse reflected from the free surface.

Subaerial volcanic rocks Overlying the submarine volcanics, these rocks were formed when the top of the volcano emerged from the ocean. They are more diverse and spatially variable than the submarine rocks. Rock types vary from massive basalts to volcanic cinder deposits.

Submarine rock falls Rock falls restricted to localised steep, near-vertical slopes.

Submarine volcanic rocks Rocks formed when the top of the volcano was still under sea level. On Mururoa and Fangataufa Atolls, these consist of pillow lavas and associated breccias, autoclastites and hyaloclastites.

Subsidence craters Following an underground nuclear test, a collapse of the cavity and formation of a chimney affecting layers up to the surface. In contrast to explosion craters, no near-surface material is expelled.

Tectonic stresses May be active, as a result of active present-day straining of the Earth's crust; or remanent, as a result of past tectonic events that have been only partially relieved by natural processes.

Thermal exchange Heat exchange by conduction and convection in a solid material.

Thermal stresses Those stresses resulting from temperature variations; they may be local in nature or may form part of the tectonic stress.

Trench An oceanic deep lying close up against the continental edge, corresponding to a destructive plate margin or subduction zone.

Transition zone Sedimentary layer, only a few metres thick, between the submarine and subaerial volcanics. The transition zone comprises two distinct layers: a sedimentary layer of calcareous, argillaceous or volcanic conglomeratic rock; and a layer of shallow submarine rocks, mainly highly brecciated lavas.

Turbidity currents or flows Submarine slope instabilities involving the down-slope transport of sediment, which is supported by the upward component of fluid turbulence within the current.

Unconfined (or uniaxial) compressive strength The uniaxial compressive strength of a sample, as determined by a compression test on a sample of rock, conducted without placing lateral confining pressure on the sample.

Vaporized zone The area in the immediate vicinity of the zero point where the rock has been melted and vaporized by the intense shock of the explosion.

Venting In the context of nuclear explosions, the transport of radioactive gases from the cavity created by the explosion to the surrounding rocks or even the biosphere via fractures or other pathways created by the explosion.

Water-saturated (rock) Rock in which the pores are filled with water.

Wavelength Distance between two consecutive points of the same phase in an undulatory movement propagating in a straight line.

Yield The effective energy released in a nuclear explosion, manifested as shock or blast, thermal radiation and nuclear radiation. The residual nuclear radiation associated with the fission products, which amounts to about 10% of the total fission energy, is not included in the yield. Yield is usually expressed as TNT equivalent — the quantity of TNT that would release the same amount of energy if exploded. TNT equivalent is usually given in kilotonnes or megatonnes, one kilotonne of TNT being defined arbitrarily as $4.18 \cdot 10^{12}$ Joules.

Zeolite A group of hydrated clay, alumina silicates of sodium potassium, calcium, and barium, which occurs in geodes, altered igneous rocks, hydrothermal veins, and some sediments.

Zero point The exact location where the nuclear testing device and measuring instrument container are positioned.

Underground Nuclear Testing in French Polynesia:

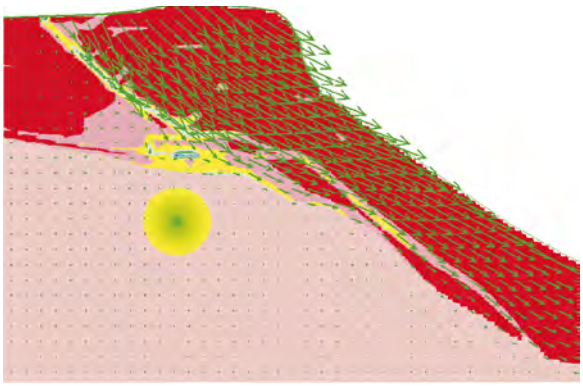

Stability and Hydrology Issues

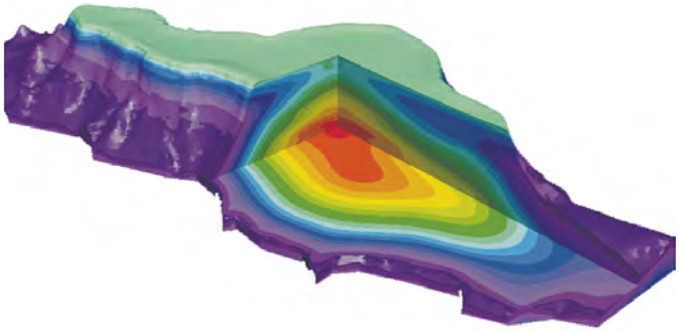

Volume III, French Translations

(from Volumes I and II)

International Geomechanical Commission

Charles Fairhurst, Chairman

Problèmes de stabilité et d' hydrologie liés aux essais nucléaires souterrains en Polynésie Française :

Volume III, Extraits en français des Volumes I et II

Rapport de la
Commission Géomécanique Internationale

présidée par Charles FAIRHURST

Rapport préparé dans le cadre d'un contrat avec l'Université du Minnesota, Minneapolis, Minnesota, U.S.A.

Un grand soin a été apporté aux traductions du Volume III avec l'intention qu'elles rendent fidèlement compte des sections correspondantes des Volumes I et II. Dans le cas que nous espérons improbable où des différences d'interprétation pourraient résulter de la comparaison des deux textes, on doit considérer que la version contenue dans les Volumes I et II constitue la position officielle de la CGI.

Ce rapport est publié en trois volumes : Volume I, *Résultats généraux* ; Volume II, *Analyses Techniques* ; et Volume III, *Les Essais Nucléaires Souterrains en Polynésie Française : Stabilité et Hydrogéologie* (Extraits en français des Volumes I et II). Ces volumes peuvent être obtenus à l'adresse suivante :

La Documentation Française
29, quai Voltaire
75344 Paris
Cedex 07
France

Imprimé aux Etats-Unis.

Membres de la
Commission Géomécanique Internationale

Président

Charles FAIRHURST (U.S.A.)

Commission

Edwin T. BROWN (Australie)

Emmanuel DETOURNAY (Belgique/U.S.A.)

Ghislain de MARSILY (France)

Victor NIKOLAEVSKIY (Russie)

J.R. Anthony PEARSON (Grande Bretagne)

Lloyd TOWNLEY (Australie)

Liaison Technique

Pierre BÉREST (France)

Une brève notice bibliographique des membres de la Commission est fournie à l'annexe A.

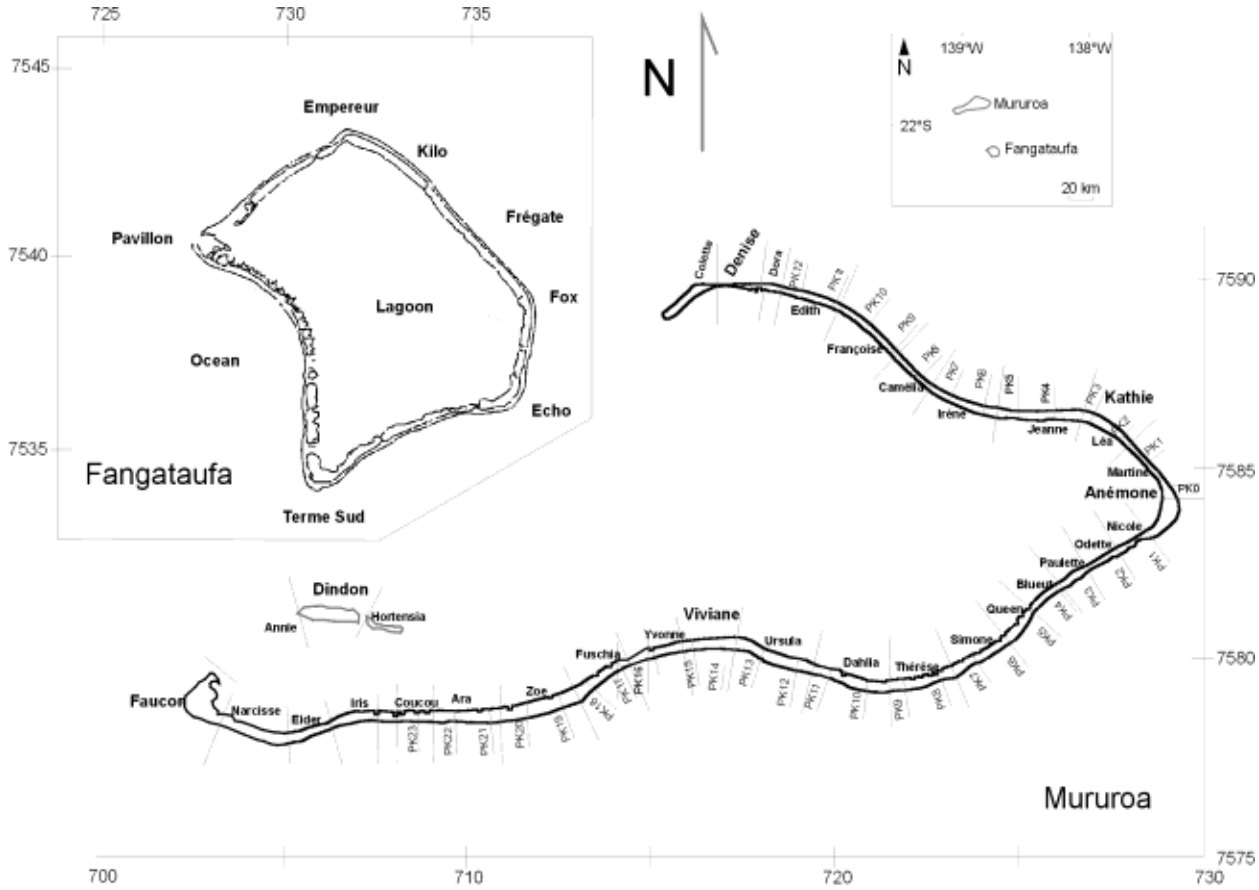

Appellations locales des différents secteurs de Mururoa et Fangataufa. Les coordonnées locales sur la figure sont indiquées (en km) dans le système Mercator Universel Transverse pour l'hémisphère sud. Les positions géographiques relatives exactes des atolls sont indiquées dans le médaillon (coin de page supérieur droit).

PRÉFACE

Le programme français d'essais nucléaires

« Gerboise bleue », une charge de relativement faible énergie (estimée à 60-70 kt *), tirée dans le désert du Sahara à Reggane, en Algérie, le 13 février 1960, faisait de la France une puissance nucléaire - quelques 15 ans après la première explosion nucléaire au monde (Trinity) à Alamagardo, Nouveau Mexique, USA, le 16 juillet 1945. Au cours de ces quinze années, les États-Unis avaient effectué 196 tirs, l'Union Soviétique 84, et le Royaume Uni 21. Ces 301 essais, à l'exception des 22 explosions souterraines du Nevada Test Site aux États-Unis (voir annexe B), avaient été conduits dans l'atmosphère. En novembre 1958, les trois pays déclaraient conjointement un moratoire sur les essais. Le moratoire dura jusqu'en septembre 1961.

En novembre 1961, après 4 essais atmosphériques à Reggane, la France procéda à une série de 13 essais souterrains tirés en profondeur dans des tunnels horizontaux creusés dans le massif granitique du Hoggar à In-Eker, à quelques 560 km de Reggane dans la direction E-SE. Cette série s'arrêta le 16 février 1966 en raison, au moins pour une part, de la situation politique en Algérie. Entre-temps, le Royaume-Uni, les USA et l'URSS avaient signé le Limited Test Ban Treaty (5 août 1963) qui interdisait les essais nucléaires dans l'atmosphère, dans l'espace ou sous l'océan.

Aldebaran, le premier essai français dans le Pacifique Sud, fut effectué le 21 juillet 1966. Il s'agissait d'une explosion nucléaire conduite depuis une barge placée dans le lagon de Mururoa, la première d'un total de 41 explosions atmosphériques : 37 à Mururoa ou dans son voisinage (dont Procyon, dont l'énergie était supérieure à 1 Mt), et 4 à Fangataufa (dont Canopus, dont l'énergie était supérieure à 1 Mt). Cinq essais de

*1 kt signifie que l'énergie libérée, ou énergie de l'explosion nucléaire, équivaut à celle obtenue dans la détonation de mille tonnes d'explosif chimique tri-nitro-toluène (TNT), soit $4,18 \cdot 10^{12}$ joules. 1 Mt signifie que l'énergie libérée correspond à un million de tonnes de TNT, soit $4,18 \cdot 10^{15}$ joules, qui est l'équivalent mécanique de 10^{15} calories d'énergie thermique. Le Threshold Test Ban Treaty (1962), résultant d'un accord entre les États-Unis et l'Union Soviétique, fixait une limite supérieure de 150 kt à l'énergie des essais souterrains. Le CEA (Bouchez et Lecomte 1996, Annexe, p. 113) affirme que tous les essais souterrains conduits par la France étaient inférieurs à la limite de 150 kt. Les résultats de la surveillance sismique internationale sont en accord avec cette affirmation (voir Volume II, annexe C).

sécurité [†] ont aussi été conduits à Mururoa, dont deux ont eu pour résultat une (faible) explosion nucléaire. Les essais atmosphériques ont pris fin le14 septembre 1974.

Les essais souterrains dans les atolls commencèrent par deux tirs de petite énergie (Achille et Hector) sous la couronne sud de Fangataufa, les 5 juin 1975 et 26 novembre 1975. Au moment où cette série d'essais s'acheva, en juillet 1991, un total de 131 essais souterrains avaient été conduits : 123 à Mururoa (73 sous la couronne et 50 sous le lagon) et 8 à Fangataufa (2 sous la couronne et 6 sous le lagon). De plus, 10 essais souterrains de sécurité, dont 3 ont eu pour résultat une faible explosion nucléaire [‡], ont été conduits à Mururoa. La France annonçait son propre moratoire sur les essais nucléaires en septembre 1991.

Localisation de Mururoa et Fangataufa par rapport aux principales terres continentales

La dernière campagne d'essais

La Grande-Bretagne, les États-Unis et la Russie avaient déjà annoncé qu'ils étaient prêts à adopter la proposition de Comprehensive Test Ban Treaty (Traité d'interdiction

[†] Un essai de sécurité consiste en la détonation d'un anneau d'explosif chimique placé autour de l'engin nucléaire en vue de vérifier si cette explosion déclenche ou non une explosion nucléaire, ou « tir ».

[‡] Il faut remarquer que les 3 essais de sécurité « nucléaires » sont inclus dans la liste des 134 essais souterrains figurant dans l'Annexe de Bouchez et Lecomte (1996). Avec les 6 essais de la campagne 1995-1996, c'est un total de (131 + 10 + 6) = 147 essais nucléaires souterrains et essais de sécurité qui ont été conduits à Mururoa et Fangataufa.

complète des essais), interdisant tout essai d'arme nucléaire, quand, en juin 1995, le Président Jacques Chirac annonçait de manière inattendue que la France conduirait à Mururoa et Fangataufa, avant de signer le Traité[¶], un nombre limité (ne dépassant pas 8) d'essais souterrains. Au total six essais complémentaires ont été effectués (4 à Mururoa et 2 à Fangataufa - tous sous les lagons) entre le 5 septembre 1995 et le 27 janvier 1996, date à laquelle la France annonçait que la série était achevée. Entre le 13 février 1960 et le 27 janvier 1996, la France a conduit 210 essais nucléaires[§], les 15 essais de sécurité étant inclus dans ce total. Le détail de tous les essais connus conduits dans le monde (USA, 1030 ; URSS 415 ; France 210 ; Chine 45 ; Royaume Uni 45 ; Inde 6 ; Pakistan 6[‖]) est donné dans le tableau de l'Annexe B. Des détails complémentaires sur les essais souterrains français du Sud Pacifique sont présentés à l'annexe C.

La décision de conduire cette dernière campagne, trois ans après que tous les pays, à l'exception de la Chine, avaient arrêté les essais, suscita des inquiétudes dans le monde entier et des protestations internationales selon lesquelles ces essais, s'ajoutant à ceux déjà conduits, pourraient avoir pour conséquences des dommages sévères à court** et à long terme. Le relâchement dans l'environnement de nucléides radioactifs dangereux produits par les explosions, et les dommages infligés à l'hydrologie des atolls et à leur stabilité mécanique, étaient les deux sujets principaux d'inquiétude.

Invitations à étudier les effets des essais souterrains

En réponse à ces inquiétudes et protestations, le Ministre français des Affaires Étrangères, Monsieur Hervé de Charette, agissant au nom du Président Jacques Chirac, invitait en septembre 1996 deux groupes internationaux distincts à conduire, en toute indépendance, des investigations relatives aux conséquences des essais souterrains de Mururoa et Fangataufa.

L'Agence Internationale de l'Énergie Atomique (AIEA), dont le siège est à Vienne, accepta d'examiner le problème du relâchement des radionucléides. Son rapport officiel a été publié à la fin du printemps 1998. Une conférence internationale ayant pour but de débattre de ses résultats s'est tenue au siège de l'AIEA, à Vienne, du 30 juin au 3 juillet 1998.

[¶] La France a signé ce Traité quand il a été adopté par les Nations Unies en 1996 ; il a été ratifié par le Parlement français en mars 1998. La Grande-Bretagne, la Chine, la Russie et les États-Unis ont aussi signé le Traité. Le Traité n'est pas encore entré en vigueur (Associated Press 1998).

[§] Les 210 essais peuvent être répartis comme suit : 45 essais atmosphériques (4 en Algérie, 41 dans le Pacifique Sud) ; 150 essais souterrains (13 en Algérie, 137 dans le Pacifique Sud) ; 15 essais de sécurité (5 en surface, 10 en souterrain - tous dans le Pacifique Sud).

[‖] L'Inde a affectué 5 tirs souterrains, du 1 au 3 mai 1998 ; le Pakistan a annoncé 5 essais, du 28 au 30 mai 1998, puis 1 essai le 30 mai 1998. Certains experts en détection sismique pensent qu'un nombre d'engins inférieur à 5 ont été tirés le 28 mai.

** « Court terme », ici, signifie la période qui s'étend jusqu'à 500 ans après la fin des essais souterrains. « Long terme » signifie une période qui s'étend jusqu'à 10 000 ans après la fin des essais souterrains.

La lettre de Monsieur de Charette (invitant le Professeur Fairhurst à conduire la seconde étude - consacrée aux questions de stabilité et d'hydrologie) est reproduite à la page suivante. Dans sa réponse à cette invitation, le Professeur Fairhurst remarquait que son mandat (d'une durée de quatre ans) de Président de la Société Internationale de Mécanique des Roches (SIMR) arrivait à son terme un mois plus tard environ, de sorte que ce ne serait pas à ce titre qu'il conduirait l'étude. Il fut alors convenu qu'il constituerait et présiderait, pour entreprendre cette étude, un groupe indépendant d'experts internationaux, sous le nom de Commission Géomécanique Internationale (CGI). Une liste des membres de la CGI et des personnes qui l'ont assistée, accompagnée d'une courte notice bibliographique de chacun des membres, sont données à l'annexe A.

Si l'essentiel des études de radiologie et de stabilité/hydrologie ont été poursuivies indépendamment l'une de l'autre, certains aspects des conséquences mécaniques et hydrologiques des essais n'en affectent pas moins directement le relâchement de radionucléides. Afin de garantir que ces conséquences soient complétement prises en compte, trois membre de la CGI ont participé à l'étude radiologique, à l'invitation de l'AIEA, en tant que membres du Groupe de Travail 4, « Transport dans la Géosphère ».

Le présent rapport expose les résultats de l'étude de la CGI.

Procédure suivie pendant l'étude de la CGI

Les autorités françaises et les membres de la Commission ont attaché une importance toute particulière à l'indépendance de l'étude de la CGI. L'objet général des investigations, la stabilité et l'hydrologie, était défini par la lettre de M. de Charette, mais la CGI a considéré qu'il lui appartenait de définir sa propre méthode de travail et le détail du contenu de ses travaux. Ainsi, bien que la lettre de mission parle de « ...l'évaluation des effets de cette série d'essais... » la Commission a rapidement décidé que l'étude des effets des expérimentations sur la stabilité et l'hydrologie des atolls devait être replacée dans le contexte de la série complète des 147 essais nucléaires souterrains réalisés à Mururoa et Fangataufa. De la même manière, le choix des questions particulières méritant d'être traitées a été effectué par la Commission. Par exemple, une certaine attention a été initialement portée au signal sismique engendré par une explosion - du point de vue à la fois de la précision des estimations de l'énergie d'un tir nucléaire (voir Annexe B) et des risques potentiels de dommage à grande distance du site d'essais, comme du point de vue de la formation de vagues par de grands glissements sous-marins. Mais, dans les deux cas, on a jugé que les questions reliées à ces effets pouvaient recevoir une réponse adéquate sans qu'une étude détaillée par la Commission soit nécessaire.

Un contrat principal a été passé entre le Commissariat à l'Énergie Atomique (CEA) et l'Université du Minnesota, Minneapolis, USA, employeur du Professeur Fairhurst. Toutes les décisions ultérieures au plan financier ont été prises par l'Université. Le choix des membres de la CGI, des consultants et contractants, a été effectué en toute indépendance vis-à-vis des autorités françaises.

14 septembre 1995

Le Ministre des Affaires Etrangères

Monsieur le Professeur,

L'engagement de la France de se joindre à la conclusion du Traité d'interdiction complète des essais nucléaires au plus tard en 1996 a conduit les autorités françaises à procéder à une ultime série d'essais. Ces essais souterrains, au nombre maximum de huit, se dérouleront au Centre d'Essais du Pacifique sur les atolls de Mururoa et de Fangataufa entre septembre 1995 et fin mai 1996.

Dans un souci de transparence, le Président de la République Française souhaite qu'une mission scientifique internationale procède a l'èvaluation des effets de cette série d'essais sur l'environnement aussi bien du point de vue radiologique qu'au plan géologique et de la stabilité des atolls. Le Gouvernement français à décidé de confier la direction de cette mission à des experts ou à des organisations internationales dont la réputation scientifique est incontestable dans les domaines considérés.

A ce titre, considérant la réputation exceptionnelle que vous avez personnellement dans la communauté scientifique internationale, les responsabilités éminentes qui sont les vôtres en tant que Président de la Société Internationale de Mécanique des Roches, j'ai l'honneur de vous demander si vous accepteriez de conduire la mission scientifique dans le domaine de la stabilité des atolls et de l'hydrogéologie.

Si vous acceptiez cette responsabilité, il vous appartiendrait de préciser la composition de cette mission scientifique dont vous seriez seul juge, s'agissant en particulier du choix des experts. J'appelle toutefois votre attention sur l'intérêt que les pays de la zone Pacifique portent à cette mission.

Les autorités francaises mettront à la disposition de la mission scientifique l'ensemble des données disponibles concernant les études antérieures liées à la situation mécanique et hydrogéologique des atolls de Mururoa et Fangataufa.

Les frais engendrés dans le cadre de cette mission seront pris en charge par la France selon un protocole à établir avec vous.

Les Services des diverses administrations françaises concernées et notamment du Commissariat à l'Energie Atomique sont à votre disposition pour apporter les précisions que vous pourriez estimer nécessaires avant de prendre une décision que le Gouvernement français souhaite positive.

Il conviendra en particulier d'arrêter avec eux les dispositions pratiques concernant le calendrier, la nature et le volume des travaux. A cet égard, je peux vous assurer que les autorités françaises auront le souci de limiter autant que possible les contraintes à prendre en considération eu égard à la confidentialité des aspects militaires des essais.

J'ajouterai enfin que si vous estimez nécessaire pour la préparation de votre mission de venir sur les atolls, éventuellement avec d'autres experts, avant la fin de notre ultime campagne d'essais, les autorités françaises feraient leurs meilleurs efforts pour rendre cela possible.

Veuillez agréer, Monsieur le Professeur, l'expression de ma haute considération.

Hervé de CHARETTE

Professeur FAIRHURST
Président de la Société Internationale
de Mécanique des Roches

Les travaux et les résultats de la Commission sont restés connus des seuls membres de la CGI jusqu'en octobre 1997, date à laquelle, plus d'un an et demi après le début des travaux, des copies de plusieurs chapitres du rapport provisoire de la CGI ont été présentées aux scientifiques du CEA. La Commission considérait que ceci était nécessaire pour s'assurer que les données fournies par le CEA n'avaient pas fait l'objet d'erreurs d'interprétation. Même si des analyses et des commentaires explicatifs ont été ajoutés depuis cette date dans le Rapport Final, ses résultats et ses conclusions n'ont pas été modifiés.

La Commission s'est efforcée d'établir un cadre scientifique solide qui permette l'évaluation des conséquences des essais nucléaires souterrains sur la stabilité et l'hydrologie de Mururoa et Fangataufa. Les résultats sont présentés de manière détaillée avec l'intention que leur validité puisse être jugée de manière indépendante par les personnes intéressées.

Sources d'information

La Commission s'est réunie à plusieurs reprises (voir l'encart ci-après) avec les scientifiques du Commissariat à l'Énergie Atomique (CEA) pendant les phases préliminaires de l'étude, pour obtenir l'information de base et poser des questions. Des échantillons carottés du sondage Zoé, effectué dans la partie centrale de la couronne sud à Mururoa, et qui a fait l'objet d'un carottage continu à travers les carbonates et les roches volcaniques, depuis la surface du sol jusqu'à une profondeur de 1100 mètres, ont été examinés dans les locaux du CEA à Bruyères le Chatel, au sud de Paris.

Les membres de la Commission ont passé trois jours à Mururoa et Fangataufa, du 10 au 12 juillet 1996, et ont examiné, en voiture ou à pied, toutes les zones accessibles des couronnes ayant servi aux essais, ou ayant été affectées par ces derniers. Les deux atolls ont également été inspectés depuis un hélicoptère volant à basse altitude. Photographies et enregistrements vidéos étaient autorisés sans restriction.

À Mururoa, une attention particulière a été portée à la zone d'essais n^{o}1, dans laquelle des volumes importants de la couronne, côté océan, subissent des déformations continues ; et à la zone d'essais n^{o}4, la plus intensivement utilisée (en termes d'énergie explosive totale par unité de volume de roche), et qui a été le siège de grands glissements sous-marins provoqués par les essais. A Fangataufa, les fractures qui ont été activées dans la couronne nord-est, au voisinage de Kilo-Frégate, ont fait l'objet d'un examen. Cette zone est exceptionnelle en ceci que les essais à Fangataufa n'ont pas été conduits dans la couronne nord-est. Ceci implique que ces fractures ont été stimulées par les ondes sismiques engendrées par les essais dans d'autres régions de l'atoll - très probablement par les essais de grande énergie effectués sous le lagon.

Bien que, comme mentionné plus haut, les localisations des essais individuels (et leur profondeurs) n'aient pas été fournies à la Commission, les emplacements à la surface du sol de nombreux essais étaient visibles des airs, notamment à Mururoa.

Réunions de la Commission Géomécanique Internationale

18-20 mars 1996, École des Mines et Bruyères le Chatel, Paris, France
Réunion plénière

27-29 mai 1996, Minneapolis, Minnesota, USA
Sous-groupe Stabilité et Consultants

30 mai 1996, Université de Paris VI, France
Sous-groupe Hydrologie et J. Hadermann

9-13 juillet 1996, Polynésie française : Tahiti ; atolls de Mururoa et Fangataufa
Réunion plénière, et représentants du CEA

6-7 septembre 1996, Université de Paris VI, France
Sous-groupe Hydrologie

21-22 septembre 1996, Chaska, Minnesota, USA
Sous-groupe Stabilité et Consultants

20-21 décembre 1996, Cambridge, Angleterre
Réunion plénière et Consultants

14 février 1997, Montlhéry, France
E. T. Brown et Pierre Bérest

7-10 mai 1997, Fontvielle, Provence, France
Réunion plénière et Consultants

28 juin 1997, New-York City, New York, USA
Sous-groupe Stabilité

15-16 août 1997, Vienne, Autriche
Sous-groupe Hydrologie et Pierre Perrochet (EPFL)

24-27 octobre 1997, Lewis, Wisconsin, USA
Réunion plénière, représentants du CEA et Consultants.

Documentation

La publication en deux volumes « Les Atolls de Mururoa et Fangataufa », Volume 1, Géologie, Pétrologie et Hydrogéologie (Guille et al., 1996) et Volume 2, Essais nucléaires, Effets mécaniques, thermo-lumineux et électromagnétiques (Bouchez et Lecomte, 1996), disponibles (en français) [††] dès le début de l'étude, ont fourni un point de vue général et complet sur les travaux du CEA, et sur les conséquences des expérimentations nucléaires sur les atolls. Cette publication était complétée par un certain nombre de thèses de doctorat et de publications de travaux liés à l'hydrologie des atolls et à leur structure. Des exemplaires des rapports des trois précédentes missions, la mission de 1982 conduite par le Professeur Haroun Tazieff (décédé depuis) (Tazieff, 1982) suivie, en décembre 1983, par un groupe originaire de Nouvelle Zélande, Australie et Papouasie Nouvelle Guinée, conduit par M. H.R. Atkinson (MoFA, Nouvelle Zélande, 1984) puis par la Mission scientifique de la Calypso, en juillet 1987, conduite par le Commandant Jacques-Yves Cousteau (décédé depuis) (Fondation Cousteau, Paris, 1988)[‡‡] ont également été fournis.

Ces documents ont été complétés ultérieurement par une série, mise à jour et plus détaillée, de 12 rapports techniques préparés par les scientifiques du CEA (de nouveau en français et en anglais). Ces documents, référencés ici comme Documents DIRCEN/CEA[¶¶] n^{o}1 à 12, ont été intensivement utilisés par la Commission et sont disponibles à la Documentation Française (voir la liste après les Références pour le détail).

Quoique la publication plus tardive que prévu de ces rapports ait été initialement une source de gêne pour les membres de la CGI, on peut estimer, rétrospectivement, qu'elle a eu un effet positif, en ceci que les membres ont été contraints de reconstruire une compréhension qui leur soit propre de la mécanique des explosions nucléaires souterraines et de leurs effets sur la stabilité et l'hydrologie des atolls. Ceci a fourni l'occasion d'une intelligence des phénomènes, formée de manière indépendante, plus profonde que ne l'aurait permis une approche qui aurait plutôt été fondée sur une revue critique des rapports du CEA quand ils eussent été disponibles.

Une information plus précise aurait permis des analyses plus détaillées dans plusieurs domaines. Les coordonnées précises des essais Nestor, Priam et Tydée, par exemple, auraient permis une meilleure compréhension des facteurs qui sont à l'origine des glissements sous-marins produits par ces essais. Pourquoi, par exemple, l'explosion Tydée

[††] Une version en anglais des passages du Volume II qui se rapportent aux essais souterrains (les parties 4 à 9, plus annexes) a été mise à la disposition des groupes de travail de l'AIEA et de l'IGC par le DIRCEN/CEA. La publication d'une version complète officielle du Volume 2 est prévue par le CEA/DASE.

[‡‡] La visite du Commandant Cousteau et les résultats concernant Mururoa constituent aussi une partie de la vidéo « Tahiti, L'eau de feu » disponible à : Équipe Cousteau, 7, rue Amiral d'Estaing, 75016 Paris (tél. 33 1 53 67 77 77 ; fax 33 1 53 67 77 71).

[¶¶] DIRCEN (Direction des Centres d'Expérimentation Nucléaire) est une direction de l'armée française qui est en charge, avec le CEA/DAM, des sites d'essais.

a-t-elle provoqué un glissement situé à 2 km (approximativement) à l'ouest de l'explosion, plutôt que sur la pente la plus proche, comme on aurait pu l'attendre ? Peut-on dire que les glissements associés à Nestor et Priam étaient de ce dernier type, plus classique, et que Tydée est une anomalie, à relier peut-être à des variations locales dans la nature des pentes sous-marines ?

Dans le même esprit, les scientifiques du CEA ont mesuré les variations de la température avec la profondeur dans les puits où étaient placés les engins, sinon systématiquement, en tout cas avant un grand nombre d'essais ; mais ces données n'ont pu être mises à la disposition de la CGI parce que, de nouveau, cette information aurait pu permettre d'identifier les localisations individuelles des essais, que le CEA ne souhaitait par révéler. Ces données auraient permis à la CGI de développer une simulation tri-dimensionnelle plus précise de l'hydrologie de Mururoa. Finalement, après que les simulations de la CGI furent achevées, des données ont été fournies sous la forme des contours de température minimale (voir Figure 6.12). La confrontation avec les données est d'ailleurs considérée comme très bonne, eu égard à l'information disponible au moment où la simulation a été effectuée.

Il faut aussi reconnaître que, même si les coordonnées précises de chaque essai avaient été rendues accessibles à la CGI, une incertitude significative serait demeurée quant aux caractéristiques géomécaniques de la roche au voisinage d'un essai - conséquence de l'hétérogénéité inhérente aux propriétés mécaniques d'un massif rocheux tel que celui constitué par les roches volcaniques des atolls.

Le CEA doit avoir eu des indications sur ces variations, à la suite des observations effectuées pendant le forage des puits destinés aux engins. L'essai Lycos par exemple, conduit sous le lagon à Fangataufa, le 27 novembre 1989, était conçu pour avoir au-dessus de la cheminée produite par l'explosion une couverture nominale de roches volcaniques intactes de 140 mètres d'épaisseur. Des relâchements de tritium provenant de cet essai ont été détectés dans les carbonates peu après l'explosion (Document DIR-CEN/CEA n^{o}9). Ceci indique que la perméabilité de la couverture (et donc aussi, la vitesse de l'eau souterraine) étaient considérablement plus élevées qu'on ne l'aurait attendu pour des roches volcaniques intactes.

Les scientifiques du CEA ont indiqué qu'ils ont rencontré des difficultés en forant le puits destiné au tir Lycos, en raison de la qualité médiocre du massif volcanique au-dessus de la région de la (future) cheminée. On pense que la zone annulaire autour du trou a pu être significativement endommagée par le forage, conduisant à la formation d'une « zone de roche perturbée » (DRZ)[§§] dans cet annulaire. De ce fait, même si la perméabilité du remplissage en béton du trou était faible, cet annulaire pourrait avoir

[§§] Le développement d'une zone de roche perturbée (« disturbed rock zone », ou DRZ) autour des excavations souterraines est un phénomène bien connu qui constitue un sujet de préoccupation dans le cas du scellement des enfouissements de déchets nucléaires souterrains.

eu une conductivité hydrologique suffisamment élevée pour permettre un relâchement précoce de tritium.

Les scientifiques du CEA considèrent que la plupart des cas de relâchement précoce de tritium sont associés aux essais CRTV (Cheminée Rejoignant le Toit du massif Volcanique). Comme indiqué dans l'Annexe C et sur le Tableau C.1 (réalisés pour l'étude de l'AIEA sur le relâchement des radionucléides), aucun relâchement n'a été détecté à ce jour pour 121 des 147 essais souterrains. Ceci suggère que les couvertures surmontant les cheminées produites par ces essais sont restées suffisamment intactes et fournissent des barrières substantielles à l'écoulement de l'eau souterraine et au transport des radionucléides contenus dans la cheminée.

Remarque finale à propos des conclusions

Dans le présent rapport, les bases scientifiques des conclusions de la CGI sont exposées de manière suffisamment détaillée pour permettre à d'autres experts de comprendre comment la Commission a tiré ses conclusions. On croit que, malgré les limitations d'accès à certaines données, la Commission a eu les moyens de parvenir à une bonne compréhension, du point de vue de leurs conséquences sur la stabilité et l'hydrologie, des essais souterrains ; et que les conclusions qui en ont été tirées sont bien fondées et robustes.

L'occasion d'une discussion ouverte du rapport de la CGI sera offerte lors de la tenue du 9ème Congrès International de Mécanique des Roches, organisé par la SIMR, qui se déroulera du 25 au 28 août 1999 à Paris. Tous les collègues intéréssés sont invités à participer à cette discussion. Les membres de l'IGC prépareront et soumettront également des articles basés sur la présente étude pour publication dans des revues scientifiques internationales à Comité de Lecture. Des précisions sur la session consacrée aux essais nucléaires souterrains seront annoncées en 1999 par la SIMR[***].

[***] Pour toute précision, contacter : Congrès SIMR, c/o G. Vouille, Ecole des Mines de Paris, 35, rue Saint-Honoré, F-77305 Fontainebleau, France (téléphone : +33-1-64.69.48.97 / fax : +33-1-64.69.47.11 / e-mail : congres-paris.99@cges.ensm.fr / internet : www.ensmp.fr/ISRM99.

REMERCIEMENTS

Ce rapport marque la conclusion de ce qui fut, officiellement, une étude d'un an et demi, dont le contenu avait été défini par un contrat passé entre le Gouvernement français et l'Université du Minnesota. En fait il a fallu près de trois années pour que cette étude soit menée à son terme par la Commission Géomécanique Internationale (CGI), un groupe international indépendant d'experts réuni spécifiquement pour cette étude.

Ce retard ne résulte pas d'un intérêt insuffisamment soutenu pour le sujet. Au contraire, ce retard est fondamentalement une conséquence de la détermination de la CGI à établir des fondations scientifiques et techniques solides sur lesquelles sont basées son examen des conséquences des essais nucléaires souterrains sur la stabilité et l'hydrologie de Mururoa et Fangataufa. Il a été nécessaire d'entreprendre des analyses fondamentales concernant une large variété de sujets, afin d'être en position d'effectuer une évaluation indépendante de l'information et des données fournies par les autorités du CEA (Commissariat à l'Energie Atomique). On peut se faire une idée de cette tâche en examinant les sujets couverts par les annexes du rapport. Dans beaucoup de cas, ces annexes ne contiennent qu'un résumé d'analyses dont le développement a souvent exigé des efforts considérables.

Cela a été un privilège, et une expérience unique, que de travailler avec les collègues de la CGI et les deux groupes principaux de consultants - Itasca Consulting Group, Inc., de Minneapolis, USA, pour les études de stabilité et le support administratif ; et l'Ecole Polytechnique Fédérale de Lausanne (EPFL), en Suisse, pour les études hydrologiques et les illustrations réalisées par ordinateur. Le professeur E. Detournay a dirigé et coordonné les études de stabilité ; le docteur L. Townley et le professeur G. de Marsily ont dirigé et coordonné les études hydrologiques.

Les consultants Branko Damjanac et Peter Cundall, d'Itasca, et Pierre Perrochet et Laurent Tacher, de l'EPFL, ont assisté à toutes les réunions de la CGI (à l'exception de la première réunion plénière de juillet 1996) et apporté des contributions inestimables, en plus d'avoir préparé des parties majeures des analyses et des résultats contenus dans ce rapport. De la même manière le professeur Pierre Bérest de l'Ecole Polytechnique à Palaiseau, France, liaison technique entre la CGI et les autorités françaises, a apporté un concours précieux.

Les membres de la CGI n'avaient pas travaillé ensemble auparavant en tant que groupe, mais un climat de travail extrêmement productif s'est rapidement mis en place. Le croisement des disciplines et le désir d'appréhender tout à la fois les principes sous-jacents aux idées présentées et les implications spécifiques à l'étude conduisirent à des échanges enrichissants et stimulants, améliorèrent la compréhension des sujets abordés et produisirent finalement un rapport mieux étayé.

Les visites de Mururoa et Fangataufa, et des installations géophysiques du CEA à Tahiti, en juillet 1996, constituèrent un moment essentiel de l'étude de la CGI ; elles permirent d'apprécier et de comprendre certains traits du programme d'expérimentation nucléaire sur les atolls, et furent à cet égard irremplaçables. Des personnels scientifiques et techniques de haut niveau du DIRCEN/CEA (voir les notes de bas de page dans la Préface) accompagnèrent à cette occasion les membres de la CGI, en fournissant des commentaires, présentant des exposés et répondant aux questions tout au long des visites. Les caméras et enregistrements vidéos étaient autorisés sans restriction. L'auteur de ces lignes a visité de nouveau les atolls en décembre 1966 en tant que membre d'un groupe d'étude de l'Agence Internationale pour l'Energie Atomique (AIEA), et eut ainsi l'occasion de réexaminer des zones qui présentaient un intérêt particulier du point de vue de la stabilité de l'atoll. Ces échanges complétèrent de manière appréciable l'information contenue dans les rapports et documents DIRCEN/CEA, comme l'ont aussi permis plusieurs discussions techniques entre l'équipe DIRCEN/CEA et la CGI (voir la Présentation d'Ensemble). Les efforts considérables consentis par l'équipe DIRCEN/CEA pour rendre ces visites utiles et agréables ont été très appréciés.

Des collègues de membres individuels de la CGI ont apporté des contributions techniques importantes à l'étude. En particulier le docteur Carlos Carranza-Torres, précédemment membre de l'Université du Minnesota, a conduit les analyses et simulations par ordinateur des annexes H.1 et I, et a préparé les illustrations. Egalement membres de l'Université du Minnesota, le docteur Igor Iankovic et Philippe Le Grand ont entrepris les analyses et simulations par ordinateur de l'annexe E, et Madame Haiying Huang a conduit les analyses tridimensionnelles discutées au chapitre 5.4 (Figures 5.12 à 5.14). Le Docteur Anthony Smith de la Division of Land and Water du CSIRO a réalisé plusieurs simulations numériques au moyen du logiciel AQUIFEM-P pour l'annexe relative à l'analyse de l'écoulement périodique de l'eau souterraine. Le Professeur P.A. Persson de l'Institute of Science and Mining Technology du Nouveau Mexique nous a fourni l'information sur l'énergie des explosifs TNT qui a été utilisée pour une note de bas de page de la Présentation d'Ensemble.

L'Université Paris VI, l'Ecole des Mines de Paris et l'Ecole polytechnique ont aimablement mis des moyens à la disposition de la CGI pour l'organisation de plusieurs réunions.

Le docteur Elena Luquet de l'Institut de Physique de la Terre de Moscou a aidé le professeur Nikolaevskiy à l'occasion de la préparation de documents destinés à la CGI.

De nombreuses personnes ayant connaissance d'aspects divers du programme d'essais nucléaires américain ont aussi fourni une information appréciée. Le docteur Charles Archambeau (TRAC, Inc., Denver, Colorado), un sismologiste éminent, a fourni une information de base extrêmement utile et des suggestions constructives lors des premières étapes de l'étude de la CGI ; Norman R. Burkhard, du Lawrence Livermore National Laboratory, à Livermore en Californie, a mis à notre disposition un ensemble non-classifié de Comptes Rendus (Proceedings) des Symposia on Containment of Underground Nuclear Explosions ; les docteurs John T. Cherry (Président de Science Horizons, Inc., Missouri) et Theodore R. Butkovich (maintenant en retraite), qui jouèrent un rôle de pionniers dans les premiers efforts de modélisation analytique et numérique des explosions souterraines, ont fourni des commentaires précieux au cours des études initiales de la CGI, à l'occasion d'entrevues avec le professeur Nikolaevskiy ; le docteur Edward W. Peterson (S- cubed, à San Diego en Californie) a fourni des aperçus extrêmement utiles sur les mécanismes d'expansion des cavités mais aussi sur l'endommagement de champ proche (voir annexe D).

Les textes provisoires de certaines sections du rapport de la CGI ont été adressés pour relecture extérieure à des experts internationaux réputés. Le docteur B. H. G. Brady, professeur de géomécanique et Doyen de la faculté d'ingénierie de l'Université d'Australie Occidentale á Perth, et le docteur Shunsuke Sakurai, professeur de génie civil à l'université de Kobé au Japon, et président actuel de la Société Internationale de Mécanique des Roches, ont tous deux fourni des commentaires précieux et indépendants sur les sections du rapport relatives à la stabilité (les chapitres 3 à 5).

Des collègues engagés dans les études techniques conduites par l'AIEA, en particulier Rober Fry (Directeur technique, étude IAC, à Vienne, Autriche), Des Levins (ANSTO à Sydney, Australie), Lars Eric de Geer (Ministère suédois de la Défense à Stockholm, Suède), Eberhardt Mittelstaedt (Agence fédérale maritime et hydrographique, à Hambourg, Allemagne) et les collègues du Groupe de travail 4 de l'AIEA, J. Hadermann (Institut Paul Sherrer à Villigen en Suisse), H. Nitsche (Institut de radiochimie, Dresde, Allemagne), A.S. Sastratenaya (Agence nationale de l'énergie atomique, Djakarta, Indonésie) et G. Warnecke (AIEA à Vienne, Autriche) ont fait part de nombreuses questions et remarques qui ont conduit à des modification et des compléments au rapport de la CGI.

Des échanges avec des responsables administratifs et techniques du Commissariat à l'énergie Atomique (CEA) et de la Direction des centres d'expérimentations nucléaires (DIRCEN) - Le général M. Boileau, les colonels P. Delcourt et G. Corion et Madame T. Delpech ; MM. Alain Barthoux, Jacques Bouchard, Jacques Bouchez, Yves Caristan, Christophe Guy et Jean François Sornein - ont été indispensables tout au long de l'étude de la CGI. En toute circonstance, les membres de la CGI ont été reçus avec une courtoisie et un sens de l'hospitalité exceptionnels, malgré la réserve et l'équilibre parfois délicat qu'appelaient la nécessité d'éviter de révéler certaines informations considérées

comme confidentielles, et la nécessité de s'abstenir à certains moments de commentaires pour respecter l'indépendance des conclusions de la CGI. Les relations particulièrement étroites entretenues avec le docteur Caristan et ses collaborateurs, J. Bouchez et J.F. Sornein, ont permis à la CGI de se faire une très haute idée non seulement de leurs compétences professionnelles, mais aussi de leur sens de la diplomatie.

Steve L. Crouch, doyen associé, a assuré le suivi du projet au nom de l'Université du Minnesota ; sa diligence a permis de résoudre rapidement divers problèmes administratifs.

Plusieurs des membres de la CGI ont accueilli des réunions de la Commission, qui ont constitué des événements privilégiés et mémorables. Anthony et Emma Pearson ont organisé la réunion de Cambridge, G.B. ; Ghislain et Gunilla de Marsily ont organisé la réunion en Provence, en France ; Kathy Sikora et ses collègues d'Itasca ont coordonné la réunion de Lewis dans le Wisconsin aux USA.

Le professeur Bérest, aidé de B. Brouard de l'Ecole polytechnique, ont pris en charge la tache formidable de traduire et assembler les éléments qui constituent le Volume III. Ce travail a été soigneusement examiné et validé par les membres de la CGI, et fait partie intégrante du rapport de la CGI. Nous mesurons notre dette vis-à-vis de MM. Bérest et Brouard pour les efforts considérables qu'ils ont proposé de prendre en charge, et qui rendent notre rapport facilement accessible á un plus grand nombre de lecteurs.

Kathy Sikora a assuré la coordination administrative de l'étude de la CGI, l'organisation de toutes les réunions, la préparation et la distribution des documents, la communication avec les membres et une multitude d'autres tâches, parmi lesquelles le fantastique défi constitué par l'intégration de tous les éléments nécessaires pour produire le présent rapport - un tour de force qui mérite l'admiration. Chad Sylvain, d'Itasca, a transcrit et assuré la présentation des fichiers graphiques, fournis sous des formats très variés par les membres de la Commission, les consultants et le DIRCEN/CEA ; on lui doit les remarquables illustrations contenues dans le rapport.

Donna Ahrens, rédacteur scientifique indépendant, a supervisé l'intégration éditoriale du rapport, la conception de la couverture, la préparation du glossaire et l'ensemble des tâches associées à la responsabilité de l'édition.

Ma femme Margaret m'a aidé de bien des manières, dont la moindre n'a pas été d'accepter les nombreux week-ends et nuits tardives (bien plus nombreuses que prévu) consacrés à l'achèvement du rapport, à sa frappe et à la relecture de plusieurs sections du texte final.

A tous, et à beaucoup d'autres, nous adressons nos remerciements et notre gratitude, et formulons l'espoir que le résultat soit à la hauteur des efforts qu'ils ont consentis.

Charles Fairhurst
Minneapolis

TABLE DES MATIÈRES

LISTE DES FIGURES

LISTE DES TABLEAUX

RÉSULTATS, CONCLUSIONS ET RECOMMANDATIONS

Le présent rapport expose les résultats d'une étude de trois ans consacrée aux effets des expérimentations nucléaires souterraines sur la stabilité mécanique et le fonctionnement hydrogéologique des atolls de Mururoa et Fangataufa, en Polynésie française. Cette étude a été conduite par la Commission Géomécanique Internationale (CGI), groupe indépendant d'experts constitué spécialement à cet effet.

La CGI s'est d'abord efforcée de comprendre, au moyen de modélisations, les phénomènes fondamentaux à l'œuvre lors d'un tir nucléaire souterrain et la manière dont ils peuvent modifier la situation préexistante. Cette étape a servi de base à l'évaluation des informations relatives aux problèmes de stabilité et d'hydrogéologie fournies par le Commissariat à l'Énergie Atomique (CEA). Les résultats, conclusions et recommandations principales sont résumés ci-dessous.

Résultats et conclusions

Les commentaires ci-après se rapportent aux effets structurels et hydrogéologiques sur les atolls provoqués par les 137 essais nucléaires souterrains et 3 essais de sûreté « nucléaires » de Mururoa[†††], et par les 10 essais nucléaires souterrains de Fangataufa, conduits entre 1975 et 1996.

Résultats généraux

1° Le volume de roche volcanique endommagée par les essais nucléaires souterrains à Mururoa et Fangataufa représente environ, dans chacun des atolls, 5% du volume total de l'intervalle compris entre les profondeurs de 500 mètres et 1500 mètres, intervalle à l'intérieur duquel sont contenus les dommages portés aux roches volcaniques par les explosions (voir l'annexe H). Aucun dommage n'a affecté les roches volcaniques au-delà d'une profondeur de 1500 mètres.

   De plus, les premiers essais (1975-1980) conduits dans le massif volcanique sous la couronne corallienne à Mururoa ont eu pour conséquence dans les 150 à 200 premiers mètres de roches carbonatées sous la surface du sol, directement à

[†††] Trois des dix essais de sûreté souterrains conduits à Mururoa ont eu pour résultat une petite explosion souterraine (voir annexe C, Tableau C4, Catégorie 3).

l'aplomb des essais, des déformations et des fracturations produites par les explosions. Des affaissements de la surface du sol atteignant jusqu'à 2 mètres et plus ont accompagné ces déformations (voir Figure 1.23). Le volume affecté représente environ 3% de l'épaisseur totale des carbonates de l'atoll, qui est de 500 mètres (voir annexe H).

2º Comme discuté ci-dessous, certains dommages portés à la couronne sud-ouest de Mururoa ont eu pour conséquence des glissements de terrain sous-marins, contemporains des explosions de 1977-1979. La couronne nord-est est affectée d'une déformation de fluage ininterrompue depuis près de deux décennies.

Certaines zones d'essais ont été plus largement affectées que d'autres (voir annexe H pour l'analyse détaillée), mais les programmes d'essais souterrains n'ont pas affecté de manière significative les régions des atolls extérieures à ces zones d'essais. À l'exception de la région nord-est de Mururoa, qui est le siège d'une déformation de fluage, toutes les parties de Mururoa et Fangataufa sont maintenant mécaniquement stables et il n'y a pas eu de modification, à l'échelle de l'atoll, que ce soit à court ou à long terme*, de la stabilité mécanique globale de Mururoa et de Fangataufa.

3º Les principales conséquences visibles des tirs souterrains sont : (a) des glissements de pentes sous-marines, (b) des fractures ouvertes observables à la surface du sol, et (c) des affaissements de surface. (Tous ces dégâts font partie du volume endommagé estimé plus haut).

4º Au moins 95% de l'énergie relâchée dans le sous-sol par l'explosion nucléaire est dissipée dans une zone délimitée par un rayon de 500 mètres (ou moins) autour de la source de l'explosion et 90% au moins de cette énergie est dissipée dans une zone délimitée par un rayon de 250 mètres (ou moins). La roche au-dessus du point d'explosion s'effondre sur une hauteur de l'ordre de 450 mètres et un rayon de l'ordre de 55 mètres (ou moins, suivant l'énergie de l'explosion), de sorte qu'une « cheminée » remplie de remblais entoure chaque point d'explosion (voir Présentation d'Ensemble).

Les fractures de surface sont en général associées à des glissements latéraux des pentes sous l'océan. Ces effets n'affectent que les carbonates. Il n'y a aucune raison de penser que des glissements de pente ou des affaissements soient survenus dans le massif volcanique sous-jacent. Les carbonates dans la couronne sud-ouest de Mururoa d'une part, dans la couronne nord-ouest de Mururoa et Fangataufa d'autre part, présentent des différences géologiques qui modifient substantielle-

*Le « court terme », ici, inclut la période qui va du début des essais jusqu'à 500 ans environ après la fin des essais. Le « long terme » implique la période allant de 500 ans à 10 000 ans, ou plus, après la fin des essais.

ment la nature des instabilités des pentes. (voir Présentation d'Ensemble, Section 1.7).

5º Il n'y a pas d'impact significatif sur le comportement hydrogéologique à long terme (500 ans et au-delà) des deux atolls provoqué par les tirs ou les essais (les estimations des modifications à long terme du débit total naturel de l'eau souterraine ne sont jamais supérieures à 1% ; voir Chapitre 7, Section 7.5).

6º L'accroissement de température au voisinage de chaque point de tir provoque une augmentation locale de la composante ascensionnelle de la vitesse de l'eau souterraine dans le massif volcanique sus-jacent. Cet accroissement diminue à peu près comme une exponentielle du temps en même temps que la chaleur de l'explosion diffuse dans le massif ; la vitesse ascensionnelle de Darcy dans le massif volcanique augmente, depuis la valeur de 8 mm par an avant le tir jusqu'à des valeurs variant de 0,1 à 1,3 m par an, (suivant les hypothèses retenues dans le modèle), après une période courte (un an après l'essai) dans tous les cas où existe une couverture volcanique intacte suffisante au-dessus de la cheminée engendrée par l'explosion. Cette vitesse décroît pour atteindre à peu près la moitié de sa valeur maximale après 10 ans et se stabiliser à 3 cm par an après 500 ans. La vitesse de Darcy dans les carbonates, au-dessus du massif volcanique, n'est pas affectée significativement par les tirs. Dans le cas de tirs pour lesquels il n'y a pas de couverture, ou pour lesquels la couverture est endommagée, on doit multiplier par un facteur voisin de 50 les valeurs indiquées ci-dessus pour les vitesses dans le massif volcanique au-dessus de la cheminée résultant de l'explosion. Ainsi, dans le cas de ces tirs, les vitesses dans les carbonates passent de 2 m par an avant l'essai à des valeurs de l'ordre de 60 m par an après une année, puis décroissent jusqu'à 5 m par an après 500 ans.

7º En utilisant les résultats sur lesquels sont fondées les conclusions (5) ci-dessus, il est possible de prévoir le transfert de radionucléides depuis les cavités résultant de l'explosion vers l'environnement. La CGI a procédé à une estimation du relâchement de tritium dans les lagons des deux atolls qui est en bon accord avec les valeurs observées, et qui conforte donc les valeurs estimées des vitesses de l'eau dans le massif volcanique et les carbonates. Le relâchement de tritium a atteint son paroxysme à Mururoa aux environs de 1997 et connaîtra son paroxysme à Fangataufa aux environs de 2000 ; il décroîtra ultérieurement. Les concentrations concernées de tritium dans les lagons sont extrêmement faibles, et sans conséquences en termes radiologiques.

8º Le relâchement des autres nucléides vers l'environnement a été estimé par l'Agence Internationale de l'Énergie Atomique (AIEA, 1998b) à partir des vitesses de l'eau souterraine fournies par la CGI. L'AIEA a trouvé que les conséquences radiologiques de ces relâchements ne méritent pas d'être considérées.

9º Dans le futur très lointain (c'est-à-dire d'ici 20 000 à 60 000 ans), une nouvelle glaciation peut faire chuter le niveau de la mer de 100 à 150 mètres. Un aquifère d'eau douce apparaîtra alors dans le niveau calcaire des îles émergées. Ces couches carbonatées pourraient être contaminées par du plutonium, avec des risques potentiels pour la population des îles. L'AIEA (1998d) a évalué ces risques et a conclu qu'ils ne constituaient pas une préoccupation significative.

Questions spécifiques

Glissement des pentes

1º Un ou plusieurs glissements de pentes sous-marines peuvent survenir au sein des carbonates, dans la zone de la couronne nord-est de Mururoa (zone d'essais 1). Une déformation continue de la pente du côté océan a été observée dans cette zone depuis la fin des années 70 et pourrait conduire à un ou plusieurs grands effondrements de pente dans le futur. Le volume total de roches soumis à cette déformation est de 0,6 km^3 environ, c'est-à-dire six fois le volume du glissement initial qui a résulté du tir Tydée en 1979.

Les mesures (effectuées par le CEA) ont clairement montré que les mouvements sont dus à des déformations localisées, de type fluage, qui affectent, à une profondeur de 500 m environ, une zone plus faible, plus fragile, de « calcaires crayeux » (voir Figure 5.9 et la discussion dans le Chapitre 5). Même s'il y a quelques indications que les vitesses de déformation diminuent actuellement, et pourraient même s'annuler, il n'en reste pas moins que les déformations accumulées dans les calcaires crayeux au cours des 20 dernières années, qui sont proches de 0,5%, peuvent avoir endommagé de manière significative les calcaires de sorte que l'éventualité d'une accélération de la déformation conduisant à une rupture ne peut être exclue.

2º On ne doit pas attendre dans la couronne sud-ouest de Mururoa de nouvelles instabilités de pente et/ou des effondrements majeurs consécutifs aux tirs. Les grandes ruptures sous-marines qui ont affecté cette zone (zone d'essais 4) sont survenues entre 1977 et 1979 et étaient directement liées, géographiquement et chronologiquement, à des tirs de grande puissance bien identifiés, tels que Nestor, Priam et Tydée. Le plus grand glissement de pente (volume estimé = 0,1 km^3) était consécutif au tir Tydée. Cet effondrement a été suivi de quelques ruptures affectant des volumes plus petits. La surveillance microsismique effectuée dans cette région indique une absence d'activité significative dans les pentes depuis la période des essais.

3º Des effondrements de pente liés au processus naturel de construction des atolls par accumulation de coraux surviendront, comme il en est survenu dans le passé (à l'échelle géologique) ce dont témoignent les accumulations sous-marines profondes de sédiments, dans cette région du Pacifique comme dans d'autres.

Affaissements

1º La simulation par ordinateur des effets dynamiques des explosions souterraines, effectuée par la Commission, permet d'expliquer les affaissements de la surface du sol observés dans les carbonates au-dessus de la couronne nord-est (zone d'essais 1) et au sud-est (zones d'essais 2, 3, 4) de Mururoa (voir Figure 1.23).

2º Les calculs effectués par la CGI montrent que le mécanisme principal à l'origine de ces affaissements est une distorsion à volume quasi constant, plutôt que la compaction superficielle invoquée par le CEA. Ce mécanisme de distorsion conduit aussi à des déformations latérales significatives et à une fracturation des carbonates dans les pentes sous-marines peu profondes (environ jusqu'à 150 à 200 m de profondeur) du côté de l'océan. Une fracturation substantielle des pentes du récif carbonaté avait été notée au cours des observations sous-marines effectuées par la mission Cousteau (Une partie des fracturations observées par le Commandant Cousteau pourrait résulter de l'effondrement naturel des pentes). Des déformations de distorsion affectent également la couronne du côté du lagon (voir Volume II, Figure 1.25).

3º Les affaissements de surface décrits ci-dessus ne surviennent que dans les parties des zones d'essais sous la couronne où les profondeurs adimensionnelles des tirs (voir Chapitre 4 et annexe D, Figure D.1) étaient relativement faibles. Les analyses de la CGI indiquent que les affaissements du fond du lagon qui résultent des essais conduits sous le lagon sont vraisemblablement beaucoup plus faibles que les affaissements correspondants qui résultent des essais conduits sous la couronne.

4º Les calculs effectués par la CGI confirment les assertions du CEA quant au caractère exclusivement superficiel des affaissements observés en surface c'est-à-dire que ces derniers restent confinés dans la partie supérieure des carbonates et ne se prolongent pas jusqu'au massif volcanique ; il n'y a pas de communication directe entre les zones affaissées de surface et l'ensemble chambre/cheminée créé par l'explosion, au contraire de ce qui a été observé au Nevada Test Site aux États-Unis.

5º Des affaissements de 2 mètres et plus sont survenus dans les zones d'essais 1 et 4 de Mururoa. Certaines parties de la zone d'essais 4 sont maintenant immergées (voir Figure 1.22). Une activité de construction corallienne vigoureuse (une accumulation de l'ordre de plusieurs cm par an) a été observée dans ces zones, de sorte que les affaissements pourraient être effacés après une période de 100 à 300 ans. Cependant une croissance active importante du corail au-dessus du niveau de l'océan est improbable, de sorte que la restauration du récif corallien à son niveau antérieur au-dessus du niveau de l'océan ne paraît pas vraisemblable.

Confinement et relâchements

1º Les modèles de calcul par ordinateur indiquent l'existence d'une couverture volcanique intacte au-dessus et autour de la plupart des cavités résultant des essais, comme dans la zone d'essais 1 à Mururoa (voir Figure 1.17). D'ailleurs, les profondeurs auxquelles sont placées les charges dans les essais souterrains à Mururoa et Fangataufa sont beaucoup plus grandes que celles jugées nécessaires pour assurer le confinement des explosions souterraines au Nevada Test Site aux États-Unis. De ce fait on pense que tous les essais de Mururoa et Fangataufa sont restés confinés (voir annexe D).

2º Les ingénieurs du CEA indiquent que le sommet de la cheminée engendrée par l'explosion a atteint la limite supérieure du massif volcanique au cours de 12 essais (appelés essais CRTV) conduits sous la couronne de Mururoa durant la période 1976-1980 (voir Figure 1.17).

3º Quoiqu'un relâchement, dans le sens classique d'une émission directe de radionucléides gazeux à l'atmosphère, ne soit probablement pas survenu dans les atolls, il y a des preuves claires, selon les observations du CEA, d'un relâchement précoce (c'est-à-dire quelques années après l'explosion) de tritium, strontium et césium à la limite supérieure du massif volcanique en direction de la base des carbonates, dans le cas d'une quinzaine environ des 147 tirs souterrains conduits sur les deux atolls. Ceci indique clairement : (1) soit que la couverture volcanique a été significativement endommagée par l'explosion, comme c'est le cas pour les essais CRTV, (2) soit que l'intégrité et/ou la perméabilité initiale de la couverture volcanique au-dessus du point de tir (par exemple, dans le cas du tir Lycos à Fangataufa) étaient significativement différentes de ce qui était attendu. À la date d'aujourd'hui, seule une petite fraction de ces relâchements de radionucléides a atteint les lagons (voir annexe S).

Hydrologie

1º Le comportement hydrologique global naturel de Mururoa et Fangataufa est typique d'un atoll ; on peut considérer qu'il est bien compris. (Une grande partie de cette compréhension résulte des études conduites par le CEA).

2º Les essais nucléaires n'auront pour l'essentiel pas d'effet à long terme sur l'hydrologie des atolls.

3º Les hétérogénéités et variations locales considérables des propriétés des roches, qui affectent aussi bien les carbonates que le massif volcanique, n'ont qu'une influence locale limitée sur la forme de l'écoulement de l'eau. Les zones karstiques des carbonates ont un effet plus global (voir 4.).

4º L'hydrologie des carbonates est considérablement compliquée par l'existence, dans différents horizons, de nombreux niveaux karstiques de grande extension et très perméables. Ces couches transmettent les influences de la marée océanique jusqu'à l'intérieur des carbonates et engendrent un brassage intense au sein de toute la couche carbonatée.

5º La complexité de l'écoulement dans les carbonates introduit une difficulté dans l'analyse de l'écoulement de l'eau du massif volcanique vers les carbonates. L'examen des concentrations de tritium dans la partie inférieure des carbonates et des relâchements dans les lagons de Mururoa et Fangataufa suggère qu'un brassage considérable des eaux s'effectue dans les carbonates (voir annexe S).

6º Une ère de glaciation mondiale survenant dans quelques dizaines de milliers d'années conduirait au développement de lentilles importantes d'eau douce souterraine sur chacun des deux atolls ; elles rendraient possible l'alimentation en eau d'une population permanente. (voir Conclusions (8) dans les Résultats Généraux et Conclusions, ci-dessus).

Volcanisme

Il n'y a aucune possibilité de réactivation du volcanisme dans les atolls à la suite des essais souterrains. Les atolls sont des volcans éteints, qui ne sont plus reliés aux « points chauds » qui avaient constitué les sources de leur développement (voir Chapitre 2).

Risque sismique

L'amplitude de l'onde sismique produite par les essais nucléaires à Mururoa et Fangataufa est bien trop petite pour avoir une influence sur le risque d'occurrence d'un tremblement de terre dans d'autres régions de la surface terrestre (voir annexe C).

Observations et recommandations

Stabilité de l'atoll et surveillance

Mururoa

Le système d'instrumentation/surveillance à distance proposé dans le Document DIRCEN/CEA nº12 (voir Présentation d'Ensemble), pour une observation continue au cours de la décennie à venir de la stabilité de la couronne nord-est de Mururoa, apparaît comme complet. Ce système de surveillance devrait permettre de prendre les dispositions adéquates permettant d'éviter tout risque sérieux résultant des effets d'un effondrement de pente dans la couronne nord-est.

La Commission recommande que le système actuel d'instruments de surveillance des déformations en place dans la région nord-est de Mururoa soit maintenu et contrôlé

pendant les vingt prochaines années ou jusqu'à l'effondrement des pentes, s'il survient pendant cette période. L'information alors disponible (dans 20 ans) devrait permettre d'évaluer de manière plus certaine la stabilité de la pente et la nécessité éventuelle de poursuivre la surveillance. Une accélération éventuelle de la vitesse de fluage fournirait largement à l'avance une mise en garde vis-à-vis d'un risque d'effondrement, qui permettrait de prendre les dispositions préventives de sécurité à Mururoa et sur les atolls voisins susceptibles d'être affectés par un petit tsunami. Des vagues de l'ordre de un à deux mètres, suivant le volume du glissement, pourraient se former, comme cela est arrivé lors du premier de la série des glissements de pente dans la zone d'essais n^{o}4 de Mururoa.

On a observé que le fluage des calcaires crayeux dans la région nord-est de Mururoa était affecté par l'onde sismique résultant des explosions survenant à l'extérieur de la zone d'essais n^{o}1 elle-même. Ceci s'applique aussi aux déformations de pente observées dans la couronne nord-est de Fangataufa.

Fangataufa

Bien qu'on ne dispose que de peu d'informations, hormis celles relatives à l'activité microsismique, quant aux déformations en cours dans la couronne nord-est de Fangataufa, le contexte géologique y paraît analogue à celui de la couronne nord-est de Mururoa.

Aucun essai n'a été conduit dans cette couronne, mais plusieurs tirs de forte puissance ont été effectués sous le lagon. Il est clair que des mécanismes de déformation de la couronne ont été activés par l'onde sismique engendrée par ces explosions. De larges (30 à 40 cm environ) fractures ouvertes, qui apparaissent comme l'élargissement et l'extension de fractures existantes, pour l'essentiel parallèles à la couronne, sont clairement visibles dans cette région.

Le volume de pente sous-marine soumis à une déformation active apparaît comme plus faible dans la région nord-est de la couronne de Fangataufa qu'à Mururoa et, selon ce que le CEA rapporte de la microsismicité locale, la masse rocheuse apparaît s'être stabilisée après les essais de 1992. Les essais de 1995-1996 n'ont pas réactivé ces déformations. Il semble prudent de tenter d'estimer le volume exact concerné, de poursuivre la surveillance de cette déformation et d'évaluer le risque d'un effondrement sous-marin significatif. La Commission recommande que le DIRCEN/CEA rende publiques des informations complémentaires sur le contexte qui lui a permis de conclure que la couronne nord-est de Fangataufa est stabilisée.

Aucune autre instabilité significative due aux expérimentations souterraines à Mururoa et Fangataufa n'est attendue par la CGI.

Le programme actuel de mesure du relâchement de radionucléides dans les carbonates inférieurs et dans les lagons de Mururoa et Fangataufa fournit des informations spé-

cifiques très intéressantes sur les processus hydrogéologiques à l'œuvre dans les atolls (voir annexes S et T). On recommande : (i) de poursuivre ces observations, (ii) de mener des études de modélisation analytique et numérique complémentaires pour mieux établir l'influence des horizons karstiques sur l'écoulement et les processus grâce auxquels a lieu un brassage à grande échelle des eaux qui circulent dans les carbonates.

Chapitre 1

CONSÉQUENCES DES ESSAIS NUCLÉAIRES SOUTERRAINS À MURURUOA ET FANGATAUFA

1.1 Introduction

La décision prise par la France, en 1995, de reprendre les essais souterrains d'armes nucléaires dans les atolls du Pacifique Sud de Mururoa et Fangataufa, a suscité dans le monde entier des protestations et des déclarations selon lesquelles les essais souterrains conduits de 1975 à 1990 avaient entraîné des dommages durables à la stabilité et à l'hydrogéologie des atolls, voire même des effets significatifs au-delà du voisinage immédiat des atolls.

En réponse à ces inquiétudes, le Président Chirac annonçait que deux Commissions composées d'experts indépendants seraient mises en place par la France avec la mission d'examiner, de ces divers points de vue, les conséquences réelles des essais.

Charles Fairhurst, Professeur à l'Université du Minnesota, USA, ancien Président de la Société Internationale de Mécanique des Roches, fut approché par le gouvernement français qui lui demanda de constituer une Commission Géomécanique Internationale (CGI). La mission de la CGI serait de conduire des investigations sur les conséquences des campagnes d'essais nucléaires souterrains entreprises par la France entre 1975 et 1996 à Mururoa et Fangataufa (désignés aussi comme Centre d'Essais du Pacifique, ou CEP), du point de vue de la stabilité et du régime hydrologique des deux atolls. L'Agence Internationale pour l'Énergie Atomique (AIEA) avait été sollicitée dans le même temps afin d'établir un rapport sur les conséquences radiologiques des essais. Du fait que les mouvements des substances radioactives sont directement reliés aux conséquences hydrologiques des essais, trois membres de la CGI ont également participé au groupe de travail de l'AIEA consacré au transport des radionucléides dans le massif rocheux. La composition de la CGI et les canaux par lesquels elle communique avec les autorités françaises (par l'intermédiaire de la DIRCEN, du CEA et du LDG) et avec la Commission mise en place par l'AIEA sont donnés sur la Figure 1.1. Une biographie succincte des membres de la CGI et de l'équipe de collaborateurs est donnée à l'annexe A du volume II.

La DIRCEN/CEA a fourni un ensemble de 12 documents (tous ces documents sont publics et désignés dans la suite comme documents n^o 1, 2, etc...), qui synthétisent toute l'information provenant du CEA (voir la liste après le Chapitre I). Selon le docu-

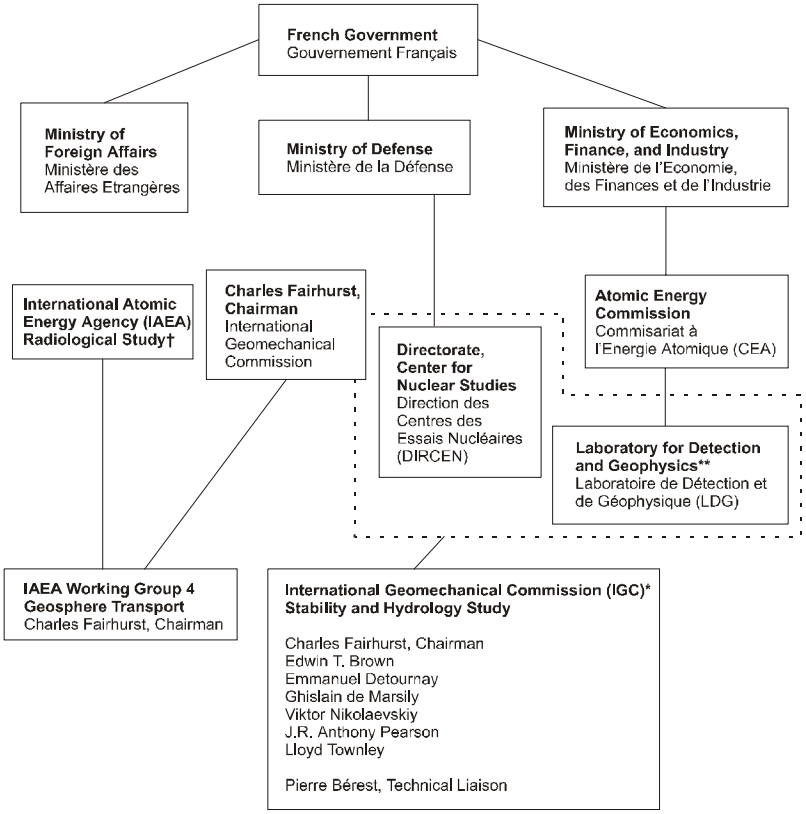

†Results of the IAEA study have been published in a series of reports (*The radiological situation at the atolls of Mururoa and Fangataufa*), prepared by an International Advisory Committee, E. Gail de Planque, Chairman, International Atomic Energy Agency, Vienna, 1998.

**Since 1996, LDG has been a division of the Département d'Analyse et de Surveillance de l'Environnement (DASE) [Department of Analysis and Surveillance of the Environment]

*The IGC was in contact with DIRCEN (for logistical aspects) and with LDG (for scientific aspects)

FIG. 1.1 Composition de l'IGC et ses relations avec d'autres organisations impliquées dans les études sur les atolls

ment DIRCEN/CEA n° 6, la DIRCEN a réalisé au total 147 essais souterrains dans les deux atolls (y compris les essais souterrains dits de sûreté effectués dans les horizons carbonatés), essais qui ont dégagé une énergie totale de 3,2 mégatonnes (Mt), essentiellement à Mururoa (137 essais totalisant 2,4 Mt pour une moyenne de 20 kt par essai). À Fangataufa un plus petit nombre d'essais ont été réalisés, mais de plus grande puissance (10 essais totalisant 0,8 Mt pour une moyenne de 80 kt). Les tirs les plus puissants n'ont pas excédé 150 kt, et plus de la moitié des tirs ne dépassaient pas 10 kt. En comparaison, il faut noter que les explosions aériennes de Hiroshima et Nagasaki étaient d'une vingtaine de kilotonnes, et que des essais thermonucléaires d'une puissance de plusieurs Mt ont été effectués.

Les deux premières explosions souterraines au CEP ont eu lieu en 1975 à Fangataufa sous la partie émergée (la couronne ou platier) de l'atoll. C'est durant cette période que les douze essais CRTV (Cheminée Rejoignant le Toit du massif Volcanique) (voir Figure 1.11) ont été effectués dans les zones d'essais 1, 2 et 3 et qu'un glissement de pente par fluage fut observé pour la première fois dans la couronne nord-est de Mururoa.

De 1981 à 1986, toutes les explosions ont été réalisées à Mururoa, sous la couronne corallienne et sous le lagon. Depuis 1987, toutes les explosions ont été effectuées sous les lagons, tant à Mururoa qu'à Fangataufa. Ces précisions proviennent du document DIRCEN/CEA n° 6 ; le détail des dates des explosions figure dans l'annexe du document DIRCEN n° 2 et dans le Volume II, annexe C du rapport de la CGI. Une évaluation indépendante de la puissance des tirs, fondée sur les données sismiques enregistrées à grande distance, est présentée dans le Volume II, annexe C, du rapport de la CGI.

La CGI fut invitée à visiter les deux atolls, ce qu'elle fit en juillet 1996. Cette visite lui permit d'examiner l'état actuel des parties découvertes des atolls, et notamment de celles sous lesquelles ont été effectués de nombreux essais. Les membres de la Commission ont pu également voir les stations sismologiques et les autres installations de surveillance qui seront maintenues en service (dans le futur) par le LDG (devenu le DASE après 1996). La Commission a été informée de manière détaillée des travaux conduits par le CEA et le LDG en relation avec les essais ; ces travaux comprennent : les expériences conduites avant et après les différents essais pour caractériser l'état mécanique et les propriétés des roches et de l'environnement hydrogéologique ; et les modèles développés pour rendre compte des changements observés. Les documents DIRCEN-CEA ne laissent pas l'impression qu'une grande attention ait été portée aux problèmes géomécaniques pendant la première phase (avant 1980) du programme d'essais. On y trouve certes une description des effets mécaniques génériques des explosions (formation de la cavité et de la cheminée, endommagement du massif rocheux et déformations) mais il y a peu de données publiées sur l'étendue et la variabilité de tels effets, La Commission a tenu cinq réunions plénières. Deux sous-groupes de la CGI ont été formés, l'un consacré à la stabilité, l'autre à l'hydrogéologie ; chacun d'entre eux s'est réuni à diverses reprises et a profité du concours d'experts et consultants extérieurs. Le détail en est donné dans le Tableau 1.1 et dans la Préface.

TAB. 1.1 Membres des deux sous-groupes de la CGI.

Sous-groupe Stabilité		
Coordinateur	Emmanuel Detournay	
Membres	Edwin T. Brown	
	Charles Fairhurst	
	Victor Nikolaevskiy	
	J.R. Anthony Pearson	
Liaison	Pierre Bérest	
Consultants	Peter Cundall	Itasca Consulting Group, Inc.
	Branko Damjanac	Itasca Consulting Group, Inc.
	Charles Archambeau	TRAC, Inc.
Sous-groupe Hydrologie		
Coordinateur	Lloyd Townley	
Membres	Charles Fairhurst	
	Ghislain de Marsily	
	J.R. Anthony Pearson	
Liaison	Pierre Bérest	
Consultants	Pierre Perrochet	École Polytechnique Fédérale de Lausanne (EPFL)
	Laurent Tacher	École Polytechnique Fédérale de Lausanne (EPFL)

TAB. 1.2 Problèmes principaux.

– Doit-on attendre une poursuite significative de l'affaissement, ou *subsidence*, de parties émergées de l'atoll ?
– Doit-on attendre que des glissements de terrains importants affectent les pentes extérieures de l'atoll ?
– Des fractures majeures ont-elles été créées en profondeur dans les atolls - notamment, les fractures visibles en surface constituent-elles la trace d'un réseau qui s'étendrait en profondeur sous l'atoll ?
– Y-a-t-il eu des changements de l'hydrogéologie naturelle de l'atoll, dont la convection d'origine thermique est un trait majeur, suffisamment importants pour accélérer significativement le transport des radionucléides de vie longue vers le lagon et l'océan ?

La CGI a pris en considération les préoccupations exprimées, avant et après les séries d'essais, par plusieurs experts, associations ou organisations nationales et internationales,. Certains groupes d'experts avaient déjà remis leurs propres rapports après des visites sur les atolls (par exemple, Tazieff (1982) ; Goguel (1982), référencé dans la suite comme le rapport Tazieff ; MoFA (Nouvelle Zélande, 1984) désigné dans la suite par : rapport Atkinson ; et Fondation Cousteau, (Paris, 1988) désigné dans la suite par : rapport Cousteau) ; par ailleurs l'hypothèse a été émise (CRII-Rad, 1995 ; Vincent, 1996) que des dommages catastrophiques, ou potentiellement catastrophiques, aient été causés aux deux atolls, (voir, dans une veine quelque peu irrévérencieuse, le dessin de la Figure 1.2, provenant de Nouvelle Zélande), qu'il s'agisse d'effondrements généralisés, d'affaissements de la surface du sol, de fracturation massive ou de profondes modifications du comportement hydrogéologique des atolls ; des craintes ont également été exprimées que les populations locales aient pu être soumises à des irradiations inacceptables. Ces rapports et commentaires ont été examinés par la CGI, qui a pris note de ces préoccupations. La Commission estime qu'une de ses responsabilités principales était d'apprécier d'un point de vue d'expert, et de manière impartiale, le bien fondé de ces préoccupations (à l'exception de la dernière qui a été examinée par l'AIEA), d'en rendre compte d'une manière qui alerte les autorités, s'il y a lieu, des risques qui n'auraient pas été identifiés ; de suggérer les dispositions nécessaires pour prévenir les évènements dommageables qui pourraient résulter des essais et pour en réduire les effets ainsi que réduire les craintes, si la Commission les considèrait infondées. Une liste des questions soulevées est donnée dans le Tableau 1.2.

Le temps et les moyens dont disposait la CGI étaient tels que la Commission a dû utiliser les seules informations déjà disponibles pour établir ses conclusions. Il ne lui a pas été possible de collecter des données nouvelles sur les sites, pour une part à cause de l'éloignement des atolls, situés au milieu du Pacifique Sud, et aussi du fait de l'accès strictement limité aux deux atolls. Ainsi toutes les interprétations auxquelles la Commission est parvenue sont-elles fondées sur les mêmes données, ou une partie des mêmes données, que celles dont a disposé le CEA/LDG. La CGI s'est efforcée d'obtenir, autant que cela était possible, des données brutes relatives aux observations factuelles effectuées, de façon à produire sa propre interprétation de ces observations. Elle a aussi utilisé les informations générales disponibles sur la structure et les propriétés des atolls, afin de réaliser sa propre estimation des valeurs des paramètres utiles aux modélisations essentielles. Elle a alors été capable de conduire de manière indépendante un ensemble de calculs, en vue de vérifier et d'étendre quelques-uns des résultats les plus importants fournis par le DIRCEN-CEA. Ces calculs intéressent :

– (i) les effets mécaniques de l'onde de choc engendrée par l'explosion d'un engin nucléaire au sein de la masse rocheuse de l'atoll ; ces effets comprennent la

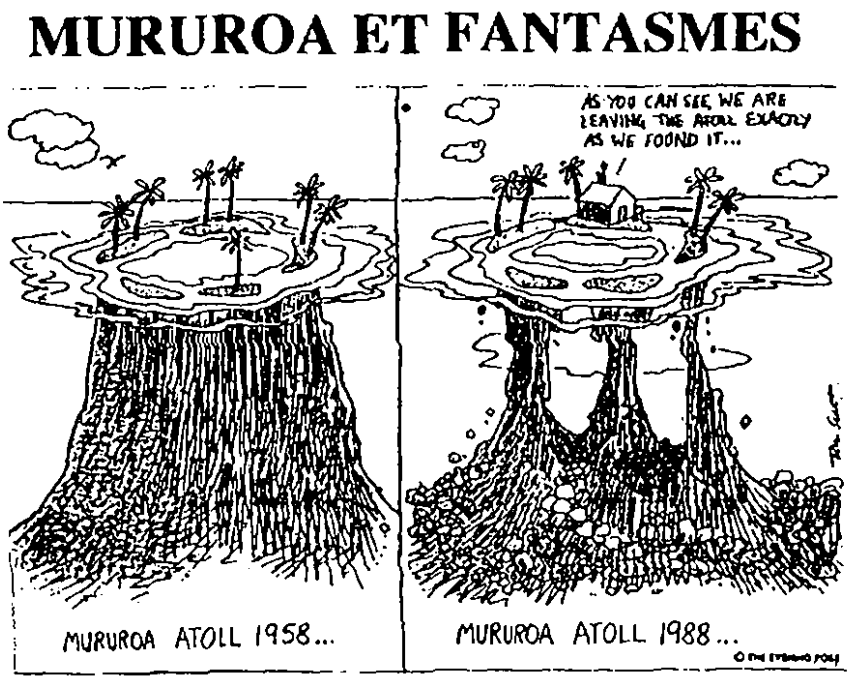

FIG. 1.2 Dessin publié dans le *Auckland Evening Post*

formation de la cavité, les déformations irréversibles qui affectent les roches environnantes, l'affaissement des couches supérieures de l'atoll et son influence sur la stabilié des pentes océaniques des récifs coralliens ;

– (ii) les écoulements de fluide dans les pores du milieu rocheux, qui résultent immédiatement de la création de la cavité et de l'échauffement du massif environnant ; et

– (iii) les modifications entraînées à long terme aux figures de convection des eaux souterraines sous les atolls.

Ces figures de convection, de court et de long terme, constituent le moteur principal de la migration (ou transport) des radionucléides depuis la cavité formée et son voisinage immédiat jusqu'à la surface de l'atoll et donc à la biosphère. Les calculs associés aux points (ii) et (iii) sont précisément ceux que l'AIEA a utilisés pour son évaluation des conséquences radiologiques des essais.

Le trait dominant de l'ensemble de l'étude -commun d'ailleurs à toutes les études consacrées aux massifs rocheux naturels- réside dans l'incertitude qui affecte toute donnée relative aux propriétés du massif rocheux, sur le site des essais et dans le milieu environnant (cette caractéristique est d'ailleurs, jusqu'à un certain point, commune à tous les travaux souterrains : tunnels, mines, exploration et production pétrolières, enfouissement de déchets). Même si de nombreux paramètres géologiques, géophysiques, mécaniques, hydrogéologiques ont été mesurés par le CEA, il résulte de l'inhomogénéité inhérente à tout massif rocheux naturel que l'estimation des valeurs moyennes des paramètres, accompagnée d'une estimation vraisemblable de leur degré de variabilité, est, dans la pratique, ce que l'on peut introduire de mieux dans les calculs. Les opinions formulées devront donc être entendues comme se rapportant aux circonstances « les plus raisonnables », à « l'intervalle possible » de résultats ou au scénario « le plus défavorable ».

Le rapport de la CGI est présenté en trois parties (coïncidant avec les trois volumes). Le présent volume, le premier, est une synthèse qui évite le détail des discussions ou analyses techniques et s'efforce plutôt de présenter les idées essentielles, les difficultés d'interprétation et les conclusions, dans un style accessible à un public large ; il ne suppose qu'une culture générale et une bonne connaissance de la méthode scientifique. Le second volume constitue une version plus longue, plus détaillée, destinée aux lecteurs spécialistes, et à tous ceux qui veulent comprendre en détail l'étude réalisée, afin qu'ils puissent, sur la base de faits connus, effectuer leur propre analyse des conséquences de la série d'essais. Le troisième volume contient la traduction en français, préparée par la CGI, du Volume I et de parties du Volume II (Préface ; Résultats, conclusions et recommandations ; et Chapitre 1, Présentation d'ensemble).

1.2 Information dont la Commission a disposé

Du fait que les deux atolls sont des zones à accès très restreint depuis le jour où le Gouvernement français a décidé de les utiliser comme centre d'expérimentation, (et qu'ils ne présentaient pas antérieurement d'intérêt scientifique ou économique remarquable), les seules données relatives aux atolls directement disponibles sont celles fournies par le Gouvernement français et ses agences. La Commission a également utilisé les informations générales disponibles relatives à des atolls analogues ou à des îles volcaniques du Pacifique, ou concernant des essais nucléaires souterrains réalisés au Centre d'Essais du Pacifique (CEP) et dans d'autres sites par d'autres pays. Parmi ces dernières informations figurent les enregistrements sismiques rassemblés et exploités en relation avec les traités d'interdiction des essais nucléaires, grâce auxquels la localisation et l'énergie des essais nucléaires souterrains peuvent être déduites des signaux sismiques émis.

À l'origine, deux rapports complets (Guille et al., 1996 ; et Bouchez et Lecomte, 1996) ont constitué les sources principales d'information. Destinés à un large public scientifique, et bien rédigés à cet égard, ces rapports s'appuyaient sur des investigations nombreuses conduites pendant des années. Même si la CGI a utilisé ces rapports, ils ne contiennent pas les renseignements détaillés que nécessite un examen critique approfondi du programme d'essais. Barrillot (1996), dont le livre récent *Les essais nucléaires français 1960-1996* s'appuie en partie sur ces deux rapports, fait la remarque suivante :

« Comme nous l'avons remarqué à plusieurs reprises dans cette étude, les documents Dircen ne fournissent que des informations parcellaires, certes précises et éclairantes, mais les conséquences les plus graves des expériences réalisées font partie des omissions constantes qui risquent d'être masquées par l'abondance et la qualité des informations données sur des points de détails » (p. 214)

Au cours des premières phases de nos investigations, nos impressions allaient dans le même sens. Toutefois, Barrillot ne disposait pas des 12 documents DIRCEN/CEA mentionnés plus haut quand il a formulé ces commentaires. Initialement, ces documents plus détaillés n'étaient pas non plus à la disposition de la Commission ; ils ont été transmis à la CGI (et à l'AIEA) après qu'ils furent achevés ; leur préparation (et traduction en anglais) en temps utile constituait un réel défi, si l'on tient compte de ce que certaines informations précises spécifiques ne pouvaient pas y figurer. Malgré les informations précieuses qu'ils contiennent, et dont l'étude de la CGI a fait son profit, certains détails importants manquent encore dans ces rapports.

Il est possible qu'une partie de l'information, dont nous pensons que le DIRCEN/CEA avait besoin et avait dû la recueillir pour parvenir à ses conclusions, n'ait pas été recueillie ou n'ait pas été interprétée de manière adéquate. Par exemple, les valeurs mesurées au laboratoire de la résistance des roches est donnée, mais les estimations de certains paramètres importants du massif rocheux ne sont pas mentionnées. On a vraisemblable-

ment conservé et analysé les enregistrements complets effectués en forage et dans les puits (réalisés en routine dans l'industrie pétrolière), qu'ils concernent les puits en grand diamètre dans lesquels les engins nucléaires étaient descendus ou les puits d'observation en plus petit diamètre forés dans les cavités créées par chaque explosion. Ils auraient contenu beaucoup d'informations utiles. Des essais en puits ont manifestement été faits, et les enregistrements des pressions et temps de remplissage de cavité ont été conservés. Une partie de l'information a été transmise, mais sans le détail complet ; cette information a été utilisée pour obtenir les valeurs des perméabilités, mais très peu de détails ou d'éléments de discussion ont été donnés quant aux méthodologies utilisées. Des estimations ont été transmises, mais, de nouveau, sans discussion de la précision que l'on peut attendre des valeurs obtenues, ni de leur unicité, ni de leur pertinence du point de vue de la formation ultérieure des figures de convection. En essayant de confirmer les résultats du CEA, la CGI a trouvé soit qu'il y avait des points du raisonnement où il fallait deviner quelles hypothèses non précisées avaient été faites, soit encore que d'autres conclusions, parfois différentes, pouvaient être tirées. Lorsque des mesures de températures ou de traceurs (tritium) sont transmises et utilisées, la même situation prévaut.

Il est vrai que la complexité des modèles mathématiques actuels et des logiciels de calcul correspondants est telle que, même dans les articles publiés dans des revues scientifiques, une partie significative doit être admise sans preuve. De plus, les paramètres et résultats français proviennent des travaux de très nombreux chercheurs, universitaires pour beaucoup d'entre eux, et dont certains peuvent avoir, sans le vouloir, omis de fournir toute l'information nécessaire dans leurs propres rapports et thèses, sur lesquels se basent largement les documents DIRCEN/CEA. Enfin, il est clair que la dernière série de documents du DIRCEN-CEA a été préparée bien après les travaux originaux (commencés il y a près de 25 ans), de sorte que les omissions ou absences de justifications peuvent être dues à ce que les auteurs ne sont plus là pour fournir les informations manquantes ; de plus les moyens informatiques ne permettaient pas, il y a dix ans, de réaliser certaines analyses possibles aujourd'hui.

Ces commentaires n'ont pas pour but de suggérer que les actions entreprises et les interprétations faites par les scientifiques du CEA aient été incorrectes, mais simplement de faire remarquer que tous les détails n'ont pas été rendus disponibles à la CGI. Confrontée à ce manque d'informations de détail, et consciente de l'incertitude générique inhérente aux données géotechniques, la CGI a été contrainte de prendre en compte dans ses analyses des situations extrêmes, afin de couvrir toutes les possibilités. Heureusement, même les hypothèses les plus pessimistes, du point de vue du confinement à court et long terme de la radioactivité, ne conduisent pas à conclure à des conséquences telles qu'elles justifieraient une évaluation plus précise.

La qualité des données dont disposait la CGI dans différents domaines est résumée de manière subjective et qualitative dans le Tableau 1.3. La raison de la faible qualité apparente de beaucoup de données est l'incertitude inévitable qui accompagne tout résultat

TAB. 1.3 Qualité des données disponibles pour la modélisation et l'analyse

Catégorie	*Sous-Catégorie*	*Qualité/Précision*
Géologie		correcte à bonne
Propriétés Physiques	Densités	bonne
	Porosités	correcte
	Conductivités thermiques	bonne
	Conductivités hydrauliques	médiocre
	Longueurs de dispersion	médiocre
	Propriétés Mécaniques	correcte
Topographie		bonne
Température		médiocre
Flux géothermique		médiocre à correcte
Flux convectif		déduite, pour l'essentiel, et médiocre
Localisation des essais		partielle
Énergie des essais		correcte à bonne
Essais par traceurs		médiocre

et plus encore toute interprétation de mesures effectuées dans un environnement naturel (comme mentionné plus haut) où l'inhomogénéité, à toutes les échelles, entraîne que plus une mesure est locale, plus la valeur mesurée peut varier avec la position du point de mesure dans l'espace. Plus de mesures auraient pu être effectuées, et une meilleure estimation aurait pu être faite de l'étendue de la variabilité à attendre. Plus de soin aurait pu être apporté à la description des modèles et calculs utilisés pour déduire les conclusions obtenues, et plus d'accent aurait pu être mis sur le degré d'incertitude impliqué. Par exemple, il n'est pas raisonnable de chercher une précision extrême quant aux effets locaux d'une explosion particulière : la taille et la forme de la cavité créée dépendront significativement des caractéristiques particulières de la proportion du massif rocheux qui n'a pas été remontée à la surface sous forme de carottes ou débris de forage, et constitue évidemment l'immense majorité du volume de ce massif ; les fractions remontées à la surface ne peuvent fournir qu'une indication des propriétés réelles des roches dans le voisinage du forage qui a permis la collecte d'échantillons. Même si l'on s'in-

téresse à des quantités plus globales, telles que le flux total de fluide transmis du massif rocheux (ou corallien) vers le lagon, ou l'énergie sismique totale et la quantité de mouvement rayonnées vers le champ lointain, une large incertitude subsistera. Les modèles ne peuvent fournir que les valeurs moyennes des variables physiques, calculées pour des valeurs moyennes des paramètres du matériau ; ces valeurs apparaissent donc indicatives plutôt que certaines. Toutefois, la CGI a examiné l'influence des divers paramètres sur les résultats utiles ; cet examen suggère que les incertitudes impliquées n'affaiblissent pas les conclusions de la Commission.

1.3 Structure et géologie des atolls

Comme expliqué dans le chapitre 2 de Bouchez et Lecomte (1996) et dans Guille et al. (1996), et discuté plus loin dans le Chapitre 2, Volume II du rapport de la CGI, les deux atolls forment une partie d'une chaîne d'îles volcaniques du Pacifique Sud. Le volcanisme qui a provoqué leur érection n'est plus actif sous les atolls, parce que ceux-ci se sont éloignés du point chaud qui a été à leur origine. En ce sens, ils sont tout aussi stables que la plaque sur laquelle ils sont placés. Certaines des îles s'élèvent au-dessus de la mer (par exemple, Tahiti) alors que Mururoa et Fangataufa sont pour l'essentiel sous la surface de l'océan ; seule émerge la couronne corallienne, plus complète à Fangataufa qu'à Mururoa. Dans les deux cas, le lagon relativement peu profond, à l'intérieur de la couronne, est relié par des hoas (passes) aux fonds océaniques extérieurs ; l'action des marées et des vents soulève et abaisse le niveau de l'eau dans le lagon et provoque des échanges journaliers de liquide à travers les hoas. Ceci conduit à un renouvellement approximativement mensuel de l'eau du lagon par l'océan.

Les couronnes coralliennes (ou les récifs dans le cas d'îles largement émergées) s'étendent au voisinage immédiat de la surface de l'océan à cause des formes de croissance du corail. S'il est trop profondément submergé, ou au contraire laissé hors d'eau pendant un certain temps, le corail meurt. À très long terme, les îles s'enfoncent très lentement dans l'océan, suivant un processus que l'on peut expliquer en considérant les mouvements globaux de la surface de la Terre ; les périodes glaciaires provoquent une descente, puis une remontée du niveau de la mer à une échelle de temps plutôt plus courte que celle du lent enfoncement ; c'est la période glaciaire la plus récente qui est à l'origine de la couronne de corail mort actuellement émergée. Le corail sous-marin, en moyenne, se développe très graduellement vers le haut, avec une vitesse légèrement supérieure dans la partie extérieure, ce qui donne la couronne visible ; comme le corail mort, fragile et hautement poreux, s'enfonce sous le corail en formation, il est écrasé par le poids des matériaux surincombants et lentement altéré par interaction chimique avec l'eau de mer qui le baigne. Dans le cas de Mururoa, le processus a duré suffisamment longtemps pour que la couche (sédimentaire) de 400 mètres environ de roches calcaires (qualifiées dans la suite de carbonates, par commodité de langage), repose sur les roches

basaltiques, moins poreuses et moins perméables, qui constituent la véritable assise des atolls. Les Figures 1.3 et 1.4 montrent sous forme simplifiée la coupe géologique et la forme de Mururoa et Fangataufa, respectivement.

Il est important de remarquer que les pentes moyennes des flancs profonds basaltiques des îles sont suffisamment douces pour assurer la complète stabilité des bases basaltiques (le diagnostic de stabilité a été remis en cause par au moins un auteur (Vincent, 1996) mais les théories classiques et toutes les données disponibles convergent pour confirmer cette stabilité). Ce n'est qu'au voisinage de la surface de l'océan, où les matériaux qui composent les flancs sont essentiellement du corail mort altéré, que l'on trouve des pentes plus raides et moins stables. Pendant la période (plusieurs millions d'années) de formation des 400 mètres de roche calcaire, de nombreux glissements ont affecté ces pentes ; c'est la raison pour laquelle le matériau constituant les flancs est partiellement calcaire à plus grande profondeur, 500 à 600 mètres de profondeur autour de Mururoa, et un peu plus autour de Fangataufa (voir Figure 1.5).

Les modifications de la topographie des deux atolls que l'on peut observer, particulièrement à Mururoa, et qui ont été provoquées par la série d'essais, résultent de modifications qui ont affecté les roches sédimentaires, et pas les basaltes sous-jacents. Une grande part de notre tâche dans ce contexte a résidé dans l'examen des explications de ces modifications données par le DIRCEN/CEA, dans le but de fournir nos propres explications et d'évaluer, sur la base des connaissances existantes et de modèles, la vraisemblance de modifications futures. Ceci est discuté dans les sections suivantes du présent rapport. Les sujets les plus importants sont :

- l'affaissement des couronnes des atolls,
- la fracturation profonde ou superficielle de la couche calcaire,
- le glissement lent ou soudain des flancs des couronnes, et
- la dispersion des radionucléides.

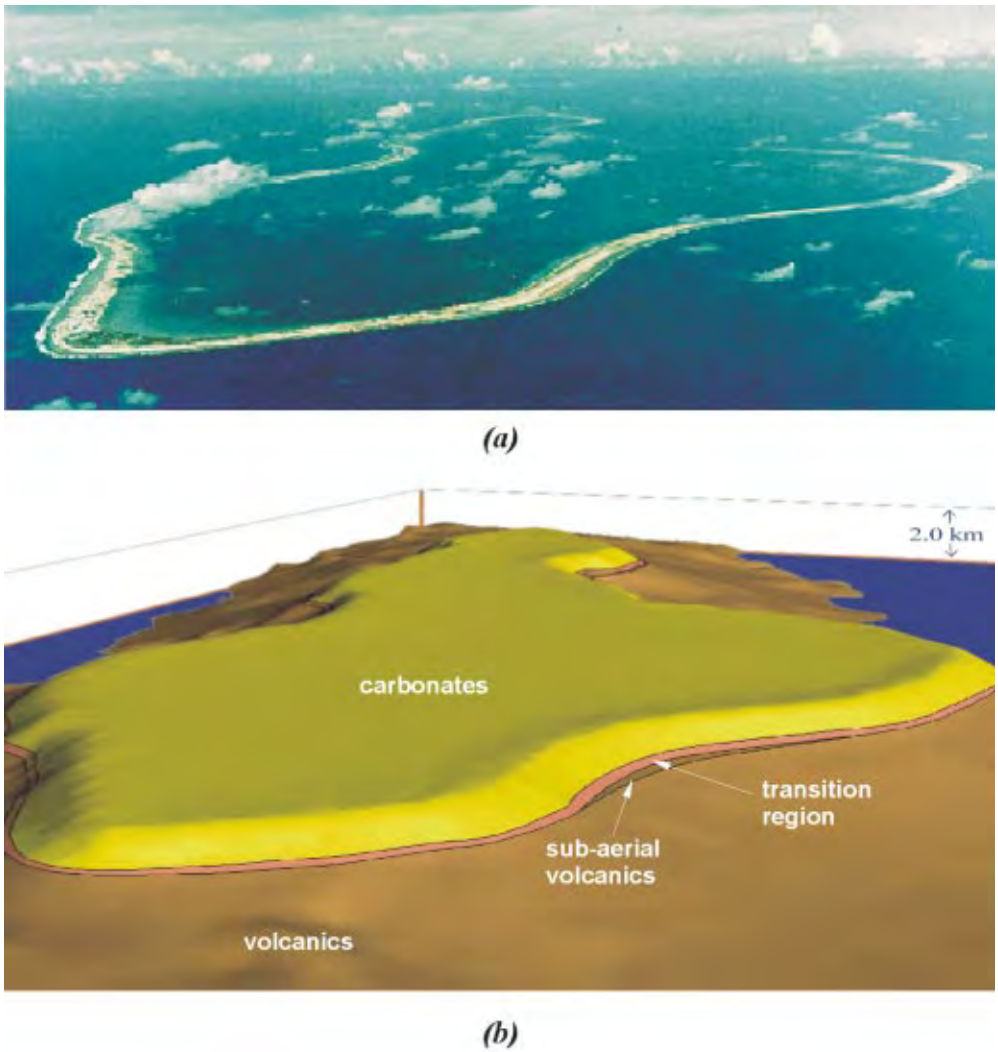

FIG. 1.3 Mururoa (a) vue aérienne - (b) perspective bathymétrique jusqu'à une profondeur de 2 km (les carbonates surmontent le massif volcanique)

(a)

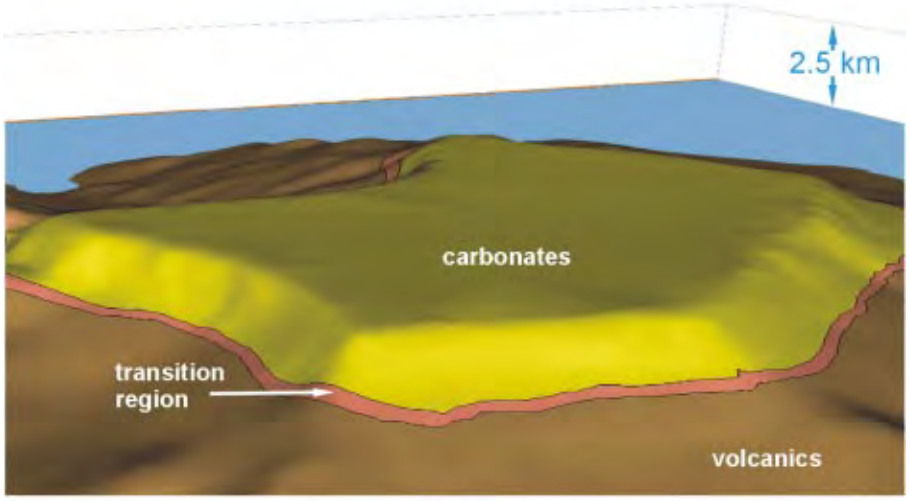

(b)

FIG. 1.4 Fangataufa (a) vue aérienne - (b) perspective bathymétrique jusqu'à une profondeur de 2,5 km (Les flancs de Fangataufa descendent plus abruptement que ceux de Mururoa ; les carbonates surmontent le massif volcanique)

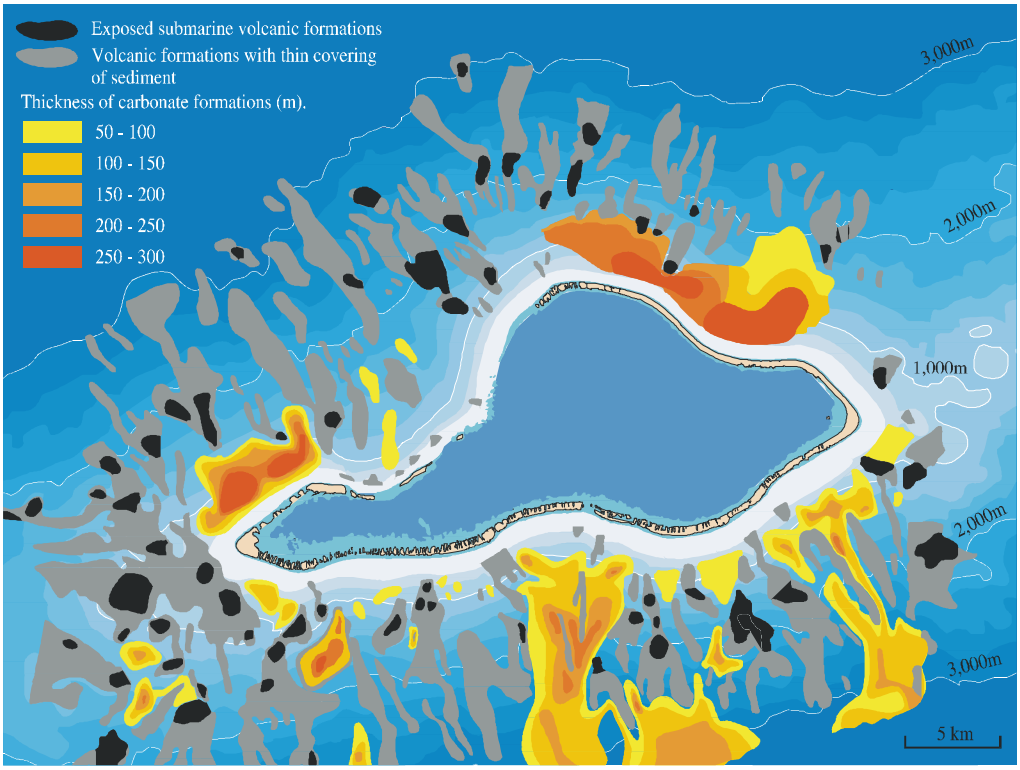

FIG. 1.5 Distribution des dépôts sédimentaires et des affleurements sous-marins sur les flancs de l'atoll de Mururoa (Guille et al. 1996, Figure 23)

1.4 Eléments d'hydrologie des atolls

A la fois les basaltes et les calcaires sont poreux et saturés d'eau de mer, le basalte étant légèrement perméable et les carbonates fortement ; les variations locales sont importantes, et la conductivité hydraulique est généralement plus grande suivant une direction horizontale que suivant la verticale. Dans les conditions naturelles, il existe un flux de chaleur dirigé des basaltes sous-jacents vers la surface et les flancs des atolls ; il s'agit du flux qu'on appelle géothermique, dont la cause réside dans les températures élevées des roches basaltiques en profondeur - le centre de la Terre étant beaucoup plus chaud que sa surface. Ce gradient vertical de température est la cause d'un mouvement ascendant de l'eau de mer contenue dans la roche, par convection naturelle, qui donne naissance à grande échelle à des rouleaux de convection. Dans le cas d'un atoll, ce processus est significativement renforcé par l'existence simultanée d'un gradient de température horizontal provoqué par (le refroidissement par) les températures plus froides de l'océan sur les flancs de l'atoll et par l'entrée d'eau de mer provenant de l'océan (voir Figure 1.6). Dans l'océan lui-même, des figures de convections à grande échelle im-

pliquent l'océan tout entier ; c'est la raison pour laquelle, dans les régions tropicales, le profil de température est positif au voisinage de la surface - c'est-à-dire que l'eau devient plus froide lorsque la profondeur croît.

Les méthodes de calcul de la circulation superficielle ou profonde de l'eau dans la croûte terrestre sont aujourd'hui bien maîtrisées, et les logiciels correspondants sont couramment disponibles, de sorte que la prévision des formes de l'écoulement stationnaire de l'eau souterraine présente une qualité qui ne dépend que de la qualité des données introduites pour représenter la masse rocheuse, telles que : porosité, perméabilité et conditions thermiques à la limite du modèle. Des arguments simples montrent que, dans les basaltes, l'essentiel du transfert de chaleur se fait par conduction et que la circulation associée du fluide dans les pores est relativement lente (de l'ordre de 1 cm par an pour la vitesse de Darcy, qui est une moyenne dans le volume, et équivaut à environ 10 cm par an pour la vitesse réelle du fluide), de sorte qu'elle n'apporte qu'une contribution mineure au transfert de chaleur ; dans les carbonates, et en particulier dans les niveaux karstiques (qui contiennent des chenaux horizontaux de grande dimension, ou des cavités, créés par des processus physico-chimiques de long terme qui sont bien connus), au voisinage de la couronne corallienne, l'écoulement du fluide dans le milieux poreux est plus important, les vitesses de Darcy associées pouvant atteindre des valeurs moyennes de 1 m par an et plus. Ces figures de circulation établies sont dites globales (c'est-à-dire qu'elles sont à l'échelle de l'atoll entier).

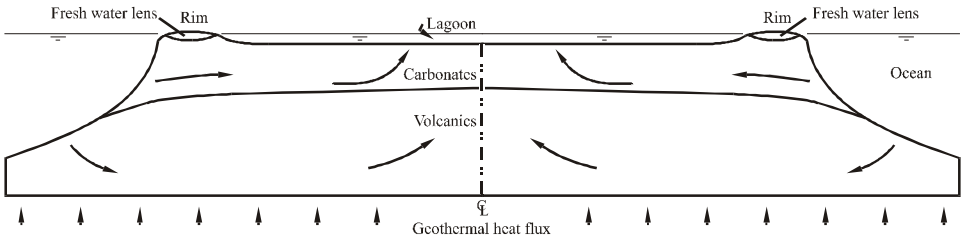

FIG. 1.6 Coupe schématique d'un atoll (d'après Perrochet et Tacher 1997a)

Le tir d'un engin nucléaire à des profondeurs comprises entre 600 et 1100 mètres implique, hormis les modifications de la perméabilité et de la porosité provoquées par l'endommagement d'origine mécanique (discuté à la Section 1.6), une augmentation soudaine de la température dans le voisinage immédiat du point d'explosion qui entraîne l'apparition de gradients de température locaux importants, de caractère transitoire, et d'un panache de fluide chauffé (une explosion de 1 kt dégage assez d'énergie pour échauffer de 1°C un million de tonnes d'eau ; en pratique, cette énergie conduit à une augmentation de la température moyenne d'environ 25°C pour une sphère de 20 mètres de rayon). Dans les basaltes, cet effet local peut simplement être superposé aux champs permanents de température et d'écoulement décrits plus haut. Dans les carbonates, où l'écoulement affecte la température de manière significative, les modifications de l'écou-

lement et de la température sont plus compliquées mais l'effet global est qualitativement le même. Une indication très grossière des échelles de temps mises en jeu peut être donnée en disant que le panache thermique met une cinquantaine d'années à traverser les 400 mètres d'épaisseur des carbonates, et que l'eau chauffée se déplace un peu plus vite que ne le fait le point où l'augmentation de température résultant de l'explosion est maximal. A ce moment, l'énergie associée à l'accroissement transitoire de température s'est en grande partie diffusée dans un environnement plus large, principalement par conduction dans le massif rocheux et convection rapide dans l'océan et l'atmosphère. Après environ 500 ans, tout effet thermique de l'explosion s'est dissipé.

1.5 Effets mécaniques d'un tir expérimental

Il y a accord général des experts sur ce qui survient lorsqu'on tire un engin nucléaire sous terre, et l'IGC a conduit ses propres calculs pour le confirmer dans le contexte particulier de Mururoa/Fangataufa. Comme discuté dans le Volume II, Chapitre 3, bien au-dessous du toit des basaltes, une grande masse de gaz à très haute pression se forme ; elle repousse le massif rocheux environnant jusqu'à former une cavité beaucoup plus grande que le volume initial occupé par l'engin avant l'explosion. Cette formation est si rapide qu'une forte onde de choc de célérité supersonique se propage à partir du point d'explosion. En s'éloignant du point zéro, l'onde de choc s'atténue jusqu'à devenir une onde sonore (sismique). Cette onde sismique se propage dans toutes les directions et dans la Terre entière ; si l'énergie dégagée dans l'explosion est suffisamment grande, le signal sismique peut être détecté et interprété dans les stations d'enregistrement sismique du monde entier. Au moment où l'onde sismique se forme, à l'exception d'une faible proportion (pour fixer les idées, de 0,5 à 5% - selon la déformation élastique extérieure finale), la quasi totalité de l'énergie totale contenue dans l'onde initiale a été perdue.

Il y a deux causes à l'atténuation de l'intensité de l'onde. La première est élémentaire et évidente : l'énergie est répartie sur une surface à peu près sphérique dont le rayon, et donc l'aire, augmentent avec le temps ; cette raison à elle seule explique que l'énergie et la quantité de mouvement par unité de surface décroissent à peu près comme l'inverse du carré de la distance -ou du temps, puisqu'une onde sonore se déplace avec une vitesse constante dans un milieu homogène. La seconde raison provient du caractère fortement non linéaire et dissipatif de l'onde de choc dans les instants qui suivent sa création ; une partie de son énergie est abandonnée sous forme de chaleur ou d'altération de l'état (énergie libre) de la roche. La part de l'atténuation qui résulte de la dissipation décroît lorsque l'intensité de l'onde diminue, et devient presque négligeable à grande distance dans la région sonique.

Lors du passage de l'onde, la roche est repoussée vers l'extérieur et se déforme. Près du centre, quand le choc est encore fort, les contraintes (ou forces par unité de surface) associées à la déformation de la roche sont grandes en comparaison de celles qui

existaient avant l'explosion -c'est-à-dire grandes en comparaison des efforts d'origine gravitaire ou tectonique- de sorte que le processus ne peut dépendre que des propriétés purement locales de la roche. Il y a donc lieu d'attendre que ce processus présente une symétrie sphérique. A plus grande distance du centre le domaine (la surface) couvert par le front d'onde présente des variations plus grandes, et la symétrie sphérique se perd ; une illustration évidente de cette idée est donnée par le moment où l'onde atteint l'océan ou l'atmosphère. A plus grande distance encore, les contraintes en place préexistantes seront bien plus fortes que celles provoquées par le passage de l'onde sonore, cette distance dépendant de la profondeur du tir considéré.

Le passage d'une onde de choc est montré sur la Figure 1.7. Les effets immédiats de l'explosion, après que l'onde s'est éloignée de l'île (il faut pour cela quelques secondes) sont représentés schématiquement sur la Figure 1.8. Une cavité dont le fond et les parois sont constitués de roche fondue (verre) est entourée d'une zone broyée au-delà de laquelle on trouve une zone beaucoup plus étendue qui est déformée de manière irréversible. La partie intérieure de cette zone déformée a été soumise à une rupture en cisaillement de type plastique, alors que la partie extérieure présente des ruptures discrètes (fractures) ; les deux parties se sont dilatées (le volume qu'elles occupent a augmenté). Au-delà de cette région déformée (ou anélastique, dans la terminologie du DIRCEN/CEA) on suppose que la roche s'est déformée élastiquement à partir de son état d'origine ; la totalité du massif est donc dans un état de contrainte modifié. Il n'y a chez les experts dans le monde que des différences mineures d'appréciation sur cette image générale, quoique, dans chaque cas particulier, il y ait eu des désaccords sur des points précis (taille de chaque zone, nature des déformations de la roche). On y reviendra plus tard. On peut supposer que les volumes de roche affectés de la manière décrite augmentent proportionnellement à l'énergie de l'explosion ; ce qui signifie que les rayons des diverses zones varient comme la racine cubique de l'énergie.

On constate que, quelques heures après l'explosion, la roche endommagée au toit de la cavité ne peut rester stable, comme il est d'observation courante lors du creusement d'un tunnel dans un matériau sec et peu résistant. En conséquence le toit s'effondre pour former une « cheminée » dans et au-dessus de la cavité. Lorsque les blocs de roche tombent dans la cavité, ou dans l'espace libre laissé par les blocs déjà tombés, ils foisonnent de sorte qu'ils occupent un volume sensiblement plus important qu'initialement ; en termes simples, les blocs de forme irrégulière qui tombent du toit ne s'ajustent pas exactement les uns aux autres quand ils s'accumulent au fond, et laissent donc entre eux des espaces libres. Au fur et à mesure de la poursuite de l'effondrement, l'espace libre initial formé par l'explosion se retrouve dans les vides laissés entre les blocs tombés ; ce processus s'arrête quand le dernier bloc à tomber reste partiellement solidaire du toit, parce qu'il repose par le bas sur les blocs accumulés. La hauteur de la cheminée foisonnée ainsi formée est à peu près égale au rayon de la zone fracturée, au-delà de laquelle est atteinte une roche suffisamment résistante pour former un toit. Dans certains

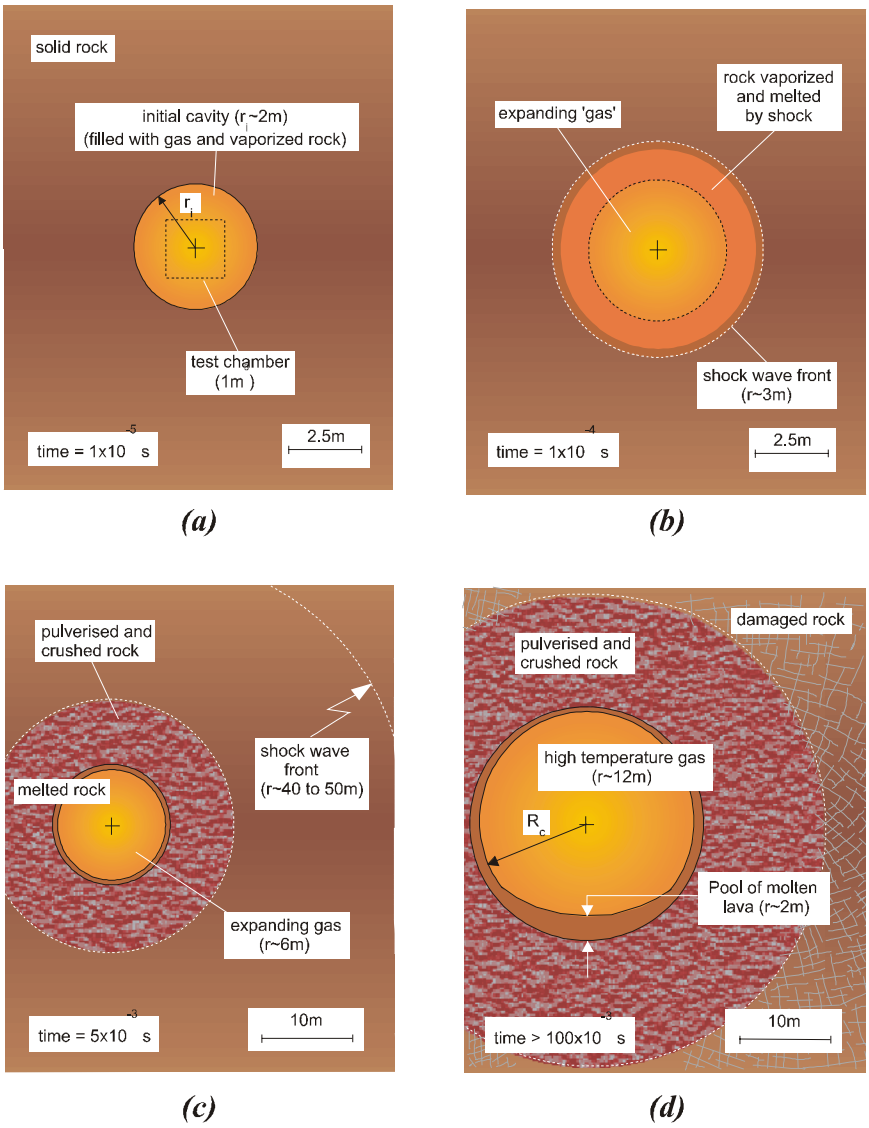

FIG. 1.7 Etapes de la formation de la cavité et de son développement pendant une explosion nucléaire (Note : r_i est le rayon de la sphère vaporisée « instantanément » ; $r_c \approx 2$ mètres pour une explosion de 1 kt) ; étapes ultérieures de l'expansion de la cavité (jusqu'à sa taille finale) et endommagement associé du massif rocheux pendant une explosion nucléaire (Note : R_c est le rayon final de la cavité complètement développée. $R_c \approx 12$ mètres pour une explosion de 1 kt (peu profonde) dans les atolls ; à plus grande profondeur $R_c \approx 10$ mètres pour une explosion de 1 kt)

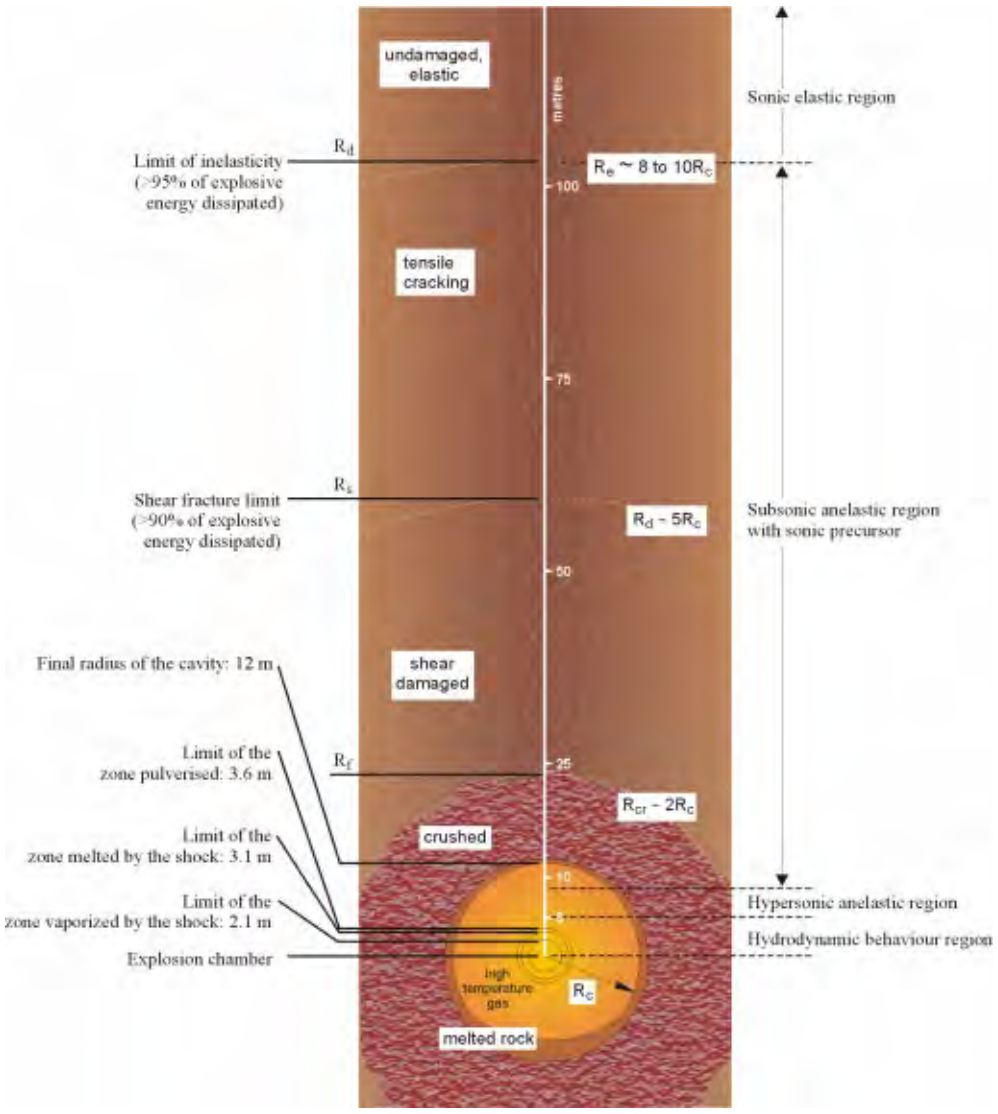

FIG. 1.8 Zones d'endommagement présumées autour d'une cavité créée par une explosion nucléaire de 1 kt dans les basaltes à Mururoa et Fangataufa (les rayons de zones endommagées sont exprimés comme des multiples du rayon final R_c de la cavité, qui augmente proportionellement à $Y^{1/3}$, où Y est l'énergie de l'explosion en kt) [modifié d'après Bouchez et Lecomte (1996) ; voir aussi Figure 3.7]

cas, la roche intacte est capable de former un toit qui n'est pas supporté par le foisonnement. Soumise à des déformations ultérieures, telles celles provoquées par des explosions proches, cette cheminée foisonnée est susceptible de transmettre les contraintes sans déformation majeure.

La formation de la cheminée est un phénomène très important, parce qu'elle accroît considérablement les effets de l'explosion en termes d'augmentation de perméabilité d'un grand volume dont la hauteur est égale à 5 à 8 fois le rayon de la cavité. Une conséquence est que les explosions dont le centre est relativement proche de la zone de transition entre le massif basaltique et les carbonates peuvent poinçonner -on sait que cela est arrivé- la couche basaltique peu perméable qui surmonte le point de tir, et faire communiquer ce dernier directement, du point de vue hydrogéologique, avec les carbonates fortement perméables. Au cours d'essais effectués à petite profondeur dans un matériau rocheux sec et non foisonnant, dans le désert du Nevada aux USA, les cheminées se sont propagées jusqu'à la surface pour former une dépression locale bien marquée à la surface. Toutefois ceci n'est pas survenu sur les atolls parce que les roches sont saturées d'eau et profondeur beaucoup plus que ne le font les alluviens du Nevada.

Des effets supplémentaires surviennent quand l'onde de choc, ou une onde sonore forte, atteint le fond du lagon puis la surface de l'océan, la surface émergée de la couronne, ou l'océan au niveau des flancs de l'atoll. La variation brutale de l'impédance mécanique (ou acoustique) entraîne la formation d'ondes réfléchies et/ou d'ondes de surface, et un affaiblissement de l'intensité de l'onde transmise. L'onde incidente est essentiellement de compression et plane ; l'onde réfléchie est donc essentiellement de traction ; l'onde de surface, d'autant plus intense que l'angle d'incidence s'écarte de la normale, contient une composante importante de cisaillement. Comme la plupart des matériaux naturels peuvent supporter des contraintes de compression bien plus importantes (souvent par un facteur de 10) que les contraintes de traction qu'ils peuvent supporter, l'onde de traction réfléchie est suffisamment forte pour détacher une plaque de matériau à la surface (écaillage). Cette dernière est projetée vers le haut jusqu'à ce que les forces de gravité la ramènent dans sa position initiale ; si le matériau soulevé est de l'eau, une cavitation survient (formation temporaire de bulles de vapeur). Ce phénomène peut expliquer l'ébullition apparente qui survient à la surface du lagon au-dessus du point de tir juste après l'explosion, alors que les irrégularités de la topographie du fond du lagon peuvent donner naissance à des jets. Le DIRCEN/CEA a de plus expliqué que le passage de l'onde de choc initiale, et de l'onde de choc secondaire provoquée par la retombée des plaques écaillées, suffisent à expliquer les affaissements manifestes au-dessus des sites d'essais sur la couronne de l'atoll (voir Figure 1.9).

La Commission trouve que les explications de l'affaissement fournies par le DIRCEN/CEA n'emportent pas la conviction, et une explication alternative par une rupture en cisaillement est donnée au Volume II, chapitre 5 du rapport de l'IGC. En termes simples, les réductions observées (suivant la verticale) de l'épaisseur des couches carbo-

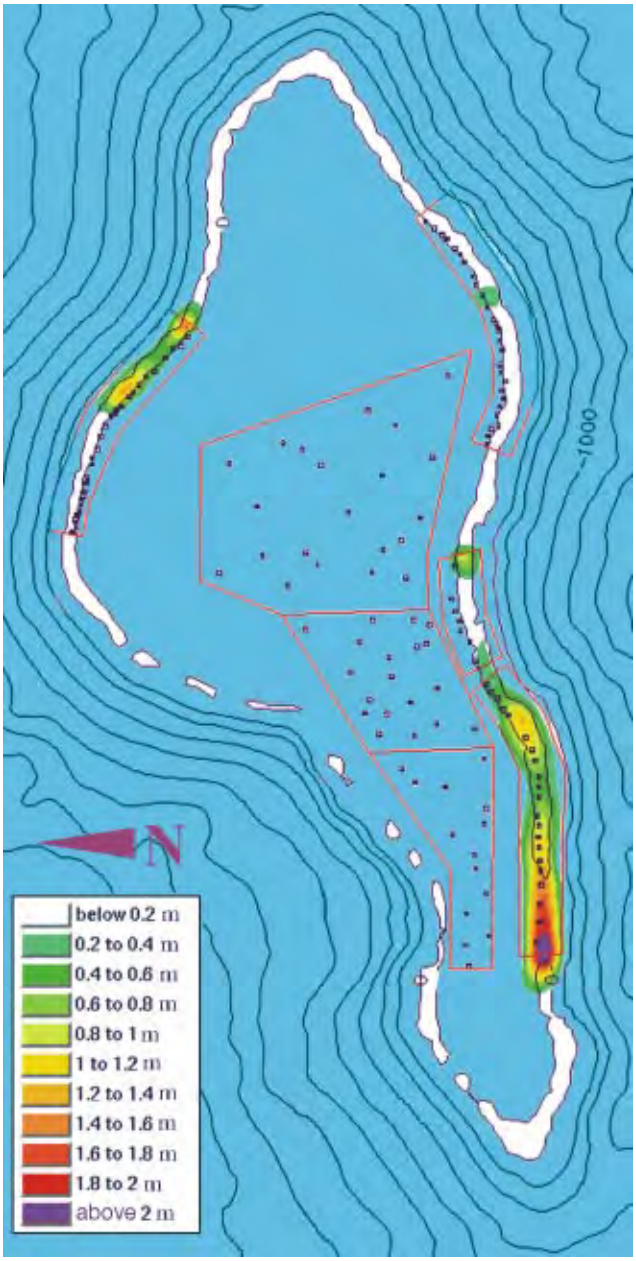

FIG. 1.9 Zones d'affaissements de la surface produites par les essais souterrains le long de la couronne corallienne à Mururoa (basé sur les données d'affaissement 1996 du DIRCEN/CEA) [selon Guille *et al.* (1996), p.69 : « les coraux qui édifient les récifs prolifèrent à l'heure actuelle avec une vitesse remarquable » (de l'ordre de 1 cm d'épaisseur par an) dans les régions affaissées. De ce fait, les zones récifiennes qui sont aujourd'hui sous l'eau auront retrouvé une altitude positive au-dessus de l'océan d'ici quelques centaines d'années]

natées supérieures surviennent parce que le passage de l'onde de choc de compression écrase les carbonates qui se déformant (horizontalement) vers l'extérieur sans changement de volume : la couronne de l'atoll est rendue un peu plus large. Une conséquence supplémentaire de ce processus est que la pente de l'atoll du côté de l'océan peut être déstabilisée ; de sorte que les glissements majeurs notés dans la zone d'essais 4 (dans la partie sud-ouest) peuvent être en partie attribués à ce mouvement, proche de la surface, dirigé vers l'extérieur. Cependant, les deux explications confortent également la conviction du DIRCEN/CEA selon laquelle les affaissements observés à la surface de l'atoll ne sont pas directement reliés aux chambres d'explosion. La Figure 1.9 montre une vue en plan des affaissements observés le long de la couronne de Mururoa (les sept zones d'essais, quatre sur le platier et trois dans le lagon, sont marquées par des lignes rouges ; voir aussi Figure 1.11).

En ce qui concerne la formation de fractures majeures, on note que les extrémités des fractures ne peuvent se déplacer aussi vite que l'onde de choc au cours du passage de cette dernière ; de sorte que les fractures créées lors de ce passage demeureront courtes et probablement isolées. Au voisinage des cavités initiales, les déformations plastiques sévères induites par l'onde de choc garantissent que les contraintes demeurent compressives ; plus loin, et notamment dans la région élastique, où des contraintes de traction peuvent apparaître du fait de la dilatation globale, de la rupture en traction et de la fracturation peuvent apparaître indépendamment de la pression régnant dans la cavité.

La relaxation de l'énergie de déformation qui accompagne la propagation des fractures limite la croissance de cette fracturation ; à plus grandes distances du centre de l'explosion, les contraintes en place préexistantes conduisent de nouveau à un environnement compressif, sauf peut-être à la surface de l'atoll. Quelques fractures de surface sont apparues du fait de l'instabilité des pentes. La Figure 1.10 montre une vue aérienne de fractures qui se sont développées à la suite de mouvements de pente dans la zone d'essais 1 de la couronne nord-est de Mururoa. Quelle que soit leur origine exacte, l'IGC croît incorrect de supposer que ces fractures de surface pénètrent profondément dans le massif rocheux de l'atoll.

FIG. 1.10 Photographie aérienne montrant des fractures en extension sous-marines, d'une largeur de l'ordre de 2 mètres, au voisinage de PK5N, section Irène (voir aussi Figure 5.6) ; une partie de la piste d'atterrissage, avec son mur protecteur, parallèle au bord du cliché, est visible dans la partie basse de la photographie ; cette région est à l'extérieur de la zone d'essais 1 [photo fournie par le DIRCEN/CEA]

1.6 Conséquences hydrologiques des explosions nucléaires

Il ne subsiste pas de modifications résiduelles de la perméabilité dans les régions qui n'ont été déformées qu'élastiquement. Dans celles qui ont été déformées de manière irréversible, la perméabilité tend à diminuer quand un écrasement survient et à augmenter quand le matériau est dilaté. Si la dilatation ne concerne que des petites micro-fractures qui n'interagissent pas entre elles, l'accroissement peut s'avérer réduit ; en revanche, si une fracturation significative survient, l'accroissement sera important (plusieurs ordres de grandeur dans le basalte). Dans la cheminée, y compris la cavité originelle, la perméabilité devient de fait (pratiquement) infinie.

Un grand nombre de sondages (puits) ont été forés dans les carbonates et les basaltes sous-jacents ; lorsqu'ils ne sont pas tubés et restent ouverts sur le massif rocheux qu'ils ont traversé, ces puits influencent la convection des eaux contenues dans les pores de leur voisinage. Pendant le forage des puits de grand diamètre (1,5 mètre), forés pour permettre la mise en place des engins nucléaires dans le basalte, de grands volumes d'eau sont prélevés dans les horizons carbonatés les plus perméables (niveaux karstiques) et sont transportés vers la tête de puits à la surface de la couronne ou au fond du lagon. Les puits effectivement utilisés pour un tir sont remplis de gravats, de sable et de laitier de ciment, afin de les boucher avant qu'on ne procède à l'explosion. Ultérieurement, ils n'ont aucune influence sur les conditions hydrologiques, quoiqu'il ait été suggéré qu'ils puissent induire dans les roches environnantes des fractures provoquées soit pendant la phase de forage soit plus tard à la suite du passage de l'onde de choc, et qu'ils offrent alors aux fluides chauds et aux radionucléides dissous un cheminement possible vers la surface significativement plus facile.

Quelques-uns de ces puits en grand diamètre n'ont pas été utilisés pour les essais et ont donc été laissés, au moins en partie, ouverts sur les roches environnantes et/ou en surface (cette information est parvenue tardivement pendant les travaux de la CGI, et les effets correspondants n'ont pas été intégrés dans la plupart des calculs détaillés). Apparemment, ces puits étaient utilisés pour faire des mesures de concentrations de radionucléides au niveau des karsts inférieurs et plus généralement dans les carbonates. Lorsqu'ils sont ouverts, du fait de leur conductivité hydraulique élevée, ils fournissent un passage plus facile -vers la surface, ou entre les couches souterraines les plus conductrices- pour le fluide contenu dans les pores qui entre par les flancs de l'atoll et se déplace vers le haut ou vers le bas sous l'effet des gradients de pression dans les roches poreuses. Des calculs grossiers suggèrent que cet effet pourrait être quantitativement significatif sur des distances égales, typiquement, à l'écart entre les points de tir dans la zone d'essais 4 de Mururoa (toutefois, l'écoulement étant normal à la ligne formée par les points d'explosions dans cette zone, on ne doit pas y attendre d'interaction notable).

D'autres puits en plus petit diamètre (0,2 m), légèrement décalés et en partie obliques, ont été forés quelques jours (ou semaines) après chaque explosion expérimentale pour

étudier (par prélèvements et diagraphies) les cavités et leur voisinage. Tous ces puits ont été rebouchés après usage, quoique certaines portions d'entre eux aient pu être laissées pleines d'eau, et ouvertes sur le massif rocheux.

Ni le DIRCEN/CEA, ni la CGI n'ont essayé d'analyser en détail les effets à court et long terme de ces ouvertures résultant de l'activité humaine sur le mouvement du fluide dans les pores de la roche. Le modèle de mélange (voir Volume II, Chapitre 7) utilisé pour calculer les concentrations de tritium (et d'autres radionucléides) et leurs mouvements dans les carbonates a virtuellement pris complètement en compte tout renforcement de la convection. De toutes les modifications créées, on peut attendre que celles provoquées par la formation de l'ensemble cavité/cheminée soient dominantes.

1.7 Historique des essais - Un commentaire

On s'est efforcé, sur les figures 1.11 et 1.12, de rassembler les seules informations disponibles de source directe, (c'est-à-dire celles fournies par le DIRCEN/CEA) concernant la distribution, la localisation, l'instant du tir et l'énergie des essais souterrains conduits à Mururoa et Fangataufa. La plupart de ces informations sont tirées du document DIRCEN/CEA n^o 6 et de l'annexe de Bouchez et Lecomte (1996). L'étude des enregistrements sismiques aide à confirmer les dates d'essais et à ajouter quelques détails sur la magnitude relative des essais individuels (voir discussion dans le Volume II, annexe C). Les photographies aériennes, dont certaines prises par des membres de la CGI, et d'autres fournies par les autorités du CEA, montrent aussi la localisation à la surface de nombreux sites de forage sur la couronne de Mururoa, particulièrement dans les zones d'essais 3 et 4, où les sites d'essais étaient espacés de manière à peu près régulière le long du périmètre intérieur de la couronne. La Figure 1.13 montre une vue aérienne, prise en juillet 1996, de la zone d'essais 4 à Mururoa. Dans quelques cas, la CGI a pu inférer quelques précisions complémentaires utiles de déclarations verbales qui lui ont été faites par le CEA/LDG, ou de statistiques et de calculs décrits dans les documents fournis par le DIRCEN/CEA.

Il est clair que, au moment de concevoir ses propres essais souterrains, le DIRCEN/CEA a porté une grande attention à l'expérience acquise au cours des dix années antérieures d'essais souterrains dans d'autres pays (voir Volume II, annexe B), notamment celle décrite dans le cas du Nevada Test Site (NTS) aux États-Unis. Les profondeurs relatives des essais au CEP étaient considérablement supérieures à celles des essais aux USA, de sorte que le relâchement direct (ou fuite) des radionucléides à l'atmosphère, qui a effectivement eu lieu dans quelques-uns des essais au NTS, a été évité (voir Volume II, annexe D).

La situation principalement sous-marine des atolls a éliminé l'option, moins coûteuse et plus riche en information, des essais conduits à l'extrémité de tunnels horizontaux, option utilisée pour certains essais US, russes, et pour les premiers essais français dans

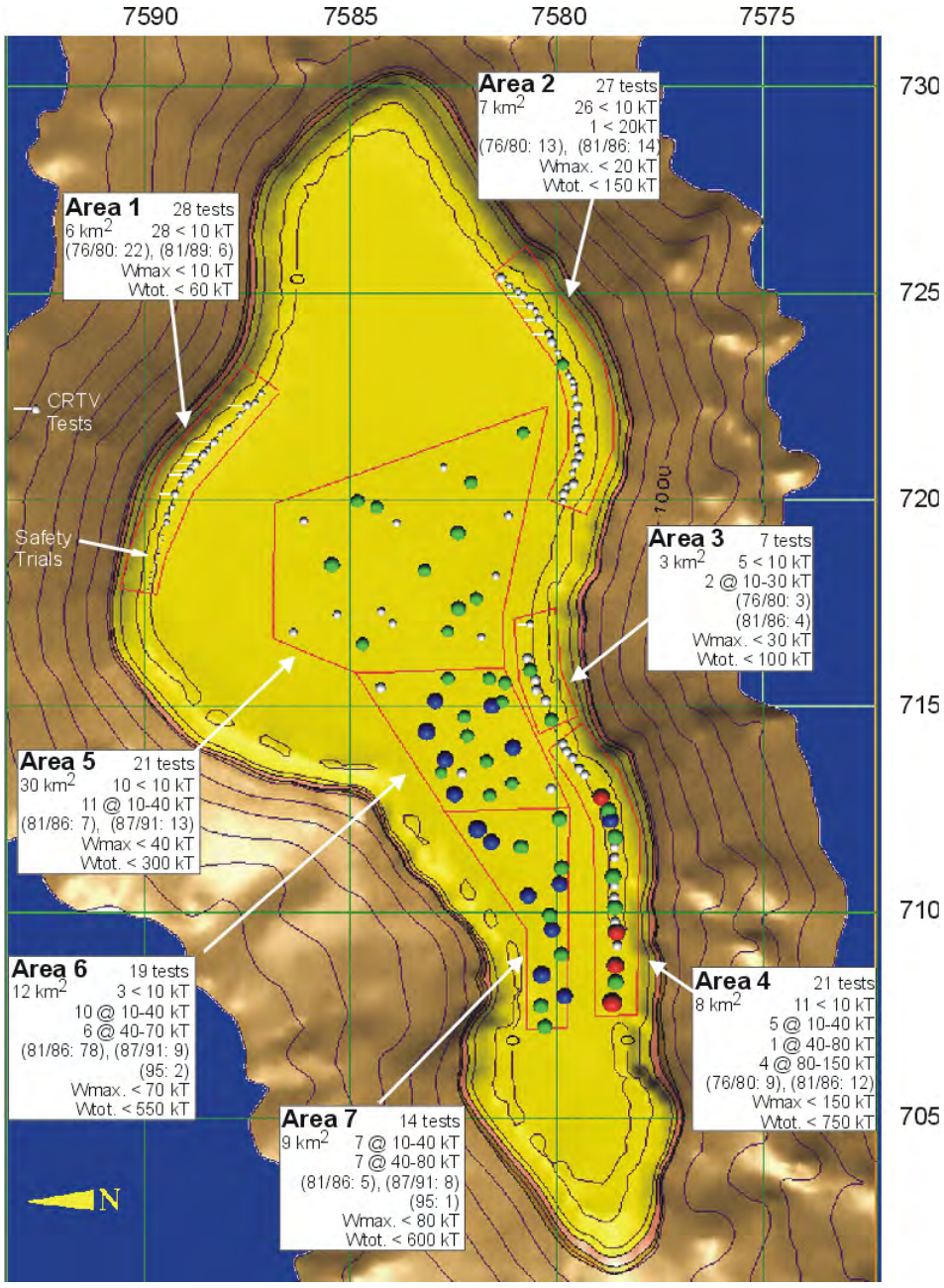

FIG. 1.11 Répartition des essais souterrains et de leurs énergies par zone d'essais à Mururoa (fournie par le DIRCEN/CEA), sur laquelle est superposée une distribution hypothétique des localisations des essais dans les zones d'essais (les contours bathymétriques figurés autour des atolls sont séparés par des intervalles de 250 mètres jusqu'à la profondeur de 2 km sous la surface)

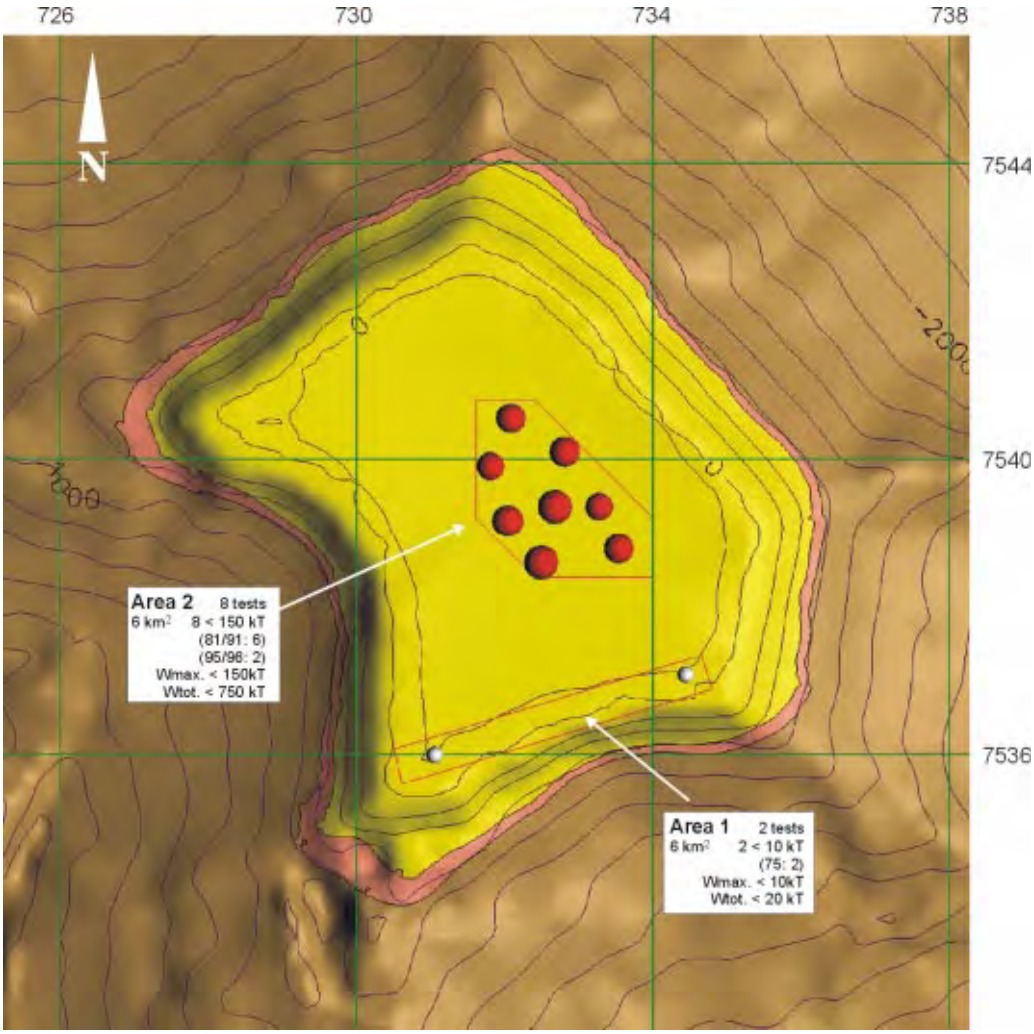

FIG. 1.12 Répartition des essais souterrains et de leurs énergies par zone d'essais à Fangataufa (fournie par le DIRCEN/CEA), sur laquelle est superposée une distribution hypothétique des localisations des essais dans les zones d'essais (les contours bathymétriques figurés autour des atolls sont séparés par des intervalles de 250 mètres jusqu'à la profondeur de 2 km sous la surface)

FIG. 1.13 Vue aérienne de la partie ouest de la zone d'essais 4 à Mururoa, prise en juillet 1996 (soit 16 ans après que les essais sur la couronne eurent cessé) ; la vue est prise de l'océan, en direction du lagon (remarquer que plusieurs sites d'essais et des zones affaissées à l'extrémité ouest de la zone d'essais 4 sont maintenant sous la mer ; voir aussi Figure 2.23)

le Hoggar (voir Préface), et qui permet des investigations ultérieures par creusement de nouveaux tunnels dans les zones endommagées autour des sites d'explosion. De ce fait, il y a relativement peu d'informations détaillées disponibles sur ces zones dans le cas du massif basaltique des atolls. Dans ce contexte, il est surprenant qu'il n'ait pas été fait et décrit une utilisation plus soigneuse des enregistrements effectués en cours de forage.

Il apparaît qu'une attention insuffisante a été portée aux problèmes géomécaniques pendant les phases initiales du programme d'expérimentation souterraine au CEP. Il est aujourd'hui évident, comme il est montré dans les Chapitres 4 et 5 du Volume II du rapport de la CGI, que des effets non désirés notables, comme l'affaissement de parties de la couronne et les glissements des flancs, auraient pu être évités si les premiers essais avaient été placés plus loin des franges extérieures des atolls, c'est-à-dire sous leur partie centrale et à plus grande profondeur. De plus, on aurait pu éviter que certaines cheminées n'atteignent la zone de transition ou les calcaires proprement dit, comme cela est

arrivé au cours de 12 des essais de la période 1976-1980*. Pour deux autres des premiers essais (Nestor et Enée) la qualité de la couverture volcanique s'est avéré insuffisante pour empêcher une fuite précoce de radionucléides contenus dans la cheminée. Il faut reconnaître toutefois que cette lucidité est plus facile après coup ; on a d'ailleurs fait remarquer que, si l'on se plaçait du point de vue de la sécurité, il était intrinsèquement plus sûr d'opérer sur terre plutôt que dans le lagon - et incidemment beaucoup moins cher.

Clairement, les effondrements de pente de la couronne sud à Mururoa†, les vagues‡ qu'ils ont provoquées et l'apparition, détectée dans les années 70, d'une lente déformation permanente affectant un large domaine de la pente de la couronne nord-est à Mururoa¶, rendirent impérative une révision complète de la stratégie d'expérimentation souterraine, le développement d'une technologie qui permette le forage de puits en grand diamètre (1,5 mètre) depuis des barges et des plates-formes opérant dans le lagon (Bouchez et Lecomte, 1996), et le basculement progressif de l'expérimentation du platier vers le lagon, qui a commencé en 1981§. L'importance de ces changements a été soulignée par la Commission Tazieff (Tazieff, 1982). A partir de 1987, tous les essais, à l'exception d'un petit essai en novembre 1989, ont été conduits sous les deux lagons. Ainsi, *depuis 1980, l'épaisseur minimale de couverture (volcanique) a été de 50 mètres puis, plus tard, de 100 mètres* (Document DIRCEN/CEA n° 6, Figure 7)‖.

A l'exception de deux cas dans lesquels la couverture volcanique était inadéquate (elle a été endommagée)** il apparaît que la totalité des 91 essais conduits depuis 1980 n'ont entraîné aucun des effets locaux non désirés expérimentés antérieurement. De ce point de vue, il est utile de répéter que tous les problèmes d'instabilité de pente et d'affaissements examinés au Volume II, Chapitres 4 et 5 et annexes associées, trouvent leur origine dans certains effets des campagnes d'essais antérieures à 1980, même s'il est clair que des accélérations temporaires des glissements de la couronne sud de Mururoa ont été déclenchées par des explosions ultérieures éloignées du rivage. De même, ni les essais CRTV ni les essais de Catégorie 2 n'ont eu de conséquences significatives du point de vue de la stabilité et ils n'ont eu que des conséquences négligeables du point de vue de l'hydrologie ou du relâchement de radionucléides (AIEA, 1998b).

---

*Voir Volume II, annexe C, Tableau C4, essais de catégorie 3 (CRTV).

†Nestor (mars 1977), Priam (novembre 1978), Tydée (juillet 1979).

‡Voir Volume II, Chapitre 5, et Document DIRCEN/CEA n° 7, Section VI.

¶Voir Volume II, Chapitre 5.

§Voir Volume II, annexe C.

‖Il s'agit des épaisseurs de dimensionnement avant essai, calculées sur la base de la profondeur réelle de l'essai dans le massif volcanique et de la hauteur prévue des cheminées déduite de la règle, donnée dans le Document DIRCEN/CEA n° 6 (page 6), qui fixe la hauteur de la cheminée en fonction de l'énergie du tir. L'épaisseur réelle de la couverture volcanique intacte au-dessus d'une cheminée n'était pas mesurée systématiquement dans les essais ultérieurs.

**Mégarée (novembre 1985), sous le lagon de Mururoa, et Lycos (novembre 1989), sous le lagon de Fangataufa (voir Volume II, annexe C, essais de Catégorie 2).

Les modifications graduelles dans la manière dont les essais ont été conduits (le choix de points zéros plus profonds, et plus largement espacés ; sous les deux lagons, plutôt qu'au voisinage des flancs des atolls) nous conduisent à conclure, même si les documents DIRCEN/CEA ne fournissent guère d'information à ce sujet, que l'équipe technique concernée a vraisemblablement analysé la situation qui se présentait à l'occasion de chaque nouvel essai avec une approche aussi prudente et objective qu'elle le pouvait.

La plus forte concentration d'énergie par unité de volume de roche a été relâchée dans la zone d'essais 4 de Mururoa, où l'on trouve les évènements non désirés les plus sévères, suivie par la zone d'essais 2 du lagon de Fangataufa et les zones d'essais 6 et 7 du lagon de Mururoa. Le glissement lent limité dans la zone d'essais 1 de Mururoa ne peut être aussi facilement attribué à un relâchement important d'énergie (voir Volume II, Chapitre 5), sauf si l'on admet qu'il s'agit d'un processus latent qui a été déclenché et accéléré par des ondes de choc relativement faibles dans une couche sédimentaire peu résistante.

1.8 Questions principales

1.8.1 Dommage mécanique local et stabilité à long terme du massif rocheux.

Il est commode de développer les raisonnements pour le cas de la zone d'essais 4 de Mururoa, où la concentration des tirs effectués a été la plus grande. On peut déduire de la Figure 1.3, par des calculs très simples, en utilisant la linéarité de la relation entre les volumes et l'énergie de l'explosion lors d'un essai, que le volume total des cavités créées a été de 5 millions de m^3 environ, le volume total des cheminées de l'ordre de 40 millions de m^3 (0,04 km^3) environ, le volume total de roche endommagée de l'ordre de 0,68 km^3 et le volume total de roche inélastiquement déformée de l'ordre de 2,3 km^3 ; ces valeurs supposent que ces tirs, qui totalisent une énergie libérée de 750 kt, ont des effets complètement indépendants les uns des autres. Le volume total de la couche de terrains dans laquelle les essais ont eu lieu peut être calculé en multipliant 8 km^2 par 600 mètres, soit environ 5 km^3, en prenant en compte que tous les tirs ont été effectués entre 500 m et 1100 m de profondeur.

Nous ne connaissons ni la localisation précise de chaque tir ni leurs énergies, de sorte que nous ne sommes pas en mesure de calculer quel recouvrement peut exister entre les régions endommagées par les différents tirs ; la seule information dont nous disposions est une figure, fournie à Tahiti par le CEA, qui donne, pour les distances séparant les tirs les plus proches voisins, la proportion de ces espacements pour lesquels on peut attendre qu'ils conduisent à un recouvrement de 25% des zones fracturées. Comme la densité des tirs dans la zone d'essais 4 est plus grande que la moyenne, on peut attendre que la proportion conduisant à des recouvrements y soit aussi plus grande. Lorsqu'on remarque la régularité de l'implantation des sites de forage le long de la ligne du récif de corail dans la zone d'essais 4, on est en droit d'estimer que, au pire, ces régions fracturées forment

une ligne continue de 7 km de long placée immédiatement sous la couche carbonatée (voir Figure 1.6 du Volume II). Ce qu'on peut affirmer avec certitude c'est que l'essentiel des 5 km^3 auxquels il est fait allusion dans le dernier paragraphe aura été déformé de manière anélastique. Jusqu'ici, nous n'avons utilisé que des considérations géométriques élémentaires sur l'emplacement de sphères à l'intérieur d'un volume donné.

Une autre question concerne les modifications de volume de la couche de 600 mètres d'épaisseur au sein de laquelle les cavités ont été créées. Si l'on suppose qu'il n'y a pas eu de changement de densité de la roche qui a été déplacée par l'explosion, la couche de basalte en question doit présenter un accroissement de volume de 5 000 000 m^3. Si l'on suppose, au contraire, que le volume repoussé pour former les cavités doit se retrouver sous la forme d'un accroissement de la densité moyenne (diminution de porosité) des 5 kilomètres cubes de roche qui constituent cette couche (c'est-à-dire s'il n'y a pas de modification du volume global de la couche), alors la porosité moyenne a diminué de 0,1%. Si l'on suppose que le volume des cavités doit se retrouver sous la forme d'un soulèvement, réparti sur les 8 kilomètres carrés de « terre » qui surmontent la couche, on obtient une montée moyenne de 0,6 mètre ; on rappelle que le mouvement réellement observé est un affaissement compris entre 1 et 2 mètres. En supposant que la pente, qui constitue le flanc de l'atoll et délimite du côté de l'océan la couche dans laquelle les essais ont eu lieu, est simplement poussée en direction de l'océan, on obtient un déplacement horizontal moyen d'un mètre ; mais en raison des glissements qui ont affecté les pentes, nous n'avons pas de preuve qui permette de conclure quant à ce qui s'est effectivement passé.

Ces considérations géométriques très simples montrent qu'une compréhension plus approfondie des variations de volume (compaction ou dilatation), associées au passage de l'onde de choc à travers le basalte et les carbonates, est nécessaire avant que des conclusions fermes puissent être tirées des changements observés sur la frange extérieure de la zone d'essais 4 de Mururoa. Le Chapitre 3 du second volume du présent rapport développe une argumentation qui conteste les explications simples par lesquelles le DIRCEN explique les affaissements ; cet aspect sera repris dans la sous-section suivante.

La question qui vient alors est de savoir si les essais ont suffisament déstabilisé la couche de carbonate pour qu'un effondrement structural puisse survenir. Il faut noter, d'abord, qu'à une profondeur moyenne de 800 mètres, la couronne érigée est confortée, du côté de l'océan, par une masse rocheuse volcanique ou sédimentaire qui présente une pente telle que les points de tirs soient distants de l'océan d'au moins un kilomètre suivant la direction horizontale ; du côté du lagon, la couche basaltique est continue jusqu'à la pente diamétralement opposée. Ainsi il est clair que la roche endommagée est entourée sur les côtés, et supportée par le dessous, par une roche basaltique saine qui n'a pas subi de déformation anélastique. Nous avons la conviction que même la masse rocheuse qui a été endommagée est aujourd'hui parfaitement capable d'assurer son propre équilibre et celui de la couche susjacente de carbonates, malgré le réseau très

étendu de cheminées et de fractures qui parcourent le volume en question. Le rôle de ce réseau pour l'hydrogéologie est discuté plus loin.

1.8.2 Affaissement de la surface

L'affaissement (ou subsidence) de la couronne de l'atoll, en particulier dans la zone d'essais 4, est la conséquence la plus immédiatement visible des campagnes d'essais (voir Figure 1.9). Des observations effectuées dans des sondages ont montré que la compaction résiduelle (réduction de porosité), et/ou la contraction verticale nécessaire pour conduire à l'affaissement de surface observé, sont réparties sur les 120 mètres supérieurs de la couche carbonatée. Comme montré plus haut, cet affaissement est de 2 mètres environ, si l'on tient compte de ce que la création des cavités a conduit à un soulèvement de 0,6 mètre. Deux mécanismes peuvent être invoqués pour expliquer cet affaissement : une réduction moyenne de la porosité de 1,5% dans la couche calcaire supérieure suffit à en rendre compte (les 2 mètres d'affaissement sont à rapporter à une épaisseur compactée de 120 mètres) sans qu'il soit nécessaire de faire appel à l'existence d'une déformation latérale ; alors qu'un déplacement latéral de 1 mètre environ des pentes du côté de l'océan conduirait au même résultat, sans qu'il soit nécessaire de faire appel à une variation de la porosité. En tout cas, un affaissement a toujours été observé au-dessus des sites d'essais (voir Figure 12 dans le document DIRCEN/CEA n° 7) de sorte qu'il est logique d'invoquer un mécanisme générique.

Les faits expérimentaux résultant de mesures directement disponibles ne sont pas conclusifs. Les documents DIRCEN/CEA n'explicitent pas complètement les raisons de leur choix, mais paraissent privilégier un mécanisme fondé uniquement sur l'effet de la compaction qui serait provoqué en partie directement par le passage de l'onde de compression, mais surtout par l'impact des écailles massives (il s'agit de plaques détachées par l'onde réfléchie par la surface du sol, qui est une onde de traction) qui retombent après leur vol balistique sur les couches carbonatées supérieures friables (voir Figures 7 à 9 de Bouchez et Lecomte (1996) et le texte qui suit page 69).

La CGI a trouvé cette explication insuffisante, parce que le massif carbonaté concerné est saturé (et l'était au moment des essais). Même si la matrice rocheuse était substantiellement endommagée par le passage de l'onde compressive et les ondes réfléchies de traction, le temps nécessaire pour expulser le volume de fluide contenu dans les pores (pour que la variation de porosité devienne effective) de la couche en question de 120 mètres d'épaisseur serait vraisemblablement long en comparaison de la durée assez brève qui caractérise l'affaissement des terrains observé. Comme mentionné plutôt, la CGI préfère un mécanisme alternatif fondé sur une déformation de distorsion rapide qui, en termes simples, implique une contraction verticale de la couche accompagnée d'une extension horizontale sans qu'il soit nécessaire d'invoquer une variation de porosité. La discussion est détaillée dans le Volume II, Chapitre 4 du présent rapport.

1.8.3 Instabilités des pentes

Les évènements les plus spectaculaires survenus pendant les campagnes de tirs ont été les glissements, immédiats ou différés, affectant de larges fractions des pentes, observés entre 1977 et 1980, à l'extrémité occidentale de la zone d'essais 4 et au-delà (à Mururoa). Pour des détails voir le document DIRCEN/CEA n° 7, Chapitre 5. Une circonstance intéressante est que les régions dans lesquelles plusieurs des glissements les plus sévères sont survenus, notamment ceux associés à Tydée, n'étaient pas les plus proches des explosions expérimentales concernées (voir Figure 1.14). Leurs conséquences ont été des grandes vagues qui ont submergé la partie de la couronne voisine du lieu des glissements. On a émis l'hypothèse que ces phénomènes aient été accompagnés d'un relâchement rapide de radioactivité dans l'océan, et même que des phénomènes volcaniques aient pu être déclenchés par ces glissements.

Des mouvements de pente ont affecté la partie nord-est de la couronne, et notamment toute la zone d'essais 1 ; ils sont toujours surveillés. Pour l'instant, le processus paraît conforme à ce que l'on peut attendre, et le mouvement se ralentit, quoique en certains endroits des glissements futurs soient possibles. La réponse en fluage du calcaire crayeux, dans lequel les mouvements sont déjà apparus, n'est pas suffisamment bien comprise pour qu'il soit assuré que le ralentissement actuel du mouvement ne s'inversera pas pour conduire à une accélération - notamment déclenchée par un événement relativement mineur à d'autres égards. L'intensité des ondes de choc qui ont atteint la pente nord-est est plus faible que celle de leurs homologues dans la zone sud-ouest ; ceci peut expliquer que le mécanisme de rupture ne soit pas allé à son terme. Cependant la roche crayeuse présente dans le sous-sol de la zone nord-est est d'une nature particulière et présente des propriétés physiques distinctes, de sorte qu'il serait dangereux de généraliser trop rapidement des conclusions relatives à l'affaiblissement des pentes et à la rupture. Ce qui paraît clair est que les glissements ne concerneront pas les roches du substrat volcanique et seront de la même nature générale que ceux survenus ailleurs dans le voisinage de la couronne dans la zone d'essais 4. La Figure 1.15 donne un résumé simplifié des divers effets d'un essai sous la couronne d'un atoll.

On peut proposer diverses explications pour les glissements qui sont survenus. Les facteurs pris en considération comprennent :

1° la médiocrité intrinsèque des caractéristiques du matériau, en partie détritique, qui constitue les pentes concernées ;

2° la forte inclinaison de la pente dans les parties supérieures des flancs de l'atoll (c'est- à-dire que les pentes sont dans une situation proche de l'effondrement) ;

3° un écaillage possible, analogue aux phénomènes observés sur les parties horizontales à la surface de l'atoll, ou, plus probablement, une rupture en traction associée à des déformations relativement petites dans la direction de propagation de l'onde ;

4° une conversion d'une partie de l'énergie de l'onde sous la forme d'une onde de

FIG. 1.14 Vue aérienne montrant le région sous-marine de Mururoa qui a été affectée par l'effondrement consécutif à Tydée (la localisation présumée du tir Tydée et les limites de la zone effondrée ont été ajoutées par la CGI) [photographies fournies par le DIRCEN/CEA]

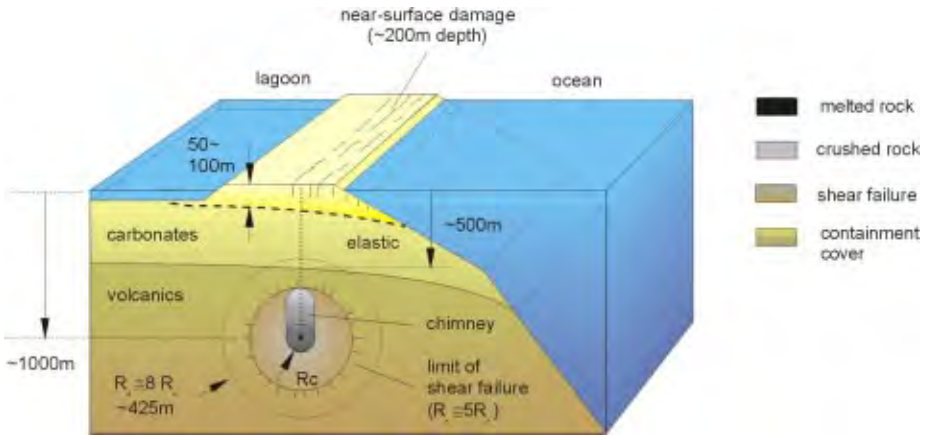

FIG. 1.15 Résumé simplifié des dommages dus à une explosion supposée de 150 kt

surface (à l'interface entre l'océan et le récif) dont l'intensité maximale survient en un point distinct du point correspondant à l'incidence normale de l'onde de compression ; et

5º un mouvement latéral (horizontal) affectant les couches supérieures carbonatées (calcaires) lorsque l'onde de choc atteint les parties immergées du récif, comme cela a été décrit plus haut à propos de l'affaissement.

Des calculs avec des hypothèses simples (réalisés pour la CGI), décrivant une onde de compression atteignant une pente régulière, uniformément plane, constituée d'une roche homogène, conduisent à la conclusion que la rupture surviendra, à condition que l'intensité de l'onde soit suffisamment forte ou que la résistance de la roche soit suffisamment faible, dans la partie de la pente la plus proche du centre de l'explosion.

Cependant certains des glissements majeurs sont survenus à plus grande distance du centre de l'explosion et la CGI a été amenée à conclure que des variations locales dans la topographie des pentes et les propriétés des roches devaient être à l'origine de ces événements qui seraient autrement paradoxaux. Ces questions ont été discutées en plus grand détail dans le Chapitre 5 du Volume II du présent rapport. On y a analysé le processus de mise en mouvement de la pente dans la zone d'essais 1 en s'efforçant de tenir compte, de manière plus réaliste qu'il n'est fait dans les documents DIRCEN/CEA,

- (a) du processus concomitant d'affaissement ;
- (b) de l'amorce et de la localisation des surfaces de glissement ;
- (c) des contributions des explosions successives ;
- (d) du caractère tri-dimensionnel du mécanisme ; et
- (e) des conséquences pour le futur.

La poursuite d'une surveillance continue est évidemment nécessaire ; même une alerte provoquée par une accélération du glissement pendant quelques jours autoriserait les autorités locales à prévenir les bateaux et les habitants des atolls habités les plus proches.

1.8.4 Accroissement des phénomènes convectifs et conséquences pour le transport des substances radioactives de l'emplacement des tirs vers la biosphère

On a fait allusion à cette question dans une section précédente. Le plus grand risque de relâchement rapide de radionucléides dans l'environnement est associé aux essais, qui sont tous des essais de sécurité (conduits avec des explosifs conventionnels, et non destinés à déclencher une réaction nucléaire), effectués dans la couche carbonatée, où les perméabilités naturelles sont les plus grandes. Pour les essais complètement confinés par le basalte (c'est-à-dire les essais dans lesquels les cheminées n'ont pas atteint l'interface entre le basalte ou la zone de transition avec les couches plus perméables), les dangers de relâchement rapide sont négligeables, même si ces relâchements croîtront à long terme. En ce qui concerne les essais, également conduits dans le basalte, pour lesquels les cheminées ont atteint les carbonates, un relâchement précoce de radioactivité a dû survenir pendant la première dizaine d'années après les tirs, c'est-à-dire un intervalle de temps aujourd'hui déjà écoulé pour la plupart des tirs. Un relâchement précoce a dû survenir, avant qu'un panache d'eau chaude engendré par l'explosion n'atteigne la surface, ou pendant qu'il l'atteignait, et ce relachement aurait dû être détecté à la surface du sol ou au fond du lagon. Les documents DIRCEN/CEA ne sont pas très précis à ce sujet, en partie parce qu'ils concluent qu'un relâchement rapide de tout le tritium mobile ne constituait pas un risque aux conséquences importantes et en partie parce que l'adsorption des isotopes à vie longue et les plus toxiques, sur les surfaces de la porosité de la roche, aurait différé les effets du processus de transport par convection de ces isotopes vers la surface assez longtemps pour que les bouffées chaudes se soient dissipées.

Des calculs ont été entrepris par la CGI pour confirmer et généraliser les estimations que le DIRCEN/CEA a faites de la convection globale avant et après les campagnes de tirs. Il n'y a pas d'effet global significatif des explosions à l'échelle de l'atoll, en ce sens que le volume total d'eau océanique qui entre dans l'atoll puis qui ressort dans les lagons est virtuellement inchangé, et que les distributions de température sont peu affectées. Cette conclusion peut être clairement tirée même s'il subsiste une incertitude considérable quant aux détails du mécanisme de convection réel. Cependant, là où la surface de la couronne s'est affaissée, dans les régions de plus grande densité de tirs, ou là où des glissements substantiels sont survenus, des changements considérables des circulations de fluide dans les pores sont apparus ; les effets de la marée ont changé à une échelle locale.

La CGI a également réalisé des calculs pour étudier les effets de plus court terme qui résultent du relâchement d'une grande quantité d'énergie et de la formation de la cheminée. Ces calculs confirment, qualitativement, les conclusions du DIRCEN/CEA, même

si l'étendue des distributions possibles de valeurs de la perméabilité après tir, compatibles avec les observations et les prévisions mécaniques, est si large, que des prédictions quantitatives précises ne peuvent être espérées. Les observations utilisées comportent les temps de remplissage des cavités par l'eau du massif environnant, les mesures de pression corrélées avec les marées, les profils verticaux de température (sondage Zoe) et les mesures de traceurs à des profondeurs et instants différents.

Une observation intéressante est que le transport vertical des fluides, et donc des traceurs radioactifs, observé dans plusieurs puits (environ 5) de Mururoa, forés en relation avec les campagnes de tirs mais non utilisés et laissés ouverts, peut ne pas être négligeable en comparaison du transport à travers le massif rocheux entre les puits, même si l'aire des sections horizontales des puits forés est négligeable en comparaison de l'extension surfacique horizontale totale de la zone d'influence de chaque explosion. La raison en est que les vitesses verticales dans un puits, engendrées par le mécanisme convectif, peuvent être de plusieurs ordres de grandeurs supérieures aux vitesses d'écoulement homologues dans le massif rocheux.

Dans le cas d'une explosion de grande énergie (100 kt) à Fangataufa (Lycos), un relâchement de tritium, clairement lié à cette explosion, a été détecté si rapidement après celle-ci qu'on ne peut en trouver une explication que dans la présence d'un chenal hydrauliquement très conducteur reliant la cavité créée par l'explosion et la couche karstique dans laquelle le tritium a été détecté. Quatre évènements de ce type au moins sont survenus à Mururoa (voir Volume II, annexe C).

Des anomalies de cette nature ne sont pas surprenantes dans un massif non homogène de grande dimension. Les calculs classiques réalisés pour de grands massifs rocheux supposent que l'écoulement du fluide poreux est régi par une propriété de la roche appelée perméabilité, qui résulte d'une approximation continue du comportement hydraulique du réseau global très complexe de connections entre les pores de la roche. Pour que les prévisions fondées sur cette notion de perméabilité soient pertinentes et réalistes, il faut que les vitesses prédites soient entendues comme des valeurs moyennes qui n'ont de sens que pour des aires ou des volumes grands en comparaison des dimensions des structures géométriques (pores, chenaux, fractures) qui sont à l'origine de la connectivité du milieu poreux. Dans la pratique, il y aura inévitablement des grandes structures (fractures majeures, conduits et chenaux karstiques, couches poreuses de grande conductivité) qui traverseront la région que l'on s'efforce de modéliser ; elles auront un effet global significatif, sinon dominant. Les valeurs de la perméabilité qui doivent être utilisées dans de tels cas se révèleront, en conséquence, dépendre à la fois des dimensions de la région en question (l'échelle des longueurs est typiquement de 1 km dans le cas des atolls) et des dimensions (typiquement de 10 à 15 mètres dans le cas du logiciel utilisé) des plus petits volumes individualisés dans les simulations numériques. Ceci reste vrai même si les propriétés de la roche sont exactement connues jusqu'à une très petite (1 mm) échelle de longueur.

Dans le cas des deux atolls qui nous préoccupent, nos connaissances sont affectées d'une grande incertitude : nous savons qu'il y aura des variations statistiques autour de n'importe quelle valeur moyenne, mais l'information quantitative à ce sujet n'est pas abondante ; nous avons des raisons de penser qu'il y aura des régions dont la conductivité hydraulique sera largement supérieure à la moyenne, mais nous ne pouvons pas les localiser précisément par rapport à l'emplacement d'un tir donné. Dans cette mesure, tous les résultats des calculs réalisés par le DIRCEN et la CGI sont indicatifs plutôt qu'exacts. Un exemple est fourni par la perméabilité accrue dans les diverses couches karstiques (dont l'existence est avérée quantitativement par les venues d'eau pendant les opérations de forage). Cette perméabilité plus forte des karsts explique que l'essentiel du flux ascendant d'eau salée sous les lagons provient de l'eau de mer qui se déplace horizontalement le long de ces couches, et que seule une faible fraction de ce flux provient du basalte sous-jacent. Dans ces couches perméables, les effets des marées sont clairement ressentis. La différence entre les effets du relâchement de la radioactivité confiné dans le basalte et les mêmes effets survenant dans les carbonates (ou, après que ceux-ci sont directement atteints) réside dans cette différence entre les échelles de temps caractéristiques de la circulation dans le basalte et les carbonates respectivement.

Dans le cas du transport du tritium, traceur passif, il y a un effet supplémentaire de dispersion cinématique, associé aux variations de vélocités, à l'échelle des pores, dans le massif poreux ; cet effet est particulièrement significatif dans des roches inhomogènes ou hautement fracturées, et est grandement renforcé par les mouvements induits par les marées océaniques. Une théorie cohérente fondée sur l'hypothèse de mélange complet dans les carbonates peut être trouvée au Volume II, Chapitre 7 du présent rapport.

1.9 Résumé des résultats, conclusions et recommandations

L'essentiel du résumé qui suit est une conséquence presque immédiate de ce qui a été exposé dans les sections précédentes de ce bref compte rendu. Quand des résultats ou conclusions complémentaires sont mentionnés, ils ont été intégrés pour reproduire ceux donnés dans la version complète du présent rapport (Volume II).

1º Environ 5% du volume total de roches volcaniques compris entre 500 mètres et 1500 mètres de profondeur sous la surface, à Mururoa aussi bien qu'à Fangataufa, a été endommagé du fait des essais nucléaires souterrains. Il n'y a eu aucun endommagement au-delà de 1500 mètres de profondeur.

   Une partie des premiers essais, conduits sous la couronne de Mururoa, ont produit un endommagement des roches carbonatées depuis le sol jusqu'à une profondeur de 200 mètres, en entraînant des affaissements de surface visibles qui atteignent jusqu'à 2 mètres ; ces effets concernent environ 3% du volume total des couches carbonatées.

2º Associés à l'endommagement des carbonates dans la couronne sud-ouest de Mururoa, on constate un ensemble de glissements de pentes sous-marines, dont la plus grande intéresse quelques 0,1 km^3 de matériaux principalement détritiques. Sur la pente nord-est de Mururoa, une déformation de fluage permanente s'est prolongée pendant presque deux décennies ; elle se manifeste par de longues fractures ouvertes de surface, parallèles à la couronne, présentes à la fois du côté du lagon et du côté de l'océan. Des fractures analogues se sont développées sur la couronne nord-est de Fangataufa.

3º Ces affaissements et fractures dans les carbonates n'affectent pas le massif volcanique sous-jacent avec lequel elles ne sont pas en communication ; elles sont particulières aux portions des carbonates les moins résistantes, ou constituant la couronne émergée.

4º A l'exception de la pente nord-est de Mururoa, qui se déforme encore par fluage (avec une vitesse qui décroît au cours du temps) et peut-être (à un moindre degré) de la pente nord-est de Fangataufa (voir Recommandation 14, ci-dessous), les deux atolls sont partout stables et les soubassements volcaniques sont structurellement sains ; les cavités et cheminées, remplies de déblais, supportent efficacement les couches sus-jacentes.

5º Il n'y a eu d'impact à long terme (500 - 10 000 ans) sur l'hydrologie globale d'aucun des deux atolls.

6º Les augmentations de température au voisinage du centre de chacune des explosions ont entraîné des accroissements détectables de la vitesse ascendante de l'eau souterraine. Cet accroissement est particulièrement marqué dans les cas où la cheminée atteint les carbonates. Les accroissements de la vitesse de l'eau s'effaceront avec le temps, et les effets de la température seront imperceptibles après 500 ans.

Si l'on revient sur les questions posées dans le Tableau 1.1, on peut plus particulièrement conclure :

7º Il n'y aura pas, à Mururoa et Fangataufa, de nouvel affaissement (ou subsidence) majeur que l'on puisse attribuer aux campagnes d'essais. Il n'y a eu, et il n'y aura, aucun danger de volcanisme induit.

8º Un ou plusieurs grands effondrements sous-marins pourraient affecter les flancs de la couronne nord-est de Mururoa, intéressant un volume total de matériaux qui pourrait atteindre 0,6 km^3. (Les mouvements des pentes dans cette région sont surveillés de près de sorte qu'on disposerait d'une alerte adéquate en cas d'accélération du fluage). Des glissements analogues sont envisageables sur la couronne nord-est de Fangataufa, mais ils n'ont pas fait l'objet de surveillance. Aucun nouveau glissement ne doit être attendu dans la couronne sud-ouest de Fangataufa, où de tels glissements sont déjà survenus.

9º On n'a pas créé de fractures majeures s'enfonçant profondément à l'intérieur des atolls, et les fractures visibles à la surface ne s'étendent pas jusqu'au massif volcanique.

10º L'hydrologie des atolls n'a pas été modifiée de manière durable. Les radionucléides produits par la plupart des explosions nucléaires réalisées sont toujours convenablement confinés par une couverture suffisante de roches volcaniques relativement imperméables. Les explosions effectuées dans les carbonates, ou les explosions qui ont engendré des cheminées ou des zones endommagées atteignant les carbonates, ont donné lieu à des relâchements précoces, mais qui ne présentent pas un risque significatif pour l'environnement, de tritium, strontium et césium, dans les portions inférieures des carbonates (et donc dans le lagon et l'océan).

11º Les modifications, mentionnées plus haut en 1. et 2., qui sont survenues, n'ont pas une importance supérieure à celle des modifications naturelles, telles que la baisse du niveau de la mer due aux glaciations, ou la croissance et la régression du corail, que l'on doit attendre à moyen terme à Mururoa et Fangataufa. Les atolls de corail se développent en permanence ; l'expérience historique montre que des changements topographiques, bien plus grands que ceux que l'on peut attribuer à la série d'essais, surviennent quand on considère de longues périodes de temps. On sait que des évènements isolés de la même ampleur que les glissements provoqués à Mururoa surviennent périodiquement.

12º Dans les régions peuplées du reste du monde, des changements de l'hydrologie et de la topographie, plus importants en termes quantitatifs, ont été induits par des activités humaines banales (et nécessaires) telles que l'agriculture de grande échelle, l'activité minière ou la construction des villes.

13º Il est recommandé que le système actuel d'instrumentation destiné à mesurer les déformations futures de la région nord-est de Mururoa soit maintenu et surveillé pendant les 20 prochaines années (ou jusqu'à l'apparition d'un effondrement, si celui-ci survenait pendant cette période), afin qu'il informe en temps utile de l'imminence possible d'un effondrement.

14º Il est recommandé que les informations complémentaires qui ont conduit le DIRCEN/CEA à conclure que le fluage observé dans le nord-est de Fangataufa était stabilisé soient rendues publiques, avec l'objectif d'obtenir une évaluation indépendante du danger que des glissements sous-marins plus importants ne surviennent dans cette région.

15º Il est recommandé que les observations relatives au relâchement de radionucléides dans les carbonates inférieurs et dans les lagons de Mururoa et Fangataufa soient poursuivies, et que des études complémentaires analytiques et numériques soient menées afin de parvenir à une meilleure explication du mélange intensif d'eaux souterraines observé dans les carbonates.

Enfin, on note que les six essais de la campagne 1995/1996 ont tous été tirés dans le massif volcanique des parties centrales des atolls. Quoiqu'aucun détail spécifique concernant ces essais n'ait été fourni à l'I.G.C., il est clair que ces essais évitaient les risques de rupture dans les pentes associés aux essais sous la couronne. La poursuite de la surveillance du tritium relâché dans les carbonates des deux atolls devrait permettre d'évaluer si le confinement des essais est effectif.

Chapitre 2

PRÉSENTATION D'ENSEMBLE

2.1 Introduction

Ce chapitre présente un compte rendu synoptique des résultats obtenus par la Commission Géologique Internationale (CGI) au cours de ses investigations techniques. Cette présentation d'ensemble ne suit pas exactement l'ordre des chapitres ; elle cherche plutôt à présenter les résultats de la CGI d'une manière globale. Ce compte rendu est complété par des illustrations graphiques et des commentaires qui visent à informer le lecteur des considérations sous-jacentes qui ont influencé les orientations données aux investigations. Il répond aussi à des préoccupations qui, quoiqu'elles ne soient pas mentionnées explicitement dans les Chapitres 2 à 7*, se sont faites jour au cours d'autres examens techniques ou publics des essais nucléaires de Mururoa et Fangataufa. Une section intitulée « Résultats, Conclusions et Recommandations » était initialement placée à la fin du présent chapitre ; toutefois, en raison de l'intérêt de cette section pour le lecteur, elle précède maintenant la Présentation d'Ensemble, en tant que résumé indépendant.

2.2 Formation des atolls

On se représente en général les atolls de Mururoa et Fangataufa, dans le Pacifique Sud, comme d'étroites bandes de récif corallien, larges de quelques mètres, s'élevant à 2 ou 3 mètres à peine au-dessus de l'océan, et délimitant un lagon. Les tempêtes les plus sévères peuvent créer des vagues qui submergent complètement les récifs.

Si l'on enlève, par la pensée, l'océan qui les recouvre (Figures 2.1.b, 2.2.b), ces structures fragiles se révèlent n'être que la limite supérieure de ce qui est, en fait, une montagne sous-marine de roches basaltiques, d'origine volcanique, surmontée de 300 à 500 mètres de calcaire, ou carbonates, s'élevant à plus de 4 kilomètres au dessus de la croûte terrestre, au fond de l'océan.

Ces édifices ont été formés il y a quelques 10 à 12 millions d'années, quand la plaque crustale est passée au-dessus d'un réservoir de magma fondu, ou « point chaud », qui, après avoir ouvert des fractures dans la croûte, s'est déversé et accumulé sur le fond de l'océan, créant des montagnes marines volcaniques qui, à leur développement maximum, s'élevaient à plus d'un kilomètre au-dessus de l'océan -avec une allure très proche

*Tous les Chapitres 2-7 et annexes cités dans cette Presentation d'Ensemble font partie du Volume II.

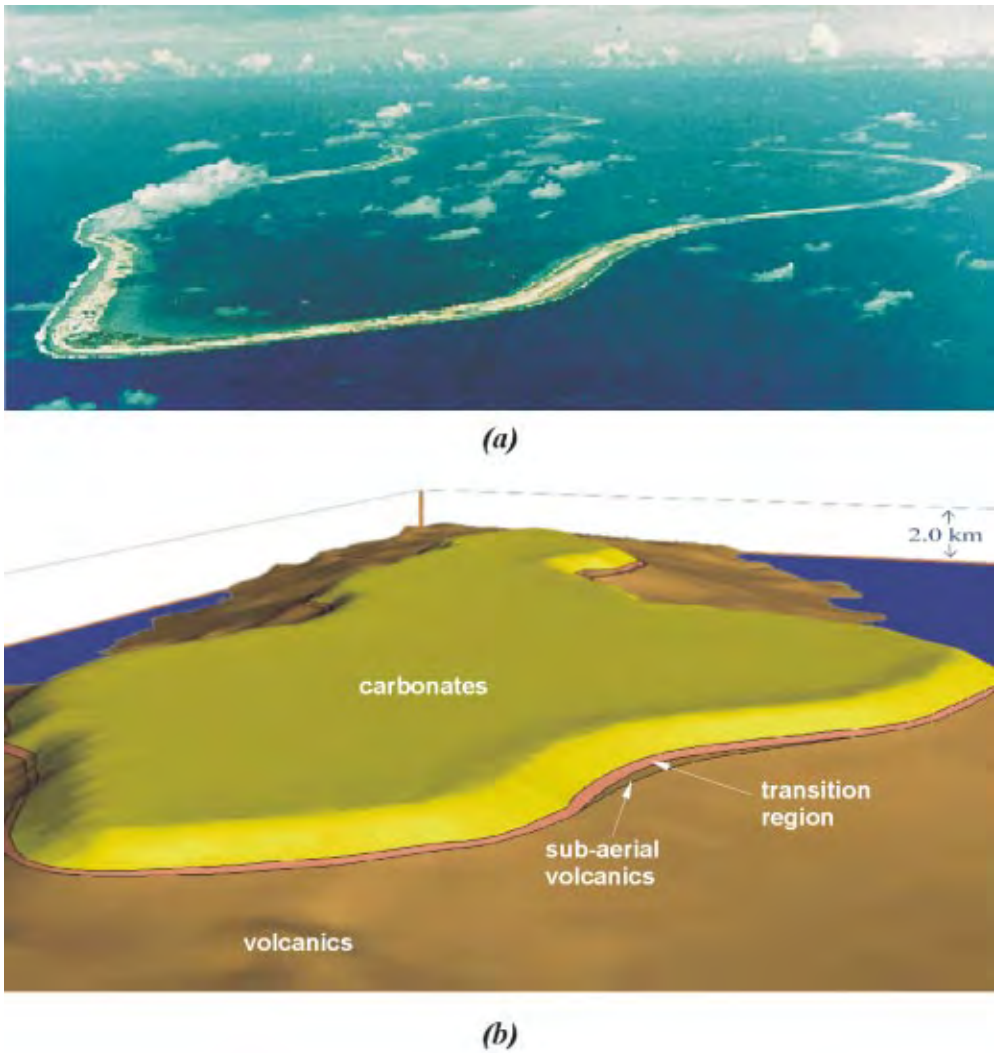

FIG. 2.1 Mururoa : (a) vue aérienne (b) vue bathymétrique (depuis le même point d'observation) jusqu'à une profondeur de 2,0 km (le massif volcanique -« volcanics/fg- est surmonté par les carbonates ; la perspective est orientée dans la direction sud-ouest (S 65^o O, altitude 21^o au-dessus de l'horizon) avec la zone d'essais 1 (voir Figure 2.17) au premier plan)

(a)

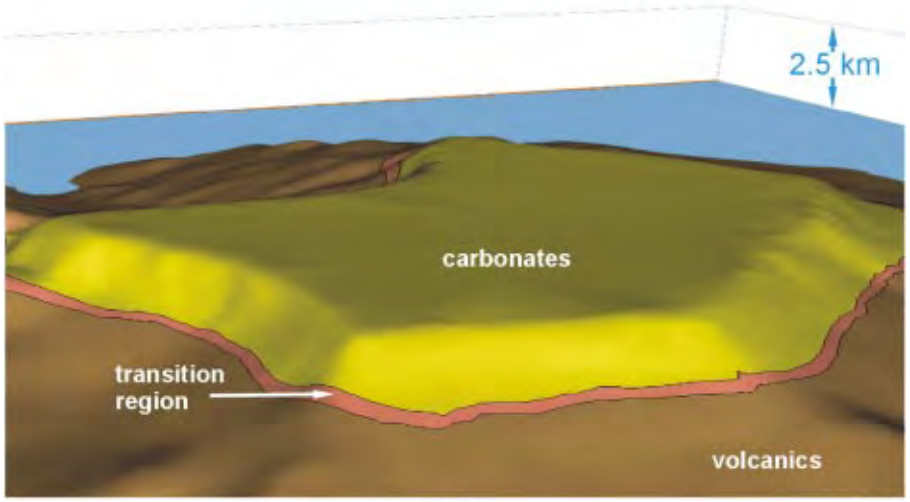

(b)

FIG. 2.2 Fangataufa : (a) vue aérienne (b) vue bathymétrique (depuis le même point d'observation) jusqu'à une profondeur de 2,5 km (Les flancs descendent beaucoup plus brutalement à Fangataufa qu'à Mururoa ; le massif volcanique - « volcanics » - est surmonté par les carbonates ; la perspective est orientée vers l'ouest (N 68^o W, altitude 27^o au-dessus de l'horizon) avec la zone d'essais 1 sur la partie gauche du récif

FIG. 2.3 Vue aérienne de Mehetia

de celle de l'île de Mehetia aujourd'hui (Figure 2.3). La lave produite par le volcan change de nature quand les écoulements sous-marins profonds font place à des dépôts moins profonds, à des explosions aériennes de cendre volcanique et, finalement, à des écoulements de lave sur l'îlot émergé.

L'activité volcanique s'arrêta après 1 à 2 millions d'années, quand la plaque, au cours de son mouvement, s'éloigna de l'influence du point chaud. Le matériel solide d'origine volcanique se refroidit graduellement et se consolide, provoquant un affaissement lent de la montagne dans l'océan. Le corail et les algues, fixés à la surface du massif rocheux qui s'affaisse, forment alors un tablier extérieur de roches carbonatées, qui se développe latéralement dans les 50 à 60 mètres d'océan dans lesquels pénètre la lumière du soleil. Finalement, quand l'île est proche dêtre submergée, la croissance du corail se généralise pour couvrir toute sa surface, et pour produire ce qui est maintenant sa couverture carbonatée. Une discussion plus complète du processus de construction de l'atoll est donnée au Chapitre 2.

Au cours de la dizaine de millions d'années qui nous sépare de la fin de leur activité, les deux îles ont dérivé de plus de 1000 km (avec une moyenne d'environ 11 cm par

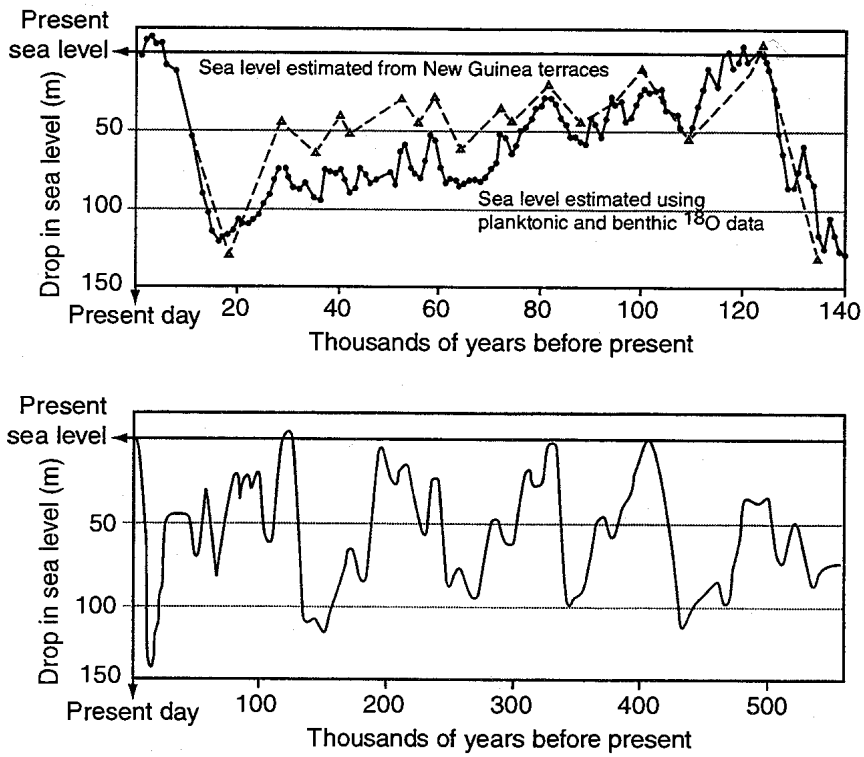

FIG. 2.4 Variations du niveau de l'océan au cours des 500.000 dernières années (en haut : Shackleton (1987), en bas : Lalou *et al.* (1988)

an) vers le nord-est du point chaud, qui est maintenant situé à 70 km au sud-est de l'île Pitcairn. Aujourd'hui, Mururoa et Fangataufa sont des volcans éteints, très éloignés de leur source magmatique (et donc, par nature, ne peuvent être réactivés).

L'affaissement progressif et lent a été interrompu par des cycles de glaciation mondiale, aux âges glaciaires, qui ont produit une descente relativement rapide du niveau de l'océan, qui a pu atteindre jusqu'à 150 mètres (Figure 2.4). L'île a de nouveau été émergée, et l'îlot carbonaté a été exposé aux effets des éléments, notamment les chutes de pluie (et les processus associés d'altération, de dissolution et de précipitation). Avec la fin de la période glaciaire, l'île de nouveau submergée redevient saturée en eau de mer.

Il y a à peu près 3000 ans, le passage d'une période chaude au climat actuel plus froid a produit une descente de 3 mètres environ du niveau de l'océan (Figure 2.4), qui explique l'élévation actuelle du récif au-dessus de la mer. Les accrétions coralliennes sont incapables de se développer beaucoup au-dessus du niveau de la mer, et se sont étendues horizontalement. Comme ces accrétions sont relativement fragiles, l'extension horizontale se limite d'elle-même, et les accrétions peuvent s'effondrer périodiquement,

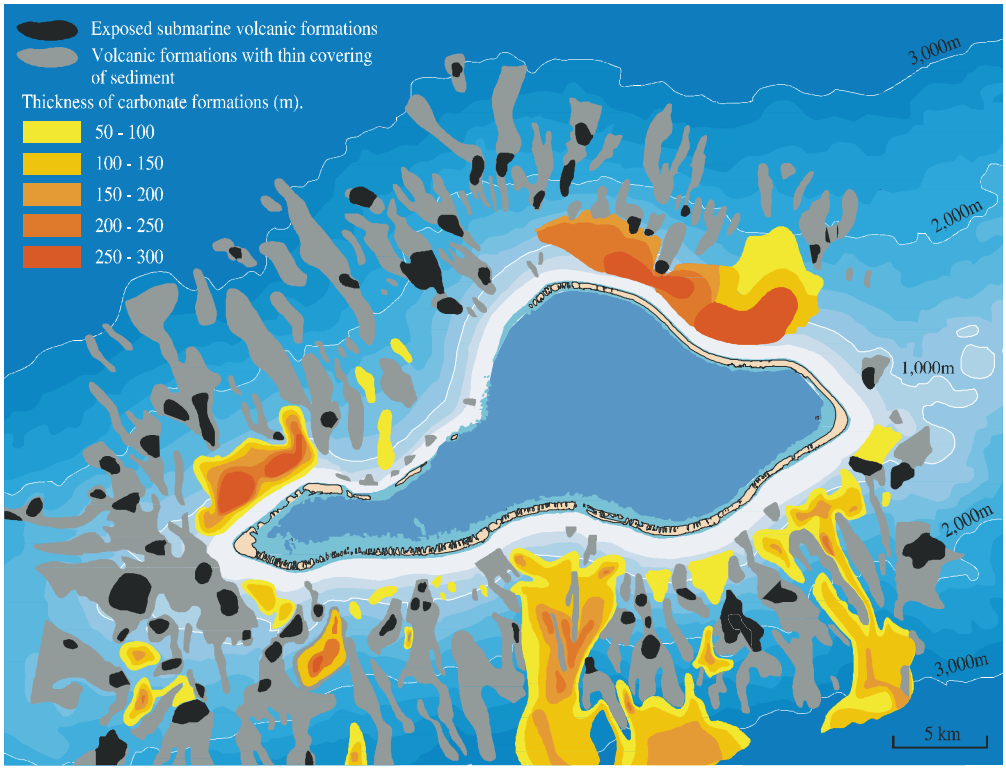

FIG. 2.5 Distribution des dépôts sédimentaires et des affleurements sous-marins sur les flancs de l'atoll de Mururoa (Guille *et al.* 1996, Figure 23)

sous leur propre poids ou sous l'effet d'excitations sismiques -ayant pour origine un tremblement de terre éloigné. La Figure 2.5 montre des accumulations de sédiments érodés et effondrés présentes autour des atolls jusqu'à des profondeurs de plus de deux kilomètres. Des instabilités plus récentes des pentes, effondrements et déplacements de la surface, conséquences des explosions souterraines, sont discutées en détail dans les Chapitres 3 et 4, et plus brièvement aux sections 2.5.3 et 2.5.4 de cette Présentation d'Ensemble.

La Figure 2.6 montre des coupes géologiques schématiques des deux atolls qui utilisent les résultats de campagnes sismiques et de forages carottés d'exploration. On doit noter que les épaisseurs réelles des différentes formations sont bien moindres que celles représentées sur les coupes, dont l'échelle verticale a été considérablement exagérée.

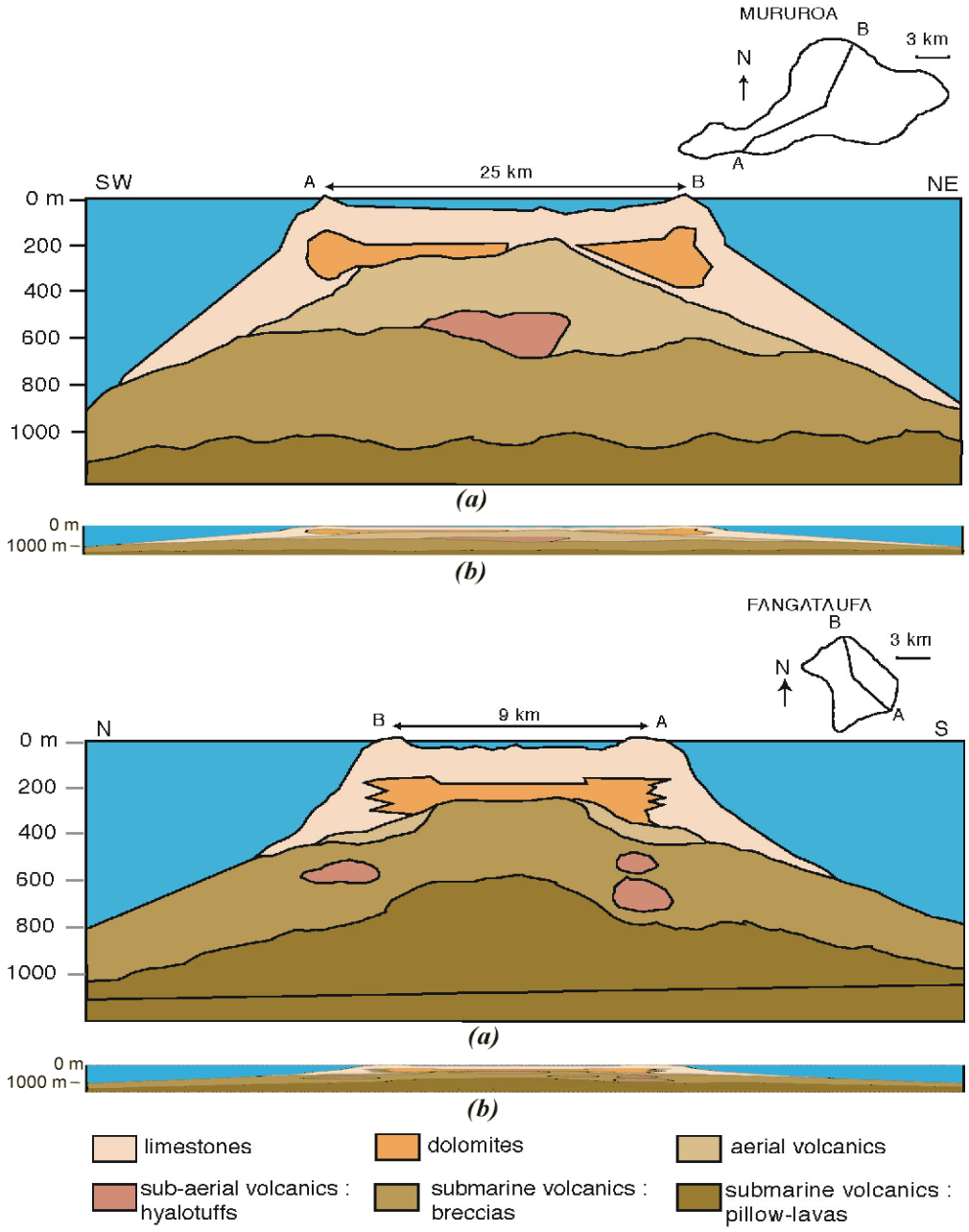

FIG. 2.6 Lithologie schématique de Mururoa et Fangataufa (modifié d'après Buigues, 1997 ; voir aussi Figures 2.5-2.8), les épaisseurs verticales sont exagérées d'un facteur 10 environ (a) et d'un facteur 2 (b). (Les dessins avec les mêmes échelles verticales et horizontales sont trop « aplatis » pour permettre une interprétation.)

2.3 Mécanique d'une explosion nucléaire souterraine

Avant d'examiner les effets des explosions nucléaires souterraines sur la stabilité et l'hydrogéologie des atolls, il est nécessaire de se faire une image correcte de la manière dont l'énergie relâchée par une explosion nucléaire répartit ses effets au sein de la masse rocheuse autour du point de tir. L'énergie produite ou simplement « énergie » d'une explosion nucléaire est généralement exprimée en termes d'énergie équivalente qui serait dégagée par l'explosif chimique TNT (trinitrotoluène) [Ainsi, on considère qu'une explosion nucléaire de 100 kt dégage autant d'énergie ($4,18.10^{14}$ joules[†]) que cent mille tonnes de TNT]. Cependant, les effets d'une explosion nucléaire sur le massif rocheux ne peuvent être considérés comme une simple transposition, à une échelle considérablement plus grande, des effets d'une explosion chimique. Le caractère pratiquement instantané d'une réaction nucléaire, et la vitesse énormément plus élevée à laquelle l'énergie nucléaire est engendrée à l'instant initial, introduisent des particularités qui rendent l'explosion nucléaire fondamentalement distincte de l'explosion chimique. L'énergie explosive d'origine chimique est dégagée à une vitesse qui est déterminée par la célérité de la détonation, qui est du même ordre de grandeur que la célérité du son dans l'explosif - en général un peu moins que 10 kilomètres par seconde. L'énergie nucléaire est engendrée à la vitesse des radiations électromagnétiques, qui se compare plutôt à la célérité de la lumière (300 000 kilomètres par seconde). Les pressions et températures initiales de l'explosion nucléaire (c'est-à-dire, dans la chambre initiale d'essai) sont aussi, en conséquence, beaucoup plus grandes, de l'ordre de 10^6 MPa et 10^6 K, ou plus.

Le déclenchement de l'explosion dans le conteneur donne naissance à la boule de feu, qui fait fondre et se vaporiser instantanément la roche (et la chambre qui contient l'engin[‡]). Le rayon de la zone vaporisée est de l'ordre de 2 mètres pour une énergie de 1 kt [¶] (ce rayon est celui de la cavité initiale, noté r_i, utilisé dans les calculs discutés au Chapitre 3 et sur la Figure 2.7). Ce rayon r_i (Figure 2.9a) est à peu près proportionnel à la racine cubique de l'énergie de l'explosion Y (c'est-à-dire $r_i \propto Y^{1/3}$).

[†] Ou 10^{14} calories d'énergie thermique (4,18 joules est l'équivalent mécanique de 1 calorie). L'énergie effectivement relâchée par une explosion de TNT varie quelque peu autour de la valeur « moyenne » supposée (10^{12} calories/kt) en fonction de plusieurs facteurs, tels que la densité initiale de la charge et la nature du milieu environnant (confinant), par exemple air ou roche.

[‡] Au Centre d'Essai du Pacifique (CEP) le volume de la partie du conteneur qui reçoit l'engin est de 1 mètre cube environ. L' « explosif » nucléaire proprement dit, qui peut avoir une énergie s'élevant jusqu'à 150 000 tonnes (cette énergie est limitée par le Threshold Test Ban Treaty, voir Préface), n'occupe qu'une petite fraction de ce volume. Un mètre cube de TNT (dont la densité est 1,65) aurait une énergie de moins de 2 tonnes. (Une liste de tous les essais souterrains réalisés au CEP, dont tous étaient inférieurs à 150 kt, peut être trouvée dans l'annexe C du présent rapport, version anglaise).

[¶] Le rayon de cette zone augmente comme $Y^{1/3}$, où Y est l'énergie de l'explosion. De ce fait, le volume de cette zone instantanément vaporisée augmente en proportion directe de l'énergie. Les pressions et températures initiales dans cette zone sont, pour l'essentiel, constantes, c'est-à-dire indépendantes de l'énergie du tir.

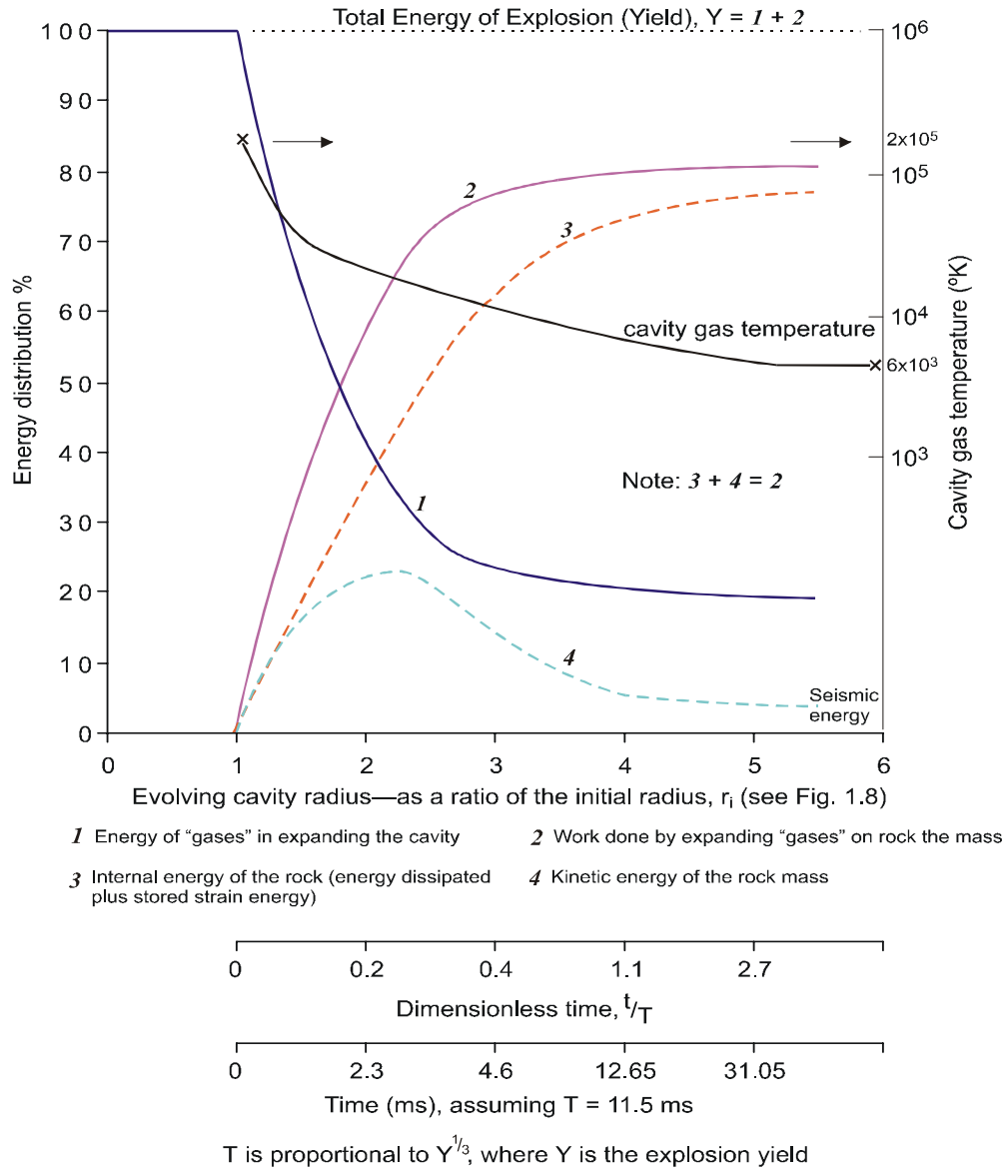

FIG. 2.7 Répartition de l'énergie dégagée par une explosion pendant les premières phases d'expansion de la cavité (Notes : (i) l'estimation du rayon final de la cavité dans le massif volcanique, soit $R_c \approx 6\, r_i$, résulte des calculs du Chapitre 3 ; (ii) cette répartition relative aux premières phases de l'expansion ne prend pas en compte une dissipation éventuelle de l'énergie. Si l'on excepte les faibles quantités produites d'énergie sismique et élastique (principalement relâchée lors du rebond de la cavité) toute l'énergie de l'explosion est en fait dissipée dans le voisinage de la cavité.)

La création pratiquement instantanée, au sein du massif rocheux, de « gaz » à haute pression (provenant de la roche vaporisée et du matériau constituant le conteneur) produit un chargement mécanique des parois de la cavité initiale par un choc de haute intensité (Figure 2.8). La Figure 2.9 illustre le développement de cette cavité dans le cas d'une énergie de 1 kt. Une onde de choc divergente à symétrie sphérique commence à se propager dans le massif rocheux. Au début, au voisinage immédiat de la cavité instantanément créée et remplie de gaz, le front du choc vaporise la roche puis, quand il a progressé dans le massif, fait fondre la roche. Selon Bouchez et Lecomte (1996) cent tonnes de roche environ sont vaporisées et deux cent dix tonnes environ sont fondues (par kt d'énergie) pendant les étapes ultérieures du chargement par le choc et de l'expansion de la cavité (Figures 2.9c et 2.9d).

Deux caractéristiques importantes de ce chargement doivent être notées.

1° La vitesse de chargement est si rapide que la roche est intensément comprimée au sein d'une coque sphérique relativement peu épaisse. L'effet est physiquement équivalent, pour la roche contenue dans cette coque, au « formage » dans une matrice extérieure infiniment rigide (c'est-à-dire non déformable). De ce fait, la roche est soumise à une compression dans toutes les directions de l'espace (tangentiellement aussi bien que radialement). Ainsi, pendant cette phase du processus explosif, il n'existe pas de possibilité de création ou propagation de fissure en extension.[§]

2° L'intensité de l'onde de choc entraîne dans le massif rocheux des processus hautement dissipatifs - c'est-à-dire qu'une large part de l'énergie explosive est absorbée par la roche dans une zone limitée à une courte distance de la source de l'explosion. Ceci est illustré sur la Figure 2.7, qui représente des résultats des analyses du Chapitre 3. On y voit que près de 70% de l'énergie de l'explosion est transférée du gaz (à forte pression et haute température) à la roche dans un temps de l'ordre de trois millisecondes. La plus grande part de cette énergie est transférée au massif rocheux sous forme d'« énergie interne ». Même si cela inclut un peu d'énergie de déformation élastique, la part élastique est vraisemblablement petite. Il apparaît donc qu'une large fraction de l'énergie d'une explosion nucléaire souterraine serait dissipée en déformation anélastique et en chaleur très près de la source explosive. Il résulte des analyses présentées au Chapitre 3 que plus de 90% de l'énergie de l'explosion est dissipée à l'intérieur d'une sphère de rayon $5R_c$, et

[§] C'est pour cette raison que la lave fondue, qui contient la très grande majorité des radionucléides engendrés par l'explosion, ou les radionucléides présents sous forme gazeuse ou vaporisée, ne s'échappent pas dans le massif rocheux et restent piégés dans la cavité. La lave fondue se solidifie ultérieurement, emprisonnant les radionucléides. Selon Bouchez et Lecomte (1996), 98% des éléments de demi-vie supérieure à 30 ans sont piégés initialement dans la lave. Les radionucléides peuvent devenir partiellement accessibles à une dissolution et à un transport par l'eau souterraine au fur et à mesure que la lave se désintègre au cours des centaines et milliers de siècles ultérieurs.

Ondes de choc et ondes plastiques

Le mot "choc" est utilisé dans le langage courant comme un synonyme de "impact" ou "secousse" (par exemple "choc sismique") mais il est utilisé, dans le présent document, dans son acception scientifique.

Une onde de choc est une onde qui se déplace plus vite que la vitesse ordinaire du son et présente un front à la forme très raide caractéristique (à la fois dans le temps et dans dans l'espace).

Toutefois, toutes les ondes présentant un front raide ne sont pas des ondes de choc – un vrai choc se forme dans un matériau qui devient plus raide quand le chargement mécanique augmente. La courbe contrainte–déformation de nombreuses roches, dans le domaine des compressions intenses, a l'allure suivante...

et la vitesse de l'onde a cette allure :

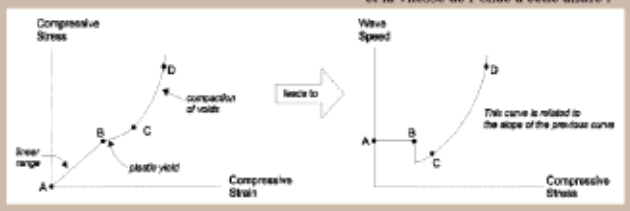

Si l'on envoie une impulsion qui traverse un tel matériau, la réponse dépend de la taille (ou "amplitude") de l'impulsion. Pour une petite impulsion (demeurant dans le domaine A–B), l'impulsion se déplace à la vitesse usuelle du son et sa forme n'évolue pas. Quand l'amplitude est plus grande (disons, au niveau de contrainte marqué par le point C) un précurseur élastique apparaît parce que la partie principale plastique se déplace plus lentement :

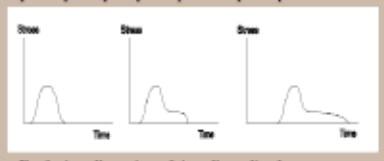

Evolution d'une impulsion d'amplitude moyenne

Pour de grandes impulsions (par exemple point D) c'est le contraire : les amplitudes élevées se deplacent plus vite que les amplitudes petites et les rattrapent de sorte que l'impulsion devient plus raide (ou "forme un choc") :

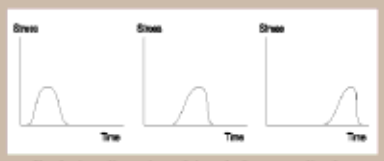

Evolution d'une impulsion de forte amplitude

La nature de l'onde engendrée par une explosion, par conséquent, se modifie quand son amplitude décroît avec la distance a la source. Elle évolue depuis une onde de choc, au voisinage de l'origine, vers une onde plastique présentant un précurseur élastique, quand on s'éloigne de l'origine. A distances encore plus grandes, on n'observe plus que des ondes sismiques élastiques.

FIG. 2.8 Ondes de chocs et ondes plastiques

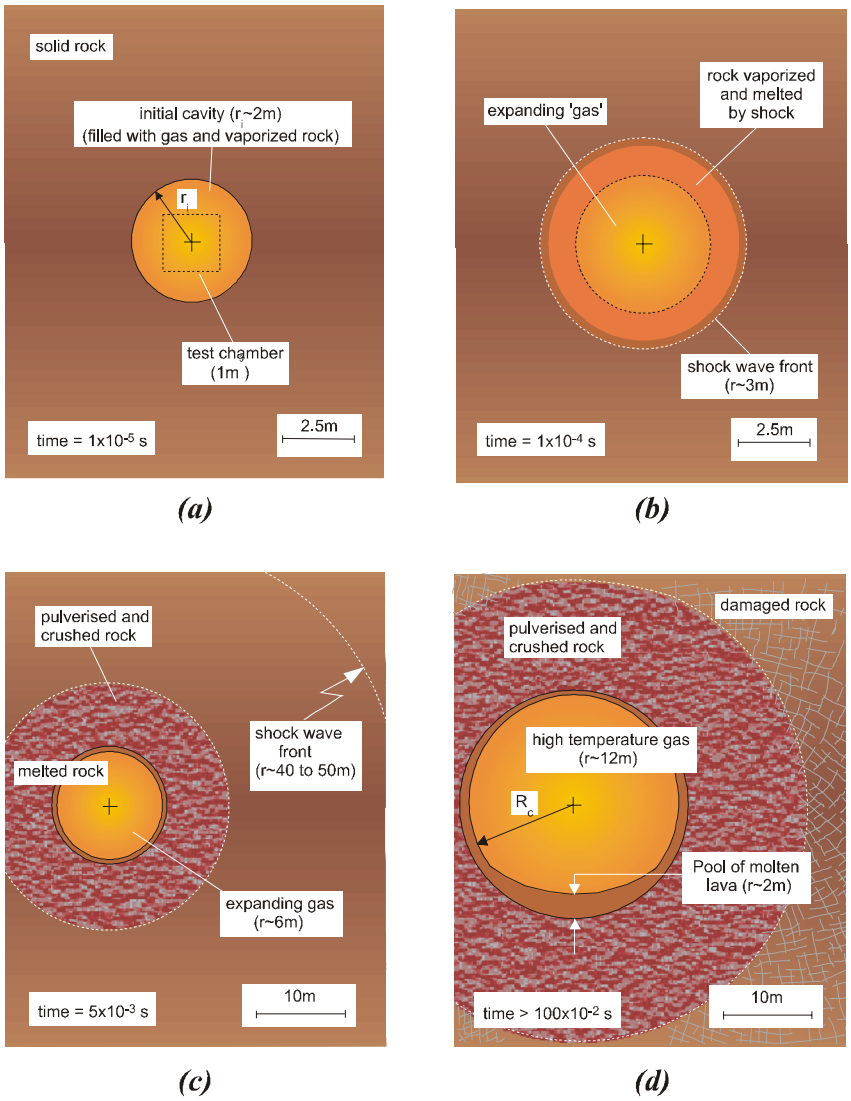

FIG. 2.9 Etapes de la formation de la cavité et de son développement pendant une explosion nucléaire (Note : r_c est le rayon de la sphère vaporisée « instantanément » ; $r_c \approx 2$ mètres pour une explosion de 1 kt) ; étapes ultérieures de l'expansion de la cavité (jusqu'à sa taille finale) et endommagement associé du massif rocheux pendant une explosion nucléaire (Note : R_c est le rayon final de la cavité complètement développée. $R_c \approx 12$ mètres pour une explosion de 1 kt (peu profonde) dans les atolls ; à plus grande profondeur $R_c \approx 10$ mètres pour une explosion de 1 kt)

plus de 95% à l'intérieur d'une sphère de rayon $10R_c$, où R_c est le rayon final de la cavité résultant de l'explosion (voir Figure 2.10).

Comme il a été noté plus haut, l'intensité du chargement initial par choc est suffisante pour produire une fusion directement au front du choc. Immédiatement au-delà de la cavité initiale (de rayon r_i) la pression moyenne de l'onde de choc dans le régime « hydrodynamique » est tellement supérieure à la résistance au cisaillement de la roche que la roche se comporte pour l'essentiel comme un fluide (visqueux). Au-delà de ce « rayon de fusion de la matrice solide »,

...l'eau interstitielle est vaporisée sur quelques mètres de distance. En se détendant, la vapeur à haute pression fait éclater la matrice qui se divise en fines particules. Lors de l'expansion ultérieure de la cavité sous l'effet de la poussée des gaz, une partie de cette zone de roche broyée est recompactée et partiellement frittée. Elle forme une coquille à faible perméabilité autour de la cavité (Bouchez et Lecomte, 1996, p.42).

Ceci suggère la possibilité que, bien que soumise à une déformation anélastique intense, la roche dans cette région pourrait être renforcée (« écrouie ») par le passage du choc. Des observations montrant que la roche au voisinage de la paroi de la cavité paraît intacte, avec des propriétés élastiques et une résistance substantielles, ont été faites au site d'essai du Nevada (Nevada Test Site) au cours d'investigations au moyen de galeries creusées après l'essai dans le voisinage immédiat de la cavité produite par l'explosion - c'est-à-dire dans la région $2R_c > R > R_c$. De telles investigations de grande échelle après essai n'ont pas été conduites à Mururoa ou Fangataufa.

Quand la pression moyenne au front du choc décline, en raison à la fois de l'atténuation (provoquée par la très forte dissipation) et de la croissance de l'aire du front de choc radialement divergent, le front initialement très raide se dégrade progressivement, et la roche est moins intensément endommagée. Au-delà d'un rayon de l'ordre de 8 à 10 R_c, plus aucun dommage n'est infligé au massif rocheux[‖].

La Figure 2.10 tente d'illustrer les évolutions de la nature de l'endommagement de la roche que l'on peut attendre, en fonction des distances à l'explosion, à la suite du passage de l'onde de choc. En réalité, bien sûr, les zones d'endommagement ne sont pas délimitées aussi nettement. Cependant, toute fracture induite dans le voisinage immédiat de l'explosion sera une fracture en cisaillement, produite par le glissement l'une sur l'autre des surfaces de la fracture sous l'effet d'un chargement compressif. Il ne s'agit pas de fractures radiales en extension, qui sont typiques des situations de chargement dynamique, dans lesquelles la contrainte nette (déviatorique) tangentielle est une traction (comme cela arrive quand le temps de montée de l'onde explosive est beaucoup plus long que dans le cas d'une explosion nucléaire), ou des situations de chargement par une pression appliquée de manière quasi statique dans la cavité.

[‖] À l'exception des fractures horizontales qui sont ouvertes par les contraintes de traction engendrées par les réflections d'onde aux interfaces entre roches dures et roches plus tendres. De telles ouvertures dues aux fractures sont fréquemment observées lors des forages qui suivent les essais.

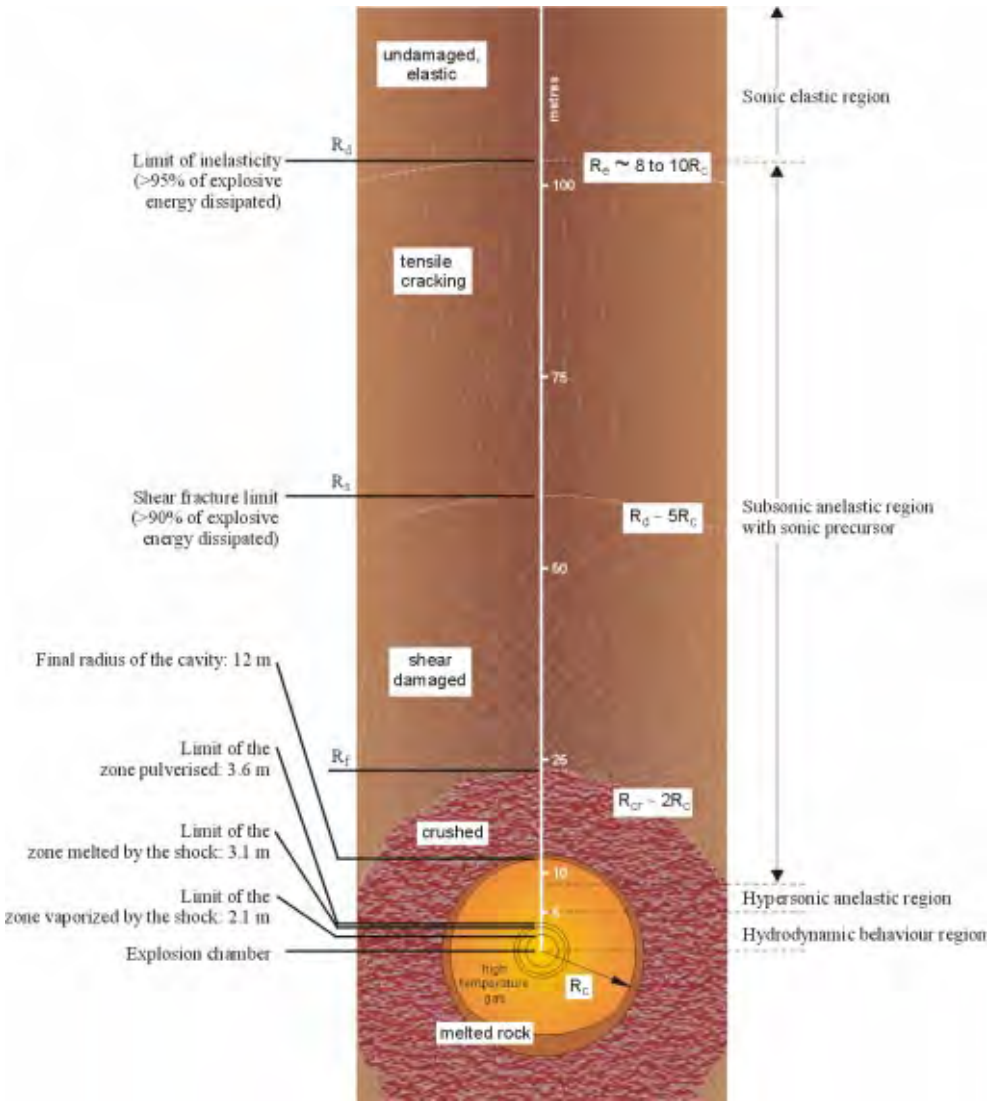

FIG. 2.10 Zones d'endommagement présumées autour d'une cavité créée par une explosion nucléaire de 1 kt dans les basaltes à Mururoa et Fangataufa (les rayons de zones endommagées sont exprimés comme des multiples du rayon final R_c de la cavité, qui augmente proportionellement à $Y^{1/3}$, où Y est l'énergie de l'explosion en kt) [modifié d'après Bouchez et Lecomte (1996) ; voir aussi Figure 3.7]

À plus grandes distances de la cavité, quand le front du choc (Figure 2.10) s'est considérablement dégradé (de telle sorte que, dans l'onde, la contrainte moyenne est devenue du même ordre de grandeur que la contrainte déviatorique, et que le temps de montée de l'onde est devenu plus long), une certaine fracturation radiale apparaîtra, provoquée par une traction tangentielle associée à la compression radiale transportée par l'onde. Plus loin encore, les fractures se dégradent en fissures, induites par les inhomogénéités préexistantes qui engendrent des tractions localisées dans la roche (comme on l'observe au cours du chargement en compression d'une éprouvette de roche soumise à une contrainte de confinement faible ou nulle). Ces fissures demeurent vraisemblablement non connectées, et sont réparties dans toute la masse rocheuse, quoique des fractures préexistantes puissent aussi croître. Dès lors, les fractures formées pendant le passage de l'onde de choc divergente ne forment vraisemblablement pas de passages connectés reliant la cavité à la masse rocheuse restée « non endommagée ». C'est dans la région la plus périphérique, où l'amplitude de l'onde approche de la limite sous laquelle elle se propage « sismiquement » (c'est-à-dire sans endommagement de la roche), que les petites inhomogénéités, dans la résistance de la roche et les contraintes en place, acquièrent de l'importance parce qu'elles contrôlent l'extension des fractures.

Dans les atolls, la contrainte horizontale in situ est moins grande que la contrainte verticale (voir Chapitre 2, section 2.6) de sorte que les fractures radiales tendront à se propager préférentiellement vers le haut, dans la direction verticale. On doit noter cependant que les fractures produites par l'onde divergente ne sont pas remplies de fluide sous pression, comme ce serait le cas si les gaz de la cavité y pénétraient directement, créant alors une situation analogue à celle rencontrée dans plusieurs situations réelles - par exemple dans le chargement mécanique par explosifs chimiques (de faible intensité), dans la technique de la fracturation hydraulique (utilisée pour stimuler la production dans les champs de pétrole), ou dans le développement de dykes volcaniques par intrusion de magma fondu. D'ailleurs, la structure en couches subhorizontales du massif volcanique tend à inhiber la propagation de fractures verticales.

Des mécanismes possibles d'extension des fractures par mise en pression de la cavité par des fluides à haute pression sont discutés à l'annexe D.

La formation d'une cavité de 12 mètres de rayon par une explosion nucléaire de 1 kt est achevée, pour l'essentiel, dans le dixième de seconde qui suit l'explosion. Ceci correspond à une vitesse moyenne de croissance du rayon de la cavité supérieure à 400 km/h ! Les vitesses initiales sont considérablement plus fortes encore, car le dixième de seconde évoqué inclut la phase de décélération qui accompagne l'arrêt de l'expansion de la cavité. Des énergies d'explosion plus grandes impliquent des vitesses elles aussi plus grandes (voir Figure 2.7). Comme le rayon final de la cavité (R_c) et la durée de la croissance de la cavité augmentent tous deux proportionnellement à Y, où Y est l'énergie de l'explosion, la vitesse de dilatation de la cavité est largement indépendante de l'énergie. Comme il y a très peu d'augmentation de la densité de la roche consécutive à

l'explosion, presque tout le volume de cavité créé doit se retrouver sous la forme d'une déformation (rapide) de la roche qui demeure élastique, à l'extérieur de la zone endommagée. Au cours de cette déformation élastique, la roche emmagasine une énergie qui est relâchée, ou déchargée, quand la pression du gaz dans la cavité chute jusqu'à, voire en-dessous de, la pression atmosphérique. La cavité « rebondit » vers l'intérieur, et une compression tangentielle, qui tend à refermer la cavité, est induite sur le pourtour de la paroi de la cavité. Ces compressions tangentielles, qui forment la « cage de contraintes », accroîssent l'étanchéité de toutes les fractures dans la zone endommagée autour de la cavité.

Il paraît probable, cependant, en raison de la fracturation naturelle qui affecte le massif volcanique à Mururoa et Fangataufa, que l'effet de cage de contraintes soit faible. Ce sujet est discuté à l'annexe E.

En même temps que le gaz refroidit, la pression du gaz dans la cavité décroît continûment au cours du temps et, après quelques minutes ou quelques heures, quand la pression de la cavité est descendue en-dessous de la valeur de la pression lithostatique (pression imposée par le poids des roches surincombantes) le toit commence à s'effondrer dans la cavité. Typiquement, l'effondrement se poursuit jusqu'à ce que le volume de morceaux cassés, ou « foudroyage », ait suffisamment progressé pour que sa hauteur atteigne 4 à 8 fois la valeur du rayon de la cavité originelle - c'est-à-dire jusqu'au moment où le volume de la cavité originelle s'est redistribué sous forme de porosité du foudroyage (voir annexe I). Les Figures H.1 et H.2 montrent quelques valeurs observées de la hauteur de la cheminée (H_c) en fonction du rayon de la cavité (R_c) [ou, de manière équivalente, en fonction de l'énergie du tir (Y)]. Une valeur de $H_c = 5R_c$ a été supposée dans la plupart des calculs présentés dans le rapport de la CGI.

2.4 Essais nucléaires sur les atolls

Des essais nucléaires atmosphériques, sur les atolls ou dans leur voisinage, ont été conduits de 1966 à 1974, date à laquelle ils ont été abandonnés en faveur d'essais souterrains dans les atolls. Les essais souterrains se sont échelonnés de 1975 à 1991, et ont repris de 1995 à 1996 (une liste complète des essais souterrains est donnée à l'annexe C, version anglaise du rapport). Les engins nucléaires ont été tirés dans les roches volcaniques, au fond de puits de 1,5 mètre de diamètre, forés jusqu'à une profondeur totale variant de 500 mètres jusqu'à 1100 mètres environ, selon l'énergie attendue de l'explosion. A l'origine, le choix des emplacements des sites d'essai était limité par la nécessité de forer les puits depuis la surface de la couronne émergée. Plusieurs ruptures majeures des flancs océaniques de l'atoll, qui ont débuté en 1977 (document DIRCEN/CEA n^o 7) et ont culminé dans le glissement de pente associé au tir Tydée en juillet 1979 (voir Figure 2.11), ont accéléré le développement de la technologie qui permet de forer des puits de diamètre 1,5 mètre depuis des barges dans les lagons. Les relevés bathymé-

triques effectués après l'effondrement consécutif à Tydée ont montré qu'une tranche de pente sous-marine, du côté océan, d'une extension latérale de quelque 2 kilomètres, se développant d'une profondeur de 1000 mètres jusqu'à la surface, et ayant en moyenne une épaisseur de l'ordre de 50 mètres (c'est-à-dire un volume total de 0,1 km^3), s'est effondrée avec une vitesse de 12 m/s (document DIRCEN/CEA n° 7, p.17). Cette descente brutale de la tranche rocheuse tend à entraîner vers le fond l'eau de mer qui est au contact de la pente. Le remplissage de la dépression créée à la surface de l'océan engendre une vague, un tsunami local, qui se brise sur la côte, et se propage, le long de l'atoll et vers l'océan (voir Bouchez et Lecomte (1996), Figure 8.3). L'effondrement de pente associé à Tydée produisit une vague, 90 secondes après l'effondrement, qui recouvrit une partie de Mururoa sous 2,5 mètres d'eau, et submergea la bande de terre à Fangataufa, distante de 40 km de l'effondrement, sous une épaisseur d'eau qui atteignit 2 mètres.

La figure 2.11 montre une vue aérienne qui indique la zone sous-marine affectée par l'effondrement lié à Tydée. La localisation présumée de l'essai Tydée est indiquée. La Figure 2.12 montre une vue analogue des zones effondrées à la suite des essais Nestor et Priam. On remarque que le centre des zones effondrées est situé à 3 kilomètres environ du point de tir présumé.

À partir de 1981, une proportion croissante des essais ont été conduits sous les lagons, à bonne distance des pentes océaniques des atolls. Tous les essais conduits depuis octobre 1986 l'ont été sous les lagons, y compris les essais de 1995-1996 (campagne finale). Selon les scientifiques du CEA, le point de tir (appelé aussi « point zéro ») de tous les essais souterrains était situé dans le massif volcanique, que ce point soit sous la couronne ou sous le lagon. Les explosions dans la zone d'essais 1 de Mururoa - « aidées » par des explosions ultérieures de grande énergie conduites sous les lagons - ont entraîné un autre type de réponse des pentes de la couronne. Les tirs dans la zone d'essais 1 étaient de bien plus faible énergie (en moyenne 2 kt) que ceux de la zone d'essais 4 (en moyenne 35 kt) et il n'y a eu à ce jour aucun effondrement spectaculaire. Cependant, en raison de la présence, dans la lithologie des carbonates de la région nord-est, d'une formation peu résistante de « calcaires crayeux » (voir Figures 5.11 et 5.12), les essais de la région nord-est ont stimulé une déformation de fluage progressive, observée d'abord en 1980, et qui a continué jusqu'à ce jour (voir Figures 5.8 et 5.9). Le volume total de roche impliqué dans ce mouvement est estimé à 0,6 km^3 environ, c'est-à-dire à peu près six fois le volume de l'effondrement consécutif à Tydée. Des fractures ouvertes de grandes dimensions produites par ces déformations des pentes sont clairement visibles dans cette région (voir Figures 2.13 et 2.14).

La couronne nord-est de Fangataufa, dont la géologie comporte aussi une formation peu résistante de calcaires crayeux, paraît avoir répondu de manière analogue, c'est-à-dire que des fractures, plus petites que celles de Mururoa, se sont développées, pour l'essentiel parallèlement au rivage, provoquées par l'onde de déformation engendrée par les essais de grande énergie dans le lagon de Fangataufa. Il n'y a eu aucun essai sous

FIG. 2.11 Vue aérienne montrant le région sous-marine de Mururoa qui a été affectée par l'effondrement consécutif à Tydée (la localisation présumée du tir Tydée et les limites de la zone effondrée ont été ajoutées par la CGI) [photographies fournies par le DIRCEN/CEA]

FIG. 2.12 Vue aérienne montrant la région sous-marine de Mururoa affectée par les effondrements consécutif aux tirs Nestor (Mars 1977) et Priam (novembre 1978) (voir aussi Figure 5.1) [photographies originales fournies par le DIRCEN/CEA, limites de l'effondrement ajoutées par la CGI]

FIG. 2.13 Photographie aérienne montrant les fractures en extension engendrées par la déformation de fluage continue qui a affecté la pente océanique de la couronne nord-est de Mururoa au voisinage de PK7-4N (zone Camélia), dans la zone d'essais 1 (voir la carte de Mururoa en Frontispice ; plusieurs fractures relativement étroites (10 à 20 cm), d'orientation E-N-E, sont visibles sur le rivage ; de plus grandes fractures, dont l'ouverture va probablement jusqu'à 2 mètres, peuvent être discernées sous plus grande profondeur d'eau) [photographie fournie par le DIRCEN/CEA]

FIG. 2.14 Photographie aérienne montrant des fractures en extension sous-marines, d'une largeur de l'ordre de 2 mètres, au voisinage de PK5N, section Irène (voir aussi Figure 5.6) ; une partie de la piste d'atterrissage, avec son mur protecteur, parallèle au bord du cliché, est visible dans la partie basse de la photographie ; cette région est à l'extérieur de la zone d'essais 1 [photo fournie par le DIRCEN/CEA]

la couronne nord-est de Fangataufa. Les déformations de fluage à Fangataufa paraissent arrêtées depuis 1992. La Figure 2.15 montre l'une des fractures dans cette région. La Figure 1.16 montre une section plane verticale, perpendiculaire à la côte, passant par l'emplacement présumé du tir Tydée (Voir Figure 2.11). Le point de tir figure à une profondeur de 987 mètres, mais le puits (le trou dans lequel l'engin est placé) avait été foré jusqu'à 1100 mètres (Bouchez et Lecomte, 1996). L'engin s'est trouvé bloqué à 987 m pendant sa mise en place dans le puits (Bouchez et Lecomte (1996) p. 25). On pense que tous les tirs souterrains dans les atolls ont eu des énergies inférieures à 150 kt (Bouchez et Lecomte, 1996), et à partir d'estimations sismiques, Tydée est considéré comme le plus grand - 115 kt (voir annexe B, version anglaise du rapport)**.

Sur la Figure 1.16, on a supposé une explosion de 150 kt qui a produit une cavité de rayon $R_c = 53$ mètres et une cheminée de hauteur $H_c = 5R_c = 265$ mètres (remarquer toutefois que des hauteurs de cheminées approchant 8 R_c semblent possibles à Mururoa et Fangataufa, voir Annexe I, Figure I.2). Le profil des pentes sous l'océan et la profondeur de l'interface carbonates-roches volcaniques sont repris des données bathymétriques détaillées fournies par l'Office Français de Liaison. Au moins deux caractéristiques importantes des atolls, du point de vue des effets des explosions souterraines, peuvent être remarquées sur la Figure 2.16.

1º Un changement clair de la lithologie (c'est-à-dire la zone de transition entre les roches volcaniques et les carbonates) survient entre la roche siège de l'explosion et la roche de surface (et ce, y compris dans les pentes). Les carbonates sus-jacents sont, d'un point de vue mécanique, plus faibles que les roches volcaniques.

2º Du fait que les deux types de roches présentent une porosité (roches volcaniques $\approx$ 20%, carbonates $\approx$ 30%, voir Chapitre 2) et une perméabilité considérables, et du fait qu'elles sont, pour l'essentiel, entièrement submergées, les roches sont complètement saturées jusqu'à la surface.

Ces caractéristiques ne sont pas présentes au Nevada Test Site (NTS) aux Etats-Unis - non plus, probablement, que dans les autres sites d'essais souterrains situés à l'intérieur des terres. Si l'on accepte, comme discuté ci-dessus, que l'onde de choc dans la roche volcanique dégénère en une onde élastique (ou « sismique ») (i.e., qui ne provoque pas d'endommagement de la roche) au-delà d'un rayon égal à 8 à 10 fois R_c, une couverture de roches volcaniques intactes existe de ce fait entre la région endommagée qui entoure la cavité créée par l'explosion et la base des carbonates. Toutefois, lorsque cette onde sismique traverse les carbonates moins résistants, elle peut de nouveau provoquer un endommagement, en particulier quand l'onde interagit avec la surface. Le fait que des affaissements de la surface du sol de l'ordre de 2 mètres ou plus aient été observés dans la couronne carbonatée au-dessus des sites de plusieurs explosions, et que des

** Hyrtacos, tiré à Fangataufa le 14 novembre 1990, a été estimé à 118 kt (Annexe C)

FIG. 2.15 Fractures en extension sous-marines d'une ouverture de l'ordre de 40 cm sur la couronne nord-est de Fangataufa au voisinage de Kilo-Frégate (aucun essai n'a été conduit sous la couronne ; les fractures ont été stimulées par les essais conduits dans le lagon de Fangataufa)

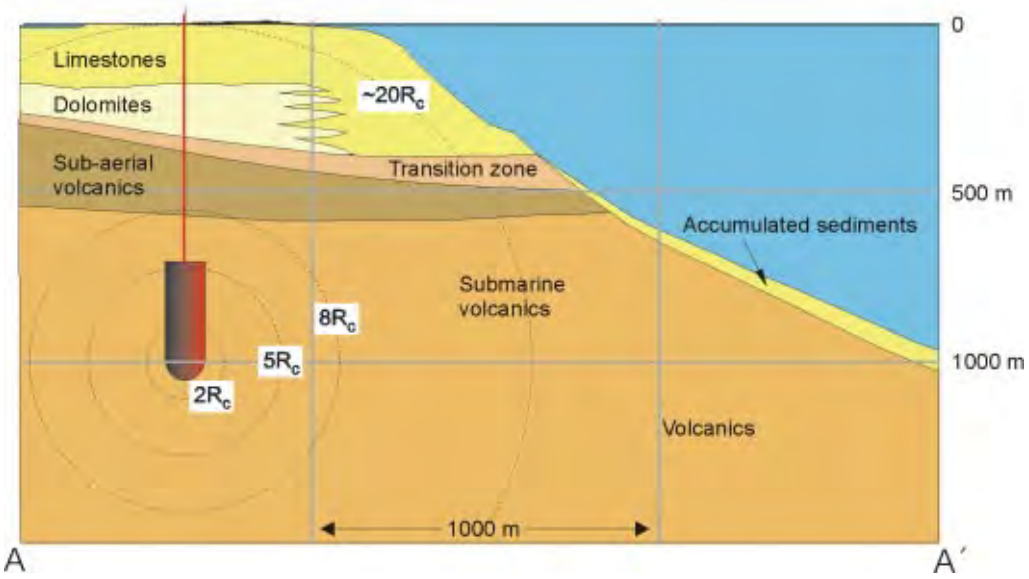

FIG. 2.16 Illustration schématique de la cheminée (avec l'hypothèse $H_c = 5R_c$) formée par un essai hypothétique de 150 kt conduit sous la couronne dans la zone d'essais 4 (voir Document DIRCEN/CEA n° 7, Figure 16) et extension radiale de l'endommagement

glissements de terrain majeurs aient été provoqués par les essais, indique que de tels endommagements sont manifestement survenus. (Une évaluation des dommages aux atolls provoqués par une explosion est présentée à l'annexe H). De ce fait la compréhension du mécanisme de l'interaction entre l'explosion et le massif rocheux tout entier jusqu'à la surface du sol est évidemment importante pour une évaluation de la stabilité de l'atoll. Les chapitres 4 et 5 du présent rapport examinent en détail ces sujets.

Les localisations et énergies exactes de chaque essai souterrain conduit à Mururoa et Fangataufa sont considérées par le CEA comme des informations militaires sensibles et n'ont pas été révélées. Des informations ont été fournies quant à la distribution des essais par zone. Des limites supérieures pour l'énergie totale, et d'autres informations présentées sous forme statistique, peuvent être trouvées dans les documents publiés par l'Office Français de Liaison. En s'appuyant sur ces sources et sur les observations visuelles, il est possible de reconstituer une distribution hypothétique des essais - comprenant l'énergie de chaque essai et sa profondeur - qui aide à visualiser l'intensité de l'endommagement des diverses zones d'essai.

Comme on l'a déjà noté, les autorités françaises affirment que la totalité des 147 essais souterrains ont été tirés dans le massif volcanique. Pour 12 de ces essais, conduits entre 1976 et 1980 (Document DIRCEN/CEA n° 6, section 1.5) la cheminée formée au-dessus de la cavité résultant de l'explosion s'étend jusqu'aux carbonates. Ces essais ap-

pelés CRTV (Cheminée Rencontrant le Toit du massif Volcanique, essais de Catégorie 3, voir annexe C) laissent au mouvement de l'eau (et des radionucléides) remontant de la cavité un obstacle moindre que celui que laissent les essais à la suite desquels demeure une couverture de roches volcaniques intactes. Ceci est pris en compte au chapitre 7 dans l'évaluation de la vitesse de l'eau qui sort de la cheminée, mais est également important pour l'estimation de la vitesse de relâchement des radionucléides contenus dans l'eau qui traverse la cavité.

Les cartouches des Figures 2.17 et 2.18 montrent la distribution des zones d 'essais à Mururoa et Fangataufa respectivement, fournie par le Document DIRCEN/CEA n^o 6.

Ces figures montrent aussi une distribution hypothétique (mais compatible avec les données fournies par le CEA) des essais souterrains (y compris les essais CRTV à Mururoa) pour les deux atolls. La zone dans laquelle les essais de sécurité ont été conduits à Mururoa est également indiquée. Des cercles de rayon $5R_c$, qui donnent une indication de l'étendue de la zone de massif endommagé associé à chaque essai (qui contient la cheminée de hauteur $5R_c$), ont été tracés autour de chaque point de tir. C'est clairement dans la zone d'essais 4 de Mururoa que l'intensité de l'endommagement de la roche est la plus élevée. La probabilité de recouvrement ou d'interaction entre les zones de roche endommagée de cavités adjacentes sera donc aussi la plus grande dans la zone d'essais 4.

La Figure 2.19 montre une section verticale parallèle à la ligne du rivage dans la zone d'essais 4, pour la distribution des essais représentée à la Figure 1.17. Cette figure illustre le recouvrement potentiel des zones de roche endommagée.

L'étude du temps requis pour qu'une cavité résultant d'une explosion se remplisse d'eau (voir Chapitre 7) suggère que la région entourant une cavité, dans laquelle la perméabilité est significativement augmentée, s'étend jusqu'à un rayon de 2,5 R_c compté à partir du point de tir et contient de plus, bien entendu, toute la cheminée. La Figure 2.20 montre la région où la perméabilité est accrue, dans le cas de la zone d'essais 4. La Figure 2.21 montre les mêmes régions pour la zone d'essais 1. On voit que, même dans la zone d'essais 4, une interaction entre régions de perméabilité accrue est peu vraisemblable. Des remarques supplémentaires sur les possibilités d'interactions structurales ou hydrogéologiques entre cavités adjacentes sont faites ci-dessous.

La question de l'interaction structurale, dans laquelle deux cavités adjacentes tendraient à se comporter comme une seule cavité plus grande, a été analysée à l'annexe H. On y montre que même dans le cas extrême où la résistance de la roche séparant les deux cavités est réduite drastiquement, l'effet sur le massif rocheux est minimal, sauf dans le voisinage immédiat des deux cavités.

L'interaction hydrogéologique entre deux cavités adjacentes est discutée à l'annexe F et au Chapitre 7, Section 3.4. Ces analyses confirment aussi que pour l'essentiel il n'y a pas d'interaction, même pour des cavités très proches l'une de l'autre.

On peut donc conclure que les effets engendrés dans le voisinage de chaque essai souterrain peuvent tous être considérés comme des évènements indépendants - c'est-à-

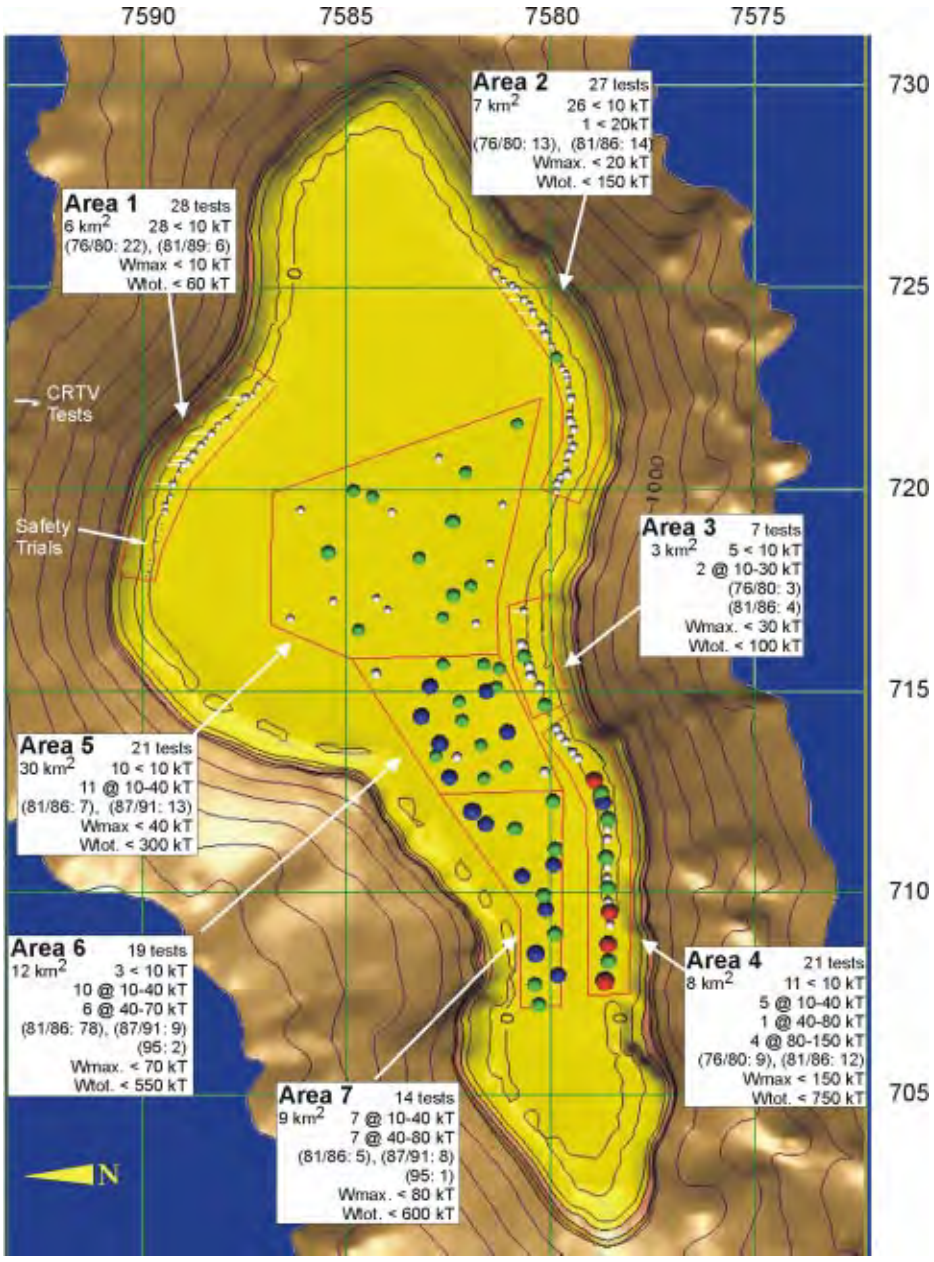

FIG. 2.17 Répartition des essais souterrains et leurs énergies par zone d'essais à Mururoa (fournie par le DIRCEN/CEA), sur laquelle est superposée une distribution hypothétique des localisations des essais dans les zones d'essais (les contours bathymétriques figurés autour des atolls sont séparés par des intervalles de 250 mètres jusqu'à la profondeur de 2 km sous la surface)

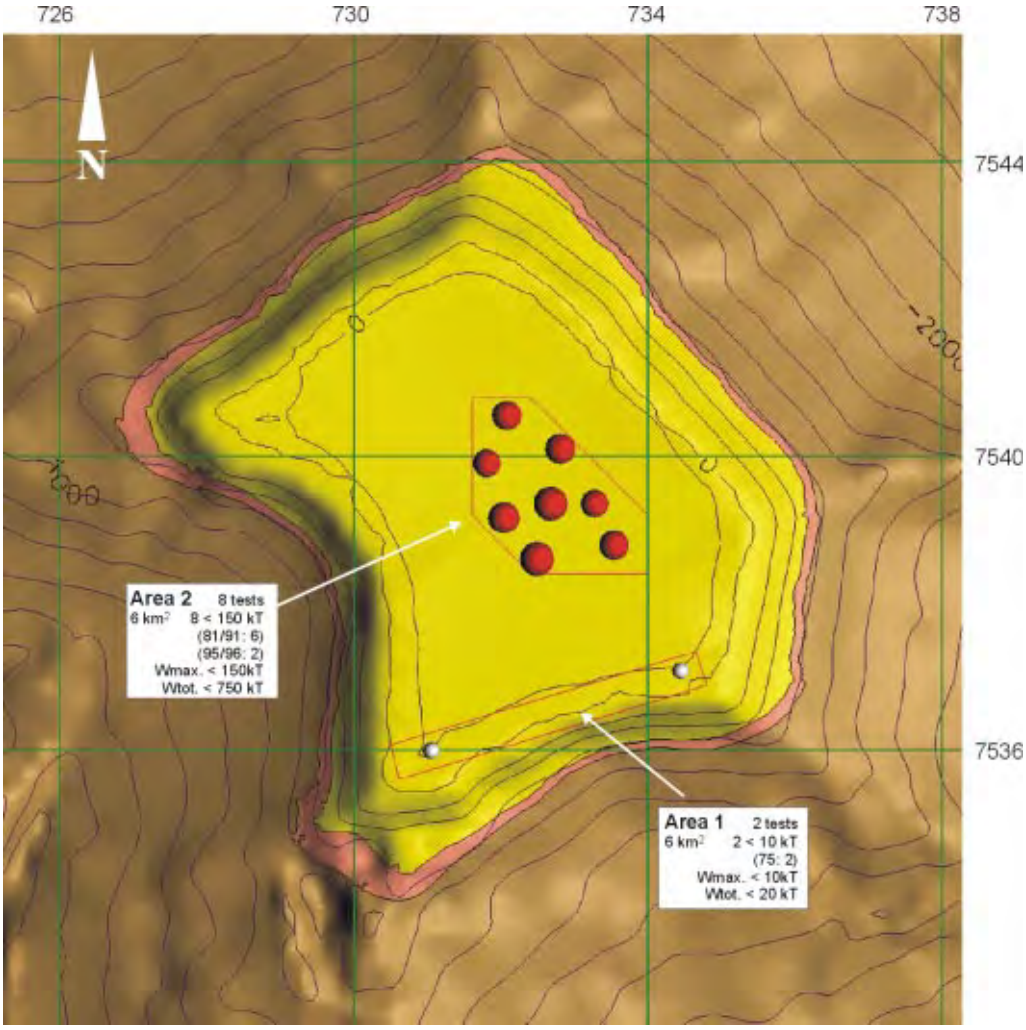

FIG. 2.18 Répartition des essais souterrains et leurs énergies par zone d'essais à Fangataufa (fournie par le DIRCEN/CEA), sur laquelle est superposée une distribution hypothétique des localisations des essais dans les zones d'essais (les contours bathymétriques figurés autour des atolls sont séparés par des intervalles de 250 mètres jusqu'à la profondeur de 2 km sous la surface)

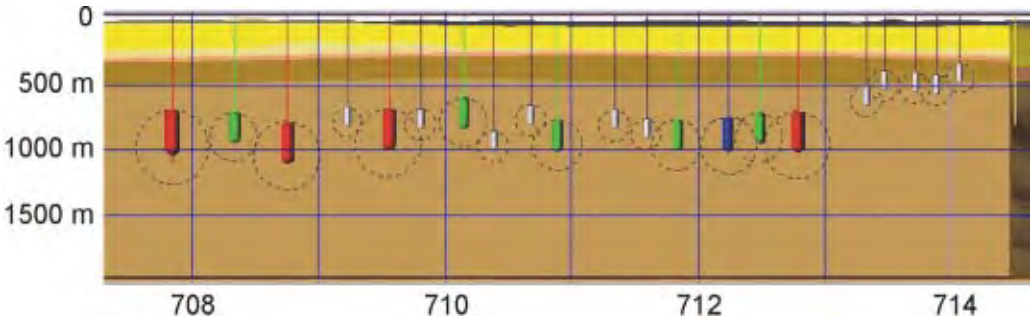

FIG. 2.19 Distribution hypothétique des essais souterrains dans la zone d'essais 4 à Mururoa (les cercles pointillés, de rayon $5R_c$, indiquent l'étendue de la zone endommagée par fractures ; les cylindres en couleur indiquent la partie effondrée ; la hauteur de la cheminée est $H_c = 5R_c$; les couleurs indiquent respectivement des explosions petites (blanc, < 5 kt), intermédiaire (vert, < 20 kt), élevées (bleu, < 80 kt), et grandes (rouge, < 150 kt) ; la coupe est approximativement parallèle à la côte, vue du côté de l'océan (voir aussi Figure 1.17)

dire qu'il n'est pas nécessaire de prendre en compte des interactions entre les essais. Les analyses produites aux Chapitres 3 à 7 ont été conduites avec cette hypothèse.

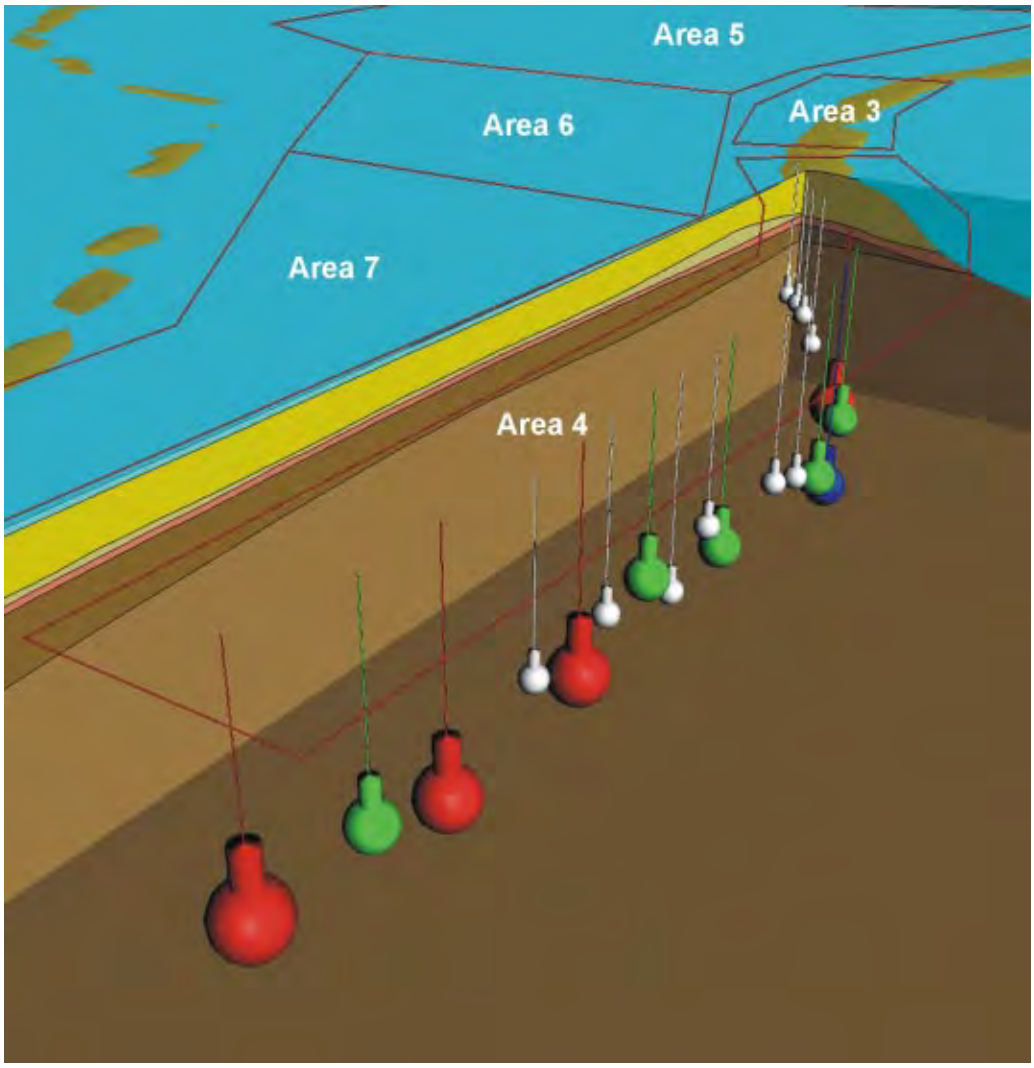

FIG. 2.20 Répartition schématique des régions de perméabilité accrue ($R_p = 2,5\ R_c$; $H_c = 5\ R_c$) associées aux essais souterrains de la zone d'essais 4 à Mururoa ; les couleurs indiquent les énergies (blanc=faible, < 5 kt ; vert=intermédiaires, < 20 kt ; bleu=élevée, < 80 kt ; et rouge=forte, < 150 kt) des explosions

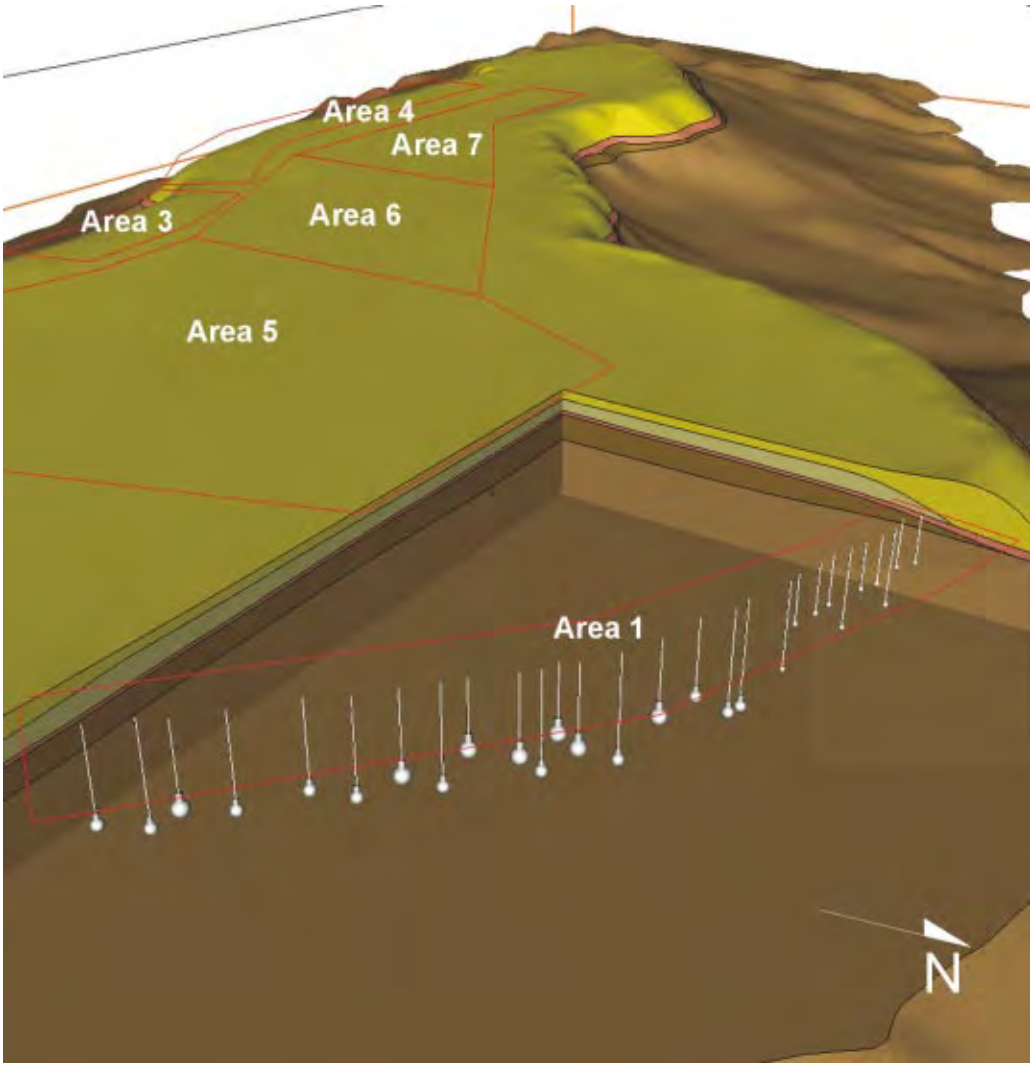

FIG. 2.21 Répartition schématique des régions de perméabilité accrue ($R_p = 2,5\ R_c$; cheminée $H_c = 5\ R_c$) associées aux essais souterrains de la zone d'essais 1 à Mururoa (le blanc indique une faible énergie (< 5 kt) ; tous les essais dans la zone d'essais 1 avaient une énergie inférieure à 10 kt ; voir Figure 2.17)

2.5 Conditions imposées à l'analyse par la géologie de l'atoll

2.5.1 Variabilité et incertitude géologiques ; leur influence sur les études de la CGI

La variabilité des propriétés mécaniques et hydrologiques des massifs rocheux est une caractéristique inhérente aux problèmes géotechniques. Les techniques d'analyse permettent de prendre en compte une variabilité *connue*, en particulier par les méthodes de calcul par ordinateur, mais la distribution et l'étendue de la variabilité dans les systèmes géologiques sont précisément largement inconnues. Ceci est dû, pour une part, à la quantité limitée de données disponibles. Mururoa et Fangataufa sont typiques à cet égard. Les coupes géologiques, comme celles de la Figure 2.6 (voir aussi Chapitre 2, Figures 2.5 à 2.8), par exemple, sont basées sur l'analyse de carottes provenant d'un nombre très limité (souvent pas plus que 5 ou 6) de sondages verticaux forés en différents endroits de l'atoll qui sont complétés, dans des cas particuliers, par des sondages inclinés et par les débris obtenus pendant le forage des puits en grand diamètre où sont placés les engins. De considérables variations spatiales de la lithologie locale resteront donc indétectées entre les sondages. Une fracturation verticale ou sub-verticale est particulièrement difficile à détecter dans les forages (verticaux). Quelques profils géophysiques ont aussi été réalisés (Guille *et al.* (1996), Figures 27 et 61 ; DIRCEN/CEA document n° 5, Figures 2 à 4) mais aucune des interprétations ne montre, de manière certaine, des détails d'échelle locale qui pourraient pourtant être significatifs pour l'analyse d'un essai particulier.

Ces limitations appellent une stratégie d'analyse ou de conception différente de celle qui convient dans le cas de problèmes relativement bien définis « à données abondantes » que l'on trouve dans d'autres branches de l'analyse appliquée (Starfield et Cundall, 1988).

L'incertitude d'origine géologique à Mururoa et Fangataufa est renforcée par l'incertitude qui résulte de ce que certaines données existantes n'ont pas été rendues disponibles pour des raisons de secret militaire.

L'ensemble de ces caractères propres à l'étude de la CGI ont commandé une approche concentrée sur l'acquisition d'une compréhension des phénomènes mécaniques et physiques sous-jacents à l'oeuvre dans le comportement du système à analyser. L'importance de la variabilité de paramètres particuliers du problème peut être plus facilement appréciée quand l'analyse, numérique ou par solutions exactes, est conduite en utilisant des grandeurs adimensionnelles convenables. C'est particulièrement intéressant dans le cas de l'étude des effets complexes des explosions nucléaires sur les massifs rocheux, comme démontré aux Chapitres 3, 4 et 5.

2.5.2 Flux de chaleur et d'eau souterraine, transport de solutés.

A un niveau fondamental, l'écoulement de l'eau à travers les fractures et les pores interconnectés du massif rocheux d'un atoll est gouverné par plusieurs processus inter-

dépendants ou « couplés ». Le moteur principal de l'écoulement est la convection ; la température dans la roche à l'intérieur de l'atoll est significativement plus élevée que celle de l'eau de mer à la même profondeur, en raison de l'existence d'un flux de chaleur, provenant de la croûte terrestre profonde, et dirigé vers la surface. La roche chauffe l'eau contenue dans les pores, provoquant sa dilatation et sa montée vers la surface.

La vitesse moyenne de l'eau (dans les pores) dépendra de plusieurs facteurs, dont les plus importants sont la résistance mécanique à l'écoulement, en général mesurée en terme de perméabilité, et l'intensité du champ convectif, qui est fourni directement par le champ de distribution des températures. On suppose en général, comme cela peut être prouvé dans le cas examiné, que le fluide contenu dans les pores est partout en équilibre thermique avec la roche dans laquelle il s'écoule ; autrement dit la roche et l'eau sont à la même température en chaque point. Le champ de distribution des températures est déterminé par deux mécanismes de transfert de chaleur : le premier, la condution de la chaleur, existe dans tout milieu immobile (ici, la roche poreuse saturée d'eau) ; le second, l'advection de la chaleur, est provoqué par l'écoulement de l'eau dans la roche. Comme tous les chenaux d'écoulement dans la roche ne sont pas équivalents, l'advection qui résulte de la vitesse moyenne n'est pas égale à l'advection réelle observée. Dès lors survient une dispersion, que l'on assimile souvent à une variation de la conductivité avec la vitesse ; l'écoulement périodique engendré par les effets de la marée introduit une complication supplémentaire, que l'on peut aussi assimiler à une dispersion.

Les processus évoqués ci-dessus peuvent être décrits rigoureusement en terme d'équations, présentées au Chapitre 6. La prise en considération complète de toutes les interactions couplées peut rendre inaccessible une solution exacte ou, dans le cas de calculs numériques, mobiliser des moyens informatiques très importants, de sorte que l'on recherche souvent des simplifications.

Dans le basalte, où la perméabilité est relativement basse, la conduction thermique domine le transport de chaleur ; aussi peut-on approximer le champ de température sans faire intervenir le transport de chaleur par advection (c'est-à-dire, lié au mouvement de l'eau) ; ce dernier ne constitue qu'une perturbation. Même quand une explosion nucléaire crée une source de convection à grande échelle dans les basaltes, la conduction thermique domine l'advection, sauf dans la cheminée et son voisinage immédiat. Dans cette mesure le champ de température est découplé du champ de vitesse de l'eau.

Dans les carbonates, toutefois, c'est le contraire, et le transport de chaleur est dominé par l'écoulement du fluide dans les pores. Les solutions pour chacun des deux champs - de température et de vitesse de l'eau dans les pores - sont fortement couplées entre elles. Un modèle mathématique adapté est donc nécessaire pour le calcul du champ de température. Le système d'équations pour le transport de chaleur est donné au Chapitre 6 en (6.3) et (6.4) ; remarquer qu'elles introduisent plusieurs paramètres (continus) supplémentaires représentant la conductivité (λ_s et λ_l), la dispersivité (α_L et α_T) et la capacité calorifique ($(\rho C)_l$, $(\rho C)_s$). La conductivité thermique et la capacité calorifique

sont, dans la pratique, bien connues au niveau de précision qui nous intéresse ici ; la conductivité thermique est représentée par un scalaire quoique, en toute rigueur, elle doive, comme d'ailleurs la perméabilité, être traitée comme un tenseur fonction de la position. Les coefficients de dispersion α_L et α_T sont des caractéristiques de la roche ; ils reflètent la connectivité (tortuosité) du milieu poreux examiné. De nouveau, en toute rigueur, ils devraient être traités comme les composantes du tenseur de dispersion (du $4^{\text{ème}}$ ordre) qui sont au nombre de deux pour un milieu isotrope.

En principe, les coefficients de perméabilité et de dispersion (dispersivités) peuvent être obtenus par inversion des données obtenues dans les essais de transfert de chaleur et de masse en régime permanent effectués dans les roches intéressées. Ni la CGI ni le CEA/DIRCEN n'ont essayé de le faire d'une manière systématique, de sorte que les valeurs des dispersivités sont tirées de la littérature, voir Tableau 6.2. Les effets de marée compliquent encore le problème (voir annexes U et V). Pendant des durées comprenant plusieurs marées (c'est-à-dire pendant des durées de plus de 10 jours), de sorte qu'une représentation moyenne continue soit adaptée, l'inversion périodique du sens de l'écoulement provoquée par les marées engendre une dispersion supplémentaire, dont la forme mathématique est, en général, différente de celle donnée en (6.4) parce que sa dépendance vis-à-vis du champ moyen de vitesse, v, n'est pas la même. Comme la force motrice pour le mouvement périodique est différente, un champ de vitesses distinct est induit. Quand on s'intéresse à un transport de solutés, ou de traceurs, (comme c'est le cas dans la discussion du relâchement des eaux tritiées provenant du massif volcanique et traversant les carbonates, que l'on trouve aux annexes S et T), des équations de transport distinctes (supplémentaires) sont nécessaires. Pour un traceur tel que le tritium, une équation de la forme (6.4) est parfois utilisée, en négligeant le terme diffusif correspondant à λ_l, et en remplaçant le terme de gauche par un opérateur plus classique de dérivation matérielle. Pour les solutés qui peuvent être adsorbés ou désorbés des surfaces internes des roches poreuses, un terme supplémentaire de source/puits est nécessaire [voir (6.5) et (6.6)]. Cependant, comme montré au Chapitre 7, une telle approche simple basée sur la notion de dispersivité ne s'avère pas fournir une représentation convenable, et l'approche beaucoup plus générale [développée par des ingénieurs chimistes en relation avec le génie des procédés des lits catalytiques poreux, voir Denbigh et Turner (1971) et Brenner et Edwards (1993)], qui introduit des distributions de temps de résidence et des échanges chromatographiques, est plus appropriée. Une version très simple, analogue au modèle de réacteur à mélange parfait, est utilisée à l'annexe S pour modéliser les concentrations transitoires et à grande échelle observées dans les carbonates et le lagon.

Les considérations générales mises en évidence plus haut forment la base d'une grande partie des analyses discutées dans les Chapitres 6 et 7.

2.6 Affaissements

Les effets principaux observables en survolant les atolls sont essentiellement de deux types - les affaissements de la surface, et l'instabilité des pentes. Des affaissements du fond du lagon doivent aussi survenir du fait des essais conduits sous le lagon, mais ils n'ont pas d'effets discernables à la surface. On pourrait penser de même que les instabilités de pente ne concernent que les essais conduits sous la couronne (c'est-à-dire dans le voisinage des pentes sous-marines du côté de l'océan). En fait, si ceci est vrai pour les instabilités de pente telles que celles produites par les explosions Priam, Nestor et Tydée sous la couronne sud-ouest de Mururoa, les conditions géologiques sous la couronne nord-est, à la fois à Mururoa et Fangataufa, sont suffisamment sensibles aux effets sismiques transitoires pour que les essais conduits sous les lagons, puissent déclencher, et aient déclenché, des glissements de pente.

L'un des effets les plus visibles des essais nucléaires souterrains sur la couronne de Mururoa est l'affaissement de la surface du sol. La Figure 2.22 montre une vue aérienne (prise en juillet 1996) de la zone d'essais 4 dans la couronne sud (on peut voir le point zéro à la surface de certains essais). Cette région, dont l'altitude au-dessus du niveau de la mer était de 2 mètres environ, (Document DIRCEN/CEA n^o 7, Figure 20), est maintenant sous la mer. Ceci indique qu'un affaissement de l'ordre de 2 mètres a été produit par les explosions. Les affaissements résultent de l'interaction entre l'onde engendrée par une explosion et les 150 à 200 mètres de carbonates les plus proches de la surface.

Selon le Document DIRCEN/CEA n^o 7 (page 10), l'onde résultant de l'explosion *...abaisse pratiquement instantanément le niveau de la couronne dans un rayon de quelques centaines de mètres autour du point zéro à la surface du sol... La fraction de la couronne corallienne qui est graduellement submergée du fait de l'accumulation de ces affaissements [l'affaissement total peut résulter des effets de plusieurs essais] (jusqu'à 2 mètres en certains endroits) représente environ 15% de la surface du sol qui était à l'origine au-dessus du niveau de la mer*.

Observées à la surface, ces cuvettes ou dénivellations (Figure 2.23) paraissent semblables aux manifestations de subsidence que l'on peut observer au-dessus de nombre des essais souterrains conduits au Nevada Test Site (NTS) aux États-Unis, en particulier ceux conduits dans les tuffs non cimentés. Les autorités du CEA soulignent, toutefois, qu'il y a des différences essentielles entre ces deux types de phénomènes (voir Figure 2.24).

De fait,

- (a) au NTS, les cuvettes de subsidence sont la manifestation en surface d'une cheminée d'effondrement qui forme un lien continu entre le point zéro souterrain et la surface du sol (Chapitre 4, Figure 4.5), dont le résultat est l'existence de passages très perméables reliant directement le point d'explosion à la surface, et donc une « fuite » possible (voir annexe D) des radionucléides les plus volatils vers la biosphère ou l'environnement accessible ; tandis que

FIG. 2.22 Vue aérienne de la partie ouest de la zone d'essais 4 à Mururoa, prise en juillet 1996 (soit 16 ans après que les essais sur la couronne eurent cessé) ; la vue est prise de l'océan, en direction du lagon (remarquer que plusieurs sites d'essais et des zones affaissées à l'extrémité ouest de la zone d'essais 4 sont maintenant sous la mer ; voir aussi Figure 2.23)

– (b) au CEP, les profondeurs auxquelles ont lieu les tirs sont considérablement plus grandes (annexe D), avec comme conséquence qu'une zone intacte de roches volcaniques subsiste au-dessus de la cheminée après un essai. De ce fait les radionucléides sont « confinés » dans la cheminée et isolés de la surface (Chapitre 4, Figure 4.3). Dès lors, les cuvettes d'affaissement au CEP n'ont qu'un caractère superficiel, et n'affectent pas plus que les 100 à 200 mètres supérieurs de carbonates. Ces assertions sont examinées dans le Chapitre 4 du présent rapport.

Comme mentionné plus haut, les configurations géologiques et hydrologiques dans les deux sites d'essais sont aussi très différentes. Au CEP, les roches volcaniques, relativement résistantes quoique fracturées, sont recouvertes par quelques 300 à 500 mètres de carbonates moins résistants (voir Figures 2.6 et 2.16). Les roches volcaniques et les carbonates sont poreux et saturés jusqu'à la surface du sol. Au NTS, les tuffs volcaniques s'étendent depuis la surface du sol jusqu'à une profondeur plus grande que les points zéros, et la surface libre de la nappe est à une profondeur de 300 mètres environ, Ű c'est-à-dire que le massif rocheux superficiel n'est pas saturé.

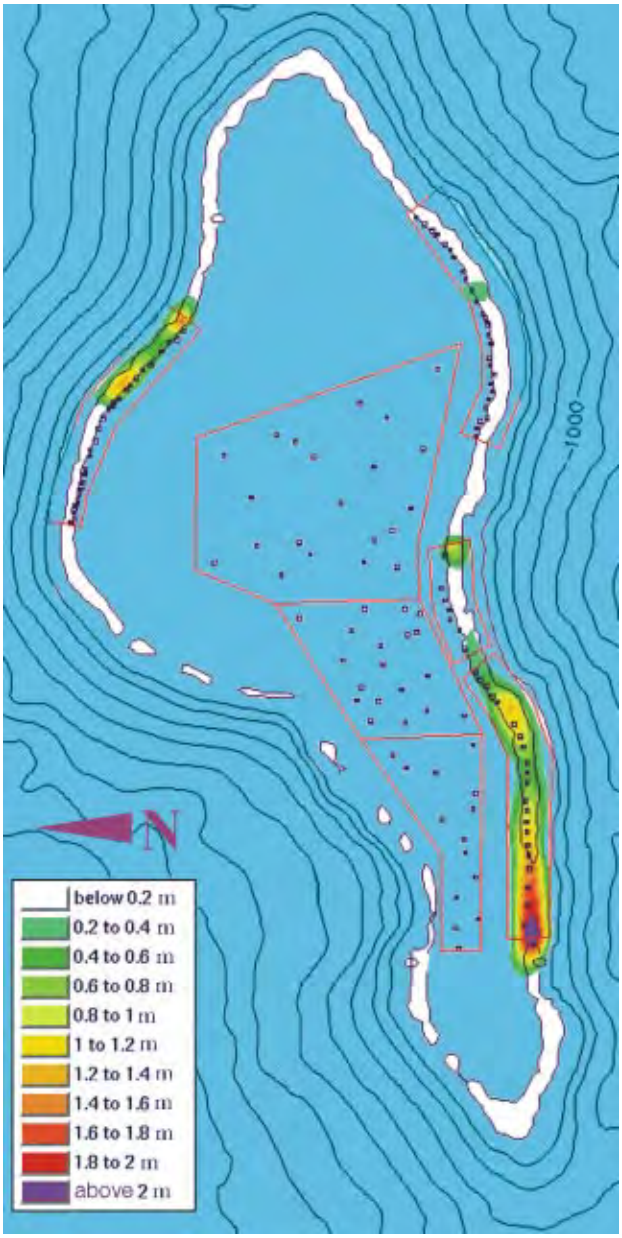

FIG. 2.23 Zones d'affaissements de la surface produites par les essais souterrains le long de la couronne corallienne à Mururoa (basé sur les données d'affaissement 1996 du DIRCEN/CEA) [selon Guille *et al.* (1996), p.69 : « les coraux qui édifient les récifs prolifèrent à l'heure actuelle avec une vitesse remarquable » (de l'ordre de 1 cm d'épaisseur par an) dans les régions affaissées. De ce fait, les zones récifiennes qui sont aujourd'hui sous l'eau auront retrouvé une altitude positive au-dessus de l'océan d'ici quelques centaines d'années]

(a) Nevada Test Site (NTS)

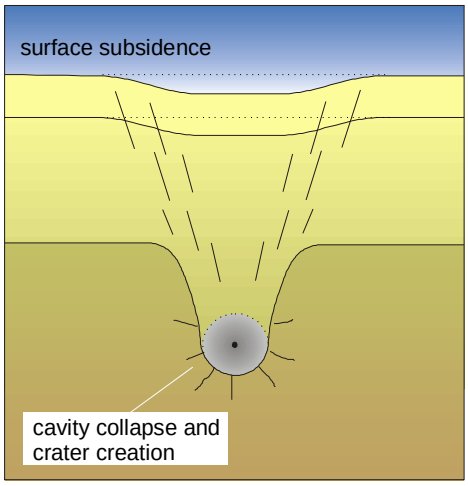

(b) Pacific Test Centre (PTC)

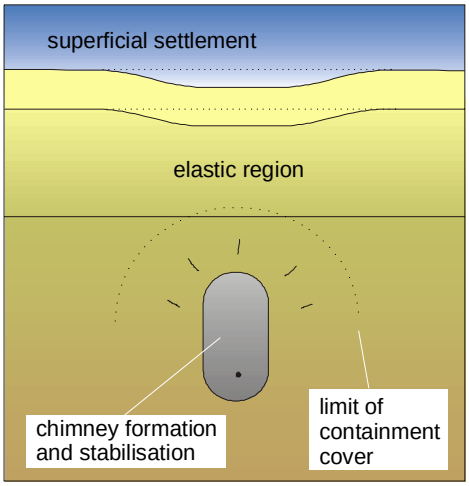

FIG. 2.24 Comparaison entre la subsidence qui survient sur le Nevada Test Site (NTS) et les affaissements produits par les essais au CEP (d'après Bouchez et Lecomte, 1996, p.77)

La configuration au CEP peut être illustrée en se référant à la Figure 2.16, qui vise à représenter le cas de l'essai Tydée dans la zone d'essais 4 : on a choisi, d'une part, une énergie approchant la valeur maximale de 150 kt, à une profondeur de 985 mètres, et d'autre part, une coupe verticale correspondant à l'emplacement présumé de Tydée. On voit que le rayon $R \approx 8Rc$, au-delà duquel le massif volcanique reste « essentiellement inchangé » par le passage de l'onde explosive, demeure à l'intérieur de (la région périphérique dans) la masse rocheuse volcanique. En passant du massif volcanique aux carbonates, mécaniquement moins résistants, l'onde peut provoquer un endommagement complémentaire. Quand l'onde s'approche de la surface, qui est située à un rayon de 20 R_c environ, l'influence du lagon et des interfaces avec l'océan devient progressivement plus importante. Une modélisation numérique de la propagation de l'onde, qui prend en compte ces influences, est décrite au Chapitre 4. On trouve que l'existence de limites latérales plus éloignées dans les carbonates inférieurs, liée à la plus grande largeur de section dans cette zone, tend à inhiber l'endommagement. En revanche, dans la section proche de la surface, plus étroite, la roche est endommagée. Sous un chargement de nature quasi statique, dans lequel l'eau peut être expulsée des pores de la roche, ou encore dans le cas où la roche n'est pas saturée (c'est-à-dire que les pores ne sont pas remplis d'eau), l'endommagement peut survenir par effondrement des pores et compaction.

La longueur d'onde (et la durée) de l'onde de l'explosion varient approximativement comme la racine cubique de l'énergie [100 mètres (20 ms) pour 1 kt ; 500 mètres

(100 ms) pour 150 kt], c'est-à-dire en suivant la même loi de similitude que le rayon de la cavité. Plus grande est l'énergie attendue, plus grande doit être la profondeur d'enfouissement de l'essai sous l'interface roches volcaniques-carbonates. Ainsi, lorsque l'onde produite par un essai de forte énergie atteint l'interface roches volcaniques-carbonates, elle est proche d'une onde plane se déplaçant vers la surface et s'étendant sur un large front. Des essais de moindre énergie, moins profonds, résulteront corrélativement en un front d'onde qui sera moins large et moins plat quand il atteindra l'interface.

Les analyses numériques des effets sur les carbonates de l'onde résultant de l'explosion sont présentées au Chapitre 4. Les résultats montrent qu'un affaissement important de la surface et des déformations latérales seront provoqués dans les carbonates supérieurs par un mécanisme de distorsion à volume constant ou isochore. Dans ce mécanisme, toute réduction de hauteur verticale des carbonates (c'est-à-dire tout affaissement) doit être accompagnée par une dilatation à un autre endroit, pour que le volume total de roche soumis à des déformations anélastiques demeure constant. La Figure 2.25 illustre cette contraction verticale, associée à une distribution complexe des déformations qui comprend des mouvements latéraux dans les carbonates, et dans les pentes côté océan et côté lagon. Les déformations anélastiques affectent les quelques 300 mètres supérieurs des carbonates. Le fait que la région déformée soit limitée en étendue est dû, pour une large part, à la proximité des pentes côté océan et côté lagon, qui autorise des déformations latérales. À plus grandes profondeurs, le confinement, imposé par le massif rocheux qui s'étend sous le lagon et vers les pentes sous plus grande profondeur d'eau (voir Figure 4.8), tend à limiter la dilatation latérale et, en conséquence, la contraction verticale. Un raisonnement analogue suggère que les explosions de faible énergie, qui n'affectent qu'un volume de roche relativement plus petit (et donc, qui sont relativement plus confinées) produiront des affaissements quelque peu moindres que ne le ferait une explosion de grande énergie, même pour des profondeurs d'enfouissement des essais respectant la règle de similitude. Il faut remarquer aussi que l'expansion latérale des pentes indiquée sur la Figure 2.25 se produit sous l'eau et n'est donc pas visible depuis la surface.

Il n'est pas possible de prévoir l'amplitude des affaissements de surface dus aux effets d'un ou plusieurs essais parce que la résistance et la déformabilité de la masse rocheuse (corail) ne peuvent être mesurées directement (comme mentionné plus haut, cette difficulté est commune à beaucoup de problèmes d'ingénierie géotechnique intéressant de grands volumes de roches). La Figure 2.26 représente une courbe cisaillement-distorsion (dynamique) « générique » pour un massif rocheux (par exemple corail). Pour une contrainte appliquée inférieure à la limite d'élasticité σ_A, la masse rocheuse présente une réponse essentiellement élastique, le chargement (OA) et le déchargement (AO) se faisant suivant le même trajet sans dissipation d'énergie (c'est la situation qui prévaut lors du passage d'une onde sismique à travers le milieu). Pour des amplitudes plus grandes de l'onde, la résistance du corail (σ_B) peut être dépassée et le corail se déforme

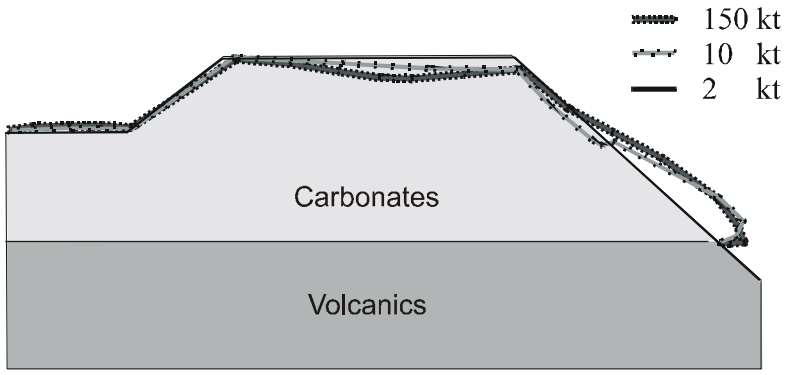

FIG. 2.25 Déformations de la surface du sol, et déformations associées des pentes côté océan et côté lagon, engendrées par un mécanisme de distorsion à volume constant pour différentes intensités de l'explosion (pour des profondeurs de tir respectant la similitude ; voir Chapitre 4.5, Figure 4.10)

en suivant le trajet OBC, jusqu'au point C atteint quand la queue de l'onde dépasse la région concernée ; alors le corail est déchargé selon le trajet « élastique résiduel » CD, jusqu'à la déformation résiduelle OD (qui se manifeste dans le cas présent par un « affaissement »). L'énergie prélevée à l'onde est proportionnelle à l'aire OABCD. Une deuxième onde (associée à un essai ultérieur) peut provoquer un « rechargement » de la même masse rocheuse le long d'un trajet D'C'EF, avec une déformation résiduelle (et donc un affaissement) augmentés, de OD' jusqu'en OF. L'énergie nécessaire pour cette augmentation (proportionnelle à DCEF) est sensiblement inférieure à celle nécessaire pour la première déformation. Comme les amplitudes des contraintes et déformations associées aux diverses étapes (A...F) montrées sur la Figure 2.26 sont inconnues a priori, il est évidemment impossible de prévoir l'amplitude exacte des déformations finales.

La Figure 2.26b donne une représentation idéalisée de la Figure 2.26a, qui est parfois utilisée dans les calculs numériques. Un choix approprié des paramètres nécessaires pour préciser la courbe de la Figure 2.26b (c'est-à-dire la résistance de pic, les déformations et résistances résiduelles, ainsi que le paramètre de radoucissement a, défini sur la Figure 1.26b, (voir aussi Chapitre 4, Section 4.4, et Tableau 4.2), permet un ajustement au comportement observé sur le terrain et donc permet de définir des propriétés « raisonnables » de la masse rocheuse utilisables pour des estimations ultérieures. La nécessité d'affiner de cette manière l'estimation des valeurs des paramètres du modèle est également discutée au Chapitre 3.5.4. en relation avec le problème de l'estimation du rayon de la cavité.

Les scientifiques du CEA (Bouchez et Lecomte, 1996 ; Document DIRCEN/CEA n° 6) estiment que les affaissements de surface résultent de la compaction du corail poreux par l'impact de la retombée des couches de surface (plaques) de corail qui ont été

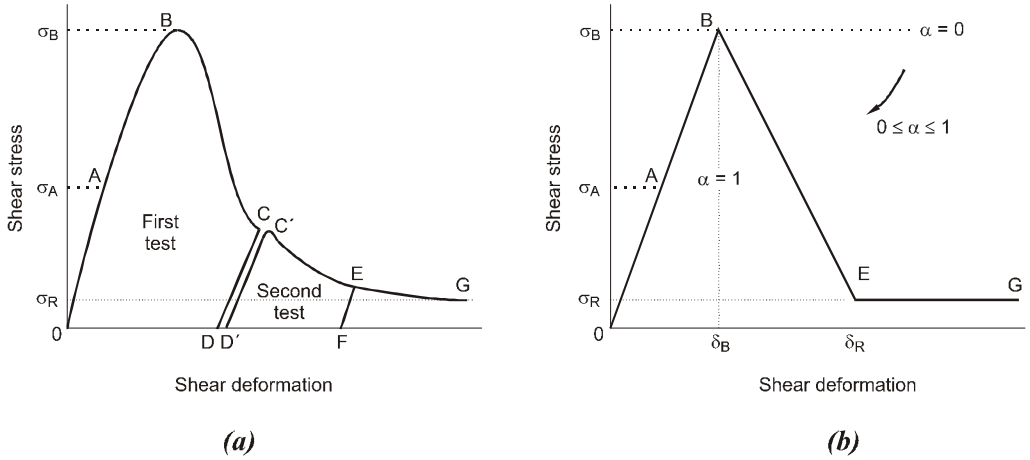

FIG. 2.26 Courbes contraintes-déformations « complètes » typique (a) et idéalisée (b) pour des roches manifestant un comportement radoucissant. DD' représente la déformation (étalée dans le temps) qui apparaît entre les deux essais

projetées en l'air par la réflection de l'onde de l'explosion à la surface. Les plaques associées à la réflection se développent bien suivant ce mécanisme, (voir annexe P), mais la CGI estime peu vraisemblable que l'impact de leur retombée sur la surface de corail ait pour résultat une compaction significative. Les carbonates sont poreux, mais ils sont également saturés, et le passage de l'onde due à l'explosion, ou de l'onde engendrée par l'impact de la plaque détachée lors de sa retombée, est si rapide (il dure quelques dixièmes de millisecondes, voir Tableau 4.1 et annexe P) que l'eau ne dispose pas d'un temps suffisant pour être expulsée des pores. De ce fait la compaction par effondrement des pores est inhibée. En fait, la réponse de la roche est celle d'un milieu non-drainé. Le passage de l'onde (compressive) due à l'explosion augmente la pression du fluide dans les pores, en réduisant la contrainte effective et la résistance au cisaillement, renforçant ainsi les conditions propices au mécanisme de distorsion isochore exposé plus haut.

Il faut aussi remarquer que, suivant le mécanisme que la CGI propose pour expliquer l'affaissement, il est peu probable que les essais conduits sous les lagons (et donc, éloignés des flancs océaniques) produisent des affaissements du fond du lagon, (c'est-à-dire de la partie supérieure des carbonates), parce que dans ce cas la zone de l'essai est surmontée par une masse de carbonates dont l'extension latérale est bien plus grande, ce qui limite la possibilité de dilatation latérale et limite donc en conséquence l'affaissement vertical. La réflexion de l'onde provoque encore le détachement de plaques, mais leur envol et leur impact à la retombée sont vraisemblablement considérablement atténués dans l'eau, en comparaison de ce qui se passe dans l'air.

Quoi qu'il en soit des différences d'interprétation des mécanismes qui sont à l'origine des affaissements de surface, il est clair que les affaissements observés au CEP sont

indubitablement un phénomène superficiel (un effet de surface) provoqué par le passage de l'onde due à l'explosion ; en d'autres termes il n'y a aucune connection directe créée entre les affaissements de surface et le sommet de la cheminée de la cavité sous-jacente.

2.7 Stabilité des pentes

2.7.1 Stabilité des flancs des atolls

Les essais conduits dans le massif volcanique sous la couronne corallienne à Mururoa ont eu pour conséquences des instabilités significatives des pentes océaniques :

- plusieurs glissements sous-marins majeurs dans la zone sud-ouest de l'atoll, pendant la période 1977-1980, dans le voisinage des zones d'essais 3 et 4 (Document DIRCEN/CEA n° 7) ;
- une instabilité se manifestant par du fluage qui affecte une région étendue de la zone nord- est et qui a été identifiée pour la première fois en 1979, (cette « région en glissement » s'étend le long de la couronne, sur toute la zone d'essais 1 et dans la section PK4 - PK6, où aucun essai n'a été conduit. Ce fluage est surveillé en permanence depuis 1979) ;
- une autre instabilité avec fluage a été identifiée dans la région nord-est de Fangataufa, près de Kilo-Frégate. Aucun essai n'a été conduit sous cette partie de la couronne. Bien que la géologie et le mécanisme de fluage soient similaires à ceux du nord-est de Mururoa, les manifestations du fluage semblent avoir diminué.

Comme discuté ci-dessous, les couronnes nord-est des atolls paraissent avoir montré, au cours des temps géologiques, une tendance à l'effondrement périodique. Une grande part de l'activité actuelle de déformation dans la couronne nord-est de Mururoa est imputable aux essais conduits sous la couronne pendant les 3 à 4 premières années d'expérimentation souterraine (1976-1980), mais quelques essais de forte puissance conduits sous le lagon ont eu aussi des effets transitoires sur les déformations (voir Figures 5.8 et 5.9 et la discussion associée à la Section 5.4.2). Les essais sous le lagon conduits à distance considérable de la couronne ont clairement été la cause originelle des déformations de fluage observées en 1988-1992 dans la région nord-est de Fangataufa dès lors que, à l'exception de deux petits essais (de moins de 10 kt tous les deux) sous la couronne sud en 1975, aucun essai n'a été conduit à Fangataufa sous la couronne corallienne.

Comme indiqué plus haut, les glissements sous-marins des zones sud-ouest de Mururoa (zone d'essais 4), particulièrement ceux associés aux essais Nestor (19 mars 1977), Priam (30 novembre 1978) et Tydée (25 juillet 1979) ont engendré de fortes vagues qui, spécialement dans le cas de Tydée, ont provoqué une inondation de parties des atolls (Document DIRCEN/CEA n° 7, Section V). Ces évènements ont entraîné une réévaluation soigneuse des procédures d'essai sur les atolls (voir Tazieff, 1982) et la décision de

déplacer les essais de la couronne vers le centre du lagon. Bien que trois essais supplémentaires de forte énergie et un essai de puissance modérée aient été conduits sous la couronne en 1980, [Thésée (énergie estimée : 78 kt ; voir annexe C) ; Asios (78 kt) ; Diomède (51 kt) ; Eurypyle (26 kt)], il apparaît que (1) aucun essai de très grande énergie (100 à 150 kt) n'a été conduit sous la couronne après 1980 (voir annexe C) et que (2) aucun des essais conduits depuis 1980 n'a provoqué de nouvelles instabilités de pente.

Les essais conduits sous la couronne sud-est, mentionnés plus haut, ont provoqué des effondrements de pente plus ou moins immédiats (Document DIRCEN/CEA n° 7), alors que ceux de la couronne nord-est n'ont eu pour résultat qu'une lente déformation qui se poursuit depuis à peu près deux décennies. La raison de cette différence de comportement peut être trouvée dans une étude détaillée de la géologie des diverses régions de la couronne.

2.7.2 Géologie de la couronne de l'atoll

L'étude détaillée du profil bathymétrique de Mururoa, complété par des photographies sous-marines et des films vidéo, révèle que les flancs océaniques de Mururoa sont constitués de crêtes volcaniques radiales étroites se développant à partir de la couronne, les vallées entre les crêtes étant remplies, à des degrés variables, par des sédiments provenant pour une grande part des carbonates sus-jacents. Les accumulations de sédiments atteignent par endroits une épaisseur de 300 mètres (Figure 2.5) et on en trouve jusqu'à 3 kilomètres de profondeur.

Les crêtes et les vallées apparaissent comme le produit d'une érosion qui commença quand l'édifice volcanique de Mururoa était émergé. On peut observer une forme analogue d'érosion qui se développe aujourd'hui sur l'île de Méhétia (Figure 2.3). L'accumulation de sédiments (carbonates) résulte, pour une part, de l'érosion consécutive à l'émersion de la montagne sous-marine, associée à une baisse du niveau de l'océan pendant les périodes de glaciation (voir Figure 2.4) et aussi, pour une autre part, à l'effondrement périodique du récif de corail quand celui-ci atteint, au cours du processus d'édification corallien, une extension qui le rend instable. Le fait que les accumulations soient les plus épaisses dans la région nord-est de la couronne (Figure 2.5) suggère que cette région est la plus encline à des effondrements périodiques. Une accumulation d'une taille analogue est observée sur la couronne nord-est de Fangataufa (Guille *et al.* 1966, Figure 80, p.101). Par contraste, exception faite d'une petite région en profondeur au voisinage de l'effondrement de pente consécutif à Tydée (Figure 2.5), la zone d'essais 4 de la couronne sud ne montre que des accumulations réduites.

Les forages d'exploration ont révélé des différences significatives dans la géologie de détail des pentes nord-est et sud-est de Mururoa. En particulier, le massif volcanique de la pente nord est recouvert d'un « tablier » de calcaires crayeux poreux, peu résistants, qui est absent sur la pente sud (Figures 5.11 et 5.12).

2.7.3 Calcul numérique de la stabilité des pentes

La CGI a conduit un ensemble de simulations numériques bidimensionnelles (2D) et tridimensionnelles (3D) en vue d'examiner :

1º la stabilité relative des pentes sud-ouest et nord-est dans les conditions naturelles, avant les expérimentations nucléaires souterraines (une analyse statique 2D a été conduite)

2º l'effet des essais souterrains sur la stabilité des pentes (une analyse dynamique 2D a été conduite)

3º l'éventualité qu'une instabilité de pente puisse être provoquée en des endroits des pentes éloignés du point d'explosion, comme cela est arrivé avec le glissement qui a résulté de l'explosion Tydée (Document DIRCEN/CEA nº 7, Section VI, p. 12 ; une analyse dynamique 3D a été réalisée).

2.7.4 Stabilité naturelle

La stabilité naturelle des deux régions a été examinée en termes de facteur de stabilité vis-à-vis de l'effondrement de la pente. On a obtenu des bornes supérieure et inférieure de ce facteur, en supposant que toutes les unités présentaient soit (i) un comportement élastique parfaitement plastique (EPP), soit (ii) un comportement élastique parfaitement fragile (EPB), respectivement. Plusieurs cas ont été testés par le calcul pour chaque hypothèse (EPP et EPB) afin de déterminer dans chaque cas si la pente était stable ou instable. Quoiqu'il soit possible de modifier d'un calcul à l'autre la valeur retenue pour la résistance du massif d'une très petite quantité, on a estimé qu'il était adapté de définir seulement le domaine approximatif à l'intérieur duquel on passe de la stabilité à l'instabilité de la pente dans chaque cas. Les résultats obtenus avec cette façon de faire sont les suivants :

Facteur de sécurité	Propriétés d'un échantillon de roche		Propriétés du massif
	Borne Sup. (EPP)	Borne Inf. (EPB)	Borne Sup. (EPP)
pente nord-est	2,0 à 2,5	1,4 à 1,7	1,5 à 1,6
pente sud-ouest	2,5 à 3,3	2,0 à 2,5	1,5 à 1,6

Comme on le voit, la pente nord-est s'est avérée significativement moins stable que la pente sud-est.

La plupart des valeurs figurant dans le tableau ci-dessus sont basées sur des valeurs de la résistance des formations rocheuses des pentes obtenues au laboratoire, car aucune valeur de la résistance du massif ne figurait dans les documents DIRCEN/CEA. Plusieurs calculs ont été effectués, pour le cas EPP seulement (c'est-à-dire $\alpha = 0$ sur la Figure 2.26b), en utilisant les estimations de la résistance du massif rocheux suggérées au Chapitre 2.5 du présent rapport. Le domaine de transition « stable-instable » a été trouvé de 1,5 à 1,67, la valeur « vraie » du seuil d'instabilité étant vraisemblablement

plus proche de 1,5. On n'a pas fait d'analyse pour le cas EPB, parce qu'il n'y avait pas de fondement solide sur lequel baser une estimation de la valeur du paramètre de radoucissement α (Figure 2.26b). Clairement, cependant, le facteur de sécurité devrait dans ce cas être inférieur à 1,5 et pourrait approcher l'instabilité intrinsèque définie par un facteur de sécurité de 1,0 ou moins. Il est donc probable que la pente nord-est, avec son profil actuel, pourrait être proche de l'instabilité ; un chargement additionnel, tel que celui qui pourrait résulter d'explosions, ou d'une future accrétion latérale de corail, pourrait avoir pour résultat un effondrement des carbonates supérieurs.

2.7.5 Stabilité sous le chargement résultant d'une explosion

L'analyse dynamique 2D a été conduite en retenant les mêmes conditions à la limite et les mêmes conditions de chargement que pour l'analyse des affaissements (voir Figure 4.8). La Figure 4.11 montre les contours des zones de distorsion plastique produites dans les carbonates par une explosion de 150 kt tirée à une profondeur de 900 mètres, comparable aux essais de plus fortes énergies conduits dans la zone d'essais 4. On voit qu'une région de distorsion plastique se développe parallèlement à la pente de l'océan dans toute l'épaisseur des carbonates. Selon les valeurs retenues pour les paramètres de résistance et de radoucissement des carbonates de la région sud-ouest, la pente pourrait être stable ou pourrait être immédiatement instable sur toute la profondeur des carbonates. Cette dernière situation peut, au moins en partie, être responsable des grands effondrements rapides qui ont résulté des essais Nestor et Priam. Ceci reste une conjecture, car la localisation de ces essais par rapport aux effondrements de pente (voir Figures 2.12 et 5.1) ne nous est pas connue.

Dans le cas de l'essai Tydée, on sait que le glissement principal est survenu approximativement à 2 km à l'ouest du point d'explosion (voir Figure 2.11). Pour examiner ce cas, une analyse dynamique 3D a été conduite. Dans ce modèle, on a supposé que toutes les unités géologiques le long de la couronne avaient la même résistance. La figure 5.14, par exemple, montre les déplacements verticaux en différents points de la pente océanique tels qu'ils résultent de l'explosion. On voit (comme il était prévisible) que les effets (les déplacements, dans ce cas) diminuent avec la distance à l'explosion. Comme on suppose que les propriétés sont uniformes dans l'espace, la rupture devrait plus vraisemblablement s'amorcer au point de la pente le plus proche du point d'explosion. La probabilité que la rupture démarre sur la pente à 2 kilomètres de distance de ce point (ce qui s'est passé en réalité) devrait être faible.

Deux hypothèses apparaissent plausibles :

1° le matériau composant la pente océanique à 2 kilomètres du « point le plus proche » est beaucoup moins résistant qu'il ne l'est dans la région du point le plus proche ;

2° des irrégularités de la surface de la pente conduisent à amplifier ou à concentrer, à cette distance de 2 kilomètres, l'amplitude de l'onde due à l'explosion, de sorte que la résistance du matériau est dépassée à cet endroit.

Une combinaison des hypothèses (1) et (2) est aussi possible. Comme noté plus haut, les sédiments s'accumulent sur les flancs de l'atoll dans les vallées entre les crêtes. L'action de l'onde sur l'interface entre les flancs pourrait produire une augmentation locale de la pression de pore dans les sédiments (qui peuvent comporter des blocs volumineux) en conduisant à une instabilité majeure, une descente rapide des sédiments et les effets associés de création de vague. Une hypothèse assez proche est présentée à l'annexe R. Le caractère en général résistant, fragile, des carbonates de la région sud-ouest, l'absence relative de sédiments en profondeur dans cette région, l'activité micro-sismique apparemment faible, se conjuguent pour indiquer que les pentes sud-ouest demeureront mécaniquement stables en l'absence de futures expérimentations sous la couronne de l'atoll.

2.7.5.1 Pente nord-est de Mururoa

Les essais conduits dans le voisinage immédiat de la zone d'essais 1 présentaient des énergies bien plus faibles (toutes inférieures à 10 kt) que celles des essais de la zone 4, mais la combinaison d'une profondeur d'enfouissement relativement réduite et de la présence de calcaires crayeux peu résistants a eu pour résultat sur les carbonates un effet de déstabilisation. La Figure 2.27c montre les contours des distorsions plastiques développées dans les carbonates, après une explosion de 10 kt à une profondeur de 650 mètres dans le massif volcanique sous la couronne nord-est. En comparant les zones plastiques de la Figure 2.27b (cas d'un chargement statique) avec celles de la Figure 2.27a (cas d'un chargement dynamique), on voit que le chargement dynamique (qui superpose aux forces de gravité du cas statique des forces issues de l'explosion, de direction radiale et orientées vers l'extérieur) engendre une zone de distorsion plus étendue. La différence est particulièrement prononcée dans la région supérieure de la couronne, avec une surface de rupture potentielle qui s'étend maintenant sous la totalité de la couronne jusqu'au lagon. La surface de rupture trouvée est cohérente avec les résultats des calculs des scientifiques du CEA (voir Figure 2.27c) et suggère que les déformations de fluage observées depuis 1980 dans la région nord-est de Mururoa sont dues, dans une considérable mesure, aux essais souterrains. L'onde dynamique a pour effet de former une fracture inclinée dans les formations carbonatées supérieures fragiles et des déformations de distorsion dans les calcaires crayeux. La fracturation des formations fragiles a pour résultat un chargement supplémentaire sur les calcaires crayeux et donc un fluage plus rapide. Les fractures verticales moins étendues du voisinage immédiat de la pente océanique [des fissures de traction visibles, avec des ouvertures jusqu'à 2 mètres et plus par endroit (sous-marines)] sont vraisemblablement provoquées initialement par chargement statique, mais évoluent du fait des mouvements induits par les effets des explosions ultérieures (voir Figure 5.6).

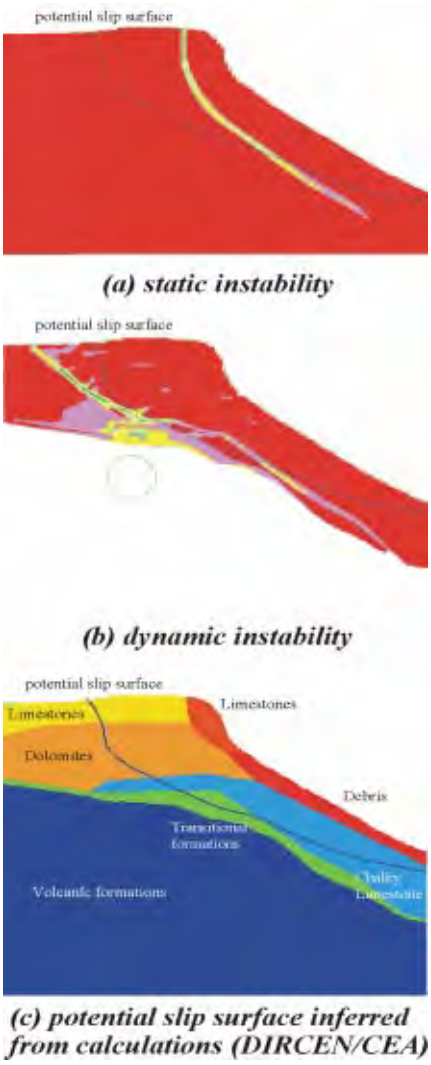

FIG. 2.27 Déformations calculées des pentes océaniques dans la zone nord-est de Mururoa, dans les cas d'un chargement statique et d'un chargement dynamique : (a) déformation statique sous chargement hydrostatique et par les forces de gravité (contours des déformations plastiques de distorsion pour un modèle radoucissant et un facteur de sécurité de 2,0 ; voir Figure 5.21) ; (b) déformation après chargement dynamique (contours des déformations plastiques de distorsion pour un modèle radoucissant après une explosion de 10 kt à une profondeur de 650 mètres ; voir Figure 5.23) ; et (c) modèle géotechnique sur lequel on a porté la surface de glissement potentielle (Document DIRCEN/CEA n° 7 ; voir Figure 5.12). Note : la surface de glissement potentielle a été déduite de calculs effectués par le DIRCEN/CEA

La modélisation des effets des explosions de grande énergie tirées à plus grande distance de la couronne (c'est-à-dire, les essais effectués sous le lagon) indique que celles-ci peuvent provoquer des effets transitoires tels que ceux observés sur les déformations mesurées de la zone nord-est (Figures 5.8 et 5.9). Les augmentations transitoires de la vitesse de fluage en novembre 1985 et 1987, par exemple, coïncident avec les essais Mégarée et Pélée respectivement, tirés dans la zone d'essais 5. Il semble également plausible que, pour des essais d'énergie encore plus grande, tels que ceux conduits sous le lagon de Fangataufa, l'effet dynamique pourrait être tel qu'il engendre des effets de déformation encore plus importants, et de durée encore plus longue. Dans les deux cas, cependant, il semble vraisemblable que ces effets tendent à s'atténuer avec le temps.

2.7.5.2 Pente nord-est de Fangataufa

Selon les scientifiques du CEA, l'observation micro-sismique et les mesures topographiques directes à Fangataufa (Document DIRCEN/CEA n° 7, Section VII) indiquent que les essais ont réactivé des déplacements de fractures préexistantes dans la région Kilo-Frégate, mais que ces mouvements paraissent, pour l'essentiel, s'être arrêtés depuis 1992 : la dernière campagne (1995/1996) n'a provoqué aucune augmentation significative de ces mouvements » [Document DIRCEN/CEA n° 7, p.38].

2.7.6 Possibilités d'instabilités ultérieures à Mururoa et Fangataufa

La CGI est en accord avec les conclusions tirées par les scientifiques du CEA quant aux points suivants :

1° les pentes du côté océan de la couronne sud-est de Mururoa sont maintenant stables et ne présenteront vraisemblablement pas de modifications dont l'origine résiderait dans le programme d'expérimentations souterraines ;

2° la couronne nord-est de Mururoa poursuivra vraisemblablement sa tendance apparente actuelle à la stabilisation. Une surveillance périodique pendant plusieurs années (environ vingt) visant à confirmer cette impression est recommandée.

En ce qui concerne la couronne nord-est de Mururoa, la CGI donne acte de ce que les déformations mesurées (voir Figures 5.8 et 5.9) montrent une tendance à la diminution des vitesses qui pourrait impliquer une éventuelle stabilisation (Bouchez *et al.* 1997). Il est également possible, cependant, si l'on a à l'esprit les déformations déjà supportées par les calcaires crayeux (environ 0,5%), que cette formation rocheuse entre dans un régime caractérisé par une chute de résistance significative, conduisant à une accélération des déformations et finalement à la rupture. Compte tenu du grand volume de roches impliqué dans ces déformations, et du risque de vagues d'amplitude comparable, ou supérieure, à celle qui a suivi l'effondrement consécutif à Tydée, on recommande qu'un programme soigneux de surveillance soit poursuivi pendant une vingtaine d'années, ou jusqu'à ce que la stabilité future de cette région puisse être évaluée de manière

plus certaine. On peut attendre que les signes d'une accélération des déformations, qui conduirait à un effondrement final, puissent être détectés quelques semaines à quelques mois avant une rupture éventuelle. Ceci laisserait un temps suffisant pour alerter toute personne qui pourrait se trouver en danger du fait de l'effondrement de pente.

En conclusion, la zone nord-est de Mururoa est fondamentalement la seule pour laquelle subsistent des préoccupations quant à la stabilité locale. Les modifications introduites en 1980 (c'est-à-dire la limitation des énergies des tirs sous la couronne et le déplacement des essais vers le sous-sol des lagons) ont supprimé l'éventualité d'une conséquence supplémentaire du point de vue de la stabilité, en un autre point des atolls, des expérimentations souterraines.

Les essais souterrains n'ont eu de conséquence globale pour la stabilité d'aucun des deux atolls. Cette conclusion est évidente quand on prend en considération l'extension géométriquement limitée des effets des tirs dans les zones d'essais, du point de vue de la stabilité ; elle est confortée par les observations (Document DIRCEN/CEA n^o 7) selon lesquelles le niveau moyen de l'océan à Mururoa pendant les 17 dernières années n'a montré aucun écart à la tendance observée pendant la même période dans d'autres régions du Pacifique Sud ; en d'autres termes il n'y a eu aucun effet des essais nucléaires souterrains sur la stabilité d'ensemble de Mururoa. La même remarque vaut très probablement pour Fangataufa, mais aucune mesure spécifique du niveau de l'océan n'est disponible pour cet atoll.

2.8 Ecoulement naturel de l'eau souterraine dans un atoll

De façon générale, l'hydrologie d'un atoll est bien comprise. (Les études conduites à Mururoa et Fangataufa par les scientifiques du CEA ont grandement contribué à cette compréhension). L'écoulement dominant de l'eau souterraine se fait de l'océan vers l'intérieur de l'atoll, dans un mouvement ascendant dirigé vers le centre du lagon de l'atoll (Figure 2.28). La composante verticale de l'écoulement a son origine dans l'« endo-upwelling ». L'eau contenue dans les pores et les fractures, à l'intérieur du massif rocheux saturé, est réchauffée par le flux de chaleur qui monte de la croûte terrestre à travers l'atoll vers la surface, et crée des forces ascensionnelles d'origine thermique qui agissent sur l'eau souterraine. L'eau de l'océan qui entoure l'atoll est plus froide et plus dense que l'eau contenue dans l'atoll, de sorte qu'une circulation se met en place, dans laquelle l'eau de mer se déplace des flancs de l'atoll vers le centre en montant vers la surface pour déboucher dans le lagon.

La combinaison de l'ascension d'origine thermique et de la perméabilité relativement beaucoup plus élevée des carbonates, en comparaison de celle du massif volcanique, produit le profil de température caractéristique observé dans les carbonates. La température de la roche (et de l'eau souterraine) décroît d'abord avec la profondeur sous la surface, puis commence à croître avec la profondeur. La température de l'eau dans l'océan présente aussi un minimum à une certaine profondeur.

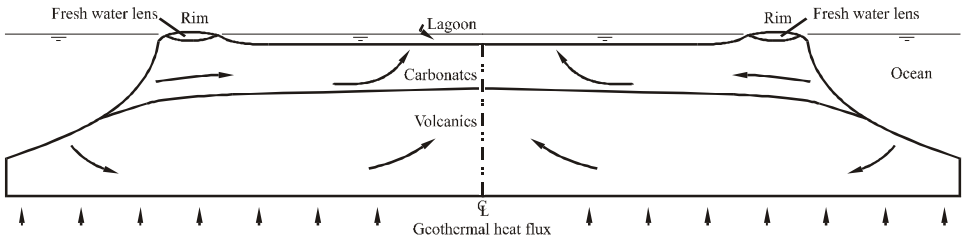

FIG. 2.28 Coupe schématique d'un atoll (d'après Perrochet et Tacher, 1997a)

2.8.1 Ecoulement de l'eau dans les carbonates

La valeur calculée de la température minimale, et de la profondeur à laquelle cette valeur est atteinte en différents endroits de l'atoll, dépendent de la perméabilité et des propriétés thermiques des carbonates et peuvent être utilisées pour « calibrer » le modèle d'écoulement de l'eau souterraine dans les carbonates. Cette technique a été utilisée par les scientifiques du DIRCEN/CEA et a été validée par la CGI ; elle est discutée au Chapitre 6, Section 3.

La conclusion principale qui peut être tirée des études par modèle numérique des profils de température conduites par la CGI est la suivante : les profils de température dans les carbonates peuvent être pratiquement aussi bien expliqués par plusieurs hypothèses différentes de régimes de perméabilité. Celle que la CGI considère comme la plus vraisemblable est l'existence d'un niveau karstique très perméable dans la partie inférieure des carbonates, interconnecté latéralement de sorte qu'il s'étend à travers tout l'atoll, présentant une transmissivité de 0,1 m^2/s (typiquement une couche de 10 mètres d'épaisseur de perméabilité 10^{-2} m/s), et surmonté par une épaisse série de coraux d'une perméabilité isotrope moyenne de 10^{-5} m/s (plusieurs horizons karstiques sont observables sur les carottes prélevées en forage). D'autres hypothèses possibles consisteraient à affecter d'une perméabilité de 10^{-4} m/s une couche unique isotrope, ou à considérer une couche unique anisotrope dont les perméabilités horizontale et verticale seraient 10^{-3} m/s et 10^{-4} m/s respectivement.

2.8.2 Perméabilité du massif volcanique

La valeur de la perméabilité naturelle à grande échelle du massif volcanique a été établie à 10^{-7} m/s ou moins. Une perméabilité plus élevée du massif volcanique donnerait un profil non linéaire de la température en fonction de la profondeur (le profil linéaire observé indique que le transfert de chaleur survient principalement par conduction thermique). Pour des perméabilités plus élevées, une part du transfert de chaleur s'effectuerait aussi par convection, ce qui produirait un profil convexe vers le haut.

La limite supérieure de 10^{-7} m/s est confirmée par le calcul inverse du temps nécessaire pour remplir d'eau la cavité formée dans le massif volcanique après une explosion souterraine (Chapitre 6).

La perméabilité mesurée sur des carottes de roches volcaniques est de l'ordre de 10^{-10} m/s, ce qui indique que l'écoulement de l'eau dans le massif volcanique s'effectue surtout par des fractures conductrices, interconnectées, qui n'apparaissent pas dans des échantillons de la dimension des carottes.

2.8.3 Vitesses de Darcy

Les résultats décrits ci-dessus conduisent aux estimations suivantes des débits de Darcy (« vitesses ») naturels :

dans les carbonates :	0,5 m par an à 2 m par an, à la fois dans les directions horizontale et verticale
dans le massif volcanique :	2 mm par an dans la direction verticale, 5 mm par an dans la direction horizontale

2.8.4 Vitesses de l'eau dans les pores

Les vitesses de Darcy (v_d) peuvent être transformées simplement en vitesses de l'eau dans les pores (v_i), si la porosité de la roche(ϕ) est connue, en utilisant la relation

$$v_i = v_d/\phi$$

Pour les carbonates, on estime que ϕ vaut environ de 30% à 40% (disons 35%). Pour le massif volcanique, une valeur de 10% est une estimation raisonnable de la porosité de matrice (ϕ_m), c'est-à-dire associée aux pores de petites dimensions dans le basalte. Toutefois, si l'écoulement a lieu dans le réseau de fractures sans qu'il y ait d'échanges de fluide entre les parois des fractures et les pores de la matrice, une valeur de la porosité de fracture (ϕ_F) beaucoup plus basse (10^{-4}, ou 0,01%) serait mieux appropriée.

Avec les valeurs précédentes [$(\phi_m)_{carb}$ = 35% ; $(\phi_F)_{volc}$ =10%], les vitesses de l'eau dans les pores (ou les fractures), soit v_i, sont :

massif volcanique

avec ϕ_m= 0,1 :	v_i = 20 mm/an dans la direction verticale 50 mm/an dans la direction horizontale
avec $\phi_F = 10^{-4}$:	v_F = 20 mm/an dans la direction verticale 50 mm/an dans la direction horizontale

carbonates

avec ϕ_m= 0,35 :	v_i = 1,5 m/an à 6 m/an, dans toutes les directions

2.9 Effet des explosions nucléaires sur la perméabilité du massif

L' « endommagement » subi par la roche à diverses distances d'une explosion nucléaire souterraine a été discuté plus haut (voir Figure 2.10, et aussi Chapitre 3). Ses manifestations vont de la vaporisation de la roche puis sa fusion (suivies d'un retour à l'état solide), la compaction et la distorsion, puis une fracturation modérée, non connectée

lorsque l'intensité des effets décroît, jusqu'à, finalement, l'absence d'effets. Il n'est pas possible d'établir, de manière fiable, la relation qui à chaque étape relie l' « endommagement » et la perméabilité résultante. On peut attendre que les régions qui ont été le plus intensivement affectées par le choc résultant de l'explosion (c'est-à-dire la « peau » qui est fondue) présentent une perméabilité beaucoup plus basse, alors que les régions à plus grande distance radiale peuvent voir leur perméabilité augmenter. Des modifications non monotones de la perméabilité peuvent s'expliquer par la compétition entre l'effondrement des pores et la fracturation, sous l'action des contraintes développées derrière l'onde de choc (Nikolaevskiy, 1996). De ce fait, l'effondrement de la cheminée qui survient peu après une explosion joue un rôle significatif en interconnectant et/ou « court-circuitant » des régions où l'endommagement est différent. Il ne semble pas que des mesures directes de la perméabilité après explosion aient été effectuées dans les diverses régions du CEP. Des estimations indirectes ont été tentées, fondées sur l'observation du temps requis pour remplir l'espace libre de la « cavité-plus-cheminée ». L'évaluation faite par la CGI (voir Chapitre 7) indique qu'une multiplication de la valeur de la perméabilité par un facteur de 10 à 100 (suivant l'extension radiale prise en compte, soit $R_{permaugm} \approx 2,5R_c$) est cohérente avec les vitesses observées de remplissage après explosion.

2.9.1 Ecoulement dans le voisinage d'un site d'essai après une explosion

L'eau qui s'écoule pour remplir la cavité-plus-cheminée produite par une explosion est rapidement chauffée et portée à une température supérieure, de 25°C à 50°C, aux températures de la roche et de l'eau avant l'explosion. Comme le volume de la cavité formée augmente proportionnllement à l'énergie du tir, la température atteinte ne dépend pas de l'énergie du tir. À l'intérieur de la cheminée, une circulation convective intense mélange intimement les eaux contenues. La chaleur se dissipe lentement, par conduction dans le massif rocheux et advection dans l'eau souterraine, qui engendrent un mouvement ascensionnel puissant et une vitesse verticale élevée en direction de la surface. Cet écoulement dirigé vers le haut voit son intensité diminuer à peu près exponentiellement avec le temps, jusqu'à atteindre au bout d'à peu près 500 ans un régime permanent de vitesses qui sont un peu supérieures à celles qui existaient avant l'essai (à cause de l'accroissement local de perméabilité).

Cet écoulement ascensionnel d'origine thermique produit par l'explosion constituant le vecteur principal du transport des radionucléides depuis la cavité et la cheminée vers la biosphère à travers le massif rocheux, on a simulé, par modélisation numérique, une grande variété de cas, impliquant plusieurs énergies distinctes, plusieurs profondeurs de tir, etc., et incluant les essais dans lesquels la cheminée a atteint les carbonates. Ces calculs sont présentés en détail au Chapitre 7. Plusieurs observations générales méritent d'être notées. Dans la situation (hypothétique) extrême d'une explosion de 150 kt, dans laquelle la cheminée atteint les carbonates, et l'accroissement de température de l'eau

dans la cavité-plus-cheminée est de 50°C, la vitesse de Darcy maximale (verticale, dirigée ver le haut) dans les carbonates a été trouvée égale à 58 mètres par an au pic, qui est atteint après un an ; la valeur moyenne sur 100 ans étant égale à 18 mètres par an. Alors les vitesses réelles (interstitielles) dans les carbonates (ϕ= 35%) seraient de l'ordre de 100 à 150 mètres par an pendant les premières années après l'explosion. Le tritium, radionucléide qui se déplace avec la vitesse de l'eau qui le transporte (c'est-à-dire qu'il n'y a pas de « retard »), pourrait arriver dans le lagon dans un délai de deux à trois ans après une telle explosion.

La présence d'un niveau karstique épais ($\approx$ 50 mètres) à la base des carbonates peut conduire à une dispersion et une atténuation considérables du panache thermique (voir Figures 7.17 et 7.18) et également à une réduction de la vitesse verticale dans les carbonates.

La Figure 2.29 montre des extraits des Figures 7.17 et 7.18 qui comparent les panaches thermiques produits par une explosion de 150 kt sous la couronne de l'atoll à des périodes de 1 an et 50 ans après l'explosion. On a supposé qu'il n'y avait pas de couverture volcanique au-dessus de la cheminée pour les deux configurations examinées : (a) il n'y a pas de niveau karstique au-dessus de la cavité, (b) il y a un niveau karstique de 50 mètres d'épaisseur au-dessus de la cavité.

Dans le cas où cette forte explosion (150 kt) survient avec une couverture volcanique résiduelle de 100 mètres au-dessus de la cheminée, la vitesse de Darcy maximale dans le massif volcanique est de l'ordre de 0,6 à 1,2 mètre par an.

Pour une petite explosion (5 kt), avec une couverture volcanique de 15 mètres, la vitesse de Darcy maximale dans le massif volcanique varie de 0,1 à 1,3 mètre par an, selon les hypothèses retenues pour les perméabilités et pour l'accroissement initial de température. Après 100 ans, une vitesse de régime permanent, variant de 0,03 à 0,3 mètre par an, est atteinte.

Les mesures effectuées par le CEA (document DIRCEN/CEA n° 9) indiquent que du tritium (^3H) a été détecté dans les carbonates inférieurs (niveau karstique) en plusieurs endroits, à Mururoa et à Fangataufa . Ceci tend à confirmer l'impression suivant laquelle l'épaisseur de couverture « intacte » au-dessus de la plupart des cheminées résultant d'une explosion a été jusqu'ici suffisante pour prévenir tout relâchement significatif de tritium (ou de tout autre radionucléide) dans les carbonates. Dans quelques cas (15 environ) cependant, les caractéristiques du massif rocheux au-dessus de la cheminée n'étaient pas telles qu'il puisse empêcher un écoulement rapide d'eau souterraine depuis la cheminée jusqu'aux carbonates, et vers le lagon.

2.9.2 Courts-circuits potentiels entre les cavités résultant des explosions et la biosphère (c'est-à-dire le lagon)

La nature hétérogène des processus de dépôt, qui caractérise aussi bien le massif volcanique que les carbonates, la création de fractures et de failles associées à la conso-

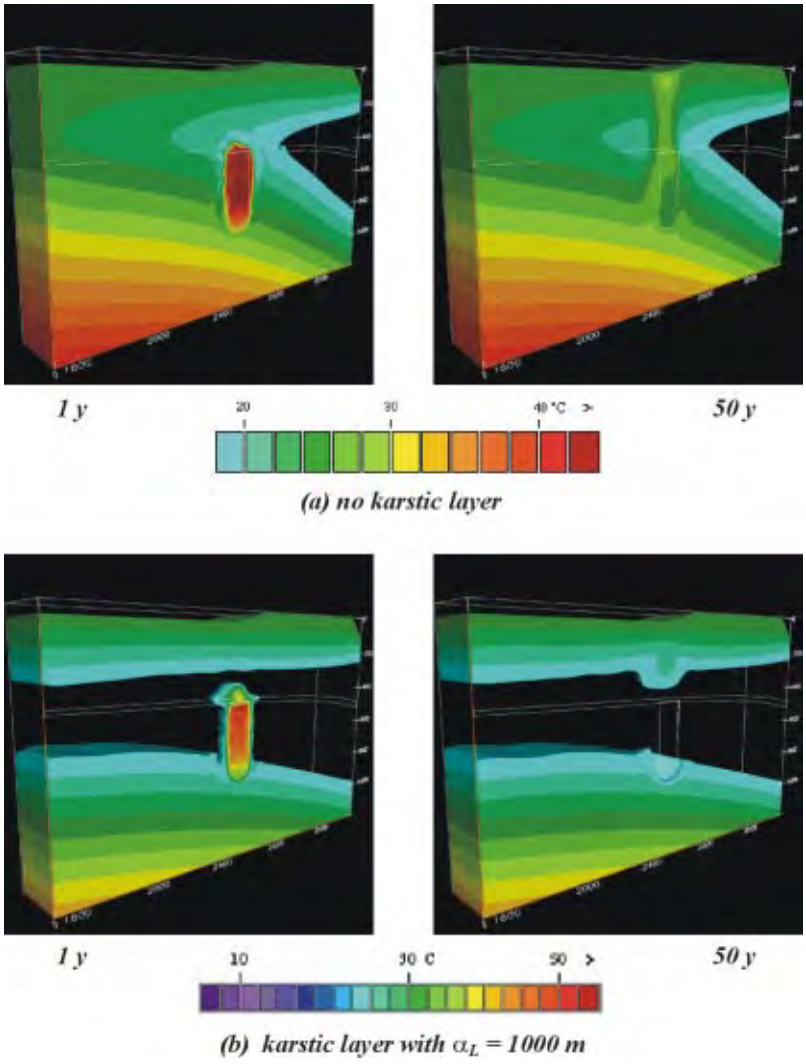

FIG. 2.29 Panache thermique engendré par une explosion hypothétique de 150 kt tirée sous la couronne, sans couverture volcanique au-dessus de la cheminée créée par l'explosion, 1 an et 50 ans après l'essai (a) en supposant qu'il n'y a pas de couche karstique à la base des carbonates et (b) en supposant l'existence d'une couche karstique à la base des carbonates [Note sur la similitude : la température du fluide dans la cheminée est indépendante de l'énergie de l'explosion, Y (et donc de la taille de la cavité)]. La largeur du panache initial (c'est-à-dire le diamètre de la cheminée) est proportionnel à $Y^{1/3}$. La vitesse de décroissance des effets thermiques est approximativement proportionnelle à $Y^{2/3}$ (c'est-à-dire que la distribution de températures dans le voisinage du panache après 1 an, pour une explosion de 150 kt, serait analogue à la distribution relative à une explosion de 10 kt après un laps de temps égal à 1 an/$(15)^{2/3}$=2 mois)

lidation dans les roches volcaniques, incluant la possibilité d'événements de type caldera (par exemple dans le secteur Viviane à Mururoa), suggèrent que des variations substantielles de la conductivité hydraulique au sein de l'atoll sont probables. Ces variations peuvent-elles être si importantes et d'une telle extension (par exemple, sous la forme de tubes de lave) qu'elles puissent constituer des « courts-circuits » efficaces entre les chambres, sièges des explosions souterraines, et la biosphère (la couronne, le lagon, l'océan) ? (Voir la discussion à l'annexe F). Les scientifiques du DIRCEN/CEA notent que, au cours du forage de plus de 300 puits qui ont traversé les carbonates et le massif volcanique (150 puits de diamètre 1,5 mètre, un nombre équivalent de sondages de prélèvement radiochimique post-tir, et un grand nombre de puits d'exploration géologique), aucun court-circuit « naturel » de cette espèce n'a été observé. Par ailleurs, ces plus de 300 sondages constituent-ils des cheminements potentiels en court-circuit vers la biosphère ?

2.9.3 Sondages de prélèvement radiochimique post-tir

S'ils étaient laissés ouverts après la récupération de carottes de lave dans chaque cavité, les sondages de prélèvement constitueraient évidemment une voie de passage direct vers la biosphère. Les scientifiques du DIRCEN/CEA indiquent que chacun de ces puits a été soigneusement rebouché au moyen de ciment sur toute la hauteur du massif volcanique après qu'on en eut retiré les cuvelages temporaires, mis en place dans les puits pour empêcher qu'ils ne se bouchent pendant qu'on les utilisait. Les puits n'ont pas été cimentés au niveau des carbonates. La CGI ne dispose d'aucune information qui ferait penser que les opérations de bouchage n'ont pas été conduites avec succès.

2.9.4 Puits où les engins sont placés

Le forage de 150 puits environ[††] verticaux, de 1,5 mètre de diamètre, destinés à la mise en place des engins nucléaires à la profondeur prescrite, introduit un court-circuit potentiel vers la biosphère. Dans chaque cas on a pris soin, comme le décrivent Bouchez et Lecomte (1996), de sceller ces trous avec un bouchon de béton, jusque cent mètres au moins au-dessus de la position du toit de la cheminée. La composition du bouchon était conçue pour assurer que l'onde de choc voyage moins vite dans le bouchon que dans la masse rocheuse, apparemment avec l'intention de développer un effet de « serrage », par dilatation de la roche qui se referme sur le bouchon pendant le passage de l'onde de

[††] Selon les scientifiques du DIRCEN/CEA, plusieurs de ces puits (de 5 à 10) ont été forés dans des régions du lagon où les essais étaient effectués, à Mururoa, mais n'ont pas été utilisés ultérieurement. Ces puits étaient fermés au moyen d'un bouchon de ciment de quelques mètres d'épaisseur disposé au sommet des carbonates, mais ont été laissés ouverts sous ce bouchon sur toute leur hauteur (c'est-à-dire au droit des carbonates et du massif volcanique). L'eau de ces puits fait maintenant l'objet de prélèvements et ces puits constituent une partie du réseau de prélèvements. Bien qu'ils ne soient pas directement liés à une source de radionucléides, comme c'est le cas quand les puits ont été utilisés pour un tir, ces trous laissés ouverts augmentent localement la perméabilité du massif rocheux dans leur voisinage.

choc consécutive à l'explosion. Ainsi, le diamètre de cheminée associé à une explosion souterraine varie de 24 mètres, pour un essai de 1 kt, à 105 mètres (c'est-à-dire 10 fois la racine cubique de l'énergie) pour un essai de 150 kt.

Si le scellement du puits lui-même a probablement été efficace pour la plupart, sinon tous les essais, le forage peut aussi altérer l'intégrité de la roche dans le voisinage du puits, c'est-à-dire dans un espace annulaire situé immédiatement autour du puits. Cette région, que l'on appelle « Disturbed Rock Zone » (ou DRZ, Zone où la Roche est Perturbée) est un sujet de préoccupation dans la conception du scellement des ouvrages destinés à l'enfouissement des déchets radioactifs. Comme l'intensité de l'état de contrainte naturel en profondeur est plutôt faible à Mururoa et Fangataufa (voir Chapitre 2), l'extension de la DRZ devrait être suffisamment petite pour être négligée, sauf dans des zones où le massif rocheux est localement moins résistant, ou a été perturbé, et/ou dans les zones où la hauteur de la couverture volcanique intacte au-dessus de la cheminée est réduite. L'existence d'une zone perturbée paraît avoir été la cause d'un relâchement précoce de tritium dans les carbonates inférieurs dans le cas de l'essai Lycos, conduit sous le lagon à Fangataufa. L'épaisseur nominale de la couverture volcanique, soit 140 mètres, aurait normalement dû être suffisante pour prévenir un tel relâchement.

Les observations faites par le DIRCEN/CEA dans les carbonates inférieures indiquent qu'il y a eu des relâchements (ou « fuites ») de tritium, césium et strontium dans un nombre relativement peu élevé d'essais souterrains (environ 15 sur les 147 essais), avec toutefois des concentrations limitées. Les scientifiques du DIRCEN/CEA affirment que plusieurs des relâchements précoces observés à Mururoa résultent des essais appelés CRTV [essais d'énergie faible ($\approx$8 kt)], peu profonds, à l'issue desquels le toit de la cheminée a atteint le sommet du massif volcanique.

L'étude de ces relâchements de tritium a permis à la CGI d'apprécier la validité d'un « modèle de mélange » (annexe S) proposé pour décrire l'écoulement dans les carbonates, et la validité de l'estimation faite des valeurs des vitesses de Darcy dans les roches volcaniques au-dessus des cheminées.

Les études de modélisation hydrogéologique, auxquelles il a été fait allusion plus tôt au cours de cette discussion, ont donné lieu à l'examen d'une gamme de situations plus extrêmes que celles qui ont résulté des essais conduits à Mururoa et Fangataufa. Le cas d'un essai de 150 kt à une profondeur telle qu'il ne subsiste aucune couverture volcanique (« no volcanic cover », voir Figure 7.18 par exemple) est beaucoup plus sévère que les cas réels des 12 essais CRTV (caractérisés par l'absence de couverture volcanique). Selon les scientifiques du DIRCEN/CEA, tous les essais CRTV ont une énergie de « moins de 10 kt ». Néanmoins, la situation que nous supposons avoir été celle résultant de l'essai Lycos et, jusqu'à un certain point peut-être, de l'essai Tydée, comme indiqué à la Figure 1.16, tendent à s'approcher de la situation décrite par la Figure 7.18.

2.10 Effets des ruptures des pentes sur l'hydrologie de l'atoll

Comme noté plus haut, les essais sous la couronne de Mururoa ont eut pour résultat des glissements de pente sous-marins substantiels de sa partie sud-ouest (zones d'essais 3 et 4), et un grand glissement potentiel dans la couronne nord-est (zone d'essais 1). A Fangataufa, de longues cassures se sont développées sur le flanc nord-est, même si aucun essai n'a été conduit directement sous cette couronne. Une activité microsismique continue de s'y produire, suggérant que de la fracturation et de la déformation se poursuivent. Le rapport 1984 de la mission Atkinson (MoFA Nouvelle Zélande, 1984) a suggéré que l'enlèvement du « tablier protecteur » extérieur de roches faiblement perméables pourrait affecter défavorablement le régime hydrologique :

« .... La Mission considère qu'un point important a été oublié [par les scientifiques du DIRCEN/CEA et la mission Tazieff (Tazieff, 1982)] concernant le risque potentiel d'effondrement, à savoir que l'effet de tout effondrement de la partie supérieure de la pente de l'atoll est de priver l'atoll de sa peau imperméable extérieure protectrice. Des recherches récentes sur les récifs des Caraïbes et du Pacifique ont montré que les réductions de porosité et les cimentations maximales surviennent le long de la marge extérieure et diminuent en direction du lagon. Les réductions de porosité et les cimentations à Mururoa sont vraisemblablement les plus grandes le long des marges au vent du sud. Les glissements sous-marins enlèveront cette zone extérieure faiblement perméable, augmentant alors la probabilité de mouvements de fluide entre l'océan et le massif rocheux sous la surface... » (p. 91/97). (Traduction)

Les études de stabilité conduites par la CGI, présentées au Chapitre 4, montrent que les ruptures des pentes déjà survenues, et les ruptures à venir, affecteront les couches carbonatées et pas le massif volcanique. L'enlèvement d'une portion de la pente océanique de la couronne, comme mentionné dans la citation ci-dessus, ne crée pas un changement majeur dans la circulation générale de l'eau souterraine dans l'atoll. Comme l'eau se déplace latéralement de l'océan vers l'intérieur des carbonates, cet écoulement est vraisemblablement légèrement augmenté (de quelques pour cent), l'épaisseur de la plaque de roche susceptible de glisser étant faible en comparaison de la quantité de carbonates qui restent en place. L'influence d'une disparition d'une portion de la pente est mineure en comparaison de l'incertitude générale qui concerne la perméabilité du massif rocheux carbonaté, qui ne constitue pas une barrière significative à la migration des radionucléides.

2.11 Influence des karsts sur l'écoulement dans les carbonates

Comme il est noté dans le rapport Atkinson [MoFA Nouvelle Zélande, (1984)],

> *« La stratigraphie des calcaires de subsurface fournit de larges passages de direction latérale et de grande extension pour des mouvements potentiels de fluide, probablement reliés à l'océan. De tels passages se trouvent aux*

profondeurs 8 à 10 mètres, 65 mètres, 90 mètres, 120 à 150 mètres, 280 à 290 mètres, 315 à 340 mètres et 422 mètres. » (Traduction)

Ces horizons karstiques, de forte perméabilité, ont une influence considérable sur l'écoulement souterrain de l'eau dans les carbonates, et, en particulier, sur l'écoulement induit par les explosions souterraines. Comme on le montre au Chapitre 7, les vitesses verticales ascensionnelles (de Darcy) de 58 mètres par an (au pic) et 18 mètres par an (moyenne sur 100 ans), calculées en négligeant toute influence des karsts, se réduisent à des valeurs de 2 à 5 mètres par an quand on suppose l'existence d'un épais horizon karstique (50 mètres) à la base des carbonates.

Le karst a aussi un effet considérable sur les phénomènes transitoires de court terme. Les mesures (Document DIRCEN/CEA n° 6) ont montré que les effets de marée dans l'océan et le lagon (pour ce dernier, avec un décalage de quelques vingt minutes par rapport à l'océan) engendrent une sollicitation sinusoïdale de pression dans l'atoll. Cette sollicitation crée un mouvement oscillatoire de l'eau dans les roches (spécialement dans les carbonates). La modélisation des conséquences de ces effets oscillatoires pour l'écoulement dans les carbonates est discutée aux annexes U et V. Même si cet effet ne modifie probablement pas énormément le flux global d'eau souterraine à travers les carbonates, il pourrait influencer la proportion de radionucléides transportés par l'eau qui arrive finalement dans le lagon, en étalant horizontalement les radionucléides provenant du massif volcanique quand ils parviennent dans les carbonates. Si l'on néglige cet étalement, la plupart des radionucléides arrivent dans le lagon ; si on représente l'étalement par un coefficient équivalent très grand de dispersion latérale (comme dans les documents DIRCEN/CEA) alors un débit de radionucléides s'élevant jusqu'à 50% du total est relâché dans l'océan, le restant étant relâché dans le lagon.

2.12 Conséquences à long terme des essais sur l'hydrologie des atolls

L'effet global à long terme des 137 essais souterrains à Mururoa a été examiné au moyen d'un modèle tridimensionnel de l'atoll. Le modèle a d'abord été mis en oeuvre pour les conditions naturelles ; il a confirmé l'allure générale de la circulation qui a déjà été discutée, mais en incluant une description plus détaillée de la morphologie complexe de l'atoll. On a introduit dans le massif volcanique, pour représenter les 137 essais souterrains, cent trente sept (137) perturbations, correspondant chacune à 7 millions de mètres cubes de roche volcanique, dont la perméabilité, en comparaison de la perméabilité de l'environnement, était multipliée (à cause de la fracturation) par un facteur de 1000 (c'est-à-dire 10^{-4} m/s au lieu de 10^{-7} m/s). Comme les localisations des essais ne sont pas exactement connues, les volumes perturbés associés à chaque essai ont reçu des localisations en partie aléatoires mais cohérentes avec les informations fournies par le DIRCEN/CEA. Le modèle a été alors mis en oeuvre de nouveau, avec les mêmes conditions à la limite que celles qui engendrent l' « endo-upwelling ». Ce calcul a montré

que le débit total dans l'atoll était augmenté de 1% seulement à la suite des 137 essais. Ce résultat est cohérent avec celui trouvé à l'annexe F. En supposant que l'aire horizontale de Mururoa est à peu près de 300.10^6 mètres carrés, et que les essais étaient effectués dans un intervalle de hauteur 600 mètres (c'est-à-dire entre les profondeurs de 500 mètres et 1100 mètres), alors le total de 137 fois 7 millions de mètres cubes, soit un milliard de mètres cubes, de « volume de forte perméabilité » (v_i) est compris dans un volume total (v_o) de l'ordre de 300.10^6 fois 600 mètres soit 180 milliards de mètres cubes. La fraction dans laquelle la perméabilité de la roche a été modifiée (augmentée, dans le cas présent) est

$$v_i / v_o = 1/180 \tag{2.1}$$

soit légèrement plus que 0,5%.

2.13 Le cas de Fangataufa

La CGI n'a pas conduit de calculs spécifiques pour le cas de Fangataufa. Compte tenu des natures très voisines de la géologie et des propriétés de la roche, la situation hydrologique est très semblable à celle de Mururoa, à la fois du point de vue de la situation naturelle et de la situation après les essais souterrains. De ce fait, le caractère plus « équi-dimensionnel » de l'atoll de Fangataufa tend à augmenter la validité des résultats de la modélisation numérique à deux dimensions axisymétrique, en comparaison du cas de l'atoll de Mururoa, plus allongé. De ce fait, les conclusions générales relatives à l'hydrologie, tirées dans le cas de Mururoa, sont considérées comme également applicables au cas de Fangataufa.

2.14 Effet d'une glaciation mondiale sur l'hydrologie de l'atoll

Comme on l'a dit au Chapitre 2, les atolls ont connu depuis leur formation de nombreux épisodes de glaciation mondiale. Le résultat net de ces glaciations est de faire descendre le niveau de l'Océan Pacifique d'une hauteur qui peut atteindre 100 à 150 mètres dans certains cas. Comme il a été noté précédemment, à l'occasion de la discussion de la Figure 1.4, une descente de 100 mètres du niveau de l'océan dans les prochains 25 000 à 60 000 ans apparaît vraisemblable. Ceci aurait pour résultat une « ré-émergence » de l'atoll au-dessus du niveau de l'eau et la formation de lentilles d'eau fraîche, d'épaisseur nulle sur les bords de l'atoll, mais atteignant une épaisseur de l'ordre de 200 mètres sous le centre de l' « île ». On peut s'attendre à ce que ceci favorise un peuplement de l'atoll, mais puisse aussi éventuellement avoir des conséquences dommageables en raison de relâchements possibles dans l'eau potable de radionucléides à vie longue présents dans le sous-sol du fait de la période d'essais. Cette possibilité a été envisagée dans l'étude de l'AIEA, qui a conclu que les conséquences n'en seraient probablement pas très sévères.

2.15 Effets à longue distance des ondes sismiques produites par les explosions au CEP

La possibilité que des explosions nucléaires puissent déclencher des tremblements de terre est une question qui a été parfois soulevée en relation avec les essais souterrains. On pourrait sans doute arguer qu'une explosion de forte puissance, au voisinage d'une faille active en situation de chargement tectonique et proche de glisser (c'est-à-dire prête à produire un tremblement de terre), pourrait fournir l'élément déclenchant le séisme, mais cette situation ne s'applique pas au cas de Mururoa et Fangataufa. La région est relativement calme sismiquement, avec une activité concentrée dans la croûte (c'est-à-dire à plus de 4 km de profondeur) autour du point chaud des Iles de la Société, situé entre Tahiti et Méhétia (au nord-ouest de Mururoa), du point chaud de l'archipel des Australes, à la montagne sous-marine de Mac Donald (au sud de Mururoa), et du point chaud de l'archipel des Gambiers-Pitcairn situé près de l'île de Pitcairn, au sud-est de Mururoa (Figure 2.30). Le point chaud de Pitcairn est à l'origine des îles de Mururoa et Fangataufa. Ces points chauds sont tous situés à plus de 1000 kilomètres de Mururoa et Fangataufa (Guille *et al.* 1996, pp. 7/8 et 33/34). De ce fait, il n'y a par nature aucune possibilité de réapparition d'un volcanisme à Mururoa et Fangataufa qui résulterait de l'activité actuelle volcanique de régions du Sud Pacifique. L'activité sismique intense de la région Pacifique est concentrée sur le pourtour des limites de plaques tectoniques qui constituent les marges de l'Océan Pacifique, appelé la « Ceinture de Feu »[‡‡] (associée aux zones de subduction montrées sur le diagramme supérieur de la Figure 2.30). Les limites de plaques sont toutes à plusieurs milliers de kilomètres au moins de Mururoa et Fangataufa et du CEP.

Comme discuté ci-dessus dans le présent Chapitre (voir Figure 2.7), dans le Chapitre 3 (Section 3.52) et dans Bouchez et Lecomte 1996 (Chapitre 5, p. 91), environ 95% ou plus de l'énergie explosive produite par un essai nucléaire souterrain est dissipée dans une sphère de roches très proches de l'explosion (par exemple un rayon de 400 mètres environ pour une explosion de 150 kt). Les 5% ou moins restant s'échappent sous la forme d'une onde élastique divergente, qui s'étale sur un front sphérique de dimension sans cesse croissante, et décroît en amplitude avec la distance à l'explosion. Si l'onde était purement élastique, l'amplitude décroîtrait proportionnellement à la distance radiale. En réalité, une dissipation d'énergie (atténuation) prend place et l'onde décroît en amplitude plus rapidement que proportionnellement à la distance.

... Les résultats montrent que ces effets deviennent extrêmement faibles quand l'onde s'éloigne des sites d'essais. Par exemple, après une explosion de 100 kilotonnes, les

[‡‡] « La Ceinture de Feu » (ou Ceinture Circum-Pacifique) tire son nom des volcans qui se sont formés sur les terres qui bordent l'Océan Pacifique, où une plaque « plonge » sous une autre dans les zones de subduction. Cette ceinture autour du Pacifique est à l'origine de plus de 90% des tremblements de terre dans le monde.

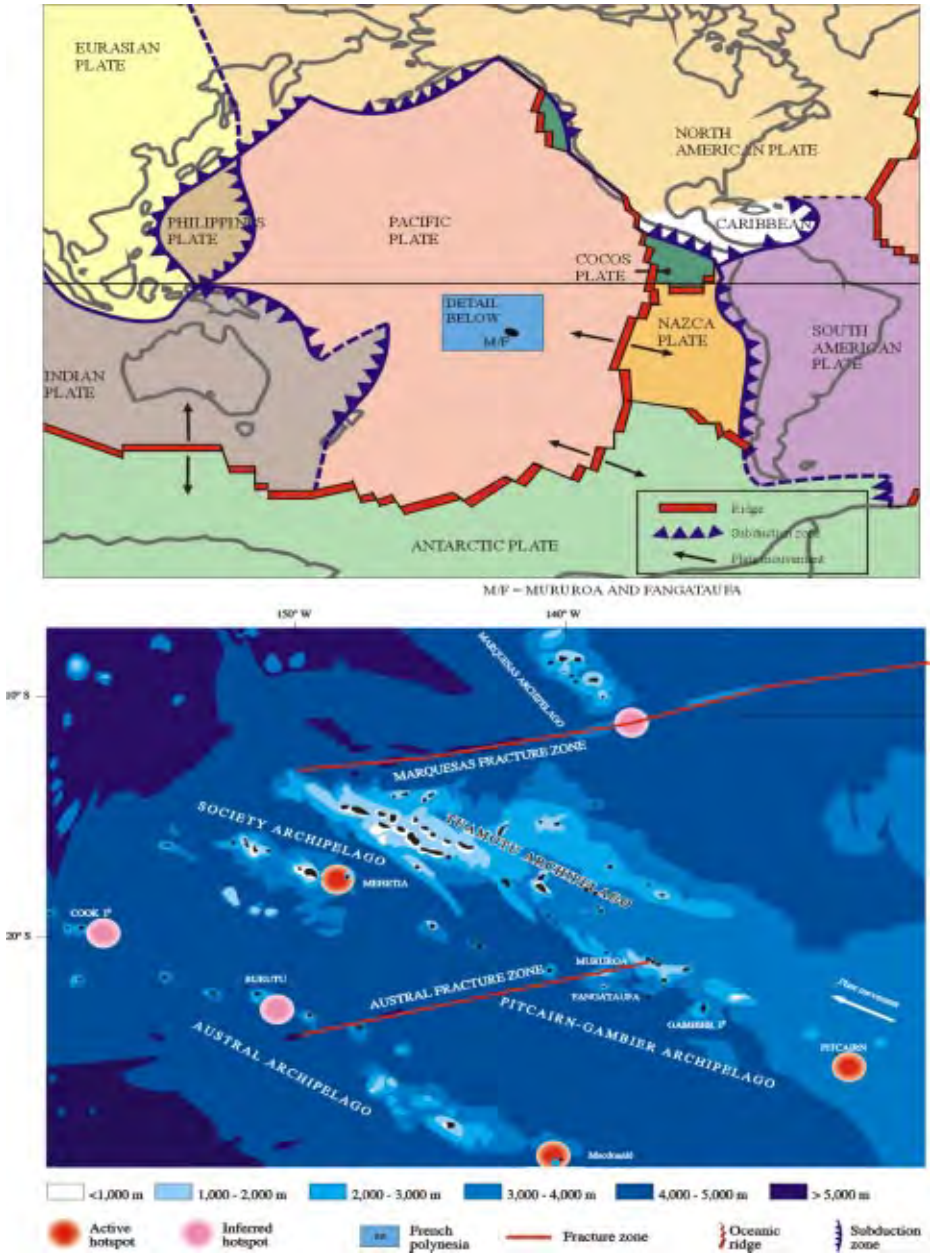

FIG. 2.30 Au-dessus : plaques lithosphériques principales, dorsales océaniques, et zones de subduction sur le contour de l'Océan Pacifique. En-dessous : détail du diagramme ci-dessus, montrant l'alignement des chapelets d'îles, les zones de fracture, et les points chauds, identifiés ou inférés, autour de Mururoa et Fangataufa (Guille *et al.* 1996)

mouvements de la surface du sol enregistrés [par des sismographes installés sur des îles de Polynésie], à 100 km de distance lors du passage de l'onde de compression, sont inférieurs à 20 micromètres [0,02 mm], et sont donc complètement imperceptibles par l'homme. Pour le même cas d'une explosion de 100 kilotonnes, le sol ne se déplace pas de plus de quelques dixièmes de micromètres à Papeete (Tahiti), située à plus de 1200 kilomètres de Mururoa. (Bouchez et Lecomte, 1996, p. 96).

L'action locale des éléments naturels (vents, vagues, tempêtes...) et des activités industrielles des régions peuplées engendrent des perturbations dynamiques du sol qui sont localement du même ordre de grandeur que les effets à longue distance des explosions. Celles-ci ne peuvent être détectées que par des séismographes sensibles placés dans des régions où le bruit de fond est faible. Il n'est donc pas crédible que des explosions au CEP puissent influencer l'activité sismique (tremblements de terre) à des milliers de kilomètres des essais.

Une discussion des estimations sismiques de l'énergie et de la localisation des essais individuels au CEP est donnée à l'annexe C.

2.16 Surveillance de la stabilité des atolls

Comme discuté plus haut dans ce Chapitre, les explosions souterraines sur les atolls ont eu pour résultat plusieurs effets structuraux importants, parmi lesquels :

1° Dans le massif volcanique

- une cavité-plus-cheminée remplie de remblais, autour de chaque point d'explosion.

  Pour la plupart d'entre elles, ces cavités-plus-cheminées sont contenues dans le massif volcanique, mais 12 essais effectués dans les premières périodes, appelés « essais CRTV » (Catégorie 3, voir annexe C) ont produit une cheminée qui a pénétré dans la base des carbonates au-dessus du massif volcanique. Bien que ces douze essais aient eu pour résultat un relâchement précoce de radionucléides (voir annexe S), aucune des cavités résultant de ces explosions ne représente une menace pour la stabilité structurelle, soit à l'échelle locale au-dessus de la cavité, soit à l'échelle de l'atoll (voir annexe H).

2° Dans les carbonates

- des affaissements de surface, atteignant 2 mètres par endroit, des récifs émergés à Mururoa (voir Figure 2.23).

  Même si la CGI estime que ces affaissements sont étroitement associés aux déformations des pentes océaniques, les affaissements ne présentent pas un risque du point de vue de la stabilité.

– des glissements de pente affectant les carbonates dans la couronne sud-ouest de Mururoa, pendant la période 1976-1979.

  Les essais souterrains ultérieurs à Mururoa ont été conduits essentiellement depuis le lagon. Il n'y a eu, apparemment, aucune activité microsismique significative dans la région sud-ouest depuis que les essais ont été déplacés vers le lagon. Ceci suggère fortement que des effets structuraux additionnels sur les flancs sud-ouest de l'atoll, liés aux essais passés, sont très peu vraisemblables.

– des déformations continues des pentes de la couronne nord-est de Mururoa.

  Le volume de roches impliqué dans ces déformations (0,6 km^3) est à peu près six fois plus grand que celui impliqué dans l'effondrement consécutif à Tydée, qui a engendré une vague de 3 mètres de haut qui a submergé une partie considérable de Mururoa (Document DIRCEN/CEA n^o 7, Section V.3) et a recouvert la partie aérienne à Fangataufa, à 45 km.

  Une inquiétude justifiée est que le glissement simultané de tout ce volume de pente océanique puisse produire une vague d'une hauteur de l'ordre de 6 à 8 mètres dans le voisinage immédiat du glissement, (Document DIRCEN/CEA n^o 12, partie 1), qui pourrait affecter l'île habitée la plus proche qui est Turéia, à 110 km au nord de Mururoa. Turéia présente une hauteur de l'ordre de 5 mètres au-dessus du niveau de la mer.

  La zone de pente qui subit des déformations consiste en plusieurs régions quelque peu distinctes, et il ne semble pas vraisemblable que le volume entier glisse en même temps (voir Figure 5.5). Il y a aussi des signes clairs que les vitesses de déformation ont diminué depuis plusieurs années, et donc peuvent se stabiliser sans qu'aucun effondrement majeur n'ait lieu. Compte tenu des incertitudes qui subsistent, et du caractère potentiellement sévère des effets, il est prudent de surveiller cette région dans les années à venir. Le système de surveillance proposé par le CEA/DASE est brièvement décrit ci-dessous.

  La géologie de la couronne nord-est de Fangataufa, dans la région comprise entre Empereur et Fox, (voir Frontispice et Document DIRCEN/CEA n^o 7, Figure 47), a été aussi sujette à des déformations de fluage et des fracturations de surface, stimulées par les essais dans le lagon de Fangataufa pendant la période 1988-1991. Selon les scientifiques du CEA, l'activité microsismique et le développement de fractures ont décliné après 1991 et ont cessé en 1993. L'activité n'est pas réapparue pendant la dernière campagne d'essais sous le lagon de Fangataufa en 1995-1996. De ce fait, une surveillance future des pentes de Fangataufa n'est pas prévue (Document DIRCEN/CEA n^o 12, Partie 1).

2.16.1 Surveillance proposée pour la pente nord-est de Mururoa

L'arrêt des essais à Mururoa et Fangataufa a été suivi par un programme d'actions visant à reconstituer, autant que cela est possible, la situation de l'environnement naturel à la surface des atolls telle qu'elle existait avant les essais. Une grande partie des infrastructures associées aux essais ont été enlevées et le personnel a été réduit au minimum. L'accès aux atolls sera strictement limité dans le futur.

Il est heureux que les développements récents dans la mesure à distance permette de lire et interpréter à distance les données des instruments de surveillance sur les atolls ; c'est-à-dire qu'il est possible de mettre en oeuvre un programme de surveillance qui ne requiert qu'une intrusion minimale dans l'environnement naturel. Le programme élaboré par les scientifiques du DIRCEN/CEA reposera très largement sur la mesure à distance. Le système d'instrumentation proposé, montré schématiquement sur les Figures 2.31 et 2.32, est pour l'essentiel analogue à celui utilisé depuis 1980 (voir Figure 5.6). Les données acquises pendant les 18 dernières années ont permis aux scientifiques du CEA de développer une très bonne compréhension des mécanismes en jeu et des vitesses qui affectent le massif qui se déforme. Ceci peut fournir un guide précieux pour la prévision du comportement futur du massif rocheux, et pour l'établissement de critères de sécurité qui assurent qu'une instabilité future ne conduira pas à un risque pour les personnels à Mururoa, ou pour qui que ce soit dans la région, notamment les habitants de Turéia (La probabilité de conséquences sérieuses d'une vague importante à 110 km de Mururoa devrait être faible, inférieure à celle d'évènements naturels dans cette région, tels que tempêtes et tsunamis).

C'est aussi une caractéristique des déformations progressives de type fluage (c'est-à-dire dépendant du temps) de grandes pentes rocheuses que l'effondrement soit précédé par une période *d'accélération du fluage* qui peut être facilement détectée par une instrumentation telle que celle qui est aujourd'hui installée à Mururoa. Ce système est maintenant très complet et comporte une redondance suffisante pour assurer une surveillance appropriée, même en cas de panne ou de dysfonctionnement de l'une de ses composantes.

La procédure à suivre pour alerter le personnel du risque d'un effondrement imminent est basée sur la vitesse relative des déformations à un instant donné, mesurée par extensométrie sur des cables horizontaux (voir diagramme supérieur de la Figure 2.32 ; voir aussi la Figure 5.18) et dans les sondages inclinés (voir diagramme inférieur sur la Figure 1.32 ; voir aussi Figure 5.9), la vitesse mesurée avant 1985 servant de référence.

Comme indiqué dans le Document DIRCEN/CEA n° 12, la vitesse de déformation relative, couramment désignée comme V.R. (Vitesse Relative) est traduite en niveau de risque, défini en termes de délai attendu avant un effondrement (imminent) majeur. Les définitions de ces niveaux de risque et des délais (avant l'effondrement) sont données ci-dessous.

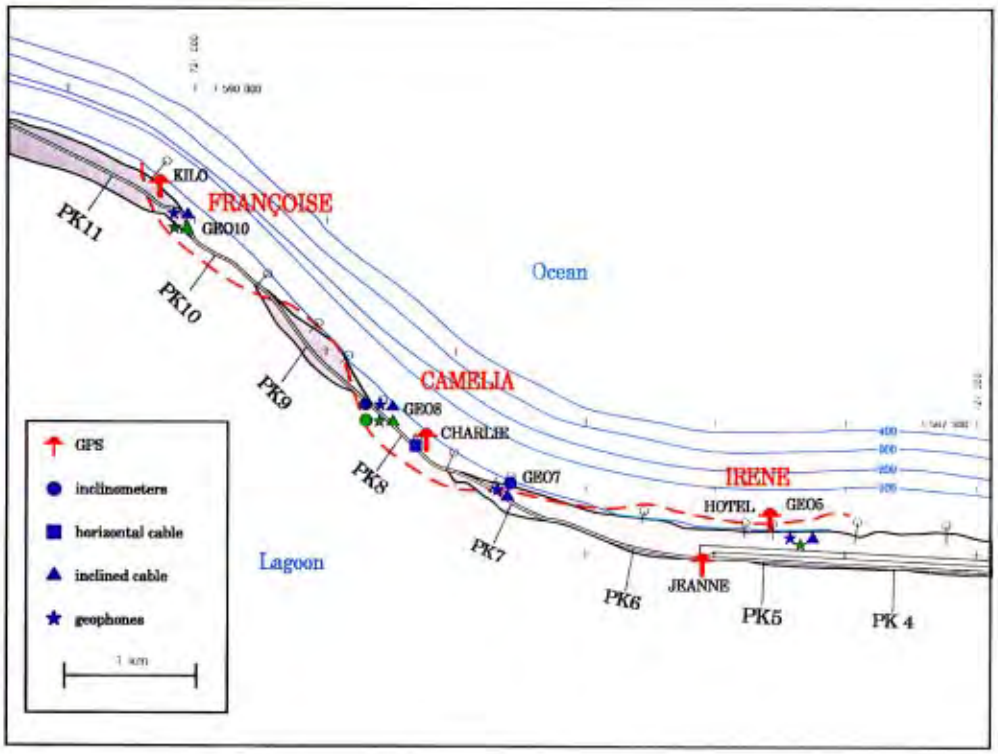

FIG. 2.31 Système de surveillance dans la zone nord-est de la couronne de Mururoa ; vue en plan (d'après Document DIRCEN/CEA n° 7)

Niveau 0	$VR < 2$	Situation normale.
Niveau 1	$2 < VR < 6$	Situation réversible. Pas de risque immédiat.
Niveau 2	$6 < VR < 12$	Situation réversible. Préavis supérieur à 1 semaine.
Niveau 3	$VR > 12$	Situation irréversible. Préavis supérieur à 1 jour.

Quoique orienté vers la surveillance de la pente nord-est, le système de surveillance comportera des composantes qui vérifieront périodiquement la situation dans d'autres parties de l'atoll. On considère que le système implique deux parties : l'une est un système permanent fonctionnant en routine ; l'autre est un système complémentaire mis en oeuvre quand une situation anormale est détectée. Les deux systèmes sont synthétisés dans les Tableaux 2.1 et 2.2.

Toute indication de risque sera rapidement communiquée au personnel du site. Le détail des procédures à suivre pour l'alerte du personnel, la réparation et la mise à jour du système, etc., est fourni dans le Document DIRCEN/CEA n° 12.

Le plan actuel envisage une période de surveillance de dix ans. À l'issue de cette période, une décision sera prise quant au maintien (ou non) du système. Si le maintien est

TAB. 2.1 Techniques utilisées pour surveiller l'évolution géomécanique normale (attendue) des atolls

Technique	Risque immédiat	Risque différé	Type de mesures	Région	Fréquence normales
Réseau microsismique séismographes et géophones	X	X	permanente	Mururoa	mesure continue
Réseau topographique de surface surveillé par le système géodétique spatial GPS		X	permanente	Nord de Mururoa	journalière
Réseau d'extensomètres		X	permanente	Nord de Mururoa	journalière
Réseau d'inclinomètres		X	permanente	Nord de Mururoa	journalière
Géomorphologie de surface par imagerie satellitaire		X	occasionnelle	Mururoa et Fangataufa	annuelle
Topographie de l'Atoll par relevé GPS		X	occasionnelle	N et SE de Mururoa	tous les 3 à 5 ans
Rattachement géodésique Régional		X	occasionnelle	atolls S. Tuamotu	tous les 3 à 5 ans
Photographie aérienne et relevés au sol de la fracturation de surface		X	occasionnelle	platier à Mururoa et Fangataufa	tous les 5 ans
Système acoustique remorqué pour déformation de surface		X	occasionnelle	récif corallien à Mururoa et Fangataufa	tous les 5 ans
Bathymétrie et sonar latéral en profondeur proche (30 à 300 m) surveillance des fractures sous-marines		X	occasionnelle	N et SE de Mururoa	tous les 5 à 10 ans
Relevé géomorphologique en eau profonde par bathymétrie (sondeur multifaisceau) et sismique haute résolution		X	occasionnelle	Flancs de Mururoa et Fangataufa	tous les 10 ans

TAB. 2.2 Actions possibles et mesures complémentaires en cas d'évolution inattendue

Technique	Type d'Intervention	Région concernée	Fréquence
Observation visuelle et photographique du platier par reconnaissance aérienne	occasionelle	Mururoa et Fangataufa	fonction du besoin
Cartographie des zones émergées par imagerie satellitaire	occasionelle	Mururoa et Fangataufa	fonction du besoin
Relevé complémentaire de la topographie de surface	occasionelle	variable	fonction du besoin
Mesure quantitative de la fracturation de surface par radar Système Acoustique Remorqué	occasionelle	Platier de Mururoa et Fangataufa	fonction du besoin

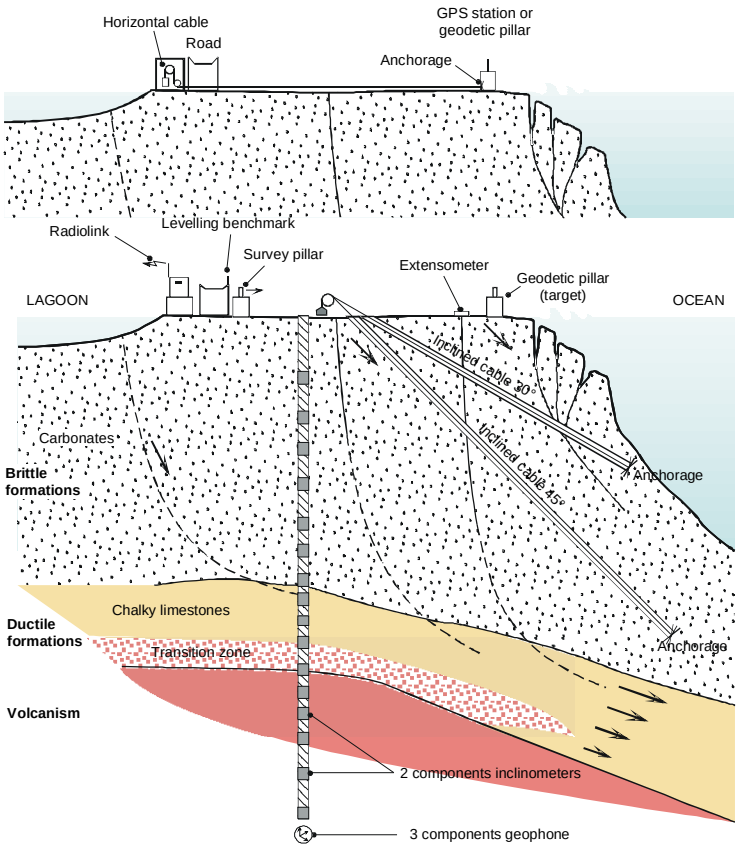

FIG. 2.32 Système de surveillance dans la zone nord-est de la couronne de Mururoa : vue en coupe (d'après Document DIRCEN/CEA n° 7)

considéré comme nécessaire, le système sera mis à jour pour incorporer les améliorations technologiques alors disponibles en télémétrie, surveillance et instrumentation.

La CGI considère que le système décrit dans le Document DIRCEN/CEA n° 12 est bien conçu, qu'il utilise des techniques conformes à l'état de l'art, et qu'il est suffisamment complet pour assurer la sécurité de toutes les personnes susceptibles d'être affectées par un effondrement de pente, et en particulier un effondrement survenant dans la couronne nord-est de Mururoa.

2.16.2 Surveillance proposée à Fangataufa

Le Document DIRCEN/CEA n° 12 indique que les observations relatives à la couronne nord-est de Fangataufa ont cessé en 1996. La CGI donne acte de ce que le volume de roches concerné par les déformations de pente et la fracturation, à Fangataufa, apparaît être plus faible qu'à Mururoa, et s'être stabilisé. Cependant, il serait bon de s'assurer

qu'aucun mouvement supplémentaire n'est effectivement survenu au moyen d'examens visuels de la fracturation de surface dans cette région, par exemple tous les deux ans. Une autre façon de faire serait que les scientifiques du DIRCEN/CEA fournissent des informations plus détaillées sur les raisons qui les conduisent à conclure que la situation à Fangataufa est stable.

Annexe A

NOTICES BIOGRAPHIQUES DES MEMBRES DE LA CGI

Pierre BEREST est diplômé de l'Ecole polytechnique (1970) et de l'Ecole des Mines de Paris (Corps technique de l'état, 1973). Il est maître de conférences (jusqu'en septembre 1998) et directeur du Laboratoire de Mécanique des Solides à l'Ecole polytechnique, France. P. BEREST est président du Comité français de Mécanique des Roches, groupe national français de la SIMR ; membre du groupe permanent Déchets et de la Commission de Sécurité des stockages souterrains.

Edwin T. BROWN est ingénieur en géomécanique, titulaire d'un Ph.D. en Mécanique des Roches obtenu à l'Université du Queensland en Australie, en 1969, et du diplôme de D. Sc. (Eng.) décerné par l'Université de Londres, G.B., en 1985, pour ses travaux publiés dans le domaine de la Mécanique des Roches de l'ingénieur. Il est présentement Second Vice-Chancelier de l'Université du Queensland et était antérieurement Professeur de Mécanique des Roches et Doyen de la Royal School of Mines au sein de l'Impérial (à cette époque) College of Science and Technology à Londres. Le Docteur BROWN est ancien Président de la Société Internationale de Mécanique des Roches (1983-1987), Fellow de l'Académie australienne des sciences technologiques et de l'ingénierie, et membre étranger de l'Académie Royale d'ingénierie de Grande Bretagne.

Ghislain de MARSILY est ingénieur des mines diplômé de l'Ecole des Mines de Paris (1963) et a obtenu un Doctorat d'état de l'Université Paris VI en 1978. Il est présentement Professeur au sein du Département des Sciences de la Terre et des Milieux Naturels de l'Université Pierre et Marie Curie (Paris VI) à Paris, France, où il enseigne l'hydrogéologie. G. de MARSILY est Fellow de l'American Geophysical Union et membre correspondant de l'Académie des Sciences de Paris. Il est Docteur Honoris Causa de l'Université du Québec et a été pendant sept ans Editeur du Journal of Contaminant Hydrology. G. de MARSILY a été membre du Committee of the U.S. National Academy of Science for Environmental Management Technologies et est membre de la Commission Nationale d'Evaluation relative aux Recherches sur la Gestion des Déchets Radioactifs.

Emmanuel DETOURNAY est ingénieur des mines diplômé de l'Université de Liège en Belgique, en 1976, et a obtenu un Ph.D. en géo-ingénierie de l'Université du Minnesota à Minneapolis, en 1983, où il est Professeur associé au Département de Génie Civil. Avant d'occuper sa position universitaire actuelle, Emmanuel DETOURNAY était Chercheur senior à Schlumberger Cambridge Research en G. B. Son domaine d'expertise est

la géomécanique pétrolière, et notamment la modélisation mathématique. Il a reçu plusieurs récompenses pour ses travaux scientifiques et technologiques, et il est membre du Comité éditorial de deux Revues internationales.

Charles FAIRHURST a obtenu un Ph.D. en génie minier à l'Université de Sheffield, Angleterre, en 1955. Il est Professeur émérite de Génie Minier et de Mécanique des Roches de l'Université du Minnesota à Minneapolis, U.S.A. ; Président de Itasca Consulting Group, Inc., Minneapolis, U.S.A., et membre de l'Advisory Committee on Nuclear Waste de la U.S. Nuclear Regulatory Commission. Ancien Président de la Société Internationale de Mécanique des Roches (1991-1995), Charles FAIRHURST est membre de la National Academy of Engineering et de la Royal Swedish Academy of Engineering Sciences. Il a été fait Docteur Honoris Causa, dans des spécialités d'ingénierie, des Universités de Saint-Petersbourg (Russie), Nancy (France) et Sheffield (Angleterre) et il est Professeur visitant Honoraire de l'Université Tongji (Shangaï, Chine).

Victor NIKOLAEVSKIY a obtenu un Ph.D. de mécanique de l'Université d'état de Moscou en Russie, en 1960 et un D.Sc. (génie minier) de l'Institut du Pétrole et du Gaz de Moscou en Russie en 1966. Il a été Postdoctoral Fellow à l'Université John Hopkins (avec C. Truesdell et J. Ericksen). Précédemment Professeur de Mathématiques Appliquées et d'Hydrodynamique à l'Université de Génie Civil de Moscou et à l'Académie Gubkin du Pétrole et du Gaz de Moscou, Victor NIKOLAEVSKIY est maintenant Directeur du Laboratoire de Géomécanique à l'Institut unifié de Physique de la Terre de l'Académie russe des sciences. Il est membre du Comité National russe de Mécanique Théorique et Appliquée de l'Académie russe des sciences naturelles. De 1965 à 1982, Victor NIKOLAEVSKIY a participé au Programme National Russe Nucléaire, dans la spécialité de la Mécanique des explosions souterraines et de la résistance dynamique des matériaux. Son domaine d'intérêt actuel est la Mécanique des processus géophysiques et les applications de la Mécanique à la récupération du pétrole et du gaz.

Anthony PEARSON a obtenu un Ph.D. en mécanique des fluides théorique de l'Université de Cambridge en Angleterre, en 1957. Il est professeur émérite de Génie chimique à Imperial College, Université de Londres, Angleterre, et consultant scientifique de Schlumberger Cambridge Research. Ancien Président et Médaille d'Or de la Société Britannique de Rhéologie, Anthony PEARSON est membre associé étranger de la U.S. National Academy of Engineering. Il est Professeur honoraire des Universités du pays de Galles et de Birmingham au Royaume Uni.

Lloyd TOWNLEY a obtenu un Ph.D. en hydrologie et hydrodynamique au Massachusetts Institute of Technology, U.S.A., en 1983. Employé jusque récemment par le Commonwealth Scientific and Industrial Research Organisation (CSIRO) à Perth, Australie occidentale, il était le Directeur pour Perth du Centre for Groundwater Studies et membre du programme de recherche sur la réhabilitation des sites miniers du CSIRO. Il

a été membre du comité éditorial de trois revues internationales et membre des comités de l'American Geophysical Union et de l'International Association for Hydraulic Research. Ancien membre de Comité national sur l'ingénierie de l'eau de The institution of Engineers, en Australie, Lloyd TOWNLEY travaille maintenant dans le secteur privé et il est professeur associé adjoint dans le département de Géologie et Géophysique de l'Université d'Australie occidentale.

Consultants

Peter CUNDALL a obtenu un Ph.D. en mécanique des roches d'Imperial College, Londres, en 1971. Il a développé des techniques et des logiciels originaux en modélisation numérique qui ont trouvé des applications dans le monde entier en géomécanique, génie civil et génie minier. Il est à l'origine de la méthode des éléments distincts qui est utilisée pour modéliser les systèmes discontinus tels que les amas de grains et les masses rocheuses, et il est chef développeur de tous les logiciels du Groupe Itasca Consulting : FLAC, UDEC, 3DEC et PFC. Peter CUNDALL a publié plus de 60 articles consacrés à divers sujets dont la genèse des bandes de cisaillement, la micromécanique des sols et des roches, la migration des fluides dans les joints rocheux et la simulation des effets des séismes sur les structures et les fondations.

Branko DAMJANAC a obtenu un Ph.D. en génie civil de l'Université du Minnesota en 1996. Il a quinze années d'expérience dans la modélisation et la simulation numérique appliquées à la Mécanique des Roches et la géomécanique pour diverses institutions de recherche et pour des consultants. Branko DAMJANAC est présentement ingénieur consultant et développeur de code pour Itasca Consulting Group, Inc., Minneapolis, U.S.A.

Pierre PERROCHET a quinze années d'expérience dans le domaine de la modélisation de l'écoulement de l'eau souterraine et du transport, au sein de diverses institutions de recherche de réputation mondiale. En 1992, il a obtenu un Ph.D. de l'Institut Suisse de Technologie (EPFL) à Lausanne où, jusque récemment, il faisait partie de l'encadrement scientifique. Les centres d'intérêt scientifiques de Pierre PERROCHET sont les interactions fluides/thermiques/chimiques à l'échelle régionale, ainsi que la conception de méthodes opérationnelles de simulation pour les grands systèmes géophysiques complexes. Il a été récemment élu Professeur d'hydrogéologie quantitative à l'Université de Neuchatel en Suisse.

Laurent TACHER a obtenu un Ph.D. d'hydrogéologie de l'Université de Neuchatel, en Suisse, en 1992. Chercheur à l'Institut Suisse de Technologie (EPFL) à Lausanne, il est principalement engagé dans les domaines de la modélisation géologique et hydrogéologique, l'infographie et le maillage.

RÉFÉRENCES DIRCEN/CEA

Les réferénces bibliographiques concernant les articles “DIRCEN/CEA documents Nos 1 – 12” cités dans le rapport CGI sont données ci-dessous. Ces documentspeuvent être obtenus des sources suivantes :

La Documentation Française
29, quai Voltaire
75344 Paris
Cedex 07
France

DIRCEN/CEA, Document No. 1

Direction des Centres d’Expérimentations Nucléaires/Commissariat à l’Energie Atomique. “Lagoon Sediment Radioactivity in Mururoa and Fangataufa,” in ***Geomechanical and Radiological Impact of Nuclear Tests at Mururoa and Fangataufa.*** Paris : La Documentation Française, 1998.

DIRCEN/CEA, Document No. 2

Direction des Centres d’Expérimentations Nucléaires/Commissariat à l’Energie Atomique. “Soil Radioactivity in Mururoa and Fangataufa,” in ***Geomechanical and Radiological Impact of Nuclear Tests at Mururoa and Fangataufa.*** Paris : La Documentation Française, 1998.

DIRCEN/CEA, Document No. 3

Direction des Centres d’Expérimentations Nucléaires/Commissariat à l’Energie Atomique. “Environmental Monitoring in French Polynesia and on the Mururoa and Fangataufa Sites, Year 1994,” in ***Geomechanical and Radiological Impact of Nuclear Tests at Mururoa and Fangataufa.*** Paris : La Documentation Française, 1998.

DIRCEN/CEA, Document No. 4

Direction des Centres d’Expérimentations Nucléaires/Commissariat à l’Energie Atomique. “Medium- and Long-Term Containment of Underground Nuclear Tests at the CEP : Source Term Inventory and Worst-Case Impact Assessment,” in ***Geo-***

mechanical and Radiological Impact of Nuclear Tests at Mururoa and Fangataufa. Paris : La Documentation Française, 1998.

DIRCEN/CEA, Document No. 5

Direction des Centres d'Expérimentations Nucléaires/Commissariat à l'Energie Atomique. "The Geological, Mechanical and Hydrogeological Environment of the Underground Nuclear Tests at Mururoa and Fangataufa," in ***Geomechanical and Radiological Impact of Nuclear Tests at Mururoa and Fangataufa.*** Paris : La Documentation Française, 1998.

DIRCEN/CEA, Document No. 6

Direction des Centres d'Expérimentations Nucléaires/Commissariat à l'Energie Atomique. "Overall Distribution and Characteristics of the Underground Nuclear Test Carried Out at Mururoa and Fangataufa and Their Effects on the Surrounding Media," in ***Geomechanical and Radiological Impact of Nuclear Tests at Mururoa and Fangataufa.*** Paris : La Documentation Française, 1998.

DIRCEN/CEA, Document No. 7

Direction des Centres d'Expérimentations Nucléaires/Commissariat à l'Energie Atomique. "Structural Integrity and Stability of the Atolls ; Data and Modelling," in ***Geomechanical and Radiological Impact of Nuclear Tests at Mururoa and Fangataufa.*** Paris : La Documentation Française, 1998.

DIRCEN/CEA, Document No. 8

Direction des Centres d'Expérimentations Nucléaires/Commissariat à l'Energie Atomique. "Experimental Data on the Mobility of the Radionuclides Deposited By the Underground Tests at Mururoa and Fangataufa - Chapters 1 (Dissolution of Lava Formed by the Underground Tests), 2 (Retention of Radioelements Deposited by Underground Tests) and 3 (Mobility of Products Deposited by the Underground Safety Tests)," in ***Geomechanical and Radiological Impact of Nuclear Tests at Mururoa and Fangataufa.*** Paris : La Documentation Française, 1998.

DIRCEN/CEA, Document No. 9

Direction des Centres d'Expérimentations Nucléaires/Commissariat à l'Energie Atomique. "Current Underground Distribution of Radionuclides at Mururoa and Fangataufa," in ***Geomechanical and Radiological Impact of Nuclear Tests at Mururoa and Fangataufa.*** Paris : La Documentation Française, 1998.

DIRCEN/CEA, Document No. 10

Direction des Centres d'Expérimentations Nucléaires/Commissariat à l'Energie Atomique. "Fangataufa : Overall Assessment of the Short, Medium and Long Term Radiological Situation of the Atolls of Mururoa and Fangataufa," in ***Geomechanical and Radiological Impact of Nuclear Tests at Mururoa and Fangataufa.*** Paris : La Documentation Française, 1998.

DIRCEN/CEA, Document No. 11

Direction des Centres d'Expérimentations Nucléaires/Commissariat à l'Energie Atomique. "Marine Data and Modelling," in ***Geomechanical and Radiological Impact of Nuclear Tests at Mururoa and Fangataufa.*** Paris : La Documentation Française, 1998.

DIRCEN/CEA, Document No. 12

Direction des Centres d'Expérimentations Nucléaires/Commissariat à l'Energie Atomique. "Guide de Surveillance Géomécanique des Atolls de Mururoa et Fangataufa," in ***Geomechanical and Radiological Impact of Nuclear Tests at Mururoa and Fangataufa.*** Paris : La Documentation Française, 1998.

Livres DIRCEN/CEA — Version Française*

Bouchez, Jacques, and Raphael Lecomte. (1995) ***Les Atolls de Mururoa et de Fangataufa (Polynésie Française),*** II. Les Expérimentations Nucléaires : Effets mécaniques. lumino-thermiques, électromagnétiques. Paris : Masson.

Guille, G., G. Goutière, J. F. Sornein, D. Buigues, A. Gachon and C. Guy. (1996) ***Les Atolls de Mururoa et de Fangataufa (Polynésie Française),*** I. Géologie - Pétrologie - Hydrogéologie : Edification et évolution des édifices. Paris : Masson.

*L'agence DIRCEN/CEA a également communiquéà l'CGI une traduction anglaise officielle du rapport de Guille et al. (1996) ainsi qu'une première ébauche de traduction des sections de tests souterrains par Bouchez et Lecomte (1996). Les numéros de pages et figures figurant dans le rapport IGC en relation avec ces ouvrages, rèferent aux versions publiées en anglais ; la traduction anglaise officielle de Bouchez et Lecomte est en cours. Les Chapitres 1–9 de la version anglaise préliminaire (dont il est fait référence dans le rapport IGC) correspondent aux Chapitres 8–16 de la version anglaise (officielle) de Bouchez et Lecomte (1996).

BIBLIOGRAPHIE

Barrillot, B. (1996) Les Essais Nucléaires Française 1960-1996 : Conséquences sur L'environment et la Santé. Lyon, France : Centre de Documentation et de Recherche sur la Paix et les Conflits.

Bouchez, J., Y. Caristan and C. Mariotti (1997) Stabilité des pentes sous-marines de l'atoll de Mururoa sous sollicitations dynamiques. *Revue Française Géotechnique*, **78**, 3–13.

Bouchez, J. and R. Lecomte (1996) The Atolls of Mururoa and Fangataufa (French Polynesia). II. Nuclear Testing, Mechanical Lumino-Thermal and Electromagnetic Effects (in Collaboration with J. Brugies, C. Guerrini, J.-F. Sornein, J.-L. Plantet and E. Blanc). Monaco : Musée Océanographique.

Brenner, H. and D. A. Edwards (1993) Macrotransport Processes. Stoneham, Mass. : Butterworth-Heinemann.

Buigues, D. (1997) Geology and hydrogeology of Mururoa and Fangataufa, French Polynesia. In H. L. Vacher and T. M. Quinn (editors), *Geology and Hydrogeology of Carbonate Islands*, vol. 1, chap. 13, pp. 433–451, Amsterdam : Elsevier.

CRII-RAD (1995a) Essais nucléaires (revue d'information de la CRII-RAD). Tech. Rep. 3, Commission de Recherche et d'Information sur la Radioactivité, Valence, France.

CRII-RAD (1995b) Revue d'Information. Technical Report, Commission de Recherche et d'Information sur la Radioactivité, Valence, France.

Denbigh, K. G. and J. Turner (1971) Chemical Reactor Theory. Cambridge : Cambridge University Press.

Fondation Cousteau, Paris (1988) Mission scientifique de la Calypso sur le site d'expérimentations nucléaires de Mururoa. Technical Report.

Goguel, J. (1982) L'évolution du cadre naturel. In *Rapport D'Haroun Tazieff*, no. Annex 2.

Guille, G., G. Goutière, J. F. Sornein, D. Buigues, A. Gachon and C. Guy (1996) The Atolls of Mururoa and Fangataufa (French Polynesia). I. Geology - Petrology - Hydrogeology, from Volcano to Atoll (translated by M.S.N. Carpenter). Monaco : Musée Océanographique.

IAEA (1998a) The radiological situation at the atolls of Mururoa and Fangataufa : Main report. Tech. rep., International Advisory Committee, Vienna.

IAEA (1998b) The radiological situation at the atolls of Mururoa and Fangataufa : Technical report, Vol. 4, Releases to the biosphere of radionuclides from underground nuclear weapon tests at the atolls, report by working group. Tech. rep., International Advisory Committee, Vienna.

IAEA (1998c) The radiological situation at the atolls of Mururoa and Fangataufa : Technical report, Vol. 3, Inventory of radionuclides underground at the atolls, report by working group. Tech. rep., International Advisory Committee, Vienna.

IAEA (1998d) The radiological situation at the atolls of Mururoa and Fangataufa : Technical report, Vol. 5, Transport of radioactive material present within the marine environment, report by working group. Tech. rep., International Advisory Committee, Vienna.

IAEA (1998e) The radiological situation at the atolls of Mururoa and Fangataufa : Technical report, Vol. 6, Doses due to radioactive material present in the environment or released from the atolls, report by working group. Tech. rep., International Advisory Committee, Vienna.

Lalou, C., J. L. Reyss and R. Boichard (1988) Relations entre certains aspects de la sédimentaion carbonatée dans le golf arabo-persique et les niveaux de stagnation concomitante de la mer au cours des 500 000 dernières années. *C. R Acad. Sci. Paris*, **307**, 1211–1216.

New Zealand MoFA (1984) Report of a New Zealand, Australian, and Papua New Guinea scientific mission to Mururoa Atoll. Tech. rep., New Zealand Ministry of Foreign Affairs, Wellington.

Nikolaevskiy, V. N. (1996) Geomechanics and Fluidodynamics. Dordrecht, The Netherlands : Kluwer.

Perrochet, P. and L. Tacher (1997a) Mathematical modeling of hydro-thermal processes in Mururoa atoll. Tech. Rep. International Geomechanical Commission (University of Minnesota), École Polytechnique Fédérale de Lausanne, Laboratoire de Géologie.

Perrochet, P. and L. Tacher (1997b) Personal communication.

Shackleton, N. J. (1987) Oxygen isotropes, ice volumes and sea level. *Quartern. Sci. Rev.*, **6**, 183–190.

Sharma, A. (1998) India sets off three nuclear blasts. *St. Paul Pioneer Press*, (May 12), Associated Press.

Starfield, A. M. and P. A. Cundall (1988) Towards a methodology for rock mechanics modelling. *Int. J. Rock Mech., Min. Sci. & Geomech. Abstr.*, **25**(3), 99–106.

Tazieff, H. (1982) Rapport d'Haroun Tazieff sur l'ensemble de la mission scientifique en Polynesie Française. Tech. rep.

Vincent, P. M. (1996) The impact of underground nuclear explosions at Mururoa Atoll (South Pacific) and associated hazards. *Médecine : Re Nucléaire*, **11**(1).

GLOSSAIRE

Advection (d'un soluté) Transport d'un soluté, par des eaux en mouvement dans un milieu poreux, s'effectuant à la vitesse de l'eau, lorsque la concentration du soluté n'est pas suffisante pour modifier la densité de l'eau.

Affaissement Dans le contexte des essais nucléaires souterrains, dépressions permanentes à la surface du sol provoquées par des déformations irréversibles des couches de surface induites par l'onde dynamique. Celle-ci se propage depuis le point d'explosion à travers le massif rocheux qui le surmonte.

Bar Unité de pression. 1 bar = 1,01972 kilogramme poids par centimètre carré, ou 10^5 pascals. La pression atmosphérique est égale à environ 1 bar (on dit souvent 1000 millibar). Multiples : 1 kilobar (kb) = 10^3 bars ; 1 Mégabar (Mb) = 10^6 bars.

Barrière (de corail) Récif de corail situé au large d'une île ou d'un continent, formant parfois un anneau. Un tel récif peut se développer tardivement dans un atoll par descente graduelle de la partie centrale.

Basalte Roche volcanique à grains fins de couleur sombre composée de feldspath plagioclase, de pyroxène et de magnétite, avec ou sans olivine, et ne contenant pas plus de 53% (en poids) de SiO_2.

Brèche Famille de roches formées principalement de fragments anguleux (taille des grains inférieure à 2 mm) cimentés par du matériau plus fin.

Calcite Forme du carbonate de calcium, contenant des fractions variables de magnésium.

Carbonates Dans les deux atolls, la couverture carbonatée comprend des calcaires et des dolomites ; son épaisseur varie entre 130 m et 450 m à Mururoa, et est environ de 230 m à Fangataufa.

Cavité Volume formé autour de la chambre d'essai à la suite d'une explosion nucléaire souterraine.

Célérité du choc Vitesse d'un front de choc se propageant dans un matériau fluide ou solide. Cette vitesse dépend de la nature du milieu et de l'énergie transportée par l'onde de choc.

Cheminée Zone de forme à peu près cylindrique, remplie de remblai rocheux, qui se forme après que la cavité créée par l'explosion nucléaire s'est effondrée. La hauteur de la cheminée est étroitement liée à l'énergie et à la profondeur du tir.

Chutes sous-marines de blocs rocheux Chutes de roches survenant exclusivement dans des pentes locales raides, quasi verticales.

Cimentation Processus par lequel des débris bioclastiques épars se lient entre eux ; ce processus contribue à la lithification du récif de l'atoll.

Compaction (des carbonates) Le fait de comprimer les matériaux carbonatés (consolidation) sous l'effet d'une pression ou d'un impact, conduisant à rendre relativement plus dense le massif.

Conduction (de la chaleur) Transport de la chaleur à travers la roche ou l'eau sans déplacement de l'eau contenue dans les pores.

Conglomérat Gravier cimenté dans lequel les galets et grains (de dimension supérieure à 2 mm) constituent plus de 50% de la roche.

Contrainte d'origine physico-chimique Contrainte résultant de modifications chimiques et/ou physiques affectant la roche (par exemple recristallisation, absorption de l'eau, fluctuation du niveau de l'eau souterraine).

Contraintes gravitaires Contraintes résultant du poids des roches surincombantes.

Contraintes induites Composantes résultant de l'activité humaine, provoquées par l'enlèvement ou l'addition de matériaux ; elles s'ajoutent aux contraintes naturelles préexistant à l'activité humaine.

Contraintes in situ Contraintes existant en un point du massif rocheux avant que le massif ne soit perturbé.

Contrainte résiduelle Contrainte subsistant dans le massif rocheux alors même que le mécanisme qui était à son origine a cessé de produire ses effets.

Contraintes tectoniques Peuvent être actives, résultat d'une déformation actuelle de la croûte terrestre ; ou rémanentes, quand elles résultent d'évènements tectoniques passés dont les effets n'ont été que partiellement effacés par les processus naturels.

Contraintes thermiques Contraintes qui résultent de variations de température ; elles peuvent être de nature locale, ou faire partie des contraintes tectoniques.

Convection (de la chaleur) Transport de la chaleur par des eaux en mouvement dans un milieu poreux ; les mouvements dans un fluide qui résultent des contrastes de densité (dus à la dilatation thermique) et de l'action de la gravité sont appelés « convection naturelle », alors que la convection forcée désigne le cas où la vitesse du fluide trouve son origine dans d'autres causes que les contrastes de densité.

Couplage Quand il se rapporte aux explosions nucléaires, ce terme désigne le mécanisme par lequel l'énergie d'une explosion nucléaire est transmise au massif rocheux environnant, et en particulier la proportion de cette énergie qui est transmise. Cette proportion est reliée directement à la quantité de gaz produite par le relâchement de l'énergie thermique.

Courants de turbidité Instabilité de pente sous-marine impliquant le transport, le long de la pente, de sédiments soulevés par l'écoulement turbulent de fluide.

Courbe d'Hugoniot Courbe représentant le lieu de tous les états thermodynamiques accessibles par choc depuis un état initial donné.

Couronne corallienne Partie du récif corallien en forme d'anneau située au-dessus du niveau de la mer et constituant la partie émergée d'un atoll.

Cratères de subsidence Suite à un essai nucléaire souterrain, effondrement de la cavité et formation d'une cheminée affectant les couches jusqu'à la surface. Contrastant avec les Cratères d'explosion, les cratères de subsidence ne donnent pas lieu à l'expulsion de matériau superficiel.

Cratères d'explosion Provoqués par l'expulsion de sol et l'effondrement de la cavité à la suite d'un essai nucléaire souterrain suffisamment proche de la surface.

CRTV Essais nucléaires à l'issue desquels la cheminée atteint le toit du massif volcanique.

Darcy Unité courante de mesure de la perméabilité, dont la dimension est celle d'une aire (L^2), caractérisant un matériau poreux dans lequel 1 cm^3 de fluide d'une viscosité de 1 centipoise s'écoule en 1 seconde, sous l'effet d'une différence de pression de 1 bar, à travers un cylindre présentant une section de 1 cm^2 d'aire et une longueur de 1 cm. Un Darcy est égal à $0,987\ 10^{-12}$ m^2.

Découplage Quand il se rapporte aux explosions nucléaires, ce terme désigne les techniques qui permettent de minimiser la proportion de l'énergie d'une explosion nucléaire qui est transmise sous forme mécanique au massif rocheux environnant (voir **Couplage**).

Densité moyenne Masse totale des fractions liquide et solide d'un échantillon de roche poreuse, divisée par le volume total de l'échantillon.

Densité saturée Quotient de la masse d'un échantillon de sol ou de roche par son volume quand tous les vides et pores sont remplis d'eau (voir aussi **Densité sèche**).

Densité sèche Quotient de la masse d'un échantillon de sol ou de roche par son volume lorsque l'échantillon est sec et que les vides et les pores ne contiennent pas d'eau (voir aussi **Densité saturée**).

Détritiques Désigne des matériaux formés de matière fragmentée provenant de l'érosion de roches pré-existantes (les dépôts détritiques forment fréquemment des inter-lits dans les formations carbonatées).

Diagraphie Mesure de caractéristiques des formations géologiques, réalisée en forage au moyen d'instruments de mesure géophysique.

Dolomite Un carbonate mixte de calcium et magnésium ; désigne aussi un type de roche sédimentaire formée de ce minéral.

Dolomitisé Affecté par un processus de dolomitisation, au cours duquel le calcaire est partiellement ou complètement transformé en dolomite ou calcaire dolomitique par substitution du carbonate de calcium (calcite) par du carbonate de magnésium.

Dyke Intrusion de roche (volcanique) perçant les couches préexistantes. La plupart des dykes sont verticaux ou proches de la verticale, étant montés à travers les roches sus- jacentes.

Eau de pore Eau contenue dans les pores d'une formation géologique.

Écaillage Déplacement vers le haut ou vers l'extérieur de couches de roche et de sédiment de surface, ou proches de la surface, provoqué par l'interaction d'une onde de compression avec la surface libre. L'onde peut provoquer une fragmentation ou une séparation momentanée de certaines couches. L'écaillage de surface associé aux explosions nucléaires survient quand une couche rocheuse de surface se sépare des roches sous-jacentes en formant une fracture horizontale, engendrée par le pulse de traction descendant qui résulte de la réflection de l'onde incidente par la surface libre.

Échange thermique Échange de chaleur par conduction et convection dans un matériau solide.

Écoulements (de sédiments) Déplacements des sédiments vers le bas d'une pente, notamment écoulements de débris, écoulement de grains et liquéfaction. Les écoulements sont parfois considérés comme une transition entre les glissements et les courants de turbidité.

Endo-upwelling Circulation géothermique qui résulte de la montée de l'eau souterraine dans la région centrale d'un atoll, et de l'entrée concomitante de l'eau froide océanique à travers les flancs de l'atoll, qui alimente cette montée.

Énergie (d'un tir) Énergie effectivement relâchée dans une explosion nucléaire, se manifestant par choc ou explosion, radiation thermique et radiation nucléaire. La radiation nucléaire résiduelle associée aux produits de fission, qui s'élève à 10% de l'énergie totale de fission, n'est pas incluse dans l'énergie. L'énergie (d'un tir) est en général exprimée en équivalent TNT Ð la quantité de TNT dont l'explosion conduirait au relâchement de la même quantité d'énergie. L'équivalent TNT est en général donné en kilotonnes ou mégatonnes, un kilotonne de TNT étant par convention égal à $4,18\ 10^{12}$ joules.

Essai de sécurité Détonation d'un anneau d'explosif chimique placé autour d'un engin nucléaire, effectuée pour vérifier si elle peut déclencher une explosion nucléaire.

Facteur de sécurité Dans l'analyse de stabilité d'une pente, la quantité (unique) par laquelle il faut, pour provoquer l'affaissement de la pente, réduire la résistance de toutes les unités géologiques impliquées.

Faille Une fracture ou zone de fractures le long de laquelle est survenu un déplacement relatif des deux surfaces parallèlement à la fracture.

Fluage Déformation continue (au cours du temps) d'un matériau sous charge constante ; comportement des matériaux terrestres en réponse à des facteurs tels que le temps, la température, la pression de pore, et le niveau de contraintes.

Fosse Étendue océanique profonde, voisine d'une frange continentale, associée à une marge de plaque active ou à une zone de subduction.

Frange récifale Plate-forme corallienne formée autour d'une île et s'étendant au voisinage immédiat du rivage.

Glissements Forme la plus fréquente prise par les instabilités de pente sous-marine, affectant la roche ou des sédiments mous.

Gradient hydraulique Mesure de la variation de la pression de l'eau dans une direction donnée pour une distance unité (voir aussi **Loi de Darcy**).

Hoa Passage entre **motus** (îlets) dans une barrière récifale, permettant les échanges d'eau de mer entre l'océan et le lagon.

Hyaloclastite Brèche volcanique formée sous l'eau, composée de fragments vitreux de taille supérieure à 4 mm et souvent associés aux pillow lavas (laves en coussin).

Hydrothermal Relatif aux fluides chauds qui circulent dans la croûte terrestre.

Karst Modifications internes de massifs rocheux apparaissant spécifiquement dans les massifs calcaires et qui résultent d'une dissolution à des degrés variables par les eaux météoriques (érosion karstique, cavité) ; elles sont caractérisées par l'élargissement de fractures, une porosité renforcée, des grottes, un drainage souterrain et, parfois, par la formation de cratères à la surface. Ces traits peuvent être reconnus à des profondeurs variées à l'intérieur d'un massif calcaire ; ils sont liés à des niveaux moins élevés qu'aujourd'hui de la mer ou de la nappe phréatique.

Kilotonne (kt) Unité utilisée pour quantifier l'énergie dégagée par des explosions nucléaires ou thermonucléaires. Elle correspond à l'énergie libérée par 1 000 tonnes d'un explosif chimique de référence, le Trinitrotoluène (TNT), soit une énergie de $4,18\ 10^{19}$ ergs ou $4,18\ 10^{12}$ joules ou 10^{12} calories. Pour les explosions thermonucléaires on utilise souvent la Mégatonne (Mt) : 1 Mt = 10^3 kt.

Liquéfaction Processus par lequel un chargement cyclique (résultant d'un tremblement de terre, d'une explosion ou de l'action d'une onde) produit un accroissement de la pression de pore, dans des conditions non-drainées ou partiellement non-drainées, conduisant à la rupture et à l'écoulement plastique de sédiments.

Loi de Darcy Loi qui décrit la vitesse du mouvement de l'eau dans les milieux poreux. Elle stipule que cette vitesse est proportionnelle au gradient hydraulique ; on peut l'écrire $u = Ki$, où u est le volume d'eau traversant une aire unité par unité de temps, K est la conductivité hydraulique (quantité proportionnelle à la perméabilité) et i est la variation de charge hydraulique par unité de longueur le long de l'écoulement (appelée aussi gradient hydraulique).

Longueur d'onde Distance entre deux points consécutifs de même phase d'un mouvement ondulatoire se propageant en ligne droite.

Mégatonne (Mt) Unité utilisée pour quantifier l'énergie dégagée par des explosions nucléaires ou thermonucléaires. Elle correspond à l'énergie libérée par 1 million de tonnes d'un explosif chimique de référence, le TNT. Le kilotonne (1 kt = 0,001 Mt) est également utilisé.

Motu Petit îlet formé de matériau bioclastique, faisant partie de la couronne récifale d'un atoll.

Nucléide Élément atomique caractérisé par son nombre de masse, son numéro atomique et son état d'énergie (voir aussi Radionucléides).

Onde de Rayleigh Onde sismique engendrée par un tremblement de terre, ou une explosion nucléaire souterraine qui n'affecte que les couches les plus superficielles du milieu.

Onde P-(primaire) Onde de compression résultant d'un tremblement de terre, ou d'une explosion nucléaire souterraine ; c'est l'onde de vibration la plus rapide.

Onde S-(secondaire) Onde de cisaillement, se propageant sous la forme d'une onde sismique, engendrée à la suite d'une explosion nucléaire souterraine.

Onde sismique Onde élastique qui se propage dans la Terre entière, sous la forme d'une vibration, et qui est engendrée par un tremblement de terre ou une explosion nucléaire souterraine.

Perméabilité Aptitude à laisser l'eau circuler (voir aussi **Loi de Darcy**) ; la perméabilité de « matrice » est déterminée principalement par le degré de communication entre les pores (voir aussi **Porosité**).

Pillow lava (coussin de lave) Écoulement volcanique sous-marin formant un entassement désorganisé d'unités en forme de coussins.

Point zéro Emplacement exact de l'engin nucléaire expérimental et du conteneur d'instrumentation.

Point zéro au sol Point de la surface du sol placé à la verticale du point zéro.

Porosité Quotient du volume de l'espace poreux par le volume total d'un échantillon de roche ou d'une formation rocheuse.

Porosité moyenne Volume des pores, exprimé en pourcentage du volume total d'un échantillon poreux.

Pression hydrostatique Pression excercée par la colonne d'eau sus-jacente en l'absence de mouvement du fluide.

Pression lithostatique Pression résultant en profondeur du poids de la colonne de terrains sus-jacents.

Pulse sismique Créé par une explosion nucléaire souterraine, le pulse se propage à grande distance dans l'environnement géologique.

Radionucléide Élément atomique radioactif.

Rai sismique Chemin suivi par une onde sismique. Dans un milieu isotrope, ce chemin est perpendiculaire au front d'onde.

Récif Voir Barrière récifale.

Relâchement Dans le contexte des explosions nucléaires, transport de gaz radioactifs hors de la cavité créée par l'explosion, en direction des roches environnantes, ou même de la biosphère, via les fractures ou d'autres cheminements créés par l'explosion.

Relations d'Hugoniot Les trois conditions de saut à la traversée d'une discontinuité qui lient les variables caractéristiques de l'état d'un matériau. Ces conditions portent le nom du savant qui les a établies ; elles traduisent la conservation de la masse, de la quantité de mouvement et de l'énergie au cours de la transition instantanée entre un état de repos et un état chargé.

Résistance à la compression non confinée (ou uniaxiale) Résistance à la compression uniaxiale d'une éprouvette, déterminée en effectuant un essai de compression sur une éprouvette dont les faces latérales sont laissées libres de tout confinement.

Résistance au cisaillement Valeur limite que peut atteindre le cisaillement, au-delà de laquelle apparaissent des déformations plastiques de la roche ; elle mesure l'aptitude de la roche à supporter les compressions. La résistance au cisaillement est influencée par la pression de pore du fluide contenu.

Roches volcaniques subaériennes Roches surmontant les roches volcaniques sous-marines qui ont été formées quand le sommet du volcan a émergé de l'océan. Elles sont plus diverses, et plus variables dans l'espace, que les roches sous- marines. Leurs types varient des basaltes massifs aux dépôts de cendres volcaniques.

Saturée en eau (roche) Roche dont les pores sont remplis d'eau.

SOFAR (canal) Sound Fixing and Ranging channel Couche d'eau de mer dans l'océan, située en général entre 500 m et 1500 m de profondeur, dans laquelle la vitesse de propagation des ondes est minimum, en raison des caractéristiques

de salinité et de température de l'océan. Les ondes guidées, piégées dans le chenal SOFAR, se propagent en restant à l'intérieur de ce dernier sur de très longues distances en demeurant peu affectées par l'atténuation.

Vitesse de Darcy Vitesse fictive d'écoulement, calculée en supposant que le débit se répartit uniformément dans la section (pores et roche) que l'on considère. En fait, l'eau ne se déplace qu'à travers les espaces poreux interconnectés, qui ne représentent qu'une certaine proportion du volume rocheux total. Bien que la constante K (voir **Loi de Darcy**) ait les dimensions d'une longueur divisée par un temps (dimensions d'une vitesse) la vitesse de Darcy s'exprime par le produit Ki.

Zéolite Famille d'argiles hydratées, alumino-silicates de sodium, potassium, calcium et barium que l'on trouve dans des géodes, dans des roches ignées altérées, des veines hydrothermales et certains sédiments.

Zone de transition Couche sédimentaire, dont l'épaisseur n'est que de quelques mètres, entre les roches volcaniques sous-marines et subaériennes. La zone de transition comporte deux couches distinctes : une couche sédimentaire de roche conglomératique calcaire, argillacée ou volcanique ; et une couche de roches sous-marines peu profondes, principalement des laves fortement brèchées.

Zone vaporisée Zone du voisinage immédiat du point zéro où la roche a été fondue et vaporisée par le choc intense résultant de l'explosion.